

به نام خدا



# مرکز دانلود رایگان مهندسی متالورژی و مواد

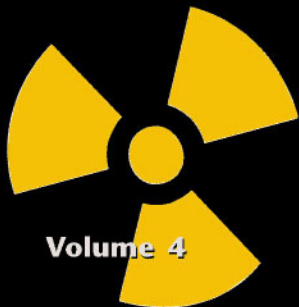
[www.Iran-mavad.com](http://www.Iran-mavad.com)



**NONDESTRUCTIVE TESTING**

Third Edition

# **HANDBOOK**



**Volume 4**

## **Radiographic Testing**

**Technical Editors**

**Richard H. Bossi**

**Frank A. Iddings**

**George C. Wheeler**

**Editor**

**Patrick O. Moore**

American Society for Nondestructive Testing

## ***Nondestructive Testing Handbook, third edition:*** **Volume 4, Radiographic Testing on CD-ROM**

The content of the printed book has been reproduced exactly in *portable document format* (pdf) files accessed with the Adobe Acrobat Reader. (*Adobe Acrobat Reader with Search* for Windows and Macintosh are provided on this CD.) Additional features of the CD-ROM version include video, more than 50 color illustrations, bookmarked links for navigating from point to point and searchable text.

All text has been indexed for electronic search. Use the *Find* tool to locate text in individual documents. Use the *Search* tool to look in all documents. *Acrobat Reader with Search* generates a list of documents containing your search request in order of greatest incidence first. Click an item in the list to open it. Every instance of the search results is highlighted. Click *Go to Next View* arrow to increment forward, *Go to Previous View* arrow to increment back. Parts within chapters contain *Article Threads* that facilitate reading from column to column. Click with the *Hand* tool within a column to automatically enlarge the view and increment text. The Adobe Acrobat Reader Guide has comprehensive instructions. [Click here](#) to open.

### **Explanation of Linking Structure**

- Open any pdf document. All are interconnected and it is not necessary to access them in any particular order.
- Each document is designed to open to the title page of a chapter or the first page of a book segment. The *Bookmark Pane* appears on the left. *Bookmarks* link to a view within the current document or to a view in another document. Click to open the view. An arrow or triangle to the left of a bookmark indicates a subhead. Click to expand for additional links. Click again to close.
- Each Bookmark Pane has these basic Bookmarks.

**User's Introduction to this CD-ROM**

**Front Matter with Table of Contents**

**Multimedia Contents**

**Links to Chapters**

**Index**

**Figure Sources**

**Movie Sources**

- **User's Introduction to this CD** — instructions for tools and linking structure.
- **Front Matter with Table of Contents** — publishing info and links to contents.
- **Multimedia Contents** — pages with text links to video files.
- **Links to Chapters** — comprehensive links to subheads, figures, tables and equations within the current document and a single link to every other chapter.
- **Index** — index for the complete volume.

## Navigation Tools

Installers for the Adobe Acrobat Reader with Search provided on this CD-ROM also install online help called *Reader Guide* under the *Help* menu (or [click this link](#)). Complete instructions for tools are there.

Acrobat Reader toolbar.



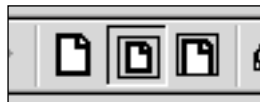
Page turners for current document — first page, previous page, next page, and last page.



Go to *Previous View* or Go to *Next View* along viewing path.



Adjust size of document in view window — 100 percent, fit in window, or fit width



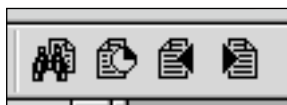
*Hand* tool moves document within window. Indicates an action by changing to pointing hand when passing over a link or article thread.



*Find* tool — enter a text string to search for a word or words within the current document.



Search all indexed documents. First icon opens *Adobe Acrobat with Search*. Click *indexes...* to select *Radiographic Testing* (browse to locate *xcatalog.pdx* on CD-ROM). Enter text string in *Find Results Containing Text* field. Click *Search*. Second icon will list all documents containing instances of search request in order of greatest incidence first. Click to select a document. Remaining two tools step forward or back to each highlighted instance of text search. For detailed instructions for this advanced search feature, [click this link](#).

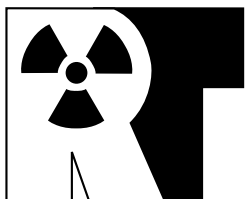




# NONDESTRUCTIVE TESTING HANDBOOK

Third Edition

Volume 4



## Radiographic Testing

Technical Editors  
Richard H. Bossi  
Frank A. Iddings  
George C. Wheeler

Editor  
Patrick O. Moore



American Society for Nondestructive Testing

[www.iran-mavad.com](http://www.iran-mavad.com)

مرجع دانشجویان و مهندسين مواد

**Copyright © 2002**  
**AMERICAN SOCIETY FOR NONDESTRUCTIVE TESTING, INC.**  
**All rights reserved.**

No part of this book may be reproduced, stored in a retrieval system or transmitted, in any form or by any means — electronic, mechanical, photocopying, recording or otherwise — without the prior written permission of the publisher. Nothing contained in this book is to be construed as a grant of any right of manufacture, sale or use in connection with any method, process, apparatus, product or composition, whether or not covered by letters patent or registered trademark, nor as a defense against liability for the infringement of letters patent or registered trademark.

The American Society for Nondestructive Testing, its employees, and the contributors to this volume assume no responsibility for the safety of persons using the information in this book.

Copyright © 2002 by the American Society for Nondestructive Testing, Incorporated. All rights reserved. ASNT is not responsible for the authenticity or accuracy of information herein, and published opinions and statements do not necessarily reflect the opinion of ASNT. Products or services that are advertised or mentioned do not carry the endorsement or recommendation of ASNT.

ACCPSM, IRRSP<sup>SM</sup>, *Level III Study Guide*<sup>SM</sup>, *Materials Evaluation*<sup>SM</sup>, *NDT Handbook*<sup>SM</sup>, *Nondestructive Testing Handbook*<sup>SM</sup>, *The NDT Technician*<sup>SM</sup> and [www.asnt.org](http://www.asnt.org)<sup>SM</sup> are service marks of the American Society for Nondestructive Testing. ASNT®, *Research in Nondestructive Evaluation*® and *RNDE*® are registered trademarks of the American Society for Nondestructive Testing.

ASNT exists to create a safer world by promoting the profession and technologies of nondestructive testing.

American Society for Nondestructive Testing, Incorporated  
1711 Arlingate Lane  
PO Box 28518  
Columbus, OH 43228-0518  
(614) 274-6003; fax (614) 274-6899  
[www.asnt.org](http://www.asnt.org)

## Errata

Errata if available for this printing may be obtained from ASNT's Web site, [www.asnt.org](http://www.asnt.org), or as hard copy by mail from ASNT, free on request addressed to the *NDT Handbook* Editor at the address above.

### Library of Congress Cataloging-in-Publication Data

Radiographic Testing / technical editors, Richard H. Bossi, Frank A. Iddings, George C. Wheeler; . -- 3rd ed.

p. cm. — (Nondestructive testing handbook ; v. 4)

Includes bibliographic references and index.

ISBN 1-57117-046-6

1. Radiography, industrial. I. Bossi, R. H. II. Iddings, F.A. III. Wheeler, G.C.

IV. Moore, Patrick O. V. American Society for Nondestructive Testing.

IV. Series: Nondestructive testing handbook (3rd ed.) ; v. 4.

TA417.25 .R32 2002

2002012672

620.1'1272--dc21

Published by the American Society for Nondestructive Testing

PRINTED IN THE UNITED STATES OF AMERICA

## NOTE:

Information presented on this page (highlighted in gray) is specific for the printed version of this publication. For Library of Congress Cataloging-in-Publication data pertaining to the CD-ROM edition, please [click this link](#).

---

---

---

---

---

# President's Foreword

The twenty-first century has now arrived and we are aware that technology will continue to accelerate at blinding speed. As these changes occur, adaptation and implementation by the end user must keep pace with proven innovations. As managers and engineers we have been quick to defend the status quo and have been slow to change when change is needed. Currently we are seeing a significant lag in the usage of such innovations as digital radiography. The new challenge for practitioners and regulatory bodies will be the acceptance and integration of this already proven technology.

The vitality and future of the American Society for Nondestructive Testing depend on the creation, improvement and sharing of information so that safety and reliability stay at the forefront of product development.

This volume represents the efforts of many dedicated professionals who have embraced change and given freely of their time with the mission of making a difference in their chosen profession. ASNT commends each and every contributor for their efforts in bridging today's technology with tomorrow's possibilities.

There were more than 100 individual contributors and reviewers, representing both volunteers and staff in an essential ongoing partnership. Each has given a piece of themselves that can never be repaid.

A special thanks is due to technical editors Richard Bossi, Frank Iddings and George Wheeler for their commitment to this project. This job requires an in-depth understanding of the component parts of the technology. The job is long and tedious and must be driven from the heart and the mind.

I must also thank the ASNT staff and *NDT Handbook* Editor Patrick Moore for their guidance and continued pursuit of excellence. Year in and year out they have made the necessary sacrifices to ensure quality and value.

Finally, reflective tribute must go to an individual who crossed paths with my

ASNT career briefly in 1974. His start in the NDT profession came as a radiographer in the Boston ship yards. His name was Philip Johnson. He was the architect and founder of this society. He was the visionary who saw the need to draw upon our collective differences and unite for a common cause.

Johnson served as the organization's Secretary from 1941 to 1965. He also assumed the dual role of editor for many of those years. In addition Johnson served as our Executive Director from 1965 through 1974. Phil provided the continuity and focus that must sustain any organization in those formative years. As you read through this book remember that it was Johnson that made possible the process of cooperative collaboration.

Stephen P. Black  
ASNT President, 2001-2002

# Foreword

## Aims of a Handbook

The volume you are holding in your hand is the fourth in the third edition of the *Nondestructive Testing Handbook*. Now is a good time to reflect on the purposes and nature of a handbook.

Handbooks exist in many disciplines of science and technology, and certain features set them apart from other reference works. A handbook should ideally give the basic knowledge necessary for an understanding of the technology, including both scientific principles and means of application.

The typical reader may be assumed to have completed three years of college toward a degree in mechanical engineering or materials science and hence has the background of an elementary physics or mechanics course. Additionally this volume provides a positive reinforcement for the use of computer based media that enhances its educational value and enlightens all levels of education and training.

Note that any handbook offers a view of its subject at a certain period in time. Even before it is published, it can begin to get obsolete. The authors and editors do their best to be current but the technology will continue to change even as the book goes to press.

Standards, specifications, recommended practices and inspection procedures may be discussed in a handbook for instructional purposes, but at a level of generalization that is illustrative rather than comprehensive. Standards writing bodies take great pains to ensure that their documents are definitive in wording and technical accuracy. People writing contracts or procedures should consult the actual standards when appropriate.

Those who design qualifying examinations or study for them draw on handbooks as a quick and convenient way of approximating the body of knowledge. Committees and individuals who write or anticipate questions are selective in what they draw from any source. The parts of a handbook that give scientific background, for instance, may have little bearing on a practical examination except to provide the physical foundation to assist handling of more challenging tasks. Other parts of a handbook are specific to a certain

industry. This handbook provides a collection of perspectives on its subject to broaden its value and convenience to the nondestructive testing community.

The present volume is a worthy addition to the third edition. The editors, technical editors and many contributors and reviewers worked together to bring the project to completion. For their scholarship and dedication I thank them all.

Gary L. Workman  
Handbook Development Director

# Preface

Radiographic testing has been a preeminent method of nondestructive testing since the discovery of X-rays in 1895. Film radiography in particular has been the backbone of industrial applications of penetrating radiation. It is fundamentally a very elegant analog process that provides an internal evaluation of solid objects. Although film radiography remains the most widely used method of radiographic testing, many other penetrating radiation techniques for nondestructive testing have been developed. In recent years the advancements in speed and capability of digital data processing have increased the application of digital methods for penetrating radiation inspections. The transition from analog to digital technology will continue into the future.

This volume of the *Nondestructive Testing Handbook*, third edition, combines essential information on the traditional penetrating radiation testing techniques and incoming techniques using digital technology. Building on material in the first edition (1959) and the second edition (1985), the many contributors of this volume have assembled the basic body of knowledge for radiographic testing. Much of the information in the second edition radiography volume has been maintained and enhanced, while some dated or rarely used material has been dropped. The first and second editions thus remain useful references — not only for historical purposes but for material that could not longer be included in the present edition.

Considerable new information has been added, particularly in the area of digital imaging, data processing and digital image reconstruction. Other material has been updated with recent information in such areas as radiation sources, standards, interpretation and applications. Techniques such as backscatter imaging and computed tomography were not covered in earlier editions but have their own chapter in this edition.

The team of contributors has tried to prepare as useful a text as possible. In many cases, items are discussed in multiple chapters to keep the continuity of the discussion in that particular chapter. This also provides multiple contexts for understanding concepts and techniques. In other cases the handbook

may rely on other chapters for details on a particular concept. The reader is encouraged to refer to the index to find information on items of interest in multiple chapters. Because of the current rate of change in technology, it is not possible to have a handbook that is completely up to date. This handbook contains the fundamental, as well as the most recent material available at the time of its writing. Where possible, tables and figures are used to serve as a quick and ready means of finding essential technical information. The references for each chapter should be helpful for the reader seeking additional material. Readers are also encouraged to use the internet and ASNT's Web site to find supplemental material on equipment and topics that are subject to change with technological advancement.

It has been the pleasure of the technical editors to work with the authors and ASNT's *Nondestructive Testing Handbook* staff to provide this third edition of the radiography handbook. We wish to thank all the contributors, including those named in the current volume, those who provided material to the contributors and may not have been named, and those whose contributions to earlier editions have been carried over to this edition. We hope this edition proves useful as both a quick reference for technical details and a source of fundamental information for comprehensive understanding.

Richard H. Bossi  
Frank A. Iddings  
George C. Wheeler

# Editor's Preface

Radiographic testing was the dominant method of nondestructive testing during the first two decades of the American Society for Nondestructive Testing (ASNT), founded in 1941. When this handbook was first envisioned in the 1940s, it was projected to be a single volume devoted entirely to radiography.

In 1959, when the first edition of the *Nondestructive Testing Handbook* finally appeared, a fourth of it was devoted to radiographic testing. In the twenty-first century, the first edition still sells scores of copies every year.

A quarter century was to pass before that presentation of radiographic testing was replaced. The second edition gave a complete volume to the method when, in 1985, ASNT published *Radiography and Radiation Testing*. Much of the volume in the present third edition is based directly on that second edition.

The process of outlining this third edition volume and recruiting volunteers for it began in 1996. Richard Bossi and George Wheeler deserve the gratitude of ASNT for the planning that launched the project. In 2001 Frank Iddings, who had already edited several chapters, was appointed as the third technical editor.

Seven ASNT past presidents participated in the writing and review of this volume, demonstrating ASNT's strength as a truly technical society.

This series is not a collection of articles but a work of collective authorship by ASNT, so authors are called *contributors*. Volunteers whose contributions to the second edition have been updated for this edition are listed if they were able to participate and to approve the product.

In the list below, people listed as contributors were also reviewers but are listed only once, as contributors.

It has been an honor to work with ASNT's volunteers, whose technical expertise is matched by their generosity in sharing it.

I would like to thank staff members Hollis Humphries and Joy Grimm for their contributions to the art, layout and text of the book and also thank Publications Manager Paul McIntire for years of encouragement.

Patrick O. Moore  
NDT Handbook Editor

## Acknowledgments

### Handbook Development Committee

Gary L. Workman, University of Alabama, Huntsville  
Michael W. Allgaier, GPU Nuclear  
Albert S. Birks, AKZO Nobel Chemicals  
Richard H. Bossi, The Boeing Company  
Lisa Brasche, Iowa State University  
William C. Chedister, Circle Systems  
James L. Doyle, Northwest Research Associates, Inc.  
Nat Y. Faransso, Halliburton Company  
François Gagnon, Vibra-K Consultants  
Robert E. Green, Jr., Johns Hopkins University  
Matthew J. Golis, Advanced Quality Concepts  
Gerard K. Hacker, Teledyne Brown Engineering  
Harb S. Hayre, Ceie Specs  
Frank A. Iddings  
Charles N. Jackson, Jr.  
John K. Keve, DynCorp Tri-Cities Services  
Lloyd P. Lemle, Jr., BP Oil Company  
Xavier P.V. Maldague, University Laval  
Paul M. McIntire, ASNT  
Mani Mina, Iowa State University  
Ron K. Miller, Physical Acoustics Corporation  
Scott D. Miller, Saudi Aramco  
Patrick O. Moore, ASNT  
Stanley Ness  
Louis G. Pagliaro, Technical Associates of Charlotte  
Emmanuel P. Papadakis, Quality Systems Concepts  
Stanislav I. Rokhlin, Ohio State University  
Frank J. Sattler  
Fred Seppi, Williams International  
Amos G. Sherwin, Sherwin Incorporated  
Kermit S. Skeie  
Roderic K. Stanley, Quality Tubing  
Holger H. Streckert, General Atomics  
Stuart A. Tison, Millipore Corporation  
Noel A. Tracy, Universal Technology Corporation  
Satish S. Udpa, Michigan State University  
Sotirios J. Vahaviolos, Physical Acoustics Corporation  
Mark F.A. Warchol, Aluminum Company of America  
Glenn A. Washer, Federal Highway Administration  
George C. Wheeler

## Contributors

Richard D. Albert, Digiray Corporation  
Richard C. Barry, Lockheed Martin  
Missiles and Space  
Garry L. Balestracci, Balestracci Unlimited  
John P. Barton  
George L. Becker  
Harold Berger, Industrial Quality,  
Incorporated  
Bruce E. Bolliger, Agilent Technologies  
Richard H. Bossi, The Boeing Company,  
Seattle  
Lisa Brasche, Iowa State University  
Roy L. Buckrop  
Clifford Bueno, General Electric Company  
William D. Burnett  
Paul Burstein, Skiametics Incorporated  
Herbert Chapman  
Francis M. Charbonnier  
Kenneth W. Dolan, Lawrence Livermore  
National Laboratory  
C. Robert Emigh  
Toshiyasu Fukui  
Donald J. Hagemaiier  
Jerry J. Haskins, Lawrence Livermore  
National Laboratory  
Charles J. Hellier III, Hellier and  
Associates  
Eiichi Hirosawa  
Frank A. Iddings  
Timothy E. Kinsella, Carpenter  
Technology Corporation  
Gary G. Korkala, Security Defense Systems  
Andreas F. Kotowski, Rapiscan Security  
Products  
Lawrence R. Lawson  
Harry E. Martz, Lawrence Livermore  
National Laboratory  
William E.J. McKinney  
Masahisa Naoe  
James M. Nelson, The Boeing Company,  
Seattle  
Stig Oresjo, Agilent Technologies  
William B. Rivkin  
Stanislav I. Rokhlin, Ohio State University  
Edward H. Ruescher  
Frank J. Sattler  
Daniel J. Schneberk, Lawrence Livermore  
National Laboratory  
Samuel G. Snow  
George R. Strabel, Howmet Research  
Corporation  
Holger H. Streckert, General Atomics  
Marvin W. Trimm, Westinghouse  
Savannah River Company  
George C. Wheeler  
Gerald C. Wicks  
William P. Winfree, National Aeronautics  
and Space Administration

## Reviewers

Arthur E. Allum, Blacksburg, South  
Carolina  
Vijay Alreja, VJ Technologies  
John K. Aman  
Ringo C. Beaumont  
Boyd D. Howard, Westinghouse Savannah  
River Company  
Mark Branecki, NRay Services  
Jack S. Brenizer, Pennsylvania State  
University  
Joseph F. Bush, Jr., NDT Training  
Richard E. Cameron, General Electric  
Nuclear Energy  
W. Dennis Cabe, Duke Energy Company  
Eugene J. Chemma, Bethlehem Steel  
Corporation  
Thomas N. Claytor, Los Alamos National  
Laboratory  
Robert L. Crane, Air Force Research  
Laboratory  
Claude D. Davis, Unified Testing Services  
John Deboo, The Boeing Company  
Donny Dicharry, Source Production and  
Equipment  
Paul Dick  
Louis J. Elliott, Lockheed Martin Tactical  
Defense Systems  
Hugh W. Evans, Amersham Corporation  
Jonathan C. Fortkamp, ABB Automation  
Incorporated  
William D. Friedman, Lockheed Martin  
Steven G. Galbraith, INEEL, Idaho Falls  
Bryan C. Goode, Faxitron X-Ray  
Corporation  
Thorsten Graeve, Rad-Icon Imaging  
Corporation  
Joseph N. Gray, Iowa State University  
Nand Gupta, Omega International  
Technologies  
David P. Harvey, Oremet-Wah Chang  
Manfred P. Hentschel, Federal Institute for  
Materials Research and Testing, Berlin,  
Germany  
Michael R. Holloway, Eastman Kodak  
Company  
James W. Houf, American Society for  
Nondestructive Testing  
Bruce G. Isaacson, ISA  
Chester W. Jackson, Westinghouse  
James H. Johnson, Varian Industrial  
Products  
Thomas S. Jones, Howmet Research  
Corporation  
Jim F. Kelly, Rivest Testing USA/IUOE  
Bradley S. Kienlen, Entergy Operations  
Richard Kochakian, Agfa Corporation  
Jeffrey Kollgaard, The Boeing Company  
James R. Korenkiewicz, Samsung  
Aerospace, Pratt and Whitney  
Joseph L. Mackin, International Pipe  
Inspectors Association  
K. Dieter Markert  
Nick Martinsen, Varian Industrial  
Products  
Robert W. McClung



Thomas E. McConomy, Special Metals Corporation  
 Claude H. McDaniel  
 Robert M. McGee, Ford Motor Company  
 Richard D. McGuire, National Board of Boiler and Pressure Vessel Inspectors  
 William D. Meade, The Boeing Company  
 John Munro III  
 Antonio G. Pascua, The Boeing Company, Canoga Park  
 J.A. Patsey, US Steel Tubular Products  
 Patrick Pauwels, Agfa-Gevaert, Mortsel  
 Thea Philliou, Thermo Eberline  
 David H. Phillips, Hytec, Incorporated  
 Robert F. Plumstead, Lucius Pitkin Incorporated  
 William C. Plumstead, Sr., PQT Services  
 Rita Pontefract, Yxlon International, Akron  
 Joergen Rheinlaender, InnospeXion ApS, Hvalsø, Denmark  
 Wade J. Richards, McClellan Air Force Base  
 Scott D. Ritzheimer, Allegheny Ludlum Steel Company  
 Morteza Safai, FMC FoodTech  
 Robert L. Schulte, Digtome Corporation  
 Russell G. Schonberg, Schonberg Research Corporation  
 Noel D. Smith, NDS Products  
 Joel Henebry, Test and Measurement Organization  
 Jana Knezovich, Agilent Technologies  
 Habeeb H. Saleh, WJE Associates  
 Fred J. Schlieper, Teradyne  
 Peter Soltani, Direct Radiography Corporation  
 Dennis S. Smith, McDonnell Douglas Aerospace  
 Richard C. Stark  
 Brian Sterling, Timco  
 Richard Z. Struk, Shellcast Foundries, Montreal, Canada  
 Barry N. Taylor, National Institute of Standards and Technology  
 Jay D. Thompson, Lockheed Martin Missiles and Space  
 Michael L. Turnbow, Tennessee Valley Authority  
 Ray Tsukimura, Aerotest Operations  
 Jerry A. Tucker, Industrial Nuclear  
 Thomas B. Turner, BWX Technologies  
 John J. Veno  
 Mark F.A. Warchol, Alcoa, Incorporated  
 Randall D. Wasberg, Amcast Automotive  
 Glenn A. Washer, Federal Highway Administration  
 Amy Waters, Varian Industrial Products  
 Gene A. Westenbarger, Ohio University  
 Dwight S. Wilson, The Boeing Company, Long Beach  
 Charles B. Winfield, Tru-Tec Services, Incorporated  
 Sik-Lam Wong, Maxwell Physics International  
 Daniel A. Wysnewski, Agfa Corporation

## Additional Acknowledgments

For Chapter 8, "Radiographic Interpretation," the contributors and editors gratefully acknowledge the contributions by Newport News Shipbuilding and Drydock Company (R.R. Hardison, L.S. Morris, D.L. Isenhour and R.D. Wallace) and by the National Institute of Standards and Technology (G. Yonemura). Appreciation is also expressed to Eastman Kodak Company, Electric Power Research Institute, ASTM International and the Southwest Research Institute for permission to use illustrations.

The applications presented in Chapter 13, "Image Data Analysis," are the result of many collaborative efforts. Thanks to Ford Nondestructive Evaluation Laboratory (R. McGee and staff); to VJ Technologies (V. Alreja, S. Nagabhushana and V. Butani); to Chrysler Kokomo Casting (R. Nicholson, D. Guthrie and W. Kendricks); to Caterpillar, Incorporated (C. Andersen and G. Happoldt); to the Boeing Company (W. Meade and M. Negley); and to Lawrence Livermore National Laboratory (D. Chinn and others).

Sources of illustrations are acknowledged in a section at the end of this book.

# CONTENTS

<b><u>Chapter 1. Introduction to Radiographic Testing</u></b> . . . . . 1	<b><u>Chapter 6. Radiation Safety</u></b> . . . . . 113
Part 1. Nondestructive Testing . . . . 2	Part 1. Management of Radiation Safety . . . . . 114
Part 2. Management of Radiographic Testing . . . . 12	Part 2. Dose Definitions and Exposure Levels . . . . . 119
Part 3. History of Radiographic Testing . . . . . 21	Part 3. Radiation Protection Measurements . . . . . 121
Part 4. Units of Measure for Radiographic Testing . . . . 29	Part 4. Basic Exposure Control . . 127
	Part 5. Shielding . . . . . 130
	Part 6. Neutron Radiographic Safety . . . . . 134
<b><u>Chapter 2. Radiation and Particle Physics</u></b> . . . . . 37	<b><u>Chapter 7. Principles of Film Radiography</u></b> . . . . . 139
Part 1. Elementary Particles . . . . 38	Part 1. Film Exposure . . . . . 140
Part 2. Properties of Radioactive Materials . . . . . 42	Part 2. Absorption and Scattering . . . . . 152
Part 3. Electromagnetic Radiation . . . . . 48	Part 3. Radiographic Screen . . . 159
	Part 4. Industrial X-Ray Films . . 163
<b><u>Chapter 3. Electronic Radiation Sources</u></b> . . . . . 55	Part 5. Radiographic Image Quality and Detail Visibility . . . . . 170
Part 1. Physical Principles . . . . 56	Part 6. Film Handling and Storage . . . . . 177
Part 2. Basic Generator Construction . . . . . 59	Part 7. Film Digitization . . . . . 180
Part 3. Megavolt Radiography . . . 67	
<b><u>Chapter 4. Isotope Radiation Sources for Gamma Radiography</u></b> . . . . . 73	<b><u>Chapter 8. Radiographic Interpretation</u></b> . . . . . 185
Part 1. Selection of Radiographic Sources . . . . 74	Part 1. Fundamentals of Radiographic Interpretation . . . . . 186
Part 2. Source Handling Equipment . . . . . 79	Part 2. Viewing in Radiographic Testing . . . . . 189
	Part 3. Densitometers . . . . . 194
<b><u>Chapter 5. Radiation Measurement</u></b> . . 89	Part 4. Radiographic Interpretation Reporting . . . . . 199
Part 1. Principles of Radiation Measurement . . . . . 90	Part 5. Radiographic Artifacts . . 202
Part 2. Ionization Chambers and Proportional Counters . . . 91	Part 6. Discontinuity Indications . . . . . 207
Part 3. Geiger-Müller Counters . . 96	
Part 4. Scintillation Detectors . . 100	<b><u>Chapter 9. Radiographic Film Development</u></b> . . . . . 219
Part 5. Luminescent Dosimetry . . . . . 102	Part 1. Radiographic Latent Image . . . . . 220
Part 6. Neutron Detection . . . . 104	Part 2. Chemistry of Film Radiography . . . . . 230
Part 7. Semiconductors . . . . . 106	Part 3. Darkroom . . . . . 237
Part 8. Film Badges . . . . . 108	Part 4. Processing Technique . . 241
	Part 5. Silver Recovery . . . . . 247

**Chapter 10. Radioscopy . . . . . 253**

- Part 1. Fundamentals of Radioscopic Imaging . . . 254
- Part 2. Light Conversion . . . . . 256
- Part 3. Image Quality . . . . . 261
- Part 4. Imaging Systems . . . . . 265
- Part 5. Cameras . . . . . 269
- Part 6. Viewing and Recording . . 275
- Part 7. System Considerations . . 277

**Chapter 11. Digital Radiographic Imaging . . . . . 283**

- Part 1. Overview of Digital Imaging . . . . . 284
- Part 2. Principles of Digital X-Ray Detectors . . . . . 286
- Part 3. Image Contrast and Signal Statistics . . . . . 289
- Part 4. X-Ray Detector Technology . . . . . 296

**Chapter 12. Computed Tomography . . . . . 303**

- Part 1. Introduction to Computed Tomography . . . . . 304
- Part 2. Laminography . . . . . 306
- Part 3. Principles of Computed Tomography . . . . . 310
- Part 4. Resolution and Contrast . . . . . 316
- Part 5. Computed Tomographic Systems . . . . . 318
- Part 6. Applications of Computed Tomography . . . . . 323
- Part 7. Reference Standards for Computed Tomography . . . . . 328

**Chapter 13. Image Data Analysis . . . 345**

- Part 1. Fundamental Properties of Digital Images and Processing Schemes . . . 346
- Part 2. Image Analysis Techniques and Radiographic Tests . . . . 353
- Part 3. Automated Testing Techniques . . . . . 354

**Chapter 14. Backscatter Imaging . . . 379**

- Part 1. Physical Principles . . . . . 380
- Part 2. Backscatter Imaging Techniques . . . . . 388
- Part 3. Reconstruction and Image Processing Techniques . . 392
- Part 4. Applications of Backscatter Imaging . . . . 394

**Chapter 15. Special Radiographic Techniques . . . . . 403**

- Part 1. Microfocus Radiographic Testing . . . . . 404
- Part 2. Flash Radiography . . . . . 409
- Part 3. Reversed Geometry Radiography with Scanning Source . . . . . 414
- Part 4. Stereo Radiography . . . . . 419
- Part 5. X-Ray Diffraction and X-Ray Fluorescence . . . . 427

**Chapter 16. Neutron Radiography . . . . . 437**

- Part 1. Applications of Neutron Radiography . . . . . 438
- Part 2. Static Radiography with Thermal Neutrons . . . . . 440
- Part 3. Special Techniques of Neutron Radiography . . 446

**Chapter 17. Radiographic Testing of Metal Castings . . . . . 453**

- Part 1. Introduction to Radiographic Testing of Metal Castings . . . . . 454
- Part 2. General Radiographic Techniques for Metal Castings . . . . . 455
- Part 3. Radiographic Indications for Metal Castings . . . . . 461
- Part 4. Radiographic Testing and Process Scheduling . . . . . 465
- Part 5. Problems in Radiographic Testing of Metal Castings . . . . . 467

**Chapter 18. Radiographic Testing of Welds . . . . . 473**

- Part 1. Introduction to Radiographic Testing of Welds . . . . . 474
- Part 2. Weld Design . . . . . 475
- Part 3. Discontinuities in Welds . . . . . 478
- Part 4. Technique Development . . . . . 482
- Part 5. Standards and Specifications for Radiographic Testing of Welds . . . . . 489
- Part 6. Radiography of Weld Discontinuities . . . . . 491
- Part 7. In-Process Radioscopy of Arc Welding . . . . . 502
- Part 8. False Indications in Radiographs of Aluminum Alloy Welds . . . . . 507

<b><u>Chapter 19. Radiographic Testing in Utility, Petroleum and Chemical Industries</u></b> . . . . .	<b>513</b>
Part 1. Overview . . . . .	514
Part 2. Pipe and Tubing Applications . . . . .	515
Part 3. Vessel and Component Applications . . . . .	526
Part 4. Nuclear Fuel Applications . . . . .	530
Part 5. Other Uses for Radiographic Testing . . .	537
<b><u>Chapter 20. Aerospace Applications of Radiographic Testing</u></b> . . . . .	<b>543</b>
Part 1. Film Radiography of Aviation Components . .	544
Part 2. Radiographic Testing of Space Flight Components . . . . .	550
Part 3. Techniques for Advanced Materials . . . . .	559
<b><u>Chapter 21. Other Applications of Radiographic Testing</u></b> . . . . .	<b>569</b>
Part 1. Radiation Gaging of Density or Thickness . . .	570
Part 2. Radioscopy of Electronics . . . . .	578
Part 3. Radiographic Testing of Consumer Goods . . . . .	584
Part 4. Radiographic Testing in Security Systems . . . . .	588
Part 5. Infrastructure Applications of Radiographic Testing . . .	591
Part 6. Radiographic Testing in Conservation of Historic Buildings and Museum Objects . . . . .	594
<b><u>Chapter 22. Attenuation Coefficients</u></b> . . . . .	<b>609</b>
Part 1. Introduction to Attenuation Coefficients . . . . .	610
Part 2. Attenuation Coefficient Tables . . . . .	612
<b><u>Chapter 23. Radiographic Testing Glossary</u></b> . . . . .	<b>653</b>
<b><u>Index</u></b> . . . . .	<b>675</b>
<b><u>Figure Sources</u></b> . . . . .	<b>691</b>

**Copyright © 2002**  
**AMERICAN SOCIETY FOR NONDESTRUCTIVE TESTING, INC.**  
**All rights reserved.**

No part of this book may be reproduced, stored in a retrieval system or transmitted, in any form or by any means — electronic, mechanical, photocopying, recording or otherwise — without the prior written permission of the publisher. Nothing contained in this book is to be construed as a grant of any right of manufacture, sale or use in connection with any method, process, apparatus, product or composition, whether or not covered by letters patent or registered trademark, nor as a defense against liability for the infringement of letters patent or registered trademark.

The American Society for Nondestructive Testing, its employees, and the contributors to this volume assume no responsibility for the safety of persons using the information in this book.

Copyright © 2002 by the American Society for Nondestructive Testing, Incorporated. All rights reserved. ASNT is not responsible for the authenticity or accuracy of information herein, and published opinions and statements do not necessarily reflect the opinion of ASNT. Products or services that are advertised or mentioned do not carry the endorsement or recommendation of ASNT.

ACCPSM, IRRSP<sup>SM</sup>, *Level III Study Guide*<sup>SM</sup>, *Materials Evaluation*<sup>SM</sup>, *NDT Handbook*<sup>SM</sup>, *Nondestructive Testing Handbook*<sup>SM</sup>, *The NDT Technician*<sup>SM</sup> and [www.asnt.org](http://www.asnt.org)<sup>SM</sup> are service marks of the American Society for Nondestructive Testing. ASNT®, *Research in Nondestructive Evaluation*® and *RNDE*® are registered trademarks of the American Society for Nondestructive Testing.

ASNT exists to create a safer world by promoting the profession and technologies of nondestructive testing.

American Society for Nondestructive Testing, Incorporated  
1711 Arlingate Lane  
PO Box 28518  
Columbus, OH 43228-0518  
(614) 274-6003; fax (614) 274-6899  
[www.asnt.org](http://www.asnt.org)

## **Errata**

Errata if available for this printing may be obtained from ASNT's Web site, [www.asnt.org](http://www.asnt.org), or as hard copy by mail from ASNT, free on request addressed to the *NDT Handbook* Editor at the address above.

## **Library of Congress Cataloging-in-Publication Data**

Radiographic Testing [computer file] / technical editors, Richard H. Bossi, Frank A. Iddings, George C. Wheeler; . -- 3rd ed.  
1 computer optical disc; 4 3/4 in. — (Nondestructive testing handbook; v. 4)  
System requirements for Windows: 486 or Pentium PC; 8 MB RAM (16 MB RAM for windows NT); Windows 95/98 or windows NT 4.0 with Service Pack 3 or later; Adobe Acrobat Reader 5.0 (included); CD-ROM drive.  
System requirements for Macintosh: Apple Power Macintosh; 4.5 MB RAM; System 7.1.2 or later; 8 MB free hard disk space; Adobe Acrobat Reader 5.0 (included); CD-ROM drive.  
Title from disc label.  
Audience: Quality control engineers and inspectors  
Summary:  
ISBN 1-57117-098-7

## **NOTE:**

Information presented on this page is specific for the CD-ROM version of this publication. For Library of Congress Cataloging-in-Publication data pertaining to the printed edition, please [click this link](#).

# MULTIMEDIA CONTENTS

<b>Chapter 4. Isotope Radiation Sources for Gamma Radiography . . . . .</b>	<b>73</b>
<a href="#">Movie. Isotopic source . . . . .</a>	74
<a href="#">Movie. Collimators . . . . .</a>	82
<b>Chapter 6. Radiation Safety . . . . .</b>	<b>113</b>
<a href="#">Movie. Radiation injury . . . . .</a>	114
<a href="#">Movie. Survey meters . . . . .</a>	117
<a href="#">Movie. Check equipment . . . . .</a>	121
<a href="#">Movie. Personnel Monitoring Devices . . . . .</a>	124
<a href="#">Movie. Warning tape and signs . . . . .</a>	128
<b>Chapter 7. Principles of Film Radiography . . . . .</b>	<b>139</b>
<a href="#">Movie. Conventional radiography gives shadow image . . . . .</a>	140
<b>Chapter 10. Radioscopy . . . . .</b>	<b>253</b>
<a href="#">Movie. Automated wheel inspection . . . . .</a>	279
<b>Chapter 12. Computed Tomography . . . . .</b>	<b>303</b>
<a href="#">Movie. Second generation (rotate and translate) . . . . .</a>	319
<a href="#">Movie. Third generation (rotate only) . . . . .</a>	319
<a href="#">Movie. Electronic device on turntable . . . . .</a>	327
<a href="#">Movie. Images of electronic device . . . . .</a>	327
<a href="#">Movie. Tomographic data image of electronic device . . . . .</a>	327
<a href="#">Movie. Image slices of device, top to bottom . . . . .</a>	327
<a href="#">Movie. Slices show delaminations in composite fastener hole . . . . .</a>	327
<a href="#">Movie. Transverse image of delaminations in fastener hole . . . . .</a>	327
<b>Chapter 13. Image Data Analysis . . . . .</b>	<b>345</b>
<a href="#">Movie. Exfoliation corrosion, thin to thick . . . . .</a>	374
<a href="#">Movie. General corrosion, thin to thick . . . . .</a>	374
<a href="#">Movie. Cracks around fasteners . . . . .</a>	374
<a href="#">Movie. Cracks around fasteners, in layers from top . . . . .</a>	374
<b>Chapter 14. Backscatter Imaging . . . . .</b>	<b>379</b>
<a href="#">Movie. Backscatter scan of undamaged area . . . . .</a>	397
<a href="#">Movie. Moving source and sensor into place . . . . .</a>	397
<a href="#">Movie. Pillowing and corrosion . . . . .</a>	397
<b>Chapter 20. Aerospace Applications of Radiographic Testing . . . . .</b>	<b>543</b>
<a href="#">Movie. Automated inspection of rocket motor . . . . .</a>	551
<b>Chapter 21. Other Applications of Radiographic Testing . . . . .</b>	<b>569</b>
<a href="#">Movie. Inspection of printed circuit boards . . . . .</a>	583
<a href="#">Movie. Radiographic inspection of light bulb . . . . .</a>	587
<a href="#">Movie. Cargo scanning . . . . .</a>	589
<a href="#">Movie. Image acquisition and evaluation . . . . .</a>	589
<a href="#">Movie. Images at 3 MV and 6 MV . . . . .</a>	589
<a href="#">Movie. Contraband in water tank . . . . .</a>	589



# 1

## C H A P T E R

# Introduction to Radiographic Testing

---

Harold Berger, Industrial Quality, Incorporated,  
Gaithersburg, Maryland (Part 3)

Holger H. Streckert, General Atomics, San Diego,  
California (Part 4)

Marvin W. Trimm, Westinghouse Savannah River  
Company, Aiken, South Carolina (Parts 1 and 2)



# PART 1. Nondestructive Testing<sup>1</sup>

*Nondestructive testing* (NDT) has been defined as comprising those test methods used to examine or inspect a part or material or system without impairing its future usefulness.<sup>1</sup> The term is generally applied to nonmedical investigations of material integrity.

Strictly speaking, this definition of nondestructive testing includes noninvasive medical diagnostics. X-rays, ultrasound and endoscopes are used by both medical and industrial nondestructive testing. Medical nondestructive testing, however, has come to be treated by a body of learning so separate from industrial nondestructive testing that today most physicians do not use the word *nondestructive*.

Nondestructive testing is used to investigate specifically the material integrity of the test object. A number of other technologies — for instance, radio astronomy, voltage and amperage measurement and rheometry (flow measurement) — are nondestructive but are not used specifically to evaluate material properties. Radar and sonar are classified as nondestructive testing when used to inspect dams, for instance, but not when they are used to chart a river bottom.

Nondestructive testing asks “Is there something wrong with this material?” In contrast, performance and proof tests ask “Does this component work?” It is not considered nondestructive testing when an inspector checks a circuit by running electric current through it. Hydrostatic pressure testing is another form of proof testing, one that may destroy the test object.

Another gray area that invites various interpretations in defining nondestructive testing is *future usefulness*. Some material investigations involve taking a sample of the inspected part for testing that is inherently destructive. A noncritical part of a pressure vessel may be scraped or shaved to get a sample for electron microscopy, for example. Although future usefulness of the vessel is not impaired by the loss of material, the procedure is inherently destructive and the shaving itself — in one sense the true *test object* — has been removed from service permanently.

The idea of future usefulness is relevant to the quality control practice of

sampling. Sampling (that is, less than 100 percent testing to draw inferences about the unsampled lots) *is* nondestructive testing if the tested sample is returned to service. If the steel is tested to verify the alloy in some bolts that can then be returned to service, then the test is nondestructive. In contrast, even if spectroscopy used in the chemical testing of many fluids is inherently nondestructive, the testing is destructive if the samples are poured down the drain after testing.

Nondestructive testing is not confined to crack detection. Other discontinuities include porosity, wall thinning from corrosion and many sorts of disbands. Nondestructive material characterization is a growing field concerned with material properties including material identification and microstructural characteristics — such as resin curing, case hardening and stress — that have a direct influence on the service life of the test object.

Nondestructive testing has also been defined by listing or classifying the various techniques.<sup>1-3</sup> This sense of *nondestructive testing* is practical in that it typically highlights methods in use by industry.

## Purposes of Nondestructive Testing

Since the 1920s, the art of testing without destroying the test object has developed from a laboratory curiosity to an indispensable tool of fabrication, construction and manufacturing processes. No longer is visual testing of materials, parts and complete products the principal means of determining adequate quality. Nondestructive tests in great variety are in worldwide use to detect variations in structure, minute changes in surface finish, the presence of cracks or other physical discontinuities, to measure the thickness of materials and coatings and to determine other characteristics of industrial products. Scientists and engineers of many countries have contributed greatly to nondestructive test development and applications.

The various nondestructive testing methods are covered in detail in the

literature but it is always wise to consider objectives before details. How is nondestructive testing useful? Why do thousands of industrial concerns buy the testing equipment, pay the subsequent operating costs of the testing and even reshape manufacturing processes to fit the needs and findings of nondestructive testing?

Modern nondestructive tests are used by manufacturers (1) to ensure product integrity and, in turn, reliability; (2) to avoid failures, prevent accidents and save human life (see Figs. 1 and 2); (3) to make a profit for the user; (4) to ensure customer satisfaction and maintain the manufacturer's reputation; (5) to aid in better product design; (6) to control manufacturing processes; (7) to lower manufacturing costs; (8) to maintain uniform quality level; and (9) to ensure operational readiness.

These reasons for widespread and profitable nondestructive testing are sufficient in themselves but parallel developments have contributed to its growth and acceptance.

### Increased Demand on Machines

In the interest of greater speed and reduced cost for materials, the design engineer is often under pressure to reduce weight. This can sometimes be done by substituting aluminum alloys, magnesium alloys or composite materials for steel or iron but such light parts may not be the same size or design as those they replace. The tendency is also to reduce the size. These pressures on the designer have subjected parts of all sorts to increased stress levels. Even such commonplace objects as sewing machines, sauce pans and luggage are also lighter and more heavily loaded than ever before. The stress to be supported is seldom static. It often

fluctuates and reverses at low or high frequencies. Frequency of stress reversals increases with the speeds of modern machines and thus parts tend to fatigue and fail more rapidly.

Another cause of increased stress on modern products is a reduction in the safety factor. An engineer designs with certain known loads in mind. On the supposition that materials and workmanship are never perfect, a safety factor of 2, 3, 5 or 10 is applied. However, because of other considerations, a lower factor is often used that depends on the importance of lighter weight or reduced cost or risk to consumer.

New demands on machinery have also stimulated the development and use of new materials whose operating characteristics and performance are not completely known. These new materials create greater and potentially dangerous problems. As an example, an aircraft part was built from an alloy whose work hardening, notch resistance and fatigue life were not well known. After relatively short periods of service some of these aircraft suffered disastrous failures. Sufficient and proper nondestructive tests could have saved many lives.

As technology improves and as service requirements increase, machines are subjected to greater variations and to wider extremes of all kinds of stress, creating an increasing demand for stronger or more damage tolerant materials.

### Engineering Demands for Sounder Materials

Another justification for nondestructive tests is the designer's demand for sounder

FIGURE 1. Fatigue cracks caused damage to aircraft fuselage, causing death of flight attendant and injury to passengers (April 1988).



FIGURE 2. Boilers operate with high internal steam pressure. Material discontinuities can lead to sudden, violent failure with possible injury to people and property.



materials. As size and weight decrease and the factor of safety is lowered, more emphasis is placed on better raw material control and higher quality of materials, manufacturing processes and workmanship.

An interesting fact is that a producer of raw material or of a finished product sometimes does not improve quality or performance until that improvement is demanded by the customer. The pressure of the customer is transferred to implementation of improved design or manufacturing. Nondestructive testing is frequently called on to deliver this new quality level.

### Public Demands for Greater Safety

The demands and expectations of the public for greater safety are apparent everywhere. Review the record of the courts in granting high awards to injured persons. Consider the outcry for greater automobile safety, as evidenced by the required automotive safety belts and the demand for air bags, blowout proof tires and antilock braking systems. The publicly supported activities of the National Safety Council, Underwriters Laboratories, the Occupational Safety and Health Administration and the Federal Aviation Administration in the United States, as well as the work of similar agencies abroad, are only a few of the ways in which this demand for safety is expressed. It has been expressed directly by passengers who cancel reservations following a serious aircraft accident. This demand for personal safety has been another strong force in the development of nondestructive tests.

### Rising Costs of Failure

Aside from awards to the injured or to estates of the deceased and aside from costs to the public (because of evacuation occasioned by chemical leaks), consider briefly other factors in the rising costs of mechanical failure. These costs are increasing for many reasons. Some important ones are (1) greater costs of materials and labor; (2) greater costs of complex parts; (3) greater costs because of the complexity of assemblies; (4) greater probability that failure of one part will cause failure of others because of overloads; (5) trend to lower factors of safety; (6) probability that the failure of one part will damage other parts of high value; and (7) part failure in an integrated automatic production machine, shutting down an entire high speed production line. When production was carried out on many separate machines, the broken one could be bypassed until repaired. Today, one machine is tied into the production

of several others. Loss of such production is one of the greatest losses resulting from part failure.

## Applications of Nondestructive Testing

Nondestructive testing is a branch of the materials sciences that is concerned with all aspects of the uniformity, quality and serviceability of materials and structures. The science of nondestructive testing incorporates all the technology for detection and measurement of significant properties, including discontinuities, in items ranging from research specimens to finished hardware and products in service. By definition, nondestructive testing methods are means for examining materials and structures without disruption or impairment of serviceability. Nondestructive testing makes it possible for internal properties or hidden discontinuities to be revealed or inferred by appropriate methods.

Nondestructive testing is becoming increasingly vital in the effective conduct of research, development, design and manufacturing programs. Only with appropriate nondestructive testing methods can the benefits of advanced materials science be fully realized. The information required for appreciating the broad scope of nondestructive testing is available in many publications and reports.

## Classification of Methods

In a report, the National Materials Advisory Board (NMAB) Ad Hoc Committee on Nondestructive Evaluation adopted a system that classified techniques into six major method categories: visual, penetrating radiation, magnetic-electrical, mechanical vibration, thermal and chemical/electrochemical.<sup>3</sup> A modified version is presented in Table 1.<sup>1</sup>

Each method can be completely characterized in terms of five principal factors: (1) energy source or medium used to probe object (such as X-rays, ultrasonic waves or thermal radiation); (2) nature of the signals, image or signature resulting from interaction with the object (attenuation of X-rays or reflection of ultrasound, for example); (3) means of detecting or sensing resultant signals (photoemulsion, piezoelectric crystal or inductance coil); (4) method of indicating or recording signals (meter deflection, oscilloscope trace or radiograph); and (5) basis for interpreting the results (direct or indirect indication, qualitative or quantitative and pertinent dependencies).

The objective of each method is to provide information about the following material parameters: (1) discontinuities and separations (cracks, voids, inclusions delaminations and others); (2) structure or malstructure (crystalline structure, grain size, segregation, misalignment and others); (3) dimensions and metrology (thickness, diameter, gap size, discontinuity size and others); (4) physical and mechanical properties (reflectivity, conductivity, elastic modulus, sonic velocity and others); (5) composition and chemical analysis (alloy identification, impurities, elemental distributions and others); (6) stress and dynamic response (residual stress, crack growth, wear, vibration and others); (7) signature analysis (image content, frequency spectrum, field configuration and others); and (8) abnormal sources of heat.

Terms used in this block are further defined in Table 2 with respect to specific objectives and specific attributes to be measured, detected and defined.

The limitations of a method include conditions required by that method: conditions to be met for method application (access, physical contact, preparation and others) and requirements to adapt the probe or probe medium to the object examined. Other factors limit the detection or characterization of discontinuities, properties and other attributes and limit interpretation of signals or images generated.

## Classification Relative to Test Object

Nondestructive testing techniques may be classified according to how they detect indications relative to the surface of a test object. Surface methods include liquid penetrant testing, visual testing, grid and moiré testing. Surface/near-surface methods include tap, potential drop, holography and shearography, magnetic particle and electromagnetic testing. When surface or surface/near-surface methods are applied during intermediate manufacturing processes, they provide preliminary assurance that volumetric methods performed on the completed object or component will reveal few rejectable discontinuities. Volumetric methods include radiography, ultrasonic testing, acoustic emission testing and less widely used methods such as acoustoultrasonic testing and magnetic resonance imaging. Through-boundary techniques described include leak testing, some infrared thermographic techniques, airborne ultrasonic testing and certain techniques of acoustic emission testing. Other less easily classified methods are material identification, vibration analysis and strain gaging.

No one nondestructive testing method is all revealing. That is not to say that one method or technique of a method is rarely adequate for a specific object or component. However, in most cases it takes a series of test methods to do a complete nondestructive test of an object

TABLE 1. Nondestructive testing method categories.

Categories	Objectives
<b>Basic Categories</b>	
Mechanical and optical	color; cracks; dimensions; film thickness; gaging; reflectivity; strain distribution and magnitude; surface finish; surface flaws; through-cracks
Penetrating radiation	cracks; density and chemistry variations; elemental distribution; foreign objects; inclusions; microporosity; misalignment; missing parts; segregation; service degradation; shrinkage; thickness; voids
Electromagnetic and electronic	alloy content; anisotropy; cavities; cold work; local strain, hardness; composition; contamination; corrosion; cracks; crack depth; crystal structure; electrical conductivities; flakes; heat treatment; hot tears; inclusions; ion concentrations; laps; lattice strain; layer thickness; moisture content; polarization; seams; segregation; shrinkage; state of cure; tensile strength; thickness; disbands
Sonic and ultrasonic	crack initiation and propagation; cracks, voids; damping factor; degree of cure; degree of impregnation; degree of sintering; delaminations; density; dimensions; elastic moduli; grain size; inclusions; mechanical degradation; misalignment; porosity; radiation degradation; structure of composites; surface stress; tensile, shear and compressive strength; disbands; wear
Thermal and infrared	anisotropy, bonding; composition; emissivity; heat contours; plating thickness; porosity; reflectivity; stress; thermal conductivity; thickness; voids; cracks; delaminations; heat treatment; state of cure; moisture; corrosion
Chemical and analytical	alloy identification; composition; cracks; elemental analysis and distribution; grain size; inclusions; macrostructure; porosity; segregation; surface anomalies
<b>Auxiliary Categories</b>	
Image generation	dimensional variations; dynamic performance; anomaly characterization and definition; anomaly distribution; anomaly propagation; magnetic field configurations
Signal image analysis	data selection, processing and display; anomaly mapping, correlation and identification; image enhancement; separation of multiple variables; signature analysis



or component. For example, if surface cracks must be detected and eliminated and the object or component is made of ferromagnetic material, then magnetic particle testing would be the obvious choice. If that same material is aluminum or titanium, then the choice would be liquid penetrant or electromagnetic testing. However, for either of these

situations, if internal discontinuities were to be detected, then ultrasonic testing or radiography would be the selection. The exact technique in either case would depend on the thickness and nature of the material and the types of discontinuities that must be detected.

TABLE 2. Objectives of nondestructive testing methods.

Objectives	Attributes Measured or Detected
<b>Discontinuities and separations</b>	
Surface anomalies	roughness; scratches; gouges; crazing; pitting; inclusions and imbedded foreign material
Surface connected anomalies	cracks; porosity; pinholes; laps; seams; folds; inclusions
Internal anomalies	cracks; separations; hot tears; cold shuts; shrinkage; voids; lack of fusion; pores; cavities; delaminations; disbonds; poor bonds; inclusions; segregations
<b>Structure</b>	
Microstructure	molecular structure; crystalline structure and/or strain; lattice structure; strain; dislocation; vacancy; deformation
Matrix structure	grain structure, size, orientation and phase; sinter and porosity; impregnation; filler and/or reinforcement distribution; anisotropy; heterogeneity; segregation
Small structural anomalies	leaks (lack of seal or through-holes); poor fit; poor contact; loose parts; loose particles; foreign objects
Gross structural anomalies	assembly errors; misalignment; poor spacing or ordering; deformation; malformation; missing parts
<b>Dimensions and metrology</b>	
Displacement; position	linear measurement; separation; gap size; discontinuity size, depth, location and orientation
Dimensional variations	unevenness; nonuniformity; eccentricity; shape and contour; size and mass variations
Thickness; density	film, coating, layer, plating, wall and sheet thickness; density or thickness variations
<b>Physical and mechanical properties</b>	
Electrical properties	resistivity; conductivity; dielectric constant and dissipation factor
Magnetic properties	polarization; permeability; ferromagnetism; cohesive force
Thermal properties	conductivity; thermal time constant and thermoelectric potential; diffusivity; effusivity; specific heat
Mechanical properties	compressive, shear and tensile strength (and moduli); Poisson's ratio; sonic velocity; hardness; temper and embrittlement
Surface properties	color; reflectivity; refraction index; emissivity
<b>Chemical composition and analysis</b>	
Elemental analysis	detection; identification, distribution and/or profile
Impurity concentrations	contamination; depletion; doping and diffusants
Metallurgical content	variation; alloy identification, verification and sorting
Physiochemical state	moisture content; degree of cure; ion concentrations and corrosion; reaction products
<b>Stress and dynamic response</b>	
Stress; strain; fatigue	heat treatment, annealing and cold work effects; residual stress and strain; fatigue damage and life (residual)
Mechanical damage	wear; spalling; erosion; friction effects
Chemical damage	corrosion; stress corrosion; phase transformation
Other damage	radiation damage and high frequency voltage breakdown
Dynamic performance	crack initiation and propagation; plastic deformation; creep; excessive motion; vibration; damping; timing of events; any anomalous behavior
<b>Signature analysis</b>	
Electromagnetic field	potential; strength; field distribution and pattern
Thermal field	isotherms; heat contours; temperatures; heat flow; temperature distribution; heat leaks; hot spots; contrast
Acoustic signature	noise; vibration characteristics; frequency amplitude; harmonic spectrum and/or analysis; sonic and/or ultrasonic emissions
Radioactive signature	distribution and diffusion of isotopes and tracers
Signal or image analysis	image enhancement and quantization; pattern recognition; densitometry; signal classification, separation; and correlation; discontinuity identification, definition (size and shape) and distribution analysis; discontinuity mapping and display

## Value of Nondestructive Testing

The contribution of nondestructive testing to profits has been acknowledged in the medical field and computer and aerospace industries. However, in industries such as heavy metals, though nondestructive testing may be reluctantly accepted its contribution to profits may not be obvious to management. Nondestructive testing is sometimes thought of only as a cost item. One possible reason is industry downsizing. When a company cuts costs, two vulnerable areas are quality and safety. When bidding contract work, companies add profit margin to all cost items, including nondestructive testing, so a profit should be made on the nondestructive testing. However, when production is going poorly and it is anticipated that a job might lose money, it seems like the first corner that production personnel will try to cut is nondestructive testing. This is accomplished by subtle pressure on nondestructive testing technicians to accept a product that does not quite meet a code or standard requirement. The attitude toward nondestructive testing is gradually improving as management comes to appreciate its value.

Nondestructive testing should be used as a control mechanism to ensure that manufacturing processes are within design performance requirements. It should never be used in an attempt to obtain quality in a product by using

nondestructive testing at the end of a manufacturing process. This approach will ultimately increase production costs. When used properly, nondestructive testing saves money for the manufacturer. Rather than costing the manufacturer money, nondestructive testing should add profits to the manufacturing process.

## Overview of Nondestructive Testing Methods

To optimize the use of nondestructive testing, it is necessary first to understand the principles and applications of all the methods. This book features radiographic testing (Fig. 3) — only one of the nondestructive testing methods. Several other methods and the applications associated with them are briefly described next.

### Visual Testing

**Principles.** Visual testing (Fig. 4) is the observation of a test object, either directly with the eyes or indirectly using optical instruments, by an inspector to evaluate the presence of surface anomalies and the object's conformance to specification.

Visual testing should be the first nondestructive testing method applied to an item. The test procedure is to clean the surface, provide adequate illumination and observe. A prerequisite necessary for competent visual testing of an item is knowledge of the manufacturing processes by which it was made, its service history, potential failure modes and related industry experience.

**Applications.** Visual testing provides a means of detecting and examining a variety of surface discontinuities. It is also

FIGURE 3. Representative setup for radiographic test.

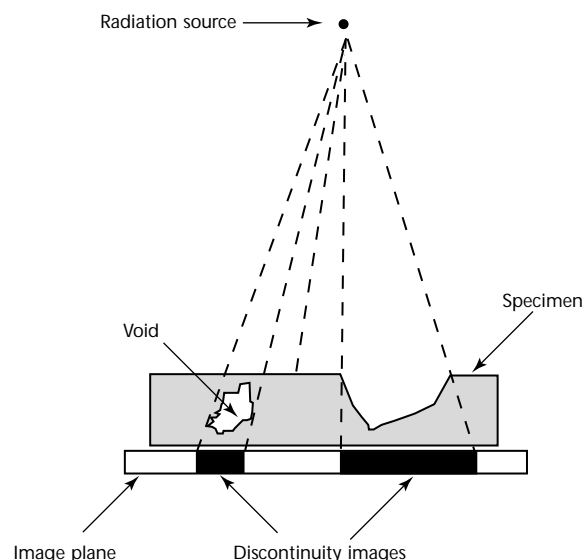


FIGURE 4. Visual test using borescope to view interior of cylinder.



the most widely used method for detecting and examining for surface discontinuities associated with various structural failure mechanisms. Even when other nondestructive tests are performed, visual tests often provide a useful supplement. For example, when the eddy current testing of process tubing is performed, visual testing is often performed to verify and more closely examine the surface condition. This verification process can impact the evaluation process associated with other nondestructive test methods being used. The following discontinuities may be detected by a simple visual test: surface discontinuities, cracks, misalignment, warping, corrosion, wear and physical damage.

### Liquid Penetrant Testing

**Principles.** Liquid penetrant testing (Fig. 5) reveals discontinuities open to the surfaces of solid and nonporous materials. Indications of a wide spectrum of discontinuity sizes can be found regardless of the configuration of the workpiece and regardless of discontinuity orientations. Liquid penetrants seep into various types of minute surface openings by capillary action. The cavities of interest can be very small, often invisible to the unaided eye. The ability of a given liquid to flow over a surface and enter surface cavities depends principally on the following: cleanliness of the surface, surface tension of the liquid, configuration of the cavity, contact angle of the liquid, ability of the liquid to wet the surface, cleanliness of the cavity and size of surface opening of the cavity.

**Applications.** The principal industrial uses of liquid penetrant testing are final testing, receiving testing, in-process testing and quality control, maintenance and overhaul in the transportation industries, in plant and machinery maintenance and in testing of large components. The following are some of the typically detected discontinuities:

FIGURE 5. Liquid penetrant indication of cracking.



surface discontinuities, seams, cracks, laps, porosity and leak paths.

### Magnetic Particle Testing

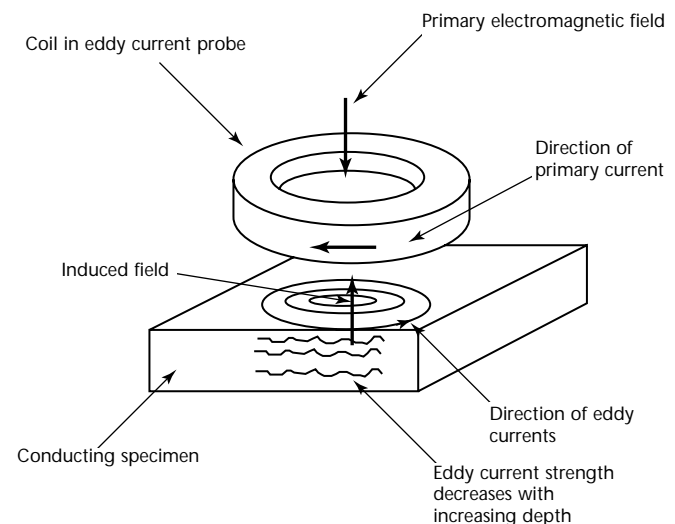
**Principles.** Magnetic particle testing is a method of locating surface and slightly subsurface discontinuities in ferromagnetic materials. It depends on the fact that when the material or part under test is magnetized, discontinuities that lie in a direction generally transverse to the direction of the magnetic field will cause a leakage field to be formed at and above the surface of the part. The presence of this leakage field and therefore the presence of the discontinuity is detected by the use of finely divided ferromagnetic particles applied over the surface, with some of the particles being gathered and held to form an outline of the discontinuity. This generally indicates its location, size, shape and extent. Magnetic particles are applied over a surface as dry particles or as wet particles in a liquid carrier such as water or oil.

**Applications.** The principal industrial uses of magnetic particle testing are for final, receiving and in-process testing; for quality control; for maintenance and overhaul in the transportation industries; for plant and machinery maintenance; and for testing of large components. Some of the typically detected discontinuities are surface discontinuities, seams, cracks and laps.

### Eddy Current Testing

**Principles.** Based on electromagnetic induction, eddy current testing (Fig. 6) is used to identify or differentiate among a

FIGURE 6. Representative setup for eddy current test.





wide variety of physical, structural and metallurgical conditions in electrically conductive ferromagnetic and nonferromagnetic metals and metal parts. The method is based on indirect measurement and on correlation between the instrument reading and the structural characteristics and serviceability of the parts being examined.

With a basic system, the part is placed within or adjacent to an electric coil in which high frequency alternating current is flowing. This *excitation current* establishes an electromagnetic field around the coil. This *primary* field causes eddy current to flow in the part because of electromagnetic induction. Inversely, the eddy currents affected by all characteristics (conductivity, permeability, thickness, discontinuities and geometry) of the part create a *secondary* magnetic field that opposes the primary field. The results of this interaction affect the coil voltage and can be displayed in a variety of methods.

Eddy currents flow in closed loops in the part or air. Their two most important characteristics, amplitude and phase, are influenced by the arrangement and characteristics of the instrumentation and test piece. For example, during the test of a tube the eddy currents flow symmetrically in the tube when discontinuities are not present. However, when a crack is present, then the eddy current flow is impeded and changed in direction, causing significant changes in the associated electromagnetic field.

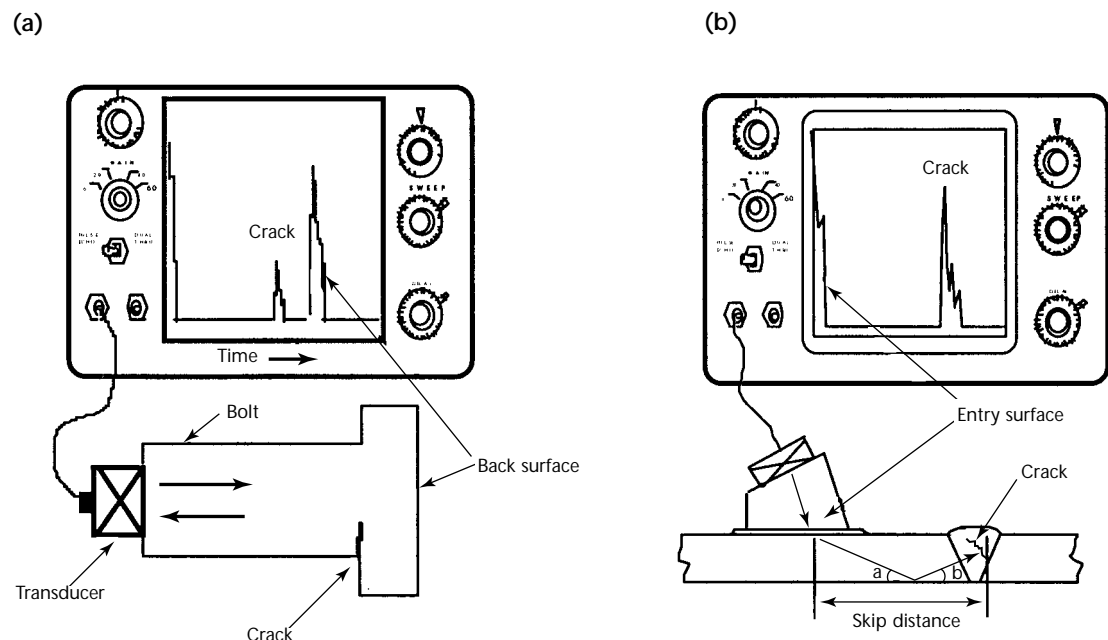
**Applications.** An important industrial use of eddy current testing is on heat exchanger tubing. For example, eddy current testing is often specified for thin wall tubing in pressurized water reactors, steam generators, turbine condensers and air conditioning heat exchangers. Eddy current testing is also used often in aircraft maintenance. The following are some of the typical material characteristics that can be evaluated by eddy current testing: cracks, inclusions, dents and holes; grain size and hardness; coating and material thickness; dimensions and geometry; composition, conductivity or permeability; and alloy composition.

## Ultrasonic Testing

**Principles.** Ultrasonic testing (Fig. 7) is a nondestructive method in which beams of sound waves at a frequency too high to hear are introduced into materials for the detection of surface and subsurface discontinuities in the material. These acoustic waves travel through the material with some attendant loss of energy (attenuation) and are reflected at interfaces. The reflected beam is displayed (or reduces the display of transmitted sound) and is then analyzed to define the presence and locations of discontinuities or discontinuities.

**Applications.** Ultrasonic testing of metals is widely used, principally for the detection of discontinuities. This method can be used to detect internal

FIGURE 7. Representative setups for ultrasonic testing: (a) longitudinal wave technique; (b) shear wave technique.



discontinuities in most engineering metals and alloys. Bonds produced by welding, brazing, soldering and adhesive bonding can also be ultrasonically examined. Inline techniques have been developed for monitoring and classifying materials as acceptable, salvageable or scrap and for process control. Other applications include testing of piping and pressure vessels, nuclear systems, motor vehicles, machinery, structures, railroad rolling stock and bridges and thickness measurement.

## Leak Testing

**Principles.** Leak testing is concerned with the flow of liquids or gases from pressurized or into evacuated components or systems intended to hold fluids. The principles of leak testing involve the physics of fluid (liquids or gases) flowing through a barrier where a pressure differential or capillary action exists. Leaking fluids (liquid or gas) can propagate from inside a component or assembly to the outside, or vice versa, as a result of a pressure differential between the two regions or as a result of permeation through a barrier. The importance of leak testing depends on the size of the leak and on the medium being leaked. Leak testing encompasses procedures that fall into these basic functions: leak location, leakage measurement and leakage monitoring.

**Applications.** Like other forms of nondestructive testing, leak testing has a great impact on the safety and performance of a product. Reliable leak testing decreases costs by reducing number of reworked products, warranty repairs and liability claims. The most common reasons for performing a leak test are to prevent the loss of costly materials or energy; to prevent contamination of the environment; to ensure component or system reliability; and to prevent the potential for an explosion or fire.

## Acoustic Emission Testing

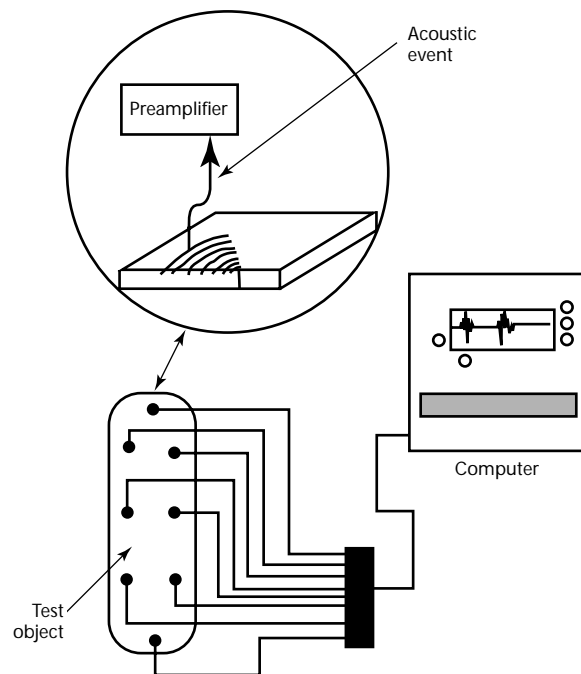
**Principles.** Acoustic emissions are stress waves produced by sudden movement in stressed materials. The classic source of acoustic emission is discontinuity related deformation processes such as crack growth and plastic deformation. Sudden movement at the source produces a stress wave that radiates out into the structure and excites a sensitive piezoelectric sensor. As the stress in the material is raised, emissions are generated. The signals from one or more sensors are amplified and measured to produce data for display and interpretation.

The source of acoustic emission energy is the elastic stress field in the material. Without stress, there is no emission. Therefore, an acoustic emission test (Fig. 8) is usually carried out during a controlled loading of the structure. This can be a proof load before service; a controlled variation of load while the structure is in service; a fatigue, pressure or creep test; or a complex loading program. Often, a structure is going to be loaded hydrostatically anyway during service and acoustic emission testing is used because it gives valuable additional information about the expected performance of the structure under load. Other times, acoustic emission testing is selected for reasons of economy or safety and a special loading procedure is arranged to meet the needs of the acoustic emission test.

**Applications.** Acoustic emission is a natural phenomenon occurring in the widest range of materials, structures and processes. The largest scale events observed with acoustic emission testing are seismic and the smallest are small dislocations in stressed metals.

The equipment used is highly sensitive to any kind of movement in its operating frequency (typically 20 to 1200 kHz). The equipment can detect not only crack growth and material deformation but also

FIGURE 8. Acoustic emission testing setup in which eight sensors permit computer to calculate location of crack propagation.



such process as solidification, friction, impact, flow and phase transformations. Therefore, acoustic emission testing is also used for in-process weld monitoring, detecting tool touch and tool wear during automatic machining, detecting wear and loss of lubrication in rotating equipment, detecting loose parts and loose particles, detecting and monitoring leaks, cavitation, flow, preservice proof testing, in-service weld monitoring and leak testing.

### Infrared and Thermal Testing

**Principles.** Conduction and convection are the primary mechanisms of heat transfer in an object or system. However, electromagnetic radiation is emitted from a heated body when electrons in that body change to a lower energy state. Thermal testing involves the measurement or mapping of surface temperatures when heat flows from, to or through a test object. Temperature differentials on a surface, or changes in surface temperature with time, are related to heat flow patterns and can be used to detect anomalies or to determine the heat transfer characteristics of an object. For example, during the operation of an electrical breaker, a hot spot detected at an electrical termination may be caused by a loose or corroded connection (see Fig. 9). The resistance to electrical flow

through the connection produces an increase in surface temperature of the connection.

**Applications.** There are two basic categories of infrared and thermal test applications: electrical and mechanical. The specific applications within these two categories are numerous. Electrical applications include transmission and distribution lines, transformers, disconnects, switches, fuses, relays, breakers, motor windings, capacitor banks, cable trays, bus taps and other components and subsystems. Mechanical applications include insulation (in boilers, furnaces, kilns, piping, ducts, vessels, refrigerated trucks and systems, tank cars and elsewhere), friction in rotating equipment (bearings, couplings, gears, gearboxes, conveyor belts, pumps, compressors and other components) and fluid flow (steam lines; heat exchangers; tank fluid levels; exothermic reactions; heating, ventilation and air conditioning systems; leaks above and below ground; cooling and heating; tube blockages; systems; environmental assessment of thermal discharge; boiler or furnace air leakage; condenser; turbine air leakage; pumps; compressors; and other system applications).

### Other Methods

There are many other methods of nondestructive testing, including optical methods such as holography, shearography and moiré imaging; material identification methods such as chemical spot testing, spark testing and spectroscopy; strain gaging; and acoustic methods such as vibration analysis and tapping.

FIGURE 9. Infrared thermography of automatic transfer switches of emergency diesel generator. Hot spots appear bright in thermogram.



## PART 2. Management of Radiographic Testing

Radiography may be considered the most effective nondestructive testing method merely because of its universal use and acceptance in industry. Radiography can be used to test most types of solid material. Exceptions include materials of very high or very low density. Neutron radiography, however, can often be used in such cases. There is wide latitude both of material thickness that can be tested and in the techniques that can be used. Usually conditions that result in a two percent or greater difference in through-section thickness can usually be detected.

Radiography has three main advantages: (1) detection of internal discontinuities, (2) detection of significant variations in composition and (3) permanent record of test data.

Compared to other nondestructive test methods, radiography can be expensive. Large capital costs and space allocations may be required for radiographic activities. Cost may be reduced if equipment of smaller size or lower energy requirement can be used. The magnitude of potential test activities, however, must be considered before limits are placed on the test facility.

There are three major limiting factors that must be considered before radiography becomes the method of choice.

1. Discontinuity detection depends on radiation beam orientation. In general, radiography can detect only features that have a thickness change in a direction parallel to the radiation beam.
2. Radiography typically involves the transmission of radiation through the part or component, in which case both sides of the part must be accessible.
3. Radiation safety is always necessary to a successful operation.

In addition, radiographic images (in the form of film or digital images) may need to be stored for years to comply with quality assurance or regulatory requirements.

### Management of Radiographic Testing Programs

Management of a radiographic testing program will require consideration of many items before a program can produce the desired results. Six basic questions must be answered before a true direction can be charted. They are as follows.

1. Are regulatory requirements in place that mandate program characteristics?
2. What is the magnitude of the program that will provide desired results?
3. What provisions must be made for personnel safety and for compliance with environmental regulations?
4. What is the performance date for a program to be fully implemented?
5. Is there a cost benefit of radiographic testing?
6. What are the available resources in personnel and money?

Once these questions are answered, then a recommendation can be made to determine the best path forward. Three primary paths are (1) service companies, (2) consultants and (3) in-house programs.

Though these are primary paths, some programs may on a routine or on as-needed bases require support personnel from a combination of two or more of these sources. Before a final decision is made, advantages and disadvantages of each path must be considered. Therefore, the following are details that must be considered.

### Service Companies

1. Who will identify the components within the facility to be examined?
2. Will the contract be for *time and materials* or have a specific *scope of work*?
3. If a *time and materials* contract is awarded, who will monitor the time and materials charged?
4. If a *scope of work* is required, who is technically qualified to develop and approve it?
5. What products or documents (test reports, trending, recommendations, root cause analysis and others) will be provided once the tests are completed?

- Who will evaluate and accept the product (test reports, trending, recommendations, root cause analysis and others) within your company?
- Do the service company workers possess qualifications and certifications required by contract and by applicable regulations? Will other contractors be required to take care of related matters such as radiation safety?
- Do the service company workers require site specific training (confined space entry, electrical safety, hazardous materials and others) or clearance to enter and work in the facility?
- If quantitative tests are performed, do program requirements mandate equipment calibration?
- Does the service company retain any liability for test results?
- What are the regulatory requirements (codes and standards) associated with program development and implementation?
- Who will develop a *cost benefit* analysis for the program?
- How much time and resources are available to establish the program?
- What are the qualification requirements (education, training, experience and others) for personnel?
- Do program personnel require additional training (radiological safety, confined space entry or others) or qualifications?
- Are subject matter experts required to provide technical guidance during personnel development?
- Are procedures required to perform work in the facility?
- If procedures are required, who will develop, review and approve them?
- Who will determine the technical specifications for test equipment?

## Consultants

- Will the contract be for *time and materials* or have a specific *scope of work*?
- If a *scope of work* is required, who is technically qualified to develop and approve it?
- Who will identify the required qualifications of the consultant?
- Is the purpose of the consultant to develop or update a program or is it to oversee and evaluate the performance of an existing program?
- Will the consultant have oversight responsibility for tests performed?
- What products (trending, recommendations, root cause analysis and others) are provided once the tests are completed?
- Who will evaluate the consultant's performance (test reports, trending, recommendations, root cause analysis and other functions) within your company?
- Does the consultant possess qualifications and certifications required by contract and by applicable regulations?
- Does the consultant require site specific training (confined space entry, electrical safety, hazardous materials and others) or clearance to enter and work in the facility?
- Does the consultant retain any liability for test results?

## In-House Programs

- Who will determine the scope of the program? Will the radiation source be isotopes or X-ray machines? Will the images be recorded on film or on digital media?

## Test Procedures for Radiographic Testing

The conduct of facility operations (in-house or contracted) should be performed in accordance with specific instructions from an expert. This is typically accomplished using written instructions in the form of a technical procedure. In many cases codes and specifications will require the use of a technical procedure to perform required tests.

The procedure process can take many forms, including general instructions that address only major aspects of test techniques. Or a procedure may be written as a step-by-step process requiring a supervisor's initial or signature after each step. The following is a typical format for an industrial procedure.

- The *purpose* identifies the intent of the procedure.
- The *scope* establishes the latitude of items, tests and techniques covered and not covered by the procedure.
- References* are specific documents from which criteria are extracted or documents satisfied by implementation of the procedure.
- Definitions* are needed for terms and abbreviations that are not common knowledge to people who will read the procedure.
- Statements about *personnel requirements* address specific requirements to perform tasks in accordance with the procedure — issues such as personnel qualification, certification, access clearance and others.



6. *Equipment* characteristics, calibration requirements and model numbers of qualified equipment must be specified.
7. *Safety* issues must be addressed because of the nature of penetrating radiation.
8. The test *procedure* provides a sequential process to be used to conduct test activities.
9. *Acceptance criteria* establish component characteristics that will identify the items suitable for service.
10. *Reports* (records) provide the means to document specific test techniques, equipment used, personnel performing activity, date performed, test results, compliance with environmental regulations and safety procedures.
11. *Attachments* may include (if required) items such as report forms, instrument calibration forms, qualified equipment matrix, schedules and others

Once the procedure is completed, typically an expert in the subject matter performs a technical evaluation. If the procedure is deemed adequate (meeting identified requirements), the expert will approve it for use. Some codes and standards also require the procedure to be qualified — that is, demonstrated to the satisfaction of a representative of a regulatory body or jurisdictional authority.

## Test Specifications for Radiographic Testing

A radiographic specification must anticipate a number of issues that arise during testing.

### Source Selection

The radiation source requirements (energy level, intensity and physical size) to detect the target discontinuities must be determined.

1. The selected means of imaging may dictate source energy and intensity levels.
2. The radiation source may need to be mobile for use in various locations.
3. The energy level (ability to penetrate) of the radiation sources affects radiographic contrast. Radiographic contrast is an element of image sensitivity.
4. The physical size of the radiation emitting surface affects the geometric unsharpness of the radiographic image.
5. High energy levels may increase safety issues because of increased shielding requirements.

6. The source intensity (total quantity of penetrating rays) will directly affect the exposure time. Increased exposure time may affect safety requirements.

## Selection of Imaging

Typically an image is the end product of a radiographic examination. The image may be the captured output of a radiosopic or electronic imaging system. Its format may be a hard copy (film or paper), a computer image file or a video monitor displaying an image in real time.

1. The first consideration is the ability to detect discontinuities of interest.
2. Examination environment.
3. Image handling requirements include provisions for processing, evaluation and transmitting of images.

## Interpretation

Interpretation may be complex. The interpreter must have a knowledge of the following: (1) the radiographic process (radiation source, exposure technique, image storage system and other means used to obtain the image); (2) the item being examined (its configuration, material characteristics, fabrication process, potential discontinuities and other aspects); and (3) the acceptance criteria.

## Standards and Specifications for Radiographic Testing

Standards have undergone a process of peer review in industry and can be invoked with the force of law by contract or by government regulation. In contrast, a specification represents an employer's instructions to employees and is specific to a contract or work place. Specifications may form the basis of standards through a review process. Standards and specifications exist in three basic areas: equipment, processes and personnel.

1. Standards for equipment include calibrated electronic radiation sources and isotope sources. Standardized reference objects such as image quality indicators (penetrameters), calibrated density strips and radiation survey meters would also fit into this category.

2. ASTM International and other organizations publish standards for test techniques. Some other standards are for quality assurance procedures and are not specific to a test method or even to testing in general. Tables 3 and 4 list some of the standards used in radiographic testing. A source for nondestructive testing standards is the *Annual Book of ASTM Standards*.<sup>5</sup>
3. Qualification and certification of test personnel are discussed below, with specific reference to recommendations of *ASNT Recommended Practice No. SNT-TC-1A*.<sup>4</sup>
2. ANSI/ASNT CP-189, *Standard for Qualification and Certification of Nondestructive Testing Personnel* resembles SNT-TC-1A but also establishes specific attributes for the qualification and certification of nondestructive testing personnel. However, CP-189 is a consensus standard as defined by the American National Standards Institute (ANSI). It is recognized as the American standard for nondestructive testing. It is not considered a *recommended practice*; it is a national standard.<sup>6</sup>
3. The *ASNT Central Certification Program (ACCP)*, unlike SNT-TC-1A and CP-189, is a third party certification process. Currently it has identified qualification and certification attributes for Level II and Level III nondestructive testing personnel. The American Society for Nondestructive Testing certifies that the individual has the skills and knowledge for many nondestructive testing method applications. It does not remove the responsibility for the final determination of personnel qualifications from the employer. The employer evaluates an individual's skills and knowledge for application of company procedures using designated techniques and identified equipment for specific tests.<sup>7</sup>

## Personnel Qualification and Certification

One of the most critical aspects of the test process is the qualification of test personnel. Nondestructive testing is sometimes referred to as a *special process*. The term simply means that it is very difficult to determine the adequacy of a test by merely observing the process or the documentation generated at its conclusion. The quality of the test is largely dependent on the skills and knowledge of the inspector.

The American Society for Nondestructive Testing (ASNT) has been a world leader in the qualification and certification of nondestructive testing personnel for many years. By 1999, the American Society for Nondestructive Testing had instituted three major programs in place for the qualification and certification of nondestructive testing personnel.

1. *ASNT Recommended Practice No. SNT-TC-1A* provides guidelines for personnel qualification and certification in nondestructive testing. This recommended practice identifies the specific attributes that should be considered when qualifying nondestructive testing personnel. It requires the employer to develop and implement a *written practice* (procedure) that details the specific process and any limitation in the qualification and certification of nondestructive testing personnel.<sup>4</sup>

### Selections from *ASNT Recommended Practice No. SNT-TC-1A*

To give an overview of the contents of these documents, the following items are specified in the 1996 edition of SNT-TC-1A. (For the purpose of this discussion the quantities cited are those that address radiographic testing only.)

**Scope.** This recommended practice has been prepared to establish guidelines for the qualification and certification of nondestructive testing personnel whose specific jobs require appropriate knowledge of the technical principles underlying the nondestructive test they perform, witness, monitor or evaluate. This document provides guidelines for the establishment of a qualification and certification program.

**Written Practice.** The employer shall establish a written practice for the control and administration of nondestructive testing personnel training, examination and certification. The employer's written practice should describe the responsibility of each level of certification for determining the acceptability of materials or components in accordance with applicable codes, standards, specifications and procedures.



**Table 3. Some radiographic standards published by ASTM International.**

C 638-92 (1997), *Standard Descriptive Nomenclature of Constituents of Aggregates for Radiation-Shielding Concrete*  
E 94-00, *Standard Guide for Radiographic Examination*  
E 155-00, *Standard Reference Radiographs for Inspection of Aluminum and Magnesium Castings*  
E 170-99e1, *Standard Terminology Relating to Radiation Measurements and Dosimetry*  
E 186-98, *Standard Reference Radiographs for Heavy-Walled (2 to 4 1/2-in. [51 to 114-mm]) Steel Castings*  
E 192-95 (1999), *Standard Reference Radiographs for Investment Steel Castings of Aerospace Applications*  
E 242-95 (2000), *Standard Reference Radiographs for Appearances of Radiographic Images as Certain Parameters Are Changed*  
E 272-99, *Standard Reference Radiographs for High-Strength Copper-Base and Nickel-Copper Alloy Castings*  
E 280-98, *Standard Reference Radiographs for Heavy-Walled (4 1/2 to 12-in. [(114 to 305-mm)]) Steel Castings*  
E 310-99, *Standard Reference Radiographs for Tin Bronze Castings*  
E 390-95, *Standard Reference Radiographs for Steel Fusion Welds*  
E 431-96, *Standard Guide to Interpretation of Radiographs of Semiconductors and Related Devices*  
E 446-98, *Standard Reference Radiographs for Steel Castings Up to 2 in. (51 mm) in Thickness*  
E 505-96, *Standard Reference Radiographs for Inspection of Aluminum and Magnesium Die Castings*  
E 592-99, *Standard Guide to Obtainable ASTM Equivalent Penetrometer Sensitivity for Radiography of Steel Plates 1/4 to 2 in. (6 to 51 mm) Thick with X Rays and 1 to 6 in. (25 to 152 mm) Thick with Cobalt-60*  
E 666-97, *Standard Practice for Calculating Absorbed Dose from Gamma or X Radiation*  
E 689-95 (1999), *Standard Reference Radiographs for Ductile Iron Castings*  
E 746-02, *Standard Test Method for Determining Relative Image Quality Response of Industrial Radiographic Film*  
E 747-97, *Standard Practice for Design, Manufacture and Material Grouping Classification of Wire Image Quality Indicators (IQI) Used for Radiology*  
E 748-95, *Standard Practices for Thermal Neutron Radiography of Materials*  
E 801 (2001), *Standard Practice for Controlling Quality of Radiological Examination of Electronic Devices*  
E 802-95 (1999), *Standard Reference Radiographs for Gray Iron Castings Up to 4 1/2 in. [114 mm]) in Thickness*  
E 803, *Standard Test Method for Determining the L/D Ratio of Neutron Radiography Beams*  
E 975-00, *Standard Practice for X-Ray Determination of Retained Austenite in Steel with Near Random Crystallographic Orientation*  
E 999-99, *Standard Guide for Controlling the Quality of Industrial Radiographic Film Processing*  
E 1000-98, *Standard Guide for Radioscopy*  
E 1025-98, *Standard Practice for Design, Manufacture, and Material Grouping Classification of Hole-Type Image Quality Indicators (IQI) Used for Radiology*  
E 1030-00, *Standard Test Method for Radiographic Examination of Metallic Castings*  
E 1032-95, *Standard Test Method for Radiographic Examination of Weldments*  
E 1114-92 (1997), *Standard Test Method for Determining the Focal Size of Iridium-192 Industrial Radiographic Sources*  
E 1161-95, *Standard Test Method for Radiologic Examination of Semiconductors and Electronic Components*  
E 1165-92 (2002), *Standard Test Method for Measurement of Focal Spots of Industrial X-Ray Tubes by Pinhole Imaging*  
E 1254-98, *Standard Guide for Storage of Radiographs and Unexposed Industrial Radiographic Films*  
E 1255-96, *Standard Practice for Radioscopy*  
E 1320-00, *Standard Reference Radiographs for Titanium Castings*  
E 1390-90 (2000), *Standard Guide for Illuminators Used for Viewing Industrial Radiographs*  
E 1411-95, *Standard Practice for Qualification of Radioscopic Systems*  
E 1441-00, *Standard Guide for Computed Tomography (CT) Imaging*  
E 1453-93 (1996), *Standard Guide for Storage of Media That Contains [sic] Analog or Digital Radioscopic Data*  
E 1475-97, *Standard Guide for Data Fields for Computerized Transfer of Digital Radiological Test Data*  
E 1496-97, *Standard Test Method for Neutron Radiographic Dimensional Measurements*  
E 1570-00, *Standard Practice for Computed Tomographic (CT) Examination*  
E 1647-98a, *Standard Practice for Determining Contrast Sensitivity in Radioscopy*  
E 1648-95 (2001), *Standard Reference Radiographs for Examination of Aluminum Fusion Welds*  
E 1672-95 (2001), *Standard Guide for Computed Tomography (CT) System Selection*  
E 1734-98, *Standard Practice for Radioscopic Examination of Castings*  
E 1735, *Standard Test Method for Determining Relative Image Quality of Industrial Radiographic Film Exposed to X-Radiation from 4 to 25 MV*  
E 1742-00, *Standard Practice for Radiographic Examination*  
E 1814-96, *Standard Practice for Computed Tomographic (CT) Examination of Castings*  
E 1815-96 (2001), *Standard Test Method for Classification of Film Systems for Industrial Radiography*  
E 1894-97, *Standard Guide for Selecting Dosimetry Systems for Application in Pulsed X-Ray Sources*  
E 1931-97, *Standard Guide for X-Ray Compton Scatter Tomography*  
E 1936-97, *Standard Reference Radiograph for Evaluating the Performance of Radiographic Digitization Systems*  
E 1955-98, *Standard Radiographic Examination for Soundness of Welds in Steel by Comparison to Graded ASTM E 390 Reference Radiographs*  
E 2002-98, *Standard Practice for Determining Total Image Unsharpness in Radiology*  
E 2033-99, *Standard Practice for Computed Radiology (Photostimulable Luminescence Method)*  
E 2116-00, *Standard Practice for Dosimetry for a Self-Contained Dry-Storage Gamma-Ray Irradiator*  
F 629-97, *Standard Practice for Radiography of Cast Metallic Surgical Implants*  
F 947-85 (1996), *Standard Test Method for Determining Low-Level X-Radiation Sensitivity of Photographic Films*  
F 1035-91 (1997), *Standard Practice for Use of Rubber-Cord Pie Disk to Demonstrate the Discernment Capability of a Tire X-Ray Imaging System*

TABLE 4. Some standards and practices for radiographic testing and for radiation safety.

Issuing Organization	Representative Standards and Related Documents
American National Standards Institute	ANSI N43.9-1991, <i>Gamma Radiography — Specifications for Design and Test of Apparatus</i> (revision and redesignation of ANSI N432-1980) ANSI PH2.8-1975, <i>Sensitometry of Industrial X-Ray Films for Energies up to 3 Million Electron Volts, Method for.</i>
American Society of Mechanical Engineers	See also ASME and ASNT. ANSI/ASME B31.1, <i>Power Piping</i> ANSI/ASME B31.3, <i>Process Piping</i> ASME <i>Boiler and Pressure Vessel Code: Section I — Power Boilers</i> ASME <i>Boiler and Pressure Vessel Code: Section III — Components</i> ASME <i>Boiler and Pressure Vessel Code: Section V — Power Boilers</i> ASME <i>Boiler and Pressure Vessel Code: Section VIII — Pressure Vessels</i> ASME <i>Boiler and Pressure Vessel Code: Section XI — Inservice Inspection of Nuclear Vessels</i> ASME PTC 19-1, <i>Performance Test Codes, Supplement on Instruction and Apparatus</i>
American Society for Nondestructive Testing	ASNT <i>Recommended Practice No. SNT-TC-1A</i> ANSI/ASNT CP-189, <i>ASNT Standard for Qualification and Certification of Nondestructive Testing Personnel</i>
American Society for Testing and Materials	See Table 3
American Petroleum Institute	API 510, <i>Pressure Vessel Inspection Code: Maintenance Inspection, Rating, Repair and Alteration</i> API 570, <i>Piping Inspection Code: Inspection, Repair, Alteration, and Rerating of In-Service Piping Systems</i> API 650, <i>Welded Steel Tanks for Oil Storage</i> API 1104, <i>Welding, Pipelines and Related Facilities</i>
American Water Works Association	AWWA D100-96, <i>Welded Steel Tanks for Water Storage</i>
American Welding Society	AWS D1.1, <i>Structural Welding Code — Steel</i> AWS D1.5, <i>Bridge Welding Code</i>
Canadian General Standards Board	CAN/CGSB-48-GP-2M, <i>Spot Radiography of Welded Butt Joints in Ferrous Materials</i> CAN/CGSB-48.3-92, <i>Radiographic Testing of Steel Castings</i> CAN/CGSB-48.5-95, <i>Manual on Industrial Radiography</i> CAN/CGSB-48.9712-95, <i>Non-Destructive Testing — Qualification and Certification of Personnel</i>
Deutsche Institut für Normung	DIN 6814, <i>Terms and Definitions in the Field of Radiological Techniques</i> DIN 6832-2, <i>Radiographic Cassettes: Test for Light-Proofness and Test for Contact between Radiographic Film and Intensifying Screen</i> DIN 25 430, <i>Safety Marking in Radiation Protection</i> DIN 54 115, <i>Non-Destructive Testing: Radiation Protection Rules for the Technical Application of Sealed Radioactive Sources</i> DIN EN 444, <i>Non-Destructive Testing: General Principles for the Radiographic Examination of Metallic Materials Using X-Rays and Gamma-Rays</i> DIN EN 12 681, <i>Founding — Radiographic Inspection</i> DIN EN 14 096, <i>Non-Destructive Testing - Qualification of Radiographic Film Digitisation Systems</i>
European Committee for Standardization	CEN 584, <i>Non Destructive Testing — Industrial Radiographic Film</i> EN 12 679, <i>Non-Destructive Testing — Determination of the Size of Industrial Radiographic Sources — Radiographic Method</i>
International Organization for Standardization	ISO 2504, <i>Radiography of Welds and Viewing Conditions for Films — Utilization of Recommended Patterns of Image Quality Indicators (I.Q.I.)</i> ISO 7004, <i>Photography — Industrial Radiographic Film — Determination of ISO Speed and Average Gradient When Exposed to X- and Gamma-Radiation</i> ISO 3999, <i>Apparatus for Gamma Radiography</i> ISO 9712, <i>Nondestructive Testing — Qualification and Certification of Personnel</i> ISO 9915, <i>Aluminium Alloy Castings — Radiography Testing</i> ISO 11 699, <i>Non-Destructive Testing — Industrial Radiographic Films</i>
Japanese Standards Association	K 7091, <i>Testing Method for Radiography of Carbon Fibre Reinforced Plastic Panels Edition 1</i> K 7521, <i>Dimensions for Photographic Film in Sheets and Rolls for Medical, Industrial and Dental Radiography</i>
Korean Standards Association	Z 4560, <i>Industrial Gamma-Ray Apparatus for Radiography</i> A 4907, <i>Film Marker of Radiography</i> A 4921, <i>Industrial X-Ray Apparatus for Radiography</i> M 3910, <i>Dimensions for Photographic Film in Sheets and Rolls for Medical, Industrial and Dental Radiography</i>
National Council on Radiation Protection Occupational Safety and Health Administration	NCRP 61, <i>Radiation Safety Training Criteria for Industrial Radiography</i> 29 CFR 1910, <i>Occupational Safety and Health Standards [Code of Federal Regulations: Title 29, Labor]</i>
Society of Automotive Engineers	SAE AMS 2635C, <i>Radiographic Inspection</i> SAE ARP 1611A, <i>Quality Inspection Procedure, Composites, Tracer Fluoroscopy and Radiography</i> SAE AS 1613A, <i>Image Quality Indicator, Radiographic</i> SAE AS 7114/4, <i>NADCAP Requirements for Nondestructive Testing Facility Radiography</i>

**Education, Training, Experience Requirements for Initial Qualification.** Candidates for certification in nondestructive testing should have sufficient education, training and experience to ensure qualification in those nondestructive testing methods for which they are being considered for certification. Table 5 lists the recommended training and experience factors to be considered by the employer in establishing written practices for initial qualification of Level I and II individuals for radiographic testing.

**Training Programs.** Personnel being considered for initial certification should complete sufficient organized training to become thoroughly familiar with the principles and practices of the specified nondestructive test method related to the level of certification desired and applicable to the processes to be used and the products to be tested.

**Examinations.** For Level I and II personnel, a composite grade should be determined by a simple averaging of the results of the general, specific and practical examinations described below. Examinations administered for qualification should result in a passing composite grade of at least 80 percent, with no individual examination having a passing grade less than 70 percent. The examination for near vision acuity should ensure natural or corrected near distance acuity in at least one eye such that applicant can read a minimum of jaeger size 2 or equivalent type and size letter at a distance of not less than 305 mm

(12 in.) on a standard jaeger test chart. This test should be administered annually.

**Written Examination for NDT Levels I and II.** The minimum number of questions that should be administered in the written examination for radiographic test personnel is as follows: 40 questions in the *general* examination and 20 questions in the *specific* examination. The number of questions is the same for Level I and Level II personnel.

**Practical Examination for NDT Level I and II.** The candidate should demonstrate ability to operate the necessary nondestructive test equipment, record and analyze the resultant information to the degree required. At least one selected specimen should be tested and the results of the nondestructive test analyzed by the candidate.

**Certification.** Certification of all levels of nondestructive testing personnel is the responsibility of the employer. Certification of nondestructive testing personnel shall be based on demonstration of satisfactory qualification in accordance with sections on education, training, experience and examinations, as modified by the employer's written practice. Personnel certification records shall be maintained on file by the employer.

**Recertification.** All levels of nondestructive testing personnel shall be recertified periodically in accordance with the following: evidence of continuing satisfactory performance; reexamination in those portions of examination deemed necessary by the employer's NDT Level III. Recommended maximum recertification intervals are three years for Level I and Level II and five years for Level III.

These recommendations from SNT-TC-1A are cited only to provide a flavor of the specific items that must be considered in the development of an in-house nondestructive testing program. However, if an outside agency is contracted for radiographic test services, then the contractor must have a qualification and certification program to satisfy most codes and standards.

## Central Certification

Another standard that may be a source for compliance is contained in the requirements of the International Organization for Standardization (ISO). The work of preparing international standards is normally carried out through technical committees of the International Organization for Standardization, a worldwide federation of national standards bodies. Each *ISO member body* interested in a subject for which a technical committee has been established

TABLE 5. Recommended training and experience for radiographic testing personnel according to ASNT Recommended Practice No. SNT-TC-1A.<sup>4</sup>

	Level I	Level II
<b>Radiographic Testing</b>		
High school graduate <sup>a</sup>	39 h	40 h
Two years of college <sup>b</sup>	29 h	35 h
Work experience <sup>c</sup>	3 mo	9 mo
<b>Neutron Radiographic Testing</b>		
High school graduate <sup>a</sup>	28 h	40 h
Two years of college <sup>b</sup>	20 h	40 h
Work experience <sup>c</sup>	6 mo	24 mo

a. Or equivalent.

b. Completion with a passing grade of at least two years of engineering or science study in a university, college or technical school.

c. Work time experience per level. Note: for Level II certification, the experience shall consist of time as Level I or equivalent. If a person is being qualified directly to Level II with no time at Level I, the required experience shall consist of the sum of the times required for Level I and Level II and the required training shall consist of the sum of the hours required for Level I and Level II.

has the right to be represented on that committee. International organizations, governmental and nongovernmental, in liaison with the International Organization for Standardization, also take part in the work.

Technical Committee ISO/TC 135, Non-Destructive Testing Subcommittee SC 7, Personnel Qualification, prepared international standard ISO 9712, *Nondestructive Testing – Qualification and Certification of Personnel*.<sup>8</sup> In its statement of scope, ISO 9712 states that it “establishes a system for the qualification and certification, by a certification body, of personnel to perform industrial nondestructive testing (NDT) using any of the following methods: (a) eddy current testing; (b) liquid penetrant testing; (c) magnetic particle testing; (d) radiographic testing; (e) ultrasonic testing” and that the “system described in this International Standard may also apply to visual testing (VT), leak testing (LT), neutron radiography (NR), acoustic emission (AE) and other nondestructive test methods where independent certification programs exist.” The applicability of ISO 9712 to radiographic testing therefore depends on activity of the national certifying body.

## Safety in Radiographic Testing

To manage a radiographic testing program, as with any test program, the first obligation is to ensure safe working conditions. The following are components of a safety program that may be required or at least deserve serious consideration.

1. Identify the safety and operational rules and codes applicable to the areas, equipment and processes being examined before work is to begin.
2. Provide proper safety equipment (protective barriers, hard hat, safety harnesses, steel toed shoes, hearing protection and others).
3. Provide necessary training in radiation safety.
4. Before the test, perform a thorough visual survey to determine all the hazards and identify necessary safeguards to protect test personnel and equipment.
5. Notify operative personnel to identify the location and specific equipment that will be examined. In addition, a determination must be made if signs or locks restrict access by personnel. Be aware of equipment that may be operated remotely or may started by time delay.

6. Be aware of any potentially explosive atmospheres. Determine whether it is safe to take your equipment into the area.
7. Do not enter any *roped off* or *no entry* areas without permission and approval.
8. When working on or around moving or electrical equipment, remove pens, watches, rings or objects in your pockets that may touch (or fall into) energized equipment.
9. Know interplant communication and evacuation systems.
10. Never let unqualified personnel operate equipment independently from qualified supervision.
11. Keep a safe distance between you and any energized equipment. In the United States, these distances can be found in documents from the Occupational Safety and Health Administration, the National Fire Prevention Association (*National Electric Code*),<sup>9</sup> the Institute of Electrical and Electronics Engineers (*National Electrical Safety Code*)<sup>10</sup> and other organizations.
12. Be aware of the personnel responsibilities before entering a *confined space*. All such areas must be tested satisfactorily for gas and oxygen levels before entry and periodically thereafter. If odors are noticed, or unusual sensations such as earaches, dizziness or difficulty in breathing are experienced, leave the area immediately.
13. Notice that the safety considerations listed above are applicable to many test methods. Because ionizing radiation can hurt people, additional precautions are needed for radiographic testing and are discussed in a separate chapter.

Most facilities in the United States are required by law to follow the requirements in the applicable standard. Two Occupational Safety and Health Standards in the United States that should be reviewed are *Occupational Safety and Health Standards* for general industry<sup>11</sup> and the *Occupational Safety and Health Standards for the Construction Industry*.<sup>12</sup>

Personnel safety is always the first consideration for every job.

## Ensuring Reliability of Test Results

When a test is performed, there are four possible outcomes: (1) a discontinuity can be found when a discontinuity is present; (2) a discontinuity can be missed even when a discontinuity is present; (3) a discontinuity can be found when none is

present; and (4) no discontinuity is found when none is present. A reliable testing process and a qualified inspector should find all discontinuities of concern with no discontinuities missed (no errors as in case 2, above) and no false callouts (case 3, above).

To achieve this goal, the probability of finding a discontinuity must be high and the inspector must be both proficient in the testing process and motivated to perform a maximum efficiency. A reckless inspector may accept parts that contain discontinuities, with the resultant consequences of possible inservice part failure. A conservative inspector may reject parts that contain discontinuities but the inspector also may reject parts that do not contain discontinuities, with the resultant consequences of unnecessary scrap and repair. Neither inspector is doing a good job.

---

## Summary

As noted in this discussion, many factors must be considered before a program of radiographic testing can begin at a facility. To manage a nondestructive testing program many options must be considered. The final decision for a path forward must be based on requirement documents (codes, standards or specifications) and what is best for your company. If a person in a position of responsibility lacks the expertise for this critical decision, the industry has many talented individuals willing to assist. The American Society for Nondestructive Testing is a place to begin the decision making process.



## PART 3. History of Radiographic Testing<sup>13</sup>

### Röntgen

Wilhelm Conrad Röntgen (Fig. 10) made his momentous discovery of X-rays on Friday, 8 November 1895, in his laboratory at the University of Würzburg in Germany. The importance of this new kind of ray was recognized immediately. The *see-through* property of X-rays created a sensation, not only in the scientific community but also in the popular press. By early January 1896, newspapers around the world carried news of these new rays and their ability to pass through flesh and other materials. The newspaper accounts correctly predicted the tremendous impact that X-rays were to have on medical diagnosis. Röntgen and other early X-ray workers showed X-ray images of *things*: Röntgen took X-ray images of his shotgun, a compass and weights in a box. Much experimental work ensued in an almost playful atmosphere, as researchers radiographed hundreds of different kinds of objects. Industrial applications of a sort were found almost immediately, in the sense that artillery shell casings were among the objects so examined. It was decades before nonmedical uses of X-rays became important.

Clearly, the practical uses for X-rays have gone well beyond the early concepts. Immediate medical uses foreseen included setting of broken bones and location of foreign objects — bullets, pins, coins and others. Medical applications have now expanded to include diagnosis of diseases such as tuberculosis, malfunctions such as blockages of the circulatory system and the detection of many abnormalities such as tumors and calcium loss in bones. X-rays are now used for medical therapy, to identify and analyze materials, to inspect industrial materials and, a use all airplane travelers recognize, to inspect baggage and packages. The methods include fluoroscopy and film radiography — the two methods Röntgen used — and more modern techniques such as electronic radioscopy, tomography, backscatter imaging, radiation gaging, diffraction, fluorescence and others.

### Preliminary Work

Röntgen was a respected scientist before the X-ray discovery, having published work on specific heat, optical phenomena

and compressibility of liquids. As a director of the Physical Institute at Würzburg, Röntgen had freedom to pursue scientific ideas that were of interest to him. In 1895, he began collecting the equipment needed to investigate luminescence effects. He studied early work by people before him — Faraday, Geissler, Hittorf and Crookes, for example — as well as the more current work of fellow German scientist Philipp Lenard. These scientists and others had studied luminescence in gases and solids using a partially evacuated tube, popularly known as a Crookes tube.<sup>14</sup> This was typically a pear shaped glass tube, containing two electrodes. When a high voltage was put between the electrodes, the positively charged ions from the gas bombarded the negative electrode, causing the release of electrons, then called *cathode rays*. The electrons caused luminescence in the partial gas filling, in the glass walls of the tube or in other materials placed in their path.

FIGURE 10. Wilhelm Conrad Röntgen.





## Discovery

Röntgen was an institute director, with graduate students and assistants available as needed. However, as was his usual custom, Röntgen did many experimental studies himself. His laboratory was only one floor down from his living quarters in the Physical Institute, so it was easily available to him as he desired. All was in readiness on the afternoon of Friday, 8 November 1895. Röntgen had his covered tube and a darkened laboratory when he energized the cathode ray tube and noticed luminescence from a barium platinocyanide screen on a table about 2 m (7 ft) away. The luminescence was definitely associated with the tube, turning on only when the tube was energized. Röntgen knew the effect could not be cathode rays, because they penetrate only a short distance in air. He was intrigued; he investigated.

He quickly learned about the penetrating power of these new rays; they penetrated paper, wood, metal and flesh. The rays made shadow pictures on fluorescent screens and on film. Nevertheless, he was skeptical about his discovery. As he became totally consumed in a seven week intensive study he commented to his friend, Theodor Boveri, "I have discovered something interesting but I do not know whether or not my observations are correct." At the same time, as a scientist, he was excited. He knew he must report his findings and obtain feedback from fellow scientists. Because the new rays darkened a photographic plate, he could take pictures and share them with others. One of these early pictures in December 1895 was a 15 min exposure showing the bones in the hand of his wife, Bertha. Other early pictures taken with the new rays included weights in a box, a compass, a piece of metal and a shotgun. He recognized that he must publish his results so that they could be shared with others in the scientific community. His first technical paper on X-rays, "On a New Kind of Rays: A Preliminary Communication," was published in the annals of the Würzburg Physical Medical Society in December 1895.<sup>15</sup> The reprints were ready by the new year. As he mailed reprints and photographs to colleagues, Röntgen said to Bertha, "Now the devil will be to pay," clearly a premonition of the coming drastic change in his life.

## Fame

Röntgen was apprehensive as he sent reprints and pictures to colleagues in January 1896, but he probably had no idea of what was in store for him. There was tremendous interest in his new rays, both from the scientific community and

the general public. One of his mailed set of reprints and photographs went to his friend Ernst Warburg in Berlin. Warburg displayed the material as a poster exhibit at the 50th anniversary meeting of the Berlin Physical Society in 1896. Many saw the exhibit in one corner of the hall.

Another of his private communications went to a second college friend, Professor Franz Exner in Vienna. Exner showed the pictures to several fellow scientists. One of them, Professor Ernst Lecher visiting from Prague, was so fascinated by the pictures that he asked Exner if he could borrow them overnight. Lecher shared the pictures with his father, Z. Lecher, editor of the *Vienna Presse* newspaper. Lecher's January 1896 article in the *Vienna Presse* newspaper extolled the potential of these new X-rays, correctly pointing out the benefits for medical diagnosis. The news quickly spread around the world, appearing in many newspapers within the following week. Röntgen received more than 1000 pieces of mail in the first week following the press announcement. Within days, scientists everywhere, using Crookes tubes, were repeating Röntgen's observations and confirming his results.

Once the news was out, there were many offers of honors, lectures and visits. However, Röntgen turned down most such overtures. One he could not refuse was a royal invitation. Röntgen gave a demonstration of X-rays before Kaiser Wilhelm II and his court in January 1896. As a result of this summons to the court, Röntgen was awarded the Royal Order of Merit, an award that permits one to use the title *von*, as an indication of nobility. Röntgen never made the formal application for the noble rank and refused to use the term *von* in his name.

Another summons he could not turn down was a call from his own university. In January 1896, he lectured on his discovery before the Physical Medical Society in Würzburg and gave the first public demonstration before an overflowing audience. The image of Röntgen's lecture was captured in a 1961 painting (Fig. 11). During the lecture Röntgen radiographed the hand of his fellow university professor and well known anatomist, Albert von Kolliker. Kolliker was so enthused by the discovery that he announced that the new rays should be called *roentgen rays*, as they are still in Europe and within the medical community. The lecture and demonstration were greeted with enthusiastic applause. It was to be Röntgen's only formal public lecture on X-rays.

The commercial community took note of Röntgen's discovery.<sup>14,16</sup> An American industrial group was said to offer Röntgen a fortune for rights to his discovery.

Röntgen was similarly approached by many industrial groups, including a documented overture by Max Levy of a German company. However, Röntgen remained true to his scientific calling, saying that discoveries and inventions belong to humanity and that they should not in any way be hampered by patents, licenses or contracts, nor should they be controlled by any one group.

Edison, the renowned American inventor, was quoted as saying about Röntgen's attitude, "After they have discovered something wonderful, someone else must look at it from the commercial point of view. One must see how to use it and how to profit from it financially." Edison was among the first of many Americans to investigate X-rays. He quickly designed and built X-ray tubes and a fluorescent screen fluoroscope, making use of the Edison discovery that a calcium tungstate phosphor screen gave very bright X-ray images. Edison exhibited an X-ray fluoroscope at the National Electrical Exposition at the Grand Central Palace in New York in May 1896. The Exposition gave the general public a rare opportunity to see X-ray pictures.

Obviously, with Crookes tubes in use in laboratories around the world, it is clear that many people before Röntgen had produced X-rays. Once the discovery was announced, many scientists recognized that X-rays had been responsible for strange effects they had noticed (but not followed up) from earlier experiments.

Crookes was always rejecting photographic plates because they were fogged, most likely from X-ray exposure. Philipp Lenard, who had helped Röntgen obtain one of his thin window tubes, had noticed that an electric charge some distance away from his Lenard tube was discharged but he did not investigate fully.<sup>17</sup>

One well documented early notice of X-rays occurred in the physics laboratory of Arthur W. Goodspeed at the University of Pennsylvania.<sup>18</sup> He was visited in February 1890, by photographer William Jennings to do some photography with spark discharges. After the young men finished with the spark equipment, Goodspeed showed Jennings his Crookes tube equipment in operation. Jennings had several unexposed, covered photographic plates on the table during the Crookes tube demonstration; he had placed several coins for his carfare on top of the stack of plates. On returning to his laboratory, he processed the plates and found a curious image of several round objects. He dated and filed the plate, only to bring it back at Goodspeed's request after the news of the X-ray discovery. They could document that they had made an X-radiograph five years before Röntgen's discovery. Goodspeed and Jennings merely brought the radiograph to public attention, never claiming any credit for discovering X-rays.

Röntgen himself published two additional scientific papers about X-rays. "On a New Kind of Rays, Continued,"<sup>15</sup> was published by the same Würzburg publication in March 1896 and was followed by "Further Observations on the Properties of X-Rays,"<sup>19</sup> published in March 1897 by the Prussian Academy of Sciences. His three scientific papers presented thorough results about X-rays.

His investigations showed the penetrating power of the new rays as related to the density of the absorber and the effect on fluorescent materials and photographic film. Röntgen took pinhole pictures to confirm that the source of the X-ray emission was the point where the cathode rays struck the glass wall or a metal target. He recognized the nonuniform distribution of the X-ray emission from the target and found the fundamentals of the inverse square law for decreasing X-ray intensity with increasing distance from the target. He tried without success to deflect the X-ray beam with a magnet or an electric field. His attempts to demonstrate reflection and diffraction were likewise without success. His experiments did produce evidence that the new rays caused electrical conductivity in air and that heavy metal targets such as platinum produced more intense X-ray beams than

FIGURE 11. Röntgen demonstrates X-rays in 1896.



glass or aluminum targets. His three papers on X-rays gave the basic information about X-rays to the world.<sup>20</sup>

### Early Medical Applications

The medical use of X-rays began immediately. It was straightforward to recognize the usefulness of X-rays to find foreign objects in the body and to help set broken bones. There are many documented instances of such applications as early as January and February 1896. The first recorded X-ray picture in the Americas was taken by Arthur W. Wright of Yale University, in January 1896. This was quickly followed by X-ray work at other universities.

Men recognized for early work in what has become medical radiology include Francis H. Williams, a doctor at the Boston City Hospital, and William J. Morton, a New York City physician.<sup>21</sup> Williams used X-rays to study anatomy, both diseased and normal. He used fluoroscopy and film radiography to study the thorax, for determining the outline of the heart, for diagnosis of tuberculosis and other medical studies. Williams had the advantage of working with two Massachusetts Institute of Technology scientists, Charles Norton and Ralph Lawrence, whose work advanced early X-ray technology. Morton's wide ranging pioneering X-ray work included the

recognition that gas in the body can help outline organs, an early concept of a contrast medium.

### Introduction of Additional Radiation Sources

In 1898 Marie Sklodowska Curie (Fig. 12) and Pierre Curie published research showing the discovery of two new radioactive elements, polonium and radium, laying the foundation for gamma radiography.

The early X-ray tubes were partially evacuated glass bulbs. Metal targets and curved cathodes were quickly added to increase X-ray output. Nevertheless, it was a challenge to operate these early gas tubes consistently. The gas pressure changed because of outgassing of the walls and other heating effects. One of the first X-ray related patents was for a technique of controlling the tube gas pressure (issued March 1896 to Siemens). Among the early uses of radioscopes, fluoroscopes similar to those at today's airports were used during World War I to inspect packages for contraband (Fig. 13).<sup>22</sup>

It was in this background that William D. Coolidge (Fig. 14) of General Electric introduced the hard vacuum, hot cathode X-ray tube, truly a significant advance in X-ray technology.<sup>23</sup> This new X-ray tube concept brought much improved reproducibility and ease of operation to X-ray technology and prepared the way for high energy X-ray use. The patent for this landmark X-ray development was issued in 1916.<sup>24</sup>

FIGURE 12. Marie Sklodowska Curie (1928).



FIGURE 13. Radioscopic system for detection of contraband (circa 1910).



## X-Rays for Nondestructive Testing

### X-Ray Diffraction

Röntgen's early X-ray work included unsuccessful attempts to show diffraction effects by directing the rays through a fine slit. This effect was successfully shown later following the 1909 work of Walter and Pohl.<sup>25</sup> It was Max von Laue who first thought of using the regular order of a crystal to diffract X-rays. Experimental confirmation of this now important and widespread use of X-rays came from Laue's work with Friedrich and

Knipping<sup>26,27</sup> and from the pioneering work of the father and son Bragg team.<sup>28,29</sup> X-ray diffraction is a widely used method to identify and analyze materials.<sup>25</sup> Some idea of the impact that X-ray diffraction has had on science is given by noting that twenty Nobel physics prizes have been awarded for achievements in crystallography.<sup>30</sup>

### Radiography

Early advances in X-ray nondestructive testing were being made in many countries around the world. Documentation of early X-ray work in the United Kingdom and in Germany describes work going back to the time of World War I. The early work in the United Kingdom, particularly the armament related X-ray nondestructive testing work of V.E. Pullin, is well described by Halmshaw.<sup>31</sup> An excellent description of early work in Germany shows many examples of radiographic nondestructive testing, including field test systems dating from the 1920s.<sup>32</sup> A recent summary of X-ray history is given in the X-ray centennial issue of *Insight*, including articles about X-ray development in the United Kingdom and in Germany.<sup>33</sup>

Early work in the United States is documented in patents.<sup>34,35</sup> Despite these early efforts and many demonstrations of X-rays for material examination,<sup>24</sup> radiographic nondestructive testing did not become important commercially until World War II. In the United States, workers in nondestructive testing cite the early work of Horace Lester (Fig. 15) at the

FIGURE 14. William Coolidge, inventor of X-ray tube: (a) posing with 1 MeV tube; (b) X-ray tube.

(a)



(b)

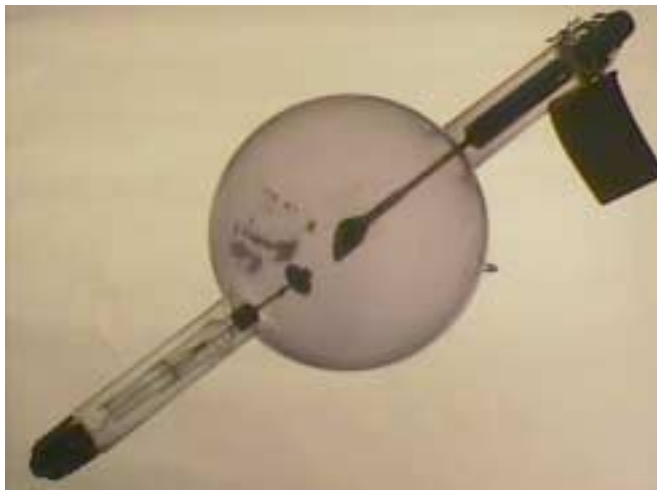


FIGURE 15. Horace Lester.





Watertown Arsenal (Fig. 16) as laying the groundwork for our present use of radiography.<sup>36,37</sup> Lester's work was significant because it clearly demonstrated that X-rays could be used to locate internal discontinuities in castings, welds and other metal forms and that these discontinuities could lead to premature failure. Lester's contributions were also important because of his preeminent position in the metallurgical field.<sup>38,39</sup> However, there was significant work done in the United States in radiographic nondestructive testing even before Lester's landmark research. An excellent review of early X-ray nondestructive testing work is given in the 1929 Fink and Archer paper for ASM International, when it was called the *American Society for Steel Treating*.<sup>40</sup> The paper cites 108 references, with 46 of these dating during the period 1915-1921. Prominent among the early citations is the work of Wheeler R. Davey, who did research on radiographic nondestructive testing at the General Electric Research Laboratory (1914 to 1926) and later at Penn State University. The Alcoa team of Fink and Archer described X-ray exposure techniques for aluminum and steel, including the use of fluorescent and lead screens. This 1929 paper is given credit for the first public description for the use of lead intensifying screens.<sup>41</sup>

FIGURE 16. Laboratory of Horace Lester at Watertown Arsenal, Watertown, Massachusetts.



Horace Lester attended this 1929 X-ray lecture and contributed to the discussion included with the published article. Lester's comment discussed the increasing use of steel forgings and welded structures instead of castings because engineers believed that "these substitutes for castings are free from hidden defects and therefore more reliable." He went on to point that his work at Watertown Arsenal showed that the assumption of soundness for forgings and welds was not true. Wheeler Davey also attended the lecture and contributed to the discussion. Davey's comment may strike a responsive chord even today: "the authors bring out the fact, previously emphasized by Lester, that there are few cases where it is good economic sense to use radiography for 100 per cent inspection."

It was in this environment of unfavorable economics for widespread use of nondestructive testing that the American Society for Nondestructive Testing began.

## American Society for Nondestructive Testing

The society was started officially by a charter from the state of Massachusetts dated August 1941. Prominent among the nine signers of the original charter are the first two names, Philip D. Johnson and Carlton G. Lutts. Lutts served as the first president of the American Industrial Radium and X-Ray Society during its initial year of operation, 1941-1942. The new society's first conference was held at Massachusetts Institute of Technology in October, 1941, highlighted by a presentation (later called the Mehl Honor Lecture) by Charles W. Briggs.

Formed as it was in late 1941, the society was in place as the United States entered World War II in December 1941. The war effort required increasing emphasis on product reliability and nondestructive testing. The fledgling society was there to provide a needed forum for the exchange of nondestructive testing information. The new society journal, first called *Industrial Radiography* and issued in the summer of 1942, played a key role in spreading knowledge about nondestructive testing.

Ralph Turner, ASNT national president during 1971-1972 and an ASNT historian, reflected on the early years of the Society: "The Society has not done badly. Perhaps the most fortunate event was its inadvertent birth just before World War II."<sup>42</sup> Clearly the war years gave a needed push to help the new society survive and grow during the crucial formative years.

An early recognition was that nondestructive testing included methods other than radiography. Liquid penetrants and magnetic particles were in wide use and other methods such as ultrasonic testing were becoming important. With Volume 5 in the summer of 1946, the journal name and mission were expanded to *Industrial Radiography & Non-Destructive Testing*. In the fall of 1947 the name of the society was changed to the Society for Non-Destructive Testing. The hyphen in the name disappeared in 1952. The journal expanded publication to bimonthly (instead of quarterly) in 1953 and became a monthly journal in 1964, at the same time changing the journal name to *Materials Evaluation*.<sup>43</sup> By 1967 many other countries had nondestructive testing societies and there had been five International Conferences on Nondestructive Testing (now called World Conferences), so it seemed appropriate to change the society name again; it became the American Society for Nondestructive Testing (ASNT).

ASNT can be proud of its role in advancing the state-of-the-art of nondestructive testing and X-ray technology. The national conferences, the section meetings for local information exchange, the topical conferences, the society's international participation, the *Nondestructive Testing Handbook* series and educational and personnel activities all provided opportunities for exchange of nondestructive testing information. The early issues of the journal were heavily weighted toward X-ray technology, reflecting the original name of the society. Early contributors to the journal included many respected engineers and scientists. Early issues contained articles by Arthur Barkow, Charles Barrett and George Clark (all of whom made early contributions to the advancement of X-ray diffraction), James Bly and Gerold Tenney (whose work included developments in high energy radiography), Donald O'Connor (whose group at the Naval Ordnance Laboratory, with colleagues Edward Criscuolo and Daniel Polansky, contributed much to the early X-ray nondestructive testing standards), Leslie Ball (an early user of X-ray technology in the aircraft field), Donald Kerst, the developer of the betatron, film research workers Herman Seeman and George Corney and many others whose names and works were well known.

Along the way there have been many noteworthy radiographic applications. *Materials Evaluation* readers may recall the following: the Vatican Pieta (June 1964), the world's largest radiograph (November 1964), the Liberty Bell (February 1976), a lighthouse (March 1980), the United

States Capitol (September 1985) and the Statue of Liberty (October 1985).

The journal has also provided an opportunity for commercial development of X-ray technology. Early advertisers in the journal included equipment suppliers such as General Electric, Keleket, North American Philips, Picker and Westinghouse, film suppliers such as Agfa-Ansco, DuPont and Eastman Kodak; and tube/accessory suppliers such as Bar-Ray Products, Machlett, Pako and Ray Proof Corporation. Only a few of these early X-ray companies continue to supply the X-ray nondestructive testing market in the 21st century; others, Keleket and Machlett, for example, have disappeared completely.

Many of the society honors and awards have had a radiation connection. The Coolidge Award, named for William D. Coolidge, the inventor of the hard vacuum X-ray tube (Fig. 14), was presented from 1953 to 1964 for outstanding contributions "to the advancement of nondestructive testing using X-rays." The Lester Honor Lecture, named for the X-ray pioneer Horace Lester (Fig. 15), has been presented since 1943. The Mehl Honor Lecture, named for Robert Mehl, an early contributor to gamma radiography,<sup>44</sup> has been presented since 1941. Although the honor lectures are named for men known for their work in radiation, the topics of the lectures cover the entire field of nondestructive testing.

Throughout the society history there has been a clear division of effort in advancing nondestructive testing between the American Society for Nondestructive Testing and the American Society for Testing and Materials Committee E-7 on Nondestructive Testing, organized in 1938.<sup>45</sup> The American Society for Testing and Materials activity produces consensus standards for nondestructive testing methods and applications. The American Society for Nondestructive Testing efforts provide a forum for information exchange, education and personnel certification. The role of the two organizations was recognized early, as indicated in a 1942 letter from Horace Lester, Chairman of American Society for Testing and Materials E-7.

There are many individuals who remain active in both the American Society for Testing and Materials Committee E-7 and the American Society for Nondestructive Testing, thereby providing a strong link between the two nondestructive testing organizations.



## Advances in Radiographic Technology

The period from 1935 to 1960 saw improvements in technology and techniques for radiation safety,<sup>46</sup> gamma radiography,<sup>47-49</sup> portable X-ray machines,<sup>49,50</sup> high voltage radiography<sup>51-53</sup> and nucleonic gaging.<sup>54</sup> Radiographic testing found new applications, in metals,<sup>55</sup> shipbuilding<sup>56</sup> and particularly in the aviation industries.<sup>57-59</sup>

Although radiographic testing is still performed essentially in the same through-transmission, direct shadowing way that Röntgen used 100 years ago, the twenty-first century has much better X-ray sources, detectors and understanding of image quality factors like scatter and unsharpness. In addition, of course, the industry today has a large arsenal of techniques — for example, electronic radioscopy, computed tomography, backscatter imaging, laminography, dual energy, microradiography, flash techniques and in-motion radiography. The commercial X-ray market for equipment, accessories and supplies is still primarily weighted toward medical fields but other X-ray applications contribute to what is estimated to be a \$12 billion annual market. In addition to the medical and traditional nondestructive testing applications, industry uses X-ray diffraction and other analytical methods such as fluorescence, radiation methods for material modification, X-ray lithography, radiation gaging and the ever expanding use of X-rays for security.

Looking toward the future, only one thing is clear — the technology will continue to advance. Obvious directions are the increasing use of computerized instrumentation, automated testing and greater use of nondestructive test techniques in process control applications. Regardless of the new directions that nondestructive testing and X-ray technology may take in the coming century the American Society for Nondestructive Testing's roles of education, information exchange and personnel certification will continue.

Thanks to the superb investigative talents of Wilhelm Conrad Röntgen, our generation enjoys many benefits from Röntgen's rays. The new edition of the *Nondestructive Testing Handbook* is a good time to remember past achievements.

## PART 4. Units of Measure for Radiographic Testing

### Origin and Use of SI System

In 1960 the General Conference on Weights and Measures established the International System of Units. *Le Système International d'Unités* (SI) was designed so that a single set of measurement units could be used by all branches of science, engineering and the general public. Without SI, this *Nondestructive Testing Handbook* volume could have contained a confusing mix of obsolete centimeter-gram-second (CGS) units, imperial units and the units preferred by certain localities or scientific specialties.

SI is the modern version of the metric system and ends the division between metric units used by scientists and metric units used by engineers and the public. Scientists have given up their units based on centimeter and gram and engineers made a fundamental change in abandoning the kilogram-force in favor of the newton. Electrical engineers have retained their ampere, volt and ohm but changed all units related to magnetism.

Table 6 lists the seven SI base units. Table 7 lists derived units with special names. Table 8 gives examples of conversions to SI units. In SI, the unit of time is the second (s) but hour (h) is recognized for use with SI.

For more information, the reader is referred to the information available through national standards organizations and specialized information compiled by technical organizations.<sup>60-63</sup>

TABLE 6. SI base units.

Quantity	Unit	Symbol
Length	meter	m
Mass	kilogram	kg
Time	second	s
Electric current	ampere	A
Temperature	kelvin	K
Amount of substance	mole	mol
Luminous intensity	candela	cd

### Multipliers

In science and engineering, very large or very small numbers with units are expressed by using the SI multipliers, prefixes of  $10^3$  intervals (Table 9). The multiplier becomes a property of the SI unit. For example, a millimeter (mm) is 0.001 meter (m). The volume unit cubic centimeter ( $\text{cm}^3$ ) is  $(0.01 \text{ m})^3$  or  $10^{-6} \text{ m}^3$ . Unit submultiples such as the centimeter, decimeter, dekameter (or decameter) and hectometer are often avoided in scientific and technical uses of SI because of their variance from the  $10^3$  interval. However,  $\text{dm}^3$  and  $\text{cm}^3$  are commonly used. Note that  $1 \text{ cm}^3$  is not equal to  $0.01 \text{ m}^3$ . Nevertheless, in equations, submultiples such as centimeter (cm) or decimeter (dm) are often avoided because they disturb the

TABLE 7. SI derived units with special names.<sup>a</sup>

Quantity	Units	Symbol	Relation to Other SI Units <sup>b</sup>
Capacitance	farad	F	$\text{C} \cdot \text{V}^{-1}$
Catalytic activity	katal	kat	$\text{s}^{-1} \cdot \text{mol}$
Conductance	siemens	S	$\text{A} \cdot \text{V}^{-1}$
Energy	joule	J	$\text{N} \cdot \text{m}$
Frequency (periodic)	hertz	Hz	$1 \cdot \text{s}^{-1}$
Force	newton	N	$\text{kg} \cdot \text{m} \cdot \text{s}^{-2}$
Inductance	henry	H	$\text{Wb} \cdot \text{A}^{-1}$
Illuminance	lux	lx	$\text{lm} \cdot \text{m}^{-2}$
Luminous flux	lumen	lm	$\text{cd} \cdot \text{sr}$
Electric charge	coulomb	C	$\text{A} \cdot \text{s}$
Electric potential <sup>c</sup>	volt	V	$\text{W} \cdot \text{A}^{-1}$
Electric resistance	ohm	$\Omega$	$\text{V} \cdot \text{A}^{-1}$
Magnetic flux	weber	Wb	$\text{V} \cdot \text{s}$
Magnetic flux density	tesla	T	$\text{Wb} \cdot \text{m}^{-2}$
Plane angle	radian	rad	1
Power	watt	W	$\text{J} \cdot \text{s}^{-1}$
Pressure (stress)	pascal	Pa	$\text{N} \cdot \text{m}^{-2}$
Radiation absorbed dose	gray	Gy	$\text{J} \cdot \text{kg}^{-1}$
Radiation dose equivalent	sievert	Sv	$\text{J} \cdot \text{kg}^{-1}$
Radioactivity	becquerel	Bq	$1 \cdot \text{s}^{-1}$
Solid angle	steradian	sr	1
Temperature, celsius	degree celsius	$^{\circ}\text{C}$	K
Time <sup>a</sup>	hour	h	3600 s
Volume <sup>a</sup>	liter	L	$\text{dm}^3$

a. Hour and liter are not SI units but are accepted for use with the SI.

b. Number one (1) expresses dimensionless relationship.

c. Electromotive force.

convenient  $10^3$  or  $10^{-3}$  intervals that make equations easy to manipulate.

In SI, the distinction between upper and lower case letters is meaningful and should be observed. For example, the meanings of the prefix *m* (milli) and the prefix *M* (mega) differ by nine orders of magnitude.

## SI Units for Radiography

The original discoveries of radioactivity helped establish units of measurement based on observation rather than precise physical phenomena. Later, scientists who worked with radioactive substances (or who managed to manufacture radioactive beams) again made circumstantial observations that were then used for measurement purposes. This practical approach was acceptable at the time, but a broader understanding of physics and the modern practice of using only one unit for a quantity has led to the modification of many of the original units (see Tables 10 to 12). In the SI system, radiation units have been given established physical foundations and new names where necessary.

TABLE 9. SI prefixes and multipliers.

Prefix	Symbol	Multiplier
yotta	Y	$10^{24}$
zetta	Z	$10^{21}$
exa	E	$10^{18}$
peta	P	$10^{15}$
tera	T	$10^{12}$
giga	G	$10^9$
mega	M	$10^6$
kilo	k	$10^3$
hecto <sup>a</sup>	h	$10^2$
deka (or deca) <sup>a</sup>	da	10
deci <sup>a</sup>	d	$10^{-1}$
centi <sup>a</sup>	c	$10^{-2}$
milli	m	$10^{-3}$
micro	$\mu$	$10^{-6}$
nano	n	$10^{-9}$
pico	p	$10^{-12}$
femto	f	$10^{-15}$
atto	a	$10^{-18}$
zepto	z	$10^{-21}$
yocto	y	$10^{-24}$

a. Avoid these prefixes (except in  $\text{dm}^3$  and  $\text{cm}^3$ ) for science and engineering.

TABLE 8. Examples of conversions to SI units.

Quantity	Measurement in Non-SI Unit	Multiply by	To Get Measurement in SI Unit
Angle	minute (min)	$2.908\,882 \times 10^{-4}$	radian (rad)
	degree (deg)	$1.745\,329 \times 10^{-2}$	radian (rad)
Area	square inch ( $\text{in.}^2$ )	645	square millimeter ( $\text{mm}^2$ )
Distance	angstrom ( $\text{\AA}$ )	0.1	nanometer (nm)
	inch (in.)	25.4	millimeter (mm)
Energy	British thermal unit (BTU)	1.055	kilojoule (kJ)
	calorie (cal), thermochemical	4.184	joule (J)
Power	British thermal unit per hour ( $\text{BTU}\cdot\text{h}^{-1}$ )	0.293	watt (W)
Specific heat	British thermal unit per pound degree fahrenheit ( $\text{BTU}\cdot\text{lb}_m^{-1}\cdot^\circ\text{F}^{-1}$ )	4.19	kilojoule per kilogram per kelvin ( $\text{kJ}\cdot\text{kg}^{-1}\cdot\text{K}^{-1}$ )
Force (torque, couple)	foot-pound ( $\text{ft}\cdot\text{lb}_f$ )	1.36	joule (J)
Pressure	pound force per square inch ( $\text{lb}_f\cdot\text{in.}^{-2}$ )	6.89	kilopascal (kPa)
Frequency (cycle)	cycle per minute	$60^{-1}$	hertz (Hz)
Illuminance	footcandle (ftc)	10.76	lux (lx)
	phot (ph)	10 000	lux (lx)
Luminance	candela per square foot ( $\text{cd}\cdot\text{ft}^{-2}$ )	10.76	candela per square meter ( $\text{cd}\cdot\text{m}^{-2}$ )
	candela per square inch ( $\text{cd}\cdot\text{in.}^{-2}$ )	1 550	candela per square meter ( $\text{cd}\cdot\text{m}^{-2}$ )
	footlambert (ftl)	3.426	candela per square meter ( $\text{cd}\cdot\text{m}^{-2}$ )
	lambert	$3\,183 (= 10\,000/\pi)$	candela per square meter ( $\text{cd}\cdot\text{m}^{-2}$ )
	nit (nt)	1	candela per square meter ( $\text{cd}\cdot\text{m}^{-2}$ )
	stilb (sb)	10 000	candela per square meter ( $\text{cd}\cdot\text{m}^{-2}$ )
Radioactivity	curie (Ci)	37	gigabecquerel (GBq)
Ionizing radiation exposure	roentgen (R)	0.258	millicoulomb per kilogram ( $\text{mC}\cdot\text{kg}^{-1}$ )
Mass	pound ( $\text{lb}_m$ )	0.454	kilogram (kg)
Temperature (difference)	degree fahrenheit ( $^\circ\text{F}$ )	0.556	kelvin (K) or degree celsius ( $^\circ\text{C}$ )
Temperature (scale)	degree fahrenheit ( $^\circ\text{F}$ )	$(^\circ\text{F} - 32)/1.8$	degree celsius ( $^\circ\text{C}$ )
Temperature (scale)	degree fahrenheit ( $^\circ\text{F}$ )	$(^\circ\text{F} - 32)/1.8 + 273.15$	kelvin (K)

## Physical Quantities

Three physical quantities in particular are widely used as measurement units — the electronvolt (eV), the speed of light ( $c$ ) and the unified atomic mass unit (u). Their precise values, however, are obtained experimentally.

**Electronvolt.** The electronvolt is the kinetic energy acquired by an electron in passing through a potential difference of 1 V in vacuum;  $1 \text{ eV} = 1.602\,176\,462 \times 10^{-19} \text{ J}$  with a combined standard uncertainty of  $6.3 \times 10^{-27} \text{ J}$ .<sup>63,64</sup> The electronvolt is accepted for use with SI.

**Speed of Electromagnetic Radiation.** The quantity  $c$  represents the speed of light, that is, the speed of electromagnetic waves in vacuum;  $1 \text{ } c = 299\,792\,458 \text{ m}\cdot\text{s}^{-1}$  exactly ( $670\,616\,629 \text{ mi}\cdot\text{h}^{-1}$ ). The speed of light is a physical quantity but can be used as a unit of measure.

**Unified Atomic Mass Unit.** The unified atomic mass unit (u) is  $12^{-1}$  of the mass of the atom of the nuclide carbon-12;  $1 \text{ u} = 1.660\,538\,7310^{-27} \text{ kg}$  with a combined standard uncertainty of  $\pm 1.3 \times 10^{-34} \text{ kg}$ .<sup>63,64</sup>

## Radiation Measurement

Because of existing practice in certain fields and countries, the International Committee for Weights and Measures (CIPM, Comité Internationale des Poids et

Mesures) permitted the units given in Table 11 (curie, roentgen, rad and rem) to continue to be used with the SI until 1998.<sup>61-63</sup> However, these units must not be introduced where they are not presently used. The National Institute of Standards and Technology strongly discourages the continued use of curie, roentgen, rad and rem.<sup>61-63</sup> The American National Standards Institute, the American Society for Testing and Materials, the Institute of Electrical and Electronics Engineers, the International Organization Standardization (ISO) and the American Society for Nondestructive Testing all support the replacement of older English units with SI units.

**Becquerel Replaces Curie.** The original unit for radioactivity was the curie (Ci), simply the radiation of one gram of radium. Eventually all equivalent radiation from any source was measured with this same unit. It is now known that a curie is equivalent to  $3.7 \times 10^{10}$  disintegrations per second. In SI, the unit for radioactivity is the becquerel (Bq), which is one disintegration per second. Because billions of disintegrations are required in a useful source, the multiplier prefix giga ( $10^9$ ) is used and the unit is normally seen as gigabecquerel (GBq).

**Coulomb per Kilogram Replaces Roentgen.** The unit for quantity of electric charge is the coulomb (C), where

TABLE 10. Physical quantities used as units. Values of physical quantities are experimentally obtained and may only be approximated in SI. Conversions are provided here for descriptive purposes.

Physical Quantity	Symbol	Multiply by	SI Unit	SI Symbol
Electronvolt <sup>a</sup>	eV	$1.6 \times 10^{-19}$	joule	J
Speed of electromagnetic waves in vacuum	$c$	$2.997\,924\,58 \times 10^8$	meter per second	$\text{m}\cdot\text{s}^{-1}$
Unified atomic mass unit <sup>a,b</sup>	u	$1.66 \times 10^{-27}$	kilogram	kg

a. Approved for use with SI.

b. Mass of unified atomic mass unit is  $12^{-1}$  of the mass of the atom of the nuclide carbon-12.

TABLE 11. Conversion to SI radiographic units.

Traditional Unit	Symbol	Multiply by	Resulting SI Unit	SI Symbol
Curie	Ci	$3.7 \times 10^{10}$ 37	becquerel gigabecquerel	Bq GBq
Rad	rad <sup>a</sup>	$10^{-2}$ 10	gray milligray	Gy mGy
Rem	rem	$10^{-2}$ 10	sievert millisievert	Sv mSv
Roentgen	R	$2.58 \times 10^{-4}$ 258	coulomb per kilogram microcoulomb per kilogram	$\text{C}\cdot\text{kg}^{-1}$ $\mu\text{C}\cdot\text{kg}^{-1}$

a. The abbreviation *rd* may be used for radiation absorbed dose where there is possibility of confusion with radian (rad), the SI unit for plane angle.

1 C = 1 A × 1 s. The original roentgen (R) was the quantity of radiation that would ionize 1 cm<sup>3</sup> of air to 1 electrostatic unit of electric charge, of either sign. It is now known that a roentgen is equivalent to 258 microcoulombs per kilogram of air (258 μC·kg<sup>-1</sup> of air). This corresponds to 1.61 × 10<sup>15</sup> ion pairs per 1 kg of air, which has then absorbed 8.8 mJ (0.88 rad, where rad is the obsolete unit for radiation absorbed dose, not the SI symbol for radian).

**Gray Replaces Rad.** The roentgen (R) was an intensity unit but was not representative of the dose absorbed by material in a radiation field. The radiation absorbed dose (rad) was first created to measure this quantity and was based on the erg, the energy unit from the old centimeter-gram-second (CGS) system. In the SI system, the unit for radiation dose is the gray (Gy). The gray is useful because it applies to doses absorbed by matter at a particular location. It is expressed in energy units per mass of matter or in joules per kilogram (J·kg<sup>-1</sup>). The mass is that of the absorbing body.

**Sievert Replaces Rem.** The SI system's unit for the dose absorbed by the human body (formerly *rem* for *roentgen equivalent man*; also known as *ambient dose equivalent*, *directional dose equivalent*, *dose equivalent*, *equivalent dose* and *personal dose equivalent*) is similar to the gray but includes quality factors dependent on the type of radiation. This absorbed dose has been given the name sievert (Sv) but its dimensions are the same as the gray, that is, 1 Sv = 1 J·kg<sup>-1</sup>.

## Compound Units

Exposure to ionizing radiation could be measured in roentgens with an ionization chamber that, when placed 1 m (39 in.) from the radiation source, provided necessary information — one roentgen per curie per hour at one meter (R·Ci<sup>-1</sup>·h<sup>-1</sup> at 1 m), for example. The numbers, however, had limited physical meaning and could not be used for different applications such as high voltage X-ray machines.

The roentgen per hour (R·h<sup>-1</sup>) was used to designate the exposure to an ionizing radiation of the stated value. Because the radiation received from 1 R·h<sup>-1</sup> was considered about equal to 1 rem, the relationship is approximated as 1 R·h<sup>-1</sup> = 0.01 Gy·h<sup>-1</sup> = 10 mGy·h<sup>-1</sup>.

A previously popular unit, roentgen per curie per hour at one meter (R·Ci<sup>-1</sup>·h<sup>-1</sup> at 1 m), is expressed in SI units as millisievert per gigabecquerel per hour at one meter (mSv·GBq<sup>-1</sup>·h<sup>-1</sup> at 1 m), such that 1 mSv·GBq<sup>-1</sup>·h<sup>-1</sup> at 1 m = 3.7 R·Ci<sup>-1</sup>·h<sup>-1</sup> at 1 m. In this relationship,

roentgen converts to millisieverts on a one-to-ten basis.

Exposure charts were often made by using curie minutes at a source-to-film distance in inches squared. This was written Ci·min·in.<sup>-2</sup>. Exposure charts made in SI use gigabecquerel minutes for a source-to-film distance in centimeters squared, where 1 Ci·min·in.<sup>-2</sup> = 50 GBq·min·cm<sup>-2</sup>. Table 12 lists some of these compound units.

TABLE 12. Compound radiographic units.

Traditional Unit	Multiply by	Resulting SI Unit
R·Ci <sup>-1</sup> ·h <sup>-1</sup> at 1 m	0.27	mSv·GBq <sup>-1</sup> ·h <sup>-1</sup> at 1 m
Ci·min·in. <sup>-2</sup>	50	GBq·min·cm <sup>-2</sup>
R·min <sup>-1</sup> <sup>a</sup>	0.01	Gy·min <sup>-1</sup>
R·min <sup>-1</sup> <sup>b</sup>	0.01	Sv·min <sup>-1</sup>
R	2.58 × 10 <sup>-4</sup>	C·kg <sup>-1</sup>

a. Absorbed dose.

b. Dose absorbed by human body.

# References

1. *Nondestructive Testing Handbook*, second edition: Vol. 10, *Nondestructive Testing Overview*. Columbus, OH: American Society for Nondestructive Testing (1996).
2. Wenk, S.A. and R.C. McMaster. *Choosing NDT: Applications, Costs and Benefits of Nondestructive Testing in Your Quality Assurance Program*. Columbus, OH: American Society for Nondestructive Testing (1987).
3. *Nondestructive Testing Methods*. TO33B-1-1 (NAVAIR 01-1A-16) TM43-0103. Washington, DC: Department of Defense (June 1984).
4. *ASNT Recommended Practice No. SNT-TC-1A*. Columbus, OH: American Society for Nondestructive Testing.
5. *Annual Book of ASTM Standards: Section 3, Metals Test Methods and Analytical Procedures*. Vol. 03.03, *Nondestructive Testing*. West Conshohocken, PA: ASTM International (2001).
6. ANSI/ASNT CP-189, *Standard for Qualification and Certification of Nondestructive Testing Personnel*. Columbus, OH: American Society for Nondestructive Testing.
7. *ASNT Central Certification Program (ACCP)*, Revision 3 (November 1997). Columbus, OH: American Society for Nondestructive Testing (1998).
8. ISO 9712, *Nondestructive Testing — Qualification and Certification of Personnel*. Geneva, Switzerland: International Organization for Standardization.
9. NFPA 70, *National Electric Code*, 2002 edition. Quincy, MA: National Fire Prevention Association (2001).
10. *National Electrical Safety Code*, 2002 edition. New York, NY: Institute of Electrical and Electronics Engineers (2001).
11. 29 CFR 1910, *Occupational Safety and Health Standards [Code of Federal Regulations: Title 29, Labor]*. Washington, DC: United States Department of Labor, Occupational Safety and Health Administration; Government Printing Office.
12. 29 CFR 1926, *Occupational Safety and Health Standards for the Construction Industry [Code of Federal Regulations: Title 29, Labor]*. Washington, DC: United States Department of Labor, Occupational Safety and Health Administration; Government Printing Office.
13. Berger, H. "100 Years of X-Rays — Industrial Use of NDT and the Role of ASNT." *Materials Evaluation*. Vol. 53, No. 11. Columbus, OH: American Society for Nondestructive Testing (November 1995): p 1253-1258, 1260.
14. Glasser, O. *Wilhelm Conrad Roentgen and the Early History of X-Rays*. Springfield, IL: Charles C. Thomas (1934). English version of an earlier biography in German published in Berlin, Germany: Springer-Verlag (1931).
15. Röntgen, W.C. "Eine Neue Art von Strahlen" ["A New Kind of Rays"]. *Verhandlungen und Sitzungsberichte der Physikalisch-Medizinische Gesellschaft zu Würzburg*. Würzburg, Germany: Physikalisch-Medizinische Gesellschaft zu Würzburg (December 1895): p 132. Continued (March 1896): p 11, 17.
16. Eisenberg, R.L. *Radiology — An Illustrated History*. Saint Louis, MO: Mosby Yearbook Publishing (1992).
17. Lenard, P. "On Cathode-Rays in Gases under Atmospheric Pressure and in the Extreme Vacuum." *Annalen der Physik*. Vol. 51. Berlin (1894): p 225-267.
18. Grigg, E.R.N. *The Trail of the Invisible Light*. Springfield, IL: Charles C. Thomas (1965).
19. Röntgen, W.C. ["Further Observations on the Properties of X-Rays."] *Berichte der Preussische Akademie der Wissenschaft*. Berlin, Germany: Berlin-Brandenburgische Akademie der Wissenschaften [formerly the Preussische Akademie der Wissenschaften] (May 1897).
20. Henning, D. "The German Röntgen Museum." *Materials Evaluation*. Vol. 45, No. 5. Columbus, OH: American Society for Nondestructive Test (May 1987): p 536-537.
21. Brecher, R. and E. Brecher. *The Rays: A History of Radiology in the U.S. and Canada*. Baltimore, MD: Williams and Wilkins (1969).



22. St. John, A. and H.R. Isenburger. *Industrial Radiography*. New York, NY: John Wiley and Sons (1934).
23. "Dr. W.D. Coolidge — The Scientist." *Industrial Radiography*. Columbus, OH: American Society for Nondestructive Testing (Summer 1944): p 33-35.
24. Coolidge, W.D. *Vacuum Tube*. United States Patent 1 203 495 (1916).
25. Ewald, P.P., ed. *Fifty Years of X-Ray Diffraction*. Utrecht, Netherlands: International Union of Crystallography (1962).
26. Friedrich, W., P. Knipping and M. Laue. *Berichte — Bayerische Akademie der Wissenschaft*. Munich, Germany: Bayerische Akademie der Wissenschaften (1912): p 303.
27. Friedrich, W., P. Knipping and M. Laue. *Annalen der Physik*. Vol. 41. Berlin, Germany: Wiley (1913): p 971.
28. Bragg, W.H. and W.L. Bragg. *Proceedings of the Royal Society of London: Series A, Mathematical and Physical Sciences*. Vol. 88. London, United Kingdom: Royal Society (1913): p 428.
29. Bragg, W.H. and W.L. Bragg. *Proceedings of the Royal Society of London: Series A, Mathematical and Physical Sciences*. Vol. 89. London, United Kingdom: Royal Society (1913): p 246.
30. Hasek, J. *X-Ray and Neutron Structure Analysis in Materials Science*. New York, NY: Plenum Press (1989).
31. Halmshaw, R. "A History of Industrial Radiography in the UK." *British Journal of Non-Destructive Testing*. Vol. 30, No. 5. Northampton, United Kingdom: British Institute of Non-Destructive Testing (September 1988): p 325-331.
32. Krüger, G. and H. Weeber. *Die Entwicklung der Technischen Durchstrahlungsprüfung in Deutschland: Streiflichter aus der Geschichte der DGZfP*. Berlin, Germany: Deutsche Gesellschaft für Zerstörungsfreie Prüfung (1983).
33. Special Feature Issue: 100 Years of X-Rays. *Insight*. Vol. 37, No. 9. Northampton, United Kingdom: British Institute of Non-Destructive Testing (September 1995).
34. Jackson, L.R., H.M. Banta, R.C. McMaster and T.P. Nordin. "A Survey of Patents, Publications on Non-Destructive Tests." *The Drilling Contractor*. Houston, TX: International Association of Drilling Contractors (April and June 1948).
35. McMaster, R.C. and S.A. Wenk. "A Basic Guide for Management's Choice of Nondestructive Tests." *Symposium on the Role of Non-Destructive Testing in the Economics of Production*. Special Technical Publication 112. West Conshohocken, PA: ASTM International (1951).
36. Lester, H.H. "Radiography of Metals." *Army Ordnance*. Vol. 3 (1922): p 210-215.
37. Lester, H.H. "X-Ray Examination of Steel Castings." *Chemical and Metallurgical Engineering*. Vol. 28, No. 6. New York, NY: McGraw-Hill (February 7, 1923). Reprint in Wenk, S.A. "The Past Perfect." *Materials Evaluation*. Vol. 27, No. 1. Columbus, OH: American Society for Nondestructive Testing (January 1969): p 1-10.
38. Wenk, S.A. "The Past Perfect." *Materials Evaluation*. Vol. 27, No. 1. Columbus, OH: American Society for Nondestructive Testing (January 1969): p 1-10.
39. Norton, M.R. "The Founder of Industrial Radiography: Personal Notes on Horace H. Lester." *Materials Evaluation*. Vol. 44, No. 3. Columbus, OH: American Society for Nondestructive Testing (March 1986): p 408-410.
40. Fink, W.L. and R.S. Archer. "Radiography as a Tool in the Metal Industry." *Transactions of the American Society for Steel Treating*. Vol. 16. Materials Park, OH: ASM International (1929): p 551-599.
41. Heidt, H. Private communication. Weimar, Germany (1994).
42. Turner, R. and D.D. Dewey. *Pictures and Passages: ASNT 1941-1991*. Columbus, OH: American Society for Nondestructive Testing (1991).
43. Berger, H. "Fifty Years of the Society Journal: A Personal Look Back." *Materials Evaluation*. Vol. 50, No. 8. Columbus, OH: American Society for Nondestructive Testing (August 1992): p 953-955.
44. Lambert, R.H. "In Memoriam: Robert F. Mehl." *Materials Evaluation*. Vol. 34, No. 7. Columbus, OH: American Society for Nondestructive Testing (July 1976): p 37A.
45. Borucki, J.S. "Overview of ASTM E-7 Nondestructive Testing Standards" *Nondestructive Testing Standards — Present and Future*. Special Technical Publication 1151. Philadelphia, PA: American Society for Testing and Materials (1992).

46. Morgan, K.Z. "History of Radiation Protection." *Materials Evaluation*. Vol. 29, No. 3. Columbus, OH: American Society for Nondestructive Testing (March 1971): p 19A-20A, 22A, 24A-27A, 32A.
47. Briggs, C.W. "Developments in Gamma Ray Radiography: 1928-41." *Industrial Radiography*. Vol. 1, No. 1. Columbus, OH: American Society for Nondestructive Testing (Summer 1942): p 7-10+. Reprinted *Materials Evaluation*. Vol. 39, No. 3 (March 1981): p 356-359.
48. Moore, P.O. "A Gamma-Radiographer of Pipeline Welds." *Materials Evaluation*. Vol. 43, No. 9. Columbus, OH: American Society for Nondestructive Testing (August 1985): p 1084-1086+.
49. Bell, R.D. "Field Radiography — Images from the Past." *Materials Evaluation*. Vol. 42, No. 7. Columbus, OH: American Society for Nondestructive Testing (June 1984): p 849-851.
50. Hovland, H. "Developments in Field X-Radiography, 1931-62." *Materials Evaluation*. Vol. 43, No. 11. Columbus, OH: American Society for Nondestructive Testing (October 1985): p 1386-1390.
51. O'Connor, D.T. and B.G. Cunningham. "Installation of the Flexible 10 MeV Betatron." *Non-Destructive Testing*. Vol. 7, No. 4. Columbus, OH: American Society for Nondestructive Testing (Spring 1949): p 20-23.
52. Straw, R. "'If I Had a Million!' The Early Years of High-Energy Radiography." *Materials Evaluation*. Vol. 42, No. 3. Columbus, OH: American Society for Nondestructive Testing (March 1984): p 264-268.
53. Straw, R. "'If I Had Ten Million!' A Man and His Laboratory." *Materials Evaluation*. Vol. 42, No. 4. Columbus, OH: American Society for Nondestructive Testing (April 1984): p 374-375.
54. Davis, R.S. "Early Development of Process Automation with Nucleonic Measurement Gages." *Materials Evaluation*. Vol. 47, No. 10. Columbus, OH: American Society for Nondestructive Testing (October 1989): p 1190-1191.
55. Henry, E.B. "The Role of Nondestructive Testing in the Production of Pipe and Tubing" [1988 Lester Honor Lecture]. *Materials Evaluation*. Vol. 47, No. 6. Columbus, OH: American Society for Nondestructive Testing (June 1989): p 714-715, 718, 720, 722-724.
56. Lutts, C.G. "Ten Years' Cooperation between the Society for Nondestructive Testing and the American Society for Metals." *Nondestructive Testing*. Vol. 12, No. 1. Columbus, OH: American Society for Nondestructive Testing (January-February 1954): p 31-36.
57. Itoh, G. "A Review of the History of Nondestructive Testing in Japan." *Materials Evaluation*. Vol. 40, No. 11. Columbus, OH: American Society for Nondestructive Testing (October 1982): p 1138+.
58. Straw, R. "Voices in the Air — The Early Days of Aircraft NDT." *Materials Evaluation*. Vol. 42, No. 2. Columbus, OH: American Society for Nondestructive Testing (February 1984): p 152-160.
59. Hagemaijer, D.J. "Aerospace Radiography — The Last Three Decades." *Materials Evaluation*. Vol. 43, No. 10. Columbus, OH: American Society for Nondestructive Testing (September 1985): p 1262-1264+.
60. IEEE/ASTM SI 10-1997, *Standard for Use of the International System of Units (SI): The Modernized Metric System*. West Conshohocken, PA: ASTM International (1996).
61. Taylor, B.N. *Guide for the Use of the International System of Units (SI)*. National Institute of Standards and Technology Special Publication 811, 1995 edition. Washington, DC: United States Government Printing Office (1995).
62. Taylor, B.N., ed. *Interpretation of the SI for the United States and Federal Government and Metric Conversion Policy*. NIST Special Publication 814, 1998 Edition. Washington, DC: United States Government Printing Office (1998).
63. Taylor, B.N., ed. *The International System of Units (SI)*, 2001 edition. NIST Special Publication 330. Washington DC: United States Government Printing Office (2001).
64. Mohr, P. J. and B.N. Taylor. "CODATA Recommended Values of the Fundamental Physical Constants: 1998." *Reviews of Modern Physics*. Vol. 72, No. 2. Melville, NY: American Institute of Physics (April 2000): p 351.



# 2

## C H A P T E R

# Radiation and Particle Physics<sup>1</sup>

---

C. Robert Emigh, Los Alamos, New Mexico

Frank A. Iddings, San Antonio, Texas

# PART 1. Elementary Particles

## Historical Background

The understanding of penetrating radiations and radioactivity begins with the discovery of X-rays by Wilhelm C. Roentgen in Germany in 1895. Detection of the natural radioactivity of uranium by Becquerel along with the separation and identification of radium and polonium by Pierre Curie and Marie Curie in France followed Roentgen's discovery in just three years.

In England by 1905, Ernest Rutherford and his students reported the identification of two kinds of radiations — alpha and beta particles — while in France, P.V. Villard and Antoine-Henri Becquerel proposed the electromagnetic nature of gamma radiation. At the same time, Einstein formulated the equation relating mass and energy as  $E = mc^2$ .

Experiments in Rutherford's labs led to the following advances in the next 15 years: (1) the nuclear atom was conceived, with the nucleus being positively charged and possessing most of the mass of the atom; (2) Niels Bohr determined that the atom's nucleus is surrounded by electrons in fixed orbits; (3) Aston separated the isotopes of neon and built a mass spectrometer that determines that atomic weights are not exact integers; and (4) nuclear transformations were performed.

The 1930s ushered in nuclear science with the invention or discovery of (1) the geiger müller tube, (2) the van de graaff and cockcroft walton accelerators and the cyclotron, (3) the neutron by James Chadwick, (4) artificial radioactivity by Irene Joliot-Curie and Frederic Joliot-Curie, (5) neutron interactions with the elements by Enrico Fermi and (6) fission by Otto Hahn and F. Strassman.

After the demonstration of the nuclear reactor and nuclear weapons in the early 1940s, peaceful uses of radioisotopes and radiation were developed for industry, medicine, agriculture and research. This contributed to the status of radiography in the world.

## Simple Atomic Structure

### Electron

Very early experiments such as rubbing various materials together gave evidence for the existence of electrical charge. The kite flying and other experiments led Benjamin Franklin to suggest, in 1750, that the flow of electricity was a flow of discrete charges. The 1833 announcement by Michael Faraday of the laws of electrolysis supported Franklin's hypothesis. By 1874, G. Johnston Stoney calculated the average charge carried by an ion in solution and named this charge the electron.

Later experiments by William Crookes, Arthur Schuster and J.J. Thomson found that the cathode rays in discharge tubes were negatively charged electrons. Thomson calculated a ratio  $e \cdot m^{-1}$  of charge to mass for the electron.

Continuing experiments by J.J. Thomson, J.S.E. Townsend and finally by Robert A. Millikan in 1909 measured the charge on an electron as  $1.5196 \times 10^{-19}$  C. This was the smallest value of charge, or multiples of it, that Millikan found on oil droplets suspended in an electric field. The value has been refined by experiments with X-ray diffraction to accurately determine Avogadro's number. The accurately known Avogadro's number is then combined with the quantity of electrical charge, called a *faraday*, which deposits one gram relative atomic mass of an element. The combination results in a very accurate value for the charge of an electron. The most recent data on electron characteristics are given in Table 1.

TABLE 1. Electron characteristics.

Quantity	Measurement
Charge	$1.602 \times 10^{-19}$ C
Rest mass	$9.109 \times 10^{-31}$ kg
Classical radius	$2.818 \times 10^{-15}$ m
Magnetic moment	$-9.285 \times 10^{-24}$ J-T <sup>-1</sup>
Compton wavelength	$2.426 \times 10^{-12}$ m

## Proton

Just as experiments in the late 1880s began to define the electron, similar experiments discovered particles with a positive charge and a mass much greater than that of an electron. Wein found that the ratio  $e \cdot m^{-1}$  of the charge to mass depended on the type of gas used at low pressures in a discharge tube and was at a maximum value for hydrogen.

Based on mass spectrograph and mass spectrometer information from Aston, Bainbridge, Dempster and others, the hydrogen ion seemed to be a basic building block for atoms. The simplest atom, hydrogen, has one proton and is atomic number one. The number of protons in the nucleus is known as the *atomic number* of the atom or element.

The name *proton* is from the Greek word  $\pi\rho\omicron\tau\omicron\varsigma$ , *protos*, which means *first*. Proton characteristics are given in Table 2.

## Neutron

For many years after the proton and electron became comfortable concepts for building models of the atoms of the elements but explanations eluded researchers for the existence of isotopes and the extremely penetrating radiation emitted by the bombardment of light elements with alpha particles. In 1932, Chadwick described a neutral particle with a mass equal to a proton that he called a neutron. The neutron explained many observations concerning radiation and particle physics and the concept was rapidly accepted. Neutron characteristics are given in Table 3.

TABLE 2. Proton characteristics.

Quantity	Measurement
Charge	$1.602 \times 10^{-19} \text{ C}$
Rest mass	$1.673 \times 10^{-27} \text{ kg}$
Classical radius	$1.534 \times 10^{-18} \text{ m}$
Magnetic moment	$+1.411 \times 10^{-26} \text{ J} \cdot \text{T}^{-1}$
Compton wavelength	$1.321 \times 10^{-15} \text{ m}$

TABLE 3. Neutron characteristics.

Quantity	Measurement
Charge	neutral
Rest mass	$1.675 \times 10^{-27} \text{ kg}$
Classical radius	$1.532 \times 10^{-18} \text{ m}$
Magnetic moment	$-9.662 \times 10^{-27} \text{ J} \cdot \text{T}^{-1}$
Compton wavelength	$1.320 \times 10^{-15} \text{ m}$

## Positron

As Chadwick was describing the neutron in 1932, Anderson discovered a particle in a cloud chamber whose tracks were identical to those of electrons except that they were deflected in the opposite direction in a magnetic field. These positrons had been predicted by Paul Adrien Maurice Dirac. Experiments by Patrick Maynard Stuart Blackett and G.P.S. Occhialini in 1933 revealed that cosmic rays interacted with matter to produce showers of electrons and positrons in about equal numbers.

The positron is now accepted to be identical to an electron in rest mass and rest energy, with a positive charge numerically equal to the electron's negative charge.

Positrons in a solid are short lived ( $10^{-7}$  to  $10^{-10} \text{ s}$ ) and combine with electrons to form annihilation radiation, which is most often two photons with energies of 0.51 MeV.

## Neutrino

Fermi postulated the neutrino in 1934 to explain an apparent contradiction of the law of conservation of energy in beta particle emission. The particle with no charge and no mass, or nearly no mass, was needed to carry away the energy missing when beta particles emerge without the full energy released in the beta decay process. Evidence to substantiate the existence of the neutrino comes from research by C.L. Cowan and F. Reines of Los Alamos National Laboratory, Los Alamos, New Mexico.

## Other Particles

In research using high energy machines and detectors such as bubble chambers and huge scintillation arrays, more particles have been discovered. These include the mesons postulated by H. Yukawa in 1934, extra heavy particles known as hyperons and the antiparticle analogs of the known particles indicated by E. Segre and his collaborators. This nuclear zoo of from 30 to 40 particles is best examined elsewhere.

## Bohr Atom

As the particles that make up an atom became known in the early 1900s, efforts to understand how the particles fit into a structure began. A structure was needed to explain some of the results of experiments performed on and properties displayed by various atoms. The English *plum duff* atom was likened to a pudding with protons and electrons evenly mixed through its volume.

Ernest Rutherford described the atom as having a nucleus containing most of the mass and described the volume of the atom as containing mostly electrons orbiting the nucleus.

Niels Bohr, Rutherford's student, then calculated that the electrons would be in discrete, calculatable orbits. Bohr postulated that the positive charged protons would be in a tiny nucleus with electrons in discrete orbits or energy levels around the nucleus. These energy levels or shells, described by quantum mechanical conditions that describe the energy, angular momentum, spin and number in each orbit, set electrons at specific energy order in the atom, as seen in neon (Fig. 1).

The shells are designated by the letters K, L, M, N, O, P and Q in order of positions farther from the nucleus. For

FIGURE 1. The bohr atom has concentric clouds or shells of electrons. The electrons in the outermost subshell are called *valence* electrons.

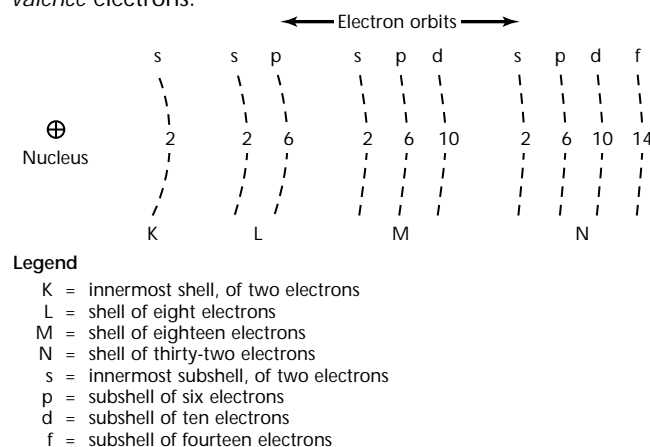


FIGURE 2. Periodic table of elements.<sup>2</sup> Three systems used to number the periods are named in the top row and are identified in the legend below. For element symbols, see Table 4.

	IUPAC	1	2	3	4	5	6	7	8	9	10	11	12	13	14	15	16	17	18
Group	Old	IA	IIA	IIIA	IVA	VA	VIA	VIIA	VIIIA	VIIIA	VIIIA	IB	IIB	IIIB	IVB	VB	VIB	VIIA	VIIIA
CAS	IA	IIA	IIIB	IVB	VB	VIB	VIIA	VIIA	VIIA	VIIA	VIIA	IB	IIB	IIIA	IVA	VA	VIA	VIA	VIA
1	AN	1																	2
	ES	H																	He
	AW	1.01																	4.00
2	AN	3	4											5	6	7	8	9	10
	ES	Li	Be											B	C	N	O	F	Ne
	AW	6.94	9.01											10.81	12.01	14.01	16.00	19.00	20.18
3	AN	11	12											13	14	15	16	17	18
	ES	Na	Mg											Al	Si	P	S	Cl	Ar
	AW	22.99	24.31											26.98	28.09	30.97	32.07	35.45	39.95
4	AN	19	20	21	22	23	24	25	26	27	28	29	30	31	32	33	34	35	36
	ES	K	Ca	Sc	Ti	V	Cr	Mn	Fe	Co	Ni	Cu	Zn	Ga	Ge	As	Se	Br	Kr
	AW	39.10	40.08	44.96	47.87	50.94	52.00	54.94	55.85	58.93	58.69	63.55	65.39	69.72	72.61	74.92	78.96	79.90	83.80
5	AN	37	38	39	40	41	42	43	44	45	46	47	48	49	50	51	52	53	54
	ES	Rb	Sr	Y	Zr	Nb	Mo	Tc	Ru	Rh	Pd	Ag	Cd	In	Sn	Sb	Te	I	Xe
	AW	85.47	87.62	88.91	91.22	92.91	95.94	(98)	101.07	102.91	106.42	107.87	112.41	114.82	118.71	121.76	127.60	126.90	131.29
6	AN	55	56	57	72	73	74	75	76	77	78	79	80	81	82	83	84	85	86
	ES	Cs	Ba	La	Hf	Ta	W	Re	Os	Ir	Pt	Au	Hg	Tl	Pb	Bi	Po	At	Rn
	AW	132.91	137.33	138.91	178.49	180.95	183.84	186.21	190.23	192.22	195.08	196.97	200.59	204.38	207.20	208.98	(209)	(210)	(222)
7	AN	87	88	89	104	105	106	107	108	109	110	111	112	(113)	114	(115)	116	(117)	118
	ES	Fr	Ra	Ac	Rf	Db	Sg	Bh	Hs	Mt	Uun	Uuu	Uub	Uut	Uuq	Uup	Uuh	Uus	Uuo
	AW	(223)	(226)	(227)	(261)	(262)	(266)	(264)	(269)	(268)	(271)	(272)	( )	—	( )	—	( )	—	( )
Lanthanide series	AN	58	59	60	61	62	63	64	65	66	67	68	69	70	71				
	ES	Ce	Pr	Nd	Pm	Sm	Eu	Gd	Tb	Dy	Ho	Er	Tm	Yb	Lu				
	AW	140.12	140.91	144.24	(145)	150.36	151.96	157.25	158.93	162.50	164.93	167.26	168.93	173.04	174.97				
Actinide series	AN	90	91	92	93	94	95	96	97	98	99	100	101	102	103				
	ES	Th	Pa	U	Np	Pu	Am	Cm	Bk	Cf	Es	Fm	Md	No	Lr				
	AW	232.04	231.04	238.03	(237)	(244)	(243)	(247)	(247)	(251)	(252)	(257)	(258)	(259)	(262)				

#### Legend

- IUPAC = period numbering system (1 to 18) used by International Union of Pure and Applied Chemistry
- Old = period system (with roman numerals) formerly used by International Union of Pure and Applied Chemistry
- CAS = period numbering system (with roman numerals) used by Chemical Abstracts Service
- AN = atomic number.
- ES = element symbol
- AW = atomic weight
- ..... = lanthanide series occurs here
- = actinide series occurs here



TABLE 4. Element symbols. (See periodic table in Fig. 2.)

Symbol	Element	Symbol	Element	Symbol	Element	Symbol	Element
Ac	actinium	F	fluorine	Ne	neon	Sr	strontium
Ag	silver	Fe	iron	Ni	nickel	Ta	tantalum
Al	aluminum	Fm	fermium	No	nobelium	Tb	terbium
Am	americium	Fr	francium	Np	neptunium	Tc	technetium
Ar	argon	Ga	gallium	O	oxygen	Te	tellurium
As	arsenic	Gd	gadolinium	Os	osmium	Th	thorium
At	astatine	Ge	germanium	P	phosphorus	Ti	titanium
Au	gold	H	hydrogen	Pa	protactinium	Tl	thallium
B	boron	He	helium	Pb	lead	Tm	thulium
Ba	barium	Hf	hafnium	Pd	palladium	U	uranium
Be	beryllium	Hg	mercury	Pm	promethium	Uub	ununbium (AN 112) <sup>a</sup>
Bh	bohrium (AN 107) <sup>a</sup>	Ho	holmium	Po	polonium	Uuh	ununhexium (AN 116) <sup>a</sup>
Bi	bismuth	Hs	hassium (AN 108) <sup>a</sup>	Pr	praseodymium	Uun	ununnilium (AN 110) <sup>a</sup>
Bk	berkelium	I	iodine	Pt	platinum	Uuo	ununoctium (AN 118) <sup>a</sup>
Br	bromine	In	indium	Pu	plutonium	Uup	ununpentium (AN 115) <sup>a,b</sup>
C	carbon	Ir	iridium	Ra	radium	Uuq	ununquadium (AN 114) <sup>a</sup>
Ca	calcium	K	potassium	Rb	rubidium	Uus	ununseptium (AN 117) <sup>a,b</sup>
Cd	cadmium	Kr	krypton	Re	rhenium	Uut	ununtrium (AN 113) <sup>a,b</sup>
Ce	cerium	La	lanthanum	Rf	rutherfordium (AN 104) <sup>a</sup>	Uuu	unununium (AN 111) <sup>a</sup>
Cf	californium	Li	lithium	Rh	rhodium	V	vanadium
Cl	chlorine	Lr	lawrencium	Rn	radon	W	tungsten
Cm	curium	Lu	lutetium	Ru	ruthenium	Xe	xenon
Co	cobalt	Md	mendelevium	S	sulfur	Y	yttrium
Cr	chromium	Mg	magnesium	Sb	antimony	Yb	ytterbium
Cs	cesium	Mn	manganese	Sc	scandium	Zn	zinc
Cu	copper	Mo	molybdenum	Se	selenium	Zr	zirconium
Db	dubnium (AN 105) <sup>a</sup>	Mt	meitnerium (AN 109) <sup>a</sup>	Sg	seaborgium (AN 106) <sup>a</sup>		
Dy	dysprosium	N	nitrogen	Si	silicon		
Er	erbium	Na	sodium	Sm	samarium		
Es	einsteinium	Nb	niobium	Sn	tin		
Eu	europium	Nd	neodymium				

a. AN = atomic number

b. Element not discovered as of 30 July 2001.

example, the uranium atom has 2 electrons in the K shell, 8 in the L, 18 in the M, 32 in the N, 18 in the O, 12 in the P and 2 in the Q or outermost shell.

The outer shell of electrons gives atoms the chemical properties exhibited by a particular element. For instance, elements whose atoms have a *full* orbit of electrons (2 for the K shell or 8 for the other shells) make up the noble gases. By arranging elements with similar electron outer orbits (or similar chemical properties), into sets of columns, a *periodic table* of the elements can be made as shown by Figure 2.<sup>2</sup> Table 4 presents a list of element symbols for use with the periodic table.

Group 1 has one electron in the outer orbit of their atoms and is the very reactive alkali metals group. Group 2 contains the alkaline earth metals, atoms having 2 electrons in the outer orbits. Group 3 is the aluminum family. Group 3

atoms have 3 electrons in the outer orbit and may have more than 8 electrons in an inner orbit. Such an organization of groups or columns of elements continues across the period table through group 7 known as the halogens with 7 electrons in the outer orbit and group 8 already identified above as the noble gases.

## PART 2. Properties of Radioactive Materials

Radioactive materials have existed since the earth was created. All elements with atomic numbers greater than 83, bismuth, exist only as radioactive elements and many elements below atomic number 83 have radioactive isotopes that exist in nature.

The difference between a stable or nonradioactive atom of an element and an unstable or radioactive atom is in the energy content of the nucleus. Most often an excess or deficiency in the number of neutrons in the nucleus provides the excess energy or instability.

As an example: most hydrogen in nature exists as atoms with only 1 proton and 1 electron. About 15 of every 100 000 atoms of hydrogen have a neutron plus the proton in the nucleus, giving the atom a mass of 2 or twice the mass of most hydrogen atoms. Mass 2 hydrogen is called deuterium or heavy hydrogen and is stable. When a second neutron is added to the nucleus of hydrogen, the atom has a mass of 3, is called tritium and is radioactive. The tritium atom is produced in nature by cosmic bombardment to produce a pre-1952 concentration in nature of between 1 to 10 tritium atoms per  $10^{18}$  hydrogen atoms.

### Radiation Units

The nucleus of a radioactive atom emits energy and most often a particle. The energy released is usually the kinetic energy of the emitted particle but also may be shared by gamma or X-ray photons. When only a single charged particle is released, the number of protons in the nucleus changes. The changed atom is an atom of a different element.

Each change in the nucleus of an atom is called a *disintegration* or *decay*. The amount of a radioactive material is measured in terms of the rate of disintegration. The first unit used to describe the quantity of radioactivity or rate of disintegration was the *curie* (Ci). The curie was  $3.7 \times 10^{10}$  disintegrations per second or  $2.22 \times 10^{12}$  disintegrations per minute.

The metric unit for quantity of radioactivity is the *becquerel* (Bq) and is defined as one disintegration per second. A useful conversion is  $1 \text{ Ci} \cong 3.7 \times 10^{10} \text{ Bq} \cong 37 \text{ GBq}$ .

### Half Life

Obviously, if the number of radioactive atoms are decreasing or decaying with time, a way of keeping track of the amount of radioactive material available is needed. The most convenient concept is that of *half life*.

Half life is the time required for half of the original number of atoms to decay or change. It is really a probability of decay but when expressed for large numbers of atoms, half life is more convenient than the probability  $\lambda$  of an atom disintegrating per unit time (also called the *decay constant*, or fraction of atoms per unit time). The number of atoms decaying per unit time can be expressed as  $\lambda$  times the total number  $N$  of parent atoms:

$$(1) \quad \frac{\text{Disintegrations}}{\text{Time}} = \lambda N$$

The half life  $T$  is related to the decay constant as shown in Eq. 1:

$$(2) \quad T = \frac{0.693}{\lambda}$$

where 0.693 is the natural logarithm of 2. The number of radioactive atoms decaying per unit time changes exponentially with time. That is, half of the original quantity at the beginning of a half life period remains at the end of the half life period. Table 5 shows this exponential property.

This exponential change with time can be expressed mathematically:

Table 5. Half lives versus remaining lives.

Elapsed Time (half lives)	Amount Remaining (percent)
0	100
1	50
2	25
3	12.5
4	6.25
5	3.12

$$(3) \quad \frac{N}{N_0} = \left(\frac{1}{2}\right)^n$$

in which  $N$  is the number of atoms or quantity of radioactive material after  $n$  half lives of decay time from an original number of atoms or quantity  $N_0$ .

A more convenient expression in terms of time  $t$  and half live  $T$  would be:

$$(4) \quad \frac{N}{N_0} = \exp(-\lambda t) \\ = \exp\left(-\frac{0.693t}{T}\right)$$

or the logarithmic form:

$$(5) \quad \ln \frac{N}{N_0} = -0.693 \frac{t}{T}$$

or

$$(6) \quad \ln \frac{N_0}{N} = 0.693 \frac{t}{T}$$

Therefore, the plot of quantity of radioactive material versus time results in a straight line if semilogarithmic coordinates are used, as in Fig. 3.

## Modes of Radioactive Decay

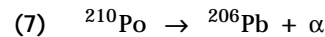
Radioactive atoms disintegrate by one or more of five primary modes: (1) emission of an alpha particle (helium nucleus), (2) emission of a beta particle (electron), (3) electron capture or positron emission, (4) emission of a gamma ray (photon) or (5) spontaneous fission.

Emission of a gamma ray photon may follow some of the first three disintegration modes and only rarely occurs alone. A few radioactive atoms decay by competing modes so that some of the parent atoms result in one daughter while others result in another. Such dual decay modes are called branching and fixed amounts of each mode or branch are observed.

### Emission of Alpha Particle

The relatively heavy nuclei of helium (2 protons and 2 neutrons) from a radioactive nucleus generally carry with them considerable *kinetic energy*, between 2 and 6 MeV. A megaelectronvolt (MeV) is the energy that would be acquired if a unit charged particle moved across a gap having a million volt potential difference. Alpha particle emitters are obviously large nuclei such as in radium, polonium

(shown below) and uranium atoms. Alpha particles are easily stopped by small amounts of matter such as a sheet of paper because they possess such large mass and high charge.

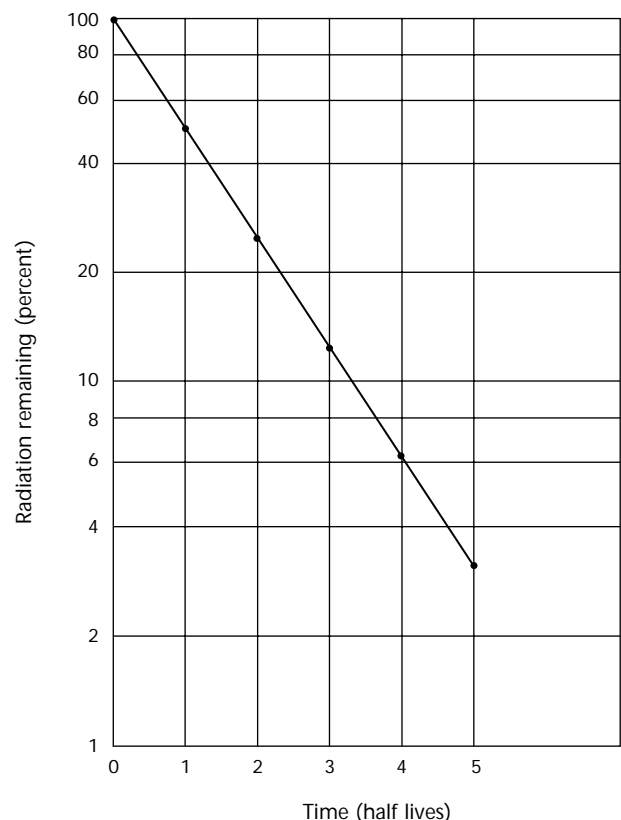


Note that there is a decrease of 4 in the mass and a decrease of 2 in the atomic number of the parent atom to form the daughter atom plus alpha.

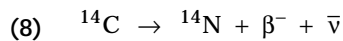
### Emission of Beta Particle

Beta particles are identical to high speed electrons, although they may be either positively charged (positrons) or negatively charged (negatrons). They are emitted with energies continuously distributed up to a maximum value characteristic of the particular isotope. The distribution of the number of beta particles, as a function of particle energy, is known as a *fermi distribution*. It typically rises to a peak at energies of one third to one half the maximum energy for that particular isotope. The radioisotopes that emit beta particles from their nucleus are neutron rich as compared to stable isotopes of the same element, such as

FIGURE 3. Radioactivity versus time.



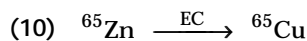
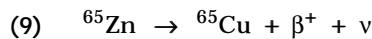
shown by the equation for decay of carbon-14 below. Beta particles are usually stopped by thin layers of metal.



Note that there is an increase of one in the atomic number of the daughter compared to the parent atom when the beta particle and neutrino are emitted.

### Electron Capture

If the nucleus is a high atomic number and is neutron deficient as compared to the stable isotopes of the element, then the nucleus can capture one of the atomic orbital electrons. Because the innermost or K shell electrons are usually caught, the process is often called *K capture*. The process creates an electron vacancy. As electrons move from outer shells to fill the vacancy, *characteristic X-rays* are released and give evidence that the process has occurred. In some moderate atomic number isotopes, the electron capture process competes with positron emission in the decay process. The daughter atom is the same for either process, as shown for the decay reactions of zinc-65.



where EC indicates electron capture.

### Gamma Ray Emission

Gamma ray emission generally follows alpha or beta decay, except for a very few radioactive isotopes where isomeric transition or release of only gamma radiation occurs. The gamma rays are released from the nucleus of an atom that contains excess energy. In some alpha and beta decay, no excess energy is left in the nucleus. Like X-rays, the gamma rays are electromagnetic radiation but the gamma rays originate in the nucleus rather than in the electron orbits and are monoenergetic. Because the gamma rays carry neither charge nor rest mass, their emission does not change the mass or atomic number of the nucleus but the nucleus is in a more stable state.

Gamma rays range in energy from a few thousand electron volts (keV) to several million electron volts (MeV). Each gamma emitter has its own unique, characteristic gamma energy or set of gamma energies and is often used to identify the isotope. The gamma rays are the chief radiation used in isotope

radiography. Three of the more familiar isotopes used in radiography are iridium-192 (over 20 different gamma rays with 0.310 MeV predominate), cesium-137 (0.661 MeV) and cobalt-60 (1.17 and 1.33 MeV). The spectra are discussed in the chapter on gamma radiography.

### Spontaneous Fission

Nuclear species with masses greater than 200 can decay by the process of spontaneous fission. Most fission processes are initiated by absorption of a neutron in the nucleus of the atom. Uranium-138 and californium-252 decay by spontaneous fission with alpha decay as competing processes. The large nucleus splits into two smaller nuclei with the release of 2 to 4 neutrons and several gamma rays. The process of spontaneous fission becomes predominant in the extremely large nuclei and they may be used as neutron sources.

### Secondary Processes

During disintegration of a nucleus by any of the preceding processes, secondary processes may take place, often resulting in emission of X-ray radiation. Internal conversion occurs when the energy of a gamma ray usually released from the nucleus is transferred to an orbital electron close to the nucleus. The electron leaves the atom with the energy of the gamma ray minus the electron's orbital binding energy. Other electrons fill the vacancy of the ejected orbital electron creating characteristic X-rays of the atom, just as in the case of electron capture.

As high speed beta particles decelerate in the matter they penetrate, a wide range (0 to the maximum energy of the beta particle) of X-ray energies are produced. This continuum of energies is also called *bremsstrahlung*. The radiation is very much like the radiation generated in an X-ray tube. In practice, the lower energy radiation is largely absorbed by the matter that produces it.

### Attenuation of Radiation

Attenuation of radiation from the point sources of radiation used in radiography occurs as the result of two processes: inverse square law (radiation intensity decreases as the square of the distance increases) and absorption of the radiation by the matter through which it passes.

### Inverse Square Law

Radiation leaves a point source of radioactive material in all directions. It

may be thought to cover the surface of a sphere with a radius equal to the distance from the source. The area of the sphere covered by the radiation from the source increases as the square of the distance from the source, so the intensity of the radiation, usually measured in sieverts per second ( $\text{Sv}\cdot\text{s}^{-1}$ ) or milliroentgens per hour ( $\text{mR}\cdot\text{h}^{-1}$ ), decreases as the square of the distance from the source. The formula used in inverse square calculations is:

$$(11) \quad I_1(d_1)^2 = I_2(d_2)^2$$

in which  $I$  is the intensity of radiation at distance  $d$ .

Distance becomes very important in decreasing the exposure of a radiographer because the radiation attenuation decrease occurs as the square of the distance from the source; that is, as compared to a unit distance  $d$  from the source, the radiation intensity is 0.25 at twice the distance ( $2d$ ), 0.11 at  $3d$  and 0.01 at  $10d$ .

## Absorption by Matter

Each kind of radiation is absorbed by matter in at least one of a variety of different ways. Alpha, beta and neutron absorption is discussed in a very simple fashion below with absorption of electromagnetic radiation being discussed in more detail.

### Alpha Particles

Alpha particles are easily absorbed by a thin layer of material such as a sheet of paper. The mass of four and the positive charge of two make interactions of the alpha particles with the electron clouds around atoms very probable. The positive charge interacts with the electrons either to move them from their atomic orbits (ionization) or to move them to higher orbits around the atom (excitation). Either process removes kinetic energy from the alpha particle equal to the energy gained by the electron. Figure 4 illustrates the ionization of an atom by an alpha particle.

As the alpha particle slows down, it interacts with more atoms and slows down faster until it slows to the molecular motion of a helium atom when it gains two orbital electrons. In air, the trail of an alpha particle will be fairly straight with tens of thousands of ion pairs (atoms deficient in electrons and the removed electrons) per centimeter along its path. This trail of high ionization is what is seen in a cloud chamber. Path length in air is about 10 mm (0.4 in.) per 1 MeV of original kinetic energy.

### Beta Particles

Beta particles, or electrons, also interact mainly with the orbital electrons of the atoms along their path. Because they are very light, they travel faster than alpha particles with equivalent energy. Because they are faster and have only half the charge of an alpha particle, they interact less frequently. Because they have little mass compared to the atoms, the path of the electrons is very *tortuous* or zigzagged with many reversals in direction.

Thin layers of metal or about 0.1 m (several inches) of air are sufficient to absorb or stop beta particles. Ionization and excitation are the major interactions with the production of X-rays likely for high energy beta particles.

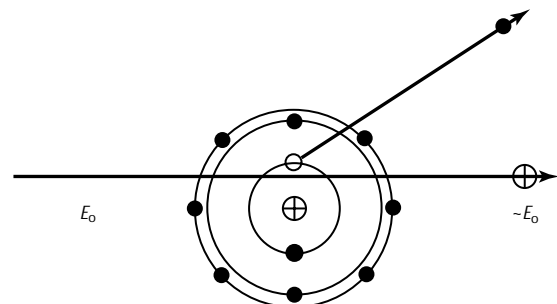
If the beta particle is positively charged, it will annihilate with an electron at the end of its path as it loses its kinetic energy. The annihilation will result in two gamma rays moving apart at 180 degrees and each having an energy of 0.51 MeV (the energy equivalent to the rest mass of an electron).

### Neutrons

Neutrons produced by fission, accelerator nuclear reactions or radioisotope sources have considerable kinetic energy. This kinetic energy is most often lost by scattering interactions with or absorption in the nuclei of the atoms in their path. Absorption of the neutron is followed by release of electromagnetic radiation or large particles such as protons, multiple neutrons, deuterons or alpha particles. Interactions with the orbital electrons contribute negligibly to the absorption of neutrons by matter.

The nucleus is much smaller than the electron orbits, so neutron interactions are less frequent than those of alpha or

FIGURE 4. Ionization by alpha particle that ejects orbital electron from atom. Specific ionization is number of ion pairs generated by particle per unit path. Total ionization designates number of ion pairs produced by particle along its entire path.





beta particles. And because the neutron has no charge, ionization and excitation are not major absorption processes.

### Elastic Scattering

For elastic scattering, the neutron collides with the nucleus and bounces off, leaving the nucleus unchanged. This type of collision can be treated straightforwardly as a mechanical billiard ball type of collision. In the collision the energy of the neutron is shared by the nucleus, thus each collision reduces the energy of the neutron. After a number of collisions with the nuclei, the energy is reduced to the same average kinetic energy as that of the absorbing medium. This energy is often referred to as the thermal energy because it depends primarily on the temperature. Neutrons at thermal equilibrium with their surroundings are thermal neutrons. At 20 °C (68 °F), a thermal neutron would have a kinetic energy of about 0.025 eV and a velocity of 2200 m·s<sup>-1</sup> (4900 mi·h<sup>-1</sup>).

The transfer of energy from the neutron to the nucleus is greater for light nuclei. Therefore, low atomic nuclei containing materials such as water, hydrocarbons, graphite and beryllium are used to reduce neutron energies. Such materials are called moderators. Hydrogen nuclei have essentially the same mass as neutrons and can undergo nearly complete kinetic energy transfer in a single collision. Energy transfer to larger nuclei require many collisions.

### Inelastic Scattering

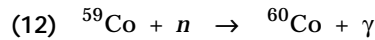
Here the neutron collides with the nucleus leaving the nucleus in an excited state. In this process, the nucleus may either stay in the excited state ( $n, n'$ ) as a metastable isomer or will immediately emit gamma radiation ( $n, \gamma n$ ) and return to the ground or original state.

### Nuclear Neutron Absorption

As the neutron has no charge, it can approach the nucleus until the close range attractive forces of the nucleus begin to operate. In this process, the neutron is captured, forming a compound nucleus. Because there is no charge barrier, even the slowest neutron can be readily captured. As the binding energy of a neutron into a compound nucleus is nearly 8 MeV, even the capture of thermal neutrons can result in a highly excited state for the nucleus. This excited nucleus can attain relative stability by ejecting a proton, ejecting an alpha particle, or emitting the excess energy as gamma radiation. When a particle is ejected, the nucleus becomes a new element; then the process is also known as *nuclear*

*transmutation*. The discovery of transmutation by slow neutrons led to the realization of nuclear fission.

The simplest capture reaction is that of capture of slow neutrons with emission of gamma rays ( $n, \gamma$ ). Thermal neutron reaction with cobalt is an example:



In heavy nuclei, the capture of a slow neutron, followed by the emission of gamma radiation, increases the neutron-to-proton ratio — usually making the nucleus radioactive with decay by electron emission likely. More information on production of radioactive material by neutron capture may be found in the discussion of radioactive materials.

As the energy of the impinging neutron is made larger, a charged particle can be ejected. However, a charged particle, because of the short range attractive forces of the nuclei, is hindered from leaving the nucleus and processes such as ( $n, p$ ), ( $n, \alpha$ ) and ( $n, d$ ) can only take place when the incident neutron supplies sufficient energy to overcome the binding energies of the particles in the nucleus. For heavy nuclei these forces are appreciable and the requisite neutron energy becomes greater. Thus, for example, a particle ejection is possible only if the neutron has sufficient energy to overcome the binding energy of the alpha particle; that is, the neutron must be a fast neutron.

In the ( $n, \alpha$ ) reaction, the product nucleus contains one neutron and two protons less than the original nucleus. The neutron-to-proton ratio is increased and the transmutation usually produces a radioactive nucleus that decays by the emission of an electron (beta disintegration).

As the energy of the incident neutron approaches 30 MeV, the compound nucleus can eject three neutrons ( $n, 3n$ ) or two neutrons and a proton ( $n, 2np$ ) as well as other combinations of particles. At even higher energies, more particles may be ejected until the nucleus essentially disappears (spallation).

Finally, nuclear fission ( $n, f$ ), where the nucleus breaks up with the release of several larger particles and several neutrons, can be induced in certain large nuclides, such as uranium-235, by neutrons of almost any energy, whereas in other nuclides, fast or energetic neutrons are required.

### Nuclear Cross Sections

Because of many reactions possible for absorbing neutrons and their complicated



energy and mass dependencies, there is no simple way to present the total absorption effect. However, the probability of any interaction between neutrons and matter can be made qualitative by means of the concept of cross sections. The cross section  $\sigma$  is the effective target area of the nucleus as seen by the impinging neutron of a given energy. The number of interactions per unit time will be  $n\nu N\sigma$ , where  $n$  is the number of neutrons per unit volume moving with velocity  $\nu$  towards the target of  $N$  nuclei. The quantity  $n\nu$  is the neutron flux density (neutrons per square centimeter second). The cross section  $\sigma$  is usually expressed in square meters ( $\text{m}^2$ ) or barns (b), where  $1 \text{ b} = 10^{-24} \text{ cm}^2 = 10^{-28} \text{ m}^2$ .

In discussing the variation of nuclear cross section with energy of the incident neutrons, certain generalizations of a broad character can be made. In general, there are three regions that can be distinguished. First is the low energy region, which includes the thermal range, where the cross section decreases steadily with increasing neutron energy. The total cross section is the sum of two terms, one due to neutron scattering is quite small and almost constant, the other representing absorption by the nucleus is inversely proportional to the velocity. This low energy range is termed the  $\nu^{-1}$  region, where the time spent by the neutron near the nucleus is proportional to  $\nu^{-1}$ . Second, following the somewhat indefinite  $\nu^{-1}$  region, many elements exhibit peaks called resonance peaks, where the neutron cross sections rise sharply to high values for certain energies, then fall to lower values again. Depending on the element, the number of such peaks

may number three or more. These peaks may be found mostly in the energy range 0.1 to 1 eV, although in a few elements like uranium-238, they may be found up to energies of 10 eV. These reactions are of the  $(\eta, \gamma)$  type. And third, with neutrons of high energy in the MeV range, the cross sections are very low, less than  $10^{-27} \text{ m}^2$  (10 b), compared to the very high cross sections of  $4 \times 10^{-25} \text{ m}^2$  (several thousand barns,  $\sim 4000 \text{ b}$ ) at low energies.

A simple example of the total absorption cross section is that of cadmium, shown in Fig. 5. The  $\nu^{-1}$  region is shown up to about 0.03 eV, the resonance at 0.176 eV and the low cross section region for energies greater than about 2 MeV.

The dramatic increase in cross sections at the resonance have been worked out by the theory of G. Breit and E.P. Wigner. In its simplicity, if the energy of the neutron is such that a compound nucleus can be formed at or near one of its energy levels, then the probability of capture of these neutrons will be exceptionally high. All elements do not show the resonant absorption effect; for example, boron has no measurable resonance and the cross section follows the  $\nu^{-1}$  law from 0.01 eV to over 1000 eV. However, its cross section for  $(n, \alpha)$  is so large for neutrons of low energy that this reaction is often used for neutron detectors. Table 6 shows the dramatic variation of cross section for absorbing thermal neutrons of some of the better neutron absorbers.

FIGURE 5. Absorption of neutrons by cadmium, showing resonance peak at 0.176 eV.

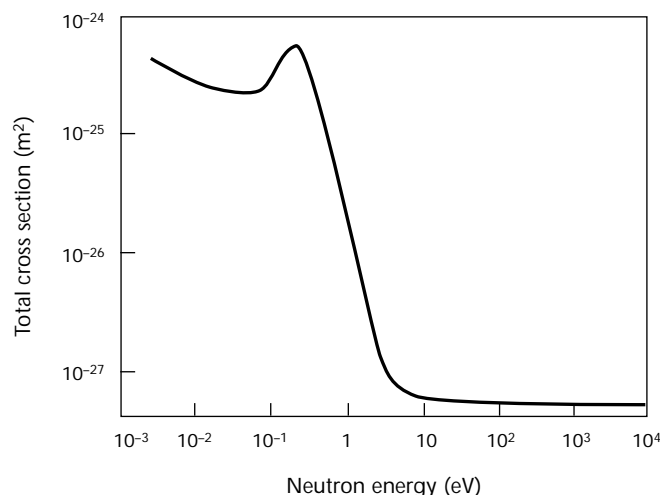


TABLE 6. Capture cross sections  $\sigma$  of strongly absorbing elements for neutrons in approximate thermal equilibrium at 300 K ( $27^\circ \text{C} = 80^\circ \text{F}$ ).

Element	Atomic Number	Cross Section ( $10^{-24} \text{ m}^2$ )
Lithium	3	65
Boron	5	540
Chlorine	17	40
Cobalt	27	35
Rhodium	45	125
Silver	47	55
Cadmium	48	3 000
Indium	49	300
Mercury	80	450
Samarium	62	4 260
Europium	63	3 400
Gadolinium	64	22 200
Dysprosium	66	1200
Holmium	67	340
Rhenium	75	90
Iridium	77	285
Gold	79	90

## PART 3. Electromagnetic Radiation

Electromagnetic radiation released during radioactive atom decay includes both X-rays and gamma rays. These *penetrating radiations* are related to other types of electromagnetic radiation (Fig. 6).

Although the X-ray and gamma ray are produced very differently, their absorption by matter is the same because there is no difference between photons of the two different kinds of radiation at the same energy once they have been generated. (X-ray generation by electronic means is discussed in another chapter.) The photons of electromagnetic radiation have no rest mass, no charge and no magnetic moment but do have a dual character in that they sometimes act like particles and other times like waves. Photon characteristics are listed in Table 7.

This dual nature of electromagnetic radiation photons was being postulated at the turn of the century and was hinted at by the quantum theory as put forth by Max Planck. Planck proposed that the photon energy was contained in a packet of energy, known as a *quantum*, and was proportional to its frequency. Photon characteristics are listed in Table 7.

$$(13) \quad E = h\nu$$

in which  $E$  is the quantum energy of the photon,  $h$  is Planck's constant ( $6.626176 \times 10^{-34} \text{ J}\cdot\text{Hz}^{-1}$ ) and  $\nu$  is the frequency of the electromagnetic radiation. This equation has helped to explain many physical phenomena.

Penetrating electromagnetic radiation interactions with matter provide the mechanics for several familiar and important applications such as medical radiology, thickness gaging, density

measurement, composition determination, industrial radiography and experimental physics. Emphasis here will be on the major interactions of X-rays and gamma radiation. The three major interactions important for the energy ranges encountered in radiography are (1) the photoelectric effect, (2) Compton scattering and (3) pair production.

Other interactions such as resonant absorption, photodisintegration and coherent scattering are not important for radiography and will not be discussed here.

### Photoelectric Effect

In a photoelectric interaction, a photon completely transfers its energy to an electron in an inner shell of an atom of the absorbing material. If the energy of the photon exceeds the binding energy of the electron, it leaves the atom with a kinetic energy  $E_k$  of the photon equal to the original energy  $E_0$  minus the binding energy  $E_b$  of the electron to the atom

TABLE 7. Photon characteristics.

Quantity	Expression
Velocity	$c$
Frequency	$\nu = c\lambda^{-1}$
Wavelength	$\lambda = c\nu^{-1}$
Energy	$E = h\nu$
Planck's constant	$E \cdot \nu^{-1}$
Mass	$h\nu \cdot c^{-2}$
Momentum	$h\nu \cdot c^{-1}$

FIGURE 6. Electromagnetic spectrum.

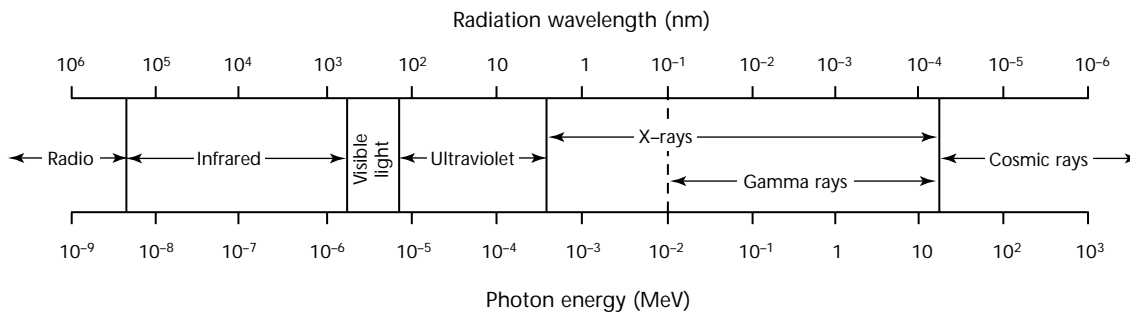


(Fig. 7). Most X-ray and gamma radiation possess sufficient energy to remove an electron from the atom — that is, to ionize the atom.

Photoelectric interactions predominate when (1) the absorbing material is of high atomic number and density, such as lead (increasing as the atomic number  $Z$  to between the fourth and fifth power), and (2) the energy of the photon is less than 1 MeV. If the binding energy of the electron is greater than the energy of the photon, the electron is temporarily moved to a higher orbit. When the photon energy equals the binding energy of a particular shell of electrons, there is a sharp increase in amount of absorption of those photons over lower and higher energies. These dramatic changes in absorption for the K and L shell electrons can be seen in photoelectric and total absorption curves in Fig. 8 and are called absorption edges.

## Compton Scattering

Above 0.5 MeV, Compton scattering becomes important in attenuating a beam of photons. As the name implies, Compton scattering is not true absorption. A part of the photon's initial energy is merely redirected, with some of the energy being taken as kinetic energy of an electron. Compton scattering occurs when the photon collides with an orbital electron and gives up part of its energy to the electron. The electron is ejected from the atom and the remainder of the photon energy leaves the atom as a lower energy photon, usually traveling in a different direction to the original photon as depicted in Fig. 9. The direction of the scattered photon may be at any angle, even 180 degrees, to the direction of the original photon, hence the scattering description for this interaction. Large angles of scatter occur and most of the photon energy goes to the electron.

Compton scattering remains the major contribution to radiation attenuation until photon energies exceed several megaelectronvolts for high atomic number absorbers, as seen in Fig. 8. For low to moderate atomic number absorbers, Compton scattering constitutes the major interaction from below 0.5 to above 10 MeV. This scatter produces the fogging of radiographic films and radiation levels higher than expected outside of a radiation beam.

FIGURE 8. Absorption and scattering curves for uranium show various components of total attenuation coefficient as function of energy.

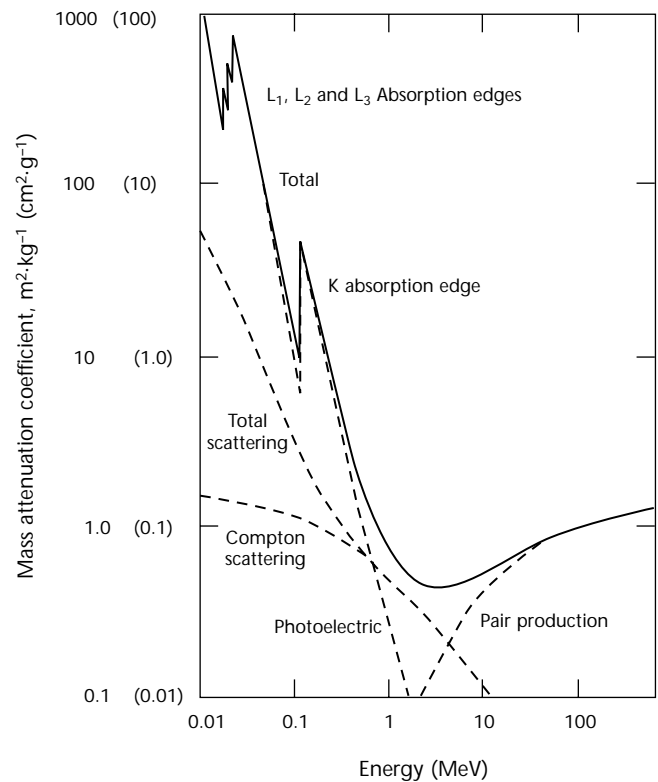
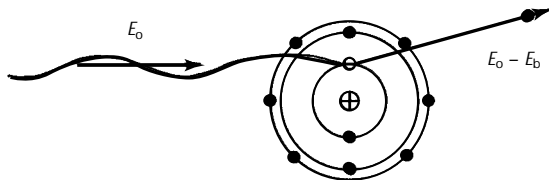


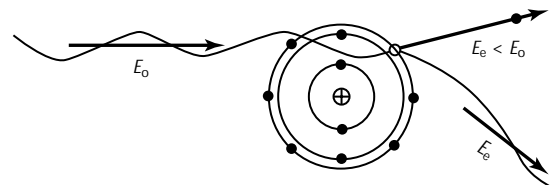
FIGURE 7. Photoelectric interaction of incident photon with orbital electron.



### Legend

$E_b$  = energy binding electron to atom  
 $E_0$  = original energy of photon

FIGURE 9. Compton scattering. Incident photon ejects electron and ejects lower energy scattered photon.



### Legend

$E_s$  = lower energy of scattered photon  
 $E_0$  = original energy of photon

## Pair Production

At 1.02 MeV the important attenuation process of pair production begins to occur. High energy photons traveling close to the nucleus with a high atomic number can convert into a pair of particles: an electron and a positron (see Fig. 10). The reason that the process begins at 1.02 MeV is that the photon has no charge and therefore must convert to a pair of particles that have equal and opposite charges to preserve neutrality. The energy needed for conversion ( $E = mc^2$ ) to the mass of an electron or a positron is 0.51 MeV each.

As the energy of photons exceeds the 1.02 MeV by greater amounts, the likelihood of the pair production reaction increases (Fig. 8) until it becomes the predominant mode of interaction. Also, the higher the atomic number of the absorber, the more likely pair production becomes. Any excess energy above 1.02 MeV possessed by the original photon becomes kinetic energy for the two particles. The particles lose energy, as described before for beta particles, with the positron annihilating at the end of its path.

## Attenuation Coefficients and Equations

Attenuation of X-ray or gamma ray photons from a beam traveling through matter follows an exponential relationship similar to that covered earlier in this section for half lives. The attenuation results from a summation or total of the radiation removed from the beam by each of the three modes of interaction just discussed. The heavy line in Fig. 8 is this total probability of interaction, or coefficient of attenuation

for each radiation energy and kind of matter involved. That is, the total probability per atom of attenuation of a photon of the original energy is the sum of the probabilities of each of the modes of interaction:

$$(14) \quad \sigma = \sigma_{pe} + \sigma_{cs} + \sigma_{pp}$$

in which  $\sigma$  is the total attenuation coefficient per atom,  $\sigma_{pe}$  is the absorption coefficient for photoelectric interactions per atom,  $\sigma_{cs}$  is the scattering coefficient for Compton scattering per atom and  $\sigma_{pp}$  is the scattering coefficient for pair production. Attenuation coefficient tables are in another chapter.

If any other modes of interaction contributed significantly, their absorption or scattering coefficient would be added to the others to produce the total attenuation coefficient. Although the attenuation coefficients are probabilities per atom, they are expressed in square centimeters and for that reason are referred to as the cross section.

The cross section is used in calculations related to the attenuation of the radiation from a narrow beam of that single energy of radiation passing through a single material. Each thickness of the material removes the same fraction of the radiation from the beam. The intensity of the original beam incident on a thickness of a material is related to the intensity of the beam transmitted through that thickness:

$$(15) \quad I = I_0 e^{-n\sigma x}$$

in which  $I$  is the transmitted intensity of radiation beam;  $I_0$  is the original intensity of radiation beam;  $n$  is the number of atoms per cubic centimeter;  $\sigma$  is the total atomic cross section ( $\text{cm}^2$ ) per atom or is the probability of interaction per atom;  $x$  is the thickness of the absorber in centimeters.

As with half life, the equation may be changed to the logarithmic form:

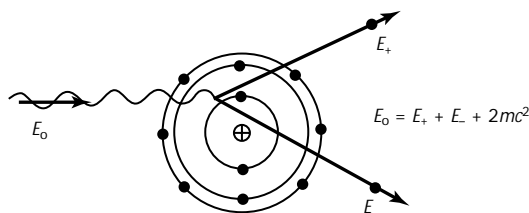
$$(16) \quad \ln\left(\frac{I}{I_0}\right) = -n\sigma x$$

or

$$(17) \quad \ln\left(\frac{I_0}{I}\right) = n\sigma x$$

Most tables of cross sections provide that information in terms of the mass attenuation coefficient  $\mu_m$  or the linear attenuation coefficient  $\mu$ . The conversion from atomic attenuation coefficient to linear attenuation coefficient is made by

FIGURE 10. Pair production of electron and positron from incident photon.



### Legend

- $c$  = speed of light
- $E$  = energy of incident photon
- $E_+$  = energy of positron
- $E_-$  = energy of negative electron
- $m$  = electron mass

using Avogadro's number  $N$ , which is the number of atoms in one gram relative atomic mass  $A$ , and by using the density ( $\text{g}\cdot\text{cm}^{-3}$ ) of the material:

$$(18) \quad n\sigma x = \frac{N}{A}\sigma\rho x = (\mu_m)\rho x$$

in which the mass attenuation coefficient  $\mu_m$  is measured in square centimeter per gram ( $\text{cm}^2\cdot\text{g}^{-1}$ ) and the linear attenuation coefficient  $\mu$  is measured as reciprocal length or reciprocal distance in centimeters ( $\text{cm}^{-1}$ ).

In many cases, the thickness of material that reduces the intensity of the radiation beam to half of its original intensity is known or is desired. This *half value thickness*, or *half value layer* as it is commonly known, can be extremely convenient to calculate the shielding thickness needed to reduce radiation intensity or to calculate the radiation

intensity that will come through a known thickness of absorber. Tables of such values are handy for common materials and for frequently used radiation energies. The equation for converting linear attenuation coefficient to half value thickness or vice versa is:

$$(19) \quad \ln\left(\frac{I_0}{I}\right) = \ln\left(\frac{1}{\frac{1}{2}}\right) = \ln(2) \\ = 0.693 = \mu x$$

Some convenient values for half value thickness are given in Table 8. These values of half thickness include attenuation of the scattered radiation outside of a narrow beam but should not be depended on for great accuracy because of the effects of scattered radiation and variations in the density and uniformity of materials.

An equation that attempts to handle scattered radiation is:

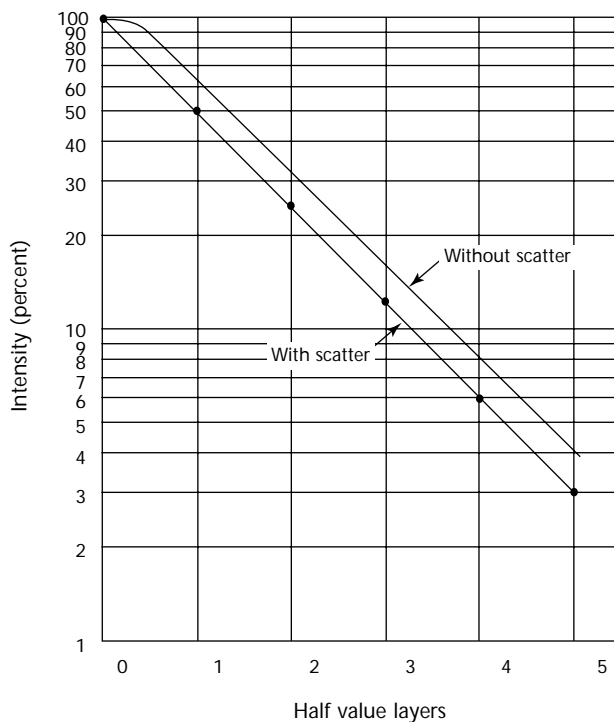
$$(20) \quad I \equiv I_0 (1 + \mu x) \exp(-\mu x)$$

The effect of Eq. 20 is to increase the radiation intensity transmitted through a thickness of material. The increased intensity is from radiation scattered back into the measurement point by the material. The effect of scatter on the radiation attenuation can be seen in Fig. 11.

TABLE 8. Half value thickness for some common materials.

Source	Energy (MeV)	Half Value Thickness (mm)		
		Lead	Iron	Concrete
Cobalt-60	1.17 and 1.33	12.5	22.1	68.6
Cesium-137	0.662	6.4	17.2	53.3
Iridium-192	0.34 average	4.8	—	48.3

FIGURE 11. Gamma attenuation with and without scatter.





## PART 4. Production of Radioactive Materials

### Natural Radioactivity

Some of the radioactive materials used in industry, medicine and research have come from those radioactive species that exist in nature. These uses have dwindled to a tiny amount except for those elements used in nuclear power and weapons where use is still quite large.

Radioactive elements found in nature come from three sources: (1) those radioactive species with half lives comparable to the age of the earth, (2) decay products of the long lived species and (3) those formed by cosmic ray bombardment.

Although all elements above atomic number 83 (bismuth) exist only in a radioactive form, only a few are or have been important commercially. Three are the precursors of many of the radioactive species found in nature and form long decay series. The *thorium* series begins with thorium-232 and ends with lead-208 after 10 decay steps. The *uranium* decay series starts with uranium-238 and stops with lead-206. Radium-226 is a decay product of the uranium decay series and one of the few radioisotopes to find large industrial and medical application. The third decay series, known as the *actinium* series, has uranium-235 at the beginning of the series with lead-207 as the stable end product. Uranium-235 is the fissionable part of uranium with an abundance in nature of 0.71 percent of the uranium.

Some 17 nuclides below bismuth in atomic number have half lives long enough to exist in nature. Potassium-40 with an abundance of only 0.0119 percent and a half life of  $1.3 \times 10^9$  years is the only one frequently encountered in radiation measurements.

Cosmic bombardment of the earth's atmosphere produces a field of fast neutrons and protons that interact with the nitrogen, oxygen and argon in the atmosphere to produce detectable amounts of such radioactive species as hydrogen-3 (tritium), carbon-14, beryllium-10, argon-39 and some 15 other nuclides. Tritium is produced at the rate of about 2500 atoms per square meter of surface area per second and carbon 14 is produced at almost ten times that rate. Until the testing of nuclear weapons in the atmosphere, cosmic production

yielded a stable concentration of these radioisotopes. At present, nuclear weapon release has increased the amount of these and other radioisotopes in the environment.

### Neutron Activation

In the section on neutron interactions with materials, neutron capture was briefly discussed. This technique, coupled with the large fields of neutrons available in nuclear reactors, produces most of the radioisotopes used in radiography. cobalt-60 and iridium-192 come from thermal neutron bombardment of the stable isotopes (cobalt-59 and iridium-191) of these two elements.

Production of the radioactivity can be predicted by Eq. 21:

$$(21) \quad A = Nf\sigma \left[ 1 - \exp\left(-0.693 \frac{t_i}{T}\right) \right]$$

in which  $A$  is the activity produced in disintegrations per second,  $N$  is number of target atoms being bombarded,  $f$  is the neutron flux (in neutrons per centimeter second),  $\sigma$  is the cross section for neutron capture (in square centimeter),  $t_i$  is the irradiation time in the same units as the half life and  $T$  is the half life of the radioisotope produced.

The exponential portion of the equation corrects the production of the radioactive material for the amount that decays away while more is being made. This leads to the point of diminishing returns for production in that after about five half lives, almost as much of the radioactive material is decaying as is being produced per each increment of neutron bombardment time.

Also, the equation is correct only for thin samples of the bombarded material. Absorption of neutrons in the outer layers of the sample (usually a metal pellet) reduces the number of neutrons incident on the interior atoms. This self-shielding of neutrons coupled with a self-absorption of gamma rays released by radioactive atoms inside of the sample gives a gamma output considerably lower than calculated.

---

## Fission Fragments

When uranium-235 or other fissionable atom undergoes fission, multiple neutrons and two major fragments of the nucleus are released. The two fragments are called *fission fragments* and are a source of radioactive materials for industrial, medical and research use. The fragments are usually of unequal size and are grouped in two distributions around mass numbers 96 and 138. One of the major products is cesium-137, which can be chemically separated from the other fission fragments for use as a gamma ray source in radiography, medical therapy and large irradiation facilities for preservation of food and for sterilization of medical supplies.

---

## Accelerator Production

Large particle accelerators such as linatrons, van de graaff generators and cyclotrons can provide appreciable neutron fluxes or streams of high energy particles including protons, deuterons and helium nuclei. When appropriate target materials are bombarded by these particles, radioactive nuclei can be produced. Although radioactive materials for medical use are being produced in this fashion, generally radiographic sources are not commercially produced in this fashion.

## References

1. *Nondestructive Testing Handbook*, second edition: Vol. 3, *Radiography and Radiation Testing*. Columbus, OH: American Society for Nondestructive Testing (1985).
  2. *CRC Handbook of Chemistry and Physics*, 80th edition. Boca Raton, FL: CRC Press (1999): inside front cover.
- 
- ### Bibliography
- Allison, S.K. and S.D. Warshaw. "Passage of Heavy Particles through Matter." *Reviews of Modern Physics*. Vol. 25, No. 4. Melville, NY: American Physical Society (1953): p 779-817.
- Bethe, H.A. and J. Ashkin. "The Passage of Heavy Particles through Matter." *Experimental Nuclear Physics*. Vol. 1, Part 2. New York, NY: Wiley (1953).
- Breit, G. and E.P. Wigner. *Physical Review*. Vol. 49, No. 7. Melville, NY: American Physical Society (1936): p 519-531.
- Bohr, N. "Neutron Capture and Neutron Constitution." *Nature*. Vol. 137. London, United Kingdom: Macmillan Publishers, Nature Publishing Group (1936): p 344-351.
- Choppin, G.R. and J. Rydberg. *Nuclear Chemistry: Theory and Applications*. New York, NY: Pergamon Press (1980).
- Emigh, C.R. "Thick Target Bremsstrahlung Theory." Los Alamos Scientific Laboratory report LA-4097-MS. Los Alamos, NM: Los Alamos National Laboratory (1970).
- Fano, U. "Gamma-Ray Attenuation: Part 1, Basic Processes." *Nucleonics*. Vol. 11, No. 8. New York, NY: McGraw-Hill (1953): p 8.
- Fano, U. "Gamma Ray Attenuation: Part 2, Analysis of Penetration." *Nucleonics*. Vol. 11, No. 9. New York, NY: McGraw-Hill (1953): p 55.
- Fano, U. "Penetration of X- and Gamma-Rays to Extremely Great Depths." *Journal of Research of the National Bureau of Standards*. Vol. 51. Gaithersburg, MD: National Institute of Standards and Technology (1953): p 95.
- Glasstone, S. *Source Book of Atomic Energy*. New York, NY: D. Van Nostrand (1950).
- Heitler, W. *The Quantum Theory of Radiation*, second edition. London, United Kingdom: Oxford University Press (1950).
- Hogerton, J.F. and R.C. Grass, eds. *The Reactor Handbook I: Physics*. AECD 3645. Washington, DC: United States Atomic Energy Commission (1955).
- Lapp, R.E. and H.L. Andrews. *Nuclear Radiation Physics*. second edition. Upper Saddle River, NJ: Prentice-Hall (1954).
- Marshall, J.S. and A.G. Ward. "Absorption Curves and Ranges for Homogeneous  $\beta$ -Ray." *Canadian Journal of Research*. Vol. 15A. Boucherville, Canada: National Research Council (1937): p 39.
- Morgan, R.H. and K.E. Corrigan. *Handbook of Radiology*. Chicago, IL: Yearbook Publishers (1955).
- Reines, F. and C.L. Cowan. "The Neutrino." *Nature*. Vol. 178. London, United Kingdom: Macmillan Publishers, Nature Publishing Group (1956): p 446-449.
- Richardson, H.D. *Industrial Radiography Manual*. Contract AT-(40-1)-3112. Washington, DC: United States Atomic Energy Commission (1964).
- Stephenson, R. *Introduction to Nuclear Engineering*. New York, NY: McGraw-Hill (1954).



# 3

## C H A P T E R

# Electronic Radiation Sources

---

George C. Wheeler, Materials and Processes  
Consultants, Schenectady, New York

## PART 1. Physical Principles

Radiation of an unknown type and origin was discovered in the year 1895 by Wilhelm Roentgen. Dubbed X-rays by their discoverer, they were soon found to be a form of electromagnetic radiation with extremely short wavelengths. The X-radiation is called *ionizing* because X-ray absorption kicks out an electron from an atom of absorption material, creating an ion. The production of ionizing radiation is well covered in the literature.<sup>1-5</sup>

Technological advances in image processing, flash radiography, real time radiography, microfocus and metal ceramic tubes have sustained interest in the electronic production of ionizing radiation. The versatility of an electronic source is difficult for an isotopic source to match, even for specific applications. The advent of solid state components has overcome many of the objections related to size, weight and durability of electronic sources.

This chapter discusses the basic physics, construction and application of electronic sources. The emphasis will be on industrial X-ray machines widely used in radiography and radiology. Where special details are significant to particular applications, these are discussed in the appropriate chapters of this volume.

### Conservation of Energy

Electromagnetic theory had long predicted that a charged particle undergoing deceleration would emit radiation. This theory can be used to qualitatively explain the continuous portion of a typical X-ray spectrum (see Fig. 1). Although a complete study of the continuous spectrum requires modern physics, an understanding of its basic principles may be gained by considering just one of the fundamental laws of physics, the conservation of energy. This law states that energy can neither be created nor destroyed, although it is possible to change it from one form to another.

In the case of X-rays, fast moving charged particles, usually electrons, strike a target material and are slowed or stopped. In some specialized applications, high energy electrons are accelerated radially by a strong magnetic field, producing X-rays without the use of a

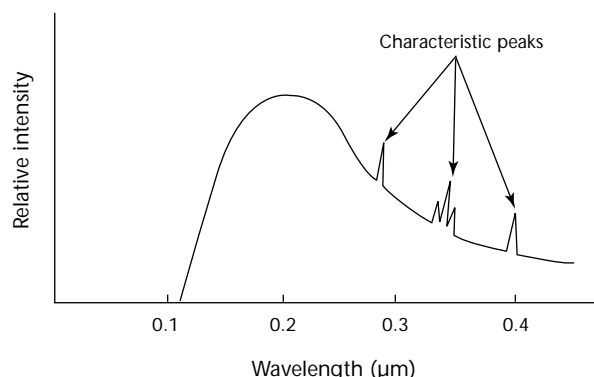
target. Much of the energy of the electrons' motion, called kinetic energy, is transformed into heat energy as the stream strikes the target. In fact, except for the case of very high energy generators, almost all of the electrons' kinetic energy (more than 97 percent) is converted into heat; disposal of this thermal energy is an important design consideration.

### Bremsstrahlung

A small portion of the energy will also be given off as packets of electromagnetic energy, called photons. The X-ray photons can have energies ranging from a few thousand volts to a maximum determined by the original kinetic energy of the electron and how rapidly the electron is decelerated by interaction with a target atom nucleus. This process produces the continuous portion of the X-ray spectrum and is known by the German term *Bremsstrahlung* for braking radiation.

Energies of the electrons (and the X-rays) are frequently given in terms of kiloelectronvolt (keV) or megaelectronvolt (MeV). The meaning of this unit becomes clear if the charged electron is considered. Under the influence of a voltage difference (technically called a potential difference), charged particles will experience a force that causes them to accelerate. A negatively charged particle, such as an electron, will move from a place of low voltage (-) to a place of higher voltage (+) and increase its kinetic

FIGURE 1. Typical X-ray spectrum.





energy as it does so. Thus the unit kiloelectronvolt (keV) corresponds to the amount of kinetic energy that an electron would gain while moving between two points that differ in voltage by 1 kV. Similarly, an electron would gain 1 MeV of kinetic energy while moving between two points that differ by 1 MV. The points of differing voltage are called the *cathode* (-) and the *anode* (+) and will be discussed later in this section.

## Characteristic X-Rays

In addition to the bremsstrahlung there are several *characteristic* peaks in a typical X-ray spectrum. These intensity spikes are caused by interaction between the impinging stream of high speed electrons and the electrons that are bound tightly to the atomic nuclei of the target material. If an atom is visualized as a planetary system, with the nucleus of protons and neutrons at the center of the system and with the electrons moving in orbits around the nucleus (see Fig. 2), the law of energy conservation can again be applied to describe the origin of characteristic radiation.

Modern physics predicts that these orbital electrons near the nucleus will have very well defined energies, with electrons in different orbits having

different energy levels. If a vacancy in a particular level were created by knocking an electron from its orbit, an electron from a higher energy level would, after a time, drop down to fill the void. To do this, it would have to lose (emit) energy. Because the energy levels of an atom are well specified, the exact amount of energy lost by an electron making such a transition would also be discrete.

According to the law of conservation of energy, the energy is not really lost but given off as electromagnetic radiation in the form of an X-ray photon. Because each atomic element has its own distinct set of energy levels, the line spectrum produced in such a manner is characteristic of the particular target material. Interest in these characteristic X-rays lies in their application to X-ray diffraction and other analytical applications. By a combination of filtration and signal processing, characteristic X-rays can be used to produce a nearly monoenergetic beam of X-rays.

## Thermionic Emission

Two final concepts are of interest in this brief treatment of the basic physics of X-ray production. The first process, thermionic emission, provides the electrons that are to be accelerated to high speeds by the voltage difference between the cathode and anode of an X-ray source.

When metal (in this case the X-ray tube filament) is heated to incandescence, a small portion of the free electrons are actually able to escape the surface of the material. Without an accelerating voltage, the electrons would form a cloudy *space charge* around the filament. Under the influence of a potential difference, however, the electrons are quickly accelerated toward the anode of the tube.

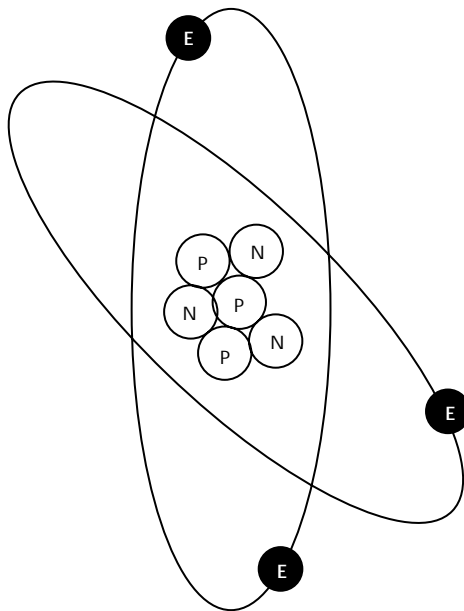
## Absorption

The second concept is X-ray absorption, discussed in greater detail in the chapter on radiation and particle physics. As X-rays pass into or through a material, they are absorbed, or attenuated, in a manner that depends on the energy of the X-radiation and on the density of the material. In equation form, the intensity  $I$  as a function of thickness has a standard exponential form:

$$(1) \quad I = I_0 e^{-\mu x}$$

where  $I$  is the intensity after passing through the material;  $x$  is the thickness of

FIGURE 2. Planetary model of atomic structure.



### Legend

E = electron  
N = neutron  
P = proton

the absorbing material;  $I_0$  is the initial intensity; and  $\mu$  is the linear absorption coefficient (characteristic of the material for a particular X-ray energy range). The importance of absorption in selection of materials for tube construction, beam filtration and shielding are discussed below.

## PART 2. Basic Generator Construction

A conventional X-ray generator consists of three main components: (1) X-ray tube, (2) high voltage source and (3) control equipment. Although each of the major components are examined in some detail, it should be remembered that all conventional units will have similar construction.

### X-Ray Tubes

Early X-ray tubes used gas filled tubes and a cold cathode from which electrons were freed by positive ion bombardment. Modern tubes used in radiography are of the high vacuum variety, allowing for reduction in size, extended tube life and more stable operation.

Electrons are supplied by thermionic emission from the filament. The accelerating potential and the tube current can then be varied independently, with the exception that, at low accelerating voltages, tube current is affected by the space charge that accumulates around the cathode.

### Envelope

Envelopes for X-ray tubes are usually glass or a combination of metal and ceramic (Figs. 3 and 4). Glass envelope tubes, although still in common use, are far more susceptible to thermal and mechanical shock than the metal ceramic

envelope and have been replaced in most industrial applications with the more durable metal ceramic tubes.

The vacuum envelope of the metal ceramic tubes consists of a metal cylinder capped on both ends with ceramic disks, usually composed of aluminum oxide. These ceramic insulators are designed to allow for more effective use of the insulation characteristics of both the ceramic and the high tension grease used in sealing connections between the high

FIGURE 3. Glass X-ray tube.

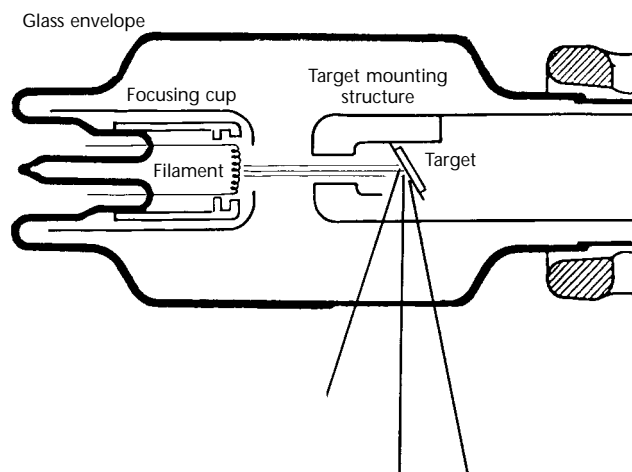
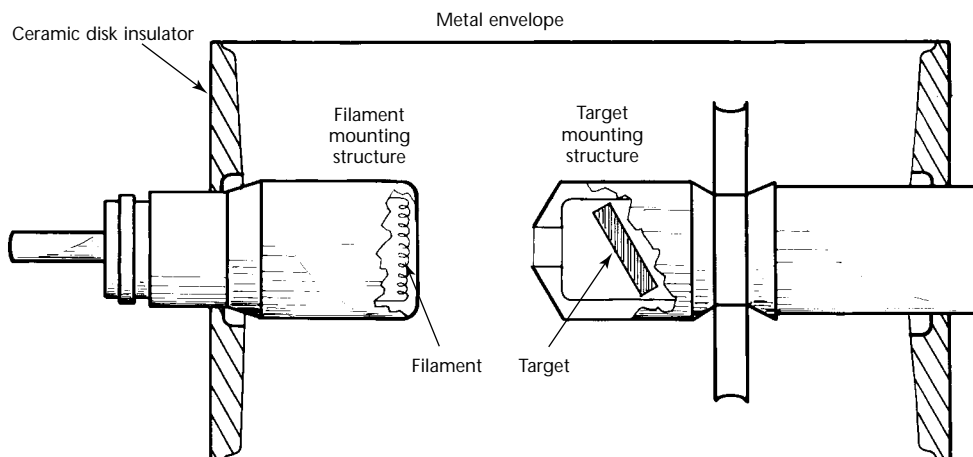


FIGURE 4. Metal ceramic X-ray tube.



voltage source and the tube. This design allows for reduction in the size of the tube housing, especially important for higher energy units.

## Cathode

The cathode includes the tungsten filament that provides the thermal electrons for acceleration. The filament is usually powered by alternating current (50 to 60 Hz) from a separately controlled transformer, although in some units the filament current is fixed or automatically controlled to maintain a constant tube current. Normally, filament currents range from 1 to 10 A. The *tube current*, passing between the cathode and anode by means of the high speed electrons, ranges from less than 300  $\mu\text{A}$  for microfocus units to over 20 mA for conventional industrial radiographic units.

## Beam Focusing

At times the filament is located in a recess in the cathode called a *focusing cup*. This surrounds the emerging beam of electrons with an electric field that repels the beam away from the cup wall and into a more localized form. The importance of a well defined beam of electrons arises from the fact that the sharpness or unsharpness of an image depends on the focal spot size (Fig. 5 and the chapter on radiographic

principles). The relationship for geometric unsharpness  $U_g$  is:

$$(2) \quad U_g = \frac{F}{D} = \frac{F \cdot t}{D}$$

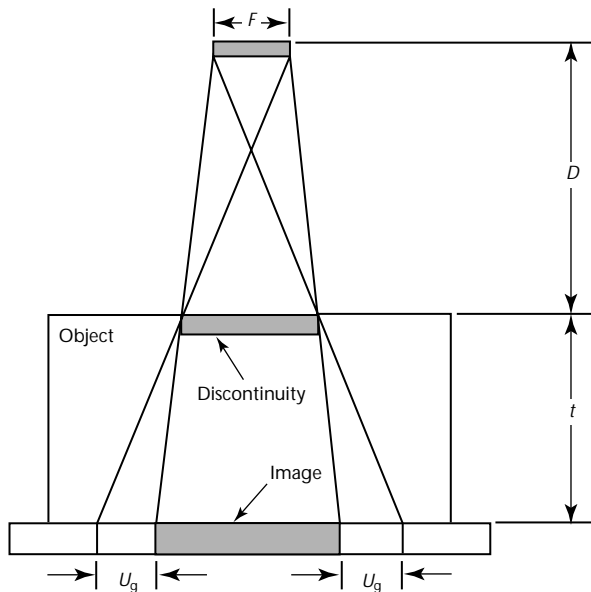
where geometric unsharpness  $U_g$  is a measure of the penumbra of the focal spot,  $F$  is the focal spot size,  $D$  is the distance from the target (focal spot to the source surface of the object) and  $t$  is the thickness of the object plus its distance to the image plane.

In accordance with Eq. 2, geometric unsharpness  $U_g$  increases directly as the focal spot size increases. Because the electron beam originates at the filament, reduction of the filament size might seem to solve geometrical unsharpness by reducing the beam size but this approach is limited by the durability of the filament.

One alternative, called *line focusing*, is to project the virtually rectangular beam produced by the filament onto a target angled with respect to the beam (about 21 degrees). By masking all of the X-ray beam except that emitted toward one side, the useful X-ray beam appears to issue from a focal spot with about equal lateral dimensions (Fig. 6). In practice, this technique allows production of units with effective focal sizes in the range of 1.0 to 3.0 mm (0.04 to 0.12 in.).

By use of a deep focusing cup, advantage can also be taken of the *screen effect* (Fig. 7). This refers to the removal of the lower energy electrons produced during that portion of the alternating current cycle where the potential difference between cathode and anode is significantly less than maximum. In practice this improvement is not without

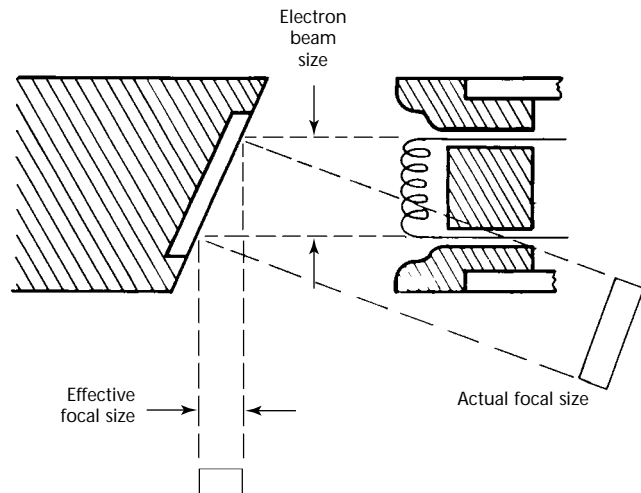
FIGURE 5. Illustration of geometric unsharpness.



### Legend

$D$  = distance from focal spot to target  
 $F$  = focal spot size  
 $t$  = thickness of test object  
 $U_g$  = geometric unsharpness

FIGURE 6. Diagram of line focusing setup.



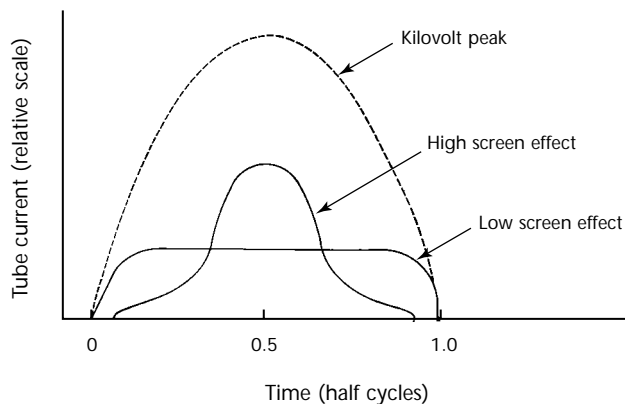
cost to the output of the unit. A loss of about 25 percent is experienced in units with high screen effect. This can be compensated for, in part, with higher filament current although this current adversely affects the lifetime of the filament. An alternate technique of removing low energy components of the electron beam is found in the discussion on constant potential units.

If still further focus of the beam is desired, as in microfocus radiography and some analytical applications, additional techniques may be used: (1) conversion of the conventional diode arrangement of cathode and anode into a triode arrangement, including a focusing electrode or grid, and (2) electrostatic or magnetic deflection systems.

For the triode arrangement used widely in the microfocus industry, a negative bias of up to  $-150\text{ V}$  is applied to the third element of the tube to further focus the beam and remove lower energy components. This configuration allows a reduction of beam size, producing focal spots at least as small as  $10\text{ }\mu\text{m}$  ( $4 \times 10^{-4}\text{ in.}$ ) and a consequent drop in tube current.

In the case of electrostatic deflection, even more elements are included within the envelope whereas a magnetic deflection system is external to the tube. These types of deflection systems have an additional advantage in that the beam may also be deflected to various areas of the target for added service life. Units that incorporate their own vacuum systems usually allow for replacement of both filament and target components. These types, though formerly limited to analytical and research units, are available off the shelf as standard microfocus and analytical units.

FIGURE 7. Graph of screen effect.



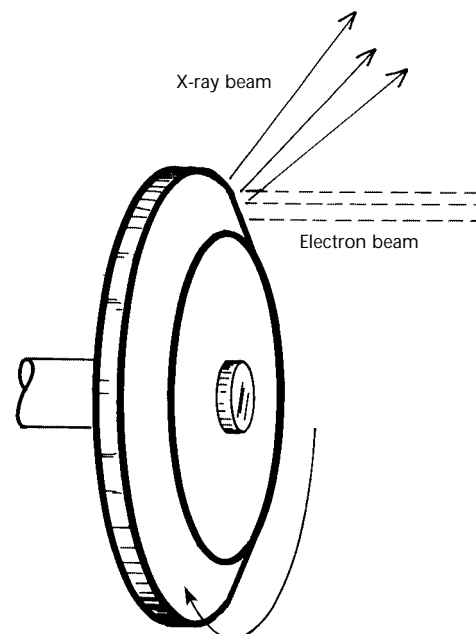
## Anode

As mentioned previously, heat is the major form of energy produced as the electrons strike the target. Uncontrolled, this heat would quickly cause the surface of the target to erode, which in turn reduces the definition of the focal spot. In addition, the vaporized target material reduces the high vacuum of the tube and leads to premature failure due to conduction within the tube. To avoid overheating of the target, the anode to which it is attached is composed of a material with high thermal conductivity, such as copper. If the cooling demands are relatively low, as for a low energy unit or intermittent use, cooling is often accomplished by means of a conductor that passes through the tube end for connection to the high voltage source; this allows for radiation of heat into an oil or gas reservoir surrounding the tube. Although such a design is not the most efficient, the weight of such a tube is minimal because pumps and heat exchangers are absent.

For higher energy units in continuous use, it is usually necessary to cool the anode by injecting coolant directly into it. This is accomplished by hollow construction of the anode conductor.

Another way of alleviating the problem of localized heating of the target is with a rotating anode in which the target, a tungsten disk, is driven as shown in Fig. 8. This allows the tube current to be increased by as much as ten times the value for a stationary target. The focal spot on such units can be reduced to less

FIGURE 8. Rotating anode.





than 1 mm (0.04 in.) for short exposure times, which is of value in medical as well as some specialized industrial applications, such as high speed imaging.

## Target

In radiographic applications, the target is usually tungsten and is bonded to the copper anode; however, analytical units use several other target materials to take advantage of the characteristic X-rays produced. Some of these materials include copper, iron and cobalt.

The orientation of the target with respect to the electron beam strongly influences the size and shape of the focal spot. Orientations from 0 degrees to 30 degrees are used for various applications. For example, zero is the angle used for panoramic units. An angle of 20 degrees is commonly selected for directional units because, in this case, the distribution of X-rays is predominantly in a direction perpendicular to the tube axis. This is shown graphically in Fig. 9. The actual maximum of intensity occurs at +12 degrees. For radiography of objects whose lateral dimensions are less than half the focus-to-film distance (objects that subtend an angle of less than 30 degrees) the variation seldom matters.

Another cause for intensity variation is the electron beam itself. A cross section of the electron beam from the filament would resemble Fig. 10a, with relative

beam intensity also shown. Figure 10b shows a similar representation for a microfocus beam. The beam distribution in Fig. 10b is said to be gaussian (bell shaped) because of the shape of the intensity curve. Such a beam profile is required when it is necessary to define very closely spaced objects, such as microcircuitry components.

## Hood

Addition of a hood to the anode provides the two fold function of (1) eliminating a portion of the X-ray beam outside the central cone of radiation and (2) electrically shielding the insulating portions of the envelope (glass or ceramic) from charge buildup due to electrons scattered from the tungsten target or released by the photoelectric effect (see Fig. 11).

Removing the unused radiation directly at the anode reduces the amount of radiation shielding that must be provided externally or incorporated into the tube housing. The hood, normally constructed of copper, may have materials with high atomic numbers, such as tungsten, incorporated to increase absorption. The electrical shielding function of the hood

FIGURE 9. X-ray distribution graph.

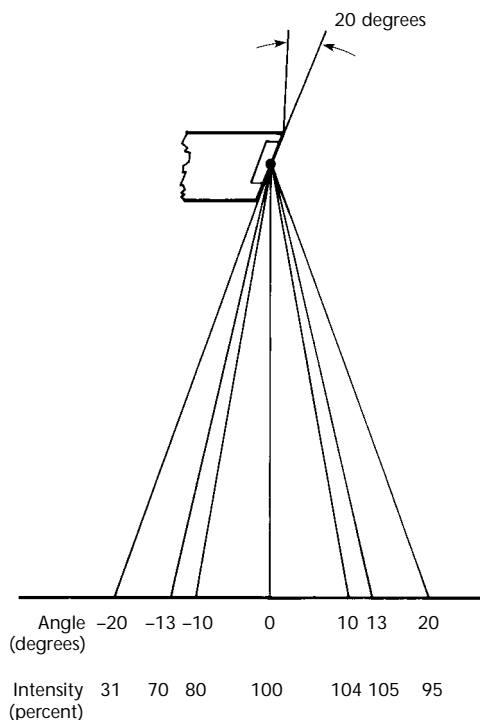
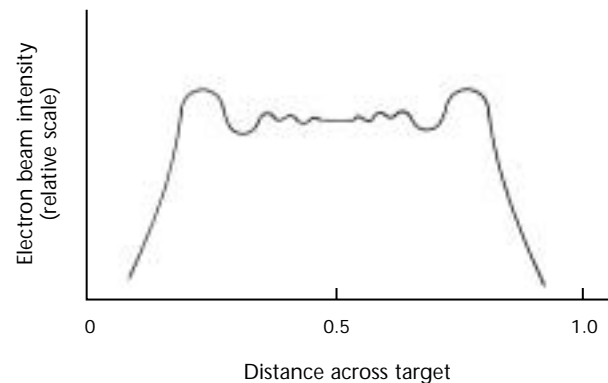
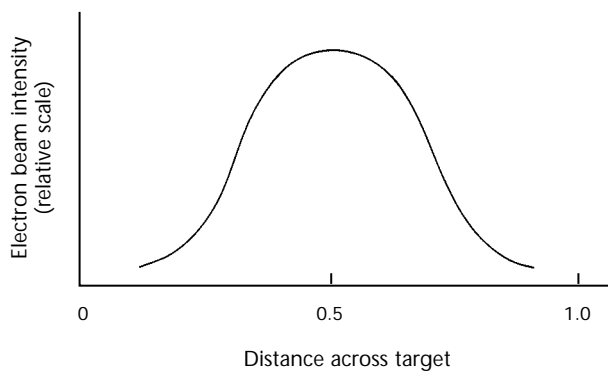


FIGURE 10. Electron beam distributions: (a) conventional beam; (b) microfocus beam.

(a)



(b)



may be improved by the addition of a beryllium window over the X-ray port. A window 3 or 4 mm (0.1 or 0.2 in.) in thickness will stop electrons with negligible effect on the overall X-ray beam.

### Rod Anode

The rod anode (sometimes referred to as an *oxtail*) is another adaptation of the anode. This type of tube arrangement requires special circuit considerations that allow the anode to be grounded. This tube, developed for use through small openings, has been partially replaced by the metal ceramic tube, which can have a diameter of less than 50 mm (2 in.) and tube head diameter as small as 75 mm (3 in.). The target of such an *end grounded* tube can be cooled by circulating water in direct contact with the anode. Beam focusing is often required for longer tubes.

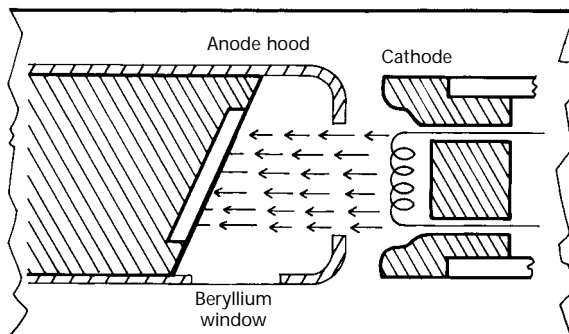
### Coolant

With the exception of the end grounded configurations and units designed for low energy output (less than 50 kV), the tube insert is surrounded by an insulating coolant and encased in a housing called the tube head.

The coolant may be highly dielectric gas or oil. If oil is used, simple convection may be sufficient for lower output units. For larger units, an oil circulating pump may be combined with a heat exchanger either internal or external to the tube head.

For units using a fixed amount of oil in the tube and a circulating pump to circulate it within the tube head, an oil resistant bellows is incorporated to allow for expansion and contraction of the oil. Because of the compressibility of insulating gases, this is not required for gas filled heads but a pressure gage is normally included to monitor possible loss of coolant insulation.

FIGURE 11. Hooded anode tube.



### Tank Head

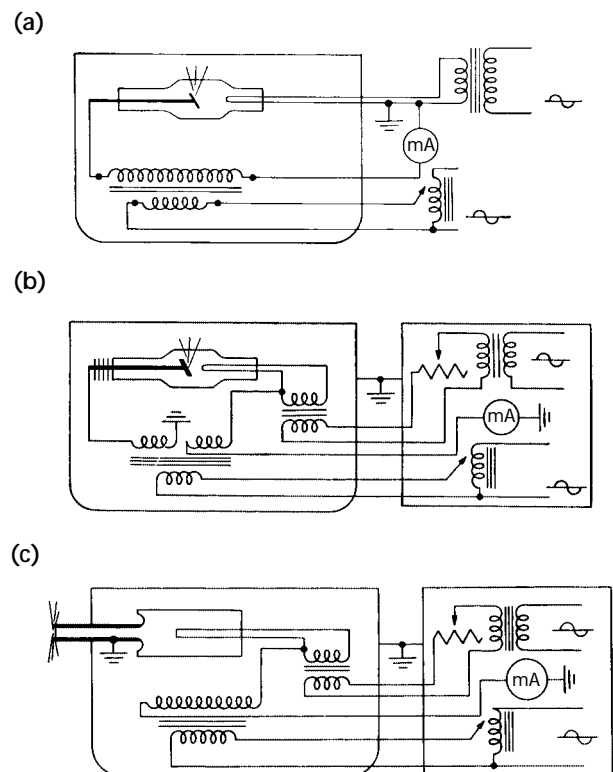
For a tank head, the housing itself structurally protects the tube, contains the coolant and forms the structural support for the tube insert, electrical connections, fittings, pumps, thermal and high voltage overload sensors and radiation shielding contained in the head. For a tank unit, the tube head also houses the high voltage and filament transformers. If the unit has separate components, the tube head will also provide for connection to the high voltage source.

### High Voltage Sources

From line voltages in the range of 100 to 460 V, the high tension circuitry supplies potential differences to the tube from 5 kV to as much as 420 kV for the larger industrial radiographic units. Several standard circuit designs are used for various applications. A portable tank unit typically uses one of the designs shown in Fig. 12.

These circuits are all self-rectified; the X-ray tube itself limits the flow of electrons to one direction in the circuit. When the anode is at negative potential

FIGURE 12. Standard high voltage circuit designs for portable tank-type units: (a) cathode grounded; (b) center grounded; (c) anode grounded.



with respect to the cathode, no tube current flows.

One drawback of the self-rectified system is the possibility of tube backfire. If the target or anode overheats, reverse conduction can occur during the negative half cycle. This type of unit is normally used for tubes producing X-rays in the range of 50 to 300 kV peak and tube currents from 2 to 8 mA.

With the addition of capacitors and diode rectifiers, the transformer is normally placed in a tank separate from the head. The additional elements allow the current to be rectified by means of valve tubes or solid state diodes and to be filtered and smoothed to provide a more nearly constant accelerating voltage. Several popular grounded circuits are shown in Figs. 13 to 15.

**Villard Circuit.** An extension of the half wave system, the villard circuit allows production of accelerating potentials of twice the transformer peak voltage. Capacitors are charged during one half of the cycle and discharged when current passes through the tube, augmenting the voltage produced by the transformer.

**Graetz Circuit.** The full wave circuit, or graetz circuit allows use of both halves of the alternating current cycle with a substantial increase in tube output per

unit time. This system is widely used in medical applications but is used less than constant potential units in industrial applications.

**Greinacker Circuit.** As can be seen from the output waveform, the greinacker circuit is of the constant potential type. Basically a variation of the villard circuit,

FIGURE 14. Graetz grounded anode circuit: (a) circuit; (b) waveform.

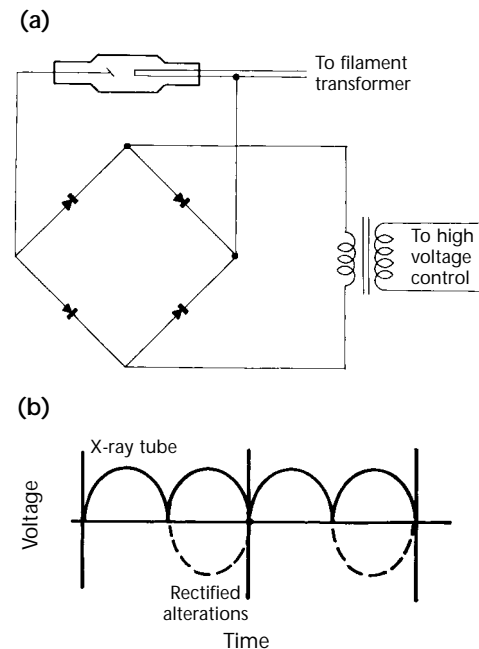


FIGURE 13. Villard grounded anode circuit: (a) circuit; (b) waveform.

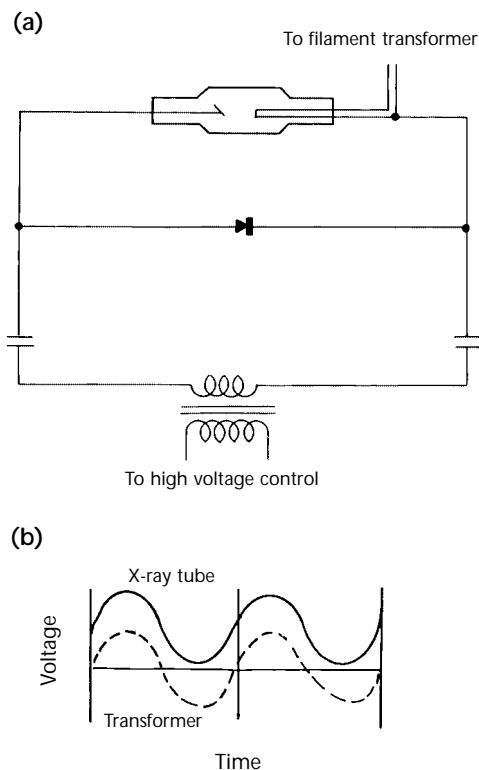
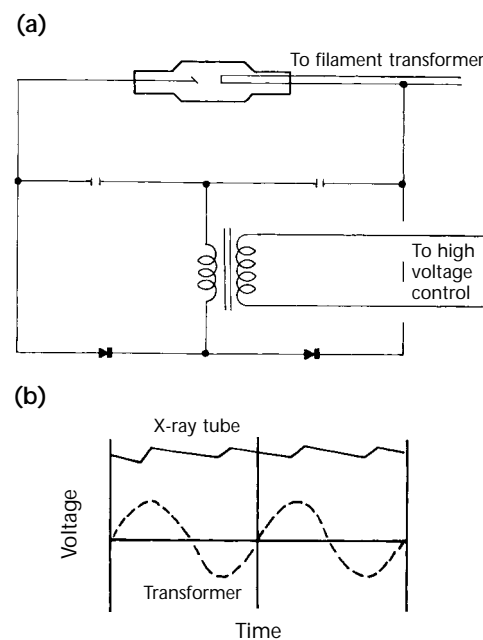


FIGURE 15. Greinacker grounded anode circuit: (a) circuit; (b) waveform.



in which capacitors are charged during both halves of the cycle, the voltage is not only doubled but remains near maximum value throughout the cycle. This gives enhanced high energy output and eliminates the electrical stress placed on the tube and insulation. Enhanced tube life, as well as about 30 percent reduction in radiographic exposure times, are the results.

A common misconception is that constant potential units provide a beam of constant energy X-rays. Although the electron beam is nearly monoenergetic, the X-rays are produced during random deceleration processes that give the statistical energy distribution shown in Fig. 1. The absence of low energy electrons reduces the quantity of low energy X-rays but does not eliminate them.

### Cathode Grounded Circuit

The main advantage of the cathode grounded configuration is that it allows the filament transformer to be external to the tank, because the cathode is at ground potential and does not require isolation. The tube head can be reduced in size and weight and is often gas filled to further decrease weight.

### Center Grounded Circuit

Both center grounded and anode grounded units require isolated filament transformers that must be insulated adequately. For the center grounded unit, this is justified by the reduction of the high tension transformer insulation. The transformer needs to supply only one half of the potential difference to each electrode, rather than having either the cathode or anode held at ground potential and supplying the entire accelerating voltage to the other electrode.

In the range of 200 to 420 kV peak with beam currents up to 15 mA, center grounded systems can be made smaller than comparable end grounded units.

### Anode Grounded Circuit

For the anode or end grounded system, the advantage lies in the specialized use of the rod anode tube or metal ceramic tube for access through small openings. As mentioned earlier, cooling of the target is also simplified. This type of unit is normally used for tubes producing X-rays in the range of 30 to 200 kV.

### Alternative Circuit Designs

A technique for improving tube output that can be used with any of the above circuits including those in tank units, is the use of a higher frequency waveform to

power the high tension transformer. Although this requires additional electronic circuitry or a motor generator, the core of the high tension transformer can be reduced in size because of increased reactance at higher frequencies. The smaller transformer can be an advantage in portable or mobile units. Also, if filtering is to be done, the variation or ripple of the output voltage can be reduced even further.

A variation of this technique is to use three phase input power with the high tension transformer. Commonly used in medical X-ray generators, this technique is used by several industrial manufacturers as well.

Another approach is to use an output waveform other than the standard sine wave. Approximate square wave outputs, in conjunction with both phase inversion circuitry and a high frequency transformer, can provide accelerating potentials with extremely low ripple characteristics. Such units are available for industrial applications.

### High Tension Connections

Also important for conventional high voltage sources is the connection of the high tension transformer to the tube. For tank units this is not a major consideration, because the transformer can be connected directly to the tube electrodes. However, for units with separate components, insulation and connection of leads (which may carry voltages in excess of 200 kV) are important considerations. The high tension cables themselves are shielded to provide protection against electrical shock. Cables used at lower energies are relatively flexible but as the amount of insulation is increased, the flexibility decreases and sharp bends during installation should be avoided.

The cables are inserted into terminations usually made of phenolic (thermosetting plastic) or ceramics and are sealed against air by use of insulating epoxy materials called *potting compound*. Figure 16 shows the phenolic termination, used primarily with glass and lower energy metal ceramic tubes.

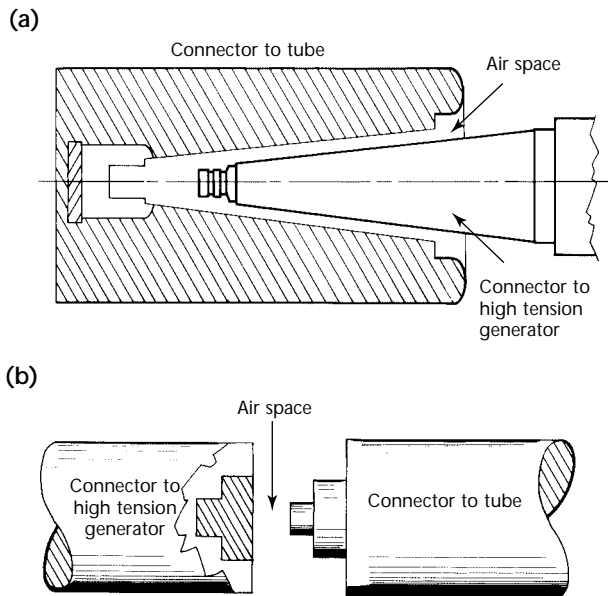
These connectors are larger than the ceramic terminations used primarily with higher energy metal ceramic tubes. Both styles use high dielectric grease to seal out air at joining surfaces. Because of the tendency for the long male-to-female connections to trap air and substantially reduce the insulation capabilities of the grease, these joints are normally rated at about one tenth their theoretical values, or at about 10 kV per 10 mm (0.4 in.). The linear dimensions of such a termination must be correspondingly

increased. At the transformer tank, this size increase is not so important but at the tube head the increase in size and weight can make the unit very cumbersome and bulky. For a 400 kV tube head, 200 kV is applied to each electrode. This requires a termination of 180 to 200 mm (7 or 8 in.) in length at each end of the tube for proper insulation.

A ceramic insulator can make full use of the dielectric strength of the insulating grease by providing rigid, flat mating surfaces that exclude air from the joint. This allows for a substantial decrease in the length of the joint. This design has been incorporated into tubes used by several equipment manufacturers for units up to 420 kV.

As stated above, a transformer is used to provide the potential difference for conventional X-ray units. As the accelerating voltages are increased toward 1 MeV, standard transformer and insulation technologies become inadequate. Higher energy X-ray generators are needed.

FIGURE 16. High voltage transformer terminations:  
(a) phenolic connection; (b) ceramic connection.



## PART 3. Megavolt Radiography<sup>6</sup>

Resonant transformer X-ray machines were developed in the late 1930s to provide X-ray energies above 500 keV. The technology of high voltage X-radiography is well documented.<sup>5-21</sup>

Resonating the high voltage circuit to the frequency of the alternating current power supply obviates an iron transformer core. In addition, insulating the high voltage sections with dichlorodifluoromethane (refrigerant-12) or sulfur hexafluoride ( $\text{SF}_6$ ) obviates transformer oil. These changes permit a large reduction in the size and weight of the machines, making them much more practical.

The resonant transformer X-ray machines, similar to Fig. 17, consist of an operating console, 180 cycles per second alternating current motor generator set, motor controller, heat exchanger and a large steel tank. An air core transformer is secured to the base of the steel tank by insulating glass rods. A multisection X-ray tube is mounted coaxially with the transformer stack. A heated filament provides the free electrons in the tube and each section of the multisectional tube is connected to an appropriate tap on the transformer. Acceleration of the electrons through the tube is accomplished by uniform voltage distribution throughout the length of the tube. The electrons strike a water cooled tungsten target at the end of the tube, thereby generating X-rays.

Most X-rays are available in the forward direction but opening ports around the lead collimator makes it

possible to extract a 360 degree circumferential beam from the machine. The focal spot size is typically as large as 10 mm (0.4 in.) in diameter in the transmitted direction. The apparent size of the target will depend on the angle that is measured from the flat plane of the target. The radiation output from these machines is about  $25 \text{ mGy}\cdot\text{s}^{-1}$  ( $150 \text{ rad}\cdot\text{min}^{-1}$ ) when measured at 1.0 m (39 in.) from the target.

These machines are very durable, many having been in service for over 30 years and one having been in daily use for over 60 years.

### Electrostatic Generators

Van de graaff X-ray machines (Fig. 18) operate on the principle illustrated in Fig. 19. The van de graaff electrostatic generator shown in Fig. 18 has undergone some changes since its origin in the early 1930s. However, the basic principles of operation presented in Fig. 19 remain the same. The machine consists of a control console and a metal tank that houses power supplies, drive motors, an insulated charging belt, a generator column, high voltage terminals and electrical connections. An accelerator tube, which is highly evacuated, extends through the generator column. This metal tank is pressurized with nitrogen, carbon dioxide and sulfur hexafluoride to about 2.6 MPa ( $375 \text{ lb}_f\cdot\text{in}^{-2}$ ) to prevent high voltage

FIGURE 17. Resotron, 2 MeV.



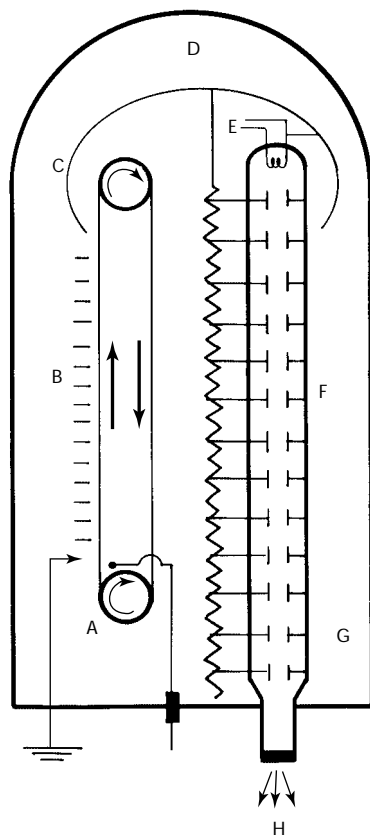
FIGURE 18. Van de graaff 2.5 MeV electrostatic generator.





arcing. Within the tank, electron sprayers deposit electrons onto a moving belt that carries them to a terminal shell. Some of these electrons are emitted into the accelerator tube as beam current through a direct connection to the filament. The filament, when properly heated, emits electrons that are replaced from the terminal shell. The electrons flow through the accelerator tube at an energy determined by the terminal shell voltage. A target is located at the end of the accelerator tube. This design results in a direct current, constant potential X-ray machine. Constant potential machines made in the 1990s are in the 2.5 MeV range, have a 2.5 mm (0.1 in.) target and produce about  $28.3 \text{ mGy}\cdot\text{s}^{-1}$  at 1 m ( $170 \text{ rad}\cdot\text{min}^{-1}$  at 40 in.).

FIGURE 19. Operation of electrostatic generator.



#### Legend

- A. Electric charge is sprayed on belt.
- B. Belt carries charge to terminal.
- C. Charge transferred from belt to terminal establishes lower voltage.
- D. Compressed nitrogen insulates terminal from accelerator shell.
- E. Heated cathode provides electrically charged particles.
- F. Charged particles escape via vacuum tube.
- G. Potential difference between terminal and lower end accelerates particles.
- H. Particle beam bombards targets to make X-rays.

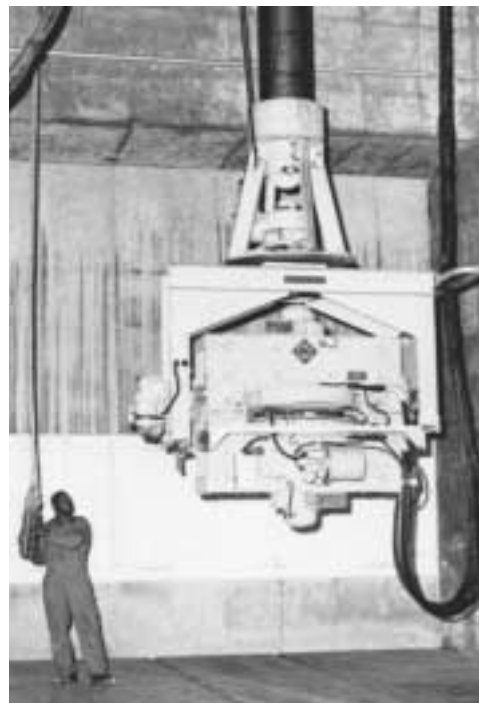
## Betatron

The first successful betatron was built in 1941. It produced 2.3 MeV X-rays and had an X-ray output equivalent to 1 g of radium. Later, machines producing X-ray energies up to 300 MeV or more were built, though the most common radiographic machines operated at 24 MeV.

To accelerate electrons to high speed, the betatron (Fig. 20) uses the magnetic induction effect used in a transformer. The primary winding in a transformer is connected to an alternating current voltage source that establishes a varying flux in an iron core. The secondary winding on this core has induced in it a voltage equal to the product of (1) the number of turns in the secondary winding and (2) the flux time rate of change. The resulting electric current is made up of the free electrons present in the wire. The betatron (as shown in Fig. 21) is essentially such a transformer except that, instead of wire, the secondary is a hollow circular tube. This tube, called a doughnut, is used to contain the electrons for many thousand revolutions.

The doughnut tube is usually made of porcelain and is coated on the inside with a conductive layer of palladium connected to a ground. The doughnut is placed between the poles of an electromagnet that produces a pulsating

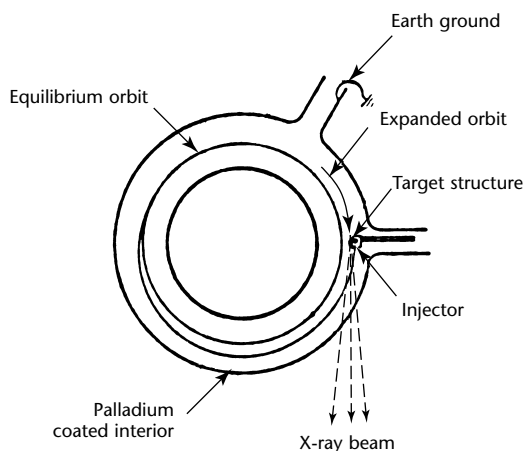
FIGURE 20. Betatron, 25 MeV.



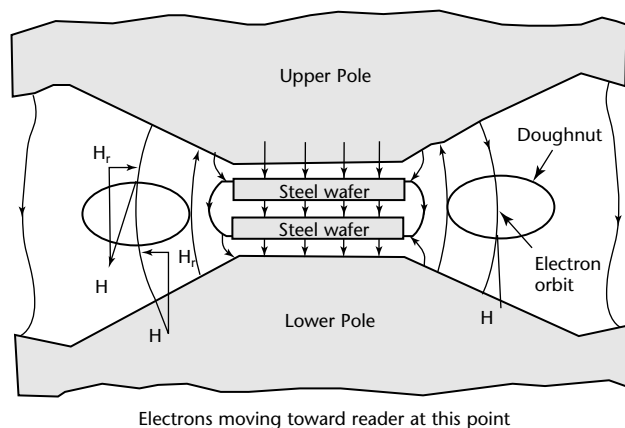
field. Electrons injected into the tube as the magnetic field increases will be accelerated in a circular path. The force acting on the particles is proportional to the rate of change of flux and the magnitude of the field. Because the electrons circle the orbit many times before striking the target, there is a large amount of energy gain. For example, in a 24 MeV betatron, the electrons circle the orbit about 350 000 times, traveling a distance of 418 km (260 mi). The average voltage gain per turn at the orbit is about 70 V, which gives about 24 MeV. As the electrons reach maximum energy, they are deflected by an electrical pulse and caused to spiral outward until they strike the target. Betatrons are equipped with platinum wire targets with dimensions of  $0.13 \times 0.25$  mm ( $0.005 \times 0.010$  in.) and have a radiation output of  $25 \text{ mGy}\cdot\text{s}^{-1}$  ( $150 \text{ rad}\cdot\text{min}^{-1}$ ) when measured at 1 m (40 in.) from the target.

**FIGURE 21.** Diagram of betatron generator: (a) top view; (b) cross section.

(a)



(b)



## Electron Linear Accelerators

Electron linear accelerators, similar to the one shown in Fig. 22, are commonly referred to as *linacs*. Linear accelerators accelerate electrons down a guide by means of radio frequency voltages. These voltages are applied so that the electron reaches an acceleration point in the field at precisely the proper time. The accelerator guide consists of a series of cavities that causes gaps when the radio frequency power is applied. The cavities have holes in each end that allow electrons to pass to the next cavity. When an electron is injected at the proper time it gains energy as it is accelerated across these gaps and out the other end of the cavity. When the radio frequency power is phased properly, increased acceleration is achieved. Figure 23 shows the general arrangement of a linear accelerator's component parts.

For research purposes, heavier particles have been accelerated by linear accelerators. An example of this type linear accelerator is the 3.2 km (2 mi) long Stanford linear accelerator. There are two general types of radiographic linear accelerators: (1) one using the principle of the traveling wave and (2) the other using a standing wave technique of acceleration.

Radiographic linear accelerators have been produced that have X-ray energies of 1 to 16 MeV and with output as high as  $4.17 \text{ Gy}\cdot\text{s}^{-1}$  ( $25 \text{ krad}\cdot\text{min}^{-1}$ ) measured at 1 m (40 in.). Although not as durable as lower voltage machines, some have been in service for over 30 years. Increased operating frequencies, up to 9.3 GHz, permit smaller, lighter X-ray heads. Configurations exist that allow for the operation of the accelerator and beam

**FIGURE 22.** Electron linear accelerator.

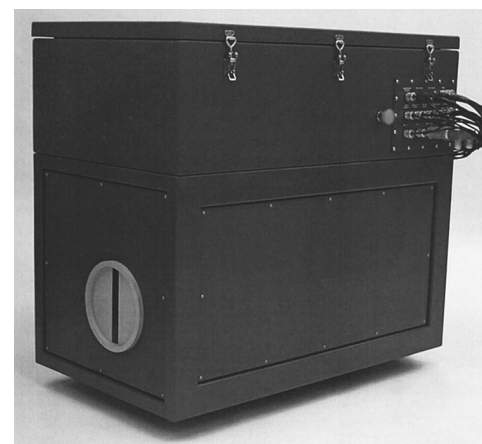
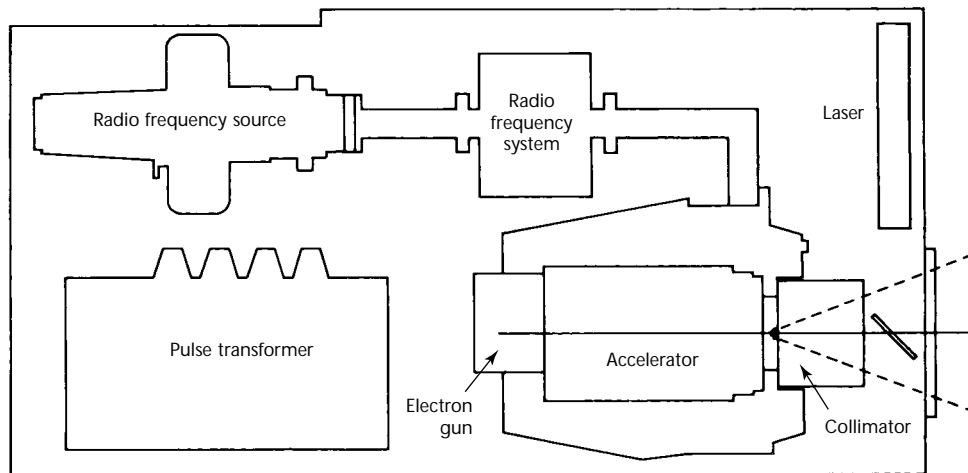


FIGURE 23. General arrangement of linear accelerator.



collimator at a distance from the radio frequency source; the source supplies power through a flexible wave guide. The total weight of the X-ray head is greatly reduced, permitting easy positioning for field inspection of pipelines, valves and other test objects of limited accessibility. One such system is being used for inservice inspection of nuclear power plants.

## References

1. Beiser, A. *Concepts of Modern Physics*, fifth edition. New York, NY: McGraw-Hill Book Company (1963).
2. Halliday, D., R. Resnick and J. Walker. *Fundamentals of Physics*, sixth edition, extended. New York, NY: John Wiley and Sons (2001).
3. *Industrial Radiography Manual*. Washington, DC: United States Office of Education, Division of Vocational and Technical Education; and United States Atomic Energy Commission, Division of Nuclear Education and Training (1968).
4. Lapp, R.E. and H.L. Andrews. *Nuclear Radiation Physics*, fourth edition. Upper Saddle River, NJ: Prentice-Hall (1972).
5. *Nondestructive Testing Handbook*, first edition. Columbus, OH: American Society for Nondestructive Testing (1959).
6. Brunty, B.J. "High-Energy Radiography." *Nondestructive Testing Handbook*, second edition. Columbus, OH: American Society for Nondestructive Testing (1985): p 256-298.
7. Wilshire, W.J., ed. *A Further Handbook of Industrial Radiology*. London, United Kingdom: Edward Arnold and Company (1957).
8. *Nondestructive Testing Handbook*, first edition. Columbus, OH: American Society for Nondestructive Testing (1959).
9. Hogarth C.A. and J. Blitz. *Techniques of Nondestructive Testing*. London, United Kingdom: Butterworth and Company (1960).
9. McGonnagle, W.J. *Nondestructive Testing*. New York, NY: McGraw-Hill Book Company (1961).
10. Halmshaw, R., ed. *Physics of Industrial Radiology*. New York: American Elsevier Publishing Company (1966).
11. *Radiography in Modern Industry*. Rochester, NY: Eastman Kodak Company.
12. Halmshaw, R. *Industrial Radiology Techniques*. London: Wykeham Publishing Company (1971).
13. *High-Energy X-Ray Applications for Nondestructive Testing*. RAD-1936. Palo Alto, CA: Varian Associates (1982).
14. Pollitt, C.G. "Radiography with High-Energy Radiation." *Journal of the British Steel Castings Research Association*. Sheffield, United Kingdom: British Steel Castings Research Association (1962).
15. O'Connor, D.T. and B.G. Cunningham. "Installation of the Flexible 10 MeV Betatron." *Non-Destructive Testing*. Vol. 7, No. 4. Columbus, OH: American Society for Nondestructive Testing (Spring 1949): p 20-23.
16. Halmshaw, R. and C.C. Pollitt. "Radiology with High-Energy X-Rays." *Progress in Nondestructive Testing*. Vol. 2. London, United Kingdom: Heywood and Company (1959).
16. Cusick, J.H. and J. Haimson. "10-MeV Rotating Target Linear Accelerator for Radiography of Large Rocket Motors." *Proceedings: Missiles and Rockets Symposium*. Concord, CA: United States Naval Ammunition Depot (1961).
18. Haimson, J. "Radiography of Large Missiles with the Linear Electron Accelerator." *Nondestructive Testing*. Vol. 21, No. 2. Columbus, OH: American Society for Nondestructive Testing (March-April 1963): p 102-112.
19. Bly, J.H. and E.A. Burrill. "High-Energy Radiography in the 6 to 30 MeV Range." Special Technical Publication No. 278. West Conshohocken, PA: ASTM International (1959).
20. Morgan, R.H. and K.E. Corrigan, eds. *Handbook of Radiology*. Chicago, IL: Year Book Publishers (1955).
21. Wheeler, G.C. "Radiography of Steel with the 25,000 R/min Linac." Paper B-41. *Conference Proceedings: The Seventh International Conference on Nondestructive Testing* [Warsaw, Poland, June 1973]. Vol. 1. Warsaw, Poland: Instytut Podstawowych Problemów Techniki Polskiej Akademii Nauk (1973): p 241-249.



# 4

## C H A P T E R

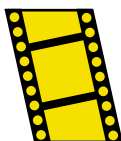
# Isotope Radiation Sources for Gamma Radiography<sup>1</sup>

---

Frank A. Iddings, San Antonio, Texas

# PART 1. Selection of Radiographic Sources

MOVIE.  
Isotopic source.



Several hundred radioactive isotopes are known to exist but only a very few find use as radiographic sources. Most of the radioactive isotopes are unsuitable for one or more reasons — short half life; undesired type, intensity or energy of radiation; difficulty of manufacture; and expense.

The isotope radiation source first used for radiography was radium-226. It was readily available from natural materials, the tailings of the uranium ore pitchblende. Radium also has a half life of 1620 years and emits several gamma energies, including 0.60, 1.12 and 1.24 MeV, that penetrate most industrial specimens. However, radium-226 decays by an alpha emission that creates helium gas pressure in the sealed capsule. To make matters worse, the radium compounds tend to corrode and crack the stainless steel capsules and the first decay product from radium is the radioactive gas radon (radon-222), which helps spread the radioactive material into the environment. The radium acts like calcium in the body and goes to the bones where some of the components of the blood are made. Once leaked into the environment, the half life of 1620 years is no longer an advantage. Radium-226 is no longer used for radiography.

The following discussion gives details on the properties, production and applications of the major radiographic isotopes used by industry. The characteristics of the three major isotopes

— cobalt-60, cesium-137 and iridium-192 — are summarized in Table 1 and discussed below. Two other isotopes, thulium-170 and selenium-75, are also discussed.

## Radiographic Isotopes and Their Properties

### Cobalt-60

Cobalt-60 comes from thermal neutron bombardment of small pieces of cobalt metal, usually 1 to 2 mm (0.04 to 0.08 in.) diameter by 1 to 2 mm (0.04 to 0.08 in.) tall, in a nuclear reactor. Neutron irradiation for about 15 days at a neutron flux of  $10^{14}$  n·cm<sup>-2</sup>·s<sup>-1</sup> results in the production of about 2.2 GBq (60 mCi) of cobalt-60 per average sized pellet or wafer. Irradiation at the same flux for about a year gives about 37 GBq (1 Ci) per piece of cobalt. As many of these pieces are placed together as needed to provide the number of curies needed for the source. They are usually encapsulated in stainless steel using a single welded capsule but may be doubly encapsulated (a welded capsule inside of another welded capsule) if conditions warrant the extra precautions to prevent loss of the radioactive material.

Cobalt exists in nature as 100 percent cobalt-59 that adds one neutron to its nucleus in the neutron bombardment to

TABLE 1. Characteristics of three isotope sources commonly used for radiography.

Characteristics	Element		
	Cobalt-60	Cesium-137	Iridium-192
Half life	5.27 years	30.1 years	74.3 days
Chemical form	cobalt metal	in glass or ceramic	iridium metal
Density, g·cm <sup>-3</sup> (oz <sub>m</sub> ·in. <sup>-3</sup> )	8.9 (5.1)	3.5 (2.0)	22.4 (12.9)
Gamma energy (MeV) <sup>a</sup>	1.17 and 1.33	0.66	0.14 to 1.2 (average 0.34)
Abundance (gamma rays per disintegration)	1.0 and 1.0	0.92	1.47 to 0.27
Beta particles (MeV)	0.31	0.5	0.6
μSv·GBq <sup>-1</sup> ·s <sup>-1</sup> at 1 m (R·Ci <sup>-1</sup> ·h <sup>-1</sup> at 1 m)	364 (1.35)	105 (0.39)	148 (0.55)
Mass absorption coefficient for lead, mm <sup>2</sup> ·g <sup>-1</sup> (cm <sup>2</sup> ·g <sup>-1</sup> )	4.8 (0.048)	11 (0.11)	33 (0.33)
Practical specific activity, TBq·g <sup>-1</sup> (Ci·g <sup>-1</sup> )	1.85 (50)	0.93 (25)	13.0 (350)
Maximum source generally in use, TBq (Ci)	1.22 (33)	2.78 (75)	5.55 (150)
Uranium shield diameter, mm (in.)	380 (15)	200 (8)	120 to 130 (4.7 to 5.1)

a. See Fig. 2 for spectra.



become cobalt-60 ([see this volume's discussion of radiation and particle physics](#)). The neutron capture cross section of  $24 \times 10^{-24} \text{ cm}^2$  makes cobalt one of the most readily available and generally useful isotopes. The cobalt is a hard, gray, magnetic metal with a melting point of  $1480^\circ\text{C}$  ( $2700^\circ\text{F}$ ) and a density of  $8.9 \text{ g}\cdot\text{cm}^{-3}$  ( $556 \text{ lb}_\text{m}\cdot\text{ft}^{-3}$ ). The metal is relatively free from oxidation and chemical attack under ambient conditions.

Cobalt-60 decays with a half life of 5.27 years by the emission of a soft beta particle followed by two gamma rays (see Fig. 1 for decay diagram and Fig. 2a for spectrum) with energies of 1.17 and 1.33 MeV. The cobalt-60 has a high output of these photons, yielding  $364 \mu\text{Sv}\cdot\text{GBq}^{-1}\cdot\text{h}^{-1}$  at 1 m ( $1.35 \text{ R}\cdot\text{Ci}^{-1}\cdot\text{h}^{-1}$  at 1 m) from the source. These high energies combined with high output let radiographers inspect iron, brass, copper and other medium weight metals with a thickness greater than 25 mm (1.0 in.).

Other more dense metals such as tantalum or uranium can be radiographed with cobalt-60. Typical range for application in steel is for a specimen with a thickness of 20 to 200 mm (0.8 to 8.0 in.). This is about radiographically equivalent to a 3 MeV X-ray generator but the cobalt-60 is not as intense a source. Use of cobalt-60 for radiography of thinner or lower density materials results in a loss of definition for any discontinuities present and use for thicker or higher density materials results in long exposure times.

### Cesium-137

Cesium-137 originally was used in the chloride form that often induces stress corrosion cracking in the stainless steel encapsulation materials. The chloride form is now usually converted into a glass or ceramic form before encapsulation. Also, it is doubly encapsulated (a welded capsule inside another welded capsule) to

prevent loss of the radioactive material to the environment. The moderate output of  $91 \mu\text{Sv}\cdot\text{GBq}^{-1}\cdot\text{h}^{-1}$  at 1 m ( $0.34 \text{ R}\cdot\text{Ci}^{-1}\cdot\text{h}^{-1}$  at 1 m) from the source per each curie from the single gamma ray on 92 percent of the decaying nuclei, as shown in Fig. 3, has not overcome the early history of leakage

FIGURE 2. Gamma spectra: (a) cobalt-60; (b) cesium-137; (c) iridium-192.

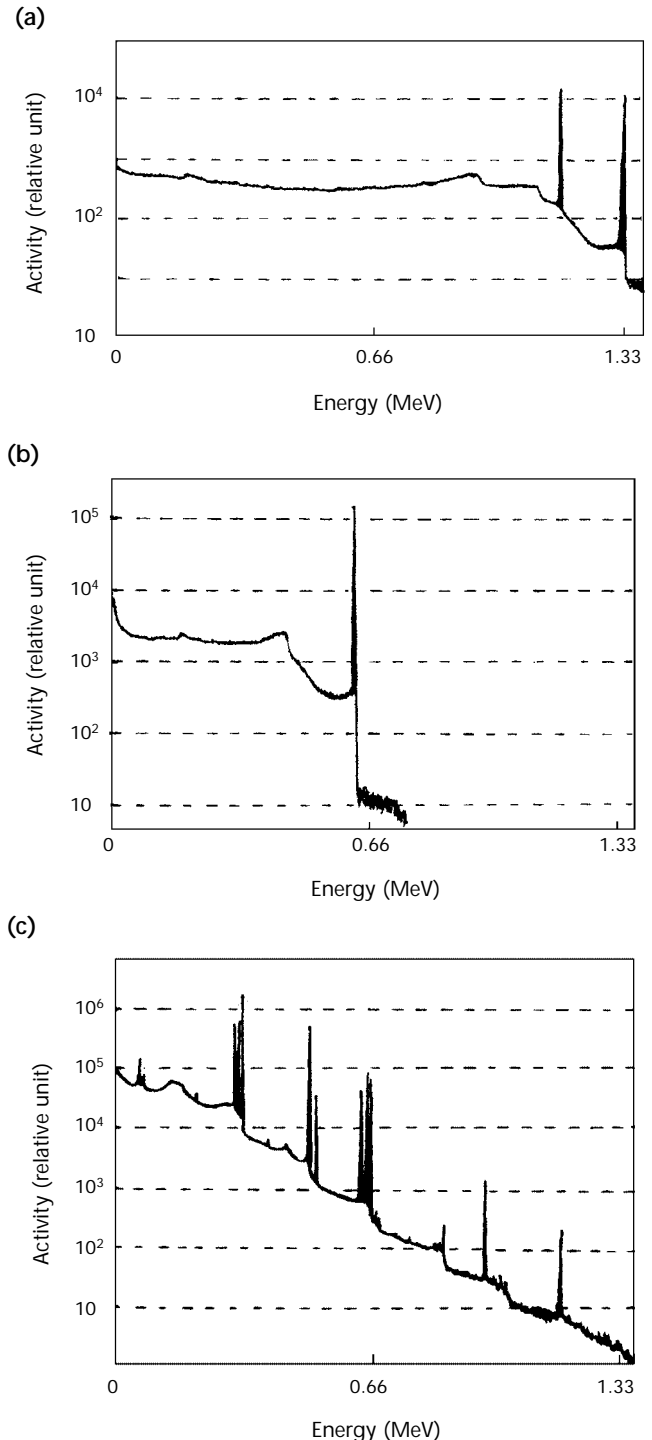
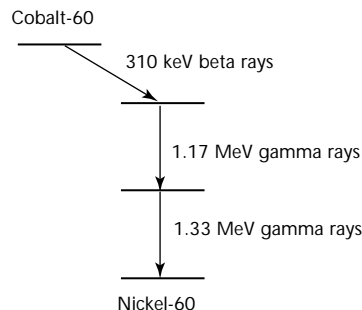


FIGURE 1. Disintegration of cobalt-60, with half life of 5.27 years.

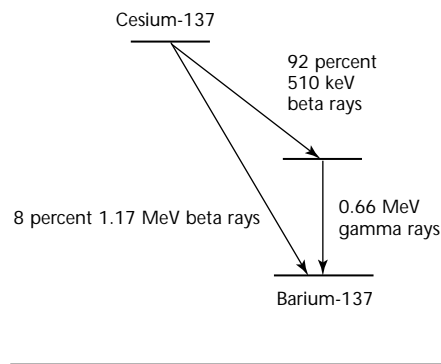


problems and bulky source size problems. Although it has a long half life of 30.1 years and has a moderate gamma ray energy of 0.66 MeV, cesium-137 is less often used as a radiographic source than either cobalt-60 or iridium-192. See Fig. 2b for gamma spectrum of cesium-137. It is frequently used as a source for industrial thickness and density gages.

Cesium-137 is not produced by neutron bombardment as are cobalt-60 and iridium-192. This radioactive material is a fission fragment from the neutron

induced fission of uranium-235 ([see this volume's section on particle physics](#)). The cesium-137 must be recovered from the unused uranium and all of the other fission fragments left in the fuel rods from a nuclear reactor. The cesium-137 is one of the most probable products of nuclear fission, resulting from about 6 percent of fission events. The cesium chloride recovered from spent fuel contains cesium-133 and cesium-135 as well as the cesium-137, limiting the specific activity to about 925 GBq (25 Ci) per gram of cesium chloride. Self-absorption and absorption by the double encapsulation may be as much as 30 percent of the intensity of a 1850 GBq (50 Ci) source.

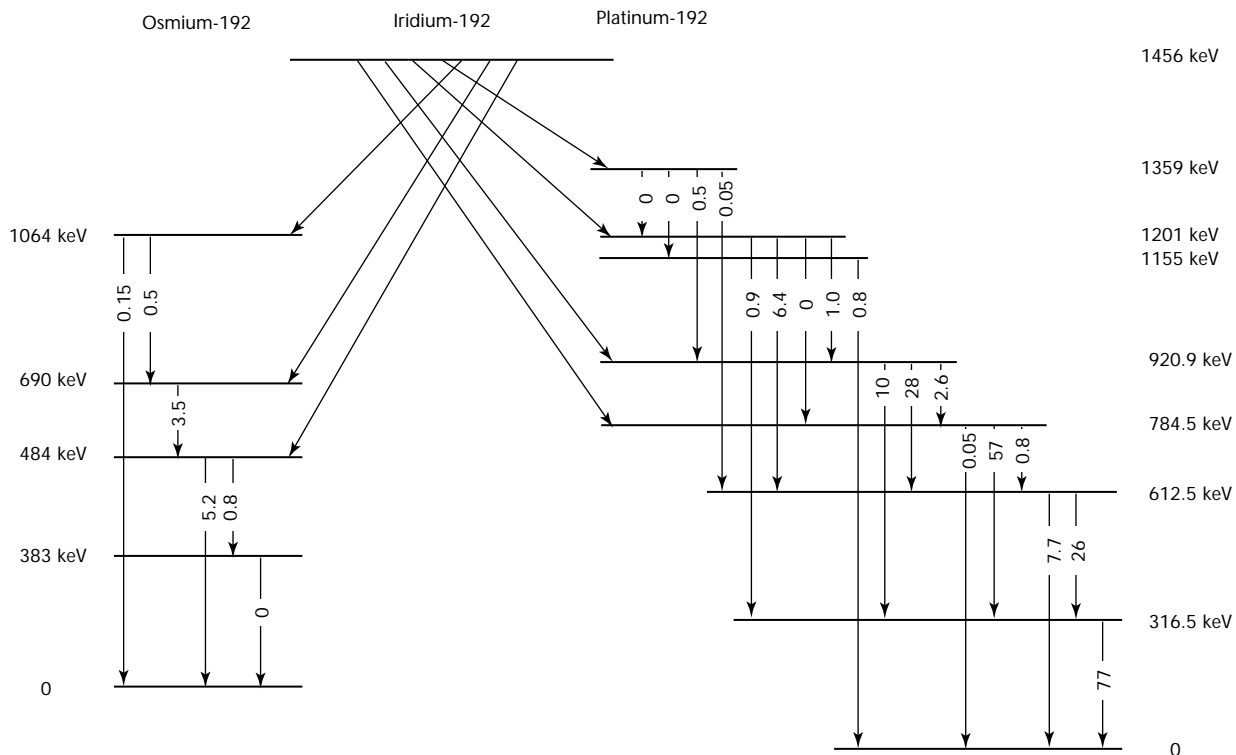
FIGURE 3. Disintegration of cesium-137, with half life of 31 years.



## Iridium-192

Iridium-192 provides a major part of the isotope radiography business. This is because of the 74.3 day half life that requires replacement of the source about every six months and because the gamma energies emitted by the source are useful for thin steel specimens that make up most of the industrial work. With an average energy of about 0.34 MeV (see Fig. 4 for the decay diagram of gamma rays actually emitted and Fig. 2c for gamma spectrum), the iridium-192 is used for the radiography of steel in the

FIGURE 4. Disintegration scheme of iridium-192. Numbers in arrows are numbers of gamma rays per 100 disintegrations.



thickness range of 3.2 to 76 mm (0.125 to 3.0 in.). Also, the low average energy of the photons requires little shielding and permits portable exposure devices weighing only 24 kg (53 lb). Useful radiographic sources of cobalt-60 or cesium-137 generally require wheels on the equipment for portability.

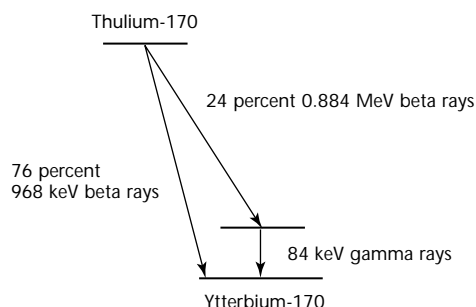
Iridium-192 is produced by neutron bombardment in a nuclear reactor. The iridium metal is a very hard, brittle, white metal of the platinum family with a density of  $22.4 \text{ g}\cdot\text{cm}^{-3}$  ( $1400 \text{ lb}_m\cdot\text{ft}^{-3}$ ) a melting point of  $2350^\circ\text{C}$  ( $4260^\circ\text{F}$ ) and a neutron cross section of  $10^{-25} \text{ m}^2$  for iridium-191. Natural iridium occurs as two isotopes, 38 percent iridium-191 and 62 percent iridium-193. Even with the 38 percent abundance, the high cross section results in most neutrons' being absorbed in the outer layers of the iridium target metal. Even with this severe self-absorption of neutrons, the wafers or pellets of iridium metal yield up to 925 GBq (25 Ci) from 2 mm diameter by 1 mm ( $0.08 \times 0.04$  in.) thick and up to 1850 GBq (50 Ci) from 3 mm diameter by 1 mm thick ( $0.12$  by  $0.04$  in.). These activities require about a six months bombardment at over  $10^{14}$  neutrons per  $1 \text{ cm}^2\cdot\text{s}^{-1}$  in a reactor. Such small sources approximate point sources to give good radiographic geometry.

Figure 2 contains the simplified gamma spectra for the following isotope sources: (a) cobalt-60, (b) cesium-137 and (c) iridium-192. Comparison of these spectra helps radiographers to understand the different uses of the isotopes that depend on the energies of the gamma rays emitted.

## Thulium-170

Thulium-170 replaces an X-ray machine in some industrial circumstances that would make the machine impractical. Such circumstances are uncommon but do exist.

FIGURE 5. Disintegration of thulium-170, with half life of 129 days.

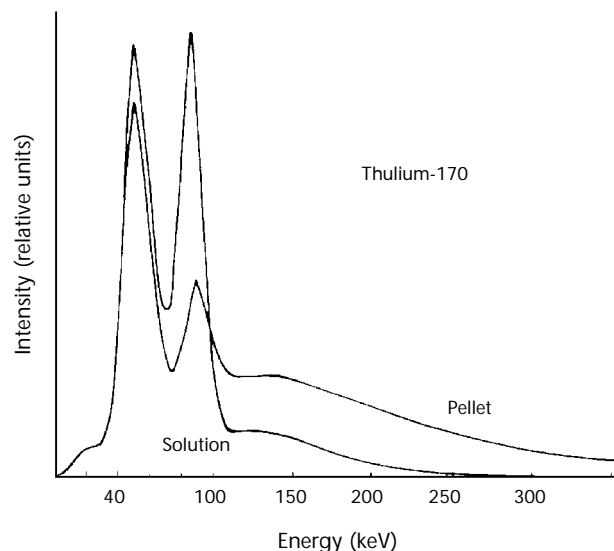


Thulium-170 decays with a half life of 129 days with the emission of a 1 MeV beta particle. In 24 percent of the disintegrations, the nucleus is left in an excited state, which becomes stable by either (1) the emission of an 84 keV gamma ray or (2) the internal conversion and ejection of an orbital electron. This decay is diagrammed in Fig. 5.

Further analysis of the decay of thulium-170 shows that 3.1 percent of the disintegrations result in the 84 keV gamma ray emission, 4.9 percent in ejection of a K shell orbital electron and 16 percent in ejection of an L shell electron or M shell electron ([see this volume's discussion of radiation and particle physics](#)). When these orbital electrons are replaced, the atom emits X-rays characteristic of ytterbium: 52 keV X-ray for the K shell, 7 keV for the L shell and 1 keV for the M shell. The lower energy photons are too weak to emerge from the source capsule. For radiographic purposes, the sources appear to produce about 3 percent of the 84 keV and 5 percent of the 52 keV radiation in the disintegrations of the thulium-170 nuclei. Two approximate spectra of the radiation from the thulium-170 are shown in Fig. 6 for pellet or solution forms.

The element thulium is chemically one of the rare earths, is physically a silver metal with a density of about  $9 \text{ g}\cdot\text{cm}^{-3}$  ( $560 \text{ lb}_m\cdot\text{ft}^{-3}$ ) and consists of the single isotope thulium-169. Because the metal is extremely difficult to produce, the material is generally handled as thulium(III) oxide ( $\text{Tm}_2\text{O}_3$ ), either as an encapsulated powder with a density of

FIGURE 6. Radiation emergent from 50 mg ( $1.76 \times 10^{-3} \text{ oz}_m$ ) thulium-170 source, compressed  $2 \times 2$  mm ( $0.08 \times 0.08$  in.), pellet in  $2 \text{ cm}^3$  ( $0.12 \text{ in.}^3$ ) solution.



about  $4 \text{ g}\cdot\text{cm}^{-3}$  ( $250 \text{ lb}_m\cdot\text{ft}^{-3}$ ) or sintered into pellets with a density of about  $7 \text{ g}\cdot\text{cm}^{-3}$  ( $440 \text{ lb}_m\cdot\text{ft}^{-3}$ ). The isotope thulium-169 has a thermal neutron cross section of  $1.2 \cdot 10^{-22} \text{ cm}^{-2}$  to produce thulium-170. No other comparable neutron reactions take place.

Source strengths of radiographic sources depend on the amount of thulium-169 irradiated in the reactor, the length of time in the reactor and the neutron flux at the site of the irradiation. An 18 weeks irradiation can yield 1.5 to 11 TBq (40 to 300 Ci) of thulium-170 from 150 mg of the oxide and slightly higher yields from metal pellets or wafers. Radiation yields are between 6 and  $56 \text{ nSv}\cdot\text{s}^{-1}$  (2 and  $20 \text{ mR}\cdot\text{h}^{-1}$ ) at 1.0 m (40 in.) from the source per 37 GBq (1 Ci). The gamma radiation intensity increases per curie as larger, more compacted source material is used. The enhanced 84 keV gamma comes at the expense of the 52 keV X-ray, which is decreased by larger, more dense source material. The thulium-170 sources approximate 600 keV X-ray machine radiation in radiographic quality because the energies are unique rather than white (all energies up to a maximum value) radiation.

Application of the thulium-170 sources includes radiography of a steel thickness as low as 0.8 mm (0.03 in.) or an aluminum thickness of 13 mm (0.5 in.) while achieving 2 percent radiographic sensitivity. It is useful for inspection of internal assemblies such as aerospace components and composite materials.

## Selenium-75

Selenium-75 has found limited use in Europe as a replacement for iridium-192. The selenium-75 has a longer half life of 120 days (versus iridium-192 at 74 days) and a lower gamma energy spectrum of 66 to 401 keV (versus iridium-192 at 206 to 612 keV with some even high gamma energies present). Besides providing a somewhat better image quality on thin specimens such as pipe, the exposure equipment is significantly lighter.<sup>2</sup>

## PART 2. Source Handling Equipment

### Encapsulation of Isotope Sources

All radiographic isotope sources must be encapsulated. This enclosure of the radioactive material in a welded shut stainless steel container prevents loss of the radioactive material to the environment when the source is exposed to make a radiograph. The radioactive materials always have tiny particles of loose source material coating their surface that are formed by oxidation or other processes. Without encapsulation, these particles can contaminate the environment with possible serious consequences. In most cases, the source will be double encapsulated. Double encapsulation means that after the radioactive material is sealed inside of a stainless steel capsule that is welded closed, that first capsule is sealed inside of another stainless steel capsule that is also welded closed.

After encapsulation according to the specifications for that source design (set up by the manufacturer under criteria established or approved by one or more of organizations such as the American National Standards Institute (ANSI), International Atomic Energy Agency (IAEA), International Organization for Standardization (ISO), Nuclear Regulatory Commission (NRC) and United States Department of Transportation.

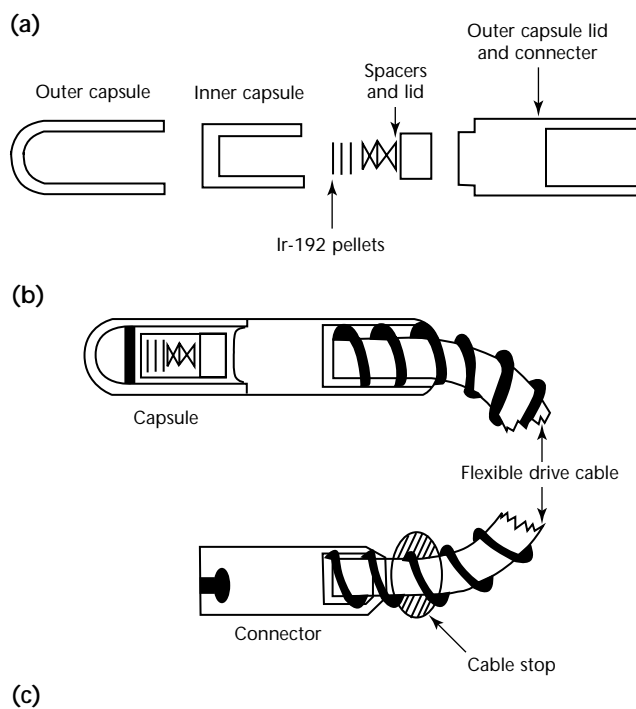
Diagrams and photographs of the capsules and their contents are featured in many manufacturers' brochures. Each capsule is tested for radioactive material leakage and for structural integrity. Each design and manufacturing technique is tested for leakage and serviceability.

The assembly and welding of the capsules occur in a special, shielded structure called a hot cell, which has thick, dense walls for radiation shielding and remote manipulators for handling the pieces in the high radiation environment. Windows in the hot cells are made of a special, high density glass. Often the windows have a dense, transparent aqueous solution of an inorganic salt, such as zinc bromide, held between the inside and outside layers of glass.

The capsule is attached to a flexible cable (pigtail) or fixed into a rotating cylinder for handling in an exposure

device by a radiographer. Figure 7 shows an idealized diagram of a double encapsulated source attached to a flexible connector to form a pigtail. This type of source holder is placed in American National Standards Institute Type I exposure devices and is discussed below.

FIGURE 7. Double encapsulated source with pigtail: (a) capsule; (b) diagram of pigtail; (c) drive cables and pigtail connectors made by different companies.



Type II devices with a rotating cylinder are discussed below, after the Type I devices.

## Exposure Devices

### ANSI Type I Exposure Devices

American National Standards Institute (ANSI) Type I exposure devices for radiography permit exposure of the source by moving it from a shielded position through a guide tube to a remote position outside the shield. Figures 8 to 11 present diagrams and photographs of exposure devices using drive cables operated by turning a hand held cranking device. In some of the diagrams, the source capsule and its attached pigtail can be seen.

The major parts of a Type I exposure device are (as can be seen in part in Fig. 8 and in more detail in Figs. 9a and 10b): (1) a rigid, wear resistant tube to guide the source pigtail through the shielding material; (2) shielding material (most often depleted uranium but tungsten may also be used for critical machined parts); (3) a metal case to protect and hold the shielding, guide tube and other components in a fixed position; (4) a lock to prevent accidental movement of the source out of the shielded position or its

removal from that end of the device; (5) connectors for the drive cable and crankout device to the pigtail end of the device and for a guide tube to the other end; (6) protectors for the connectors with one having a short flexible cable to prevent movement of the source out of that end of the device; and (7) a handle to carry the device and radiation, warning and information tags to identify the device and its hazardous nature.

The design of an exposure device for radiography shows great improvement and increase in safety for the radiographer and the public. Earliest techniques were

FIGURE 9. Exposure device for up to 7.4 TBq (200 Ci) of iridium-192: (a) cross section; (b) photograph.

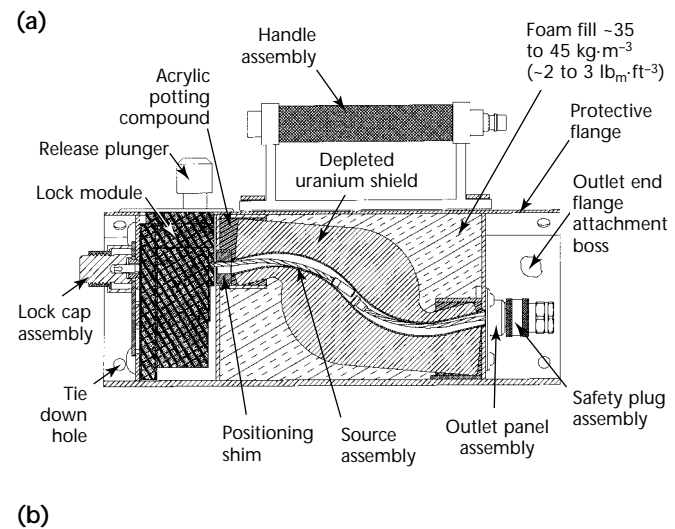
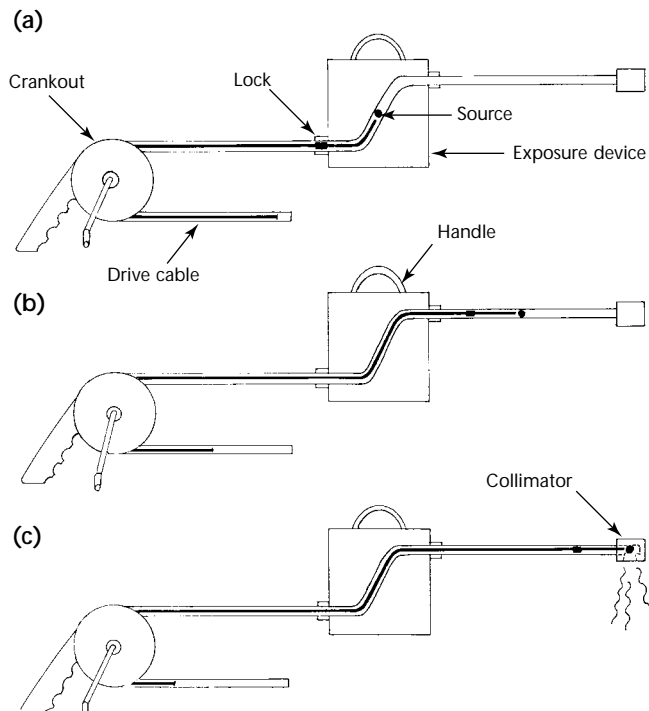


FIGURE 8. Operation of ANSI Type I source handling device: (a) stored position; (b) source in transit; (c) exposure position.





nothing more than bamboo poles with a string running from tip of the pole to the source. Shielding was completely ignored or just a lead bucket in the corner of the office. Now the design includes the features noted in the above list.

The tube inside of the shielding material is now a hard, wear resistant material such as titanium metal or zirconium alloy. This hardness keeps the tube from wearing out early because of movement of the drive cable for source exposure. Earlier materials wore away early in the life of an exposure device and exposed the shielding material. When the shielding material is depleted uranium, a worn out tube allows this radioactive material to be carried into the environment. Leak tests suggested that the encapsulated source was leaking.

Why use a radioactive material, depleted uranium, to shield a radiation source? The depleted uranium provides more shielding of the radiographic source per unit of mass than the original shielding material, lead. Also, most of the radiation from the uranium is alpha radiation and is stopped by the case of the device. A coating of paint prevents loss of the uranium from the shield just as an intact inner tube does.

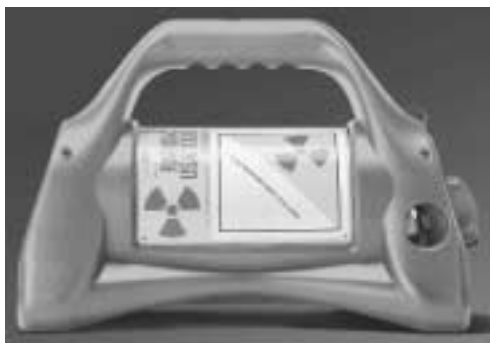
Depleted uranium is the uranium-238 that remains when the fissionable uranium-235 is removed for nuclear reactor fuel or nuclear weapon manufacture. The uranium-238 is 98.28 percent of the natural uranium and uranium-235 is only 0.72 percent so considerable uranium-238 remains after depletion of the uranium-235. This depleted uranium allows the exposure device to be carried by hand and be relatively portable with lower external radiation hazard than if the device were made from lead. Also, the uranium shield gives better protection from fire than lead shielding would. Commercial exposure devices do not use lead shielding. The uranium shield is generally cast around the inner tube ready to be fitted into the case without any machining. If machining is required, a piece of tungsten metal is machined and used with uranium to complete the necessary shielding.

The metal case protects the uranium shield from loss of the uranium and stops the alpha radiation from reaching the environment as long as the inner tube is intact. Also, the case protects the alignment of parts, the lock and connections from likely damage. The cases are made from heavy gage aluminum or stainless steel in most of the commercial devices available today. This is to prevent broken locks and connectors that might allow the source capsule to escape from the shielding accidentally.

All exposure devices require a locking device that uses a key. A regulatory requirement is that the lock cannot be opened unless the drive cable is attached to the pigtail. Often, this is accomplished by requiring a reverse cranking motion to release the lock. This prevents the source being moved out of the shield to the end of the guide tube without a good physical connection between the two. If the drive cable is not connected to the pigtail, the source could be driven to the end of the guide tube but not retrieved when the drive cable is returned. Several severe accidental overexposures have occurred in the past and the above regulatory requirement works to reduce such

FIGURE 10. Exposure device for up to 5.6 TBq (150 Ci) of iridium-192: (a) photograph; (b) diagram.

(a)



(b)

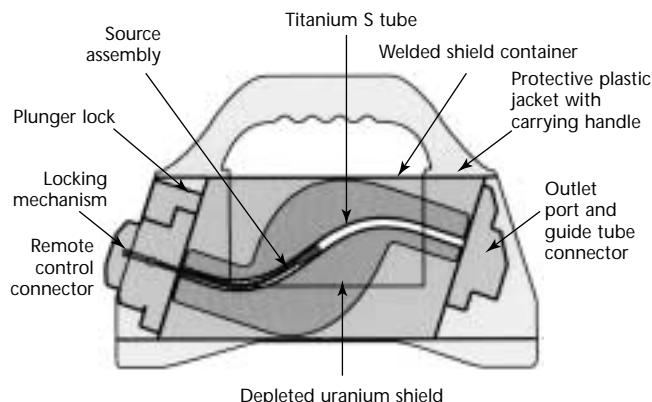


FIGURE 11. Exposure device with crankout and guide tube.



*disconnects* as they were called. Also, the lock should automatically lock the source in its stored position when it is returned to the shield. If the source is locked, it cannot be moved to an exposed position.

Special connectors, often of a proprietary design as shown in Fig. 7c (pig tails) permit the drive cable and guide tube to be connected to the exposure device. Connectors or protective caps, similar to those of the drive cable and guide tube, stay on the device to protect the connection to the lock and exit points and to prevent movement of the source from its shielded position. This is best seen in Fig. 9a.

The handle of the device may simply serve as a convenient handle for carrying the device and may also serve to store the protective connectors. In Figs. 9 to 11 can be seen the various radiation, warning and information tags that identify the device and potential hazards. One tag gives information for calling the proper authorities should the device be found when not in the direct custody of a radiographer.

The guide tube that carries the source from the shielded position in the exposure device to the place where radiographic exposure is made should meet applicable codes or specifications,

such as those in ANSI N43.9.<sup>3</sup> The end of the guide tube is a metal part that aligns the source for exposure. A collimator (Fig. 12) may be added to the end of the guide tube to reduce radiation in all directions except as needed for exposure of the radiograph. By reducing extraneous radiation, closer boundaries for exclusion of nonradiation workers may be set up making the radiographer's job much easier and more efficient.

Capacity of the exposure devices shown in Figs. 9 to 11 vary from about 4.4 to 5.5 TBq (120 to 150 Ci) of iridium-192. Regulations and design changes may alter these values at any time.

Cobalt-60 exposure devices are not so portable but they may be wheeled from place to place for exposures in the field. Movement of cobalt-60 exposure devices over a few yards generally requires cranes or other large lifting and transport equipment. Figure 13 shows two

MOVIE.  
Collimators.

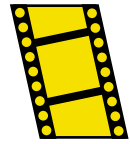
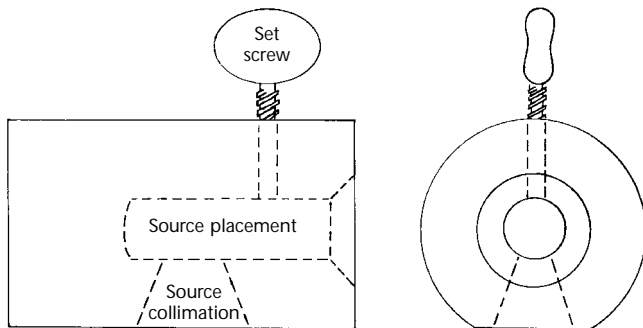


FIGURE 12. Guide tube collimators for reducing personnel exposure: (a) cross sections; (b) photographs.

(a)



(b)



FIGURE 13. Photographs of two American National Standards Institute Type I cobalt-60 exposure devices: (a) on two-wheeled dolly, for up to 9.25 TBq (250 Ci) of cobalt-60; (b) on four-wheeled dolly.

(a)



(b)



photographs of American National Standards Institute Type I cobalt-60 exposure devices available for field radiography. Capacity of these and similar devices ranges from 1.2 to 12.2 TBq (33 to 330 Ci).

### Source Exchanger Equipment

When short lived sources such as iridium-192 have decayed to an unusable level, a new source may be exchanged with the old source in the field (usually at the facilities of the exposure device's owner). Figure 14 shows a pair of photos an exposure device fitted with a short exchange tube and the closed exchanger showing (Fig. 14a) and the exposure device connected to the exchanger ready for source transfer from exchanger to the exposure device (Fig. 14b). Note the old, used source pigtail can be seen in the storage position on the left. The crankout handle and cable cannot be seen in the photo but are attached to the other end of the exposure device. Both the exposure device and the exchanger must be unlocked to make the source movements, first the old source into the exchanger and second the new source from the exchanger into the exposure device. Other designs are available to accomplish the same procedure.

### ANSI Type II Exposure Devices

One design representative of ANSI Type II exposure devices moves the source capsule from the storage position in the center of

the shield in the exposure device to a position on the outside surface of the shield (see Fig. 15). The 180 degree rotation of the eccentric cylinder carrying the source may be made manually (1) with a the operator remaining behind the exposure device shield relative to the aperture for the exposed source or (2) by turning a crank attached to the device by a metal drive cable. Again, the shield material is usually depleted uranium (uranium with almost all of the fissionable uranium-235 removed, leaving uranium-238).

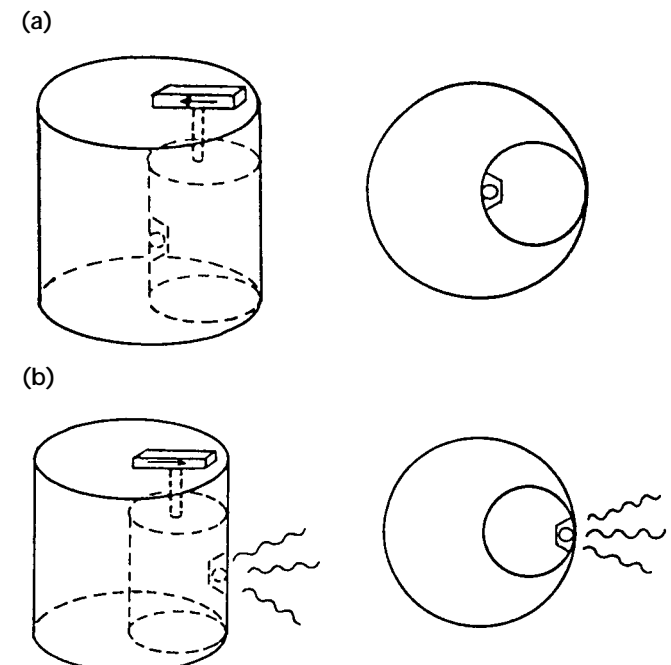
Depleted uranium offers more shielding per unit mass than similar shields made of lead. A lead shield for 100 Ci of iridium-192 might weigh over 30 kg (66 lb); a uranium shield would be closer to 20 kg (44 lb). The eccentric cylinder may be tungsten, which can be machined more easily than depleted uranium, or a precision cast uranium wheel or disk that is then attached to the rotation handle or knob.

Figure 16 shows a diagram and photograph of an American National Standards Institute Type II exposure device. Note that the device has a stainless steel housing with carrying handle. There is also a lock to prevent rotation of the source into an exposed position as well as indication on the *on/off* knob as to the position of the source. Such devices most often find use for radiography of piping and can carry as

FIGURE 14. Exposure device with source exchanger: (a) exchanger (left) closed, exposure device fitted with short exchange tube; (b) exchanger open and attached, ready for source transfer to exchanger (note source pigtail in storage position, on the left).



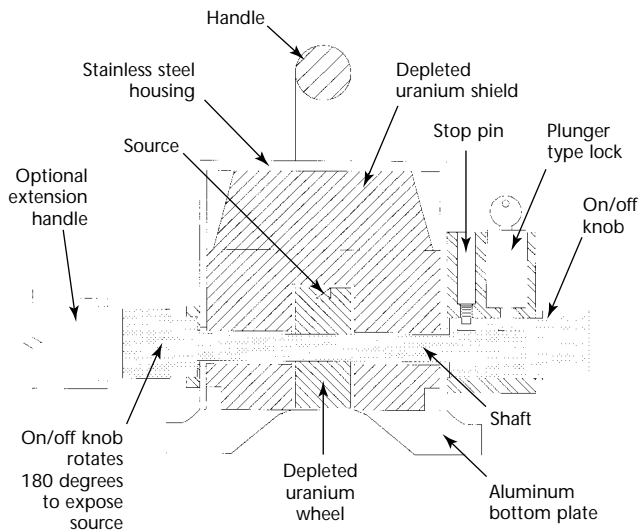
FIGURE 15. Diagram of one type of American National Standards Institute Type II exposure device: (a) source stored; (b) source exposed.



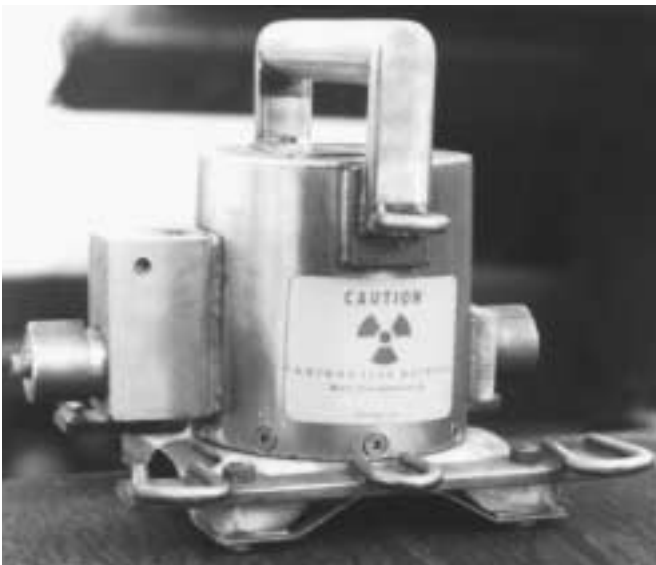
much as 3.7 TBq (100 Ci) of iridium-192. The manufacturer or other licensed company must do source replacements for American National Standards Institute Type II devices. The exchange of sources requires a hot cell for remote, shielded handling.

FIGURE 16. American National Standards Institute Type II exposure device; (a) diagram; (b) photograph.

(a)



(b)



# References

1. *Nondestructive Testing Handbook*, second edition: Vol. 3, *Radiography and Radiation Testing*. Columbus, OH: American Society for Nondestructive Testing (1985).
2. Ewert, U. and J. Stade. "Comparative Analysis of Image Quality from X-Ray Radiography and Gamma Radiography Using Selenium 75 and Iridium 192." *Materials Evaluation*. Vol. 57, No. 2. Columbus, OH: American Society for Nondestructive Testing (February 1999): p 117-121.
3. ANSI N43.9, *Gamma-Radiography — Specifications for Design and Testing Apparatus*. New York, NY: American National Standards Institute (1991).

## Bibliography

- Anderson, M.B. "Radiographic Sensitivity Data for the Isotopes Cobalt-60, Iridium-192, Cesium-137, Thulium-170 and Thorium-228." *Nondestructive Testing*. Vol. 17, No. 6. Columbus, OH: American Society for Nondestructive Testing (November-December 1959): p 365-370.
- Berger, H. "Nuclear Methods for NDT." *National Bureau of Standards in Instrumentation Technology*. Vol. 23, No. 8 (1976): p 45-50.
- Berman, A.I. "Radioactivity Units and Radiography." *Non-Destructive Testing*. Vol. 9, No. 2. Columbus, OH: American Society for Nondestructive Testing (Fall 1950): p 11-15.
- Blair, J.S. "Iron and Steel Works Applications of Radioactive Isotopes for Radiography." *Iron and Coal Trades Review*. Vol. 163. London, United Kingdom: Industrial Newspapers (1951): p 1349, 1405.
- Bokshpan, S. and D. Kedem. "Detection of Imperfections by Means of Narrow Beam Gamma Scattering." *Materials Evaluation*. Vol. 33, No. 10. Columbus, OH: American Society for Nondestructive Testing (October 1975): p 243.
- Clarke, E.T. "Investigation of Isotopes for Aircraft Radiography." Wright Air Development Center Technical Report; ASTIA Document No. AD 118224 (1957): p 56-440.
- Clack, B.N. "Natural and Artificial Sources for Gamma Radiography." *Engineer*. Vol. 194. London, United Kingdom: Office for Advertisements and Publication (1957): p 329.
- Cosh, T.A. "An Exposure Calculator for Isotope Radiography." *Journal of Scientific Instrumentation*. Vol. 34 (1957): p 329.
- Doan, G.E. and S.S. Yound. "Gamma-Ray Radiography." *ASME Proceedings*. Vol. 38, Pt. 2. New York, NY: American Society of Mechanical Engineers (1938): p 292.
- Evans, R.D. *The Atomic Nucleus*. New York: McGraw-Hill Book Company (1955).
- Evans, R.D. and R.O. Evans. "Studies of Self-Absorption in Gamma-Ray Sources." *Reviews of Modern Physics*. Vol. 20. Melville, NY: American Physical Society (1948): p 305.
- Faulkenberry, B.H., R.H. Johnson and C.E. Cole. "Radioautographs Show Quality of Panel Brazing." *Nucleonics*. Vol. 19, No. 4. New York, NY: McGraw-Hill (1961): p 126-130.
- Fletcher, L.S. "Radiographic Inspection Assures Good Welds in Providence Distribution Line." *Welding Engineer*. Vol. 38, No. 6. Chicago, IL: Jefferson Publications (June 1953): p 50-52.
- Frazier, P.M., C.R. Buchanan and G.W. Morgan. "Radiation Safety in Industrial Radiography with Radioisotopes." Report AECU 2967. Washington, DC: United States Atomic Energy Commission (1954).
- Gardner, R.P. and R.L. Ely, Jr. *Radioisotope Measurement Applications in Engineering*. New York, NY: Reinhold Publishing Corporation (1967).
- Gilbert, E. "Applications of Nondestructive Testing in the Petroleum Industry." *Nondestructive Testing*. Vol. 21, No. 4. Columbus, OH: American Society for Nondestructive Testing (July-August 1963): p 235-237.
- Goldstein, H. and J.E. Wilkins, Jr. "Calculation of Penetration of Gamma Rays." Report NYO-3075. Washington, DC: United States Atomic Energy Commission (1954).



- Halmshaw, R. "The Factors Involved in an Assessment of Radiographic Definition." *Journal of Photographic Science*. Vol. 3. Bury Saint Edmunds, Suffolk, United Kingdom: Professional Engineering Publishing, for the Royal Photographic Society (1955): p 161.
- Handbook on Radiography*, revised edition. Ottawa: Atomic Energy of Canada, Ltd. (1950).
- Harrington, E.L., H.E Johns, A.P. Wiles and C. Garrett. "The Fundamental Action of Intensifying Screens in Gamma Radiography." *Canadian Journal of Research*. Vol. 28. Boucherville, Canada: National Research Council (1948): p 540.
- Iddings, F.A. "Editorial" [Back to Basics]. *Materials Evaluation*. Vol. 37, No. 11. Columbus, OH: American Society for Nondestructive Testing (October 1979): p 20.
- "Interpreting Weld Radiographs." *Welding Engineer*. Vol. 56, No. 6. Chicago, IL: Jefferson Publications (June 1976).
- Karrer, C.A. "Safe and Economical Use of Isotopes in the Steel Industry." *Nondestructive Testing*. Vol. 13, No. 2. Columbus, OH: American Society for Nondestructive Testing (March-April 1955): p 29-31.
- Kiehle, W.D. "Radiography." *Nondestructive Testing*. Vol. 16, No. 4. Columbus, OH: American Society for Nondestructive Testing (July-August 1958): p 313-318.
- Landalt, J.F. "A Technique for Placing Known Defects in Weldments." *Materials Evaluation*. Vol. 31, No. 10. Columbus, OH: American Society for Nondestructive Testing (October 1973): p 214-216.
- Mehl, R.F. "How Gamma Ray Radiography Came About" [1971 Mehl Honor Lecture]. *Materials Evaluation*. Vol. 30, No. 3. Columbus, OH: American Society for Nondestructive Testing (March 1972): p 17A-19A.
- Memorandum on Gamma-Ray Sources for Radiography*, revised edition. London, United Kingdom: Institute of Physics (1954).
- "Methods and Limitations for In Service Inspection of Nuclear Power Plant." *Nuclear Engineering International*. London, United Kingdom: Heywood-Temple Industrial Publications Limited (October 1976): p 61-64.
- O'Connor, D.T. and E.L. Criscuolo. "The Quality of Radiographic Inspection." *ASTM Bulletin*. No. 213. West Conshohocken, PA: ASTM International (1956): p 53.
- Polansky, D., D.P. Case and E.L. Criscuolo. "The Investigation of Radioisotopes for the Inspection of Ship Welds." *Nondestructive Testing*. Vol. 17, No. 1. Columbus, OH: American Society for Nondestructive Testing (1959): p 21.
- "Radiographic Inspection — An Adaptable Tool." *Quality Progress*. Vol. 7, No. 6. Milwaukee, WI: American Society for Quality (June 1974): p 10-11.
- Radiography in Modern Industry*, third edition. Rochester, NY: Eastman Kodak Company (1969).
- Radioisotope Techniques*. Vol. 2. London: Her Majesty's Stationery Office (1952).
- Reiffel, L. "Beta-Ray Excited Low-Energy X-Ray Sources." *Nucleonics*. Vol. 13, No. 3. New York, NY: McGraw-Hill (1955): p 22.
- Richardson, H.D. *Industrial Radiography Manual*. Catalog Number FS 5.284:84036. Washington, DC: Superintendent of Documents (March 1968).
- Rummel, W.D. and B.E. Gregory. "'Ghost Lack of Fusion' in Aluminum Alloy Butt Fusion Welds." *Materials Evaluation*. Vol. 23, No. 12. Columbus, OH: American Society for Nondestructive Testing (December 1965): p 586-588.
- "Take a Look at Nuclear Gages." *Instrumentation and Control Systems*. Vol. 49. Radnor, PA: Chilton Company (December 1976): p 41-44.

## Cesium-137

- Dutli, J.W. and G.M. Taylor. "Application of Cesium 137 to Industrial Radiography." *Nondestructive Testing*. Vol. 12, No. 2. Columbus, OH: American Society for Nondestructive Testing (March-April 1954): p 35-38.
- Dutli, J.W. and D.E. Elliott. "The Application of Cesium-134 to Industrial Radiography." *Nondestructive Testing*. Vol. 14, No. 2. Columbus, OH: American Society for Nondestructive Testing (March-April 1956): p 24-27.
- Rhoten, M.L. "Cesium-137 As a Versatile Radiographic Tool." *Nondestructive Testing*. Vol. 16, No. 3. Columbus, OH: American Society for Nondestructive Testing (May-June 1958): p 261-264.
- Thompson, J.M. and P.A. Glenn. "Cesium Radioisotope — New Tool for Parts Inspection." *Iron Age*. Vol. 172, No. 11. Newton, MA: Cahners Business Information, Division of Reed Elsevier (1953): p 174.

## Cobalt-60

- "Exposures for Cobalt-60 Radiography of Steel." *Metals Progress*. Vol. 58. Materials Park, OH: ASM International (1950): p 80.



- Hile, J. "Automatic Radiography with Cobalt-60." *Materials and Methods*. Vol. 40. New York, NY: Reinhold Publishing Corporation (1954): p 108.
- Isenburger, H.R. "Exposure Charts for Cobalt-60 Radiography." *Modern Castings [American Foundryman]*. Vol. 18. Des Plaines, IL: American Foundrymen's Society (1950): p 48.
- Kastner, J. "Units Used in Industrial Radiography to Describe Strength of Cobalt-60 Sources." *Nondestructive Testing*. Vol. 11, No. 1. Columbus, OH: American Society for Nondestructive Testing (Fall 1952): p 21-23.
- "Material Required to Carry Out Radiography with Cobalt-60 or Radium." Report 2008. Boucherville, Canada: National Research Council (1949).
- Morrison, A. "Radiography with Cobalt-60." *Nondestructive Testing*. Vol. 9, No. 4. Columbus, OH: American Society for Nondestructive Testing (1951): p 14.
- Nir-El, Y. "Accurate Calibration of a Co-60 Gamma Radiographic Source." *Materials Evaluation*. Vol. 54, No. 2. Columbus, OH: American Society for Nondestructive Testing (February 1996): p 138-139.
- O'Conner, D.T. and J.J. Hirschfield. "Some Aspects of Cobalt Radiography." *Nondestructive Testing*. Vol. 10, No. 1. Columbus, OH: American Society for Nondestructive Testing (Summer 1951): p 33-39. Errata, Vol. 11, No. 1 (Summer 1952): p 34.
- "Radiography with Cobalt-60." *Nucleonics*. Vol. 5, No. 6. New York, NY: McGraw-Hill (1949).
- Reed, M.E. *Cobalt-60 Radiography in Industry*. Boston, MA: Tracerlab Incorporated (1954).
- Schwinn, W.L. *Economics and Practical Applications of Cobalt-60 in Radiographic Inspection of Steel Weldments*. ASME Special Technical Publication 112. New York, NY: American Society of Mechanical Engineers (1951): p 112.
- Landauer, R.S., Jr., and E.T. Clarke. "Field Determination of Output and Effective Size of Iridium-192 Radiographic Sources." *Materials Evaluation*. Vol. 37, No. 12. Columbus, OH: American Society for Nondestructive Testing (November 1979): p 35-37.
- Larabie, P. "Iridium-192 Production." *Materials Evaluation*. Vol. 50, No. 9. Columbus, OH: American Society for Nondestructive Testing (September 1992): p 1022-1023, 1025-1026.
- Morrison, A. "Iridium 192 for Gamma-Ray Radiography." *Nondestructive Testing*. Vol. 10, No. 1. Columbus, OH: American Society for Nondestructive Testing (Summer 1951): p 26-28.
- Munro, J.J. "Calculation of Scattered Radiation Intensities of 192 Iridium Gamma Rays from a Steel Slab." *Materials Evaluation*. Vol. 35, No. 2. Columbus, OH: American Society for Nondestructive (February 1977): p 51-53.
- Rigby, J.V. and C.F. Baxter. "Iridium-192 in Industrial Radiography." *Nondestructive Testing*. Vol. 11, No. 1. Columbus, OH: American Society for Nondestructive Testing (Fall 1952): p 34-40.
- Ritz, V.H. "Broad and Narrow Beam Attenuation of Iridium-192 Gamma Rays in Concrete, Steel and Lead." *Nondestructive Testing*. Vol. 16, No. 3. Columbus, OH: American Society for Nondestructive Testing (1958): p 269.
- Wolf, R.V. and K.P.W. Wolf. "An Investigation of the Application of Iridium 192 Gamma Radiation to the Radiography of Light Metal Castings." *Nondestructive Testing*. Vol. 12, No. 1. Columbus, OH: American Society for Nondestructive Testing (January-February 1954): p 26-29.
- Yeomans, C. and S. Bellanca. "Iridium-192 Proves Useful Inspection Tool in the Aircraft Industry." *Nondestructive Testing*. Vol. 14, No. 4. Columbus, OH: American Society for Nondestructive Testing (July-August 1956): p 32, 34.

## Iridium-192

- Halmshaw, R. "Use and Scope of Iridium-192 for the Radiography of Steel." *British Journal of Applied Physics*. Vol. 5. London, United Kingdom: Institute of Physics (1954): p 238.
- Johns, M.W. and S.V. Nablo. "Disintegration of Iridium 192 and Iridium 194." *Physics Review*. Vol. 96, No. 6. Melville, NY: American Physical Society (1954): p 1599-1607.

## Selenium-75

- Grimm, R. and J.J. Munro III. "Gamma Radiography Using the Radioisotope Selenium 75 in the Chemical and Petroleum Industry." *ASNT's International Chemical and Petroleum Industrial Inspection Technology (ICPIIT) IV Topical Conference* [Houston, TX]. Columbus, OH: American Society for Nondestructive Testing (June 1995): p 51-53.

McCutcheon, D. "Experimental Work Employing Radioisotopes Cobalt and Selenium." *Non-Destructive Testing*. Vol. 7, No. 3. Columbus, OH: American Society for Nondestructive Testing (Winter 1948-49): p 7-14.

### Thallium-204

Kereiakes, J.G. and G.R. Kraft. "Thallium-204 X-Radiography." *Nondestructive Testing*. Vol. 16, No. 6. Columbus, OH: American Society for Nondestructive Testing (1958): p 490.

### Thulium-170

Carpenter, A.W. "Complete Portable Field X-Ray Unit." Army Medical Research Laboratories Report No. 168 (1954).

Clarke, E.T. "Gamma Radiography of Light Metals." *Nondestructive Testing*. Vol. 16. Columbus, OH: American Society for Nondestructive Testing (1958): p 265.

Graham, R.L., J.L. Wolfson and R.E. Bell. "The Disintegration of Thulium-170." *Canadian Journal of Physics*. Vol. 30. Boucherville, Canada: National Research Council (1952): p 459.

Halmshaw, R. "Thulium-170 for Industrial Radiography." *British Journal of Applied Physics*. Vol. 6. London, United Kingdom: Institute of Physics (1955): p 8.

West, R. "Low-Energy Gamma Ray Sources." *Nucleonics*. Vol. 11, No. 2. New York, NY: McGraw-Hill (1953): p 20.

### Radium

"Exposures for Radium Radiography of Steel." *Metals Progress*. Vol. 57. Materials Park, OH: ASM International (1950): p 780.

Gezelius, R.A. and C.W. Briggs. *Radium for Industrial Radiography*. New York, NY: Radium Chemical Co., Inc. (1946).

Johns, H.E. and C. Garrett. "Sensitivity and Exposure Graphs for Radium Radiography." *Nondestructive Testing*. Vol. 8, No. 3. Columbus, OH: American Society for Nondestructive Testing (Winter 1949-50): p 16-25.

Kahn, N.A., E.A. Imbembo and J. Bland. *A Universal Exposure Calculator for Radium Radiography and Its Application to Current Radiographic Films and Techniques*. ASME Special Technical Publication 96. New York, NY: American Society of Mechanical Engineers (1950).

*Radiological Health Handbook*, revised edition. PB 121784R. Washington, DC: United States Department of Health, Education and Welfare (1960).

Morrison, A. and E.M. Nodwell. "Radium Radiography of Thin Steel Section." *ASTM Bulletin*. No. 127. West Conshohocken, PA: ASTM International (1944): p 29.

### Radon

Morrison, A. "Use of Radon for Industrial Radiography." *Nondestructive Testing*. Vol. 6, No. 2. Columbus, OH: American Society for Nondestructive Testing (Fall 1947): p 24-26.

Pullin, V.E. "Radon, Its Place in Nondestructive Testing." *Welding*. Vol. 18. London, United Kingdom: Institute of Welding (1950): p 166.



# 5

## C H A P T E R

# Radiation Measurement<sup>1</sup>

---

Frank A. Iddings, San Antonio, Texas

William B. Rivkin, Highland Park, Illinois

Gerald C. Wicks, Durham, North Carolina

# PART 1. Principles of Radiation Measurement

Emissions from radioactive nuclei and radiation from that portion of the electromagnetic spectrum beyond the ultraviolet energies can cause the ionization of atoms and molecules.

Ionizing radiation occurs as three forms: (1) charged particles such as alpha particles, beta particles and protons, (2) uncharged particles such as neutrons and (3) electromagnetic radiation in the form of X-rays and gamma rays.

## Radiation Detection Systems

Some forms of radiation, such as light and heat, can be detected by human sense organs; ionizing radiation, however, can be detected only by the aftereffect of its ionizing properties. If ionizing radiation does not interact with matter, its detection and measurement is impossible. For this reason, the detection process uses substances that respond to radiation, as part of a system for measuring the extent of that response.

The ionization process is used by a large class of detection systems, including ion chambers, proportional chambers, geiger-müller counters and semiconductor devices (Table 1).

Some systems depend on the excitation and molecular dissociation that occur with ionization. These processes are useful in scintillation counters and chemical dosimeters. Although other types of detection systems exist, they are not generally used in radiation survey instruments.

## Radiation Detection for Safety

Several widely used technologies for personnel dosimetry are discussed in the [chapter on radiation safety](#).

TABLE 1. Effect of detected and measured ionization.

Effect	Type of Instrument	Detector
Electrical	ionization chamber	gas
Electrical	proportional counter	gas
Electrical	geiger müller counter	gas
Electrical	solid state	semiconductor
Chemical	film emulsion	photographic
Chemical	chemical dosimeter	solid or liquid
Light	scintillation counter	crystal or liquid
Light	cerenkov counter	crystal or liquid
Thermoluminescence	dosimeter	crystal
Heat	calorimeter	solid or liquid

## PART 2. Ion Chambers and Proportional Counters

### Principles of Ionization

The mechanism most widely used in radiation survey applications is the ionization principle: charged particles producing ion pairs by direct interaction. These charged particles may (1) collide with electrons and remove them from their atoms or (2) transfer energy to an electron by the interaction of their electric fields (Fig. 1). If the energy transfer is not sufficient to completely remove an electron, the atom is left in a disturbed or excited state.

Gamma and X-ray photons interact with matter mainly by photoelectric absorption, Compton scattering and pair production, each of which produces electrons and ions that may be collected and measured. The average energy expended in the creation of an ion pair, in air and most gases, is about 34 eV.

The number of ion pairs produced per unit of path length is called specific ionization. Specific ionization is affected by the energy of the particle or photon by its change and by the nature of the ionized substance.

### Ionization Chambers

In an ionization chamber, an electric field is applied across a volume of gas, between two electrodes. Often the chamber's

geometry is cylindrical, a cylindrical cathode enclosing the gas and an axial, insulated rod anode (Fig. 2).

Charged particles, photons or both pass through the chamber and ionize the enclosed gas. When an electric field is applied to the gas, ions drift along the electrical lines of force to produce an ionization current. Under normal conditions, electrons drift at speeds of about  $10^4 \text{ m}\cdot\text{s}^{-1}$  (22 000  $\text{mi}\cdot\text{h}^{-1}$ ). The drift velocity of positive ions is many orders of magnitude less.

When the electric field is increased slightly from zero and a detector is placed in the constant radiation field the collected ions still will be few in number because many recombine. As the voltage is further increased, recombination yields to ionization, where all ions are collected (Fig. 3).

FIGURE 2. Basic ionization chamber with high value resistance  $R$  and voltage  $V$ .

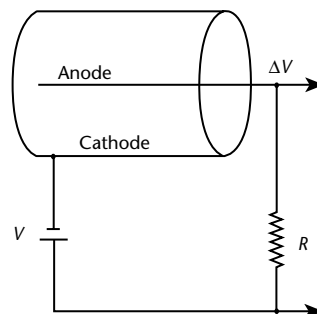


FIGURE 1. Ion pair (showing ejected electron and vacancy in electron orbit of atom).

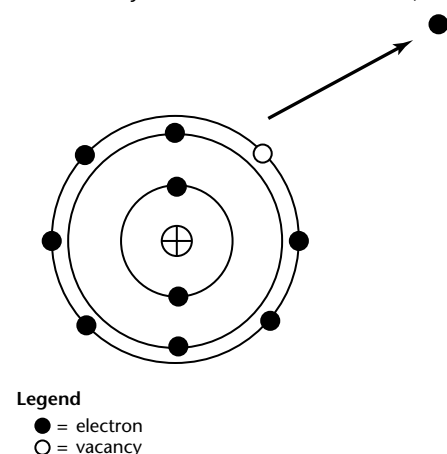
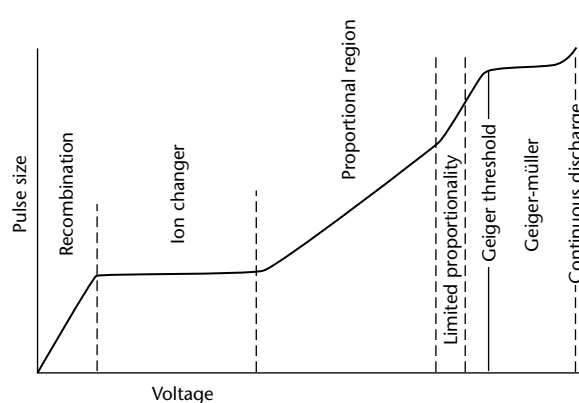


FIGURE 3. Pulse size as function of voltage in gas ion chamber.



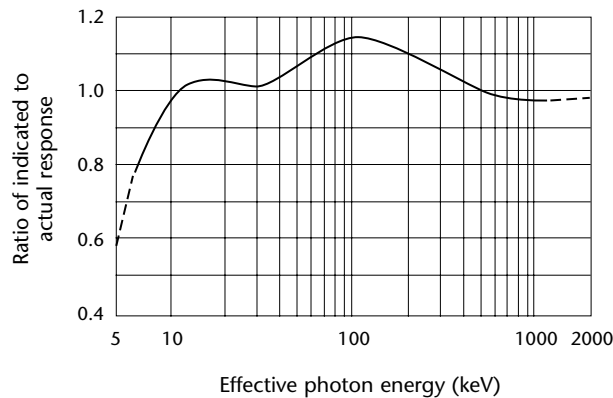
Ion current chambers have a response magnitude proportional to the absorbed energy and are therefore widely used for making dose measurements. When (1) recombination is negligible, (2) gas amplification does not occur and (3) all other charges are efficiently collected, then the steady state current produced is an accurate measurement of the rate at which ion pairs are formed within the gas. Measurement of this ionization current is the principle behind the direct current ion chamber.

Ion chambers may be constructed of several different materials and, because

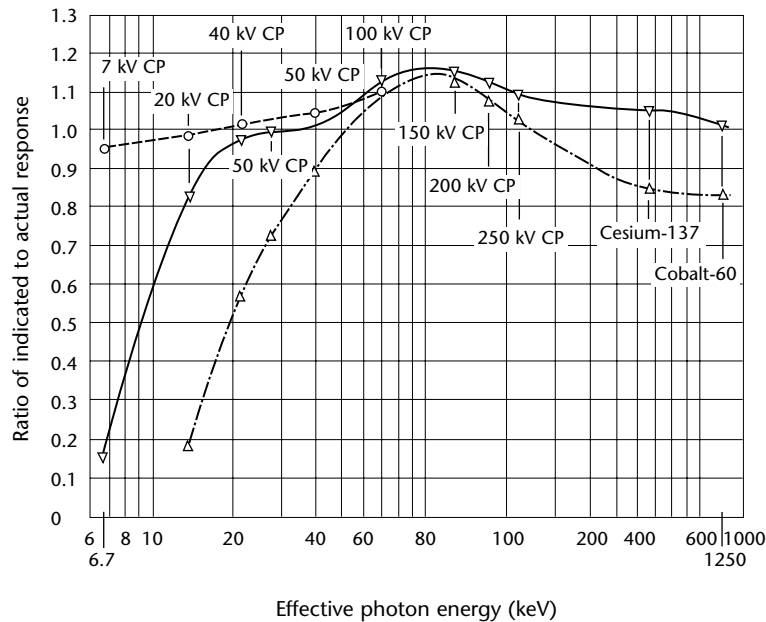
radiation must penetrate the wall of the chamber to ionize the gas volume, chambers are chosen for the specific radiation energy being evaluated. When considering a particular instrument the energy response curve should always be consulted (Fig. 4). Some instruments may also have an angular dependence (more sensitivity in some directions), which should also be considered when making measurements. Radio frequency shielded ionization chambers are available for measurements made near high level radio frequency sources.

**FIGURE 4.** Energy and directional response of typical ion chamber survey meters: (a) example of response curve; (b) comparison of several response curves.

(a)



(b)



**Legend**

- = Parallel to long axis, cap on
- ▽ = Parallel to long axis, cap off
- Δ = Perpendicular to long axis
- CP = constant potential



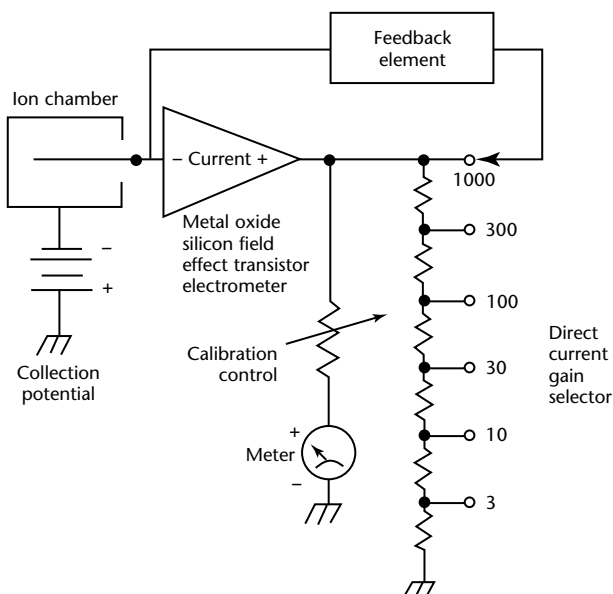
## Output Current Measurements

The ionization current collected in the ion chamber flows through an external circuit for measurement. Although in principle an ammeter could be placed in the external circuit to read the ion current, in practice the ammeter is not placed there, for the current is very small. A 440 cm<sup>3</sup> (27 in.<sup>3</sup>) ion chamber typically produces about  $4 \times 10^{-15}$  A·μSv<sup>-1</sup> ( $4 \times 10^{-14}$  A·mR<sup>-1</sup>) at standard temperature and pressure. A high valued load resistor (on the order of  $10^{10}$  Ω) is placed in the circuit and the voltage drop across the resistor is measured with a sensitive electrometer. A metal oxide silicon field effect transistor (MOSFET) is used in some electrometers. The metal oxide silicon field effect transistor produces an input impedance on the order of  $10^{15}$  Ω to amplify the collected current (Fig. 5).

## Vibrating Reed Electrometers

An alternative approach to ion current measurement is to convert the signal from direct current to alternating current at an early stage. This allows a more stable amplification of the alternating current signal in subsequent operations. The conversion is accomplished in a dynamic capacitor or vibrating reed electrometer, by collecting the ion current across a resistive capacitive circuit. The capacitance is then changed rapidly,

FIGURE 5. Operational configuration of current amplifier.



compared to the time constant of the circuit. The induced alternating current voltage is proportional to the ionization current (Fig. 6).

## Integrating Instruments

The instruments described above (Fig. 7) are generally rate meters; that is, they indicate the radiation at the time of exposure and, depending on its time constant, will return to background levels as the source is removed.

Some instruments may have an integration switch that introduces a capacitor to the circuit to accumulate the charge. Leaving such an instrument at an operator's location will indicate the total amount of ionizing radiation that area has received, from the time the instrument is engaged.

## Personnel Monitoring Instruments

### Pocket Chambers

Personnel monitoring instruments, some the size of a ball point pen, are usually

FIGURE 6. Principle of vibrating reed electrometer; oscillations of capacitance induce alternating current voltage proportional to steady state signal current.

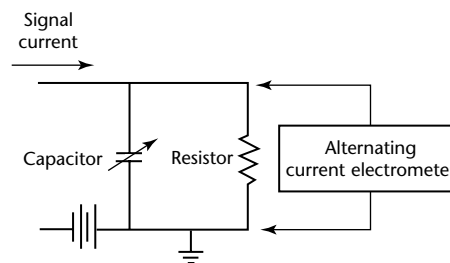
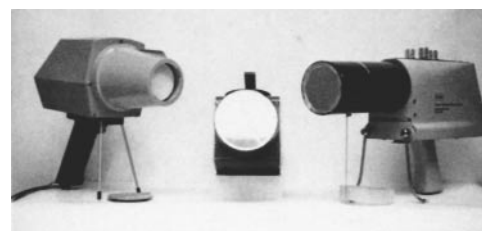


FIGURE 7. Examples of ionization chambers located externally on survey instruments. Protective caps are removed, showing thin windows for low energy X-ray or beta detection.



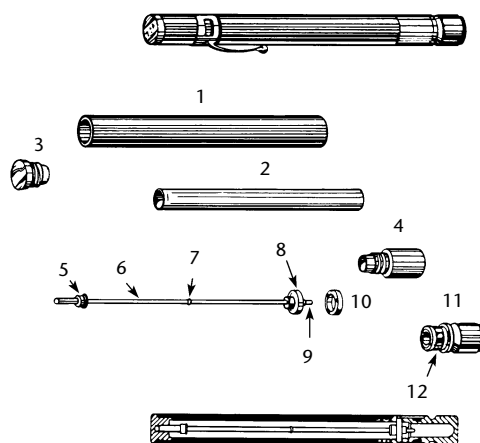
the integrating type and contain an ionization chamber. One version, the pocket chamber, requires the application of an initial charge of 150 to 200 V by an external instrument. Zero dose is then indicated on a scale contained in the charging unit. Exposure of the chamber to ionization decreases the initial charge. When the chamber is reconnected to the charging unit the reduced charge is translated to the level of exposure (Fig. 8).

### Direct Reading Dosimeters

The direct reading dosimeter operates on the principle of the gold leaf electroscope (Fig. 9). A quartz fiber is displaced electrostatically by charging it to a potential of about 200 V. An image of the fiber is focused on a scale and viewed through a lens at one end of the instrument. Radiation exposure of the dosimeter discharges the fiber, allowing it to return to its original position. Personnel dosimeters may have a full scale reading of 1 to 50 mSv (100 mR to 5 R) and may have other scales according to applicable regulations.

Chambers are available with thin walls for sensitivity to beta radiation over 1 MeV and may be coated on the inside with boron for neutron sensitivity.

**FIGURE 8.** Cross section of quartz fiber pocket dosimeter.



#### Legend

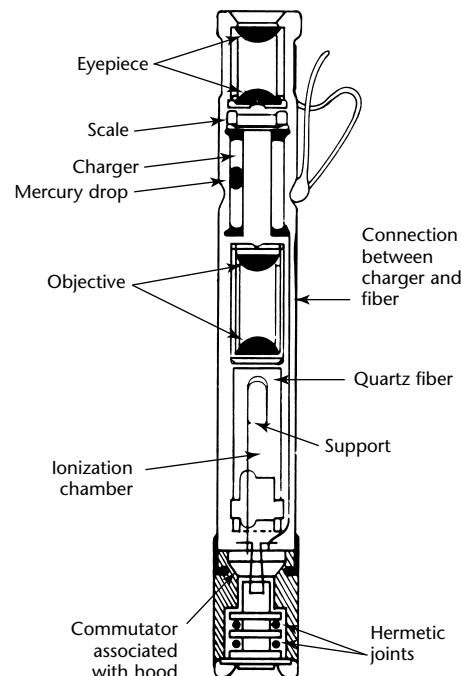
1. Low atomic number wall
2. Graphite coated paper shell
3. Aluminum terminal head
4. Aluminum terminal sleeve
5. Polystyrene support bushing
6. Central electrode, graphite coated
7. Polyethylene insulating washer
8. Polystyrene fixed bushing
9. Electrode contact
10. Retaining ring
11. Aluminum base cap
12. Polyethylene friction bushing

Figure 10 demonstrates the energy response of self-reading pocket dosimeters. Table 2 lists performance specifications of dosimeters in general.<sup>2</sup>

### Proportional Counters

If the electric field in an ion chamber is raised above the ionization potential but below saturation potential, enough energy is imparted to the ions for production of secondary electrons by collision and gas amplification.

**FIGURE 9.** Cross section of pocket (direct reading) ionization chamber.



**FIGURE 10.** Energy dependence of response of different commercial self-reading dosimeters.

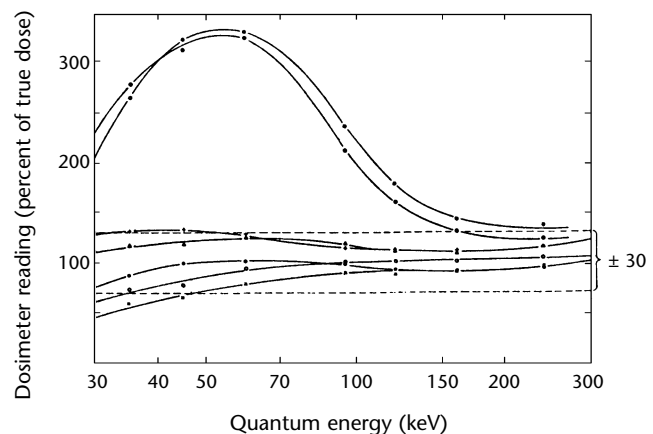


**TABLE 2. General performance specifications for dosimeters.<sup>2</sup>**

Characteristic	Performance Specification
Accuracy	±12 percent at 95 percent confidence
Energy dependence	±10 percent over given range
Sensitivity adjustment	sealed
Exterior surface	smooth
Ruggedness	withstands drop of 1.2 m (4 ft)
Temperature	+50 to -10 °C (+122 to +14 °F)
Humidity	0 to 90 percent
Discharge	no more than 2 percent of full scale in 24 h
Angular dependence	more than 70 percent at angles greater than 50 degrees from direction of maximum response

Operation at this electric potential overcomes the difficulty of the small currents in the ionization region yet takes advantage of pulse size dependence for separating various ionizing energies. When an ionization chamber is operated in this region it is called a proportional counter.

The size of the output pulse is determined by, and proportional to, the number of electrons collected at the anode and the voltage applied at the detector. By careful selection of gases and voltages, a properly designed proportional counter can detect alphas in the presence of betas, or higher energy beta and gamma radiation in the presence of lower energies. Proportional counters are often used in X-ray diffraction applications.

## PART 3. Geiger-Müller Counters

### Operating Voltage Level

Increasing voltage beyond the proportional region (Fig. 3) will eventually cause the gas avalanche to extend along the entire length of the anode wire. When this happens, the end of the proportional region is reached and the geiger-müller region begins.

An instrument operating in this voltage range, using a sealed gas filled detector, is referred to as a *geiger-müller counter*, a *GM counter* or simply a *geiger tube*. This instrument was introduced in 1928 and its simplicity and low cost have made it the most popular radiation detector since then. Geiger-müller counters complement the ion chamber and proportional counter and comprise the third category of gas filled detectors based on ionization.

### Properties

Extension of the gas avalanche increases the gas amplification factors so that  $10^9$  to  $10^{10}$  ion pairs are formed in the discharge. This results in an output pulse large enough (0.25 to 10 V) to require no sophisticated electronic amplification circuitry for readout. At this voltage, the size of all pulses, regardless of the nature of the ionization, is the same.

When operated in the geiger-müller region, a counter cannot distinguish among the several types of radiation and therefore is not useful for spectroscopy or for the detection of one energy event in the presence of another. An external shield is often used to filter out alpha and beta particles in the presence of gamma energies.

### Resolving Time

As an ionizing event occurs in the counter, the avalanche of ions paralyzes the counter. The counter is then incapable of responding to another event until the discharge dissipates and proper potential is established. The time it takes to reestablish the electric field intensity is referred to as the resolving time. Average resolving time for a geiger-müller counter

is about 100 ms, which must be corrected at high level readings.

Resolving time  $\tau$  of a counter may be determined by counting two sources independently ( $R_1$  and  $R_2$ ), then together ( $R_{1,2}$ ). The background count is  $R_b$ .

$$(1) \quad \tau = \frac{R_1 + R_2 - R_{1,2} - R_b}{R_{1,2}^2 - R_1^2 - R_2^2}$$

Correct counting rate  $R$  can be calculated from observed counting rate  $R_o$  and resolving time  $\tau$  in the following equation for nonparalyzable systems:

$$(2) \quad R = \frac{R_o}{1 - R_o \tau}$$

### Dead Time

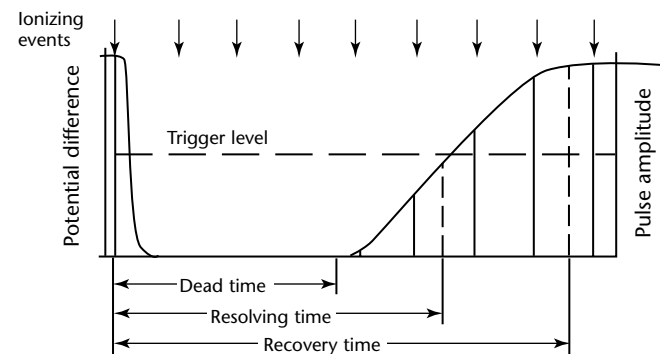
The relationship of resolving time to dead time and recovery is illustrated in Fig. 11. Resolving time may be a function of the detector alone or of the detector and its signal processing electronics. Its effect on the real counting rate depends on whether the system design is paralyzable or nonparalyzable.

### Nonparalyzable Systems

In Fig. 12, a time scale is shown indicating six randomly spaced events in the detector.<sup>3</sup>

At the bottom of the illustration is the corresponding dead time behavior of a

FIGURE 11. Resolving time, dead time and recovery time for geiger-müller system.



detector assumed to be nonparalyzable. A fixed time  $\tau$  follows each event that occurs during the live period of the detector. Events occurring during the dead time have no effect on the detector, which would record four counts from the six interactions.

### Paralyzable Systems

The top line of Fig. 12 illustrates a paralyzable system. Resolving time  $\tau$  follows each interaction, whether it is recorded or not. Events that occur during resolving time  $\tau$  are not recorded and further extend the dead time by another period  $\tau$ . The chart indicates only three recorded events from the six interactions. In this case,  $\tau$  increases with increased number of interactions.<sup>3</sup>

It can be demonstrated that with a paralyzable system (at increasingly higher interaction rates), the observed counting rates can actually decrease with an increased number of events. When using a counting system that may be paralyzable, extreme caution must be taken to ensure that low observed counting rates correspond to low interaction rates, rather than very high interaction rates with accompanying, long dead time. It is possible for a paralyzable system to record the first interaction and then be paralyzed, recording zero counts in high radiation fields.

## Quenching

As positive ions are collected after a pulse, they give up their kinetic energy by striking the wall of the tube; ultraviolet photons and/or electrons are liberated, producing spurious counts. Prevention of such counts is called quenching.

Quenching may be accomplished electronically (by lowering the anode voltage after a pulse) or chemically (by using a self-quenching gas).

### Electronic Quenching

Electronic quenching is accomplished by introducing a high value of resistance into the voltage circuit. This will drop the anode potential until all the positive ions have been collected.

### Self-Quenching Gas

A self-quenching gas is one that can absorb ultraviolet (UV) photons without becoming ionized. One way to use this characteristic is to introduce a small amount of organic vapor, such as alcohol or ether, into the tube. The energy from the ultraviolet photons is then dissipated by dissociating the gas molecule. Such a tube is useful only as long as it has a sufficient number of organic molecules to dissociate, generally about  $10^8$  counts.

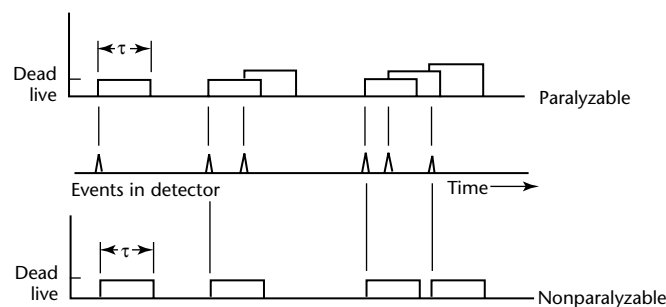
To avoid the problem of limited lifetime, some tubes use halogens (chlorine or bromine) as the quench gas. The halogen molecules also dissociate in the quenching process but they are replenished by spontaneous recombination at a later time. Halogen quench tubes have an infinite lifetime and are preferred for extended applications.

Reaction products of the discharge often produce contamination of the gas or deposition on the anode surface and generally limit the lifetimes of geiger-müller tubes.

## Design Variations

Geiger-müller counters (Fig. 13) are available in various shapes and sizes. The most common form is that of a cylinder with a central anode wire. If low energy beta or alpha particles are to be counted, a

**FIGURE 12.** Processing of detector interactions in paralyzable and nonparalyzable systems.<sup>3</sup>



**Legend**

$\tau$  = resolving time



**FIGURE 13.** Assortment of geiger-müller counters demonstrating availability of sizes and shapes. Smallest counter shown is about 30 mm (1 in.) long.

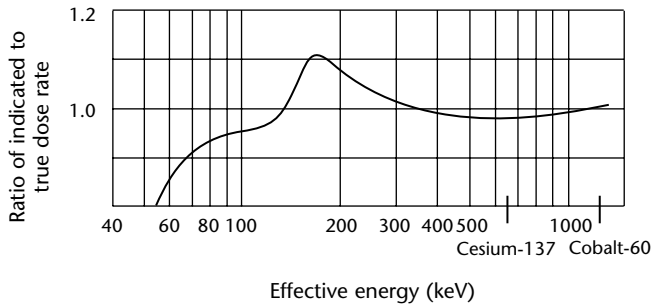
unit with a thin entrance window (1 to 4 mg.cm<sup>-2</sup>) should be selected.

For surveying large surfaces, pancake or large window counters are available. High count rate instruments, greater than 0.14 mSv.s<sup>-1</sup> (50 mR.h<sup>-1</sup>), generally

contain a small tube to minimize resolving time of the system; large volume detectors may require significant correction.

A geiger-müller counter response to gamma rays occurs by way of gamma ray interaction with the solid wall of the tube. The incident gamma ray interacts with the wall and produces a secondary electron that subsequently reaches the gas. The probability of gamma ray interaction generally increases with higher density wall material.

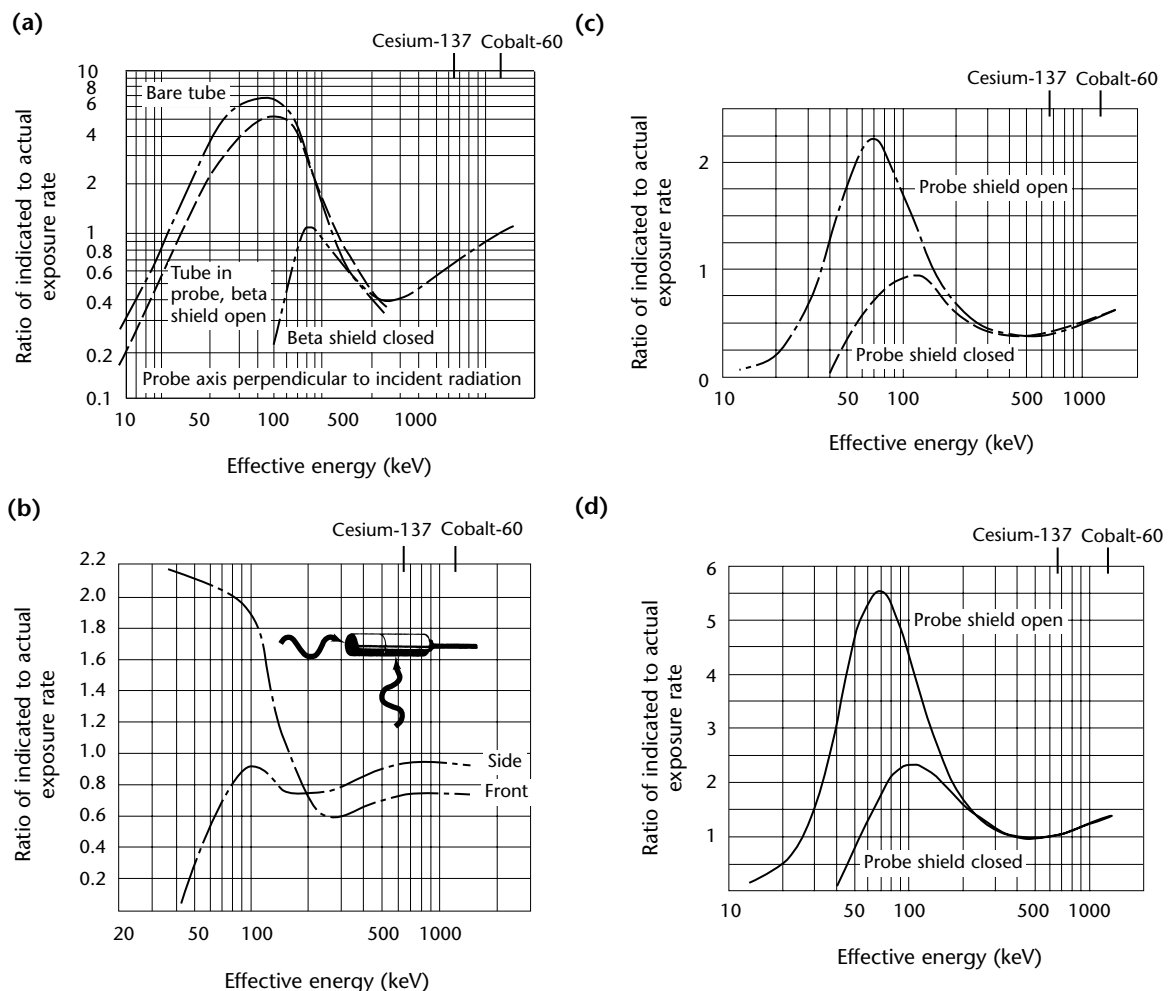
**FIGURE 14.** Dose rate ratio versus effective energy for personnel radiation monitor.



## Alarming Rate Meters (Personnel Monitors)

Small geiger-müller tubes are used in pocket-sized units for personnel monitoring. They generally emit a high frequency chirp at a rate proportional to the subjected dose rate. United States

**FIGURE 15.** Typical energy response curves for geiger-müller counters (a) shielded versus unshielded; (b) radiation incident on side versus front; (c) exposure ratio close to ideal with radiation incident normal to long axis of probe; (d) radiation incident normal to long axis of probe.





regulations specify an alarm threshold of  $500 \text{ mSv}\cdot\text{h}^{-1}$  ( $500 \text{ mR}\cdot\text{h}^{-1}$ ) for field gamma radiography. The energy dependence curve for one such instrument is shown in Fig. 14.

---

## Applications

Geiger-müller counters are the most widely used, general purpose radiation survey instruments. It must be remembered that geiger-müller counters, unlike current ionization chambers, read pulses (regardless of their energy or ionizing potential) and register in counts per minute. Some instruments have a scale calibrated in milliroentgens per hour ( $\text{mR}\cdot\text{h}^{-1}$ ); however, this is an arbitrary scale calibrated on the radiation from radium-226, cesium-137 or some other energy (Fig. 15). Another scale is microsieverts per second ( $\mu\text{Sv}\cdot\text{s}^{-1}$ ). A sensitivity versus energy table should always be consulted before making measurements with a geiger-müller instrument.

## PART 4. Scintillation Detectors

Soon after the discovery of X-rays and radioactivity, it was observed that certain materials emit visible light photons after interacting with ionizing radiation. These light photons appear to flash or sparkle and the materials are said to scintillate. Scintillators commonly used with radiation survey instruments are solid materials. Being denser than gases, these scintillators have greater detection efficiencies and are useful for low level measurements. For gamma photons, scintillators have detection efficiencies  $10^6$  times greater than typical gas ionization chambers. Detection of alpha and beta particles, neutrons and gamma photons is possible with various scintillator systems (Table 3).

### Scintillation Process

Radiation interactions with matter produce excitation as well as ionization. Ionization refers to the removal of an electron from an atom and excitation refers to the elevation of an electron's energy state. The return of excited electrons to their normal, lower energy state is called deexcitation. Scintillators excited by ionizing radiation return to lower energy states quickly and emit visible light during the deexcitation process. Radiation detection is possible by measuring the scintillator's light output (Fig. 16).

### Materials and Characteristics

Scintillation materials come in gaseous, liquid and solid forms. Organic liquids

and solids, as well as inorganic gases and solids, are common scintillators. Organic, solid scintillators are available as crystals, plastics and gels. Inorganic solid scintillators are usually alkali halide crystals. The scintillation process in inorganic materials requires the presence of small amounts of an impurity, or activator. Inorganic solid scintillators are commonly used with radiation survey instruments and are listed in Table 3.

### Desirable Scintillator Characteristics

A useful and practical scintillator needs to have most of the characteristics listed below. Not all of these characteristics are ideally satisfied by each scintillator and often a compromise is acceptable.

1. The scintillator should be of high density and large enough to ensure adequate interaction with the ionizing radiation.
2. Efficient conversion of the electron's kinetic energy into visible light is required and the light yield should be linearly related to the deposited electron kinetic energy.
3. The scintillator should be of good optical quality, transparent to its emitted light and free of hygroscopic effects, and should have an index of refraction close to that of glass.
4. The wavelength of the emitted light should be appropriate for matching to a photomultiplier tube.

### Photomultiplier Tubes

Before the advent of photomultiplier tubes (PMTs), scintillation light photons had to be visually counted. This limited the use and development of scintillators. In the 1940s, the photomultiplier tube

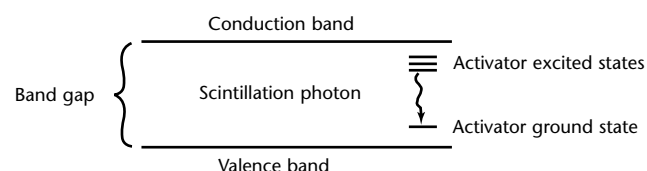
TABLE 3. Common scintillators.

Scintillator <sup>a</sup>	Chemical Symbol <sup>b</sup>	Radiation Type Detected
Sodium iodide	NaI(Tl)	gamma
Lithium iodide	LiI(Eu)	gamma, neutrons
Zinc sulfide	ZnS(Ag)	alpha
Bismuth germanate	Bi <sub>4</sub> Ge <sub>3</sub> O <sub>12</sub>	gamma

a. Many other scintillators are available but are not commonly used with radiation survey instruments.

b. Parentheses indicate impurity used as activator.

FIGURE 16. Energy diagram of scintillation process.



was developed and dramatically increased the use of scintillators, to the point where scintillators are preferred over other radiation detectors for many survey applications.

The photomultiplier tube's function is to convert the scintillator's light output into an electrical pulse. The photomultiplier tube is composed of a photosensitive layer, called the *photocathode*, and a number of electron multiplication structures called dynodes. Conversion of the scintillation light into photoelectrons is accomplished by the photocathodes through the photoelectric effect. To maximize the information contained in the scintillation light, the photomultiplier tube photocathode should be matched to the scintillator; the scintillator and photomultiplier tube should be optically coupled to minimize light losses.

Electron multiplication, or gain, is accomplished by positively charging the dynodes in successive stages, so that the total voltage applied to the photomultiplier tube is around 1000 V. Electrons emitted by the photocathode are focused toward the first dynode; more electrons are emitted than were initially incident on the dynode. This is repeated at each dynode stage. The photocathode and dynodes are positioned in a glass enclosed vacuum so that air molecules will not interfere with the collection of electrons. The net result of the photomultiplier tube may be an electron

gain up to  $10^{10}$  per emitted photoelectron. Figure 17 illustrates the structure of a photomultiplier tube.<sup>4</sup>

## System Electronics

Once the output pulse from a photomultiplier tube is generated, it is amplified and analyzed. The pulse height, or amplitude, is proportional to the amount of energy deposited within the scintillator and can be correlated to a count rate or scale of microsievert per second ( $\mu\text{Sv}\cdot\text{s}^{-1}$ ) or milliroentgen per hour ( $\text{mR}\cdot\text{h}^{-1}$ ) when calibrated against a known energy source. (See Fig. 18.)

**FIGURE 18.** Comparison of sodium iodide (thallium activated) and germanium detectors for gamma spectroscopy.

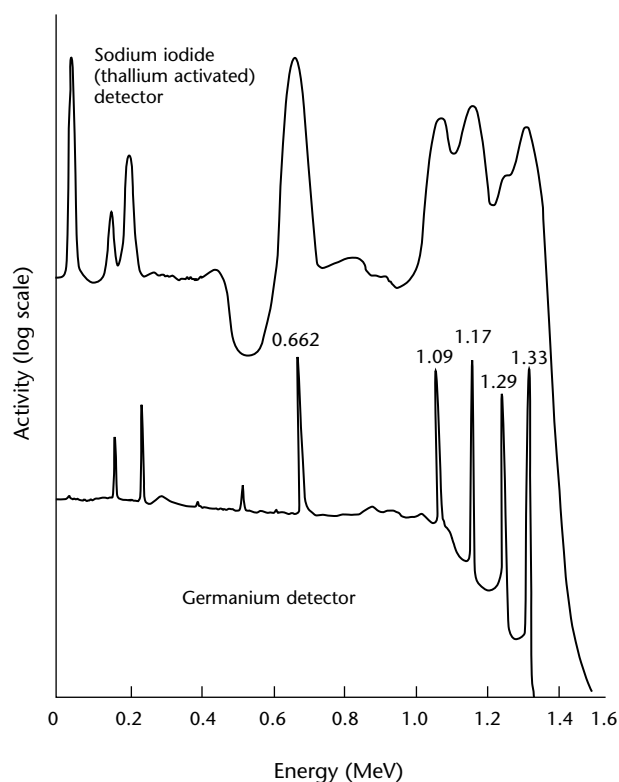
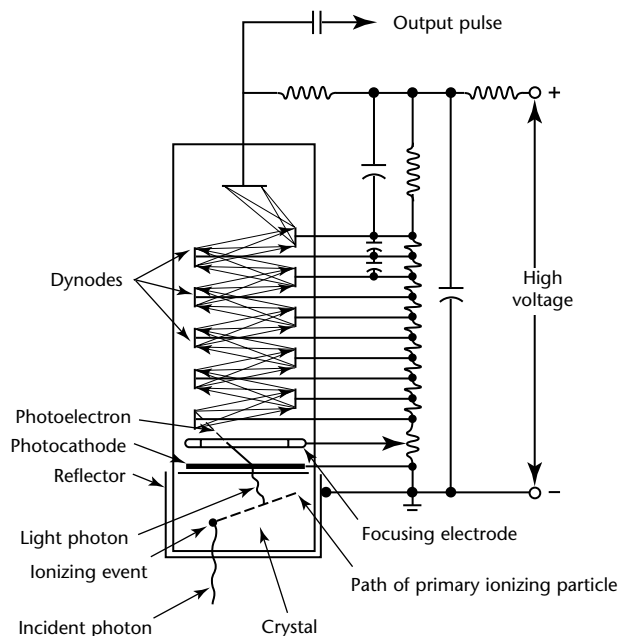


**FIGURE 17.** Cutaway drawing of photomultiplier tube, showing crystal, photocathode, collecting dynodes and voltage divider network.<sup>4</sup>



## PART 5. Luminescent Dosimetry

### Thermoluminescent Dosimetry

Thermoluminescence is the emission of light from previously irradiated materials after gentle heating. The radiation effect in thermoluminescent (TL) materials is similar to that observed in scintillators, except that light photon emission does not occur in thermoluminescent materials until some heat energy is supplied (Fig. 19).<sup>5</sup> Measurement of the light photons emitted after heating permits correlation to the amount of ionizing radiation energy that was absorbed in the thermoluminescent material. Thermoluminescent dosimetry (TLD) is possible for beta, gamma and neutron radiations, if the appropriate thermoluminescent material is used.

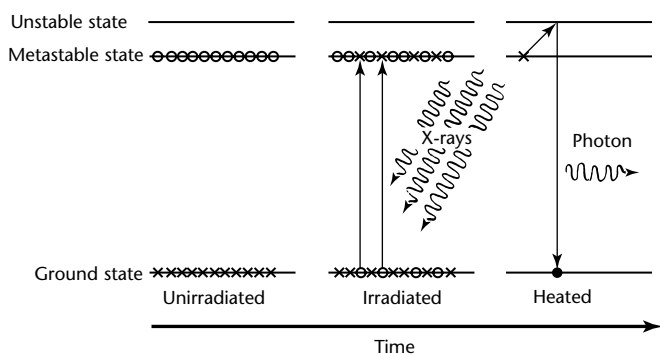
### Lithium Fluoride Properties

The most common thermoluminescent phosphor used in gamma and neutron personnel dosimetry is lithium fluoride. Other thermoluminescent phosphors are available for personnel dosimetry but, for various reasons, are not as well suited as lithium fluoride. The advantages of lithium fluoride include its (1) usefulness over a wide dose range, (2) linear dose response, (3) near dose rate independence, (4) reusability, (5) stability, (6) short

readout time and (7) near tissue equivalence. Disadvantages include the loss of information after readout and lack of information about the incident radiation energy.

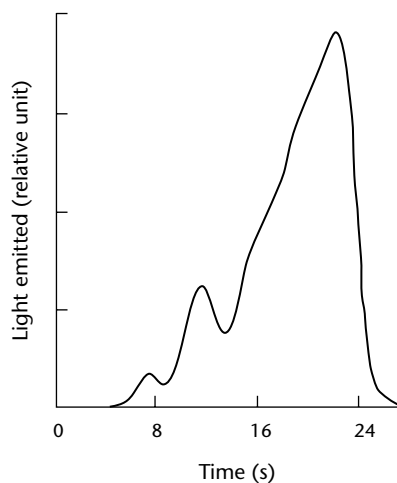
Both gamma photons and neutrons produce ionization indirectly. Gamma photons interact with matter, releasing electrons that in turn cause ionization. Lithium fluoride undergoes interactions with gamma photons and is therefore used in gamma dosimetry. Slow neutrons require the presence of the lithium fluoride enriched with lithium-6 for detection of the  $(n, \alpha)$  nuclear reaction. Fast neutron detection with lithium fluoride would only be possible if the fast neutrons were slowed down to thermal energies before reaching the lithium fluoride thermoluminescent dosimeter. Nearly complete elimination of neutron response in lithium fluoride is possible with lithium fluoride enriched with lithium-7. In a mixed gamma and slow neutron field, distinction of gamma and neutron doses is possible by comparing the readings of two lithium fluoride thermoluminescent dosimeters with different lithium-6 contents.

FIGURE 19. Thermoluminescence process.<sup>5</sup>



Legend  
x = electron  
o = electron vacancy

FIGURE 20. Typical glow curve. Integrated area under curve is measure of radiation exposure.<sup>5</sup>



## Thermoluminescent Dosimetric Readout Systems

Thermoluminescent dosimetric readout systems are commonly made up of a sample holder, heating system, photomultiplier tube (light detector), high voltage supply, signal amplifier and a recording instrument. The thermoluminescent dosimetric sample is heated indirectly, using electrical resistance heat applied to a pan or planchette. The photomultiplier tube converts the light output into an electronic pulse that is then amplified before recording. The recording instrument may be a plotter or any other instrument that can measure the amplified photomultiplier tube output signal. A plot of the output signal versus time is equivalent to emitted light intensity versus heat and results in a glow curve. The area under the glow curve is proportional to the absorbed dose (Fig. 20).<sup>5</sup>

Uses of thermoluminescent measurement of radiation include personnel dosimetry, medical dosimetry, environmental monitoring and archeological and geological dating.

---

## Optically Stimulated Luminescence Dosimetry

Optically stimulated luminescence dosimeters typically have aluminum oxide detectors and are available in plastic holders, or *body badges*, that are worn at collar level to measure full body dose. They can measure gamma ray and X-ray doses from 10 $\mu$ Sv to 10Sv (1 mrem to 1 krem).

## PART 6. Neutron Detection

### Characteristics

The neutron is a part of the nucleus, has no charge and is somewhat larger in mass than the proton. It is similar to the photon in that it has no charge and produces ionization indirectly; it is different from the photon because it is a nuclear particle and not a unit of electromagnetic energy. Because the neutron is an uncharged particle, its interactions with matter are different from those of charged particles or photons.

Ionization by neutrons is indirect: as a result of neutron interactions with matter, recoil nuclei, photons or charged particles are produced and then interact with matter by various mechanisms that cause ionization.

### Neutron Sources

Neutrons are classified according to their energies as shown in Table 4.

Some radionuclides (such as californium-252) may decay by spontaneous fission and emit neutrons with fission fragments, photons and electrons. Induced fission reactions, such as those occurring in a nuclear reactor with uranium, emit about 2.5 neutrons per fission. Fission neutrons range in energy from 0.025 eV to about 16 MeV. Other neutron sources are the result of various nuclear reactions and produce either a spectrum of neutron energies or monoenergetic neutrons. Common neutron producing nuclear reactions are the  $(\gamma, n)$ ,  $(\alpha, n)$ ,  $(p, n)$ ,  $(d, n)$  and  $(\alpha, 2n)$  reactions and may use radionuclide emissions or accelerated particles to initiate the reaction. Neutron radiography

usually uses radionuclides that emit alpha or gamma photons and produce neutrons by  $(\alpha, n)$  and  $(\gamma, n)$  reactions with various target materials.

### Neutron Detectors

There are several mechanisms and devices used to detect neutrons of various energies. Ionization chambers, proportional counters, scintillators, activation foils, track etch detectors, film emulsions, nuclear emulsions and thermoluminescent phosphors are some of the many devices used to detect neutrons. The main mechanisms used to detect neutrons in these devices are the  $(n, \alpha)$ ,  $(n, p)$ ,  $(n, d)$ ,  $(n, f)$  and  $(n, \gamma)$  nuclear reactions.

### Proportional Neutron Detectors

Many fast and slow neutron counters use proportional counting chambers filled with boron trifluoride ( $\text{BF}_3$ ) gas, often enriched in boron-10. The interaction of thermal (slow) neutrons with boron gas releases an alpha particle of several megaelectronvolts that is easily detected in the proportional mode. Fast neutrons are detected by a similar counter, in which thermal neutrons are absorbed in an external cadmium shield; the fast neutrons that pass through the shield are thermalized in hydrogen rich material and counted in the proportional chambers.

### Scintillation

Scintillators containing lithium-6, boron-10 and hydrogenous plastics have been used as neutron detectors. Lithium-6 is used as lithium iodide (europium activated) and in lithium glasses to detect slow and fast neutrons. Scintillators loaded with boron-10 are used for slow neutron detection. Plastic scintillators with high hydrogen content are used in fast neutron detection and spectroscopy by measuring the energy deposited by recoil protons.

### Activation Foils

Introducing certain materials to an incident neutron flux will result in these materials becoming radioactive. The

TABLE 4. Neutron classification.

Class	Energy
Thermal	< 0.3 meV
Epithermal	> 1 eV
Slow	30 meV to 100 eV
Intermediate	100 eV to 10 keV
Fast	10 keV to 10 MeV
Relativistic	greater than 10 MeV



process is called activation and gaining information about the incident neutron flux and energy is possible by analyzing the radiations emitted from the activated foil. Activation foils rely on  $(n, \gamma)$ ,  $(n, p)$ ,  $(n, \alpha)$ ,  $(n, f)$  and other nuclear reactions to cause the activation. Selection of the proper activation foil can give a rough estimate of the neutron energy spectrum. In high neutron flux fields, where instruments would fail, activation foils are used as integrating detectors.

### Miscellaneous Neutron Detectors

Track etch detectors, nuclear emulsions and film have all been used to detect neutrons. Various neutron interactions with the detector material or foils in intimate contact with the detectors allow these systems to operate as integrating dosimeters.

## PART 7. Semiconductors

Certain semiconductor crystals, when exposed to ionizing radiation, become conductors and may be used as radiation detectors. Semiconductors are most often used for low level spectroscopic measurements of alpha particles, beta particles and gamma rays in laboratory settings and in X-ray diffraction equipment (Table 5).

The most widely used semiconductor devices are diffused  $p$ - $n$  junction, surface barrier and lithium drifted detectors. Semiconductor detectors have found their broadest application in the field of spectroscopy, although lithium drifted detectors are also being used for gamma ray detection.

natural movement of electrons and holes (reverse bias), the potential barrier across the junction is increased and a depletion region is produced.

This depletion region is the sensitive part of the detector and is analogous to the gas volume in a gas ionization detector. Charged particles, on entering the depletion region, produce electron hole pairs analogous to the ion pairs produced in gas ionization chambers. Because an electric field exists in this region, the charge produced by the ionizing particle is collected, producing a pulse of current. The size of the pulse is proportional to the energy expended by the particle.

### Diffused $p$ - $n$ Junction Detector

The diffused  $p$ - $n$  junction detector (Fig. 21a) gets its name from its manufacturing process. A slice of  $p$  type (electron depleted) silicon or germanium crystal, with a layer of  $n$  type (electron rich) impurity (usually phosphorus) deposited on the surface, is heated to form a  $p$ - $n$  junction just below the surface. The phosphorus may also be painted onto the silicon and made to diffuse into it by applying heat. Because the  $n$  type material has an excess of electrons and the  $p$  type has an excess of holes (holes may be thought of as unit positive charges), the natural action of the combined materials tends to align the electrons on one side of the junction and the holes on the other. Thus a difference of potential is built up across the junction.

By applying an external voltage to the crystal of such polarity as to oppose the

### Surface Barrier Detectors

The operation of surface barrier and lithium drifted detectors is the same as for the  $p$ - $n$  junction: a depletion region is produced, in which there exists an electric field. The means of producing the depletion region (as well as its dimension and location within the crystal) vary from one type of detector to another.

The operation of a surface barrier detector (Fig. 21b) depends on the surface conditions of the silicon or germanium. At the surface of a piece of pure crystal, an electric field exists such that both holes and electrons are excluded from a thin region near the surface. For  $n$  type crystals, the field repels free electrons. If a metal is joined to the crystal, the free electrons are still repelled but a concentration of holes is produced directly under the surface. If a reverse bias is then applied, a depletion region is produced.

TABLE 5. Radiation detector types.

Radiation Type			Detector Type
Charged Particle	Gamma Ray	X-Ray	
x	—	—	Silicon surface barrier detectors
—	—	x	Silicon (lithium activated) detector systems for X-ray detection exclusively below 30 keV
—	x	—	Coaxial germanium (lithium activated) detectors
—	x	x	Coaxial pure germanium detectors
—	x	x	Planar, pure germanium detectors: low energy photon spectrometer for energy range of 2 to 200 keV

Surface barrier detectors give better resolution for particle spectroscopy than  $p$ - $n$  junctions but wider depletion regions are possible with the latter. (The wider the depletion region, the higher the energy of particles can be analyzed because a particle must expend all its energy in a depletion region.)

## Lithium Drifted Detectors

The lithium drifted detector (Fig. 22) is produced by diffusing lithium into low resistivity  $p$ -type silicon or germanium. When heated under reverse bias, the lithium ions serve as an  $n$  type donor. These ions drift into the silicon or germanium in such a way that a wide layer of the  $p$  type material is compensated by the lithium, yielding an effective resistivity comparable to that of the intrinsic material. Wider depletion regions can be obtained with the lithium drift process than by any other means. Consequently, lithium drifted detectors are most useful in gamma spectroscopy work.

Silicon detectors can be operated at room temperatures but exhibit low efficiency for gamma rays. Germanium detectors have higher gamma efficiencies

but must be operated at liquid nitrogen temperatures. For these reasons, coupled with the small sensitive volumes obtainable to date, semiconductor detectors have not received widespread application in radiation survey instruments.

FIGURE 22. Cross section of lithium drifted detector.

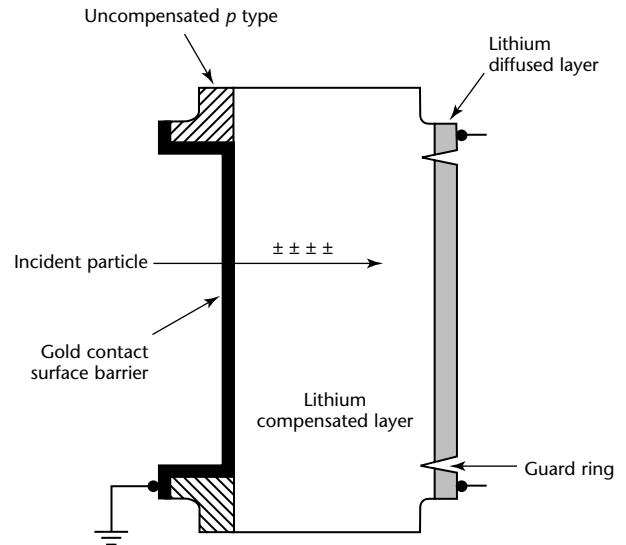
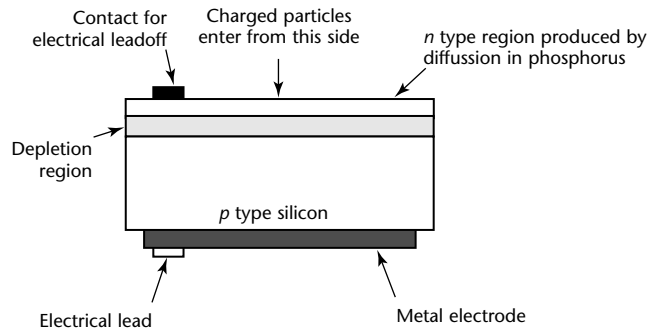
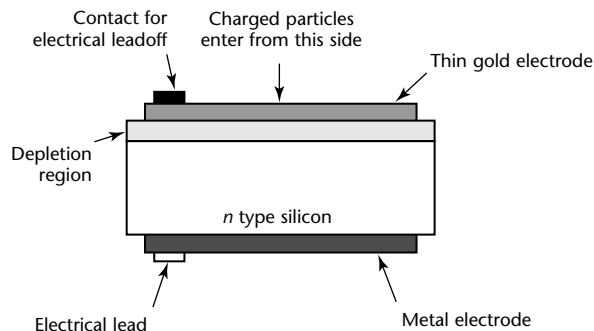


FIGURE 21. Cross sections: (a) diffused  $p$ - $n$  junction detector; (b) surface barrier detector.

(a)



(b)



## PART 8. Film Badges<sup>1,5-7</sup>

One of the most important uses of radiographic film as a means of measuring radiation is in film badges. Individuals who work with isotope radiation sources and X-ray machines are required by codes to wear badges indicating cumulative exposure to ionizing radiation. [Film badges are discussed in this volume's chapter on radiation safety](#) and elsewhere.<sup>2,5,6</sup>

### Latent Image Formation

Latent image formation is a very subtle change in the silver halide grain of film. The process may involve the absorption of only one or, at most, a few photons of radiation and this may affect only a few atoms out of some  $10^9$  or  $10^{10}$  atoms in a typical photographic grain. Formation of the latent image, therefore, cannot be detected by direct physical or analytical chemical means. The process that made an exposed photographic grain capable of transformation into metallic silver (by the mild reducing action of a developer) involved a concentration of silver atoms at one or more discrete sites on the photographic grain.

In industrial radiography, the image forming effects of X-rays and gamma rays, rather than those of light, are of primary interest. The agent that actually exposes a film grain (a silver bromide crystal in the emulsion) is not the X-ray photon itself but rather the electrons (photoelectric and Compton) resulting from an absorption event.

The most striking difference between X-ray and visible light exposures arises from the difference in the amounts of energy involved. The absorption of a single photon of light transfers a very small amount of energy to the crystal — only enough energy to free a single electron from a bromide ( $\text{Br}^-$ ) ion. Several successive light photons are required to make a single grain developable (to produce within it, or on it, a stable latent image). The passage of an electron through a grain can transmit hundreds of times more energy than the absorption of a light photon. Even though this energy is used inefficiently the amount is enough to make the grain developable.

In fact, a photoelectron or Compton electron can have a fairly long path

through a film emulsion and can render many grains developable. The number of grains exposed per photon interaction varies from one (for X-radiation of about 10 keV) to 50 or more (for a 1 MeV photon).

Because a grain is completely exposed by the passage of an energetic electron, all X-ray exposures are, as far as the individual grain is concerned, extremely short. The actual time that an electron is within a grain depends on the electron velocity, the grain dimensions and the squareness of the hit. A time on the order of  $10^{-13}$  s is representative. (In the case of light, the exposure time for a single grain is the interval between the arrival of the first photon and the arrival of the last photon required to produce a stable latent image.)

### Development

Many materials discolor with exposure to light (some kinds of wood and human skin are examples) and could be used to record images. Most of these materials react to light exposure on a 1:1 basis — one photon of light alters one molecule or atom. In the silver halide system of radiography, however, a few atoms of photolytically deposited silver can, by development, be made to trigger the subsequent chemical deposition of some  $10^9$  or  $10^{10}$  additional silver atoms, resulting in an amplification factor on the order of  $10^9$  or greater. This amplification process can be uniform and reproducible enough for quantitative radiation measurements.

Development is essentially a chemical reduction in which silver halide is converted to metallic silver. To retain the photographic image, however, the reaction must be limited largely to those grains that contain a latent image; that is, to those grains that have received more than a prescribed minimum radiation exposure.

Compounds that can be used as photographic developing agents are those in which the reduction of silver halide to metallic silver is catalyzed (speeded up) by the presence of metallic silver in the latent image. Those compounds that reduce silver halide, in the absence of a catalytic effect by the latent image, are not suitable developing agents because

they produce a uniform overall density on the processed film.

---

## Closing

More [information on the radiographic latent image, its formation and processing are available elsewhere](#).<sup>1,7</sup> The correct use of film badges is especially important for safety in the conduct of radiographic testing programs and is [discussed in this book's chapter on radiation safety](#) and elsewhere.<sup>2,5,6</sup>

# References

1. Rivkin W.B. and G. Wicks. Ch. 4, "Radiation Detection and Recording." *Nondestructive Testing Handbook*, second edition: Vol. 3, *Radiography and Radiation Testing*. Columbus, OH: American Society for Nondestructive Testing (1985): p 152-185.
2. ANSI N13.5-1972 (R1989), *Direct Reading and Indirect Reading Pocket Dosimeters for X- and Gamma-Radiation, Performance, Specifications for*. New York, NY: American National Standards Institute (1989).
3. Knoll, G.F. *Radiation Detection and Measurement*, second edition. New York, NY: John Wiley and Sons (1989).
4. Cember, H. *Introduction to Health Physics*, second edition. New York, NY: Pergamon Press (1983).
5. Cameron, J.R., N. Suntharalingam and G.N. Denney. *Thermoluminescent Dosimetry*. Madison, WI: University of Wisconsin Press (1968).
6. Bush, J. *Gamma Radiation Safety Study Guide*, second edition. Columbus, OH: American Society for Nondestructive Testing (2001).
7. Quinn, R.A. and C.C. Sigl, eds. *Radiography in Modern Industry*, fourth edition. Rochester, NY: Eastman Kodak Company (1980).

## Bibliography

### Radiation Measurement

- Attix, F.H. and W.C. Roesch. *Radiation Dosimetry*. Vol. 2. New York, NY: Academic Press (1966).
- Attix, F.H., ed. *Luminescence Dosimetry*. Symposium Series No. 8. Washington DC: Atomic Energy Commission (1967).
- A *Handbook of Radioactivity Measurements Procedures*. NCRP Report 58. Washington, DC: National Council on Radiation Protection and Measurements (1978).
- Lapp, R.E. and H.L. Andrews. *Nuclear Radiation Physics*. Upper Saddle River, NJ: Prentice-Hall (1972).
- Price, W.J. *Nuclear Radiation Detection*, second edition. New York, NY: McGraw-Hill (1964).

### Radiation Safety

- Aerna, V. *Ionizing Radiation and Life*. Saint Louis, MO: C.V. Mosby Company (1971).
- Alpen, E.L. *Radiation Biophysics*. Upper Saddle River, NJ: Prentice Hall (1990).
- Basic Radiation Protection Criteria*. NCRP Report 39. Washington, DC: National Council on Radiation Protection and Measurements (1971).
- Hine, G. *Instrumentation in Nuclear Medicine*. New York, NY: Academic Press. Vol. 1 (1967).
- Instrumentation and Monitoring Methods for Radiation Protection*. NCRP Report 57. Washington, DC: National Council on Radiation Protection and Measurements (1978).
- International Commission on Radiological Protection. Ann. ICRP 21 (1-3), 1990 *Recommendations of the International Commission on Radiological Protection*. ICRP Publication 60. Oxford, United Kingdom: Pergamon Press (1991).
- Ionizing Radiation: Sources and Biological Effects*. New York, NY: United Nations Scientific Committee on the Effects of Atomic Radiation (1982).
- Martin, A. and S.A. Harbison. *An Introduction to Radiation Protection*, third edition. London, United Kingdom: Chapman and Hall (1986).
- Moe, H.J. *Radiation Safety Technician Training Course*. Prepared for the United States Atomic Energy Commission under contract W-31-109-Eng-38. Argonne, IL: Argonne National Laboratory (May 1972).
- Morgan, K.Z. and J.E. Turner. *Principles of Radiation Protection*. New York, NY: John Wiley and Sons (1973).
- National Research Council, Committee on the Biological Effects of Ionizing Radiations. *Health Effects of Exposure to Low Levels of Ionizing Radiations*. Washington, DC: National Academy Press (1990).
- Personnel Dosimetry Systems for External Radiation Exposures*. Technical Report Series No. 109. Vienna, Austria: International Atomic Energy Agency (1970).



- Rivkin, W.B. *Personnel Monitoring Radiation Safety and Protection in Industrial Applications: Proceedings of a Symposium*. DHEW Publication No. (FDA) 73-8012. Washington, DC: Department of Health, Education and Welfare (1973).
- Rollo, F.D., ed. *Nuclear Medicine Physics, Instrumentation and Agents*. Saint Louis, MO: C.V. Mosby and Company (1977).
- Shapiro, J. *Radiation Protection: A Guide for Scientists and Physicians*. Cambridge, MA: Harvard University Press (1990).
- Shleien, B. and M. Terpilak. *The Health Physics Handbook*. Olney, MD: Nuclear Lectern Associates (1984).
- Simmons, G.H. *A Training Manual for Nuclear Medicine Technologists*. DMRG 70-3. Washington, DC: Bureau of Radiological Health [1970].
- Turner, J. *Atoms, Radiation, and Radiation Protection*, second edition. New York, NY: John Wiley and Sons (1995).
- ASTM E 666-97, *Standard Practice for Calculating Absorbed Dose from Gamma or X Radiation*. West Conshohocken, PA: ASTM International (1997).
- IEEE/ANSI N323-1978, *American National Standard Radiation Protection Instrumentation Test and Calibration*. New York, NY: Institute of Electrical and Electronics Engineers (1978).
- IEEE 309-1999 / ANSI N42.3-1999, *IEEE Standard Test Procedures and Standard Bases for Geiger-Mueller Counters*. New York, NY: Institute of Electrical and Electronics Engineers (1999).
- IEEE N42.20-1995, *ANSI Performance Criteria for Active Personnel Radiation Monitors*. New York, NY: Institute of Electrical and Electronics Engineers (1995).
- Occupational Safety and Health Administration: 29 CFR 1910, *Occupational Safety and Health Standards [Code of Federal Regulations: Title 29, Labor]*. Washington, DC: United States Government Printing Office.

## Standards

- ANSI N13.15-1985, *Dosimetry Systems, Performance of Personnel Thermoluminescence*. New York, NY: American National Standards Institute (1985).
- ANSI N13.2-1969 (R1982), *Administrative Practices in Radiation Monitoring (A Guide for Management)*. New York, NY: American National Standards Institute (1982).
- ANSI N13.27-1981 (R1992), *Dosimeters and Alarm Ratemeters, Performance Requirements for Pocket-Sized Alarm*. New York, NY: American National Standards Institute (1992).
- ANSI N13.7-1983 (R1989), *Photographic Film Dosimeter Performance, Criteria for*. New York, NY: American National Standards Institute (1989).
- ANSI N42.5-1965, *American National Standard for Bases for GM Counter Tubes*. New York, NY: Institute of Electrical and Electronics Engineers (1965).
- ANSI N43.3-1993, *General Radiation Safety — Installations Using Non-Medical X-Ray and Sealed Gamma-Ray Sources, Energies up to 10 MeV*. New York, NY: American National Standards Institute (1993).
- ASTM E 1894-97, *Standard Guide for Selecting Dosimetry Systems for Application in Pulsed X-Ray Sources*. West Conshohocken, PA: ASTM International (1997).
- ASTM E 2116-00, *Standard Practice for Dosimetry for a Self-Contained Dry-Storage Gamma-Ray Irradiator*. West Conshohocken, PA: ASTM International (1900).



# 6

## C H A P T E R

# Radiation Safety<sup>1</sup>

---

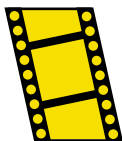
William D. Burnett, Albuquerque, New Mexico

Garry L. Balestracci, Balestracci Unlimited,  
Charlestown, Rhode Island

Frank A. Iddings, San Antonio, Texas

# PART 1. Management of Radiation Safety

MOVIE.  
Radiation  
injury.



## Introduction

There are many considerations involved in setting up and outfitting a safe radiographic facility. Commercial consulting firms specializing in personnel dosimetry and radiation protection may help with this goal. Regardless of who establishes or monitors the program, it is vitally important that radiation exposures to personnel be reduced to as low a level as is practical. To this end, each radiographic facility should appoint a *radiation safety officer*, who is responsible for systematically assuring management that a safe operation exists. The functions of the radiation safety officer are discussed later in this part.

In the twenty-first century, some publications of the 1970s<sup>2-5</sup> are still useful to document information in later publications. However, all guidelines, standards, regulations and handbooks have a shelf life beyond which some of their information is obsolete. It is the duty of inspectors and safety personnel to become familiar with the literature and refer to up-to-date documents for critical decisions.

Because of potential changes in safety requirements, radiation safety officers and all personnel active in the field of radiography should consult the most up-to-date publications and regulations before making a determination on the safety of a radiographic facility. Many publications are written specifically to describe in detail the requirements and techniques involved. The following discussion is an *overview* of radiation safety and personnel protection and does not attempt to duplicate the information available elsewhere — for example, in the works cited in the references and bibliography at the end of this chapter. Unsealed radioactive sources and the associated health protection requirements, internal dosimetry, instrumentation and related subjects are not covered in this chapter. Note also that safety regulations may vary with locality.

## Radiation Safety Inspections and Audits

### Government Licensing<sup>6</sup>

Most manufacturers specify that radiation producing devices should be operated only by qualified personnel. Most states require the *registration* of radiation machines and provide survey services during compliance audits. *Licenses to possess byproduct materials* (radioisotopes other than radium) are issued by the Nuclear Regulatory Commission (NRC) or states operating under its rules (*agreement states*).

### Radiation Safety Officer

Personnel responsible for work with radiation are also responsible for radiation safety. A *radiation safety officer* (RSO) needs to be appointed if fields may be experienced in excess of 1 mSv (100 mrem) per work week in accessible regions inside or outside externally applied shielding. The radiation safety officer is responsible for: (1) technical assistance in planning and execution of work insofar as radiation safety is concerned, (2) appraisal of safe operation of the radiation source through surveys and personnel monitoring, (3) notification of personnel working around the source of any special hazards, (4) reporting of radiation hazards or unsafe practices to the proper authorities, (5) seeking advice from qualified experts when necessary, (6) keeping records of personnel exposures and area dose levels, (7) keeping informed of any changes in the mode of operation of the source and (8) periodically providing radiation safety training.

A good radiation safety officer has the confidence and support of company management and the radiography personnel. Fair and honest treatment, knowledge of the regulations and open mindedness to ideas and needs of those involved builds a good working relationship. This relationship helps to ensure that corrective actions are taken, however unsavory. The radiation safety officer must have access to any level of management necessary to ensure the compliance with regulations and

procedures to provide for a safe work environment.

### Written Procedures

All radiographic work must be covered by written procedures that are reviewed and updated annually. The radiation safety officer needs to work with operating personnel and management in preparing these procedures so that adequate safety procedures are integrated with the needs and goals of the workplace environment. The radiation safety officer can *recommend* approval of a written procedure but only management can *approve* the procedure with a signature.

The level of management required for approval depends on the level of risk for operation. Where first level management is delegated to approve some procedures, a written delegation of authority from top management should be on file in the radiation safety officer's records.

### Emergencies

Written procedures should exist for actions to be taken in case of an emergency. While the radiation safety officer may have considerable authority in a radiation emergency situation, the written procedures should make it clear that management is responsible for assuming the level of risk for any action taken in case of an emergency.

The case of a radiographic source that because of mechanical problems cannot be returned to its storage container provides an example. In this situation, all personnel should know from existing general procedures to evacuate to a safe distance or location where a specific, written procedure, even handwritten, can be prepared and approved for restoring the source.

In a case where an injured or unconscious person is exposed to a hazardous radiation dose rate, time is very important. Written procedures prepared in advance with assignments of roles and responsibilities, combined with periodic training and practice scenarios, can facilitate the rapid recovery of an immobile person without unacceptable radiation exposures to recovery personnel.

### Internal Inspections<sup>7</sup>

An internal inspection system is essential to maintaining a quality industrial radiography program. Internal inspection programs are mandated by regulations and are vital to ensure safe operations and the welfare of radiography workers as well as of the general public.

Required internal inspections consist of semiannual radiographer audits, an annual overview audit of the entire

radiation protection program, an annual review of the quality assurance program and a continuous review of the company program to keep personnel exposures as low as reasonably achievable (ALARA). Audit procedures for gamma radiography or X-radiography are basically the same, just as observations of temporary field sites are conducted in a manner similar to cell or permanent facility audits. These components make up the internal inspection system.

The single most important part of the internal inspection system is the radiation safety officer. The radiation safety officer should have sufficient experience and expertise to observe radiography operations and immediately recognize infractions or violations as well as good practices. The radiation safety officer should be able to make a valid assessment of the conditions observed and provide corrective actions or recommendations to those involved. Any and all discrepancies should immediately be pointed out to the responsible individuals with a followup notification to the appropriate supervision.

The radiation safety officer should conduct audits in person and take appropriate actions to stop violations or unsafe practices. Unfortunately some regulations are instituted as a result of the actions of a few individuals. The integrity of the radiation safety officer and the radiographers are important to a good radiation safety program. A good relationship between regulators and licensees is also important to a quality program. Regulators should not be feared or shunned: avoidance gives the impression that people have something to hide.

A number of factors can affect how an individual reacts to situations. Very few people start out with the intention to break the rules. But good intentions, lack of training, lack of proper equipment or misunderstanding of the requirements can result in problems. Many factors can contribute to the situation, such as tight schedules, cost implications and the mental health or morale of the persons involved. Maybe there is a bonus offered to finish the job early. Radiographers that circumvent the regulations or take short cuts around procedural requirements run greater risk of accidents or overexposures than those that continuously operate *by the book*. Audits are necessary to detect and correct breaches of safety procedure.

What makes up an audit or observation varies. Simply questioning a radiography crew can often provide a false idea of how the crew normally operates. An experienced auditor can usually perceive more while approaching a radiography job site and observing the normal work

practices than can be obtained by spending eight hours sitting on a job and interviewing radiographers. During that amount of time when the auditor's presence is not known, work ethics are demonstrated and the real story is told. Followup interviews should be conducted to verify the details that must be noted: serial numbers, calibration dates and items that need to be checked and validated.

This is not to suggest in any way that observations should be conducted, as some audits are conducted, from a long distance by hidden auditors with binoculars. Audits should be open exchanges of information. All parties involved should be treated with the dignity and respect expected in any business encounter. All involved should participate in a professional manner.

The radiographers should be aware that the sole purpose of the radiation safety officer, observer or auditor at the job site is to validate that the radiography team is operating to the established procedures and within the restraints of governing regulations, not to try to catch the participants committing infractions. Systematic or generic deficiencies should be addressed to appropriate management for long term corrective actions. The audit process should be a positive experience rather than a traumatic one. A more casual, relaxed, audit allows an opportunity to experience the way things are done.

Careful observation of details, such as radiation levels at the posted boundaries, can be conspicuously determined while approaching the job site. Proper surveillance techniques, area control procedures and adherence to proper operating procedures should become obvious as the auditor approach the radiography operation.

The better the auditor understands operations, the better the ability to identify existing or potential problems. Experience provides a higher potential to ensure the safety of personnel involved as well as the general public. Large scale operations with many radiographers or multiple locations may require assistant radiation safety officers or radiation safety officer delegates to be assigned to provide the support and coverage needed to ensure compliance.

### **Temporary Field Sites versus Permanent Facilities for Isotopic Sources<sup>7</sup>**

At temporary field sites specific restraints apply. Generally each field site operation offers a new challenge. The site should be examined and assessed to determine problems that might arise. Location and

overall conditions at the work site affect the operations. Distances to radiation area boundaries need to be calculated and posted as required to prevent unauthorized entry into the radiography area. Conditions may require that nonradiography personnel must work in close proximity to the radiography boundaries. Surveillance is required to maintain control of the established area. Specific transportation requirements and regulations mandate how the radiographic exposure device and equipment are transported to the work location. Radiation surveys must be performed to ensure compliance with established procedural requirements. Peak readings need to be documented. Emergency procedures and points of contact should be reviewed to afford timely response in the event of an accident or emergency. By the nature of the operation, an overexposure or other accident is more likely during a temporary field operation.

Permanent facilities are constructed and evaluated to determine restrictions for use. These restrictions allow some relaxation of the requirements associated with temporary field site operations. If permanent cells are used within the parameters established, radiation levels outside the facility will always be at acceptable limits. The safety inspector must confirm that activities are within the established parameters. Exposure cells must be outfitted with alarms and warning devices and these devices now require a daily operability check. Accesses to the facility must be locked or guarded while exposures are being completed.

In industrial radiography operations, high radiation exists in permanent exposure cells — for example, facilities equipped with cobalt-60 exposure devices of 14 TBq (385 Ci). Some permanent facilities also serve as long term storage areas for radiography exposure devices. When established as a storage area, additional radiation surveys and postings are required and should be checked. When it is necessary to operate an exposure cell outside of the established parameters for use, the cell can be established as a temporary field site. Additional considerations needed for a temporary site will then apply. If an alarm or warning device malfunctions, a permanent facility may be used as a temporary field site but current regulations must be checked to find out how long.

### **Semiannual Isotopic Source Audits<sup>7</sup>**

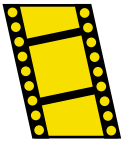
Field audits of radiography are required to be conducted semiannually, quarterly in some locations. Every person,



radiographer, radiographer's assistant or radiation safety officer that operates radiography equipment or participates directly in a radiography operation must be observed. A checklist should be used to ensure that each specific point is properly addressed. A regular semiannual inspection should cover the following.

1. Determine the source and exposure device being used. Verify the serial number of the source and the exposure device.
2. Check that the source is safe from unauthorized removal or tampering.
3. Check the condition of the equipment in use. Are a sufficient number properly functioning, calibrated survey meters available on the job site? Are the exposure device, control assembly and source guide tubes in good working condition? Does the equipment appear to have received adequate inspection and maintenance for the conditions of use?
4. Check to ensure that the equipment is being operated properly and in accordance with established procedures. Are good collimators and shielding being used? Are practices being followed to keep exposures as low as reasonably achievable? Are trainees and assistants being properly supervised?
5. Do all persons involved with the operation have required personnel monitoring devices? Is each dosimeter within calibration, not discharged beyond its range? Is a thermoluminescent dosimeter badge or film badge available and being used? Is an alarming rate meter available and within calibration?
6. Ensure that the area is adequately posted in accordance with applicable procedures. Signs must be posted for restricted and high radiation area boundaries.
7. Check to ensure that the high radiation is under constant direct surveillance at all times while the source is exposed. Are adequate controls established to keep unauthorized personnel out of the radiography area?
8. Are procedures being properly followed? Are surveys being taken as required? Do the people involved display adequate competence for the tasks involved?
9. Check the records to ensure that the source use log agrees with the source and equipment in use. Is all required information properly documented? Are the transportation records in order?

**MOVIE.**  
Survey meters.



## Personnel Certification for Radiation Safety

The United States Nuclear Regulatory Commission (NRC) has published rules that govern the use of nuclear, or gamma, radiation in those states that choose to follow federal regulations, the *NRC states*. In contrast, states that wish to use their own regulations, which must meet or exceed Nuclear Regulatory Commission requirements, are known as *agreement states* and their regulations are in force for nuclear radiation in those states. Because X-rays (unlike gamma rays) are not generated by nuclear materials, the Nuclear Regulatory Commission does not have jurisdiction over X-ray radiography and each state is responsible for regulating X-radiography. Radiographers working in any state must be aware of who has jurisdiction over radiation safety and must adhere to the requirements that govern in that state. In some instances, large metropolitan areas also have requirements and these must also be met when working in those areas.

### Safety Personnel Certification

In May 1997, the Nuclear Regulatory Commission published a rule requiring that all industrial radiographers using radioactive materials be certified through either an approved independent certifying organization (ICO) or an agreement state program that complied with the criteria in 10CFR [Code of Federal Regulations: Title 10], Part 34, Appendix A.<sup>8</sup> The final deadline for compliance was set as July 1999 for Nuclear Regulatory Commission states and as July 2000 for agreement states.

The American Society for Nondestructive Testing (ASNT), in an effort to provide a service to industry, developed the American Society for Nondestructive Testing's Industrial Radiography Radiation Safety Personnel (IRRSP) program,<sup>9,10</sup> which was sent to the Nuclear Regulatory Commission for review in late 1997. In May 1998, The Nuclear Regulatory Commission formally approved the American Society for Nondestructive Testing as an independent certifying organization and accepted the radioactive materials (RAM) portion of the Industrial Radiography Radiation Safety Personnel examinations.

The Nuclear Regulatory Commission does not take responsibility for radiation producing machines, such as X-ray machines used in radiographic testing. Each individual state was responsible for determining their own certification requirements for radiographers using X-radiation. The agreement states, to



minimize duplication and establish uniformity between the States' certification requirements, formed the Conference for Radiation Control Program Directors (CRCPD). In early 1998, the American Society for Nondestructive Testing asked the Conference for Radiation Control Program Directors to review the Industrial Radiography Radiation Safety Personnel program to determine if it would meet the requirements of the agreement states.

In September 2001, after detailed review and some revision of the program, the Conference for Radiation Control Program Directors formally approved the American Society for Nondestructive Testing as an independent certifying organization and recommended acceptance of the radioactive materials examinations and X-ray examinations for use by agreement states. This decision was sent to all agreement states, because each state makes its own decision whether or not to accept recommendations of the Conference for Radiation Control Program Directors.

### Radiographer Certification

Radiographers are generally required to carry two types of certification, one based on technical competence and the other based on the knowledge of safety regulations. The requirements listed in commercial codes, standards and specifications are predominantly technical and rely on the contractor (the radiographer's employer) to ensure that all applicable safety requirements are met. The safety requirements are detailed by the local, state or federal government regulatory agencies that have jurisdiction over radiography in the locale where the work is to be performed.

Technical certification is required by the code or standard governing a specific project. The purpose of this certification is to ensure that the radiographer can make proper exposures and accurately interpret radiographs in accordance with the requirements of the governing code or specification. Each code or specification has varying technical requirements and each will specify that a radiographer be certified somehow before working on projects governed by those documents. A certified radiographer will be able to produce acceptable radiographs that accurately show that the quality of workmanship required by the designer has been achieved.

Safety certification is required by local, state and federal regulatory agencies. Because of the dangers of penetrating radiation, these agencies want to ensure the safety of the general public and require that all radiographers demonstrate

their knowledge of safety regulations by successfully completing a safety examination on the type of radiation to be used in the course of their work. To be eligible to sit for these safety examinations, radiographers must be able to show that they have had adequate training and experience in performing radiography.

---

## Transportation of Radioactive Materials

Radioactive material is considered hazardous material. As a result its shipment within the United States is controlled by the Department of Transportation under the *Code of Federal Regulations*, Title 49, Subtitle B, Parts 171-177.<sup>11</sup> These regulations prescribe the rules and procedures for packaging, marking, labeling, placarding and shipping.

Additional requirements for the international shipment of such materials by air are set forth by the International Air Transport Association (IATA).

Except for very minor quantities, use of the Postal Service for transport of radioactive materials is prohibited.

Finally the Inter-Governmental Maritime Consultative Organization (IMCO) and the International Atomic Energy Agency (IAEA, an office of the United Nations) represent the collection of nations around the world that regulate the international transport of dangerous goods by sea.

### Disposal

The disposal of leaking sources, contaminated equipment or sources decayed below useful levels must be according to the *Code of Federal Regulations*, Title 10.<sup>12</sup> Generally, a commercial radioactive waste disposal service licensed by the Nuclear Regulatory Commission is used for this purpose, either directly by the owner of the source or indirectly by returning the source to the manufacturer.

## PART 2. Dose Definitions and Exposure Levels

### Radiation Quantities and Units

Radiation is measured by the International System of Units (SI), [described elsewhere in this volume](#). SI units include the becquerel, coulomb, sievert and gray. The literature for radiation safety also uses older units, such as roentgen, curie, rad and rem. Because of the widespread use of the older units in the United States, especially in regulatory documents dealing with health and safety, the United States Department of Commerce in 1998 accepted these older units with SI.<sup>13</sup> All these units are discussed briefly below.<sup>1,14</sup>

**Disintegration Rate.** *Disintegration rate* is the rate at which a radionuclide decays. In SI, the unit for radioactivity is the becquerel (Bq), one disintegration per second. Because billions of disintegrations are required in a useful source, the multiplier prefix *giga-* ( $10^9$ ) is used and the unit is normally seen as gigabecquerel (GBq). An older unit is the *curie* (Ci), simply the radiation of 1 g of radium. A curie is equivalent to 37 GBq, that is, to  $3.7 \times 10^{10}$  disintegrations per second.

**Exposure.** Exposure is a measure of X-radiation or gamma radiation based on the ionization produced in air by X-rays or gamma rays. The unit for quantity of electric charge is the coulomb (C), where  $1 \text{ C} = 1 \text{ A} \times 1 \text{ s}$ . The original roentgen (R) was the quantity of radiation that would ionize  $1 \text{ cm}^3$  of air to 1 electrostatic unit (ESU) of charge (where  $1 \text{ ESU} = 3.3356 \times 10^{-10} \text{ C}$ ) of either sign. A roentgen is equivalent to 258 microcoulombs per kilogram of air ( $1 \text{ R} = 258 \mu\text{C}\cdot\text{kg}^{-1}$  of air). This corresponds to  $1.61 \times 10^{15}$  ion pairs per 1 kg of air, which has then absorbed 8.8 mJ (0.88 rad, where rad is the obsolete unit for radiation absorbed dose, not the SI symbol for radian).

**Absorbed Dose.** Absorbed dose is the mean energy imparted to matter by ionizing radiation per unit mass of irradiated materials at the place of interest. The roentgen (R) was an intensity unit but was not representative of the dose absorbed by material in the radiation field. The radiation absorbed dose (rad) was first created to measure this value and was based on the erg, the energy unit

from the old centimeter-gram-second (CGS) system. In the SI system, the unit for radiation dose is the gray (Gy). The gray is useful because it applies to doses absorbed by matter at a particular location. It is expressed in energy units per mass of matter or in joules per kilogram ( $\text{J}\cdot\text{kg}^{-1}$ ). The mass is that of the absorbing body. One gray equals 100 rad equals 10 000 ergs per gram ( $1 \text{ Gy} = 100 \text{ rad} = 10\,000 \text{ erg}\cdot\text{g}^{-1}$ ).

**Dose Equivalent.** Dose equivalent *H* is a quantity used for radiation protection that expresses on a common scale for all irradiation incurred by exposed persons. The SI unit of dose equivalent is the *sievert*, equal to 100 rem ( $1 \text{ Sv} = 100 \text{ rem}$ ). The SI system's unit for the dose absorbed by the human body (formerly rem for *roentgen equivalent man*; also known as *ambient dose equivalent*, *directional dose equivalent*, *dose equivalent*, *equivalent dose* and *personal dose equivalent*) is similar to the gray but includes quality factors dependent on the type of radiation. This absorbed dose has been given the name sievert (Sv) but its dimensions are the same as the gray ( $\text{J}\cdot\text{kg}^{-1}$ ), that is,  $1 \text{ Sv} = 1 \text{ J}\cdot\text{kg}^{-1}$ .

**Quality Factor.** Quality factor<sup>15-18</sup> is a modifying factor used in determining the dose equivalent. The quality factor corrects for the dependence of biological factors on the energy and type of the radiation. A formerly commonly used term, *relative biological effect*, is restricted in use to radiobiology. For practical

TABLE 1. Radiation weighting factors.<sup>31</sup>

Radiation Type	Quality Factor <sup>a</sup>
X-rays	1
Gamma rays	1
Beta rays	1
Neutrons	2 to 11 <sup>b</sup>
Neutrons of unknown energy	10
High energy protons	10
Alpha particles	20
Multiple charged particles	20
Fission fragments	20
Heavy particles of unknown charge	20

a. Value of quality factor at point where dose equivalent is maximum in 300 mm (12 in.) diameter cylinder tissue equivalent phantom.

b. Quality factor depends on energy of neutron.

purposes the quality factors in Table 1 are conservative. For example, consider an absorbed dose in the lens of the eye of 1 mGy (0.1 rad) from 2 MeV neutrons. The dose equivalent is:

$$\begin{aligned} (1) \quad H &= \left[ \begin{array}{c} \text{Dose in} \\ \text{milligray} \end{array} \right] \times \left[ \begin{array}{c} \text{Quality} \\ \text{factor} \end{array} \right] \\ &= 1 \text{ mGy} \times 10 \\ &= 10 \text{ mSv} \end{aligned}$$

### Compound Units

Roentgens could be measured with an ionization chamber that, when placed 1.0 m (39 in.) from the radiation source, provided necessary information — one roentgen per hour at one meter ( $1 \text{ R}\cdot\text{h}^{-1}$  at 1 m), for example. The roentgen per hour ( $\text{R}\cdot\text{h}^{-1}$ ) was used to designate the exposure to an ionizing radiation of the stated value. The SI unit used for this exposure rate is the sievert (Sv), 100 times as large as the compound unit it replaces:  $1 \text{ Sv}\cdot\text{h}^{-1} = 100 \text{ R}\cdot\text{h}^{-1}$ . The radiation received from  $1 \text{ R}\cdot\text{h}^{-1}$  appeared equal to about 1 rem, so the relationship is approximated as  $1 \text{ R}\cdot\text{h}^{-1} = 0.01 \text{ Gy}\cdot\text{h}^{-1} = 10 \text{ mGy}\cdot\text{h}^{-1}$ .

A previously popular unit, roentgen per curie per hour at one meter ( $\text{R}\cdot\text{Ci}^{-1}\cdot\text{h}^{-1}$  at 1 m), is expressed in SI units as millisievert per gigabecquerel per hour at one meter ( $\text{mSv}\cdot\text{GBq}^{-1}\cdot\text{h}^{-1}$  at 1 m), such that  $1 \text{ mSv}\cdot\text{GBq}^{-1}\cdot\text{h}^{-1}$  at 1 m =  $3.7 \text{ R}\cdot\text{Ci}^{-1}\cdot\text{h}^{-1}$  at 1 m. In this relationship, roentgen converts to millisievert on a one-to-ten basis.

Exposure charts were often made by using curie minutes at a squared distance from source to sensor in inches. This was written  $\text{Ci}\cdot\text{min}\cdot\text{in}^{-2}$ . Exposure charts made in SI use gigabecquerel minutes for a squared distance from source to sensor in centimeters, where  $1 \text{ Ci}\cdot\text{min}\cdot\text{in}^{-2} = 50 \text{ GBq}\cdot\text{min}\cdot\text{cm}^{-2}$ .

## Permissible Doses

### Concept of ALARA (As Low As Reasonably Achievable)<sup>19</sup>

All persons should make every reasonable effort to maintain radiation exposures as low as is reasonably achievable, taking into account the state of technology and the economics of improvements in relation to benefits to the public health and safety. In this sense, the term *permissible dose* is an administrative term mainly for planning purposes.

### Prospective Annual Limit for Occupationally Exposed Personnel

The maximum permissible prospective dose equivalent for *whole body irradiation* is 50 mSv (5 rem) in any one year.<sup>15</sup> The Nuclear Regulatory Commission<sup>19</sup> has further restricted for its licensees the rate at which this planned annual dose may be received by averaging over calendar quarters rather than calendar years. This maximum dose and limits for other parts of the body are summarized in Table 2.

### Permissible Levels of Radiation in Unrestricted Areas<sup>19</sup>

Nonoccupationally exposed personnel or all personnel in unrestricted areas (see below) shall not receive more than 1.0 mSv (0.1 rem) to the whole body in any period of one calendar year.

### Restricted Areas

A *restricted area* needs to be established where either (1) a dose in excess of 20  $\mu\text{Sv}$  (2 mrem) can be received in any 1 h or (2) a dose in excess of 1.00 mSv (100 mrem) can be received in a calendar year.

### Exposure of Minors<sup>19</sup>

An individual under 18 years of age must not be exposed to greater than 10 percent of the limits for occupationally exposed workers, that is, 10 percent of 12 mSv (1.25 rem) per quarter to the whole body and similarly for the hands, forearms, feet, ankles and skin of the whole body.

### Exposure of Females

During the entire nine months of gestation the maximum permissible dose equivalent to the fetus from occupational exposure of the declared pregnant woman should not exceed 5 mSv (0.5 rem) evenly distributed over the entire pregnancy.<sup>15-21</sup>

TABLE 2. Maximum permissible dose per quarter of calendar year (3 mo) for whole body irradiation.<sup>19</sup>

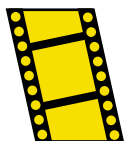
Radiation Workers	Dose per Quarter <sup>a</sup>	
	mSv	(rem)
Whole body; head and	12	(1.25)
Active blood forming organs	12	(1.25)
Lens of eyes	12	(1.25)
Gonads	12	(1.25)
Hands and forearms <sup>b</sup>	188	(18.75)
Feet and ankles	188	(18.75)
Skin of whole body	75	(7.5)

a. These numbers are obtained by dividing annual doses of 5, 75 and 30, respectively, by 4.

b. All reasonable efforts should be made to keep exposure of hands and forearms within the general limit for skin.<sup>2,15-18</sup>

## PART 3. Radiation Protection Measurements

MOVIE.  
Check  
equipment.



### Personnel Dosimetry<sup>21,22</sup>

#### Requirements

Personnel monitoring must be performed on all occupationally exposed persons who may receive in a calendar quarter more than one fourth of the applicable doses in Table 2. Occasional visitors to restricted areas, including messengers, servicemen and deliverymen, can be regarded as nonoccupationally exposed persons who do not need to be provided personnel monitors when it is improbable that they would receive in one year a dose equivalent exceeding the nonoccupational limit of 5 mSv (0.5 rem). Long term visitors in an installation should be regarded as occupationally exposed if they are likely to receive a dose equivalent greater than 5 mSv (0.5 rem) per year.

#### X-Rays, Gamma Rays and Electrons

For radiation protection measurement, the choice lies among ionization chambers, film badges, photoluminescent glasses and thermoluminescent dosimeters.

[\(These and other dosimetric technologies are discussed in the chapter on radiation measurement.\)](#)

**Ionization Chambers.** The principal advantages of ionization chambers (Fig. 1), particularly those of the self-reading type, are the simplicity and speed with which readings are made. They are useful, therefore, particularly for monitoring exposures during nonroutine operations or during transient conditions or for monitoring short term visitors to an installation. Chambers should be tested for leakage periodically and those that leak more than a few percent of full scale over the period of use should be removed from service. Most of these ionization chambers are small, about the size of a pencil, and are charged on a separate device. They read from a few hundredths to a few sievert (a few tens to a few hundred milliroentgen) of exposure.

**Film Badges.** Small badges containing special X-ray films are popular personnel dosimeters (Fig. 2a). The sensitivity of available emulsions is sufficient to detect about  $2.6 \mu\text{C}\cdot\text{kg}^{-1}$  (10 mR) of cobalt-60

gamma radiation and about  $0.8 \mu\text{C}\cdot\text{kg}^{-1}$  (a few mR) of 100 keV X-rays. A useful range is from about  $0.8 \mu\text{C}\cdot\text{kg}^{-1}$  (a few mR) to  $500 \text{ mC}\cdot\text{kg}^{-1}$  (2 kR) can be covered by two commonly available films or two emulsions of different sensitivity on one film base. For energies below 200 keV, film overresponds where, for example, the photographic density per roentgen at 40 keV is about 20 times higher than for 1 MeV photons. Metallic filters covering portions of the film provide additional readings that help determine the incident radiation energy and afford a means of computing a dose from appropriate calibration curves. Film has several undesirable characteristics. Fogging may result from mechanical pressure, elevated temperatures or exposure to light. Fading of the latent image may result in

**FIGURE 1.** Radiation survey meter incorporates air filled ionization chamber vented to atmosphere, with five selectable linear ranges: 0 to 50  $\mu\text{Sv}\cdot\text{h}^{-1}$  (0 to 5  $\text{mR}\cdot\text{h}^{-1}$ ), 0 to 500  $\mu\text{Sv}\cdot\text{h}^{-1}$  (0 to 50  $\text{mR}\cdot\text{h}^{-1}$ ), 0 to 5  $\text{mSv}\cdot\text{h}^{-1}$  (0 to 500  $\text{mR}\cdot\text{h}^{-1}$ ), 0 to 50  $\text{mSv}\cdot\text{h}^{-1}$  (0 to 5  $\text{R}\cdot\text{h}^{-1}$ ), 0 to 500  $\text{mSv}\cdot\text{h}^{-1}$  (0 to 50  $\text{R}\cdot\text{h}^{-1}$ ).





decreased sensitivity but may be minimized by special packaging to exclude moisture and by storage in a refrigerator or freezer before distribution. Film dosimeters also exhibit directional dependence, particularly for the densities recorded behind metal filters.

**Photoluminescent Glasses.** Silver activated metaphosphate glasses, when exposed to ionizing radiation, accumulate fluorescent centers that emit visible light when the glass is irradiated with ultraviolet light. The intensity of the light is proportional to radiation exposure up to  $250 \text{ mC}\cdot\text{kg}^{-1}$  (1000 R) or more. Glass dosimeters exhibit energy dependence below 200 keV and are also subject to fading. They are useful down to only  $250 \mu\text{C}\cdot\text{kg}^{-1}$  (1 R).

**Thermoluminescence.** A common technique of personal radiation exposure measurement is thermoluminescent dosimetry (Fig. 2b). The desirable characteristics of thermoluminescent dosimeters (TLDs) include their wide linear range; short readout time; relative insensitivity to field conditions of heat, light and humidity; reusability; and for some phosphors, energy independence. Response is rate independent up to  $1 \text{ GSv}\cdot\text{s}^{-1}$  ( $100 \text{ GR}\cdot\text{s}^{-1}$ ), which can be useful in flash X-ray radiographic

installations. Very small thermoluminescent dosimeters can be used to measure exposure to specific parts of the body. They probably represent the technique of choice for measurement of finger, hand or eye dose. They have a useful range down to  $1 \mu\text{C}\cdot\text{kg}^{-1}$  (several mR) for lithium fluoride and even lower for more exotic thermoluminescent dosimetric materials.

**Others.** Electronic dosimeters and hybrid technologies are also available.

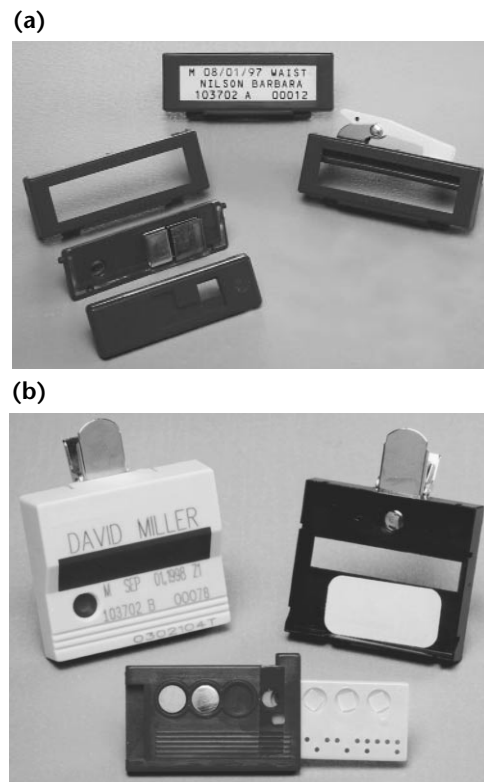
## Neutrons

For neutron fields the practical devices are nuclear track film, thermoluminescent dosimeters containing lithium-6 fluoride and fission track counting systems. The nuclear track films do not respond to neutrons below 0.5 MeV in energy; in practice, a substantial fraction of the neutrons may be below this energy. Track counting is a relatively insensitive technique of neutron dosimetry. For low doses, counting of a statistically significant number of tracks is too time consuming to be warranted. On the other hand, at high doses it is difficult to distinguish tracks from one another so that they can be counted. Fading occurs and, as a result, short tracks may disappear. For these reasons, nuclear track film is more useful in demonstrating that large neutron doses have not been received than in measuring actual low doses.

The lithium-6 fluoride and fission track counting systems do not suffer from these disadvantages and will provide measurements at permissible dose levels. These techniques are sensitive down to doses of about 30 or 40  $\mu\text{Gy}$  (3 or 4 mrad) and down to thermal neutron energies.

Boron trifluoride neutron radiation detector tubes provide high gamma rejection up to about  $5 \text{ Sv}\cdot\text{h}^{-1}$  ( $500 \text{ R}\cdot\text{h}^{-1}$ ) and detect neutrons with energies from thermal to about 10 MeV (Fig. 3).<sup>23</sup> Other means of neutron dosimetry, including ion chambers, have been investigated or developed.<sup>23-25</sup>

**FIGURE 2.** Clip-on personal radiation dosimeters: (a) film badges; (b) thermoluminescent dosimeters (TLDs).<sup>21</sup>



## Radiation Detection and Measurement<sup>22</sup>

In an area survey, measurements are made of radiation fields to provide a basis for estimating the dose equivalents that persons may receive. Changes in operating conditions (such as beam orientations and source outputs) can cause changes both in field intensity and pattern. The number of measurements depends on how much the radiation field varies in space and time and on how

much people move about in the field. Measurements made at points of likely personnel occupancy under the different operating conditions are usually sufficient to estimate dose equivalent adequately for protection purposes.

Detection instruments are used in radiation surveys and area monitoring to warn of the existence of radiation or radiation hazard and, as distinct from measuring instruments, usually indicate count rate rather than dose rate or exposure rate. They should be used only to indicate the existence of radiation.

## Measurement

At points of particular interest, individual determinations of dose or exposure rate should be made with calibrated measuring instruments. Dose integrating devices (dosimeters) may be mounted at points of interest and left for an extended period of time to improve the accuracy of the measurement.

Information concerning the dimensions, dose rate and location of primary beams of radiation in relation to the source is important in determining direct external exposure from the beam and the adequacy of protective measures. The dose or exposure rates within the beam at specific distance from the source should be measured and compared with expected values.

Measurements close to radiation sources of small dimensions or of radiation transmitted through holes or cracks in shielding require special attention. The general location of discontinuities in shielding should be determined by scanning with sensitive detection instruments. More precise delineation of the size and configuration of the discontinuities can be obtained by using photographic film or fluorescent screens for X-ray, gamma ray or electron leakage. Measurements may then be made in any of three ways:

1. Film may be used at the point of interest, provided it has been properly calibrated for the types and energies of the radiations present.
2. An instrument may be used that has a detector volume small enough to ensure that the radiation field throughout the sensitive volume is substantially uniform.
3. An instrument with a large sensitive volume may be used, if an appropriate correction factor is applied. Only when  $A_{\text{chamber}}$  is larger than  $A_{\text{beam}}$ , multiply the reading by the ratio of the instrument chamber cross section area to the beam cross section area:

$$(2) \quad \text{Reading} \times \frac{A_{\text{chamber}}}{A_{\text{beam}}} = \text{Corrected reading}$$

## Choice of Instruments<sup>22</sup>

The following general properties should be considered.

**Energy Response.** If the energy spectrum of the radiation field differs significantly from that of the calibration field, a correction may be necessary.

**Directional Response.** If the directions from which the radiations arrive at the instrument differ significantly from those in the calibration field, correction may be necessary. If the dose equivalents being determined are small in comparison to permissible doses, large errors are acceptable and correction may not be necessary.

**Rate Response.** Instruments that measure dose or exposure are called *integrating instruments*; those that measure dose rate or exposure rate are called *rate instruments* or *rate meters*. If the dose rate or exposure rate differs significantly from that in the calibration field, correction may be necessary. Ordinarily, an integrating instrument should be used only within the rate ranges for which the reading is independent of the rate. Rate instruments, similarly, should be used only within the rate ranges in which the reading is proportional to the rate. A few instruments will become saturated at very

**FIGURE 3.** Boron trifluoride neutron radiation detector tube provides high gamma rejection up to about  $5 \text{ Sv} \cdot \text{h}^{-1}$  ( $500 \text{ R} \cdot \text{h}^{-1}$ ) and detects neutrons with energies from thermal to about 10 MeV.





high rates; that is, they will cease to function and the reading will drop to zero or close to zero. It is particularly necessary to know the rate response of instruments to be used near machines that produce radiation in short pulses. Rate instruments used near repetitively pulsed machines

need only to indicate the average rate for radiation protection purposes.

**Mixed Field Response.** Because some radiations (such as neutrons) have higher quality factors than others, mixed field monitoring is necessary. This can be done either by using two instruments that are

**FIGURE 4.** Gamma and X-radiation sensing devices incorporating geiger-müller tubes: (a) survey meter for range selectable from 0 to 20 mSv·h<sup>-1</sup> (0 to 2 R·h<sup>-1</sup>) and automatic aural alarm over 2.5 mSv·h<sup>-1</sup> (250 mR·h<sup>-1</sup>); (b) survey meter with on/off switch for aural monitoring; (c) for high noise areas, personal rate alarm with flashing light and optional earplug for aural alarm; (d) area monitor with standard 20 μSv·h<sup>-1</sup> (2 mR·h<sup>-1</sup>) trip point, audio piezo alert and large red strobe warning light; (e) visual alarm for gamma and X-rays from 80 keV to 1.5 MeV and adjustable alarm threshold.

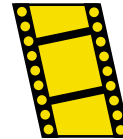
(a)



(c)



**MOVIE.**  
Personnel  
monitoring  
devices.



(d)



(b)



(e)



each sensitive to only one radiation or by using two instruments that are sensitive to both but to a different extent.

**Unwanted Response.** Interference by energy forms that an instrument is not supposed to measure can be a problem. Response to heat, light, radiofrequency radiations and mechanical shock are examples.

**Fail Safe Provision.** To avoid unknowingly exposing personnel to radiation, malfunctions of an instrument should be readily recognizable or should always result in readings that are too high.

**Precision and Accuracy.** Typically, *precision* of a few percent should be obtained on successive readings with the same survey instrument. At the level of a maximum permissible dose a measurement *accuracy* specified by regulations should be achieved. At levels less than 0.25 the maximum permissible dose a lower level of *accuracy* (say, a factor of 2) is acceptable.

**Calibration.** Instruments used for radiation protection are not absolute instruments; that is, they require calibration in a known radiation field or comparison with instruments whose response is known. Many users of radiation protection instruments must rely on the manufacturer to calibrate their instruments properly. Users should arrange a reproducible field in which the instruments are placed and read frequently — at least semiannually. The possibility of reading error due to imprecision is minimized by computing the mean of several readings. If changes in the mean reading are detected, the instruments should be recalibrated promptly.

**Time Constant.** An important characteristic of a rate instrument is the time constant, an indication of the time necessary for the instrument to attain a constant reading when suddenly placed in a constant radiation field. Time constants are generally given as the time required to arrive at  $1 - e^{-1}$  (that is, 0.63) of the final reading. Typical time constants of good rate meters are 1 s or less. The *response time* of a rate instrument is defined as the time necessary for it to reach 90 percent of full response. It is equal to 2.3 time constants.

## Radiation Surveying and Area Monitoring

Various technologies for radiation surveying and area monitoring are available. The following can be used for sealed gamma ray sources and for sources of X-rays. (More information on these technologies can be found in the chapter on radiation measurement.)

**Ionization Chambers.** Many gamma ray and X-ray exposure rate measurements are made with portable ionization chambers (Fig. 1). Ionization chambers with separate readers are useful for measuring either very high or very low exposure rates. Ion chambers made of plastic or other low atomic number materials usually give exposure readings independent of photon energy down to 50 keV. Ionization chambers are available for exposure rates to over  $20 \text{ Sv}\cdot\text{h}^{-1}$  (3 or 4  $\text{kR}\cdot\text{h}^{-1}$ ).

**Geiger-Müller Counters.** The dead time in geiger-müller counters (Fig. 4) sets a limit to their count rate that, in turn, limits their use to exposure rates up to about 0.03 nSv (a few  $\mu\text{R}\cdot\text{h}^{-1}$ ). The counters respond to the number of ionizing events within them independent of energy and thus do not yield equal count rates for equal exposure rates of different energies. Geiger-müller counters are better suited for radiation detection than for measurement.

**Scintillation Instruments.** Scintillation devices (Fig. 5) also have count rate limitations because of the duration of the light flashes but can count much faster than geiger-müller counters. In the same exposure field, scintillation count rates are higher than geiger-müller count rates, so scintillation counters are useful for locating weak X-ray and gamma ray fields.

FIGURE 5. Radiation detector with scintillation counter measurement of low energy gamma radiation.



## Instrument Calibration

The National Institute of Standards and Technology (NIST) is the point of record for reference standards. Laboratories calibrate according to the National Institute of Standards and Technology. Laboratory standard instruments for measuring exposure from photons of higher energies from 1 to 1000 mSv (0.1 to 100 R) or exposure rate from 0.1 to 150 mSv·min<sup>-1</sup> (0.01 to 15 R·min<sup>-1</sup>) can be calibrated by the National Institute of Standards and Technology by comparison with either cesium-137 or cobalt-60 calibrated sources. These laboratory standard instruments or secondary standards may then be used to calibrate radiation protection survey instruments by comparison in radiation fields of similar quality. Consideration must be given to beam width, uniformity of radiation over the calibration area and changes in radiation quality caused by scattered radiation.

Neutron instrument calibration can be afforded by exposure to fields from National Institute of Standards and Technology calibrated neutron sources. One type of such a source is made by mixing a radionuclide such as plutonium, polonium or radium with a material such as beryllium or boron. The neutrons are produced in ( $\alpha$ ,  $n$ ) reactions in the latter materials. Radium sources are difficult to use because they also emit intense gamma radiation.

## Leak Testing of Isotope Sealed Sources<sup>26</sup>

All sealed sources must be tested for leakage of radioactive material before initial use, at intervals not exceeding six months, whenever damage or deterioration of the capsule or seal is suspected or when contamination of handling or storage equipment is detected.

The leak test should be capable of detecting the presence of 185 Bq (5 nCi) of removable activity from the source. Sources that are in the United States and that are leaking greater than 185 Bq (5 nCi) of removable activity, based on the tests described below, should be reported to the Nuclear Regulatory Commission within five days. Records of leak test results should be specific in units of disintegrations per minute or microcuries. Leak test records should be kept until final disposition of the source is accomplished.

A small sealed capsule may be tested by washing for a few minutes in a detergent solution. An aliquot of this solution should then be counted. An absorbent liner in the storage container normally in

contact with the source will also reveal leakage if it is contaminated.

Leak tests of devices from which the encapsulated source cannot be removed or is too large to handle should be made by wiping the accessible surface or aperture of the device nearest to the storage position of the source.

Detection of contaminants on the housing or surface of a neutron source may not indicate source leakage but may be due to induced activity. Confirmation of leakage may require identification of the contaminant.

In leak testing of radioactive sources, special equipment may be necessary for radiation exposure control. Depending on the activity of the source, shielding may be required to keep the leak tester's exposure as low as possible. The actual leak test wipe should be done by using tongs or forceps and not the fingers. Rubber gloves should be used to minimize hand contamination. The wipes should be taken quickly and the source returned to its designated container.

## PART 4. Basic Exposure Control

### Physical Safeguards and Procedural Controls<sup>22</sup>

As long as the radiation source remains external, exposure of the individual may be terminated by removing the individual from the radiation field, by removing the source or by switching off a radiation producing machine. If the external radiation field is localized, exposure to individuals may be limited readily by shielding or by denying access to the field of radiation.

#### Physical Safeguards

Physical safeguards include all physical equipment used to restrict access of persons to radiation sources or to reduce the level of exposure in occupied areas. These include *shields, barriers, locks, alarm signals* and *source shutdown mechanisms*.

Planning and evaluation of physical safeguards should begin in the early phases of design and construction of an installation. Detailed inspection and evaluation of the radiation safety of equipment are mandatory at the time of the installation's initial use. Additional investigations are necessary periodically to ensure that the effectiveness of the safeguards has not decreased with time or as a result of equipment changes.

#### Procedural Controls

Procedural controls include all instructions to personnel regarding the performance of their work in a specific manner for the purpose of limiting radiation exposure. *Training programs* for personnel often are necessary to promote observance of such instructions. Typical instructions concern *mode of use* of radiation sources, limitations on *proximity* to sources, *exposure time* and *occupancy* of designated areas and the sequence or kinds of *actions permitted* during work with radiation sources.

*Periodic area surveys* and *personnel monitoring* are necessary to ensure the adequacy of and compliance with established procedural controls.

### Classes of Installations for X-Rays and Gamma Rays

There are four types of nonmedical X-ray and gamma ray installations: *protective, enclosed, unattended* and *open*.<sup>3,26</sup>

#### Protective Installation

This class provides the highest degree of inherent safety because the protection does not depend on compliance with any operating limitations. The requirements include the following.

1. Source and exposed objects are in a permanent enclosure within which no person is permitted during irradiation.
2. Safety interlocks are provided to prevent access to the enclosure during irradiation.
3. If the enclosure is of such a size or is so arranged that occupancy cannot be readily determined by the operator, the following requirements should also be provided: (a) fail safe audible or visible warning signals to indicate the source is about to be used; (b) emergency exits; (c) effective means within the enclosure of terminating the exposure (sometimes called scrambling).
4. The radiation exposure 50 mm (2.0 in.) outside the surface of the enclosure cannot exceed 5  $\mu\text{Sv}$  (0.5 mR) in any 1 h.
5. Warning signs of prescribed wording at prescribed locations.
6. No person may be exposed to more than the permissible doses. The low allowable exposure level necessitates greater inherent shielding. At high energies in the megavolt region with high workloads, the required additional shielding may be extremely expensive. For example, in the case of cobalt-60, the required concrete thickness will have to be about 0.3 m (1 ft) greater than for the enclosed type.

#### Enclosed Installation

This class usually offers the greatest advantages for fixed installations with low use and occupancy. With *proper supervision* this class offers a degree of protection

similar to the protective installation. The requirements for an enclosed installation include items 1, 2, 3, 5 and 6, above, plus a different item 4.

4. The exposure at any *accessible* and *occupied* area 0.3 m (1 ft) from the outside surface of the enclosure does not exceed 100  $\mu\text{Sv}$  (10 mR) in any 1 h. The exposure at any accessible and *normally unoccupied* area 0.3 m (1 ft) from the outside surface of the enclosure does not exceed 1 mSv (100 mR) in any 1 h. This class of installation requires administrative procedures to avoid exceeding the permissible doses. The tradeoff between (1) the intrinsic but initially expensive safety of a protective installation and (2) the required continuing supervision and consequences of an overexposure in an enclosed installation should be carefully considered in the planning stages of a new facility.<sup>22</sup>

### Unattended Installation

This class consists of automatic equipment designed and manufactured by a supplier for a specific purpose that does not require personnel in attendance for operation. The requirements for this class include the following.

1. The source is installed in a single purpose device.
2. The source is enclosed in a shield, where the closed and open positions are identified and a visual warning signal indicates when the source is on.
3. The exposure at any accessible location 0.3 m (1 ft) from the outside surface of the device cannot exceed 20  $\mu\text{Sv}$  (2 mR) in any 1 h.
4. The occupancy in the vicinity of the device is limited so that the exposure to any individual cannot exceed 5 mSv (0.5 R) in a year.
5. Warning signs are used.

6. Service doors to areas where exposure can exceed the measurements in items 3 and 4 above must be locked or secured with fasteners requiring special tools available only to qualified service personnel.

### Open Installation

This class can only be used when operational requirements prevent other classes, such as in mobile and portable equipment where fixed shielding cannot be used. Mobile or portable equipment used routinely in one location should be made to meet the requirements of one of the fixed installation classes. Adherence to safe operating procedures is the main safeguard to overexposure. The requirements include the following.

1. The perimeter of any area in which the exposure can exceed 1 mSv (100 mR) in any 1 h must be posted as a *very high radiation area*.
2. No unauthorized or unmonitored person may be permitted in the high radiation area during irradiation. In cases of unattended operation, positive means, such as a locked enclosure, shall be used to prevent access.
3. The perimeter of any area in which the radiation level exceeds 50  $\mu\text{Sv}$  (5 mR) in any 1 h must be posted as a radiation area.
4. The equipment essential to the use of the source must be inaccessible to unauthorized use, tampering or removal. This shall be accomplished by the attendance of a knowledgeable person or other means such as a locked enclosure.
5. No person can be exposed to more than the permissible doses.
6. For reasons of safety and security, restricted areas must be clearly defined and marked. Means of surveillance to enforce the restrictions are needed.

**MOVIE.**  
Warning tape  
and sign.

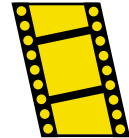


TABLE 3. Gamma ray sources.<sup>3,15,27</sup>

Radionuclide	Atomic Number (Z)	Half Life	Energy (MeV)	Gamma Ray Constant	
				mSv-GBq <sup>-1</sup> ·h <sup>-1</sup> at 1 m	(R·Ci <sup>-1</sup> ·h <sup>-1</sup> at 1 m)
Cesium-137	55	30 yr	0.662	0.086	(0.320)
Chromium-51	24	28 d	0.323	0.005	(0.018)
Cobalt-60	27	5.3 yr	1.17, 1.33	0.351	(1.300)
Gold-198	79	2.7 d	0.412	0.062	(0.230)
Iridium-192	77	74 d	0.136, 1.065	0.135	(0.500)
Radium-226	88	1622 yr	0.047 to 2.4	0.223	(0.825)
Tantalum-182	73	155 d	0.066 to 1.2	0.162	(0.600)



## Output of Radiation Sources

Table 3 lists some data on gamma ray sources of interest for industrial purposes.

Table 4 lists some typical radiation machine outputs for varying voltages.

## Working Time

This is the allowable working time in hours per week for a given exposure rate. For example, for an exposure rate of  $100 \mu\text{Sv}\cdot\text{h}^{-1}$  ( $10 \text{ mR}\cdot\text{h}^{-1}$ ) to the whole body:

$$\begin{aligned} (3) \quad \text{Working time} &= \frac{\text{Permissible occupational dose per week}}{\text{Exposure dose rate}} \\ &= \frac{1000 \mu\text{Sv} \cdot \text{wk}^{-1}}{100 \mu\text{Sv} \cdot \text{h}^{-1}} \\ &\left( = \frac{100 \text{ mR} \cdot \text{wk}^{-1}}{10 \text{ mR} \cdot \text{h}^{-1}} \right) \\ &= 10 \text{ h} \cdot \text{wk}^{-1} \end{aligned}$$

## Working Distance

The inverse square law applied to radiation states that the dose rate from a point source is inversely proportional to the square of the distance from the origin of the radiation source provided that

(1) the dimensions of the radiation source are small compared with the distance and (2) no appreciable scattering or absorption of the radiation occurs in the media through which the radiation travels. In practice, the first requirement is satisfied whenever the distance involved is at least ten times greater than the largest source dimension. In situations where there is

insignificant scattering or absorption, the primary beam is the total radiation field.

For example, consider a  $3.7 \text{ GBq}$  ( $100 \text{ mCi}$ ) iridium-192 source in air in the shape of a pencil,  $6.3 \text{ mm}$  ( $0.25 \text{ in.}$ ) diameter and  $0.13 \text{ m}$  ( $5.0 \text{ in.}$ ) long. What would the working time be at  $3.0 \text{ m}$ ? First, solve for  $1 \text{ m}$ . From Table 3, the gamma ray constant for iridium-192 is  $135 \mu\text{Sv}\cdot\text{GBq}^{-1}\cdot\text{h}^{-1}$  at  $1 \text{ m}$  ( $0.5\text{-Ci}^{-1}\cdot\text{R}\cdot\text{h}^{-1}$  at  $1 \text{ m}$ ). Therefore:

$$\begin{aligned} (4) \quad \text{Exposure rate} &= \left[ \frac{0.135 \text{ mSv}\cdot\text{GBq}^{-1}\cdot\text{h}^{-1}}{\text{at } 1 \text{ m}} \right] \\ &\times 3.7 \text{ GBq} \\ &= 0.5 \text{ mSv}\cdot\text{h}^{-1} \end{aligned}$$

$$(5) \quad \left( \begin{aligned} \text{Exposure rate} &= \left[ \frac{0.5 \text{ R}\cdot\text{Ci}^{-1}\cdot\text{h}^{-1}}{\text{at } 1 \text{ m}} \right] \\ &\times 0.1 \text{ Ci} \\ &= 0.05 \text{ R}\cdot\text{h}^{-1} \end{aligned} \right)$$

Because  $3.0 \text{ m}$  is obviously more than 10 times  $0.13 \text{ m}$  ( $5.0 \text{ in.}$ ), the inverse square law applies. Also, scattering is not a problem. Using the inverse square law gives the exposure rate at  $3 \text{ m}$ :

$$\begin{aligned} (6) \quad \text{Exposure rate} &= \left[ \frac{0.5 \text{ mSv}\cdot\text{h}^{-1}}{\text{at } 1 \text{ m}} \right] \\ &\times \left( \frac{1 \text{ m}}{3 \text{ m}} \right)^2 \\ &= 55 \mu\text{Sv}\cdot\text{h}^{-1} \end{aligned}$$

$$(7) \quad \left( \begin{aligned} \text{Exposure rate} &= \left[ \frac{0.05 \text{ R}\cdot\text{Ci}^{-1}\cdot\text{h}^{-1}}{\text{at } 1 \text{ m}} \right] \\ &\times \left( \frac{1 \text{ m}}{3 \text{ m}} \right)^2 \\ &= 5.5 \text{ mR}\cdot\text{h}^{-1} \end{aligned} \right)$$

Equations 8 and 9 finally give the working time at  $3 \text{ m}$ :

$$\begin{aligned} (8) \quad \text{Working time} &= \frac{1 \text{ mSv}\cdot\text{wk}^{-1}}{55 \mu\text{Sv}\cdot\text{h}^{-1}} \\ &= 18 \text{ h}\cdot\text{wk}^{-1} \end{aligned}$$

$$(9) \quad \left( \begin{aligned} \text{Working time} &= \frac{100 \text{ mR}\cdot\text{wk}^{-1}}{5.5 \text{ mR}\cdot\text{h}^{-1}} \\ &= 18 \text{ h}\cdot\text{wk}^{-1} \end{aligned} \right)$$

TABLE 4. Forward X-ray intensity from optimum target.<sup>3,27,32</sup>

Peak Voltage (MV)	Intensity at 1 m (40 in.)	
	$\text{kSv}\cdot\text{min}^{-1}\cdot\text{mA}^{-1}$	$(\text{R}\cdot\text{min}^{-1}\cdot\text{mA}^{-1})$
0.050	0.005	(0.05)
0.070	0.01	(0.1)
0.100	0.04	(0.4)
0.250	0.2	(2.0)
1.000	2.0	(20)
2.000	28	(280)
5.000	500	(5000)
10.000	3000	(30 000)
15.000	10 000	(100 000)
20.000	20 000	(200 000)



## PART 5. Shielding

### Protective Enclosures

Because of scattered radiation, protection for the operator and other personnel working in the neighborhood often requires shielding of the part being radiographed and any other material exposed to the direct beam, in addition to the shield for the source itself. Preferably the source and materials being examined should be enclosed in a room or hood with the necessary protection incorporated into the walls (Fig. 6).

Shields can be classified as either primary or secondary. Primary shields are

designed to shield against the primary radiation beam; secondary shields are only thick enough to protect against tube housing leakage and scattered radiation. Therefore, the X-ray tube or source should *not* be pointed toward secondary shields. For this reason, mechanical stops should be used to restrict tube housing orientations toward primary barriers. Operating restrictions, such as not pointing the beam at certain walls or the ceiling, should be spelled out in the operating procedures.

Protective materials are available in panels so that radiation barriers may be customized for work areas of various sizes. Mobile work rooms with modular designs are also available, offering the same flexibility in size and location (Fig. 6b).

When changes in operating conditions are contemplated, the radiation safety officer (RSO) should be contacted for consultation and for surveys as needed to determine additional shielding requirements.

For design purposes, the primary beam should not be pointed at a high personnel occupancy space and the distance from the radiation source to any occupied space should be as great as is practical. Scattered radiation usually has a lower effective energy than the primary beam and may, therefore, be easier to shield.

### Skyshine<sup>28</sup>

In the design of facilities, there is often a question concerning the magnitude of shielding required for the roof over the building. As an ordinary weather roof

FIGURE 6. Rooms offering radiation shielding: (a) concrete shooting booth; (b) modular radiation enclosure.

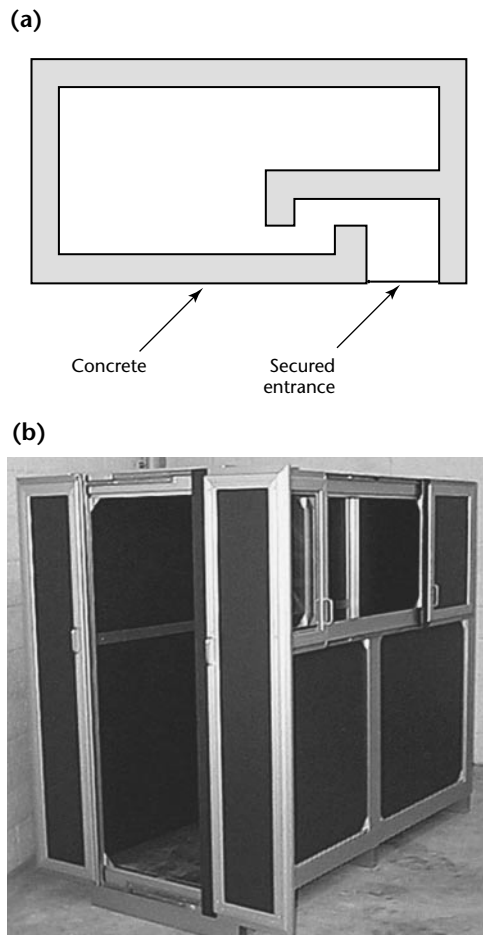
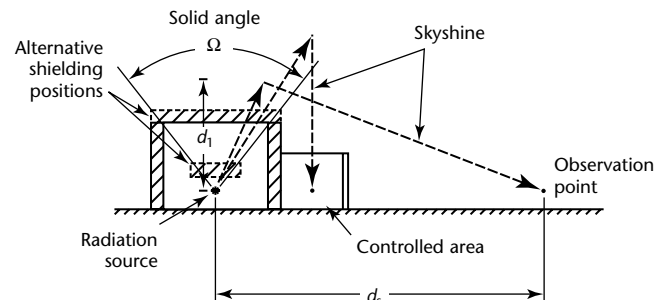


FIGURE 7. Shielding above radiation source reduces radiation reflected from atmosphere. Such radiation is called skyshine.<sup>28</sup>



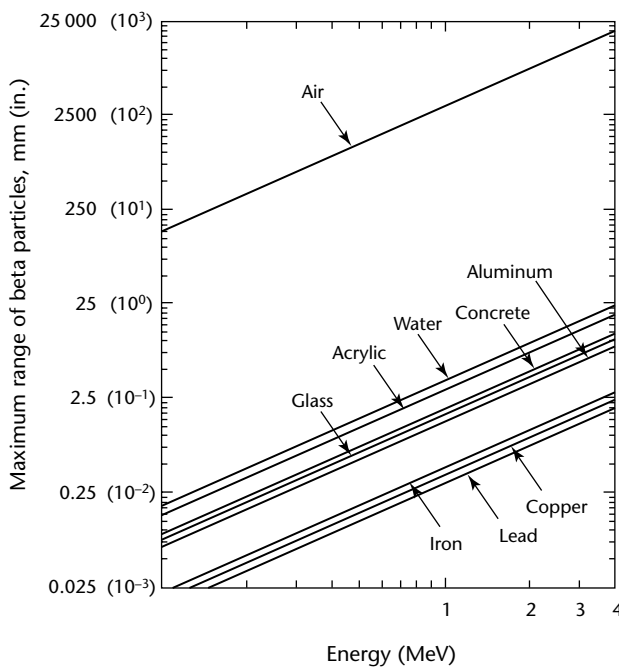
provides little if any attenuation for radiation directed up, there is a significant probability that radiation reflected back from the atmosphere will be unacceptable in the immediate area of the facility. See Fig. 7 for X-rays and gamma rays this radiation (1) increases roughly as  $\Omega^{1.3}$ , where  $\Omega$  is the solid angle subtended by the source and shielding walls, (2) decreases with  $(d_s)^2$ , where  $d_s$  is the horizontal distance from the source to the observation point and (3) decreases with  $(d_i)^2$ , where  $d_i$  is the vertical distance from the source to about 2 m (6.5 ft) above the roof.

The shield thickness necessary to reduce the radiation to an acceptable level may be calculated according to published techniques<sup>28</sup> and may alternatively be designed into the roof structure or mounted over the source with a lateral area sufficient to cover the solid angle  $\Omega$ . Similar statements apply to neutron skyshine, except that the functional dependences of the radiation at  $d_s$  are slightly different for  $\Omega$  and  $d_s$ .

## Materials

Common materials such as concrete and lead can be used as absorbers or shields to reduce personnel exposures.<sup>29</sup> Beta or electron radiation is completely stopped by the thicknesses of material shown in Fig. 8.<sup>30</sup> The thickness of any material that will halve the amount of radiation passing through the material is referred to

FIGURE 8. Maximum range of beta particles as function of energy in various materials indicated.<sup>30</sup>



as the *half value layer* (HVL). Similarly, the thickness that will reduce the radiation to one tenth is referred to as the *tenth value layer* (TVL). (See Tables 5 and 6 and see Figs. 9 and 10.<sup>1,3</sup>)

FIGURE 9. Transmission through lead of gamma rays from selected radionuclides.<sup>3</sup>

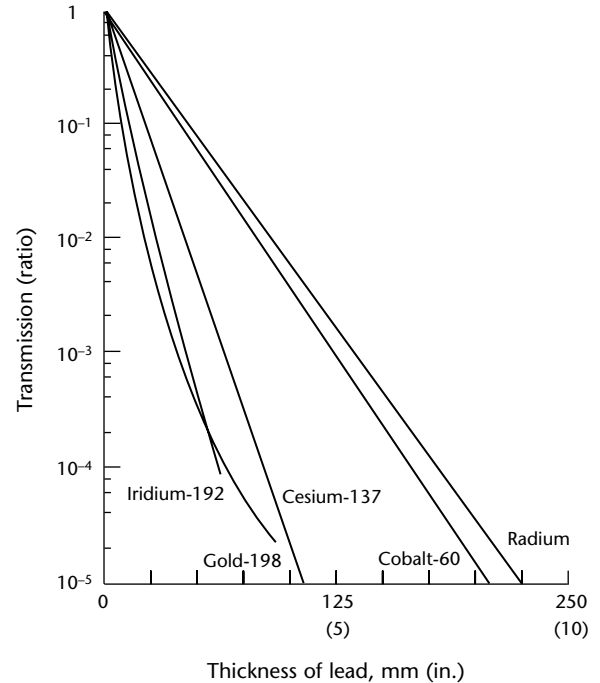
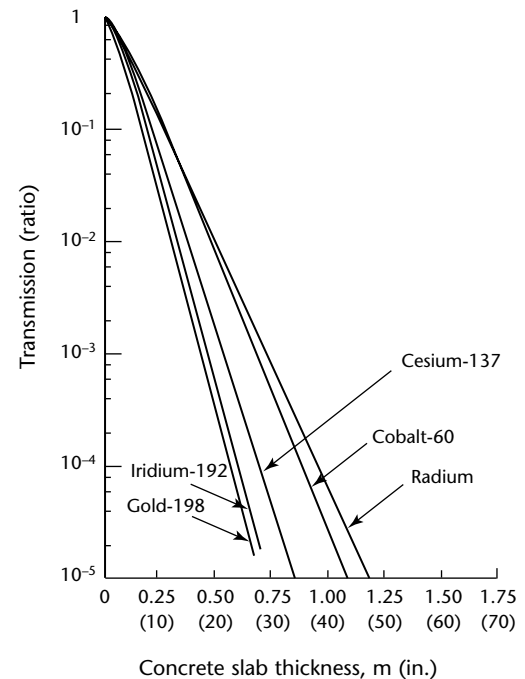


FIGURE 10. Transmission through concrete (density of 2.35 g·cm<sup>-3</sup> [147 lb<sub>m</sub>·ft<sup>-3</sup>]) of gamma rays from radium, cobalt-60, gold-198 and iridium-192.<sup>3</sup>



These terms imply an exponential function for transmitted radiation in terms of shield thickness. Figures 9 and 10, however, show that the transmission curves are not completely linear on a semilogarithmic plot.<sup>1,3</sup> Hence, the listed half value layers and tenth value layers in Tables 5 and 6 are approximate, obtained with large attenuation.

Table 7 lists densities of commercial building materials. For X-radiation and gamma radiation, the absorption process depends largely on Compton absorption and scattering, which in turn increase with the atomic electron density. As a first approximation, electron density varies directly with the mass density of a material. Hence, the denser building materials are usually better shielding materials for a given thickness of material. On a mass basis, shielding materials are much the same above about 500 keV. Where space is a problem, lead is often used to achieve the desired shield

attenuation. Lead, however, requires extra structural support because it is not self-supporting. Concrete is by far the most commonly used shielding material for economic, structural and local availability reasons — in addition to desirable shielding characteristics. Where space considerations are important depleted uranium shields are expensive but offer excellent solutions to difficult problems.

Table 5 lists half value layers and tenth value layers for several commonly used gamma ray emitting radionuclides.

Table 6 lists similar information for X-ray peak voltages. Figures 9 and 10 show actual transmission through lead and concrete for the gamma ray emitting radionuclides. Figure 11 shows a representative transmission through concrete. Similar charts are available for steel, lead and other materials for X-ray beams of various peak energies.<sup>1,28</sup>

**Table 5. Shielding equivalents: approximate tenth (TVL) and half value (HVL) layer thicknesses in lead and concrete for several gamma ray sources.<sup>3,27</sup>**

Source	Lead				Concrete			
	Half Value Layers		Tenth Value Layers		Half Value Layers		Tenth Value Layers	
	mm	(in.)	mm	(in.)	mm	(in.)	mm	(in.)
Radium-226	56	(2.20)	16	(0.65)	234	(9.2)	69	(2.7)
Cobalt-60	41	(1.60)	12	(0.49)	218	(8.6)	66	(2.6)
Cesium-137	21	(0.84)	6	(0.25)	157	(6.2)	48	(1.9)
Iridium-192	20	(0.79)	6	(0.24)	140	(5.5)	41	(1.6)
Gold-198	11	(0.43)	3	(0.13)	140	(5.5)	41	(1.6)

**TABLE 6. Shielding equivalents: approximate half value layers (HVL) and tenth value layers (TVL) for lead and concrete for various X-ray tube potentials.<sup>3,27</sup>**

Peak Voltage (kV)	Lead				Concrete			
	Half Value Layers		Tenth Value Layers		Half Value Layers		Tenth Value Layers	
	mm	(in.)	mm	(in.)	mm	(in.)	mm	(in.)
50	0.05	(0.002)	0.16	(0.006)	4.32	(0.170)	15.10	(0.594)
70	0.15	(0.006)	0.50	(0.020)	8.38	(0.330)	27.95	(1.100)
100	0.24	(0.009)	0.80	(0.031)	15.10	(0.594)	50.80	(2.000)
125	0.27	(0.011)	0.90	(0.035)	20.30	(0.799)	66.00	(2.598)
150	0.29	(0.011)	0.95	(0.037)	22.35	(0.880)	73.60	(2.898)
200	0.48	(0.019)	1.60	(0.063)	25.40	(1.000)	83.80	(3.299)
250	0.90	(0.035)	3.00	(0.118)	27.95	(1.100)	94.00	(3.701)
300	1.40	(0.055)	4.60	(0.181)	31.21	(1.229)	104.00	(4.094)
400	2.20	(0.087)	7.30	(0.287)	33.00	(1.299)	109.10	(4.295)
500	3.60	(0.142)	11.90	(0.469)	35.55	(1.400)	116.80	(4.598)
1000	7.90	(0.311)	26.00	(1.024)	44.45	(1.750)	147.10	(5.791)
2000	12.70	(0.500)	42.00	(1.654)	63.50	(2.500)	210.40	(8.283)
3000	14.70	(0.579)	48.50	(1.909)	73.60	(2.898)	241.20	(9.496)
4000	16.50	(0.650)	54.80	(2.157)	91.40	(3.598)	304.48	(11.987)
6000	17.00	(0.669)	56.60	(2.228)	104.00	(4.094)	348.00	(13.701)
10000	16.50	(0.650)	55.00	(2.165)	116.80	(4.598)	388.50	(15.295)

These charts present *broad beam shielding* information, which includes all scattered radiation resulting from deflection of the primary gamma or X-rays within the shield as well as absorption of the primary radiation. Most engineering applications need to consider broad beam geometry. *Narrow beam geometry*, where only the primary beam needs consideration, is seldom encountered in practice.

## Thickness of Shielding Walls

The shielding in the walls of the enclosures should be of sufficient thickness to reduce the exposure in all occupied areas to a value *as low as reasonably achievable* (ALARA). In the design the desired thickness can be determined with reasonable accuracy by

TABLE 7. Densities of commercial building materials.<sup>3,27</sup>

Material	Average Density	
	g·cm <sup>-3</sup>	(lb <sub>m</sub> ·ft <sup>-3</sup> )
Aluminum	2.7	(169)
Bricks: fire clay	2.05	(128)
Bricks: kaolin clay	2.1	(131)
Bricks: silica	1.78	(111)
Bricks: clay	2.2	(137)
Cement: colemanite borated	1.95	(122)
Cement: portland and sand <sup>a</sup>	2.07	(129)
Concrete: barite	3.5	(218)
Concrete: barite with boron frit	3.25	(203)
Concrete: barite with limonite	3.25	(203)
Concrete: barite with other <sup>b</sup>	3.1	(194)
Concrete: iron portland	6.0	(375)
Concrete: portland <sup>c</sup>	2.2	(137)
Glass: borosilicate	2.23	(139)
Glass: lead (high density)	6.4	(399)
Glass: plate (average)	2.4	(150)
Iron	7.86	(491)
Lead	11.34	(708)
Acrylic (polymethyl methacrylate)	1.19	(74)
Rock: granite	2.45	(153)
Rock: limestone	2.91	(182)
Rock: sandstone	2.40	(150)
Sand	2.2	(137)
Sand plaster	1.54	(96)
Steel: Type 347 stainless	7.8	(487)
Steel: 1 percent carbon	7.83	(489)
Uranium	18.7	(1167)
Uranium hydride	11.5	(718)
Water	1.0	(62)

a. One part portland cement and two parts sand.

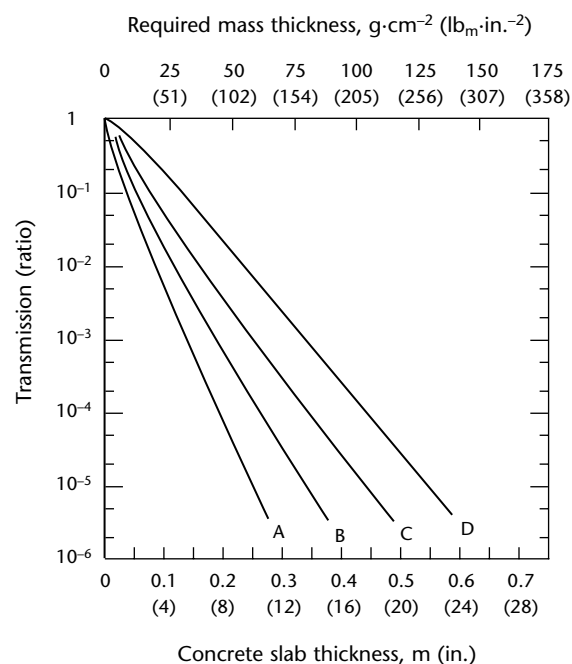
b. Barite with calcium aluminate and colemanite.

c. One part cement, two parts sand and four parts gravel.

reference to tables or by calculations. See the applicable standard.<sup>3,28,29</sup>

In many cases an additional tenth value layer can be induced at little extra cost and will increase the margin of safety considerably. A series of measurements of transmitted radiation in occupied areas, called a *radiation survey*, is necessary to document the adequacy of the facility's design. Such a radiation survey can be derived from a combination of portable instrument readings and personnel dosimeters placed at appropriate locations in the facility (called *badge plants*).

FIGURE 11. Transmission through concrete (density of 2.35 g·cm<sup>-3</sup> [147 lb<sub>m</sub>·ft<sup>-3</sup>]) of X-rays produced by 0.1 to 0.4 MeV electrons under broad beam conditions. Four curves shown represent transmission in dose equivalent index ratio. First three electron energies were accelerated by voltages with pulsed wave form. Fourth electron energy (0.4 MeV) was accelerated by constant potential generator. Top scale indicates required mass thickness, or mass per unit area, g·cm<sup>-2</sup> (lb<sub>m</sub>·in.<sup>-2</sup>). Concrete of different density may be used if required mass thickness is achieved. Where weight is considered, this scale can be used in selection of optimum shielding material.<sup>28</sup>



### Legend

- A. 0.10 MeV.
- B. 0.15 MeV.
- C. 0.25 MeV.
- D. 0.40 MeV.

## PART 6. Neutron Radiographic Safety

### Introduction

Neutrons are of interest in radiography because their interaction with matter is significantly different from X-rays or gamma rays. Neutrons are absorbed and scattered more in low atomic numbered (low  $Z$ ) materials than high  $Z$  materials. Thus, plastics, explosives and some organic materials can be examined for discontinuities with little interference from encapsulating metals and electronic parts and wiring.

### Neutron Sources<sup>24</sup>

#### Radioactive Neutron Sources

[Radiation measurement techniques specific to neutron radiation are discussed elsewhere.](#)<sup>23-25</sup>

#### Spontaneous Fission Neutron Sources

These sources are attractive because of their fissionlike spectrum, relatively low gamma ray yield and their small mass. Californium-252 has been used for stationary and mobile systems.

#### Accelerator Sources

Constant voltage accelerators such as van de graaff and cockcroft-walton accelerators can produce energies up to about 20 MeV for protons and deuterons and still higher energies for alpha particles and heavy ions. Small accelerators using deuterons of 100 to 200 keV energy can produce large numbers of 14 MeV neutrons when using a tritiated target. High frequency positive ion accelerators include the cyclotron, synchrocyclotron, proton synchrotron and heavy ion linear accelerator. These are capable of producing a wide range of neutron energies. Protons above 10 MeV will produce neutrons when striking almost any material.

High frequency electron accelerators such as the betatron produce X-rays through the interaction of the accelerated electrons with the target. The X-rays in turn produce photoneutrons, most with energies of a few MeV but with some

neutrons having energies up to near the maximum energy of the accelerator.

### Nuclear Reactor Sources

Neutron production in reactors occurs as a result of the fission process. In the usual operating mode the number of fissions (and neutrons) is essentially constant in time. The neutron energies range from thermal to 15 MeV with the number over 10 MeV being small.

### Shielding

#### Fast Neutrons

Adequate shielding against neutrons will often attenuate gamma radiation to acceptable levels at both reactors and accelerators. Water and other hydrogenous shields may constitute an important exception to this rule. Ordinary or heavy aggregate concrete or earth are the recommended materials in most installations. Any economy achieved by water filled tanks is likely to be offset by maintenance difficulties. Both paraffin and oil, although good neutron absorbers, are fire hazards and should not be used in large stationary shields. Techniques of shielding calculations are discussed in detail elsewhere.<sup>24</sup>

The importance of concrete as a structural and shielding material merits special mention. Its use for gamma and X-ray shielding has been previously discussed. Because of its relatively high hydrogen and oxygen content, it is also a good neutron shield. The subject of shielding calculations for neutrons is complex and should be performed by specialists. Benchmarks include approximate tenth value layers of 250 mm (10 in.) of concrete for 14 MeV neutrons and 150 mm (6 in.) for 0.7 MeV neutrons.

#### Thermal Neutrons

Generally the energies associated with thermal neutrons are less than 1 eV. For radiation protection the most important interaction of thermal neutrons with matter is radioactive capture. In this process, the neutron is captured by the nucleus with the emission of gamma

radiation. A shield adequate for fast neutrons usually will be satisfactory for thermal neutrons. The low quality factor ( $QF = 2$ ) for thermal neutrons (0.025 eV) makes their biological consequence considerably less than for fast neutrons.



# References

1. Burnett, W.D. "Radiation Protection." *Nondestructive Testing Handbook*, second edition: Vol. 3, *Radiography and Radiation Testing*. Sec. 18. Columbus, OH: American Society for Nondestructive Testing (1985): p 732-758.
2. NCRP Report No. 39, *Basic Radiation Protection Criteria*. Bethesda, MD: National Council on Radiation Protection and Measurements (1971).
3. *General Safety Standard for Installations Using Non-Medical X-Ray and Sealed Gamma-Ray Sources, Energies up to 10 MeV*. NBS Handbook 114, United States Department of Commerce/National Bureau of Standards (1975). United States Government Printing Office, Washington, DC 20402 (SD Catalog No. C13.11: 114).
4. American College of Obstetricians and Gynecologists. DHEW publication (NIOSH) 78-118, *Guidelines on Pregnancy and Work*. Washington, DC: United States Department of Health, Education, and Welfare [DHEW], National Institute for Occupational Safety and Health [NIOSH]; Superintendent of Documents, United States Government Printing Office (1978). Superseded by NTIS PB 83-179-952. Springfield, VA: National Technical Information Service (1983).
5. Nuclear Regulatory Guide 8.10, *Operating Philosophy for Maintaining Occupation Radiation Exposures As Low As Reasonably Achievable, 1975*. Revised. Washington, DC: United States Nuclear Regulatory Commission (1977).
6. 10 CFR 30, *Rules of General Applicability to Licensing of Byproduct Material* [Code of Federal Regulations: Title 10, *Energy*]. Part 30. Washington, DC: United States Government Printing Office (2001).
7. Balestracci, G.[L.] "Industrial Radiography Internal Inspections." *Industrial Radiography Radiation Safety Personnel (IRRSP) Program Regulatory Compliance Seminar: Post-Conference Seminar* [Pittsburgh, PA, October 1997]. Columbus, OH: American Society for Nondestructive Testing (1997): p 5-8.
8. 10 CFR 34, *Licenses for Industrial Radiography and Radiation Safety Requirements for Industrial Radiographic Operations* [Code of Federal Regulations: Title 10, *Energy*]. Part 34, Appendix A. Washington, DC: Nuclear Regulatory Commission; United States Government Printing Office (2001).
9. ASNT Practice No. ASNT-CP-IRRSP-1A, *Industrial Radiography Radiation Safety Personnel*. [This recommended practice is revised frequently. The current version is available from the American Society for Nondestructive Testing.] Columbus, OH: American Society for Nondestructive Testing.
10. *Industrial Radiography Radiation Safety Personnel (IRRSP) Program Regulatory Compliance Seminar: Post-Conference Seminar* [Pittsburgh, PA, October 1997]. Columbus, OH: American Society for Nondestructive Testing (1997).
11. 49 CFR [Code of Federal Regulations: Title 49, *Transportation*]. Subtitle B, *Other Regulations Relating to Transportation*: Parts 171-176. Washington, DC: Department of Transportation; United States Government Printing Office (2000).
12. 10 CFR, *Code of Federal Regulations*: Title 10, *Energy*. Washington, DC: Department of Energy; United States Government Printing Office (2001).
13. Taylor, B.N., ed. *The International System of Units (SI)*. NIST Special Publication 330, 2001 edition. Gaithersburg, MD: National Institute of Standards and Technology (2001): p iii.
14. IEEE/ASTM SI 10-1997, *Standard for Use of the International System of Units (SI): The Modern Metric System*. New York, NY: Institute of Electrical and Electronics Engineers (1997).
15. NCRP Report 58, *A Handbook of Radioactivity Measurements Procedures*, second edition. Bethesda, MD: National Council on Radiation Protection and Measurements (1985).
16. NCRP Report 59, *Operational Radiation Safety Program*. Bethesda, MD: National Council on Radiation Protection and Measurements (1978).
17. NCRP Report 127, *Operational Radiation Safety Program*. Bethesda, MD: National Council on Radiation Protection and Measurements (1998).

18. NCRP Report 134, *Operational Radiation Safety Training*. Bethesda, MD: National Council on Radiation Protection and Measurements (2000).
19. 10 CFR 20, *Standards for Protection against Radiation* [Code of Federal Regulations: Title 10, Energy]. Part 20. Washington, DC: United States Government Printing Office (2001).
20. NCRP Report 128, *Radionuclide Exposure of the Embryo/Fetus*. Bethesda, MD: National Council on Radiation Protection and Measurements (1998).
21. Bush, J.[F., Jr.]. *Gamma Radiation Safety Study Guide*, second edition. Columbus, OH: American Society for Nondestructive Testing (2001).
22. NCRP Report 57, *Instrumentation and Monitoring Methods for Radiation Protection*. Bethesda, MD: National Council on Radiation Protection and Measurements (1978).
23. Wernli, C. *Advanced Methods of Active Neutron Dosimetry for Individual Monitoring and Radiation Field Analysis*. Report, Project BBW 95.0560. Bern, Switzerland: Federal Office for Education and Science (1998).
24. NCRP Report 38, *Protection against Neutron Radiation*. Bethesda, MD: National Council on Radiation Protection and Measurements (1971).
25. NCRP Report 25, *Measurement of Absorbed Dose of Neutrons, and of Mixtures of Neutrons and Gamma Rays*. Bethesda, MD: National Council on Radiation Protection and Measurements (1961).
26. NCRP Report 40, *Protection against Radiation from Brachytherapy Sources*. Bethesda, MD: National Council on Radiation Protection and Measurements (1972).
27. ANSI N43.3-1993, *General Safety — Installations Using Non-Medical X-Ray and Sealed Gamma-Ray Sources, Energies up to 10 MeV*. McLean, VA: Health Physics Society (1993).
28. NCRP Report 51, *Radiation Protection Design Guidelines for 0.1-100 MeV Particle Accelerator Facilities*. Bethesda, MD: National Council on Radiation Protection and Measurements (1977).
29. NCRP Report 49, *Structural Shielding Design and Evaluation for Medical Use of X Rays and Gamma Rays of Energies up to 10 MeV*. Bethesda, MD: National Council on Radiation Protection and Measurements (1976).
30. SRI Report No. 361, *The Industrial Uses of Radioactive Fission Products*. Stanford, CA: Stanford Research Institute.
31. 10 CFR 20.1004, *Units of Radiation Dose* [Code of Federal Regulations: Title 10, Energy]. Part 20. *Standards for Protection against Radiation*. Washington, DC: United States Government Printing Office (2001).
32. Patterson, H.W. and R.H. Thomas. *Accelerator Health Physics*. New York, NY: Academic Press (1973).

## Bibliography

- 10 CFR 20, *Standards for Protection against Radiation* [Code of Federal Regulations: Title 10, Energy]. Part 20. Washington, DC: United States Government Printing Office.
- 10 CFR 34, *Licenses for Industrial Radiography and Radiation Safety Requirements for Industrial Radiographic Operations* [Code of Federal Regulations: Title 10, Energy]. Part 34. Washington, DC: United States Government Printing Office (2001).
- 29 CFR 1926, *Occupational Safety and Health Standards for the Construction Industry* [Code of Federal Regulations: Title 29, Labor]. Part 1926. Washington, DC: United States Department of Labor, Occupational Safety and Health Administration; Government Printing Office (2001).
- Centers for Disease Control and Prevention (CDC) Radiation Safety Committee. *Radiation Safety Manual*. Atlanta, GA: United States Department of Health and Human Services, Office of Health and Safety, Public Health Service, Centers for Disease Control and Prevention (August 1999).
- DOE-STD-1095-95 (proposed), *DOE Standard Department of Energy Laboratory Accreditation Program for Personnel Dosimetry Systems*. Washington, DC: United States Department of Energy Laboratory Accreditation Program (1995).
- Draft DG-8010, *Nuclear Regulatory Guide 8.34, Monitoring Criteria and Methods to Calculate Occupational Radiation Doses*. Washington, DC: United States Nuclear Regulatory Commission (1991).
- Health (Radiation Safety) Regulations 1994*. Version No. 011, incorporating amendments as at 27 April 1998. S.R. No. 165/1994. Victoria, Australia: State Government of Victoria (1998).
- Knoll, G.F. *Radiation Detection and Measurement*, third edition. New York, NY: John Wiley and Sons (2000).
- McGuire, S.A. and C.A. Peabody. *Working Safely in Gamma Radiography: A Training Manual for Industrial Radiographers*. NUREG/BR-00024. Washington, DC: United States Nuclear Regulatory Commission; United States Government Printing Office (1982; reprinted 1995).

- NCRP Report 101, *Exposure of the U.S. Population from Occupational Radiation*. Bethesda, MD: National Council on Radiation Protection and Measurements (1989).
- NCRP Report 102, *Medical X-Ray, Electron Beam and Gamma-Ray Protection for Energies Up to 50 MeV*. (Supersedes NCRP Report No. 33). Bethesda, MD: National Council on Radiation Protection and Measurements (1989).
- NCRP Report 104, *The Relative Biological Effectiveness of Radiations of Different Quality*. Bethesda, MD: National Council on Radiation Protection and Measurements (1990).
- NCRP Report 112, *Calibration of Survey Instruments Used in Radiation Protection for the Assessment of Ionizing Radiation Fields and Radioactive Surface Contamination*. Bethesda, MD: National Council on Radiation Protection and Measurements (1991).
- NCRP Report 114, *Maintaining Radiation Protection Records*. Bethesda, MD: National Council on Radiation Protection and Measurements (1992).
- NCRP Report 115, *Risk Estimates for Radiation Protection*. Bethesda, MD: National Council on Radiation Protection and Measurements (1993).
- NCRP Report 116, *Limitation of Exposure to Ionizing Radiation*. (Supersedes NCRP Report No. 91). Bethesda, MD: National Council on Radiation Protection and Measurements (1993).
- NCRP Report 117, *Research Needs for Radiation Protection*. Bethesda, MD: National Council on Radiation Protection and Measurements (1993).
- NCRP Report 126, *Uncertainties in Fatal Cancer Risk Estimates Used in Radiation Protection*. Bethesda, MD: National Council on Radiation Protection and Measurements (1997).
- NCRP Report 130, *Biological Effects and Exposure Limits for "Hot Particles."* Bethesda, MD: National Council on Radiation Protection and Measurements (1999).
- NCRP Report 136, *Evaluation of the Linear-Nonthreshold Dose-Response Model for Ionizing Radiation*. Bethesda, MD: National Council on Radiation Protection and Measurements (2001).
- NCRP Report 30, *Safe Handling of Radioactive Materials*. Bethesda, MD: National Council on Radiation Protection and Measurements (1964).
- NCRP Report 32, *Radiation Protection in Educational Institutions*. Bethesda, MD: National Council on Radiation Protection and Measurements (1966).
- NCRP Report 52, *Cesium-137 from the Environment to Man: Metabolism and Dose*. Bethesda, MD: National Council on Radiation Protection and Measurements (1977).
- NCRP Report 61, *Radiation Safety Training Criteria for Industrial Radiography*. Bethesda, MD: National Council on Radiation Protection and Measurements (1978).
- NCRP Report 82, *SI Units in Radiation Protection and Measurements*. Bethesda, MD: National Council on Radiation Protection and Measurements (1985).
- NCRP Report 88, *Radiation Alarms and Access Control Systems*. Bethesda, MD: National Council on Radiation Protection and Measurements (1987).
- NCRP Report 96, *Comparative Carcinogenicity of Ionizing Radiation and Chemicals*. Bethesda, MD: National Council on Radiation Protection and Measurements (1989).
- "Nuclear Regulatory Commission's Report on Radiography Control Assembly Drive Cable Failures." *Materials Evaluation*. Vol. 58, No. 6. Columbus, OH: American Society for Nondestructive Testing (June 2000): p 715.
- OSH Answers: *Radiation — Quantities and Units of Ionizing Radiation*. Hamilton, Ontario, Canada: Canadian Centre for Occupational Health and Safety (1999).



# 7

## C H A P T E R

# Principles of Film Radiography<sup>1-3</sup>

---

Timothy J. Kinsella, Carpenter Technology Corporation,  
Reading, Pennsylvania (Part 7)

Parts 1 to 6 from *Radiography in Modern Industry*. © 1980, Eastman Kodak Company.  
Reprinted with permission by the American Society for Nondestructive Testing.

[www.iran-mavad.com](http://www.iran-mavad.com)

مرجع دانشجویان و مهندسين مواد

## PART 1. Film Exposure

### Making Radiographs

Radiography is one of the oldest and most widely used of nondestructive testing techniques. Despite its established position, new developments are constantly modifying the radiographic techniques applied by industrial and scientific users, thereby producing technical or economic advantages, or both, over previous techniques. This progressive trend continues with such special equipment and techniques as microfocus X-ray generators, portable linear accelerators, radioscopy, neutron radiography, imaging on paper, digital image analysis and image enhancement.

A *radiograph* is a photographic record produced by the passage of penetrating radiation through an object onto a film (Fig. 1). When film is exposed to X-rays, gamma rays or light, an invisible change called a latent image is produced in the film emulsion. The areas so exposed become dark when the film is immersed in a developing solution, the degree of darkening depending on the amount of exposure. After development, the film is rinsed, preferably in a special bath, to stop development. The film is next put into a fixing bath, which dissolves the unexposed parts of the emulsion's sensitive salt. The film is washed to remove the fixer and dried so that it may be handled, interpreted and filed. The developing, fixing and washing of the exposed film may be done manually or in automated processing equipment.

The diagram in Fig. 1 shows the essential features in the exposure of a radiograph. The focal spot is a small area in the X-ray tube from which the radiation emanates. In gamma radiography, it is the capsule containing the radioactive material that is the source of radiation (for example, cobalt-60). In either case the radiation proceeds in straight lines to the object; some of the rays pass through and others are absorbed — the amount transmitted depending on the nature of the material and its thickness. For example, if the object is a steel casting having a void formed by a gas bubble, the void produces a reduction of the total thickness of steel to be penetrated. Hence, more radiation will pass through the section containing the void than through the surrounding metal.

A dark spot, corresponding to the projected position and shape of the void, will appear on the film when it is developed. Thus, a radiograph is a kind of shadow picture — the darker regions on the film representing the more penetrable parts of the object and the lighter regions representing those more opaque to gamma radiation or X-radiation.

Industrial radiography is tremendously versatile. Radiographed objects range, in size, from microscopic electronic parts to mammoth missile components, in product composition through virtually every known material and in manufactured form over an enormously wide variety of castings, weldments and assemblies. Radiographic examination has been applied to organic and inorganic materials, to solids, liquids and even to

**MOVIE.**  
Conventional radiography gives shadow image.

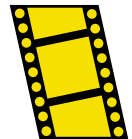
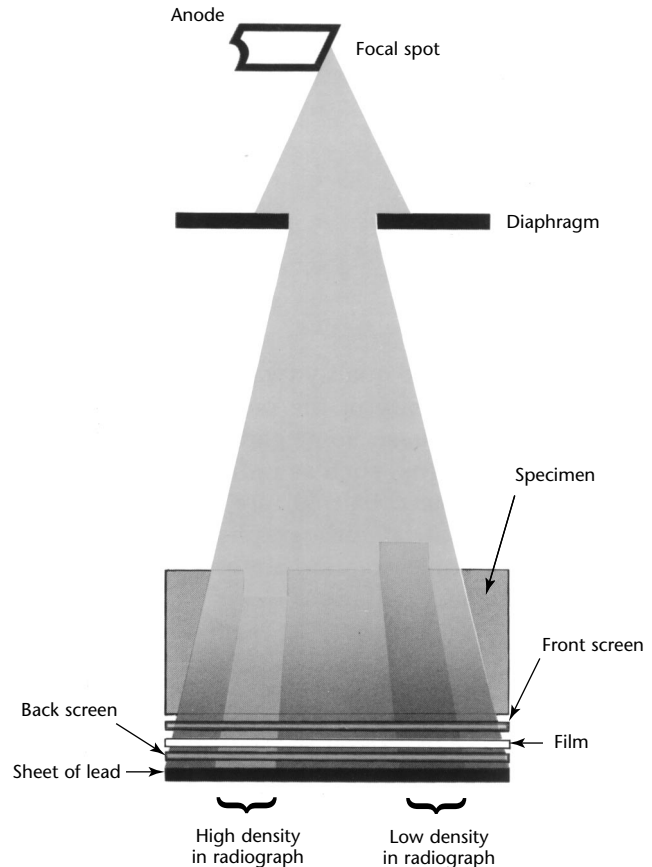


**FIGURE 1.** Diagram of setup for making industrial radiograph with X-rays.





gases. An industry's production of radiographs may vary from the occasional examination of one or several pieces to the examination of hundreds of specimens per hour. This wide range of applications has resulted in the establishment of independent, professional X-ray laboratories as well as radiographic departments within manufacturing plants. Radiographic testing performed by industry uses customer specifications or industry standards provided by technical societies and regulatory bodies.

To meet the growing and changing demands of industry, research and development in the field of radiography are continually producing new sources of radiation such as neutron generators and radioactive isotopes; lighter, more powerful, more portable X-ray equipment as well as multimegavolt X-ray machines designed to produce highly penetrating radiation; new and improved radiographic films and automatic film processors; and improved or specialized radiographic techniques. These factors, plus the activities of many dedicated people, broadly expand radiography's usefulness to industry.

## Factors Governing Exposure

Generally speaking, the optical density (called *photographic density* or simply *density*) of any radiographic image depends on the amount of radiation absorbed by the sensitive emulsion of the film. This amount of radiation in turn depends on several factors: the total amount and type of radiation emitted by the X-ray tube or gamma ray source; the amount of radiation reaching the specimen; the amount of radiation specifically absorbed that is characteristic of the test material; secondary and scattered radiation; filtration; and the intensifying action of screens, if used. [Photographic density is discussed elsewhere in this chapter.](#)

## Emission from X-Ray Source

The total amount of radiation emitted by an X-ray tube depends on tube current (milliamperage), voltage, target (source) material and the time the tube is energized.

When the other operating conditions are held constant, a change in milliamperage causes a change in the *intensity* (quantity of radiation leaving the X-ray generator per unit time) of the radiation emitted, the intensity being approximately proportional to the milliamperage. The high voltage

transformer losses and voltage waveform can change with tube current but a compensation factor is usually applied to minimize the effects of these changes. In normal industrial radiographic practice, the variation from exact proportionality is not serious and may usually be ignored.

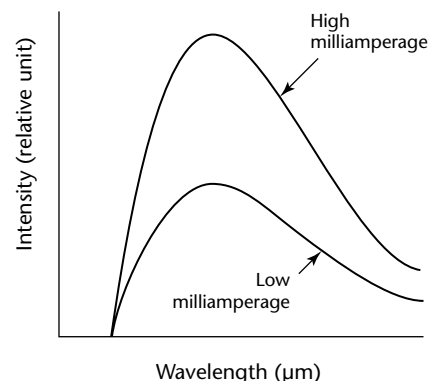
Figure 2 shows spectral emission curves for an X-ray tube operated at two different currents, the higher being twice the milliamperage of the lower. Therefore, each *wavelength* is twice as intense in one beam as in the other. Note that no wavelengths present in one beam are absent in the other. Hence, there is no change in X-ray quality or penetrating power.

As would be expected, the total amount of radiation emitted by an X-ray tube operating at a certain kilovoltage and milliamperage is directly proportional to the time the tube is energized.

Because the X-ray output is directly proportional to both milliamperage and time, it is directly proportional to their product. (This product is often referred to as the *exposure* in units such as milliamperere minutes.) Algebraically, this may be stated  $E = MT$ , where  $E$  is the exposure,  $M$  the tube current and  $T$  the exposure time. The amount of radiation will remain constant if the exposure remains constant, no matter how the individual factors of tube current and exposure time are varied. This permits specifying X-ray exposures in terms such as milliamperere minutes (mA·min) or milliamperere seconds (mA·s), without stating the specific individual values of tube current and time.

The kilovoltage applied to the X-ray tube affects not only the quality but also the intensity of the beam. As the kilovoltage is raised, X-rays of shorter wavelength and hence of more penetrating power, are produced as well as more X-rays of the same wavelength as at

FIGURE 2. Curves illustrating effect of change in milliamperage on intensity of X-ray beam.





lower voltages. Shown in Fig. 3 are spectral emission curves for an X-ray tube operated at two different kilovoltages but at the same milliamperage. Notice that some shorter wavelengths present in the higher kilovoltage beam are absent from the lower kilovoltage beam. Further, all wavelengths present in the lower kilovoltage beam are present in the more penetrating beam and in greater amount. Thus, raising the kilovoltage increases both the penetration and the intensity of the radiation emitted from the tube.

### Emission from Gamma Ray Source

The total amount of radiation emitted from a gamma ray source during a radiographic exposure depends on the activity of the source (in becquerels or curies) and the time of exposure. For a particular radioactive isotope, the intensity of the radiation is approximately proportional to the activity (in becquerels or curies) of the source. If it were not for absorption of gamma rays within the radioactive material itself, this proportionality would be exact. In normal radiographic practice, the range of source sizes used in a particular location is small enough so that variations from exact proportionality are not serious and may usually be ignored.

Thus, the gamma ray output is directly proportional to both activity of the source and time and hence is directly proportional to their product. Analogously to the X-ray exposure, the gamma ray exposure  $E$  may be stated  $E = MT$ , where  $M$  is the source activity in becquerels or curies and  $T$  is the exposure time; the amount of gamma radiation remains constant so long as the product of source activity and time remains

constant. This permits specifying gamma ray exposures in becquerel hours or curie hours without stating specific values for source activity or time.

Because the gamma ray energy depends on the isotope, there is no variable to correspond to the kilovoltage factor encountered in X-radiography. The only way to change the radiation penetrating power when using gamma rays is to change the source, for example, higher penetration cobalt-60 in place of lower penetration iridium-192.

### Geometric Principles

Because X-rays and gamma rays obey the common laws of light, their shadow formation may be simply explained in terms of light. It should be borne in mind that the analogy is not perfect because all objects are, to a greater or lesser degree, transparent to X-rays and gamma rays and because scattering presents greater problems in radiography than in optics. However, the same geometric laws of shadow formation hold for both light and penetrating radiation.

Suppose that, as in Fig. 4a, there is light from a point  $L$  falling on a white card  $C$  and that an opaque object  $O$  is interposed between the light source and the card. A shadow of the object will be formed on the surface of the card.

This shadow cast by the object will naturally show some *enlargement* because the source is smaller than the object and the object is not in contact with the card; the *degree of enlargement* will vary according to the relative distances of the object from the card and from the light source. For a point source, or one much smaller than the object, the law governing the size of the shadow may be stated: *the diameter of the object is to the diameter of the shadow as the distance of the light from the object is to the distance of the light from the card.*

Mathematically, the degree of enlargement may be calculated with the following equations:

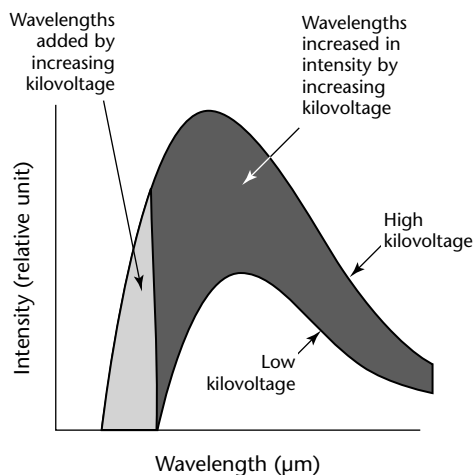
$$(1) \quad \frac{S_o}{S_i} = \frac{D_o}{D_i}$$

which may also be expressed as Eq. 2:

$$(2) \quad S_o = S_i \left( \frac{D_o}{D_i} \right)$$

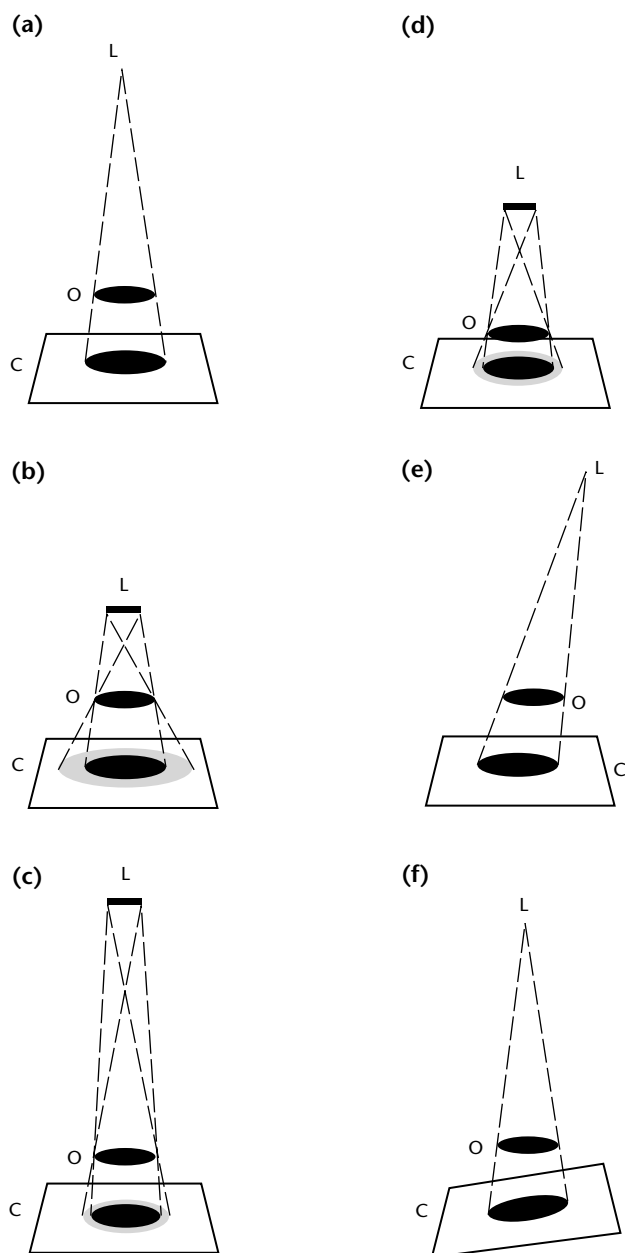
where  $D_o$  = distance from radiation source to object;  $D_i$  = distance from radiation source to image recording surface (or radiographic film);  $S_o$  = size of object; and  $S_i$  = size of shadow (or radiographic image).

**FIGURE 3.** Curves illustrating effect of change in kilovoltage on composition and intensity of X-ray beam.



The degree of *sharpness* of any shadow depends on the size of the light source and on the position of the object between the light and the card — whether nearer to or farther from one or the other. When

**FIGURE 4.** Geometric principles of shadow formation: (a) planes of object and film perpendicular to X-ray direction from point source; (b) perpendicular, near nonpoint source; (c) perpendicular, distant nonpoint source; (d) perpendicular, midrange nonpoint source; (e) oblique, parallel object and film planes, point source; (f) oblique, object and film planes not parallel, point source.



**Legend**  
C = film plane  
L = radiation source  
O = test object

the source of light is not a point but a small area, the shadows cast are not perfectly sharp (Figs. 4b to 4d) because each point in the source of light casts its own shadow of the object and each of these overlapping shadows is slightly displaced from the others, producing an ill defined image.

When the source is larger than the object, as when imaging a crack, the shadow will be smaller than the object. Depending on the distance from object to film the image may be undetectable because only the black shadow is usually detectable.

The *form* of the shadow may also differ according to the angle that the object makes with the incident light rays. Deviations from the true shape of the object as exhibited in its shadow image are referred to as distortion or misalignment.

Figure 4a to 4f shows the effect of changing the size of the source and of changing the relative positions of source, object and card. From an examination of these drawings, it will be seen that the following conditions must be fulfilled to produce the sharpest, truest shadow of the object.

1. The source of light should be small, that is, as nearly a point as can be obtained (compare Fig. 4a and 4c).
2. The source of light should be as far from the object as practical (compare Fig. 4b and 4c).
3. The recording surface should be as close to the object as possible (compare Fig. 4b and 4d).
4. The light rays should be directed perpendicularly to the recording surface (see Fig. 4a and 4e).
5. The plane of the object and the plane of the recording surface should be parallel (compare Fig. 4a and 4f).

## Radiographic Shadows

The basic principles of shadow formation must be given primary consideration to ensure satisfactory sharpness and freedom from distortion in the radiographic image. A certain degree of distortion will exist in every radiograph because some parts will always be farther from the film than others, the greatest magnification or image shrinkage being evident in the images of those parts at the greatest distance from the recording surface.

Note, also, that there is no distortion of shape in Fig. 4e — a circular object having been rendered as a circular shadow. However, under circumstances similar to those shown in Fig. 4e, it is possible that spatial relations can be distorted. In Fig. 5 the two circular objects can be rendered either as two circles (Fig. 5a) or as a figure

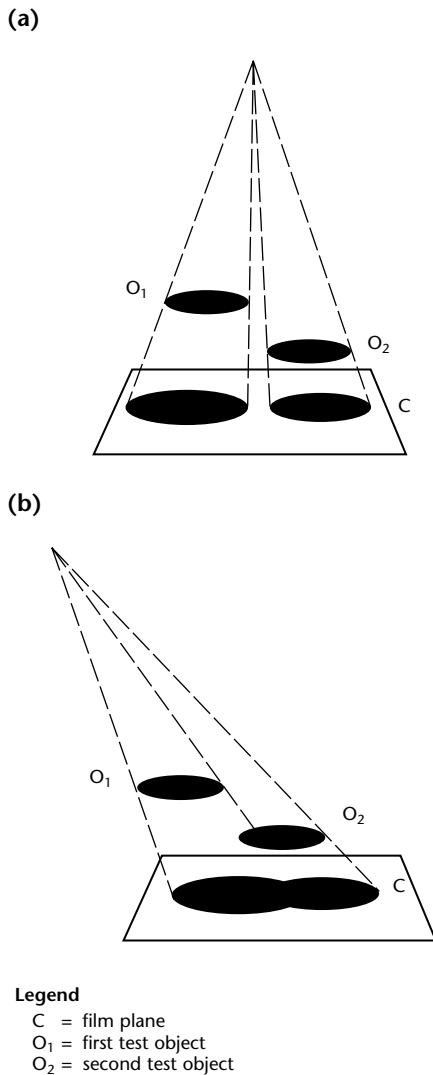
eight shaped shadow (Fig. 5b). It should be observed that both lobes of the figure eight have circular outlines.

Distortion cannot be eliminated entirely but, with an appropriate source-to-film distance, can be lessened to a point where it will not be objectionable in the radiographic image.

### Application to Radiography

The application to the geometric principles of shadow formation to radiography leads to five general rules. Although these rules are stated in terms of radiography with X-rays, they also apply to gamma radiography.

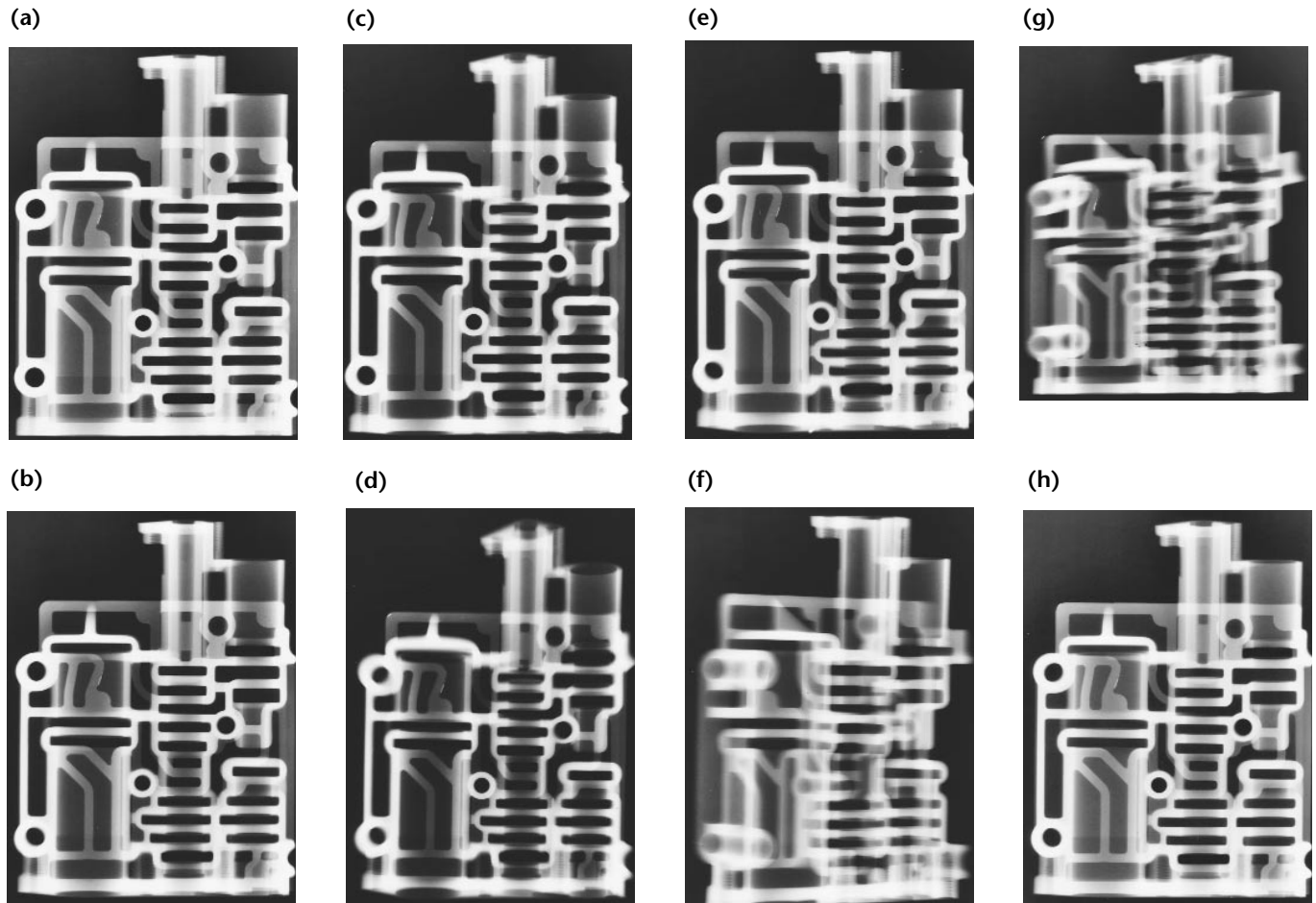
**FIGURE 5.** Depending on direction of radiation, two circular objects can be rendered: (a) as two separate circles; (b) as two overlapping circles.



1. The focal spot should be as small as other considerations will allow, for there is a definite relation between the size of the focal spot of the X-ray tube and the *definition* in the radiograph. A large focus tube, although capable of withstanding large loads, does not permit the delineation of as much detail as a small focus tube. Long source-to-film distances will aid in showing detail when a large focus tube is used but it is advantageous to use the smallest focal spot permissible for the exposures required. Figures 6b and 6h show the effect of focal spot size on image quality. As the focal spot size increases from 1.5 mm (0.06 in.) in Fig. 6b to 4.0 mm (0.16 in.) in Fig. 6h, the definition of the radiograph starts to degrade. This change is especially evident at the chamber edges that are no longer sharp.
2. The distance between the anode and the material examined should always be as great as practical. Comparatively long source-to-film distances should be used in the radiography of thick materials to minimize the fact that structures farthest from the film are less sharply recorded than those nearer to it. At long distances, radiographic definition is improved and the image is more nearly the actual size of the object. Figures 6a to 6d show the effects of source-to-film distance on image quality. As the source-to-film distance is decreased from 1730 mm (68 in.) to 305 mm (12 in.) the image becomes more distorted until at 305 mm (12 in.) it is no longer a true representation of the casting. This is particularly evident at the edges of the casting where the distortion is greatest.
3. The film should be as close as possible to the object being radiographed. In practice, the film (in its cassette or exposure holder) is placed in contact with the object. In Fig. 6b and 6e, the effects of object-to-film distance are evident. As the object-to-film distance is increased from zero to 102 mm (4 in.), the image becomes larger and the definition begins to degrade. Again, this is especially evident at chamber edges that are no longer sharp.
4. The central ray should be as nearly perpendicular to the film as possible to preserve spatial relations.
5. As far as the shape of the specimen will allow the plane of maximum interest should be parallel to the plane of the film.

In Fig. 6f and 6g, the effects of object-film-source orientation are shown. When compared to Fig. 6b, the image in Fig. 6f is extremely distorted; although the

FIGURE 6. Effects on image quality when geometric exposure factors are changed: (a) 1.75 m (68 in.) source-to-film distance, 0 mm (0 in.) object-to-film distance; (b) 1.5 mm (0.06 in.) focal spot, 0 mm (0 in.) object-to-film distance; (c) intermediate focal spot size, intermediate source-to-film distance; (d) 0.30 m (12 in.) source-to-film distance; (e) 100 mm (4 in.) object-to-film distance; (f) perpendicular film-to-source angle and 45 degree object-to-film angle; (g) perpendicular film-to-source angle, parallel object-to-film angle; (h) 4.0 mm (0.10 in.) focal spot.



film is perpendicular to the central ray, the casting is at a 45 degree angle to the film and spatial relationships are lost. As the film is rotated to be parallel with the casting (see Fig. 6g), the spatial relationships are maintained and the distortion is lessened.

### Calculation of Geometric Unsharpness

The width of the *fuzzy* boundary of the shadows in Fig. 4c and 4d is known as the *geometric unsharpness*  $U_g$ . Because the geometric unsharpness is a calculable measure of the sharpness of the image and can strongly affect the appearance of the radiographic image, it is frequently necessary to determine its magnitude. From the laws of similar triangles (see Fig. 7), it can be shown that:

$$(3) \quad \frac{U_g}{F} = \frac{d}{D_o}$$

or

$$(4) \quad U_g = F \frac{d}{D_o}$$

where  $D_o$  = source-to-object distance;  
 $F$  = size of radiation source;  $d$  = the object-to-film distance; and  
 $U_g$  = geometric unsharpness.

Because the maximum unsharpness involved in any radiographic procedure is usually the significant quantity, the object-to-film distance  $d$  is usually taken as the distance from the *source side* of the specimen to the film.

$D_o$  and  $d$  must be measured in the same units — say, millimeters or inches. So long as  $D_o$  and  $d$  are in the same units, Eq. 3 or

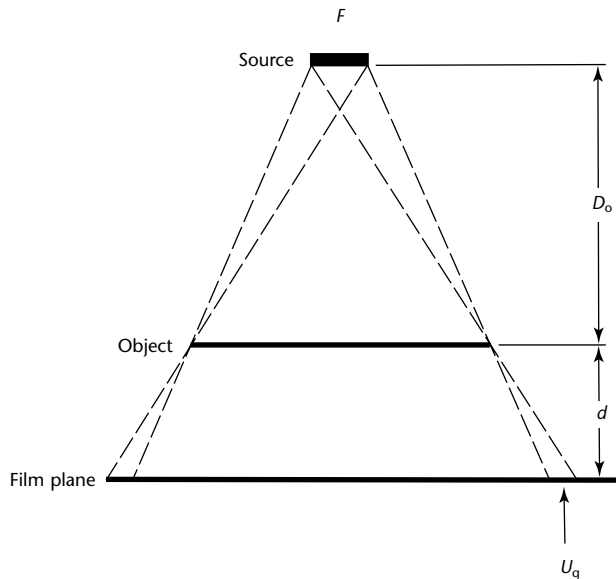
4 will always give the geometric unsharpness  $U_g$  in whatever units were used to measure the dimensions of the source. The projected sizes of the focal spots of X-ray tubes are usually stated in millimeters and  $U_g$  will also be in millimeters. If the source size is stated in inches,  $U_g$  will be inches.

For rapid reference, graphs of the type shown in Fig. 8 can be prepared with these equations. The graphs relate source-to-film distance, object-to-film distance and geometric unsharpness. Note that the lines of Fig. 8 are all straight. Therefore, for each source-to-object distance, it is only necessary to calculate the value of  $U_g$  for a single specimen thickness and then draw a straight line through the point so determined and the origin. It should be emphasized, however, that a separate graph of the type shown in Fig. 8 must be prepared for each size of source.

### Geometric Enlargement

In most radiography, it is desirable to have the specimen and the film as close together as possible to minimize geometric unsharpness. An exception to this rule occurs when the source of radiation is extremely minute, that is, a fraction of a millimeter, as in a microfocus source or betatron. In such a case, the

**FIGURE 7.** Geometric construction for determining geometric unsharpness  $U_g$  where source is smaller than object. See Eq. 4.



#### Legend

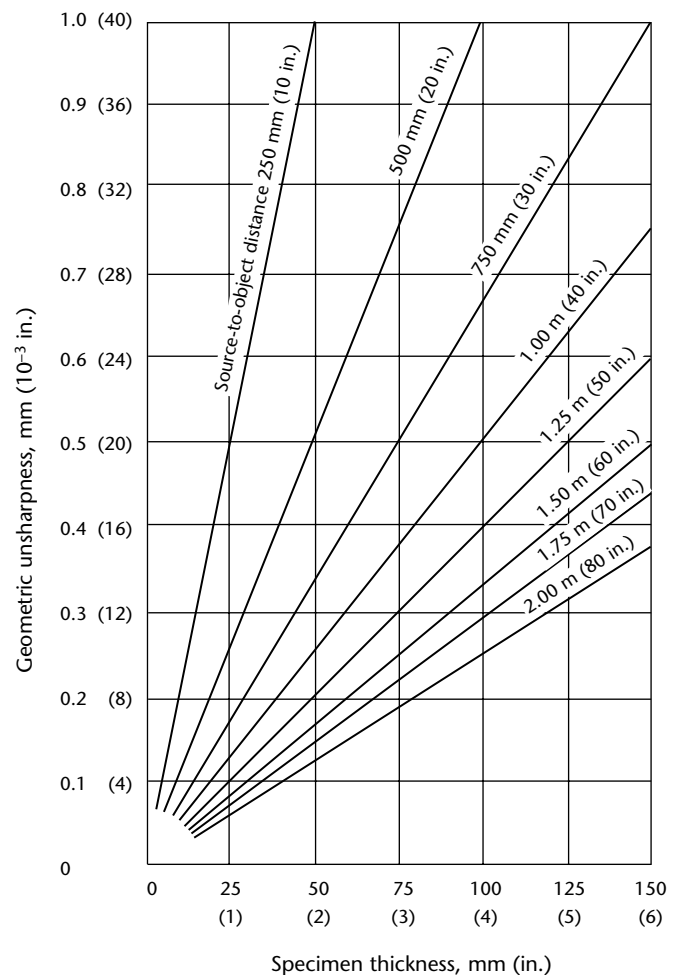
$D_o$  = source-to-object distance  
 $d$  = object-to-film distance  
 $F$  = radiation source  
 $U_g$  = geometric unsharpness

film may be placed at a distance from the specimen rather than in contact with it (Fig. 9). Such an arrangement results in an enlarged radiograph without introducing objectionable geometric unsharpness. Enlargements of three to ten diameters by this technique are useful in the detection of fine structures otherwise invisible radiographically. As the enlargement increases, the effective field of view (inspection area) decreases. This can result in the requirement of multiple exposures to cover an entire part. A benefit of geometric enlargement is a decrease in the amount of object scattered radiation reaching the image plane. This effect can improve contrast sensitivity.

### Inverse Square Law

When the X-ray tube output is held constant or when a particular radioactive source is used, the radiation intensity reaching the specimen (object) is

**FIGURE 8.** Graph relating geometric unsharpness  $U_g$  to specimen thickness and source-to-object distance, for 5 mm (0.2 in.) source size.





governed by the distance between the tube (source) and the specimen, varying inversely with the square of this distance. The explanation that follows is in terms of X-rays and light but applies to gamma rays as well.

Because X-rays conform to the laws of light they diverge when they are emitted from the anode and cover an increasingly larger area with lessened intensity as they travel from their source. This principle is illustrated in Fig. 10. In this example, it is assumed that the intensity of the X-rays emitted at the anode A remains constant and that the X-rays passing through the aperture B cover an area of 25.8 cm<sup>2</sup> (4 in.<sup>2</sup>) on reaching the recording surface C<sub>1</sub>, which is 305 mm (12 in.) from the anode (distance D).

When the recording surface is moved 305 mm (12 in.) farther from the anode, to C<sub>2</sub>, so that the distance (2D) from the anode is 610 mm (24 in.) or twice its earlier value, the X-rays will cover 103.4 cm<sup>2</sup> (16 in.<sup>2</sup>) — an area four times as great as that at C<sub>1</sub>. It follows, therefore, that the radiation per square centimeter on the surface at C<sub>2</sub> is only one fourth of

that at the level C<sub>1</sub>. The exposure that would be adequate at C<sub>1</sub> must be increased four times to produce at C<sub>2</sub> a radiograph of equal density. In practice, this can be done by increasing the time or by increasing the milliamperage.

The inverse square law can be expressed algebraically as follows:

$$(5) \quad \frac{I_1}{I_2} = \frac{D_2^2}{D_1^2}$$

where  $I_1$  and  $I_2$  are the intensities at distances  $D_1$  and  $D_2$ , respectively.

## Relations of Source Strength (Milliamperage), Distance and Time

With a given kilovoltage of X-radiation or with the gamma radiation from a particular isotope, the three factors governing the exposure are the milliamperage (for X-rays) or source strength (for gamma rays), time and

**FIGURE 9.** With very small focal spot, enlarged image can be obtained. Degree of enlargement depends upon ratio of source-to-film and source-to-specimen distances.

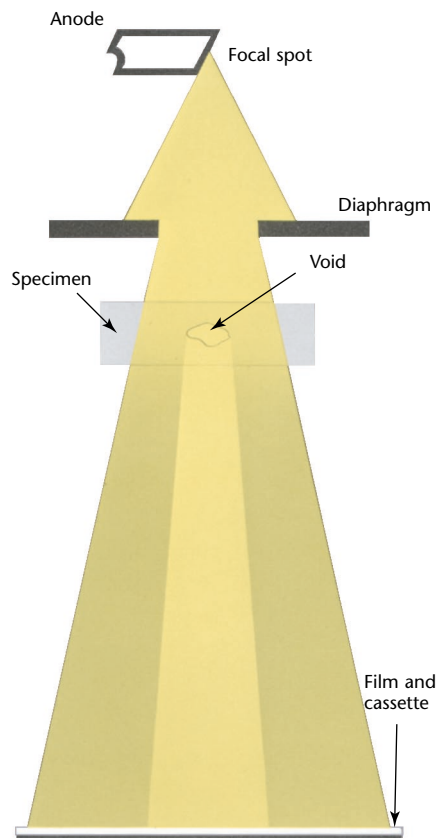
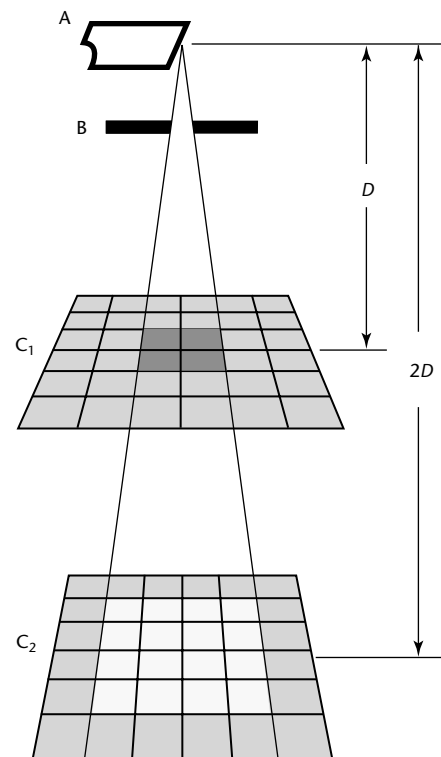


**FIGURE 10.** Schematic diagram illustrating inverse square law.



### Legend

- A = radiation source
- B = focal point
- C<sub>1</sub> = first film plane
- C<sub>2</sub> = second film plane
- D = source-to-film distance



source-to-film distance. The numerical relations among these three quantities are demonstrated below, using X-rays as an example. The same relations apply for gamma rays, provided the number of becquerels (curies) in the source is substituted wherever milliamperage appears in an equation.

The necessary calculations for any changes in focus-to-film distance  $D$ , milliamperage  $M$  or time  $T$  are matters of simple arithmetic and are illustrated in the following example. As noted earlier, kilovoltage changes cannot be calculated directly but must be obtained from the exposure chart of the equipment or the operator's log book.

### Relationship of Source Strength and Distance

Rule: If exposure time is held constant, the milliamperage ( $M$ ) required for a given exposure is directly proportional to the square of the source-to-film distance ( $D$ ). The equation is expressed as follows:

$$(6) \quad M_1 : M_2 = D_1^2 : D_2^2$$

or

$$\frac{M_1}{M_2} = \frac{D_1^2}{D_2^2}$$

For example, suppose that with a given exposure time and kilovoltage, a properly exposed radiograph is obtained with 5 mA ( $M_1$ ) at a distance of  $D_1$  of 120 mm (30 in.) and that it is desired to increase the sharpness of detail in the image by increasing the focus-to-film distance  $D_2$  to 240 mm (60 in.). The correct milliamperage  $M_2$  to obtain the desired radiographic density at the increased distance  $D_2$  may be computed from the proportion:

$$(7) \quad 5 : M_2 = 30^2 : 60^2$$

or

$$\frac{5}{M_2} = \frac{30^2}{60^2}$$

or

$$\begin{aligned} M_2 &= 5 \times \frac{60^2}{30^2} = 5 \times \frac{3600}{900} \\ &= 5 \times 4 = 20 \text{ mA} \end{aligned}$$

When very low kilovoltages, say 20 kV or less, are used, the X-ray intensity decreases with distance more rapidly than

calculations based on the inverse square law would indicate because of absorption of the X-rays by the air. Most industrial radiography, however, is done with radiation so penetrating that the air absorption need not be considered. These comments also apply to the time-to-distance relations discussed below.

### Relationship of Time and Distance

Rule: If tube current (mA) is held constant, the exposure time  $T$  required for a given exposure is directly proportional to the square of the focus-to-film distance  $D$ :

$$(8) \quad T_1 : T_2 = D_1^2 : D_2^2$$

or

$$\frac{T_1}{T_2} = \frac{D_1^2}{D_2^2}$$

### Relation of Milliamperage to Time

Rule: If distance is held constant but exposure must be changed, the milliamperage  $M$  required for a given exposure is inversely proportional to the time  $T$ :

$$(9) \quad M_1 : M_2 = T_2 : T_1$$

or

$$\frac{M_1}{M_2} = \frac{T_2}{T_1}$$

Another way of expressing this is to say that for a given set of conditions (voltage, distance and others), the product of milliamperage and time is constant for the same photographic effect. Thus:

$$\begin{aligned} (10) \quad M_1 T_1 &= M_2 T_2 = M_3 T_3 \\ &= C \text{ (a constant)} \end{aligned}$$

This commonly referred to as the *reciprocity law*. (Important exceptions are discussed below.)

### Tabular Solution of Source Strength, Time and Distance Problems

Problems of the types discussed above may also be with a table similar to Table 1. The factor between the new and the old exposure time, milliamperage, or milliamper minute (mA·min) value appears in the box at the intersection of the column for the new source-to-film distance and the row for the old source-to-film distance.

Note that some approximation is involved in such a table because the

values in the boxes are rounded off to two significant digits. However, the errors involved are always less than 5 percent and, in general, are insignificant in actual practice. Also, a table of this type cannot include all source-to-film distances. However, in any one radiographic department, only a few source-to-film distances are used in the great bulk of the work and a table of reasonable size can be made using only these few distances.

## Reciprocity Law

In the preceding text, it has been assumed that exact compensation for a decrease in the time of exposure can be made by increasing the milliamperage according to the relation  $M_1T_1 = M_2T_2$ . This may be written  $MT = C$  and is an example of a general photochemical law: the same effect is produced for  $IT = \text{constant}$ , where  $I$  is intensity of the radiation and  $T$  is the time of exposure. This is called the *reciprocity law* and is true for direct X-ray and lead screen exposures. For exposure to light, it is not quite accurate and, because some radiographic exposures are made with the light from fluorescent intensifying screens, the law cannot be strictly applied.

Formally defined, the Bunsen-Roscoe reciprocity law states that the result of a photochemical reaction is dependent only on the *product* of radiation intensity  $I$  and the duration of the exposure  $T$  and is independent of absolute values of either quantity.

Errors that result from assuming the validity of the reciprocity law are usually so small that they are not noticeable in examples of the types given here.

Departures may be apparent, however, if the intensity is changed by a factor of 4 or more. Because intensity may be changed by changing the source-to-film distance, failure of the reciprocity law may appear to be a violation of the inverse square law. Applications of the reciprocity law over a wide intensity range sometimes arise and the relation between results and calculations may be misleading unless the possibility of reciprocity law failure is kept in mind. Failure of the reciprocity law means that the efficiency of a light sensitive emulsion in responding to the light energy depends on the light intensity.

## Exposure Factor

The *exposure factor* is a quantity that combines milliamperage (X-rays) or source strength (gamma rays), time and distance. Numerically the exposure factor equals

$$(11) \quad \frac{\text{Milliamperes} \times \text{Time}}{\text{Distance}^2} = \text{X-ray exposure factor}$$

and

$$(12) \quad \frac{\text{Activity} \times \text{Time}}{\text{Distance}^2} = \text{Gamma ray exposure factor}$$

Activity is measured in becquerels (Bq) or curies (Ci), where  $3.7 \times 10^{10} \text{ Bq} = 37 \text{ GBq} = 1.0 \text{ Ci}$ .

Radiographic techniques are sometimes given in terms of kilovoltage and exposure factor, or radioactive isotope and exposure factor. In such a case, it is necessary merely to multiply the exposure factor by the square of the distance to

**TABLE 1. Value of source strength–time (mA-min) is multiplied by factor shown in this table when source-to-film distance is changed. (The same factors apply regardless of unit of distance — for example, multiply by same factor if both old and new distance are measured in inches instead of millimeters.)**

Old Source-to-Film Distance (mm)	New Source-to-Film Distance (mm)											
	250	300	350	400	450	500	550	600	650	700	750	800
250	1.0	1.4	2.0	2.6	3.2	4.0	4.8	5.6	6.8	7.8	9.0	10.0
300	0.70	1.0	1.4	1.8	2.3	2.8	3.4	4.0	4.8	5.4	6.3	7.1
350	0.51	0.74	1.0	1.3	1.6	2.0	2.5	3.0	3.4	4.0	4.6	5.2
400	0.39	0.56	0.77	1.0	1.3	1.6	1.9	2.2	2.6	3.1	3.5	4.0
450	0.31	0.45	0.60	0.79	1.0	1.2	1.5	1.8	2.1	2.4	2.8	3.2
500	0.25	0.36	0.49	0.64	0.81	1.0	1.2	1.4	1.7	2.0	2.2	2.6
550	0.21	0.30	0.40	0.53	0.67	0.83	1.0	1.2	1.4	1.6	1.9	2.1
600	0.17	0.25	0.34	0.44	0.56	0.69	0.84	1.0	1.2	1.4	1.6	1.8
650	0.15	0.21	0.29	0.38	0.48	0.59	0.72	0.85	1.0	1.2	1.3	1.5
700	0.13	0.18	0.25	0.33	0.41	0.51	0.62	0.74	0.86	1.0	1.1	1.3
750	0.11	0.16	0.22	0.28	0.36	0.45	0.54	0.64	0.75	0.87	1.0	1.1
800	0.10	0.14	0.19	0.25	0.32	0.39	0.47	0.56	0.66	0.77	0.88	1.0

find, for example, the milliamperere minutes or the curie hours required.

## Determination of Exposure Factors

### X-Rays

The focus-to-film distance is easy to establish by actual measurement, the milliamperage can conveniently be determined by the milliammeter supplied with the X-ray machine and the exposure time can be accurately controlled by a good time switch. The tube voltage, however, is difficult and inconvenient to measure accurately. Furthermore, designs of individual machines differ widely and may give X-ray outputs of a different quality and intensity even when operated at the nominal values of peak kilovoltage and milliamperage.

Consequently, although specified exposure techniques can be duplicated satisfactorily in the factors of source-to-film distance, milliamperage and exposure time, one apparatus may differ materially from another in the kilovoltage setting necessary to produce the same radiographic density. Because of this, the kilovoltage setting for a given technique should be determined by trial on each X-ray generator. In the preliminary tests, published exposure charts may be followed as an approximate guide. It is customary for equipment manufacturers to calibrate X-ray machines at the factory and to furnish suitable exposure charts. For the unusual problems that arise, it is desirable to record in a logbook all the data on exposure and techniques. In this way, operators will soon build up a source of information that will make them more competent to deal with difficult situations.

For developing trial exposures, a standardized technique should always be used so that any variation in the quality of the trial radiographs may then be attributed to the exposure alone. This technique obviates many of the variable factors common to radiographic work.

Because an increase of kilovoltage produces a marked increase in X-ray output and penetration (see Fig. 3), it is necessary to maintain a close control of this factor to secure radiographs of uniform density. In many types of industrial radiography where it is desirable to maintain constant exposure conditions for source-to-film distance, milliamperage and exposure time, it is common practice to vary the kilovoltage in accordance with the thickness of the material to be examined to secure proper density in the radiographic image.

Suppose, for example, it is desired to change from radiographing 38 mm (1.5 in.) thick steel to radiographing 50 mm (2 in.) thick steel. For a given X-ray machine, the 50 mm (2 in.) thick steel will require more than 10 times the exposure in milliamperere minutes at 170 kV than the 38 mm (1.5 in.) thick steel requires. However, increasing the kilovoltage to a little more than 200 will yield a comparable radiograph with the same milliamperere minutes.

Therefore, kilovoltage is an important variable because economic considerations often require that exposure times be kept within fairly narrow limits. It is desirable, as a rule, to *use as low a kilovoltage as other factors will permit*. In the case of certain high voltage X-ray machines, the technique of choosing exposure conditions may be somewhat modified. For instance, the kilovoltage may be fixed rather than adjustable at the will of the operator, leaving only milliamperage, exposure time, film type and focus-to-film distance as variables.

### Gamma Rays

With radioactive materials, the variable factors are more limited than with X-rays. Not only is the quality (energy or wavelength) of the radiation fixed by the nature of the radiation emitter, but also the intensity is fixed by the amount of radioactive material in the particular source. The only variables under the control of operators and the only quantities they need to determine are the source-to-film distance, film type and the exposure time. As in the case of X-radiography, it is desirable to develop trial exposures using the gamma ray sources under standardized conditions and to record all data on exposures and techniques.

## Radiographic Contrast

In a radiograph, the various intensities transmitted by the specimen are rendered as different densities in the image. The density differences from one area to another constitute *radiographic contrast*. Details in the image are visible by reason of the contrast between them and their background. Within appropriate limits, the greater the contrast or density differences in the radiograph, the more definitely various details will stand out. However, if overall contrast is increased too much, there may be an actual loss in detail visibility in both the thick and the thin regions of the specimen as the image is too light or too dark to display useful contrast (see discussion of film contrast, below).

Radiographic contrast is the result of both subject contrast and film contrast. Subject contrast is governed by the range of radiation intensities transmitted by the specimen. A flat sheet of homogeneous material of nearly uniform thickness would have very low subject contrast. Conversely, a specimen with large variations in thickness, which transmits a wide range of intensities, would have high subject contrast. Overall subject contrast could be defined as the ratio of the highest to the lowest radiation intensities falling on the film. The subject contrast is affected by the X-ray kilovoltage. As shown in Fig. 11, a lower kilovoltage will increase subject contrast and so increase sensitivity to small variations in the object. Contrast is also affected by scattered radiation, removal of which increases subject contrast, and by the energy of the primary radiation.

### Choice of Film

Different films have different contrast characteristics. Thus, a film of high contrast may give a radiograph of relatively low overall contrast if the subject contrast is very low; conversely, a film of low contrast may give a radiograph of relatively high overall contrast if the subject contrast is very high. With any given specimen, the contrast of the radiograph will depend on the kilovoltage or quality of the X-rays or gamma rays, the contrast characteristics of the film, the type of screen, scatter, the

density to which the radiograph is exposed and film processing.

The classification of film types and their speeds are discussed in the chapter on film processing.

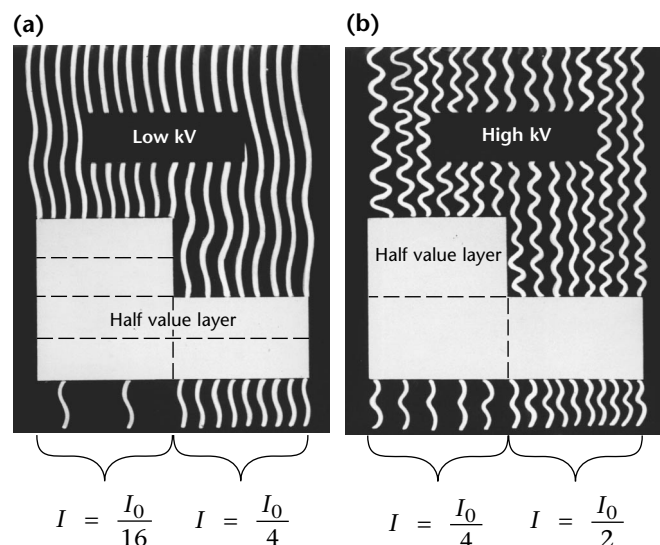
## Radiographic Sensitivity

Radiographic sensitivity refers to the size of the smallest detail that can be seen in a radiograph or to the ease with which the images of small details can be detected.

Sensitivity depends on the sharpness and the contrast of the radiograph. Thus, the grain size of the film, as well as its contrast and other factors such as the exposure geometry and radiation energy, affect sensitivity.

In radiography of materials of approximately uniform thickness, where the range of transmitted X-ray intensities is small, a technique producing high contrast may satisfactorily render all portions of the area of interest and the radiographic sensitivity will usually be greater than with a technique producing low contrast. If, however, the part radiographed transmits a wide range of X-ray intensities, then a technique producing lower contrast may be necessary to achieve radiographic sensitivity in all regions of the part.

**FIGURE 11.** As kilovoltage increases, subject contrast decreases. More wavelengths penetrate subject in both thick and thin sections, thus reducing overall difference in exposure between them: (a) low kilovoltage selected for four half value layers in thick section; (b) kilovoltage increased to get two half value layers in thick section.



## PART 2. Absorption and Scattering

### Radiation Absorption in Specimen

When X-rays or gamma rays strike an absorber (Fig. 12), some radiation is absorbed or deflected and some passes through undeviated. It is the intensity variation of the undeviated radiation from area to area in the specimen that forms the useful image in a radiograph. The radiation that is scattered is not image forming. Scattered radiation will expose the film and thus tend to obscure the useful radiographic image. Therefore, scatter must be carefully controlled. (Scattered radiation and the means for reducing its effects are discussed in detail below.) Another portion of the original beam's energy is spent in liberating electrons from the absorber. The electrons

from the specimen are usually unimportant radiographically; those from materials in contact with the film, such as screens of lead or other materials, are very important.

### Radiographic Equivalency of Materials

Because various wavelengths exist in X-rays and gamma rays and because considerable scattered radiation reaches the film, the laws of radiation absorption must be given in a general way.

The absorption of a specimen depends on its thickness, on its density and on the atomic composition of the material. Comparing two specimens of the same composition, the thicker or the more dense will absorb more radiation and so require more kilovoltage or exposure, or both, to produce the same photographic result.

However, the atomic elements in a specimen often exert a far greater effect upon X-ray absorption than either the thickness or the density. For example, lead is about 1.5 times as dense as ordinary steel but at 220 kV, 2.5 mm (0.1 in.) of lead absorbs as much as 30.5 mm (1.2 in.) of steel. Brass is only about 1.1 times as dense as steel, yet, at 150 kV, the same exposure is required for 6.4 mm (0.25 in.) of brass as for 8.9 mm (0.35 in.) of steel.

Table 2 gives approximate radiographic equivalence factors. It should be emphasized that this table is approximate and is intended merely as a guide because it is based on a compilation of data from many sources. In a particular instance, the exact value of the radiographic equivalence factor will depend on the quality of the X-radiation and the thickness of the specimen. It will be noted from this table that the relative absorptions of the different materials are not constant but change with kilovoltage and that as the kilovoltage increases the differences between all materials tend to become less. In other words, as kilovoltage is increased, the radiographic absorption of a material becomes less dependent on the atomic numbers of its constituents.

For X-rays generated at voltages more than 1 MeV and for materials not differing too greatly in atomic number (steel and copper, for example), the

**FIGURE 12.** Schematic diagram of some ways X-ray or gamma ray energy is dissipated on passing through matter. Electrons from specimens are usually unimportant radiographically; those from lead foil screens are very important.

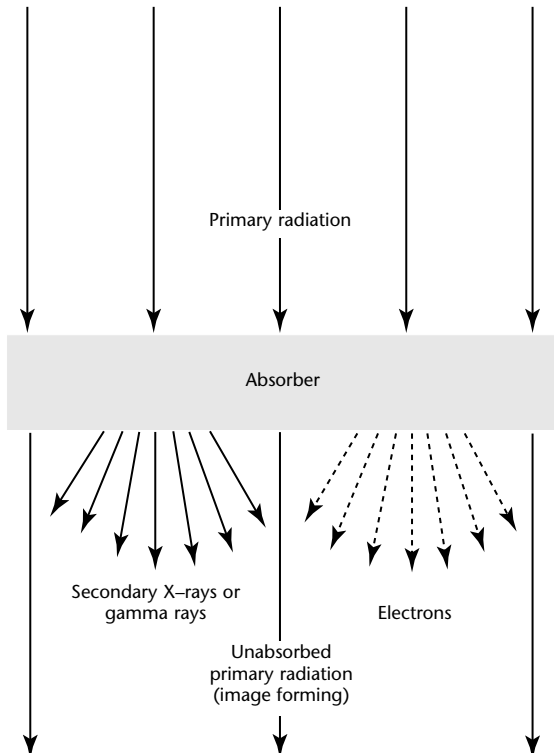




TABLE 2. Approximate radiographic equivalence factors.<sup>a</sup>

Material	X-Rays (kV)								Gamma Rays			
	50	100	150	220	400	1000	2000	4 to 25 <sup>b</sup>	Iridium-192	Cesium-137	Cobalt-60	Radium
Magnesium	0.6	0.6	0.5	0.08								
Aluminum	1.0	1.0	0.12	0.18					0.35	0.35	0.35	0.40
2024 aluminum alloy	2.2	1.6	0.16	0.22					0.35	0.35	0.35	
Titanium			0.45	0.35								
Steel		12.0	1.0	1.0	1.0	1.0	1.0	1.0	1.0	1.0	1.0	1.0
Steel alloy <sup>c</sup>		12.0	1.0	1.0	1.0	1.0	1.0	1.0	1.0	1.0	1.0	1.0
Copper		18.0	1.6	1.4	1.4			1.3	1.1	1.1	1.1	1.1
Zinc			1.4	1.3	1.3			1.0	1.1	1.0	1.0	1.0
Brass <sup>d</sup>			1.4	1.3	1.3	1.2	1.2	1.0	1.1	1.1	1.1	1.1
Nickel alloy <sup>e</sup>		16.0	1.4	1.3	1.3	1.3	1.3	1.0	1.3	1.3	1.3	1.3
Zirconium			2.3	2.0		1.0						
Lead			14.0	12.0		5.0	2.5	3.0	4.0	3.2	2.3	2.0
Uranium				25.0				3.9	12.6	5.6	3.4	

a. Aluminum is the standard metal at 50 kV and 100 kV; steel is the standard metal with high voltages and gamma rays. The thickness of another metal is multiplied by the corresponding factor to obtain the approximate equivalent thickness of the standard metal. The exposure applying to this thickness of the standard metal is used. Example: to radiograph 12.7 mm (0.5 in.) of copper at 220 kV, multiply 12.7 mm (0.5 in.) by the factor 1.4, obtaining an equivalent thickness of 17.8 mm (0.7 in.) of steel.

b. 4 to 25 MeV.

c. Alloy consisting of 18 percent chromium, 8 percent nickel.

d. Tin or lead alloyed in brass will increase these factors.

e. Alloy consisting of 73 percent nickel, 15 percent chromium.

radiographic absorption for a given thickness of material is roughly proportional to the density of the material. However, even at high voltages or with penetrating gamma rays, the effect of composition on absorption cannot be ignored when dealing with materials that differ widely in atomic number. For instance, the absorption of lead for 1 MeV X-rays is about five times that of an equal thickness of steel, although its density is only 1.5 times as great.

## Scattered Radiation

When a beam of X-rays or gamma rays strikes any object, some of the radiation is absorbed, some is scattered and some passes straight through. The electrons of the atoms constituting the object scatter radiation in all directions, much as light is dispersed by fog. The wavelengths of much of the radiation are increased by the scattering process and hence the scatter is of longer wavelength and is somewhat *softer*, or less penetrating, than the unscattered primary radiation. Any material — whether specimen, cassette, tabletop, walls or floor — that receives the direct radiation is a source of scattered radiation. Unless suitable measures are taken to reduce the effects of scatter, it will reduce the contrast over the whole image or parts of it. Scatter forms *fog* of nonuniform density.

Scattering of radiation occurs and is a problem in radiography with both X-rays and gamma rays. In the text which follows, the discussion is in terms of X-rays but the same general principles apply to gamma radiography.

In the radiography of materials that are thick relative to the radiation energy, scattered radiation forms most of the total radiation. For example, in the radiography of a 19 mm (0.75 in.) thickness of steel, the scattered radiation from the specimen is almost twice as intense as the primary radiation; in the radiography of a 50 mm (2 in.) thickness of aluminum, the scattered radiation is 2.5 times as great as the primary radiation. Preventing scatter from reaching the film markedly improves the quality of the radiographic image.

As a rule, the greater portion of the scattered radiation affecting the film is from the specimen under examination (A in Fig. 13). However, any portion of the film holder or cassette that extends beyond the boundaries of the specimen and thereby receives direct radiation from the X-ray tube also becomes a source of scattered radiation that can affect the film. The influence of this scatter is most noticeable just inside the borders of the image (B in Fig. 13) and is often referred to as *undercut*. In a similar manner, primary radiation striking the film holder or cassette through a thin portion of the specimen will cause scattering into the shadows of the adjacent thicker portions.



Another source of scatter that may undercut a specimen is shown as C in Fig. 13. If a filter is used near the tube, this too will scatter X-rays. However, because of the distance from the film, scattering from this source is negligible. Any other material, such as wall or floor, on the film side of the specimen may also scatter an appreciable quantity of X-rays back to the film, especially if the material receives the direct radiation from the X-ray tube or gamma ray source (Fig. 14). This is referred to as *backscattered radiation*.

## Reduction of Scatter

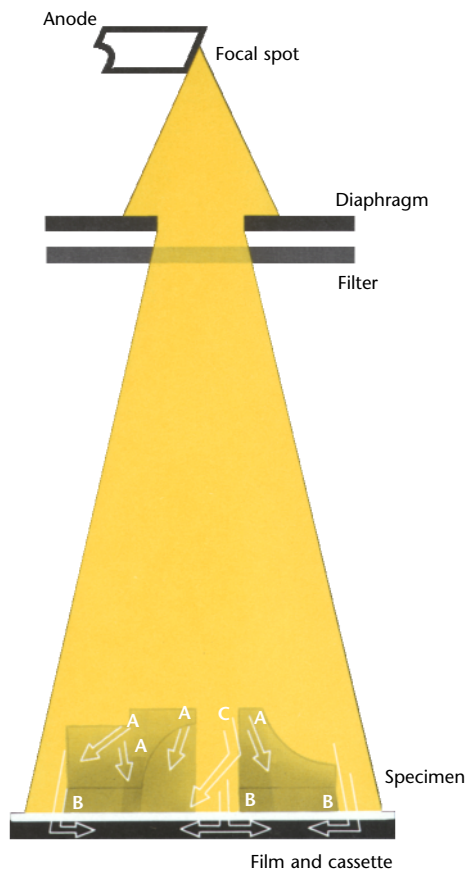
Although scattered radiation can never be completely eliminated, a number of means are available to reduce its effect. The various techniques are discussed in terms of X-rays. Although most of the same principles apply to gamma and megavolt X-ray radiography, differences in application arise because of the highly penetrating radiation emitted by megavolt

and gamma ray sources. For example, a mask (see Fig. 15) for use with 200 kV X-rays could easily be light enough for convenient handling. A mask for use with cobalt-60 radiation, on the other hand, would be thick, heavy and probably cumbersome. In any event, with either X-rays or gamma rays, the means for reducing the effects of scattered radiation must be chosen on the basis of cost, convenience and effectiveness.

## Lead Foil Screens

Lead screens, mounted in contact with the film, diminish the effect on the film of scattered radiation from all sources. They are beyond doubt the least expensive, most convenient and most universally applicable means of combating the effects of scattered radiation. Lead screens lessen the scatter reaching the films regardless of whether the screens permit a decrease or necessitate an increase in the radiographic exposure. The nature of the action of lead

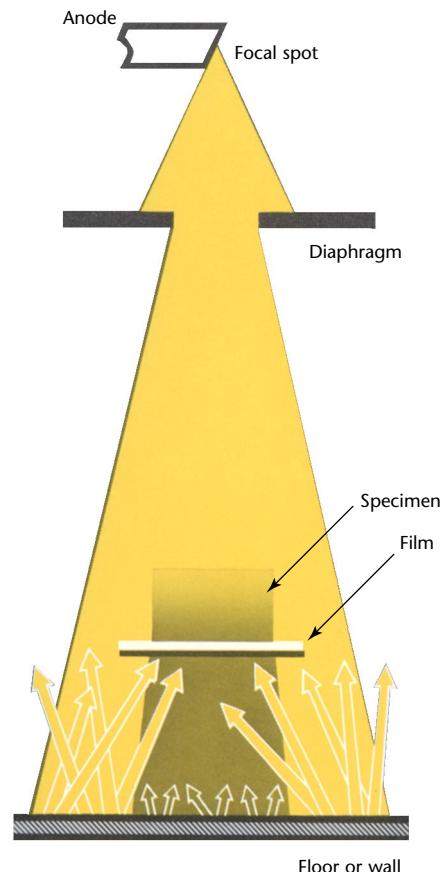
FIGURE 13. Sources of scattered radiation.



### Legend

- A = transmitted scatter
- B = scatter from cassette
- C = diffraction scatter

FIGURE 14. Intense backscattered radiation may originate in the floor or wall. Collimating, masking or diaphragming should be used. Backing the cassette with lead may give adequate protection.

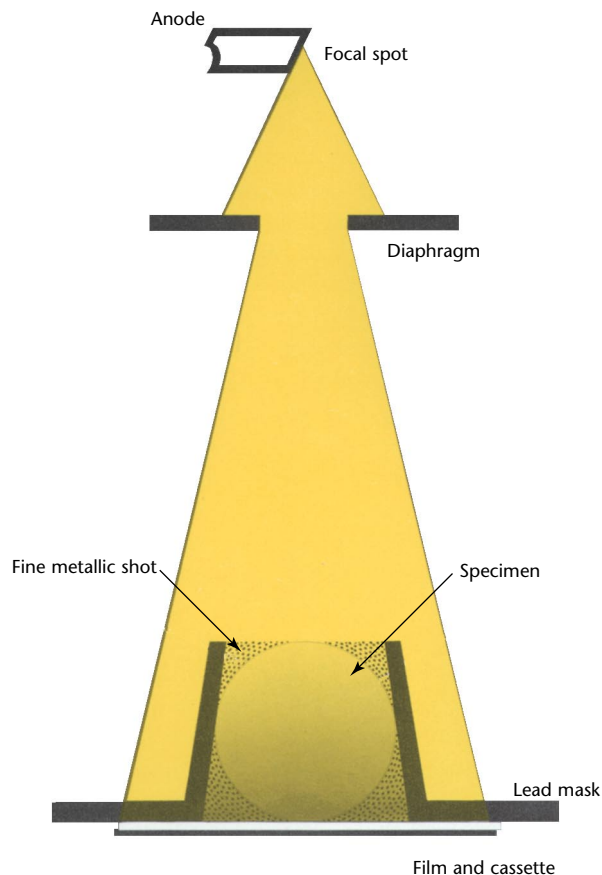


screens is discussed more below. Definite means must be provided to ensure good contact with the film to ensure image sharpness.

Many X-ray holders or cassettes incorporate a sheet of lead foil in the back for the specific purpose of protecting the film from backscatter from the table or other objects. This lead will not serve as an intensifying screen — first because it usually has a paper facing and second because it often is not lead of *radiographic quality*.

When radiographic film cassettes fitted with a sheet of lead foil in the back for protection against backscatter are used with gamma rays or with X-rays above 200 kV, the film should always be enclosed between double lead screens; otherwise, the secondary radiation from the lead backing is sufficient to penetrate the intervening felt or paper and cast a shadow of this material on the film giving a granular or mottled appearance.

**FIGURE 15.** Combined use of metallic shot and lead mask for lessening scattered radiation is conducive to good radiographic quality. If several round bars are to be radiographed, they may be separated along their lengths with lead strips held on edge by wooden frame and voids filled with fine shot.



## Masks and Diaphragms

Scattered radiation originating in matter outside the specimen is most serious for specimens that have high absorption for X-rays because the scattering from external sources may be large compared to the primary image forming radiation that reaches the film through the specimen. If many specimens of the same article are to be radiographed, it may be worthwhile to cut an opening of the same shape, but slightly smaller, in a sheet of lead and place this on the object. The lead serves to reduce the exposure in surrounding areas and thus to reduce scattered radiation from this source. Because scatter also arises from the specimen itself, it is good practice, wherever possible, to limit the cross section of an X-ray beam to cover only the area of the specimen that is of interest in the examination.

For occasional pieces of work with low energy radiation, where a cutout diaphragm would not be economical, barium clay packed around the specimen may serve the same purpose. The clay should be thick enough so that the film density under the clay is somewhat less than that under the specimen. Otherwise, the clay itself contributes appreciable scattered radiation.

One of the most satisfactory arrangements, combining effectiveness and convenience, is to surround the object with copper or steel shot having a diameter of about 0.25 mm (0.01 in.) or less (Fig. 15). Steel is best for objects of low atomic number; copper, for steel and objects of higher atomic number than iron. The materials flow and are effective for filling cavities or irregular edges of objects, such as castings, where a normal exposure for thick parts would result in an overexposure for thinner parts. Of course, it is preferable to make separate exposures for thick and thin parts but this is not always practical.

In some cases, a lead diaphragm or lead cone on the tube head may be a convenient way to limit the area covered by the X-ray beam. Such lead diaphragms are particularly useful where the desired cross section of the beam is a simple geometric figure, such as a circle, square or rectangle.

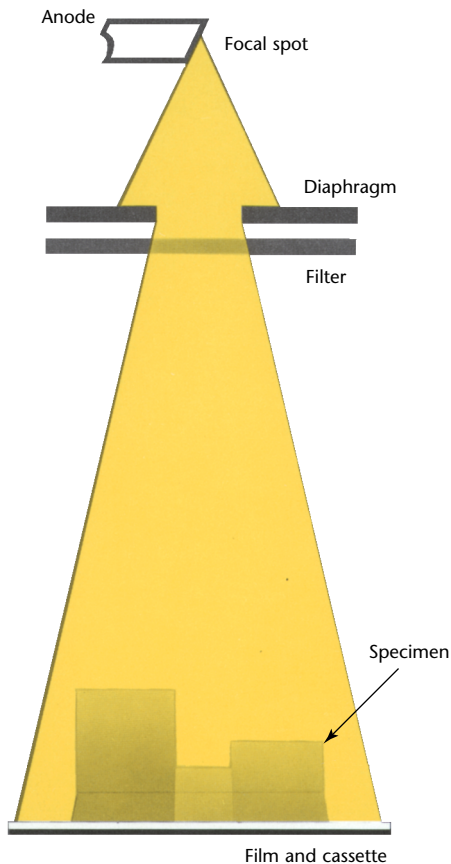
## Filters

In general, filters are limited to radiography with X-rays below 1 MeV. A simple metallic filter mounted in the X-ray beam near the X-ray tube (Fig. 16) may adequately serve the purpose of eliminating overexposure in the thin regions of the specimen and in the area surrounding the part (Table 3). Such a filter is particularly useful for reducing scatter undercut in cases where a mask

around the specimen is impractical. Of course, an increase in exposure of kilovoltage will be required to compensate for the additional absorption.

The underlying principle of the technique is that the filter absorbs more of the softer radiation of the primary beam than it does the harder radiation. This causes a greater change in the amount of radiation passing through the thin parts than through the thicker parts.

**FIGURE 16.** Filter placed near X-ray tube reduces subject contrast and eliminates much of secondary radiation, which tends to obscure detail in periphery of specimen.



In regions of strong undercut, the contrast is *increased* by a filter because the only effect of the undercutting radiation is to obscure the desired image. In regions where the undercut is negligible, a filter has the effect of *decreasing* the contrast in the finished radiograph.

A filter reduces excessive subject contrast (and hence radiographic contrast) by hardening the radiation. The longer wavelengths do not penetrate the filter to as great an extent as do the shorter wavelengths. Therefore, the beam emerging from the filter contains a higher proportion of the more penetrating wavelengths (see Fig. 17).

The choice of a filter material should be made on the basis of availability and ease of handling. For the same filtering effect, the thickness of filter required is less for those materials having higher absorption. In many cases, copper or brass is the most useful, because filters of these materials will be thin enough to handle easily yet not so thin as to be delicate (see Fig. 18).

Rules for filter thicknesses are difficult to formulate exactly because the amount of filtration required depends not only on the material and thickness range of the specimen but also on the distribution of material in the specimen and on the amount of scatter to be eliminated. In the radiography of aluminum, a filter of copper about 4 percent of the greatest thickness of the specimen should provide the thickness necessary. With steel, a copper filter should ordinarily be about 20 percent, or a lead filter about 3 percent, of the greatest specimen thickness for the greatest useful filtration. The foregoing values are maximum values; depending on circumstances, useful radiographs can often be made with far less filtration.

**FIGURE 17.** Curves illustrating effect of filter on composition and intensity of X-ray beam.

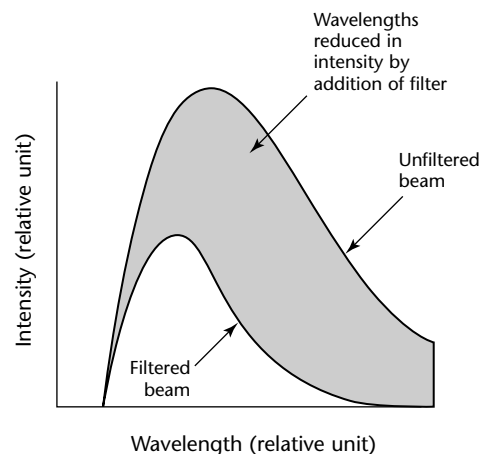


**TABLE 3.** Effect of metallic filter on X-ray intensity.

Region	Specimen Thickness		Original X-Ray Intensity Remaining after Addition of Filter (percent)
	mm	(in.)	
Outside specimen	0	(0)	< 10
Thin section	6.4	(0.25)	~ 30
Medium section	12.7	(0.50)	~ 40
Thick section	25.4	(1.0)	~ 55

In radiography with X-rays up to at least 250 kV, a 0.125 mm (0.005 in.) front lead screen is an effective filter for the scatter from the bulk of the specimen. Additional filtration between specimen and film only tends to contribute additional scatter from the filter itself and harden the beam unnecessarily.

### Grid Diaphragms

One of the most effective ways to reduce scattered radiation from an object being radiographed at energies up to 400 kV is with a potter-bucky diaphragm. This apparatus (Fig. 19) consists of a moving grid, composed of lead strips held in position by intervening strips of a material transparent to X-rays. The lead strips are tilted, so that the plane of each is in line with the focal spot of the tube. The slots between the lead strips are several times as deep as they are wide. The lead strips have the function of absorbing the very divergent scattered rays from the object being radiographed, so that most of the exposure is made by the primary rays emanating from the focal spot of the tube and passing between the lead strips. During the course of the exposure, the grid is moved, or oscillated (out of synchronization with the X-ray pulse) in a plane parallel to the film as shown by the

black arrows in Fig. 19. Thus, the shadows of the lead strips are blurred to the point that they do not appear in the final radiograph.

The potter-bucky diaphragm complicates industrial radiographic testing and necessarily limits the flexibility of the arrangement of the X-ray tube, the specimen and the film. Grids can, however, be of great value in the radiography of beryllium more than 75 mm (3 in.) thick and in the examination of other low absorption materials of moderate and great thicknesses.

Special forms also have been designed for the radiography of steel with voltages as high as 200 to 400 kV. These diaphragms are not used at higher voltages or with gamma rays because relatively thick lead strips would be needed to absorb the radiation scattered at these energies. This in turn would require a potter-bucky diaphragm, with

FIGURE 18. Maximum filter thickness for aluminum and steel.

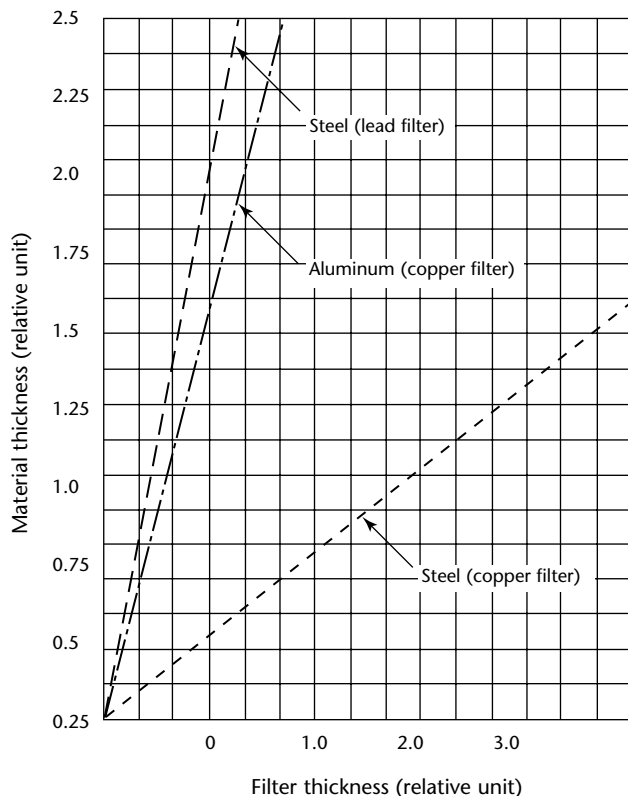
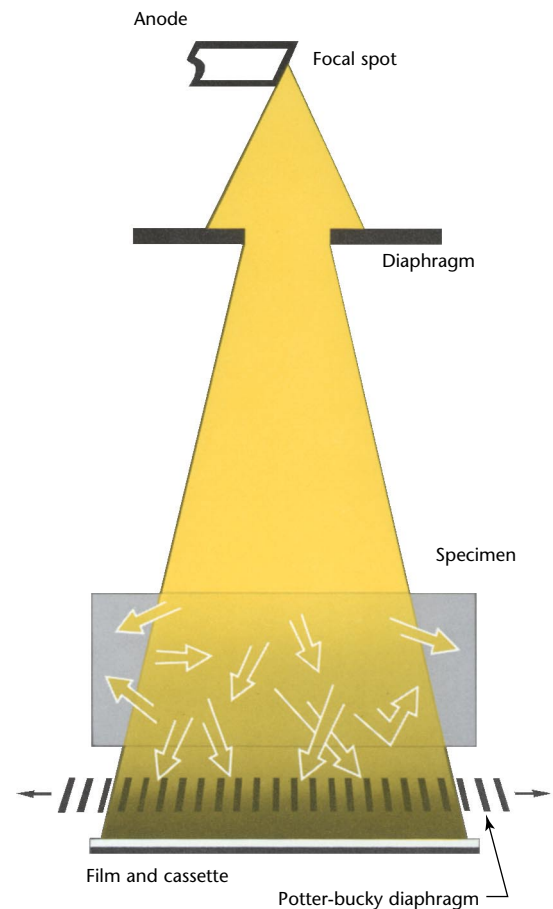


FIGURE 19. Schematic diagram showing how primary X-rays pass between lead strips of potter-bucky diaphragm. Most of scattered X-rays are absorbed because they strike sides of strips.



the associated mechanism, of an uneconomical size and complexity.

## Mottling Caused by X-Ray Diffraction

A special form of scattering caused by X-ray diffraction is encountered occasionally. It is most often observed in the radiography of fairly thin metallic specimens whose grain size is large enough to be an appreciable fraction of the part thickness. The radiographic appearance of this type of scattering is mottled and may be confused with the mottled appearance sometimes produced by porosity or segregation. It can be distinguished from these conditions by making two successive radiographs, with the specimen rotated slightly (1 to 5 degrees) between exposures, about an axis perpendicular to the central beam. A pattern caused by porosity or segregation will change only slightly; however, one caused by diffraction will show a marked change. The radiographs of some specimens will show a mottling from both effects and careful observation is needed to differentiate between them.

Relatively large crystal or grain in a relatively thin specimen may in some cases diffract an appreciable portion of the X-ray energy falling on the specimen, much as if it were a small mirror. This will result in a light spot on the developed radiograph corresponding to the position of the particular crystal and may also produce a dark spot in another location if the diffracted, or reflected, beam strikes the film. Should this beam strike the film beneath a thick part of the specimen, the dark spot may be mistaken for a void in the thick section. This effect is not observed in most industrial radiography, for most specimens are composed of a multitude of very minute crystals or grains variously oriented; hence scatter by diffraction is essentially uniform over the film area. In addition, the directly transmitted beam usually reduces the contrast in the diffraction pattern to a point where it is no longer visible on the radiograph.

The mottling caused by diffraction can be reduced and in some cases eliminated by raising the kilovoltage and by using lead foil screens. The former is often of positive value even though the radiographic contrast is reduced. Because definite rules are difficult to formulate, both approaches should be tried in a new situation and perhaps both used together.

It should be noted, however, that in some instances, the presence or absence of mottling caused by diffraction has been used as a rough indication of grain size

and thus as a basis for the acceptance or the rejection of parts.

## Scattering in High Voltage Megavolt Radiography

Lead screens should always be used in the 1 or 2 MeV range. The common thicknesses, 0.125 mm (0.005 in.) front and 0.25 mm (0.010 in.) back, are both satisfactory and convenient. Some users, however, find a 0.25 mm (0.010 in.) front screen of value because of its greater selective absorption of the scattered radiation from the specimen.

At these voltages filtration at the tube offers no improvement in radiographic quality. Filters at the film improve the radiograph in the examination of uniform sections but give poor quality at the edges of an image because of undercut of scattered radiation from the filter itself. Hence, filtration should not be used in the radiography of specimens containing narrow bars, for example, no matter what the thickness of the bars in the direction of the primary radiation. Also, filtration should be used only where the film can be adequately protected against backscattered radiation.

Lead filters are most convenient for this voltage range. When used between specimen and film, filters are subject to mechanical damage. Care should be taken to reduce this to a minimum, lest filter anomalies be confused with structures in or on the specimen. In radiography with megavolt X-rays, specimens of uniform sections may be conveniently divided into three classes. Below 38 mm (1.5 in.) of steel, filtration affords little improvement in radiographic quality. Between 38 and 100 mm (1.5 and 4.0 in.) of steel, the thickest filter, up to 3 mm (0.125 in.) lead, that allows a reasonable exposure time, may be used. Above 100 mm (4.0 in.) of steel, filter thicknesses may be increased to 6.3 mm (0.25 in.) of lead, economic considerations permitting. It should be noted that in the radiography of extremely thick specimens with megavolt X-rays, fluorescent screens may increase the photographic speed to a point where filters can be used without requiring excessive exposure time.

A very important point is to block off all radiation except the useful beam with heavy (12.7 to 25.4 mm [0.5 in. to 1 in.]) lead at the tubehead. This step is called *collimation*. Unless this is done, radiation striking the walls of the X-ray room will scatter back enough to seriously affect the quality of the radiograph. This will be especially noticeable if the specimen is thick or has parts projecting relatively far from the film.



## PART 3. Radiographic Screens

### Functions of Screens

Radiographic screens help radiographers to use more fully the X-ray or gamma ray energy reaching the film. The [physical principles underlying the action of both lead foil and fluorescent screens are discussed elsewhere](#) and only the practical applications are discussed here.

When an X-ray or gamma ray beam strikes a film, usually less than one percent of the energy is absorbed. Because the formation of the radiographic image is governed by the absorbed radiation, more than 99 percent of the available energy in the primary radiation reaching the film performs no useful photographic work. Obviously, any means of more fully using this wasted energy, without complicating the technical procedure, is highly desirable. Three types of radiographic screens are commonly used for this purpose — lead, fluorescent and fluorometallic (metal phosphor). Metals other than lead are sometimes used in megavolt radiography. Lead screens may be in the form of thin foil, usually mounted on a thin cardboard or plastic sheet, or in the form of a lead compound, usually lead oxide, evenly coated on a thin support. The lead compound screens are usually used only for radiography below 150 kV.

### Lead Foil Screens

For radiography with X-ray or gamma ray energies between 150 kV and 2 MeV, lead foil screens in intimate contact with both sides of the film, within the film holder, will reduce exposure times and improve radiographic quality by reducing scatter. Foils as thin as 0.10 to 0.15 mm (0.004 to 0.006 in.) are commonly used. To reduce backscatter from the table or floor of the room an additional lead sheet 3 to 6 mm (0.12 to 0.25 in.) thick is usually placed behind the film holder.

The choice of screens and filters for radiography above 1 to 2 MeV is more complicated, as discussed in the section on high energy radiography.

### Effects of Lead Screens

Lead foil in direct contact with the film has three principal effects: (1) it increases

the photographic action on the film, largely by reason of the electrons emitted and partly by the secondary X-rays emitted by the lead; (2) it absorbs the longer wavelength scattered radiation more than the primary; and (3) it intensifies the primary radiation more than the scattered radiation. The differential absorption of the secondary radiation and the differential intensification of the primary radiation result in diminishing the effect of scattered radiation, producing greater contrast and clarity in the radiographic image. This reduction in the effect of the scattered radiation decreases the total intensity of the radiation reaching the film and lessens the net intensification factor of the screens. The absorption of primary radiation by the front lead screen also diminishes the net intensifying effect; and, if the incident radiation does not have sufficient penetrating power, the actual exposure required may be even greater than without screens. At best, the exposure time is one half to one third of that without screens but the advantage of screens in reducing scattered radiation still holds.

The quality of the radiation necessary to obtain an appreciable intensification from lead foil screens depends on the type of film, the kilovoltage and the thickness and nature of the material through which the rays must pass (Fig. 20). In the radiography of aluminum, for example, using a 0.125 mm (0.005 in.) front screen and a 0.25 mm (0.010 in.) back screen, the thickness of aluminum must be about 150 mm (6 in.) and the kilovoltage as high as 160 kV to secure any advantage in exposure time with lead screens. In the radiography of steel, lead screens begin to give appreciable intensification with thicknesses in the neighborhood of 6.3 mm (0.25 in.), at voltages of 130 to 150 kV. In the radiography of 32 mm (1.25 in.) steel at about 200 kV, lead screens permit an exposure of about one third of that without screens (intensification factor of 3). With cobalt-60 gamma rays, the intensification factor of lead screens is about 2. Lead foil screens, however, do not detrimentally affect the definition or graininess of the radiographic image to any material degree so long as the lead and the film are in intimate contact.



Lead foil screens also diminish the effect of scattered radiation. Scattered radiation from the specimen itself is cut almost in half by lead screens, contributing to maximum clarity of detail in the radiograph; this advantage is obtained even under conditions where the lead screen makes an increase in exposure necessary.

In radiography with gamma rays or high voltage X-rays, films loaded in metal cassettes without screens are likely to record the effect of secondary electrons generated in the lead covered back of the cassette. These electrons, passing through the felt pad on the cassette cover, produce a mottled appearance because of the structure of the felt. Films loaded in the customary lead backed cardboard exposure holder may also show the structure of the paper that lies between the lead and the film (Fig. 21). To avoid these effects, film should be enclosed between double lead screens, care being taken to ensure good contact between film and screens. Thus, lead foil screens are essential in practically all radiography with gamma rays or megavolt X-rays. If, for any reason, screens cannot be used with these radiations, a lightproof plastic holder with no metal backing should be used.

Contact between the film and the lead foil screens is essential to good radiographic quality. Areas lacking contact produce fuzzy images, as shown in Fig. 22b.

**FIGURE 21.** Upper area shows decreased density caused by paper between lead screen and film. Electron shadow picture of paper structure has also been introduced.

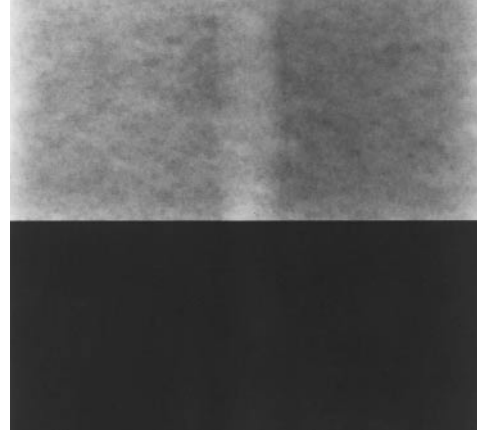


**FIGURE 22.** Between film and lead foil screens: (a) good contact gives sharp image; (b) poor contact gives fuzzy image.

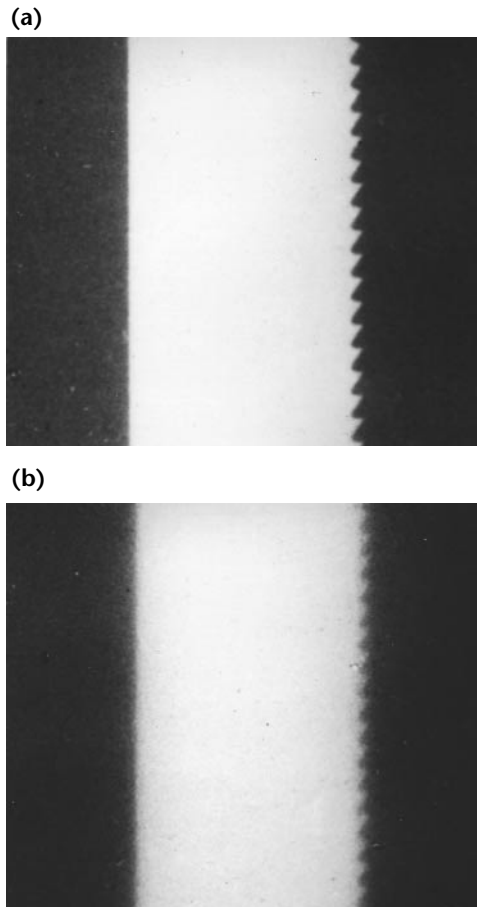
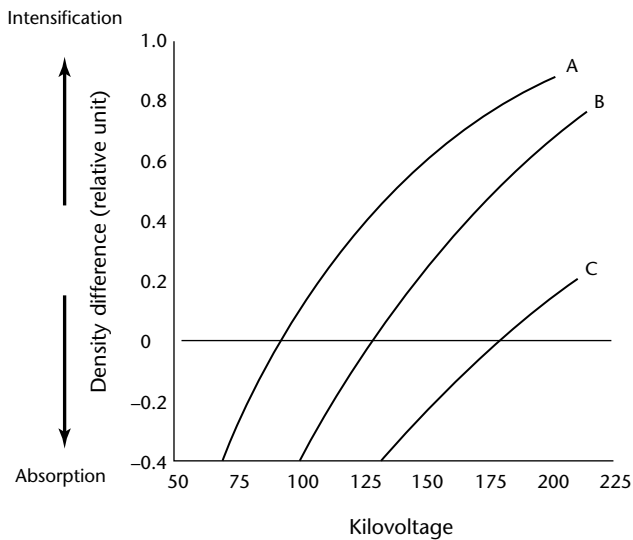


**FIGURE 20.** Effects of kilovoltage on intensification properties of lead screens.



**Legend**

- A. 0.05 mm (0.002 in.) lead oxide, 0.01 mm (0.0004 in.) lead equivalent.
- B. 0.12 mm (0.005 in.).
- C. 0.25 mm (0.01 in.) lead.

## Selection and Care of Lead Screens

Lead foil for screens must be selected with extreme care. Commercially pure lead is satisfactory. An alloy of 6 percent antimony and 94 percent lead, being harder and stiffer, has better resistance to wear and abrasion. Tin coated lead foil should be avoided, because irregularities in the tin cause a variation in the intensifying factor of the screens, resulting in mottled radiographs. Minor blemishes do not affect the usefulness of the screen but large *blisters* or cavities should be avoided.

Most of the intensifying action of a lead foil screen is caused by the electrons emitted under X-ray or gamma ray excitation. Because electrons are readily absorbed even in thin or light materials, small flakes of foreign material — for example, dandruff or tobacco — will likewise produce light spots on the completed radiograph. For this same reason, protective coatings on lead foil screens should be removed before use. The coating should not produce static electricity when rubbed against or placed in contact with film (see Fig. 23).

Deep scratches on lead foil screens, on the other hand, will produce dark lines on the radiograph (Fig. 24).

Surface contaminants may be removed from lead foil screens with a mild household detergent or cleanser and a soft, lint-free cloth. If more thorough cleaning is necessary, screens may be very gently rubbed with the finest grade of

steel wool. If this is done carefully, the shallow scratches left by the steel wool will not produce dark lines in the radiograph.

Films could be fogged if left between lead foil screens longer than is reasonably necessary, particularly under conditions of high temperature and humidity. When screens have been freshly cleaned with an abrasive, this effect will be increased; prolonged contact between film and screens should be delayed for 24 h after cleaning.

## Fluorescent Screens

Certain chemicals fluoresce; that is, they have the ability to absorb X-rays and gamma rays and immediately emit light; the intensity of the emitted light depends on the intensity of the incident radiation. These fluorescent materials can be used in radiography by first being finely powdered, mixed with a suitable binder, then coated in a thin, smooth layer on a special cardboard or plastic support.

For the exposure, film is clamped firmly between a pair of these fluorescent screens. The photographic effect on the film, then, is the sum of the effects of the X-rays and of the light emitted by the screens. For example, in the radiography of 12.7 mm (0.5 in.) steel at 150 kV, a factor as high as 125 has been observed.

**FIGURE 23.** Static marks result from poor film handling. Static marks may also be treelike or branching.

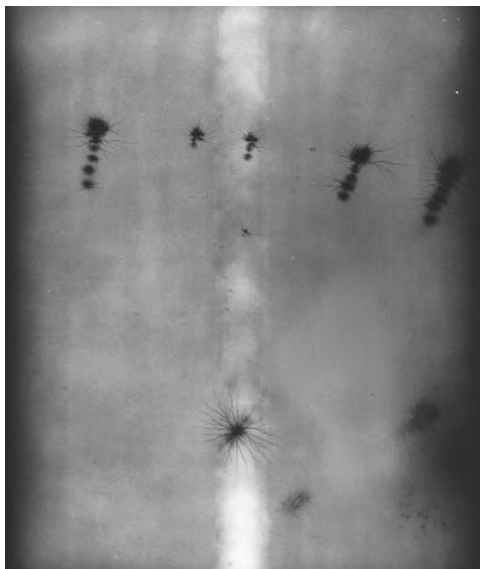
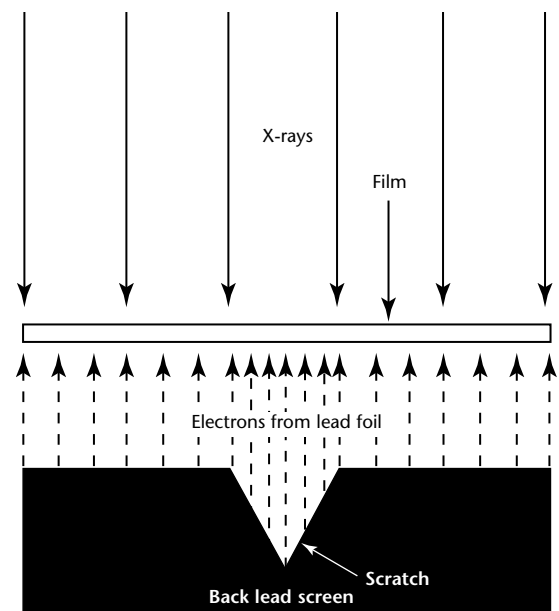


**FIGURE 24.** Number of electrons emitted (per surface unit of lead) is essentially uniform. More electrons can reach film in vicinity of scratch, resulting in dark line on radiograph. (For illustrative clarity, electron paths have been shown as straight and parallel; actually, electrons are emitted diffusely.)



In radiography of 19.1 mm (0.75 in.) steel at 180 kV, factors of several hundred have been obtained experimentally.

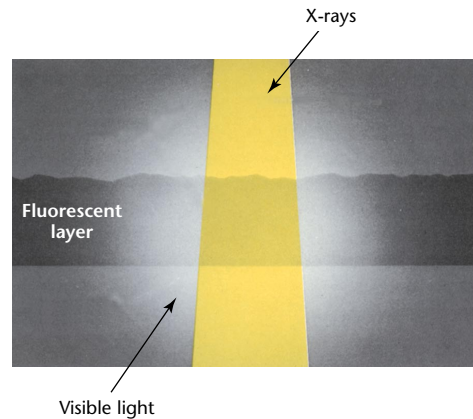
Under these latter conditions, the intensification factor has about reached its maximum and diminishes both for lower voltage and thinner steel and for higher voltage and thicker steel. Using cobalt-60 gamma rays for very thick steel, the factor may be 10 or less.

### Limitations

Despite their great effect in reducing exposure time, fluorescent screens are not widely used in industrial radiography. This is mainly because they may give poor definition, compared to a radiograph made directly or with lead screens. The poorer definition results from the spreading of the light emitted from the screens, as shown in Fig. 25. The light from any particular portion of the screen spreads out beyond the confines of the X-ray beam that excited the fluorescence.

The other reason fluorescent screens are seldom used in industrial radiography is because they may produce *screen mottle* on the finished radiograph. This mottle is characteristic in appearance, very much larger in scale and much softer in outline than the graininess associated with the film itself. Screen mottle is associated with purely statistical variations in the numbers of absorbed X-ray photons, from one tiny area of the screen to the next. Thus, screen mottle tends to become greater as the kilovoltage of the radiation increases. The higher the kilovoltage, the more energetic, on the average, are the X-ray photons. Therefore, on absorption in the screen, a larger *burst* of light is produced. The larger the bursts, the fewer that are needed to produce a given density and the greater is the purely statistical variation in the number of photons from one small area to the next.

**FIGURE 25.** Light and ultraviolet radiation from typical fluorescent screen spreads beyond X-ray beam that excites fluorescence.

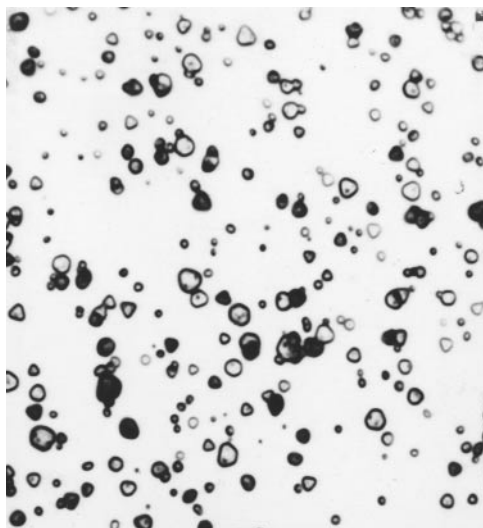


## PART 4. Industrial X-Ray Films

Modern radiographic films for general radiography consist of an emulsion (gelatin containing a radiation sensitive silver halide compound) and a flexible, transparent base that sometimes contains a tint. Usually, the emulsion is coated on both sides of the base in layers about 0.0125 mm ( $5 \times 10^{-4}$  in.) thick (see Fig. 26 and 27). Putting emulsion on both sides of the base doubles the amount of radiation sensitive silver compound and thus increases the speed. At the same time, the emulsion layers are thin enough so that developing, fixing and drying can be accomplished in a reasonable time. However, some films for radiography in which the highest detail visibility is required have emulsion on only one side of the base.

When X-rays, gamma rays or light strike the grains of the sensitive silver compound in the emulsion, a change takes place in the physical structure of the grains. This change cannot be detected by ordinary physical techniques. However, when the exposed film is treated with a chemical solution (called a developer), a reaction takes place, causing the formation of black, metallic silver. It is

**FIGURE 26.** Silver bromide grains of radiographic film emulsion (2500 diameters). Grains have been dispersed to show shape and relative sizes more clearly; in actual coating, crystals are much more closely packed.



this silver, suspended in the gelatin on both sides of the base, that constitutes the image (see Fig. 28).

**FIGURE 27.** Cross section of unprocessed emulsion on one side of radiographic film (2000 diameters). Note greater quantity of grains as compared to developed grains of Fig. 28.

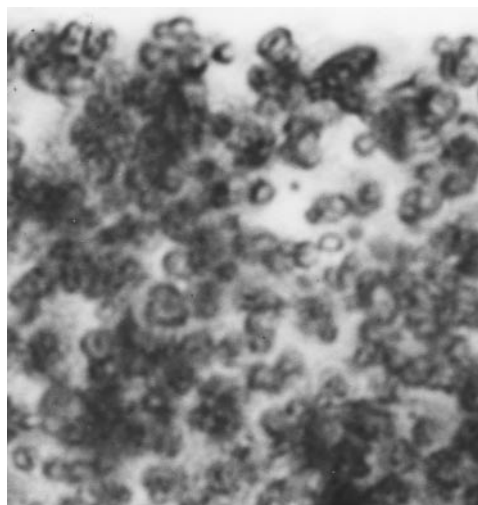
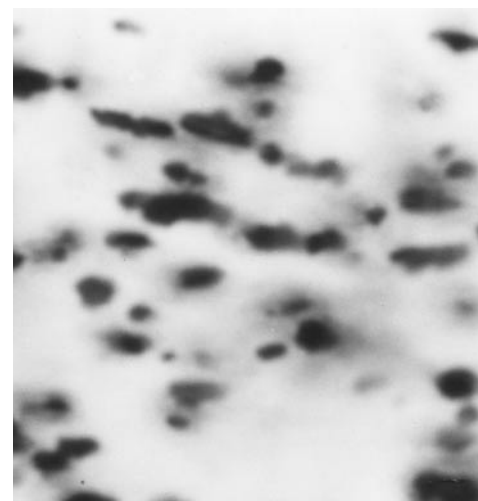


**FIGURE 28.** Cross section showing distribution of developed grains in radiographic film emulsion exposed to give moderate density.



Although an image may be formed by light and other forms of radiation, as well as by gamma rays or X-rays, the properties of the latter two are of distinct character and, for this reason, the sensitive emulsion must be different from those used in other types of photography.

## Selection of Films for Industrial Radiography

As pointed out above, industrial radiography now has many widely diverse applications. There are many considerations to be made in obtaining the best radiographic results, for example: (1) the composition, shape and size of the part being examined — and, in some cases, its weight and location as well; (2) the type of radiation used — whether X-rays from an X-ray machine or gamma rays from a radioactive material; (3) the kilovoltages available with the X-ray equipment; (4) the intensity of the gamma radiation; (5) the kind of information sought — whether it is simply an overall inspection or the critical examination of some especially important portion, characteristic or feature; and (6) the resulting relative emphasis on definition, contrast, density and time required for proper exposure. All of these factors are important in the determination of the most effective combination of radiographic method and radiographic film.

The selection of a film for the radiography of any particular part depends on the thickness and material of the specimen and on the voltage range of the available X-ray machine. In addition, the choice is affected by the relative importance of high radiographic quality or short exposure time. Thus, an attempt must be made to balance these two opposing factors. As a consequence, it is not possible to present definite rules on the selection of a film. If high quality is the deciding factor, a slower (less sensitive) and finer grained film should be substituted for a faster (more sensitive) one — for instance, for the radiography of

steel up to 6.3 mm (0.25 in.) thick at 120 to 150 kV, film Y might be substituted for film X. If short exposure times are essential, a faster film (or faster combination of film and screen) can be used. For example, 38 mm (1.5 in.) steel might be radiographed at 200 kV using fluorescent screens with a film particularly sensitive to blue light, rather than a direct exposure film with lead screens.

Figure 29 indicates the direction that these substitutions take. The direct exposure films may be used with or without lead screens, depending on the kilovoltage and the thickness and shape of the specimen.

Fluorescent intensifying screens must be used in radiography requiring the highest possible photographic speed. The light emitted by the screens has a much greater photographic action than the X-rays either alone or combined with the emission from lead screens. To secure adequate exposure within a reasonable time, screen type radiographic films sandwiched between fluorescent intensifying screens are often used in radiography of steel in thicknesses greater than about 50 mm (2 in.) at 250 kV and greater than 75 mm (3 in.) at 400 kV.

## Photographic Density

*Photographic density* refers to the quantitative measure of film blackening and is also called *optical density* and *sensitometric density*. When no danger of confusion exists, photographic density is usually spoken of merely as *density*. Density is defined by the equation:

$$(13) \quad D = \log \frac{I_0}{I_t}$$

where  $D$  = density;  $I_0$  = light intensity incident on film; and  $I_t$  = light intensity transmitted.

Table 4 illustrates some relations between transmittance, percent

FIGURE 29. Choice of film depends on relative emphasis on high speed or high radiographic quality.

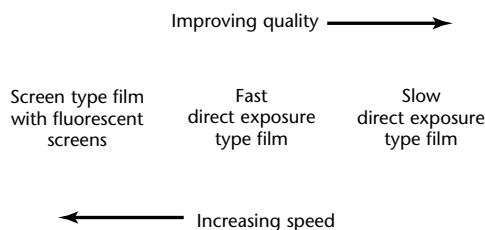


TABLE 4. Transmittance, percent transmittance, opacity and density relationships.

Transmittance $I_t \cdot I_0^{-1}$	Percent Transmittance $I_t \cdot I_0^{-1} \times 100$	Opacity $I_0 \cdot I_t^{-1}$	Density $\log I_0 \cdot I_t^{-1}$
1.00	100	1	0
0.50	50	2	0.3
0.25	25	4	0.6
0.10	10	10	1.0
0.01	1	100	2.0
0.001	0.1	1000	3.0
0.0001	0.01	10 000	4.0



transmittance, opacity and density. It shows that an increase in density of 0.3 reduces the light transmitted to half of its former value. In general, because density is a logarithm, a certain *increase* in density always corresponds to the same *percentage decrease* in transmittance.

## Densitometers

A densitometer is an optical instrument for measuring photographic densities. Film density to a required range is usually specified in radiographic procedures. The densitometer must be available to see that specifications are met. [The densitometer is essential for creating characteristic curves, discussed elsewhere.](#)

Different types of densitometers, both visual and photoelectric, are available commercially. For purposes of practical industrial radiography there is no great premium on high accuracy in a densitometer. A much more important property is reliability, that the densitometer should reproduce readings from day to day.

## X-Ray Exposure Charts

An exposure chart is a graph showing the relation between material thickness, kilovoltage and exposure (Figs. 30 to 32). In its most common form, an exposure chart resembles Fig. 30. These graphs are adequate for determining exposures in the radiography of uniform plates but they serve only as rough guides for objects, such as complicated castings, having wide variations of thickness.

Exposure charts are usually available from manufacturers of X-ray equipment. Because, in general, such charts cannot be used for different X-ray machines unless suitable correction factors are applied, individual laboratories sometimes prepare their own.

### Preparing an Exposure Chart

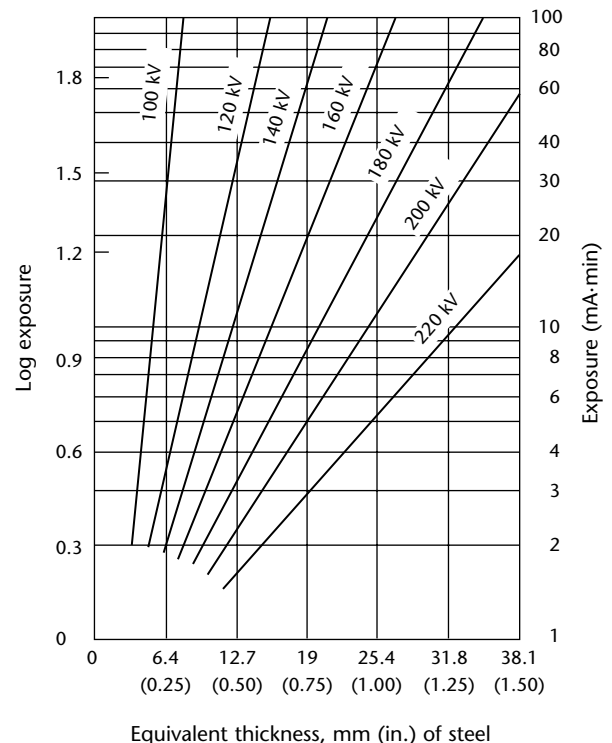
A simple technique for preparing an exposure chart is to make a series of radiographs of a pile of metal plates (of equal thickness but different lengths) consisting of a number of steps. This step tablet, or stepped wedge, is radiographed at several different exposure times at each of a number of kilovoltages. The exposed films are all processed under conditions identical to those that will later be used for routine work. Each radiograph consists of a series of photographic densities corresponding to the X-ray intensities transmitted by the different thicknesses of metal. A certain density, for example 1.5, is selected as the basis for the preparation

of the chart. Wherever this density occurs on the stepped wedge radiographs, there are corresponding values of thickness, milliamperere minutes and kilovoltage. It is unlikely that many of the radiographs will contain a value of exactly 1.5 in density but the correct thickness for this density can be found by interpolation between steps. Thickness and milliamperere minute values are plotted for the different kilovoltages in the manner shown in Fig. 30.

Another technique, requiring fewer stepped wedge exposures but more arithmetical manipulation, is to make one step tablet exposure at each kilovoltage and to measure the densities in the processed stepped wedge radiographs. The exposure that would have given the chosen density (in this case 1.5) under any particular thickness of the stepped wedge can then be determined from the characteristic curve of the film used. The values for thickness, kilovoltage and exposure are then plotted.

Note that thickness is on a linear scale and that milliamperere minutes are on a nonlinear scale. The logarithmic scale is not necessary but is very convenient because it compresses an otherwise long scale. A further advantage of the logarithmic exposure scale is that it usually allows the location of the points

**FIGURE 30.** Typical X-ray exposure chart for steel may be applied to film X (see Fig. 33), with lead foil screens, at 1.5 film density and 1.0 m (40 in.) source-to-film distance.





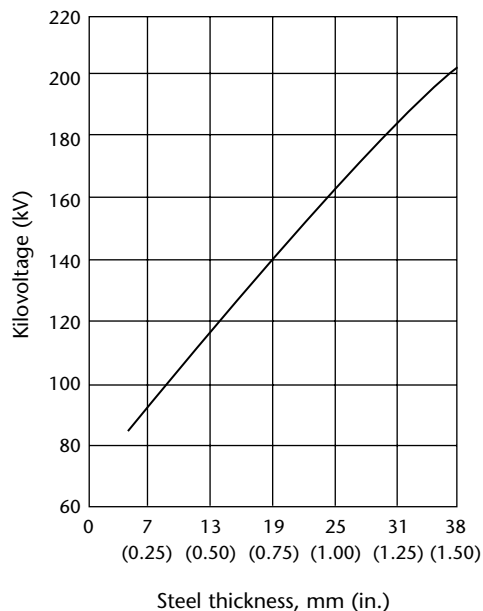
for any one kilovoltage to be well approximated by a straight line.

An exposure chart usually applies only to a single set of conditions, determined by (1) the X-ray machine used; (2) a certain source-to-film distance; (3) a particular film type; (4) processing conditions used; (5) the film density on which the chart is based; (6) the type of screens (if any) that are used; and (7) the material tested.

Only if the conditions used in making the radiograph agree in all particulars with those used in preparation of the exposure chart can values of exposure be read directly from the chart. Any change requires the application of a correction factor. The correction factor applying to each of the above conditions is discussed separately.

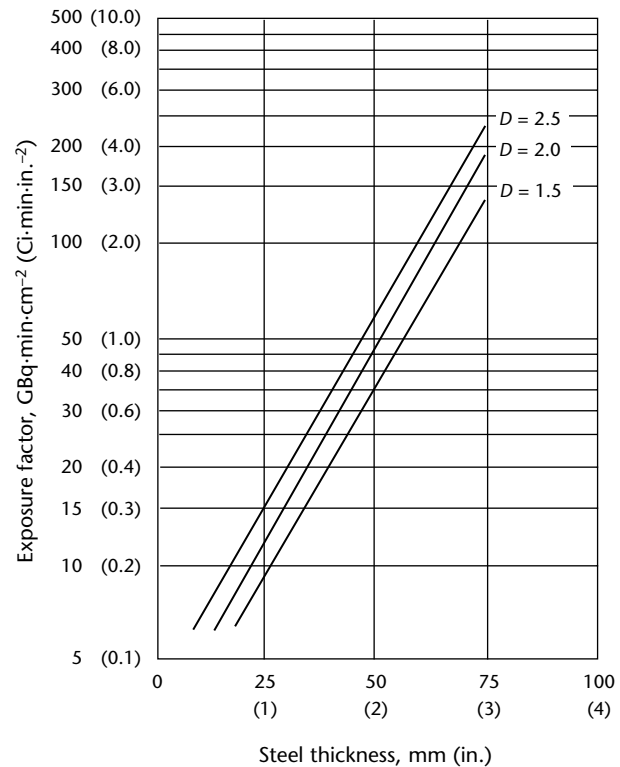
1. It is sometimes difficult to find a correction factor to make an exposure chart prepared for one X-ray machine applicable to another. Different X-ray machines operating at the same nominal kilovoltage and milliamperage settings may give not only different intensities but also different qualities (energies) of radiation.

**FIGURE 31.** Typical X-ray exposure chart for use when exposure and distance are held constant and kilovoltage is varied to conform to specimen thickness. Film X (see Fig. 33), exposed with lead foil screens to density of 1.5, source-to-film distance is 1.0 m (40 in.) and exposure is 50 mA-min.



2. A change in source-to-film distance may be compensated for by the inverse square law. Some exposure charts give exposures in terms of *exposure factor* rather than in terms of milliamperere minutes or milliamperere seconds. Charts of this type are readily applied to any value of source-to-film distance.
3. A different type of film can be corrected by comparing the difference in the amount of exposure necessary to give the same density on both films (from relative exposure charts such as those described below). For example, to obtain a density of 1.5 using film Y, 0.6 more log exposure is required than for film X (Fig. 33). This log exposure difference corresponds to an exposure factor of 3.99. To obtain the same density on film Y as on film X, multiply the original exposure by 3.99 to get the new exposure. Conversely, if going from film Y to film X, divide the original exposure by 3.99 to obtain the new exposure.

**FIGURE 32.** Typical gamma ray exposure chart for iridium-192, based upon the use of film X (see Fig. 33).



These procedures can be used to change densities on a single film as well. Simply find the log E difference needed to obtain the new density on the film curve; read the corresponding exposure factor from the chart; then multiply to increase density or divide to decrease density.

4. A change in processing conditions causes a change in effective film speed. If the processing of the radiographs differs from that used for the exposures from which the chart was made, the correction factor must be found by experiment.
5. The chart gives exposures to produce a certain density. If a different density is required, the correction factor may be calculated from the film's characteristic curve.
6. If the type of screen is changed — for example, from lead foil to fluorescent — it is easier and more accurate to make a new exposure chart than to determine correction factors
7. Material can be changed by using the material equivalence table (Table 2).

In some radiographic operations, the exposure time and the source-to-film distance are set by economic considerations or on the basis of previous experience and test radiographs. The tube current is, of course, limited by the design of the tube. The specimen and the kilovoltage are variables. When these conditions exist, the exposure chart may take a simplified form as shown in Fig. 31, which allows the kilovoltage for any particular specimen thickness to be chosen. Such a chart will be particularly useful when uniform sections must be radiographed in large numbers by relatively untrained persons. This type of exposure chart may be derived from a chart similar to Fig. 30 by following the horizontal line corresponding to the chosen milliamperere minute value and noting the thickness corresponding to this exposure for each kilovoltage. These thicknesses are then plotted against kilovoltage.

## Gamma Ray Exposure Charts

A typical gamma ray exposure chart is shown in Fig. 32. It is somewhat similar to Fig. 30; however, with gamma rays, there is no variable factor corresponding to the kilovoltage. Therefore, a gamma ray exposure chart contains one line, or several parallel lines, each of which corresponds to a particular film type, film density or source-to-film distance. Gamma ray exposure guides are also available in the form of linear or circular slide rules.

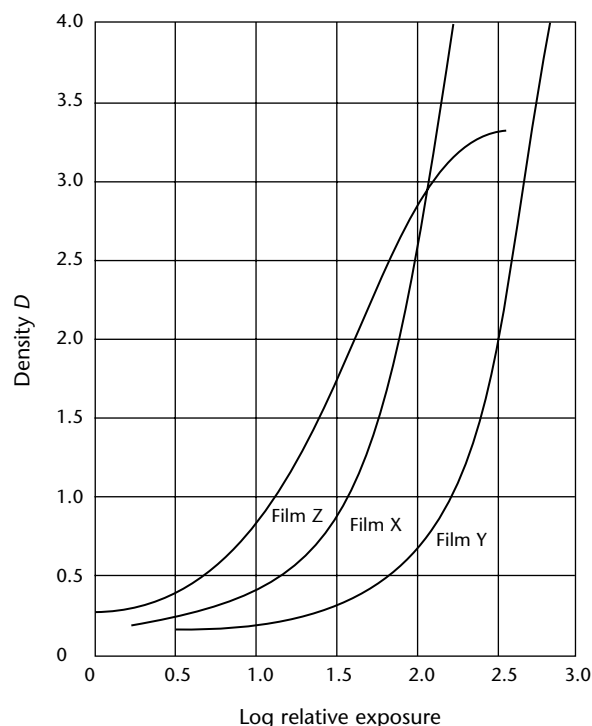
These contain scales on which the various factors of specimen thickness source strength and source-to-film distance can be set and from which exposure time can be read directly.

## Characteristic Curve

The characteristic curve, sometimes referred to as the *sensitometric curve* or the *H and D curve* (after Hurter and Driffield, who first used it in 1890), expresses the relation between the exposure applied to a photographic material and the resulting photographic density. The characteristic curves of three typical films, exposed between lead foil screens, are given in Fig. 33. Such curves are obtained by giving a film a series of known exposures, determining the densities produced by these exposures and then plotting density against the logarithm of relative exposure.

Relative exposure is used because there are no convenient units, suitable to all kilovoltages and scattering conditions, in which to express radiographic exposures. The exposures given a film are expressed in terms of some particular exposure, giving a relative scale. In practical radiography, this lack of units for X-ray intensity or quantity is no hindrance, as will be seen below. The logarithm of the

FIGURE 33. Characteristic curves of three typical X-ray films, exposed between lead foil screens.



relative exposure, rather than the relative exposure itself, has a number of advantages. It compresses an otherwise long scale. Furthermore, in radiography, ratios of exposures or intensities are usually more significant than the exposures of the intensities themselves. Pairs of exposures having the same ratio will be separated by the same interval on the log relative exposure scale, no matter what their absolute value may be.

Consider the pairs of exposures in Table 5.

As can be seen in Fig. 33, the slope (or steepness) of the characteristic curves is continuously changing throughout the length of the curves. For example, two slightly different thicknesses in the object radiographed transmit slightly different exposures to the film. These two exposures have a certain small log  $E$  interval between them; that is, they have a certain ratio. The difference in the densities corresponding to the two exposures depends on just where on the characteristic curve they fall; the steeper the slope of the curve, the greater is this density difference. For example, the curve of film Z (Fig. 33) is steepest in its middle portion. This means that a certain log  $E$  interval in the middle of the curve corresponds to a greater density difference than the same log  $E$  interval at either end of the curve. In other words, the film contrast is greatest where the slope of the characteristic curve is greatest. For film Z, as has been pointed out, the region of greatest slope is in the central part of the curve. For films X and Y, however, the slope — and hence the film contrast — continuously increases throughout the useful density range. The curves of most industrial radiographic films are similar to those of films X and Y.

### Use of Characteristic Curve

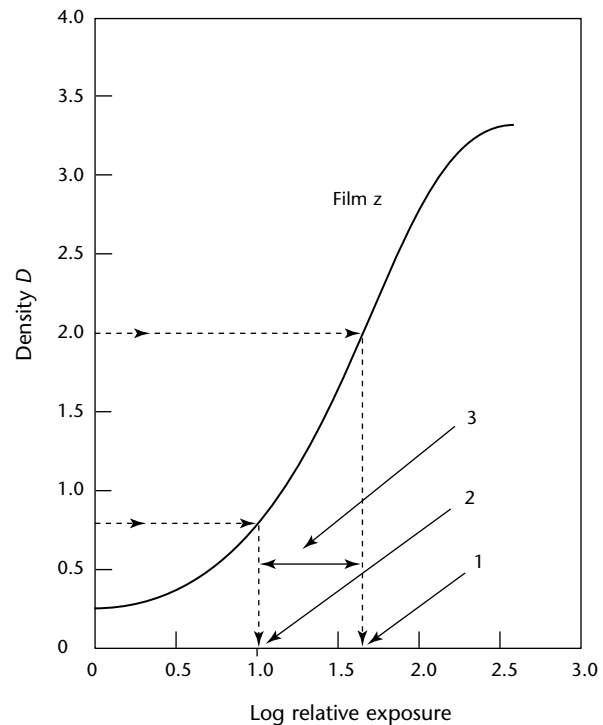
The characteristic curve can be used in solving quantitative problems arising in radiography, in the preparation of technique charts and in radiographic research. Characteristic curves made

under actual radiographic conditions *should* be used in solving practical problems. However, it is not always possible to produce characteristic curves in a radiography department and curves prepared elsewhere must be used. Such curves prove adequate for many purposes although it must be remembered that the shape of the characteristic curve and the speed of a film relative to that of another depend strongly on developing conditions. The accuracy attained when using *ready made* characteristic curves is governed largely by the similarity between the developing conditions used in producing the characteristic curves and those for the films whose densities are to be evaluated.

Quantitative use of characteristic curves are worked out in Figs. 34 and 35. Note that  $D$  is used for density and log  $E$  for logarithm of relative exposure.

In the first example (Fig. 34), suppose a radiograph made of film Z with an exposure of 12 mA·min has a density of 0.8 in the region of maximum interest. It is desired to increase the density to 2.0 for the sake of the increased contrast there available.

FIGURE 34. Characteristic curve of film Z (see Fig. 33).



#### Legend

1. Log  $E = 1.62$  at  $D = 2.0$ .
2. Log  $E = 1.00$  at  $D = 0.8$ .
3. Difference in log  $E$  is 0.62.

TABLE 5. Equivalent exposure ratios.

Relative Exposure	Log Relative Exposure	Interval in Log Relative Exposure
1	0.0	0.70
5	0.70	
2	0.30	0.70
10	1.00	
30	1.48	0.70
150	2.18	

1. Log  $E$  at  $D = 2.0$  is 1.62.
2. Log  $E$  at  $D = 0.8$  is 1.00.
3. The difference in log  $E$  is 0.62. The antilogarithm of this difference is 4.2.

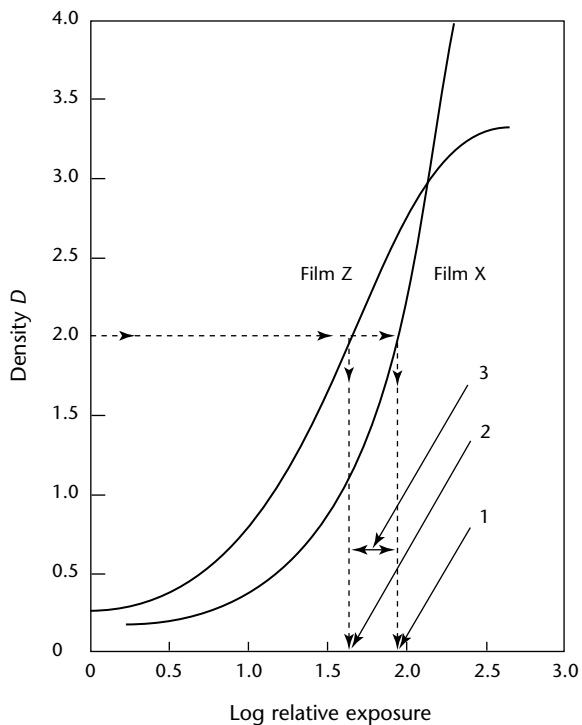
Therefore, the original exposure is multiplied by 4.2 giving 50 mA·min to produce a density of 2.0.

In the second example (see Fig. 35), film X has higher contrast than film Z at  $D = 2.0$  and also a finer grain. Suppose that, for these reasons, it is desired to make the radiograph on film X with a density of 2.0 in the same region of maximum interest.

1. Log  $E$  at  $D = 2.0$  for film X is 1.91.
2. Log  $E$  at  $D = 2.0$  for film Z is 1.62.
3. The difference in log  $E$  is 0.29. The antilogarithm of this difference is 1.95.

Therefore, the exposure for  $D = 2.0$  on film Z is multiplied by 1.95, giving 97.5 mA·min for a density of 2.0 on film X.

**FIGURE 35.** Characteristic curves of two X-ray films exposed with lead foil screens.



**Legend**

1. Log  $E = 1.91$  at  $D = 2.0$ .
2. Log  $E = 1.62$  at  $D = 2.0$ .
3. Difference in Log  $E$  is 0.29.

## PART 5. Radiographic Image Quality and Detail Visibility

### Controlling Factors

Because the purpose of most radiographic testing is to examine specimens for heterogeneity, a knowledge of the factors affecting the visibility of detail in the finished radiograph is essential. Table 6 shows the relationships of the various factors influencing image quality and radiographic sensitivity; following are a few important definitions.

*Radiographic sensitivity* is a general or qualitative term referring to the size of the smallest detail that can be seen in a radiograph or to the ease with which the images of small details can be detected. Phrased differently, it is a reference to the amount of information in the radiograph. Note that radiographic sensitivity depends on the combined effects of two independent sets of factors: radiographic contrast (the density difference between a small detail and its surroundings) and definition (the abruptness and the smoothness of the density transition). See Fig. 36.

*Radiographic contrast* is the difference in density between two areas of a radiograph. It depends on both subject contrast and film contrast.

*Subject contrast* is the ratio of X-ray or gamma ray intensities transmitted by two selected portions of a specimen. Subject contrast depends on the nature of the specimen, on the energy (spectral composition, hardness or wavelengths) of the radiation used and on the intensity and distribution of the scattered radiation but is independent of time, milliamperage or source strength, distance and the characteristics or treatment of the film (Fig. 11).

*Film contrast* refers to the slope (steepness) of the characteristic curve of the film. It depends on the type of film, on the processing it receives and density. It also depends on whether the film's exposure is direct, with lead screens or with fluorescent screens. Film contrast is independent, for most practical purposes, of the wavelengths and distribution of the radiation reaching the film and hence is independent of subject contrast.

The steepness of the characteristic curve is sometimes referred to as gamma ( $\Gamma$ ). Higher gamma films have more contrast.

*Definition* refers to the sharpness of outline in the image. It depends on the types of screens and film used, the radiation energy (wavelengths) and the geometry of the radiographic setup.

### Subject Contrast

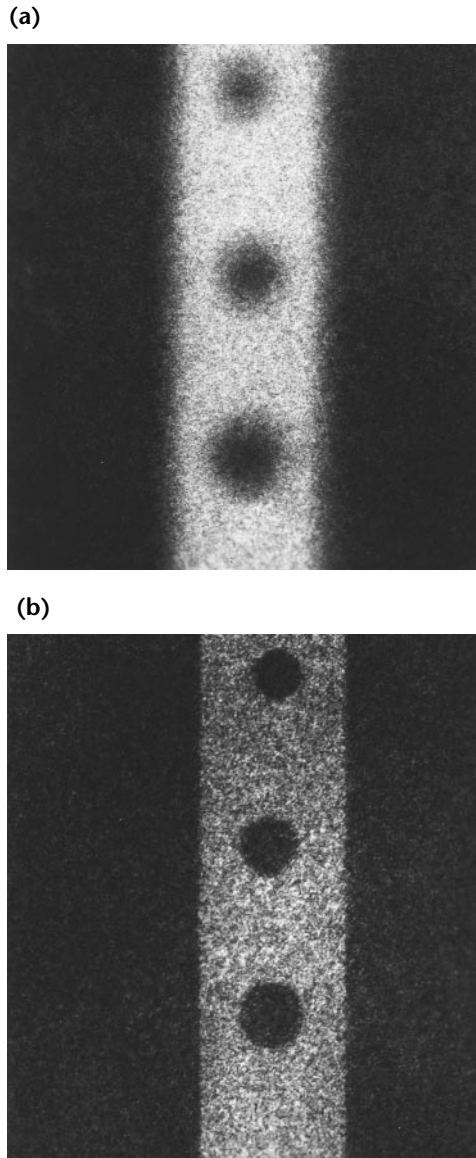
Subject contrast decreases as the kilovoltage is increased. The decreasing slope (steepness) of the lines of the exposure chart (Fig. 30) as kilovoltage increases illustrates the reduction of subject contrast as the radiation becomes more penetrating. For example, consider a steel part containing two thicknesses, 19 and 25 mm (0.75 and 1 in.), which is radiographed first at 160 kV and then at 200 kV.

In Table 7, column 3 shows the exposure in milliamperere minutes required to reach a density of 1.5 through each thickness at each kilovoltage. These data are from the exposure chart in Fig. 30. It is apparent that the milliamperere minutes required to produce a given density at any

TABLE 6. Factors controlling radiographic sensitivity.

Radiographic Contrast		Radiographic Definition	
Subject Contrast Affected by	Film Contrast Affected by	Geometrical Factors Affected by	Graininess Factors Affected by
Specimen thickness variations	Type of film	Focal spot size	Type of film
Radiation quality	Development time, temperature and agitation	Distance from focal point to film	Type of screen
Scattered radiation	Density	Distance from specimen to film	Radiation quality
	Activity of the developer	Abrupt specimen thickness variations	Development
		Contact of screen to film	

**FIGURE 36.** Radiographic definition: (a) advantage of higher contrast is offset by poor definition; (b) despite lower contrast better rendition of detail is obtained by improved definition.



kilovoltage are inversely proportional to the corresponding X-ray intensities passing through the different sections of the specimen. Column 4 gives these relative intensities for each kilovoltage. Column 5 gives the ratio of these intensities for each kilovoltage.

Column 5 shows that, at 160 kV, the intensity of the X-rays passing through the 19 mm (0.75 in.) section is 3.8 times greater than that passing through the 25 mm (1 in.) section. At 200 kV, the radiation through the thinner portion is only 2.5 times that through the thicker. Thus, as the kilovoltage increases, the ratio of X-ray transmission of the two thicknesses decreases, indicating a lower subject contrast.

## Film Contrast

The dependence of film contrast on density must be kept in mind when considering problems of radiographic sensitivity. In general, the contrast of radiographic films, except those designed for use with fluorescent screens, increases continuously with density in the usable density range. Therefore, for films that exhibit this continuous increase in contrast, the best density to use is the highest that can be conveniently viewed with the illuminators available. Adjustable high intensity illuminators are commercially available and greatly increase the maximum density that can be viewed.

High densities have the further advantage of increasing the range of radiation intensities that can be usefully recorded on a single film. In X-radiography, this in turn permits use of the lower kilovoltage, resulting in increased subject contrast and radiographic sensitivity.

The slope of screen film contrast becomes steep at densities greater than 2.0. Therefore, other things being equal, the greatest radiographic sensitivity will be obtained when the exposure is adjusted to give this density.

**TABLE 7.** Exposure of steel part containing two thicknesses.

Voltage (kV)	Thickness mm (in.)	Exposure to Give $D = 1.5$ (mA-min)	Relative Intensity	Ratio of Intensities
160	20 (0.75)	18.5	3.8	3.8
	25 (1.0)	70.0	1.0	
200	20 (0.75)	4.9	14.3	2.5
	25 (1.0)	11.0	5.8	

## Film Graininess and Screen Mottle

The image on an radiographic film is formed by countless minute silver grains, the individual particles being so small that they are visible only under a microscope. However, these small particles are grouped together in relatively large masses visible to the naked eye or with a magnification of only a few diameters. These masses result in a visual impression called *graininess*.



All films exhibit graininess to a greater or lesser degree. In general, the slower films have lower graininess. Thus, film Y (Fig. 33) would have a lower graininess than film X.

The graininess of all films increases as the radiation energy increases, although the rate of increase may be different for different films. The graininess of the images produced at high kilovoltages makes the slow, inherently fine grain films especially useful in the megavolt and multimegavolt range. When sufficient exposure can be given, fine grain films are also useful with gamma rays.

Lead screens have no significant effect on film graininess. However, graininess is affected by processing conditions, being directly related to the degree of development. For instance, if development time is increased for the purpose of increasing film speed, the graininess of the resulting image is likewise increased and vice versa. However, adjustments in development technique made to compensate for changes in temperature or activity of a developer will have little effect on graininess, because they are made to achieve the same degree of development as would be obtained in the fresh developer at a standard processing temperature.

Another source of irregular density in uniformly exposed areas is the screen mottle encountered in radiography with fluorescent screens. The screen mottle increases markedly as hardness of the radiation increases. This mottle limits the use of fluorescent screens at high voltage and with gamma rays. Yet another source of mottle occurs when some films are exposed to megavolt radiation. This is most noticeable in radiography of materials of uniform thickness.

## Image Quality Indicators

A standard test piece is usually included in every radiograph as a check on the adequacy of the radiographic method. The test piece is commonly referred to as a *penetrameter* or an *image quality indicator* (IQI). The image quality indicator is a simple geometric form made of the same material as, or a material similar to, the specimen being radiographed. It contains some small structures (holes, wires and others), the dimensions of which bear some numerical relation to the thickness of the part being tested. The image of the image quality indicator on the radiograph is permanent evidence that the radiographic examination was conducted under proper conditions.

Codes or agreements between customer and vendor may specify the type of image

quality indicator, its dimensions and how it is to be employed. Even if image quality indicators are not specified, their use is advisable because they provide an effective check on the quality of the radiographic inspection and evidence that radiographic sensitivity is achieved.

## Hole Image Quality Indicators

A common image quality indicator in the United States consists of a small rectangular piece of metal, containing several (usually three) holes, the diameter of which are related to the thickness of the image quality indicator (Fig. 37).

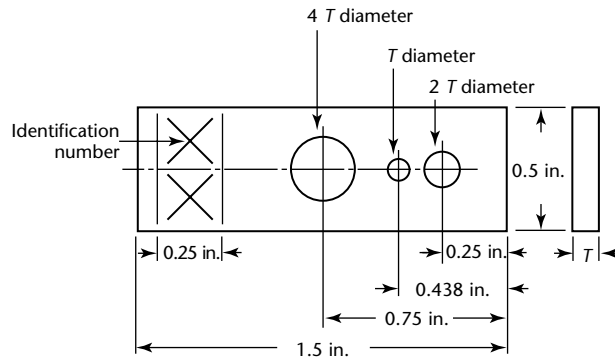
The ASTM International plaque type image quality indicator<sup>4</sup> contains three holes of diameters  $T$ ,  $2T$ , and  $4T$ , where  $T$  is the thickness of the image quality indicator. Because of the practical difficulties in drilling tiny holes in thin materials, the minimum diameters of these three holes are 0.25, 0.50 and 1.00 mm (0.01, 0.02, and 0.04 in.), respectively. Thick image quality indicators of the hole type would be very large because of the diameter of the  $4T$  hole. Therefore, image quality indicators more than 0.46 mm (0.180 in.) thick are in the form of disks, the diameters of which are four times the thickness ( $4T$ ) and which contain only two holes, of diameters  $T$  and  $2T$ . Each image quality indicator is identified by a lead number showing the thickness in thousandths of an inch.

The ASTM International image quality indicator permits the specification of a number of levels of radiographic sensitivity, depending on the requirements of the job. For example, the specifications may call for a radiographic quality level of 2-2T. The first symbol, 2, indicates that the image quality indicator shall be 2 percent of the thickness of the specimen; the second symbol (2T) indicates that the hole having a diameter twice the image quality indicator thickness shall be visible on the finished radiograph. The quality level 2-2T is probably the one most commonly specified for routine radiography. However, critical components may require more rigid standards and require a level of 1-2T or 1-1T. On the other hand, the radiography of less critical specimens may be satisfactory if a quality level of 2-4T or 4-4T is achieved. The more critical the radiographic examination — that is, the *higher* the level of radiographic sensitivity required — the *lower* the numerical designation for the quality level.

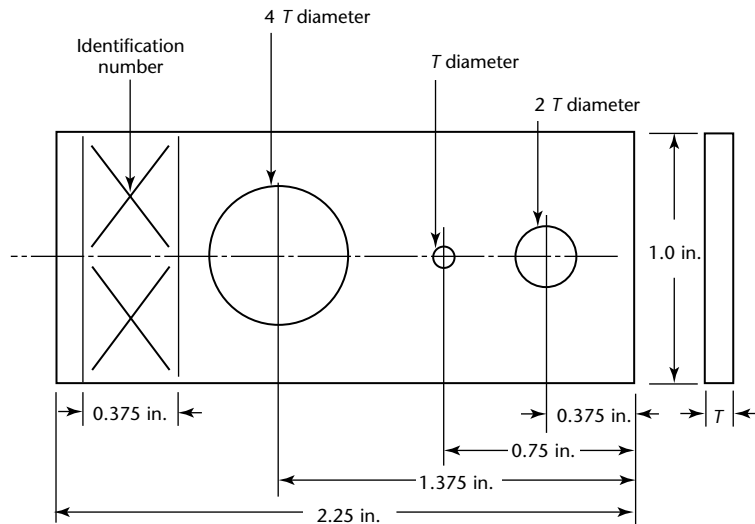
Another ASTM International image quality indicator design required by some specifications is the wire type that consists of sets of wires arranged in order of increasing diameter (Fig. 38).

**FIGURE 37.** Image quality indicator of ASTM International, according to ASTM Standard E 1025: (a) design for image quality indicator type numbers 5 to 20, with tolerances of  $\pm 0.0005$ ; (b) design for image quality indicator type numbers 21 to 59 with tolerances of  $\pm 0.0025$  in. and for image quality indicator type numbers 60 to 179, with tolerance of  $\pm 0.005$  in.; (c) design for image quality indicator type numbers over 180, with tolerances of  $\pm 0.010$  in. (Except for relative thickness  $T$ , all measurements in these diagrams are in inches; 1.00 in. = 25.4 mm.)

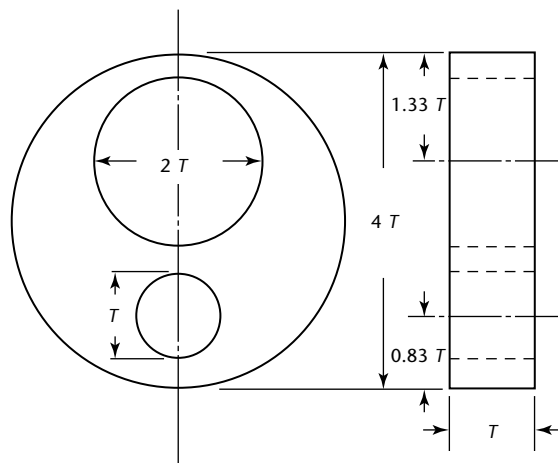
(a)



(b)



(c)



All sections of the *ASME Boiler and Pressure Vessel Code* require an image quality indicator identical to the ASTM plaque or wire type image quality indicator.<sup>5</sup>

### Equivalent Image Quality Indicator Sensitivity

Ideally, the image quality indicator should be made of the same material as the specimen. However, this is sometimes impossible because of practical or economic difficulties. In such cases, the image quality indicator may be made of a radiographically similar material — that is, a material having the same radiographic absorption as the specimen but which is better suited to the making of image quality indicators. Tables of radiographically equivalent materials have been published, grouping materials with similar radiographic absorptions. In addition, an image quality indicator made of a particular material may be used in the radiography of materials having *greater* radiographic absorption. In such a case, there is a certain penalty on radiographic technicians because they are setting more rigid radiographic quality standards for themselves than those which are actually required. This penalty is often outweighed by avoiding the problems of obtaining image quality indicators for an unusual material.

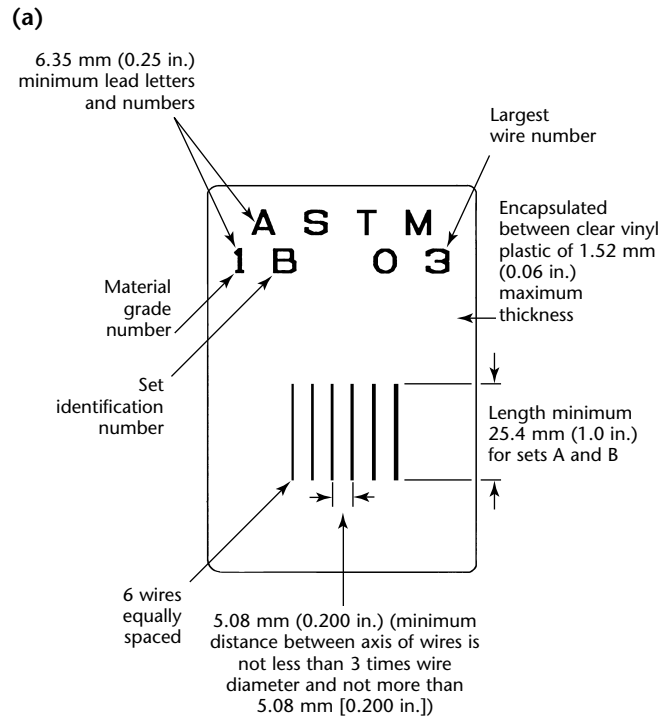
In some cases the materials involved do not appear in published tabulations. Under these circumstances the comparative radiographic absorption of two materials may be determined experimentally. A block of the material under test and a block of the material proposed for image quality indicators, equal in thickness to the part being examined, can be radiographed side by side on the same film with the technique to be used in practice. If the film density under the proposed image quality indicator material is equal to or greater than the film density under the specimen material, that proposed material is suitable for fabrication of image quality indicators.

In practically all cases, the image quality indicator is placed on the source side of the specimen, in the least advantageous geometric position. In some instances, however, this location for the image quality indicator is not feasible. An example would be the radiography of a circumferential weld in a long tubular structure, using a source position within the tube and film on the outer surface. In such a case *film side* image quality indicator must be used. Some codes specify the *film side* image quality indicator that is equivalent to the *source*

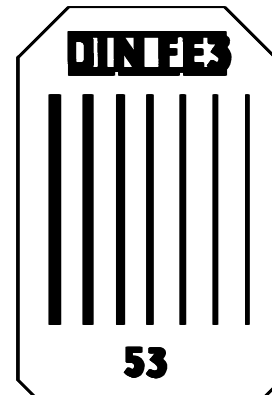
*side* image quality indicator normally required.

When such a specification is not made, the required *film side* image quality indicator may be found experimentally. In the example above, a short section of tube of the same dimensions and materials as the item under test would be used in the experiment. The required image quality indicator would be placed on the *source side* and a range of image quality indicators on the *film side*. If the *source side* image quality indicator indicated that the required radiographic sensitivity was being achieved, the image of the smallest

**FIGURE 38.** Examples of wire type image quality indicators: (a) ASTM Standard E 747 (set B, Alternate 2); (b) Deutsche Industrie Norm 54109, German standard image quality indicator.



(b)



visible hole or wire size in the *film side* image quality indicators would be used to determine the image quality indicator and the hole or wire size to be used on the production radiographs.

Although the *smallest visible hole* criterion is the best one in most cases for plaque image quality indicators, in some cases the best criterion is the *smallest visible hole in the thinnest image quality indicator*. In rare cases neither of these rules of thumb is correct. Therefore, for critical applications, the best criterion for equivalent sensitivity should be determined by calculations based on the visible features of the film side image quality indicators and using the equations given in the appendix to ASTM E 1025.<sup>4</sup>

Sometimes the shape of the part being examined precludes placing the image quality indicator on the part. When this occurs, the image quality indicator may be placed on a block of radiographically similar material of the same thickness as the specimen. The block and the image quality indicator should be placed as close as possible to the specimen.

### Wire Image Quality Indicators

A number of wire image quality indicator designs are in use. The ASTM E 747 image quality indicator<sup>6</sup> and the European wire image quality indicator<sup>7,8</sup> (Fig. 38) are widely used. These consist of a number of wires of various diameters sealed in a plastic envelope that carries the necessary identification symbols. The image quality is indicated by the thinnest wire visible on the radiograph. The system is such that only three image quality indicators, each containing seven wires, can cover a very wide range of specimen thicknesses. Sets of Deutsche Industrie Norm image quality indicators are available in aluminum, copper and steel whereas ASTM image quality indicators are available in three light metal and five heavy metal groups.

### Comparison of Image Quality Indicator Designs

The hole type image quality indicator is, in a sense, a *go/no-go* gage; that is, it indicates whether or not a specified quality level has been attained but, in most cases, does not indicate whether requirements have been exceeded or by how much. The wire image quality indicator on the other hand is a series of image quality indicators in a single unit. As such, they have the advantage that the radiographic quality level achieved can often be read directly from the processed radiograph.

The hole image quality indicator can be made of any material that can be formed into thin sheets and drilled but

the wire image quality indicator is only made from materials that can be formed into wires. A quality level of 2-2T may be specified for the radiography of, for example, commercially pure aluminum and 2024 aluminum alloy, even though these have appreciably different compositions and radiation absorptions. The hole image quality indicator would, in each case, be made of the appropriate material. To achieve the same quality of radiographic inspection for equal thicknesses of these two materials, it would be necessary to specify different wire diameters — that for 2024 alloy would probably have to be determined by experiment.

### Special Image Quality Indicators

Special image quality indicators have been designed for certain classes of radiographic testing. An example is the radiography of electronic components in which some of the significant factors are the continuity of fine wires or the presence of tiny balls of solder. Special image quality indicators have been designed consisting of fine wires and small metallic spheres within a plastic block.<sup>9</sup>

The block is covered on top and bottom with steel about as thick as the case of the electronic component.

### Image Quality Indicators and Visibility of Discontinuities

It should be remembered that even if a certain hole in an image quality indicator is visible on the radiograph, a cavity of the same diameter and thickness may not be visible. The image quality indicator holes, having sharp boundaries, result in abrupt, though small, changes in metal thickness whereas a natural cavity having more or less rounded sides causes a gradual change. Therefore, the image of the image quality indicator hole is sharper and more easily seen in the radiograph than is the image of the cavity.

Similarly, a fine crack may be of considerable extent but if the X-rays or gamma rays pass from source to film in a direction other than parallel to the plane of the crack, its image on the film may not be visible because of the very gradual or small transition in photographic density. Thus, an image quality indicator is used to indicate the quality of the radiographic method and not to measure the size of flaw which can be shown.

In the case of a wire image quality indicator, the visibility of a wire of a certain diameter does not ensure that a discontinuity of the same cross section will be visible. The human eye perceives much more readily a long boundary than

it does a short one, even if the density difference and the sharpness of the image are the same. However, the equivalency between the hole and wire ASTM International image quality indicators was developed on the basis of empirical data as well as theoretical numbers.

---

## Viewing and Interpreting Radiographs

[The viewing of the finished radiograph is discussed elsewhere in this volume.](#)

## PART 6. Film Handling and Storage

### Film Handling

Radiographic film should always be handled carefully to avoid physical strains, such as pressure, creasing, buckling, friction and others. The normal pressure applied in a cassette to provide good contacts is not enough to damage the film. However, when films are loaded in semiflexible holders and external clamping devices are used, care should be taken to ensure that this pressure is uniform. If a film holder bears against a few high spots, such as those that occur on an unground weld, the pressure may be great enough to produce desensitized areas in the radiograph. Precaution is particularly important when using envelope packed films.

Crimp marks or marks resulting from contact with fingers that are moist or contaminated with processing chemicals can be avoided if large films are grasped by the edges and allowed to hang free. A convenient supply of clean towels is an incentive to dry the hands often and well. Envelope packed films avoid these problems until the envelope is opened for processing. Thereafter, of course, the usual care must be taken.

Another important precaution is to avoid withdrawing film rapidly from cartons, exposure holders or cassettes. Such care will materially help to eliminate objectionable circular or treelike black markings in the radiograph, the results of static electric discharges.

The interleaving paper must be removed before the film is loaded between either lead or fluorescent screens. When using exposure holders without screens, the paper should be left on the film for the added protection that it provides. At high voltage, direct exposure techniques are subject to the problems mentioned earlier: electrons emitted by the lead backing of the cassette or exposure holder may reach the film through the intervening paper or felt and record an image of this material on the film. This effect is magnified by lead or fluorescent screens. In the radiography of light metals, direct exposure techniques are the rule and the paper folder should be left on the interleaved film when loading it in the exposure holder.

Ends of a length of roll film factory packed in a paper sleeve should be sealed

in the darkroom with black pressure sensitive tape. The tape should extend beyond the edges of the strip 7 to 13 mm (0.25 to 0.5 in.) to provide a positive light tight seal.

### Identifying Radiographs

Because of their high absorption, lead numbers or letters affixed to the film holder or test object furnish a simple means of identifying radiographs. They may also be used as reference marks to determine the location of discontinuities within the specimen. Such markers can be conveniently fastened to the film holder or object with adhesive tape. A code can be devised to minimize the amount of lettering needed. Lead letters are commercially available in a variety of sizes and styles. The thickness of the chosen letters should be great enough so that their image is clearly visible on exposures with the most penetrating radiation routinely used. Under some circumstances it may be necessary to put the lead letters on a radiation absorbing block so that their image will not be *burned out*. The block should be considerably larger than the legend itself.

Flash box identification should be included where a corner of a radiograph is blocked with lead to minimize exposure. The unexposed corner is flashed with light transmitted through typed or hand written information exposed onto the film.

### Shipping of Unprocessed Films

If unprocessed film is to be shipped, the package should be carefully and conspicuously labeled, indicating the contents, so that the package may be segregated from any radioactive materials, high heat or pressure. It should further be noted that customs inspection of shipments crossing international boundaries sometimes includes fluoroscopic inspection. To avoid damage from this cause, packages, personnel baggage and the like containing unprocessed film should be plainly marked and the attention of inspectors drawn to their sensitive contents.



## Storage of Unprocessed Film

### X-Ray Film Storage

With X-rays generated up to 200 kV, it is feasible to use storage compartments lined with a sufficient thickness of lead to protect the film. At higher kilovoltages, protection becomes increasingly difficult; film should be protected not only by the radiation barrier for protection of personnel but also by increased distance from the source.

At 100 kV, a 3 mm (0.125 in.) thickness of lead should normally be adequate to protect film stored in a room adjacent to the X-ray room if the film is not in the line of the direct beam. At 200 kV, the lead thickness should be increased to 6.4 mm (0.25 in.).

With megavolt X-rays, films should be stored beyond the concrete or other protective wall at a distance at least five times farther from the X-ray tube than the area occupied by personnel. The storage period should not exceed the times recommended by the manufacturer.

These rules of thumb may be ignored if suitable radiation surveys indicate radiation levels low enough to avoid fogging during the maximum time period that the film will be stored.

### Storage near Gamma Rays

When radioactive material is not in use, the shielding container in which it is stored helps provide protection for film. In many cases, however, the container for a gamma ray source will not provide satisfactory protection to stored radiographic film. In such cases, the emitter and stored film should be separated by a sufficient distance to prevent fogging.

### Heat, Humidity and Fumes

The effects of heat, humidity and fumes on stored film are discussed elsewhere.<sup>2</sup>

## Storage of Exposed and Processed Film

*Archival storage* is a term commonly used to describe the keeping quality of radiographic film. It has been defined by the American National Standards Institute (ANSI) as *those storage conditions suitable for the preservation of photographic film having permanent value*. The American National Standards Institute does not define archival storage *in years* but in terms of the thiosulfate content (residual

fixer) permissible for storage of radiographs.

Although many factors affect the storage life of radiographs, one of the most important is the residual thiosulfate left in the radiograph after processing and drying. Determined by the methylene blue test, the maximum level is  $2 \text{ mg}\cdot\text{cm}^{-2}$  on each side of coarse grain radiographic films. For short term storage requirements, the residual thiosulfate content can be at a higher level but this level is not specified by the American National Standards Institute.

Washing of the film after development and fixing, therefore, is very important. The methylene blue test and silver densitometric test are laboratory procedures performed on clear areas of the processed film.

Temperature and humidity should be carefully controlled. Radiographic film should be stored with precautions specified in ASTM E 1254.<sup>10</sup>

### Storage Suggestions

Regardless of the length of time a radiograph is to be kept, these suggestions should be followed to provide for maximum stability of the radiographic image.

1. Avoid storage in the presence of chemical fumes.
2. Avoid short term cycling of temperature and humidity.
3. Place each radiograph in its own folder to prevent possible chemical contamination by the glue used in making the storage envelope (negative preserver). Several radiographs may be stored in a single storage envelope if each is in its own interleaving folder.
4. Never store unprotected radiographs in bright light or sunlight.
5. Avoid pressure damage caused by stacking a large number of radiographs horizontally in a single pile or by forcing more radiographs than can comfortably fit into a single file drawer or shelf.

Radiographic film offers a means of precise discontinuity detection and documentation. Despite the introduction of digital means of image capture, display and storage, film radiography will continue to be an important part of nondestructive testing well into the twenty first century.

## Microfilm

Radiographic film images can be copied to microfilm and microfiche for storage. A microfiche the size of a postcard can store more than a hundred radiographic

images. Like film negatives, microfilm and microfiche require climate control to prevent degradation of the medium when stored for years.

In the twenty-first century, microfilming services offer image digitization and will provide the images on compact disks or digital video disks. Film digitization is discussed below.

## PART 7. Film Digitization

Film digitization is the conversion of existing radiographic film images to a digital format for electronic image analysis, management, transmission and storage. Film digitization also permits disposal of film that would degrade over time.

In film digitization, film densities are converted into digital values by measuring light transmitted through the film and assigning each measurement a digital value and a particular location. Three primary parameters affect the resulting image quality of film digitization: density range, density resolution and spatial resolution (pixel size).

Optical density (OD) is a logarithmic function. This means that at optical density 0, 100 percent of the incident photons are transmitted through the film; at 1.0 optical density, only 10 percent make it through; at 2.0 optical density, only 1 percent; and at 3.0 optical density, only 0.1 percent. It is difficult to measure higher densities with the same accuracy and precision as lower densities.

There are two basic methods of digitizing film. The first method makes the measurement using a diffuse light source and a charge coupled device (CCD) whereas the second uses a combination of a laser and a photomultiplier tube (PMT).<sup>11,12</sup>

### Charge Coupled Device Film Digitization Systems

A charge coupled device film digitizer illuminates the full width of the film with a diffuse light source and then uses a lens system to focus the light down to the size of the charge coupled device elements. The charge coupled device is a silicon semiconductor device consisting of a large number of gridlike elements sensitive to light. When light energy impinges on the charge coupled device elements, the photons generate a charge within each element. Periodically, the element is discharged and the amplitude of the charge is measured. In this way, light amplitude can be converted to a proportionate electrical signal related to the density at any given point.

In film digitization systems, a linear array of charge coupled device elements is used with optics to focus the film image

onto the much smaller charge coupled element. A narrow line of diffuse light is passed through the film and the transmitted light is focused onto the charge coupled device array, one line at a time. Once one line of data is collected, a second line is then scanned.

The total density range of charge coupled devices can be affected if, when there is a rapid and drastic change in light level, the charge coupled device momentarily becomes saturated. The image may be corrected by changing the sampling time (integration period). At high light levels, the integration period is reduced to avoid saturation of the charge coupled device whereas at low light levels, the integration period is increased to achieve an adequate ratio of signal to noise. To obtain optical density dynamic ranges up to five, multiple scans may be performed at varying charge coupled device integration periods and scan speeds.

The density resolution of charge coupled device digitizers is determined by the conversion of the logarithmic density scale to a linear voltage scale. For example, at an optical density of zero, maximum light passes through the film, so the charge coupled device element produces the maximum voltage. Because optical density is a logarithmic function, only 10 percent of the light transmitted at an optical density of 0 will be detected at an optical density of 1. If the charge coupled device's maximum voltage is calibrated to be 10 V, then the voltage output at an optical density of 1 is 1.0 V, at 2 it is 0.1 V, at 3 it is 0.01 V and at 4 it is 0.001 V. Therefore, if the charge coupled device output of 10 V is digitized at 12 bits or 4096 density levels, then an optical density from 0 to 1 will produce an output of 9 V, which equates to 3686 density levels (90 percent of 4096). The output of densities from 1 to 2 will equate to 369 levels; densities from 2 to 3, to 37 levels; and densities from 3 to 4, 4 levels. While this results in a nonlinear density resolution, it is similar to the original image and as a result is adequate for many purposes. It is important that the application and image analysis requirements are thoroughly understood before a particular digitizer is used.

Another aspect of charge coupled devices is spatial resolution. The elements

can be arrayed along one or two dimensions. The array's resolution is sometimes given as the element size because all charge coupled device chips have a large number of elements (for example, 4000 or 6000) that in theory can be digitized into a like number of pixels. For example, the 1 cm<sup>2</sup> chip in a video camera is said to have a resolution of about 20  $\mu$ m. Once the various focusing lens aberrations are coupled together, the true resolving capability of the charge coupled device chip is low. A home video camera is surely not able to discern objects 20  $\mu$ m apart.

Therefore, it is important to differentiate between the chip specifications versus those of the imaging system. The resolution of the imaging system depends in part on the quality of the focusing optics and in part on the cross talk between charge coupled elements (as when one photon activates more than one element).

---

## Laser Film Digitization Systems

Laser scanners use a nonimaging photomultiplier tube to detect light transmitted through the film. The laser beam is a focused beam of coherent light of known value and is transmitted through the film at one discreet point. The transmitted light is then detected by the photomultiplier tube and digitized into a value directly proportional to the density of the film at that point.

The photomultiplier tube has a wide dynamic range, a good ratio of signal to noise and uses a log amplification process such that a uniform density resolution is maintained over the entire range. The log amplifier normalizes the extremely high number of photons detected at low optical densities versus the relatively low number of photons detected at high optical densities. For example, if a laser film digitizer converts each optical density measurement into a pixel value 1000 $\times$  the optical density at that point, then there are 1000 levels from 0 to 1 optical density, from 1 to 2 optical density, from 2 to 3 optical density, and so on. This would provide a density resolution of 0.001 optical density at all levels.

The spatial resolution of a laser scanner is determined by the point of laser light that impinges on the film. Because there is only a single beam, there is no cross talk between pixels and a true limiting resolution equal to the laser spot size can be achieved. Typical laser spot sizes are 100  $\mu$ m (0.004 in.) and 50  $\mu$ m (0.002 in.). However, the actual resolution will

depend on overall laser beam quality, detector noise and electronic noise.

It is important that the application and image analysis requirements of a particular digitizer are thoroughly understood before it is used. There are several ways to determine experimentally the performance of a film digitizer. One method is to scan a modulation transfer function (MTF) pattern to validate performance. Another, simpler method, is to place a strip of cellophane tape over the image of a step wedge. This translucent tape will produce a density difference of about 0.03 optical density. The idea here is to demonstrate (1) the dynamic range of the system (when the steps begin to be difficult to differentiate) and (2) the density resolution (at what density the tape can no longer be seen).

---

## Other Considerations

Beyond the technical issues of the scanning scheme, other issues are related to image size relative to the display and storage medium. All the information may be captured in memory, but both the processor size and monitor size limit what can be worked with or displayed.

For example, let us assume that each pixel contains 12 bits of grayscale information plus 4 bits of header information. This equates to 16 bits or 2 bytes. The image size then, is the total number of pixels times two bytes. If the scan resolution is 100  $\mu$ m (0.004 in.), then a 14  $\times$  17 in. image would contain 3500 pixels (14 in.  $\div$  0.004 in.)  $\times$  4300 pixels (17 in.  $\div$  0.004 in.) or a total of about  $1.5 \times 10^7$  pixels. Having 2 bytes of information per pixel results in an image size of 30 megabytes. If the scan resolution were increased to 50  $\mu$ m (0.002 in.), then the image size would increase by 4 $\times$  to 120 megabytes.

Some monitors may not be able to display the entire image. For example, cathode ray tubes may have display resolutions of 1200  $\times$  1600 or 2000  $\times$  2500. Therefore, it is important to remember that, depending on the magnification of the image on the monitor, there may actually be more raw data available than are displayed. To display an image that has either more or fewer data displayed than are in the raw image, pixel mapping techniques are used. Pixel replication or pixel interpolation are used when magnifying beyond the image resolution. When reducing the image size, pixel averaging is used.


Digital images may contain 12-bit (or more) digital data that must be displayed on a monitor that only displays 8 bits (about what the human eye can discern).

A method must then be employed to map the original 4096 gray scale levels of data onto the available 256 display levels. This is commonly done either (1) by selecting which 256 levels of the original 4096 are displayed or (2) by equally dividing the 4096 levels over the available 256.

## References

1. Quinn, R.A. and C.C. Sigl, eds. *Radiography in Modern Industry*, fourth edition. Rochester, NY: Eastman Kodak Company (1980).
2. *Nondestructive Testing Handbook*, second edition: Vol. 3, *Radiography and Radiation Testing*. Columbus, OH: American Society for Nondestructive Testing (1985).
3. *Nondestructive Testing Handbook*, second edition: Vol. 10, *Nondestructive Testing Overview*. Columbus, OH: American Society for Nondestructive Testing (1996).
4. ASTM E 1025, *Standard Practice for Design, Manufacture, and Material Grouping Classification of Hole-Type Image Quality Indicators (IQI) Used for Radiology*. Philadelphia, PA: American Society for Testing and Materials.
5. ASME Boiler and Pressure Vessel Code. New York, NY: American Society of Mechanical Engineers.
6. ASTM E 747, *Standard Practice for Design, Manufacture and Material Grouping Classification of Wire Image Quality Indicators (IQI) Used for Radiology*. West Conshohocken, PA: ASTM International.
7. DIN 54109. *Non-Destructive Testing; Image Quality of Radiographs; Recommended Practice for Determining Image Quality Values and Image Quality Classes*. Berlin, Germany: Deutsche Institut für Normung [German Institute for Standardization] (1989). Superseded by EN 462 (DIN).
8. EN 462 P1 (DIN), *Non-Destructive Testing — Image Quality of Radiographs — Image Quality Indicators (Wire Type) and Determination of Image Quality Value*. Brussels, Belgium: European Committee for Standardization (1994).
9. ASTM E 801, *Standard Practice for Controlling Quality of Radiological Examination of Electronic Devices*. West Conshohocken, PA: ASTM International (2001).
10. ASTM E 1254, *Standard Guide for Storage of Radiographs and Unexposed Radiographic Film*. West Conshohocken, PA: ASTM International (1998).
11. "CCD Versus Laser Film Digitization Systems." Liberty Technologies, Incorporated, Imaging Systems Division.
12. Soltani, P.K., C.R. Chittick, T. Chuang, M.J. Dowling, G.R. Kahley and T.E. Kinsella. "Advances in 2D Radiography for Industrial Inspection." Presented at the *International Conference on Quality Control by Artificial Vision*. Le Creusot, France: Institut Universitaire de Technologie (May 1997).





# 8

## C H A P T E R

# Radiographic Interpretation

---

Charles J. Hellier III, Hellier and Associates, Niantic,  
Connecticut

George C. Wheeler, Materials and Processes  
Consultants, Schenectady, New York

# PART 1. Fundamentals of Radiographic Interpretation

Radiographic interpretation is the art of extracting the maximum pertinent information from a radiographic image. This requires subjective judgment by the interpreter and is influenced by the interpreter's knowledge of (1) the characteristics of the radiation source and its energy levels with respect to the material being examined; (2) the characteristics of the recording media in response to the selected radiation source and its energy levels; (3) the processing of the recording media with respect to resultant image quality; (4) the object being radiographed; (5) the possible and most probable types of discontinuities that may occur in the test object; and (6) the possible variations of the discontinuities' images as affected by radiographic technique and other factors.

Accurate interpretation is strongly influenced, not only by the viewing conditions and by the interpreter's vision acuity, but also by the interpreter's knowledge and experience. Therefore, training of the interpreter is essential to the reliability of the results of the interpretation. Because the experience and knowledge of interpreters vary widely, training is also an essential factor in improving the agreement level between interpreters.

In a program conducted by a research laboratory,<sup>1,2</sup> a comparison was made among five certified film interpreters who were trained by a master apprentice program. These five certified film interpreters reviewed 350 radiographs and reached agreement on 238 radiographs or disagreed 32 percent of the time.

The results of this research were then incorporated into a unified training program, using discontinuity categories from the welding process. Subsequently, a procedure was developed wherein nine certified film interpreters trained under the unified training program were compared to nine certified film interpreters trained under the master apprentice program. Using 96 radiographs, the master apprentice group disagreed 44 percent of the time; the unified training group disagreed only 17 percent of the time.

In a similar study of medical radiology,<sup>3</sup> the reproducibility of a tuberculosis diagnosis was examined. This study revealed an average disagreement in

one out of three cases or 67 percent agreement. On a second independent reading of the same radiographs, a physician would disagree with his or her own previous diagnosis in an average of one out of five cases or 80 percent agreement.

Under the best circumstances of training and experience, qualified film interpreters may disagree. Therefore, in all applications where quality of the final product is critical for safety or reliability, a minimum of two qualified interpreters should evaluate and pass judgment on the radiographs.

Reference radiographs are a valuable training and interpretation aid. An in-house library of radiographs and accompanying photographs of macrosections of various discontinuities are also recommended.

## Steps of Radiographic Testing

The five essential steps of radiographic nondestructive testing are the following:

- (1) supplying a suitable form and distribution of radiation from an external source to the object being tested;
- (2) modification of the radiation distribution within the test object as a result of the variations in radiation absorption within the object caused by discontinuities or differences in material properties that correlate with serviceability of the object;
- (3) detection of these changes in radiation distribution by a sensitive detector such as photosensitive film or paper or an electronic system;
- (4) recording this radiation distribution in a form, such as a radiographic image, suitable for interpretation; and
- (5) interpretation of the image to comply with applicable codes and standards or to provide other information sought about the object.

## Specifying Nondestructive Tests<sup>4-6</sup>

Nondestructive tests must be designed and specified for validity and reliability in each individual application. The tests are specific to the problem; no nondestructive

test is applicable to every kind of material, part, structure, function, or operating condition. Instead, each nondestructive test must be based on a thorough understanding of (1) the nature and function of the part being tested, (2) workmanship standards during manufacturing and fabrication, and (3) the conditions of the part's service.

These fundamentals are part of the basic experience and knowledge that a radiographic interpreter must possess. Specific radiographic procedures must be prepared and adhered to in both the production and the interpretation of the resultant radiographic image. These procedures should be based on applicable specifications, codes and standards and the interpreter must be thoroughly familiar with their requirements to properly assess the image and product quality.

## Interpretation of Radiographic Images

The basic steps in interpretation of images produced by radiography, whether film, paper or electronic images, are the following.

1. Ensure by appropriate tests that the interpreter has adequate vision acuity under proper viewing conditions.
2. Establish proper viewing conditions to ensure that the interpreter can use that vision acuity in interpreting the images.
3. Assess the quality of the radiographic images that are to be interpreted, including presence of required identification information, freedom from artifacts that might mask discontinuities, display of the required penetrameter (image quality indicator) quality level and display of the correct station/location markers.
4. Assess the quality of the object being tested in the areas of interest. This is the step that requires the greatest training, experience and knowledge, particularly in understanding of the radiographic process and its effects on the radiographic image.

Some aids useful in detection and identification of discontinuities include the following.

1. Slowly moving the radiograph back and forth often helps in detecting small or low contrast details, because the eye is sensitive to moving objects.
2. Tilting the film or changing the viewing angle will also improve the apparent contrast of low contrast details. This may aid in differentiating film artifacts from discontinuity images.

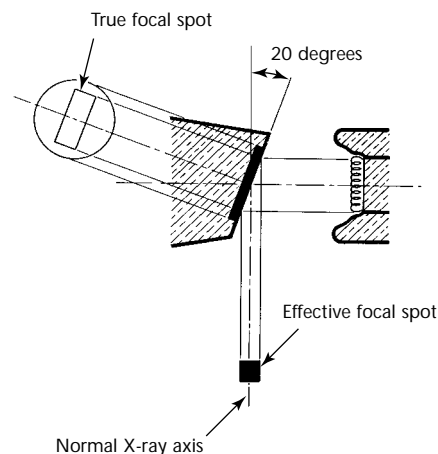
3. Limiting the area being viewed may improve detection of fine details.
4. Use a good 2× or 3× magnifying glass to assess some indications.
5. Use a transparent scale or ruler to measure indications may be useful in differentiating acceptable from rejectable indications.
6. Visually examine the test object, if possible, whenever there is any question as to whether an indication represents a surface condition.
7. When evaluation of an image or detail is uncertain, radiograph the area again, if possible, for verification. Change the exposure geometry if a discontinuity may be unfavorably oriented or is near the edge of the film (Figs. 1 and 2) except for *transmitted beam* radiographs.
8. When the depth of a discontinuity (within the thickness of the object) is important use triangulation exposures to determine its depth.

## Standards, Codes and Specifications

All radiography (except research and development) should be performed in accordance with written procedures developed from applicable standards, codes or specifications, as required by contractual agreement. This means that the radiographic interpreter must have both a working knowledge of and ready access to pertinent documents to verify the technique and quality level requirements of (1) the radiography and (2) the product.

However, radiographic personnel should understand that specified quality

FIGURE 1. Schematic diagram of effective (or projected) focal spot of X-ray tube.



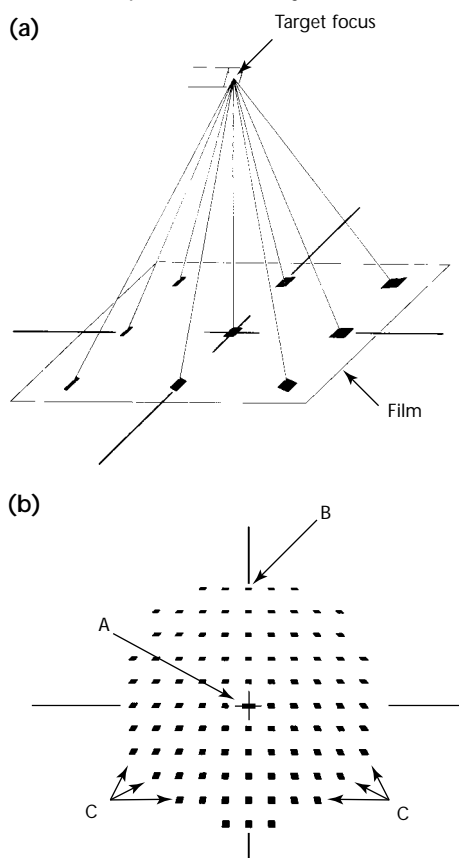
levels may vary depending on the specifications in effect and that radiographic quality levels are considered minimum requirements that may be exceeded.

Product quality levels should be based on the service (use) of the component being examined, even though this is not always addressed in the governing code or specification. Ideally, the product quality level should be established by appropriate engineering personnel in conjunction with the radiographic specialist, thus providing the maximum degree of inspectability and ensuring that the most critical discontinuities can be detected.

Carlton H. Hastings succinctly defined *material* as a "collection of defects, with acceptable material being a [fortunate] arrangement of defects and rejectable material being an unfortunate arrangement of defects."<sup>7</sup> The message is

clear: regardless of the radiographic technique used, there can never be the assurance of a component totally free of discontinuities. Hence, a thorough understanding of radiography's limitations is essential for choosing the optimum techniques to achieve the desired radiographic quality level.

FIGURE 2. Diagram showing change of shape and size of projected X-ray focal spot as function of position in X-ray field.



#### Legend

- A. Nominal center film, directly in line with orthogonal projection from X-ray tube window, may give average sized focal spot projection.
- B. Optimum focal spot projection in this example.
- C. Poor projection

## PART 2. Viewing in Radiographic Testing

### Vision Acuity and Perception

Vision acuity as it applies to radiography requires both the observation of fine detail and the detection of small differences in brightness or contrast. It is significantly affected by environmental, physiological and psychological variables. The major controllable factors are the ambient light level in the viewing area and the light level illuminating the radiographic image, that is, passing through the film, falling on the paper or emitted from a fluorescent or real time display.

The vision acuity of an individual may vary from moment to moment, hour to hour and day to day, as well as over longer time periods, depending on many variables. These include emotions, fatigue, light levels and wavelength of the light, light and dark adaptation of the eyes and the characteristics of the images being sought, that is, their shape, size and contrast.

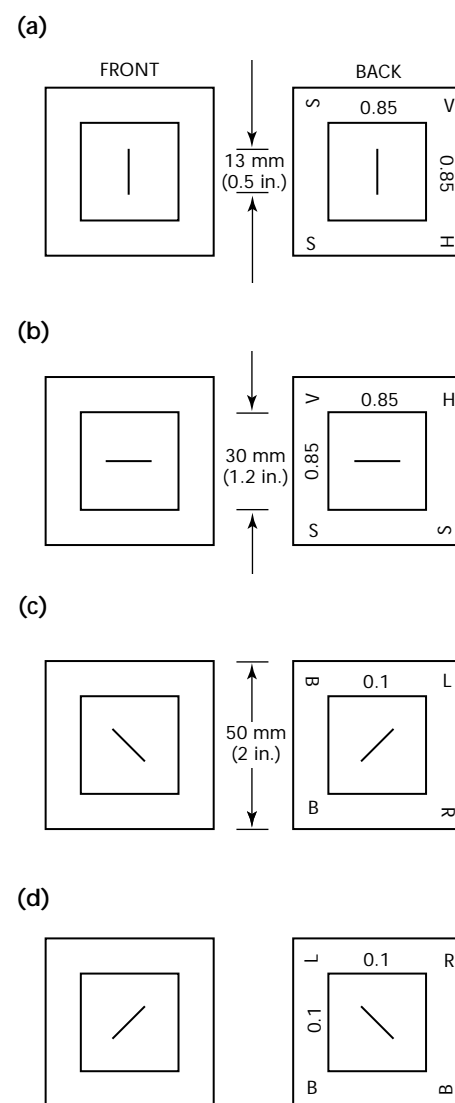
Acuity alone, as usually measured, does not guarantee detection. The eye and the brain together must discriminate patterns from the background. This requires thorough knowledge of the target patterns and how they may vary as a function of radiographic exposure technique variables. Discrimination also depends on the scanning technique, which includes, as in ultrasonic testing, the pattern, coverage and speed of scanning.

Annual vision examinations cannot account for all of these variables. They establish only the ability, at the time of the examination, to detect known targets with simple shapes (letters, numbers and others) that *usually have high contrast relative to their background*. This suggests that, for highly critical work, more frequent examinations with more variables should be used or that multiple interpreters should be used for such work.

The vision test described below was developed using microdensitometer scans of discontinuities taken from actual radiographs.<sup>8</sup> Samples of the acuity test slides are presented in Fig. 3. The optotype (acuity test target) is a thin line darker than the background. Line orientation serves two important functions: (1) it increases the number of

possible responses (two with no orientation, four with orientation) and (2) it includes astigmatic effects. The four orientations are horizontal *H*, vertical *V*, oblique right *R* and oblique left *L*.

FIGURE 3. Examples of reference acuity tests showing line orientations and dimensions: (a) vertical, contrast 0.85, sharp; (b) rotated 90 degrees, horizontal, contrast 0.85, sharp; (c) oblique/left, contrast 0.1, blurred; (d) oblique, rotated 90 degrees, contrast 0.1, blurred.



The recommended parameters for this test are summarized in Table 1. The background luminance (brightness) of the test chart is kept constant at  $85 \pm 5 \text{ cd}\cdot\text{m}^{-2}$  or  $25 \pm 1.5 \text{ ftl}$  (see footnotes to Table 1 for definitions of these units). Three contrast levels and line widths are recommended. The length of the lines is kept constant at 107 min of arc. These angular measures are based on a viewing distance of 400 mm (16 in.). Two levels of line sharpness are included: one with a sharp edge similar to most optotypes used in vision testing and one with a blurred edge like that in many actual radiographs.

These slides are designed for self-testing as well as testing by designated examiners. The front of the slides contain only the optotypes (Fig. 3) with all necessary information given on the reverse side. This procedure assumes that for self-testing the examinee will look at the side giving the correct response (*H*, *V*, *R* or *L*) only after evaluating the target orientation.

## Viewing Conditions and Equipment

Viewing conditions are important for achieving good interpretation and evaluation results. Interpretation and evaluation of radiographic images should be done under conditions that afford maximum visibility of detail together with a maximum of comfort and a minimum of fatigue for the interpreter.

In most cases subdued lighting in the viewing area is preferable to total darkness. However, when relatively broad areas, about 6 mm (0.25 in.) wide or more, of very low contrast and low sharpness, such as shallow, blended depressions or microshrinkage, must be detected or their dimensions measured, it may be desirable or even necessary for the interpreter to practice extended dark adaptation. Adaptation times of as much as 30 to 45 min have sometimes been found necessary to ensure adequate vision to resolve such features.<sup>9,10</sup>

The room lighting must be arranged so that there are no reflections from the surface of the image being interpreted. Adequate table surface must be provided on either side of the viewing device to accommodate film and to provide a writing surface for recording the interpretation. Quick and easy access should be provided to a suitable densitometer; reference radiographs; and applicable codes, standards and specifications. In addition, it is important for the film interpreter to be free of distractions, including telephone and visitors, to maintain concentration.

For radiosopic techniques that require viewing of a computer screen or electronic imaging console, the same general conditions apply but may vary depending on the specific system being used. Direct viewing generally requires dark adaptation: 20 min of dark adaptation is considered good practice. Red light up to 30 times brighter than white will not affect dark adapted eyes. Red goggles outside the viewing area and red light in the viewing rooms are useful to maintain eye sensitivity. A remote viewing system with a video presentation allows individual control of brightness and contrast for maximum vision acuity.<sup>9</sup>

If the interpretation of the radiographic image is to be meaningful, it is essential that proper viewing equipment be in good working condition. If slight density variations in the radiographs are not observed, rejectable conditions may go unnoticed. In many cases, various types of discontinuities are barely distinguishable even with optimized techniques and fine grained film. To optimize the interpreter's ability to properly evaluate the radiographic image, appropriate viewing conditions and suitable equipment are absolutely necessary.

## High Intensity Illuminators

A radiograph that meets the density requirements of current codes and specifications will permit only a small fraction of the incident light to pass through it. The optical density of a

TABLE 1. Vision acuity test parameters.

Variable	Quantity of Conditions	Conditions
Figure and ground	1	Dark on light
Background luminance <sup>a</sup>	1	$85 \pm 5 \text{ cd}\cdot\text{m}^{-2}$ ( $25 \pm 1.5 \text{ ftl}$ )
Contrast	3	0.1, 0.3, 0.85
Line width (plane angle)	3	220 $\mu\text{rad}$ (0.75 min), 290 $\mu\text{rad}$ (1.0 min) and 440 $\mu\text{rad}$ (1.5 min)
Line width (plane angle)	1	31.13 mrad (107 min)
Viewing distance	1	400 mm (16 in.)
Blur	2	sharp, blurred
Line orientation	4	perpendicular or horizontal, oblique right, oblique left
Light source (viewer)	1	Incandescent, fluorescent
Total (combinations)	72	

a. The unit for luminance in the International System of Units (SI) is candela per square meter ( $\text{cd}\cdot\text{m}^{-2}$ ). The English unit for luminance, the footlambert (ftl), is equal to  $3.426 \text{ cd}\cdot\text{m}^{-2}$ .

b. The unit for plane angle in the International System of Units (SI) is radian (rad), equal to 3437.75 minutes (min) and equal to 57.296 degrees (deg), where  $1 \text{ deg} = 60 \text{ min} = 1.745 \times 10^{-2} \text{ rad}$ .



radiographic film can be expressed as a logarithmic function:

$$(1) \quad \text{Density} = \log \frac{I_0}{I_t}$$

where *Density* is the degree of blackness resulting from radiographic exposure;  $I_0$  is the incident light intensity (from the high intensity illuminator or densitometer); and  $I_t$  is the light transmitted through a specific region of the radiograph.

If a film is perfectly clear, the optical density will be 0:

$$\text{Density} = \log \frac{100}{100} = \log(1) = 0$$

A film that permits 1 percent of the incident light to be transmitted will have an optical density of 2.0.

Following the same procedure, it can be seen that a film optical density of 3.0 permits only 0.1 percent of the incident light to pass through and a film optical density of 4.0, a mere 0.01 percent.

Typically, radiographic density requirements through the area of interest range between 2.0 (1 percent light transmission) and 4.0 (0.01 percent light transmission); this explains the need for a source of high intensity viewing light.

There are many types and styles of high intensity illuminators, although they are generally classified into four groups: (1) spot viewers, (2) strip film viewers, (3) area viewers and (4) combination spot and area viewers.

Spot viewers provide a limited field of illumination, typically 76 to 102 mm (3 to 4 in.) in diameter. These viewers are usually the most portable and least expensive.

The strip film viewer (Fig. 4) permits interpretation of strip film including 90 × 430 mm (3.5 × 17 in.), 115 × 430 mm (4.5 × 17 in.), 100 × 250 mm (4 × 10 in.) and 125 × 175 mm (5 × 7 in.) and the 35 mm or 70 mm sizes. The

FIGURE 4. High intensity illuminator designed for viewing strip film.



viewing area is rectangular and the area of illumination may be adjusted to conform to the film dimension by using metal or cardboard masks.

The area viewers are designed to accommodate large films up to 360 × 430 mm (14 × 17 in.). The illumination is generally provided by fluorescent lights or a bank of photographic flood bulbs. The fluorescent light intensity may not have suitable brightness to permit effective examination through the higher densities and this could result in a serious limitation. The combination spot and area viewers (Fig. 5) provide the interpreter with spot capability while allowing the viewing of a large area of film. A switch determines which light source will be activated.

**Heat.** Because light of high intensity also generates significant amounts of heat, it is necessary that the illuminator have a means of dissipating or diverting the heat to avoid damaging the radiographic film while viewing. Light sources in illuminators of typical film viewers consist of one or more photographic flood bulbs. Other light sources such as flood lights and tungsten halogen bulbs are also used.

**Diffusion.** To minimize variation in the intensity of light across the area being viewed it is also important that the light be diffused over the area used for viewing. This diffusing is accomplished with a diffusing glass, usually positioned between the light source and the viewing area, or with a white plastic screen at the front of the viewer.

**Intensity Control.** Another essential feature of the illuminator is the variable intensity control. This permits subdued intensity when viewing lower densities and maximum intensity as required for the high density portions of the radiograph.

FIGURE 5. High intensity combination illuminator with iris diaphragm spot viewer and large viewer.



**Masks.** Masks can be extremely helpful when attempting to evaluate a small portion of a larger radiograph or when the radiograph is physically small. The intent is to illuminate that portion of the radiograph identified as the area of interest, while masking other light from the eyes of the interpreter. Some spot viewers are equipped with an iris diaphragm that permits the spot size to be varied with the simple adjustment of a lever. This feature is especially helpful when small areas or fine details must be examined.

**Precautions.** The illuminator's front glass or screen touches the film and should always be clean and free of blemishes on both sides. Scratches, nicks, dirt or other imperfections on the front glass or screen will cast shadows on the radiograph, causing unnecessary images.

Another precaution will help minimize film scratches. The front of the viewer should be carefully examined to ensure that there are no sharp edges or other obstructions; these could cause scratches to the sensitive surface of the radiograph as it is moved or positioned on the viewer.

## Magnifiers

Normally, radiographs can be effectively evaluated without magnification devices. There may be occasions, however, when such devices are helpful. For example, if the article being radiographed contains very small discontinuities or consists of minute components, magnification may be essential. This application will generally require fine grained film that can be suitably magnified. Some of the coarser grained films are difficult to view with magnification because the graininess is also enlarged; this can make discernment of slight optical density changes impossible.

There is a wide assortment of magnifiers appropriate for the evaluation of radiographs. The most common is the handheld magnifying glass, available in many shapes, sizes and powers. For convenience, a gooseneck magnifier may be employed. Because this magnifier is free standing and attached to a weighted metal base, it leaves the interpreter's hands free during use. One device that offers magnification *and* measuring capabilities is a comparator with an etched glass reticle (Fig. 6).

If any form of magnification is employed, it should be done with caution and limited to only those applications where it is necessary.

## Viewing Accessories

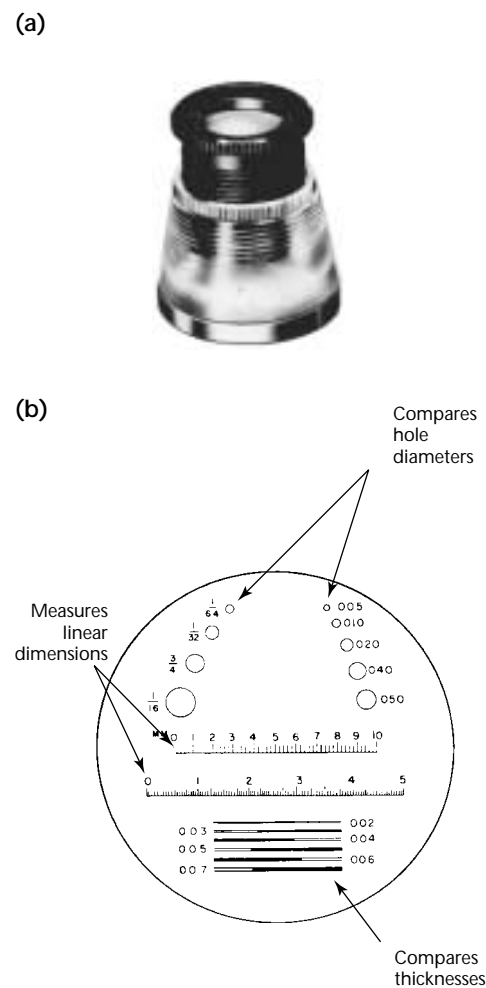
Additional accessories that aid the interpreter and should be available in the

film reading area, include (1) supply of wax marking pencils to mark the film; (2) rulers (the most appropriate would be clear, flexible plastic); (3) a small flashlight to reflect light off the radiographic film to assist in the identification of film artifacts such as scratches, roller marks, dirt and others; (4) gloves, usually cotton or nylon, to minimize direct contact between the film and the fingers of the interpreter; (5) charts, tables and other technical aids that will assist in the prompt establishment of density range (for example, see Table 2), determination of geometric unsharpness and other data related to the applicable codes or specifications.

## Viewing Paper Radiographs

Typically, paper radiographs are reviewed under normal lighting conditions using white light reflected from the radiograph. It is essential that the light be of suitable

FIGURE 6. Comparator with etched glass reticle: (a) comparator; (b) reticle.



intensity and, in some cases, positioned at an angle to prevent glare. Various lighting sources have been successful, including the high intensity reading lamps and specular lights (light focused from a reflector). Magnifiers containing fluorescent bulbs also provide an effective means of evaluating the paper radiograph, while magnifying the image. High magnification (above 5×) is not usually beneficial because of the normal graininess and lack of sharpness inherent in the paper radiograph. [See discussions of paper radiography elsewhere for more information.](#)

TABLE 2. Density range table based on densities of +30 percent and -15 percent. Densities less than 2.0 and more than 4.0 are considered unacceptable by some codes and specifications.

Density through Penetrameter	Maximum (+30 percent)	Minimum (-15 percent)
1.5	1.95	1.28
1.6	2.08	1.36
1.7	2.21	1.45
1.8	2.34	1.53
1.9	2.47	1.62
2.0	2.60	1.70
2.1	2.73	1.79
2.2	2.86	1.87
2.3	2.99	1.96
2.4	3.12	2.04
2.5	3.25	2.13
2.6	3.38	2.21
2.7	3.51	2.30
2.8	3.64	2.38
2.9	3.77	2.47
3.0	3.90	2.55
3.1	4.03	2.64
3.2	4.16	2.72
3.3	4.29	2.81
3.4	4.42	2.89
3.5	4.55	2.98
3.6	4.68	3.06
3.7	4.81	3.15
3.8	4.94	3.23
3.9	5.07	3.32
4.0	5.20	3.40

## PART 3. Densitometers

The densitometer is an instrument that measures film density (Figs. 7 and 8). Before the invention of portable densitometers, densities were estimated by comparing the radiographic density to a comparator strip. The strip contained a series of densities established by cumbersome and unwieldy early densitometers. Many of these early radiographic density determinations were simple, visual estimates.

FIGURE 7. Digital transmission densitometer.



FIGURE 8. Battery powered densitometer.



The operation of modern densitometers is quite simple. After calibration, using a density strip with known values for a number of different densities, the radiograph is positioned between the light source, usually located at the base of the densitometer, and the head, which contains a photomultiplier. Because the transmitted light intensity decreases as radiographic film density increases, less light reaches the photosensitive surface in the head and the voltage output from the photomultiplier (to the meter or digital display) will indicate a higher density reading. Conversely, as more light passes through a lower density region of the radiographic film and interacts with the photosensitive surface in the head, a lower density is indicated on the meter or digital display.

An aperture is installed near the light source to establish the precise region of the film that is being measured. Changing apertures requires recalibration.

### Procedure

The first step in the proper use of the densitometer is warmup. Most instruments now contain solid state circuitry and warmup time is minimal. It is good practice to wait at least five minutes after the densitometer has been turned on before taking density readings. This provides ample time for electronic stabilization.

The next step is the most important one. No matter how simple the densitometer may appear to be, it must be calibrated. Calibration is accomplished with a calibrated density strip. Because different densitometers have different controls and procedures for calibration, the specific instruction manuals should be consulted. After calibration is accomplished, a series of readings for a number of density steps should be taken using the calibrated strip. This should be repeated frequently during the densitometry to detect electrical shifts or inadvertent changes to the controls.

It is good practice to record calibration readings in a daily log book. Some codes and specifications require a master density strip traceable to a standards organization. The master strip can be used to calibrate

other density strips that are typically used for daily calibration. As the daily calibration strips wear out or become damaged from use, new ones can be prepared by comparison to the master strip.

After calibration, the densitometer is ready to use.

## Precautions

Several precautions should be kept in mind.

1. The densitometer is a sensitive electronic instrument and must be treated with care.
2. The densitometer must be kept clean at all times. The aperture, glass portions of the head and the reflective mirror (if used) should be cleaned with care using a cotton swab moistened with alcohol.
3. To avoid damaging the densitometer and to ensure accurate readings, never take density readings if the film is not completely dry. (Wet film density is not the same as dry film density.)
4. When replacing the bulb, exercise extreme care; make sure the densitometer is unplugged and take time to remove smudges resulting from handling.
5. Keep both the daily and master calibration strips in a protective cover or envelope.

It is reasonable to expect readings with an accuracy of  $\pm 0.02$  when the densitometer is properly maintained. Repeatability should generally fall within  $\pm 0.01$ . If the readings vary from these tolerances, the equipment should be checked for possible corrective action.

## Optical Density of Paper Radiographs

Density readings of radiographic film are made using a transmission densitometer. In the case of paper radiographs, density must be measured with a reflection densitometer because light cannot be transmitted effectively through paper.

Reflection density can be determined by using Eq. 2:

$$(2) \quad D_R = \log \frac{I_0}{I_R}$$

where  $D_R$  is the reflection density,  $I_0$  is the incident light intensity and  $I_R$  is the reflected light intensity.

While this equation is similar to the one used to determine the transmission density in radiographic film, density

readings of paper radiographs are achieved by measuring reflected light. There are a number of commercially available reflection densitometers and several transmission densitometers that also have the ability to read reflected densities.

## Scanning Microdensitometers

Densitometry for conventional radiographic equipment and procedures is done with the transmission densitometer. This instrument is generally suitable for ensuring compliance with radiographic technique requirements. However, it may not provide sufficient information for certain specialized radiographic analyses. The transmission densitometer is limited, in certain respects, by its relatively large aperture and by its inability to automatically scan a film or produce a permanent record. These limitations may dramatically affect the accuracy of relative density determinations, especially if the area of interest on a film is small (two or three millimeters). The scanning microdensitometer (SMD), which is also called a recording microdensitometer, was designed to overcome these limitations.

The scanning microdensitometer automatically scans a predetermined area on a film and produces a graphic depiction of the density changes occurring in the scan path. The accuracy of the scanning microdensitometer is greatly enhanced by its adjustable aperture, which may be set for openings as small as  $3 \mu\text{m}$  ( $1.2 \times 10^{-4}$  in.), hence the prefix *micro*. The scanning microdensitometer concept is based on the synchronous combination of an elaborate densitometry system and a compatible scanning/recording system.

## Description of Equipment and Operation

The principle of operation for conventional scanning microdensitometer equipment (Fig. 9) is based on a true double beam light system, in which two beams, emanating from a single light source, are switched alternately to a single photomultiplier. One of the light beams is directed, through a series of prisms and mirrors, to the aperture that actually scans the film; the other light beam is directed to an aperture that sends it through a mobile calibrated *gray wedge*.

Any differences in light intensity are automatically corrected so that both apertures transmit the same light quantity. During a scan, the film is placed on an automatically propelled carriage

that transports the film across the aperture's light beam (the aperture remains stationary). As the film traverses the light beam, continuous density readings are transmitted to a computer that feeds these readings to the gray wedge portion of the apparatus.

The mobile gray wedge (which is calibrated based on degree of density change per centimeter) will shift its position so that the density through the gray wedge matches the density of the film being scanned. The mobile gray wedge is mechanically attached to a recording pen assembly; the recording pen is in contact with graph paper that is mounted on a graph carriage moving at the same rate as the film carriage. The end result of this system is a graphic depiction of the density changes occurring in the scan path of the film:

$$(3) \quad \frac{A}{\Delta D_1} = \frac{B}{\Delta D_2}$$

where  $A$  is shim thickness;  $\Delta D_1$  is film density change from area of base metal to that of base metal plus shim;  $\Delta D_2$  is the film density change from base metal to total weld thickness; and  $B$  is thickness difference between weld area and base material. The definition of  $B$  is further specified in Eq. 4:

$$(4) \quad B = FR + RR$$

where  $FR$  is face reinforcement thickness and  $RR$  is root reinforcement thickness. These values are shown in the cross sectional drawing of Fig. 10 and the scanning microdensitometric graphs of Fig. 11.

## Advantages and Limitations of Scanning Microdensitometry

The scanning microdensitometer was designed to overcome the scanning, recording and accuracy limitations of conventional densitometry equipment. With these limitations eliminated, a broad array of information can be derived from the scanning microdensitometer.

The instrument provides numerous means by which accuracy can be enhanced or optimized. The aperture opening may be set as small as three micrometers to provide information associated with film grain dispersion and grain size. The ratio arm will allow for graph-to-scan path ratios of 1:1, 2:1, 5:1 and so on, which is very beneficial for scanning small areas. The ratio arm setting can also be used to optimize accuracy, provided other equipment adjustments are set accordingly. The scan graph itself can be incorporated into radiographic records to demonstrate verification of dimensional tolerances or adherence to density tolerances. The scanning microdensitometer can be a very useful and cost effective radiographic tool; however, its limitations should not be overlooked.

The major limitation of this equipment is ensuring that it will produce interpretable results. Some graph peaks

FIGURE 9. Double beam microdensitometry schematic.

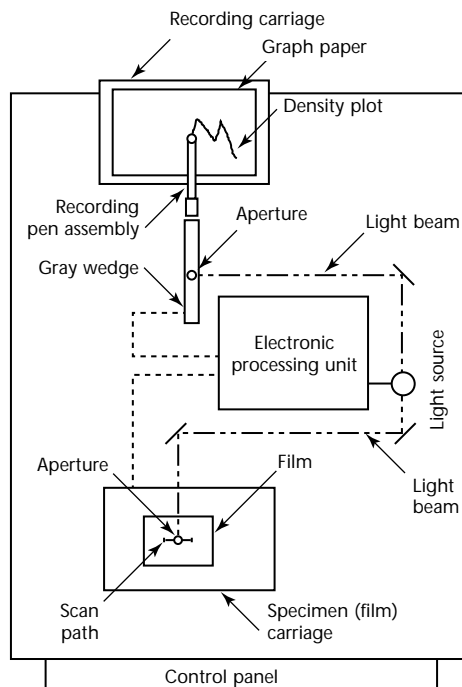
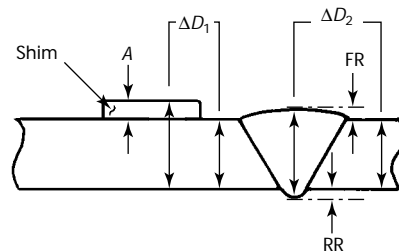


FIGURE 10. Typical convexity scan path.



### Legend

- $A$  = shim thickness
- $B$  = total material thickness difference between weld area and base metal
- $FR$  = additional thickness at face reinforcement
- $RR$  = additional thickness at root reinforcement
- $\Delta D_1$  = film density change from base metal to shim
- $\Delta D_2$  = film density change from base metal to total weld thickness



are signals (relevant) and others are noise (nonrelevant). The ability to distinguish between signal and noise is highly dependent on the aperture opening and its relation to the film being scanned. If a very grainy high contrast film is scanned, a large aperture ( $90\text{ }\mu\text{m}$ , or  $3.5 \times 10^{-3}\text{ in.}$ ) should be used. Otherwise, the signal-to-noise ratio of the scan graph will make interpretation difficult. Conversely, if a fine grained film is scanned, a small aperture opening is appropriate.

The scanning microdensitometer operator should be thoroughly familiar with the variables of the equipment so that the scanning technique can be optimized on the basis of the objective of the scan and the data producing capabilities of the film.

### Applications

Scanning microdensitometry equipment can be very useful for certain industrial radiography applications. Among these applications are X-ray focal spot measurements and determination of total radiographic unsharpness. A common application of the scanning microdensitometer in industrial radiography is verification of dimensional tolerances of questionable piping weld root conditions.

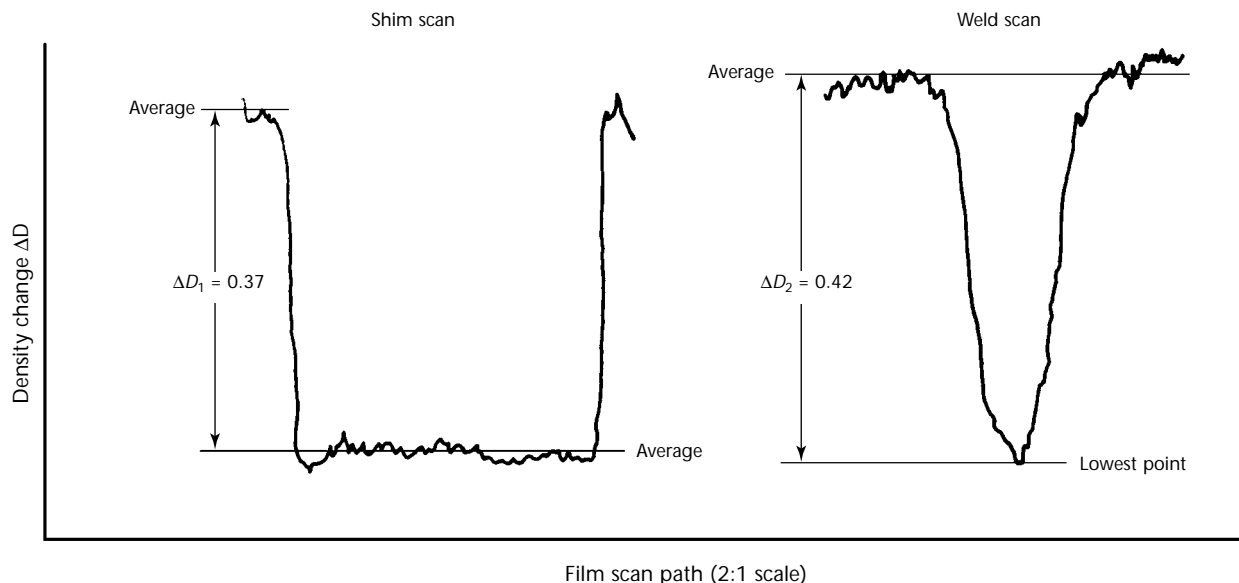
The ideal technique for verifying the dimensional tolerances of a given weld root condition is by performing a visual test and actually measuring the condition

involved. Ideal situations are infrequent in pipe radiography, however, and the majority of pipe weld joints are inaccessible for visual testing of the weld root. In a large portion of these situations, an additional radiograph, showing a profile view of the questionable condition, will provide the information necessary to support or determine the film interpreter's judgment. Additional radiography is normally an effective means for determining the accept/reject status of a radiograph; however, the additional time, cost and material required with this technique frequently make scanning microdensitometry more suitable.

The scanning microdensitometer graph (Fig. 11) allows conversion of density differences to material thickness differences (provided there is an item of known thickness on the radiograph, such as a shim). This, in turn, allows the X-ray film interpreter to determine the degree of the weld condition without additional radiography. (A shim of known thickness can be used as a visual reference for go/no-go thicknesses of reinforcements on welds.)

The scanning microdensitometer is also used for determining adherence to dimensional tolerances of assemblies such as nuclear fuel elements, artillery fuses and other assemblies where hidden component tolerances are critical. Where physical density variations are a matter of concern, the scanning densitometer is

FIGURE 11. Scanning microdensitometry graph.



#### Legend

$\Delta D_1$  = film density change from base metal to shim

$\Delta D_2$  = film density change from base metal to total weld thickness

useful for controlling the density of matrix and composite materials.

In an unusual application, high voltage radiography and a microdensitometer with a double light beam source were used to measure the stress in rock specimens when mine rock anchor bolts of various types were inserted.<sup>11</sup>

The scanning microdensitometer will generally transfer certain information from a radiograph to a medium (a graph) that can be understood by nonradiographic personnel. It should be noted, however, that some degree of interpretation is necessary to understand fully the information provided by the microscan graph. Therefore, the microscan graph should only be interpreted by knowledgeable and qualified personnel.

The limitations of scanning microdensitometer systems must be realized. The actual scanning technique must be devised based on the objective of the resultant graph.

## PART 4. Radiographic Interpretation Reporting

When reporting and documenting the results of radiographic film interpretation, complete and accurate information must accompany the radiographs.

Consistent with the importance of accurate information is correct terminology. Slang should be discouraged in any formal reports. Furthermore, interpretation reports should use terminology consistent with acceptance criteria. As an example, where the acceptance criteria limit *rounded indications*, a report identifying *porosity* may be misleading or even incorrect — a small void with a tail may meet the description of an elongated or linear indication (and rounded and linear indications may have different size limits).

Subsequent customer review and regulatory agency review may not occur until long after the completion of the radiographic test and acceptance by the fabricator or supplier. Lack of explanatory information and documentation can result in costly delays for resolving apparent or suspect indications on the radiographs. This information is typically documented on the film reader's *interpretation report*, sometimes called a *reader's sheet*.

Suppose, for example, that there is a surface discontinuity in a casting mold and this results in a number of castings that have the same discontinuity. The castings are subsequently radiographed and the radiographs reveal the same indication. The condition of the mold is well known to the initial film interpreter, who might therefore neglect to make note of it. Later reviewers will not have this basic information and must then develop it. This generally requires reconstruction of the shooting sketch and visual examination of the casting, frequently a time consuming task, particularly if the shooting sketch does not adequately identify reference points and the indication is on an inside surface. To further complicate matters, the casting may be unavailable for routine visual examination.

Documentation needed to minimize confusion during interpretation includes, but is not limited to, the following items.

1. The contract or purchase order should clearly delineate the applicable codes, standards, specifications and procedures, including acceptance criteria and personnel qualification requirements. Exceptions to codes, standards or specification requirements, if any, should also be noted.
2. Required quality levels and techniques as referenced in the applicable codes, multifilm techniques if used, section thicknesses, penetrometer (image quality indicator) selection and placement for each thickness range covered.
3. General exposure techniques used include the following: (a) shooting sketches, including film coverage and identification; (b) kilovoltage, time, milliamperage, target-to-film distance and target size (for X-rays); source type and becquerel (or curie) strength, source-to-film distance and physical source size (for gamma rays); (c) film types and intensifying screens used; (d) calculated geometric unsharpness; (e) blocking and masking; (f) manual or automatic processing; (g) quality level required and obtained; and (h) film density required and obtained.
4. Repairs should be documented so that the ultimate reviewer knows the cause and corrective action as an aid to interpretation. Radiographs taken after repair should be so indicated. Also, indications determined to be surface conditions on the test object should be recorded as such, together with any corrective action. If not radiographed after corrective action, that fact should be noted.
5. Disposition of each radiograph should be noted. All relevant indications (indications requiring evaluation) within the allowable acceptance criteria should be classified and sized (for example, "Station No. 7, slag, 6 mm long") and entered on the interpretation report.

These data are typically entered on the interpretation report. Figure 12 is an example of such a form for weld interpretation; Fig. 13, for castings.

FIGURE 12. Typical radiographic interpretation report (reader's sheet) for welds.

<b>COMPANY OR LABORATORY NAME</b> <b>ADDRESS      PHONE NUMBER</b>									
CUSTOMER ID _____ WELD ID/LOCATION _____ PART ID/LOCATION _____				RT REPORT NO. _____ DATE _____					
<b>PART DATA</b>				<b>TECHNIQUE DATA</b>					
WELD THICKNESS _____ BASE MATERIAL THICKNESS _____ MATERIAL TYPE _____ WELDING TECHNIQUE _____ WELD STATUS _____ WELD JOINT CONFIGURATION _____ DIAMETER OR WELD LENGTH _____ APPLICABLE CODE/STANDARD _____ RT PROCEDURE _____				<div style="display: flex; justify-content: space-between;"> <div>             PENETRATOR ID/NUMBER _____              SHIM THICKNESS _____              FILM TYPE _____              FILM SIZE _____              SINGLE _____ MULTIPLE (NO.) _____              KV _____ OR CURIE STRENGTH _____              RADIATION SOURCE TYPE _____              TARGET OR SOURCE SIZE (EFFECTIVE) _____              SFD _____ UNSHARPNESS _____              FILM PROCESSING: MANUAL _____ AUTOMATIC _____           </div> <div style="text-align: center;"> <b>SCREENS</b>              TYPE _____              FRONT THICKNESS _____              BACK THICKNESS _____              CENTER THICKNESS _____           </div> </div>					
<b>SHOOTING SKETCH</b>									
<div style="text-align: right; font-size: small;">             SHOW SOURCE/TUBE LOCATION, DIRECTION OF RADIATION, POSITION AND LOCATION OF PART, FILM, PENETRATOR, SHIM AND LEAD NUMBER/LETTER ID.           </div>									
<b>INTERPRETATION DATA</b>									
VIEWED SINGLE <input type="checkbox"/> VIEWED SUPERIMPOSED <input type="checkbox"/>									
PART NUMBER	WELD ID	STATION	ACC.	REF.	DISCONTINUITY CODE	QUALITY LEVEL	DENSITY	ARTIFACT	REMARKS
<b>DISCONTINUITY CODE</b>									
<div style="display: flex; flex-wrap: wrap; font-size: x-small;"> <div style="width: 33%;">             POR - POROSITY              S.I. - SLAG INCLUSION              S.L. - SLAG LINE              IP - INCOMPLETE PENETRATION           </div> <div style="width: 33%;">             LOF - LACK OF FUSION              UC-EX - UNDERCUT OUTSIDE              UC-IN - UNDERCUT INSIDE              CONC - CONCAVITY           </div> <div style="width: 33%;">             CONV - CONVEXITY              HILo - HIGH LOW              BT - BURN-THROUGH              IC - ICICLES           </div> <div style="width: 33%;">             W - TUNGSTEN INCLUSION              CR(L) - LONGITUDINAL CRACK              CR(T) - TRANSVERSE CRACK              CR(R) - ROOT CRACK           </div> <div style="width: 33%;">             CR(C) - CRATER CRACK              AB - ARC BURN              UI - UNCONSUMED INSERT              OR - OXIDIZED ROOT              SURF - SURFACE           </div> </div>									
<div style="display: flex; justify-content: space-between;"> <div>             REVIEWED BY _____              NAME _____           </div> <div>             LEVEL _____              DATE _____           </div> </div>									
<div style="display: flex; justify-content: space-between;"> <div>             CUSTOMER OR              CUSTOMER REPRESENTATIVE _____              NAME _____           </div> <div>             LEVEL _____              DATE _____           </div> </div>									

FIGURE 13. Typical radiographic interpretation report (reader's sheet) for castings.

<b>COMPANY OR LABORATORY NAME</b> <b>ADDRESS      PHONE NUMBER</b>										
CUSTOMER ID _____ CASTING ID/LOCATION _____ PART ID/LOCATION _____				RT REPORT NO. _____ DATE _____						
<b>PART DATA</b>				<b>TECHNIQUE DATA</b>						
MATERIAL THICKNESS _____ MATERIAL TYPE _____ APPLICABLE CODE/STANDARD _____ RT PROCEDURE _____				<div style="display: flex; justify-content: space-between;"> <div>             PENETRATOR ID/NUMBER _____              SHIM/BLOCK THICKNESS _____              FILM TYPE _____              SINGLE _____ MULTIPLE (NO.) _____              KV _____ OR CURIE STRENGTH _____              RADIATION SOURCE-TYPE _____              TARGET OR SOURCE SIZE (EFFECTIVE) _____              SFD _____ UNSHARPNESS _____              FILM PROCESSING: MANUAL _____ AUTOMATIC _____           </div> <div style="text-align: center;"> <b>SCREENS</b>              TYPE _____              FRONT THICKNESS _____              BACK THICKNESS _____              CENTER THICKNESS _____           </div> </div>						
<b>SHOOTING SKETCH</b>										
<div style="display: flex; justify-content: space-between;"> <div style="flex-grow: 1; border: 1px solid black; min-height: 150px;"></div> <div style="font-size: 0.8em; padding-top: 10px;">           SHOW SOURCE/TUBE LOCATION, DIRECTION OF RADIATION, POSITION AND LOCATION OF PART, FILM, PENETRATOR, SHIM AND LEAD NUMBER/LETTER ID.         </div> </div>										
<b>INTERPRETATION DATA</b>										
VIEWED SINGLE <input type="checkbox"/> VIEWED SUPERIMPOSED <input type="checkbox"/>										
PART NUMBER	CASTING ID	STATION	ACC.	REJ.	DISCONTINUITY CODE	QUALITY LEVEL	DENSITY	ARTIFACT	REMARKS	
<b>DISCONTINUITY CODE</b>										
<div style="display: flex; flex-wrap: wrap; font-size: 0.8em;"> <div style="width: 33%;">MP - MICROPOROSITY</div> <div style="width: 33%;">SI - SAND INCLUSION</div> <div style="width: 33%;">MS - MICROSHRINKAGE</div> <div style="width: 33%;">HT - HOT TEAR</div> <div style="width: 33%;">CS - CORE SHIFT</div> <div style="width: 33%;">POR - POROSITY</div> <div style="width: 33%;">SL - SLAG INCLUSION</div> <div style="width: 33%;">SH - SHRINKAGE</div> <div style="width: 33%;">UC - UNFUSED CHAPLET</div> <div style="width: 33%;">SEG - SEGREGATION</div> <div style="width: 33%;">WP - WORM HOLE POROSITY</div> <div style="width: 33%;">DI - DENSE INCLUSION</div> <div style="width: 33%;">DR - DROSS</div> <div style="width: 33%;">MR - MISRUN</div> <div style="width: 33%;">SURF - SURFACE</div> <div style="width: 33%;">BH - BLOW HOLE</div> <div style="width: 33%;">SS - SPONGE SHRINKAGE</div> </div>										
REVIEWED BY _____ NAME _____ LEVEL _____ DATE _____ CUSTOMER OR CUSTOMER REPRESENTATIVE _____ NAME _____ LEVEL _____ DATE _____										

## PART 5. Radiographic Artifacts

### Indication Description

Because most *nonrelevant indications* can be readily related to their actual causes, this category of indications is comparatively easy to interpret. False and actual discontinuity indications will be presented here to provide guidance for the radiographic film interpreter.

The interpretation of radiographs is not a precise science. As mentioned earlier in this chapter, even those qualified film interpreters with years of experience will often disagree on the nature of discontinuities and their disposition. The descriptions and illustrations<sup>12</sup> contained in this chapter may be used as a general guideline to help identify similar indications encountered during the interpretation process.

### False Indications (Film Artifacts)

The radiographic process is very intolerant of dirt and careless handling of the recording media. Violations of good darkroom practice in film loading, unloading and processing will result in artifacts that must be recognized for what they are, not what they may appear to be.

Erroneous interpretations may be made as the result of not recognizing artifacts. Emulsion scratches are a common cause of such misinterpretation. These and many other artifacts are quickly recognizable by viewing both surfaces of the film with reflected light.

The double film technique is one of the most effective steps in recognizing artifacts, by simply comparing the area of interest on both films. If the indication is on one film and not the other, is not in the same place or has changed in appearance, it is an artifact.

There are many different types of artifacts, some of which can be confused with actual discontinuities. It is extremely important to identify these false indications and to note their presence in the film interpreter's report. In some cases the existence of artifacts in the area of interest may require reradiography. It is therefore important to take every reasonable step to minimize artifacts.

### Artifacts Caused before Processing

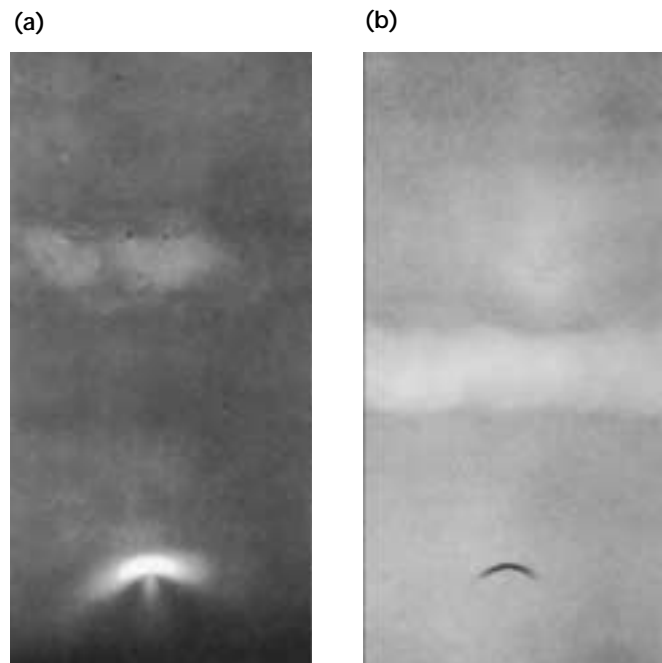
#### Film Scratches

Radiographic film emulsion is quite sensitive and scratches can be caused by most abrasive materials; fingernails and rough handling during loading or unloading are examples. Film scratches can be identified by reflecting light at an angle to the film surface.

#### Crimp Marks

*Crimp marks* are caused by bending the film abruptly, usually when loading and unloading the film holder. If the film is crimped before exposure, it will produce a crescent shaped indication that is lighter in density than the adjacent film density (Fig. 14). If crimped after exposure, the film will produce an indication that is darker than the adjacent film density.

FIGURE 14. Crimp marks resulting from poor handling of individual sheet of film: (a) before exposure; (b) after exposure.





## Pressure Marks

*Pressure marks* are caused by severe localized applications of pressure to the film. For example, a part may be dropped on the film holder during setup. This will produce an artifact on the processed film (Fig. 15).

## Static Marks

Static charges may develop when the radiographic film is handled roughly or moved rapidly during loading or unloading the film holder. It may also be caused by rapid removal of the paper wrapper used as an interleaf. The appearance of *static marks* will range from branchlike, jagged dark lines to irregular, abrupt dark spots.

## Screen Marks

Scratches and other blemishes in a lead screen will become intensified and can create significant indications on the film image. This may be especially noticeable when the film holder containing the lead screens is bent to accommodate part configuration. Dirt on fluorescent screens will interfere with light transmission to the film and a light area will result after the film is processed. Dirt on lead screens interferes with electron bombardment of the film and also produces a light area in the image (Fig. 16). Screens should have a unique serial number inscribed in a corner to identify these problems and to make it easier to locate the faulty screen.

Small bits of foreign material (such as lint, tobacco, paper or dandruff) between the film and fluorescent or lead screens will cause light spots in the processed film. To minimize false indications from

screens, it is imperative that they be absolutely clean, smooth, free of imperfections and foreign matter.

A word of caution: manufacturers of screens often apply a thin plastic coating to protect the screen from scratches during processing. This coating must be removed before using a new screen as it will absorb much of the emissions that would otherwise provide the desired intensification.

## Fog

Fog is an overall, small density increase caused when unexposed film is exposed to some chemicals, low levels of radiation, high humidity, small darkroom light leaks or an inadequate safelight. Information regarding safe light intensity limits can be obtained from the film manufacturer.

## Light Leaks

Exposure to light usually results in noticeable local film blackening (Fig. 17).

FIGURE 15. Pressure mark caused before exposure, visible as low density.

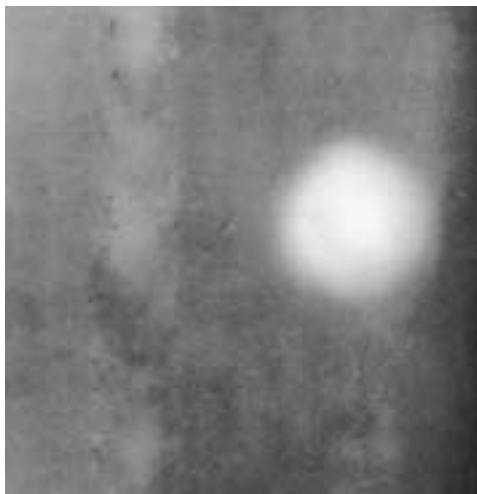


FIGURE 16. Words *front* and *back* scratched in the surface of front and back lead foil screens before radiography of a 25 mm (1.0 in.) welded steel plate. Hairs placed between respective screens and film are visible as light marks preceding inscribed words.



FIGURE 17. Light leaks.



Film holders should be examined regularly to eliminate the problem.

### Finger Marks

Marks such as fingerprints are normally easy to recognize. They may be darker or lighter images on the film.

## Artifacts Caused during Processing

### Chemical Streaks

During manual processing, streaks on the film may result if chemicals from previous processing are not adequately removed from the hanger clips (Fig. 18). Overall film streaking may also result when the film is placed directly into a water rinse without first placing it into the stop bath solution. Developer carryover into the fixer may cause an overall streaking condition. A further cause of streaking is insufficient agitation of the film hanger during development.

### Spotting

If fixer solution comes in contact with the film before development, light areas or spots will result (Fig. 19). If drops of developer or water inadvertently reach the film before placing it into the developer, dark spots can result (Fig. 20).

FIGURE 18. Streaking caused by inadequately cleaned film hangers.



FIGURE 19. Light spots caused before development: (a) by stop bath splashed on film; (b) by fixer splashed on film.

(a)

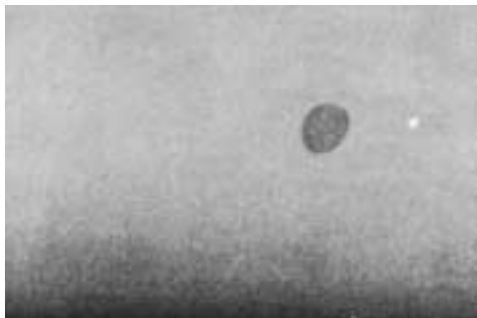


(b)

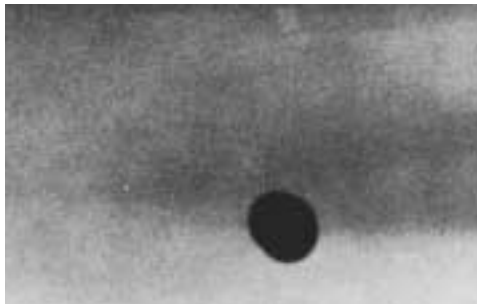


FIGURE 20. Dark spots caused before development: (a) by water splashed on film; (b) by developer splashed on film.

(a)



(b)



Another spotting condition may occur from water droplets on the film surface. During the drying process, these droplets take longer to dry and leave a distinct circular pattern on the film surface. Water spots can be reduced by using a wetting agent before drying.

### Delay Streaks

These are uneven streaks in the direction of film movement through an automatic processor. A delay in feeding successive films may result in the drying of solutions on the processor rollers. Cleaning the exposed rollers with a damp cloth should eliminate *delay streaks*.

### Air Bells

*Air bells* are caused by air bubbles clinging to the surface of the film when it is immersed in the developer. An air bell prevents developer from reaching the film surface, thus causing light spots on the film image. If the film hanger is tapped abruptly against the side of the tank then properly agitated, the air bubbles should become dislodged.

### Dirt

If dirt or other contaminants accumulate on the surface of the developer or fixer, a noticeably dirty pattern will probably appear on the film. If the rinse water is not adequately replenished, it can also cause a similar problem, especially if the water coming into the wash tank is dirty and filtration is not used (Fig. 21). This condition can be verified by observing the surface of the film in reflected light.

FIGURE 21. Surface deposits caused by contaminated wash water in automatic processor.



### Pi Lines

These lines run across the film, perpendicular to the direction of rolling, when an automatic processor is used. They occur at regularly spaced intervals, 3.14 times the roller diameter. This condition is apparently caused by a slight deposit of chemicals on the rollers by the leading edge of the film (Fig. 22).

### Pressure Marks

*Pressure marks* may be caused by a buildup of foreign matter on rollers in an automatic processor or by inadequate clearances between rollers. Rollers should be thoroughly cleaned and properly adjusted to minimize this condition (Fig. 23).

### Kissing

Film that comes in contact with other film, especially in the developer during manual processing, will result in a severe blotch in the area of contact.

FIGURE 22. Pi lines. Two or more lines recur at interval of  $\pi \times$  roller diameter.

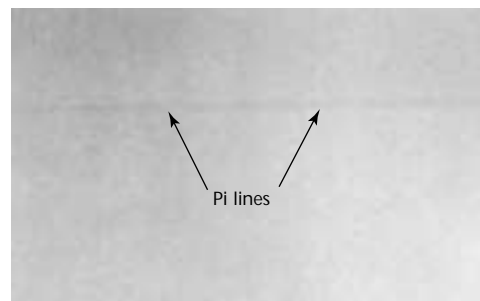


FIGURE 23. Pressure marks caused by foreign matter on rollers or improper roller clearance.



## Artifacts Caused after Processing

### Scratches

Scratches result from rough handling. Even after processing, the emulsion is sensitive to all types of abrasion and care should be taken to minimize damage to the emulsion.

### Fingerprints

These occur when improperly handling the film, as can happen during interpretation. Film should be handled with care by the edges or corners whenever possible. To prevent fingerprints, radiographs should be handled with cotton or nylon gloves.

### Radioscopic Artifacts

Radioscopic artifacts are also operator dependent and must be recognized. They are caused primarily by electronic noise generated in video systems and can be corrected by filtering. Dust on the lens surface is another common cause of real time artifacts. When using image enhancement techniques on radiographs, a very careful examination of the film should be made to identify all artifacts before enhancement. Otherwise, the artifacts will also be enhanced and could possibly be difficult to identify in subsequent evaluations. This is also true when radiographs are duplicated or microfilmed.

## PART 6. Discontinuity Indications

### Discontinuity Indications for Welds

The various discontinuities found in weldments are illustrated and described here strictly as representative conditions. Cross sectional photographs or sketches are also shown. These examples are for illustrative purposes; actual discontinuities vary in shape, size and severity.

#### Porosity

These are voids that result from gas being entrapped as the weld metal solidifies (Fig. 24). Porosity is generally spherical but may be elongated. In some cases, porosity may appear to have a tail as a result of the gas attempting to escape or move while the weld metal is still in the liquid state. Porosity is often uniformly scattered to different degrees of severity but may also appear as a cluster where there is a concentration of pores in a relatively small area. *Linear porosity* is a condition that involves a number of pores aligned and separated by a distance usually stipulated in the acceptance standards. *Piping porosity* is severely elongated gas holes that are well defined and may vary in length from very short to as long as 380 mm (15 in.) or more. This type of porosity is sometimes referred to as *worm hole porosity*. *Hollow bead* (Fig. 25) is an elongated gas void that is usually centrally oriented in the root pass and may also extend for a significant length.

In general, porosity is not considered a critical discontinuity unless (1) it is present in large quantities (a percentage, according to specification, of the cross section in which it occurs), (2) it contains sharp tails or (3) it is aligned in significant numbers in a relatively short distance. The severity of piping and wormhole porosity or hollow bead conditions is generally determined by length and amount.

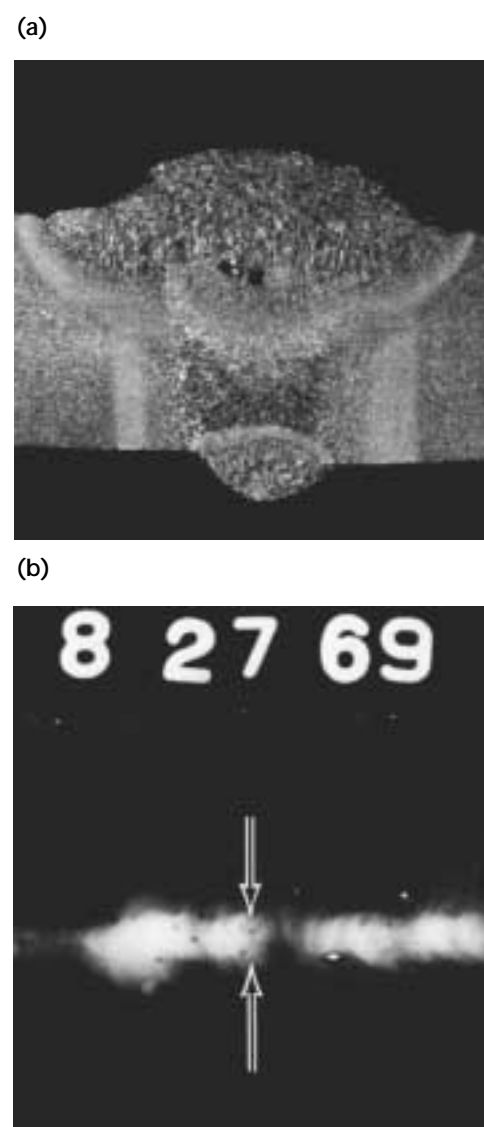
#### Slag or Inclusions

Also referred to as *nonmetallics*, these indications are caused by nonmetallic materials — usually silica or complex sulfides or oxides — entrapped in the weld metal between weld passes or between weld metal and base metal (Fig. 26). Inclusions occur in all shapes

and sizes but can be generally categorized as an inclusion (short, isolated piece) or as a slag line (relatively narrow but having length). Inclusions are evaluated based on size, quantity and length.

In welds, slag inclusions are often elongated or linear, often aligned with the length of a weld. This condition is associated with multipass welding

FIGURE 24. Porosity: (a) photomacrograph; (b) radiographic image.

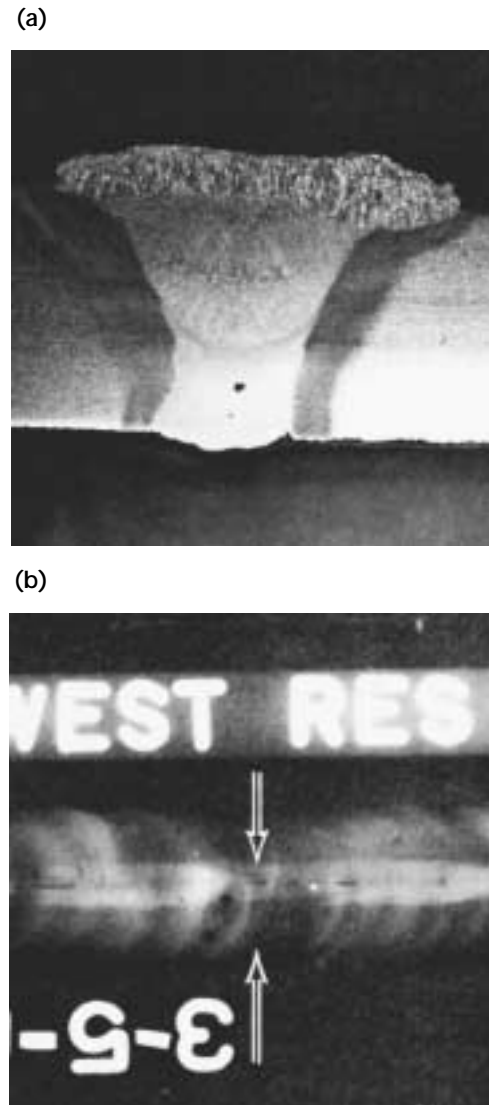


processes that provide a slag covering to retard heat loss. When this slag layer is not properly cleaned it becomes trapped between weld layers.

### Dense Inclusions

Dense inclusions have greater radiographic density than the weld metal, so they appear as light spots in the radiograph. They are generally rounded in shape and sharply defined but sometimes may blend gradually into the surrounding metal. The most common dense inclusions are pieces of tungsten electrode that have broken off and been entrapped in the weld metal (Fig. 27).

FIGURE 25. Hollow bead:  
(a) photomacrograph; (b) radiographic image.



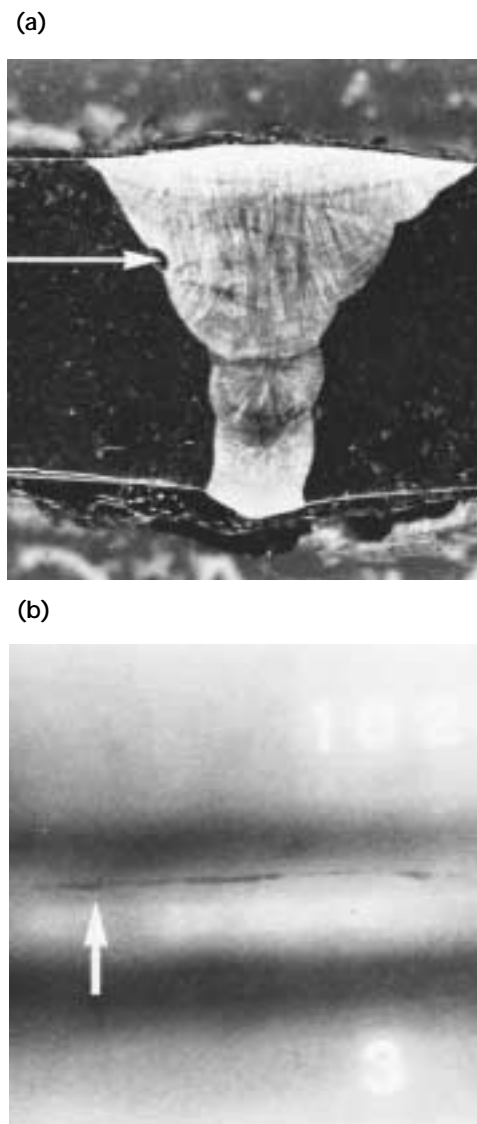
### Incomplete Penetration

*Incomplete penetration* or *inadequate penetration* is an area of nonfusion in the root area (Fig. 28).

Incomplete penetration is characterized by one or both weld joint sides' not being melted and fused at the toe or toes of the root. For double-sided weld joints incomplete penetration occurs near the midpoint through the weld thickness, or weld throat.

This may result from inadequate heat while the root pass is being deposited. It may also be caused by faulty joint design or problems with the welding procedure. This condition is considered more severe

FIGURE 26. Slag inclusion:  
(a) photomacrograph at 4.7 $\times$ ;  
(b) radiographic image at 1.1 $\times$ .





than the porosity or slag discontinuities because it is more of a *stress raiser*. Incomplete penetration is usually easy to detect and identify radiographically because of its location in the weld and its relatively straight, well defined image.

### Lack of Fusion

*Lack of fusion* is an area of nonadhesion between successive weld passes or between a weld pass and the side wall of the base material (Fig. 29). It is primarily the result of improper welding techniques or poor joint design. Many lack-of-fusion conditions are relatively narrow and in some cases angularly oriented, so this

discontinuity is not always readily detected by radiography. When it is observed, it may not be clearly defined but will have a telltale linear alignment, running in the same direction that the weld was deposited.

### Underfill

*Underfill* is a condition where the weld joint is not completely filled, as evidenced by a depression or lack of weld metal at the face of the weld. This condition is readily observed by an increase in the film density in the weld area; the extent should be confirmed by physical measurement.

FIGURE 27. Tungsten inclusion:  
(a) photomacrograph at 4.5 $\times$ ;  
(b) radiographic image at 1.2 $\times$ .

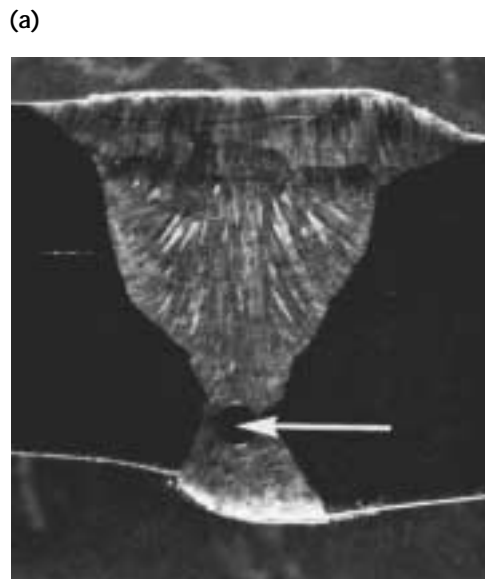
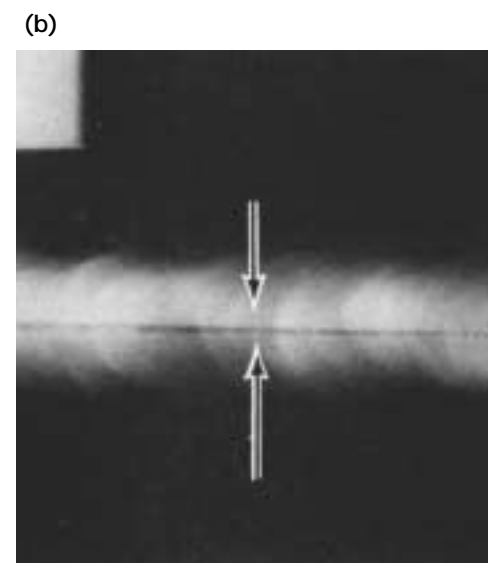
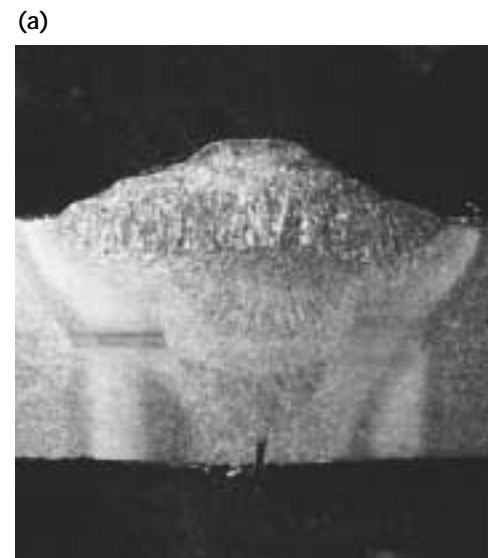


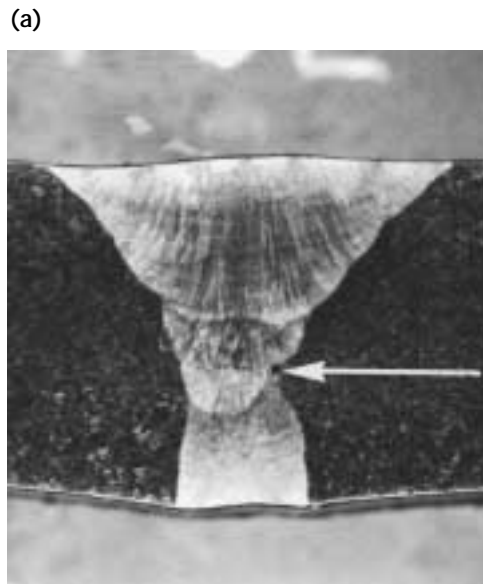
FIGURE 28. Incomplete or inadequate penetration: (a) photomacrograph;  
(b) radiographic image.



## Undercut

*Undercut* is generally described as a groove or depression located at the junction of the weld and base material (the fusion zone) on the weld surface (Fig. 30). This depression is caused by a melting away of the base metal during the welding process and can occur at the weld root. Undercut can be readily seen and identified on a radiograph but the extent should be measured physically, if possible. Generally, undercut is not considered to be a serious condition if it is relatively shallow (within specification requirements) and not sharp.

FIGURE 29. Side wall incomplete fusion:  
(a) photomacrograph at 4.5×;  
(b) radiographic image at 1.1×.



## Overlap

*Overlap* is an extension of unfused weld metal beyond the fusion zone. In many cases the overlap forms a tight stress riser notch and is not easily seen in the radiograph. It is generally considered severe when it is detected and confirmed visually.

## Excessive Penetration

This is sometimes referred to as *convexity* and results from excessive heat input while the root pass is being deposited

FIGURE 30. Undercut on outside diameter:  
(a) photomacrograph at 4.6×;  
(b) radiographic image at 1×.



(Fig. 31). The reinforcement of the root becomes excessive and, in some cases, results in a corner or notch condition on the inside surface at the toe of the weld. When excessive penetration occurs in short or intermittent droplets, it may be referred to as *icicles* and is usually accompanied by a burnthrough area that lacks weld metal (Fig. 32).

### Concavity

*Concavity* is a concave condition in the root pass face that results from insufficient heat input while depositing the root pass (Fig. 33). Concavity causes a dimensional change in the thickness of

the weld that may then be less than the required thickness. Because the condition is usually a gradual dimensional change, it shows as a slight and gradual density change in the radiograph. The extent should be determined by physical measurement but may be estimated by density measurements.

### High Low

*High low* and *mismatch* are terms that denote a misalignment in pipe welds that results in an offset union of the two sections being welded (Fig. 34).

FIGURE 31. Excessive penetration:  
(a) photomacrograph at 4.5×;  
(b) radiographic image at 1.2×.

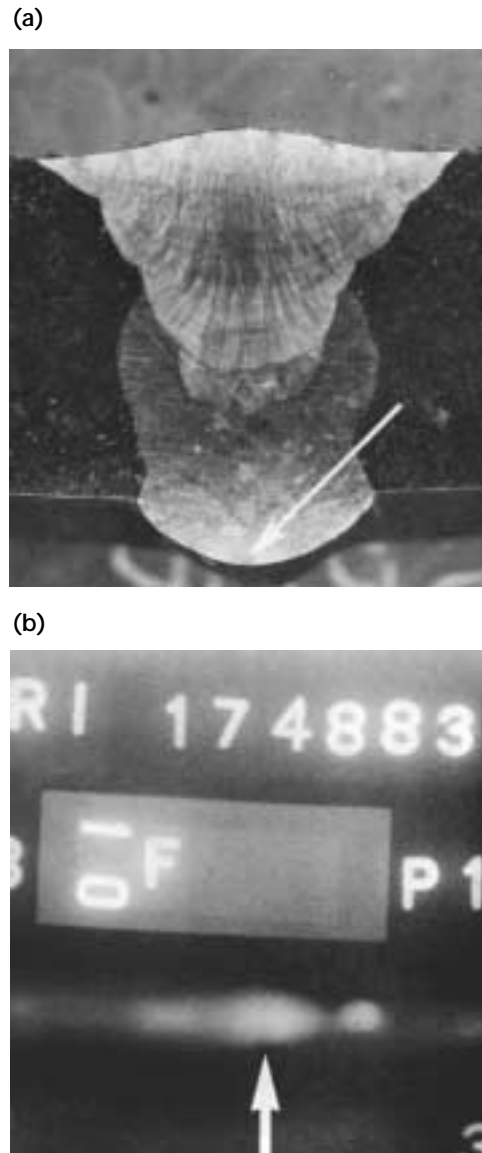
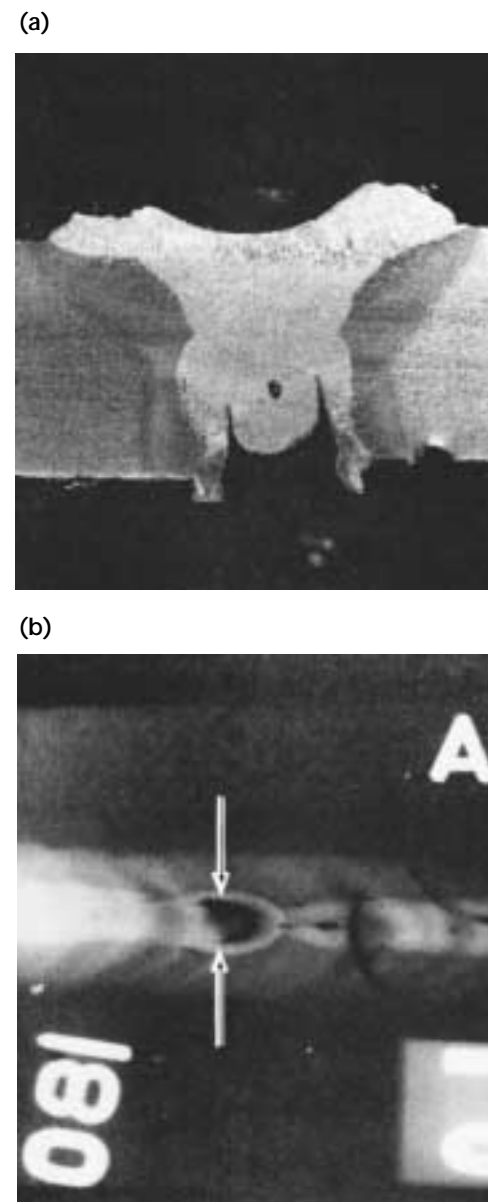


FIGURE 32. Burnthrough area:  
(a) photomacrograph; (b) radiographic image.



## Cracks

Cracks are fractures or ruptures of the weld metal occurring when the stresses in a localized area exceed the weld metal's ultimate tensile strength. *Hot cracks* occur as tears while the weld metal is in the plastic condition whereas *cold cracks* and *delayed cracks* occur after the weld metal has cooled. Delayed cracks are cold cracks that may occur hours after the weldment has cooled. There are a number of crack types associated with weldments.

**Longitudinal Crack.** *Longitudinal cracks* (Fig. 35) are oriented along the length or approximately parallel to the longitudinal axis, of the weld.

**Transverse Crack.** *Transverse cracks* (Fig. 36) are approximately perpendicular to the longitudinal axis of the weld.

**Underbead Crack.** *Underbead cracks* form in the heat affected zone and are usually short but may also be an extensive network.

**Toe Crack.** *Toe cracks* begin at the toe of the weld and propagate along the plane of highest stress.

**Root Crack.** *Root cracks* (Fig. 37) are longitudinal cracks located in the root pass.

**Crater Crack.** *Crater cracks* are usually star shaped patterns that occur in the crater (a depression at the end of a weld bead).

FIGURE 33. Concave root surface:  
(a) photomacrograph at 4.3×;  
(b) radiographic image at 1.2×.

(a)



(b)



FIGURE 34. High low defect, also called  
*mismatch*: (a) photomacrograph at 4.4×;  
(b) radiographic image at 1.1×.

(a)



(b)

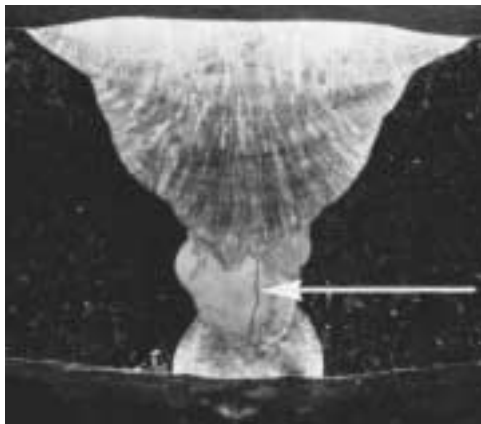


## Discontinuity Indications for Castings

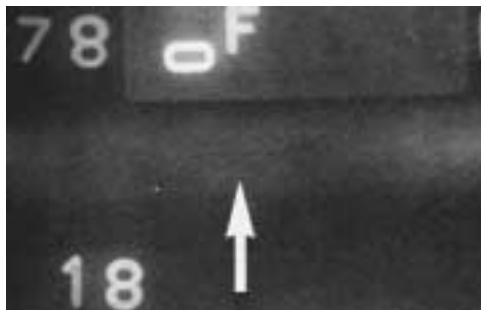
Casting discontinuities, as with weld discontinuities, will vary in shape, size and appearance depending on many variables, including material type, mold design, casting process, casting size and foundry control. The examples used to illustrate the various discontinuities found in castings are typical and are not

FIGURE 35. Longitudinal crack:  
(a) photomacrograph at 4.5×;  
(b) radiographic image without collimated source at 1.1×; (c) radiographic image at 1.1× with same conditions as Fig. 35b but with collimation.

(a)



(b)



(c)



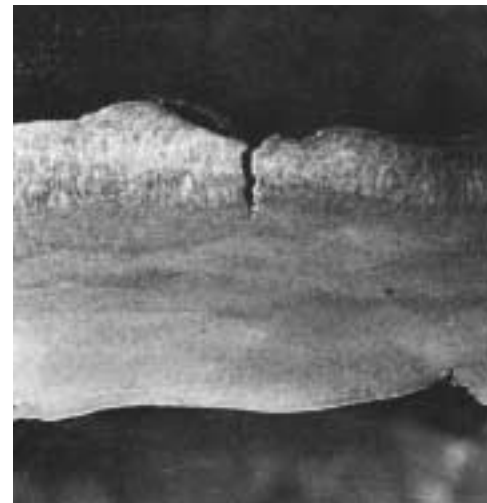
intended for any purpose other than guidance.

## Porosity

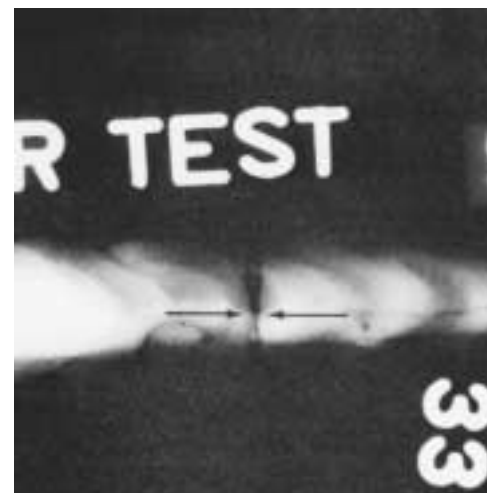
*Porosity* occurs when gas dissolved in the metal, entrained by turbulence during pouring or given off by the mold material, is entrapped in the casting during solidification. Porosity can be individually identified and defined in the radiograph as distinct, globular gas voids (Fig. 38). Individual pores may vary in size and concentration and these characteristics are used for classification of porosity. Such voids may be present at the surface of the casting or throughout the cross section.

FIGURE 36. Transverse crack:  
(a) photomacrograph; (b) radiographic image.

(a)



(b)





## Gas Voids

The most serious gas voids are referred to as *gas holes* (Fig. 39), *wormhole porosity* or *blow holes*. A larger, darker (film density) porosity condition is called a gas hole to distinguish it as a more severe condition compared to typical porosity. Wormhole porosity is so named because of its likeness to a wormhole. The shape is caused by the tendency of entrapped gas to escape during solidification and this, in turn, occurs because the gas is considerably lighter in density than the cast metal. During its escape attempt, the gas forms a tail like linear pattern resembling a wormhole.

The most severe gas voids are called blow holes: severe, well defined cavities

that occur when the hot, molten metal is deposited into a mold containing moisture or other impurities. The extremely hot metal causes the moisture or impurity to change rapidly to steam or gas that develops a series of linear voids extending into the metal from the surface.

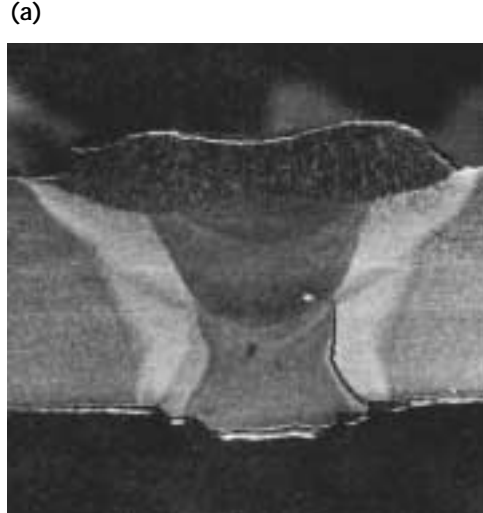
## Inclusions

**Sand Inclusion.** *Sand inclusions* are pieces of sand that have broken off the sand mold. Radiographically, they resemble a pocket of sand with a granular appearance if observed closely.

**Slag Inclusion.** *Slag inclusions* (Fig. 40) are impurities introduced into the mold with the molten metal. They may also be the result of oxide or impurities that did not rise to the surface before metal solidification.

**Dross.** *Dross* is sometimes referred to as the scum of the melt. Dross may become entrapped, resulting in a general zone of

FIGURE 37. Crack adjacent to root: (a) photomacrograph; (b) radiographic image.



(a)

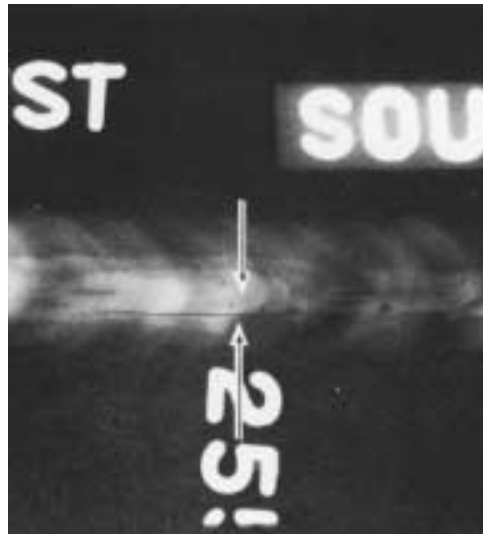
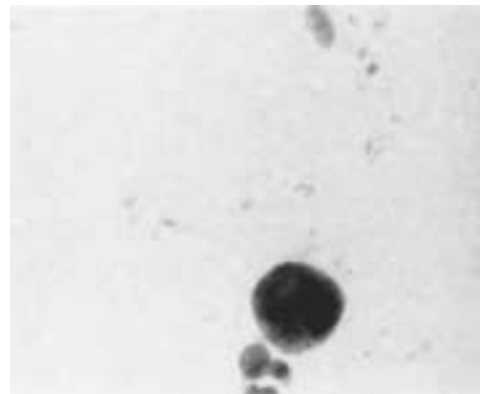


FIGURE 38. Porosity.



FIGURE 39. Gas holes, also called blow holes.





impurities. Dross is usually irregular compared to slag and may be accompanied by gas voids.

**Dense Inclusion.** *Dense inclusions* (Fig. 41) can result from the inadvertent addition of more dense objects (such as core wire, bits of metal or other high density materials) to the molten cast metal. These dense inclusions will result in a lighter area of film density in the radiograph.

## Shrinkage and Shrinks

The term *shrinkage* is common but can cause confusion about the source of this type of discontinuity. A useful term for an individual discontinuity is a *shrink*.

Shrinks are voids that occur when there is insufficient liquid metal to compensate for the reduction in volume of the metal as it solidifies. The cast molten metal solidifies from the mold inward, shrinking as it freezes and continuing to contract as the solidified

metal cools further below the melting point. When a large section is being fed through a section having a smaller volume, the smaller will usually freeze before the larger one, thus choking off the supply of molten metal needed to fill the larger volume. This results in a shrink or shrinkage cavity.

There are several forms of shrinks. They may be open to the casting surface or totally beneath the surface. They may lie at the center line or be associated with a chaplet, core, gate or other feature of the casting. Large, individual voids will often have a rough, jagged surface of dendritic (treelike) metal grains and appear in the radiograph as large, irregular voids (Fig. 42) or as rough, branching indications that may be mistaken for cracks or hot tears.

**Microshrinks and Sponge Shrinkage.** Shrinks may also occur as arrays of small voids (*microshrinks* or *microshrinkage*) having a feathery (Fig. 43) or spongelike (Fig. 44) radiographic appearance. The feathery form is most often seen in magnesium castings. The sponge form

FIGURE 40. Slag inclusions.



FIGURE 41. Dense inclusions.

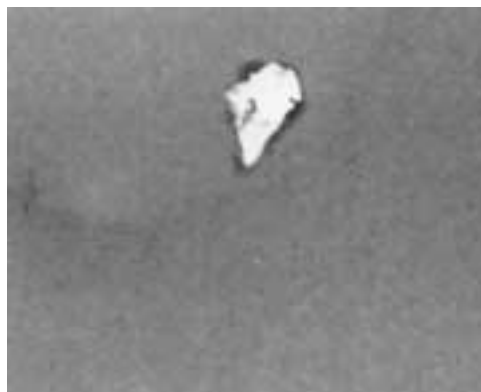


FIGURE 42. Shrinkage.



FIGURE 43. Microshrinkage.



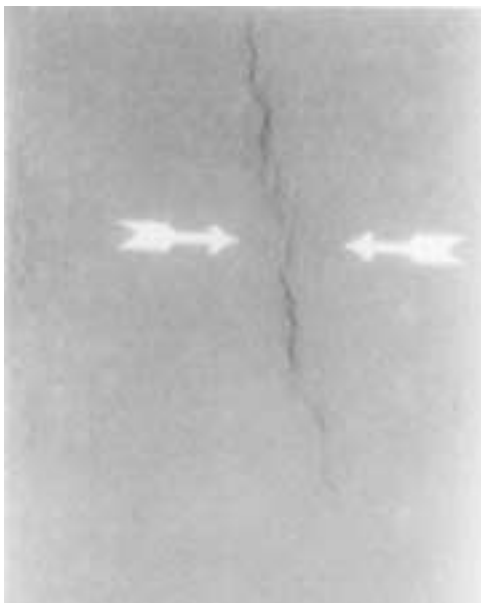
often occurs in nickel base and cobalt base alloys. The small voids forming these shrinks are sometimes difficult for the naked eye to see on a polished surface. Relatively large areas of such shrinks may produce only faint, barely detectable radiographic images. In coarser form, sponge shrinkage occurs in many metals.

**Hot Tears.** Hot tears (Fig. 45) are cracks that form before complete solidification of the metal section. They are usually caused by stresses resulting from uneven cooling of a large volume of metal adjacent to a smaller volume of metal, such as where a thick flange meets the wall of a valve body. They are almost always open to the surface and have rounded edges at the surface. When exposed, the crack face often shows a rough, heavily oxidized, dendritic surface.

FIGURE 44. Sponge shrinkage.



FIGURE 45. Hot tears.



Radiographically, hot tears appear as jagged linear indications, sometimes branching.

**Cracks.** Cracks (Fig. 46) are formed after the metal has completely solidified and while it is cooling to ambient temperature. If open to the surface, they will have sharp edges. When exposed they display oxidized surfaces if cracking occurred while the casting was still quite hot or no oxidation if cracking occurred near room temperature. Radiographically, they will be less open (narrower) than hot tears and usually show little if any branching.

### Cold Shuts

Cold shuts are essentially a lack of fusion between adjoining portions of the cast metal. They may be caused by excessive oxidation of one or more portions of the molten metal, by too low a temperature of the molten metal or by entrapment of a thin layer of slag or dross between the adjoining portions of molten metal. In a radiograph, cold shuts usually appear as smooth straight or curved lines.

### Unfused Chaplets and Inserts

Chaplets are metal devices used to support the core inside the mold or to separate parts of the mold to fit a wall thickness or other dimension of the casting. Chaplets are usually made of the same material as the casting and generally will be consumed when the molten metal comes in contact with them. If this does not occur or if only part of the chaplet melts, the condition that results is referred to as an *unfused chaplet*.

Unfused chaplets and other *unfused inserts* are special cases of cold shuts in that they exhibit a lack of fusion. However, in these cases it is lack of fusion of the casting metal with solid metal portions of the mold structure that had been intended to be fused into the

FIGURE 46. Cracks.



finished casting. Unfused chaplets appear as circular (Fig. 47) or short rectangular lines, depending on the shape of the chaplet post or as segments of circles or rectangles. Unfused inserts appear as straight or curved lines corresponding to all or part of the shape of the insert.

### Shifts

A *shift* is a mismatch of two parts of a casting at the parting line or an unintended variation in wall thickness because of a core having shifted during casting (Fig. 48). Both are often clearly evident on radiographs unless the shift is slight or only one wall is imaged on the radiograph.

### Misruns

A *misrun* is failure of the metal to fill the mold, either because of trapped gas or insufficient molten metal reaching a part of the mold cavity. Misruns (Fig. 49) are easy to identify radiographically and,

when the surface can be observed are visually apparent.

### Segregation

*Segregation* is a local deviation from the average composition of the metal in the casting. Certain alloys of some metals such as copper, often exhibit segregation because some constituents of the alloy freeze at a substantially higher temperature than other constituents. Radiographically, segregation may appear as mottled areas or banded areas of greater or lesser density, depending on the materials that have segregated. Radiographically detectable segregation may be of engineering concern, depending on its severity and location, as well as the intended use of the casting.

### Conclusion

There are many of structures, assemblies, materials and components that can be effectively radiographed. Interpretation, if it is to be meaningful, must only be attempted with a complete understanding of the following: (1) material, (2) part dimensions and configuration, (3) radiographic technique used, (4) processing used on test object, (5) applicable code, (6) acceptance standard and (7) other information desired from the examination.

The key to successful interpretation, after all other variables are optimized, rests with the individual doing the interpretation. Judgment must be based on complete knowledge of the radiographic process and a thorough understanding of the test object, coupled with extensive radiographic interpretation experience and training.

FIGURE 47. Unfused chaplet.



FIGURE 48. Core shift.

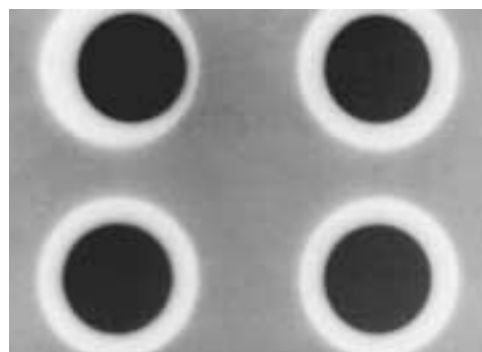
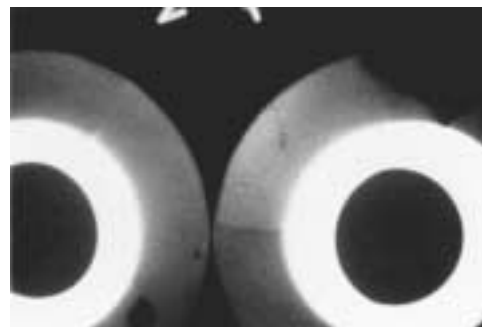


FIGURE 49. Misrun.



## References

1. Megling, R.C. and M.L. Abrams. *Relative Roles of Experience/Learning and Visual Factors on Radiographic Inspector Performance*. Research Report SRR73-22. San Diego, CA: Naval Personnel and Training Research Laboratory (June 1973).
2. Berock, J.F., R.G. Wells and M.L. Abrams. *Development and Validation of an Experimental Radiographic Reading Training Program*. Report AD-782-332. San Diego, CA: Navy Personnel Research and Development Center (June 1974).
3. Lusted, L.B. "Signal Detectability and Medical Decision-Making." *Science*. Vol. 171 (March 1971): p 1217-1219.
4. McMaster, R.C. and S.A. Wenk. *A Basic Guide for Management's Choice of Nondestructive Tests*. Special Technical Publication No. 112. Philadelphia, PA: American Society for Testing Materials (1951).
5. *Nondestructive Testing Handbook*, first edition. Vol. 1, Sections 1 and 4. Columbus, OH: American Society for Nondestructive Testing (1959).
6. McClung, R.W. "An Introspective View of Nondestructive Testing" (1974 ASNT Lester Honor Lecture). *Materials Evaluation*. Vol. 33, No. 2. Columbus, OH: American Society for Nondestructive Testing (February 1975): p 16A-19A, 43A-45A.
7. Hastings, C.H. "Nondestructive Testing As an Aid to Fracture Prevention Mechanics." *Journal of the Franklin Institute*. Vol. 290, No. 6. Philadelphia, PA: Franklin Institute (December 1970).
8. Yonemura, G.T. Report NBS-TW 1143. Washington, DC: National Bureau of Standards (June 1981).
9. *Nondestructive Testing Handbook*, second edition: Vol. 3, *Radiography and Radiation Testing*. Columbus, OH: American Society for Nondestructive Testing (1985): p 610-611.
10. *Nondestructive Testing Handbook*, second edition: Vol. 8, *Visual and Optical Testing*. Columbus, OH: American Society for Nondestructive Testing (1993): p 36.
11. Foster, B.E., S.D. Snyder, R.W. McClung and W.J. Godzinsky. "Development of High Voltage Radiography and Dual Microdensitometric Techniques for Evaluating Stressed Rock Specimens." *Materials Evaluation*. Vol. 31, No. 11. Columbus, OH: American Society for Nondestructive Testing (November 1973): p 229-236.
12. Quinn, R.A. and C.C. Sigl, eds. *Radiography in Modern Industry*, fourth edition. Rochester, NY: Eastman Kodak Company (1980): p 147-153.



# 9

## C H A P T E R

# Radiographic Film Development<sup>1</sup>

---

William E.J. McKinney, Naples, Florida (Parts 2 to 5)

Part 1 adapted from *Radiography in Modern Industry*. © 1980, Eastman  
Kodak Company. Reprinted with permission.

## PART 1. Radiographic Latent Image<sup>1,2</sup>

More information on the radiographic latent image, its formation and processing are available elsewhere.<sup>1-4</sup>

### Introduction

Throughout much of photography's history, the nature of the latent image was unknown. The first public announcement of Daguerre's photographic process was made in 1839 but it was not until 1938 that a satisfactory and coherent theory of photographic latent image formation was proposed.<sup>5</sup> That theory has been undergoing refinement and modification ever since.

Some of the investigational difficulty arose because latent image formation is actually a very subtle change in the silver halide grain. The process may involve the absorption of only one or, at most, a few photons of radiation and this may affect only a few atoms out of some  $10^9$  or  $10^{10}$  atoms in a typical photographic grain. Formation of the latent image, therefore, cannot be detected by direct physical or analytical chemical means.

A good deal was known about the latent image's physical nature. It was understood, for example, that the latent image was localized at certain discrete sites on the silver halide grain. If a photographic emulsion was exposed to light, developed, fixed and then examined under a microscope (Fig. 1), the change of silver halide to metallic silver was visible at only a limited number places on the crystal. Because small amounts of silver sulfide on the surface of the grain were known to be necessary for high photographic sensitivity, it seemed likely that the spots where the latent image formed were also concentrations of silver sulfide.

It was further known that the material of the latent image was probably silver. For one thing, chemical reactions that oxidized the silver also destroyed the latent image. It was also a common observation that photographic materials given prolonged exposure to light darkened spontaneously, without the need for development. This darkening was known as the printout image. The printout image contained enough material to be identified chemically as metallic silver. By microscopic

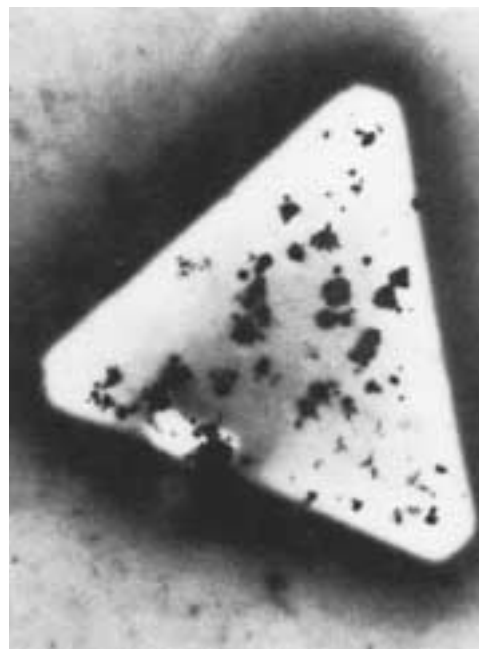
examination, the silver of this image was also discovered to be localized at certain discrete areas of the grain (Fig. 2), just as the latent image.

Thus, the process that made an exposed photographic grain capable of transformation into metallic silver (by the mild reducing action of a developer) involved a concentration of silver atoms

FIGURE 1. Localized sites on grains.



FIGURE 2. Localized silver in printout image. This is a T grain, a form used with soft intensifying screens.





at one or more discrete sites on the photographic grain.

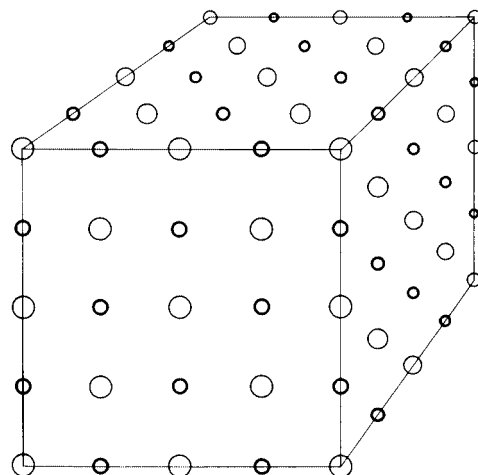
Any theory of latent image formation must account for the way that light photons, absorbed at random within the grain, can produce isolated aggregates of silver atoms. Most current theories of latent image formation are modifications of the mechanism proposed by R.W. Gurney and N.F. Mott in 1938.<sup>5,6</sup> To understand the Gurney-Mott theory of the latent image, it is necessary to consider the structure of crystals, in particular, the structure of silver bromide crystals.

### Silver Bromide

When solid silver bromide is formed, as in a photographic emulsion, the silver atoms each give up one orbital electron to a bromine atom. The silver atoms, lacking one negative charge, have an effective positive charge and are known as silver ions ( $\text{Ag}^+$ ). The bromine atoms, on the other hand, have gained an electron and become bromine ions ( $\text{Br}^-$ ). The plus and minus signs indicate, respectively, one fewer or one more electron than the number required for electrical neutrality of the atom.

A crystal of silver bromide is a regular, cubic array of silver and bromine ions, as shown in Fig. 3. It should be emphasized that the magnification used in the illustration is very high; the average grain in an industrial film may be about 0.001 mm ( $4 \times 10^{-5}$  in.) in diameter. Despite its small size, the grain will contain several billion ions.

FIGURE 3. Silver bromide crystal is rectangular array of silver and bromine ions.



#### Legend

- = silver ( $\text{Ag}^+$ ) ion
- = bromine ( $\text{Br}^-$ ) ion

A crystal of silver bromide in a photographic emulsion is not perfect. First, within the crystal, there are silver ions that do not occupy the lattice positions shown in Fig. 3 but rather are in the spaces between. These are known as interstitial silver ions (Fig. 4). The number of interstitial silver ions is small compared to the total number of ions in the crystal. In addition, there are distortions of the uniform crystal structure. These may be (1) foreign molecules, within or on the crystal, produced by reactions with other components of the emulsion, or (2) distortions of the regular array of ions shown in Fig. 3. These anomalies are classed together and called latent image sites.

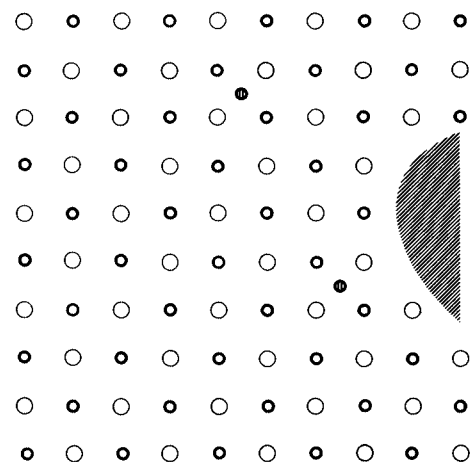
### Radiographic Latent Images

In industrial radiography, the image forming effects of X-rays and gamma rays, rather than those of light, are of primary interest.

The agent that actually exposes a film grain (a silver bromide crystal in the emulsion) is not the X-ray photon itself but rather the electrons (photoelectric and Compton) resulting from an absorption event.

The most striking difference between X-ray and visible light exposures arises from the difference in the amounts of

FIGURE 4. Plan view of layer of ions of crystal latent image site is shown schematically. Two interstitial silver ions are indicated.



#### Legend

- = silver ( $\text{Ag}^+$ ) ion
- = bromine ( $\text{Br}^-$ ) ion
- ⦿ = interstitial silver ion
- /// = latent image site

energy involved. The absorption of a single photon of light transfers a very small amount of energy to the crystal — only enough energy to free a single electron from a bromide ( $\text{Br}^-$ ) ion. Several successive light photons are required to make a single grain developable, that is, to produce in or on it a stable latent image.

The passage of an electron through a grain can transmit hundreds of times more energy than the absorption of a light photon. Even though this energy is used inefficiently, the amount is sufficient to make the grain developable.

In fact, a photoelectron or Compton electron can have a fairly long path through a film emulsion and can render many grains developable. The number of grains exposed per photon interaction varies from one (for X-radiation of about 10 keV) to 50 or more (for a 1 MeV photon).

For higher energy photons, there is low probability for a single interaction that transfers all the photons' energy. Most commonly, high photon energy is imparted to several electrons by successive Compton interactions. Also, high energy electrons usually pass out of a film emulsion before all of their energy is transferred. For these reasons, there are, on the average, five to ten grains made developable per photon interaction at high energy.

For lower exposure values, each increment of energy exposes (on the average) the same number of grains. This, in turn, means that a curve of net density versus exposure is a straight line passing through the origin (Fig. 5). This curve is nonlinear only when the exposure is so great that appreciable energy is wasted on previously exposed grains. For commercially available fine grain films, for example, the density versus exposure curve may be essentially linear up to densities of 2.0 or higher.

The fairly extensive straight line relation between exposure and density is very useful for determining exposure values and for interpretation of densities observed on the resulting films.

If the curves shown in Fig. 5 are replotted as characteristic curves (density versus the logarithm of exposure), both characteristic curves are the same shape (Fig. 6) and are separated along the log exposure axis. The similarity in the shape has been experimentally observed for conventional processing and many commercial photographic materials.

Because a grain is completely exposed by the passage of an energetic electron, all X-ray exposures are, as far as the individual grain is concerned, extremely short. The actual time that an electron is within a grain depends on the electron velocity, the grain dimensions and the squareness of the hit. (In the case of light, the exposure time for a single grain is the interval between the arrival of the first photon and the arrival of the last photon required to produce a stable latent image.)

FIGURE 5. Typical net density versus exposure curves for direct X-ray exposures.

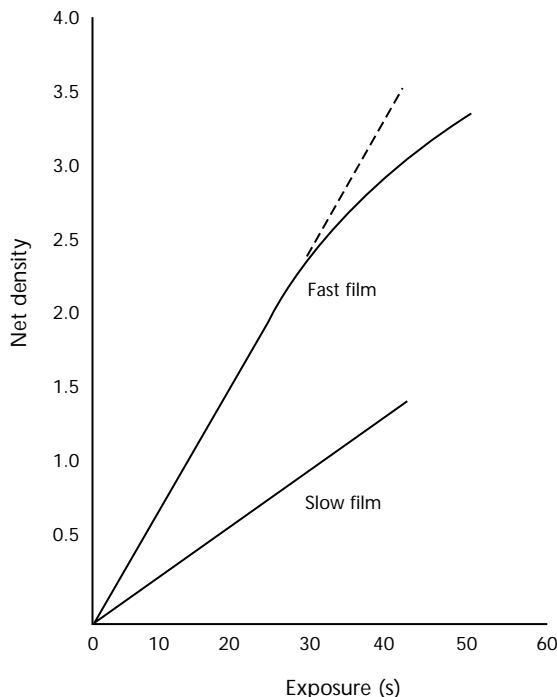
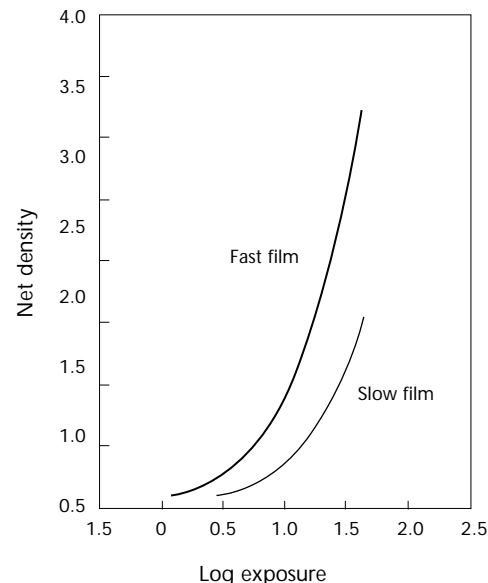


FIGURE 6. Characteristic curves plotted from data of Fig. 9.



## Development

Many materials discolor with exposure to light (some kinds of wood and human skin are examples) and could be used to record images. Most of these materials react to light exposure on a 1:1 basis: one photon of light alters one molecule or atom.

In the silver halide system of radiography, however, a few atoms of photolytically deposited silver can, by development, be made to trigger the subsequent chemical deposition of some  $10^9$  or  $10^{10}$  additional silver atoms, resulting in an amplification factor on the order of  $10^9$  or greater. This amplification process can be performed at a time convenient to the user and, with sufficient care, can be uniform and reproducible enough for quantitative radiation measurements.

Development is essentially a chemical reduction in which silver halide is reduced from the molecular state to elemental metallic silver. To retain the photographic image, however, the reaction must be limited largely to those grains that contain a latent image — that is, to those grains that have received more than a prescribed minimum radiation exposure.

Compounds that can be used as photographic developing agents are those in which the reduction of silver halide to metallic silver is catalyzed (speeded up) by the presence of metallic silver in the latent image. Those compounds that reduce silver halide, in the absence of a catalytic effect by the latent image, are not suitable developing agents because they produce a uniform overall density on the processed film.

Many practical developing agents are relatively simple organic compounds (Fig. 7) and their activity is strongly

dependent on molecular structure and composition. The developing activity of a particular compound may often be predicted from a knowledge of its structure.

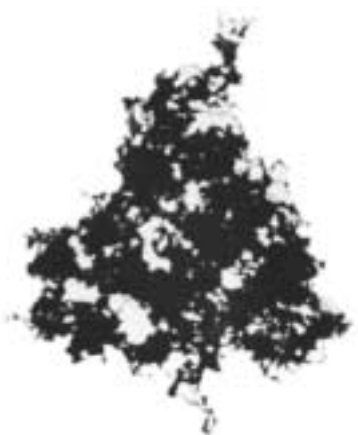
The simplest concept of the latent image's role in development is that it acts merely as an electron conducting bridge, by which electrons from the developing agent can reach the silver ions on the interior face of the latent image. Experiment has shown that this simple concept is inadequate for explaining many phenomena encountered in practical film development.

The exact mechanisms of most developing agents are relatively complex. A molecule of developing agent can easily give up an electron to an exposed silver bromide grain (one that carries a latent image) but not to an unexposed grain. This electron combines with a silver ion ( $\text{Ag}^+$ ) in the crystal, neutralizing the positive charge and producing an atom of metallic silver. The process can be repeated many times until all the billions of silver ions in a photographic grain have been turned into metallic silver.

Development and latent image formation involve the union of a silver ion and an electron to produce an atom of metallic silver. In latent image formation, the electron is freed by the action of radiation and combines with a silver ion. In development, the electrons are supplied by a chemical electron donor and combine with the silver ions of the crystal lattice.

The physical shape of the developed silver has little relation to the shape of the silver halide grain from which it is derived. Very often the metallic silver has a tangled, filamentary form, the outer boundaries of which can extend far beyond the limits of the original silver halide grain. The mechanism for this filament formation is still in doubt. It is probably associated with another phenomenon, where filamentary silver is produced by vacuum deposition of silver atoms in the vapor phase onto suitable nuclei.

FIGURE 7. Electron micrograph of developed silver bromide grain.



## Contrast

The slope of the characteristic curve for film can change continuously along its length. It has been shown qualitatively that a density difference, corresponding to a difference in specimen thickness, depends on the region of the characteristic curve where the exposure falls. The steeper the slope of the curve in this region, the greater the density difference and hence the greater the visibility of detail (assuming an illuminator bright enough so that a

reasonable amount of light is transmitted through the radiograph to the eye of the observer.)

The slope of a curve at any particular point may be expressed as the slope of a straight line drawn tangential to the curve at that point. When applied to the characteristic curve of a photographic material, the slope of such a straight line is called the gradient of the material at that particular density.

Consider a specimen with two slightly different thicknesses that transmit slightly different radiation intensities to the film; there is a small difference in the logarithm of the relative exposure to the film in the two areas. Assume that, at a certain kilovoltage, the thinner section transmits 20 percent more radiation than the thicker section. The difference in logarithm of relative exposure ( $\Delta \log E$ ) is 0.08 and is independent of the milliamperage, exposure time or distance from source to film.

If this specimen is now radiographed with an exposure that puts the developed densities on the toe of the characteristic curve (where the gradient is 0.8), the intensity difference of 20 percent is represented by a density difference of 0.06 (Fig. 8). If the exposure is such that the densities fall on the curve where the

gradient is 5.0, the 20 percent intensity difference results in a density difference of 0.4.

A minimum density is often specified for radiographs. This is not because of any virtue in a particular density but rather because of the gradient associated with that density; the minimum useful density is that density at which the minimum useful gradient is obtained. In general, gradients lower than 2.0 should be avoided whenever possible.

The ability of the film to amplify subject contrast is especially significant in radiography, where penetrating radiations of higher energy and shorter wavelength produce low subject contrast. Good radiographs depend on the enhancement of subject contrast by the film.

The gradients of film curves have been calculated from the characteristic curves and are plotted in Fig. 9 against the density. The gradients of films X and Y increase continuously, up to the highest densities convenient for radiography.

The gradient versus density curve of film Z is different from the others in that the gradient increases, then becomes constant over the range of 1.5 to 2.5, beyond which it decreases. With this film, the greatest density difference (corresponding to a small difference in transmission of the specimen) is obtained in the middle range of densities. The maximum, as well as the minimum, useful density is governed by the minimum gradient that can be tolerated.

It is often useful to have a single number to indicate the contrast property

FIGURE 8. Characteristic curve of typical industrial radiographic film. Density differences corresponding to 20 percent difference in radiographic exposure.

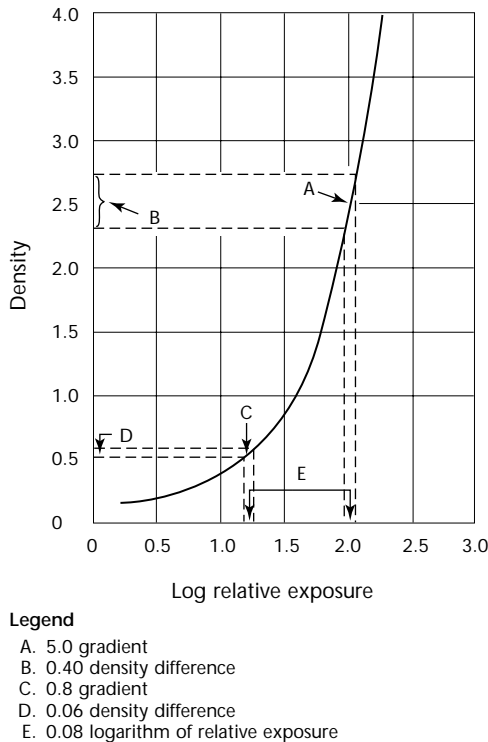
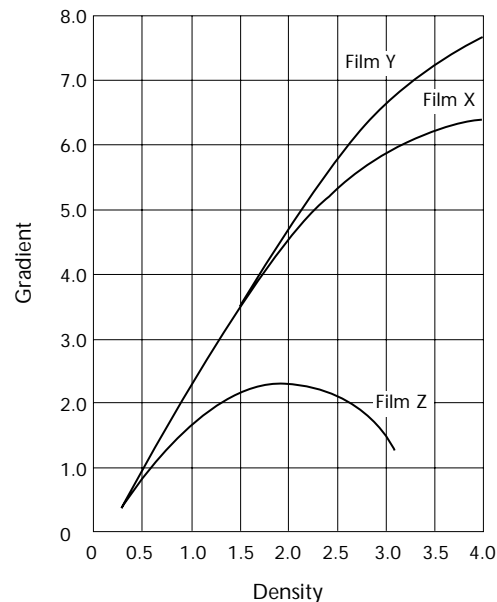


FIGURE 9. Gradient versus density curves of typical industrial radiographic film.



of a film. This need is met by a quantity known as the average gradient, defined as the slope of a straight line joining two points of specified densities on the characteristic curve (Table 1).

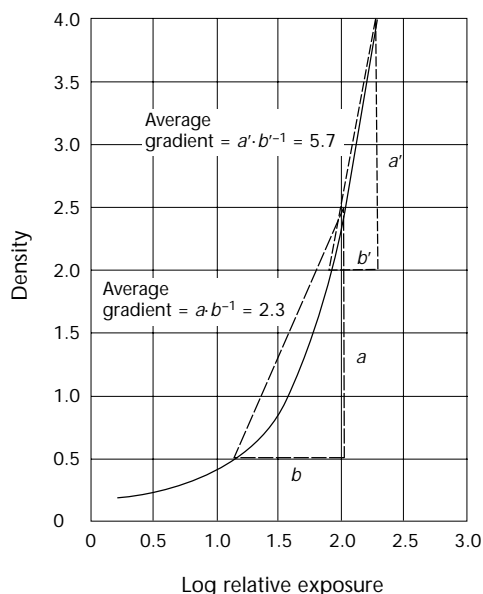
These two densities are often the maximum and minimum useful densities for a particular application. The average gradient indicates the average contrast properties of the film over this useful range; for a given film and development technique, the average gradient depends on the density range chosen.

Experiments have shown that the shape of the characteristic curve is, for practical purposes, largely independent of the radiation wavelength (Fig. 10 for the characteristic curve of a typical industrial film). Therefore, a characteristic curve based on any radiation quality may be applied to exposures based on another quality, to the degree of accuracy usually required in practice; the same is true for values of gradient or average gradient derived from the curve.

TABLE 1. Average gradient.

Film	Density Range	
	0.5 to 2.5	2.0 to 4.0
X	2.3	5.7
Y	2.6	6.3
Z	1.7	—

FIGURE 10. Characteristic curve of typical industrial radiographic film. Average gradient is calculated over two density ranges.



The influence of kilovoltage or gamma ray quality on contrast in the radiograph, therefore, is the result of its action on the subject contrast and only very slightly, if at all, the result of any change in the contrast characteristics of the film.

Radiographic contrast can also be modified by choosing a film of different contrast or by using a different density range with the same film. Contrast is also affected by the degree of development but in industrial radiography, films are developed to their maximum or nearly maximum contrast.

In the early stages of development, both density and contrast increase quite rapidly with time of development. In manual processing, the minimum recommended development time gives most of the available density and contrast. With certain of the direct film types, somewhat higher speed and, in some cases, slightly more contrast are gained by extending the development; in no case should the maximum time recommended by the manufacturer be exceeded because silver halide molecules may break down and produce *fog*.

A special situation arises when, for technical or economic reasons, there is a maximum allowable exposure time. In such cases, an increase in kilovoltage increases the radiation intensity penetrating the specimen and the film will contain a higher density. This may result in a decrease in radiographic contrast.

Table 2 lists densities obtained through 13 to 16 mm (0.5 to 0.6 in.) sections, using an exposure of 8 mA·min. These data show that, when the exposure time is fixed, the density difference between the two sections increases. The contrast also increases as the kilovoltage is raised.

The improvement in detail visibility occurs in spite of the decrease in subject contrast (caused by the increase in kilovoltage) and is the direct result of using higher densities where the film gradient is higher. In this particular case, the film contrast increases (as a result of increased density) faster than the subject contrast decreases (as a result of increased kilovoltage).

TABLE 2. Densities obtained through 13 to 16 mm (0.5 to 0.6 in.) steel sections by using exposure of 8 mA·min.

Energy (kV)	Density		Radiographic Contrast	Relative Radiographic Contrast
	$D_B$	$D_A$		
120	0.50	0.27	0.23	20
140	1.20	0.67	0.53	46
160	2.32	1.30	1.02	88
180	3.48	2.32	1.16	100



## Influence of Film Speed

It has been shown that the film contrast depends on the shape of the characteristic curve. The other significant value obtained from the characteristic curve is the relative speed governed by the location of the curve, along the log E axis, in relation to the curves of other films.

The spacing of the curves along the log E axis arises from differences in relative speed; the curves for the faster films lie toward the left, slower films toward the right. From these curves, relative exposures for producing a fixed photographic density can be determined. For some industrial radiographic purposes, a density of 1.5 is an appropriate level at which to compute relative speeds. However, the increasing trend toward high densities, with all radiographs viewed on high intensity illuminators, makes a density of 2.5 more suitable for most industrial radiography. Relative speed values derived from characteristic curves, for two given density levels, are shown in Table 3, where film X has been assigned a relative speed of 100 at both densities. Note that the relative speeds computed are not the same; this is because of the differences in curve shape from one film to another.

Although the shape of the characteristic curve is practically independent of changes in radiation quality, the location of the curve along the log relative exposure axis, with respect to the curve of another film, does depend on radiation quality. Thus, if characteristic curves were prepared at a different kilovoltage, the curves would be differently spaced — that is, the films would have different speeds relative to the film that was chosen as a standard of reference.

## Relation of Density to Exposure

The most common way of expressing the relation between film response and radiation intensity is the characteristic curve (the relation between the density

and the logarithm of the exposure). If density is plotted against relative exposure to X-rays or gamma rays, in many cases there is a linear relation over a more or less limited density range (Fig. 11). If net density (density above base density and fog), rather than gross density, is plotted against exposure, the straight line passes through the origin.

The linear relation cannot be assumed but must be checked for the particular application because of variations in film and processing conditions. The linear relation between density and exposure may be extremely useful in the interpretation of diffraction patterns and the evaluation of radiation monitoring films, provided that the limited linear range of the curve is considered.

## Effect of Development Time on Speed and Contrast

Although the shape of the characteristic curve is relatively insensitive to changes in X-ray or gamma ray quality, it is affected by changes in degree of development. Degree of development, in turn, depends on the type of developer, its temperature and its activity; the time of development increases the speed and contrast of any radiographic film. If, however, development is carried too far, the contrast of the film, based on a certain net density, ceases to increase and

FIGURE 11. Density versus exposure curve for typical industrial radiographic film exposed to direct X-rays or with lead screens.

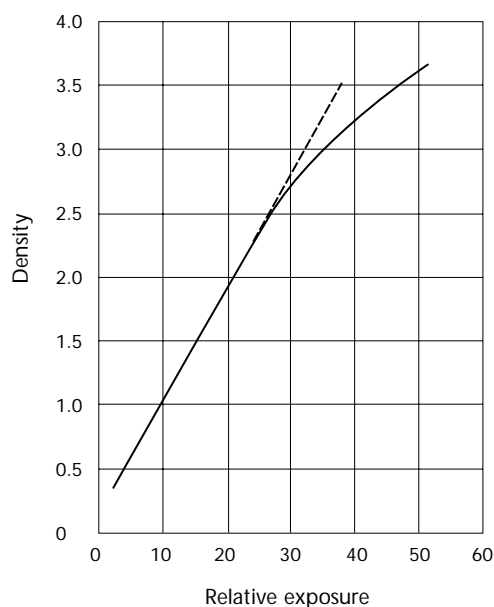


TABLE 3. Relative speed values.

Film	Density = 1.5		Density = 2.5	
	Relative Speed	Relative Exposure	Relative Speed	Relative Exposure
X	100	1.0	100	1.0
Y	24	4.2	26	3.9
Z	250	0.4	150	0.7



may even decrease. In this case, fog increases and contrast may decrease.

## Graininess

Graininess is defined as the visual impression of nonuniformity in the density of a radiographic (or photographic) image. With fast films exposed to high kilovoltage radiation, graininess is easily visible with unaided vision; with slow films exposed to low kilovoltage X-rays, moderate magnification may be needed. In general, graininess increases with increasing film speed and with increasing radiation energy.

The clumps of developed silver responsible for the impression of graininess do not each arise from a single developed photographic grain. The particle of black metallic silver caused by the development of a single photographic grain in an industrial radiographic film is rarely larger than  $1.0\text{ }\mu\text{m}$  ( $4 \times 10^{-5}\text{ in.}$ ) and is usually less. The unaided human eye cannot see an individual grain.

The visual impression of graininess is caused by the random, statistical grouping of these individual silver particles. Each quantum (photon) of X-radiation or gamma radiation absorbed in the film emulsion exposes one or more tiny crystals of silver bromide. These absorption events occur at random. Even in a uniform radiographic beam, the number of absorption events will differ from one small area of the film to the next, for purely statistical reasons. Thus, the exposed grains will be randomly distributed and their numbers will have a statistical variation from one area to the next.

With a very slow film, it might be necessary for 10 000 photons to be absorbed in a small area to produce a density of, for example, 1.0. With an extremely fast film it might require only 100 photons in the same area to produce the same density. When only a few photons are required to produce the density, the random positions of the absorption events become visible in the processed film as film graininess. On the other hand, the more X-ray photons that are required, the less noticeable the graininess in the radiographic image, when all other conditions are equal.

In general, the silver bromide crystals in a slow film are smaller than those in a fast film and thus will produce less light absorbing silver when they are exposed and developed. At low kilovoltages, one absorbed photon will expose one grain, of whatever size. Thus, more photons will have to be absorbed in the slower film

than in the faster film to produce a particular density.

The increase in graininess with increasing kilovoltage can also be understood on this basis. At low kilovoltages, each absorbed photon exposes one photographic grain; at high kilovoltages, one photon will expose many grains. At high kilovoltages, then, fewer absorption events are required to produce a given density. Fewer absorption events, in turn, mean a greater relative deviation from the average and hence greater graininess.

## Screens

The above discussion of graininess applies also to exposures made with lead screens. As stated earlier, the grains in a film emulsion are exposed by high speed electrons. Silver bromide cannot distinguish between electrons from an absorption event within the film emulsion and those from a lead screen.

The quantum mottle observed in radiographs made with fluorescent intensifying screens has a statistical origin similar to that of film graininess. In this case, however, the number of photons absorbed in the screens is significant. The grain size of a fluorescent crystal is greater than that of silver bromide, so a spread function also contributes to nonuniformity.

## X-Ray Spectral Sensitivity

The shape of the characteristic curve of a radiographic film is unaffected, for practical purposes, by the wavelength of the exposing X-rays or gamma rays. However, the sensitivity of the film (the number of coulombs per kilogram, or roentgens, required to produce a given density) is strongly affected by the wavelength of the exposing radiation.

Figure 12 shows the number of roentgens needed to produce a density of 1.0, for a particular radiographic film and specific processing conditions (exposures were made without screens).

The spectral sensitivity curves for all radiographic films have roughly the same features as the curves shown in Fig. 12. Details, among them the ratio of maximum to minimum sensitivity, differ with film type.

The spectral sensitivity of a film or differences in spectral sensitivity between two films, need rarely be considered in industrial radiography. Usually such changes in sensitivity are automatically taken into account in the preparation of exposure charts and tables of relative film speeds. The spectral sensitivity of a film is very important in radiation monitoring,

because here an evaluation of the number of roentgens incident on the film is required.

ISO 11699-1<sup>9</sup> are examples of two film classifications. Table 4 compares films listed according to the ASTM classification with the corresponding ISO classification level.<sup>7</sup>

## Film Classification

Radiographic film systems can be classified on the basis of their image quality performance. The classification of films provides a means of specifying radiographic film and film systems without mentioning film brand names.

This specifying of film is according to measurable physical characteristics such as the minimum film gradient at film density 2.0, minimum film gradient at film density 4.0, maximum granularity and the minimum ratio of film gradient to granularity.<sup>7</sup> ASTM E 1815<sup>8</sup> and

## Reciprocity Law Failure

The Bunsen-Roscoe reciprocity law states that the density of a photochemical reaction depends only on the product of the radiation intensity and the duration of the exposure and is independent of the absolute values of either quantity. Applied to radiography, this means that the developed density in a film depends only on the product of X-ray or gamma ray intensity reaching the film and the time of exposure.

FIGURE 12. Typical X-ray spectral sensitivity curve of radiographic film, showing radiation required to produce density of 1.0 for various radiation qualities.

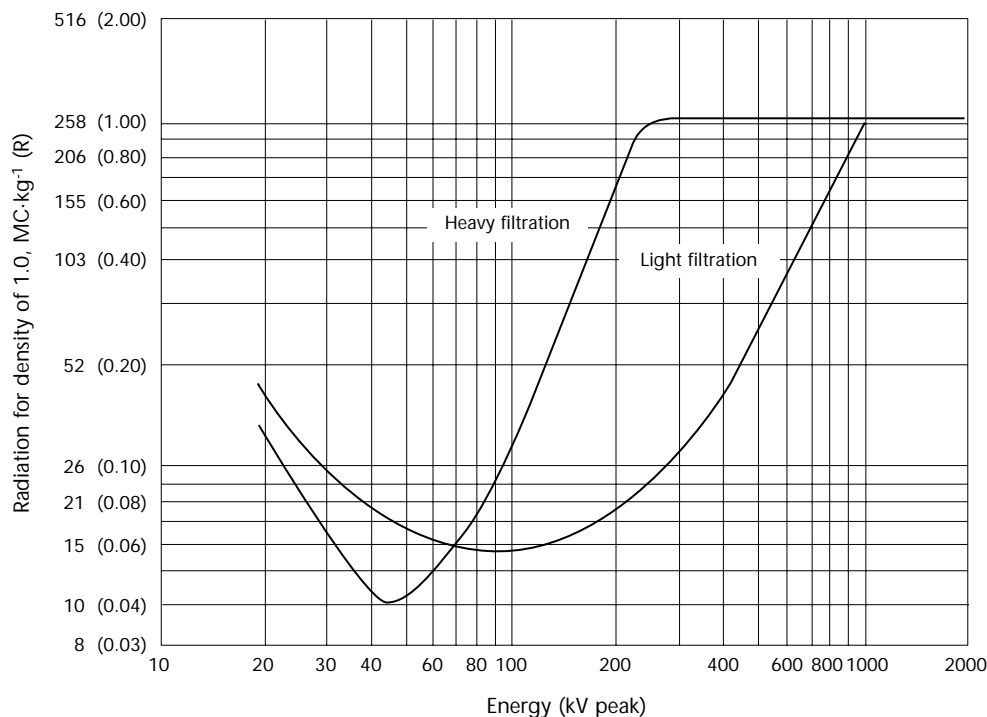


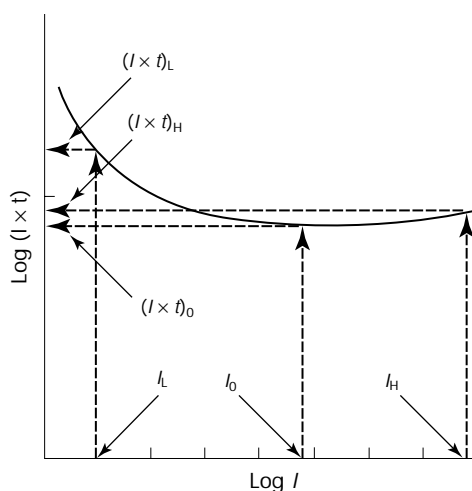
Table 4. Classification of industrial X-ray films.<sup>7</sup> *D* = density.

Image Quality Factor			Classification		Minimum Gradient		Granularity	Ratio of Gradient to Granularity
Speed	Contrast	Granularity	ASTM <sup>8</sup>	ISO <sup>9</sup>	<i>D</i> = 2.0	<i>D</i> = 4.0	<i>D</i> = 2.0	<i>D</i> = 2.0
—	—	—	special	T1	4.5	7.5	0.018	300
Low	very high	very low	I	T2	4.1	6.8	0.028	150
Medium	high	low	II	T3	3.8	6.4	0.032	120
High	medium	high	III	T4	3.5	5.0	0.039	100

The reciprocity law is valid for direct X-ray or gamma ray exposures or those made with lead foil screens, over a range of radiation intensities and exposure times much greater than those normally used in practice. Reciprocity fails, however, for exposures to light and therefore for exposures using fluorescent intensifying screens. Figure 13 shows a conventional reciprocity curve.

The vertical axis in Fig. 13 has been considerably expanded to make the curvature more apparent. The logarithms of the exposures that produce a given density are plotted against the logarithms of the individual intensities. It can be seen that, for a particular intensity, the exposure required to produce the given density is a minimum. It is for this intensity of light that the film is most efficient in its response.

FIGURE 13. Reciprocity curve for light exposures. Corresponding curve for direct radiographic or lead screen exposures would be straight line parallel to  $\log I$  axis.



#### Legend

$I$  = intensity of light or electromagnetic radiation  
 $O$  = subscript denoting particular value  
 $H$  = subscript denoting higher value  
 $L$  = subscript denoting lower value  
 $t$  = exposure duration

## PART 2. Chemistry of Film Radiography<sup>3</sup>

Most radiographers are highly skilled, motivated and generally interested in the challenges of creating an image on film. Much training goes into being able to select the correct exposure. However, the image or exposure is useless until it is developed. This invisible image is called a *latent image*. It is through the chemical process called development that the hidden (latent) image is transformed into the useful visible image. For a radiographer or laboratory personnel to know only about latent image formation and not visible image formation is to know only half of film radiography. Film radiographers must be knowledgeable and skilled in both areas if they are to control the efficiency, economics and the quality they are responsible for.

The basic steps in processing are (1) development (to transfer the latent image into the visible image); (2) fixation (to stop development and remove all remaining underdeveloped crystals and unexposed crystals); (3) washing (to remove fixer to ensure archival quality); and (4) drying.

All of the chemical reaction steps are controlled by elements of (1) time (immersion time in solution); (2) temperature (of the solution); and (3) activity (replenishment, agitation, moisture).

Time, temperature and activity, in turn, depend on six electromechanical systems: (1) transport (time factor); (2) temperature control; (3) replenishment; (4) circulation and filtration (agitation, uniformity of chemicals), (5) electrical systems; and (6) dryer systems. These six electromechanical systems constitute the processor (manual or automatic), which support a seventh system: chemistry (developer, fixer and wash).

Though the developer has its own relationship of time, temperature and activity (as do the fixer and wash), one of the controlling factors of the developer is the fixer. If the fixer is not washed out properly the film is damaged. Also, if the fixer is weak, the developer is not neutralized quickly and development is protracted. Thus the chemistry system includes developer, fixer and wash.

How does the radiographer know that the processor is working right? How is it known that the processing is correct? Will the radiographer get a good radiograph? If

a technically accurate exposure (exposed radiograph with a latent image) is put into a processor, will it come out okay? Will it be free of artifacts and have the correct density and contrast? What if the radiographer is unsure that the exposure technique is optimal or that the quality achieved on the visible film is the result of bad exposure, bad processing or both? The answer to all of these questions, which are quite common in industrial radiography, is in two parts.

1. There is no condition better than correct exposure with full development. Overdevelopment, underdevelopment, overexposure and underexposure are inappropriate and inefficient. The processing completes what the exposure started; it cannot add information.
2. The sum total of the radiographer's efforts is to produce a useful visible image, whose density levels and contrast may be measured. To monitor and control processing and the total visible image production, *sensitometry* is used. *Sensitometry* is the quantitative measure of the film's response to exposure and development.

The total value of the visible image is the result of exposure and development. To know only how to make exposures is to know only half of the technology required.

### Latent Image

When a radiographic film is exposed to a radiation energy source, it forms what is called a *latent image*. When the film is processed in chemicals, a visible image appears. This is, in its simplest terms, the chemistry of radiography. Because the chemistry actually allows radiography to exist, however, it is most important that it be better understood. *Radiographic chemistry* means the total concept of the chemical constituents and mechanisms of film, processing chemistries and the reactions during exposure.

## Chemistry of Film

### Film Base

Modern plastic bases such as polyethylene terephthalate have important features: strength, clarity, superior transport characteristics, stability and the fact that they do not absorb water.

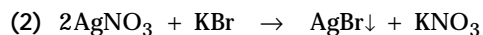
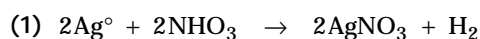
Polyester bases require an adhesive so that the emulsion will adhere properly to the smooth surface. The adhesive is applied to both sides of the base as a substrate layer. The tint, composed of a delicate balance of many dyes, is usually found as an integral part of the base.

### Film Emulsion

Once the film base is made ready to receive the emulsion, the emulsion is applied to both sides of the base. The emulsion is composed of a silver halide recording media and a binder of gelatin manufactured from collagen. Collagen is a naturally occurring fibrous protein and is a major component of animal skin, bone and certain tissues. Collagen is treated with lime or an acid that breaks down the protein into a very pure gelatin. The gelatin has a great affinity for water; that is, it can absorb great quantities of water by swelling and is very important in film processing.

To the gelatin is added a sensitized silver halide. Silver halide is usually silver bromide. Other useful members of the halide group are chlorine and iodine. The halide might also be a combination such as chlorobromide or iodobromide.

Silver bromide is formed in this way:



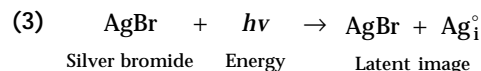
The silver bromide is sensitized with a sulfur compound and mixed into the gelatin. Several washing operations follow until the emulsion is ready to be coated onto the base. And, of course, all of these steps must be carried out in total darkness.

## Exposing of Film

### Latent Image Formation

Gurney and Mott developed a theory that is the accepted basis for explaining image formation.<sup>4</sup> In the above formula, the latent image is composed of metallic silver and the crystalline silver bromide is

undisturbed. Gurney and Mott found that crystals (silver bromide) sensitized with a foreign sulfur compound were easier to expose. They called these sensitizers *sensitivity specks*. At the moment of exposure the energy of exposure initiates an autocatalytic (self-completing) reaction:



where  $\text{Ag}_i^{\circ}$  is interstitial silver. The crystal is coated with an excess of bromide ions containing excess electrons. At exposure, some of these electrons are released and are trapped at the sensitivity specks — now termed *sensitivity sites*. The bromine becomes gas and is absorbed in the gelatin. Because the sensitivity site contains numerous electrons, it is of a negative value and exerts a magnetic pull on silver ions floating in the crystal lattice structure. This unbonded silver, which needs one or more electrons and is termed *interstitial silver* ( $\text{Ag}_i^{\circ}$ ), will deposit and thereby constitute a *development site*. Without this site the crystal will not develop.

## Chemistry of Processing

After the exposure has been made and before development, both exposed and unexposed silver bromide crystals exist within the film emulsion. This is the *latent image*. The exposed crystals will be made visible as black metallic silver by reducing the structural silver bromide to simple metallic silver and by clearing away the *unexposed* crystals. This action is the basis of chemical processing and has an important role in the field of radiography.

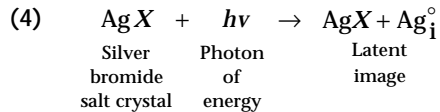
In this discussion *speed* denotes the film's sensitivity, that is, its response to exposure;  $D_{\text{max}}$  is the maximum density for the maximum exposure;  $D_{\text{min}}$  is the minimum density for the minimum exposure; and *contrast* is a difference in densities for a range of exposures.

### Development

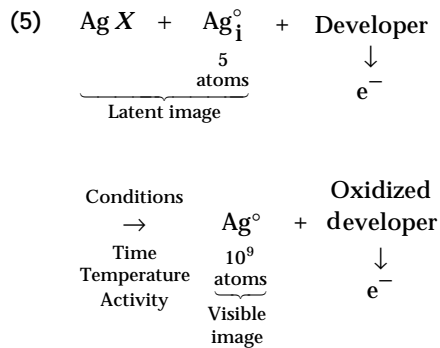
The film emulsion is now composed of two types of crystals: unexposed and exposed. The developer selectively seeks out the exposed crystals containing a development site made up of five atoms of interstitial silver and converts them to black metallic silver. The entire crystal becomes metallic silver and now contains  $1 \times 10^9$  atoms of silver. The amplification factor of about  $10^9$  is the result of the oxidation reduction reaction whereby the developer is consumed (oxidation) and

the crystal is reduced from a compound to a simple element (reduction).

Equations 4 and 5 describe this sequence of events:



and



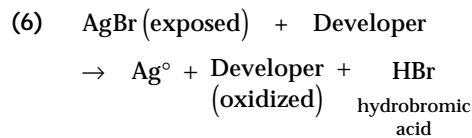
where  $\text{Ag}_i^\circ$  is interstitial silver and  $X$  is one or more halides, such as chlorine, iodine, bromine or hybrids.

This reaction is controlled, as are all chemical reactions, by elements of time, temperature and activity. To keep the developer chemical strength (activity) at a constant level a manual or automatic replenishment system is used. Constituents of a typical radiographic developer can be seen in Table 5.

The primary function of the developer is to reduce silver ions to black metallic silver. However, there are five criteria for a modern developing agent:

1. It should provide a reducing agent for silver ions; that is, a source of electrons to reduce silver ions ( $\text{Ag}^+$ ) to black metallic silver ( $\text{Ag}^\circ$ ).
2. It should provide reduction of the exposed silver halide in preference over the unexposed crystals.
3. It should be water soluble or soluble in an alkaline media.
4. It should be reasonably stable and resistant to aerial oxidation.
5. It should yield colorless, soluble oxidation products.

**Reducing Agents.** Developers composed of methylaminophenol sulfate and hydroquinone are referred to as *MQ developers*. Modern developers are composed of phenidone and hydroquinone and are called *PQ developers*. The basic reaction might be written:



It is important to notice that the developer is oxidized. Oxidized developer becomes a deep brown color and this indicates exhaustion. Because the rate of development is pH dependent, pH is standardized with buffers against the effect of different water supplies and working conditions. *Buffering* means that the formulas are designed so that additional hydrogen or hydroxyl groups cause an internal rearrangement that prevents any appreciable alteration of pH.

The single most important function of the developer is the action of the reducing agents. The reducing agent or developing agent supplies the electrons necessary to enable the essential reaction of development to occur.

In addition to aiding and controlling the developer agent reactions under normal conditions, buffering agents also retard the influences of oxidation and different solvent conditions. The general hardness solvent is tap water, which varies in pH and general hardness depending on the city.

**Solvent.** Water is the solvent and is over 80 percent of the developer solution. Water should be of *drinking quality* with a carbonate hardness of between 40 and 150 parts per million. Metal ions in water can accelerate developer oxidation and result in high fog.

**Temperature Influence on Developer Action.** Developing agents are temperature dependent, resulting in temperature coefficients. There is about a  $\pm 0.05$  pH change per each temperature difference of  $10^\circ\text{C}$  ( $18^\circ\text{F}$ ). Sensitometrically the optimal developer temperature occurs when it produces the maximum or a specific gamma (contrast) level. *Optimal* means achieving the best levels of speed,

TABLE 5. Developer components.

Chemical	General Function	Specific Function
Phenidone	reducer	quickly produces gray tones
Hydroquinone	reducer	slowly produces blacks
Sodium carbonate	activator	provides alkaline media; swells emulsion
Potassium bromide	restrainer	prevents reduction of unexposed crystals
Sodium sulfite	preservative	maintains chemical balance
Water	solvent	dissolves chemicals
Gluteraldehyde	hardener	permits transport of films by controlling swelling



$D_{\max}$  and  $D_{\min}$  for optimum contrast. Deviation in either direction because of temperature change will generally result in lower contrast (see Fig. 14).

**Agitation.** Agitation increases both the rate of development and the rate of reduction. To clarify, development rate is increased because agitation permits a constant mixing of the solution and aids in washing bromine and the oxidized developers out of the emulsion. Agitation aids reduction by constantly swirling the reducing agents in and around the silver halide crystal lattice. When replenishment systems are used, agitation helps keep the stronger replenishment solution properly mixed into the working solution.

Agitation also helps in the filtration of reaction byproducts, mostly gelatin, by circulating the chemicals through a filter. Finally, agitation keeps the temperature uniform.

**Replenishment.** Chemically defined, *replenishment* is only a replacement of quantity, of volume, a maintenance of a preset amount. *Regeneration* is the second function of an adequate replenishment system and its job is to ensure consistent activity by a replacement of spent chemicals. It is the purpose of developer regeneration to ensure that the characteristics of the finished radiograph — its speed, contrast level, fog level and maximum density — remain substantially constant.

A good replenishment and regeneration system will prolong the life of chemistries, aid in the maintenance of consistent quality and may lead to improved sensitometric quality. The proper replenishment or regeneration system means that chemicals need to be changed less often. Although replenishment keeps the chemical conservation constant the system

chemicals should be changed periodically to eliminate particulates and contaminants from accumulating. Changing out chemistry once a month or every two to six weeks should be by choice and convenience and never because the activity has been lost.

**Starter Solution.** This is an acid solution (pH 2 approximately) containing bromides that is added to fresh developer each time the automatic processor is filled. Between 20 and 25 mL·L<sup>-1</sup> (2.5 and 3.2 oz per 1 gal) of developer are added to the processor, depending on the manufacturer. Each manufacturer's brand of starter should be used with the corresponding brand of developer. Starter is not normally added to the replenishment chemistry.

Starter gets its name from the fact it is used when a fresh batch of developer is first used. Its acid nature primarily deactivates the developer to help control fog. Its bromides are added to simulate used developer and thereby provide consistent, reproducible quality from batch to batch. For Class I films, which benefit from higher bromide levels, the starter both lowers pH and increases the development rate.

The developer chemistry manufacturer provides guidance on the amount of time and temperature to use with its product. The manufacturer's recommendations are based on the assumption that all instructions have been carefully followed, including the addition of the correct amount of the correct brand of starter.

**Faults from Developer.** Types of faults due to developer include too much or too little density (toe, straight line, shoulder areas), too much contrast or too little contrast. See Table 6 for faults related to the developer.

**Automatic versus Manual Processing and Chemistry.** Automatic developers contain glutaraldehyde as a hardening agent to control emulsion (gelatin) swelling. Because manual developers have no

FIGURE 14. Gamma versus temperature response curve.

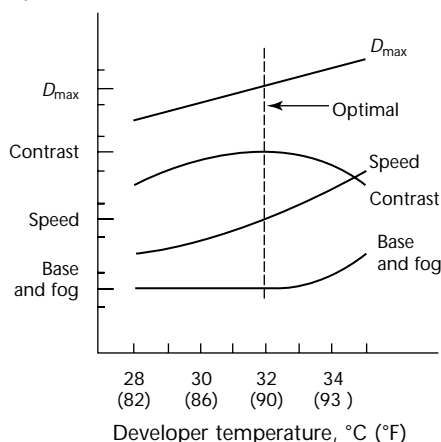


TABLE 6. Faults from developer.

Processing Action	Underdevelopment	Overdevelopment
Temperature	low	high
Transport rate	fast	slow
Solution level	low	not applicable
Agitation	low	not applicable
Chemical reaction; oxidation	high	not applicable
Contamination	high	high
Class I film replenishment	over	under
Class II film replenishment	under	over
Class III film replenishment	under	over
Class IV film replenishment	under	over

hardeners the gelatin carries out more of the developer volume. In automatic processing, in addition to developer hardener, the processor uses squeegee rollers to remove excess developer and an automatic replenishment system to sustain both volume and activity levels of all chemicals. Of course the processor has no short stop and this reduces the overall size by about 20 percent. Automatic developers can generally operate at higher temperatures than manual developers.

Manual processing uses a short stop, first rinse or acid bath between the developer and fixer to stop development or prevent excess developer from carrying into the fixer and diluting or contaminating it (to prolong the fixer life). Fixers are generally the same for both automatic and manual processing.

**Manual Acid Stop Bath.** The acid stop bath, normally 2 to 3 percent acetic acid solution, functions in several ways: it neutralizes alkaline developer by rapidly lowering the pH to the point where development stops; it helps prevent aerial oxidation of the developer agent, which otherwise could form staining products; it dissolves or retards the formation of calcium scum and preserves the acidity of the fixer and helps control gelatin swelling. Some commonly used agents are acetic acid, citric acid, diglycolic acid and sodium bisulfite.

The rate of neutralization for the acid stop bath of the fixer depends on (1) nature and thickness of emulsion; (2) pH value of stop bath, fixer or both; (3) total acidity of the stop bath and fixer; (4) agitation; (5) developer alkalinity; (6) developer pH; (7) type of developer agents used; (8) age, a function of replenishment; and (9) temperature.

## Fixer

Standard fixers are composed of chemicals listed in Table 7.

**Fixing Agent.** The function of the fixing agent is to form soluble stable complexes of silver salts that can be removed readily from the emulsion. Fixing agents should have no effect on the emulsion binder or on the already developed silver.

Thiosulfate, in the form of sodium or

ammonium salts, is the usual fixing agent. Sodium thiosulfate is best known as *hypo*. However, all of the terms *hypo*, *fixer*, *clearing agent*, *fixing agent* and *thiosulfate* are generally synonymous. The basic reaction between thiosulfate and silver halide is that of dissolving and carrying away the undeveloped silver. Thiosulfate can, however, attack the developed silver if the pH is decreased (moved toward a neutral or basic pH). Thus, replenishment is important to the fixer in regeneration of chemical strengths. The developer carryover into the fixer replaces what fixer is carried out but also reduces the pH slightly. If left within the emulsion, thiosulfate reacts with silver particles to form silver sulfide ( $\text{Ag}_2\text{S}$ ), which has a characteristic objectionable yellow brown stain. This is referred to as *residual hypo* or *hypo retention*.

**Hardener.** The hardener shrinks and hardens the emulsion. Aluminum chloride is frequently used but any aluminum compound, such as potassium alum or chrome alum, will work. The hardener has several functions: (1) to increase resistance to abrasion; (2) to minimize water absorption by the gelatin (this reduces drying time); and (3) to reduce swelling to permit roller transport.

**Activator.** Acetic acid provides acid media of about pH 4.0 and aids in the hardening of the emulsion. However, the most important function is the neutralizing of developer carryover and of the developer trapped within the emulsion. The reducers of the developer require high basic or alkaline media in which to react and they will continue to react, even after the film is removed from the developer solution, until they are neutralized. Because a very small part of the fixer (acid) will neutralize or at least lower the pH or a larger volume of developer, greater care is required when mixing chemistries so that contamination of the developer with fixer does not occur.

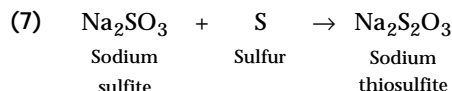
Acetic acid is usually used because it is a *weak acid*. It achieves good buffering and a slightly acid medium permits aluminum hardeners.

**Preservative.** Sodium sulphite is also the preservative for the fixer but its general function is to prolong the life of

TABLE 7. Fixer components.

Chemical	General Function	Specific Function
Ammonium thiosulfate	clearing agent	clears away unexposed, undeveloped silver bromide
Aluminum chloride	hardener	shrinks and hardens emulsion
Acetic acid	activator	acid media that neutralizes developer
Sodium sulfite	preservative	maintains chemical balance
Water	solvent	dissolves chemicals

thiosulfate in the fixer by reacting with free sulphur in the presence of the activator to regenerate the thiosulfate complex.



**Solvent.** Water is again the solvent and as with the developer it need be only of drinking quality.

**Rate of Fixation.** The rate of fixation depends primarily on: (1) the diffusion rate of the fixing agent into the emulsion; (2) the solubility of the silver halide grains; and (3) the diffusion rate of the complex silver ions out of the emulsion. Thus it can be seen that adequate agitation and replenishment are important to proper fixation.

The rate of fixation is the amount of time required to totally *fix* the emulsion, including clearing of all unexposed silver halide from the emulsion and hardening of the emulsion. In general it is said that the fixer clears and fixes. The rate is determined by this rule of thumb: the total fixing time is twice the clearing time. A simple clearing time test might be: using a 70 × 30 mm (3 × 1 in.) strip of fresh unexposed, unprocessed film, place a drop of fixer on both sides of the film, wait for 10 s, then dunk the strip into the fixer, agitate gently and watch for the spot to disappear. The clearing time is the time until the overall film is as clear as the spots, which had a head start. Additional time will not make it any clearer. Clearing time is critical for industrial films, especially in automatic processors where immersion time is fixed. Normally films will clear in 20 °C (70 °F) fixer in 20 to 60 s, depending on brand and class of film.

Faults from fixer include (1) rise in pH (decreased hardening), wet films and poorer archival quality; (2) dichroic stain (reaction of developer with silver loaded fixer); (3) streaks from nonuniform removal (that is, from nonuniform neutralization of the developer); (4) precipitation resulting from too low pH; (5) brown stain (produced by the formation of hydroquinone monosulfanate) from electrolytic oxidation of carryover developer, with low sulfite content.

## Water

Wash water is a photographic processing chemical whose purpose is to dilute or wash out the residual fixer chemicals. Water's action is to swell the emulsion and the rate is usually 11 L·min<sup>-1</sup> = 180 mL·s<sup>-1</sup> (3 gal·min<sup>-1</sup>).

Washing steps are included in photographic processing to remove reagents that might adversely affect later operations — and at the end of processing to eliminate all soluble compounds that might impair the stability of the film. Water removes fixing salts contaminated with dissolved silver compounds in the form of complexes with the thiosulfate. Failure to remove these silver compounds eventually causes stain in the highlights and the unexposed areas, whereas the presence of thiosulfate, its oxidation product *tetrathionate* and other *polythionates* will, with time, cause slow sulfiding of the image. This stain is silver sulfide (Ag<sub>2</sub>S) and is called *hypo retention stain*. The rate of diffusion of thiosulfate from emulsion is affected by (1) amount of silver image present, (2) pH of the fixer, (3) type of thiosulfate, (4) degree of fixer exhaustion, (5) temperature of wash, (6) agitation rate, (7) water flow rate and (8) wash apparatus design.

In the *counter current principle*, the water enters at the point where the films exit, the films leave uncontaminated water. One thousand square feet of film will deposit about four troy ounces of silver in a stagnant water tank. Agitation is normally supplied as a function of the water volume (replenishment flow rate) and directly affects efficiency.

**Hypo Retention.** Hypo retention is the amount of residual hypo or thiosulfate remaining in the emulsion after the film is processed. Hypo retention levels will vary with different brands of film. The type of processor, processing cycle and the situation of the chemistries have influence on hypo retention levels. The amount of residual hypo, which affects the archival qualities of the radiograph, is measured in microgram of thiosulfate per square inch of film (μg·in.<sup>-2</sup>) or microgram per square centimeter (μg·cm<sup>-2</sup>). The upper limit of 4 μg·cm<sup>-2</sup> (25 μg·in.<sup>-2</sup>) of retained thiosulfate is accepted for storage in excess of five years. A retention level higher than this may cause a general brown stain to appear on the film. Film with a level of 500 will usually last only one year before stain appears and the film becomes legally useless.

Hypo retention tests, requiring the normal processing of an unexposed film, should be made twice a year. Write down the processing conditions (time, temperature, chemical age, processor number, date and so on) and submit to a technical representative to have an analytical test made. Hypo estimator kits are available from X-ray film dealers and are used on a daily basis to indicate a general *go/no-go* status. These kits are convenient and very useful but are only estimators. It is important to have an

analytical test made periodically and to compare the test results to the estimates.

However, the most important aspect of silver sulfide formation is the storage conditions. Films held in long term storage require the same ambient conditions as fresh film: 21 °C (70 °F) or cooler and ≤60 percent relative humidity. Even with low hypo retention levels, unwanted stain can result from improper storage — for example, 32 °C (90 °F) and 90 percent relative humidity. If films must be kept, then they must be kept without stain.

**Water's Mechanical Function.** Water is required primarily to wash the fixer out of the film; this is its chemical function. Mechanically, the wash water is either the source of heat for the developer solution or the primary developer temperature stabilizer in automatic processors. In manual processors, the developer and fixer tanks sit in a larger tank filled with circulating water at a selected temperature. The water controls the temperature of the other chemistries. In automatic processors, the wash water flows through a heat exchanger at about 3 °C (5 °F) less than the desired developer temperature. The cooler water and the warmer developer are in proximity with a common steel wall. The cooler water picks up heat from the developer, causing the developer thermostat and heater to respond more rapidly and thereby provide greater stability. The fixer tank in an automatic unit is usually heated by the developer on one side and cooled by the wash on the other side. The wash water tank also provides an insulation barrier between the hot dryer section and the chemical section.

## Summary of Film Development Chemistry

Chemistry necessitates reaction controls, such as the time and temperature technique of processing. Filtration, circulation, pumping, metering, replenishment system, emulsion characteristics, transport systems, aerial oxidation, contamination and chemistry aging are all various aspects of the chemistry system in the processing of radiographs. It is these things that greatly influence the processing of radiographs to obtain optimal informational integrity. It has been rightly stated that “radiography begins and ends in the darkroom” and that “processing completes what the exposure started.”

The only real difference between manual and automatic processing chemistries is the developer hardener and the only real difference in the two techniques is the increased degree of consistency derived from the machine.

Manual processing can be as fast as automatic but there are many variables with the human operator controlling time, agitation, replenishment and other factors. On the other hand, the automatic processor, although consistent, is not entirely automatic and may produce consistently good or consistently bad product depending on the knowledge of and control by the operator.

## PART 3. Darkroom<sup>3</sup>

### Darkroom Technique

#### Principle

The radiographic darkroom is two things: a scientific laboratory and a *dark* room. A darkroom, where the lighting is kept at a very low level with special filters, must be constantly tested to ensure that it is indeed dark. The reason is that the X-ray film is sensitive to light and will turn black when developed. X-ray or radiographic film can be affected by heat, light, humidity, static electricity, pressure, chemical fumes and radiation. To establish and maintain a desired level of quality, all variables that can alter the scientific processes in the darkroom must be known and eliminated. A routine system of checking these variables must be made.

To reinforce the idea that the darkroom is indeed a scientific laboratory, even though it exists in the dark, two points may be considered.

1. Radiographers strive to make radiographs with excellent quality. The most common cause of unsatisfactory radiographs is fog, a noninformational density or blackness from silver deposits that occur in the wrong place and mask over the visibility of detail. As mentioned above, many forms of energy cause radiographic film to become black when developed. Once radiation exposure has been made the radiographic film becomes at least *twice* as sensitive to all types of energy, so extreme care is required in working in the darkroom laboratory.
2. The darkroom laboratory exists because processing in a very precise manner is required to change the latent image formed by the exposure into the useful visible image. Processing is an exact science based on a scientific principle called the *time and temperature* technique of processing. This time and temperature principle is based on a controlled level of chemical activity monitored by the technician. Processing is completely vital to radiography and must be performed completely.

The darkroom laboratory should be, by its descriptive name, light tight and should have all of the requirements and equipment of a laboratory. Most laboratories are well ventilated, well organized, clean, pleasant and safe places to work.

#### Design

The basic requirement for designing a darkroom is usually available space. It is most unfortunate when the darkroom is considered so unimportant that it is crowded into a former closet or basement area. Any darkroom must be designed so that there is a smooth and orderly work flow pattern.

The layout of a darkroom is generally considered to be either for centralized processing or decentralized (dispersion) processing. Centralized processing has, until recently, been the most advantageous system. However, some large industrial facilities have found that, with the convenience of automatic processors, dispersion processing and darkroom location are suited to the needs and requirements of increased workloads.

Darkroom layout should first be designed for convenience and safety. Consideration must be given to saving steps and time for the darkroom personnel, because darkroom efficiency is directly related to exposure planning efficiency. Because the darkroom is a laboratory, every applicable safety standard must be followed. Separate the darkroom into a wet and a dry area and keep these areas as far apart as possible. Keep surfaces dry and clean. There should be adequate ventilation to provide a sufficient supply of fresh, clean air. Dust is very destructive in the darkroom because it scratches films, salt screens and equipment, resulting in permanent damage. Metal filings (carried by radiographers' hair or clothes into the darkroom) can adversely affect the developer and cause artifacts on the film.

Near the darkroom should be a *viewing room*, sometimes referred to as the *lightroom*, in which processed films are sorted and organized and some supplies may be stored. The most important aspect of this area is the availability of view boxes.



## Equipment and Practice

### Maintenance

It is a recommended practice to sponge off routinely the outside and inside of a manual solution tank cover. Always replace tank covers when solutions are not in use to minimize oxidation, contamination and dust. Dust sticks to a wet surface, so always wipe up spills as they occur and buff surfaces dry. Periodically wipe down walls and shelves (including side walls of shelves). Make sure the room is light tight, free of strong chemical fumes and radiation protected through the establishment and continuation of a regular maintenance schedule. Time, money and effort are saved through a few minutes of preventive maintenance per day.

Inspect the darkroom at the beginning and end of each shift or work day. Clean up and put things in their places. Make sure adequate supplies are on hand for each day's workload.

Every darkroom should have a mop and bucket for floors and sponges for cleaning walls, surfaces and the processing equipment. A source of hot water is necessary for cleaning, lintless rags for wiping surfaces dry, a calibrated bimetallic or electronic thermometer for checking temperature and nonmetallic scouring pads for removing chemical encrustations. Do not use soaps or detergent around the processing solutions. Protective waxes can be applied to the *exterior* surface. Spare safelight bulbs, laboratory brushes, beakers, funnels, graduates and carrying buckets are all useful. Keep everything in its place so that it is easy to locate, even in the dark.

### Darkroom Lighting

For general darkroom lighting, either direct or indirect sources of light are satisfactory. White or light colored walls and tested ceiling safelight fixtures give good overall illumination. Direct safelights may be located over the loading bench and processing tanks or the processors.

### Safelights

All illuminators should be tested thoroughly and frequently to avoid light fog. This testing procedure is suggested: expose a film to very low intensity radiation to produce an approximate density of 0.50. Unload the film in total darkness and place it under a mask under one safelight. Turn on the safelight. Uncover sections of the film at one minute intervals until a maximum

exposure of ten minutes has been given. Turn off the safelight. Develop the film normally but in total darkness. Process and test the film. The time required to produce an increased trace of fog indicates the time limit for the safelight fixture.

Extraneous light in the darkroom is just as bad as stray X-radiation and must be eliminated. Possible sources of white light leaks are doors, windows, keyholes, ventilators, joints in walls and partitions. To monitor monthly for stray light, enter the darkroom and wait for the eyes to adjust for 15 min. Move around looking for light leaks. Look high and low. Make sure *all* lights are on in adjacent rooms. Correct any leaks and retest. Keep records.

The highest sensitivity of X-ray film is in the blue region of the spectrum. Therefore, safelights should be made with amber or red filters. Filters specially designed for X-ray darkrooms are available from X-ray film dealers.

### Unwanted Radiation

Because X-ray films are highly sensitive, they must be protected from accidental exposure to sources of X-rays and gamma rays.

If fogging of film occurs, the storage room, if located near sources of radiation, should be checked for possible stray radiation coming from radium, radon needles, radioactive isotopes, X-ray tubes or other sources. It is advisable to perform this test every six months as a precaution.

The following is a simple, inexpensive test. Attach a small coin or equivalent penetrometer with adhesive tape to each of several X-ray films (use fastest speed) in plastic bags or cardboard holders (day pack works very well) and place them on the bin and on the walls or the room in which films are stored. The coin is toward each possible source of radiation. After two weeks, develop the films. If an image of the coin appears on any of them, radiation may be reaching the stored films and should be eliminated.

Another technique is to use normal radiation testing devices such as a personnel film badge or an ion chamber device. In the latter case, tests must be made during full exposure. Film as a testing device provides indication of accumulated dose, if any.

### Ventilation

It is important that the darkroom be well ventilated. Ventilation provides comfort to the darkroom personnel and makes the darkroom a better place to work. Ventilation helps to maintain proper ambient (room) temperature and relative conditions vital to the proper storage of film. Ventilation also helps to prevent



artifacts from static electricity, handling or moisture. In addition, adequate ventilation is needed to keep harmful chemical fumes from accumulating and affecting either the darkroom personnel or the radiographic film.

## Cleaning Tanks

Corrosion seldom occurs when the tanks are full of normal chemical solutions and are kept *clean*.

Deposits often form on the walls of the developer tanks because of the action between mineral salts dissolved in the water and carbonate in the developing solutions. These deposits can be removed by using commercially prepared stainless steel tank cleaner. Follow the directions of the manufacturer, being sure to rinse the tank walls with fresh water. Wipe the tank out with a clean cloth or cellulose sponge.

Clean the exterior stainless steel before any deposits can attack the surface. Wipe with a cloth and warm soapy water and then rinse, making sure no soap deposits get into the chemistry. Once a week, use a stainless steel cleaner according to the directions on the label.

Always give special attention when cleaning welds and corners where deposits can cling. If deposits are heavy, remove the worst of them with fiber brush or plastic cleaning pad, then polish with a stainless steel cleaner. If an abrasive is required, use a very fine sandpaper.

Use caution never to use metallic abrasives, steel wool or wire brushes, as they can contaminate the surface of stainless steel. Any foreign metal particles will cause corrosion and may contaminate chemicals. Do not use commercial steel wool pads or strong detergents, because these are hard on the stainless steel and could react unfavorably with the chemistry.

## Cleaning Illuminators

Quite frequently, good radiographs will appear dull because they are viewed on faulty illuminators. Illuminators are faulty when the glass plate is dirty or bulbs of different wattage, age, color or size are used. Old interior paint that is dull or dusty will cause the radiograph to appear dull. Use a regular photographic exposure meter to test the illuminator. Identical radiographic studies should be viewed at the same intensity. An amperage meter can be installed to control uniform output.

Wash the outside of the viewing glass plate every day. Once a month wash out the inside of the view box. Always use bulbs with similar intensities. When conditions indicate paint deterioration, unplug the illuminator, remove the front

diffuser and wash it. Then paint the inside with a good, durable white enamel finish.

## Avoiding Static

There are two ways to avoid markings on X-ray films. One is to prevent the generation of static electricity; the other is to cause such charges, once generated, to leak off gradually rather than to discharge rapidly, which is what causes damage.

The most successful procedure is to keep a high relative humidity in the surrounding atmosphere. An accurate instrument for measuring relative humidity, called a *psychrometer*, is a valuable addition to any radiographic darkroom. Periodic checks on prevailing darkroom humidity enable one to take special precautions necessary to minimize the generation and discharge of static electricity. The relative humidity in the darkroom should be between 40 and 60 percent.

The following precautions will be of assistance in overcoming the most common causes of static:

1. If using X-ray film that has interleaving paper, handle film gently. Let the interleaving paper fall away from the film and place film in the cassette gently, without sliding it over the screen.
2. Following X-ray exposure, the cassette or holder should be opened slowly and the film removed carefully. The reason for careful handling is that the film is more than twice as susceptible to an energy source once it is exposed. Thus, a film will react to much smaller electrical discharges after exposure.
3. Move slowly when handling the film.
4. Make sure everything is grounded.
5. Use X-ray antistatic salt screen cleaner regularly.
6. Avoid static generating synthetic clothing.

**Grounding.** Electrically ground the metal top of the film loading bench, film bin, X-ray table, pass boxes and other equipment such as processors. In the darkroom, avoid nonconductive floor covering (rubber tile), hard floor waxes on concrete, rubber soled and plastic soled shoes, intensifying salt screens with worn surfaces and using a dry cloth to clean intensifying screens. A camel hair brush or vacuum cleaner should be used for dusting and a lintfree cloth and screen cleaner with antistatic solution should be used for washing intensifying salt screen surfaces. In periods of low ambient humidity (winter time or northern climates), when static is prone to occur, antistatic solution can be applied to

intensifying screens as added protection against static discharges.

**Common Static Marks.** Three kinds of static markings are illustrated in Fig. 15. *Crown* and *tree* are considered to be results of heavier electric discharges. They can be generated by very rapid motions, such as occur when film is removed from interleaving paper, when interleaving paper breaks contact with the film or when the film is touched by fingers. Smudge static markings may result from photographic exposure to visible light produced by sparks in air next to the film. Smudge static is produced when relatively low potential discharges occur over a large area.

### Color Conditioning

Surfaces above the working area should be finished with a dark matte paint to minimize reflected light.

### Storing X-Ray Film

Recommended storage conditions for all types of X-ray films are temperatures between 18 and 24 °C (65 and 75 °F) and 40 to 60 percent relative humidity.

Usually most radiographic facilities will have two storage areas. One area is for long term supplies and another, usually the darkroom, is for short term needs. In either case, it is required that a stock rotation plan be instituted. The plan is quite simple in that as new film arrives, it is placed on the right side of the supply. As the film is needed, it is removed from the left side. This is called a *FIFO* system: *first in, first out*. To assist in rotating film boxes, remember that all film boxes have an emulsion number and an expiration date on the end label. A system many

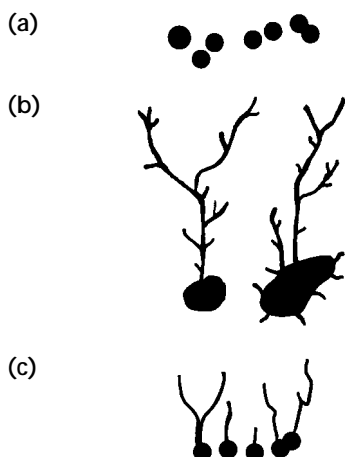
people use is to write on each box the date when it is received. Whatever system is used, be sure to keep records and always use the oldest film first. Film must be stored and inventoried by expiration date, film brand, type (class) and speed.

Film boxes should be stored on their edges. This distributes the weight and helps protect the film from pressure marks.

When using one box at a time or when there is no film bin, always be sure to fold over or close the bag and to replace the lid after each film is removed. Film is packaged in hermetically sealed light tight and moisture proof pouches — for example, black polyethylene or aluminized plastic. Once the pouch is opened to expose the fresh film there is still enough bag remaining to fold over to make the bag light tight again. This feature is not to obviate the box top or film bin but is an added safeguard.

Cassettes should not be stored for prolonged periods of time loaded with film. Load cassettes and holders with fresh film before each use.

FIGURE 15. Static electricity markings: (a) smudge; (b) tree; (c) crown.



## PART 4. Processing Technique<sup>3</sup>

### Principle

Processing completes what the exposure starts. After the exposure is made, the film is removed from the cassette and placed on a hanger. The film is processed. This is the simplicity of radiographic processing but there is obviously more to forming a visible image radiograph.

There is indeed an exactness to manual processing. This is a controlled scientific process in which something in one form (the latent image) is converted into another form (the visible image). No matter how superior the exposure techniques are, if anything less than optimal processing technique is permitted then an image less than optimal will result.

### Equipment and Practice

#### Thermometers

In developing X-ray films by the time and temperature system, an accurate thermometer is of the utmost importance. Service thermometers should be checked at regular intervals against a thermometer whose accuracy is known. They should be graduated in degrees or, better, in half degrees.

A thermometer should be read while it is inserted in the thoroughly mixed solution. To avoid parallax, the thermometer should be held so that an imaginary line from the eye forms a right angle to the axis of the thermometer. To further avoid this problem, a bimetallic or electronic thermometer might be considered.

**Safety Warning.** Never use glass thermometers containing mercury or iodine. If the glass breaks, the mercury or iodine can be hazardous to personnel and developer.

#### Mixing Solutions

Make sure the solution tanks are clean. Carefully read the instructions on the chemical container. Mix as recommended at the suggested temperature to ensure satisfactory performance. Avoid high temperatures, inclusion of air and contamination during preparation. Stir

thoroughly but not too violently or too long.

If the processing solutions do not seem to be working well enough, answer these four questions.

1. Are the tanks really clean?
2. Are solutions properly mixed? Were they mixed in the right sequence? Were they overagitated?
3. Are temperature and timer accurate?
4. Are the exposure techniques accurate?

### Water for Processing

The water temperature for mixing should be  $\pm 3^\circ\text{C}$  ( $\pm 5^\circ\text{F}$ ) of the manufacturer's recommendation.

The rule of thumb is to use water of drinking quality. In spite of the variety of impurities in water supplies, most city water in the United States is pure enough for photographic processes.

### Time and Temperature Technique

The time and temperature technique provides the controlled basis for obtaining consistent, optimal radiographic information. This scientific technique also permits alteration of the processing cycle to suit specific needs and requirements.

Regardless of the optimal time and temperature recommendations for a given chemistry and film, it must be remembered that everyone has different likes and desires. With this in mind, consider that faster processing, higher or lower contrast, greater speed, less density and other considerations can be altered through the judicious use of the time and temperature technique. At a given temperature, longer times will overdevelop the film, increasing density. At a given time, higher temperatures will cause overdevelopment fogging (increased noninformational density) of the film. This does not mean that *sight* development is advocated. No one should use anything but the specific time and temperature technique.

### Developers

Optimal radiographs require correct development. The developing time to be followed differs with the processed film type, the developer type and the processing solution temperature.

Radiographs require just the right amount of contrast. Too much reduces the range of densities covered by a single exposure; the thinner parts become too dark and the thickness ones too light. Conversely, insufficient contrast, though it affords more latitude in exposure, lessens the total differentiation, thereby obscuring fine details. To achieve an ideal contrast, a given type of X-ray film should be developed in the same brand of solutions using the time and temperature and replenishment characteristics supplied by the manufacturer.

### Compensating for Developer Exhaustion

**Replenisher Technique.** Replenishers replace the reducing agents as they are exhausted and, if added correctly, obviate adjustment of developing time to maintain constant density and contrast over the useful life of the developer. Replenishers should be mixed as directed on the label and should be added frequently and in small amounts to maintain the developer level; if an amount greater than 10 percent of the developer tank volume is added at one time, fog may increase. The remaining replenisher should be kept in a tightly stoppered bottle or in a plastic jug or tank with a floating lid and dust cover.

Because developer exhaustion depends on the type of film emulsion and the film density as well as the film area, the quantity of replenisher per  $355 \times 430$  mm ( $14 \times 17$  in.) film will not be constant. As a rule, about  $90 \text{ cm}^3$  (3 oz) of replenisher are required for each  $355 \times 430$  mm ( $14 \times 17$  in.) film processed.

---

### Quality Control of Processing

Maintenance of the time and temperature technique of processing depends on some system of quality control. Quality control kits are available to give experience to operators and help them set up their own program. A simple quality control test is to use the same cassette or film holder and a step wedge with known exposure, film and processing techniques. Establish a *control* film and routinely make test films that can be compared to the control film. Keep exact records as a personal teaching and record file.

Processing of a radiograph is done in an automated processor to achieve consistent quality. The processing system is a chemical process with specific conditions of time and temperature based on a given chemical activity. Good processing makes good radiographs.

Processing quality control is a procedure of monitoring to see if, and to what extent, there is consistency. Consistency is necessary before *quality* can be improved, because the variables of processing must be identified, their degree of fluctuation and cycling patterns noted and the limits of acceptability established. Once the uncontrolled variables are identified, the best control measure will be more apparent. Sometimes, the variable may have to be compensated for, minimized or eliminated. Also, in this process of identifying and controlling the variables, indications are often provided as to the best way to consistently achieve optimum quality.

### Sensitometry

The study and measurement of relationships between exposure, processing conditions and film response to exposure are known as *sensitometry*. The properties of a film that affect or govern the relationships are known as sensitometric properties. *Quality* is defined by the sensitometry of the visible image. Processing is the vital link between the latent image and the visible image radiograph; careful control of the many factors involved is essential. Establishing processor quality control to maximize uniformity is desirable.

**Control Strips.** Each day control strips are processed periodically and read on a densitometer. The changes in density levels of the exposure are plotted and the characteristic curve is generated. Speed and contrast can be determined. This system is the professional approach to quality control. The matched exposure radiographs are easily duplicated from day to day. Check the processor, note the conditions mentioned below and process the control strip. This control strip becomes the master and subsequent daily strips are simply matched to it. Deviations from the master strip necessitate interpretation, investigation, and corrective actions. The master test strip should be processed under optimum conditions of chemistry and processor performance.

**Density.** Density and adequate differences in density (contrast) are considered the most important of all properties in the radiograph. Proper densities and adequate contrast make visible the structural details within the image of the object.

*Radiographic density* has been defined as the amount of film blackening that is the result of metallic silver deposits remaining on the film after exposure and processing. A useful way to measure the amount of film blackening is to measure its interference with a beam of light passing through a radiograph. The amount of

light absorbed by the film is measured with a densitometer.

Sensitometrically, density is defined as the common logarithm of the ratio of the amount of light striking one side of the radiograph compared to the amount of light that passes out the other side. When the metallic silver in the emulsion allows one tenth of the light to pass through, this ratio is 10:1. The common logarithm of 10 equals 1 and the silver deposit is said to have a density of 1. Density can now be defined by the equation:

$$(8) \quad D = \log \frac{I_i}{I_t}$$

where  $D$  is density,  $I_i$  is intensity of light incident to the film and  $I_t$  is intensity of light output transmitted through the film.

The data obtained by sensitometric procedures are usually plotted in the form of graphs. Figure 16 shows a typical characteristic curve of an X-ray film exposed with intensifying salt screens. The portion of the curve designated as the *toe* demonstrates the nonlinear response of the emulsion to relatively small amounts of radiant energy. With uniform increases in exposure, the density builds up slowly until the linear response part of the curve. Along this straight line the density increases uniformly with the logarithm of the exposure until the nonlinear *shoulder* of the curve is reached. The shoulder is produced when slat screens are used. Additional exposure results in smaller increases in density to a point where additional exposure does not produce greater density.

**Contrast.** Contrast by definition is the difference between two densities. As a radiograph is viewed on an illuminator, the difference in brightness of the various parts of the image is called *radiographic contrast*. This is the product of two distinct factors: (1) film contrast, inherent in the film and influenced by the developing process; and (2) subject contrast, a result of differential absorption

of radiation by the subject. Although radiographic contrast can be altered by changing one or both of these factors, it is good practice to standardize the film and processing procedure and to control radiographic contrast by changing subject contrast. Contrast can be changed easily by adjusting the kilovoltage or general exposure technique to alter the quality of radiation. Sensitometrically, contrast refers to the slope or steepness of the characteristic curve of the film; this is also called gamma.

**Gamma.** Gamma is the slope or steepness of the straight line portion of the characteristic curve. In plotting a characteristic curve, *density* (a logarithmic value) is most often plotted against log relative exposure. *Exposure* is defined as the intensity multiplied by the time; it can be expressed in exposure units, such as  $\text{J}\cdot\text{cm}^{-2}$  ( $10^7 \text{ erg}\cdot\text{cm}^{-2}$ ) of X-radiation. Relative exposure is much more convenient and equally useful. X-radiography exposure is expressed in terms of milliamperere seconds (mA·s) or milliamperere minutes (mA·min). Then if the amperage is doubled, the exposure is doubled, kilovoltage peak remaining constant. If the kilovoltage remains constant, the ratios of the exposure reaching the film through two different regions of the subject are always the same, no matter what the values of milliamperage, time or distance from focal point to film. For example, two exposures, one of which is twice the other, will always be separated by 0.3 on the logarithmic exposure scale (the logarithm of 2 being 0.3).

**Speed.** It has been determined that the contrast of a film is indicated by the *shape* of the characteristic curve. Speed is indicated by the *location* of the curve along the exposure axis. The *faster* film will lie toward the left of the graph. In Fig. 17, film A is faster than film B but has

FIGURE 16. Characteristic curves.

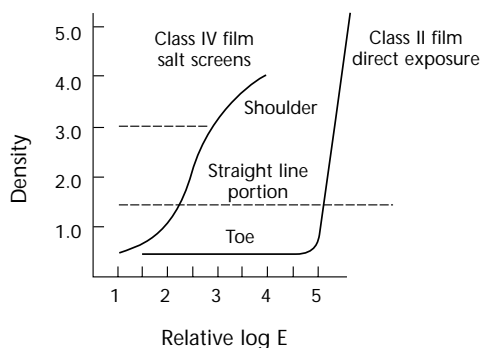
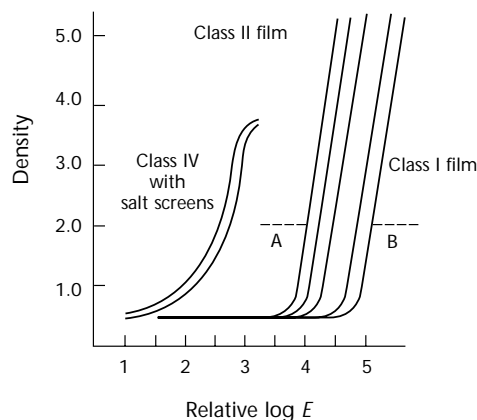


FIGURE 17. Speed shifts.





the same contrast. The separation of the films is a measure of the speed difference. Film A requires less exposure to achieve a speed point of density 2.00 above base plus fog. Film B requires more exposure, so it is said to respond slower or be less fast. The convenience of using relative exposure also applies to speed. The speed of one film can be expressed on a basis relative to another film when one is made the standard of comparison. This reference film can be assigned any arbitrary speed value, such as 100. If another film requires only half the exposure to reach the same density as the reference film, the faster film will have a *relative speed* of 200. A density of 2.00 above base plus fog has been designated as the density to compute film speed. This density has been chosen because it represents the minimum useful density range for much of radiography. For lower density films, speeds are often calculated at the lower density of 1.00.

### Fixer

Failure to fix a film sufficiently results in its discoloring with age. A good rule of thumb for determining the minimum fixing time is as follows. After a film has cleared, leave it in the fixer an additional two times as long as it took to clear. For example, if it takes 1 min for a film to clear, then it should be left in the fixer at least an additional 2 min or a total period of 3 min.

To prepare fixing baths from liquid concentrate fixer, it is essential that directions on the container be followed. Attention is paid only to the temperature of the developer, because fixer temperature is less critical; however, at high temperatures, it is important that the processing baths be maintained at about the same temperature. Changes in temperature cause the gelatin of the emulsion to swell and contract. When the temperatures of two baths differ excessively, this change in the gelatin takes place so abruptly that unevenness is likely to result. The effect produced on the film is known as *reticulation* — the gelatin breaks, producing fine cracks.

**Archival Quality.** The importance of adequate fixing to archival keeping quality cannot be overemphasized. Poorly fixed films will not deteriorate until many months after processing. The lighter portion of a radiograph may become yellow and the image may tend to fade. This delayed action may be traced back to the nature of the fixing process, which is believed to consist of two steps. Undeveloped silver halide is first converted to silver thiosulfate complexes that are only slightly soluble. The reaction

then proceeds to form soluble compounds that are removed by washing.

Inadequate fixing leaves small amounts of these complexes that cannot be removed by normal washing. In time, these residues break down and react with the silver image to form silver sulfide ( $\text{Ag}_2\text{S}$ ). This sulfide is usually yellow but may range from pink to brown. It cannot be easily removed from the radiograph. Extremely minute amounts of residual thiosulfates are sufficient to cause serious deterioration. Therefore, the radiograph may appear transparent and at the same time be inadequately fixed. For this reason, close attention to recommended fixing technique is mandatory.

### Washing

Radiographs must be washed thoroughly to prevent discoloration with age and to ensure preservation of the image.

### Drying

Avoid temperatures above 49 °C (120 °F) in drying and maintain a steady volume of air across the film surface. An excessively low relative humidity within the dryer may cause water spot drying marks and streaks on the film surface.

---

## Safety

Developer, with its hydroquinone and alkalinity, forms a very hazardous solution. Always use good ventilation when mixing chemicals. A nose filter or respirator is suggested when powdered chemicals are mixed. Goggles are required by the United States Occupational Safety and Health Administration to protect the eyes.<sup>10</sup> In addition an eye wash station is required. If developer gets into the eye the worker must begin washing within 15 s and continue washing for 15 min minimum. Washing for 1 h is preferred.

The developer is most hazardous but care must be taken when working with fixers also. In addition to the above, rubber gloves will protect the skin and keep chemicals out of cuts; rubberized or plastic aprons will protect the worker and clothing.

### Clearing Film Base

Liquid laundry bleach will dissolve the gelatin and produce a clean, clear sheet of base plastic. Warm solutions work faster. Enzymes could be used but are very hazardous.



## Removing Developer Stains from Hands

Developer solutions should be considered hazardous and hands should not be routinely submerged in them. Rubber gloves should be worn. When manually processing or working on automatic processor rack components where contact is prevalent, be sure to rinse hands frequently in fresh water. In manual processing make sure hands are rinsed while rinsing or fixing the film.

## Automatic Processing

Automatic processing is a chemical reaction performed in a machine; it is often spoken of as if the machine were the important part. However, since the introduction in 1957 of a roller transport processor, processors have provided improved consistency over manual processing. But humans control the machine as they control manual processing, only less frequently. Keep in mind that automatic processing produces consistent quality; the quality will be consistently good or bad depending on the operator.

There are three distinct advantages to automatic processing: consistent quality, improved quality and economy of time and labor. Given a well functioning, properly adjusted machine, film after film will be of better quality from the machine than from a person *sight developing*. As a result, processors have found their way into small and large laboratories, trailers and the backs of pickup trucks.

Automatic processing developer chemistry has a hardener that is extremely important in controlling the amount of emulsion swell. An overswollen film can result in overdevelopment fog, uncleared films, poorer archival quality, wet films and increased transport problems. Automatic chemistry is usually replenished automatically to sustain volume and activity.

In an institution or laboratory all the processors may be located in one central darkroom and processing area or in several areas. The major advantage of centralization is that one darkroom person can feed several processors, saving space and manpower. The main advantage of dispersed or decentralized processing is that the processor can be placed in different areas, such as production, quality control and research, to reduce down time and the confusion of intermixed films. The major disadvantage is increased space and manpower. It is a good idea, with dispersed processing, to centralize the mixing and distribution of

chemicals to various locations and to return spent fixer to central collection and recovery area.

**Daylight Installation.** In daylight, a film dispenser dispenses films into hard cassettes. After exposure the film is fed directly into a processor, sitting in a lighted area, by means of an unloading, feeding device. Film is never touched by humans until after processing. Processors can be placed virtually anywhere there are utilities. There is no darkroom or associated personnel.

**Darkroom Installation.** In a conventional darkroom, the processor may be installed totally inside the darkroom. The best way is to put the bulk of the unit outside the darkroom to reduce heat inside. Some people put the bulk of the unit inside the darkroom so that any jams can be cleared in the dark. The disadvantage of this system is that all service requiring white light necessitates closing down the darkroom. An alternative would be to put the bulk of the unit in the outer room but construct the room so that it can become a darkroom.

All processors should have a minimum of 600 mm (24 in.) access on a side. If this is not possible the processor can be made portable on wheels or skids with quick disconnects to allow easy service. Near the processor there should be a floor sink for washing racks or the entire processor may be placed over a large grill work with a drain below.

**Automatic Feeders.** Automatic feeders are available for some makes of processors, which allow a stack of films to be placed in the feeder and the lid closed; the operator can do other jobs as the feeder automatically feeds films. Feeders require adjustment and periodic monitoring. In addition, it may take twice as long to feed one sheet of film automatically as it would manually, because of the cycle time and delay of the mechanism, especially at the faster processing times (in excess of 7 min).

## Darkroom Workflow

An automatic processing darkroom shares many of the features of a conventional darkroom but there are significant differences. No provision need be made for hangers or hanger storage. Deep tanks for developing and fixing solutions and for washing and drying may be eliminated, because these operations take place within the automatic processor; however, deep tanks may be retained for training and emergency use. Only the input end of the processor needs to be located within the darkroom. Dual processor installation is convenient. To handle peak loads, both machines are

operated simultaneously; one suffices at other times.

## Processing Chemicals

Processing chemicals for automatic equipment differ from deep tank chemicals. Never attempt to use conventional chemicals in automatic processors. Although the basic chemical reactions are similar, automatic processing chemicals are especially formulated for high speed roller operation. Modern automatic processing chemicals make possible maximum ease of use and uniformity of finished radiographs, regardless of the make of processor.

Although all chemicals operate efficiently with any make or speed of film, they generally provide best results with the same brand of film. In addition, using companion products causes fewer variables and is better understood by a manufacturer.

All ingredients, plus full instructions, are included in each package of developer, fixer and starter solution. These chemicals are prepared in strict conformity with basic formulas known to produce excellent results. When properly mixed and cared for, they operate efficiently over long periods of time.

Finally, clean the work area and equipment and put the equipment away. Then install the crossovers and prepare the processor for operation. This installation of fresh chemistry should be entered in the processor log book.

---

## Cleanup and Inspection

Operating instructions for each processor also include suggestions for cleaning and inspection. In general, these procedures require little time and trouble but this does not minimize their importance. They contribute substantially to efficient operation and to maintenance of optimum film quality.

---

## Solution Services

In many localities, specialized organizations handle the mixing and maintenance of chemicals for automatic processing equipment. These services include routine inspection, cleaning and refilling. Although the services are provided by professionals, it is still good policy for each X-ray department to have its own in-house specialists and to perform routine, daily inspection.

## PART 5. Silver Recovery<sup>3</sup>

The scarcity and high price of silver make its recovery from fixing baths important for ecological, environmental and economic reasons. Fixer contains about 40 percent of the original silver in the film. Laws and standards in the United States establish limits for dissolved silver and forbid its disposal in drains.<sup>10,11</sup> This consideration is in addition to silver's scarcity and value. Even the smallest user should treat the used fixer to remove silver — the money recovered will pay for the effort.

### Recovery Techniques

The techniques of recovery are chemical (which includes precipitation and metallic replacement) and electrolytic. Metallic replacement is simplest but requires a low volume continuously. Electrolysis is recommended for higher volume processors.

**Metallic Replacement.** If a fixer solution containing silver ions is brought into contact with a metal, the less noble metal (such as steel wool, zinc, copper or steel turnings) is replaced by the silver. The silverless fixer cannot be reused.

Metallic replacement units, also called buckets or cartridges, contain steel wool or zinc screen and are usually used in tandem. As the acid fixer breaks down the less noble steel, the more noble silver metal precipitates as metallic silver. A sludge of iron oxide and silver forms in the bottom of the container.

This technique is both inexpensive and efficient. It can remove 60 to 95 percent of the silver: 1 kg (2.2 lb<sub>m</sub>) of steel wool will collect 3 to 4 kg (6 to 9 lb<sub>m</sub>) of silver. However, efficiency is based on a slow, steady, continuous flow of silver laden fixer. Efficiency is about perfect for the first 25 percent of the unit's life expectancy, 400 to 800 L (100 to 200 gal) of silver laden fixer and then often becomes only 30 percent effective. Also, the sludge produced by this technique is expensive to ship and refine.

**Chemical Precipitation.** Precipitation is a chemical reaction that separates the silver from the solution in an insoluble, solid form. This type of unit, particularly those that use sodium sulfide and zinc chloride, produces toxic and volatile fumes and so should be avoided. The units using sodium borohydride are very efficient and

safe but require constant pH adjustment by a technician.

**Electrolytic Recovery.** Silver is recovered by passing an electric current (direct current) through the silver laden fixer. Electrolytic recovery systems (called cells) are classified as agitated or nonagitated, high or low current density units. The two terminals (electrodes) are a positively charged anode (usually graphite) and a negatively charged cathode of stainless steel. Positively charged silver ions ( $\text{Ag}^+$ ), are attracted to the cathode, where they plate out as metallic silver ( $\text{Ag}^0$ ), called flake. This is the most efficient technique for medium or larger installations.

### Efficiency of Silver Recovery Equipment

During processing, the developer converts the latent image bearing silver halide crystals into a visible image — black metallic silver. Those crystals exposed but not developed and those not exposed are washed out in the fixer. In industrial radiography the silver is dissolved into the fixer in a ratio of more than 6 g·L<sup>-1</sup> (1 troy oz·gal<sup>-1</sup>) of fixer. Silver recovery or reclamation is the process of converting the silver to metallic silver. Understanding the factors that control the efficiency of this operation will help in understanding and upgrading existing systems or in generating specifications for new systems. **Dwell Time.** Sufficient time is required for the reaction to occur. Electrolytic units (cells) are rated in troy ounce per hour capacity. Buckets are rated in cubic centimeters per minute or gallons per hour of fixer flow. Exceeding these limits will result in silver going through the unit and down the drain.

**Agitation.** Buckets provide agitation by flowing the fixer over the many wire filaments. Electrolytic cells use pumps or impellers. Greater physical agitation increases the unit's efficiency in producing metallic silver and allows higher plating currents to be used. However, agitation should not be so violent as to cause splatter, spillover or excess evaporation.

**Surface Area.** The larger the surface area the higher the plating current can be in a cell. In any unit, increased area increases recovery rate.

**Edge Effect.** The edge effect is related to surface area and electron flow efficiency; the more edges or surface area, the better the efficiency.

**Electrolysis.** As the acid fixer enters the bucket the steel wool is attacked, producing chemical electrolysis. The steel becomes oxidized to iron oxide and the silver in solution becomes metal. Cells contain an anode and a cathode, a rectifier and a transformer to pass direct current through the solution. The higher the current, the greater the efficiency. Too high a current (usually when little silver is present) can break down the fixer, this is called sulfurization and is to be avoided.

**Maintenance.** All units require records, regular inspection and regular maintenance to ensure proper use. Buckets can clog, back up or leak. Cells can become too loaded with silver, short out, blow a fuse or burn up an agitation pump. The amperage should be automatically or manually adjusted according to the film (silver) volume during the day.

**Centralization.** Centralized recovery is the most efficient system where three or more units are involved. A holding tank feeds a single cell a continuous supply for optimal efficiency.

## Silver Estimation

Silver estimating paper, which indicates the relative amount of silver per gallon of used fixer, can be readily purchased from most silver reclaimers. The test strips are used just like pH paper strips. Industrial radiography usually operates at a level of about  $10 \text{ g}\cdot\text{L}^{-1}$  ( $1.2 \pm 0.2 \text{ troy oz}\cdot\text{gal}^{-1}$ ).

An even simpler technique of determining if there is any silver in the solution is to put a brightly polished copper tube in the solution. Any silver in the used fixer will quickly adhere to the copper tube and give it a gray color.

Purchase tailing or central electrolytic units according to the calculated capacity in gram per second. Collect the fixer in the processor at cleaning time. If a silver recovery unit malfunctions, disconnect it or isolate it so that it cannot ruin radiographs being processed.

## Silver Recovery Installations

**Tailing units** may be buckets or cells placed individually or in tandem on each processor. Usually buckets are used in tandem, with the second becoming the first after every 400 to 1300 L (100 to 300 gal) of fixer, depending on brand and size. Properly sized cells should not require a tailing unit.

**Recirculation cells** take the fixer from the processor, remove most of the silver and return the fixer to the processor. This

reduces fixer consumption and silver lost into the wash. The major disadvantages are increased cost of the cell and potentially higher hypo retention levels because of reduced fixer efficiency. Fixer can only be recirculated from cells — never from buckets or precipitation. The following precautions should be observed when installing or operating any silver recovery units:

1. Make sure that fixer overflow to the silver recovery unit is a continuous downward flow.
2. Clean the standpipe on metal exchange units regularly.
3. Ensure against air locks in electrolytic units.
4. Be sure there is an air break (electrolytic break) between the solution in the electrolytic recovery unit and the incoming fixer. Without one, there is danger of plating silver in the processor fixer tank.
5. Use the highest amperage possible for optimal recovery — but keep it short of sulphurization (characterized by yellow color and smell of rotten eggs). High amperage produces soft, black silver; low amperage produces hard, shiny silver but of approximately equal quality. The higher amperage helps to ensure removal of most of the silver.

## Scrap Film

Films that are to be discarded also have value for their silver content. About 60 percent of the original silver remains in the film to form the visible image. Both waste film and outdated records are valuable and should be sold for their silver content.

## Security and Selling Recovered Silver

In radiography, business economics revolve around the cost of producing a visible image versus the value or price of the product. The single largest budget item is manpower, which must be used efficiently.

Radiographic film is expensive. It must be kept in the best possible condition and protected against abuse and theft, whether in its fresh or used form, through inventory controls such as records, policy procedures and security. Such programs will pay for themselves in improved earnings.

Silver should be recovered from used fixer and used films to reduce the cost of the original fresh stock. Because a substantial value is represented by recovered silver, it is important to impose inventory and security controls.

Fresh green (unexposed) film and black or scrap (processed or discarded green) film represent money that is easily transported or lost. Both conditions of X-ray film require inventory controls including records, proper storage conditions and security.

Of all the silver in the film, 40 percent goes into the fixer and 60 percent remains on the film. Ninety percent of the silver from the fixer and 70 percent of the film silver may be recovered, giving a total of about 75 percent of the original silver that is recoverable. Considering that the film costs are about five times the price of silver, only 10 to 15 percent of the film's retail price may be recovered.

### Specific Suggestions

*Silver flake* is derived from scraping off the collection plate of an electrolytic silver recovery unit (cell). There is little significance whether it is silver colored and hard (result of low current levels) or black and soft (result of high current levels). A properly sized cell will collect 90 to 95 percent of the silver, which will be 95 percent pure. Dry the silver before weighing. (If weighed wet, deduct five percent of the weight for trapped moisture).

*Silver sludge* from buckets should be shipped in solution in the bucket. Draining the fixer exposes the sludge to air and an exothermic reaction produces heat. If possible, the sludge should be dried in a large open pan and then shipped. The sludge damages the refiner's crucibles and the refiner charges more to handle sludge than flake.



# References

1. Rivkin, W.B. and G. Wicks. Sec. 4, "Radiation Detection and Recording." *Nondestructive Testing Handbook*, second edition: Vol. 3, *Radiography and Radiation Testing*. Columbus, OH: American Society for Nondestructive Testing (1985): p 174-185.
2. Quinn, R.A. and C.C. Sigl, eds. *Radiography in Modern Industry*, fourth edition. Rochester, NY: Eastman Kodak Company (1980).
3. McKinney, W.E.J. Sec. 7, "Radiographic Latent Image Processing." *Nondestructive Testing Handbook*, second edition: Vol. 3, *Radiography and Radiation Testing*. Columbus, OH: American Society for Nondestructive Testing (1985): p 299-376.
4. McKinney, W.E.J. *Radiographic Processing and Quality Control*. Philadelphia, PA: J.B. Lippincott Company (1988).
5. Gurney, R.W. and N.F. Mott. *Proceedings of the Royal Society of London: Series A, Mathematical and Physical Sciences*. Vol. 164. London, United Kingdom: Royal Society (1938): p 151.
6. Gurney, R.W. and N.F. Mott. *Electronic Processes in Ionic Crystals*. Oxford, United Kingdom: Clarendon Press (1940).
7. Marstbloom, K., R. Kochakian, B. Vaessen and P. Willems. "Analog Film Radiography Technology Advancements." *ASNT Fall Conference and Quality Testing Show 2001 Paper Summaries Book*. Conference [Columbus, OH, October 2001]. Columbus, OH: American Society for Nondestructive Testing (2001): p 165-167.
8. ASTM E 1815-96, *Standard Test Method for Classification of Film Systems for Industrial Radiography*. West Conshohocken, PA: ASTM International (2001).
9. ISO 11699-1, *Non-Destructive Testing — Industrial Radiographic Films*. Geneva, Switzerland: International Organization for Standardization (1998).
10. 29 CFR 1210, *Occupational Safety and Health Standards*. Code of Federal Regulations: Title 29, Labor. Washington, DC: United States Department of Labor, Occupational Safety and Health Administration; Government Printing Office.
11. *2001 TLVs® and BEIs®*. Cincinnati, OH: American Conference of Governmental Industrial Hygienists (2001).

## Bibliography

### Books

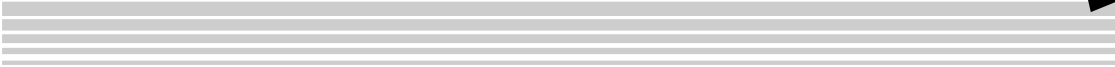
- Bruce, H.F. *Your Guide to Photography*, second edition. New York, NY: Barnes and Noble (1974).
- Bunting, R.K. *The Chemistry of Photography*. Normal, IL: Photoglass Press (1987).
- Control Techniques in Film Processing*. New York, NY: Society of Motion Picture and Television Engineers (1960).
- Eaton, G.T. *Photographic Chemistry in Black-and-White and Color Photography*, fourth edition, revised. Dobbs Ferry, NY: Morgan and Morgan (1986).
- Feininger, A. *Darkroom Techniques*. Garden City, NY: Amphoto (1974).
- Folts, J.A., R.P. Lovell and F.C. Zwahlen, Jr. *Handbook of Photography*, fifth edition. Albany, NY: Delmar Thomson Learning (2001).
- Gray, J.E. *Photographic Processing, Quality Control and the Evaluation of Photographic Materials*, Vol. 2. HEW Publication 77-8018. Rockville MD: Bureau of Radiologic Health (1977).
- Gray, R.H., ed. *Applied Processing: Practice and Techniques*. Washington, DC: Society of Photographic Science and Engineering (1968).
- Gregg, D.C. *Principles of Chemistry*, third edition. Boston, MA: Allyn and Bacon (1968).
- Haist, G. *Modern Photographic Processing*, Vols. 1 and 2. New York, NY: Wiley Interscience (1979).
- Herz, R.H. *The Photographic Action of Ionizing Radiations in Dosimetry and Medical, Industrial, Neutron, Auto- and Microradiography*. New York, NY: Wiley Interscience (1969).
- James, T.H., ed. *The Theory of the Photographic Process*, fourth edition. New York, NY: Macmillan (1977).
- James, T.H. and G.C. Higgins. *Fundamentals of Photographic Theory*, second edition. New York, NY: Morgan and Morgan (1960).



- John, D.H.O. *Radiographic Processing in Medicine and Industry*. London, United Kingdom: Focal Press (1967).
- Marcus, A. *Basic Electricity*. Upper Saddle River, NJ: Prentice-Hall (1958).
- Mason, L.F.A. *Photographic Processing Chemistry*. New York, NY: Focal Library (1975).
- Mitchell, J.W., ed. *Fundamental Mechanisms of Photographic Sensitivity* [Bristol, United Kingdom, March 1950]. London, United Kingdom: Butterworths Scientific Publications (1951).
- Pauling, L. *College Chemistry: An Introductory Textbook of General Chemistry*, fourth edition. San Francisco, CA: W.H. Freeman (1964).
- Silver Recovery for Hospitals*. Chicago, IL: American Hospital Association (1980).
- Stiles, E. *Handbook for Total Quality Assurance*. Waterford, CT: National Foreman's Institute (1965).
- Todd, H.N. *Photographic Sensitometry: A Self-Teaching Text*. New York, NY: Wiley-Interscience (1976).
- Todd, H.N. and R.D. Zakia. *Photographic Sensitometry: The Study of Tone Reproduction*. New York, NY: Morgan and Morgan (1969).
- ANSI IT9.9-1990, *American National Standards Institute. Standard for Imaging Media (Film) — Stability of Color Photographic Methods*. New York, NY: American National Standards Institute (1990).
- ANSI PH1.28-1984, *Specifications for Photographic Film for Archival Records, Silver Gelatin Type on Cellulose Ester Base*. New York, NY: American National Standards Institute (1984).
- ANSI PH4.32-1986, *American National Standard for Photography (Processing) — Methods for Evaluating Processing with Respect to the Stability of the Resultant Image — Black-and-White Papers*. New York, NY: American National Standards Institute (1986).
- ANSI PH1.41-1984, *Photographic Film for Archival Records, Silver Gelatin Type on Polyester Base, Specifications for; When Tested by ANSI Standard PH4.8-1984, Methylene Blue Method for Measuring Thiosulfate and Silver Densitometric Method for Measuring Residual Chemicals in Films, Plates, and Papers; and Stored in Accordance with ANSI Standard PH1.43-1983, Storage of Processed Safety Photographic Film, Practices for*. New York, NY: American National Standards Institute (1984).
- ANSI PH4.8-1985, *American National Standard for Photography (Chemicals) — Residual Thiosulfate and Other Chemicals in Films, Plates, and Papers — Determination and Measurement*. New York, NY: American National Standards Institute (1985).
- ANSI/AIIM MS26-1990, *American National Standard for Determining Illumination Uniformity*. New York, NY: American National Standards Institute (1990).
- ASTM E 999-99, *Standard Guide for Controlling the Quality of Industrial Radiographic Film Processing*. West Conshohocken, PA: ASTM International (2002).
- ASTM E 1254-98, *Standard Guide for Storage of Radiographs and Unexposed Industrial Radiographic Films*. West Conshohocken, PA: ASTM International (2002).
- FED-STD-125D, *Film, Photographic and Film, Photographic Processed (for Permanent Records Use)*. Federal Standard. Washington, DC: General Services Administration (1977).

## Standards

- ANSI IT1.15, *Photography (Films) — Industrial Radiographic Film (Roll and Sheet) and Metal Intensifying Screens — Dimensions*. New York, NY: American National Standards Institute (1994).
- ANSI IT1.48, *Photography (Films) — Medical Hard Copy Imaging Film — Dimensions and Specifications*. New York, NY: American National Standards Institute (1997).
- ANSI IT2.46, *Photography — Industrial Radiographic Film — Determination of ISO Speed and Average Gradient When Exposed to X- and  $\gamma$ -Radiation*. New York, NY: American National Standards Institute (1997).
- ANSI IT9.1-1988, *American National Standard for Imaging Media (Film) — Silver Gelatin Type — Specification for Stability*. New York, NY: American National Standards Institute (1988).
- ANSI IT9.18, *Imaging Materials — Processed Photographic Plates — Storage Practices*. New York, NY: American National Standards Institute (1996).
- ANSI IT9.2-1991, *American National Standard for Photography (Processing) — Processing Films, Plates, and Papers — Filing Enclosures and Containers for Storage*. New York, NY: American National Standards Institute (1991).



# 10

## C H A P T E R

# Radioscopy<sup>1</sup>

---

Kenneth W. Dolan, Lawrence Livermore National  
Laboratory, Livermore, California

Jerry J. Haskins, Lawrence Livermore National  
Laboratory, Livermore, California

# PART 1. Fundamentals of Radioscopic Imaging

## Principles

Radioscopy is a nondestructive testing technique, a subset of the radiographic testing method, that uses penetrating radiation to produce images viewed during irradiation. *Radioscopic imaging* and *real time radiography* mean the same as *radioscopy*.

The arrangement of radiation source, object and image plane in radioscopic imaging are similar to film radiography. Whereas traditional radiography uses film as the imaging medium, radioscopy uses a fluorescent screen to convert radiation to light for direct viewing or electronic imaging. With electronic imaging systems, the image signal is amplified and presented as an analog signal for viewing on a television monitor, video recording, analog processing or for converting to digital for computer display, storage and analysis.

Radioscopy is a powerful and versatile technique for rapid testing of objects and structures and for imaging dynamic events. For assembly line inspection, robotics and remote positioning allow rapid testing at many locations or orientations of an object and provide an inspector the freedom to review details of interest or to move on to other locations. Accept or reject decisions may be made immediately without the delay or expense that would be incurred in film processing. The same applies to large structures such as aircraft or pipelines where robotics positioning systems can be applied to testing of large areas. For dynamic events, radioscopic imaging is typically used at television frame rates of 30 frames per second, providing time resolution in a fraction of a second. High rate events can be captured with high speed cameras that operate at tens of thousands of frames per second.

Fluorescent screens consist of a phosphor material deposited on a substrate. Radiation interacts with the phosphor to produce light. The thickness of the phosphor coating and the coarseness of the grains affect both light conversion efficiency and resolution. Fine grain, thinner coatings provide higher resolution but lower light output. Screen brightness or light conversion efficiency also depends on the energy of the incident radiation. Light conversion

efficiency is generally lower for higher energy radiation.

Light from fluorescent screens may be viewed directly by the human eye, amplified in an image intensifier tube with video output, or imaged directly by a low light level video camera. Low brightness level, operator dependent vision acuity and radiation safety are significant disadvantages for viewing by the human eye. Electronic imaging by image intensifiers and low light level video provides both remote viewing for radiation safety and improved signal. Image intensifier tubes amplify the light signal by converting the light to electrons in a photocathode layer adjacent to the input phosphor layer, accelerating the electrons and then converting back to light in an output phosphor layer. A video camera provides output signal by imaging the output phosphor. Low light level video cameras are more recent developments that provide additional options for imaging higher output phosphor screens.

Many of the principles of film radiography apply directly to radioscopic imaging. The geometric rules for unsharpness and magnification are examples. Radioscopic imaging technology, however, is significantly different from film based imaging and therefore the emphasis in some of the radiographic principles is different. Dynamic range and sensitivity, for instance, are examples of differences between these techniques. This chapter presents radioscopic imaging based image acquisition by fluoroscopic screen and video technology. Digital imaging systems that use [discrete detectors](#) and [image analysis](#) are discussed elsewhere.

## Background

Radioscopic imaging has its roots in the discovery of X-rays. Roentgen used phosphorescent (or fluorescent) screens for X-ray detection. The earliest form of the radioscopic imaging technique was called fluoroscopy. With this technique, X-rays from a source pass through an object and strike a fluorescent screen. The screen emits light observed by the human eye. Human vision acuity and dark adaptation were very important for

optimum interpretation. Modern phosphors developed for fluoroscopy systems have changed dramatically over the years, resulting in improvements in both quantum efficiency and resolution.

The advent of image intensifiers, video cameras and television systems in the 1950s provided dramatic improvements in the radioscopic imaging technique and improved safety by allowing the operator to be remote from the X-ray source. Digital imaging and computer systems have further increased the possibilities of image acquisition, enhancement, information storage and display. Robotic systems, automated data acquisition systems and both online and offline image processing have made radioscopic imaging a very versatile, sensitive, rapid and safe technique for radiographic testing in both industry and medicine.

An industrial radioscopic test system is shown in Fig. 1. The source (X-ray tube), part manipulator and detector (image intensifier tube) are located in a shielded radiation chamber. The parts, already on a tray, are introduced into the chamber by conveyor belt and positioned by robotics. The source and detector system are located on radial arms and are repositioned in fixed orientation to each other to provide different angular views including different geometric magnifications. The controls for the X-ray source, part manipulator, image processing and image display are located at a computer workstation (not shown). Variations in the size of the radiation chamber make it possible to image smaller or larger items such as castings, transmission cases and wheels for the automotive industry, munitions and rocket motors for the defense and aerospace industries and electronic components and assemblies for the

electronics industry. This chapter discusses the fluorescent screens for conversion of X-rays to light, image intensifier tubes and video camera technologies and how they can be effectively used for radioscopic imaging.

FIGURE 1. Radioscopic imaging system.



## PART 2. Light Conversion

### Fluorescent Screens

#### Principles of Operation

Fluorescent screens consist of phosphor particles dispersed in a binder and coated on a reflecting, supporting base. The basic function of the fluorescent screen is to convert X-ray energy to light. This happens in three steps.

1. Absorbed X-ray energy is converted to high energy electrons.
2. Part of the kinetic energy of the high energy electrons is used to produce excited states within the phosphor material.
3. Light emission occurs when the excited states return to their normal state.

As shown in Fig. 2, an X-ray or gamma ray photon striking the screen deposits energy in a grain of phosphor at the point  $z$  releasing high energy electrons, which cause formation of excited states and emission of light photons. Typical paths followed by the photons are illustrated.

A light photon generated in the screen phosphor has a probability of leaving the emitting surface, depending on (1) the number of scattering events; (2) the probability of absorption at each collision with phosphor particles; (3) the depth at

which the light photon originates (dependent on the X-ray stopping power of the phosphor); and (4) the spatial orientation of the free path lengths between collisions.

Light emitted simultaneously with the excitation energy (X-ray absorption) is called fluorescence. By contrast, light that persists after the excitation source is removed is called phosphorescence.

#### Screen Types and Construction

Fluorescent screens use a variety of supports, depending on the application. Typical screens have a white plastic or cardboard base, about 0.4 mm (0.02 in.) thick, as a support for the phosphor material layer. The screen base must be chemically inert so as not to react unfavorably with the luminescent material. It must be uniformly radiolucent and cannot contain radiopaque inclusions, which might cause shadows on the fluorescent image. The support must also be durable enough for use in the radiation fields to be encountered.

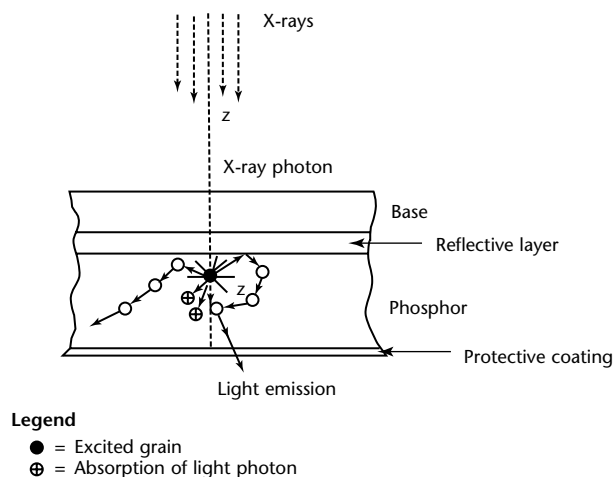
The phosphor material is in the form of small grains. This material is combined with a suitable binder and is coated on the support in a uniform layer. Grain size and thickness of the phosphor layer are construction parameters affecting performance. The final packing density of the phosphor particles is usually on the order of 50 percent. A protective surface is often added to the screen to help it resist markings and abrasive wear and to permit cleaning.

In X-ray image intensifier tubes, the fluorescent layer is deposited on the inside of a vacuum tube envelope. In this case, phosphors whose physical properties are unacceptable for use in air, such as hygroscopic sodium activated cesium iodide (CsI[Na]), can be used. The depositing technique is often proprietary.

#### Screen Characteristics

Fluorescent screens are characterized by their efficiency, spectral emission, persistence, unsharpness and gamma. Table 1 contains parameters of typical screen phosphors.

FIGURE 2. Structure of typical X-ray intensifying screen and typical paths followed by light photons.



## Efficiency

The overall efficiency of the fluorescent screen in converting X-rays to light, is composed of three terms: (1) the incident X-ray absorption efficiency  $n_a$ ; (2) the intrinsic absorbed X-ray to light conversion efficiency  $n_c$ ; and (3) the light transmission efficiency  $n_t$  determined by the path length of light in the screen coatings.

Hence the overall efficiency can be expressed in Eq. 1 as:

$$(1) \quad n = n_a \times n_c \times n_t$$

The absorption efficiency  $n_a$ , which is the fraction of the incident flux absorbed by the screen, can be calculated when the incident X-ray spectrum and the composition of the screen are known. At low energy, where X-ray absorption predominates over scatter, the absorption efficiency is about equal to the attenuation of the radiation beam. A high absorption efficiency is important for maximizing the signal-to-noise ratio in the detection process.

The conversion efficiency  $n_c$  is about equal to the phosphor efficiency under cathode ray excitation, which can be measured separately. The transmission efficiency  $n_t$  can be estimated if the scattering and absorption parameters of the screen are measured and if surface conditions are known. Experimental measurements of light photon output for X-ray photon input with typical fluorescent screen materials results in an energy efficiency in the range of 1 to 7 percent at low X-ray energies (20 to 100 kV peak).<sup>2</sup>

## Spectral Emission

Although the spectral emission of phosphors is broad band the emission spectra are characterized by a maximum intensity at a characteristic wavelength. Spectral emission is used to match the phosphor to application, whether for human eye in a direct viewing fluoroscopy system, a low light level camera in a camera based fluoroscopy system or photocathode for an image intensifier tube. Figure 3a is a plot of the spectral emission of four types of screens: calcium tungstate ( $\text{CaWO}_4$ ), lanthanum oxybromide ( $\text{LaOBr}$ ), gadolinium oxysulfide ( $\text{Gd}_2\text{O}_2\text{S}$ ) and zinc cadmium sulfide ( $\text{ZnCdS}$ ).

The effect of spectral emission is demonstrated in Table 2 where the relative light yield for different phosphors at 140 kVp X-ray energy are compared for photopic response (the human eye) and a multialkali photocathode. When measured with a multialkali photocathode, the calcium tungstate and lanthanum oxybromide screens (which emit in the blue) show an increase in response over the photopic response, which has a maximum in the green.

## Persistence

The persistence of a fluorescent screen is the time over which it continues to emit light following excitation. Persistence curves are a characteristic of phosphors. Some curves have an exponential decay, whereas others have long decay tails. An estimate of the persistence can be made by assuming an exponential decay and then assigning a decay constant (time for

TABLE 1. Phosphor parameters.

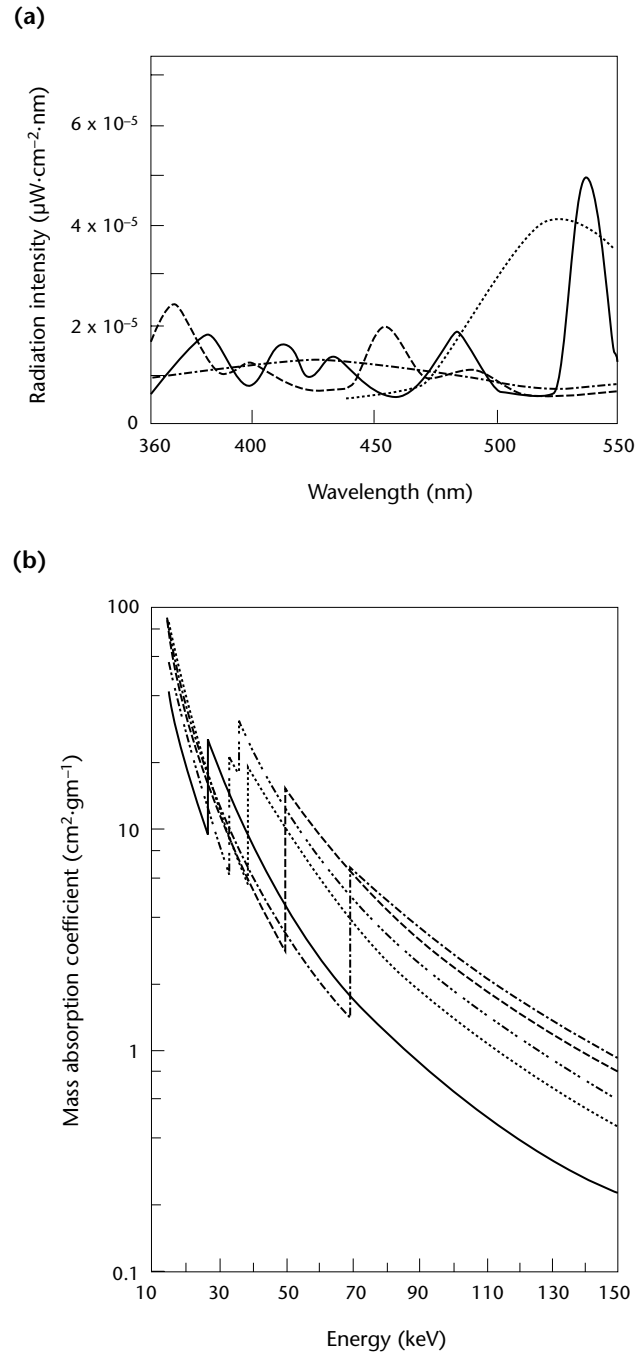
Phosphor	Chemical Symbol	Density ( $\text{g}\cdot\text{cm}^{-3}$ )	Emission Peak (nm)	Decay Constant ( $\mu\text{s}$ )
Zinc sulfide	$\text{ZnS}(\text{Ag})$	4.1	450	0.060
Zinc cadmium sulfide	$\text{ZnCdS}(\text{Ag})$	4.5	550	0.085
Sodium activated cesium iodide	$\text{CsI}(\text{Na})$	4.5	420	0.650
Calcium tungstate	$\text{CaWO}_4$	6.1	430	6.00
Terbium activated gadolinium oxysulfide	$\text{Gd}_2\text{O}_2\text{S}(\text{Tb})$	7.3	544	480.0

TABLE 2. Relative light yield as function of detector measurement.

Screen	Chemical Symbol	Emission Color	Photopic (relative yield)	Multialkali Photocathode (relative yield)
Zinc cadmium sulfide	$\text{ZnCdS}$	green	100	100
Gadolinium oxysulfide	$\text{Gd}_2\text{O}_2\text{S}$	yellow green	50	50
Calcium tungstate	$\text{CaWO}_4$	violet	7	32
Lanthanum bromide	$\text{LaOBr}$	blue	4	25



**FIGURE 3.** Fluorescent screen phosphors: (a) spectral emission; (b) mass absorption coefficient as function of energy.

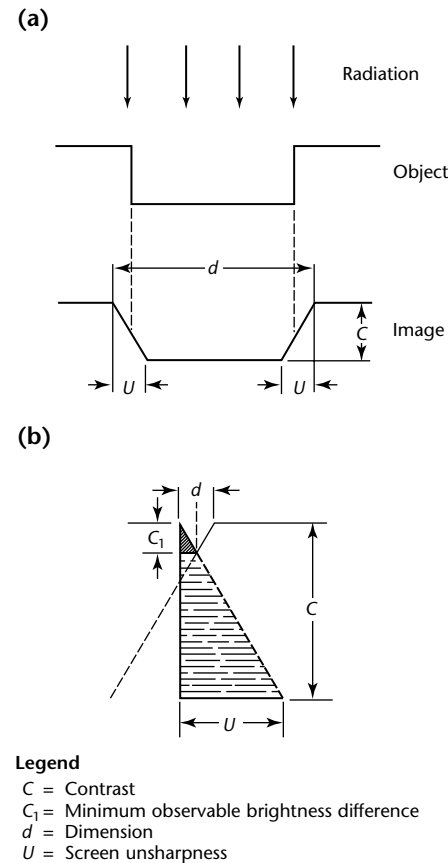


the phosphor to decay by a factor of  $e^{-1}$ , where  $e$  is the natural logarithmic base). A few typical decay constants are listed in Table 1. The persistence, particularly with rapid decay phosphors, can vary significantly depending on the purity and the manufacturing process.

### Unsharpness

Unsharpness in images formed by fluorescent screens is primarily a function of the grain size of the phosphor and the screen thickness, increasing as the parameters increase. Light transmission characteristics of the screen can also affect the unsharpness. Figure 4a demonstrates how unsharpness can affect the detection of a sharp edged discontinuity by spreading the edge shape. Here,  $C$  represents the contrast in percentage of brightness change,  $d$  represents width of discontinuity and  $U$  represents screen unsharpness. For a fixed value of  $U$ , a change in contrast  $C$  produces a change in the slope of the unsharp edge. It can be seen from Fig. 4b that when  $d$  is smaller than  $2U$ , the discontinuity will vanish

**FIGURE 4.** Effect of unsharpness on discontinuity detection: (a) spread of edge shape; (b) discontinuity above minimum contrast level.



unless  $C_1$  is above the minimum observable contrast level. Equations 2 to 4 show the relationships among variables in Fig. 4:

$$(2) \quad C_1 \leq C$$

$$(3) \quad d \leq \frac{2C_1U}{C}$$

$$(4) \quad \frac{\frac{d}{2}}{C_1} = \frac{U}{C}$$

The following relationship may be obtained from Fig. 4b:

$$(5) \quad d = \frac{2C_1U}{C} \quad \text{for } C_1 \leq C$$

Typical values of screen unsharpness for commercially available screens vary from  $U = 0.50$  mm (0.02 in.) to  $U = 1.0$  mm (0.04 in.).

### Screen Gamma

The fluorescent screen gamma  $\gamma$  is a measure of the contrast ratios between the output screen image brightness  $B$  and the input X-radiation intensity  $I$ :

$$(6) \quad \frac{\Delta B}{B} = \frac{\gamma \Delta I}{I}$$

As in film radiography, the output image must have a minimum brightness ratio between adjacent image areas for detection by an observer or an image intensifying component. For most fluorescent screens at industrial radiography energies, the screen gamma is very close to 1.0. So the fluorescent screen itself is very seldom the limiting factor as far as the total imaging system gamma is concerned.

### Radiation Energy Effects

The efficiency of fluorescent screens is a function of the energy of the radiation. This is shown in Fig. 3b where the mass absorption coefficient is plotted as a function of X-ray energy for different phosphor materials. These data are calculated from X-ray cross section tabulations.<sup>3</sup> The K absorption edge of the heaviest element in each phosphor is indicated by the step in the coefficient plot. Other than at the K absorption edge, the absorption coefficient (and hence efficiency) decreases with increasing photon energy.

The absorption efficiency is given by Eq. 7:

$$(7) \quad n_a = 1 - \exp\left[-\frac{\mu}{\rho} TP\right]$$

where  $\mu \cdot \rho^{-1}$  is the mass absorption coefficient,  $T$  the phosphor thickness and  $P$  the packed phosphor density.

The energy spectrum of the source, such as the continuum spectrum of an X-ray machine, must be considered when determining screen efficiency. The total absorption efficiency  $n_a$  is found by integrating the absorption efficiency and photon intensity over energy.

The X-ray energy spectrum incident on the screen will be changed by the presence of an object; the direct transmitted beam is hardened. At the same time, lower energy scattered radiation is generated in the object for which screens generally have higher absorption efficiency.

## Special Screens

### Neutron Sensitive Screens

Real time radiography may be performed using neutron beams when the fluorescent screen is a good neutron absorber. Elements with high thermal neutron cross sections, such as lithium-6, boron-10 and gadolinium are used in neutron sensitive screens. Plastic scintillation materials can be used for radiography with fast neutrons.

The characteristics of screen composition and construction are more important in neutron imaging than in X-ray imaging because the intensity of available neutron sources is generally lower than for X-ray sources. It is important that the screen absorb a sufficient quantity of neutrons to obtain an acceptable light yield for adequate contrast.

### High Energy Screens

Some materials, when absorbing X-rays, emit secondary electrons copiously. The phosphor materials used in fluorescent screens are generally more sensitive to electrons than to primary X-rays. At high X-ray energies, the electrons from suitable secondary electron emitters can be used to enhance the imaging process. Heavy metals such as lead, tungsten or tantalum are often used in MeV radiography, serving both as secondary electron emitters and low energy X-ray filters. Along with the production of secondary electrons to increase the absorbed energy in the adjacent fluorescent screen, the heavy metal will shield the screen from

TABLE 3. Scintillator materials and some of their properties.

Scintillator	Chemical Symbol	Density (g·cm <sup>-3</sup> )	Emission Maximum (nm)	Light Yield (10 <sup>3</sup> photons × MeV <sup>-1</sup> ·g <sup>-1</sup> )	Primary Decay (ns)	Afterglow (percent)
Bismuth germinate (BGO)	Bi <sub>4</sub> Ge <sub>3</sub> O <sub>12</sub>	7.13	480	8 to 10	300	—
Europium activated calcium fluoride	CaF <sub>2</sub> (Eu)	3.18	435	19	0.94	< 0.3 after 6 ms
Cadmium tungstate	CdWO <sub>4</sub>	7.9	470/450	12 to 15	20/5	0.1 after 3 ms
Thalium activated cesium iodide <sup>a</sup>	CsI(Tl)	4.51	550	52 to 56	1	0.5 to 5.0 after 6 ms
Thalium activated sodium iodide <sup>b</sup>	NaI(Tl)	3.67	415	38	250	—
Terbium activated high density glass	—	3.5 to 3.8	543	—	3400	<0.5 after 300 ms

a. Slightly hygroscopic.

b. Hygroscopic.

low energy scattered X-rays. Both of these processes improve the contrast sensitivity.

### Scintillator Plates

Scintillators are optically clear, generally single-crystal, phosphor materials that produce very short pulses of light as a result of X-ray interactions. In addition, the amount of light emitted is generally proportional to energy deposited in the X-ray interaction. Because scintillators are optically clear (that is, transparent to their own emission wavelengths) and single-crystal components, they can be used in thicknesses not possible with polycrystalline phosphor materials that form the light emitting coatings for fluorescent screens. Scintillators can be made as single crystals, monolithic plates or fiber optic plates. The increased thickness provides a more efficient means for absorbing X-ray energy, which is particularly important for high energy (megavolt) X-rays. In addition, scintillators are not limited in spatial resolution by material grain size as are fluorescent screens. Some scintillator types are available in sizes up to 0.30 m (12 in.) diameter or more, with thicknesses ranging from 2 mm (0.1 in.) to 100 mm (4.0 in.) or more. Typical scintillator materials and their properties are given in Table 3.

To be useful for radioscopic imaging, the scintillator must be nearly flawless and must be large enough in area to provide the desired field of view. The scintillator plate must be thin enough to allow lens focusing at limited depth of field associated with fast lenses and thick enough for adequate conversion of X-ray energy to light. Light emission must be in the wavelength compatible with camera imaging and afterglow must be low.

One of the highest density scintillators with emission in the green is cadmium tungstate (CdWO<sub>4</sub>). This scintillator is available nearly flaw free in diameters of 10 to 20 mm (0.4 to 0.8 in.) and

thicknesses of 1 to 2 mm (0.04 to 0.08 in.). It provides an efficient imaging medium at high resolution for small fields of view. Features as small as 4 μm have been resolved with this material using a plate thickness of 0.7 mm (0.03 in.).<sup>4</sup>

The terbium activated high density glass is an innovation that provides a large area imaging, 250 to 300 mm (10 to 12 in.) diameter, and thicknesses from 2 mm (0.08 in.) to 12 mm (0.5 in.) and greater. This is available as a monolithic plate and as a fiber optic plate with fiber diameter as small as 10 μm. Spatial resolution with these materials has been demonstrated in excess of 20 line pairs per millimeter for low X-ray energies (less than 120 kV).<sup>5</sup>

## PART 3. Image Quality

The factors that limit resolution in radioscopic imaging are similar to those in normal film radiography. Some aspects of radioscopic image quality are given in Table 4.

In radioscopic imaging only the X-ray energy absorbed during the scan time of the image pickup system will add to each single image. For a direct viewing fluoroscopic system, this is the image summation time of the human eye (0.2 s). With the increased sophistication of radioscopic imaging systems, the limits of object thickness penetrated and contrast of details detected are only restricted by the quantum structure of the radiation and the noise introduced by each stage of the imaging process.

Each detail, as defined by size and contrast, can be described by a number of radiation quanta that is proportional to the intensity of the radiation. The relative statistical fluctuation of radiation intensity is proportional to the reciprocal of the square root of intensity. In general, radiation contrast in the image element must exceed the value of this fluctuation to yield detail.

### Contrast

#### Subject Contrast

*Subject contrast* for fluorescent screens is defined as the fractional change in brightness resulting from a change  $\Delta x$  in absorber thickness. The nearly linear relationship between screen brightness  $B$  in candela per square meter (or millilambert) and X-ray intensity  $I$  on the screen in gray (or roentgen) per minute may be written as:

$$(8) \quad B = mI$$

or

$$(9) \quad \Delta B = m \Delta I$$

where  $m$  is the proportionality constant. The absorption law for monochromatic radiation is:

$$(10) \quad I = I_0 \exp[-\mu x]$$

Differentiating Eq. 10 gives:

$$(11) \quad \Delta I = -\mu I \Delta x$$

where  $\mu$  is the linear absorption coefficient and  $x$  is the absorber thickness. Combining the above equation gives Eq. 12:

$$(12) \quad \frac{\Delta B}{B} = -\mu \Delta x = C$$

where  $C$  is contrast.

The effect of X-ray energy on subject contrast  $C$  manifests itself through the absorption coefficient  $\mu$ , which varies with X-ray energy. The efficiency of the fluorescent screen affects subject contrast by its ability to convert the incoming X-ray photons to light and manifests itself through the screen brightness response  $B$ .

#### Observed Contrast

The *observed contrast* in radioscopic imaging is affected by several factors beyond the screen response. The effects of all system components must be included. This is done by defining proportionality factor  $\gamma$  for the contrast ratio of output intensity  $B$  to the input intensity  $I$  (see also Eq. 6):

$$(13) \quad \gamma = \frac{\frac{\Delta B}{B}}{\frac{\Delta I}{I}}$$

or

$$(14) \quad \frac{\Delta B}{B} = -\gamma \mu \Delta x$$

TABLE 4. Image quality.

Aspect	Factor
Subject contrast	thickness, scatter, radiation hardening
System contrast	screen gamma, intensifier, camera, monitor
Definition, geometric	source focal spot size, source-to-object distance, object-to-screen distance, screen thickness, motion
Definition, mottle	quantum fluctuations, screen gain, raster scan of monitor

where  $\mu$  is the linear absorption coefficient and  $\Delta x$  is the change in the thickness of the absorber material. The combined system gamma is the product of the individual components in the imaging chain. In a vidicon television chain, for example, the system gamma would be given by:

$$(15) \quad \gamma = \gamma_a \gamma_c \gamma_k \gamma_s$$

where  $\gamma$  = overall system gamma,  $\gamma_a$  = electron amplifier chain gamma,  $\gamma_c$  = vidicon tube gamma,  $\gamma_k$  = television picture tube gamma and  $\gamma_s$  = fluorescent input screen gamma.

For a typical case, the fluorescent screen gamma is taken as  $\gamma_s = 1.0$ , a conventional closed circuit television amplifier chain provides  $\gamma_a = 1.0$  (maximum), the vidicon tube provides a  $\gamma_c = 0.9$  and the television picture tube gamma is typically  $\gamma_k = 3.0$ .<sup>6</sup> Although it appears that considerable contrast gain is possible in a television chain, the final imaging element, the human eye, must also be considered. The human eye gamma is nonlinear and is less than one. A typical value of the human eye gamma is 0.3. With increased viewing room brightness or glare, this value drops rapidly.

### Effects of Scatter

Scattered radiation affects contrast in fluorescent screens by effectively raising the background brightness level. The scattered radiation affects only the primary imaging component of a radioscopic system, the fluorescent screen. Here, the contrast is defined as:

$$(16) \quad C = \frac{\Delta B}{B} = \frac{\Delta I}{I}$$

If however, scattering is not eliminated, the equation for contrast becomes

$$(17) \quad C = \frac{\Delta I}{I + I_s}$$

where  $I_s$  is the scattered radiation intensity. Now, if  $I_s = KI$ , where  $K$  is the scattering factor, the equation for screen contrast becomes

$$(18) \quad C = \frac{\frac{\Delta I}{I}}{K + 1}$$

As this equation illustrates, it is important to keep the scattered radiation incident on the fluorescent screen to a minimum to keep the contrast at an acceptable level.

## Control of Scatter

Scattered radiation comes from many sources in a radioscopic imaging setup. There is scatter from the room, object, fixtures and air path in the primary radiation beam and scatter from objects placed in the path of the beam. The control of scatter for radioscopic imaging is the same as for normal radiography. Specific techniques to reduce scatter are listed below.

1. Collimate the primary beam to the minimum viewing area necessary.
2. Shield the setup to reduce room scatter from walls, ceiling and floor.
3. Filter the primary beam to remove the low energy portion of the spectrum.
4. Filter the radiation beam between the object and the fluorescent screen because many filters preferentially remove the lower energy scattered radiation.
5. Use antiscatter grids, both fixed and moving, between the object and the fluorescent screen.
6. Use projection magnification to increase the distance of the fluorescent screen from the object scatter.

In general, it is very important in radioscopic imaging to consider all areas where scattered radiation can be introduced and to attempt to eliminate or reduce their effect to improve image contrast.

## Definition

### Unsharpness and Optimum Magnification

The same rules that apply for unsharpness and optimum magnification in film radiography apply to radioscopic imaging. Unsharpness and optimum magnification are discussed elsewhere.<sup>1</sup>

### Motion Blur

In radioscopic imaging, unsharpness due to object movement can limit image definition. Determining factors for this are the X-ray excitation rate, the decay time of the fluorescent screen phosphor and the delay time or scan time of the imaging system components. Typically, radioscopic systems are used with continuous or rapid pulse rate X-ray excitation (120 pulses per second or greater), rapid decay phosphor (on the order of milliseconds or faster) and frame rates of 30 frames per second.

## Quantum Mottle

*Quantum mottle* is the statistical fluctuation of brightness on fluorescent screens and is due to the randomness of X-ray production and absorption and needs to be considered in any radioscopic imaging. The following list shows the numerous sources of this fluctuation: (1) X-ray photon production, (2) X-ray photon absorption in the object, (3) X-ray photon absorption in the screen, (4) conversion of X-ray photons to light photons, (5) fraction of the light photons reaching the eye after traversing the imaging system and (6) light photon absorption in the retina.

These fluctuation obey poisson statistics so that the standard deviation  $\sigma$  is equal to the square root of the intensity  $n$ :

$$(19) \quad \sigma = \sqrt{n}$$

Because radioscopic imaging involves a series of processes, the standard deviation for the total sequence is:

$$(20) \quad \sigma^2 = \sigma_1^2 + \sigma_2^2 + \dots + \sigma_n^2$$

Certain stages in the process will cause either an increase or decrease in the intensity. The relationship can be shown to a first approximation:

$$(21) \quad \sigma^2 = gn$$

where  $g$  is the amplification of the process (from the state of lowest intensity to the final observation by the retina) and  $n$  is the final intensity.<sup>7</sup>

To observe detail in the light image reaching the retina, there must be a detail intensity difference greater than the standard deviation:

$$(22) \quad \Delta n = k\sigma$$

where  $\Delta n$  is the smallest difference in the number of detectable photons in the retinal image and  $k$  is a constant termed the threshold contrast to standard deviation ratio.

Contrast is defined as:

$$(23) \quad C = \frac{\Delta n}{n}$$

Then:

$$(24) \quad C = \frac{k\sqrt{g}}{\sqrt{n}}$$

Because  $n$  is the total photon intensity in the retinal camera image, it is equal to the

number of photons arriving per second, times the storage time of the detector  $t$ . Therefore:

$$(25) \quad n_t t = n$$

where:

$$(26) \quad n_t = \frac{\pi d^2 n_0}{4}$$

Here  $d$  is the diameter of the object under observation and  $n_0$  is the number of photons reaching the detector per unit area of the fluorescent screen per second.<sup>7</sup>

Now contrast is defined again:

$$(27) \quad C = \frac{2k\sqrt{g}}{d\sqrt{\pi t n_0}}$$

or

$$(28) \quad d = \frac{2k\sqrt{g}}{C\sqrt{\pi t n_0}}$$

The smallest discernible object size that can be detected is seen from Eq. 28 to improve with increasing contrast and number of stimulating photons. Detail sensitivity in an image will be limited by statistical fluctuations as long as  $d$  is greater than the unsharpness of the system.

The statistical fluctuations of fluorescent screen brightness, which are due to the randomness of the process, are important at low brightness levels, which usually occur with low intensity sources. Most industrial X-ray machines produce sufficient intensity to render the statistical fluctuation unimportant for most applications. Much of the effect of quantum fluctuation in cases where it is important can be removed in near real time by video frame averaging or summing.

## Radiation Sources

The radiation source plays an important role in radioscopic imaging. In choosing a radiation source, consideration must be given to the types of materials to be tested, densities, thicknesses, smallest feature size to be resolved, smallest thickness change to be detected, response of the radioscopic imaging system and rate of image acquisition. High output, high stability, constant potential X-ray systems are available for these applications. Minifocus and microfocus X-ray tubes expand the possibilities of radioscopic imaging to include high spatial resolution applications.



Limitations of generator wave form are no longer a consideration with the availability of high frequency generators.

Projection magnification is one of the most advantageous applications of radioscopic systems. A small focal spot permits the object to be moved away from the detector, allowing easy robotic manipulation. The projection increases magnification so that fine detail can be imaged with a detector whose resolution is relatively poor. Magnifications of 2× to 50× are common in microfocus radioscopic systems.

Linear accelerators for high energy applications, for example, greater than 1 MeV, use resonant waveguides to accelerate electrons to a target. The radiation is produced in pulses typically of 3 to 4 μs width and at repetition rates of 60 to 420 Hz. Radioscopic imaging components may need shielding from radiofrequency fields produced by accelerator operation and from direct high intensity X-rays. Setup configuration, synchronization of the imaging system to the accelerator pulse rate and image frame averaging can be used to reduce or eliminate these effects.

Neutron radioscopic imaging is accomplished with portable accelerator neutron sources and neutron reactors with beam ports suited for radioscopic imaging. The effective focal spot of neutron sources is typically large. For most neutron sources, whether accelerator type or reactor type, the focal spot is defined by the collimator opening at the neutron source. To transport a reasonable number of neutrons down the beam tube, these collimator openings are necessarily larger than the focal spots possible with X-ray machines and linear accelerators.

## Radiation Energy

The size of the object to be imaged and the material type will determine the radiation type and energy to be used. As a general rule, the radiation type and energy should be selected so that the object thickness to be penetrated is three to five half value layers. One half value layer reduces the transmitted radiation intensity by 50 percent. Satisfactory results can also be obtained if deviation from the rule is no greater than a factor of 2 (that is, in the range from 1.5 to 10 half value layers). Configuration of the part is of some importance because scattering from the part will reduce contrast.

The half value layer (HVL) can be equated with values of  $\mu x$  from the absorption law stated in Eqs. 10 and 11:

$$(29) \quad I = I_0 \exp(-\mu x)$$

or

$$(30) \quad \frac{\Delta I}{I} = -\mu \Delta x = -\mu x \cdot \frac{\Delta x}{x}$$

Table 5 presents this result in tabular form. The image contrast, or detection percentage, given in this table is based on a subject contrast of  $\Delta x \cdot x^{-1} = 2$  percent. The image contrast is seen to increase considerably for larger thicknesses expressed as  $\mu x$ . This improvement is only realized in practice if the transmitted intensity is large enough to produce a statistically accurate measurement.

**TABLE 5. Half value layer thicknesses associated with different values of  $\mu x$ .**

Thickness (half value layers)	Value of $\mu x$	Contrast $\Delta I \cdot I^{-1}$ (percent)	Transmission $I_0 \cdot I^{-1}$ (percent)
1.45	1.0	2	36
2.17	1.5	3	22
2.89	2.0	4	13
3.62	2.5	5	8
4.33	3.0	6	5
5.05	3.5	7	3
5.78	4.0	8	1.8
6.50	4.5	9	1.1
7.22	5.0	10	0.67
7.94	5.5	11	0.41
8.66	6.0	12	0.25
9.40	6.5	13	0.15
10.00	7.0	14	0.09

## PART 4. Imaging Systems

### Introduction

Imaging systems with video pickup for remote viewing offer advantages of radiation shielding for operator protection, display monitor with lighting adjusted for vision acuity, video signal for image enhancement and computer analysis. The fluorescent screen converts radiation to light and either an image intensifier is used to boost light intensity to a level suitable for pickup by a solid state or television camera or a low light level camera is used to image the screen directly. The signal from the camera is sent to a television monitor or computer video card and monitor for viewing. A video or digital recorder is used to provide permanent record of the test.

At X-ray energies above 1 MeV, shielding is used to protect the electronic components from radiation with camera placed out of the direct line of radiation by use of folding mirrors. Below 300 kV, the intensifier and camera can be placed in the direct line of the radiation.

Typically, radiation damage occurs in electronics such as transistors at  $10^3$  Gy ( $10^5$  rad) and will discolor optical components at  $10^3$  to  $10^4$  Gy ( $10^5$  to  $10^6$  rad). Table 6 lists radiation damage thresholds for a few components. Given time outside the radiation field, most materials will recover from the damage. Specialized equipment such as camera tubes can be made to tolerate up to  $10^6$  Gy ( $10^8$  rad).

Glass may fluoresce under strong irradiation resulting in undesired light signals. Noise may also be generated in the electronics, increasing with the radiation intensity. Good shielding practice is desirable for medium energy

systems and very important in high energy operations. Shielding for personnel protection is a necessary feature.

### Image Intensifier Tubes

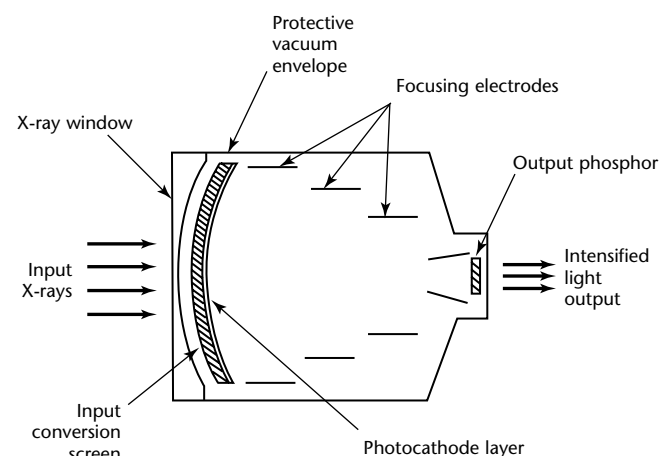
The image intensifier tube converts photons to electrons, accelerates the electrons and then reconverts them to light. Figure 5 shows a generalized diagram of an intensifier tube. Intensifiers typically operate in the range of 30 to 10 000 light amplification factors. The intensification is not necessarily solely electronic but may also include a reduction in image area where electrons from a large area input screen are focused on a small area output screen.

The earliest type of image intensifiers for X-ray applications used a zinc cadmium sulfide (ZnCdS) layer inside the glass envelope to convert the X-rays to light. The photocathode adjacent to the fluorescent layer converted the light to electrons. The original X-ray tube used a 25 kV potential between the photocathode and output phosphor. Even though only 10 percent of the light photons from the fluorescent screen would generate electrons at the photocathode and only 10 percent of the accelerated electrons would produce light at the output phosphor, a  $10\times$  to  $15\times$  increase in luminous flux was generated by the acceleration. The tube had a curved input screen with a 130 mm (5 in.)

TABLE 6. Radiation damage thresholds.

Component	Threshold	
	kGy	(Mrad)
Silicon semiconductor	70.0	(7.00)
Germanium semiconductor	0.50	(0.05)
Capacitors	3000 to 7000	(300 to 700)
Resistors	2000 to 5000	(200 to 500)
Ceramics, glass, optical	0.20	(0.02)
Plastics	0.20	(0.02)

FIGURE 5. X-ray image intensifier tube design.



diameter and an output screen with a 15 mm (0.6 in.) diameter. The ninefold reduction in diameter from the fluorescent screen to the viewing screen provided an additional factor of 80 in brightness gain. The total gain was between 800 and 1200.<sup>8</sup>

Technical improvements in electronic gain, fluorescent and photocathode layer efficiencies and electron optics have made modern X-ray image intensifiers very useful in both medical and industrial applications.<sup>9-13</sup> Sodium activated cesium iodide (CsI[Na]) is now commonly used as the fluorescent layer because it has twice the X-ray absorption of zinc cadmium sulfide and because its crystalline structure minimizes lateral light diffusion. Rare earth phosphors such as gadolinium oxysulfide ( $Gd_2O_2S$ ) are also found to be superior to zinc cadmium sulfide. At X-ray energies below 100 kV, sodium activated cesium iodide is very good; at higher X-ray energies, the rare earths are more useful.<sup>13</sup>

Modern tubes are available with 100 to 400 mm (4 to 16 in.) input diameters, multiple modes that electronically select variable field size of the input and fiberoptic output for direct camera coupling. A typical 210 mm (8 in.) tube performs with resolution on the order of 4 line pairs per millimeter and gains on the order of 10 000. Resolution is at a maximum at the center of these intensifiers and decreases somewhat at the edges.

The advantages of these tubes are the relatively low cost, generally compact size and high resolution and contrast. A disadvantage is that minification will increase image unsharpness. Also, because a ratio of length to diameter of from 1.0:1.0 to 1.5:1.0 is required for the electron optics, large diameter inputs require large tubes. This requirement not only increases bulk but creates a potential implosion hazard. The curved input screens in these tubes cause distortion. The tubes are sensitive to voltage drifts, stray magnetic fields and space charge defocusing at high dose levels.<sup>12</sup> Electron scattering, thermionic emission and light reflection on interior surfaces are causes for loss of contrast from intensifiers. Fabrication techniques in the latest generation tubes minimize these problems.

Tubes with 360 mm (14 in.) input have been manufactured.<sup>14</sup> The advanced vacuum tube technology requires a metal tube body. A titanium membrane is used for the entrance window to withstand atmospheric pressure and maintain transparency to X-rays. The titanium produces less scatter than a glass window that improves contrast. An acceleration voltage of 35 kV is used. Limiting

resolution in the large format is specified at 3.6 line pairs per 1 mm (91 line pairs per 1.0 in.). Tubes as large as 400 mm (16 in.) diameter have also been marketed.

## Channel Electron Multiplier

The *channel electron multiplier* or *microchannel plate* (MCP) is an assembly of small tubes for amplifying an electron signal using secondary emission. The channels are glass coated or ceramic coated with a high resistance material on the inside. A potential difference of 500 to 1000 V is applied across the channel plate. An electron entering the channel will strike a wall causing one or more secondary electrons to be released. These will continue to strike the channel wall yielding more electrons as they are accelerated by the electric field along the channel. The gain of the channel multiplier depends on the applied voltage and the ratio of length to diameter.

Channel electron multipliers are limited only by the technology for fabricating small diameter channels that do not break down in the electron field. With 10 kV and a length-to-diameter ratio of 50, a typical gain is about  $10^4$ . The resolution of the device is limited by the size of the channel spacing.<sup>15,16</sup> Figure 6 shows a diagram for a microchannel electron multiplier.

The channel electron multiplier is used in conjunction with an electrostatic image intensifier tube to form what is called a *second generation* or *third generation image converter*. In these devices, a photocathode is coated on the inside surface of the input window. A voltage applied between the photocathode and the microchannel plate accelerates the photoelectrons to the input surface of the small channels that make up the electron multiplier. Electron multiplication occurs as described above. A high voltage applied between the output of the microchannel plate and a phosphor screen coated and the inside surface of the output window accelerates the electrons between the two. The electron image is converted back into a photonic image at the output window.

The simplest electron optics for focusing electrons in second generation and third generation microchannel electron multiplier image intensifiers is based on proximity planar electrode design. The proximity image intensifier consists of an input window (photocathode surface), microchannel plate and the output window (phosphor surface), all parallel and in close relative position to each other. Appropriate

voltages are applied between the elements to provide minimum electron spread for a distortion free image at the output window. Proximity focused image intensifiers offer small size with little increase in length as the diameter is made larger.

Direct X-ray sensitive microchannel plates can be made. A metallic converter that emits secondary electrons following a high energy photon excitation (200 kV and above) serves as the input. These electrons are amplified in the channels.<sup>17</sup>

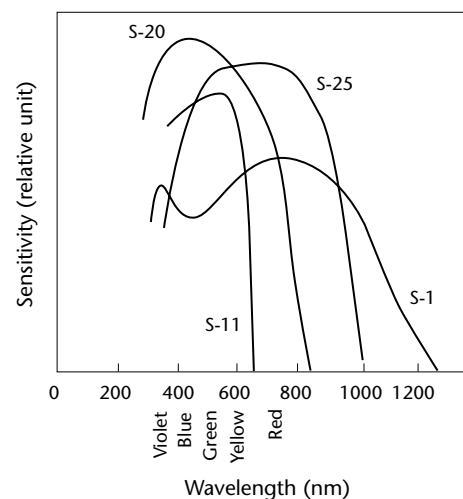
## Spectral Matching

Image intensifiers rely on a photocathode to convert input light radiation to electrons. The X-ray image intensifiers have a fluorescent screen ahead of the photocathode to convert X-rays to light. The spectral response and sensitivity varies among photocathode materials. See Fig. 7 for the spectral response of several

typical photocathodes. Desirable characteristics include high efficiency at the wavelength of light being observed and a low dark current (the signal level when no light is falling on the photocathode).

The light emitted from the intensifier is generated by the action of electrons on a phosphor. The spectral emission characteristics of some common phosphors are shown in Fig. 8.

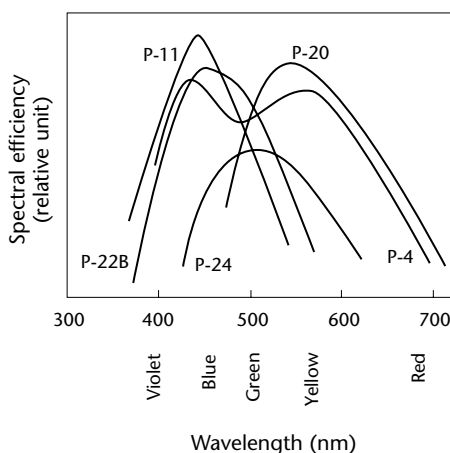
FIGURE 7. Photocathode response spectrum.



### Legend

S-1 =  $\text{Ag} + \text{Cs}_2\text{O}$ ,  $10^{-10}$  to  $10^{-13} \text{ A}\cdot\text{cm}^{-2}$   
 S-11 =  $\text{Cs}_3\text{Sb}$ ,  $10^{-14}$  to  $10^{-15} \text{ A}\cdot\text{cm}^{-2}$   
 S-20 =  $\text{Na}_2\text{KSb} + \text{Cs}$ ,  $10^{-15} \text{ A}\cdot\text{cm}^{-2}$   
 S-25 =  $\text{Na}_2\text{KSb} + \text{Cs}_3\text{Sb}$ ,  $10^{-15} \text{ A}\cdot\text{cm}^{-2}$

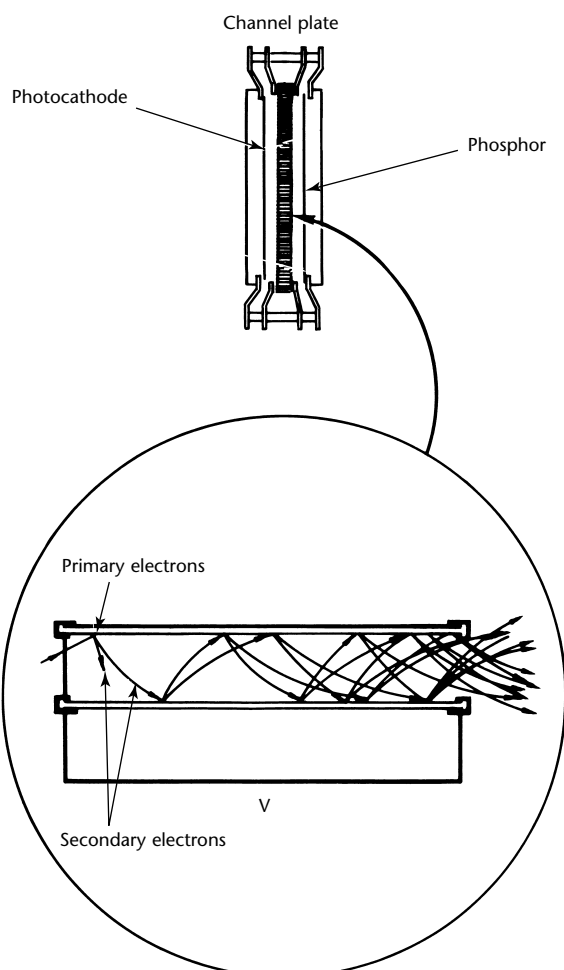
FIGURE 8. Phosphor spectrum.



### Legend

P-4 =  $\text{ZnS}:\text{Ag} + \text{ZnCdS}:\text{Ag}$   
 P-11 =  $\text{ZnS}:\text{Ag} (\text{Ni})$   
 P-20 =  $\text{ZnCdS}:\text{Ag}$   
 P-22B =  $\text{ZnS}:\text{Ag}$   
 P-24 =  $\text{ZnO}:\text{Zn}$

FIGURE 6. Microchannel plate.



## Statistics

The image intensifier system can improve imaging by boosting the light output so that the statistical limitation in the image process is not at the eye but at the input fluorescent screen. The intensifier itself operates on a statistical process for the generation of electrons and the regeneration of light. The sources of fluctuation are essentially independent, so the Eqs. 19 and 20 apply.

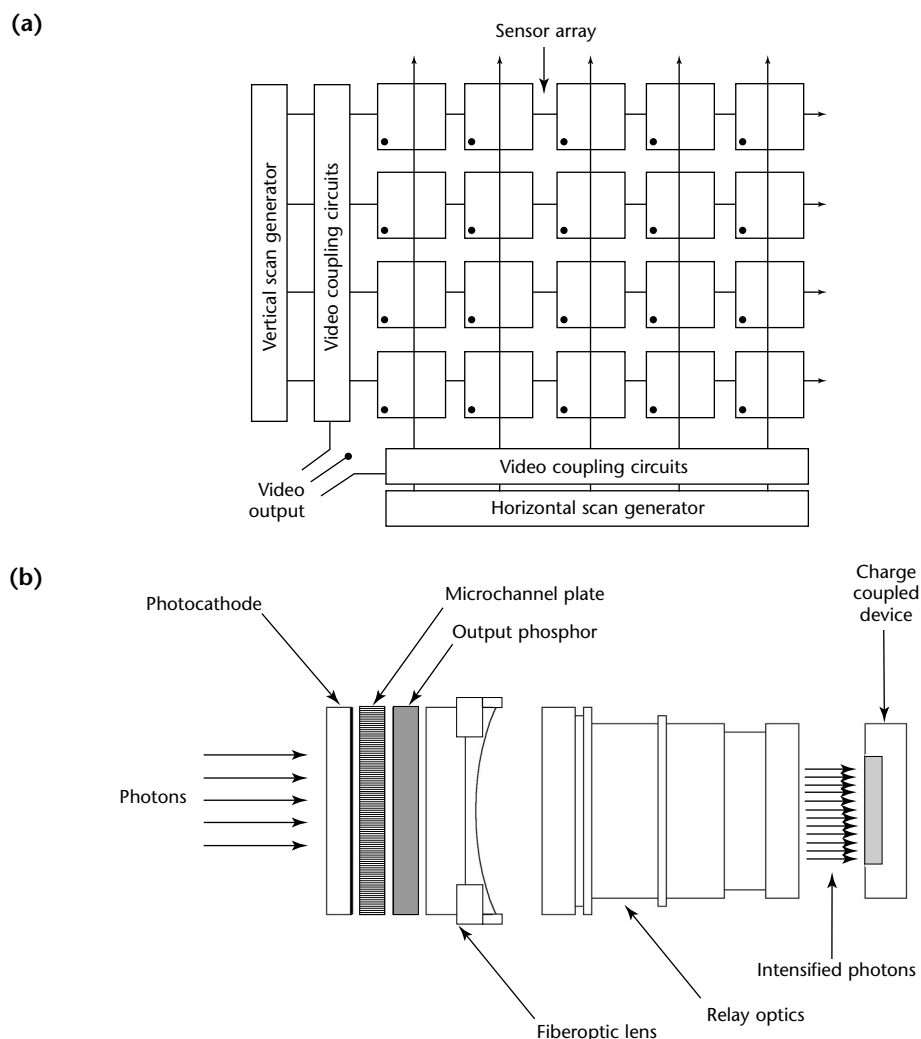
Amplification  $g$  (where  $g = \sigma^2 \cdot n^{-1}$ , per Eq. 20) may be used for improving detail sensitivity in an intensifier system. This improvement is accomplished by choosing that amplification that makes the number of light quanta (used by the observer's eye) equal to the number of radiation quanta used by the input fluorescent screen.

## PART 5. Cameras

Up until the last few years, real time X-ray imaging systems (fluoroscopic or radiosopic systems) typically used a television camera in combination with a device (such as an image intensifier tube or phosphor screen) to convert incident X-rays into visible light at wavelengths compatible with the response of the camera. Television cameras with image tubes were the common implementation. Systems introduced at the beginning of the twenty-first century, however, use *charge coupled device* (CCD) cameras almost exclusively. Charge coupled

devices and related solid state devices have advantages over image tubes in stability, geometric accuracy, signal uniformity and size. Conversion of X-radiation to visible light image is provided by a phosphor screen or scintillator plate. The light image is collected by the charge coupled device camera by either lens coupling (with or without folding mirrors) or by fiber optic bundle coupling (Fig. 9b). A more recent advance in the field of radiosopic X-ray imaging is flat panel solid state arrays.

FIGURE 9. Charge coupled device: (a) array schematic; (b) intensified camera.





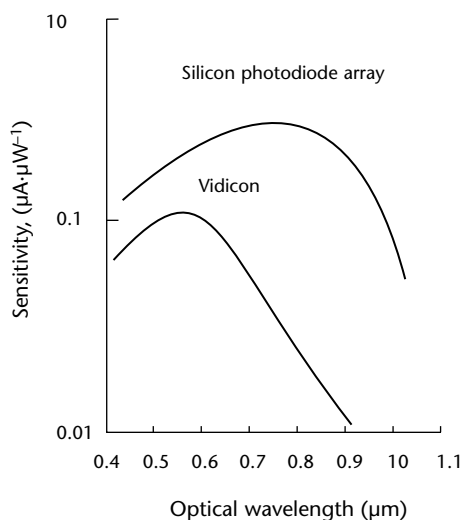
[These devices are discussed in with digital imaging elsewhere in this volume.](#)

## Charge Coupled Devices

Charge coupled devices and related solid state cameras use an array of photodiodes or charged coupled devices as the sensitive layer. These arrays may be linear or area arrays of individually addressable elements. The solid state cameras are small and have wide spectral response (Fig. 10), reduced lag, higher quantum yields (50 percent) and (depending on the application) may have equivalent resolution capabilities when compared to commercially available vidicon cameras. Solid state cameras are rugged, are not damaged by intense light images and do not require the scanning electron beam found in vidicons.

The photodiode arrays in solid state cameras are simple photon detectors, typically reverse biased silicon photodiodes, that absorb incident photons and liberate current carriers. This gives rise to a current referred to as the *photocurrent signal*, proportional to the arrival rate of the incident photon. The efficiency of the photodiode strongly depends on its material and construction as well as the wavelength of the incident photons. The diodes consist of *p* type islands in an *n* type substrate. Standard arrays are available with  $128 \times 1024$  diodes with a center spacing as small as  $25 \mu\text{m}$ . A dynamic range of 100:1 is typical.<sup>18</sup>

**FIGURE 10.** Sensitivity of a photodiode array (solid state) camera versus vidicon camera.



Charge coupled devices work like photodiodes.<sup>19-21</sup> A photon, incident on the depletion region of a charge coupled device, will create an electron hole pair if absorbed. This creates a current flow that, in a charge coupled device, is stored in the potential well of the device. The amount of charge collected at the potential well is in direct proportion to the amount of local light intensity.

The charge coupled device is fabricated with a combination of thin film technology and silicon technology. Arrays are available in a variety of configurations, such as  $768 \times 512$ ,  $1536 \times 1472$  and  $2184 \times 1472$  with photoelement center spacing typically ranging from 9 to  $23 \mu\text{m}$ . More recently, diode arrays as large as  $4000 \times 4000$  and even  $8000 \times 8000$  have become available. A dynamic range of 1000:1 (10 bits) is typical but 4000:1 (12 bits), 16 000:1 (14 bits) and 64 000:1 (16 bits) are common.

The image on the solid state array is coupled to video circuitry by horizontal and vertical scan generators that read the charge level at the detector elements. Figure 9 shows the schematic of a charge coupled device array. The output of the video can be specified to fit a particular video format. The clock sequence, which sequentially reads the charge level on each device, is started after a suitable image integration time. This integration time can be adjusted, making solid state cameras useful for low light level applications, provided the detection element can retain the charge over the integration period.

The interesting feature of solid state cameras is that individual pixel elements may be addressed and the signals processed digitally. With individually addressable elements, the integration time and the video output format may be simply specified. The cost of solid state cameras increases significantly with increasing array size and the electronic circuit complexity required to scan large arrays. Each element must be individually calibrated for uniform response throughout the field. This feature can be used to correct nonuniform fields in radiography. Because each element is independent, blooming can be controlled; a bright element does not spill over into a neighboring dark element.

The imaging in real time radiographic applications may be accomplished with optical focusing of the light from a scintillation screen onto the solid state detector. In this case, the image format and resolution are similar to conventional television cameras. Also, scintillation materials may be deposited directly on the array. Each element becomes an independent radiation detector and the

resolution is dependent on the element spacing.

## Intensified Charge Coupled Device Cameras

Intensified charge coupled device cameras consist of a microchannel plate image intensifier tube with relay optics to a charge coupled device incorporated into a single camera body. Proximity focused microchannel plate image intensifiers offer smallest camera body size as described above. Relay optics transmits the image by exiting the intensifier to the charge coupled device image array as shown in Fig. 9. Typical luminance gain is 18000 at 20  $\mu\text{lx}$  ( $2 \times 10^{-6}$  ftc) input. The limiting resolution of the intensifier is typically 30 line pairs per millimeter.

Automatic brightness control can be built into the electronics to automatically limit the maximum output of the intensifier to prevent saturating the charge coupled device array. The output can be limited by sensing the current in the microchannel plate and adjusting the microchannel plate voltage accordingly. Automatic brightness control is used not only to protect the charge coupled device from saturation but also allows intrascene dynamics (very dark and bright areas in the same image) to be viewed with good contrast at both extremes.

## Optical Coupling

To couple optical signals between components, real time imaging systems use fluorescent screens for conversion from X-radiation to light and systems use chains connecting intensifiers to television camera. Mirrors or lenses are the most common means of coupling.

Front faced silver mirrors must be used to avoid ghost images caused by multiple reflections in back faced mirrors. Optical lenses provide good coupling, depending on the  $f$  number and transmission characteristics. The illuminance  $E$  on a pickup surface, coupled by a lens in a simple optical system, is given by:

$$(31) \quad E = \frac{\pi BT}{4f^2(1 + M)^2}$$

where  $B$  is the luminance of the output phosphor,  $T$  is the lens transmission,  $M$  is the magnification and  $f$  is the  $f$  number, or relative aperture of the lens — that is, the ratio of focal distance to aperture diameter. The lower the  $f$  number, the more light is collected for imaging.

Simple lenses are not often used in coupling because of the low optical efficiency. For example, if a reduction in image size by a factor of 2 is required from the coupling, the distance from phosphor to lens must be twice the distance from lens to pickup surface. From the lens formula, the distance from phosphor to lens will be three times the focal length of the lens, giving poor light collection efficiency. With a coupling of one to one, this distance is still twice the focal length.

Collimated optics are superior because the objective lens, focused at infinity, is located at its focal length from the phosphor. Collection efficiency is nine and four times greater, respectively, for the two magnifications discussed above ( $2\times$ ,  $1\times$ ). The second lens will determine the image size at the pickup surface by the ratio of its focal length to the focal length of the objective lens. Vignetting, a reduction in light intensity at the edges, does occur in collimated optics. This reduction is minimized when the lenses are close to each other. Some real time imaging systems in the 1980s used specialized optics such as bouwers-schmidt lenses, where concentric mirrors provide a low  $f$  number<sup>22</sup> — for example, 0.65. Since then, the light collection efficiency of cameras have obviated extreme lens coupling systems.

Fiber optics may also be used for coupling. Intensifier tubes often have fiber optic input and output surfaces. These may be coupled directly to other components with similar surfaces by using an optical gel. Fiber optic light guides can be considered for moving light from one location to another (that is, from the fluorescent or phosphor screen to the camera). The potential advantages of this are greater retention of the light, one-to-one size transfer, improved contrast by suppression of undesirable reflections and shortening of the system dimensions. Fiber optic connections can also be used over considerable distance or around unusual obstructions.

Fibers for fiber optic systems are glass or plastic with diameters of 1 or 2  $\mu\text{m}$  to 50  $\mu\text{m}$ . The fiber optic array operates on total internal reflection. To reduce leakage each fiber is coated with a material having a lower index of refraction. Losses in the fiber optic system are due mainly to the opacity of the fibers in long systems or the acceptance angle of the light in short lengths.

## Image Tubes

A wide variety of television cameras and image tubes are available for use on real time imaging systems. Many different

camera configurations can be used to accommodate test requirements. On one extreme is the small compact camera with no user adjustments. At the other extreme is the larger, two-piece camera, with many controls for optimizing image quality. In addition to solid state cameras as discussed above, a variety of image tubes are also available. The most common types for radioscopic applications are (1) vidicons, (2) silicon intensifier targets, (3) image isocons and (4) X-ray sensitive tubes.

### Vidicons

The vidicon is a small, rugged and simple tube. An electron beam scans a light sensitive photoconductive target. A signal electrode of transparent material is coated onto the front of the photoconductor. The scanning electron beam charges the target to the cathode potential. When light is focused on the photoconductor, the target conductivity increases, changing the charge to more positive values. The signal is read by the electron beam that deposits electrons on the positively charged areas, causing a capacitively coupled signal at the signal electrode (Fig. 11).

The vidicon has a number of variations, depending on the selection of the photoconductive material. The standard vidicon uses an antimony trisulphide layer. The plumbicon uses a lead oxide junction layer. The newvicon

uses cadmium and zinc telluride and the silicon diode tube uses a silicon diode array target structure.

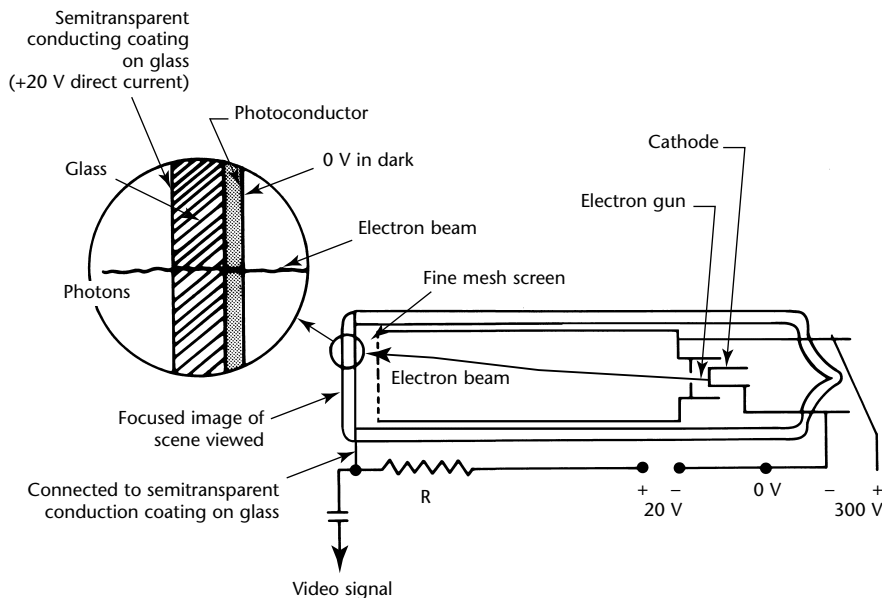
### Silicon Intensifier Targets

Another type of tube called the *silicon intensifier target* (SIT) uses a photocathode as an image sensor and focuses the photoelectrons onto a silicon mosaic diode target. Readout is similar to the vidicon. The design allows for very high light gains in the pickup by accelerating the photoelectrons to high energies (perhaps 10 keV) before they strike the target. The silicon intensifier target tube and *intensified silicon intensifier tubes* (ISIT) are used extensively for low light level applications.

### Image Isocons

The *image isocon tube* (Fig. 12) was widely used in radioscopic applications in the 1980s. The image on its photocathode forms a photoelectron pattern focused by an axial magnetic field onto a thin, moderately insulating target. The photoelectrons striking the target cause secondary emission electrons collected in a nearby mesh, leaving a net positive charge on the target. The beam from an electron gun scans the target, depositing electrons on the positively charged areas. The scattered and reflected components in the return beam are separated. Only the scattered component enters the electron multiplier surrounding the electron gun.

FIGURE 11. Vidicon television camera.



This signal is amplified to become the video output.

### X-Ray Sensitive Cameras

Although the usual input to a television camera is a light signal, for radioscopic purposes it is possible to make the camera sensitive directly to X-radiation. The vidicon camera in particular may be modified for X-ray sensitivity and has been found useful for obtaining direct real time radiographic images. Two alterations of the vidicon are needed for good results: an X-ray window and an efficient target. Thin glass or beryllium X-ray windows located close to the target replace the heavy optical glass windows in conventional tubes. Although the normal vidicon photoconductive targets will respond to X-ray, they are so thin that absorption of radiation is minimal. Suitable thick targets must be used. Selenium has been found to be very effective, having adequate response and low lag.<sup>6</sup> Lead oxide targets are more common, having a high density for good X-ray absorption and resulting sensitivity.<sup>23</sup>

The X-ray sensitive vidicon is an imaging system for small objects and low kilovoltages, 150 kV or less. The X-ray intensity must be high, in the range of 8 to 80 mSv·s<sup>-1</sup> (50 to 500 R·min<sup>-1</sup>). The vidicon tube typically has a sensing area of only 9.5 × 12.5 mm (0.37 × 0.5 in.). Presentation of the image on a 480 mm (19 in.) television screen results in better than 30 times magnification. With a 525-line scan rate, the resolution in the object is better than 0.02 mm (0.0008 in.). The X-ray sensitive vidicon camera has a gamma on the order of 0.7 to 1.0. Image

quality indicator sensitivities of two percent have been obtained. The cameras have experienced problems with deterioration, possibly due to local overheating in the target layer, poor bonding to the heat sink layer, substrate irregularities or incompatibility between beryllium and target materials.

### Camera System Characteristics

The performance criteria for camera tubes are based on the sensitivity, dynamic range, resolution, dark current and lag. A plot of signal output versus faceplate illuminance for some typical camera tubes is shown in Fig. 13 and the slope of these curves is called the *tube gamma*. The light source for illuminance is important in the response characteristics of the tubes.

In X-ray imaging applications, image isocon television tubes are commonly used because of their low light level sensitivity and high dynamic range; unfortunately, isocons are very expensive. Vidicons are often used in combination with X-ray sensitive image intensifier tubes; vidicons are simple as well as inexpensive. The newvicon is more sensitive than the plumbicon or the antimony trisulfide vidicon. Silicon intensifier target tubes are used with low light level systems when high dynamic range is not required. Table 7 lists characteristics for television tubes used in real time radiographic applications. Lag is given as the percentage of the original signal present after 50 ms.

FIGURE 12. Image isocon television camera.

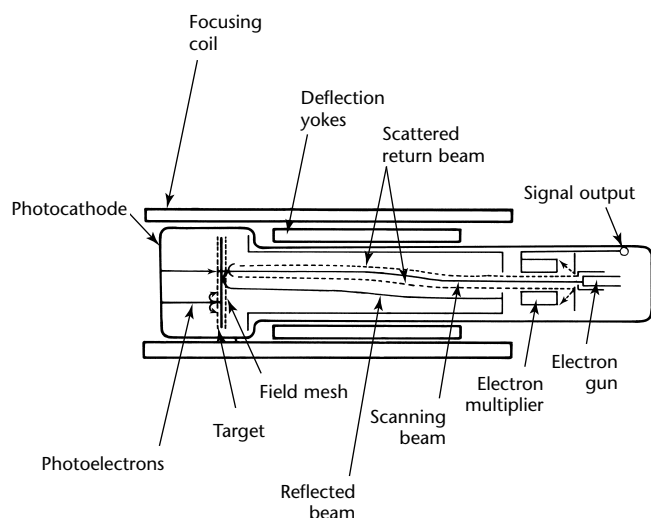


FIGURE 13. Television camera output versus light input with 2856 K tungsten source.

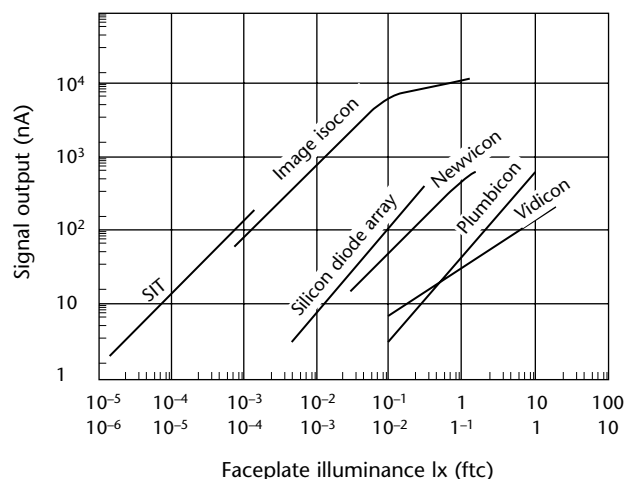


TABLE 7. Typical characteristics of television camera tubes.

Tube Type	Dynamic Range	Typical Resolution (television lines)	Current (nA)	Lag (percent)	Gamma
Image Isocon	2000	1000	0	7	1.0
Antimony trisulfide vidicon	300	900	20	20	0.65
Newvicon	100	800	8	20	1.0
Lead oxide vidicon	300	700	3	4	0.95
Silicon intensifier target	100	700	8	12	1.0

## Camera Matching

The standard scanning rate for camera tubes is 30 frames per second. Each frame image is created in a 33 ms exposure time. The frame is composed of two fields in which the electronically scanned 525 vertical lines are interlaced. The first field in 60<sup>-1</sup> s contains the odd numbered lines and the second field contains the even numbered lines.

In some applications, where very low radiation intensities are experienced, it is necessary to use a slower scanning rate. The target of the television camera can be made to integrate the incoming signal for several minutes and then scan it to provide one frame of information. Faster scanning rates may be used to image rapid dynamic systems, provided a sufficient light intensity is present and the lag features are acceptable.

Television cameras require electrical adjustments to set up the operating parameters of the image tube and signal processing electronics. Cameras may be one-piece or two-piece systems. The one-piece camera is usually self-contained with few (or no) user adjustable controls. The two-piece camera is much more versatile. The camera head can be made much smaller, decreasing bulk and weight for restricted mounting requirements. The camera control unit will have all controls readily accessible to the user for optimizing image quality. Common adjustable controls or switches found in most cameras are described in Table 8.

The beam, target and focus controls optimize the image tube's performance. Other control features (such as pedestal, gamma correction and polarity reversal) enhance image quality and ease of operation. The polarity reverse feature, for example, is a comparatively simple and advantageous option. Small detail against a bright background is difficult to detect; however, inverting the polarity and having details appear against a dark background makes them more visible to the observer.

TABLE 8. Common adjustments for television cameras.

Control	Effects
Beam current	controls electron beam in image tube; usually set only to discharge picture highlights
Focus	electrostatic focus adjustment for electron beam
Gamma correction	electronic change of slope characteristic (gamma) of tube
Pedestal level	voltage adjust for black level of picture
Polarity reverse	inverts black and white areas of image
Target voltage	sets positive potential on image tube target fixed voltage for most tubes; is variable on sulfide vidicons and controls sensitivity



## PART 6. Viewing and Recording

### Monitors

Television monitors for observing video signals are cathode ray tubes using a modulated electron beam to write on the output phosphor. In North America the standard format is 525 lines, interlaced. *Interlacing* means that the total picture frame is composed of two fields: the first field uses every other line on the screen; the second writes between the lines of the first. The television camera provides the monitor with the appropriate operating format in the video signal.

Other systems are used routinely in Europe and have various numbers of lines that can be as high as 1200, triple interlaced. The tubes vary in size, deflection system and component design. Contrast controls can be adjusted to increase or decrease the gamma over a range of values, typically 0 to 10.

To see an object, there must be a sufficient number of scan lines in the television image; following is one description of scan line requirements.<sup>22</sup> To visualize  $n$  objects there must be  $2n$  lines. Allowing for random orientation, this should be increased by a factor of 2 percent. To see a mesh with 5 holes per 1 mm (125 holes per 1.0 in.) would require 14 lines per 1 mm (350 holes per 1.0 in.) scan rate. Horizontally, the resolution is determined by the bandwidth of the signal. One cycle of bandwidth is required to see the mesh (half cycle for the holes and half cycle for the spacing between holes). In a conventional system, the viewing matrix uses a  $3 \times 4$  aspect ratio, the horizontal being larger than the vertical. If 525 scan lines are used, then the horizontal will require  $4 \times 525 \times (\sqrt{2})^{-1}$  half cycles, or about 250 cycles, to maintain the same resolution. Using 30 frames per second scanning and a factor of 1.2 for retrace time, the required bandwidth is on the order of  $525 \times 250 \times 30 \times 1.2 = 4.7$  MHz.

Although it may appear that resolution could be improved by increasing the number of scan lines, two problems result: (1) the charge capacity on the camera's target elements will be reduced in proportion to the area change that may reduce the sensitivity and (2) an increase in bandwidth will be required that increases the noise in the electronics in proportion to the square root of the

bandwidth. The result is that the standard number of scan lines is often as good as or superior to higher scan line systems.<sup>22,24</sup>

Many cameras and television monitors are designed for higher bandwidth operation (10 MHz and greater). This provides greater resolution horizontally (800 lines or more) than vertically. Because the 525-line vertical is standard, the resolution of video systems is often quoted by the horizontal resolution value, a function of bandwidth.

### Recording Equipment

Recording the video signal provides a permanent record of the radioscopic results. Technology in this area changes rapidly with new options appearing frequently.

Recording of video data generally occurs in either of two ways. It can be recorded as an analog signal on some form of video tape or it can be recorded digitally. When the output of the video system is analog the signal is first converted to digital form and then recorded on some form of digital media such as digital audio tape (DAT), compact disk (CD), digital video disk (DVD) or hard disk.

Cassette video tape recorders are still the most common means of saving video information. They are easily operated but are limited to about 2 h of playback. The ratio of signal to noise in the record improves with tape width, which varies from 13 to 51 mm (0.5 to 2.0 in.).

Video tape recorders may be equipped with pause and slow motion modes. The pause mode, however, shows only one field rather than the full two-field frame. This limitation results in a reduction of information by half.

In place of the second field, some expensive recording equipment repeats the first field of information in the pause mode. This improves the visual display but still represents a reduction in information. The reason for showing only one field is to eliminate interfield jitter caused by movement between field scans of the camera.

Slow motion modes are quite useful for replaying rapid events. Unfortunately in slow motion replay a broadband



synchronizing signal is reproduced on the video screen, sweeping by at each frame. This signal is not easily removed and can be very distracting when evaluating images; removal of the synchronizing signal noise is possible with further investment in video replay equipment.

All video recording devices alter the video signal in some way. When linking the output of the recording camera to monitors and recorders, the strength of the signal is reduced in proportion to the number of devices. This results in a weaker signal at the recorder and a poorer record. Repeated copying results in a degradation of the image as the signal becomes successively reduced. Playback from recorded images will be inferior to the original image. It is also important to consider the bandwidth capability of recording equipment. To maintain as much information as possible, bandwidth should be matched to the bandwidth required in the original image. The standard television broadcast is 4.2 MHz, to which many video recording devices are matched.

Digital recording of the video signal is generally more expensive but has the potential of providing a high quality record if the digital signal has a large dynamic range. Digital video disk (DVD) technology offers a high quality recording in a compact storage medium capable of holding large amounts of data (4 to 10 gigabytes).

The technology of digital storage media in the two decades from 1982 to 2002 has undergone the following developments.

1. Optical media have been supplementing or replacing magnetic media.
2. Media have become more economical.
3. Media have become able to store more bytes of data.
4. Media have become more compact.
5. Platforms have become mutually intelligible, so media formatted by one computer or program are more likely to be able to be read by another computer.

Similar trends affect instruments as well as media. These trends seem likely to continue in the twenty-first century.

## Electronic Soft and Hard Copy

Hard copy of a single frame image is often desirable and a radioscopic system should be capable of generating hard copy. Photographic imagers that capture a single frame from a video input are available. Using a video capture card or similar hardware enhancements in a computer, however, is very useful. The

captured image can then be displayed on the computer monitor for image enhancement. It can be processed into a number of digital formats (see Table 9) that can be output to any printer.

The images can also be stored or transmitted as electronic files. Multiple frame averaging with video capture can improve the image quality. Noise is reduced by the square root of the number of frames averaged.

The frame averaging technique is commonly a running average:

$$(32) \quad F = \frac{F_c}{n} + \frac{F_p(n-1)}{n}$$

where  $F$  is the displayed image frame,  $F_c$  is the current row frame,  $F_p$  is the previous averaged frame and  $n$  is the number of frames in the running average. When viewed in real time, running averages reduce noise but create image lag or blur for moving objects, depending on the number of frames averaged.

TABLE 9. File formats widely used for bitmapped graphics.

Abbreviation	Format
BMP	bit mapped picture
DIB	device independent bitmap
GIF	graphics interchange format <sup>a</sup>
JFF	JPEG file format <sup>b</sup>
JIF	JPEG image format <sup>b</sup>
JPEG	Joint Photographic Experts Group
JPG	JPEG <sup>b</sup>
PIC	PICS <sup>b</sup>
PICS	platform for internet content selection
PICT	picture
PNG	portable network graphics
RLE	run length encoding
TIF	TIFF <sup>b</sup>
TIFF	tagged image file format

a. GIF<sup>SM</sup> is a service mark of CompuServe Incorporated.

b. For compatibility with the disk operating system (DOS) many file names end with a file extension consisting of a period followed by three letters. For this reason, some format abbreviations consist of three letters or have been shortened to three letters so the format abbreviation can be appended as an extension to the file name.

## PART 7. System Considerations

### System Evaluation

#### Image Quality Indicators

The most common means for evaluation of radiographic sensitivity is to use a penetrameter, or image quality indicator. The penetrameter is a thin plaque of the same material as the object. The plaque thickness is a certain percentage of the object thickness. The penetrameter has holes with diameters one, two and four times its thickness. The radiographic quality of the imaging system is then listed as the smallest percentage penetrameter detectable and the smallest hole detectable. Other types of penetrameters are in use, such as the German Industry Standard, Deutsche Industrie Norm (DIN), penetrameter in Europe.<sup>26</sup> This penetrameter uses wires of graded diameters, made of the same material as the object. The smallest wire detected is the quality level.

Many experimenters use their own measurement systems for evaluating the quality of an imaging system. These are generally called an *image quality indicator* (IQI). Image quality indicators vary in design but commonly contain a step wedge of material from which the smallest percentage change (in material or contrast level) can be determined. Resolution may be measured by the smallest hole size detectable. Because the ability to observe a certain diameter hole is a function of the depth of the hole, it is common to specify resolution using a high contrast object.

Wire meshes are commonly used to evaluate real time imaging systems. The wire mesh is an object whose fine structure is repetitive. Wire meshes are often used to indicate the quality level of inspection at certain speeds of movement.

#### Modulation Transfer Function

Another technique of system evaluation, more rigorous in its approach, is the modulation transfer function (MTF). The modulation transfer function is the ratio of the image amplitude to the object amplitude, as a function of sinusoidal frequency variation in the object:

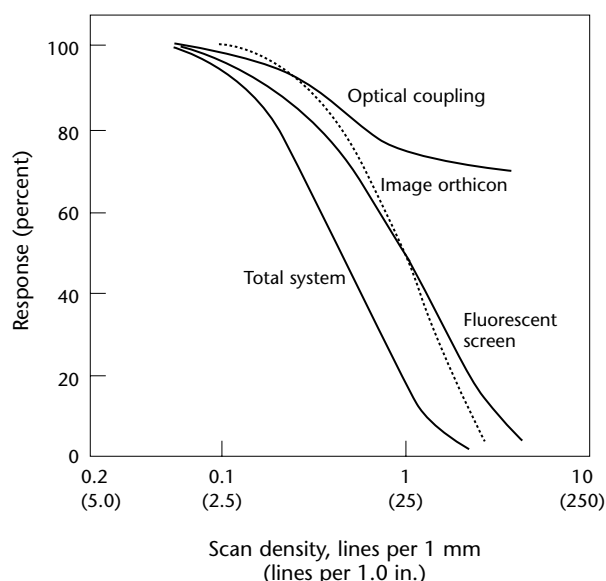
$$(33) \quad R(\omega) = \frac{I(\omega)}{O(\omega)}$$

where  $I(\omega)$  is the image amplitude,  $O(\omega)$  the object amplitude and  $R(\omega)$  is the sine wave response.

This approach to system evaluation can be understood by imagining a bar pattern. As the pattern becomes finer and finer, the image response begins to lose contrast. A plot of this response is called the square wave response (when a bar pattern is used) and is very similar to the modulation transfer function. Square wave response factors can be used to evaluate imaging systems and under certain conditions may be corrected to the sine wave response or modulation transfer function equivalence.<sup>27,28</sup>

The true modulation transfer function, generated by an object having sinusoidal variations in intensity, is measured routinely for optical components such as lenses, intensifiers and cameras. Normally, in radiography, determining the modulation transfer function for such an object is prohibitively difficult. Instead, the modulation transfer function is derived by generating the edge spread function, differentiating to obtain the line

FIGURE 14. Modulation transfer function of system.



spread function and fourier transforming to yield the modulation transfer function. Derivations of this and examples may be found in the literature.<sup>29-33</sup>

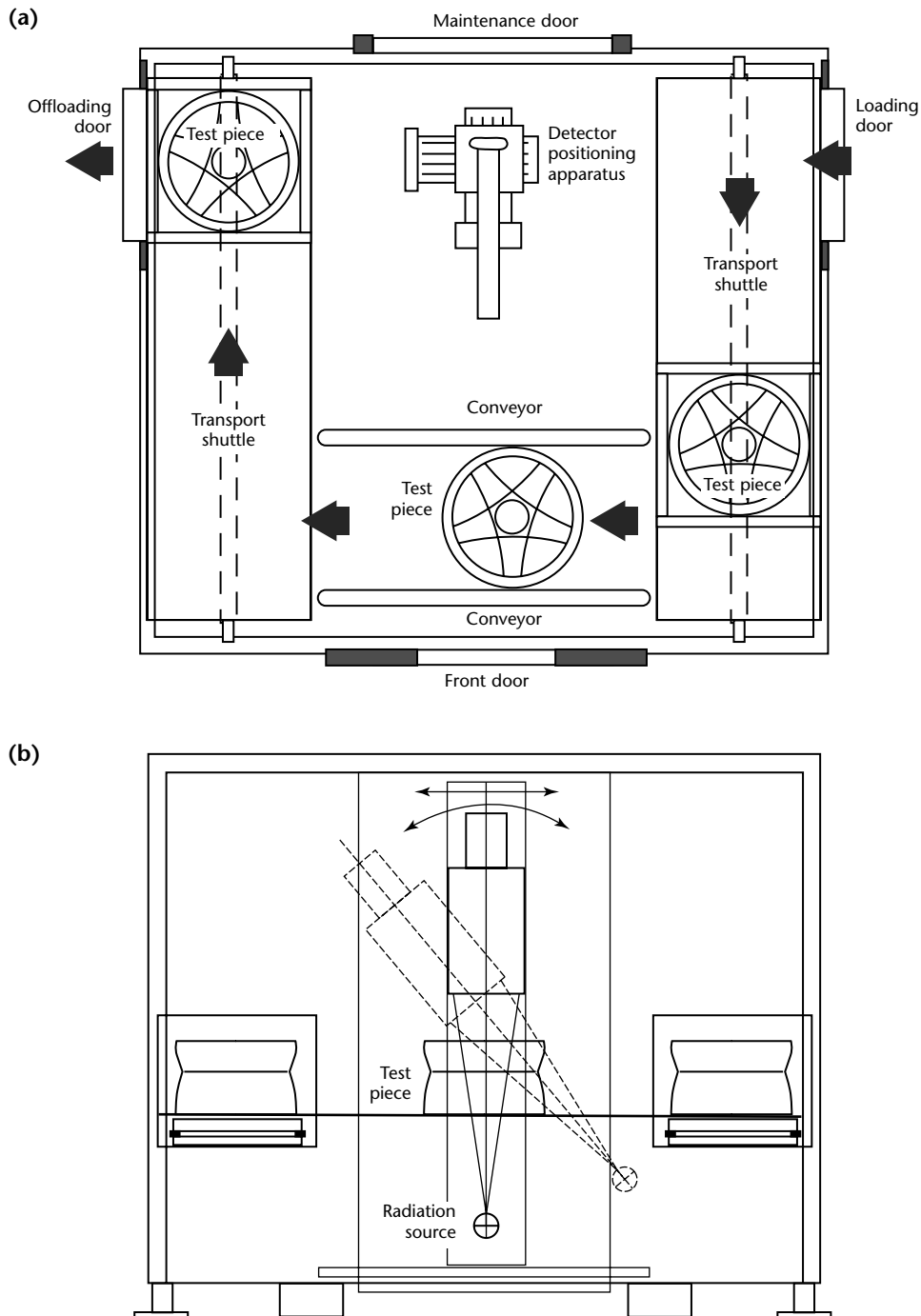
The importance of the modulation transfer function in evaluating systems is that the total system modulation transfer function is the product of the individual

modulation transfer functions of the components:

$$(34) \text{MTF}_{\text{system}} = \text{MTF}_1 \times \text{MTF}_2 \times \text{MTF}_3$$

This is shown in Fig. 14, where the modulation transfer functions for the

**FIGURE 15.** Assembly line radiography for automotive parts using automated part positioning: (a) top view; (b) front view.



fluorescent screen, optical coupling, image orthicon camera and total system are shown.<sup>34,35</sup> The components of a system are analyzed quantitatively and the poorest is easily determined. This technique allows for the prediction of a proposed system's performance from data on the individual components.

## System Design

General purpose remote reviewing systems are usually of three types: X-ray image intensifier with charge coupled device or vidicon camera; fluorescent screen with intensified charge coupled device or isocon camera; and scintillator plate with charge coupled device camera. Amorphous silicon digital flat panels (discussed elsewhere in this volume) have been implemented in remote viewing radioscopic systems. Additional equipment should include a high quality video monitor, a video tape recorder, a video disk for dynamic recording and a computer based frame digitizing and image enhancement system for real time summing, running average or contrast adjustments plus edge enhancement and subtraction techniques. The computer data acquisition system provides digital data storage and hard copy output capabilities.

The X-ray image intensifier systems are usually less expensive. They operate best at the low and intermediate X-ray energies for which they are designed. Scintillator plates are appropriate for both low to intermediate range and megavolt X-ray energies but may not provide enough sensitivity for video framing rates.

The intensified charge coupled device and isocon camera systems are more versatile. Because the fluorescent screen is changeable, the system can be adjusted for optimum performance at any energy. Intensified charge coupled device and

isocon camera systems may also be used for X-ray or neutron detection. Both systems can perform in the 1.5 to 2.0 percent sensitivity range. The resolution limit will generally depend on the input field size, the video bandwidth used and the input phosphor.

The digital flat panel detectors are generally more expensive than traditional radioscopic imaging components. They are expected, however, to command a large share of the market because of their performance advantages.

A cabinet system incorporates many of the modern features of radioscopic imaging, using an image intensifier tube with remote viewing and radiation protection for the operator. Assembly line radioscopy in a larger enclosure using robotics to position automotive parts is shown in Fig. 15 and a radioscopy system for automotive wheel inspection is shown in Fig. 16.

**MOVIE.**  
Automated  
wheel  
inspection.

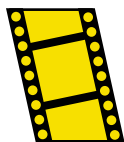


**FIGURE 16.** Radioscopy systems for automotive wheel inspection.



# References

1. Bossi, R.H., C. Oien and P. Mengers. Sec. 14, "Real-Time Radiography." *Nondestructive Testing Handbook*, second edition: Vol. 3, *Radiography and Radiation Testing*. Columbus, OH: American Society for Nondestructive Testing (1985): p 593-640.
2. Ludwig, G.W. and J.S. Prener. "Evaluation of  $Gd_2O_3:S:Tb$  as a Phosphor for the Input of X-Ray Image Intensifier." Schenectady, NY: General Electric Corporate Research and Development (1972).
3. Storm, E. and H.E. Israel. "Photon Cross Sections from 0.001 to 100 MeV for Elements 1 through 100." Report LA-3753. Los Alamos, NM: Los Alamos National Laboratory (1967).
4. Kinney, J.H. and M.C. Nichols. "X-Ray Microscopy (XTM) Using Synchrotron Radiation." *Annual Review of Materials Science*. Vol. 22. Palo Alto, CA: Annual Reviews (2002): p 121-152.
5. Placious, R.C., D. Polansky, H. Berger, C. Bueno, C.L. Vosberg, R.A. Betz and D.J. Rogerson. "High-Density Glass Scintillator for Real-Time X-ray Inspection." *Materials Evaluation*. Vol. 49, No. 11. Columbus, OH: American Society for Nondestructive Testing (November 1991): p 1419-1421.
6. McMaster, R.C., L.R. Merle and J.P. Mitchell. "The X-Ray Vidicon Television Image System." *Materials Evaluation*. Vol. 25, No. 3. Columbus, OH: American Society for Nondestructive Testing (March 1967): p 46-52.
7. Sturm, R.E. and R.H. Morgan. "Screen Intensification Systems and Their Limitations." *American Journal of Roentgenology and Radium Therapy*. Vol. 62, No. 5. Leesburg, VA: American Roentgen Ray Society (1949).
8. Teves, M.C. and T. Tol. "Electronic Intensification of Fluoroscopic Images." *Philips Technical Review*. Vol. 14, No. 2. Eindhoven, Netherlands: Philips Research Laboratory (1952): p 33-43.
9. Bates, C.W., Jr. "Concepts and Implementation in X-Ray Image Intensification." *Real-Time Radiologic Imaging; Medical and Industrial Applications*. Special Technical Publication 716. West Conshohocken, PA: ASTM International (1980): p 45-65.
10. Diakides, N.A. "Phosphors." SPIE Proceedings, Vol. 42. Bellingham, WA: International Society for Optical Engineering (1973): p 83-92.
11. Schagen, P. "X-Ray Imaging Tubes." *NDT International*. Vol. 14, No. 1. Guildford, United Kingdom: Butterworth-Heinemann (1981): p 9-14.
12. Wang, S.P., D.C. Robbins and C.W. Bates, Jr. "A Novel Proximity X-Ray Image Intensifier Tube." SPIE Proceedings, Vol. 127: *Optical Instruments in Medicine VI*. Bellingham, WA: International Society for Optical Engineering (1977): p 188-194.
13. Vosburg, K.G., R.K. Swank and J.M. Houston. "X-Ray Image Intensifiers." *Advances in Electronics and Electron Physics*. Vol. 43. Orlando, FL: Academic Press (1977).
14. Kuhl, W. and J.E. Schrijvers. "A New 14-Inch X-Ray Image Intensifier Tube." *Medicamundi*. Vol. 22. Eindhoven, Netherlands: Philips Electronics (March 1977).
15. Fink, D.G. and D. Christiansen, eds. *Electronic Engineers' Handbook*, third edition. New York, NY: McGraw-Hill (1989).
16. Woodhead, A.W. and G. Eschard. "Microchannel Plates and Their Applications." *Acta Electronica*. Vol. 14, No. 2. Limeil Brévannes, France: Laboratoires d'Électronique et de Physique Appliquée (1971): p 181-200.
17. Chalmetron, V. "Microchannel X-Ray Image Intensifiers." *Real-Time Radiologic Imaging; Medical and Industrial Applications*. Special Technical Publication 716. West Conshohocken, PA: ASTM International (1980): p 66-89.
18. Hobson, G.S. *Charged Transfer Devices*. New York, NY: Holsted Press (1978).
19. Biberman, L.M. and S. Nudelman, eds. *Photoelectric Imaging Devices*. New York, NY: Plenum Press. Vol. 2 (1971).
20. Howe, M.J. and D.V. Morgan. *Charge Couple Devices and Systems*. New York, NY: Interscience (1979).
21. Titus, J. "How Do CCDs Capture Images?" *Test and Measurement World*. Newton, MA: Cahners Business Information (April 1999).




22. Siedband, M. "Electronic Imaging Devices II." *Physics of Diagnostic Radiology*. USDHEW Publication No. (FDA) 74-8006. Washington, DC: United States Department of Health, Education, and Welfare [DHEW] (1971).
23. Jacobs, J.E. "X-Ray-Sensitive Television Camera Tubes." *Real-Time Radiologic Imaging: Medical and Industrial Applications*. Special Technical Publication 716. West Conshohocken, PA: ASTM International (1980): p 90-97.
24. Webster, E.W. "Electronic Imaging Devices I." *Physics of Diagnostic Radiology*. USDHEW Publications No. (FDA) 74-8006. Washington, DC: United States Department of Health, Education, and Welfare [DHEW] (1971).
25. Webster, E.W., R. Wipfelder and H.P. Prendergrass. "High Definition versus Standard Television in Televised Fluoroscopy." *Radiology*. Vol. 88, No. 2. Easton, PA: Radiological Society of North America (1967): p 355-357.
26. ASTM E 1647-98a, *Standard Practice for Determining Contrast Sensitivity in Radioscopy*. West Conshohocken, PA: ASTM International (1998).
27. Bossi, R.H., J.L. Cason and C.N. Jackson, Jr. "The Modulation Transfer Function and Effective Focal Spot As Related to Neutron Radiography." *Materials Evaluation*. Vol. 30, No. 5. Columbus, OH: American Society for Nondestructive Testing (May 1972): p 103-108, 112.
28. Coltman, J.W. "The Specification of Imaging Properties by Response to a Sine Wave Input." *Journal of the Optical Society of America*. Vol. 44. Washington, DC: Optical Society of America (June 1954): p 468.
29. Klingman, E. "Theory and Application of an Edge Gradient System for Generating Optical Transfer Functions." NASA TN D-6424. Washington, DC: National Aeronautics and Space Administration (1971).
30. Mees, C.K. *Theory of the Photographic Process*. New York, NY: MacMillan Company (1942).
31. Morgan, R.H. "The Frequency Response Function." *American Journal of Roentgenology and Radium Therapy*. Vol. 88. Leesburg, VA: American Roentgen Ray Society (January 1962): p 175.
32. Morgan, R.H., L.M. Bates, U.V. Gopalarao and A. Marinaro. "The Frequency Response Characteristics of X-Ray Films and Screens." *American Journal of Roentgenology, Radium Therapy and Nuclear Medicine*. Vol. 92. Leesburg, VA: American Roentgen Ray Society (February 1964): p 426.
33. Smith, F.D. "Optical Image Evaluation and the Transfer Function." *Applied Optics*. Vol. 2, No. 4. Washington, DC: Optical Society of America (1963): p 335.
34. Halmshaw, R. "Direct-View Radiological Systems." *Research Techniques in Nondestructive Testing*. Vol. 1. Orlando, FL: Academic Press (1970): p 241-268.
35. Halmshaw, R. "Fundamentals of Radiographic Imaging." *Real-Time Radiologic Imaging: Medical and Industrial Applications*. Special Technical Publication 716. West Conshohocken, PA: ASTM International (1980): p 5-21.

## Bibliography

- Bates, C.W., Jr. "New Trends in X-Ray Image Intensification." *Application of Optical Instrumentation in Medicine III*. SPIE Proceedings, Vol. 47. Bellingham, WA: International Society for Optical Engineering (1974): p 152-158.
- Cassen, B. and R.C. McMaster. "Fluoroscopic Methods of Inspection of Metallic Materials, Part VII." WPB Contract W-138. Pasadena, CA: California Institute of Technology (1945).
- Chamberlain, W.E. "Fluoroscopes and Fluoroscopy." *Radiology*. Vol. 38. Easton, PA: Radiological Society of North America (1942): p 383-412.
- Coltman, J.W. "Fluoroscopic Image Brightening by Electronic Means." *Radiology*. Vol. 51. Easton, PA: Radiological Society of North America (1948): p 359-367.
- Criscuolo, E.L. and D. Polansky. "Improvements in High Sensitivity Fluoroscopic Technique." *Nondestructive Testing*. Vol. 14, No. 1. Columbus, OH: American Society for Nondestructive Testing (January 1956): p 30-31, 40.
- Csorba, I.P. *Image Tubes*. Indianapolis, IN: Howard W. Sams and Company (1985).
- Curtis, L.R. "Fluoroscopic Inspection of Aluminum and Magnesium Castings." *Nondestructive Testing*. Vol. 7, No. 4. Columbus, OH: American Society for Nondestructive Testing (Spring 1949): p 24-27.
- Dalberg, R.C. "Real-Time Digital Image Filtering and Shading Correction." *Applications of Digital Image Processing III*. SPIE Proceedings, Vol. 207. Bellingham, WA: International Society for Optical Engineering (1979)



- Halmshaw, R. *Physics of Industrial Radiography*. London, United Kingdom: Heywood Books. New York, NY: American Elsevier Publishing Company (1966).
- Hampe, W.R. "Modern Fluoroscopy Practices." *Nondestructive Testing*. Vol. 14, No. 1. Columbus, OH: American Society for Nondestructive Testing (January 1956): p 36-40.
- Hecht, S. and Yun Hsia. "Dark Adaptation Following Light Adaptation to Red and White Light." *Journal of the Optical Society of America*. Vol. 35. Washington, DC: Optical Society of America (1945): p 261.
- Klasens, H.A. "Measurement and Calculation of Unsharpness Combinations in X-Ray Photography." *Philips Research Reports*. Eindhoven, Netherlands: Philips Research Laboratories (1946): p 241.
- O'Connor, D.T. "Industrial Fluoroscopy." *Nondestructive Testing*. Vol. 11, No. 2. Columbus, OH: American Society for Nondestructive Testing (Fall 1952): p 11-22.
- Rossi, R.D. and W.R. Hendree. "Some Physical Characteristics of Rare-Earth Imaging Systems." *Application of Optical Instrumentation in Medicine IV*. SPIE Proceedings, Vol. 70. Bellingham, WA: International Society for Optical Engineering (1975): p 224.
- Smith, W.J. *Modern Optical Engineering: The Design of Optical Systems*. New York, NY: McGraw-Hill (1976).
- Wagner, R.E. "Noise Equivalent Parameters in General Medical Radiography: The Present Picture and Future Pictures." *Photographic Science and Engineering*. Vol. 21, No. 5. Springfield, VA: Society for Imaging Science and Technology (1977).



# 11

## C H A P T E R

# Digital Radiographic Imaging

---

Clifford Bueno, General Electric Company, Niskayuna,  
New York

# PART 1. Overview of Digital Imaging

## Definition

The digital imaging chapter of this volume presents approaches available to obtain digital radiographs by electronic means. The discussion and examples in the present chapter include techniques of conversion of X-rays to light and then to electronic images, photoconductive conversion of X-rays to electronic images, photostimulable phosphors, array detectors, line scan imaging and scanning electron beams.

Radioscopic digital imaging is related to radioscopy. In radioscopic imaging the major emphasis is on the conversion of X-rays to analog electronic data that are viewed as video signals in real time. Digitization of these analog signals is a technique of digital imaging. Many of the principles for X-ray detection are identical, particularly where digital based cameras such as charge coupled device cameras are used. The present chapter, on digital radiographic imaging, differs from radioscopic imaging in that the systems are not video based (although in some cases video could be output). Rather, digital systems use discrete sensors with the data from each detection pixel being read out into a file structure to form the pixels of the digital image file.

An exception to the discrete sensor based systems discussed in this chapter is the photostimulable phosphor system that forms a latent image (similar to film) on a storage phosphor imaging plate. The screen is read out electronically using a special laser scanner. The pixelization in this case is based not on the X-ray sensitive phosphor but in the laser scanner process.

## Development

The ability to develop digital imaging technology that would be useful for radiographic testing is due in large part to the growth in the speed and memory of computer systems. In the 1980s images of  $512 \times 512$  pixels 8 bits deep of data (256 kilobytes) were considered large and created storage and display problems for the computer systems at that time. By the twenty-first century, image files of  $1500 \times 2000$  with 16 bits of data (6 megabytes) are common and can be

transported, stored and displayed with relatively inexpensive computer systems.

The medical community has led the development of digital X-ray imaging, where the demand for imaging systems allows significant investment in the development of the tools. Spinoff from the medical community has occurred, allowing the introduction of digital imaging technology for the industrial radiography community.

In the early 1980s, digital imaging for radiographic purposes was primarily done by electronic digitization of the video signal from a radioscopic system.<sup>1</sup> Charge coupled device cameras were available but the most common application was as a video output camera. Developments in direct digital image output for these cameras resulted in charge coupled device arrays in the 1990s that consisted of millions of pixels.

Also developed in the 1970s and 1980s were digital imaging systems using line scan detector arrays. To form the image, either the part or the detector array was physically scanned in the dimension perpendicular to the array. In the late 1970s to early 1980s the photostimulable phosphor array was developed for medical use and was used in industry in the 1990s.

In the 1990s the development of large thin film transistor arrays provided the tool that could make large area X-ray imagers using either amorphous silicon or amorphous selenium possible.

## Detectors for Digital Imaging

Digital radiographic detectors are used in numerous industries from airport baggage scanning to medical diagnosis. In addition to these widely used applications, digital radiography is finding an increasing role for inservice nondestructive testing, as a diagnostic tool in the manufacturing process, for online production line testing and with conveyer handling systems. Digital radiographic detectors are also being used as hand held devices for pipeline inspections, as film replacement devices, in industrial and medical computed tomography systems and as part of large robotic scanning systems for coverage of large structures.

The digital image by its nature will provide numerical results important for metrology and thickness measurements. The development of a wide range of digital X-ray imaging products complements the recent digital revolution and provides digital image data and results that can be incorporated into the massive digital manufacturing and services databases that have emerged to help manage the life cycles of products and structures.

In the field of industrial digital radiography, there is really no single standard X-ray system to address all applications. Economics, speed, quality and the impact on the overall manufacturing or service processes are key in designing and building digital radiographic systems. A large aspect of that design is the consideration of the digital X-ray detection device itself. For this selection, there are almost as many choices of detectors as there are ways to configure the overall test system. [The different digital detector technologies available are discussed below.](#)

## PART 2. Principles of Digital X-Ray Detectors

The detection devices that support the larger imaging systems already mentioned are the following: (1) phosphors deposited on amorphous silicon thin film transistor diodes; (2) photoconductors such as amorphous selenium deposited on thin film transistors; (3) phosphors deposited or coupled through fiber optic lenses onto charge coupled device based detectors and complementary metal oxide silicon based detectors; (4) photostimulable storage phosphors; (5) phosphors deposited on linear array systems; and (6) X-ray scanning source reversed geometry detectors. Further details are provided in Table 1.

Each of these devices has an X-ray capture material as its primary means for detecting X-rays. This material is either an X-ray phosphor material combined with a photoelectric device (diode, photomultiplier tube or charge coupled device) or is an X-ray photoconductor material that is then followed by an electronic readout device. The most common of these detection systems in operation today are the flat panel detection systems based on amorphous silicon and amorphous selenium structures, the camera systems based on charge coupled device technology and the storage phosphor systems. The

amorphous silicon, amorphous selenium and charge coupled device technologies are described below.

Each of these devices can be used to replace film radiographic techniques depending on the size of the application and on the spatial resolution, image contrast and speed required. As noted in Table 1, the detectors have variable modes of operation or are available in different architectures to address diverse applications. There are numerous pixel architectures of amorphous silicon detectors but it is important to note that currently not all detector choices allow real time operation of 30 frames per second.

### Charge Coupled Devices

Scientific charge coupled devices, although they are typically small in size, have been made with high pixel densities. The fields of photography, astronomy and microscopy have demanded this and the nondestructive testing industry has been a beneficiary of these developments. Table 1 illustrates these small pixel dimensions (9 to 50  $\mu\text{m}$  pixels).

Charge coupled devices have not been fabricated into larger arrays because the

TABLE 1. Properties of digital radiographic detectors.

Detector	Size Range (mm)	Pixels	Square Pixel Size ( $\mu\text{m}$ )	Image Acquisition Speed (min)	Conversion Material	Atomic Number Z of Conversion Material
Amorphous silicon	200 $\times$ 200, 230 $\times$ 190, 410 $\times$ 410 or 280 $\times$ 410	1024 $\times$ 1024, 2304 $\times$ 1920, 2048 $\times$ 2048 or 2304 $\times$ 3200	100, 127 or 200	< 1 (real time)	thallium activated cesium iodide or terbium activated gadolinium oxysulfide	55/53 or 64
Amorphous selenium	350 $\times$ 430	to 2560 $\times$ 3072	139	< 1.0 to 1.5	selenium	34
Charge coupled devices	small to 100 $\times$ 100; larger with lenses	to 4096 $\times$ 4096	9 to 50; effectively larger with other optics	< 1 (real time)	thallium activated cesium iodide or terbium activated gadolinium oxysulfide	55/53 or 64
Storage phosphors	small to 1550 $\times$ 430	to 15 500 $\times$ 4300	25 to 250	< 1 to 4	europium activated barium fluorobromide	56/35
Linear arrays	small to 500	to 4096	10 to 200	< 1 (real time)	thallium activated cesium iodide or terbium activated gadolinium oxysulfide	55/53 or 64
Reversed geometry	small to 450 $\times$ 450	to 2048 $\times$ 2048	25 to 200	< 1 (real time)	thallium activated sodium iodide	11/126

charge coupled device is based on crystalline silicon, which has traditionally been cut from silicon wafers available in sizes only as large as 100 to 150 mm (4.0 to 6.0 in.) in diameter or less. A larger field of view can be accomplished with charge coupled devices through tiling of the charge coupled devices or through a lens or a fiber optic transfer device to view an X-ray conversion (phosphor) screen. The downside of the lens approach is that it has very poor light collection efficiency. Fiber optics or tiling do not provide large fields of view but will result in more efficient light collection. A more detailed discussion of charge coupled device technology may be found elsewhere.<sup>2</sup>

---

## Thin Film Transistor

Larger amorphous silicon and amorphous selenium detectors based on thin film transistor technology have been made commercially available with a pixel pitch smaller than 75  $\mu\text{m}$ . Amorphous silicon through large area amorphous silicon deposition and processing/etching techniques offers a solution to the size constraints of charge coupled devices while maintaining good light collection efficiency from the phosphor or photoconductor (selenium) material. Because the phosphor layer is typically deposited directly onto the silicon, efficient light transfer is easily obtained. However, the readout circuitry ([described elsewhere](#)) in these devices requires a large pixel space to accommodate the thin film transistor (TFT) and data lines and scan (gate) lines required for operation, thus limiting how small a pixel this device can permit.

## Light Collection Technology

The amorphous silicon thin film transistor circuitry has a fill factor of active photodiode ranging from 65 to 90 percent. Charge coupled devices use a transparent polysilicon gate structure for reading out the device and have a fill factor of close to 100 percent.<sup>2</sup> On a per pixel basis, the charge coupled device is therefore more efficient in collecting the light produced from the phosphor material. For small field of view applications, the directly coupled charge coupled device approach will provide high spatial resolution and high light collection efficiency. For large field of view applications, the amorphous silicon approach offers excellent light collection efficiency (no lenses), in a thin, compact, robust package.

## Radiation Conversion Material

The amorphous selenium device is similar to the amorphous silicon based detector. They both use thin film transistor readout circuitry. The difference lies in the X-ray conversion material. The amorphous selenium detector relies on the selenium photoconductive material (not a phosphor layer) as a means to detect X-rays. The selenium converts X-rays to electron hole pairs that then get separated by the internal bias of the device and captured by an electrode structure. The amorphous silicon thin film transistor circuitry beneath the selenium layer provides readout of the charge with the aid of field effect transistors (FETs) in a similar manner to that of the amorphous silicon detectors. The selenium layer is typically 500  $\mu\text{m}$  (0.02 in.) thick.<sup>3</sup>

For applications with large fields of view, amorphous selenium offers direct X-ray collection efficiency in a compact, robust package.

---

## Storage Phosphors

Storage phosphors trap X-ray induced charge carriers in the color centers of such phosphor materials as europium activated barium fluorobromide ( $\text{BaFBr:Eu}$ ).<sup>4</sup> Although prompt phosphorescence occurs during X-ray exposure, some of the charge trapped in the phosphor material is stored in these discontinuity color centers in the crystalline structure. The carriers stored at these discontinuity centers can be released when stimulated by infrared or red laser light. The rerelease of trapped carriers subsequently creates photostimulated luminescence of the same emission wavelength that the prompt emission process produces.

A photomultiplier tube converts the emitted photostimulated luminescence to an electrical signal that is then amplified and sampled.<sup>5</sup> These systems have a practical spatial resolution and contrast sensitivity and have been widely used in production radiography. Additionally, they are used like film and are somewhat flexible (moldable about parts), portable like film in the field and fully reusable. Similarly these screens have to be transferred to a laser processor before they can be interpreted. This removal process step is where this technology departs from the other digital approaches. Photostimulable luminescence techniques can be more productive when imaging plates can be used in the field in a collection or batch that covers large areas for each exposure.

The main advantage of phosphor screens over film is the reduction of film use, the ability to digitally acquire a film



quality image, the dynamic range and the corresponding benefits of that digital image file, such as easy archival and retrieval.

## Linear Arrays

Linear array detectors are much like charge coupled devices, except that they typically only have pixels in 1 dimension or they may be composed of a small rectangular array such as a  $32 \times 1024$  pixel array. The advantage of linear arrays is their intrinsic scatter rejection capability. X-ray scatter exiting a specimen under examination can be a large contribution to the degradation of the contrast in the image. The linear array system acquires its image by being scanned one line (or a group of lines) at a time across an object.<sup>6,7</sup> The key is that the radiation beam is masked or collimated to match the size of the detector. This dramatically decreases the object's scatter field. The scatter detected at each of those lines is substantially less than that of individual lines in an area array. Linear arrays have been successfully used in computed tomography applications and have also been found to be effective for digital radiographs.

## Scanning Beam, Reversed Geometry

The reversed geometry system<sup>8-10</sup> goes one step further in reducing X-ray scatter in the examination. In this case the data are acquired with a small thallium activated sodium iodide (NaI:Tl) scintillator coupled to a photomultiplier tube. A large scanned X-ray source with a target diameter of about 250 mm (10 in.) is used to define the image. The X-ray source operates in a manner similar to a video monitor. An electron beam is electronically rastered over the inner surface of the front of the X-ray source. Where the electrons collide with the inner surface of the tube, X-rays are generated. By electronically scanning the electron beam, the instantaneous position of the X-ray source is scanned over an area of the front surface of the tube. The size and location of the scanned region is user definable, variable from 0.25 to 16 s. The acceleration voltage is also user definable from 55 to 160 kV with an electron beam current up to about 0.5 mA. The diameter of the electron beam spot at the inner surface of the tube is about 25  $\mu\text{m}$  (0.001 in.).

The specimen under examination is placed on top of the X-ray source. This is the opposite of conventional radiography where the object is placed near the

imaging detector and the source is about the size of a point source. The data acquisition computer also controls the rastering of the electron beam. By acquiring the output of the detector as a function of electron beam position, the computer can generate a real time radiograph of the specimen under examination.

Because a single small area detector is used and the object is placed at the source, not at the detector, the X-ray scatter from the object is essentially nil. The disadvantage of this approach is that, because it is reversed geometry, the effective focal spot size is that of the detector size. The detector size is typically much larger than a typical industrial X-ray focal spot. So that any specimen that has some thickness will show significant unsharpness as the feature of interest moves away from the X-ray source.

## Detection Efficiency

With the exception of the photoconductive selenium based detector, all detectors listed use a phosphor layer of one sort or another to capture and convert the X-ray intensity. The selection of the phosphor or photoconductive material, its thickness and effective atomic number will impact the total number of X-rays absorbed in the conversion material. Once energy is absorbed each material, phosphor or photoconductor, has its own efficiencies for conversion of this energy into either light or charge carriers. There are other coupling steps following this to transfer the signal onto the pixelized readout circuitry. The performance of the X-ray detector to convey the information in the radiation beam is then dependent on the efficiency of each step in the X-ray conversion process leading to an electronic signal. The signal-to-noise ratio of the detector and thus the image contrast are therefore dependent on the transfer of information along the imaging chain. Digital imaging chain statistics and the relation with image contrast are discussed immediately below.

## PART 3. Image Contrast and Signal Statistics

The transmitted X-ray beam signal propagates through various energy conversion stages of an imaging system, as discussed elsewhere.<sup>11,12</sup> In Fig. 1,  $N_0$  quanta are incident on a specified area of the detector surface (stage 0). A fraction of these, given by the absorption efficiency (quantum efficiency) of the phosphor material, interact (stage 1). Here it is important that the absorption efficiency be high, or a larger X-ray dose would be needed to arrive at a desired signal level.

The mean number  $N_1$  of quanta interacting represents the primary quantum sink of the detector. The fluctuation about  $N_1$  is  $\sigma_{N1} = \sqrt{N_1}$ . This defines the signal-to-noise ratio of the imaging system, which increases as the square root of the number of quanta interacting with the detector. Regardless of the value of the X-ray quantum efficiency, the maximum signal-to-noise ratio of the system will occur at this point. If the signal-to-noise ratio of the imaging system is essentially determined there, the system is said to be X-ray quantum limited in performance. The

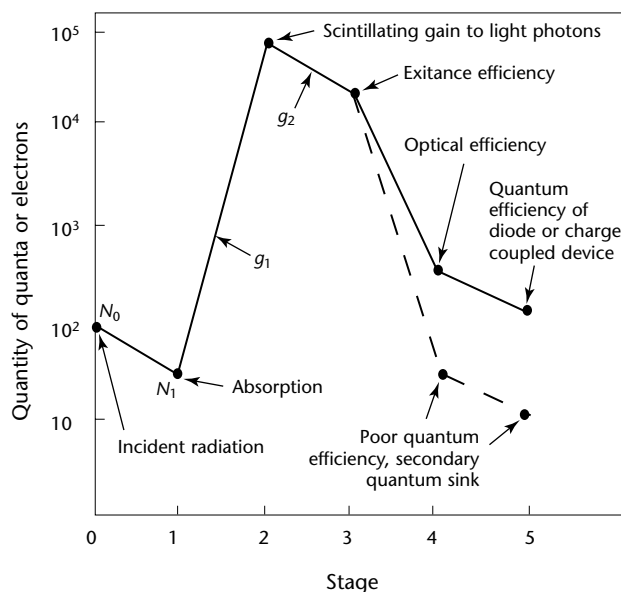
phosphor layer typically creates a large gain factor at this point. Following this, any subsequent inefficiencies in emitting the light and capturing it by the photodiode will result in losses and additional sources of noise. If the number of quanta falls below the primary quantum sink, then a secondary quantum sink will be formed and becomes an additional important noise source.

For most detection systems discussed here, where the phosphor is in direct contact with the diode as in the flat panel detectors, the limiting source of noise is the quantum efficiency of the X-ray conversion material. Noise characteristics of digital detectors are discussed elsewhere.<sup>12</sup>

In efficient systems, because the noise is related to the square root of the number of X-ray quanta absorbed, it is crucial to have a sufficient signal level to avoid quantum mottling. Quantum mottling makes detection of smaller features more difficult. In medical imaging, regulations allow a certain maximum dose to the patient and optimal signal levels may not be obtainable. In this scenario, it is critical to absorb as many X-ray photons as possible and not to allow secondary quantum sinks. In nondestructive testing, it may be possible to increase signal levels by selecting any or all of the following: a longer exposure time, a higher beam flux, a higher radiation beam energy (assuming absorption is still high at those energies) or a closer working distance between source and detector. These techniques will provide improved image contrast throughout the spatial frequency spectrum of the device. Some of these techniques, however, may not meet other goals, such as throughput or allowable space needed for a specimen between the detector and the X-ray tube and tradeoffs must be made.

As just discussed, the phosphor is therefore an important component of the system. For the amorphous silicon detector, the phosphor of choice has been cesium iodide with thallium as the luminescent activator in the material (see Fig. 2).<sup>13</sup> This phosphor is ideal because it has the following beneficial properties.

FIGURE 1. Quantum statistics of X-ray imager.



### Legend

$g$  = gain  
 $N$  = quanta

1. Cesium iodide can be formed into needles on top of the diode structure to direct the light to the photodiodes without significant light scatter. The needles are separated by small air gaps and the high refractive index mismatch between the cesium iodide needles and air ensures a high total internal reflection of the light as it is directed to the photodiode.
2. The needle structure enables thick phosphor layers, which improves X-ray absorption.
3. The cesium iodide has a high effective atomic number ( $Z$ ) which also contributes to good X-ray absorption efficiency.

One disadvantage of the thallium activated cesium iodide material is that it is sensitive to moisture and this hygroscopic nature can degrade the spatial resolution of the phosphor and therefore the device over time if allowed to be in contact with ambient humid conditions. Manufacturers of cesium iodide based systems provide sealed enclosures. A sealed enclosure may typically add 20 percent or more to the cost relative to other phosphors and may reduce the robustness of the system. Another disadvantage is that the phosphor is prone to afterglow and potential variations in light output as a function of increasing X-ray dose.

Nevertheless, the thallium activated cesium iodide phosphor has shown increasing use on the amorphous silicon detector,<sup>13</sup> the charge coupled device detector and the linear array detector. Other inorganic phosphor materials, such as terbium activated gadolinium oxysulfide ( $\text{Gd}_2\text{O}_2\text{S:Tb}$ ),<sup>14</sup> high density glass fiber optic scintillators (FOSs)<sup>15</sup> and hybrid combinations of gadolinium oxysulfide and fiber optic scintillators<sup>16</sup> have also been used successfully as X-ray

phosphor material on these same detector structures. The fiber optic scintillator structure and the hybrid analogs (Fig. 3) provide a similar light guiding capability, provide high X-ray absorptivity without sensitivity to moisture and permit control of afterglow<sup>17-19</sup> but are not as bright an X-ray converter as is the cesium iodide.

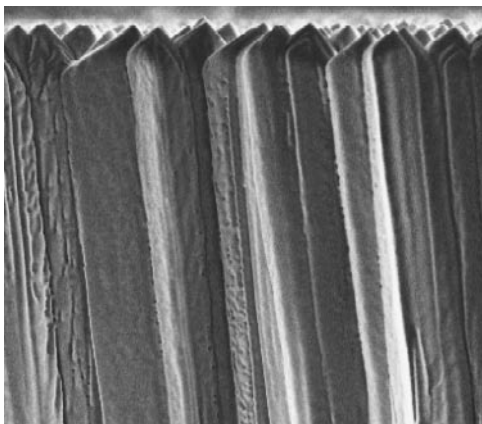
Because the gain in the fiber optic scintillators materials is not as high as in cesium iodide, a potential secondary quantum sink is possible especially in a lens based charge coupled device system. This lower gain will clearly lead to a higher noise level for a given exposure or to a much longer exposure time to generate similar statistics. If the detection system used leads to a strictly quantum limited configuration for any of the phosphor systems mentioned, then they all should provide similar image quality, assuming the resulting signal levels are high enough above the noise floor of the detection system to render the detector noise negligible.

On the other hand, if a phosphor is too bright under a range of X-ray conditions, then it is possible for the diodes to be filled too quickly and a mottled image can result simply because of the low number of X-ray photons actually transmitting the part. One way to solve this problem is to use a lower gain phosphor or the fiber optic scintillators and use an extended exposure in a single frame. Another way is to average multiple frames with the faster phosphor until the desired image quality is produced.

To summarize, the selection of the phosphor is as important as the selection of the readout electronics and image acquisition software. All three have to be considered together in the design and purchase of a system, as well as in the operation of the system.

The selenium photoconductive material has been the photoconductive material of choice as a direct means of converting X-rays directly into charged carriers and avoiding the production of light.<sup>3</sup> [This is described in more detail elsewhere.](#) The obvious advantage here is that the image forming carriers can be more effectively and efficiently directed to the electrode structure than is possible with light. The image sharpness and speed that results can be very high. The modulation transfer function can in principle be higher than that of phosphor based systems for a given pixel pitch. The disadvantage of the selenium material, however, is that it does not have as high an atomic number as cesium iodide or gadolinium oxysulfide. For nondestructive testing applications where the X-ray energy is typically above 50 kV, to obtain similar X-ray sensitivity to the higher  $Z$  phosphor materials, the selenium layer

**FIGURE 2.** Photograph of cesium iodide fibers grown onto a photodiode array.



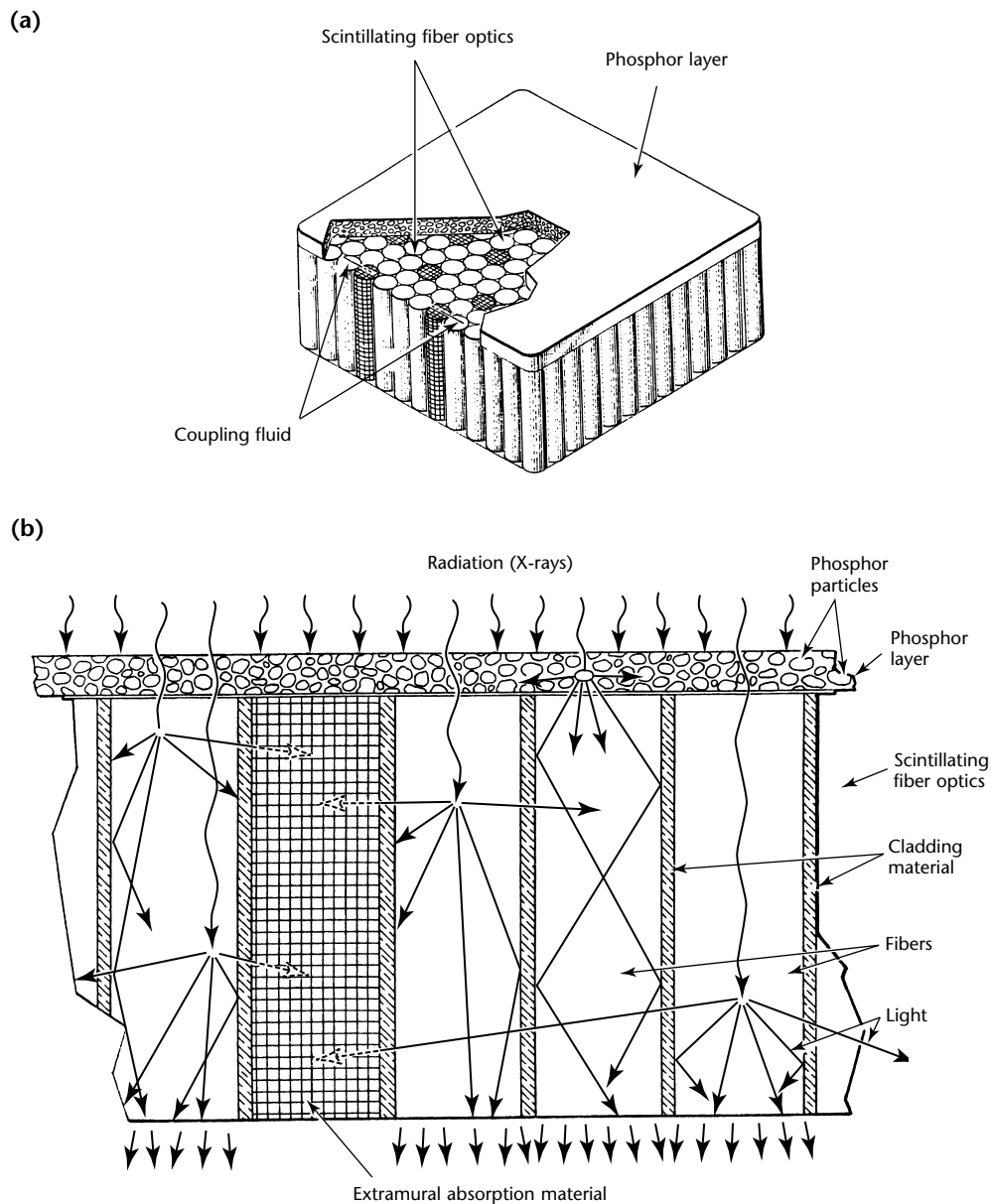
needs to be substantially thicker than the phosphor material. This means that the X-ray energy will be deposited in a thicker region than in these phosphor configurations. The downfall here is that X-ray scatter and the diverging X-ray beam can reduce the resulting spatial resolution in the image, reducing some of the benefit of the electrostatic transfer.

A problem for the selenium approach in the 1990s was that the speed of the selenium process was too high in some circumstances and the pixels were filled with charge at a relatively low X-ray exposure. This overcharging resulted in quantum mottling and a reduced

signal-to-noise ratio. This problem has been corrected through reduction of gain amplification during electronic readout.

Clearly, the debate of photoconductor versus phosphor will remain an interesting topic for discussion and both approaches will continue to be used successfully. If system noise or other artifacts in the system begin to compete with statistical noise, then in addition to proper selection of the converter, the detection system electronics needs to be carefully evaluated. The systems discussed here have a wide range of system noise values, some from different sources and some not necessarily correctable. As a

**FIGURE 3.** Hybrid scintillator — phosphor attached to fiber optic scintillator.



final check, it is best to test the system for the application at hand.

## Spatial Resolution Considerations

The efficiency of the energy conversion process relates to the speed of the test, the throughput and the tradeoff with contrast sensitivity (the ability to detect a small change in thickness or density).

### Detector Resolution

The spatial resolution of the detector determines if features in the object are detectable from a pixel sampling consideration. The selection of the spatial resolution of the detector is also important in designing or selecting a detection system. From the aspect of image contrast and spatial resolution, it is desirable to have the largest pixel that will allow detection of the features of interest in the radiographic examination. For example, it is not necessary to select a 39  $\mu\text{m}$  pixel pitch if the application is for the detection of large foreign objects left behind in an engine nacelle. Similarly, fatigue crack detection is probably not going to be too successful with a pixel pitch of 200  $\mu\text{m}$  or larger.

### Pixel Pitch

The predominant factor that governs the spatial resolution of a detector is the pixel pitch. The pixel size of a number of digital detectors is provided in Table 1. The selection of the X-ray conversion screen then becomes important. Here the architecture of the X-ray conversion material will dictate to what degree the full spatial resolution of the detector can be realized.

As the pixel pitch is reduced to increase resolution, the total number of pixels in the image increases for a constant field of view. The file sizes for typical images run from 2 to 8 megabytes. However, for digital images at radioscopic (real time) frame rates of 30 frames per second, the image size must be closer to about 1 megabyte at current technology. Therefore tradeoffs are made in selecting larger pixels for smaller fields of view for digital radioscopy.

The selection of a high atomic number X-ray conversion material that can provide a signal gain sufficient to not allow secondary quantum sinks following absorption is critical. Forming this material into a shape that directs the signal onto a single pixel, as is done with cesium iodide, is then crucial to maintaining good image detail. As the atomic number of the conversion material

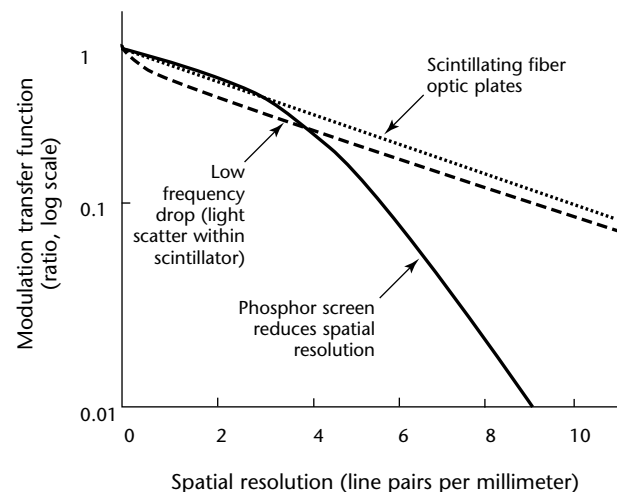
selected goes down, the percentage of X-ray information in the radiation beam will diminish and poor image contrast will result.

To compensate for this image degradation, the conversion material can be made thicker or, if time permits, a longer total exposure time can be selected to capture more X-ray quanta. Making the conversion layer thicker can impact the spatial resolving power of the device because both X-ray cross talk and signal (light or electron hole carriers) cross talk will yield a breakdown in the modulation of the signal somewhere in the spatial frequency range of the detector.

## Modulation Transfer Function

A good measure of the spatial resolution therefore is the modulation transfer function (MTF). The modulation transfer function measures the signal modulation as a function of spatial frequency and is typically computed using a fourier transform of a line spread function acquired on an angled tungsten edge placed directly on the detector.<sup>13</sup> Figure 4 shows the power of a modulation transfer function for revealing a breakdown in spatial resolution throughout the spatial frequency regime of the detector. If the spatial resolution drops near the 0 line pairs per millimeter spatial frequency regime, this drop can be interpreted as a severe degradation in image contrast and will result in poor density discrimination. If the modulation transfer function is low at high spatial frequencies, near the sampling limit of the detector, this

**FIGURE 4.** Examples of modulation transfer function curves, showing localized variations in modulation transfer function curve in some regions of spatial frequency domain. Maximum spatial resolution for detector is 10 line pairs per millimeter.





indicates that the conversion material is not a good choice for detection of the fine features that the system was designed to detect. Another choice should be selected. Balancing the spatial resolving powers of a conversion material with its quantum efficiency has been an active area of research and development in digital radiography since 1985.

### Gain and Offset Correction

Imagery from digital detectors are frequently normalized for pixel-to-pixel gain variations and also adjusted to subtract out the background or offset. The offset or background signal is usually a small percentage of the maximum signal and is common to all digital detectors. It is important to subtract this background signal to provide a wider linear range and to subtract any latent images on the detector. In performing a gain correction, not only are pixel-to-pixel variations reduced but also variations in the optical components feeding these pixels will be diminished. Performing this gain correction can also be used to flatten the radiation intensity distribution across the detector panel. Making the radiation beam intensity more uniform across the detector can result in wider latitude (viewable thickness range) in the image. This normalization is really not possible with film radiography.

The gain correction is accomplished by taking an image with a radiation technique similar to that planned for production but without an object in the beam (an *air* image) and with a much reduced X-ray intensity. By simply performing an image division by the gain factor on a pixel-by-pixel basis, the offset corrected *air* image is then used to correct each subsequent image of an object. Following gain and offset correction, detection sensitivity improves in relation to an image that does not have this correction. For the *air* image, it is critical that the image be free of transient latent images, have the correct intensity and also not contain an object of any sort (such as a fixture) in the beam. If any of these occur, then every subsequent corrected object image will contain artifacts and the correction will do more damage than good.

## Radiation Damage

In digital imaging devices, there are numerous elements of the detector assembly that can be damaged by the ionizing radiation. Every component in the imaging chain not shielded appropriately from X-rays or gamma rays can be damaged. The term radiation

damage is a general term that can refer to any range of damage to a component in the detection chain. The damage can lead to subtle changes in performance, all the way to failure. Most digital detectors are designed so that the electronic components behind the X-ray conversion material are either shielded from the X-rays (for example, by the conversion material itself or by fiber optic transfer components behind it) or are sufficiently thin to absorb only a small portion of the X-rays that impinge on the component. The damage that occurs in the electronic circuitry can result in an increase in the electronic noise of the device and eventually to failure as the accumulated dose to the component increases. Each manufacturer uses proprietary circuitry and various forms of shielding elements to prevent these effects. Each system is different, so the reader is referred to a general text on radiation effects on silicon circuitry.<sup>20</sup>

The X-ray conversion material, being the primary X-ray absorption component, is exposed to the highest levels of radiation within the imaging chain. Phosphors such as cesium iodide and photoconductive materials such as selenium have discontinuity centers within their band structures that will trap electron and hole carriers produced by the ionizing radiation. In many circumstances, thermally released carriers from these traps will yield a delayed luminescence or a delayed release of charge. This form of radiation damage known as *afterglow* or *lag* usually increases as a function of radiation dose until an equilibrium occurs where the number of carriers being trapped equals the number being thermally released.

Another form of radiation damage to X-ray conversion materials that occurs is when the carriers are permanently trapped in deep centers within the band gap. This trapping is sometimes associated with a darkening of the conversion material and usually results in a rapid decrease in signal that can only be healed by heat annealing of the material or by slow thermal release at room temperature. This form of damage is known as a *gain decrease*. In other materials, it is possible to observe a rapid signal gain increase as a function of increased radiation dose. Although the mechanism of gain decrease is not widely understood, both gain changes can impart spatial artifacts into a current image created by the variation in radiation intensity across a prior specimen image. In most cases these gain changes are not long term or permanent. If the system is prone to these radiation induced gain changes, it is important to continually update gain and offset data, even if the actual examination is not



changing, so that these artifacts can be reduced. If the problem becomes severe it might warrant a new phosphor.

The storage phosphor used in computed radiography systems, europium activated barium fluorobromide (BaFBr:Eu), inherently has discontinuity centers when prepared under certain reducing conditions in the presence of a partial pressure of hydrogen ( $H_2$ ) gas in an otherwise inert atmosphere.<sup>4,21,22</sup> In this phosphor, this radiation damage has been used in a novel way by storing these charge carriers in the phosphor material and then later reexciting those carriers (with red light emitting diodes or a helium neon laser) to produce a delayed luminescence. In storage phosphors, this radiation damage is beneficial but, in promptly emitting materials such as cesium iodide, is to be avoided if possible.

## Selection of Systems to Match Application

Some of the key characteristics that might be considered in the selection of a digital radiographic imaging system are the following: (1) detection precision and accuracy; (2) system speed to match that of manufacturing and test processes; (3) area of the detector to match manufacturing throughput needs; (4) volume of the device for access to tight locations in an assembly; (5) presence of artifacts that can impact detection capability.

If a large area detector is needed and there is a requirement to work at real time frame rates of 30 frames per second, then an amorphous silicon detector or charge coupled device based detector should be selected.<sup>23</sup> Note that technology in 2002 may limit digital radioscopy frames to about one million pixels. If static imaging is required but the highest spatial resolution is needed and the object size is not large, then a system using a low noise phosphor or charge coupled device should be selected. For this same application, a large area flat panel detector operating in static mode can also be selected if used in combination with a microfocus X-ray tube but only if the application can withstand the longer exposure times associated with magnification radiography.<sup>24</sup>

If super high resolution is required, for example, very tight small crack detection, then magnification may be required with the high resolution charge coupled device devices.

As mentioned above, it is important to have the largest pixel that can be accepted from a feature detection (spatial resolution) standpoint. This parameter then provides the highest throughput

possible because larger pixels can produce a higher signal-to-noise ratio for a given X-ray exposure. Larger pixels will also allow a lower exposure for a constant signal-to-noise ratio. Larger pixels permit thicker X-ray conversion materials, again potentially adding speed to the test. Finally larger pixels will result in a larger overall field of view (larger throughput). For example, a four million pixel array of 200  $\mu m$  pixels will have 16 $\times$  the field of view of a four million pixel array of 50  $\mu m$  pixels. As mentioned earlier, the size of the detector and the size of the pixel still go hand in hand using today's technology. It is possible to have a 10 000  $\times$  10 000 pixel array of 25  $\mu m$  pixels resulting in a 250  $\times$  250 mm device. That said, if a smaller pixel device is selected, it might be possible to average pixels into larger superpixels to enhance speed and part throughput. The minor drawbacks of such superpixels is that the X-ray conversion material may not be of optimal thickness for the larger size pixel and the percent of active pixel (because the amorphous silicon approach may be summing four field effect transistors) may not be as great as if the pixel were designed with a single set of readout circuitry. Finally, the noise of averaging four pixels is a little higher than the noise of a similar detector element of the same size.

For tight locations, small detectors based on charge coupled device or complementary metal oxide silicon technology can be used. Some of these devices are being used for dental radiography and they are beginning to find application in nondestructive testing.

Where the requirement is to simply replace film in favor of a lower cost digital solution, then storage phosphors can be used quite successfully. However, if access is not an issue, then the other digital approaches may be more cost effective over the long term because they are more amenable to high speed mechanized automation of the detector and X-ray tube to scan about a part or conversely for the part to be scanned through the stationary tube and detector configuration.

Linear arrays can be used in an assembly line configuration, as can the real time flat panel and charge coupled device detector based systems. Line scanners offer the advantage of reduced sensitivity to X-ray scatter in relation to area array systems.<sup>22</sup>

The scanning beam, reversed geometry system has shown promise in reduced access applications. This detector is natural because the detector module is quite small. The reversed geometry system is probably the best system for reduced sensitivity to X-ray scatter because the detector is essentially a point based

sensor. However, it is important to note that the detector is typically much larger than an X-ray tube focal spot. Because of the effective focal spot size of the system, there may be some geometric constraints placed on this system in terms of image unsharpness.

Artifacts have been prevalent in digital radiographic systems. The presence of artifacts, therefore has to be evaluated almost on a detector-to-detector basis.

## PART 4. X-Ray Detector Technology

### Amorphous Silicon Detectors<sup>23</sup>

Most new amorphous silicon designs are based on a flat glass panel that has undergone a deposition process resulting in a coating on one side that contains several million amorphous silicon transistors. These transistors are arranged in a precise array of rows and columns. Bias and control lines are brought to the edge of the panel for each individual transistor. The length and makeup of these control lines play a role in how fast image data can be scanned out of the array. On large receptors the control lines are typically brought out from the middle to both sides of the panel to minimize the track lengths.

Figure 5 illustrates a cutaway view of a typical panel design. This configuration is typical of a receptor incorporating a phosphor conversion layer. The phosphor layer converts the X-ray photons to light photons. The light photons are in turn converted to electrons by the amorphous silicon array and the readout electronics.

The next layer of the assembly (shown in Fig. 5) is the amorphous silicon transistor array. Deposited on a glass substrate to provide a rigid and very flat surface, this layer converts the light photons, from the phosphor, into electrons that can be read out, amplified, digitized and stored as an image. Each element of the amorphous silicon array is made up of a transistor and a photo diode. See Fig. 6 for a schematic representation of a small section of the receptor. The light from the phosphor is captured by the photodiode and then read out through the transistor in a very high

speed and synchronized process. Each charge is digitized by an analog to digital converter and then stored in a precise memory location in the image processing computer. Once every transistor is sampled and read out, a complete image will be displayed on the viewing monitor.

With regard to flat panel receptors, a pixel is the area of one transistor and one photo diode.<sup>24</sup> Typically these pixels range in size from  $100 \times 100 \mu\text{m}$

FIGURE 6. Circuitry of amorphous silicon detector array.

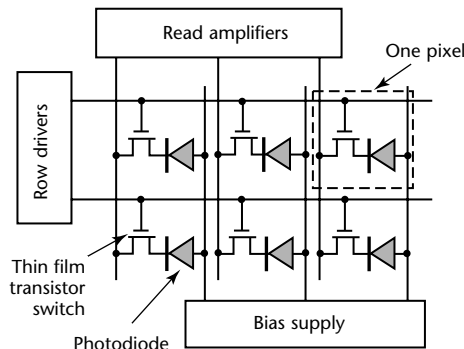


FIGURE 7. Photomicrograph of amorphous silicon detector circuitry.

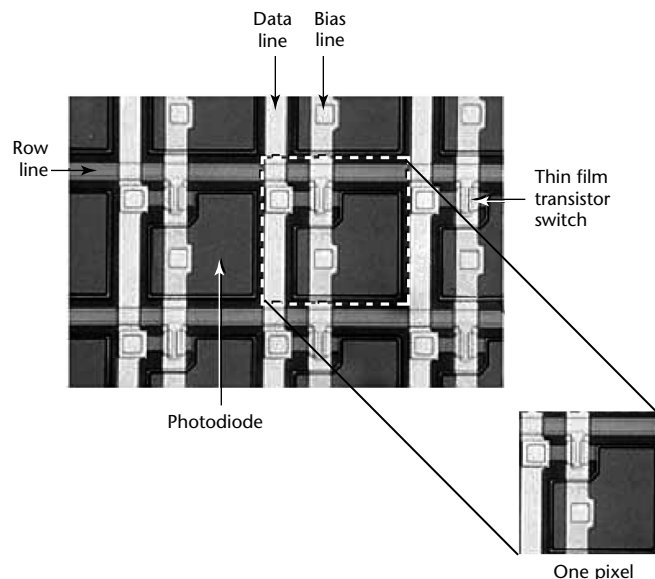
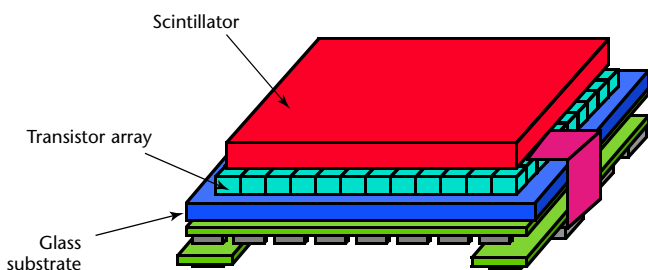


FIGURE 5. Scintillator attached to amorphous silicon array.



( $0.004 \times 0.004$  in.) to  $400 \times 400$   $\mu\text{m}$  ( $0.016 \times 0.016$  in.). A typical pixel is shown in Fig. 7.

Figure 8 shows a cross sectional view of an amorphous silicon receptor that uses a cesium iodide scintillator. This view suggests the path taken by the X-ray beam as it exits the object being tested and enters the input of the receptor. Figure 9 shows an image receptor assembly with the electronics folded out from behind the panel during assembly and testing. The large dark area at the right center of the picture is the amorphous silicon array. Around the edges of the array are all the electronics required to control and read out the image data.

The micrograph in Fig. 7 shows the mechanical makeup of the amorphous silicon layer. The bias and data lines provide the ability to properly control

**FIGURE 8.** Schematic cross section of photodiode X-ray detector using amorphous silicon receptor with cesium iodide scintillator.

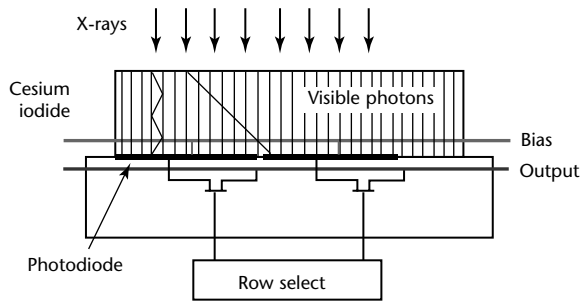
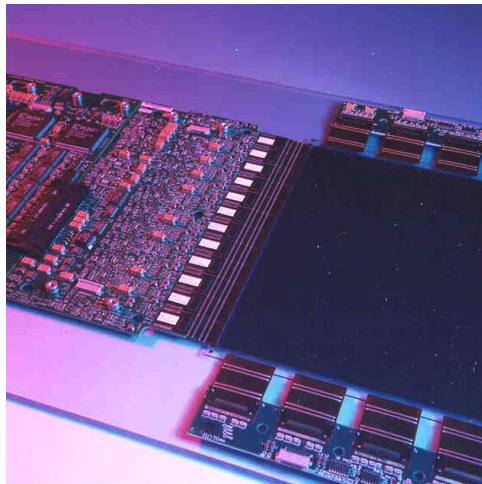


**FIGURE 9.** Photograph of amorphous silicon detector with electronics mounted to side of panel in position where they can be shielded from X-rays.

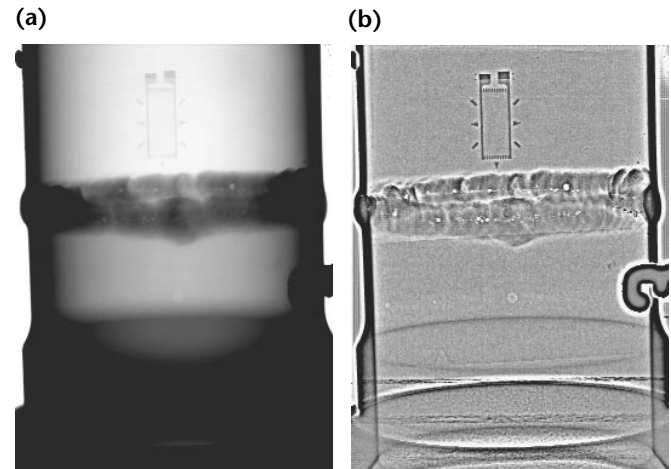


each pixel and the connections used to get the image data out.

The high resolution view of an aluminum tube weld in Fig. 10 was obtained with an amorphous silicon panel originally acquired at 4 $\times$  geometric magnification with a microfocus X-ray source. In the lower portion of the image is the placement of a 75  $\mu\text{m}$  (0.003 in.) thick ASTM aluminum plaque image quality indicator. The central hole in this plaque is 250  $\mu\text{m}$  (0.010 in.) in diameter and is clearly visible through the thin aluminum walls, about 1.25 mm (0.050 in.) thick. This image illustrates that very small diameter porosity can be detected in these structures: comparing the gray scale and size of the pores in the weld with the holes of the image quality indicator reveals porosity much smaller in diameter than the 1T (250  $\mu\text{m}$  [0.010 in.]) hole. Figure 10b provides a high pass filter rendition of this image. Once filtered, contrast may be added to the image so that high contrast can be observed across the entire thickness range of the object. This now provides information on the weld almost to the tangent point and assists the operator in identifying discontinuities over a wider range of thickness in a single view.

Most flat panel receptors available today are designed to provide radiographic acquisition capability at a rate of one image about every 5 to 10 s. Some designs take more or less time to put the image on the monitor but most fall into this range. This speed is certainly

**FIGURE 10.** Aluminum tube weld image acquired with amorphous silicon detector with 4X geometric magnification. (a) porosity as small as 125  $\mu\text{m}$  (0.005 in.) can be detected in gray scale image; (b) high pass filter provides high contrast over wider thickness range in single view, making porosity evident almost to tangent point of weld.



much faster than what can be achieved with film cassettes. This technology represents an advance in practicality since the 1990s.

## Amorphous Selenium Detectors

In flat panel arrays using an amorphous selenium converter (or other photoconductors), the X-ray to electrical charge conversion process is referred to as direct because no intermediate steps are required. As shown in Fig. 11, the high voltage bias field applied to an amorphous selenium layer creates vertical

field lines. Because the field lines are parallel to the incident X-ray beam (other than for oblique angles), the field prevents the charge from lateral *scattering* and thus there is virtually no blur.

Intuitively, this would seem to suggest that the amorphous selenium conversion layer (excluding the pixel electrodes) should exhibit extremely high resolution. In fact, measurements prove this to be the case.

## Charge Coupled Device Radiographic Systems

Charge coupled devices are used in X-ray imaging systems in combination with X-ray phosphors or scintillators without the need for electronic image intensification. A charge coupled device is an integrated circuit formed by depositing a series of electrodes, called gates on a semiconductor substrate to form an array of metal oxide semiconductor (MOS) capacitors. By applying voltages to the gates, the material below is depleted to form charge storage *wells*. These store charge injected into the charge coupled device or generated within the semiconductor by photoelectric absorption of optical quanta. If the voltages over adjacent gates are varied appropriately, the charge can be transferred from well to well under the gates, much in the way that boats will move through sets of locks as the potential (water heights) are adjusted.<sup>12</sup>

FIGURE 11. Schematic cross section of amorphous selenium X-ray detector.<sup>12</sup>

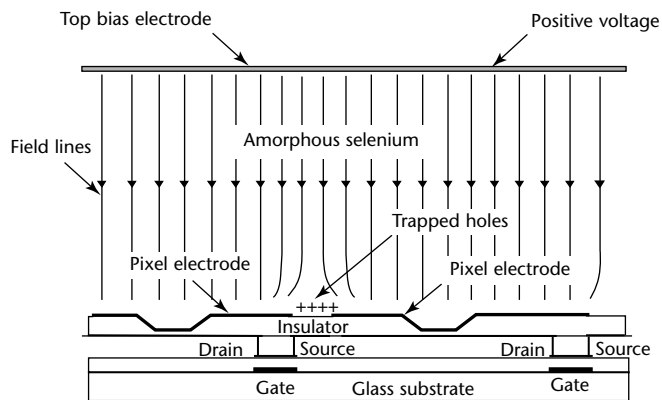
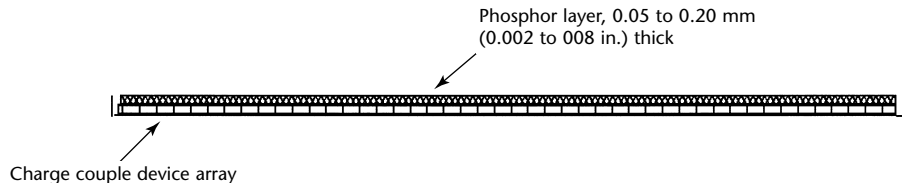
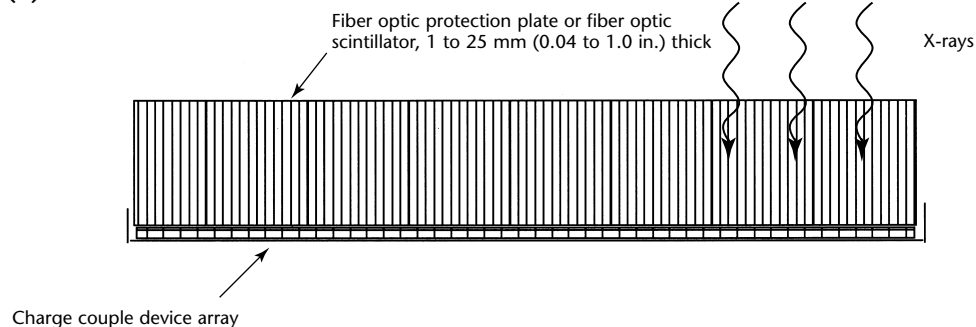


FIGURE 12. Charge couple device based X-ray detector: (a) X-rays directly excite charge coupled device through phosphor (phosphor does not provide enough shielding); (b) fiber optic scintillator coupled directly to charge couple device provides shielding to sensor.

(a)



(b)





In the simplest charge coupled device systems, the charge coupled device is rapidly scanned to provide television frame rates with typical exposures per frame of 33 ms. In this mode, the signal captured can be very low and the resulting signal-to-noise ratio will therefore also be low because of the small number of photons impinging on the phosphor in the time allotted and the high noise level of the charge coupled device. The noise of the device increases as a function of the square root of the readout speed and is quite high at real time frame rates. The image quality can be improved by averaging multiple frames in a digital processor but the high noise of the device operating at these speeds does not provide film quality images.

The better way to improve signal-to-noise ratio using charge coupled devices, is to integrate the charge produced by light from the phosphor directly on the charge coupled device cells. The *wells* generated by the readout approach can be sufficiently deep to capture three to four orders of magnitude in equivalent light levels. Because the exposure times are now much slower than the real time rates of traditional charge coupled device video cameras, the readout speed can be reduced to obtain lower camera noise levels. On a frame-by-frame basis, the signal levels have been increased while the additive noise from the camera has been decreased. In this mode, further electrostatic image intensification is not needed.

Charge coupled devices are now available with image formats as large as  $4096 \times 4096$  pixels and 16 bits. Some devices have been made as large as  $60 \times 60$  mm ( $2.4 \times 2.4$  in.). A phosphor screen can be coupled directly to the charge coupled device itself but even if the phosphor has good X-ray quantum efficiency, those X-ray photons not absorbed by the phosphor (even if it is a small percentage) can still be absorbed in the silicon layer of the charge coupled device and yield a significant direct excitation speckle noise in the image. To avoid this noise a fiber optic image transfer plate or a scintillating fiber optic plate may be used<sup>16</sup> to absorb the transmitted X-rays before being absorbed in the silicon (see Fig. 12).

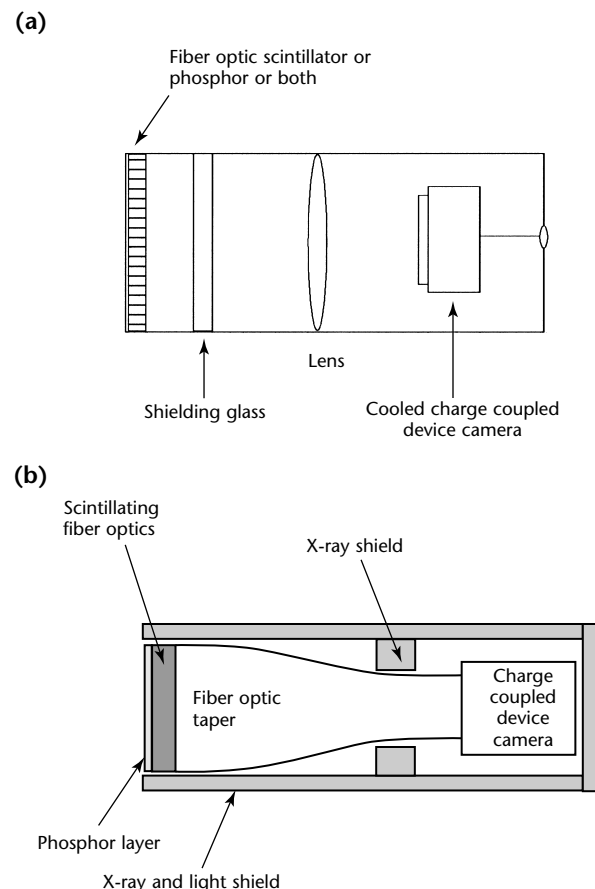
The field of view of the charge coupled device based X-ray systems can be expanded with a fiber optic taper or a lens system. These configurations are shown in Fig. 13.

Fiber optic tapers are fiber optic face plates in which the size of each fiber in the face plate is reduced so that an image deposited at the input surface may be transferred to a smaller device such as a charge coupled device at the output

surface. Fiber optic tapers thereby increase the field of view, provide efficient light collection (with respect to a lens), offer shielding of the charge coupled device from direct X-ray hits and can yield a compact, light weight rigid design. Fiber optic tapers have now been incorporated with a  $100 \times 100$  mm ( $4.0 \times 4.0$  in.) active area.<sup>25</sup>

A lens as an optical coupling device has the drawback that it is a very inefficient light collection device. Relative to a fiber optic taper a lens system is less efficient by a factor roughly of ten or more. This inefficiency can lead to secondary quantum sinks and additional noise in the image. Secondly, the lens does not provide adequate shielding to the charge coupled device, so an additional shielding glass is needed directly in front of the charge coupled device to reduce direct X-ray hits on the device. In addition, a mirror can be used to move the camera out of the radiation beam. The charge coupled device can then be shrouded in lead to reduce excitation by tangentially scattered X-rays. One advantage of a lens is the increased flexibility it offers to

**FIGURE 13.** Coupling of light from phosphor to charge couple device in X-ray detector system: (a) lens coupling; (b) fiber optic coupling.





adjust the field of view for testing of both large and small objects.

The amorphous silicon, the amorphous selenium (Fig. 14) and the charge coupled device approach each provides image characteristics of interest. Charge coupled devices can provide high resolution with a small field of view whereas the larger amorphous detectors will provide moderate resolution with a large field of view.

## Linear Detector Arrays

The linear detector array based systems are ideally suited for production environments. Many industries — including automotive manufacture, cargo transport, food inspection, munitions, security and nuclear waste containment — use linear arrays of X-ray detectors for their inspection needs. Thousands of these units have been installed. Figure 15 shows images of various objects suspended in barrels and detected with linear arrays.

**FIGURE 15.** X-radiographic images of barrels and contents made with linear detector arrays: (a) first barrel; (b) second barrel.

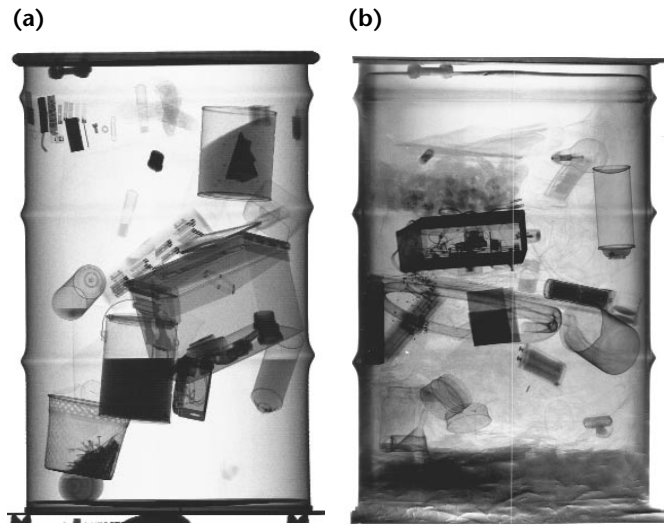
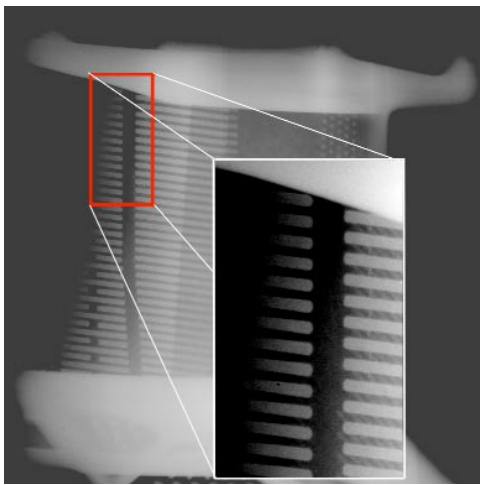


**FIGURE 14.** Radiographic image of nickel alloy bucket blade with enlarged view of finning effect. Image was acquired with 400 kV exposure of 350 × 430 mm (14 × 17 in.) field of view with part on amorphous selenium detector.



# References

1. *Nondestructive Testing Handbook*, second edition: Vol. 3, *Radiography and Radiation Testing*. Columbus, OH: American Society for Nondestructive Testing (1985).
2. Janesick, J. and T. Elliot. "History and Advancement of Large Area Array Scientific CCD Imagers." *Astronomical CCD Observing and Reduction* [Tucson, AZ]. *Conference Series* 91. Vol. 23. Chelsea, MI: Bookcrafters (1992): p 1.
3. Soltani, P.K., D. Wysnewski and K. Swartz. "Amorphous Selenium Direct Radiography for Industrial Imaging." *Proceedings — Computerized Tomography for Industrial Applications and Image Processing in Radiology* [Berlin, Germany]. DGZIP Proceedings BB 67-CD. Berlin, Germany: Deutsche Gesellschaft für Zerstörungsfreie Prüfung (March 1999): p 1-10.
4. Takahashi, K., J. Miyahara and Y. Shibahara. "Photostimulable Luminescence (PPL) and Color Centers in BaFX:Eu<sup>2+</sup>(X=Cl,BrI) Phosphors." *Journal of the Electrochemical Society*. Vol. 132, No. 6. Pennington, NJ: Electrochemical Society (1985): p 1492-1494.
5. ASTM E 2007-00, *Standard Guide for Computed Radiology (Photostimulable Luminescence (PSL) Method)*. West Conshohocken, PA: ASTM International (2002).
6. Spees, G., B. Munier, G. Roziere, P. Prieur and H. Rougeot. "Solid-State Linear Detector for X-Ray Digital Imaging." *Materials Evaluation*. Vol. 48, No. 3. Columbus, OH: American Society for Nondestructive Testing (March 1990): p 326-327.
7. Koskinen, J. "LDA Technology Today and Possibilities in the Future." Paper presented at *Digital Imaging 4* [Mashantucket, CT]. Columbus, OH: American Society for Nondestructive Testing (August 2001).
8. Albert, R.D. "X-Ray Scanning Method and Apparatus." United States Patent 3 949 229 (April 1976).
9. Winfree, W.P., N.A. Cmar-Mascis and F.R. Parker. "Enhanced Imaging of Corrosion in Aircraft Structures with Reverse Geometry X-Ray ®." Paper 7C2. *Third Joint Conference on Aging Aircraft* [Albuquerque, NM]. Arlington, VA: Galaxy Scientific, for the Federal Aviation Administration, Airworthiness Assurance Nondestructive Inspection Validation Center, Sandia National Laboratories, Albuquerque, NM (September 1999).
10. Albert, R., W. Pember, J. Garrison and D. Reyna. "Aircraft Inspection with a Portable, Filmless X-Ray System Using Reverse Geometry." *Materials Evaluation*. Vol. 58, No. 5. Columbus, OH: American Society for Nondestructive Testing (May 2000): p 634-638.
11. Ter-Pogossian, M.M. *The Physical Aspects of Diagnostic Radiology*. New York, NY: Harper and Row Publishers, Hoeber Medical Division (1967).
12. Yaffe, M.J. and J.A. Rowlands. "X-Ray Detectors for Digital Radiography." *Physics in Medicine and Biology*. Vol. 42. London, United Kingdom: Institute of Physics in association with the American Institute of Physics and the American Association of Physicists in Medicine (1997): p 1-39.
13. Granfors, P.R. and R. Aufrichtig. "Performance of a 41 × 41-cm<sup>2</sup> Amorphous Silicon Flat Panel X-Ray Detector for Radiographic Imaging Applications." *Medical Physics*. Vol. 27, No. 6. Melville, NY: American Institute of Physics for the American Association of Physicists in Medicine (June 2000): p 1324-1331.
14. Weisfeld, R.L., M.A. Hartney, R.A. Street and R.B. Apte. "New Amorphous-Silicon Image Sensor for X-Ray Diagnostic Medical Imaging Applications." *Medical Imaging 1998: Physics of Medical Imaging*. SPIE Proceedings, Vol. 3336. Bellingham, WA: International Society for Optical Engineering (July 1998): p 444-452.
15. Bueno, C., M.D. Barker, P.E. Condon and R.A. Betz. "Solid State X-Ray Imaging Methodology." Final Report, Contract No. F33615-89-C-5617, WL-TR-92-4003. Wright-Patterson Air Force Base, OH: Wright Laboratory, Materials Directorate, Air Force Systems Command (March 1992).

16. Placious, R.C., D. Polansky, H. Berger, C. Bueno, C.L. Vosberg, R.A. Betz and D.J. Rogerson. "A High Density Glass Scintillator for Real-Time X-Ray Inspection." *Materials Evaluation*. Vol. 49, No. 11. Columbus, OH: American Society for Nondestructive Testing (November 1991): p 1419-1421.
17. Bueno, C., R.L. Rairden, R.A. Betz, R.W. Mead and J. Ellis. "Hybrid Luminescent Device and Method for Imaging Penetrating Radiation." United States Patent 5 636 299 (June 1997).
18. Bueno, C., R.L. Rairden and R.A. Betz. "Hybrid Luminescent Device for Imaging of Ionizing and Penetrating Radiation." United States Patent 5 594 253 (January 1997).
19. Bueno, C., R.A. Betz and R.L. Rairden. "Hybrid Scintillators for X-Ray Imaging." *Medical Imaging 1996: Physics of Medical Imaging*. SPIE Proceedings, Vol. 2708. Bellingham, WA: International Society for Optical Engineering (1996): p 469-481.
20. Messenger, G.C. *The Effects of Radiation on Electronic Systems*. New York, NY: Van Nostrand Reinhold (1986).
21. Crawford, M.K., L.H. Brixner and K. Somaiah. "X-Ray Excited Luminescence Spectroscopy of Barium Fluorohalides." *Journal of Applied Physics*. Vol. 66, No. 8. Melville, NY: American Institute of Physics (October 1989): p 3758-3762.
22. Crawford, M.K. and L.H. Brixner. "Photostimulable Phosphors for X-Ray Imaging: Applications and Mechanism." *Journal of Luminescence*. Vol. 48-49, Part 1. New York, NY: Elsevier (January-February 1991): p 37-42.
23. Budner, G. "High Energy Digital Imaging Techniques with aSi Flat Panel Imagers." Paper presented at *Digital Imaging 4* [Mashantucket, CT]. Columbus, OH: American Society for Nondestructive Testing (August 2001).
24. Gilblom, D., R. Colbeth, M. Batts and B. Meyer. "Real-Time X-Ray Imaging with Flat Panels." *Process Control and Sensors for Manufacturing*. SPIE Proceedings, Vol. 3399. Bellingham, WA: International Society for Optical Engineering (1998): p 213.
25. Bueno, C., M. Barker, K. Lauraitis, R. Barry and J. Ryder. "High Resolution Real-Time X-Ray Radiography Advanced Development." Vol. 1, Final Report, Contract No. F33615-91-C-5623, WL-TR-97-4035. Wright-Patterson Air Force Base, OH: Air Force Research Laboratory, Air Force Materiel Command (February 1997).

## Bibliography

- ASTM E 1000-98, *Standard Guide for Radioscopy*. West Conshohocken, PA: ASTM International (1998).
- ASTM E 1255-96, *Standard Practice for Radioscopy*. West Conshohocken, PA: ASTM International (2002).
- ASTM E 1453-93, *Standard Guide for Storage of Media That Contains Analog or Digital Radioscopic Data*. West Conshohocken, PA: ASTM International (1996).
- ASTM E 2033-99, *Standard Practice for Computed Radiology (Photostimulable Luminescence Method)*. West Conshohocken, PA: ASTM International (1999).
- Kano, T. "X-Ray Imaging System Utilizing Photostimulable Phosphor Detector." *Medical Imaging Technology*. Vol. 5. Tokyo, Japan: Japanese Society of Medical Imaging Technology (1987): p 179.



# 12

## C H A P T E R

# Computed Tomography

---

Richard H. Bossi, The Boeing Company, Seattle,  
Washington

Paul Burstein, Skiametics Incorporated, Winchester,  
Massachusetts

James M. Nelson, The Boeing Company, Seattle,  
Washington

## PART 1. Introduction to Computed Tomography

Standard radiography uses superposition of information to create two-dimensional images of three-dimensional objects. For a great many objects, this effect is acceptable. However, in complicated objects this superposition can cause difficulty in interpretation. It is desirable in such cases to be able to view interior regions of interest without interference. The term tomography comes from the Greek  $\tau\omicron\mu\omicron\varsigma$ , *tomos*, "cut" or "slice." Several techniques of tomographic imaging have been developed to *slice* or *section* an object radiographically.

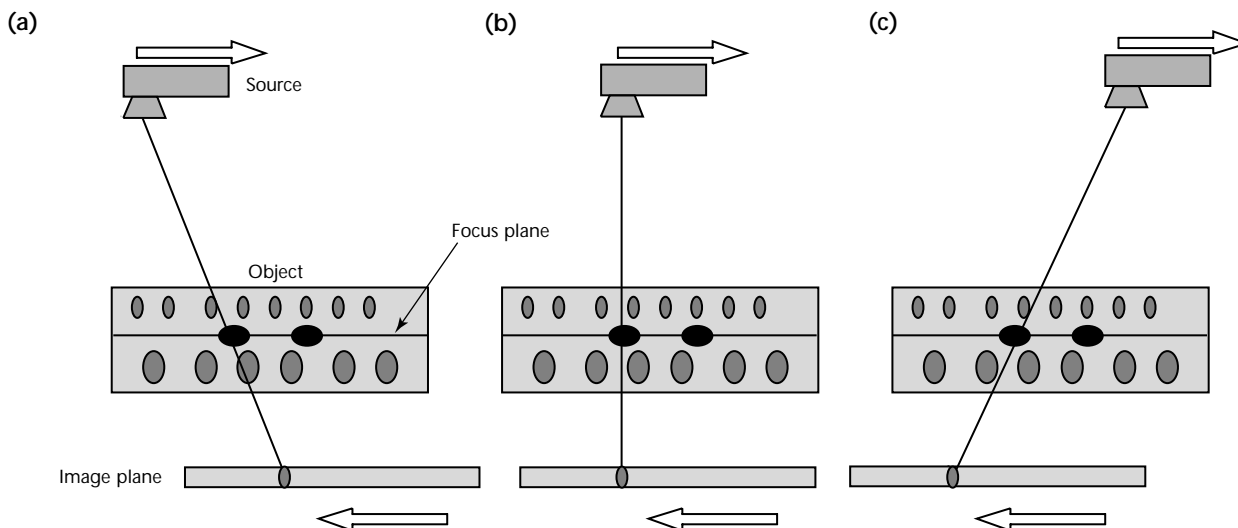
Classical body scan tomography has been used for many years in the medical field. In this technique the source, object and detector planes can be manipulated during the imaging process in a synchronous manner such that a single plane of interest remains in focus while other planes in the object are blurred. Figure 1 is a simple schematic of the approach where the object remains stationary while the source and image plane detector are moved synchronously, keeping one plane of the object in focus. The source and image plane need not necessarily be moved in a linear fashion but may have a circular or other motion

pattern, so long as one plane remains in focus.

This approach has not been widely applied for industrial objects, although there has been interest in the electronics industry for circuit board inspection. Multiple applications of synchronous motion are required to focus on different planes in the object. With the application of digital imaging, however, it is possible to generalize the technique as shown in Fig. 2. By using a digital imager and collecting multiple data sets at different projection views from the source, the data may be reconstructed digitally to create a series of focused planes through the object. Again, the position of the source, object and detector may be manipulated in a number of ways, so long as registration is maintained for digital focusing on a plane of interest. This technology is sometimes referred to as *laminography* or *tomosynthesis*. Commercial equipment can be purchased to perform this data acquisition and reconstruction. The reconstruction can include not only the laminar planes but other reconstruction surfaces as desired.

Computed tomography (CT) is a powerful digital data reconstruction technique for radiographic information

FIGURE 1. Classical body scan tomography method where source and image detector are moved synchronously such that one plane of interest remains in focus: (a) early in scan; (b) interrogating beam normal to plane of interest; (c) late in scan.



that was conceived in the early 1960s. Computed tomography uses measurements of X-ray transmission from many angles about a component to compute the relative X-ray linear attenuation coefficient of small volume elements and presents them in cross sectional image maps (tomograms). Computed tomography can provide quantitative information about the density or constituents and dimensions of the features imaged.

Computed tomography is used for both medical and industrial applications. Medical systems are designed for high throughput and low dosages specifically for humans and human sized objects. These systems can be applied to industrial objects that have low atomic number and are less than 0.5 m (20 in.) in diameter.

Industrial computed tomographic systems do not have dosage and size constraints. They are built in various sizes for applications ranging from evaluation of small (millimeter scale) material samples using low energy X-ray sources, to the inspection of small jet engine turbine blades using medium energy (hundreds of kilovolt) X-ray sources, to the inspection of large intercontinental ballistic missiles requiring high (megavolt scale) X-ray energies.

A typical computed tomographic configuration is shown in Fig. 3. The

X-ray beam is collimated to a narrow slit and aligned with a detector array to define a computed tomographic slice plane in the component. The slit collimation reduces scatter and improves the signal-to-noise ratio in the image. For 100 percent coverage of an object, multiple, contiguous slices must be taken over the entire component. It is possible to perform volume computed tomography or cone beam computed tomography, where the source is uncollimated and the entire cone of radiation passing through the object is measured using an area detector. This is potentially a higher throughput technique than the standard single slice, high collimation technique, although there are limitations in the reconstruction and an increase in scatter signal level.

FIGURE 2. Digital laminographic method where 1 to  $n$  images are taken with various orientations of source object and detector, allowing multiple focus planes in part to be reconstructed from data set.

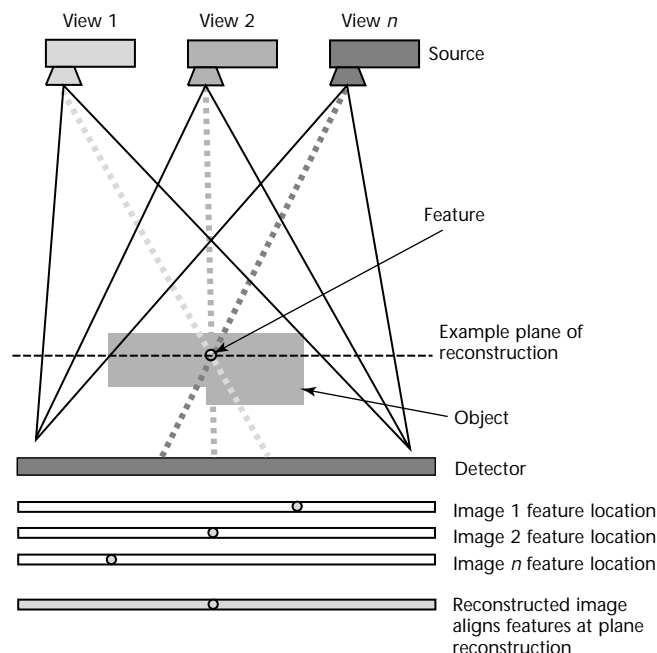
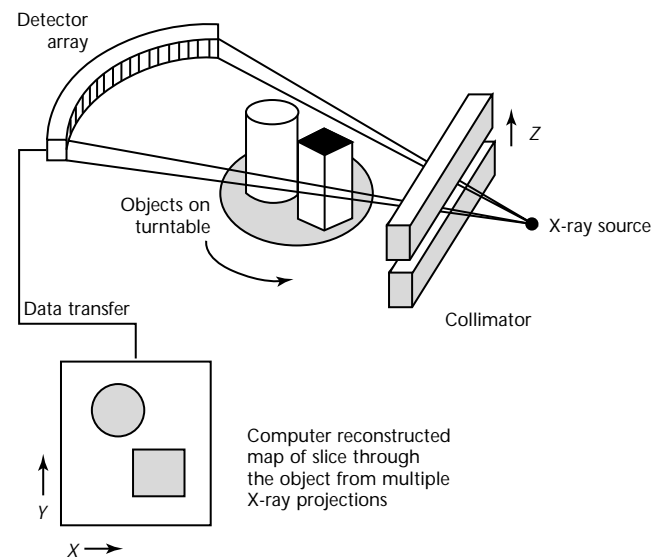


FIGURE 3. Computed tomography using a collimated fan beam and linear detector array data acquisition to reconstruct cross section of object.





## PART 2. Laminography

In the body scan tomography or laminographic technique as shown in Fig. 1, at any given position a standard radiograph consisting of a summation of feature effects along the projected lines of sight to the film is made. If, however, the source and detector are moved simultaneously about a pivot point located in a plane of interest in the test specimen, only that plane will remain in focus on the film. Everything above or below the focal plane blurs. The information outside the plane of interest contributes to the overall noise in the image of the plane but does not add any small scale (that is, high spatial frequency) information. In this classical tomography, all features in the test specimen are present in the image but in a blurred form. The farther away the features are from the plane of interest, the more blurred they are.

Classical tomography is a strictly mechanical technique. It does not rely on computation, except insofar as the mechanical registration of source and detectors with respect to the plane is calculated.

The technique has been applied to electronic multiplayer circuit boards by using a combination of a moving source and radiosopic imaging system. In particular, by using a scanning electron beam source and radiosopic imaging system a very fast system can be developed as shown in Fig. 4.<sup>1</sup> The circuit board is inspected by mounting it on an XYZ table and positioning the region of interest in the field of view. The scanning beam source rotates in a circular motion, synchronous with a rotating motion of the mirror system. The radiographic image of the object is detected by the fluorescent screen and subsequently captured by the camera detector. High speed rotation (600 rotations per minute for example) causes a narrow plane of interest in the object to be in focus based on the geometry of the system. Movement of the object in the Z direction will cause planes of interest to be brought into focus. Objects with high contrast, uniform size and shape and laminar in nature are good candidates for the technique.

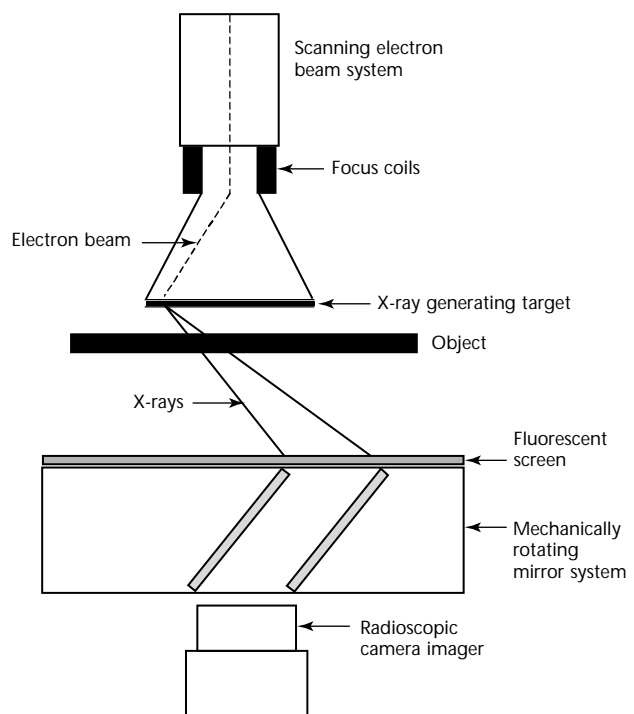
### Tomosynthesis

The basic form of classical tomography can be accomplished with digital radiography, in which case, the plane of interest is specified and the response image is calculated. This technique, referred to as *laminography* or digital *tomosynthesis*, has the advantage of allowing multiple planes of interest to be calculated from a few digital images. A number of variations of digital *laminography* or *tomosynthesis* have been developed by various researchers.<sup>2,3,5-10</sup> Figure 5 shows the generalized mathematical solution to the problem of tomosynthesis on any plane.

Equation 1 shows the notational convention for vectors, unit vectors and their components in the following equations.

Equations 2 to 22 refer to variables and coordinates diagrammed in Fig. 5.<sup>4</sup> Vector  $R$  represents the XYZ coordinate system fixed with respect to the part being inspected:

FIGURE 4. Scanned beam laminography system.



$$(1) \quad R = \begin{bmatrix} X \\ Y \\ Z \end{bmatrix}, \quad r = \frac{R}{|R|} = \begin{bmatrix} r_1 \\ r_2 \\ r_3 \end{bmatrix}$$

The view image raster is  $(I + 1) \times (J + 1)$  pixels. The laminogram image raster is  $(M + 1) \times (N + 1)$  pixels, where  $I, J$  and  $M, N$  represent the horizontal and vertical sizes, respectively, of each image in units of pixel spacings. The laminography integration steps are as follows. First, pick a destination pixel in the laminogram  $(m, n)$ , then solve Eqs. 2 to 4 for the constants  $c_1, c_2$  and  $c_3$ :

$$(2) \quad Zp_1 = c_1 * Xp_1 + c_2 * Yp_1 + c_3$$

$$(3) \quad Zp_2 = c_1 * Xp_2 + c_2 * Yp_2 + c_3$$

$$(4) \quad Zp_3 = c_1 * Xp_3 + c_2 * Yp_3 + c_3$$

Define  $U, V$  and  $W$ :

$$(5) \quad U = Rp_2 - Rp_1$$

$$(6) \quad V = Rp_3 - Rp_1$$

$$(7) \quad W = V - (V \cdot u)u$$

Then solve the  $3 \times 3$  system of Eqs. 8 to 10 for  $R_B$ :

$$(8) \quad \frac{m}{M} = (R_B - Rp_1) \cdot \frac{u}{|U|}$$

$$(9) \quad \frac{n}{N} = (R_B - Rp_1) \cdot \frac{w}{|W|}$$

$$(10) \quad Z_B = c_1 * X_B + c_2 * Y_B + c_3$$

Continuing with reference to variables and dimensions in Fig. 5, the remaining steps are performed for each image ( $k$  of  $K$ ). Solve  $3 \times 3$  Eqs. 11 to 13 for  $e_i$ :

$$(11) \quad Zd_1 = e_1 * Xd_1 + e_2 * Yd_1 + e_3$$

$$(12) \quad Zd_2 = e_1 * Xd_2 + e_2 * Yd_2 + e_3$$

$$(13) \quad Zd_3 = e_1 * Xd_3 + e_2 * Yd_3 + e_3$$

Define  $T$ :

$$(14) \quad T = R_A - R_S$$

Solve  $4 \times 4$  Eqs. 15 and 16 for  $R_A$  and  $d$ :

$$(15) \quad R_A = R_S + dt$$

$$(16) \quad Z_A = e_1 * X_A + e_2 * Y_A + e_3$$

Then compute the vectors:

$$(17) \quad F = Rd_2 - Rd_1$$

$$(18) \quad G = Rd_3 - Rd_1$$

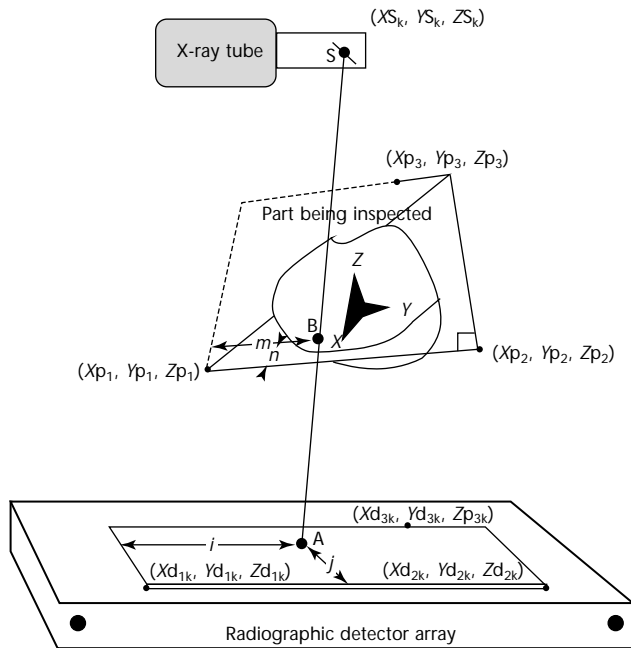
$$(19) \quad H = G - (G \cdot f)f$$

Finally, calculate the indices of the image pixel to be summed:

$$(20) \quad i = I(R_A - Rd_1) \cdot \frac{f}{|F|}$$

$$(21) \quad j = J(R_A - Rd_1) \cdot \frac{h}{|H|}$$

FIGURE 5. Generalized laminography mathematical solution.<sup>4</sup>



#### Legend

- A = point in detector surface
- B = point in laminographic focus plane
- d = subscript designating detector
- $i, j$  = position in detector surface
- k = subscript designating source/detector configuration
- $m, n$  = position in laminographic focus plane
- p = subscript designating corner points of laminographic focus plane
- S = radiation source
- $X, Y, Z$  = cartesian coordinates

And perform the sum into the completed laminogram  $L$ :

$$(22) \quad L(m,n) = L(m,n) + I_k(i,j)$$

## Implementation of Laminographic Techniques

Laminography of this type can be performed in a variety of ways. Computed tomography (see below) is one technique where the geometry is known because of precision of the stage mechanisms. By using the digital radiographic imaging mode of computed tomographic scanning systems a series of digital images at various geometric locations can be obtained and reconstructed for the data set.<sup>6</sup> The computed tomographic system provides precise encoding of the geometry locations for the reconstruction. It is possible however to simply use fiducials in the image to generate the required geometry data and reconstruction.<sup>7</sup> Techniques of laminography using an object motion apparatus with fixed source and detector positions have been devised.<sup>8,9</sup> These techniques provide a relatively simple implementation of the methodology.

The key issue for laminography is the effective image aperture. Figure 6 demonstrates how the position of the X-ray source affects the aperture. In the case of the single source position of a conventional radiograph, the image can be considered to have an effective infinite depth of field and the entire object is the slice (compression of all information into one plane). As the angles of the laminographic data acquisition become larger, an effectively narrower depth of

field is created. Computed tomography is the limiting case for the effective slice thickness through the object. The resulting images from the techniques show an increase in contrast sensitivity for features as the depth of field is narrowed.

Figure 7 is an example of laminographic reconstruction from only

FIGURE 7. Digital laminographic reconstructions of pocket army knife: (a) first layer; (b) second layer; (c) third layer.<sup>10</sup>

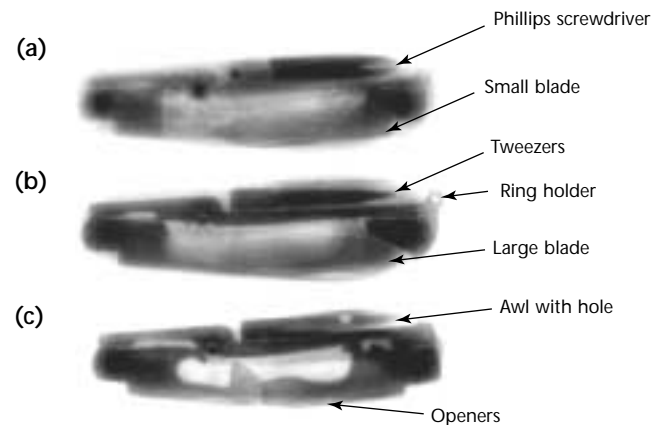


FIGURE 8. Digital tomosynthesis reconstructions of weld shows vertical reconstructions through pores and notch to determine depth information: (a) plan view; (b) vertical view through both pores; (c) vertical view through notch.<sup>10</sup>

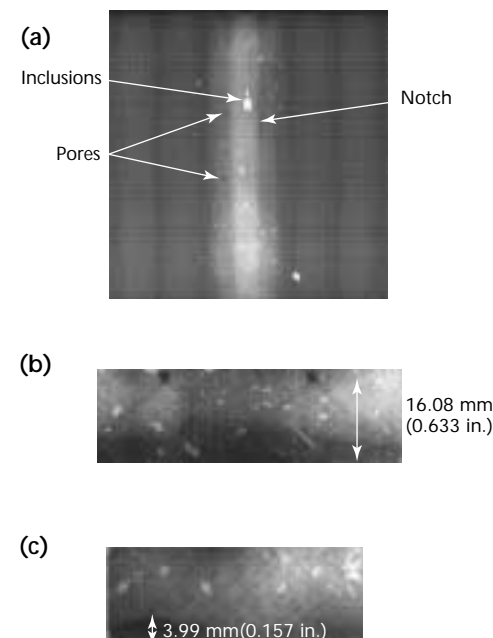
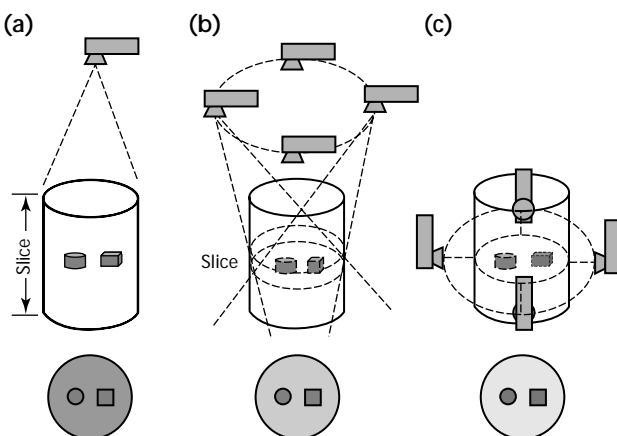


FIGURE 6. Graphical representation of effective apertures: (a) radiography; (b) laminography; (c) computed tomography.<sup>45</sup>



eight digital images.<sup>10</sup> In this example, several layers of a pocket knife are imaged by focusing on the several different depths in the object. Figure 8 is an example of a weld radiograph with two digital tomosynthesis reconstructions. By reconstructing a series of laminographic planes through the object, the volume information on the part is obtained. Tomosynthesis of any arbitrary surface through that volume is now possible. In Fig. 8 two vertical planes have been reconstructed to demonstrate the ability to obtain depth information on features.

## PART 3. Principles of Computed Tomography

### Background

The development of modern computed tomography hinges on advances in a number of different fields. X-rays had been known since before the turn of the century. Medical X-ray films were routinely made as early as 1900. As the technology improved, these projection radiographs became better and better, with reasonably good diagnostic quality being reached in the 1930s. The images returned by those medical systems contained useful information but much information was obscured by tissue and bone on either side of the region of interest. This was especially true in making images of the brain and other interior sections of the skull. Early medical researchers reasoned, that if a series of X-ray absorption measurements could be made around the periphery of the head, the X-ray density of the interior could be reconstructed. This would remove the superposition difficulties inherent in projection radiography. The problem could be viewed as a giant matrix of equations; however, solving the equation matrix for useful spatial resolution would require too much computation unless an algorithm could be found.

The existence theorem for that algorithm was proved by J.H. Radon in 1917. He showed that an arbitrary distribution of material can be reconstructed on a point-by-point basis by measuring the line integrals — that is, summing the elements of the distribution along a series of lines through the distribution — and plugging them into a formula. Unfortunately, although Radon proved the existence of the formula, he needed a mathematical transformation that would make the problem tractable.

Although this existence theorem for computed tomography had been known since World War I, there was no impetus to find a technique of reconstruction, because it was clear that whatever technique was used, the number of calculations would be staggering. In the mid-1950s, however, the impetus to find a set of basis functions for the practical solution to the problem came from radio astronomy. Ronald N. Bracewell had taken a series of radioastronomy measurements. These amounted to long, narrow apertures

on the sky — strip integrations that provided measurements of a number of point sources but integrated over these apertures. Bracewell solved this problem using Fourier transforms for a relatively small number of sources and passes. The important point, however, is that he had found a transformation that worked. Bracewell deconvolved the data and was able to derive the positions of the multiple point radio sources in his data.

In the period from 1957 to 1963, Alan M. Cormack, a mathematical physicist, was struck by the fact that the child of a friend had died of a brain tumor that was inoperable, perhaps because it could not be detected or delimited by conventional X-ray projection radiography. Cormack, convinced that he could provide a solution, proposed a set of mathematical basis functions — the Jacobi polynomials. Cormack actually conducted a crude experiment, tabulated the results by hand and reconstructed a crude line of voxels in a phantom. The seminal papers appeared in 1963 and almost escaped notice.<sup>11,12</sup>

In the late 1960s Geoffrey Hounsfield built a computed tomographic system. Hounsfield was very much a hands-on experimenter who was absolutely convinced that he could provide a reconstruction means, whether rigorously mathematical or not. Before the convolve-and-backproject technique was generally used, Hounsfield experimented with algebraic reconstruction and other iterative solutions. Hounsfield's original instrument is the basis of all modern medical computed tomography.<sup>13</sup> (Cormack and Hounsfield shared the Nobel Prize in Medicine for their work on computed tomographic scanning.)

The two main drivers for computed tomography are development of good mathematical algorithms for reconstruction and inexpensive computers. The combination of the availability of both was what allowed the field to develop technically. The promise of a strong United States market for computed tomographic equipment is what prompted the sponsors to provide the capital. Much work on codes has evolved at various institutions for all sorts of specialized applications. But what gave scientific experimenters access to

nonmedical computed tomography was the availability of codes in the public domain. These codes, such as *SNARK* or the Berkeley Donner Laboratory package, could be run on a general purpose minicomputer.<sup>14,15</sup> These codes allowed anybody who wanted the opportunity a chance to try computed tomography.

The other successful implementations of reconstructive schemes are positron emission tomography (PET) and nuclear magnetic resonance imaging (MRI). Positron emission tomography uses an injected radioactive chemical that is metabolized in certain organs. The degree of uptake of that chemical in the body depends on how well (or poorly) the organ functions. The radioactive tracer element undergoes a decay, resulting in a positron electron pair product. The positron goes only a short distance before annihilating by collision with another electron, emitting two 511 keV photons. Positron emission tomography detects these photons. The algorithms are somewhat different, because the *source* is distributed. Some algorithms look for single 511 keV photons; some look only for coincidences. All require a reconstructive geometry along line integrals.

*Nuclear magnetic resonance imaging* is really a radio frequency measurement that uses gradient alternating magnetic fields superimposed on a static magnetic field at right angles. The nuclear magnetic moment of atoms will allow absorption and subsequent decay only at certain frequencies. Following excitation the atoms will emit radio waves at specific frequencies dependent on their gyromagnetic constant and the strength of the magnetic field. By proper manipulation of magnetic fields it is possible to effectively measure line integrals representing the presence of specific atoms (for example, hydrogen) in an object. These integrals may be treated similarly to computed tomographic data for image reconstruction.

## Physical Principles

Computed tomography differs from conventional radiographic imaging in that it uses X-ray transmission information from numerous angles about an object to computer reconstruct cross sectional images (that is, slices) of the interior structure. To generate a computed tomographic image, X-ray transmission is measured by an array of detectors (see Fig. 3). Data are obtained by translating and rotating the object so that many viewing angles about the object are used. A computer mathematically reconstructs the cross sectional image from the

multiple view data collected. This reconstructed image is a two-dimensional presentation of a two-dimensional cross sectional cut through the object. A primary benefit of computed tomography is that features are not superimposed in the image, thus making it easier to interpret than radiographic projection images. The image data points are small volumetric measurements directly related to the X-ray attenuation coefficient of the material present in the volume elements defined by the slice thickness and the image plane resolution of the computed tomographic system. The computed tomographic image values and locations provide quantitative data for dimensional measurements and measurements of material density and constituents.

The computed tomography process is fundamentally different from other forms of radiographic imaging. Ordinary projection radiography makes intuitive sense. It is relatively straightforward to imagine X-rays coming off an anode or a gamma source, being absorbed and scattered by the test specimen and finally interacting in a film. The image on film is a projection of everything along the line of sight between the source and the film. You can imagine the film to be a kind of murky image, with objects close to the film being clearer than those farther away. All the associated details of projection radiography — for example, geometric unsharpness due to finite source size — make good sense.

What happens when the depth location of a feature found in a radiograph is important? The most common technique for discovering the position along the line of sight where the feature lies is to use triangulation. This consists of obtaining a second film of the area in question but with the source in a different angular position relative to the test specimen than was obtained on the first exposure. The geometry is carefully laid out on a piece of paper; measured positions of source, test specimen anomalous feature on the films are noted; and the position of the anomalous feature along the intersecting lines of sight is determined as shown in Fig. 9. Distances from discontinuities to the image plane are calculated by using triangulation as shown in Eqs. 23 and 24.

$$(23) \quad h_1 = \frac{d\delta_1}{s + \delta_1}$$

$$(24) \quad h_2 = \frac{d\delta_2}{s + \delta_2}$$

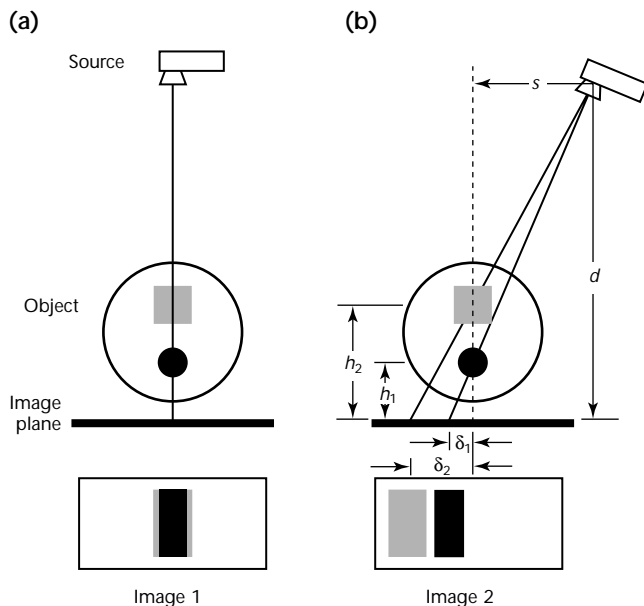
Triangulation is a rudimentary tomographic reconstruction that contains



the essentials elements of computed tomography. The first step is to recognize the features of interest. When more than one image is used, the mind can detect and locate these features as being somehow different. The eye-and-brain system filters out the other information, so that the mind is left only with the features of interest in both radiographs. The second step is to correlate the test specimen, the source position the radiographic image together for both exposures. This correlation in space allows the information from the two exposures to be overlaid constructively. Finally, the third step is to note the position of the attenuation corresponding to the anomalous feature to project it back to the source along the original attenuation line. This backprojection is performed for each exposure and the combined effects of these two backprojections is the constructive interference of the two attenuation patterns.

In computed tomography the basic methodology can be considered in a similar manner. The X-ray beam is collimated to a narrow slit and aligned with a solid state X-ray detector array to define a computed tomographic slice

FIGURE 9. Example of triangulation as basis for computed tomography: (a) first image, with line of interrogation normal to sensor plane; (b) second image, with line of interrogation oblique to sensor plane.



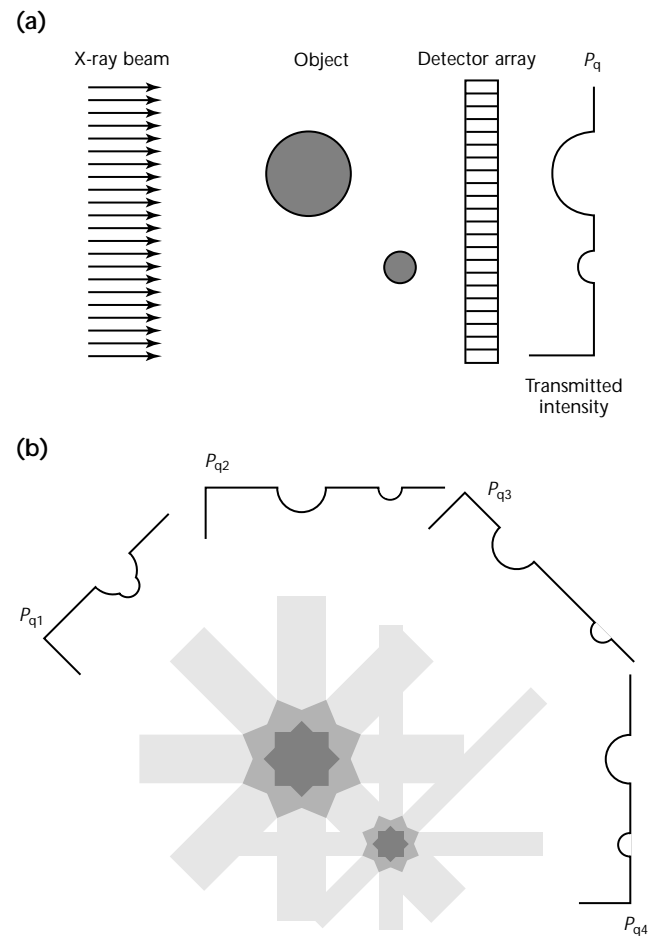
#### Legend

$d$  = distance from source to image plane  
 $h_1$  = distance from round discontinuity to image plane  
 $h_2$  = distance from square discontinuity to image plane  
 $s$  = source travel distance  
 $\delta_1$  = apparent travel distance of round discontinuity in image plane  
 $\delta_2$  = apparent travel distance of square discontinuity in image plane

plane in the object. The slit collimation reduces scatter, improving the signal to noise in the image. Data are obtained by translating and rotating the object so that many viewing angles about the object are acquired.

Figure 10a shows how a data projection can be taken through a part. The transmitted X-ray intensity at each detector element position in the detector array is converted to a digital output level and transmitted to a computer as a projection for the particular angle through the object. The projection data are analogous to a series of slit radiographs taken at numerous orientations (projections) about the object. The resulting slit radiographs yield an attenuation that is an average over the slit thickness.

FIGURE 10. Computed tomography data acquisition and back projection reconstruction: (a) source-object-detector geometry; (b) back projection reconstruction from multiple views.



#### Legend

$p$  = projection  
 $q$  = subscript that designates angle

When a series of projections are taken from many angles about a part, the projection data can be backprojected as shown in Fig. 10b to create an image. As the number of projections increase, the ability to more exactly reconstruct the object increases. In a computed tomographic system, the projections are actually subjected to an incredible amount of mathematical massaging but the steps are effectively the same as involved in the manual triangulation.

The computed tomography image, the cross sectional representation of the densities within an object, depends on the three basic processes: (1) convolution or filtering of the data with special mathematical operators; (2) correlation of the projection data in an absolute space; (3) backprojecting the convolved attenuation data along its original spatial vectors. The mathematics of the image reconstruction can be found in a number of references.<sup>4,16-18</sup>

The intensity of an attenuated X-ray beam passing through an object is given by the line integral:

$$(25) \quad I = \int \left\{ I_0(E) \exp[-\mu(E, x)] dx \right\} dE$$

where  $I$  is the beam intensity at the detector,  $I_0(E)$  is the beam intensity with no object,  $E$  is energy of the X-rays,  $\mu(E, x)$  is the linear attenuation coefficient and  $x$  is the transmitted distance through the object. Most computed tomographic systems use X-rays generated by a bremsstrahlung source that creates a broad spectrum defined here as  $I_0(E)$ . The transmitted intensity is an integration over the energy spectrum and along the ray path through the object as a function of the distribution of linear attenuation coefficient  $\mu(E, x)$ . For predictive purposes, it is useful to change Eqs. 25 to 26:

$$(26) \quad I = I_0 \exp[-\mu(E_{\text{eff}})x]$$

where  $E_{\text{eff}}$  is an effective energy and a uniform material is assumed. The effective energy is that specific energy, where the transmitted intensity of a monoenergetic beam would be equivalent to that of an integrated spectrum. The effective energy is influenced by the type and amount of material penetrated because, as the attenuation or path length increases, the lower energy photons are preferentially attenuated, resulting in higher effective energies or *harder* beams. In computed tomographic applications, attenuations of  $10^4$  and higher are not uncommon, although attenuations of  $10^1$  to  $10^2$  are preferred.

The measured intensity at the detector is normalized based on the calibration of the detector array and the measured intensity for no object in the beam. By taking the logarithm of the normalized intensity, the value of the projection  $P_q(R)$  is proportional to the linear attenuation coefficient:

$$(27) \quad P_q(R) = \ln \frac{I}{I_0} \propto \mu$$

where  $P_q$  is the projection at angle  $q$  and  $R$  is the position of the ray along that projection (see Fig. 10b).

The backprojection of the data will therefore create an image distribution where the values in the image are proportional to the linear attenuation coefficient. The backprojection is given by Eq. 28:

$$(28) \quad b_q(x, y) = \int P_q(R) \times \delta(x \cos q + y \sin q - R) dR$$

where  $\delta$  is the dirac delta function. This equation effectively distributes the values of the projections  $P_q(R)$  to all points  $(X, Y)$  that lie on the projection line. By integrating over angle  $q$  the total reconstructed image will be formed:

$$(29) \quad f(x, y) = \iint P_q(R) \times \delta(x \cos q + y \sin q - R) dR dq$$

This reconstruction is crude because, intuitively, a point object (or delta function) will be reconstructed with the crossing of radial lines creating a star effect. This is evident in Fig. 10b and is shown in Fig. 11. This point response can be shown to be a  $1 \cdot r^{-1}$  blurring of the image points (where  $r$  is the distance from the point). Reconstructions must therefore use filtering to remove this effect.

The filtering is usually performed by a convolution function  $C(R)$  such that:

$$(30) \quad f(x, y) = \iint P_q(R) * C(R) \times \delta(x \cos q + y \sin q - R) dR dq$$

Each projection is convolved with a function and the result is backprojected. Figure 11 demonstrates the benefit of the filtering. The convolution function  $C(R)$  is a filtering operation that can be selected to enhance various characteristics of the image. Innumerable filters are possible for use in the convolution. The two most popular (and extreme) filters are the ramachandran filter, used to emphasize sharpness, and the shepp and logan filter,

used to emphasize contrast. It is also convenient in some cases to perform the filtering by fast fourier transforming the projection, multiplying by a filter function, inverse transforming and backprojecting. The mathematics of the filtering is easier to visualize in the frequency domain but is equivalent to the convolution technique of Eq. 30.

Alternative reconstruction techniques to the filtered backprojection technique are available including fourier transform techniques and iterative reconstruction. The fourier transform technique fills a two-dimensional frequency space with the transform of each projection. A two-dimensional inverse transform is required to create the reconstructed image. The two-dimensional fourier transform technique requires that all the

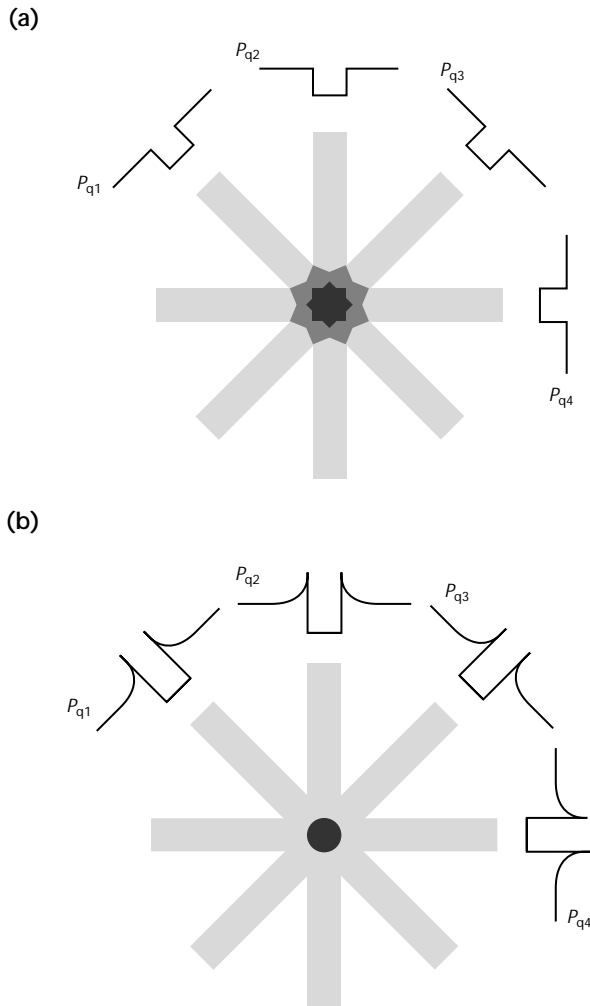
data be taken before reconstruction, whereas filtered backprojection has the advantage of allowing reconstruction to begin on each projection data set. The iterative reconstruction technique assumes a solution for the image matrix and iteratively compares projections through the image to the measured projection data. With each iteration the image matrix is altered until a match of the calculated and measured projections are within an acceptable accuracy. This technique is useful when limited angles are available but can become very time consuming for data taken from many angles.

X-ray computed tomography can be considered the high end application of radiation measurements because the data obtained are quantitative measures (directly related to the X-ray linear attenuation coefficient) for each volume element throughout an object. The computed tomographic image is digital with an image intensity value assigned to each pixel of the image. The pixel is actually a voxel because it represents the two-dimensional cross section plus a third dimension (depth) defined by the slice thickness. The medical field uses the hounsfield notation for the image data:

$$(31) \quad H = 1000 \frac{\mu - \mu_w}{\mu_w}$$

where  $H$  is the hounsfield number,  $\mu$  is the measured attenuation coefficient and  $\mu_w$  is the attenuation number coefficient for water. Using this scale, water takes on the value of zero, vacuum (or air) is -1000 and bone is 1000. This range used in medical computed tomographic scanners corresponds to a density range of about 0 to 2.0 g.cm<sup>-3</sup>. A change of one integer in the hounsfield scale is a 0.1 percent change in attenuation value. Medical facilities maintain a regular calibration schedule of their equipment to maintain proper hounsfield readings. Table 1 shows a numerical scale for hounsfield units. Medical scanners can be used for higher

FIGURE 11. Filtering of back projection: (a) backprojection of original profiles: (b) backprojection of filtered profiles.



Legend  
 $p$  = projection  
 $q$  = subscript that designates angle

TABLE 1. Hounsfield units.

Material	Hounsfield Value
Air	-1000
Water	0
Bone	1000
Acrylic	110
Carbon	580
Aluminum	1900
Iron	24 000

density materials than bone but readings beyond 4000 hounsfield units are usually not suitable.

Industrial computed tomographic systems do not use the hounsfield scale but use the numerical values from their reconstructions. For most scanners the data will be 16 bit or represent an image gray scale range from 0 to 64 000 K values (K values being increments of blackness in the image). Calibration of the reconstructed values to true density must be performed by scanning a standard.

## PART 4. Resolution and Contrast

The basic resolution of a computed tomographic system is determined by the effective beam width of the X-ray beam in the object. The effective beam is a function of the source and detector dimensions and the position of the object with respect to them. The vertical resolution of the slice volume will be determined by the effective slice thickness of the collimation apertures.

Figure 12 shows the configuration of a source and detector for the horizontal resolution of a computed tomographic slice through an object. In Fig. 12a, a source and detector of equivalent aperture size have an object positioned midway between them. With this configuration the effective beam width is minimized at the center. At the edges of the object the effective beam width will be slightly larger and the resolution is decreased. When the source and detector apertures differ in size, as shown in Fig. 12b, the best resolution will be off center. In this case the rotation of the computed tomographic system, whether 180 or 360 degrees, could make a difference on

the resolution of details on either side of the object.

Figure 12c shows the case of a very small source (microfocus) and larger detector. By using projection magnification, very fine resolution may be possible in the object. The resolution can be estimated by taking an average of the effective beam size in millimeter (mm), multiplying by two and inverting to obtain resolution values in line pairs per 1 mm.

The number  $N$  of data points necessary to achieve the highest resolution from a particular scanner geometry can be estimated from the effective beam width. If the field of view (circle of reconstruction) has a diameter  $D$ , then the number of data points in each projection across the object should be:

$$(32) \quad N = \frac{2D}{w}$$

where  $w$  is the effective beam width. This allows two samples per beam width. The number of projection views is estimated by allowing a ray through each beam width on the outer radius of the field of view:

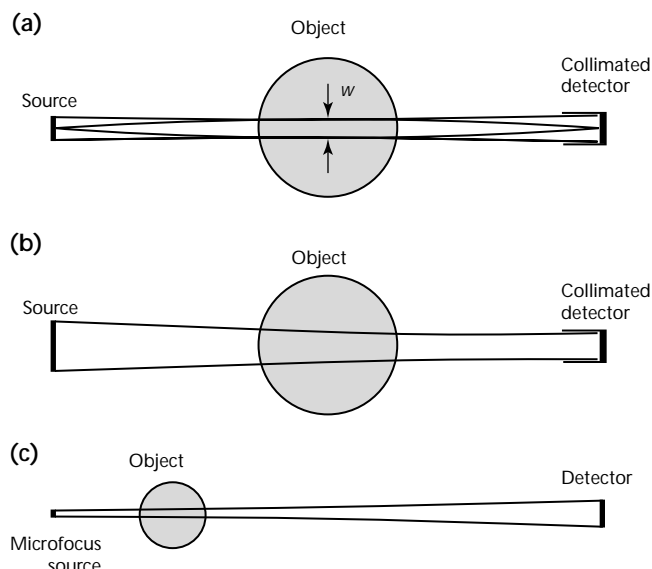
$$(33) \quad v = \frac{\pi D}{w}$$

The total number of data points used for the computed tomographic data acquisition will be  $2\pi D^2 \cdot w^{-2}$ .

Manufacturers of computed tomographic systems may use a variation on the above assumptions to establish the number of projections and data points per projection used for their equipment.

The slice thickness is the third dimension that defines the inspection volume. The operator will normally select this value. Increasing the slice thickness will allow more photons for better imaging statistics or greater scanning speed. However it will increase the smearing of sloping edges on objects or features and decrease sensitivity to details that may be thinner than the slice thickness. Narrowing the slice provides finer detail sensitivity to axial variations in the object but at the cost of scan time and increased statistical noise.

FIGURE 12. Examples of source-object-detector configurations and effective beam widths ( $w$ ): (a) source and detector of equivalent aperture size; (b) source larger than detector; (c) source smaller than detector.



The contrast sensitivity in computed tomographic images is inherently high because each reconstructed volume element is composed of backprojected rays from many orientations about the object. Equation 34 shows an estimate of the signal-to-noise ratio (SNR) in a voxel element as a function of various computed tomographic system characteristics for a reconstruction of cylindrical object:<sup>19</sup>

$$(34) \quad \text{SNR} = 0.665 \mu w^{1.5} \sqrt{\frac{vnt}{\Delta p}} \exp(-2\pi R)$$

In this equation,  $\mu$  is the linear attenuation coefficient,  $w$  is the X-ray beam width,  $v$  is the number of views,  $n$  is the photon intensity rate at the detector,  $t$  is the integration time of the detectors,  $\Delta p$  is the ray spacing and  $R$  is the radius of the object. The contrast ratio will be given by:

$$(35) \quad \text{Contrast ratio} = \frac{6}{\sqrt{\text{SNR} \times Z}}$$

where  $Z$  is the number of pixels over which the contrast is observed. Table 2 shows an example of calculations based on Eqs. 34 and 35. Computed tomographic systems often provide contrast sensitivity measurements in the range of 0.1 to 1.0 percent. What the equations show is that the signal-to-noise ratio improves with increases in computed tomographic system characteristics of X-ray beam width, number of views, X-ray beam intensity and integration time. The signal-to-noise ratio will also be improved by decreasing the ray spacing and object diameter. These computed tomographic system characteristics reflect the tradeoffs in optimizing a computed tomographic system. Fast scan times, fine resolution, high contrast sensitivity and

large object size are mutually exclusive, requiring compromise in system design.

Because of the high signal-to-noise ratio in any voxel, computed tomography can detect features below the resolution limit of the image. For features that are larger than a single voxel the contrast sensitivity improves by the square root of the number of pixels making up the feature. For a feature smaller than a pixel, the apparent density is averaged over the image voxel and therefore the signal for that image voxel is reduced. This is called a partial volume effect. Although the signal is reduced by the partial volume effect, the feature may still be detected. This is a significant point about the application of computed tomography because very often relatively large image voxels (compared to very fine discontinuities) may be used — the very small features are still detected but not necessarily resolved.

TABLE 2. Computed tomography contrast ratio calculation.

Parameter	Symbol	Quantification
Object diameter	$D$	150 mm (6.0 in.)
Attenuation coefficient	$\mu$	0.24 cm <sup>-1</sup>
Beam width	$w$	0.08 mm (0.003 in.)
Number of views	$v$	588
Photon rate	$n$	10 <sup>8</sup> s <sup>-1</sup>
Integration time	$t$	10 ms
Ray spacing	$\Delta p$	2 mm (0.08 in.)
Signal to noise ratio	SNR	324
Number of pixels	$Z$	9
Contrast ratio	CR	0.0062 = 0.62 percent



## PART 5. Computed Tomographic Systems

The computer reconstructed computed tomographic image is a two-dimensional image of a two-dimensional plane in the object. The data in the image is composed of information in small voxel units that are composed of the  $X, Y$  reconstruction matrix element sizes and averaged over the slice thickness of the computed tomographic collimation scheme. By taking a series of contiguous computed tomographic slices through the object a volumetric data set can be created from which cross section images in any plane through the object may be extracted. The slice thickness used determines the vertical resolution of the volume data set. The horizontal resolution is determined by the effective X-ray beam size in the object and the reconstruction matrix size.

Computed tomography requires more sophisticated equipment for data acquisition and reconstruction than conventional radiography. The total time required to inspect an object volumetrically can also be relatively long, making computed tomography a significantly more expensive inspection. However, for many structures computed tomography provides unique information.

### System Configurations

Computed tomography has several variations from its basic concept of Fig. 3. Figure 13 shows four generations of computed tomographic system configurations.

1. The essential characteristics of first generation geometry are a single source and a single detector. The source and detector are locked together (or at least their relative positions are constant) and the entire source and detector unit made to traverse the test specimen. A single traverse yields a series of attenuation measurements (recall that each attenuation measurement is a ray and that the series across the test specimen is a view), thus generating a single view. The most important characteristic of this view is that it is a series of parallel rays. If the test specimen is rotated by an angle  $\theta$  and another such traverse is made, another view of attenuation data but displaced by angular rotation  $\theta$  will be made.

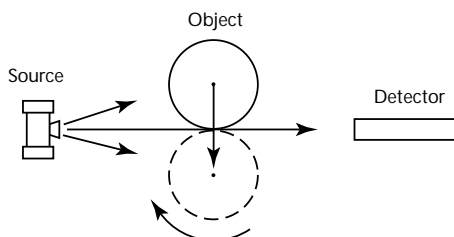
The entire test specimen can be covered if the procedure is repeated  $n$  times where  $n = 180 \cdot \theta^{-1}$  in theory (in practice, 360 rather than 180 is sometimes required.)

2. Second generation geometry uses the same principle as first generation geometry. The difference is that instead of having only a single detector, there is typically a bank of detectors arranged to subtend a fan beam of the source. (The fan beam is collimated so that the fan lies in the plane of interest.) Thus the central detector acquires the same data on a single traverse as the first generation system described above. The next detector might be placed so that its center as seen from the source focal spot is displaced by angle  $\theta$  from the central detector. Simultaneously with the first traverse, that next detector gathers the identical information that would, in a first generation configuration, be gathered sequentially on the second traverse. In fact, second generation geometry lets all views in the fan angle of the source be obtained on the same traverse. After traversing the fan, the object rotates the number of degrees of the fan and transverses back across the fan beam. Rotations continue until 180 or 360 degrees have been covered.
3. Third generation geometry uses a single source and a bank of detectors that span the test specimen as seen from the source. The detectors provide a single view simultaneously of a series of fan shaped measurements rather than parallel ray measurements. By continuously turning the test specimen and taking data, many fan views are acquired for reconstruction. In third generation scanning each detector will not see all of the object as in second generation. Thus detector imbalance causes ring artifacts in the image.
4. Fourth generation geometry uses a single moving source and a bank of stationary detectors configured into a circular ring. As the source rotates inside the detector ring, a single view might be made at one time; instead, the view data is constructed from simultaneous positions of the source with respect to a single detector. Like

the third generation geometry, this fourth generation configuration uses a fan beam view structure. The main reason for using the fourth generation geometry is that each view is made

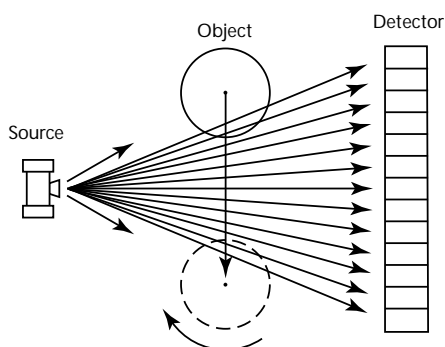
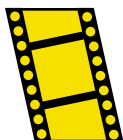
FIGURE 13. Computed tomographic system generations: (a) first generation; (b) second generation (rotate and translate); (c) third generation (rotate only); (d) fourth generation.

(a)



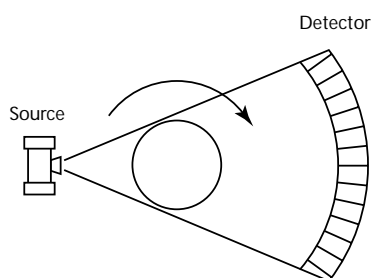
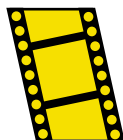
(b)

MOVIE.  
Second  
generation  
(rotate and  
translate).

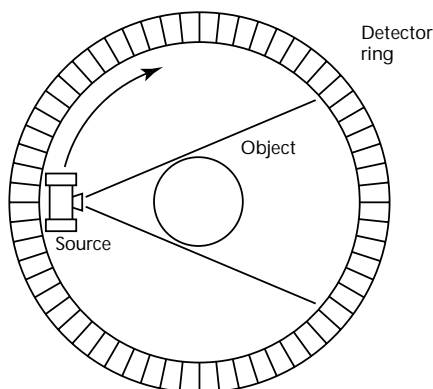


(c)

MOVIE.  
Third  
generation  
(rotate only).



(d)



with a single detector; this presents an advantage over third generation geometry where searching for changes in small scale signals is frequently overwhelmed with interdetector normalization problems. The fourth generation use of one detector for each view obviates interdetector detector normalization problem.

The most useful forms for industrial computed tomography are second generation and third generation. Both techniques use a collimated fan beam of X-rays and one-dimensional array of detectors.

### Rotate-and-Translate Configuration Advantages

The second generation scheme, the rotate-and-translate scheme, is commonly used for industrial objects because objects larger than the X-ray beam fan angle can be accommodated. The main reasons for this implementation are three:

1. The spatial resolution is determined by the spacing between sampling positions and is not dependent on the number of detectors or the interdetector spacing.
2. The problems of false large scale radial density variations (*cupping* or *capping* — very common in third generation geometry) are largely avoided. Hence, true absolute densities, an important factor for nondestructive test systems, especially for composites, are easily obtained.
3. The interdetector normalization requirements compared with third generation systems are relaxed by a factor of about 100.

This last point is especially important because, in gathering the series of ray measurements necessary for a single view (one-dimensional projection), it is the small scale variations in response that determine the visibility of any particular feature. In second generation geometry, a view is made by successive measurements with the same detector element.

### Third Generation Configuration

In third generation geometry, a view is made by the simultaneous measurements of all the detector elements. Thus, variations in response between adjacent detectors can mimic the response of a small feature present in the object. In third generation systems, complex smoothing algorithms usually are used to mitigate the effects of the second and third objections.

The third generation, or rotate only, scanning approach is used on small industrial objects because it is faster than

second generation. Both the second and third generation techniques only image in a single computed tomography scan one slice location through the part. That slice inspection volume is the size of the fan beam height collimation.

## Other Configurations

**Volume Computed Tomography.** Another technique, *volume* computed tomography or *cone beam* computed tomography, uses a two-dimensional area detector and an uncollimated cone of radiation such that the entire object may be inspected in one scan. This technique sacrifices some detail in the image quality for a higher throughput when the entire object must be inspected with computed tomography and has limitations on the applicable part size. It also generally works well only for relatively small objects.

**Limited Angle Tomography.** Limited angle, tangential and annular reconstruction computed tomography are also techniques that can be beneficial to large composite structure. Limited angle computed tomography does not require that the computed tomographic data be taken from all angles completely about the part. This can be particularly advantageous for large planar composite structure. Tangential and annular reconstruction offer advantages for large cylindrical structures where information is only needed along annular rings, particularly near the outside of the structure.

## Mechanical Handling

The primary technical considerations for computed tomographic system configurations are X-ray source, detectors, computer processing hardware and software, algorithms, speed and visibility of anomalous conditions. Mechanical handling systems for computed tomographic systems are mature. The advent of microprocessor control, high resolution encoder and feedback systems and the ability to use *fire-on-position* data acquisition rather than a freerunning clock have actually eased the mechanical handling tasks.

Mechanical handling has been eased because the smoothness of motion and accuracy of position required of previous era systems have been supplanted by *knowledge-of-position* systems. In many modern computed tomographic systems for nondestructive testing, especially those that are designed with a range of applications, incorporation of the knowledge of position is done routinely and results in considerably more flexibility than is possible with systems

relying on strictly mechanical motions. The penalty is in a more complex interface between motion subsystems and the control computer and in a more computationally intensive algorithm for arriving at a reconstructed image.

Mechanical handling system tolerance budgets are almost always expressed in terms of the spatial resolution. For second generation geometry, the total stacking tolerance is given as  $0.25\times$  to  $0.33\times$  the spatial resolution. Thus, for a resolution corresponding to good spatial discrimination of adjacent pixels of size 1.0 mm (0.04 in.) the nominal tolerance stackup would be 0.33 mm (0.013 in.). This means that all the imprecisions in the individual mechanical components must, when added together, be less than this absolute tolerance. This applies to random errors — for example, runout in a bearing. The limit for systematic errors tends to be about ten times more stringent although each individual contributor must be analyzed separately. Because the reconstruction process adds data taken from many different positions a systematic error produces an artifact that is characteristic of the selective reinforcement of the particular error.<sup>20</sup>

## System Design

Because computed tomographic systems require more precise equipment and data processing than traditional nondestructive evaluation hardware, it is important to consider the components in a computed tomographic system and discuss their ramifications.

Figure 14 shows a generic design of computed tomographic system components. The major subsystems that go into a computed tomographic system include the mechanical handling subsystem, the data acquisition subsystem and the computer interface and software subsystem. These major subsystems categories can be further broken down into components and characteristics that are essential for a computed tomographic system to operate for the desired output. The selection of certain component attributes or system characteristics will affect the selection of other components or the overall performance and cost of a computed tomographic system.

Table 3 lists key attributes of a computed tomographic system and the ramifications of selections of the attributes on system component selection. In the selection of a computed tomographic system to perform nondestructive inspections it is important to be able to define the desired inspection characteristics, particularly specimen (size, type, weight), inspection parameters

FIGURE 14. Generic computed tomographic system components.

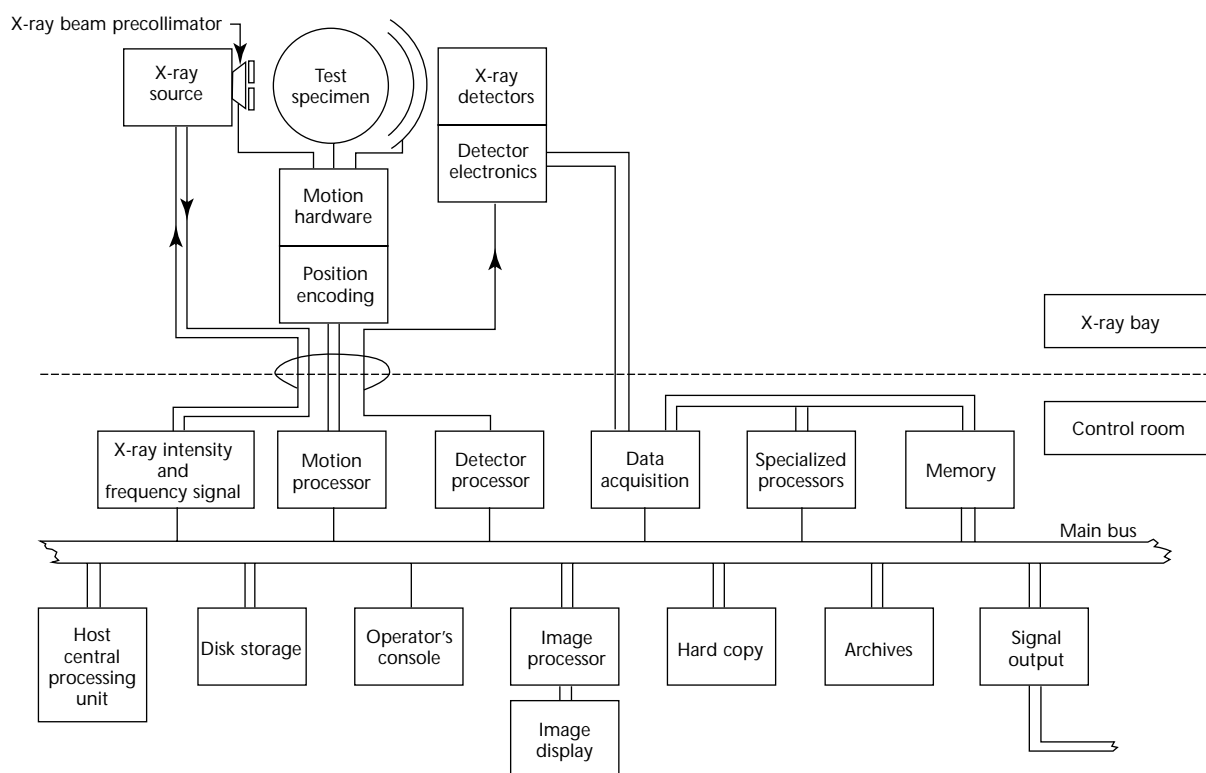


TABLE 3. Computed tomography system attributes and their major ramifications.

Attribute	Ramifications
Test specimen size, weight and shape	mechanical handling equipment, loading and unloading
Test specimen X-ray penetrability	X-ray source X-ray detector type dynamic range of detector and front end electronics
Spatial resolution	accuracy of mechanical handling equipment configuration of source, object and detector source and detector aperture size
Contrast sensitivity	strength of X-ray source integration time
Artifact level	reconstruction algorithm software accuracy of mechanical handling equipment
Speed of computed tomographic process	size of object X-ray source strength number and configuration of detectors bus structure speed and architecture of processors mechanical hardware — motors, brakes and others
Number of pixels in image	number and configuration of detectors amount of data acquired choice of computer and hardware
Slice thickness range	detector configuration system dynamic range
Operator interface	instrument control panel image processing system control software interface to remote workstation
Archival requirements	choice of computer and hardware

(spatial resolution, contrast sensitivity, slice thickness, time for inspection) and the operator interface (system control panel, image display, processing functions and data archiving).

The most significant point of Table 3 is how the specimen to be inspected determines many of the principle characteristics of the computed tomographic system. For this reason, different computed tomographic systems are designed for different sized objects. The object size and X-ray penetrability determines the mechanical handling characteristics. As the object becomes larger, higher energy X-ray sources and larger mechanical systems are required. The result of this is higher cost for the computed tomographic system. Figure 15 shows the effect of object size and energy on the cost of a computed tomographic system.

The sensitivity to fine detail of computed tomographic systems is a function of resolution and contrast sensitivity. The computed tomographic resolution is fundamentally determined by the beam width of the X-ray optics design and is driven by the selection of source and detector aperture sizes and the source, object and detector distances. The beam width, size of the object computed tomographic image reconstruction matrix must all be considered in a system design.

A typical reconstruction matrix size for computed tomography at the turn of the century was  $1024 \times 1024$ . A first approximation would make the resolution limit roughly one part in 1000 and the system would be designed to match the X-ray optics to  $0.001 \times$  the size of the part. For example, a system designed to handle a 0.5 m (20 in.) size part might allow for 0.5 mm (0.02 in.) size beam width and a system designed for a 10 mm (0.4 in.) size

part might have a 0.01 mm (0.0004 in.) beam width.

It is of course possible, and routinely performed, to reconstruct the  $1024 \times 1024$  matrix over subregions of a component so that a higher resolution beam width finer than 1 part in 1000 of the object can be used effectively. However, the scan must still cover the full size of the part. As the part size increases, the distance from source to detector increases and X-ray intensity at the detector falls off quadratically. Thus, it is impractical to use a very small beam width on large parts because of the very long scan time that will result. Practical resolutions for computed tomographic systems that handle large components greater than 0.30 m (12 in.) in diameter are in the range of 1 to 2 line pairs per 1 mm (25 to 50 line pairs per 1.0 in.). For components less than 300 mm (12 in.) diameter, 2 to 4 line pairs per 1 mm (50 to 100 line pairs per 1.0 in.) can be obtained. For higher resolution, greater than 4 line pairs per 1 mm (100 line pairs per 1.0 in.) and feature sensitivity on the order of 0.125 mm (0.005 in.), the computed tomographic systems are designed to handle objects of only 30 or 40 mm (about 1 or 2 in.) in size.

Figure 16 shows how the size and detail sensitivity of computed tomographic systems are related by the design. Each type of system (A through D) represents a range of capability that can be found in commercially available computed tomographic systems but no one computed tomographic system can provide both large object inspection and very fine resolution.

FIGURE 15. Computed tomographic system size versus cost.

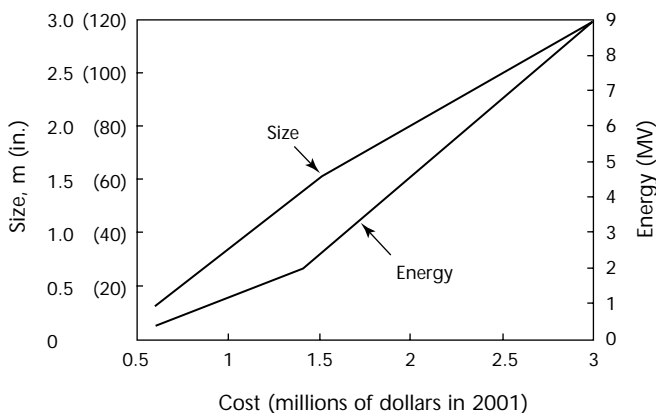
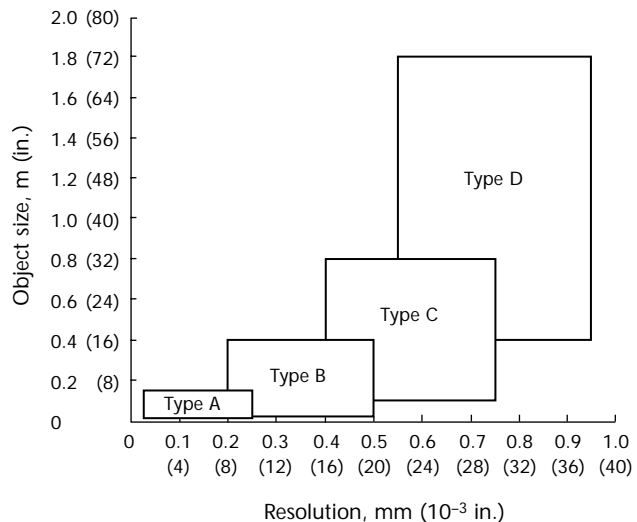


FIGURE 16. Computed tomographic system size versus sensitivity to detail.



## PART 6. Applications of Computed Tomography

Computed tomographic data allows accurate evaluation of dimensions, locations in three-dimensional object space or material density (as related to X-ray linear attenuation coefficient) to be performed in any orientation throughout the volume of an object that has been scanned with the computed tomographic system. Table 4 summarizes computed tomography's capability and typical sensitivity ranges and limitations.

In general, the benefit of X-ray computed tomography over alternative nondestructive evaluation methodologies is its ability to map the relative X-ray linear attenuation coefficient of small volume elements throughout a component, permitting the extraction of dimensional and material characteristics of features and anomalies. With these characteristics, derived from the computed tomographic data, engineers can perform a variety of analyses to arrive at quantitative measurements of parameters to improve the overall product. For objects that fit the constraints of size and shape for proper computed tomographic examination, the computed tomographic data offer unparalleled capability for feature detection and measurement. As complexity of design increases, the value of computed tomographic measurement capability increases.

Present computed tomographic technology is relatively expensive. The value of computed tomography is therefore realized in applications where the objects are of critical value or adequate measurements cannot be made by other means. A primary example is rocket motors. Computed tomography is used extensively on rocket motors because the objects are very valuable and are used in critical applications, so that the cost of computed tomography remains a small fraction of the overall mission value. Complex, high value turbine blades are another example where computed tomography is worth the cost because of dimensional accuracy better than that from other techniques.

Beyond these few examples, computed tomography is not routinely applied to objects as a final inspection process. Rather, computed tomography is applied as an engineering tool and enabling technology to support product development activities, speeding products to market. Table 5 summarizes cost effective applications for computed tomography.

The application of computed tomography as a measurement tool for engineering and manufacturing provides a cost benefit to a number of processes. Computed tomography is used by engineers on prototypes to fully

TABLE 4. Capabilities of computed tomography.

Point of Interest	Technical Capability
<b>Volumetric Measurement</b>	
Quantitative features	volumetric feature detection and configuration control
Data	digital; three-dimensional
Disbond detection	must have separation
<b>Detail Sensitivity</b>	
Resolution	large structures: typically 0.5 mm (0.02 in.) features are resolved, smaller high contrast features can be detected small structures, <250 $\mu$ m (10 in.): typically 0.002 to 0.004 parts per thousand are resolved
Density measurement	multiple materials must differ in X-ray linear attenuation coefficients (density and atomic number) for detection (0.01 to 0.1 percent for large areas, >1.0 mm (0.04 in.) diameter
Artifacts	large aspect ratios cause streak artifacts (>15:1 is difficult) detail sensitivity in low density material near high density features is compromised
<b>Parts Handling</b>	
Penetration	X-ray transmission is limited by size, density and atomic number of the part and by the available X-ray energy
Size and shape	Access to 360 degrees around the part



characterize the object. Computed tomography measurements can be performed on test articles to validate prototypes and models before testing, during certain types of testing and post testing, including noninvasive micrographic evaluations. Computed tomography permits geometry acquisition (often referred to as reverse engineering), providing a direct cost saving over traditional approaches to translating existing components into digital models in computer aided design (CAD) workstations and computer aided engineering (CAE) workstations. Computed tomography is particularly effective during product failure analysis by noninvasively inspecting the interior condition of articles, including scans under various operational conditions. Computed tomography evaluation of materials also is useful in performance prediction based on the measurements obtained from the computed tomographic data. This is where engineering and nondestructive evaluation need to collaborate to create the most cost effective products.

Computed tomography can be an important tool in the manufacturing and process development stages of product life cycles by providing feature and anomaly location, configuration control and the direct measurement of dimensions for engineering acceptance. The value of computed tomographic evaluation is high for ensuring a development process has been brought into control. For routine production quality control the application of computed tomographic depends on the relation between the object value, computed tomographic scanning cost and the cost of alternatives. The more complex and costly an assembly, the more likely that computed tomography can be a cost effective tool.

Ultimately computed tomography can allow the acceptance of a product on the basis of quantitative measurements and engineering criteria. Such an engineering

analysis rather than qualitative inspection standards has considerable potential for reducing scrap and increasing component reliability. Maintenance, repair and failure analysis activities benefit from computed tomography measurements by providing information for making decisions on irreversible steps and/or eliminating disassembly or destructive testing to obtain critical data. The long range value of computed tomography technology is that it closes the loop between the engineering and the manufacturing operations by providing quantitative data that can be accessed by engineers at their workstations.

Because the output of computed tomography is a digitized, quantitative map of the density, the computed tomographic image can be analyzed by quantitative, computer based techniques. Subtle deviations in density from a host density can be identified and measured much more precisely than with any other means. The important point about computed tomography is its data presentation: a clear, unambiguous image in digital, computer readable format. Although traditional projection radiography does deliver an image, foreground and background material can obscure the clarity of the image in the region of interest. Computed tomography provides great sensitivity to the most subtle variations in density; typically, computed tomography provides 10 to 100 times greater sensitivity to density than projection radiography. Compared to other inspection modalities, computed tomography works best in complex, thick objects. Figure 17 and Table 6 show how object geometry influences the test technique.

The major disadvantage to conventional computed tomography lies in having to make X-ray measurements over the entire periphery of a test specimen for each slice. Thus, as shown in Fig. 17, graphic slices that do not have to penetrate through much material present the best computed tomographic images; computed tomographic slices that suffer massive amounts of absorption do not provide images as good as those taken with projection radiographs taken from a different perspective where the path is not so heavily absorbed, as shown in the flat pancake shape of Fig. 17.

An important point, usually overlooked, is illustrated by the pancake shape: computed tomographic images and projection radiography images that present substantially the cross sectional picture are taken from entirely different perspectives. In this case, the projection radiography would be taken with the source above and the recording film below (or vice versa) so that the X-ray

TABLE 5. Beneficial application areas for computed tomography.

Field	Application
Engineering	prototype evaluation
	geometry acquisition
	failure analysis
	performance prediction
Manufacturing	process development
	feature and anomaly location
	configuration control
	acceptance by engineering criteria

paths are essentially perpendicular to the pancake plane. The computed tomographic image would be acquired with source and detectors confined to the pancake plane and relative motion would be induced between them so that the X-ray paths are always within the plane.

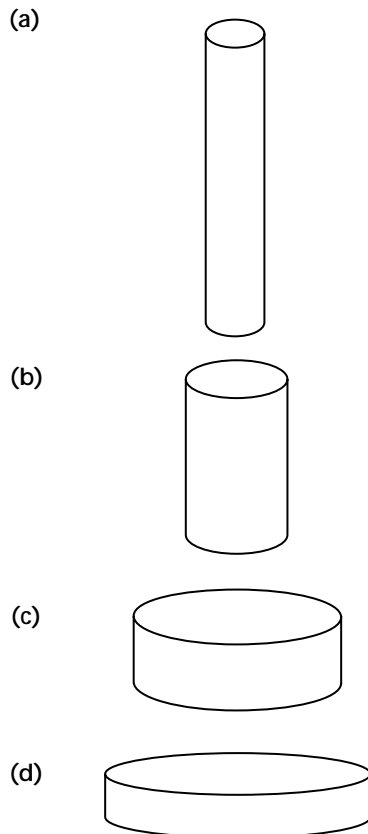
The test specimen diversity in sizes, materials, anomalies and time constraints of industrial objects is such that no single X-ray computed tomographic system is appropriate for even a major fraction of the range of applications. Thus, the investment required in the development of a single computed tomographic system design for nondestructive testing cannot, in general, be amortized over a variety of applications. Computed tomographic systems are slow and expensive. With several exceptions, nondestructive testing computed tomography has been developed in several very specific sets of circumstances: (1) the finished product is very expensive, such as a ballistic missile,<sup>21</sup> (2) a relatively inexpensive component becomes a critical item in a

larger assembly, such as rocket nozzles, and (3) computed tomographic sampling yields information as an engineering tool for process control, such as geometry acquisition for dimensional control.

Because computed tomography is a direct, full imaging mode, many developed systems, especially those conceived with a more general use, provide the capability for inspections based on techniques derivative of computed tomography. Among these capabilities are laminography and other techniques based on reconstructive imaging, such as limited angle (incomplete views) computed tomography or high resolution annular computed tomography.

Other nonimaging modes peculiar to the particular problem at hand are also possible — for example, precise measurement of an internal seal clearance. Indeed, such computed tomography derivative techniques may present the most fruitful of approaches for solving specific inspection problems. Why? In most nondestructive testing problems, there is a great deal of *a priori* knowledge and anomalies tend to fall in very narrow, well defined categories. Thus, digital signal processing of nonimaged signature data may provide quick, efficient schemes for specific kinds of anomalies that traditional computed tomographic imaging cannot provide. Some of these applications are discussed below.

FIGURE 17. Object shapes referred to in comparison of computed tomography with conventional radiography: (a) oblong cylinder; (b) regular cylinder; (c) short and wide cylinder; (d) flat or *pancake* cylinder. See Table 6.



## Computed Tomography Examples

Figures 18 to 21 show examples of computed tomographic images of materials and structures.

The detailed evaluation of complex castings is an excellent application of computed tomographic technology.<sup>22-26</sup> Figure 18 shows a comparison of computed tomography with conventional

TABLE 6. Shape inspectability by computed tomography versus conventional radiography. See Fig. 17.

Object Shape		Radiographic Technique	
Description	Figure	Computed Tomography	Conventional Radiography
Cylinder, oblong	17a	satisfactory <sup>a</sup>	satisfactory
Cylinder, regular	17b	excellent	poor
Cylinder, short and wide	17c	excellent	poor
Cylinder, flat ( <i>pancake</i> )	17d	poor	excellent

a. With sensor plane parallel to test object.

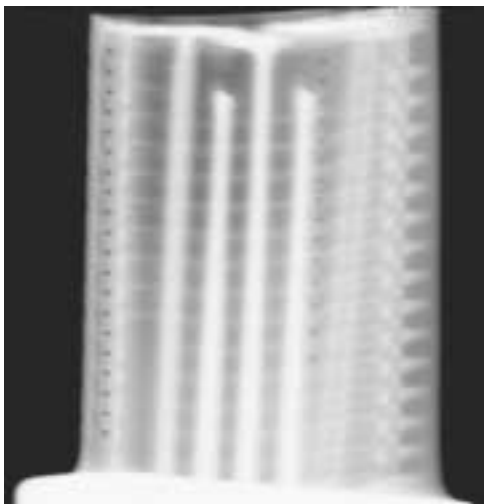
radiography for a turbine blade casting. The part contains a complex internal geometry. The radiograph is unable to evaluate the internal cross sectional configuration of the part. The computed tomographic slice shows the wall thickness of the casting directly and will show discontinuities in the cast material if they are present at the location of the slice plane.

The ability of computed tomographic images to show internal material variations is particularly advantageous for composite material inspection.<sup>27-33</sup>

Figure 19 shows a computed tomographic image of a composite J stiffener, where the variations in the consolidation and the ply layups can be evaluated, particularly at T junctions.

FIGURE 18. Computed tomographic evaluation of casting turbine blade with 400 kV computed tomographic system showing internal feature condition and wall thickness measurement: (a) digital radiograph; (b) computed tomographic slice.

(a)



(b)

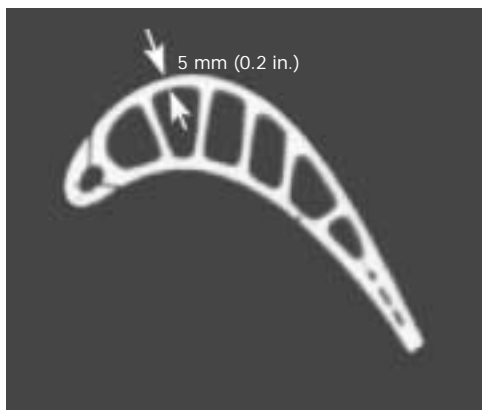


FIGURE 19. Computed tomographic image of graphite epoxy woven J stiffener showing ply condition and consolidation.<sup>31</sup>

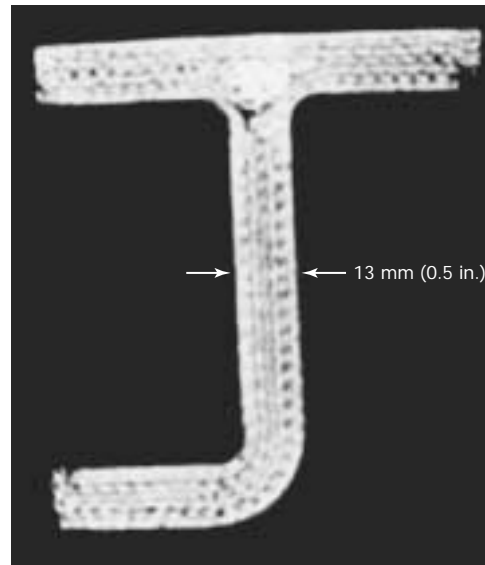
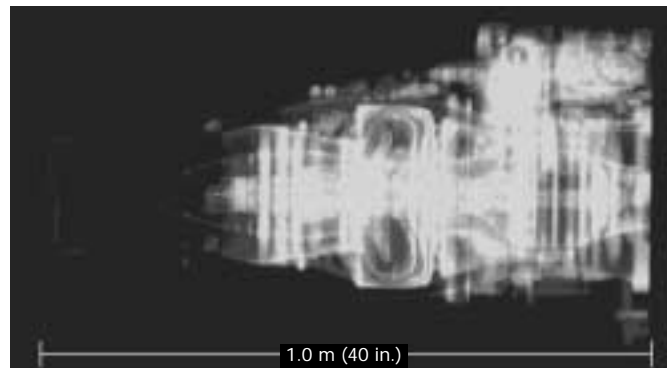


FIGURE 20. Cruise missile engine: (a) projection radiograph showing complex superposition of information; (b) longitudinal computed tomographic slice along axis of engine obtained with 2.5 MV computed tomographic system showing internal details.<sup>49</sup>

(a)



(b)

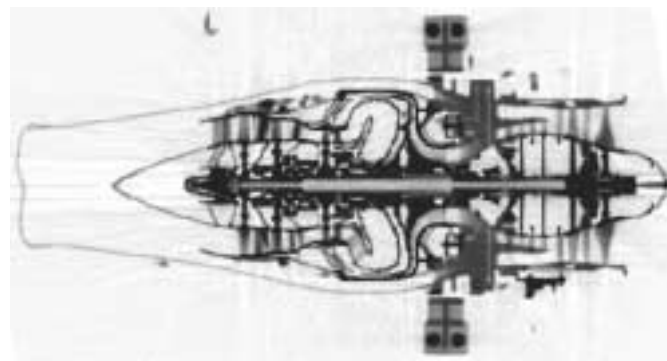
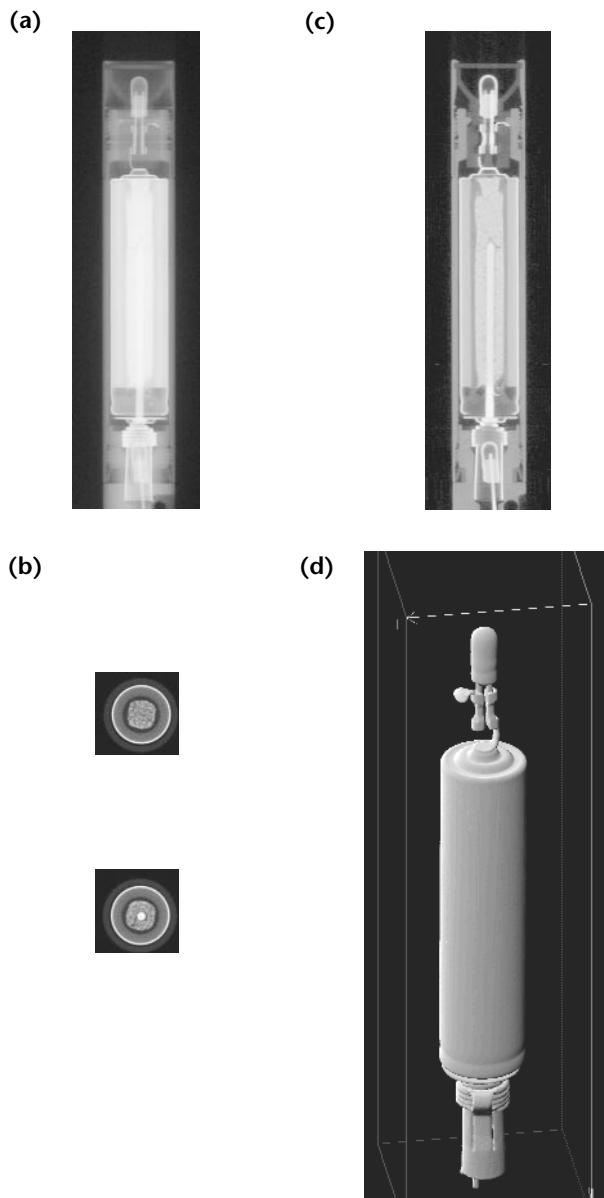


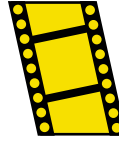
Figure 20 shows a radiograph and a longitudinal computed tomographic slice through a cruise missile engine using a 9 MV X-ray source. This example demonstrates the power of computed tomography for complex structure evaluation overcoming superposition common in radiography to reveal superior information about the internal configuration of systems.

Figure 21 is an example of volumetric computed tomographic scanning.

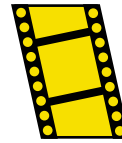
**FIGURE 21.** Volumetric computed tomographic system data of small single battery flashlight data by using area array detector. Multiple slice reconstruction and three-dimensional surface rendering are possible: (a) digital radiograph; (b) horizontal slices; (c) vertical slice; (d) three-dimensional surface rendering.<sup>49,50</sup>



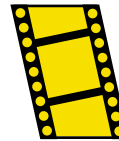
**MOVIE.**  
Electronic  
device on  
turntable.



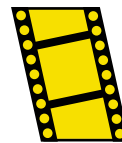
**MOVIE.**  
Image slices of  
device, top to  
bottom.



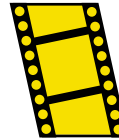
**MOVIE.**  
Images of  
electronic  
device.



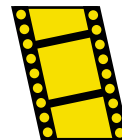
**MOVIE.**  
Slices show  
delaminations  
in composite  
fastener hole.



**MOVIE.**  
Tomographic  
data image of  
electronic  
device.



**MOVIE.**  
Transverse  
image of  
delaminations  
in fastener hole.



## PART 7. Reference Standards for Computed Tomography

### Background

The initial developments of computed tomography were directed at medical diagnostic applications. The medical community has generated comprehensive literature on the theory and performance of computed tomography for biomedical applications. The basic references on the fundamentals of computed tomography come from medical users.

Medical computed tomographic system performance measurement requirements have been described with the development of appropriate phantoms. McCullough and others,<sup>34</sup> Payne and others<sup>35</sup> and Bergstrom<sup>51</sup> discuss measurements for performance evaluation, for acceptance testing and for ongoing quality assurance of computed tomographic scanning systems. They discuss possible phantom types that can be constructed to test parameters of interest. Goodenough and others<sup>36</sup> and White and others<sup>37</sup> describe the developments of phantoms to be used in measuring various parameters. The American Association of Physicists in Medicine (AAPM) also describes a phantom.<sup>38</sup> Table 7 indicates the parameters, generally agreed on in the literature, that require evaluation in medical computed tomographic systems.

The phantoms used in medical computed tomographic evaluation have various components that test these parameters.

The theory of image quality considers the modulation transfer function (MTF) and the noise power spectrum as the essential defining characteristics of imaging systems.<sup>39</sup> These principles have been applied to medical computed tomographic imaging. Judy describes using the line spread function<sup>40</sup> to obtain the modulation transfer function and Bischof and Ehrhardt describe the point spread function<sup>18</sup> to obtain it. Hanson<sup>41</sup> describes the noise power spectrum measurement. Hansen considers probability distributions to indicate signal detection probabilities in computed tomographic imaging. Resolution and noise can be combined in detectability limit curves that plot contrast needed to detect an object versus the object size for different dose levels of medical imaging. These are referred to as contrast detail dose (CDD) curves. Bergstrom<sup>51</sup> shows an example contrast detail dose curve from research data and discusses the difficulties in creating a phantom for such measurement. Cohen and Di Bianca<sup>42</sup> use the contrast detail dose diagram to evaluate a computed tomographic scanner.

As computed tomography has expanded from the medical to industrial

TABLE 7. Parameters of interest for computed tomography standards.

Parameter	Notes
Alignment	image artifacts caused by mechanical alignment; dimensional accuracy
Slice thickness and geometry	vertical coverage; alignment and uniformity of computed tomographic plane in object
Spatial uniformity	variation of computed tomography measurement across scan plane
Noise	random variation in attenuation measurements (measured by statistical variation or noise power spectrum)
Low contrast sensitivity	ability to detect small contrast changes (mainly limited by noise)
Spatial resolution	ability to distinguish two objects as separate (measurement should be under noise free conditions)
Modulation transfer function	quantitative measurement of high contrast spatial resolution
Effective energy and linearity of tomography numbers	monochromatic photon energy that would give result equivalent to results from polychromatic spectrum used
Accuracy and precision	reliability and stability of computed tomography measurements
Dose	patient exposure (for medical computed tomography)



applications, industrial users have discussed the issue of standards. Dennis<sup>43</sup> describes computed tomographic fundamentals and the image quality parameters from an industrial computed tomography perspective. The American Society for Testing and Materials (ASTM) CT Standardization Committee E7.01.03 has also developed a document describing the basic principles of industrial computed tomography and advocates the modulation transfer function and contrast detail dose for measurement of system performance.<sup>44-46</sup> For industrial applications, the contrast detail dose curve is referred to the contrast discrimination curve (CDC). Sivers and Silver have described the theoretical background and experimental results of using modulation transfer function measurements and contrast discrimination curves on industrial computed tomographic systems.<sup>47</sup> Jacoby and Lingenfelter describe the use of a test phantom for monitoring industrial computed tomographic system performance over time.<sup>48</sup>

The parameters listed in Table 7 may be measured from data taken by a phantom that contains features that represent the parameter. A single phantom unit may contain a variety of subsections that will measure various parameters. The parameters themselves are not independent but often are different manifestations of the fundamental performance characteristics of the system. Table 8 lists some key categories for a phantom and potential techniques of obtaining the measurements.

TABLE 8. Phantom categories and measurement technique.

Type	Construction or Technique
Resolution	holes squares line pairs pins and wires calculation of modulation transfer function
Contrast	signal to noise in a uniform material sample small density variation
Material and density	various solids liquids of different mixture percentages porous material compaction
Dimensional accuracy and distortion	pin sets hole sets
Slice thickness	pyramids cones slanted edges spiral slit

## Resolution

Resolution refers to the ability to sense that two features are distinct. Measurements of resolution with a phantom can be performed in a wide variety of ways. Holes in a uniform material of either fixed diameter and changing separation, or decreasing diameter with separations that also decrease accordingly, are very common. The resolution is defined as the minimum separation detectable.

Plates of alternating high and low density material (that is, plastic to air, metal to air or metal to plastic) can be used to make line pair gages. The resolution limit is determined by the ability to see the line pairs. The loss in sensitivity is due to a loss of modulation between the high and low density features of the line pairs as the plate thickness becomes smaller. This can be monitored numerically by a data trace across the image of the line pairs to measure the modulation as a function of line pair size. A plot of the modulation values as a function of the line pair value is the square wave response of the system. This is related but not equivalent to the modulation transfer function.

The modulation transfer function is defined for a sinusoidal varying test pattern; however, such a pattern is very difficult to construct for use with X-rays. Because of the definition of the modulation transfer function, it can be measured by mathematical calculation of the fourier transform of the one-dimensional line spread function (LSF) or the two-dimensional point spread function (PSF). The line spread function and/or point spread function is obtained by measurement of the spreading of the image from a delta function input such as a pin or wire. If the pin is small enough the point spread function is given directly. If not, the size of the pin must be deconvolved from the results. Because of the problem of finding an adequate line or point source phantom, the line spread function is very often measured by differentiation of the edge spread function (ESF). The edge spread function is readily obtained from a data trace across a sharp edge in the image.

The modulation transfer function output is a curve of the response of a system as a function of frequency. It is often useful to have a single numeric value to be used for relative comparison of performance. In the case of the modulation transfer function an arbitrary value from the curve may be taken, such as the frequency at which the modulation is decreased to 10 percent. The width of the line spread function or point spread

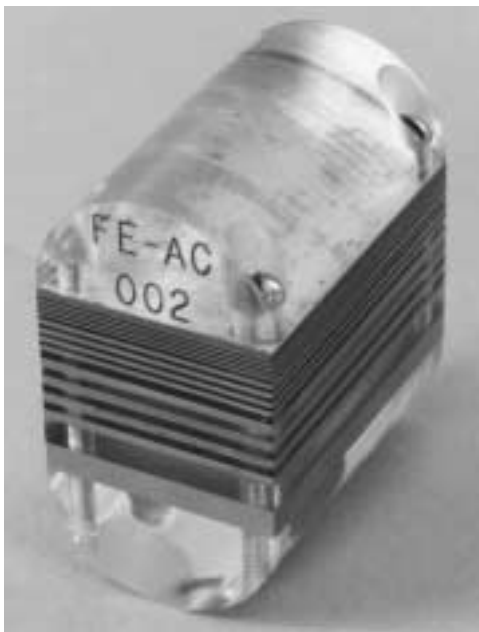


function can also be used as a single numeric value for comparison of resolution. By measuring the full width at half maximum (FWHM) of the line spread function a relative value that is related to the system resolution is obtained.

Resolution is most commonly measured in the computed tomographic image, which is a slice through the object. However, computed tomographic data are fundamentally volumetric in nature, multiple contiguous computed tomographic slices result in a volume data base. Depending on the use of the data, it may be important to consider the resolution in the axial orientation of the computed tomographic data acquisition. This resolution will be for the most part determined by the effective slice thickness and axial step spacing used in the scanning sequence and may be quite different from the individual slice resolution. In addition, the effective slice thickness often will vary over the field of view, leading to additional resolution characterization requirements. In the case of direct volume computed tomographic imaging using cone beam geometries, the data are usually taken and reconstructed so that resolution is about the same in all directions in the volume.

Figure 22 is a photograph of a line pair resolution phantom. The phantom consists of sets of metallic and acrylic plates of specified thickness. Line pairs of 0.5, 1, 2 and 4 line pairs per 1 mm (12, 25, 50 and 100 line pairs per 1.0 in.) are formed by the phantom. The entire

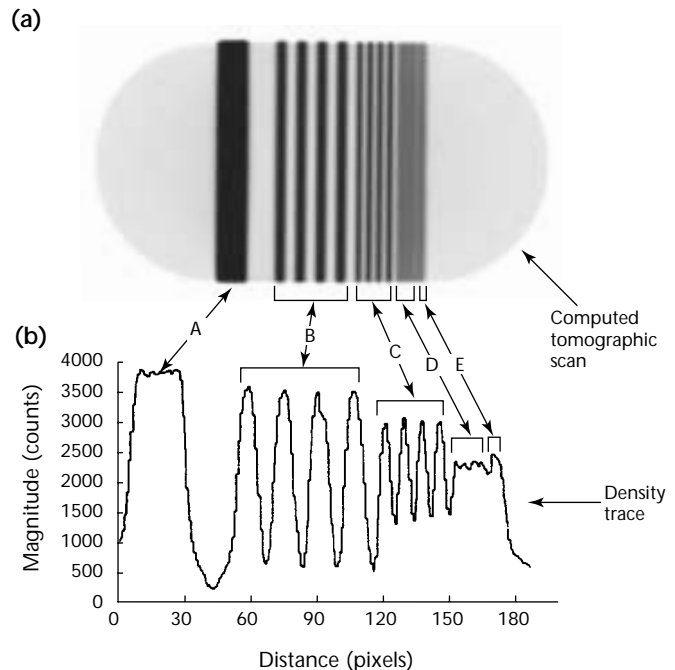
FIGURE 22. Photograph of line pair phantom.



assembly is bolted together and the line pair plates can be changed if additional or a different range of line pairs is desired. After computed tomography scanning the reconstructed image is analyzed by measuring the modulation of the computed tomography numbers obtained from a trace across the line pairs. The modulation at each line pair set is measured as a percentage, where the modulation measured between the 3 mm (0.12 in.) thick metal and 3 mm (0.12 in.) thick acrylic steps is taken to be 100 percent. The resolution phantom has been fabricated in two forms: (1) steel and acrylic and (2) aluminum and acrylic. The steel and acrylic phantom is for systems of 300 kV and up, the aluminum and acrylic phantom is for systems under 300 kV.

Figure 23 shows a computed tomographic image of the steel resolution phantom obtained from a relatively high resolution computed tomographic system. The computed tomographic image density contour line across the phantom indicates modulation for the respective line pair measurements at about 82 percent at

FIGURE 23. Computed tomography of line pair phantom: (a) tomographic image; (b) density trace evaluation.



#### Legend

- A. Reference bar.
- B. 0.5 line pairs per 1 mm (13 line pairs per 1 in.).
- C. 1 line pairs per 1 mm (25 line pairs per 1 in.).
- D. 2 line pairs per 1 mm (50 line pairs per 1 in.).
- E. 4 line pairs per 1 mm (100 line pairs per 1 in.).

0.5 line pairs per 1 mm (12 line pairs per 1.0 in.), 46 percent at 1 line pair per 1 mm (25 line pairs per 1.0 in.), 4 percent at 2 line pairs per 1 mm (50 line pairs per 1.0 in.) and 0 percent at 4 line pairs per 1 mm (100 line pairs per 1.0 in.).

The modulation transfer function provides a measurement of the resolution of a system by plotting the signal modulation that the system can provide as a function of frequency. The modulation transfer function characterization can be obtained by different techniques. One of the easiest techniques is to calculate the modulation transfer function from line trace data across the edge of a phantom. In the following, the edges used for the measurement are from the contrast sensitivity disk phantom discussed in below. The process involves using multiple traces across the edge of the disk from numerous angles. This provides edge traces from all orientations in the computed tomographic image. These traces are averaged to form the edge spread function, then differentiated to form the line spread function and finally fourier transformed to generate the modulation transfer function.

Figure 24 shows the line spread function for each of three different computed tomographic systems. The shape of the line spread function is an important characteristic of the system. The full width at half maximum (FWHM) of the line spread function is a measure of the relative resolution capability of each system. The shape of the line spread function should be symmetric. In Fig. 24 data System I is symmetric, System K is slightly asymmetric and System D is very asymmetric. The asymmetry may be due to a variety of causes. Aliasing in the data acquisition — that is, under sampling, truncating or clipping the edge spread

function — and detector cross talk are all possible causes.

The modulation transfer function may be calculated directly from the asymmetric line spread function or the line spread function may be processed to form a symmetric function. Figure 25 shows three possible modulation transfer functions for System D data. By taking the line spread function and mirroring it at the peak, symmetric line spread functions are generated for the *air* and *aluminum* halves of the edge spread function. Figure 25 shows that modulation transfer function curves for each of these three approaches to handling the System D data will create significantly different curves.

Figure 26 shows the results of modulation transfer function measurements for several computed tomographic systems. The modulation transfer function measurements were

FIGURE 25. Modulation transfer function of system D, showing effects of asymmetric and symmetric line spread functions.

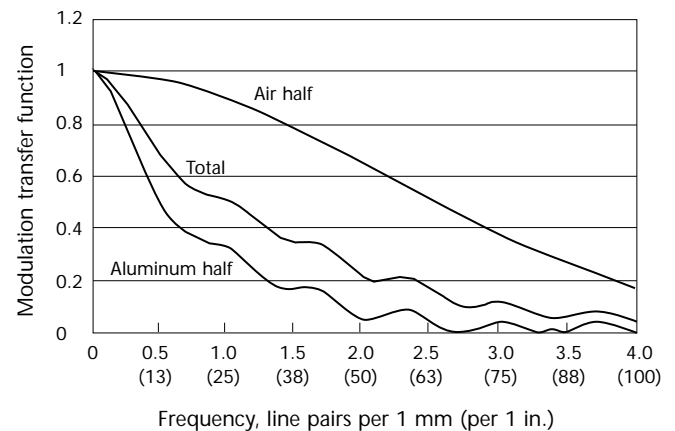


FIGURE 24. Line spread function for three computed tomographic systems.

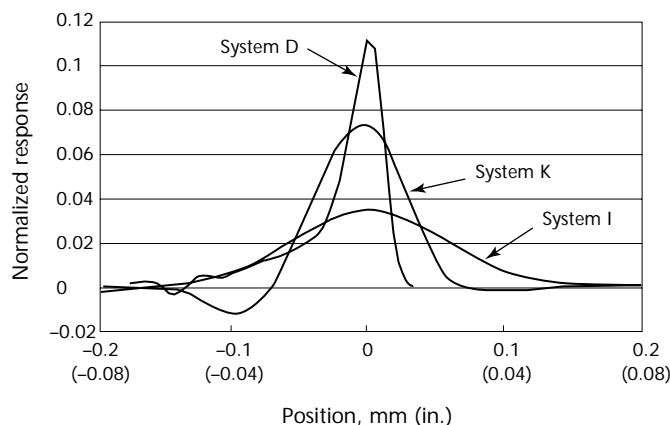
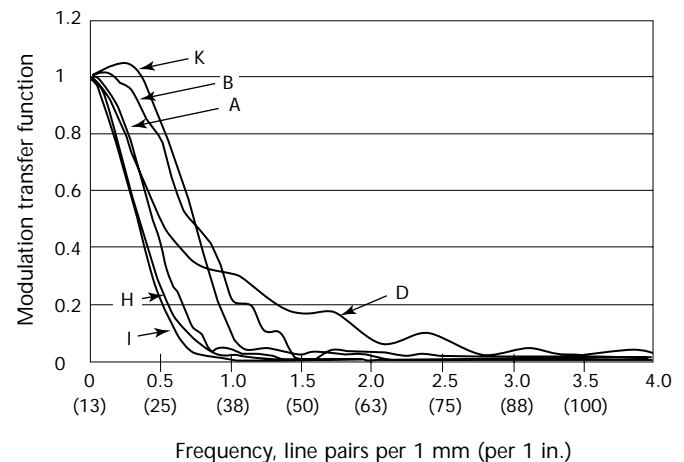


FIGURE 26. Modulation transfer function measurements of several computed tomographic systems.



analyzed by obtaining an average edge spread function, using a three point running average over the curve, differentiating, repeating a three point running average and then taking the fourier transform. For Systems B and D, the line spread function has been modified to be symmetric by mirroring the aluminum side of the edge spread function. One system demonstrates modulation transfer function values greater than expected, which can be caused by frequency enhancement in the reconstruction algorithms.

Table 9 tabulates the modulation transfer function values for 5, 10 and 20 percent contrast from the two sets of modulation transfer function calculations of Fig. 26. Five percent contrast is usually considered the limit of resolution. The

FWHM values of the line spread functions are also listed. The modulation transfer functions are less than 1 line pair per 1 mm (25 line pairs per 1.0 in.) for lower resolution systems, typically for test objects greater than 750 mm (30 in.) in diameter. The higher resolution systems (B and D) are designed for smaller test objects, that is, 150 to 300 mm (6 to 12 in.) in diameter.

## Contrast Sensitivity

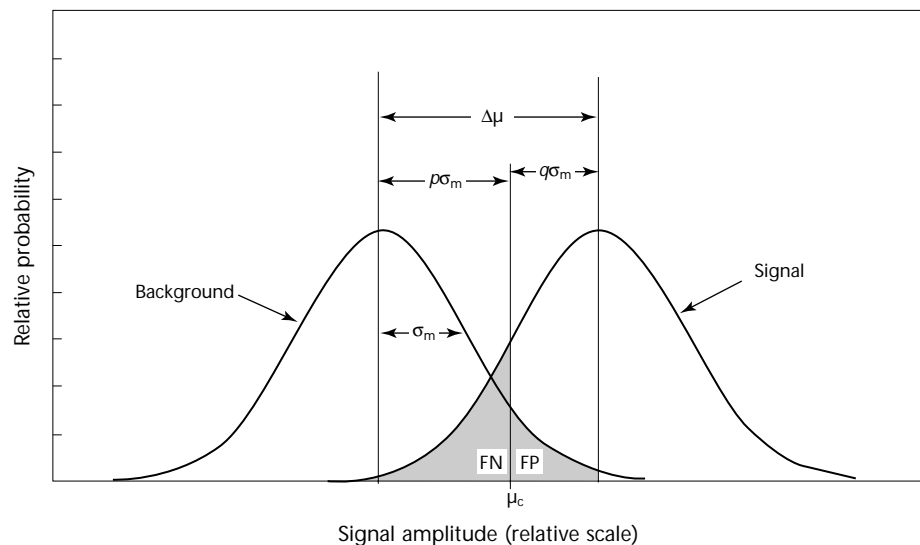
Contrast sensitivity refers to the graininess in an image. The best way to measure contrast sensitivity is to obtain a histogram of pixel values in a region of uniform density of a test specimen. Contrast sensitivity is then defined as the fractional standard deviation of the distribution. The inverse of this contrast sensitivity value is also commonly referred to as a signal-to-noise measurement of the system. The best contrast sensitivity phantom is an absolutely featureless uniform disk composed of a material whose X-ray absorption and density mimic those of the actual class of inspection objects.

In practice it is of interest to measure the contrast sensitivity as a function of the feature size. Materials of very close but differing densities can be used for this. Normally plugs of slightly different densities are inserted into a background

TABLE 9. Modulation transfer function frequency for 5, 10 and 20 percent contrast.

System	Frequency (line pairs per 1 mm) for Contrast Levels			Full Width at Half Maximum	
	5 percent	10 percent	20 percent	mm	(in.)
A	0.84	0.77	0.67	1.10	0.043
B	1.41	1.28	1.05	0.60	0.024
D	2.10	1.93	1.31	0.30	0.012
H	0.80	0.70	0.56	1.10	0.043
I	0.70	0.58	0.51	1.30	0.051
K	1.08	1.00	0.92	0.80	0.031

FIGURE 27. Probability distribution analysis for feature detection.



### Legend

- FN = false negative
- FP = false positive
- $p$  = FP level units of  $\sigma_m$
- $q$  = FN level units of  $\sigma_m$
- $\Delta\mu$  = contrast discrimination
- $\mu_c$  = signal threshold in decision process
- $\sigma_m$  = standard deviation of mean over some specified feature size

material. The size of the plugs is a variable. Evaluators then determine which level of contrast they can detect as a function of feature size. This type of phantom can cause a contrast discrimination curve. By plotting the size of feature with its percentage contrast for detectability, the curve is generated. Numerous samples, however, may be required. The contrast detectability will change with exposure and multiple curves are created as a function of the patient (or object) dose. The visual perception of the detectability of features will be different for different individuals. Thus a large number of interpreters should be used to develop a curve where, for example, 50 percent of the interpreters sense the contrast level for detection of various feature sizes.

An alternative technique to obtain the contrast discrimination curve is to calculate it on the basis of noise measurements as a function of region of interest size in a uniform phantom and weight the curve for loss of contrast as a function of resolution by using the modulation transfer function. The contrast required to detect a feature will depend on the statistical confidence, in terms of false positive or false negatives, that one is willing to accept. Figure 27 shows the statistical variation in the background and signal that could be observed in an image. The contrast discrimination  $\Delta\mu$  necessary for detection depends on the values of acceptable false positive (FP) and false negative (FN), respectively, where  $\sigma_m$  is the standard deviation of the mean over some specified feature size,  $p$  is the false positive,  $q$  is the FN level in units of  $\sigma_m$  and  $\mu_c$  is the critical value used in the decision process to decide if a signal is present or not. A contrast discrimination curve can be created for any combination of false positive and false negative values by multiplying the  $\sigma_m$  values in the noise curve by the sum of  $p$  and  $q$  and dividing by the modulation transfer function modulation. The contrast discrimination curve determines the minimum contrast that a feature must have to be detectable at the statistical discrimination levels selected. The exposure level is a variable in data acquisition, which is a factor in the noise measurements as a function of feature size.

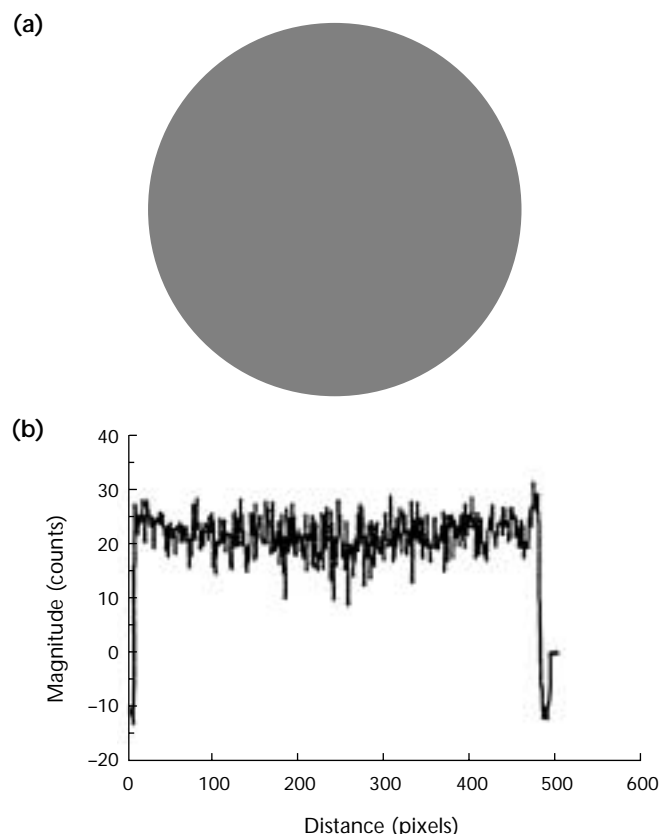
A contrast sensitivity phantom can be made from a uniform disk of material such as aluminum, 25 mm (1.0 in.) thick. Different sizes such as 140 mm (5.5 in.) in diameter and 70 mm (2.8 in.) in diameter may be appropriate for different computed tomographic systems. The smaller diameter size is used on systems with small fields of view or low kV. Figure 28 shows an example of a

computed tomographic slice of the large aluminum contrast sensitivity phantom with the corresponding density trace.

The measurement of contrast sensitivity is obtained by taking a region in the center of the reconstructed image and determining the average and standard deviation for all computed tomographic numbers in the region. A typical region size of 10 mm (0.4 in.) diameter is used. Readings are usually taken at the center of the disk. The ratio of the average to the standard deviation is used as a signal to noise measurement. The inverse is a measure of contrast sensitivity. The measurement of signal to noise for the image shown in Fig. 28 is about 6.

The signal-to-noise ratio is an important measure of system performance. The values improve with higher signal strengths. Large slice thickness and longer scan times will also improve signal to noise. The signal-to-noise ratio will also improve with smoothing algorithms in the reconstruction; however, this will decrease the resolution. Thus, the signal-to-noise ratio and resolution must be considered together in assessing performance.

FIGURE 28. Computed tomographic image of aluminum contrast sensitivity phantom: (a) slice image; (b) density trace.



A means of combining signal-to-noise ratio and resolution is the contrast discrimination curve. The contrast discrimination is affected by the feature size. Low contrast changes are easier to detect over larger areas than in small areas where they are easily masked by noise. This effect can be calibrated by measuring the statistical variations in the values of the means of the computed tomographic numbers as a function of the size of the region of interest. Figure 29 plots the error in the mean of the computed tomographic value (standard deviation  $\sigma_m$  of the mean) for a number of readings as a function of the feature size (size of the region of interest) on several computed tomographic systems.

From this curve and the modulation transfer function, it is possible to generate the contrast discrimination curve as discussed above. The conversion of modulation transfer function line pair values to the feature size is obtained by multiplying the line pair per millimeter by two and inverting to provide modulation as a function of feature size.

Figure 30 shows the contrast discrimination curve for five computed tomographic systems. The contrast discrimination curves are plotted for 10 percent false positive and false negative discrimination levels. The lower the contrast discrimination value on the curve, the easier it should be to detect features. Thus, systems such as *H* and *K* would be most likely to detect low contrast changes in an object. It is interesting that system *K*, a medical scanner, has excellent contrast discrimination. Medical systems can play a useful role in industrial computed tomography for components that can be penetrated with the lower kV and that fit within the medical gantry system size. The contrast discrimination curve data are

scan time dependent. Thus scanning longer or with larger slice thickness should drive the curves lower. The systems shown in this figure, of course, have been operated at different scan times, slice thicknesses and X-ray energies or intensities that are appropriate for the goal of that particular computed tomographic system design.

Figure 31 shows the effects of the false positive and false negative discrimination levels on the contrast discrimination curve.

## Material Density

An important phantom function is to establish the correlation between computed tomographic value and material density. Such a phantom can be quite difficult to manufacture because it is difficult to change density significantly

FIGURE 30. Contrast discrimination curves for several computed tomographic systems (A, B, H, I, K) at 10 percent false positive and false negative values.

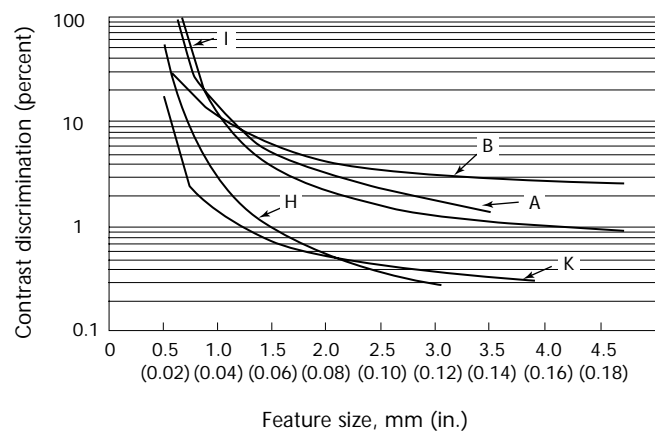


FIGURE 29. Standard deviation  $\sigma_m$  of mean of computed tomographic readings, as function of feature size.

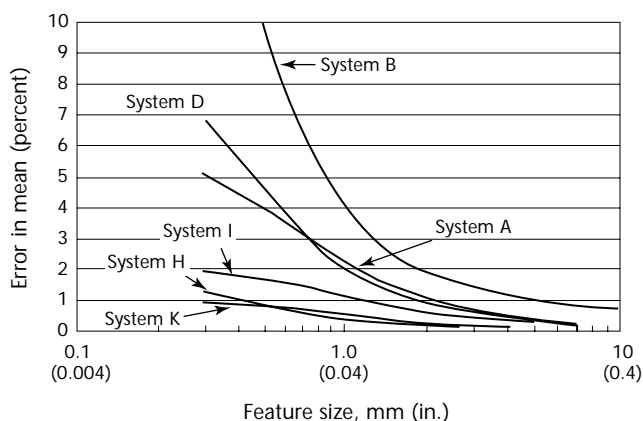
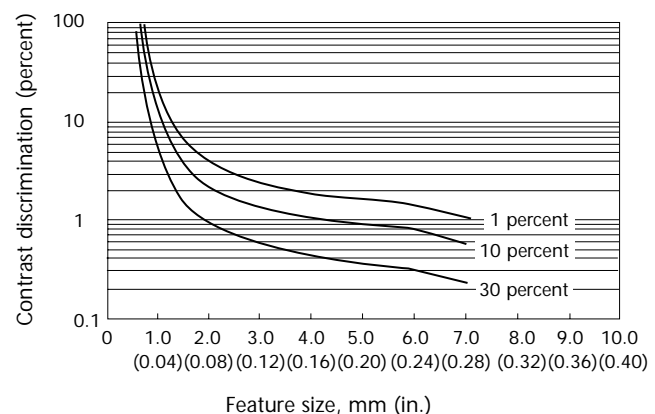


FIGURE 31. Contrast discrimination curves at 1, 10 and 30 percent false positive and false negative values.





without changing atomic number. The X-ray attenuation coefficient is dependent on both density and atomic number. At high X-ray energies where the Compton effect dominates the attenuation, the calibration is not difficult. At low energies, where photoelectric effects are involved in the attenuation, it is a real problem. The range of high or low energy depends on the material being tested. At medical computed tomographic energies of 80 keV effective, carbon materials can be used for density calibration. At 150 keV effective for a 300 kV X-ray system, even magnesium and aluminum may distort the density calibration.

The traditional density phantoms used in medical computed tomography have been liquid mixtures, such as glycerin and

isopropyl alcohol or dilutions of potassium iodide. These can be used to create steps of density over a very narrow range. Various polymers, such as acrylic and nylon, have also been used. They have inherent manufacturing variations that will result in differing attenuation measurements between samples that can be used to develop a phantom.

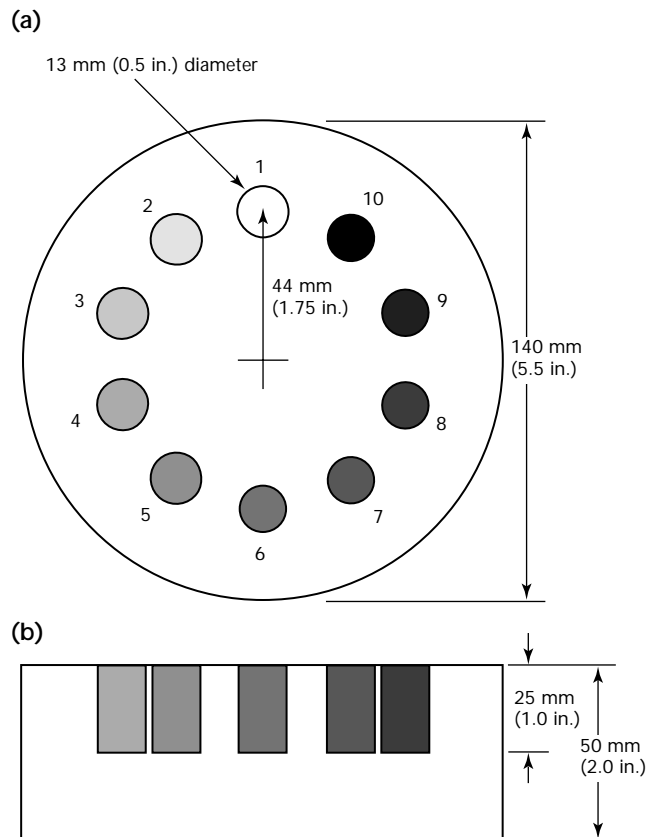
Carbon-to-carbon composite specimens can be manufactured to varying levels of densification in the range of about 1.3 to 1.8 g·cm<sup>-3</sup>, which makes a useful phantom for low density calibration. Densification of ceramic powders is also feasible for ranges of about 60 percent to full densification.

A phantom that consists of differing materials of significant density variation for a wide range of industrial material applications may be fabricated. However, the evaluation of the results from such a phantom must consider the X-ray energy and the atomic elements involved when extrapolating to other materials not included in the phantom.

An example material calibration phantom is shown in Fig. 32. It consists of an acrylic disk of 140 mm (5.5 in.) diameter with inserts of ten various materials. The inserts are machined to specific tolerances and weighed to obtain the density. The accuracy of the density value is estimated to be better than one percent. The acrylic disk is 50 mm (2.0 in.) thick but the inserts are only 25 mm (1.0 in.) long, which leaves in the phantom a uniform acrylic disk area that can be used for other measurements, such as the modulation transfer function and the contrast detail dose.

A computed tomographic scan of the material calibration phantom is shown in Fig. 33. The computed tomographic numbers for each insert from the reconstructed image are plotted against the measured densities to serve as a calibration curve for the system. The insert materials vary in atomic number that adds another variable in the process when the X-ray energy is such that the photoelectric effects are significant. The phantom is useful for generating a general density calibration curve for a computed tomographic system. Figure 34 shows a plot of material density versus computed tomographic density for one system.

FIGURE 32. Example of material density phantom: (a) top view; (b) side view. Each density phantom is a cylinder measuring 13 mm (0.05 in.) diameter x 25 mm (1.0 in.) ±0.0025 mm (0.001 in.).



#### Legend

1. Air gap.
2. High molecular weight polyethylene, density 0.95 g·cm<sup>-3</sup>.
3. Nylon, density 1.16 g·cm<sup>-3</sup>.
4. Nylon, lubricant filled, density 1.17 g·cm<sup>-3</sup>.
5. Acrylic plexiglas (core material), density 1.19 g·cm<sup>-3</sup>.
6. Acetal homopolymer, density 1.51 g·cm<sup>-3</sup>.
7. Magnesium, density 1.78 g·cm<sup>-3</sup>.
8. Fluorocarbon resin, density 2.18 g·cm<sup>-3</sup>.
9. Aluminum, density 2.70 g·cm<sup>-3</sup>.
10. Titanium, density 4.42 g·cm<sup>-3</sup>.

## Other Functions of Phantoms

Numerous phantoms of all sizes and shapes have been made to evaluate various characteristics of a system. Most commonly, pyramids or slanting edges of some type or other have been used to



assess the slice plane thickness and field uniformity of computed tomographic systems. Phantoms that represent actual parts that are discontinuity free or have anomalies of known dimensions are excellent for monitoring inspection sensitivity day to day and should be implemented if possible.

Artifacts are features present in the image that are not present in the object. All imaging systems, even the human eye, will have artifacts at some level. Artifacts in computed tomographic systems range from those associated with the particular computed tomographic configuration such as circular rings in third generation (rotate-only computed tomography) to those that are computed tomographic process dependent such as partial volume streaks. Beam hardening is a primary source of artifacts from polychromatic sources. Mechanical inaccuracies, material densities and partial voluming effects can also produce artifacts. It is important to be able to recognize an artifact as such and to understand the limitation the artifact places on the recognition of anomalies or measurement of some critical characteristic. Artifacts must not mask the presence of anomalies for unambiguous interpretation. This is accomplished if the artifact noise level can be kept below the required signal level for anomaly detection. No particular

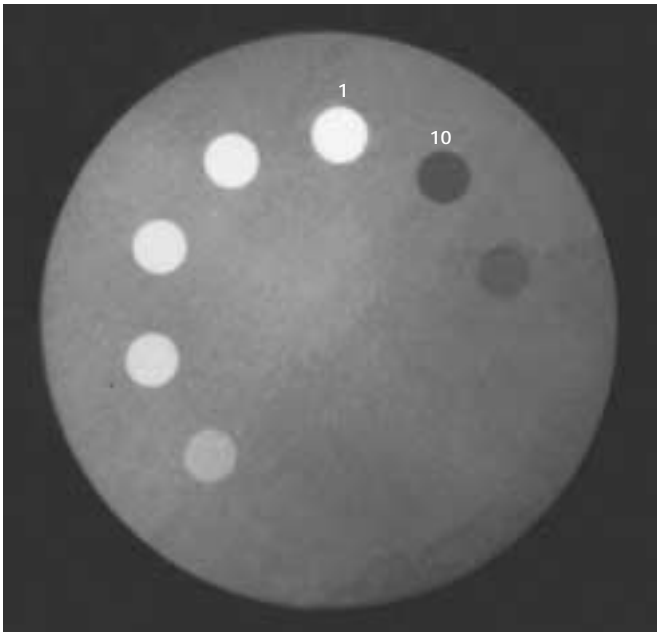
phantoms are necessary to monitor artifacts, although pin phantoms are normally used for mechanical system alignment. The artifact pattern generated from the pin is used to adjust the computed tomographic system configuration for minimal artifacting.

Extraction of positional and dimensional information from complex assemblies represents an important application of X-ray computed tomography. Examples include noninvasively measuring gaps and measuring deformations under mechanical load. Such information is extracted also where no photogrammetry or mechanical technique is possible to produce accurate, dimensioned representations of assemblies.

A basic assumption made in these calculations is the absolute equivalence of the computed tomographic image frame of reference and the scanned object frame of reference. Because this equivalence depends on a variety of factors including mechanical, motion, physical element, analysis techniques, software implementation and calibration techniques, this assumption of equivalence may introduce significant errors. A dimensional measurement phantom (DMP) is needed to establish precision of a computed tomographic imaging system.

An example of a dimensional measurement phantom consists of a 16.5 mm (0.65 in.) thick disk, 200 mm (7.87 in.) in diameter with forty-nine 8.6 mm (0.34 in.) diameter precision drilled holes forming a rectangular matrix at equal spacings of 20.0 mm (0.787 in.) plus or minus 0.006 mm ( $2.5 \times 10^{-4}$  in.). Three additional, precisely located, small holes were drilled adjacent to two corners of the large hole matrix, two at one

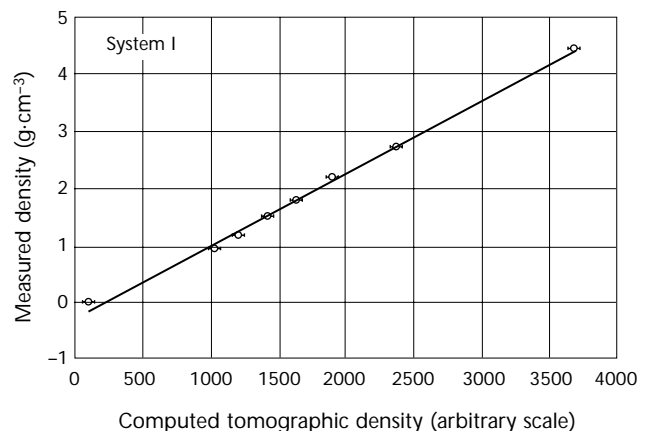
FIGURE 33. Computed tomographic scan of material density phantom<sup>49</sup>.



**Legend**

- 1. Most dense.
- 10. Least dense.

FIGURE 34. Plot of material density versus computed tomographic density for material density phantom.



corner and one at the adjacent corner to serve as reference points during image analysis. Figure 35 shows a computed tomographic scan of the dimensional measurement phantom in the nominal orientation used for the measurements discussed below.

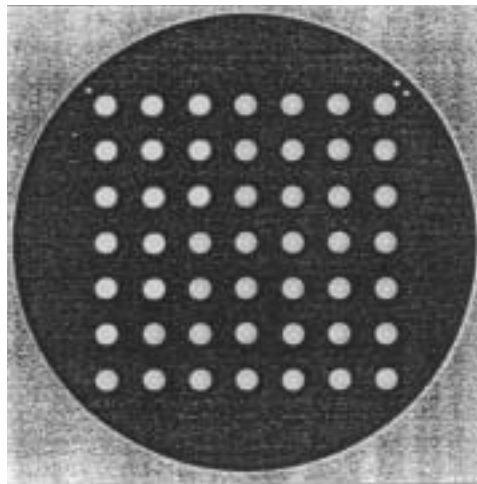
The dimensional phantom provides a metric for the precise dimensional analysis of scanned parts. Figure 36 and Eq. 36 show the concept of the metric  $\Gamma$ , which measures distortion.

$$(36) \quad \Gamma = \left( \det \begin{bmatrix} \frac{\partial X}{\partial x} & \frac{\partial X}{\partial y} \\ \frac{\partial Y}{\partial x} & \frac{\partial Y}{\partial y} \end{bmatrix} - 1 \right)^2$$

The metric uses the local jacobian of the transformation matrix between the part and its computed tomographic image representation to provide a quantitative means of assessing the inherent geometric accuracy of any given computed tomographic system.

Table 10 summarizes the outcome of phantom measurements for three computed tomographic systems. The first column identifies the system. The second shows the mean value of the dimensional distortion metric ( $\Gamma_{ij}$ ) measured for each of the systems. This index of the overall image distortion shows that it was extremely small. The third column gives the ratio of the  $6\sigma$  width of the deduced distribution of principal diagonal measurements ratioed to the nominal dimension. It is a measure of system precision. The last column indicates system accuracy. It is the offset of the peak of the probability distribution for the diagonal length from the nominal value.

FIGURE 35. Computed tomographic image of dimensional metric phantom.



It probably overstates the inaccuracy for system L that had a *forced offset* because of probable slight misalignment and the calibration technique used. The accuracy determined for the other two systems falls well within the uncertainty in part dimension that would be associated with

FIGURE 36. Dimensional phantom metric  $\Gamma$ : (a) image; (b) object; (c) example  $\Gamma$  map for particular test.

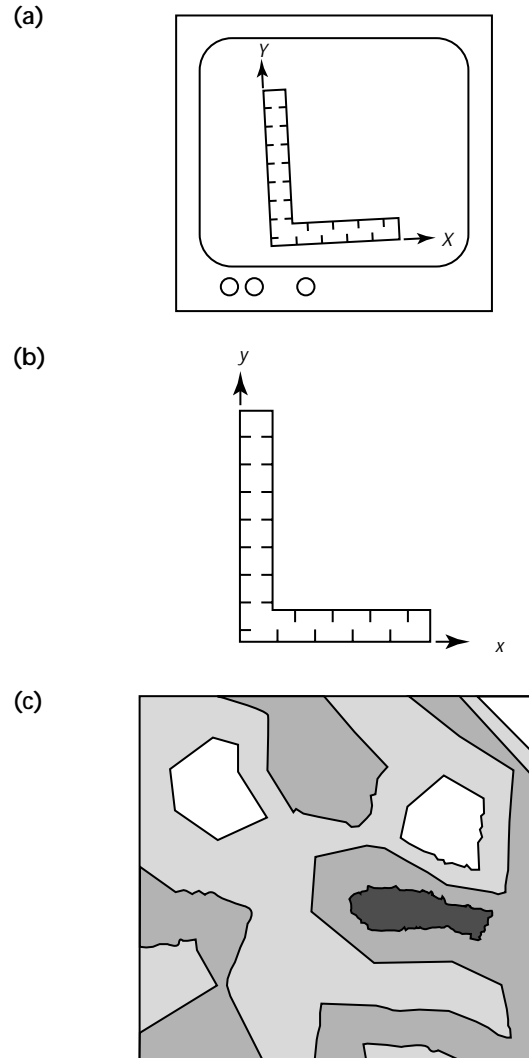


TABLE 10. Summary of dimensional fidelity measurements metric on dimensional measurement phantom.

System	Average Distortion $G^*$ (dimensionless)	Dimensional Precision, $6\sigma$ (percent)	Maximum Dimensional Inaccuracy in 170 mm (6.7 in.)	
			$\mu\text{m}$	$(10^{-3} \text{ in.})$
A	$4.0 \times 10^{-6}$	0.93	15.2	0.6
H	$3.5 \times 10^{-6}$	0.04	2.54	0.1
L	$4.2 \times 10^{-6}$	0.05	55.9	2.2

normal temperature variations in the working environment,  $\pm 6^{\circ}\text{C}$  ( $\pm 10^{\circ}\text{F}$ ), for a coefficient of thermal expansion of aluminum of  $1.22 \times 10^{-5}$ .

The methodology adopted in this study should be easily transportable to other systems for which an inherent geometry accuracy (IGA) is desired. Location of the centers of an array of precision machined holes in the computed tomographic image of a test article for comparison with the location of the holes in the part itself is an excellent means of deriving the elements of the local transformation matrix for inherent geometry accuracy determination. The success of the technique relies on the fact that the hole center location is insensitive to the criterion used for finding the hole edge, particularly because the hole center coordinates are highly overdetermined. Techniques that rely on precise determination of edges (for example, finding the absolute diameter of the test article) will be less successful because they are sensitive to the definition of an edge in the image.

# References

1. Adams, J. "Scanned-Beam Laminography Breaks through the 3-D Barrier." *Proceedings of the Technical Program — National Electronic Packaging and Production Conference (West)* [NEPCON West '89] (Anaheim, CA, March 1989). Des Plaines, IL: Cahners Exposition Group (1989).
2. Grant, D.B. "Tomosynthesis: A Three-Dimensional Radiographic Imaging Technique." *IEEE Transactions on Biomedical Engineering*. Vol. 19. New York, NY: Institute of Electrical and Electronics Engineers (1972): p 20-28.
3. Miller, E.R., E.M. McCurry and B. Hruska. "An Infinite Number of Laminograms from a Finite Number of Radiographs." *Radiology*. Vol. 98. Oak Brook, IL: Radiological Society of North America (1971): p 249-255.
4. Nelson, J. and H.H. Tat. "Web Deployed Design for Radiography." JANNAF [Joint Army-Navy-NASA-Air Force] *Propulsion Meeting Proceedings* [Salt Lake City, UT, July 2001]. Baltimore, MD: Johns Hopkins University, Chemical Propulsion Information Agency, for the JANNAF Interagency Propulsion Committee (2001).
5. Maravilla, K.R., R.C. Murry, Jr. and S. Horner. "Digital Tomosynthesis: Technique for Electronic Reconstructive Tomography." *American Journal of Roentgenology*. Vol. 141. Leesburg, VA: American Roentgen Ray Society (1983): p 497-502.
6. Buchele, S.F., H. Ellinger and F. Hopkins. "Forming Laminograms on Object-Dependent Surfaces." *Materials Evaluation*. Vol. 48, No. 5. Columbus, OH: American Society for Nondestructive Testing (May 1990): p 618-622.
7. Webber, R., R. Horton, D. Tyndall and J. Ludlow. "Tune-Aperture Computed Tomography (TACT)." Winston-Salem, NC: Cerberus Technologies (1996).
8. Kirchner, T., P. Burstein, M. Barker and F. Sequin. "High-Resolution Areal Tomosynthesis for Rapid Nondestructive Inspection of Large-Scale Aerospace Materials, Structures and Components." Columbia, MD: Johns Hopkins University, Chemical Propulsion Information Agency (1994).
9. Gondrom, S. and S. Schröpfer. "Digital Computed Laminography and Tomosynthesis — Functional Principles and Industrial Applications." *Proceedings — Computerized Tomography for Industrial Applications and Image Processing in Radiology* [Berlin, Germany]. DGZfP Proceedings BB 67-CD. Berlin, Germany: Deutsche Gesellschaft für Zerstörungsfreie Prüfung (March 1999).
10. Schulte, R. "Full Volumetric X-Ray Imaging Using a Digital Flat Panel Detector." Presented at ASNT Fall Conference and Quality Testing Show [Columbus, OH, October 2001].
11. Cormack, A.M. "Representations of a Function by Its Line Integrals, with Some Radiological Applications." *Journal of Applied Physics*. Vol. 34, No. 9. Melville, NY: American Institute of Physics (September 1963): p 2722-2727.
12. Cormack, A.M. "Representations of a Function by Its Line Integrals, with Some Radiological Applications, II." *Journal of Applied Physics*. Vol. 35, No. 10. Melville, NY: American Institute of Physics (October 1964): p 2908-2913.
13. Hounsfield, G.N. "Computerized Transverse Axial Scanning (Tomography): Part 1, Description of System." *British Journal of Radiology*. Vol. 46. London, United Kingdom: British Institute of Radiology (1973): p 1016-1022.
14. Herman, G. and S. Rowland. "SNARK: A Programming System for Image Reconstruction from Projections." Technical Report Number 130. Buffalo, NY: State University of New York at Buffalo (1978).
15. Huesman, R., G. Gullberg, W. Greenberg and T. Budinger. "RECLBL Library Users Manual, Donner Algorithms for Reconstruction Tomography." Publication 214. Berkeley, CA: Lawrence Berkeley Laboratory, University of California (October 1977).
16. ASTM, E 157-93, *Standard Guide for Computed Tomography (CT) Imaging*. West Conshohocken, PA: ASTM International (1993).

17. ASTM E 1570-95, *Standard Practice for Computed Tomographic (CT) Examination*. West Conshohocken, PA: ASTM International (1995).
18. Bischof, C.J. and J.C. Ehrhardt. "Modulation Transfer Function of the EMI CT Head Scanner." *Medical Physics*. Vol. 4, No. 2. Melville, NY: American Institute of Physics, for American Association of Physicists in Medicine (1977): p 163-167.
19. Barret, H.H. and W. Swindell. *Radiological Imaging: The Theory of Image Formation, Detection and Processing*. Vols. 1 and 2. New York, NY: Academic Press (1981).
20. Shepp, L.A. and J.A. Stein. "Simulated Reconstruction Artifacts in Computerized X-Ray Tomography." *Reconstruction Tomography in Diagnostic Radiology and Nuclear Medicine*. Baltimore, MD: University Park Press (1977).
21. Burstein, P., R. Mastronardi and T. Kirshner. "Computerized Tomography Inspection of Trident Rocket Motors: A Capability Demonstration." *Materials Evaluation*. Vol. 40, No. 11. Columbus, OH: American Society for Nondestructive Testing (November 1982): p 40.
22. Bossi, R.H. and G.E. Georgeson. "Computed Tomography Analysis of Castings." Report WL-TR-91-4121. Wright-Patterson Air Force Base, OH: Air Force Research Laboratory (January 1992).
23. Bossi, R.H., J.L. Cline, E.G. Costello and B.W. Knutson. "X-Ray Computed Tomography of Castings." Report WRDC-TR-89-4138. Wright-Patterson Air Force Base, OH: Air Force Research Laboratory (March 1990).
24. Georgeson, G.E. and R.H. Bossi. "X-Ray Computed Tomography of Full-Scale Castings." Report WL-TR-91-4049. Wright-Patterson Air Force Base, OH: Air Force Research Laboratory (October 1991).
25. Georgeson, G.E. and R.H. Bossi. "Computed Tomography for Casting Development." Report WL-TR-92-4032. Wright-Patterson Air Force Base, OH: Air Force Research Laboratory (September 1992).
26. Georgeson, G.E., R.H. Bossi and R.D. Rempt. "Computed Tomography Demonstration for Castings." Report WL-TR-93-4048. Wright-Patterson Air Force Base, OH: Air Force Research Laboratory (May 1993).
27. Friddell, K.D., A.R. Lowrey and B.M. Lempriere. "Application of Medical Computed Tomography (CT) Scanners to Advanced Aerospace Composites." *Review of Progress in Quantitative Nondestructive Evaluation*. Vol. 4. New York, NY: Plenum Press (1985): p 1239-1246.
28. Bossi, R.H., K.K. Coopridge and G.E. Georgeson. "X-Ray Computed Tomography of Composites." Report WRDC-TR-90-4014. Wright-Patterson Air Force Base, OH: Air Force Research Laboratory (July 1990).
29. Bossi, R.H., K.D. Friddell and A.R. Lowrey. "Computed Tomography." *Non-Destructive Testing of Fibre-Reinforced Plastics Composites*. Ch. 4. London, United Kingdom: Elsevier Science Publishers (1990).
30. Georgeson, G.E. and R.H. Bossi. "Computed Tomography for Advanced Materials and Processes." Report WL-TR-91-4101. Wright-Patterson Air Force Base, OH: Air Force Research Laboratory (June 1992).
31. Bossi, R.H., G.E. Georgeson and R.D. Rempt. "X-Ray Computed Tomography for Emerging Aerospace Materials and Processes Development." Report WL-TR-93-4054. Wright-Patterson Air Force Base, OH: Air Force Research Laboratory (May 1993).
32. Bossi, R.H. and G.E. Georgeson. "Composite Structure Development Decisions Using X-Ray CT Measurements." *Materials Evaluation*. Vol. 53, No. 10. Columbus, OH: American Society for Nondestructive Testing (October 1995): p 1198-1203.
33. Boyd, J.E. "Limited-Angle Computed Tomography for Sandwich Structures Using Data Fusion." *Journal of Nondestructive Evaluation*. Vol. 14, No. 2. New York, NY: Plenum Press (1995): p 61-76.
34. McCullough, E.C., J.T. Payne, H.L. Baker, Jr., R.R. Hattery, P.F. Sheedy, D.H. Stephens and E. Gedgaudas. "Performance Evaluation and Quality Assurance of Computed Tomography Scanners, with Illustrations from the EMI, ACTA, and Delta Scanners." *Radiology*. Vol. 120. Oak Brook, IL: Radiological Society of North America (July 1976): p 173-188.
35. Payne, J.T., E.C. McCullough, T. Stone and E. Gedgaudas. "Acceptance Testing of a Computerized Tomographic Scanner." *Optical Engineering*. Vol. 16, No. 1. Bellingham, WA: International Society for Optical Engineering (January-February 1977): p 28-31.



36. Goodenough, D.J., K.E. Weaver and D.O. Davis. "Development of a Phantom for Evaluating Assurance of Image Quality in CT Scanning." *Optical Engineering*. Vol. 16, No. 1. Bellingham, WA: International Society for Optical Engineering (January-February 1977): p 62-65.
37. White, D.R., R.D. Speller and D.M. Taylor. "Evaluating Performance Characteristics in Computerized Tomography." *British Journal of Radiology*. Vol. 54. London, United Kingdom: British Institute of Radiology (1981): p 221-231.
38. AAPM 1977, *Phantoms for Performance Evaluation and Quality Assurance of CT Scanners*. Report No. 1. New York: American Institute of Physics, for American Association of Physicists in Medicine (1977).
39. Mees, C.K. *Theory of the Photographic Process*. New York, NY: MacMillan Company (1942).
40. Judy, P.F. "The Line Spread Function and Modulation Transfer Function of a Computed Tomography Scanner." *Medical Physics*. Vol. 3, No. 4. Melville, NY: American Institute of Physics, for American Association of Physicists in Medicine (1976): p 233-236.
41. Hanson, K.M. "Detectability in Computed Tomographic Images." *Medical Physics*. Vol. 6, No. 5. Melville, NY: American Institute of Physics, for American Association of Physicists in Medicine (1979): p 441-451.
42. Cohen, G. and F. Di Bianca. "The Use of Contrast-Detail-Dose Evaluation of Image Quality in a CT Scanner." *Journal of Computer Assisted Tomography*. Vol. 3, No. 2. New York, NY: Raven Press (1979): p 189-195.
43. Dennis, M.J. "Industrial Computed Tomography." *Metals Handbook*, ninth edition: Vol. 17, *Nondestructive Evaluation and Quality Control*. Materials Park, OH: ASM International (1989): p 358-386.
44. ASTM E 1441-95, *Standard Guide for Computed Tomography (CT) Imaging*. West Conshohocken, PA: ASTM International (1995).
45. ASTM E 1672-95, *Standard Guide for Computed Tomography (CT) System Selection*. West Conshohocken, PA: ASTM International (1995).
46. ASTM E 1695-95, *Standard Test Method for Measurement of Computed Tomography (CT) System Performance*. West Conshohocken, PA: ASTM International (1995).
47. Sivers, E.A. and M.D. Silver. "Performance of X-Ray Computed Tomographic Imaging Systems." *Materials Evaluation*. Vol. 48, No. 6. Columbus, OH: American Society for Nondestructive Testing (June 1990): p 706-713.
48. Jacoby, M.H. and D.E. Lingenfelter. "Monitoring the Performance of Industrial Computed Tomography Inspection Systems." *Materials Evaluation*. Vol. 47, No. 10. Columbus, OH: American Society for Nondestructive Testing (October 1989): p 1196-1199.
49. Bossi, R.H., J.L. Cline and B.W. Knutson. "Computed Tomography of Thermal Batteries and Other Closed Systems." Report WRDC-TR-89-4113. Wright-Patterson Air Force Base, OH: Air Force Research Laboratory (December 1989).
50. Hytec Incorporated. "Small Flashlight Results." Technical Report, HT 107990-0003. Los Alamos, NM: Hytec Incorporated (February 2001).
51. Bergstrom, M. "Performance Evaluation of Scanners." *Radiology of the Skull and Brain: Vol. 5, Technical Aspects of Computed Tomography*. Chapter 123. Saint Louis, MO: C.V. Mosby Company (1981): p 4212-4227.

## Bibliography

- Armistead, R.A. "CT: Quantitative 3D Inspection." *Advanced Materials and Processes*. Materials Park, OH: ASM International (March 1988): p 42-48.
- Bossi, R.H. and B. Knutson. "The Advanced Development of X-Ray Computed Tomography Applications." Report WL-TR-93-4016. Wright-Patterson Air Force Base, OH: Air Force Research Laboratory (May 1993).
- Bossi, R.H. and R.J. Kruse. "X-Ray Tomographic Inspection of Printed Wiring Assemblies and Electrical Components." WRDC-TR-90-4091. Wright-Patterson Air Force Base, OH: Air Force Research Laboratory (October 1990).
- Bossi, R.H. and W. Shepherd. "Computed Tomography for Failure Analysis Investigations." Report WL-TR-93-4047. Wright-Patterson Air Force Base, OH: Air Force Research Laboratory (May 1993).



- Bossi, R.H., A.R. Crews and G.E. Georgeson. "X-Ray Computed Tomography for Failure Analysis." Report WL-TR-92-4017. Wright-Patterson Air Force Base, OH: Air Force Research Laboratory (August 1992).
- Bossi, R.H., J.L. Cline and G.E. Georgeson. "High Resolution X-Ray Computed Tomography." Report WL-TR-91-4102. Wright-Patterson Air Force Base, OH: Air Force Research Laboratory (July 1992).
- Bossi, R.H., R.J. Kruse and B.W. Knutson. "Computed Tomography of Electronics." Report WRDC-TR-89-4112. Wright-Patterson Air Force Base, OH: Air Force Research Laboratory (December 1989).
- Brooks, R.A. and G. Di Chiro. "Principles of Computer Assisted Tomography (CAT) in Radiographic and Radioscopic Imaging." *Physics in Medicine and Biology*. Vol. 21, No. 5. London, United Kingdom: Institute of Physics in association with the American Institute of Physics and the American Association of Physicists in Medicine (1976).
- Bueno, C., M.D. Barker, R.A. Betz, R.C. Barry and R.A. Buchanan. "Nondestructive Evaluation of Aircraft Structures Using High-Resolution Real-Time Radiography." *Nondestructive Evaluation of Aging Aircraft, Airports, Aerospace Hardware and Materials*. SPIE Proceedings, Vol. 2455. Bellingham, WA: International Society for Optical Engineering (June 1995).
- Burstein, P. and R.H. Bossi. "A Guide to Computed Tomography System Specifications." Report WRDC-TR-90-4026. Wright-Patterson Air Force Base, OH: Air Force Research Laboratory (August 1990).
- Copley, D., J. Eberhard and G. Mohr. "Computed Tomography: Part 1, Introduction and Industrial Applications." *JOM*. Warrendale, PA: Minerals, Metals and Materials Society [TMS] (January 1994): p 14-26.
- Crews, A.R. and R.H. Bossi. "X-Ray Computed Tomography for Whole System Evaluation (Small Jet Engines)." Report WL-TR-91-4109. Wright-Patterson Air Force Base, OH: Air Force Research Laboratory (May 1992).
- Crews, A.R., R.H. Bossi and G.E. Georgeson. "X-Ray Computed Tomography for Geometry Acquisition." Report WL-TR-93-4036. Wright-Patterson Air Force Base, OH: Air Force Research Laboratory (March 1993).
- Feldkamp, L.A. and G. Jesion. "3D X-Ray Computed Tomography." *Review of Progress in Quantitative Nondestructive Testing*. IS-4923. New York, NY: Plenum Press (1986): p 555-566.
- Gupta, N. and V. Alreja. "Tangential Scanner for Waste Drum Inspection." *ASNT Industrial Computed Tomography Topical Conference* [Huntsville, AL, May 1996]. Columbus, OH: American Society for Nondestructive Testing (1996): p 85-88.
- Hendee, W.R. *The Physical Principles of Computed Tomography*. Boston, MA: Little, Brown and Company (1983).
- Herman, G.T. *Image Reconstructions from Projections: The Fundamentals of Computerized Tomography*. New York, NY: Academic Press (1980).
- Kak, A.C. and M. Slaney. *Principles of Computerized Tomographic Imaging*. New York, NY: IEEE Press (1987).
- Kropas, C.V., T.J. Moran and R.N. Yancey. "Effects of Composition on Density Measurement by X-Ray Computed Tomography." *Materials Evaluation*. Vol. 49, No. 4. Columbus, OH: American Society for Nondestructive Testing (April 1991): p 487-490.
- Macovski, A. *Medical Imaging*. Upper Saddle River, NJ: Prentice-Hall (1983).
- Mandelkorn, F. and H. Stark. "Computerized Tomosynthesis, Stereoscopy and Coded-Scan Tomography." *Applied Optics*. Vol. 17. Washington, DC: Optical Society of America (1978): p 175-80.
- Marshall, C. *The Physical Basis of Computed Tomography*. Saint Louis, MO: Warren H. Green, Incorporated (1982).
- Newton, T.H. and D.G. Potts, ed. *Radiology of the Skull and Brain: Vol. 5, Technical Aspects of Computed Tomography*. Saint Louis, MO: C.V. Mosby (1981).
- Perceptics Corporation. High-Resolution Three-Dimensional Computed Tomography. Wright Laboratory Final Report, WLTR-96-4117. Wright Patterson Air Force Base, OH: United States Air Force (October 1996).
- Radon, J.H. "Über die Bestimmung von Funktionen durch ihre Integralwerte längs gewisser Mannigfaltigkeiten." *Berichte Sächsische Akademie der Wissenschaften [Berichte über die Verhandlungen der Königlich Sächsischen Gesellschaft der Wissenschaften zu Leipzig]*. Vol. 69. Leipzig, Germany: Math.-Phys. Klasse (1917): p 262-277.
- Schneberk, D.J., S.G. Azevedo, H.E. Martz and M.F. Skeate. "Sources of Error in Industrial Tomographic Reconstructions." *Materials Evaluation*. Vol. 48, No. 5. Columbus, OH: American Society for Nondestructive Testing (May 1990): p 609.

- Seeram, E. *Computed Tomography Technology*. Philadelphia, PA: W.B. Saunders Company (1982).
- Smith, B.D. "Cone-Beam Tomography: Recent Advances and a Tutorial Review." *Optical Engineering*. Vol. 29, No. 5. Bellingham, WA: International Society for Optical Engineering (May 1990).
- Stanley, J. "Standards for Computed Tomography." *ASNT 1993 Fall Conference and Quality Testing Show* [Long Beach, CA]. Columbus, OH: American Society for Nondestructive Testing (November 1993).
- Stanley, J. and J. LePage. "CT System Performance Evaluation." Joint Army-Navy-NASA-Air Force 1990 NDE Subcommittee Meeting [Idaho Falls, ID, April 1990].



# 13

## C H A P T E R

# Image Data Analysis

---

Daniel J. Schneberk, Lawrence Livermore National  
Laboratory, Livermore, California

Harry E. Martz, Lawrence Livermore National  
Laboratory, Livermore, California

# PART 1. Fundamental Properties of Digital Images and Processing Schemes

Image analysis can be described as the process that relates the features in the image to the state of the object being tested. Not all features in an image carry the same significance for the test, nor are all features in an image necessarily related to the object. Operations applied to images can highlight, enhance and sometimes remove certain features in the image. Image analysis proceeds by developing a sensible rationale for the steps and procedures connecting features in an image to an interpretation about the state of the object. Depending on the situation the amount of image analysis applied to a particular image can be minimal or very extensive.

The goal of the test drives the image data analysis for any image. Tests are always about measuring a property of an object, with some precision and repeatability. Operator based tests use image analysis techniques to extract the necessary information about the object from the image. Automated test systems embed an analysis of the image in the processing. The role of image analysis is to develop the techniques for manipulating the image data and at the same time assess the weaknesses of the procedure. It is best when an image analysis technique can be reduced to a set of image quality standards for the input images. These standards can also highlight some fundamental aspect of the radiographic method, for that radiographic source and that detector. Consequently, evaluating an image analysis technique and its potential for conveying reliable information about the object involves a whole matrix of issues — from the fidelity of the image in space, the particular detector used and the procedures used for evaluating the digital image. Problem areas and limitations of image analysis schemes can result from detector choices as well as processing schemes. For an understanding of these issues some recognition of the fundamentals of digital images and the landscape of acquisition and processing for digital images is useful.

Three properties of digital images are fundamental: (1) signal-to-noise ratio, (2) spatial resolution and (3) contrast sensitivity (defined below). Each identifiable feature corresponds to some change in measured intensity in the

image. To decide whether this change in intensity derives from the state of the object or is some artifact of the scanning modality requires an assessment of these three properties of the imaging system.

The image performance achieved on any acquisition is the result of a number of factors. Digital radiographic images or computed tomographic images are the combined result of the radiographic technique used, the detection scheme and all the processing steps that result in the image used for the test.

The entire imaging process for digital radiography and computed tomography can be represented in sequential phases, with digital radiography requiring fewer steps than computed tomography (Fig. 1). Indeed, the properties of the computed tomographic reconstructed image depend strongly on the properties of the underlying digital radiographic images.

## Components of X-Ray Transmission Images

The radiographic beam is the starting point for all radiographic scanners. The properties of the beam, its shape and energy content and the geometry of the object with respect to the beam are crucial determinants of imaging quality. The beam generates an image in space and the detector samples the X-ray intensity of this beam. The sampling has both a spatial and energy discriminating aspect for some position in space. Before the introduction of any detector or detector and collimation scheme a number of different sources of signal are present in the transmission measurements. For any detector position (some three-dimensional position on the other side of the object from the X-ray beam), the transmitted X-ray photons intersecting this solid angle divide into different types as follows:

$$(1) \quad N_T[S(E),d] = N_P[S(E),d] + N_S[S(E),d]$$

$$(2) \quad N_S[S(E),d] = N_{Sbk}[S(E),d] + N_{Sobj}[S(E),d]$$

$$(3) \quad N_{TO}[s(E),d] = N_{PO}[s(E),d] + N_{Sbk}[s(E),d]$$

The schema above decomposes the total photon flux from an X-ray source  $S(E)$ , for the solid angle subtended by detector position  $d$ , into primary photons  $N_p$  and scattered photons  $N_s$ . Further there are two types of scattered photons: background scatter  $N_{Sbk}$  and object scatter  $N_{Sobj}$ . Most X-ray measurements have a means for taking into account the radiation field independent of the object,  $N_{TO}$ . Typically this measurement contains some background scattered photons from the supporting fixtures in the radiographic scanner or in the detection hardware, as well as the primary photons launched by the X-ray source  $N_{PO}$ .

The attenuation of electromagnetic radiation — for example, X-rays passing through matter — involves three mechanisms, each accompanied by secondary processes. The three

mechanisms are photoelectric effect, compton scattering and pair production.

1. In the photoelectric effect an X-ray dissipates its entire energy by knocking out an electron from an atom.
2. In compton scattering, the X-ray imparts some energy to an electron but survives with a lower energy and different direction.
3. In pair production an X-ray is absorbed to create an electron positron pair. For pair production to occur the incident X-ray must have an energy equal to or greater than the rest mass of an electron positron pair. This energy is 1.02 MeV because the rest mass of each is 0.511 MeV.

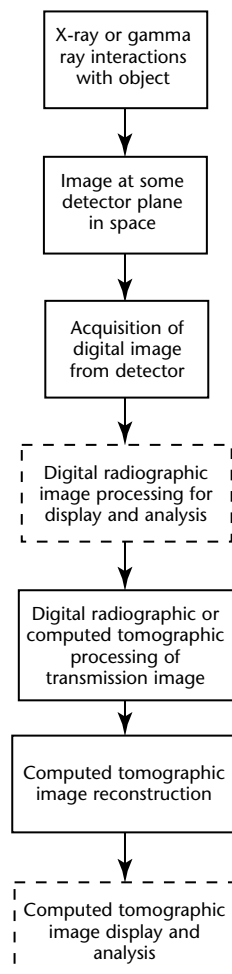
[A more complete discussion of these processes can be found elsewhere in this volume](#) and in books by Evans and Heitler.<sup>1,2</sup>

The different attenuation mechanism combine in any scan to produce signal from a variety of secondary processes. For example, a photoelectric electron interacts with the material and creates scattered X-rays. Likewise, scattered X-rays at lesser energy than the initial flux undergo photoelectric attenuation before reaching an exit plane in the object. At lower energies the secondary processes are not prominent. However, at medium to higher energy regimes the secondary and ancillary processes can dominate imaging quality.

The performance of imaging techniques using penetrating radiation follows from the properties and the proportions of the different classes of X-ray photons in the image. The *primary* X-ray photons account for the performance of the transmission image. These *straight line* projections through the materials best conform to the *idealized* ray path implicit to computed tomographic reconstruction algorithm textbooks.<sup>3,4</sup> Spatial resolution of the primary photons is bounded by the spot size blur and in the case of heavily collimated systems the effective width of the source and detector apertures. The contrastive properties of the primary photons have the distribution of an X-ray gage with standard deviation proportional to the inverse of the square root of  $N$ .

Primary photon flux  $N_p$  includes the total X-ray photons emitted by the X-ray source and transmitted straight through the object, undergoing the different attenuation processes. As shown elsewhere, photons emitted from the X-ray source are a poisson random variable and total X-ray attenuation is represented as distributed binomial. The two variables taken together result in Eq. 4:

FIGURE 1. Imaging process for digital radiography and computed tomography.



$$(4) \quad N_P[s(E), d] = N_{PO}[s(E), d] \times \exp[-\sum \mu_i(\rho, Z) x_i]$$

where  $\mu_i(\rho, Z)$  is the X-ray attenuation coefficient of the  $i$ th material with thickness  $x_i$  in the direction subtended by the detector element looking back at the X-ray source through the object. Following this development  $N_T$  is a poisson random variable with mean  $N_T$ , variance also equal to  $N_T$  and standard deviation  $N_T^{-1}$ .<sup>3</sup>

Contrastive performance of a transmission image is that ability to detect intensity changes due to some change in the attenuation of the object along some ray path. All measurement systems involve some noise. One bound on the contrast in an image is the ratio of the change in intensity of the signal to the random intensity variations caused by the noise in the system. For some change in attenuation  $\Delta$  and by using the poisson variable  $N$ , the signal-to-noise ratio can be written:

$$(5) \quad \frac{S}{N} = \frac{\Delta N_P}{\sqrt{N_P}} = \Delta \sqrt{N_P}$$

Feature contrast in an object is directly related to the number of transmitted and detected photons. In the limit too few photons (weak signal) will always result in poor contrast.

The photons scattered in the object are more difficult to interpret. The line or path of the scattered photons is energy dependent, usually forward peaked and always broader than the path of the primary photons.<sup>3</sup> Object scatter can vary throughout the image because of the change in the lengths and types of material in the specimen. Highly attenuating sections of an object adjacent to low attenuating elements will generate substantial signal for the image of the low attenuating sections. In radiography the contrast in the low attenuating sections is simply compromised and this effect is independent of the detector. For computed tomographic reconstructed images scatter results in *streak* artifacts along the directions of the longest chord lengths or highest attenuation.<sup>4</sup> The spatially variant character of object scatter makes removal of this source of artifacts difficult.

*Background scatter* is the fluence that arises from the detector and its environment, for example, cabinet and room hardware, independent of the object. If there was no detector or cabinet hardware there would be no photons of this type but then there would be no image. Consequently, this category is included as always part of any acquired

image, even though the photons are present because of the detector itself. The detector hardware includes all the aspects of collimation, scatter from adjacent parts of the cabinet or detector enclosure, fluence from the fixturing from the object, as well as sources of scatter within the detector (blooming in the scintillator and other sources). Background scatter fills up the detector dynamic range with counts that do not carry information about the object.

As indicated above, contrast is also affected by the types of photons detected at that position in the image. A signal that arrives at the detector element from adjacent ray paths will blur the contents of the ray in straight lines through the object. Consequently, certain features in the object will be masked by adjacent features. By substituting Eqs. 1 to 3 into Eq. 5, this effect can be quantified:

$$(6) \quad \frac{S}{N} = \frac{\Delta N_P}{\sqrt{N_T}} = \frac{\Delta \sqrt{N_P}}{\sqrt{1 + \frac{N_{Sobj}}{N_P} + \frac{N_{Sbk}}{N_P}}}$$

Contrast is reduced in two ways, from the presence of object scatter and background scatter in the detector package. The two quantities in the denominator of Eq. 6 are usually referred to as *scatter-to-primary* ratios. Here the effects of the two different types of scatter are separated out because of their separate physical mechanisms. A couple of different techniques are available for measuring these quantities<sup>5</sup> and these measurements are recommended as elements in any standard image calibration procedure.

Spatial resolution is nominally defined as the size of the smallest detectable feature. Notice the necessary involvement of contrastive performance. The feature must be detectable to be *sized* or be attributed some dimensionality. Image contrast must be at some minimal level in order for spatial resolution to be assessed at all. Alternatively, poor spatial resolution because of some source of uncontrolled blur (background scatter or object scatter) can compromise the best contrastive performance. The *modulation transfer function* (MTF)<sup>6</sup> for a system provides a good view of the contrastive performance at different spatial frequencies. The point spread function (PSF), the fast fourier transform pair to the modulation transfer function, also provides a useful measure of the spatial resolution of a digital radiographic or computed tomographic imaging system. Good estimates of these functions for an



imaging system are invaluable for subsequent image analysis.<sup>6</sup>

Obtaining good estimates for these functions for a system requires careful procedures.

1. All procedures for digital radiography and computed tomography involve obtaining an image containing a *material edge*, where the edge spread is due only to the imaging system not the object. For radiographic systems this requires a perpendicular orientation of the flat aspect of the object to the X-ray beam.
2. There should be some transmission through the object or the edge sharpness is artificially created by the opaqueness of the object and masks the imaging of the edge by the system.
3. Data acquisition for the image should be typical of system operations. It is important to know and monitor the properties of the *regular* image being acquired every day.

The photons arising in the course of X-ray attenuation mechanisms can be organized into classes and the different classes do not have the same properties for imaging the object. The contrastive performance and spatial resolution for the different classes of photons are different and the system performance will reflect the proportions of the different types of photons. Better imaging performance will enable more reliable image data analysis and interpretations. Lastly, much of the image processing for digital radiographic and computed tomographic images is based on an *idealized* ray path model of X-ray attenuation. This is the kind of imaging one would expect if the received signal was composed exclusively of *primary* photons. Imaging artifacts are often the result of this mismatch between theory and actual measurement. This mismatch varies with each particular scanner. Whereas the actual properties of the photons in space before digitization can be somewhat elusive, it is important to know the general properties of the different photons. Hopefully this knowledge can guide the analyst in deciding whether a particular image effect is *just the radiation doing its job* or whether some particular source of the effect can be remediated.

## Digitizing Transmission Images

Acquiring digital radiographic and computed tomographic data involves some mechanism for digitizing the image in space, which involves its own set of issues. Whereas the performance of digital radiographic and computed tomographic

systems can be accounted for by analyzing the properties of the different types of photons, images and tests are built on the measured intensities,  $I[S(E),d]$  and  $I_0[S(E),d]$ , the digitized version of  $N_T$  and  $N_{T0}$ . Digitization of the photon flux has two aspects: (1) a change into a more measurable energy deposition (for example, X-rays converted by a scintillator into visible light or X-rays converted by high purity germanium crystal into current) and (2) some readout of the energy deposition into a digitized quantity (bit depth). The issues for converting the X-ray energy pivot about the treatment of the incoming X-ray energy spectrum.

Scintillators differ in their sensitivity to different energy ranges and their ability to record much of the signal for high energy X-rays. On occasions, the energy windowing character of X-ray detectors is an advantage. For computed tomography the choice of scintillator directly affects the amount of *beam hardening* in the reconstructed image. This effect can be more significant for industrial computed tomography where the energies are substantially higher than in medical computed tomography. The act of digitizing the signal adds noise to the signal and can be more significant for systems involving signal amplification as part of digitization (such as image intensifiers). Independent of other considerations lower noise and higher bit depth will provide the most faithful acquisition of X-ray images in space.

The physical configuration of the detector fundamentally affects the proportions of the above quantities detected for X-ray imaging. Indeed the detector performs a sampling of the X-ray image for both the *intensity* of the spectrum and the spatial landscape of the transmission through the object. Additionally, the internal configuration of the X-ray detector determines important practical performance properties. In general, there are three types of X-ray detectors (1) highly collimated single-detector systems, (2) linear detector arrays and (3) area detector systems. By their physical arrangement each of these detector modalities treats the classes of photons in the transmission differently.

1. For the single-detector system, both the source and detector are highly collimated. This is the closest physical realization of the *idealized* ray path used in computed tomographic theory texts.
2. Linear detector arrays use collimation on both sides of the short aspect of the array. Background scatter and object scatter are much reduced from the collimation.

3. Area detectors use less collimation and are susceptible to more effects of scatter. However, area detectors make good use of the radiation envelope generated by the X-ray source and have inherent speed advantages over single detectors or linear array detectors for the same source output. For three-dimensional applications, system speed is limited by the efficient use of source output.

The best detector for the application is the choice that best meets the specific goals, which involves all kinds of practical considerations. However to clearly describe the strengths and weaknesses of specific modalities, imagers can be categorized according to five properties: (1) ratio  $N_p \cdot N_s^{-1}$  of primary to scattered photon flux, (2) detector blur, (3) number of internally scattered photons, (4) source efficiency and (5) quantum efficiency. Together these properties define important tradeoffs that result from the different detector designs (Table 1).

The greater range of choices for industrial scanners provides opportunities and tradeoffs for a particular application. For data quality, the best choice is the spectroscopy digital radiographic and computed tomographic based systems.<sup>7</sup> This is the experimental analogue of imaging with the *primary* photons. Sources of scatter are removed by collimation or from the energy resolution in the detector. However, the impact on system speed is dramatic (factor of a thousand).

Slit collimated linear detector array (LDA) systems offer the next best alternative for acquiring digital radiographic and computed tomographic data with the greatest proportion of primary photons.<sup>8</sup> The difficulty is when the focus of the application is on obtaining higher spatial resolution or full three-dimensional test data. In this case

area detectors can improve system speed by a factor of 20. However, all types of area detectors include varying amounts of scatter blur, which directly reduces the dynamic range of the system.<sup>9</sup>

Contrastive performance for any scanner is limited by the system dynamic range that varies by the scanner and by the application. The dynamic range of the system is not simply the number of bits in the detector or the number of bits subtracting the readout noise. Rather, dynamic range in a particular area of the image is bit depth minus readout noise, minus the background scatter signal in the system. For certain medium energy systems the proportion of background scatter signal can be as high as 20 percent of the detected fluence, reducing the effective dynamic range greatly. These kinds of considerations are important for scanner selection and for interpreting scans of objects with high scatter fractions.

Depending on the system, different procedures have been developed to correct for some of the effects in the measured signals resulting from the particular scanner configuration. The goal of these procedures is to process the transmission data into the *ray path* model that is the basis for image reconstruction. Industrial computed tomographic scanners can be classified according to how many processing steps are applied to transmission data before reconstruction (see Table 1). Only minimal processing is needed for single-detector spectroscopy systems, because they are the closest physical realization of the ideal *ray path*. Linear detector arrays require a bit more processing but much less than area detector arrays.

It is typical for linear detector array scanners to involve some detector balancing or detector linearity corrections. Area arrays involve at least the application

TABLE 1. Performance characteristics of different detector designs.

Detector	Ratio $N_p \cdot N_s^{-1}$ of Primary to Scattered Photons	Detector Blur	Quantity $N_s$ of Scattered Photons	Quantum Efficiency	Source Efficiency
<b>Area Array</b>					
Film	low	small	low	low	medium
Flat panel	low	small to medium	medium	high	high
Camera or scintillator with small cone	low	medium to high	high	low	high
Camera or image intensifier with large cone	medium	high	high	high	high
<b>Linear Array</b>					
Slit collimated with septa	high	small	low	high	low
Slit without septa	medium	medium to small	low	medium	low
<b>Single Detector</b>					
Single detector with spectroscopy	highest	smallest	smallest	medium	lowest

of some detector balancing correction and in some cases involve a correction for spatial distortions. Each one of these corrections can create scanning artifacts (ring artifacts or spatial distortions) in itself and can mask features in the object, depending on the location of the feature.

Fundamental issues for applications of computed tomography to industrial objects involve this recognition of artifact content in different computed tomographic scanners. All of the different types of scanners can provide quality test data for a particular application (see below). At the same time different applications are better suited for different types of scanners. As indicated above, some artifacts (for example, object scatter) are part of the transmission image in space independent of the detection scheme. A fully optimized scanner still has some artifacts that sometimes compromise test performance. At best they are benign features in the image. Also, the detector configuration can contribute its own set of artifacts that mask the imaging of object features. The importance of scanner characterization through computed tomographic phantoms (well known three-dimensional objects) cannot be overestimated. Phantoms are the main means for distinguishing artifacts from features within the object.

In summary, the different industrial digital radiographic and computed tomographic scanners can be plotted on a four axis scale as in Fig. 2. At the four axes are spatial resolution, contrast resolution, energy resolution and system speed. Experience suggests that improvement in any two of the parameters results in a worsening of at least one of the other two. More collimation will improve image contrast and with smaller apertures better spatial resolution can be obtained. However, the cost in system speed can be prohibitive for even the hottest X-ray source. Obtaining more scanning speed usually sacrifices image contrast and

resolution. Reducing the energy spectrum for the scanning makes for slower scans for most conventional X-ray sources. Making tradeoffs is required — the test designer must understand the application well enough to make the best choice.

## Practical Considerations for Digital Imaging

There are a number of practical limits on the performance of digital imagery. For spatial resolution, the performance of all techniques applied to digital images are bounded in the limit by the pixel sizes and spacing.<sup>6</sup> Features at the detector that are smaller than a detector element or on the size of the pixel spacing are difficult to image. If the spatial fidelity of the image in space is less than a digitized pixel the contrast change for the feature will be averaged over the pixel and only some fraction of the change in intensity will be recorded in that pixel. The modulation transfer function arising from a particular size of a rectangular discrete detector element has been [described in detail elsewhere](#).<sup>6</sup>

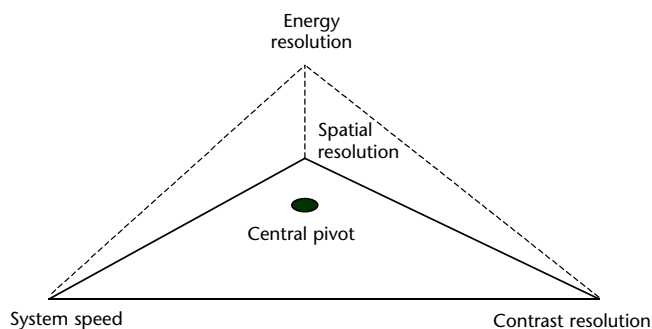
Contrastive performance is limited by the effective dynamic range of the imaging system.<sup>10</sup> Implicit in the above decomposition of the photons in space into the different types, determining the dynamic range of a system requires measurements with standards for the particular technique. The first bound for dynamic range for any image is bit depth, that is, the range of discrete digital counts possible in the detector system. Digitization generates some noise in the image, which subtracts from the total range of counts. Lastly, for the particular technique, the contrastive performance of the system is limited by the number of background scattered counts recorded by the detector.

$$(7) \quad EDR = +BD - N_R - N_{Sbk}$$

where EDR = effective dynamic range, BD = bit depth,  $N_R$  = readout noise and  $N_{Sbk}$  = background scatter. Effective dynamic range defines the best an inspector can do with a particular system for a particular technique. Actual results will likely include less performance.

From the above it would seem the limits of digital X-ray detection would be advanced by smaller pixel sizes, lower readout noise and higher bit depth. This is certainly true but there are a number of practical issues to consider. As mentioned earlier smaller pixels will require more X-ray flux. Cutting the pixel size in half in both dimensions reduces the solid angle by one fourth. For the same

**FIGURE 2.** Tradeoffs in industrial digital radiographic versus computed tomographic detectors.



detection scheme the X-ray flux needs to be four times greater to obtain equivalent signal in the smaller pixel in the same amount of time. Likewise, if more bit depth increases the readout time by some factor (this is usually the case) or if the detector cost increases by a factor, the greater dynamic range may be no bargain. On another level, if the background scatter in the particular cabinet or physical configuration is large, no increase in bit depth can provide the necessary dynamic range.

One practical technique for obtaining greater dynamic range on any image frame based system is frame averaging or summation. Readout noise is mostly random, with some exceptions. For the random components, image averaging reduces the variation leaving more bit depth for the changes in the transmission image through the object. One of the differences in systems is in the amount of frame averaging required to achieve a certain contrastive performance. These kinds of measurements have to be acquired on the particular system and the performance metered with the appropriate standards of the American Society for Testing and Materials. Frame averaging always requires more time but is a straightforward technique for increasing imaging performance. Averaging frames is not to be confused with integration time, the duration of time the sensor is exposed to the X-ray flux. Effective dynamic range is ultimately driven by the number of photons arriving at a detector position in space. In circumstances where only a small number of photons are available, frame averaging may be of marginal utility.

## PART 2. Image Analysis Techniques and Radiographic Tests

The following discussion supposes an *in-hand* digital image, which includes enough fidelity to convey something about the object. Analysis techniques divide into groups depending on the technique for final determination of the test: (1) visual evaluation of the raw image, (2) visual evaluation of a transformed image, (3) computer evaluation with a human visual checkpoint and (4) computerized automated inspection.

Also, analysis techniques get more or less complicated depending on the intrinsic characteristics of the test object: (1) discontinuity or dimensions of a feature in a single-thickness single-material section of an object, (2) discontinuity or dimensions of a feature in a single-material varying thickness section of an object, (3) discontinuity or dimensions of a feature in a single-thickness but multiple-material section of an object and (4) discontinuity or dimensions of a feature in a multiple-material multiple-thickness section of an object. The simplest type of image analysis to configure is the visual evaluation for a discontinuity in a single-material single-thickness section of an object. At the other end of the spectrum is automated inspection of a multiple-material object, through a section of multiple-material thicknesses. Image analysis techniques play a role in each of these different types of tests.

The following discussion pertains to the performance and oversight of the test. Suppliers of digital radiographic test equipment have access to an ever increasing array of image processing and image manipulation technologies. As well, the choices of modalities in digital imaging are changing rapidly. New and novel image transform and analysis algorithms are being developed equally fast for a wide variety of imaging applications. However, not all techniques developed for other imaging modalities apply well to radiographic transmission images. As described above, the content of radiometric images follows from the physical mechanisms of X-ray interaction. This results in images with some peculiar and subtle properties. These differences should be carefully noted.

Recent advances in detector technology have resulted in rather extensive *calibration* schemes for generating more radiometric images free of artifacts. Many tests are performed on *calibrated* images configured to resemble film or the output of an image intensifier. The process has become more explicit: specialized gain corrections that were the task of analog hardware have become digital transforms. However, this has introduced another variable into the whole job of system maintenance and optimization; maintain the source, maintain the detector and maintain a good set of calibration data. Because system calibration is crucial it is best to develop quick measurements of image degradation due to *calibration drift*. If planned for ahead of time, image quality indicators can be imbedded in part holders, or procedures for *salting* the test can be inserted into the process.

### Visual Enhancement of Digital Images

Image enhancement encompasses a wide variety of techniques for evaluating, manipulating and transforming images. The image enhancement for visualization is divided into two types: (1) interactive techniques and (2) transform based techniques. The first class includes the variety of interactive operations to extract pixel information, colorize the content of the image and accentuate the features of an image to enable a better visual determination.

The second class of techniques transform the image with the interest of amplifying a certain class of features, at the expense of other features in the image. In the present discussion the organizing principle for image enhancement is visualization, and quantitative properties of the enhanced image are not of central importance.

### Interactive Tools

Interactive image enhancement techniques are usually provided in *toolbars* that can be accessed on the desktop display of the control information for the software package. There are three types of toolbars of which two are important in this discussion: (1) point processing



toolbars, (2) color manipulation toolbars and (3) image modification, drawing or text annotating tool sets.

**Point Processing.** Point processing tool sets at a minimum should include pixel value query, lineout extraction, image zoom and region-of-interest extraction. With these tools, the values of the images can be directly examined.

1. The pixel query tool makes it possible to click on a position in the image and see the values or a neighborhood of values.
2. The lineout extraction tool makes it possible to draw line across a position in the image, extract the values along that line and view the extracted signal as a vector plot.
3. Image zoom tools display resampled or pixel replicated versions of an image or region of the image.

The pixel query and lineout extraction tools permit the operator to view the values in the image and make it possible to change intensity in the region of interest. In images with a lot of detail these kinds of tools can verify the nature of the intensity change in the image.

**Statistics.** Related to these tools is some statistics capability, which can calculate means and standard deviations of small or selected areas.

**Archiving.** It is advantageous if the software allows for archiving some extracted part of an image for later comparison.

Access to these tools is crucial for evaluating the state of an inspection. It is important to know the fundamental difference in pixel value that accounts for the identification of a feature. Algorithms for visual or computerized testing can highlight very small changes in pixel intensity that indicate real changes in the object. Actually looking at the numbers in the image is the only way to assess the state of the imaging system. Experience shows that most test systems degrade in the field over time. The antidote for this possibility is to be able to accurately track image quality in a rigorous way [as discussed below and elsewhere](#).

## Color Tools and Lookup Tables

Tools for manipulating the colorizing of an image fall into two categories. First, the type that manipulates the color lookup table (LUT) in the display for the computer (see Figs. 3 to 8). Second the types that rescale the intensities of the image to a particular display minimum — display maximum, selected by the user or by selecting a region of interest and thereby restrict the number of colors to a small range in the image.

The schema in Fig. 3 contains the different data structures and elements for colorizing a digital image in computer memory.

The process for viewing an image on a computer monitor involves two steps, scaling the image for copying to the display hardware and manipulating the lookup table that maps the pixel values of the image in the display hardware into colors displayed on the monitor. One added feature here is the particular state of the display as configured in the operating system. The simplest type of mapping is a linear lookup table over the minimum and maximum of the image. This kind of display is shown in Fig. 4, where the same image is displayed with three different color lookup tables. The image is a 0 to 255 linear ramp with the display minimum is set to 0, the display maximum is set to 255 (the total range of the image) and the 256 gray scale colors are mapped directly from the minimum to the maximum, one gradation of color for each value of the image.

Most color tools allow for a way to change the slope of the transfer function for applying the color map to the image

**FIGURE 3.** Different data structures and elements for colorizing of digital image in computer memory.

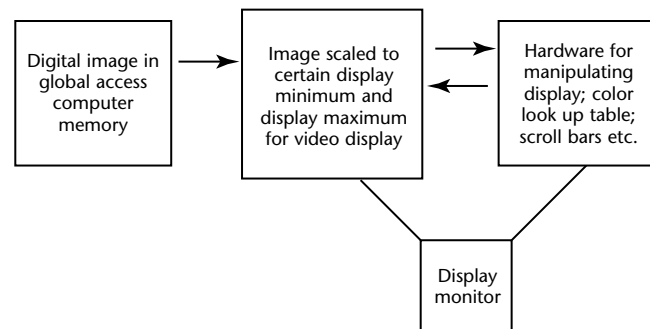


**FIGURE 4.** Linear lookup table with gamma = 1.0 applied to image (valued 0 to 255) for three different color maps.





being displayed. In Fig. 5 the display minimum has been increased, the display maximum reduced and the slope increased to 2. For this state of the color map the values in the higher ranges of the image have been set to one value, as have the values in the lower ranges. The colors are now distributed over a smaller range of the total intensity of the image allowing a more detailed look at those pixel values in the middle of the intensity range of the image. The intensity values of the image have been bundled up into a smaller set of colors. A segmentation of the image has been performed and features that differ along those segmentation boundaries are easier to view.

To illustrate the significance of this type of image enhancement Fig. 6 contains a radiograph of a synchronous dynamic random access memory (SDRAM) memory chip acquired with an amorphous silicon flat panel. The effective dynamic range of this particular

system is about 2500 to 1, with spatial resolution on the order of four line pairs per millimeter. With the slope of the transfer function set to one and the full range of colors spread over the minimum and maximum of the image a wide range of details of this electronic component can be viewed.

Choosing different lookup tables or different display minimum and display maximums can make the difference between seeing a feature or missing the feature completely. It is often the case that an automated visual evaluation will have a number of lookup tables for inspecting the different features in an image. In Fig. 7, the same image is displayed with different lookup tables (color based segmentation) applied and the operator makes a judgement as to the presence or absence of a feature. Figure 8

FIGURE 5. Linear lookup table with gamma = 2.0 applied to image (valued 0 to 255) for three different color maps.

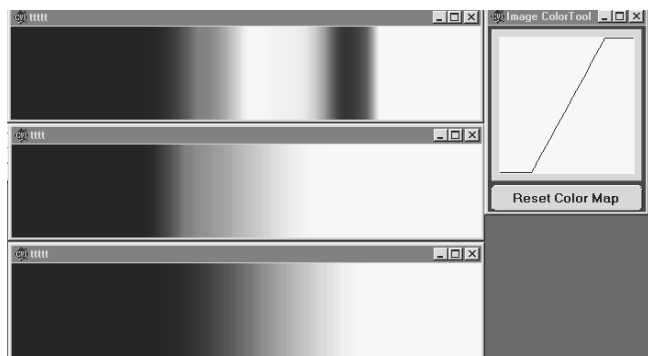


FIGURE 6. Digital image of synchronous dynamic random access memory chip with linear lookup table.



FIGURE 7. Image of synchronous dynamic random access memory chip with gamma = 2.0, linear lookup table.

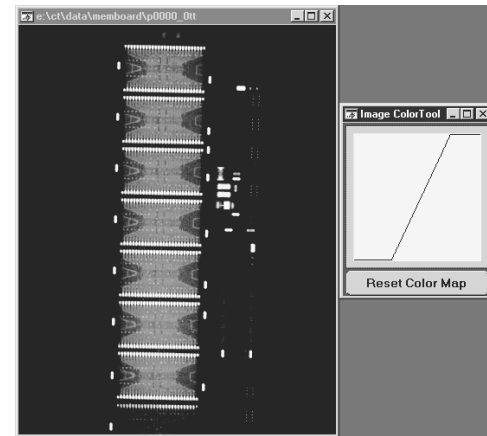
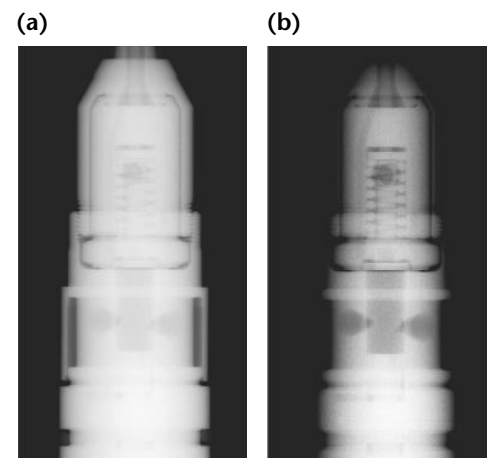


FIGURE 8. Digital radiograph of steel fuel injector with two different lookup table settings: (a) high intensity, low contrast setting; (b) high contrast setting.



shows a similar result for a different application.

Repeatability of visual evaluation depends on a variety of physical components, not to mention the alertness of the operator. Monitors can and do degrade over time. Perhaps more importantly, calibrating monitors to ensure operators in different places at different times are viewing the *same* image is not a simple task. As expected, small degradations in image quality, (that is, larger noise content) can undo the visual content of any lookup table segmented image. Similarly, growth in the spot size can lower spatial resolution, thereby masking features. For any particular test that uses the colorization of an image it is a good idea to calculate the smallest difference that accounts for the visual identification. Next, it is a good idea to calculate a local standard deviation for the image values and compare this value to the difference in the pixel values being accentuated by the lookup table.

## Image Transform Techniques

Digital images have the distinct advantage of residing in a memory location enabling direct manipulation by a wide variety of algorithms. Image transforms directly manipulate the values of the image to emphasize certain features and suppress others. Some image transforms proceed by decomposing the image into a particular *feature space* where aspects of the image are sifted for relevant information about the object. The importance of image transforms follows from their availability, the easy way in which commonplace computers can perform the operations and the interesting way transforms can easily show discontinuities or image features in certain circumstances.

Moreover, transforms can be strung together in a sequence to perform sophisticated image enhancement. Transforms can be particularly useful for exploratory analyses of digital radiographs. This is especially true for high bit depth (14 to 16 bit) digital radiographic data where everyday monitors and lookup table techniques are hard pressed to reflect the large dynamic range of the data.

In an important sense the interactive operations discussed above are simple *thresholding* transforms. The image viewed through the lookup table organizes the pixel intensities in such a way as to make all pixels lower than a certain value one color. Also, at the high end, all values greater than a certain pixel intensity are

likewise one color. The value of this threshold is an estimate of some property of the object. Consequently, this value has some real significance — in its mean and variance and error properties. These transforms are considered more explicitly below, evaluating the resultant image for information about the test object.

The present discussion classifies image transforms used for digital radiographic and computed tomographic data into five groups.

1. Low level transforms are used to calibrate or account for artifactual features in the raw image.
2. Spatially invariant transforms are applied through image kernel based processing.
3. Morphological transforms involve erosion and dilation operators.
4. Specialized numerical processing algorithms involve taking projections on a single axis of an image, shrinkwrap operations and freeman chain code algorithms for finding curvilinear boundaries.
5. There are multiscale, multiresolution transforms.

Many good texts and papers are available on these different transform options. The following illustrative examples may help to focus the investigation for any particular test at issue. Table 2 compares the transform techniques discussed below.

## Calibration and Low Level Transforms

Many properties of an X-ray image are not a result of some property of the object. The barrel distortion or *veiling glare* in image intensifier images<sup>5</sup> is a result of the inner workings of the image intensifier and is not related to the object. Bad pixels in X-ray panel images are discontinuities in the detector. Saturated pixels in charge coupled device scintillator images are stray X-rays that have come in contact with the charge coupled device chip (and this can occur from any direction). Readout lines or bands in some amorphous silicon detectors are part of the structure of the detector. Finally, intensity differences and edge distortion due to beam divergence and large cone angles are the result of the X-ray source-to-detector geometry. The artifacts in images from these sources can mask features of interest and make image interpretation difficult.

One approach to removing these types of artifacts from image data is to acquire additional data that include the source of these artifacts and divide out, subtract or calibrate out those aspects of the image. Figure 9 includes two images of nine balls of a ball grid array from a charge coupled

device camera scintillator system, one with no correction applied, one with an attenuation correction applied from an image of the radiation without the object in the field. This digital radiograph is from a system with a microfocal source and magnification of 20. Notice how the attenuation correction flattens the intensity of the beam divergence. Also notice how the transform in the logarithmic scale enables a clearer view of the higher attenuating features in the image. The attenuation correction proceeds by dividing the object image  $I_{obj}$  with the image of the radiation (no object)  $I_{rad}$  and taking the natural logarithm of the result. In terms of the digitized quantities  $I[S(E),d]$ , and  $I_o[S(E),d]$ , the attenuation image  $A$  can be defined as

$$(8) \quad A[S(E),d] = -\ln \frac{I[S(E),d]}{I_o[S(E),d]}$$

where the expression  $[S(E),d]$  merely designates the digitized  $d$  signal  $S$  of the energy  $E$ .

It is common for flat panel based detector manufacturers to provide schemes for calibrating their detectors. The calibration scheme requires the acquisition of images at differing levels of detector saturation. From these images a much clearer and more linear image is generated. Bad pixels or errant pixels are those intensity values in the image that carry no information about the object or have received a hit from the radiation. A number of reliable bad pixel removal

routines exist, most based on local neighborhood statistics for the pixels in the image. Figure 10 contains images of an aluminum casting before and after calibration and bad pixel correction.

Properly acquired calibration data can produce much clearer images. Artifacts of

FIGURE 9. Ball grid arrays: (a) raw image; (b) image after attenuation transform.

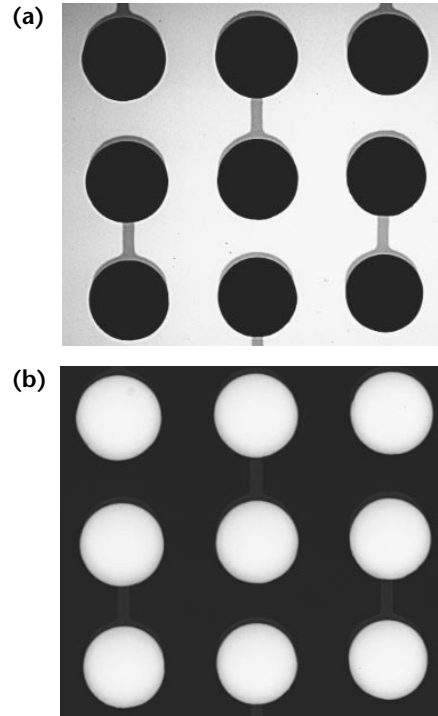


TABLE 2. Comparison of transform techniques.

Transform Technique	Resources Required for Use	Time Required for Application	Advantages for Application	Drawbacks
Spatially invariant kernel based transforms	hardware and software readily available	with specialized hardware, time required is almost insignificant	many proven choices with well known properties	will not handle spatially varying aspects of radiographs
Image calibration transforms	significant maintenance	can be substantial — must be applied to every image	eliminates troublesome artifacts correctly	errors or problems in calibration data have big impacts
Morphological operators	hardware and software readily available	more significant than standard kernels	can show important features independent of single-pixel noise	large changes to image content — will simply remove certain features from the image
Specialized numerical transforms	input requirements can be demanding	can be computer intensive and disk intensive	will address a specific analysis need in image data	algorithms are not well known and error properties are not readily available
Wavelet based transforms	software packages must be evaluated relative to application	pyramidlike application structure provides many choices	different and novel transforms of images	difficult to assess the error properties of these transforms
Multiscale multiresolution transforms	software packages must be evaluated relative to application	usually more significant than standard kernels	good decomposition of images into their component parts	difficult to assess the error properties of the different multiscale transforms

the detector are removed using the characteristic patterns within the detector. Beam divergence artifacts can be reduced by acquiring background images. When combined with the natural logarithmic transform, artifact reduction can easily reveal detail on the more attenuating parts of the object. Bad pixel corrections are usually recommended and mask the effects of troublesome pixels, enabling a clearer view of the rest of the image.

Proper calibration is both critical and problematic for tests. In many cases the best image analysis routines are the simplest. For the single-material, single-thickness test image, *thresholding* can help identify discontinuities in a straightforward and reliable way. In this type of operation a pixel value is chosen that represents the *not anomalous* intensity level and pixels on one side or the other of that value are identified indicating the presence of a discontinuity.

Figure 11 includes a calibrated image, background corrected image and processed image of the casting in Fig. 10. Without calibration the identification of a useful threshold is complicated by the beam divergence in this particular

technique. The outer edges of the image would require a different threshold than the inner parts of the image because the pixel intensities are different with the beam divergence of the X-ray source. This is even more important for some image intensifiers where distortion can account for a 30 percent change in the pixel values independent of the object. Dividing out the background image sufficiently flattens the image to enable the subsequent application of a simple threshold technique.

**FIGURE 11.** Images of casting in Fig. 10: (a) calibrated image; (b) attenuation image; (c) unsharp mask image.

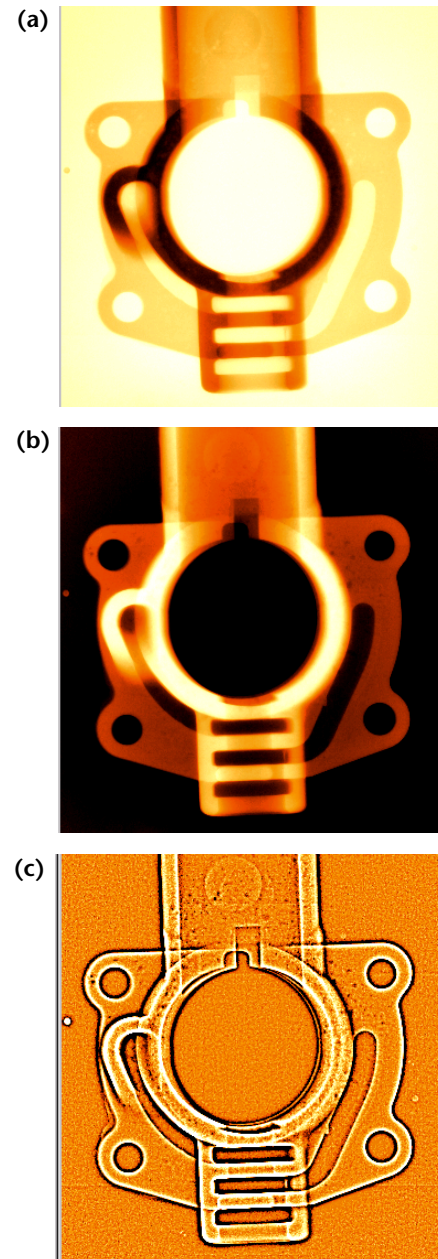
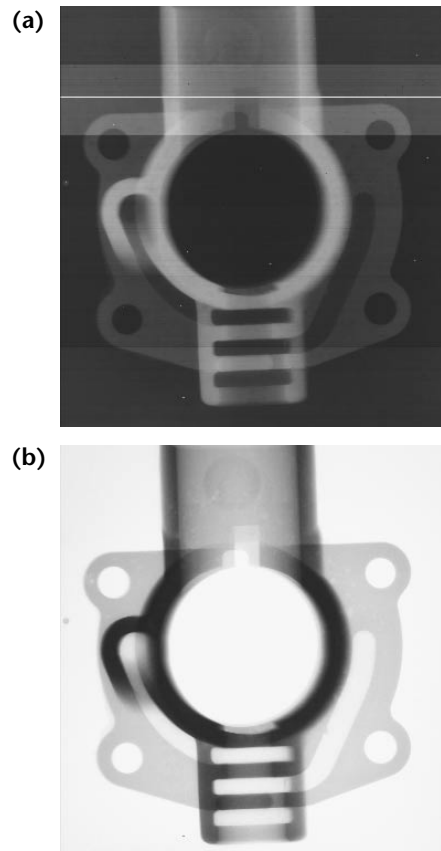


**FIGURE 10.** Aluminum casting: (a) raw flat panel image; (b) image after calibration and bad pixel correction.





Extensive calibration schemes bring their own set of issues. To acquire an image for testing it is necessary to acquire many different images. Tests take more time and resources. Both the images for testing and the calibration images need to be maintained and possibly archived to track system performance over time. More importantly, the image being used to test the object now includes the error variance of all the calibration images. Poorly acquired calibration data can ruin a test. Consequently, it pays to take very good calibration images (that is, lots of frame averages). Also, there is a limit to bad pixel removal. Clusters of pixels greater than  $3 \times 3$  are problematic. It is best to specify a limit on the number of bad pixels clusters and bad lines in the detector before purchase.

Image *thresholding* techniques are used throughout image analysis in a wide variety of contexts, on raw, calibrated and transformed images. There are two basic types: (1) fixed thresholds and (2) histogram derived thresholds. Fixed thresholds are determined from a set of considerations, usually an analysis of this class of images, and are independent of the particular image being analyzed. The value of the threshold is known before the analysis of the image. For histogram derived thresholds, the value of the threshold is not known before analysis. Rather, the histogram of the image is calculated first and a threshold value is determined from an analysis of the histogram. Consequently, the threshold will vary with the particular image. There are a variety of rules and approaches for choosing the value of the threshold from the histogram.<sup>11</sup> Histogram based techniques have the advantage of correctly changing with small intensity changes due to X-ray source fluctuations but are more complicated to develop and apply. As indicated above, the viability of thresholding techniques strongly depends on consistent quality in the analyzed images. This implicates the raw and calibration data.

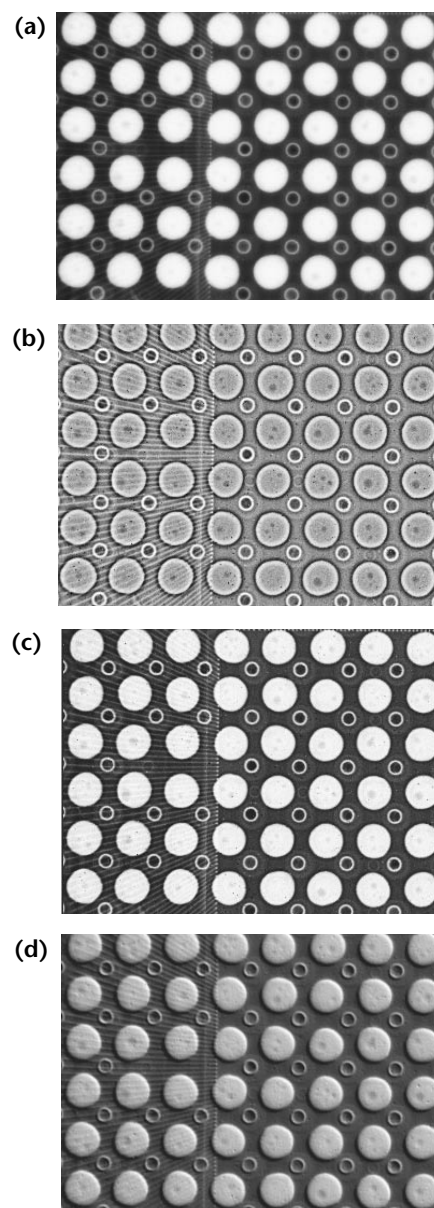
### Spatially Invariant Kernel Based Transforms

This class of image transforms afford the most variety. This is the class of image transforms covered in most signal and image processing books.<sup>12-14</sup> Within this class of transforms are the most commonly referred to routines for smoothing, edge detection and image sharpening. Figure 12 contains images of a section of a digital radiograph with transforms applied: original image, unsharp mask image, sharpened image and gradient transform image. These different representations of this image

emphasize the different aspects of this object — the position of the grid array balls, the porosity in the balls and the array of bond wires to the left of the image.

For digital radiographic imaging, lookup tables and interactive visual enhancement tools can be very time consuming on multiple-material, multiple-thickness images. Field flattening transforms can be useful in quickly inspecting different regions of an image in a single view. This is especially true for high bit depth detectors (12 bits or

**FIGURE 12.** Four different kernel based transforms of digital radiograph of electronic component: (a) original image; (b) unsharp mask image; (c) sharpened image; (d) gradient transform image.



greater). Figure 13 includes raw and *field flattened* (also called *unsharp mask* transforms) images of objects with multiple thickness and multiple materials. The transformed image provides an easier identification of indications in different regions of the objects. The output of these *field flattened* transforms can be then thresholded for more detailed or automated identification of features (see Fig. 13).

A large variety of kernel based transforms have been developed for a number of different types of radiographic testing. In most cases, these different kernels were developed to sift a particular feature from the image. As such, these different transforms apply to a certain class of images where that feature is present. Specific to radiographic data some analyses have led to kernel based transformations for removing the effects of veiling glare<sup>5</sup> and in some cases the effect of background scatter. These types of transforms have been shown to result in an image that shows features difficult to visualize with more standard techniques.

Automated and semiautomated tests often involve one or more of these transforms as one step in the process. The laplacian gaussian transforms are

commonly used for edge detection and in combination with some thresholding operation discontinuities and the edges of an object can be identified. Once edges are identified the object can then be segmented out of the image or some background feature taken out to enable clearer processing of the parts of the image of interest. Automated processing for many different visible light tests have been developed using these tools and these results are illustrated in different texts and articles.<sup>4</sup> These transforms will be mentioned again in the discussion on automated processing.

Limitations for this whole class of transforms stems from the spatially invariant character of how the transform goes about its work. The effects of each of the transforms in this class can be explained from the fourier representation of the processed image. To the extent noise is substantial in the image, emphasizing the high frequency components of the image will increase the proportion of noise in the image. To the extent the high spatial frequency content is suppressed, noise is reduced, the *edges* of the object in the image will be somewhat compromised. This difficulty can usually be addressed by acknowledging the tradeoff in processing. The fundamental problem in radiographic images is the presence of artifacts in both the high frequency and low frequency content of the image.

The various kinds of noise present in radiographic images are mostly high frequency. However, background scatter, beam hardening and object scatter are all low frequency effects. Consequently, image regions through long chords of material contain more noise and contain more blur (object scatter).

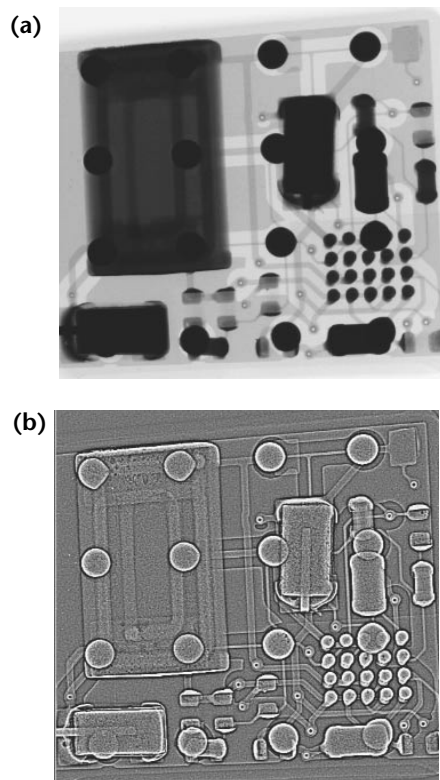
In spite of the nonspatially invariant character of some effects in radiographic images, useful kernel based transforms will continue to emerge as useful tools in many circumstances. Many software packages include highly developed options for kernel based processing. Hardware for performing the operations is commonplace and will continue to perform this kind of imaging operation with more ease and accuracy.

## Morphological Transforms

Image morphological operators are important tools for the identification of a variety of features of an image. Many good texts are available on morphological operators and image analysis.<sup>15</sup>

Single-pixel noise (also called *quantum noise*) in computed tomographic images can make the process of extracting features from computed tomographic reconstructed images difficult.<sup>3</sup> For digital

**FIGURE 13.** Electronic circuit board: (a) raw image; (b) field flattened image.





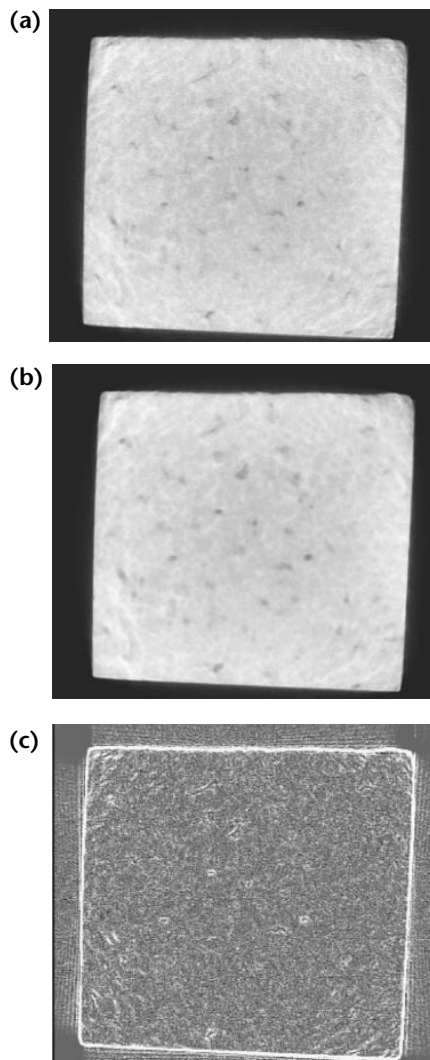
radiographic and computed tomographic data images, erosion and dilation are useful techniques for reducing the single-pixel noise, for labeling the different regions and for extracting component objects and segments of image regions from images. In a binary image, each pixel is assigned a value of one (1) or zero (0). *Dilation* of a binary image means that a pixel in the output image is a one if *any one* of its eight closest neighbors is a one in the input image. *Erosion* means that the pixel in the output image is a one if *all* of its eight neighbors are ones in the input image.

Figure 14 contains a computed tomographic slice through a metal sample for a new casting process and an image processed with  $3 \times 3$  kernel gray scale erosion dilation operators. The pixel size

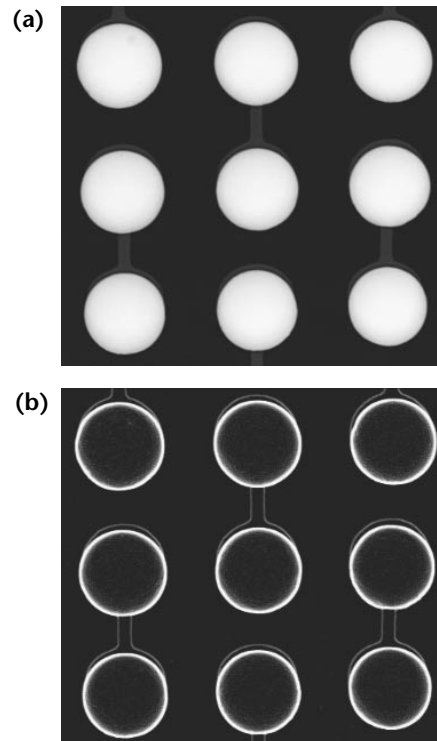
for this particular computed tomographic slice is 0.038 mm ( $1.5 \times 10^{-3}$  in.). This particular material is a mixture of low-Z and high-Z materials and a certain amount of porosity. In this case the erosion operator replaced each voxel with the minimum of the  $3 \times 3$  neighborhood around that voxel. In this way the intensities in the regions with more porosity are leveled to a fewer number of values. Also, the voxels on the edge of the porous sections are replaced with values closer to the center of the porous regions. The high-Z regions in the image are likewise leveled in intensity and connectivity in the high-Z areas is easier to identify.

Morphological operators can be connected together to perform many tasks useful in the analysis of images. Calculating or estimating boundaries of objects in digital radiographic or computed tomographic images is useful in many different contexts: assembly verification or to qualify a process or to track the movement of different components in an assembly. Subtracting an eroded image from the original, subtracting a dilated image from the original or subtracting the dilated image from an eroded image can provide a good estimate of the boundary of attenuating objects. Figure 15 contains an image of

**FIGURE 14.** Metal sample: (a) computed tomography slice; (b) gray scale morphological transform; (c) difference image.



**FIGURE 15.** Radiographs of ball grid array: (a) attenuation radiograph; (b) boundary image.



the electronic component radiograph in Fig. 9 and an image of the boundaries of the different materials generated by subtracting the eroded image from an image of the digital radiograph.

Morphological operators are used in selected steps in automated image analysis contexts. As objects get more complicated (multiple-material, multiple-thickness), automated analysis routines use a number of processing steps to generate the identification of a discontinuity or to find some feature out of tolerance in an object. Erosion and dilation operations can generate an image by showing connectivity between pixels or by grouping a number of pixels together in a binary image.

Issues surrounding the application of morphological operators depend on the test. Erosion and dilation operators can significantly change the values of the pixels in the transformed image. For larger kernels (greater than  $3 \times 3$ ), smaller features are completely removed. Although this can be crucial for an analysis of larger features in an image, it is important to be aware of just what image content was left behind. It is best when the motivation for the image analysis can be developed into a determination of a kernel size and a justification applied to the extracted image content. It is also useful if a residual image is calculated and saved to track the features excluded.

### Specialized Numerical Transforms

A number of specialized image operations have been developed for particular tasks common in image analysis of digital radiographic data. Only a few of the possibilities are mentioned here but each addresses particular problems in radiographic tests. Also, each showcases some possibilities of digital data.

In many circumstances the region of the object to be tested sits on top of a structure in the material that is not of interest to the test. A number of approaches have been developed to subtract out the structure independent of the object to be tested. One class of these techniques involves curve fitting the structure with some function that leaves the important part of the test alone. In one example of this technique, third degree polynomials were used to subtract out the underlying structure for the automated testing of welds in railroad rails<sup>16</sup> (see the discussion of automatic discontinuity recognition for an example of subtracting trends). A second approach involves using prior knowledge of the discontinuity types to generate synthetic profiles or templates of discontinuities for extraction or identification of

discontinuity signatures within a structure of an object.<sup>17,18</sup>

Weld testing often involves features organized in a vertical or horizontal dimension of the digital radiograph. In some of these circumstances it can be an advantage to sum the contents of the image into a single vector by averaging the rows or columns of a region of the digital image. The average vector has better signal to noise properties than the individual rows (columns) of the image and it can turn out that the signature of the discontinuities are preserved in the single vector. This vector can be used for correlation to signatures of discontinuities or can be decomposed into suspect discontinuity sites.

A number of radiographic tests involve numbers of the same structures organized in some way in the image. Sometimes this is by design where a large area detector is used to test large numbers of small objects (that is, film radiographs of spark plugs, small aluminum castings and other objects). In these circumstances it is an advantage if the computer can pick the objects out of the image and either present them for analysis or provide some analysis of the constituent parts.

One such example are the ball grid array images in Figs. 9, 12 and 15. In these images the constituent balls are a central component for the test. Blob analysis<sup>19</sup> can be an important tool for the analysis of these images. This algorithm finds contiguous groups of pixels satisfying a pixel intensity threshold, then identifies and extracts those segments for further processing. For the automated analysis of ball grid array images this routine finds the balls in the circuit board and extracts the image segments from the rest of the image. These image segments can then be subsequently passed on to other analysis algorithms.

In some tests, neither segmentation or pixel classification is the important feature for the analysis; rather the boundary of an object or object component is central to the test. This kind of analysis is applied more often to computed tomographic reconstructed images where the boundaries of object components are not obscured by other structures in the path of the X-rays. As such these techniques can be applied to two-dimensional or three-dimensional data. A number of different techniques have been developed to find boundaries in complicated objects.

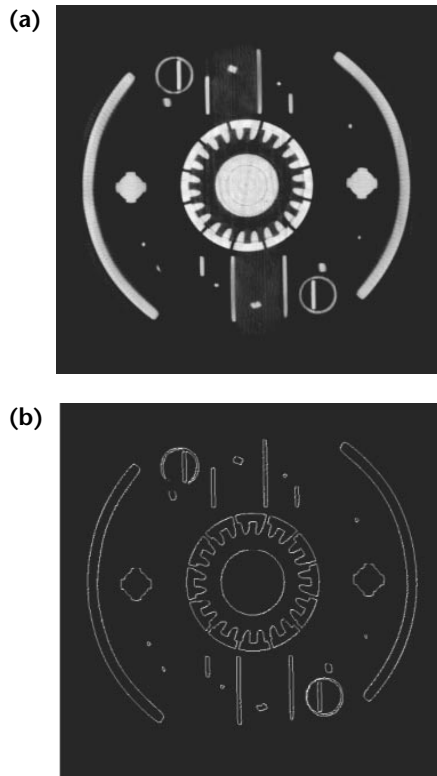
This operation is different than the above transforms. By using other transforms edges of high attenuating or low attenuating materials can be highlighted. Likewise, with morphological transforms images can be generated that

show the outline of material boundaries. In these transforms the output is not an image but a set of boundary points (sometimes referred to as a *point cloud*).

*Shrinkwrap* codes are one way to estimate material boundaries in computed tomographic scans. The routines work by expanding some kind of wave front through the pixels or voxels in the image; then at a particular threshold the expansion stops, resulting in a set of coordinates measuring where the wave front stopped. There are different means for expanding the wave front and different means for controlling the positions for stopping around curved surfaces.

A second type of technique used is the *freeman chain code*, which finds a boundary point and then uses a circular *sewing* operation to find the next boundary point and this process continues until the original boundary point is found. This type of routine can find boundaries of many different types of objects. Figure 16 illustrates the operation of this code applied to the computed tomographic scan of an automotive part.

**FIGURE 16.** Computed tomographic images: (a) shrink wrap routine applied; (b) freeman chain code routine applied.



## Advanced Transforms for Multiscale, Multiresolution Analysis

The need for a different kind of image analysis has arisen out of the different problems encountered by the above techniques. Just how to determine the diameter of the kernels used is a matter of some controversy in medical and industrial imaging. The question of optimal kernel size is difficult within a particular application and completely intractable across different tests. Digital images are getting deeper in bit depth, possess greater latitude, are lower in noise, are larger in extent (sometimes larger than any available monitor) and can include substantial spatial resolution. Viewing these images on devices having much less dynamic range is a challenge. Techniques covered above each glean some set of features from the image at the expense of others. Unsharp mask transforms highlight the high frequency content of the image but can amplify the noise to overwhelm the low contrast features. It is often the case that the choice of kernel, lookup table or imaging transform is a compromise between competing and legitimate testing requirements and the losses in any one choice can be significant.

The process in multiscale, multiresolution analysis is one way of dealing with the image content at different scales in a more explicit fashion. The first step involves transforming the original image into a family of images. Each of the decomposed images contains a subband of the scale and contrast space of the image. In different terms, the image is split into *componentlike* images, each component represents a class of features of the image at a particular scale. The *component images* can then be manipulated, transformed or amplified and then recombined to obtain a transformed image with a contrastive performance matching the viewing range of the monitor or making the best of the contrast in the image (taking into account the noise). The low contrast features of the image, mostly found in some of the component images can be amplified somewhat independently of the noise content. Figure 17 is a pictorial representation of this process used in a commercial image enhancement process.<sup>20</sup>

Wavelet based transforms also feature this concept of decomposing images into different *scales* and *resolutions*. Although this varies with the particulars of the wavelet generating transform, different numbers of subimages are obtained from a particular transform.<sup>21</sup> Depending on the image each subimage contains

information at a different scale or in a different region. Matched filters can be applied to the sets of subimages, or filters can be applied that are derived from templates of an object of interest.<sup>22</sup> The subimages are combined and the inverse transform results in a transformed image.

*Multiscale, multiresolution analysis* provides the best context for explicit manipulation of both the spatial content and the contrastive information in a particular image. The transformed image is built up of the weighted and transformed subimages and this provides a means for enhancing images and taking into account the radiation contrast of a set of features. A number of different studies have shown the benefit of these transforms for object identification and optimal image contrast.

All of this image manipulation can be implemented in a compact and computationally efficient way. Once the initial transform is complete the bulk of the computations are performed on smaller, less complicated pieces of the image. This aspect of the analysis can be a big advantage for images with large numbers of pixels (that is,  $3000 \times 2000$ ), where even fast computers are hard pressed to repeatedly process the image at its full size.

The benefits of multiscale, multiresolution analysis notwithstanding, there are issues with this class of techniques. These techniques may provide the best means for managing the tradeoff inherent in showing high bit depth images on monitors with much less range or in providing a means for extracting low contrast features without losing edge

definition. However, making the most of image contrast for display purposes is different from reliably indicating the size or even the presence of a discontinuity. Low signal-to-noise images make poor input data for qualitative work. Compromises like these exist at all levels of the image formation and analysis process (see Fig. 2).

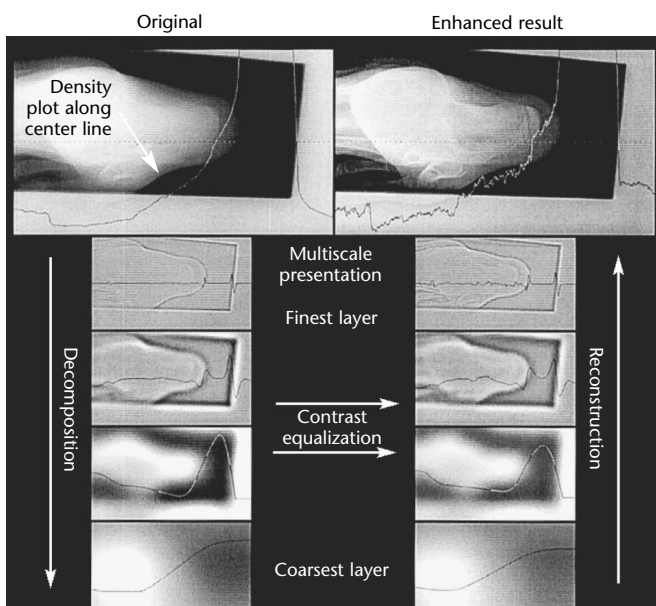
Furthermore, at this juncture the statistical properties of these transforms are not well understood. Low contrast features wrestled out of the noise have a tendency to disappear with changes in the scanner. As indicated above, image formation is a statistical process. Radiographic scanners degrade in the field over time. Running a large number of samples through a scanner and an algorithm to establish the error properties of a routine may miss the point.

### Subtleties of Radiographic Images

Transmission images from X-ray sources include a number of subtle features not found in other imaging modalities. As explained above, each pixel in a radiographic image includes content from the scatter in the detector and scatter in the object. Neither the scatter profile of the detector nor the scatter profile for the object at that particular orientation to the X-rays is necessarily spatially invariant. Perhaps more important, these effects occupy both high and low spatial frequencies in the image. Figure 18 includes an image of a step wedge from a camera scintillator system and a lineout through the step wedge. This particular radiograph was acquired with the step wedge at 1.17 m (46 in.) from the source whereas the detector was 1.22 m (48 in.) from the X-ray source. The wedge was shot at 200 kV peak to ensure good transmission through all the steps in this wedge. The step sizes are 3.175 mm (0.125 in.) and the image has been processed by dividing out the background image and taking the natural logarithm of the result (units of the image are in attenuation units).

Notice the sharpness of the edges for the different levels in the step wedge and the noise levels in the steps as indicated in the lineout. The crispness of the edges decreases and the noise over the flat portions of the steps increases with attenuation. The noise levels are easily explained by the fewer photons transmitted through the steps (and this is a circumstance in which there is ample transmission through each of the steps). The more blurry edges and some of the increased noise can be explained as greater proportions of background and object scatter in the pixels behind the thicker sections of aluminum. Also, notice

FIGURE 17. Multiresolution multiscale image enhancement.





the nonlinearity in the relative attenuation value of each step thickness.

Figure 19 contains the image of the wedge and the histogram of the image. This is another way of showing the same result. Notice the spacing between the peaks and the width of each peak. As the attenuation increases, the noise in the flat sections of the wedges also increases as shown by the larger width of the peaks. Also, the spacing of the peaks gets slightly closer together with larger attenuation values. This is the combined effect of small amounts of scatter in the object, scatter in the detector and beam hardening.

Kernel based processing techniques, applied to the entire image, operate on all the spatial frequencies in an image in a uniform fashion (spatial invariance). As shown in many texts,<sup>23</sup> the effects of any particular kernel based transform can be evaluated from the fourier representation of the transform. From this representation it can be seen just what gets multiplied to what spatial components of an image, the sharp features of an image (high frequency) and the smoother more

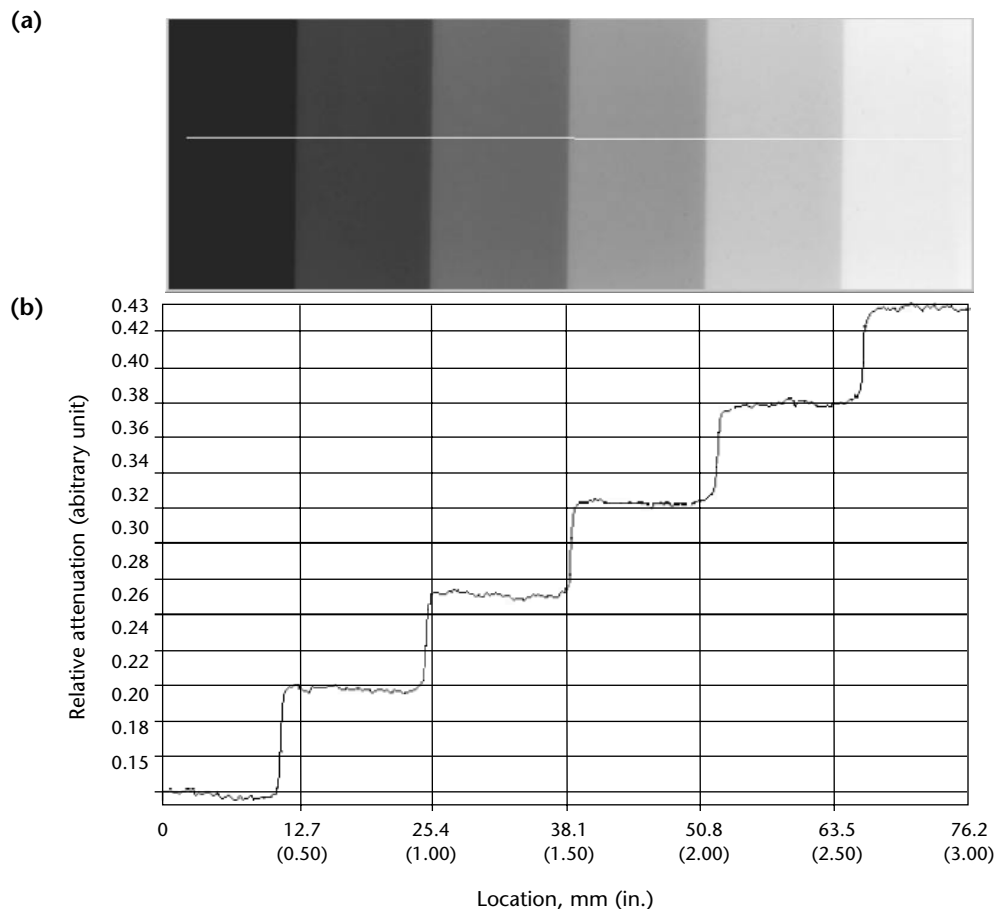
constant intensity parts of the image (low frequency).

The problem with these techniques for radiometric transmission images is the artifactual image content at nearly all frequency components of the image. Techniques that apply processing kernels to the entire image to enhance a particular feature will invariably do the wrong thing to other components in the image.

The subtleties of digital radiographic images mentioned here do not make these transforms a uniformly bad choice for processing and analysis. Many successful processing schemes have been developed for digital radiographs and computed tomography images based on these techniques. The most important aspects of particular image transforms are their limitations. All transforms emphasize some features and suppress or eliminate others. Depending on the nature of the test this selectivity can be good or bad.

The point is to understand the nature of why some procedures do not perform and how this might relate to the nature of these images. A technique developed for reflected light images is not always a good

FIGURE 18. Step wedge: (a) attenuation image; (b) lineout through wedge.



choice for transmission images. There is no substitute for thorough testing of image analysis operations. Thoroughness entails running a sufficient number of images of different types through a particular algorithm to enable some statistical evaluation of image analysis performance.

Although it is typical to perform a variety of tests for any algorithm this strategy may have limitations. It is often the case that digital radiographic or computed tomographic systems degrade in the field. There are a number of reasons for this degradation. Scintillators become less sensitive over time and produce less light. Cameras, intensifier tubes and amorphous panels become increasingly noisy with extensive use.

The degradation is not fast but is persistent. Consequently, the images fed to an algorithm when the system is fresh may not be typical of the images fed to the system after it has been operating for a while.

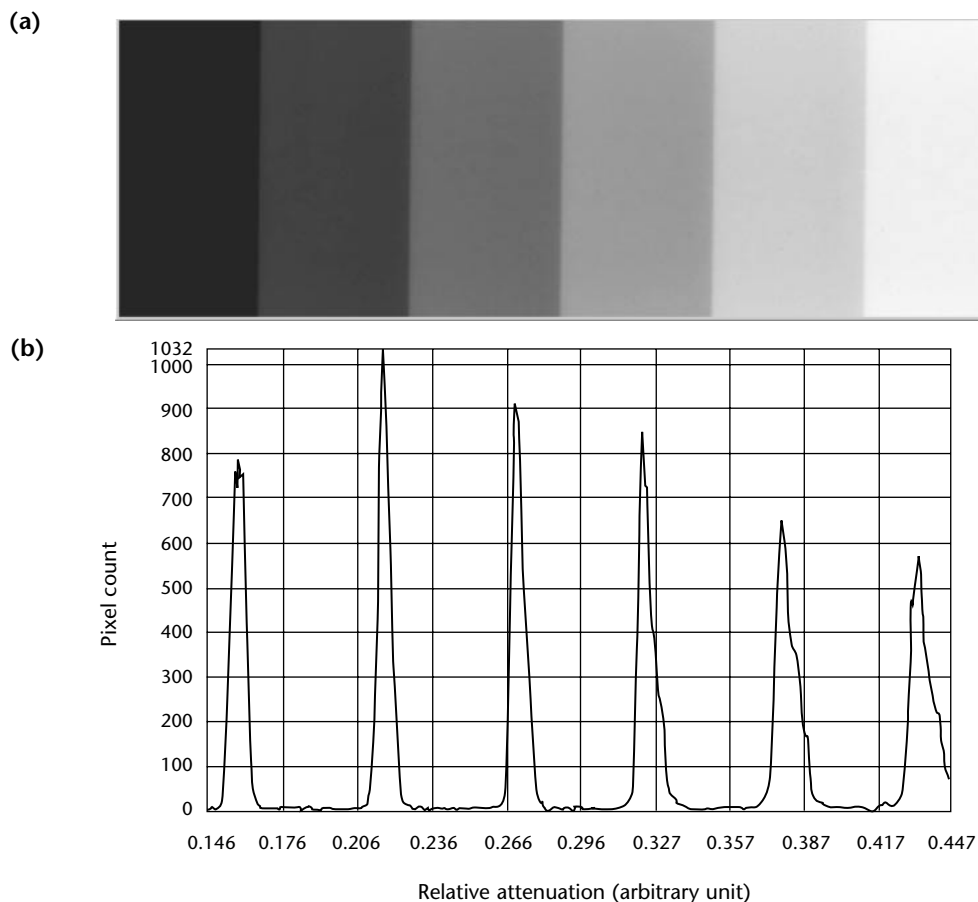
Simulated radiographic images can help the operator to assess the degradation. A set of simulated images

like the features to be detected or measured can be produced and later degraded with computer generated noise and blur in a precise way without running the system. In this way the point at which the algorithm stops working can be determined. By increasing the amount of noise and blur in a particular image in a graduated and precise way the effects likely to occur over time can be estimated and maintenance intervals adjusted.

## Dimensional Measurements

There are a variety of techniques for obtaining dimensional measurements from digital radiographic or computerized tomographic images. Three types of techniques are common: (1) interactive point and click procedures, (2) lineout extraction techniques with some algorithm applied to the lineout after extraction from the image and (3) boundary identification techniques for contour estimation. The first two types of

FIGURE 19. Step wedge: (a) attenuation image; (b) histogram of image.





techniques are common for obtaining wall thickness measurements, although the third set of techniques are used mostly in obtaining boundaries from three-dimensional computed tomographic data. All three of these different techniques produce a dimensional measurement of a component in an image, with more or less accuracy.

### Application to Copper Pipe

To illustrate these techniques and compare accuracy a flat panel computed

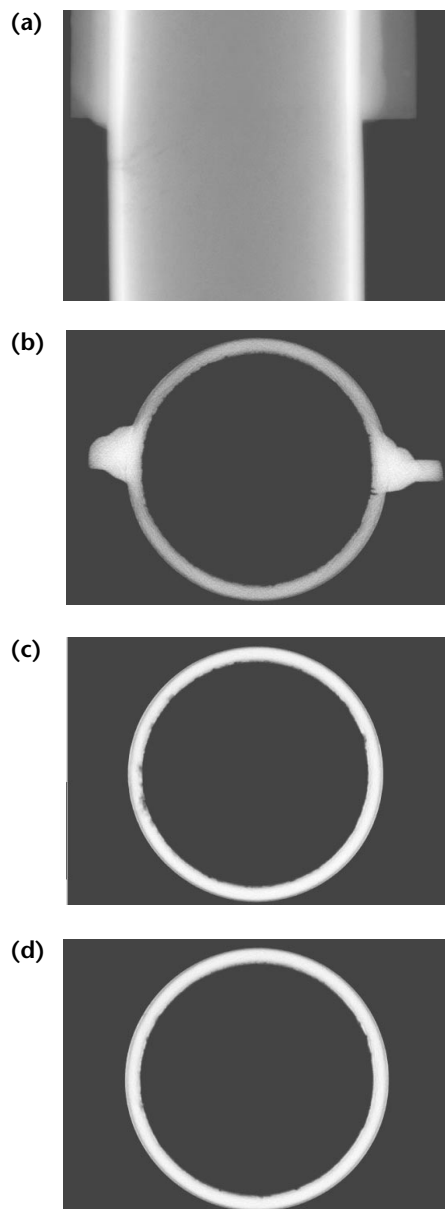
tomographic data set for a 75 mm (3 in.) outside diameter copper pipe was evaluated. This type of data set includes both digital radiographic and computed tomographic data and more importantly allows easy access for a physical measurement of the wall thickness as a reference. The data consist of 360 digital radiographic images acquired with a  $300 \times 400$  mm ( $12 \times 16$  in.) flat panel and a 9 MeV linear accelerator. The computed tomographic scan was performed with rotational scanning only. The detector was 6 m (20 ft) away from the source and the object 0.50 m (20 in.) away from the detector.

Digital radiographic images were calibrated with the *two-gain coefficient* technique and then processed into attenuation radiographs by dividing out the background image in the logarithmic scale. For this scan the digital radiographic data generate a volume of computed tomographic data with width and height roughly corresponding to the width and height of the digital radiographs (the computed tomographic data set will be a little smaller because of magnification but this is small in this data set). Figure 20 contains digital radiographic and computed tomographic images from this scan; these images are adduced in subsequent discussion.

Interactive point and click techniques measure the number of pixels between two clicks of a mouse or pointer. For each click the closest  $x,y$  coordinate is returned from the interaction and the cartesian distance calculated between the two sets of  $x,y$  pairs of points. After this operation, the pixel distance is converted to object distance by multiplying by the pixel size at that magnification of the object. For digital radiographic images orientation is important: only walls 90 degrees to the X-ray beam-to-detector envelope can be measured. The goal for this operation is to pick the position of maximum chord length (the position of the inner wall) and the position of the outer edge of the part (the outer boundary). For computed tomographic images the goal is simply to pick the inner and outer edges.

Using these techniques a number of measurements of wall thickness were taken on the digital radiograph and computed tomographic slices in Fig. 20. The positions of these measurements are indicated in Fig. 21 (these are not the lines drawn for the measurements — just indicators of the position). Because there is substantial porosity in this particular sample an explicit attempt was made to avoid taking computed tomographic measurements in locations of porosity or corrosion on the inner wall. Six different measurements of wall thickness were made for the digital radiographic and

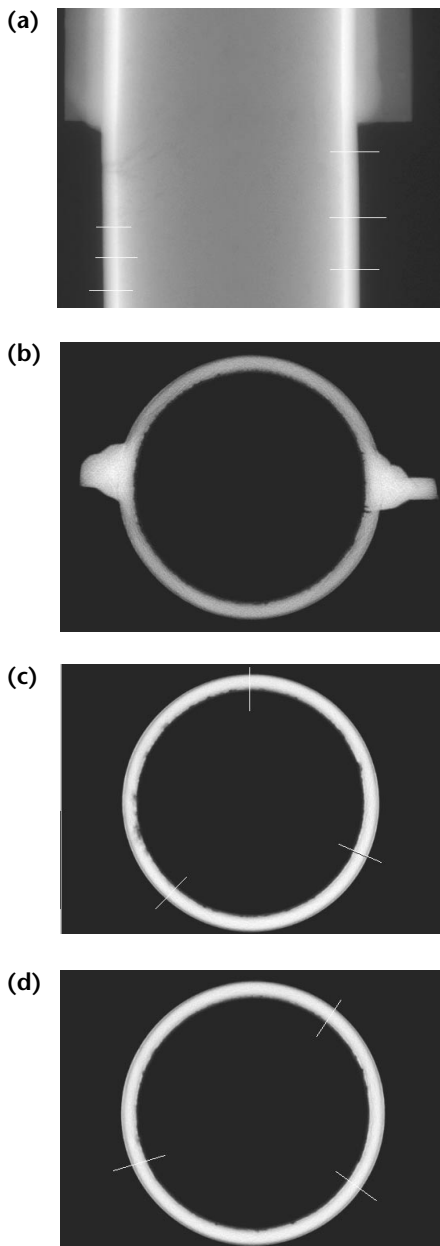
**FIGURE 20.** Digital radiograph and computed tomographic slices of copper pipe: (a) digital radiograph; (b) cross section; (c) cross section; (d) cross section.



computed tomographic data. Results for the digital radiographic measurements were 4.53, 4.65, 4.76, 4.88, 4.76 and 4.65 mm (0.178, 0.183, 0.187, 0.192, 0.187 and 0.183 in.). Results for the computed tomographic measurements are 4.332, 4.55, 4.3, 4.13, 4.46 and 4.36 mm (0.1706, 0.179, 0.169, 0.163, 0.176 and 0.172 in.).

Error variance for measurements performed with point-and-click

**FIGURE 21.** Digital radiographic image and computed tomographic slices of copper pipe with locations of measurements identified: (a) digital radiograph; (b) cross section; (c) cross section; (d) cross section.



techniques depend strongly on the accuracy of the operator, precision of the measurements of pixel size at the object and somewhat on pixel size itself. In the hands of a seasoned operator these techniques can produce accurate results. Alternatively, cavalier clicks on the image result in sloppy estimates and lack of precision. It is best to train operators with a standards set of images, with different levels of noise, contrastive performance and spatial resolution.

Pixel size at the object is determined from a measurement of the pixel size at the detector and the X-ray magnification or from the radiograph of an object that includes a dimensional standard. It is best when both techniques are used to produce an estimate of pixel size at the object and used for comparison. For digital data, the operation of pointing-and-clicking will only be good to a pixel, because everything is in terms of pixels. Given these sources of error, it's difficult to understand how this measurement can be better than a couple of pixels, with substantial variation from operator to operator. At the same time, for some tests, this accuracy may be good enough.

A second more rigorous technique involves the extraction of a lineout across the feature and then an analysis of that lineout. The typical example of this type of approach is for measuring a wall thickness from a computed tomographic slice image of a cylinder. There are three steps.

1. The user draws a lineout across the wall, taking care to orient the lineout as perpendicular to the wall as possible.
2. The extracted lineout is processed with a code combining derivative calculation and fitting.
3. The pixel distance between the selected positions in the lineout are calculated and the physical size of the pixel is applied to the pixel distance.

Knowing the physical pixel size is still a source of measurement error in this technique. Also, not orienting the lineout perpendicular to the wall to be measured will result in some variability from measurement to measurement. Lastly, the noise in the lineout can be problematic for the processing applied to the lineout. Most processing schemes apply a derivative filter to the lineout, resulting in two peaks, each measuring the line spread function of the system. The two peaks are then put through some kind of fitting code to determine the center of the peak and the distance between the two fitted values is the pixel distance. This technique was applied to the different lineouts around the wall in the computed

tomographic scan and resulted in measurements with an average of 4.3 mm (0.17 in.). When properly extracted, these techniques can produce subpixel accuracy for wall thicknesses imaged clearly by computed tomographic scanners.

Figures 22 and 23 display one of the computed tomographic slices from the copper pipe scan and illustrate the results of transforming and fitting the vector drawn across the wall of the copper pipe.

The last technique — in this case, a class of techniques — builds on some of the transform techniques mentioned above. Any transforms mentioned that can convert the inner and the outer edges of the computed tomographic data to boundary measurements qualify as a dimensioning techniques. For example the shrinkwrap, freeman chain code algorithm was applied to one of the computed tomographic slices in the copper pipe data set. Figure 24 shows the results of the application of this algorithm to this data set. Using these boundary points and taking distances the average wall thickness was measured at 4.45 mm (0.175 in.).

It is hard to assess the accuracy of the different techniques. A variety of measurements were acquired around the pipe with a micrometer. The physically measured thickness values ranged from 4.2 to 4.7 mm (0.165 to 0.185 in.). This object is a copper pipe with substantial pitting and corrosion on its inner wall. The corrosion can be seen in the computed tomographic scans. The measurements of the wall thickness from the digital radiographic images are hard pressed to account for the loss of material on the inner wall and this explains why the measurements are a little high.

Indeed, the very nature of the integration over the tangent to the wall performed by the radiation is an averaging operation. The computed tomographic point-and-click measurements were a little higher than the fitted measurements because of the subpixel estimation done by the nonlinear fitting to the lineout. The average measurements from the boundary image are close to all the other computed tomographic measurements. On a point by point basis the boundary image techniques used in this comparison overestimate the wall thickness because of the *stopping at a pixel boundary* inherent in the routine.

This class of techniques generates sets of boundary points from three-dimensional computed tomographic volumes. The sets can be used in a variety of applications. The boundary points can be used in the process of generating three-dimensional solid models, computer aided design and computer aided

manufacture models or models can be input to finite element analysis mesh generating codes. It is important to emphasize here that these sets of boundary points (often referred to as *point clouds*) are performing a measurement operation and have an error variance possibly greater than the above techniques and the error variance is not constant throughout the computed tomographic volume data.

There is a special character to blurs in computed tomographic reconstructed images. It is usually the case that the inner edges of computed tomographic reconstructed images include more blur than the outside edges. The reason for this is in the nature of X-ray imaging, the beam that is imaging the inner edges has more scatter than the beam that images the outer edges. This *greater blur on the inside edges* is less true for highly

FIGURE 22. Computed tomographic slice with lineout indicated and line trace with derivative displayed.

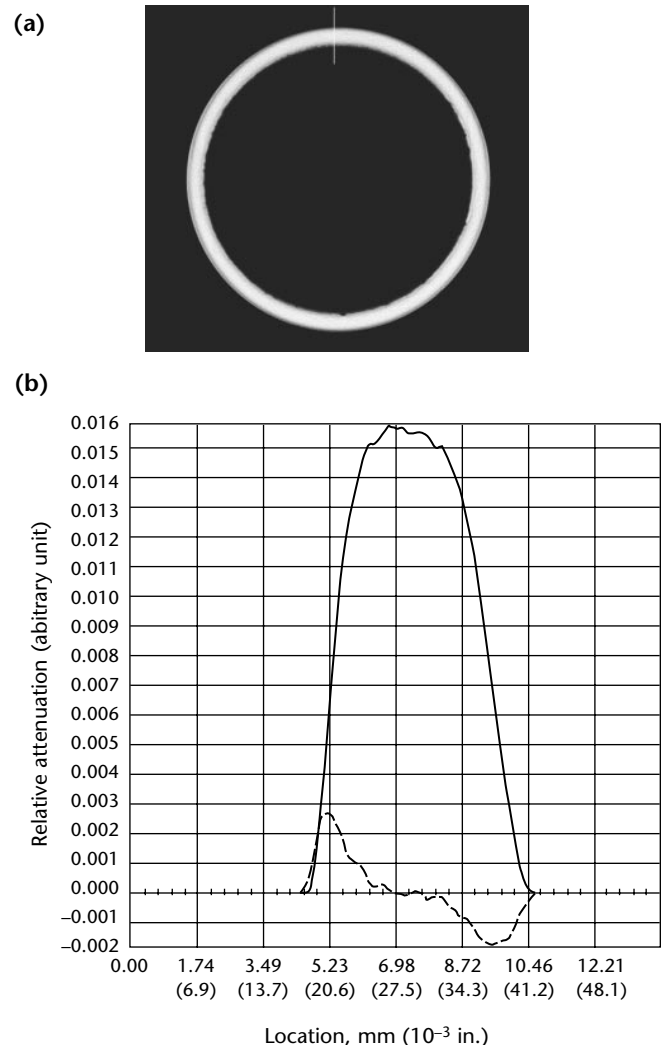
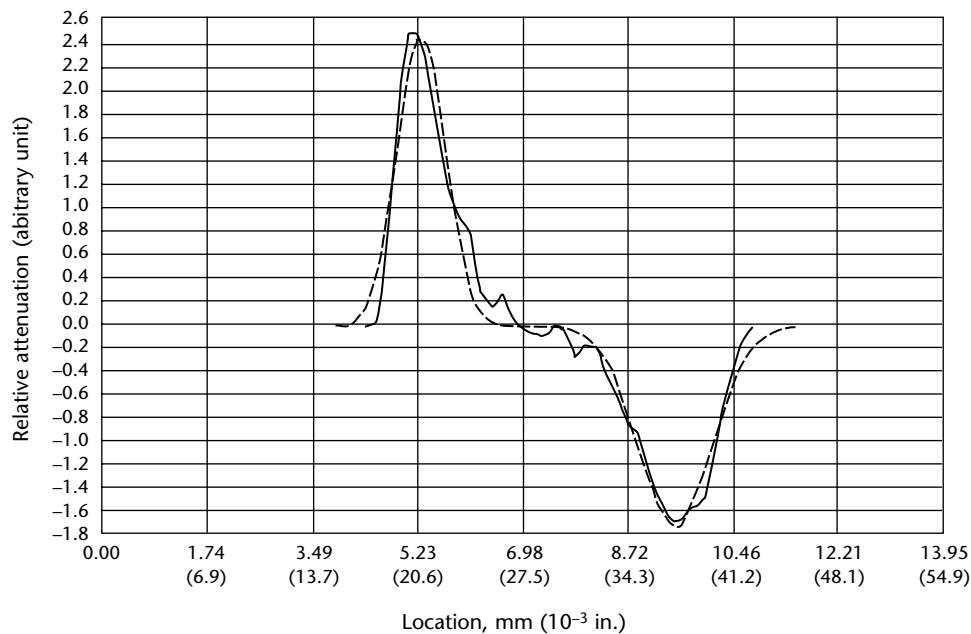


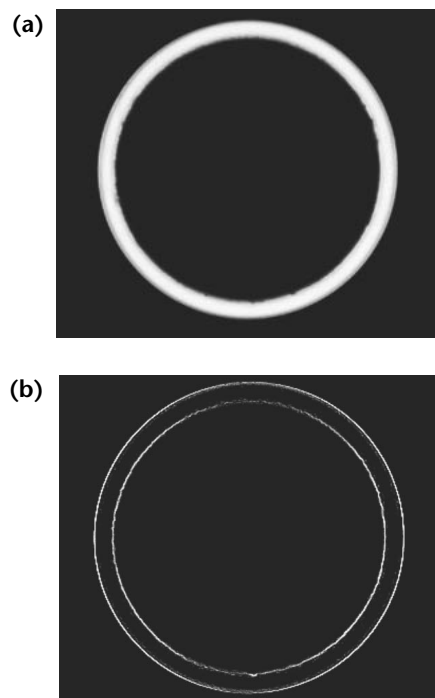
FIGURE 23. Derivative of line trace and levalier-marquart gaussian fit.



collimated computed tomographic scanners and more true for area detector scanners with less collimation, that is, area detector based scanners. This property is present in the copper pipe data and can be seen in the skew of the lineouts on the inner edge. Consequently thickness of walls and inner features can easily be overestimated.

The problem with all of these techniques is the absence of a *real* error bar connected to any of these measurements. All of the measurements are interesting and suggestive. Also, some studies have been performed comparing lots of computed tomographic wall thickness measurements to other modalities.<sup>7</sup> In the first case computed tomographic measurements were found to be lacking in measurement accuracy, in the second the accuracy was equal to any of the other techniques used. Both of these studies were conducted on real objects, not standards blocks (although standards blocks were used in the calibration). In each case it was very difficult to get a physical measurement of a physically concealed feature. For computed tomographic dimensional measurements to emerge from an interesting technique to a metrology tool more quantitative investigations are necessary. This problem gets worse for automated three-dimensional tools that find the boundaries of inner walls and attribute a physical significance to an estimate of unknown accuracy.

FIGURE 24. Cross section images; (a) computed tomographic slice; (b) freeman-chain code estimate of inner and outer boundaries.



## PART 3. Automated Testing Techniques

### Need for Automated Systems

The need for fast tests, the added cost of operators and the known issues with variability in operator scoring have emphasized the need for automated test systems. Improvements in computer speeds and increased detector sensitivity have made automated techniques a good possibility for many applications.

Despite the relatively large bibliography of articles on automated discontinuity recognition techniques, the number of successful automated discontinuity recognition systems remains small. There are a variety of reasons for this, many of which are not part of the image analysis for a test. Design changes and changes in criteria are increasingly common in manufacturing operations. The effective lifetime for parts and components is getting smaller. In the automotive industry, continuous quality improvement programs and weight reduction programs can change the properties of a component to the point where a new test is required. Developing *robust* test techniques can be expensive in time and resources. For nondestructive testing systems, it is difficult to be responsive to every new change in a part or component. Consequently, there is a disinclination to enter expensive development programs with short payoff lifetimes.

Automated X-ray nondestructive testing systems face a growing list of expectations. Fielded systems in manufacturing operations are increasingly more connected to the other systems on the factory floor. Statistical process control functions are part of this connection with each component system reporting status and results. X-ray nondestructive testing systems are not always as connected as other systems.

Furthermore, reporting functions within a system are not common and maintenance intervals can be problematic. It is rare for radiographic nondestructive testing systems to include recognition of an *error variance* in their measurements even though these measurements include substantial variability. Radiographic nondestructive testing systems are often treated as a special case and this is

expensive in both factory floor time and part flow. Radiographic nondestructive testing systems will be a mature part of manufacturing operations when they more easily fit into factory operations and possess the same reliability for both the automated testing and connectivity as other systems.

In spite of all of these issues the demand for automatic discontinuity recognition systems is high and growing. The details of any particular automatic discontinuity recognition system are usually proprietary. What follows is an overview of the elements in most automatic discontinuity recognition routines followed by an example and recommendations for fielding and maintenance.

### Discontinuity Recognition

Automated testing techniques are intentionally application specific. Just as it is difficult to decide on *one kernel diameter*, no single automatic discontinuity recognition routine works for all tests. Tests involving penetrating radiation can be classified into four classes: (1) single material, single thickness, (2) single material, multiple thickness, (3) multiple material, single thickness and (4) multiple material, multiple thickness. A second layering on this classification is whether the test involves digital radiography or computed tomography. Automatic discontinuity recognition routines are more common for the first two types of tests and much more common for digital radiography than computed tomographic systems.

Automatic discontinuity recognition routines include a similar number of steps. Underneath each system is some definition of a suspect pixel within the object.

1. The first step usually involves *subtracting out* or *extracting out* the portions of the object that get in the way of clearly identifying the discontinuity. In digital radiography this is usually referred to as *trend removal* or *subtracting out* the object. Other algorithms compare indication signals to some template of an acceptable object at this point.



2. After trend removal the processed image is in the best scale to identify the discontinuity. Some segmentation routine is applied at this point, usually guided by a threshold, to pick out the pixels that are part of some segment of a discontinuity.
3. Next, a connectivity routine is applied to bundle pixels that are close together and have been identified as anomalous. At the end of this step a binary image of the anomalous and not anomalous pieces of the radiograph can be generated to show the results of the operation.
4. Lastly, the discontinuity criteria are applied to the different segments of *discontinuity* locations and decisions are made about whether the object is *good* or *bad*.

The different steps in automatic discontinuity recognition routines are built up from the transforms covered above. The same *thresholding* transforms are used throughout the process on the

processed images. Connectivity analysis routines like *blob analysis* mentioned above can be useful as well. In different applications *trend removal* is performed by a least squares fit to a simple function to take out the changing lengths in the part at that place. The automatic discontinuity recognition routine is the sum of all the steps combined and the robustness of the entire routine is a function of the match between the data presented and the routines used.

## Evaluation of Indications

### Application to Pipe Welds

To illustrate this process, a technique similar to work presented by Doering and Basart<sup>16</sup> is applied to digital radiographs of pipe welds. In this case the welds are in small tubes, 25 mm (1.0 in.) outside diameter. Figure 25 contains two digital

FIGURE 25. Tube weld: (a) 0 degree view; (b) 90 degree view.

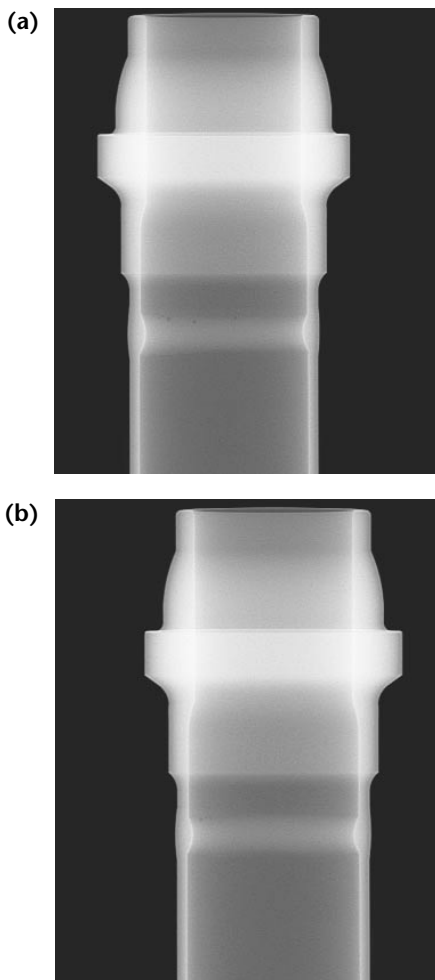
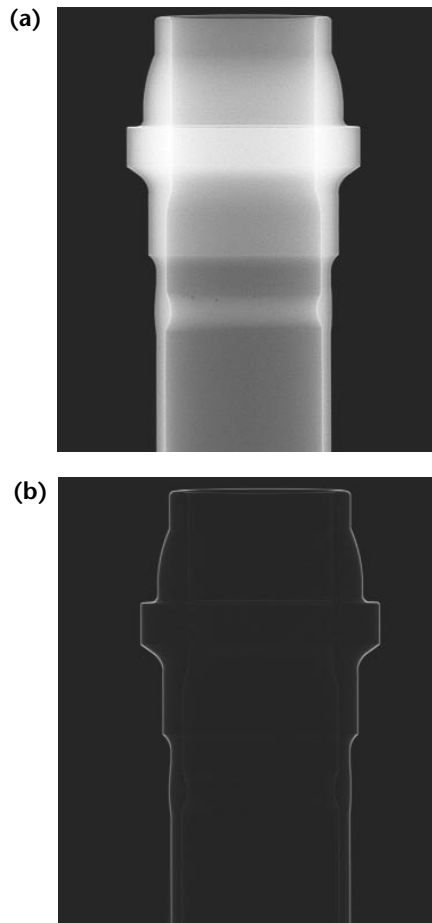


FIGURE 26. Digital radiographic image of tube weld: (a) 0 degree view; (b) boundary image.





radiographs of the tubes taken at 0 and 90 degrees. Because evaluating the discontinuities on the long tangent chords of the tube is more difficult, the two views will be used and those sections of the object will be avoided. The first step is an automated extraction of the center portion of the tube. To extract from the center of the tube in an automated way the boundary points are used to calculate an extracted inner rectangle.

Figure 26 includes one of the digital radiographs and the boundary point image. The discontinuities that sit on the integration through the double walls without the tangents can be identified with a polynomial least squares fit applied row wise to the extracted pieces. The result is the discontinuities on an otherwise flat image.

Now that the discontinuities have been isolated from the tube shape, a fixed threshold of minus two standard deviations of the noise calculated from the center of the tube in an unwelded area. Pixels less than this value are considered to be reliable indicators of less mass in the weld of the object. After the threshold is applied only the discontinuities are left against a binary image. Figure 27 contains the results of this operation.

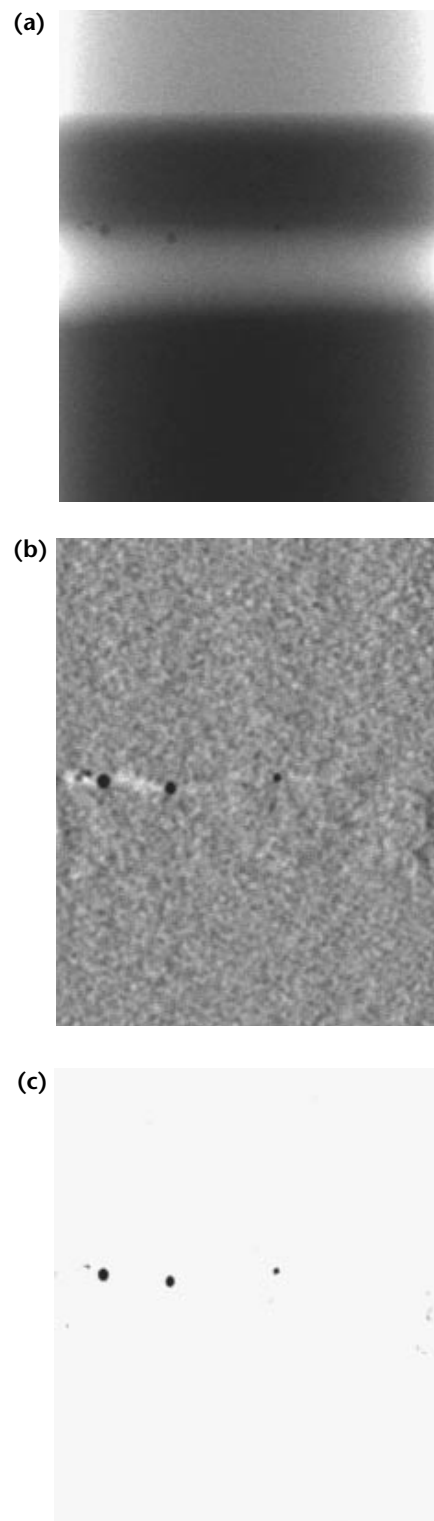
At this point the image has been processed to identify discontinuities with a two-sigma fixed criterion. In this case a number of different segmentation schemes (that is, blob analysis) can be applied to extract out the discontinuities. From these extracted segments, a number of different quantities can be calculated: total discontinuity area, largest discontinuity and others. If the images have been calibrated into material length, it is also possible to calculate the total mass lost, in total and per discontinuity area. In spite of all these calculations, more information is needed to classify these different image segments into categories. Then still more information is required to accumulate the different discontinuity indications in the different categories and make a determination of a *good* or *bad* weldment.

### Discontinuity Detection Criteria

In the automatic discontinuity recognition process there are a number of important roles for product engineers.

1. It is important to specify the discontinuity or discontinuities to be detected. Full part drawings are useful as well as any assistance in precise mounting that can be offered.
2. Developing the criteria for finding *discontinuity indications* should be a cooperative effort.

**FIGURE 27.** Extracted portion of tube weld: (a) before processing ; (b) results of fit; (c) result of 2 sigma fixed threshold.



3. It is most useful if the product engineer is involved in the selection or acquisition of realistic sample images for analysis work.
4. *Standard* parts need to be fabricated with known discontinuities. These parts are essential for system verification and are equally useful for *salting* the regular operation of the scanner.

---

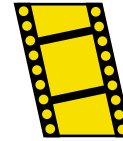
## Summary

In spite of the many issues with radiographic automatic discontinuity recognition systems the nature of radiographic testing makes this modality particularly attractive. Radiographic testing is a noncontact test method that can adapt to design changes better than contact based methods. Radiographic sources can cover a wide range of energies, letting a single system be used on a variety of parts. Sometimes only software needs to be changed to inspect a new part. Advances in computer hardware makes more extensive automatic discontinuity recognition algorithms more tractable within the strict time requirements for factory floor cycle times.

Although some of the promise of radiographic automatic discontinuity recognition depends on more general purpose tools for stitching together automatic discontinuity recognition routines, it is reasonable to expect radiographic automatic discontinuity recognition machines to be more commonplace and achieve the reliability and repeatability obtained in other factory floor equipment.

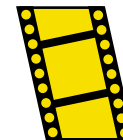
---

**MOVIE.**  
Exfoliation corrosion, thin to thick.



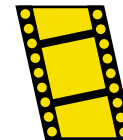
---

**MOVIE.**  
General corrosion, thin to thick.



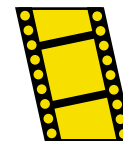
---

**MOVIE.**  
Cracks around fasteners.



---

**MOVIE.**  
Cracks around fasteners, in layers from top.



# References

1. Evans, R.D. *The Atomic Nucleus*. New York, NY: McGraw Hill (1955).
2. Heitler, W. *Elementary Wave Mechanics with Applications to Quantum Chemistry*, second edition. Oxford, United Kingdom: Clarendon Press (1955).
3. Barrett, H.H. and W. Swindell. *Radiological Imaging*. New York, NY: Academic Press (1981).
4. Kak, A.C. and M. Slaney. *Principles of Computerized Tomographic Imaging*. New York: IEEE Press (1987).
5. Bushberg, J.T., J.A. Seibert, E.M. Leidholdt, Jr. and J.M. Boone. *The Essential Physics of Medical Imaging*, second edition. Philadelphia, PA: Lippincott Williams & Wilkins (1994).
6. Dainty, J.C. and R. Shaw. *Image Science: Principles Analysis and Evaluation of Photographic Type Imaging Processes*. New York, NY: Academic Press (1974).
7. Martz, H., D. Schneberk, C. Logan and J. Haskins. "New Modalities in X-Ray Detection and Their Use for Industrial DR/CT." Presented at *International Symposium on Computerized Tomography for Industrial Applications and Image Processing in Radiology* [Berlin, Germany, March 1999]. Berlin, Germany: Deutsche Gesellschaft für Zerstörungsfreie Prüfung (March 1999).
8. Macovski, A. *Medical Imaging Systems*. Upper Saddle River, NJ: Prentice-Hall (1983).
9. Martz, H.E., D.J. Schneberk, G.P. Roberson and S.G. Azevedo. *Computed Tomography*. UCRL-ID-112613. Livermore, CA: Lawrence Livermore National Laboratory (September 1992).
10. Johns, H.E. and J.R. Cunningham. *The Physics of Radiology*, fourth edition. Springfield, IL: Charles C. Thomas (1983).
11. Sahoo, P.K., S. Soltani and A.K.C. Wong. "A Survey of Thresholding Techniques." *Computer Vision, Graphics, and Image Processing*. Vol. 41. San Diego, CA: Academic Press (1988): p 233-260.
12. Oppenheim, A.V. and R.W. Schaffer. *Discrete-Time Signal Processing*. Upper Saddle River, NJ: Prentice Hall (1999).
13. Lim, J.S. *Two-Dimensional Signal and Image Processing*. Upper Saddle River, NJ: Prentice Hall (1990).
14. Bracewell, R.N. *The Fourier Transform and Its Applications*, third edition. Boston, MA: McGraw-Hill (2000).
15. Serra, J. and P. Soille, eds. *Mathematical Morphology and Its Applications to Image Processing*. Dordrecht, Netherlands: Kluwer Academic Publishers (1994).
16. Doering, E.R. and J.P. Basart. "Trend Removal in X-Ray Images." *Review of Progress in Quantitative Nondestructive Evaluation*. Vol. 7. New York, NY: Plenum Press (1988): p 785-794.
17. Gayer, A., A. Saya and A. Shiloh. "Automatic Recognition of Welding Defects in Real-Time Radiography." *NDT International*. Vol. 23, No. 3. Oxford, United Kingdom: Elsevier Science Limited (1990): p 131-136.
18. Kaftandjian, V., A. Joly, T. Odievre, M. Courbière and C. Hantrais. "Automatic Detection and Characterisation of Aluminium Weld Defects: Comparison between Radiography, Radioscopy and Human Interpretation." *7th European Conference on Non-Destructive Testing* [Copenhagen, Denmark]. Vol. 2. Copenhagen, Denmark: 7th ECNDT Copenhagen (May 1998): p 1179-1186.
19. Davis, K. and C. Lazinsky. "The Quest for Speed, Precision and High Yield." *Imaging Insight*. Vol. 2, No. 3. Dorval, Quebec, Canada: Matrox Electronic Systems Limited (Fall 2000): p 4-5.
20. Vuylsteke, P. and E. Shoeters. "Image Processing in Computed Radiography." *International Symposium on Computerized Tomography for Industrial Applications and Image Processing in Radiology* [Berlin, Germany, March 1999]. DGZfP Proceedings BB 67-CD. Berlin, Germany: Deutsche Gesellschaft für Zerstörungsfreie Prüfung (March 1999): p 87-101.
21. Jawerth, B.D., M.L. Hilton and T.L. Huntsberger. "Local Enhancement of Compressed Images." *Journal of Mathematical Imaging and Vision*. Vol. 3, No. 1. Norwell, MA: Kluwer Academic Publishers (1993): p 39-49.

22. Strickland, R.N. and H.I. Hahn. "Wavelet Transform Methods for Object Detection and Recovery." *IEEE Transactions on Image Processing*. Vol. 6, No. 5. New York, NY: Institute of Electrical and Electronics Engineers (May 1997).
  23. Brigham, E.O. *Fourier Transforms*. Upper Saddle River, NJ: Prentice Hall (1974).
- 
- ## Bibliography
- Azevedo, S.G., H.E. Martz, D.J. Schneberk and G.P. Roberson. "Quantitative Measurement Tools for Digital Radiography and Computed Tomography Imagery." UCRL-53868-94. Livermore, CA: Lawrence Livermore National Laboratory (1994).
- Berger, H. *Neutron Radiography — Methods, Capabilities and Applications*. Amsterdam, Netherlands: Elsevier (1965).
- Berger, H., ed. *Practical Applications of Neutron Radiography and Gaging*. Special Technical Publication 586. West Conshohocken, PA: ASTM International (1976).
- Bossart, P.-L., H.E. Martz, H.R. Brand and K. Hollerbach. "Application of 3D X-Ray CT Data Sets to Finite Element Analysis." *Review of Progress in Quantitative Nondestructive Evaluation*. Vol. 15. New York, NY: Plenum Press (1996): p 489-496.
- Brand, H.R., D.J. Schneberk, H.E. Martz, P.-L. Bossart and S.G. Azevedo. *Progress in 3-D Quantitative DR/CT*. UCRL-53868-95. Livermore, CA: Lawrence Livermore National Laboratory (1995).
- Chinn, D., J. Haskins, C. Logan, D. Haupt, S. Groves, J. Kinney and A. Waters. "Micro-X-Ray Computed Tomography for PBX Characterization, Engineering Research, Development and Technology." UCRL-53868-98. Center for Nondestructive Characterization, UCRL-ID 132770. Livermore, CA: Lawrence Livermore National Laboratory (February 1999).
- Dolan, K.W., H.E. Martz, J.J. Haskins and D.E. Perkins. "Digital Radiography and Computed Tomography for Nondestructive Evaluation of Weapons." *Thrust Area Report*. UCRL-53868-94. Livermore, CA: Lawrence Livermore National Laboratory, Engineering Research, Development and Technology (1994).
- Dolan, K.W., J.J. Haskins, D.E. Perskins and R.D. Rikard. "X-Ray Imaging: Digital Radiography." *Thrust Area Report*. UCRL 53868-93. Livermore, CA: Lawrence Livermore National Laboratory, Engineering Research, Development and Technology (1993).
- Espinal, F., T. Huntsberger, B.D. Jawerth and T. Kubota. "Wavelet-Based Fractal Signature Analysis for Automatic Target Recognition." *Optical Engineering*. Vol. 37, No. 1. Bellingham, WA: International Society for Optical Engineering (1998): p 166-174.
- Feldkamp, L.A. L.C. Davis and J.W. Kress. "Practical Cone-Beam Algorithm." *Journal of the Optical Society of America*. Vol. 1. Washington, DC: Optical Society of America (1984): p 612-619.
- Freedman, M. and N.H. Strickland. "Digital Radiology and PACS: Image Processing in Computed Radiography." *Grainger & Allison's Diagnostic Radiology: A Textbook of Medical Imaging*. Edinburgh, United Kingdom: Churchill Livingstone (1997).
- Goebbels, J., U. Zscherpel and W. Bock. *Computertomographie und Bildverarbeitung [Proceedings, International Symposium on Computerized Tomography for Industrial Applications and Image Processing in Radiology]*, Berlin, Germany, 1999]. DGZfP Proceedings BB 67-CD. Berlin, Germany: Deutsche Gesellschaft für Zerstörungsfreie Prüfung (1999).
- Goodman, D.M., E.M. Johansson and T.W. Lawrence. Chapter 11, "On Applying the Conjugate Gradient Algorithm to Image Processing Problems." *Multivariate Analysis: Future Directions*. New York, NY: Elsevier Science Publishers (1993).
- Grangeat, P. "Analysis d'un Systeme d'Imagerie 3D par Reconstitution á Partir de Radiographies X en Géométrie Conique." Ph.D. Dissertation. Grenoble, France: L'Ecole Nationale Supérieure des Telecommunications (1987).
- Grodzins, L. "Optimum Energies for X-Ray Transmission Tomography of Small Samples." *Nuclear Instruments and Methods in Physics Research*. Vol. 206. Amsterdam, Netherlands: North-Holland Publishing Company (1983): p 541.
- Grodzins, L. "Critical Absorption Tomography of Small Samples." *Nuclear Instruments and Methods in Physics Research*. Vol. 206. Amsterdam, Netherlands: North-Holland Publishing Company (1983): p 547.

- Haddad, W.S., I. McNulty, J.E. Trebes, E.H. Anderson, R.A. Levesque and L. Yang. "Ultrahigh-Resolution X-Ray Tomography." *Science*. Vol. 266. Washington, DC: American Association for the Advancement of Science (1994): p 1213.
- Herman, G.T. *Image Reconstruction from Projections: The Fundamentals of Computerized Tomography*. New York, NY: Academic Press (1980).
- Hollerbach, K. and A. Hollister. "Computerized Prosthetic Modeling." *BioMechanics*. Albany, NY: CMP United Business Media (September 1996): p 31-38.
- Horstemeyer, M., K. Gall, A. Gokhale, M. Dighe and K. Dolan. "Visualization, Quantification and Prediction of Damage Evolution in Cast A356 Aluminum using High Resolution Experimental and Numerical Techniques." Manuscript (1999).
- Jain, A.K. "Image Data Compression: A Review." *Proceedings IEEE*. Vol. 69, No. 3. New York, NY: Institute of Electrical and Electronics Engineers (March 1981): p 349-389.
- Jain, A.K. *Fundamentals of Digital Image Processing*. Upper Saddle River, NJ: Prentice Hall (1989).
- Keswani, R., S. Gangotra, S. Muralidhar, P.M. Ouseph, K.C. Sahoo and D.S.C. Purushotham. "Computed Tomography of Irradiated Nuclear Fuel Elements." *15th World Conference on Nondestructive Testing* [Rome, Italy, October 2000]. Brescia, Italy: Associazione Italiana Prove non Distruttive e Monitoraggio Diagnostica (2000).
- Kinney, J.H., S.R. Stock, M.C. Nichols, U. Bonse et al. "Nondestructive Investigation of Damage in Composites Using X-Ray Tomographic Microscopy (XTM)." *Journal of Materials Research*. Vol. 5, No. 5. Pittsburgh, PA: Materials Research Society (May 1990): p 1123-1129.
- Kinney, J.H. and M.C. Nichols. "X-Ray Tomographic Microscopy Using Synchrotron Radiation." *Annual Reviews of Materials Science*. Vol. 22. Palo Alto, CA: Annual Reviews (1992): p 121-152.
- Kinney, J.H., D.L. Haupt, M.C. Nichols, T.M. Breunig, G.W. Marshall and S.J. Marshall. "The X-Ray Tomographic Microscope: 3-Dimensional Perspectives of Evolving Microstructure." *Nuclear Instruments and Methods in Physics Research: Section A, Accelerators, Spectrometers, Detectors and Associated Equipment*. Vol. 347. Amsterdam, Netherlands: Elsevier Science Publishers (1994): p 480-486.
- Kinney, J.H., T.M. Breunig, T.L. Starr, D. Haupt et al. "X-Ray Tomographic Study of Chemical Vapor Infiltration Processing of Ceramic Composites." *Science*. Vol. 260, No. 5109. Washington, DC: American Association for the Advancement of Science (1993): p 789-792.
- Knoll, G.F. *Radiation Detection and Measurement*. New York, NY: John Wiley and Sons (1989).
- Logan, C., J. Haskins, K. Morales, E. Updike, D.J. Schneberk, K. Springer, K. Swartz, J. Fugina, T. Laviates, G. Schmid and P. Soltani. "Evaluation of an Amorphous Selenium Array for Industrial X-Ray Imaging." *Engineering NDE Center Annual Report*. UCRL-ID-132315. Livermore, CA: Lawrence Livermore National Laboratory (1998).
- Martz, H.E. "Computed Tomography of Bridge Pins, Cast Aluminum Automotive Components and Human Joints." Report No. UCRL-JC-133573. *6th Nondestructive Evaluation Topical Conference* [San Antonio, TX, April 1999]. New York, NY: American Society of Mechanical Engineers (April 1999).
- Martz, H.E. "The Role of Nondestructive Evaluation in Life Cycle Management." *Frontiers of Engineering: Reports on Leading Edge Engineering from 1997 NAE Symposium on Frontiers of Engineering* [Third Annual Symposium on Frontiers of Engineering]. Washington DC: National Academy Press (1998) p 56-71.
- Martz, H.E., S.G. Azevedo, D.J. Schneberk, M.F. Skeate, G.P. Roberson and D.E. Perkins. *Computerized Tomography*. UCRL-53868-90. Livermore, CA: Lawrence Livermore National Laboratory (October 1991).
- Physics Today*. Special issue celebrating the centenary of Röntgen's discovery of X-rays. Vol. 48, No. 11. Melville, New York: American Institute of Physics (November 1995).
- Pontau, A.E., A.J. Antolak, D.H. Morse, A.A. Ver Berkmoes, J.M. Brase, D.W. Heikkinen, H.E. Martz and I.D. Proctor. "Ion Microbeam Microtomography." *Nuclear Instruments and Methods in Physics Research: Section B, Beam Interactions with Materials and Atoms*. Vol. B40/41. Amsterdam, Netherlands: Elsevier Science Publishers (1989): p 646.
- Proceedings of ASNT Topical Conference on Industrial Computerized Tomography* [Seattle, WA, July 1989]. Columbus, OH: American Society for Nondestructive Testing, (1989).



- Real-Time Radioscopy Radioscopy and Digital Imaging* [Manshantucket, Connecticut, August 1998]. Topical Conference Paper Summaries Book. Columbus, OH: American Society for Nondestructive Testing (1998).
- Rowlands, J. and S. Kasap. "Amorphous Semiconductors Usher in Digital X-Ray Imaging." *Physics Today*. Vol. 50, No. 11. Melville, NY: American Institute of Physics (1997): p 24.
- Savona, V., H.E. Martz, H.R. Brand, S.E. Groves and S.J. De Teresa. "Characterization of Static- and Fatigue-Loaded Carbon Composites by X-Ray CT." *Review of Progress in Quantitative Nondestructive Evaluation*. Vol. 15. New York, NY: Plenum Press (1996): p 1223-1230.
- Scott, V.D. and G. Love. *Quantitative Electron-Probe Microanalysis*. Chichester, United Kingdom: Ellis Horwood Limited (1983).
- Seibert, J.A., O. Nalciglu and W.W. Roeck. "Removal of Image Intensifier Veiling Glare by Mathematical Deconvolution Techniques." *Medical Physics*. Vol. 12, No. 3. Melville, NY: American Institute of Physics, for the American Association of Physicists in Medicine (May/June 1985).
- Sengupta, S.K. "IMAN-3D: A Software Tool-Kit for 3-D Image Analysis." Engineering Research, Development and Technology, UCRL 53868-98. Livermore, CA: Lawrence Livermore National Laboratory (1998).
- Smith, B.D. "Cone-Beam Tomography: Recent Advances and a Tutorial Review." *Optical Engineering*. Vol. 29, No. 5. Bellingham, WA: International Society for Optical Engineering (1990): p 524-534.
- Soltani, P.K., D. Wysnewski and K. Swartz. "Amorphous Selenium Direct Radiography for Industrial Imaging." DGZfP Proceedings BB 67-CD, *Computerized Tomography for Industrial Application and Image Processing in Radiology* [Berlin, Germany, March 1999]. Berlin, Germany: Deutsche Gesellschaft für Zerstörungsfreie Prüfung (1999).
- Strickland, R.N. and H.I. Hahn. "Wavelet Transforms for Detecting Microcalcifications in Mammograms." *IEEE Transactions on Medical Imaging* [1995]. Vol. 15, No. 2. New York, NY: Institute of Electrical and Electronics Engineers (April 1996): p 422-425.
- Tabb, M. and N. Ahuja. "Multiscale Image Segmentation by Integrated Edge and Region Detection." *IEEE Transactions on Image Processing*. Vol. 6, No. 5. New York, NY: Institute of Electrical and Electronics Engineers (May 1997).
- Tonner, P.D. and J.H. Stanley. "Supervoltage Computed Tomography for Large Aerospace Structures." *Materials Evaluation*. Vol. 12, No. 12. Columbus, OH: American Society for Nondestructive Testing (December 1992): p 1434-1438, 1445.
- Van der Meulen, M.C.H. "Mechanical Influences on Bone Development and Adaption." *Frontiers of Engineering: Reports on Leading Edge Engineering from 1997 NAE Symposium on Frontiers of Engineering* [Third Annual Symposium on Frontiers of Engineering]. Washington DC: National Academy Press (1998): p 12-15.
- Varian Corporation. *Flashscan 30 Manual*. Palo Alto, CA: Varian Corporation [no date].
- Waters, A.M., H. Martz, K. Dolan, M. Horstemeyer, D. Rikard and R. Green. "Characterization of Damage Evolution in an AM60 Magnesium Alloy by Computed Tomography." *Proceedings of Nondestructive Characterization of Materials IX. AIP Conference Proceedings 497* [Sydney, Australia, June-July 1999]. Melville, NY: American Institute of Physics (1999): p 616-621.
- Weisfield, R.L., M.A. Hartney, R.A. Street and R.B. Apte. "New Amorphous-Silicon Image Sensor for X-Ray Diagnostic Medical Imaging Applications." *SPIE Medical Imaging: Physics of Medical Imaging*. Vol. 3336. Bellingham, WA: International Society for Optical Engineering (1998): p 444-452.





# 14

## C H A P T E R

# Backscatter Imaging

---

Lawrence R. Lawson, Bradford, Pennsylvania

## PART 1. Physical Principles

Backscatter imaging involves the single-sided collection of scattered radiation rather than the transmitted radiation to form an image. Although in a typical X-ray test configuration at least as many photons are scattered as are transmitted, imaging with them is much more difficult. Consequently, backscatter imaging is usually a digital technique. The development of backscatter imaging has followed the evolution of digital radiography.

The motivations for backscatter imaging have been several. Perhaps the foremost has been the desire to image from one side. Furthermore, the backscatter technique can image a volume rather than a plane. For these reasons, backscatter imaging has been found useful for such applications as aircraft pressure bulkhead inspections where access to both sides of the bulkhead is impracticable.

Other motivations for using backscatter imaging include its ability to be configured for direct measurement of the electron density of the object being measured. This property has been used in medical measurements of bone density. It was soon recognized that this property could be exploited to detect the difference between filled and unfilled voids within steel casings. The case in point was that of artillery shells. The shells themselves are of heavy material while detonators are nearly transparent radiographically. Transmission radiography could not always detect whether or not ordnance shells were armed. Backscatter radiography could. In fact, inspection of baggage for explosives and contraband has been the major driving force in the development of backscatter radiography.

Another motivation for using backscatter radiography is that it can perform a certain amount of chemical analysis on the object being imaged. This faculty is most acute at very low (1 keV) and very high (>2 MeV) energies. At energies around 60 keV, the dual energy technique permits the estimation of the atomic number of the material being inspected through comparison of scattering and absorption coefficients.

Scattering takes place through the interaction of an X-ray or gamma ray photon's oscillating electromagnetic field with either the charge of an electron or of the nucleus. For imaging purposes

interaction with electrons is most important. In most interactions, there is a transfer of energy between the photon and the electron.

### Types of Scattering

There are four scattering processes currently used for backscatter imaging in the broadest sense. These are *elastic*, *fluorescence*, *compton* and *resonance fluorescence*.

*Elastic* scattering involves no energy loss. It is also called *rayleigh scattering* or coherent scattering. It is significant when the photon wavelength is on the order of atomic dimensions. Because it is coherent, the wave function of the scattered photon is predictably related to that of the incident photon, it gives rise to diffraction effects. The entire field of X-ray diffraction is based on elastic scattering. Elastic scattering from crystalline materials takes place only at certain angles. Hence it is possible to measure the amount of some crystalline constituent using elastic scattering at selected angles. In noncrystalline materials, statistical parameters describing the spatial distribution of neighboring atoms can be determined from analyzing the scattered X-rays using techniques such as X-ray absorption spectroscopy. By measuring small changes in the scattering angles, elastic strains and hence residual stresses can be measured. But because the energies involved are on the order of a couple thousand electronvolts, penetration is limited. Elastic scattering is used primarily for one-dimensional measurements at a point. An example is the measurement of thin coatings with low energy X-rays. In this case, the source detector geometry can be configured to exclude reflection from the (steel) substrate, because that reflection will occur only at specific angles.

Similar to elastic scattering *compton* scattering is also scattering by the electrons that surround the nuclei of atoms. In this case there is energy loss from the incident photon to the electron that recoils in what amounts to a collision. Compton scattering is important in the range of tens to hundreds of thousands of electronvolts. It is the basis for most of the attenuation of

high energy photons, for example, gamma rays. It is also the basis of most backscatter imaging techniques.

There are definite relations between the amount of energy lost and the angle of scatter. Phase information is essentially lost in the scattering process. So, unlike elastic scattering, diffraction effects do not take place detectably. Compton scattering is not isotropic but varies with the energy. At high energies, forward scattering predominates. Compton scattering competes with the photoelectric effect as a means of consuming photon energy. Hence, in low  $Z$  materials, where the photoelectric effect for X-rays is weak, Compton scattering is relatively intense compared with high  $Z$  materials in which photons are actually lost because of photoelectric absorption. Thus Compton scattering is particularly useful for detecting electronically dense low  $Z$  materials such as opiate drugs and high explosives.

In the event that a photon is absorbed in a photoelectric process, a high energy electron is generated. This secondary electron may itself be a K or L shell electron. It may also interact with other atoms to eject K or L shell electrons. The cascade that results to refill the missing K or L shell electron may result in the emission of a photon of the energy corresponding to the difference between that and some higher shell. For high  $Z$  materials these photons can have energies in thousands of electronvolts. This process is called *fluorescence*.

As with radiation used for elastic scattering, fluorescence radiation has limited penetration. Backscattered X-ray fluorescence imaging is the basis of several chemical analysis tools used by surface scientists. Most of these require placing the part to be examined in a vacuum chamber and are therefore destructive testing. X-ray and gamma ray fluorescence has also been used in probes to sort alloys, to detect and measure the lead in paint coatings and to perform similar tasks.

Another type of fluorescence occurs at very high energies and is called *resonance fluorescence*. At energies in the vicinity of 10 MeV, incident photons can cause changes in the energy of the nuclei of atoms. After absorption of a photon the nucleus relaxes emitting other photons at lower energies but still in the millions of electronvolts range. These fluorescence photons, like their lower energy counterparts, are emitted at random angles nearly isotropically. This isotropy means that nuclear resonance fluorescence makes backscatter imaging possible at energies above those where Compton scattering would only take place in the forward direction. This technique

has advantages for the examination of thick or dense structures and like low energy fluorescence facilitates chemical analysis from the backscatter energy spectrum.

The resonance fluorescence technique has drawbacks. Particle accelerators are required to generate the incident X-ray illumination. These are bulky and expensive. Another drawback is that above 500 keV, it is possible to generate residual radioactivity. This residual radioactivity problem is significant at 10 MeV for some materials.

## Compton Scatter

Compton scattering is the type most often used in backscatter imaging. In this type of scattering the electron receives energy from the incident photon and recoils. Momentum is conserved and a lower energy scattered photon emerges. Because momentum is conserved, it is possible to relate the scattering angle to the amount of energy lost by the photon. This gives rise to the relationship:

$$(1) \quad \frac{v_0}{v'} = 1 + \frac{hv_0}{mc^2} [1 - \cos(2\theta)]$$

where  $v_0$  is incident photon frequency (reciprocal second),  $v'$  is scattered photon frequency,  $hv_0$  is incident photon energy,  $mc^2$  is about 500 keV and  $2\theta$  is the scattering angle (in the sense used in diffractometry). Multiplying up and down by  $h$ , Planck's constant, shows that the expression is equal to the ratio of incident to scattered photon energies. The Compton scattering process is described by the well known Klein-Nishina formula, which for ray pencils can be written, apart from specific geometry factors:

$$(2) \quad \Psi_{\text{out}} = \Psi_{\text{in}} \frac{r_0^2}{2} Z N \Omega_d \left( \frac{v'}{v_0} \right)^2 \times \left( \frac{v_0}{v'} + \frac{v'}{v_0} - \sin^2(2\theta) \right) t \times \exp(-\mu \ell)$$

where  $\ell$  is the total path length (meter),  $N$  is the number of atoms per cubic meter,  $r_0^2$  is the classical electron radius constant (where  $r_0^2 = 7.94 \times 10^{-30} \text{ m}^2$ ),  $t$  is the thickness (meter) of the scattering element in the incident beam direction,  $Z$  is the average atomic number,  $\mu$  is the linear attenuation coefficient ( $\text{m}^{-1}$ ),  $\theta$  is the beam angle (radian is preferred but degree is conventional, depending on choice of sin),  $\Psi$  is the photon flux (photons per second) and  $\Omega_d$  is the detector solid angle (steradian) into which the photon is scattered. Figure 1a

illustrates the scattering pattern given by Eq. 2. It gives the number scattering cross section per electron per unit of solid angle in units of  $10^{-30} \text{ m}^2$ .

Because the solid angle per increment of scattering angle at the poles is zero, this graph may be confusing. Figure 1b replots the data for 50 keV in terms of increment of scattering angle where the solid angle increment is in terms of the scattering angle  $2\theta$ :

$$(3) \quad d\Omega = 2\pi \sin(2\theta) d(2\theta)$$

The units are again  $10^{-30} \text{ m}^2$ .

Compton scatter also contributes to attenuation in that it scatters photons out of a beam and consumes energy at the same time. The total linear attenuation coefficient  $\mu_T$  is composed of compton

component  $\mu_c$ , and of elastic scattering  $\mu_e$  (significant at low energies) of photoelectron component  $\mu_p$ :

$$(4) \quad \mu_T = \mu_c + \mu_p + \mu_e$$

Compton scattering is, in fact, the main cause of attenuation at energies over about 55 keV. In Fig. 1a., a polar plot of the differential scattering cross section, scattering is very roughly isotropic at the energy of 50 keV and below. The amount of backscatter however becomes diminished at 200 keV. Further increases in energy result in further reductions in backscatter intensity by the compton mechanism.

Because the amount of scattering in a volume element depends on the incoming flux, proportional to the area of the element, times the thickness of the element, the intensity of the radiation scattered from a material volume element of  $\Delta V$ , a voxel, inside an object, can be expressed as

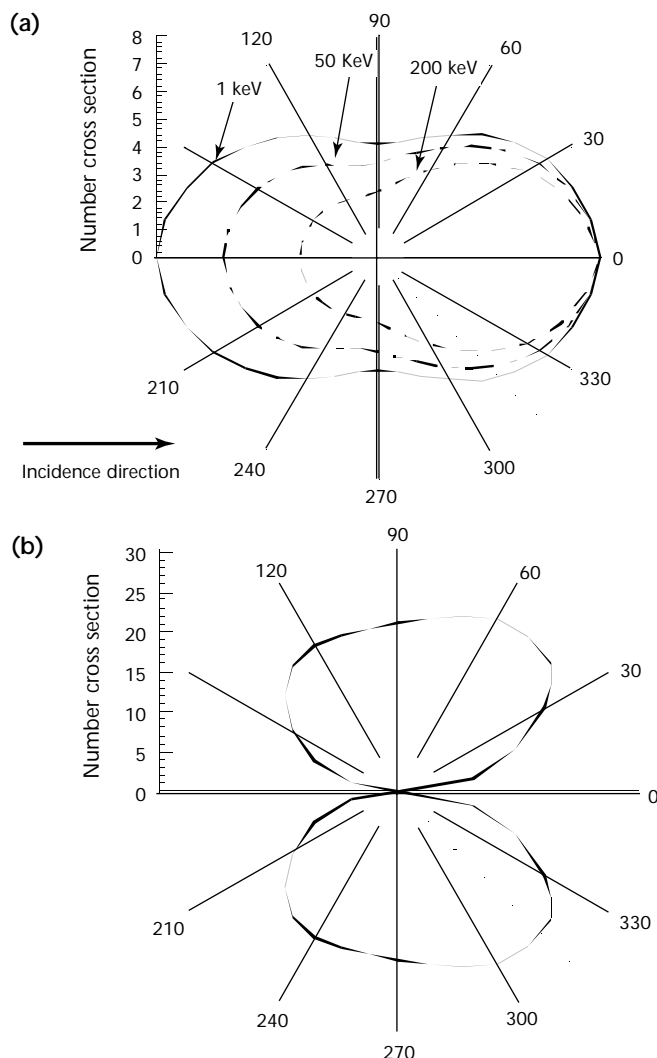
$$(5) \quad I_{sc} = K N_e \Delta V \exp(-\bar{\mu} \ell)$$

where  $K$  is a constant including the strength of the incident beam,  $N_e$  is the electron density of the material within the voxel and  $\bar{\mu}$  is an average linear attenuation coefficient over the total path of length  $\ell$ , starting where the to-be-scattered photon enters the material and ending where it leaves it. The attenuation coefficient not only is a function of the material through which the photons pass but also is affected by the compton shift, that is, by the energy change on scattering. In addition to the flux intensity  $I_{sc}$  given above, there are also background and a component resulting from multiple scatter, photons scattered more than once. Multiple scatter within the voxel may augment the signal but a system would probably be poorly designed if that were significant because it implies a great deal of fuzziness in the image. The balance of the multiple scatter appears as enhanced background or noise. In fact, most of the background in backscatter scanning appears to result from multiple scatter rather than natural radioactivity and X-ray leakage. Making the multiple scatter background negligible is a matter of good design, proper choice of energies (frequencies) and software corrections.

### Scatter As Function of Material

During their passage through material, X-rays are both absorbed and scattered. Figures 2 and 3 illustrate the relative amounts of these two processes for lead and aluminum respectively. The curve

FIGURE 1. Compton scattering pattern: (a) polar plot of differential scattering cross section; (b) incremental scattering angle for 50 keV. Unit of angle is the degree.



shown for scattering is composed of both elastic and inelastic scattering but the former is not significant at energies near 100 keV and above.

Lead has a high atomic number and shows considerable photoelectric absorption relative to compton scatter at energies of 1 MeV. Another absorption mechanism is also shown: pair production. This occurs in all materials but is only significant at energies greater than 1 MeV above the usual range for backscatter imaging. Aluminum has a low atomic number and consequently photoelectric absorption exceeds compton scattering only at very low energies. This makes aluminum a suitable material for inspection by backscatter imaging.

Figure 4 compares the significance of compton scattering to photoelectric absorption by showing the compton

fraction of total scattering. Notice that even near 120 keV, compton scattering remains the minority process in iron. At low incident photon energies, the binding of the electron to the nucleus becomes significant. The klein-nishina formula given as Eq. 2 is no longer strictly accurate, because electrons cannot all be regarded as being free.

At high incident energies, the binding energy of the electron is trivial compared with its recoil energy. When the incident energy is so low that the binding energy is close to the recoil energy, two types of effects are observed. Line broadening is one effect that can in principle be observed up to several tens of keV depending on the energy sensitivity of the detector and the monochromatic purity of the source.

Much chemical information can be gained about the bonding of electrons through studies of compton broadening. At still lower energies the scattering coefficients themselves vary. Figure 5 illustrates this effect through comparing the scattering coefficients for two ions having the same total number of electrons, 21, but different nuclear charges.<sup>1</sup> The ions are titanium ( $Ti^{+}$ ) and vanadium ( $V^{+2}$ ). The compton scattering intensity (divided by the breit recoil factor) is plotted versus an energy loss parameter,  $\sin(\theta) \cdot \lambda^{-1}$  where  $\lambda$  is the wavelength in units of 0.1 nm. At large energy losses, the scattering intensities are nearly the same for both ions. But at low energies, they differ. Such differences can in principle be observed by comparing images made at two different energies. In practice, these effects are not easily observed in backscatter.

FIGURE 2. Scattering and absorption for lead.

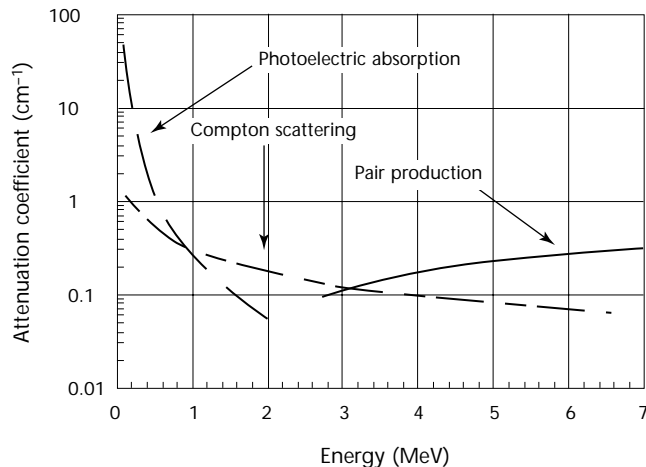


FIGURE 3. Scattering and absorption for aluminum.

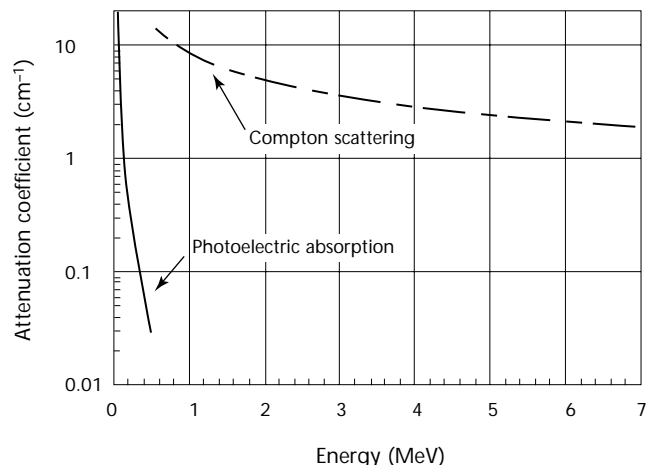
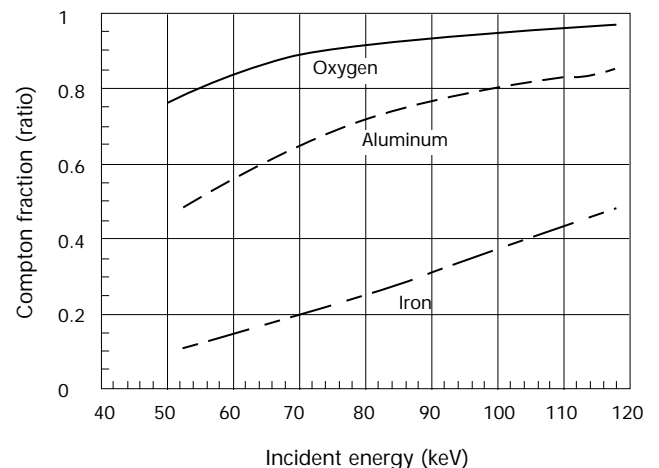


FIGURE 4. Compton fraction of total scattering compared to photoelectric absorption. Even near 120 keV, compton scattering remains the minority process in iron.



Other modalities such as fluorescence and coherent scattering are less often used for nondestructive testing. Coherent scattering, X-ray diffraction, is often a reflection technique. Because of the low energies involved, however, penetration is minimal.

X-ray diffraction also tends to be slow. Scans can be performed but they are even slower. For this reason X-ray diffraction is seldom used as an imaging technique except in the highly specialized task of inspecting large crystals for discontinuities in structure.

The main advantage of X-ray diffraction is that it measures composition by crystal structure. Hence, it is used commercially to detect diamonds in diamond mining. Low energy X-ray or gamma fluorescence has been used in commercial paint gages to detect and measure lead paint. Resonance fluorescence is a high energy technique recently developed.

Resonance fluorescence involves transitions between energy levels within the nucleus itself. It was predicted before it was discovered. Early attempts using isotope sources to detect it were not highly successful because the narrow energy ranges of these sources did not match the energies favorable for resonance transitions. The development of small accelerators providing broad band bremsstrahlung in the 10 MeV range has made resonance fluorescence available as an imaging tool. The techniques involved use flying spot scanning (to be discussed) in combination with broad area detectors. The primary advantage of resonance fluorescence lies in the large amount of backscatter obtained at high energies where the Compton process

would allow only forward scatter. The second advantage is that the backscattered photons have energies characteristic of the atoms from which they originated. This allows chemical analysis to be performed — even of light elements — of materials within heavy absorptive enclosures.

## Single and Multiple Scattering

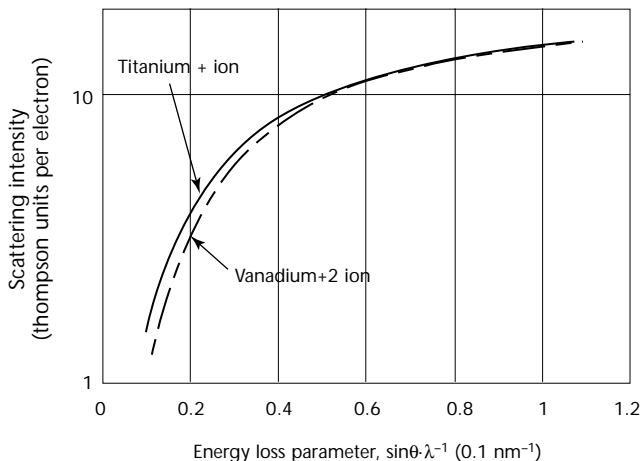
There are basically two scattering models useful for backscatter imaging. They will be discussed only for Compton scatter but in the single scattering case, the same remarks apply qualitatively to elastic scatter as well. In the first, single scattering model, an incident photon travels with some probability of absorption to a region within the material. It is there scattered and returns along a straight path with some probability of absorption to a detector. The simplicity of this model allows closed form calculations and has proven extremely useful in the service of nondestructive testing. Computations are based on geometry and are relatively simple compared with the corresponding computations for visible light because the wave nature of X-rays can generally be ignored because of their small wavelengths.

The second model is multiple scattering. Two entirely different approaches may be used but both involve solving the Boltzmann transport equation. Historically, the first approach was to solve the Boltzmann transport equation directly. Except in a very few special cases, this approach was fraught with errors and disappointments due to the simplifying assumptions that were needed.

What emerged as the most successful approach is solution by Monte Carlo simulation. The overall energy transfer is estimated from averaging over many such paths generated by random numbers. This computationally intensive approach is greatly facilitated by digital computers. Unlike early attempts at solving the Boltzmann transport equation directly, Monte Carlo methods usually show excellent agreement with experiment. In either single or multiple scattering, the theoretical treatment depends somewhat on the detector model. Detectors may count photons or respond to photon energy. The following discussion of backscatter presumes photon counting. The energy of the counted photons is measured separately in modern detectors and provides supplementary information.

The single scattering model is applicable, at least as an initial estimate, to almost all backscatter imaging applications to date. The reason for this is that most imaging is done with photons

FIGURE 5. Compton scattering intensity (divided by Breit recoil factor) is plotted versus energy loss parameter ( $\sin\theta/\lambda^{-1}$ ), where  $\lambda$  is wavelength in units of  $10^{-10}$  m.



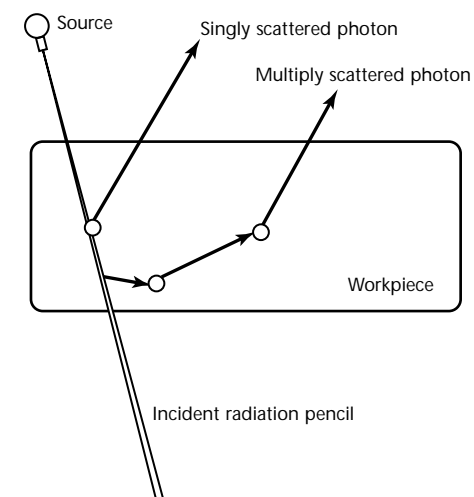


in the 30 to 100 keV energy range. In most materials, for example, transition metals, there is significant absorption in this energy range. Consequently, multiple-scattered photons have lost more energy because of the Compton process and are therefore better targets for photoelectric absorption. In addition, they are laterally displaced. In systems with both collimated sources and collimated detectors, multiple-scattered photons must follow very specific paths that undo the lateral displacement effect to reach the detector. Because these paths are specific, their associated probabilities are low.

Consider an X-ray pencil beam entering a uniform material (Fig. 6). A particular set of photons passes through the upper layer of material, is scattered in some volume element and returns back through the material to the detector. There is a round trip path that contributes to the attenuation of photons. This is the first element of the process. In the second element, the scattering itself, the reciprocal of the linear dimension of the interrogated area (scattering zone) defines the resolution. This dimension is related to the solid angle subtended by the pencil beam. The throughput or fraction of available photons participating is proportional to this solid angle. If uncollimated detectors are used, then by this reasoning, the throughput is inversely proportional to the square of the resolution. Under such circumstances the resolution is in two dimensions only; the beam interrogates more or less the entire depth of the specimen at once and the resulting signal is an integral over the depth.

As an example consider a configuration where a narrow pencil enters a uniform

FIGURE 6. Scattering model.



material (see Fig. 7). Presume that the detector is configured to collect all photons on paths for which the cosine of the angle between them and the incident pencil is unity (implied is that the solid angle of the detector is not a factor); this would be about 180 degree scatter. The probability of scattering in a volume element of thickness  $t$  is  $\sigma t$ , where  $\sigma$  is the linear scattering coefficient. If  $z$  is the distance from the scattering element to the surface, the amount of scattering in that element is  $I_0 \sigma t \exp(-\mu z)$ , taking into account attenuation on the way in. Including attenuation on the way out gives:

$$(6) \quad \text{Scattering} = I_0 \sigma t \exp(-2\mu z)$$

Taking the limit as  $t$  becomes infinitesimal and integrating over the entire specimen give:

$$(7) \quad \text{Scattering} = \frac{I_0 \sigma}{2\mu} [1 - \exp(-2\mu z)]$$

where now  $z$  is the thickness of the specimen, as proportional to the strength of the signal at the detector. For an infinitely thick specimen, the signal is simply proportional to the ratio of the scattering coefficient and the linear attenuation coefficient.

A frequent type of measurement is to estimate the density of a material from its backscatter signal. But, given this expression, backscatter can be expected to reveal very little about the density of absorptive materials, because both the linear scattering coefficient  $\sigma$  and the linear attenuation coefficient  $\mu$  are proportional to density. A way around this limitation is to use multiple detectors to provide different path lengths for the scattered photon. This allows  $\mu$  to be decoupled from  $\sigma$ . More commonly in density measurements a different approach separates the source and detector; its application to concrete is discussed below. If the material is a weak absorber, then expanding in a series makes the signal instead proportional:

$$(8) \quad \text{Scattering} = I_0 \sigma x + O(\mu x^2)$$

where  $x$  is the material's thickness.

When a collimated detector is used, its solid angle relative to the point of scattering becomes important. The throughput is then proportional to the solid angles of both the source pencil and that of the detector. This proportionality suggests that geometry could result in the signal's being inversely proportional to the fourth power of the resolution. Practical volume imaging systems make

one of the imaging elements a slit so that the throughput is inversely proportional to the cube of the resolution. This is still a severe limitation. In some systems, the resolution requirement is relaxed in less important dimensions to overcome this restriction. For example, in a commercially developed backscatter tomography system,<sup>2,3</sup> resolution in the direction perpendicular to the plane of the tomograms has been somewhat reduced. In depth profiling backscatter schemes, the resolution in directions perpendicular to depth is considerably reduced.

This resolution problem is shown in Fig. 7. The scattering volume is assumed to be roughly spherical. Referring to the scattered rays approaching the detector, it should be apparent that the resolved dimension can be no smaller than the diameter of the aperture shown between the scattering volume and the detector; imagine the aperture at first located at the scattering volume itself and then while adjusting the size of the detector withdraw it in steps toward the detector to visualize. The solid angle  $\Omega$  is subtended by the detector aperture:

$$(9) \quad \Omega = \frac{\pi d^2}{16 r^2}$$

where  $d$  is both the aperture diameter and proportional to (if not identical to) the resolved dimension and  $r$  is the distance from the scattering volume to the detector. If the source is large in diameter compared to the resolved dimension, then the same construction can be applied to the source resulting in the fourth power relationship mentioned. If the source is smaller than the resolved dimension, the power of aperture diameter  $d$  in the

throughput may diminish but the overall efficiency would be improved by making the source larger. Were it possible to replace the detector aperture by an annular slit, the power would then be reduced to three. The single scatter geometry has been extensively modeled in the literature.

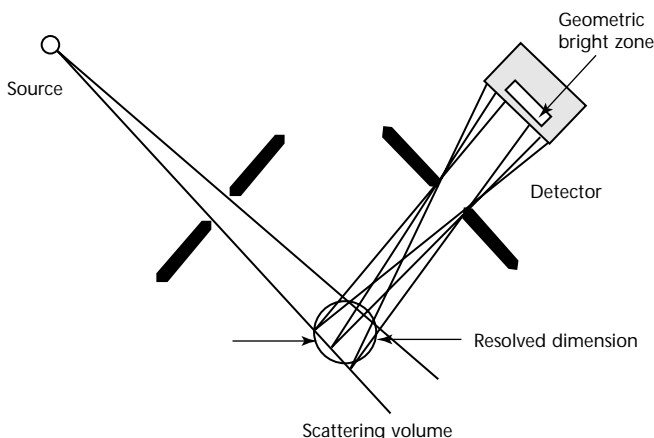
The multiple scattering model is of primary importance only in those techniques that use detectors collimated to exclude singly scattered photons, because single scattering usually dominates even when uncollimated detectors are used. The multiple scattering model can be described through the transport equation. This equation states that in any element or particular region in space, the rate of change in the number of photons within the region equals the fluxes integrated over that element's boundary.

These surface fluxes come from two sources. First are those arising from photons passing through the element unscattered (the convection term). Second are those arising from photons being scattered into the element. A third flux is proportional to the volume of the element and comes from photons created or absorbed in the element. Generally, the creation of photons within the element can be neglected. A monte carlo solution of the transport equation might divide the space into discrete elements and track hypothetical photons, scattered or not depending on generated random numbers as they pass from element to element. Summing over many trial incident photons allows calculation of the expected fraction of them in any volume element at any time going in any particular direction with any particular energy.

Apart from monte carlo and other numerical methods, many approaches have been tried to obtain solutions in closed form. The most common of these has been to assume that the scattering angles are small. These have resulted in a number of so called *straight ahead* approximations, useful when the energies of the incident photons are very high. An example is Yang's method, which allows calculation of the average lateral displacement because of scattering of a photon passing through a thin layer.<sup>4</sup>

These methods are of little use under imaging conditions. If the convection term is made very small, absorption negligible, scattering isotropic, source term zero and the number of photons in any volume element independent of time, then it is possible to convert the transport equation into a form of Laplace's equation. This give the *diffusional approximation*. Diffusional approximations could yield closed form estimates to some

FIGURE 7. Resolved dimension can be no smaller than diameter of aperture shown between scattering volume and detector.



flying spot scanning problems that might be useful under fortuitous conditions. But generally diffusional assumptions would seldom be realistic. Retaining the diffusional assumptions and reintroducing the convection term would give rise to a fokker-planck equation for which there is an extensive literature of solutions. However, the consistently good accuracy reported for monte carlo methods has largely obviated closed form approximations.

Multiple scattering may be significant in the detection of low density regions or regions of low atomic number in materials. In the case of low density regions, initially scattered photons may travel the length of the region before being rescattered out of the material. In the case of low  $Z$  materials, the relative absence of photoelectric absorption may allow a single photon to exist through many scattering events. It has been reported that when nearly monochromatic cobalt-60 radiation is backscattered from steel containing an air gap, a detectable energy peak varies in energy as a function of the size of the air gap. This effect is enhanced at small scattering angles and probably results from multiple scatter within the air gap.<sup>5</sup>

Cracks can be detected through a combination of multiple scattering and fluorescence. By placing a film in contact with a metal surface and illuminating the part obliquely, Hasenkamp was able to visualize small cracks.<sup>6</sup> Just as a deep notch in a red hot part will usually appear brighter than its surrounding surface, a crack will appear brighter than its surroundings when the part is illuminated with X-rays in a direction such that only scattered X-rays can reach the detector.

## PART 2. Backscatter Imaging Techniques

### Pinhole

One of the earliest examples of industrial scatter imaging was performed using a pinhole camera. Pinhole cameras have been used to image sources such as X-ray tube anode spots or isotopes. The pinhole camera technique gives a two-dimensional image on film. Its simplicity is offset by the very small throughput obtainable because of the small solid angle subtended by a pinhole. Illumination of the object to be examined by a fan beam confined to a plane parallel to the film plane can be used as a form of laminography.<sup>7</sup>

Closely related to the pinhole camera is the multiple aperture collimator. This is essentially a plurality of pinholes and masks designed to image a selected volume element repeatedly onto a detector. For that particular volume element, the efficiency improves by the number of times that there are apertures. Because typically only one volume element is imaged at a time, no actual image is formed unless the aperture assembly is scanned. This technique was first developed for radioisotope scans in nuclear medicine and later adapted to the checking of ordnance detonators where

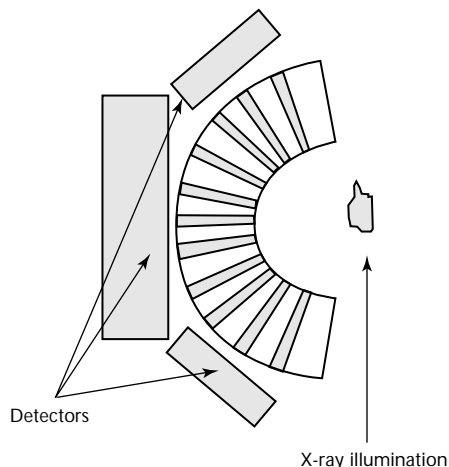
only one volume element needed to be checked. Figure 8 illustrates one form of multiaperture detector. Conical holes are drilled radially in a shielding material such as lead. The specimen, shown in gray, is illuminated from the side. Only those photons scattered at the geometric center of the collimator are detected.

### Moving Slits

By elongating a pinhole into a slit, its solid angle may be significantly increased without sacrificing resolution in one direction. Imaging slits have long been used for X-ray diffraction to create one or even two-dimensional images in reciprocal space. Reciprocal space, the fourier transform of ordinary space, is of great interest to crystallographers because it defines the periodicities of crystals. By selecting a certain region of reciprocal space with slits, two- and even three-dimensional images of a selected crystal periodicity can be obtained in ordinary space by scanning the part to be examined relative to the configuration of fixed source to slit detector. A major application is the mapping of residual stresses in machined parts.

When applied to compton scattering, slit imaging has been used in several depth profiling schemes. In these, the slits are configured to give high resolution in a direction defined as the *depth* at the sacrifice of resolution in other directions. This configuration allows a maximization of throughput. In one case the source slit detector assembly is a rigid assembly and is physically moved relative to the surface of the object under study. This makes positional accuracy independent of X-ray parameters or construction accuracy. In a second configuration, the source and one slit are stationary while the detector and an imaging slit are moved across the surface to collect scatter from progressively deeper layers (Fig. 9). Both systems have their advantages. The former is easily calibrated for depth because it is inherently a 1:1 system. It is usually configured so that the angles of both the incident and scattered photon paths are about or less than 45 degrees with respect to the surface normal. The latter is usually configured so that the scattered photon makes an angle much larger than

FIGURE 8. Multiaperture collimator. In one type of multiaperture collimator, conical holes are drilled radially in shielding material such as lead. Specimen is illuminated from side and only photons scattered at geometric center of collimator are detected.



45 degrees with respect to the surface normal.

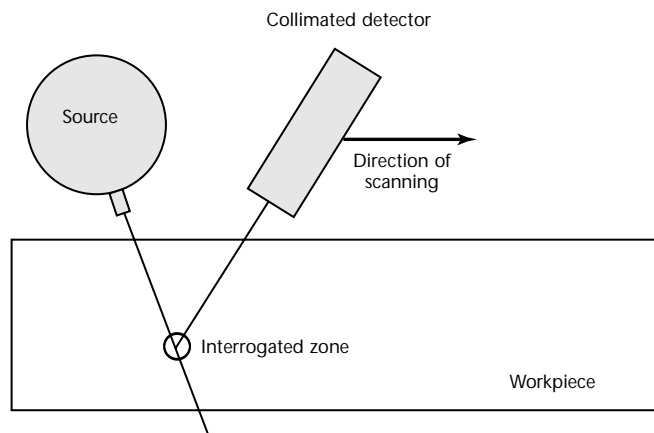
In principle, three-dimensional images can be obtained through a combination of depth scanning and lateral displacement of the imaging apparatus to create three-dimensional scanning. However, when high resolution is required in the depth direction, scanning in other directions as well is likely to be impracticable from the standpoint of the time required. Such methods have been used in the laboratory to examine organic composites.

## Flying Spot

Flying spot scanning is by far the most popular backscatter modality because of the large throughput obtainable. The detector solid angle can reach nearly  $2\pi$  steradians. Flying spot scanning was used in the very earliest forms of television, which antedated broadcast television. It was rediscovered as a means of reducing unwanted scatter in transmission X-rays in the early 1970s and soon thereafter was applied to backscatter imaging.<sup>8</sup>

The most common technique involves placing a chopper wheel in front of a long and often semicircular slot (Fig. 10).<sup>8</sup> The combination of the slot in the chopper wheel and the fixed slot together form a moving mask that limits the incident X-ray beam to whatever will pass through the mask. Usually a raster is scanned. The test object moves on a conveyor or in extreme cases the entire scanning apparatus moves. Because no reciprocating motion is needed, the speed of scanning can be correspondingly rapid and free of vibration.

FIGURE 9. Moving detector depth scanning. In slit imaging configuration, source and one slit are stationary while detector and imaging slit are moved across surface to collect scatter from progressively deeper layers.



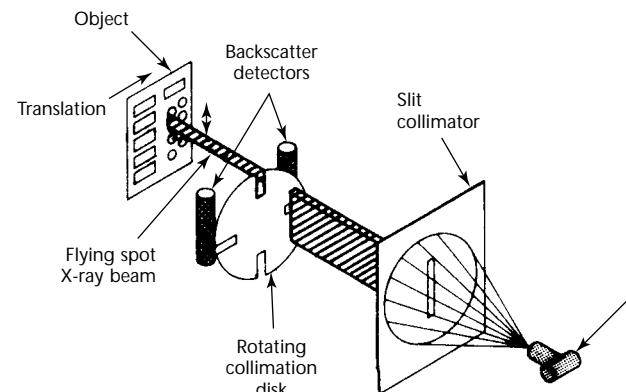
The backscattered photons are usually detected with broad area uncollimated detectors. This technique is used extensively in luggage scanners to test for bombs. As previously discussed, resolution is limited by the size of the hole formed by the moving mask while throughput increases with the square of its linear dimension.

Using a detector in conjunction with the beam catcher (safety shield), transmission and backscatter images are often collected simultaneously. These can be processed to enhance features associated with dense materials of low atomic number such as heterocyclic drugs and explosives.

Flying spot scanners have been scaled up to sizes that allow the inspection of entire trucks and freight cars. They have been adapted to mine detection by directing the beam into the ground. A recent adaptation has been the addition of collimated detectors to detect only multiple scattered photons as a means of further highlighting low Z materials having high densities. By making the hole in the mask quite large, for example, 30 mm (1.2 in.), and by using very large area detectors, the technique has been adapted for scanning humans for concealed drugs and explosives at a low X-ray dosage. Collecting data at two or more different energies allows estimation of the ratio of the scattering cross section to the linear absorption coefficient. This may be used to estimate the effective atomic number of the material being scanned to partially identify explosives, drugs or water in metal and other materials.

A significant variation on the flying spot scanner has been its combination with an imaging slit and segmented detectors. In one such configuration,<sup>2</sup> a reciprocating aperture formed by a rotating slotted cylinder placed very close

FIGURE 10. Flying spot X-ray backscatter system.<sup>8</sup>





to the anode of an X-ray tube scans the beam in one direction. Calling that direction  $X$ , the raster is completed by a drive that moves the detectors, tube and  $X$  direction scanner in the  $Y$  direction. A long imaging slit (actually two, one on each side of the scanner) parallel to the  $X$  direction images the  $Z$  direction onto segmented detectors. Thus a true three-dimensional imaging system is formed. To increase speed, three scanning slits and sets of detectors can be worked simultaneously off one tube. This system's resolution is best in the  $X$  and  $Y$  directions, about 2 line pairs per 1 mm (0.04 in.). The  $Z$  direction is divided into about 1 mm (0.04 in.) thick slices. The scanned area is about  $50 \times 100$  mm ( $2 \times 4$  in.). It has been found useful for aircraft bulkhead inspections and is one of the many backscatter techniques used for testing aircraft honeycomb.

A different approach to flying spot scanning has been to use magnetic coils to move the electron beam back and forth along the anode in an X-ray tube. This technique has been tried with a fixed aperture to move the X-ray beam back and forth or with a film anode tube to scan a raster in low energy X-rays for micro examination of thin objects. Scanning the beam would allow a higher spot intensity than would otherwise be possible in a fixed anode tube. Difficulties with this technique as a means of beam steering include the problem of keeping the electron beam in focus over a significant angular deflection, providing a tube, anode and window wide enough for significant deflection.

[The scanning beam, reversed geometry technique is discussed elsewhere in this volume.](#)

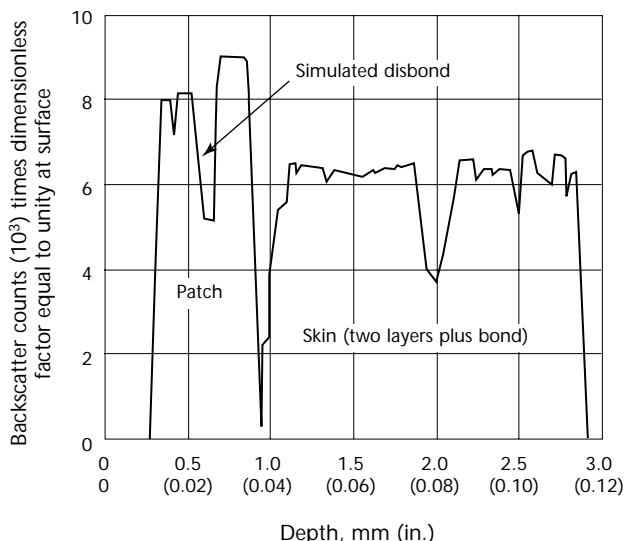
## Depth Profiling

Depth profiling has already been discussed under moving slit techniques where the moving detector technique was discussed. Here the fixed detector technique will be treated. In either case, a major issue in depth profiling is the simultaneous optimization of flux and resolution in the depth direction.<sup>9</sup> The exact solution depends on the source collimation, the linear absorption coefficient and the depth being scanned. For materials having small absorption coefficients, the angle between the source and the detector should exceed 90 degrees, permitting for a very high throughput at a given resolution. For absorptive materials, a symmetrical configuration having about a 90 degree separation between source and detector is a good choice although others including asymmetrical configurations may perform as well with compensating advantages.

The fixed detector technique has the detector in a fixed position relative to the source and both combined into a single assembly. Slits are used to control the degree of collimation and the source and detector angles. Lead screws move the assembly perpendicular to the surface of the material being probed. An array of optical gages measures the true location of the surface. Because the interrogated region is at a fixed depth with respect to the assembly, the gages return the exact depth being scanned. Depth accuracy of  $13 \mu\text{m}$  (0.0005 in.) has been achieved under field conditions. Actual accuracy in measuring the thickness of a layer depends on the size of the interrogated zone, the roughness of the surfaces involved and the amount of noise. Typical accuracies are in the range of  $\pm 0.04$  mm ( $\pm 0.0015$  in.).

Figure 11 shows a depth profile of a boron fiber composite patch applied to an aluminum aircraft skin. The scan was made on an aircraft in the field. The chart shows a parameter roughly proportional to the electron density times a factor that decreases with increasing photoelectric absorption. As expected, the organic material containing the low  $Z$  element, boron, gives a higher signal than the aluminum substrate. Each flat topped peak corresponds to a layer of material. When needed, layer thicknesses are measured at half the height of the peak using a least squares fit to the data. The simulated disbond is a thin layer of fluorocarbon polymer introduced to test ultrasonics. Commonly noise increases

FIGURE 11. Depth profile of boron fiber composite patch on cold bonded aluminum aircraft skin.





with depth because the actual number of photons is less for a scan at a constant speed. Measuring the time required to achieve a constant count would reduce noise but is impracticable where voids may be encountered. Increasing the counting time with depth is the usual practice to reduce noise.

## PART 3. Reconstruction and Image Processing Techniques

*Reconstruction* is the term for extracting an image from data that do not themselves form a proper image. Reconstruction has been used in backscatter ultrasonography and has been important in computed tomography. Except for the crude form used in depth profiling, however, reconstruction has seen little application in X-ray backscatter imaging.

Classically, reconstruction recovers a two-dimensional cross sectional slice in the plane of a fan beam from many one-dimensional projections of an object taken at regular angles. Central to Fourier techniques of reconstruction is the central section theorem that permits calculation of the Fourier transform of the cross sectional slice from the Fourier transforms of the projections. But access to all sides of the object in question is usually required to reconstruct the slice. Back projection techniques regard the reconstruction problem as one of linear algebra in which the image to be found is a matrix and the projections are analogous to row, column or diagonal sums. Such schemes are in principle more flexible and could be adapted to a variety of new problems.

Backscatter imaging has been mostly used when access is highly restricted or the specimen can be treated as two-dimensional. In luggage scanning there is no particular restriction to access and hence no reason why a back projection scheme could not develop a three-dimensional image from combined transmission and backscatter data acquired in different planes at the same time. Inspection of aircraft imposes more restrictions. Besides reconstruction, there are techniques of deconvolution to remove the blurring caused by finite apertures and similar techniques common to all image processing. These find wide use in all digital radiography.

Backscatter tomography as described above generates basically a three-dimensional data set. The only limitation to these data is that features nearer the surface cast shadows on those underneath them. These shadows may result from either enhanced absorption or enhanced scatter. However, even with the problem of beam hardening (changes in the incident photon energy distribution resulting from passing through intervening material), elimination of most

shadows would be relatively straightforward by using back projection. In principle a similar approach might be applied to flying spot scanning, especially where multiple detectors may be disposed about the periphery of the object being scanned.

In certain configurations the integrated scatter from a single pencil of X-rays or gamma rays may contain useful, quantitative chemical information. A simple example is the case when scattering is weak and the energies involved are high so that absorption can be neglected as in the common bone density measurement used in medicine. The constituents of bone — calcium, carbon, hydrogen and oxygen — have small atomic numbers and hence absorb little in proportion to their Compton scattering. The photon count can be accurately related to the amount of bone present.

Applying this principle are backscatter thickness gages for sheet stock. In most cases the photon count is not precisely linear with the thickness of the metal. Because the metal is uniform in its constitution, however, the only contribution would be from changes in thickness. Dual energy techniques depend on the atomic number of the material examined because photoelectric absorption changes much more quickly with photon energy than does Compton scattering. In depth profiling the same type of information is obtained using a single energy or band of energies. This is because it allows a comparison of the attenuation of the incident X-rays with the amount of backscatter given off.

Another reason computed tomography has not been extensively applied to backscatter tomography is that it does not significantly improve the image in most cases. A test was performed with a commercial backscatter tomography system<sup>2,3</sup> on a phantom composed of aluminum sheets, rivets and a pellet of aluminum corrosion product (Fig. 12). Figures 12b and 12c show respectively a section through the pellet area and another section through the upper surface of the bottom plate. The bottom plate itself was inherently featureless because the rivets filled the rivet holes. However, the rivet heads, the corrosion pellet and sides of the bulged region of the top plate

appear as shadows. These shadows could have been removed through reconstruction but have weak contrast in comparison with the strong contrast of the backscatter itself. The added noise from the reconstruction could possibly have been more detrimental than the shadows.

Reconstruction has been applied in depth profiling because it leads to a more readable chart. The one-dimensional nature of the problem simplifies the reconstruction problem significantly. It also provides a simple way of explaining what is needed in backscatter reconstruction. As the X-radiation passes into the material it is both scattered and absorbed. Thus as the probe penetrates deeper, there is less of it. Also, as it penetrates deeper, the lower energy photons are absorbed or scattered preferentially over those with higher energies. Thus the average energy of the photons in the probe tends to increase with depth. This is why these changes are called beam hardening. Similarly, after the probe has been scattered at some point

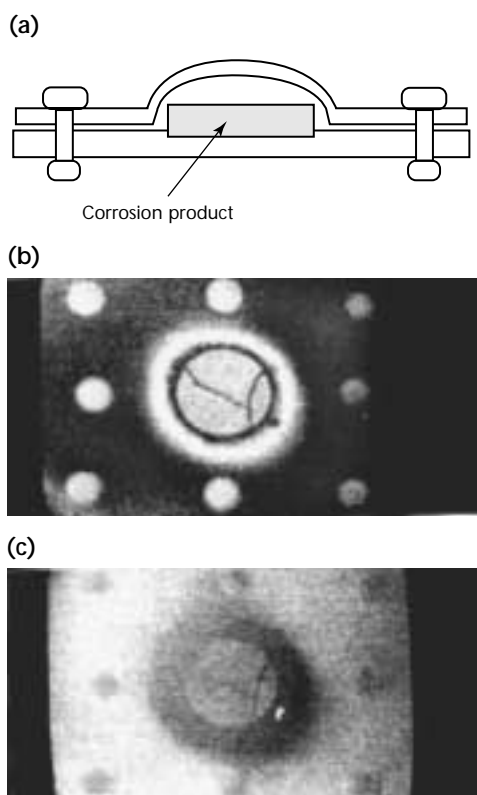
under study, the same effects also act on the photons as they return to the detector.

Essentially the reconstruction problem is how to boost the signal to compensate for increasing depth. A first order approach is to boost it in proportion to the amount of signal collected including any previous boost. If photoelectric absorption were not a factor, such a technique could easily guarantee that the resulting scan would be a chart of electron density versus depth. But absorption is significant and varies from material to material. In addition to boosting the signal in proportion to the integrated backscatter, an empirical power law has been used to compensate for beam hardening. When the composition of the structure being studied is known, the correction constants are known *a priori*. In other cases, it may be assumed that the appropriate material constants will result in essentially level, flat topped peaks as shown in Fig. 11. Different constants may be applied to different layers.

Besides reconstructions there are also other techniques of image processing that can be applied to backscatter signals. One of these is deconvolution to remove the aperture function. These techniques are extensively discussed in their own literature.

Salient to backscatter imaging is the problem of quantum noise. Because deconvolution is essentially high pass filtering, it tends to exaggerate quantum noise. Experimentally, fourier techniques have met with only limited success. Iterative techniques in the spatial domain work better because unrealistic excursions can be trimmed along the way. Von Citer's technique<sup>10</sup> is the starting point for a variety of iterative techniques.

FIGURE 12. Backscatter tomography of phantom composed of aluminum sheets, rivets and pellet of aluminum corrosion product: (a) schematic of side view, showing pellet and dome; (b) slice through pellet and dome; (c) slice through bottom plate.



## Sensitivity

In transmission shadowgraphic radiography, sensitivity is generally defined as being the smallest change in material thickness that can be detected on film. This type of sensitivity is measured with an image quality indicator. In volume imaging or depth profiling, the voxel size is a measure of resolution and roughly corresponds to sensitivity in transmission shadowgraphic radiography. By analogy, sensitivity for integrated backscatter techniques may be defined as the minimum detectable change in thickness.

Other possible *sensitivities* can be defined, too. Minimum detectable change in density is one. In backscatter radiography, quantum noise is the usual limiting factor in any density measurement. For a given material, test

configuration and source intensity, the number of counts will not be constant but will be poisson distributed. The poisson distribution has the convenient property that its mean is also its variance. Thus the expected deviation in the number of counts is the square root of that number of counts.

If a plot or image is examined and a step or dip or contrasting region is seen, the null hypothesis that the perceived change is only the result of noise must first be tested. The subject of statistics is a long one but one well treated in texts. If a rule of thumb is needed, the null hypothesis may be rejected if the change is more than two standard deviations of the noise level. The contribution of background radiation to noise is low if equipment is well designed. For example, consider a volume element that contributes 8100 counts. The square root of that number is 90, the expected standard deviation. Thus if an adjacent element has more than  $8100 + 180 = 8280$  counts, it would be presumed to represent no fluctuation in density. Thus the sensitivity to changes in density would be on the order of  $180/8100 = 0.02$  or 2 percent.

Sensitivity in terms of dimensions has previously been mentioned. Where dimensional measurements are based on edge location, the size of the interrogated volume (Fig. 7), is important in determining dimensional sensitivity. However, the dimensional accuracy is better than the resolved dimension shown because edges can be located by numerical fitting. The problem again reverts to one of quantum noise and its effect on the fit. In the case of very small gaps, these appear in the image or chart convolved with the aperture function, that is, the transmission of the aperture. In fact they look like an image of the aperture. Measurement of such small features is based on the size of the dip they produce in the intensity of the surrounding image. For example, if an aperture function were rectangular, a gap one tenth the width of the aperture function (essentially the resolved dimension of Fig. 7) would produce ideally a 10 percent dip in the signal. Whether a 10 percent dip is detectable depends on the number of photons counted.

## PART 4. Applications of Backscatter Imaging

The principles and techniques described above have evolved in different ways to meet the needs of numerous applications. It is not possible to describe them all here. What follows is a sampling of applications selected to bring out major points of interest.

### Ordnance

X-ray backscatter has proven itself useful in two areas related to ordnance. The most direct is the checking of fuses and detonators in artillery shells and similar devices. There is a need to routinely check these to see whether they have been fused at the beginning of a mission and defused afterward. For obvious reasons of safety, a noncontact technique of checking ordnance fuses is preferred. Transmission radiography has been used to check the contents of food cans and other applications similar to the checking of ordnance fuses. However, artillery shells are typically made of thick steel and other relatively heavy metals. The fuses are made of organic materials and show little contrast in transmission radiography. But, being relatively dense organic materials, the composition of the fuses does scatter radiation well and absorbs little. This has allowed the construction of automatic fuse checking equipment.

The second area of use for X-ray backscatter in relation to ordnance is mine detection. The problem and technology of mine detection are, not surprisingly, similar to baggage scanning. Early mine detectors often relied on the metallic nature of the housing of a mine to detect it. As with most of the apparatus of contemporary life, the need for a metallic housing has been obviated in antipersonnel mines — contributing little to the mine besides weight and detectability. As with the ordnance fuses, the high density of low atomic number elements needed to make an explosive facilitates detection of mines by X-ray backscatter. It is perhaps fortunate to those faced with cleaning up nonoperative mine fields that an absolutely undetectable mine is of little use to any military force.

For checking ordnance fuses a narrowly collimated incident beam has been configured with a multiaperture

collimator similar to that shown in Fig. 8. One example was configured to identify cracks voids and anomalies in the filler on the order of 1.6 mm (0.063 in.) through a 13 mm (0.5 in.) thick steel case.<sup>11</sup> An isotope source of cobalt-60 yielding gamma rays of 1.17 and 1.33 MeV was used to penetrate the steel case. The detector collimator was oriented roughly 90 degrees to the incident beam. The same configuration was also evaluated to check for the presence of explosives in demilitarized practice bombs.

Mine detectors using compton backscatter have evolved along much the same lines as luggage scanners. Some may use isotope sources (anecdotal) for portability. Others use small X-ray machines.<sup>12</sup> These use the principle of flying spot scanners although the scanning of the spot may be semimanual via a gantry. The spot size is usually on the order of 10 to 20 mm (0.4 to 0.8 in.). Usually uncollimated detectors are used to maximize throughput. Mines are recognized primarily by their shape and scattering characteristics. Antipersonnel mines are usually made of plastic while heavier antitank mines are made of metal to provide more tamping. In the event that a mine uses lead azide or mercury fulminate as a detonator, fluorescence radiation in the 80 keV range may be detected. These high energy fluorescence photons can escape through earth, plastic and thinner metal housings. This is the subject of a United States Patent.<sup>13</sup>

Recently the concept of lateral migration radiography has been applied to land mine detection.<sup>14</sup> Lateral migration radiography is imaging of specifically multiple-scattered photons. As mentioned previously, explosive materials and plastics are expected to favor multiple scatter. To accomplish multiple scatter imaging, detectors collimated to exclude singly scattered photons are used. In practice the multiple scatter detectors are augmented with noncollimated detectors to provide an image conventional for mine detectors. It is reported that the air volumes in the land mines give them *unique signatures* apart from their multiple scatter characteristics. The air volume is necessary to the functioning of the mine because it gives something to compress to translate applied pressure into mechanical displacement that activates the mine. The

air volume also gives free flight to the photons that appear through rescattering at some distance from their point of entry. This double scattering is the rationale behind lateral migration radiography.

## Corrosion, Aircraft

Second only to the interdiction of drugs and bombs in suitcases, no other application has stimulated the imaginations of inventors more than aircraft inspections. The need for techniques of corrosion detection and evaluation that require access only to the outside of an aircraft has drawn attention to X-ray backscatter as a desirable choice. That X-ray backscatter can be especially good at detecting voids is an additional bonus.

Transmission shadowgraphic radiography remains the technique commonly used for corrosion evaluation around windows and door frames. While adequate to the task, removing a plane's interior furnishings is usually required. Lap splices are often checked by ultrasonic, eddy current or visual testing. Again, these techniques have been proven adequate to the task of detecting corrosion but evaluation of the damage in terms of metal loss still requires dismantling the joint. Also, ultrasound is only useful for inspecting the first layer in commercial aircraft because their construction often involves faying strips that create benign air gaps in older planes. Air gaps block ultrasound. Military aircraft are usually constructed without faying strips; the air gap problem is less acute with military planes. The ability of X-ray backscatter depth scans to gage the thickness of subsurface layers has suggested its use to measure metal loss.

Commuter aircraft designed to be commissioned on the *safe life* basis were expected to fly only so many cycles. Because they were not expected to require airframe inspections, they often have *uninspectable* areas — especially in the tail. Recommissioning them to extend their life requires a means of inspecting these areas. What makes them *uninspectable* is limited access. Adding ports for borescopes has helped solve the inspectability problem. However, X-ray visualization requiring only single side access would also be helpful.

X-ray backscatter tomography has been introduced for the purpose of general inspection. Two systems that have been tried are a commercial system<sup>2,3</sup> and another system developed by an aviation manufacturer.<sup>15</sup> The former has gradually gained some acceptance and is used for the inspections of aft pressure bulkheads

in aircraft for corrosion and large cracks.<sup>3,16</sup> X-ray backscatter tomography, while unable to resolve fine cracks that may result from fatigue corrosion processes, is able to visualize the mechanical distortions that take place in corroding aircraft as a result of accumulated corrosion product.

Commercial aircraft alloys, generally aluminum copper, are susceptible to corrosion but fortunately most structural members are made of alloys not particularly susceptible to stress corrosion or fatigue corrosion (environmental fatigue). This means that the enhancement of fatigue by corrosion results almost entirely from metal loss. High strength alloys in landing gear are likely to experience fatigue cracking in advance of discernible corrosion damage but these parts are easily accessed for inspection. Military aircraft are more likely to use higher strength and therefore less forgiving alloys. Aluminum alloys containing magnesium are among those susceptible to exfoliative corrosion, a type of intergranular corrosion that can be very damaging before it is noticed. Hence the inspection requirements differ for the two classes of aircraft.

The corrosion products of aluminum are hydrated aluminum oxides. They are rarely crystalline and have comparatively low densities, being roughly half water by weight.<sup>17</sup> Electron density correlates with density. Furthermore, aircraft corrosion products *in situ* appear to contain many voids and are surprisingly difficult to isolate when parts are dismantled. In depth profiling, artificially grown corrosion products scatter less than the parent aluminum. A similar relation is suggested by Fig. 12b when the brightness of the dome is compared with that of the pellet. Table 1 compares some sample densities.<sup>18</sup> The aircraft skin corrosion products listed were measured in a dry and essentially void free condition. Gibbsite is not a primary aircraft corrosion product and is included for reference.

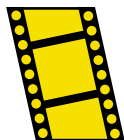
A characteristic of aircraft corrosion is swelling caused by the formation of corrosion products. Corrosion within lap splice joints causes swelling between the rivets leading to a phenomenon called *pillowing*. Exfoliative corrosion causes the

TABLE 1. Aircraft corrosion products.

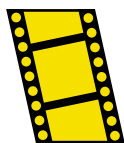
Material	Density (g·cm <sup>-3</sup> )
Aluminum	2.71
Commercial aircraft corrosion product	2.0
Military aircraft corrosion product	2.1
Crystalline gibbsite (Al <sub>2</sub> O <sub>3</sub> ·3H <sub>2</sub> O)	2.42



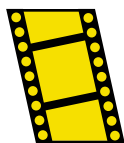
MOVIE.  
Backscatter  
scan of  
undamaged  
area.



MOVIE.  
Moving  
source and  
sensor into  
place.



MOVIE.  
Pillowing  
and  
corrosion.



metal itself to swell and in extreme cases burst in pocklike eruptions.

Apart from three-dimensional backscatter tomography, a number of two-dimensional techniques are in use. These have their origins in thickness gaging and flying spot scanning techniques. One example is the compact backscatter gage developed by an aviation manufacturer.<sup>19</sup> This hand held device incorporates a collimated americium-241 isotope source of 60 keV low level gamma radiation. Surrounding the source is a scintillator. The device also includes a position sensor. As it is manually swept over the surface to be examined, the location of the source is recorded allowing the accumulation of a two-dimensional image in a manner similar to that mentioned for mine detectors. It may be operated in any of several modes: as a thickness gage, as a two-dimensional imager, as a profile scanner and as an edge locator. For automated edge location, a gantry is used.

To detect corrosion, the technique detects gaps. In forming, corrosion products separate metal members. Often the corrosion product is leached out or dries leaving behind gaps. The presence of subsurface gaps reduces the count rate. When the position encoder is engaged, subsurface gaps can be mapped. This mapping has facilitated the use of the gage to detect blistering and pitting of aircraft skins because of corrosion. A related application is the detection of water in honeycomb. Should water invade honeycomb, it corrodes rapidly losing strength. The additional material in the form of trapped water has been visualized in detail using backscatter tomography but is more easily detected with the hand held backscatter probe. Hand held nonimaging backscatter probes have also been used for the detection of contraband. A gantry mounted version of this configuration, more directly resembling a mine detector, has been reported.<sup>20</sup>

One-dimensional scanning techniques have also been applied in the form of depth profiling to measuring metal loss due to corrosion. One-dimensional scanning has the advantage that the thickness measurement depends on thickness only and is unrelated to the material's X-ray constants.<sup>21</sup> The integrated backscatter techniques of thickness measurement depend strongly on the properties of what is being measured and must be specifically calibrated for the material. They are of little value when layers of different materials are present simultaneously. One-dimensional scanning is best when maximum resolution in the thickness direction is needed, as discussed above.

## Corrosion, Pipeline

Pipelines for carrying petroleum are subject to corrosion and need inspection. These pipes often have metal clad insulating jackets. If the jackets can be removed and the pipes can be drained for inspection, there is little problem with using ultrasonic techniques or film radiography using a radioisotope. However, when the pipes are full of oil, there is very little backwall reflection in ultrasonic inspection and no way of introducing an isotope. The reflection problem is further aggravated when corrosion product adheres to the interior of the pipe.

Fortunately, corrosion much more frequently takes place on the outside of the pipe. This creates a rough surface problem for ultrasound. Integrated backscatter thickness gaging is useful when pipes are dry and corrosion products are not present. It is of little value when pipes are filled with oil. Attempts to use tomographic backscatter imaging have met with only limited success because the limited photon energy available did not allow good imaging of steel. Depth profiling using the moving detector technique discussed above also met with little success when pipes were filled with oil. Similar problems are also met in offshore oil lines.<sup>22</sup>

An innovative approach is to use multiple scattering within the oil to illuminate the pipe from the inside.<sup>23</sup> Thickness may then be gaged by a calibration process or thin areas visualized with film or detector arrays placed on the outside of the pipe. It should be emphasized that when iron corrosion products adhere to the pipe, thickness measurements of any sort are unreliable. It is conceivable that the amount of corrosion product could be determined through the 6.92 MeV resonance fluorescence of oxygen.

## Composites

Composite materials formed of resins and fibers are highly dispersive to ultrasound transmission. Thick sections are extremely difficult to inspect with ultrasound. There is also a masking effect: surface layer disbands prevent penetration of the ultrasound and hide the extent of damage. Organic fiber composites are usually dielectric and so unsuitable for eddy current testing. Because most damage involves little change in volume, transmission radiography has difficulty finding it. Because Compton scattering is relatively strong in low Z materials and because backscatter techniques are more

sensitive to small changes in density than are transmission techniques, X-ray backscatter imaging shows considerable promise for detecting damage in composite structures too thick for ultrasonic testing.

Commercially available backscatter tomography has been evaluated in comparison with ultrasonic techniques for testing of joints in composite materials.<sup>24</sup> In any test technique using optical radiation, the resolution of an incoherent or energy technique can be no better than the wavelength. While coherent phase based techniques can improve on this, they are not practicable for ultrasonic testing of composites — to a large extent because they are composites. Reducing the ultrasonic wavelength substantially reduces the penetration depth in these materials. In contrast, X-ray techniques are not limited by their wavelengths because these are extremely short. The resolution tradeoff appears to favor backscatter tomography for depths greater than several millimeters in many cases.

Besides the issue of resolution there is the problem of shadows created by surface damage that hide damage underneath. This is especially important when imaging delaminations, internal cracks in the plane of the material caused by impact damage or faulty layup. A backscatter depth profiler with an  $X, Y$  translation stage has shown that very tiny delaminations can be studied and compared with ultrasonic microscopy.<sup>25</sup> The special advantage of backscatter is that it can resolve delaminations underneath other delaminations. Ultrasonic microscopy in common with other ultrasonic techniques can only resolve those delaminations in a direct line of sight from the surface.

## Concrete

Compton backscatter has proven itself useful as a means of measuring density. For this reason there is considerable interest in using gamma backscatter to measure the density of concrete. Because the actual density of concrete depends on its flow during pouring, poured concrete may be nonuniform in strength. The results obtained from testing samples of the mix poured into containers may not be representative — especially of consolidation in the vicinity of reinforcement. This has motivated the development of backscatter techniques for the purpose for which it seems well suited.

Another area of interest, the testing of concrete structures for rebar corrosion, is still difficult by any means. In the laboratory, X-ray measurements of

concrete specimens for segregation has long been practiced. Recently computed tomography has obviated the sectioning of samples. Where surface measurements suffice, many of these same techniques seem applicable in the field using X-ray backscatter techniques with the flying spot or other<sup>2,3</sup> configuration. For measuring metal loss in rebar corrosion, where the corrosion product remains in place, experience suggests that this is outside the reach of the present resolution versus depth tradeoff because the scale of measurement is in tens of micrometers at a depth of tenths of meters (thousandths of an inch at a depth of inches). On the other hand, sampling the average density of concrete may actually benefit from low resolution because this means a larger sample of the aggregate. Similar remarks also apply to asphalt pavings.

A major factor in the strength of concrete is the fraction of air that becomes entrapped in the mix. Nuclear gaging of several types is used to test concrete largely with this problem in mind. One technique is gamma backscatter imaging. The American Society for Testing and Materials provides a standard for the testing of concrete by gamma backscatter.<sup>26</sup> This technique measures only an average density and represents the state of the art at the turn of the millennium. The backscatter technique has been criticized for giving too much weight to top layers, for being too sensitive to chemical effects and for being susceptible to interference from rebars. The American Society for Testing and Materials standard attempts to address these issues. Similar standards have been issued by several state governments. Location of rebars and voids through flying spot techniques has been proposed and is under investigation.

The evaluation of concrete is a good place to examine the principles of backscatter density measurement. The essential idea is deceptively simple. A cesium-137 (662 keV) source is used to emit gamma photons into the concrete. A photon detector is placed at some small distance from the source. The response of the detector is a function of the density of the concrete. The function is not a simple one, however — the geometry is simple but the integrals involved are not. To get a qualitative picture of the process simplifying assumptions are needed. The source and the detector are separated by a distance  $d$ , called the *sonde length*. If the penetration is shallow relative to the sonde length, the total round trip path  $z$  from the source to depth to the detector is about  $z + d$ . If the change in the solid angle of the detector with depth is neglected, an expression similar to that given before is obtained:

$$(10) \quad \text{Scattering} = \frac{I_0 \sigma}{d^2 \mu} \exp(-\mu d)$$

for an infinitely thick section. Let  $\sigma = c_1 \rho$ , where  $\rho$  is density and  $\mu = c_2 \rho$ . Then expanding the exponential gives the following result:

$$(11) \quad \frac{I_0}{d^2} \left( \frac{c_1}{c_2} - c_1 d \rho + c_1 c_2 d^2 \frac{\rho^2}{2} - \dots \right)$$

which is a power series in the density. Of course the assumptions made are too simple. A typical calibration formula takes the form of Eq. 12:

$$(12) \quad \begin{aligned} \text{Scattering} = & A_1 \rho \exp(-B_1 \rho) \\ & + A_2 \rho^2 \exp(-B_2 \rho) + \dots \end{aligned}$$

When this equation is plotted it gives zero for zero density, then reaches a peak at some intermediate density and, following that, tails off to give zero for infinite density. Thus for any reading obtained, there are two possible densities. The densitometer is designed to make one of these unrealistic for the expected conditions of use.

## Closing

Backscatter imaging is a powerful technique with a growing list of applications. Additional publications document its capabilities.<sup>27-30</sup>

## References

1. International Union of Crystallography. *International Tables for X-Ray Crystallography*, Vol. C: *Mathematical, Physical and Chemical Tables*. Dordrecht, Netherlands: Kluwer Academic Publishers (1999).
2. Kosanetzky, J.M., G. Harding, K.H. Fischer and A. Meyer. *Compton Backscatter Tomography of Low Atomic Number Materials with the ComScan System*. Philips Technical Information Bulletin. Hamburg, Germany: Philips GmbH (1988).
3. Kosanetzky, J.M. *Inspection of the Pressure Bulkhead of an Aircraft*. ComScan Application Note. Hamburg, Germany: Philips GmbH (undated, ca. 1990).
4. Yang, C.N. "Actual Path Length of Electrons in Foils." *Physical Review*. Vol. 84. Melville, NY: American Physical Society (1951): p 599-600.
5. Archipov, G.A., E.G. Golukov, B.L. Dvinyaninov, P.P. Zol'nikov, Y.A. Kovyazin and K.A. Sukhanova. "Using Scattered Gamma Radiation for Detecting Subsurface Defects in Metal" [translation]. *Defektoskopiya - The Soviet Journal of Nondestructive Testing*. No. 3. New York, NY: Consultants Bureau (1976): p 55-60.
6. Hasenkamp, F.A. "Radiography Using Scattered Radiation." Presented at ASNT's *Conference on Innovative and Advanced NDT Radiography* [Wilmington, DE] (August 1977).
7. Strecker, H. "Scatter Imaging of Aluminum Castings Using an X-Ray Fan Beam and a Pinhole Camera." *Materials Evaluation*. Vol. 40, No. 10. Columbus, OH: American Society for Nondestructive Testing (September 1982): p 1050-1056.
8. R.H. Bossi, K.D. Friddell and J.M. Nelson. "Backscatter X-Ray Imaging." *Materials Evaluation*. Vol. 46, No. 11. Columbus, OH: American Society for Nondestructive Testing (October 1988): p 1462-1467.
9. Lawson, L. "Flux Maximization Techniques for Compton Backscatter Depth Profilometry." *Journal of X-Ray Science and Technology*. Vol. 4. Amsterdam, Netherlands: IOS Press (1993): p 18-36.
10. Qiu, F., W.L. Anderson and P.S. Ong. "Deconvolution of X-Ray Backscatter Diffraction Data for NDE of Corrosion." *Progress in Quantitative Nondestructive Evaluation*. Vol. 12. New York, NY: Plenum (1993): p 1979-1985.
11. Stokes, J.A., K.R. Alvar, R.L. Corey, D.G. Costello, J. John, S. Kocimski, N.A. Lurie, D.D. Thayer, A.P. Trippe and J.C. Young. "Some New Applications of Collimated Photon Scattering for Nondestructive Examination." *Nuclear Instruments and Methods*. Vol. 193. Amsterdam, Netherlands: North Holland Publishing Company (1982): p 261-267.
12. Lockwood, G., S.L. Shope, J.C. Wehlberg, M.M. Selph, J.M. Jojola, B.N. Turman and J.A. Jacobs. "Field Tests of Xray Backscatter Mine Detection." *Proceedings of the 2nd International Conference on the Detection of Abandoned Land Mines* [Edinburgh, United Kingdom, 1998]. IEE Conference Publication No. 458. Stevenage, United Kingdom: Institute of Electrical Engineers (1998): p 160-163.
13. Annis, M. and P. Bjorkholm. *Shadowgraph Imaging Using Scatter and Fluorescence*. United States Patent 4 839 913 (1989).
14. Su, Z., A. Jacobs, E.T. Dugan, J. Howley and J. Jacobs. "Lateral Migration Radiography, Application to Land Mine Detection and Classification." *Optical Engineering*. Vol. 39. Bellingham, WA: International Society for Optical Engineering (2000): p 2472-2479.
15. Black, G.L. *Advanced Development of Backscatter Imaging Tomography*. Final Report, WL-TR-93-4015. Wright Patterson Air Force Base, OH: Air Force Wright Laboratory (November 1995).
16. "Midcoast Purchases ComScan 160 II X-Ray System to Complete Gulfstream 580 Bulkhead Inspections." Press release. Saint Louis, MO: Midcoast Aviation (May 1999).
17. "The Analysis and Composition of Aluminum Corrosion Products." NACE Publication 60-5. *Annual Conference: Corrosion*. Vol. 16. Houston, TX: NACE International (1960): p 181t-187t.

18. Lawson, L. *X-Ray Backscattering*. Final Report, National Aging Aircraft Research Program (NAARP), NDI 4, Subtask D, Radiographic Methods for Corrosion Inspection. Washington, DC: Federal Aviation Administration (2001).
19. Schulte, R.L. *Two-Dimensional Imaging Backscatter Probe*. United States Patent 5 763 886 (1998).
20. Dunn, W.L. and A.M. Yacout. "Corrosion Detection in Aircraft by X-Ray Backscatter Methods." *Applied Radiation and Isotopes*. Vol. 53. New York, NY: Pergamon Press (2000): p 625-632.
21. Lawson, L. "Compton X-Ray Backscatter Depth Profilometry for Aircraft Corrosion Inspection." *Materials Evaluation*. Vol. 53, No. 8. Columbus, OH: American Society for Nondestructive Testing (August 1995): p 936-941.
22. Bridge, B. "A Theoretical Feasibility Study of the Use of Compton Backscatter Gamma-Ray Tomography for Underwater Offshore NDT." *British Journal of Non-Destructive Testing*. Vol. 27. Northampton, United Kingdom: British Institute of Non-Destructive Testing (1985): p 357-363.
23. Ong, P.S., W.L. Anderson, B.D. Cook and R. Subramanyan. "Transscatter X-Ray Technique for the Inspection of Insulated, Oil-Carrying Pipelines." *Review of Progress in Quantitative Nondestructive Evaluation*. Vol. 12. New York, NY: Plenum (1993): p 295-301.
24. Roye, W. "The Reliability of Nondestructive Techniques within the Field of Modern Composite Materials." *British Journal of Non-Destructive Testing*. Vol. 33, No. 11. Northampton, United Kingdom: British Institute of Non-Destructive Testing (November 1991): p 549-550.
25. Kim, N. and J. Achenbach. "Quantitative Characterization of Multiple Delaminations in Laminated Composites Using the Compton Backscatter Technique." *Journal of Nondestructive Evaluation*. Vol. 17. New York, NY: Plenum (1998): p 53-65.
26. C 1040-93 (2000), *Standard Test Methods for Density of Unhardened and Hardened Concrete in Place by Nuclear Methods*. West Conshohocken, PA: ASTM International (2001).
27. Evans, R. *The Atomic Nucleus*. New York, NY: McGraw-Hill (1955).
28. Huddleston, A. and J. Sackler. "Determination of Electron Density by the Dual-Energy Compton Scatter Method." *Medical Physics*. Vol. 12. New York, NY: American Institute of Physics, for the American Association of Physicists in Medicine (1985): p 13-19.
29. MacKenzie, I.K. *Method and Apparatus for Measuring Thickness of Paint Layers on Substrates Using Backscattered X-Rays*. United States Patent 5 862 199 (1999).
30. Williams, B.G. *Compton Scattering*. New York, NY: McGraw Hill (1977).

## CHAPTER

# Special Radiographic Techniques<sup>1</sup>

Richard D. Albert, Digiray Corporation, Danville,  
California (Part 3)

Richard C. Barry, Lockheed Martin Missiles and Space,  
Palo Alto, California (Part 4)

Francis M. Charbonnier, McMinnville, Oregon (Part 2)

Edward H. Ruescher, Coeur d'Alene, Idaho (Part 4)

William P. Winfree, National Aeronautics and Space Administration, Hampton, Virginia (Part 3)



## PART 1. Microfocus Radiographic Testing<sup>2</sup>

Projection radiography can be accomplished with a true microfocus X-ray source — that is, an X-ray tube or other source with an electron focal spot smaller than 0.1 mm (0.004 in.). In practice, focal spots from 0.002 to 0.025 mm (0.0001 to 0.001 in.) have proven to be the most useful for radiosopic systems<sup>3</sup> whereas spots from 0.025 to 0.075 mm (0.001 to 0.003 in.) have proven satisfactory for film techniques using moderate magnification levels. Film techniques have been documented previously in the literature.<sup>3-5</sup> Successful radiosopic projection using microfocal equipment was limited before the mid-1980s by a combination of low X-ray output, marginal X-ray system reliability and a total lack of real time performance specifications other than the quality indicators generally required for film radiography.<sup>5</sup> Since then the technique has continued to develop in various applications.<sup>6-13</sup> New imaging technologies using screens of amorphous silicon, amorphous selenium and other materials offer a variety of solutions for industrial real time imagery. Engineers and researchers will continue to introduce designs and integrate new materials to adapt the technology for field use.

### Projection Microfocus Radioscopy

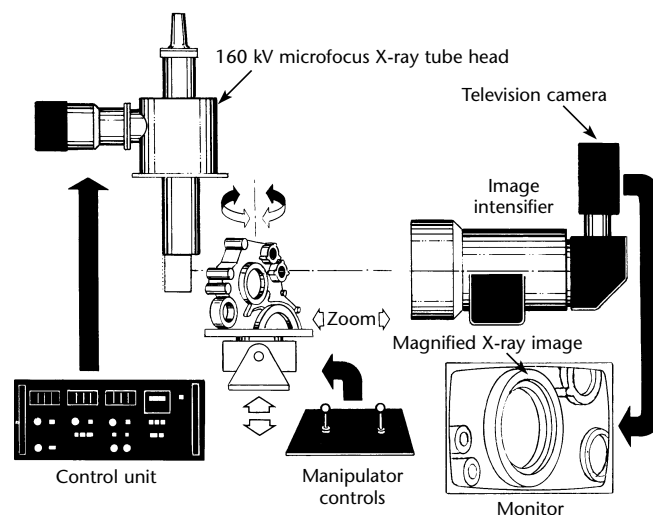
A typical system for testing of smaller objects contains digital radiosopic components. One type of system that has shown versatility in many applications has been remote video viewing systems like those in Fig. 1. The X-ray source is a 160 kV constant potential microfocus unit capable of 300 W operation at a focal spot size of 0.25 mm (0.01 in.). It can also operate continuously at 80 W with a focal spot of 0.012 mm (0.0005 in.). This means that the X-ray unit can operate continuously at 160 kV and 0.5 mA with a 12  $\mu\text{m}$  ( $5 \times 10^{-4}$  in.) focal spot size and, in this configuration, can resolve details as small as 25  $\mu\text{m}$  (0.001 in.) at a 1:1 geometric relationship without magnification.

Low light level imaging cameras combined with high resolution fluors or X-ray image intensifiers and camera

combinations are capable of resolving ten to two line pairs per millimeter (250 to 50 line pairs per inch), respectively, as measured by resolution test pattern, with good contrast (better than 50 percent modulation of the composite video signal). Accordingly, these video systems cannot resolve the fine details (0.1 mm [0.004 in.] or less) available in the X-ray image at 1:1 magnification. However, if projection magnification techniques of 10 $\times$  or greater are used, even the two line pair per millimeter system can resolve a 20 line pair per millimeter (500 line pair per inch) test pattern as shown in Fig. 2 (these images are radiographic positives).

The geometry used for the test data was a distance from source to detector of 1.50 m (60 in.) and a distance from source to object of 0.15 m (6.0 in.), producing the 10 $\times$  projection magnification. The radiosopic imaging system used a 0.23 m (9.0 in.) X-ray image intensifier optically coupled with a 15 MHz closed circuit television fitted with a 25 mm (1.0 in.) vidicon image tube. With low absorbing materials, projection magnifications of 50 $\times$  or more can be obtained; 100 $\times$  projections have been achieved. The arrangement shown, or others, can also use deposited rare earth screens or crystal fluors if the camera is equipped with a sufficiently sensitive image tube such as a silicon intensified target or an intensified

FIGURE 1. Microfocus X-ray video system.



vidicon tube. These combinations of camera, screen and crystal can be less expensive than a cesium iodide image intensifier but the images produced are usually much noisier.

## Zoom Technique

A useful technique that can be achieved with radiosopic projection microfocus radiography is that of *zooming*, or dynamically positioning the object with a manipulator between the X-ray tube and image receptor. In this technique, the object is moved between the X-ray tube and the image intensifier (Fig. 1). The effect of this motion is shown in Fig. 3. The object illustrated is a single integrated circuit initially situated for low projection magnification (about 5 $\times$ ). The resultant image is shown as it appeared on the television monitor in Fig. 3a. The integrated circuit was then zoomed toward the X-ray tube through 10 $\times$  as shown in Fig. 3b, 20 $\times$  in Fig. 3c and finally to about 50 $\times$  in Fig. 3d. It is evident that the higher the projection magnification, the more detail one can see in the integrated circuit, even down to the solder joint voids in the bond of the silicon chip to the substrate, the individual soldered leads and the etching of the metal substrate. The total length of the metal components of the integrated circuit is 18 mm (0.7 in.).

A similar test, done on a metal jet engine turbine blade, is shown in Fig. 4. The entire blade as shown in Fig. 4a displays no obvious discontinuities.

**FIGURE 2.** Lead resolution tester, showing 20 line pairs per millimeter (500 line pairs per inch).

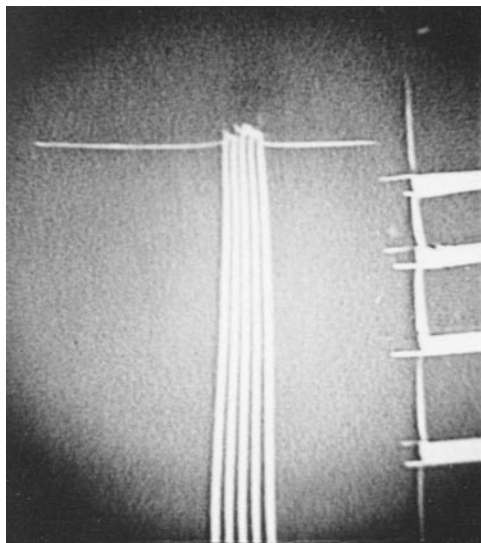


**FIGURE 3.** Sequence of radiographic video magnifications of integrated circuit: (a) low magnification; (b) medium magnification; (c) high magnification; (d) ultrahigh magnification.

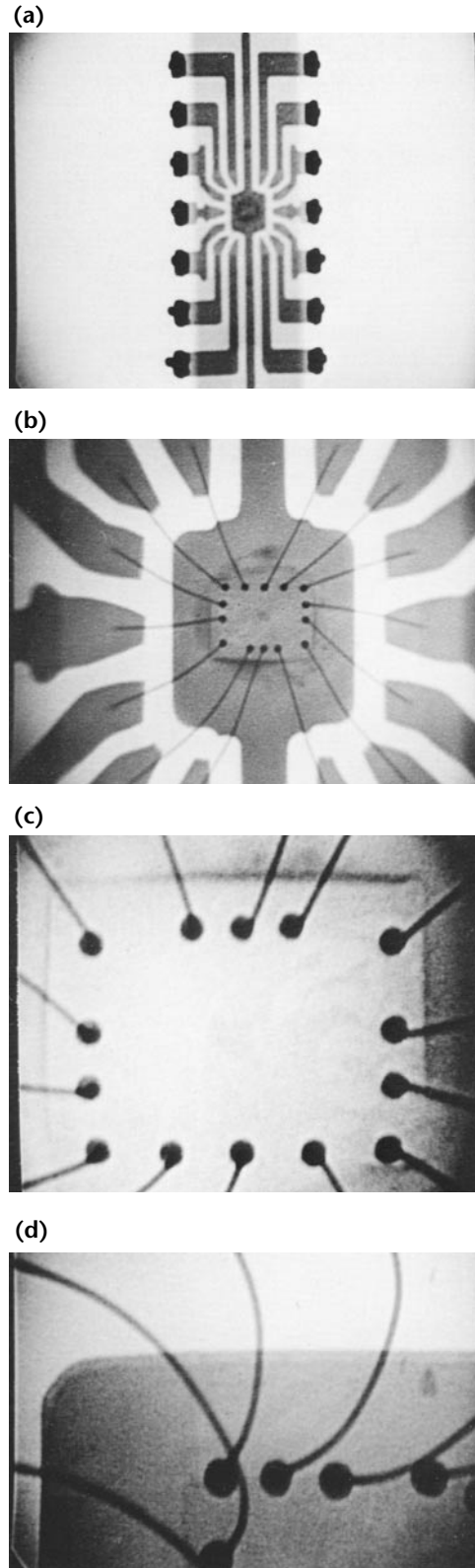
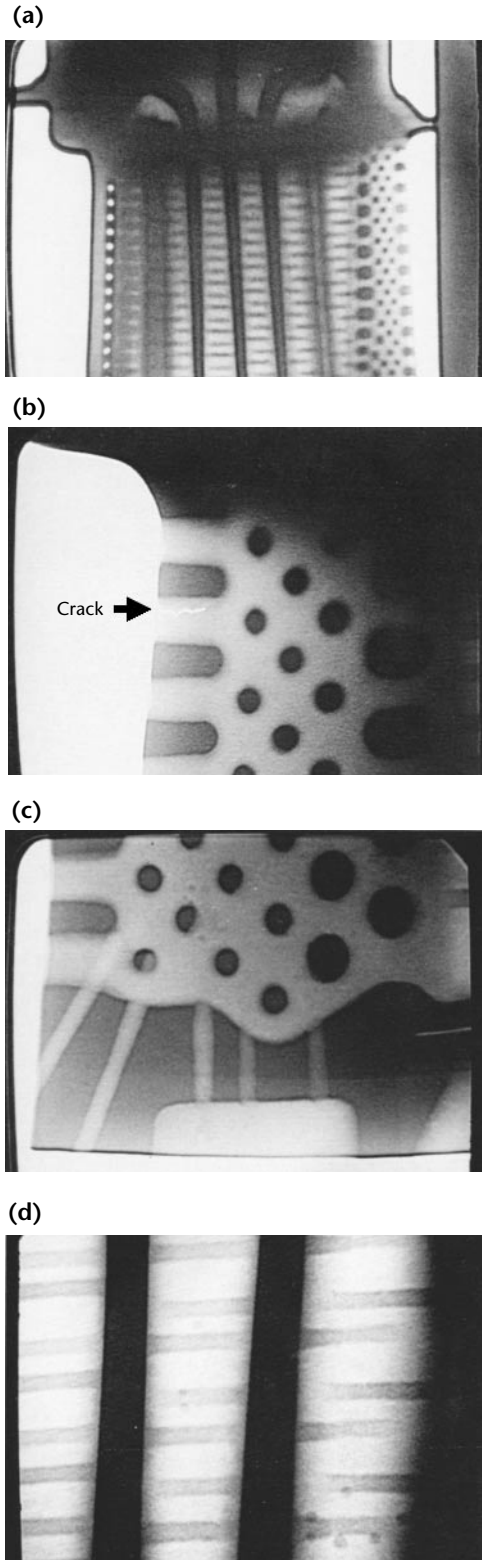


**FIGURE 4.** Sequence of radiographic magnifications of turbine blade: (a) low magnification view; (b) high magnification view of cracked metal in turbine blade; (c) high magnification view of drilling faults in blade; (d) high magnification view of 0.3 mm (0.01 in.) steel shot.



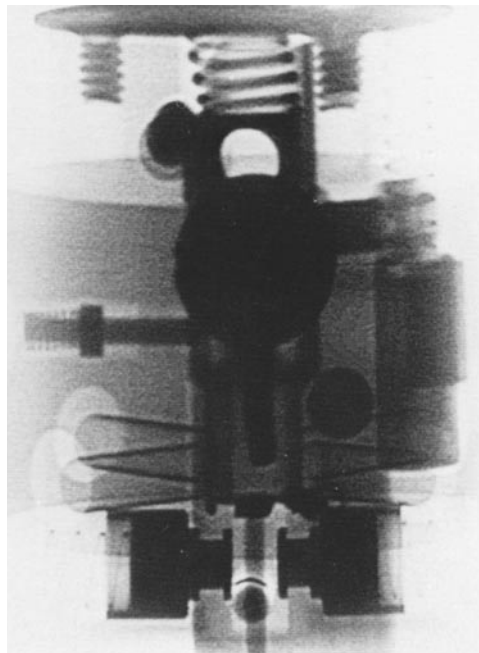
However, on close inspection at about 12 $\times$  magnification (Fig. 4b), a small crack at the trailing edge of the blade is visible. Note that drilling undercuts are present at the blade tip in Fig. 4c and that the body of the blade (Fig. 4d) also contains small steel shot sized about 0.25 mm (0.01 in.).

Another important benefit of projection techniques is the greatly improved image contrast level that results by eliminating all but very low angle scatter at the image plane.

## Automatic Defect Recognition Applications

Automatic defect recognition (ADR) is applied to parts that must be tested for the presence or absence of certain components or for the presence or absence of bonding agents such as solder and brazing. Automatic defect recognition may also be used at very high speed for objects that can be scanned and interrogated by intensity statistics, pixel statistics or similar window techniques for voids, inclusions or other anomalies with good contrast against the surrounding material. The picture in Fig. 5 shows the ease of achieving a test for the presence, absence or correct location of components in a small armaments arming device. The diameter of the device is about 25 mm (1.0 in.) and, when imaged at 10 $\times$

**FIGURE 5.** Munitions safety and arming device details visible with microfocus radiography.



magnification, it can be tested by a series of window scans that give the computer a signature for the correct location and presence of components. The speed of a standard 525 line television system equipped with a flash analog-to-digital converter allows the window scans to be done in 0.016 s, giving an automatic test capability up to 60 parts per second.

A second example of a specimen that lends itself to automatic defect recognition is the small tantalum capacitor shown in Fig. 6. This capacitor, manufactured in batches of ten thousand or more, can be tested at about 20 $\times$  magnification to reveal centering of the electrode, solder filling and voids in the hermetic seals around the top of the can and around the lead wire. Here, a video window is positioned in the appropriate area and an automatic intensity comparison (accept/reject) is made.

The third example, also manufactured in very large quantities, is the resistor spark plug shown in Fig. 7. The spark plug is typical of parts that can be tested automatically for homogeneity of core material. In this case, area measurement and intensity measurement can be used to detect voids in the resistive sealing compound inside the ceramic insulating shell. The magnification required for adequate resolution of voids as small as 0.05 mm (0.002 in.) is about 25 $\times$ .

Microfocus benefits automatic defect recognition by greatly increasing the image quality and reducing the band width, stability and repeatability

tolerances required of automatic defect recognition positioning and imaging equipment.

New systems boast geometrical magnification up to 2400 $\times$  and total magnification up to 7200 $\times$ , offering nanofocus technology with <900 nm ( $4.5 \times 10^{-5}$  in.) resolution and 500 nm ( $2.5 \times 10^{-5}$  in.) feature recognition.

---

## High Power Applications

The usefulness of a microfocus X-ray system is greatly enhanced if the system can be used to penetrate dense, thick objects as well as small, highly detailed objects. The need for systems to penetrate fairly thick specimens with enough X-ray flux to produce a useful image in the video system requires high output microfocus equipment. Systems based on microfocus and nanofocus technology have been produced in a variety of configurations using interchangeable targets and sophisticated handling systems.

---

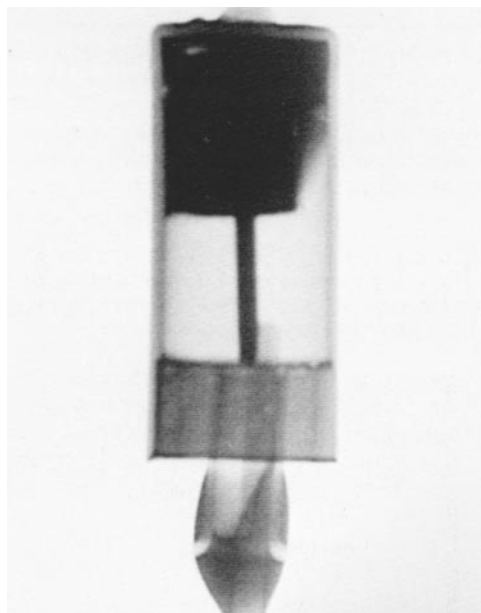
## Limited Field of View

Various image intensifiers and direct digital detector technology are available to achieve the radiographic sensitivity required for some applications. Amorphous silicon screen sensitivity is at least 5 $\times$  greater than conventional image intensifier X-ray converters.

A major concern with projection radiography is the limited field of view. For small objects this is rarely an issue. As objective size increases, however, the limited field of view requires multiple exposures to obtain coverage. The number of exposures required to cover an object

---

**FIGURE 6.** Medium magnification of solder faults in miniature tantalum capacitor, less than 6.3 mm (0.25 in.) in diameter.



---

**FIGURE 7.** Medium magnification view of electrode seal in resistor spark plug.





that would just fill the detector field of view is increased by the magnification squared. For example, if 3× is used then nine exposures are required to cover all of the original test object. Thus, optimization of the level of magnetization to bring out detail yet limit the number of exposure positions is an important challenge in projection radiographic testing.

### Penetrameter Compatibility

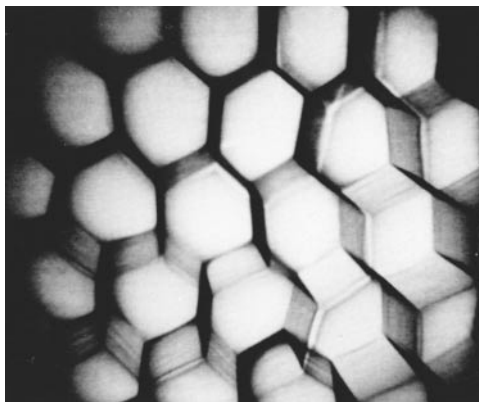
The limited field of view in high magnification images also presents a problem for penetrameters or image quality indicators. A requirement to simultaneously display an appropriate image quality indicator may tax the system when combined with a requirement to produce an acceptable video and hard copy image or digital record for archival purposes. Often standard penetrameters are too large, covering a large fraction of the image area.

### Special Applications

Some objects that do not fit in a volume convenient to a system's fixed enclosure can also be tested by using high magnification microfocus with remote displays or automated video systems.

Systems have been constructed for objects as varied as honeycomb core aircraft parts as shown in Fig. 8 and for dental X-rays as shown in Fig. 9. Aircraft sections naturally require a very large manipulator to properly align the microfocus source, imager and parts to show subtle discontinuities such as crushed core cells. This application places severe demands on the microfocus unit's mechanical and electrical design.

**FIGURE 8.** Crushed core cells in aluminum honeycomb.



Likewise, the dental application requires a special rod anode to permit interoral location for panoramic radiography of the teeth. The results of these two applications show the capability of microfocus to detect minute detail: cracked enamel in the teeth and the crushed honeycomb cell ends in the aircraft structure. Also, it shows the flexibility of the equipment to adapt to specialized requirements.

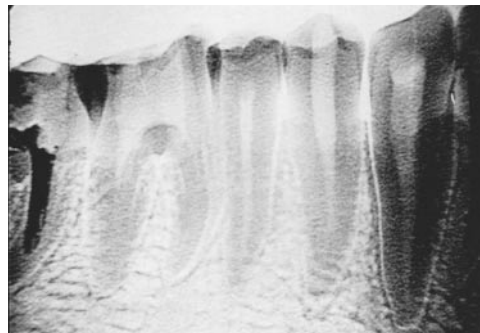
### Projection Microfocus Radioscopy

The literature describes previous developments in film projection radiography and contains many high quality photographs showing results achieved with microfocal radiography.<sup>1-14</sup>

### Closing

Projection microfocus radiography using both digital and film sensors is very practical for detecting minute details in objects ranging from tiny integrated circuits to large steel structures having 13 mm (0.5 in.) thick walls. The major impediment to wide acceptance of projection microfocus radioscopy in the 1980s was the tardiness of industry in accepting a slightly modified penetrameter that can be fitted into the small field of view of a highly magnified projection X-ray image.

**FIGURE 9.** View of dental work with microfocus rod anode.



## PART 2. Flash Radiography<sup>15</sup>

### Development of Flash Radiography

Flash radiography is a special type of radiography used to produce a single stop motion image or a series of sequential images of high speed dynamic phenomena. In conventional radiography, the subject is motionless during exposure. The exposure time can therefore be lengthened as necessary to obtain proper detector exposure once the tube-to-detector distance, the focal spot size and the tube voltage have been adjusted for optimum sharpness (lateral resolution) and contrast (depth resolution). In flash radiography, a stop motion requirement places an upper limit on the exposure time, that is, on the duration of the X-ray pulse or the duration of X-ray detector activation. This time limit in turn depends on the velocity of the object being radiographed. For instance, millisecond exposures may be adequate to stop motion in vibration studies whereas submicrosecond exposures are generally required for ballistic or shock wave studies and subnanosecond exposures may be required for extremely high speed or extremely short duration events such as nuclear fuel pellet implosion.

Real time radiography, using X-ray image intensifiers and cameras or television display systems, represents another type of radiography that produces an essentially continuous display of a dynamic event. In real time, however, the event's rate of motion or change must be sufficiently slow to allow millisecond exposures at a video tape frame rate of 60 frames per second.

Flash radiography provides time resolution or stop motion, which is not present in conventional radiography. This added capability, however, carries some limitations.

1. The exposure time and radiation intensity must generally be preset and there is no opportunity to change them while the exposure is in progress.
2. Relatively high voltages are required to achieve useful X-ray intensities during a very short pulse. Hence, image contrast is more limited than in conventional radiography.

3. Even at high voltages, the total radiation intensity per pulse is relatively low, typically an incident dose of  $2.58 \times 10^{-7}$  to  $1.29 \times 10^{-5}$  C·kg<sup>-1</sup> (1 to 50 mrem) at 3 m (10 ft) from the X-ray source; the intensity is much less after penetration of a thick object. Consequently very fast combinations of sensor and screen must be used, resulting in a loss of sharpness and an increase in quantum noise.
4. Because the target cannot be cooled effectively during the submicrosecond pulse, the X-ray target must be physically large (1 to 5 mm (0.04 to 0.20 in.) to absorb the electron beam energy. The large focal spot places an additional limitation on the sharpness of the radiographic image.
5. During the observation of very violent events, such as large explosive detonations or impact phenomena, suitable shields and a substantial physical distance from the event must be used to protect the sensor from damage. This further degrades the contrast and sharpness of the image.

The ability to control and optimize technique factors is much more limited in flash radiography than it is in conventional static radiography and the same image quality cannot generally be attained. However, in many situations involving high speed events, flash radiography represents the only available technique for imaging or observation and its limitations are tolerated because of its unique ability to freeze motion and provide time resolved information. It is possible to gate an X-ray detector system to get the equivalent of a fast shutter for stop motion image acquisition. Charge coupled device systems are available in gated configurations.

### History and General Principles

The general principles that govern the production and the imaging characteristics of X-rays are identical for conventional static radiography and flash radiography. Subjects have been widely discussed in the literature, such as the energy and intensity of X-ray brehmsstrahlung and characteristic radiation (as a function of tube voltage and target material); X-ray penetration



and image contrast (as a function of tube voltage); or the relation of image sharpness to geometry and focal spot size.

Extensive references to flash radiography may be found in other publications<sup>16-19</sup> and in the *Nondestructive Testing Handbook*, second edition: Vol. 3, *Radiography and Radiation Testing*.<sup>15</sup>

Several general observations may suggest the range of future developments in and applications for flash radiography.

1. Flash radiography has been used for ballistic studies to track the detonation of explosives and especially the projection of shells and rockets. (Incidentally, because the test objects were removed from service upon detonation, these tests were strictly speaking not nondestructive testing.)
2. Increases in the memory and speed of microprocessors have made it possible for digital radiography to be used in circumstances where flash radiography was formerly used, that is, successive exposures at frame rates faster than video. Digital radiography obviates the mechanical systems of switches that were necessary for film flash radiography.
3. Some flash radiography research has not been released for publication because of its military sponsorship.
4. The quantity of published research studies on flash radiography has sharply diminished since 1990.

## Means of X-Ray Generation

In X-ray tubes for conventional radiography, a thermionic cathode is used to produce an electron beam that is accelerated and focused to strike a small spot on a metal plane target. This basic mechanism of generating X-rays by impact of high energy electrons on a metal target is also used in flash radiography. However, because thermionic cathodes cannot produce the very high peak current densities and total currents required for flash radiography, different electron sources must be used. These sources do not allow effective focusing of the electron beam, so different X-ray tube and target geometries must be designed for achieving the necessary confined focal spot.

**Gas Discharge Tubes.** In early designs, *gas discharges* were used to accelerate electrons into the target and produce X-rays. Gas discharges can produce very large electron currents. However, electrons lose energy by collision or ionization and the average energy of the electrons striking the target is considerably less than the voltage applied to the tube; a severe loss in X-ray generating efficiency and X-ray hardness is the result. For these reasons gas

discharge tubes are no longer used in flash X-ray systems.

**Field Emission.** *Field emission* is a process in which electrons are emitted into high vacuum by applying an extremely high electric field (30 to 100 MV·cm<sup>-1</sup>) at the surface of a cold metal cathode, generally made of tungsten. The cathode is electrolytically etched into a very sharp needle so that the high electric field necessary for emission can be concentrated at the tip of the needle and can be produced at a reasonable applied voltage. The electric field applied at the cathode surface thins and lowers the potential energy barrier at the surface and, when the applied electric field is sufficiently high, electrons at or slightly below fermi energy can tunnel through the surface energy barrier with a probability (described by quantum mechanical theory) that increases exponentially with field strength

**Vacuum Discharges.** Vacuum discharges occur in a residual gas pressure low enough so that the electron mean free path is many times larger than the gap spacing between the electrodes; under these conditions, the avalanche breakdown and collisions of electrons with gas molecules are essentially eliminated. In a vacuum discharge tube, a finite time is required for the discharge to develop even though the discharge initiation time can be short at high voltages and can be affected by proper choice of voltage, pulse duration and gap spacing. Once initiated, a vacuum discharge is terminated only by removing the voltage applied to the tube and there is then a finite recovery time required for the plasma to recombine and the metal vapor in the gap to condense and disappear. This recovery time, which depends on prior discharge current and energy as well as gap spacing and electrode material, sets the minimum time interval between successive X-ray pulses from a given discharge tube; it is typically on the order of microseconds.

## Flash X-Ray Tubes

Flash X-ray tube designs are based on basic mechanisms and principles. Figure 10 illustrates a typical design for a high vacuum sealed field emission flash X-ray tube, operating at relatively high voltages (100 to 2000 kV).

The simple sealed tube of Fig. 10 uses a multiple needle field emission cathode consisting of six linear arrays surrounding a conical target made of tungsten. The focal spot and resolution characteristics of this flash X-ray source have been discussed.<sup>20</sup> The sharpness of the X-ray image is determined by the base diameter of the cone, the effective focal spot

diameter being about two thirds of the cone base diameter. The pulsed heat absorption capability of the target is proportional to the lateral area of the cone (and also to the electron range into the target).

For a given resolution, the X-ray intensity can be increased by using a cone with a small half angle  $\theta$ . If  $\theta$  becomes too small, X-rays are reabsorbed more heavily in the target and the effective X-ray beam coverage is reduced. In practice, a nominal  $\theta$  value of seven degrees is found to be about optimum for flash radiography. The maximum X-ray intensity increases very rapidly with increasing voltage, both because the electron range increases rapidly with voltage and because the efficiency of X-ray generation also increases with voltage; hence it is difficult to achieve large X-ray intensities at low voltages without excessive evaporation and rapid destruction of the target.

### Pulsed High Voltage Sources for Flash Radiography

A number of techniques have been used to generate the pulsed high voltage and to accommodate the high current, low impedance characteristics of flash X-ray tubes.

The oldest and simplest technique is to charge a capacitor to a high voltage, then discharge the capacitor through a low impedance pressurized gas triggered spark gap. This technique is limited to 100 to 150 kV, in practice.

Capacitive energy storage at relatively low voltage (15 to 100 kV) followed by voltage multiplication is routinely used to generate high voltages. The voltage multiplication is achieved by means of a pulse transformer of a marx-surge generator. Pulse transformers are suitable for output voltages up to 400 kV. Marx-surge generators can be used over a broad range of voltages, up to several megavolts, and have been commonly used in flash X-ray systems.

**Marx-Surge Generators.** In the simplest form of a marx-surge generator, a bank of  $N$  capacitors (of individual capacitance  $C$ ) is charged in parallel to a direct current

voltage  $V_0$  (typically 15 to 100 kV) then discharged in series by means of cross connected spark gaps. The open circuit output voltage is then  $NV_0$ . The output voltage waveform into a resistive load  $R$  is an exponential:

$$(1) \quad V = NV_0 \exp\left(-\frac{NT}{RC}\right)$$

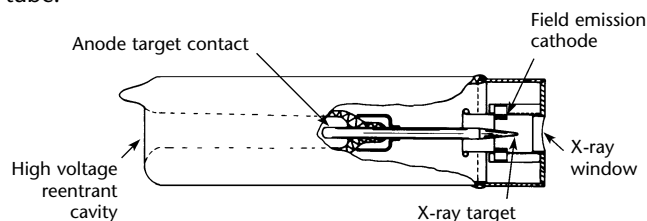
where  $T$  is trigger voltage.

For flash radiography applications, the capacitor in each stage of the marx-surge generator is replaced by a pulse forming network to produce a more effective, more nearly rectangular output waveform.<sup>15</sup>

**Blumlein Line Generators.** The rise time of the voltage pulses delivered by a marx-surge generator is not easily reduced below 5 ns. The difficulty in designing a device with sufficiently low inductance puts a lower limit of about 15 ns on the X-ray pulse length. The design also limits the maximum current intensity and the minimum characteristic impedance of the pulser, particularly for high voltage systems that contain a large number of stages. For these reasons, more complex high voltage generating circuits are used for applications that require output pulses of very short duration, very high current or very low impedance. The blumlein line generator is pulse charged by a marx-surge generator. A blumlein generator generally consists of three coaxial cylinders that behave as two transmission lines connected through a resistive load (the flash X-ray tube). The blumlein and the tube are designed to have approximately equal impedance, about 60  $\Omega$ , yielding a 600 kV, 10000 A, 3 ns electron or X-ray pulse.

**Electron Accelerators.** Linear accelerators are sometimes used to produce very high electron energies for flash radiographic applications requiring moderately short (about 0.1 to 10  $\mu$ s) repetitive pulses of very high energy X-rays. A unique design for high energy flash radiography system, built in 1965, used three large cylindrical cavities, resonant at 50 MHz, arranged in series and excited by input radiofrequency energy at 50 MHz. Standing waves developed and increased in amplitude during the excitation period. When the standing wave amplitude reaches its maximum (about 5 MV·cm<sup>-1</sup> axial field), a high current pulsed electron gun produced an intense, relatively low energy (500 keV) electron beam. The beam was injected into the radio frequency cavities and accelerated to 27 MV. The emerging electron beam was focused onto a transmission X-ray target, producing a very high energy X-ray source only 1 mm (0.04 in.) in diameter. The system was

FIGURE 10. High voltage, sealed, field emission, flash X-ray tube.



suited for flash radiographic applications demanding very high penetration and high image quality.

**Commercial Flash X-Ray Systems.** The different available outputs provide additional flexibility and imaging capability. Soft X-ray output, achieved with special flash X-ray tubes using a thin beryllium or polyester film window, allows much higher X-ray dose and contrast. Soft X-rays are useful in the observation of low density media or in flash X-ray diffraction studies.

**Others.** A number of other flash X-ray systems have also been designed, built and used, particularly for very high penetration studies, for a variety of ballistic and diffraction applications,<sup>16</sup> and for soft X-ray and characteristic X-ray

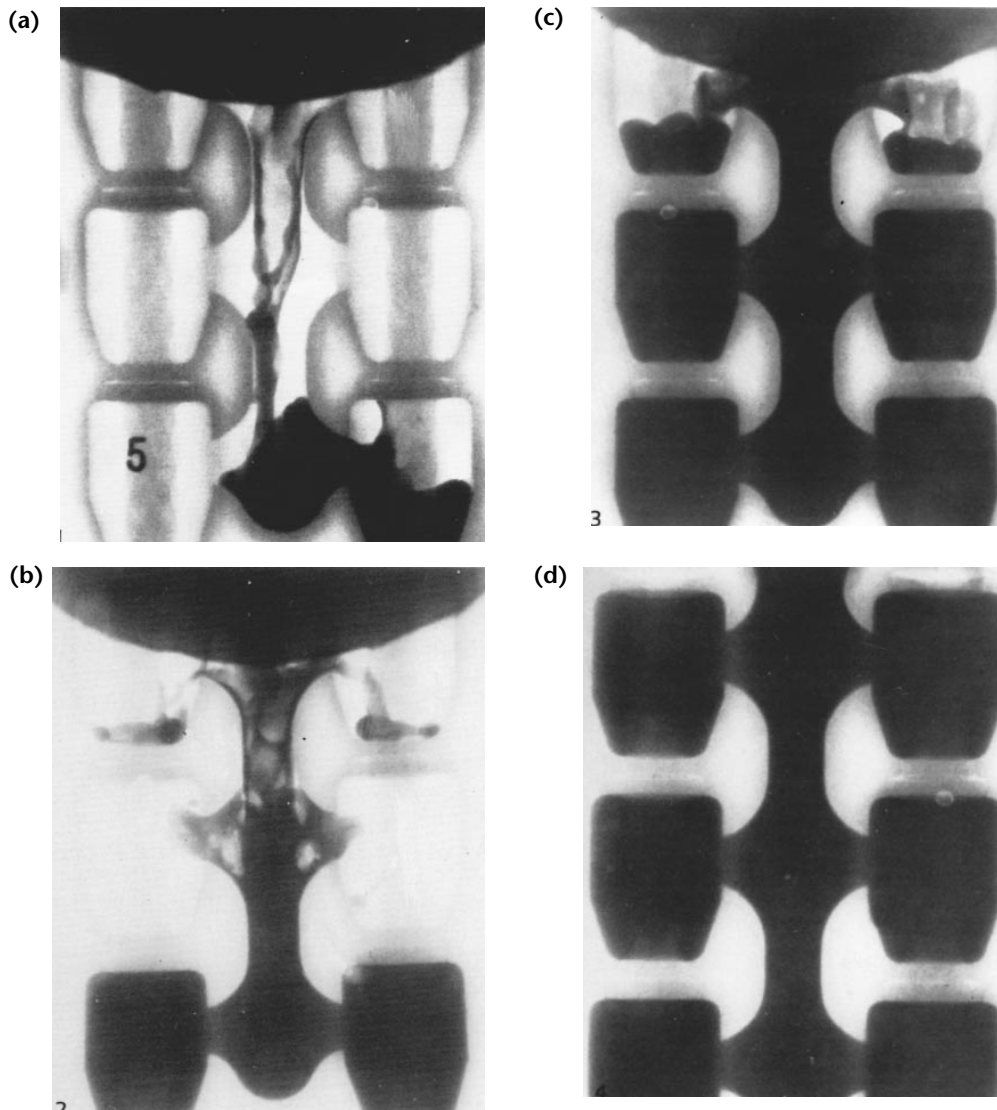
generation for flash X-ray diffraction studies.

## Industrial Applications

Industrial applications are not yet as widespread as applications to ballistics and detonics. A dynamic study of liquid filled high voltage power switches (10 kV, 600 A) was made to investigate arc initiation and quenching during switch opening.

Arc welding and electron beam welding<sup>21</sup> have also been studied by flash radiography and flash cineradiography. Another application is to the metal casting process, as illustrated in Fig. 11. This sequence of four radiographs was

**FIGURE 11.** Application of high voltage slow video flash radiography system to study casting process. Sequential radiographs of filling of multicavity shell mold: (a) first image; (b) second; (c) third; (d) fourth, cavities filled.



obtained with a 600 kV slow cineradiographic system. The four radiographs illustrate successful phases during a test pour of a multiple cavity shell mold for steel fittings and shows the gating characteristics as well as casting discontinuities due to premature partial filling of the upper cavities.

High voltage cine flash radiography has also been used successfully to study dynamic conditions inside gas turbines and jet engines.<sup>18</sup> The main purpose of such studies is to obtain accurate engineering data on clearances between the rotating and static parts of gas turbines, at all steady state or transient running conditions, between cold static and maximum power. A 2 MV flash X-ray system capable of delivering five pulses in 15 s was used in early experiments on large jet engines. Better results were subsequently obtained using a linear accelerator as the pulsed X-ray source for an X-ray image intensifier coupled to a 16 mm rotating prism camera for image recording.

### Nuclear Technology

High speed radiography has been applied to nuclear technology, particularly to the imaging of stainless steel clad fuel elements. Another important application is the investigation of interactions of fuel with coolant in safety studies of liquid sodium cooled fast breeder reactors. Both a flash X-ray system (250 to 350 kV peak, 1000 pulses per second) and a direct current X-ray source (420 kV, 15 mA) have been used in these studies. The imaging system consists of an X-ray image intensifier (gated when used with the direct current X-ray source) and a 16 mm pin registered framing camera or rotating prism camera. Both systems have produced useful cineradiographs of simulated safety failures (fuel coolant interactions) in steel pipe test sections.

### X-Ray Backlighting for Pellet Implosion Studies

One of the elements of controlled nuclear fusion research involves the study of pellet implosion to produce high density, high temperature plasmas. The pellets are small hollow glass, plastic or metal spheres filled with a deuterium tritium gas mixture under pressure. Bombardment by intense, short pulse ion beams or, more commonly, laser beams causes the pellet to implode, generating the very high densities, temperatures and pressures required to initiate thermonuclear fusion reactions. Flash radiography of imploding pellets, using an external X-ray source (backlighting), is exceptionally difficult because it requires extremely short pulses, very precise timing and very high

resolution. A three-channel high voltage system meets these requirements and has been used successfully for flash radiography of high density metal pellets.

Very low energy X-rays are required for glass and plastic pellets and it is possible to produce the necessary flash X-ray source characteristics by bombarding a metal target with a very short duration, very high power, sharply focused laser beam; this evaporates the target and produces a plasma that radiates X-rays. The X-rays emitted are predominantly L shell characteristic radiation from the target and the X-ray energy is thereby controlled through choice of the target material. By this means a 0.1 mm (0.004 in.), 1.5 keV, 50 ps duration plasma source has been produced<sup>18</sup> by bombarding a brass target with a 50 ps, 1 J glass laser pulsed beam. The technique was improved by using two separate laser bombarded targets (copper and molybdenum) to produce two X-ray microsources 250 ps apart. By using a small copper wire instead of a plane target, a point X-ray source only 6  $\mu\text{m}$  ( $2.4 \times 10^{-4}$  in.) in diameter was produced.

### Flash X-Ray Diffraction

X-rays are used to record diffraction patterns that yield detailed information about the crystal structure, texture, residual stresses and discontinuity distribution of various materials. X-ray diffraction studies normally use fine beams of low energy, continuous or monochromatic X-rays and require the long exposure times that restrict such studies to static situations. However, it is of great interest to obtain information about the crystal structure of materials under very high dynamic stresses or other rapidly changing conditions that could produce significant changes in the crystalline state. Intensive efforts have been made to produce the very high intensity, short pulse, low energy X-ray beams required for flash X-ray diffraction with very short exposure times.

## Closing

It can be said, in summary, that successful flash radiography demands the good practices of conventional radiography as well as its own specialized practices (triggering and protection from potentially violent test environments, for example).

Flash X-ray equipment and techniques are available for obtaining single or sequential images. A variety of flash X-ray generators have been built to provide different degrees of penetration, intensity, portability and pulse duration.



## PART 3. Reversed Geometry Radiography with Scanning Source<sup>22,23</sup>

### Reversed Geometry System

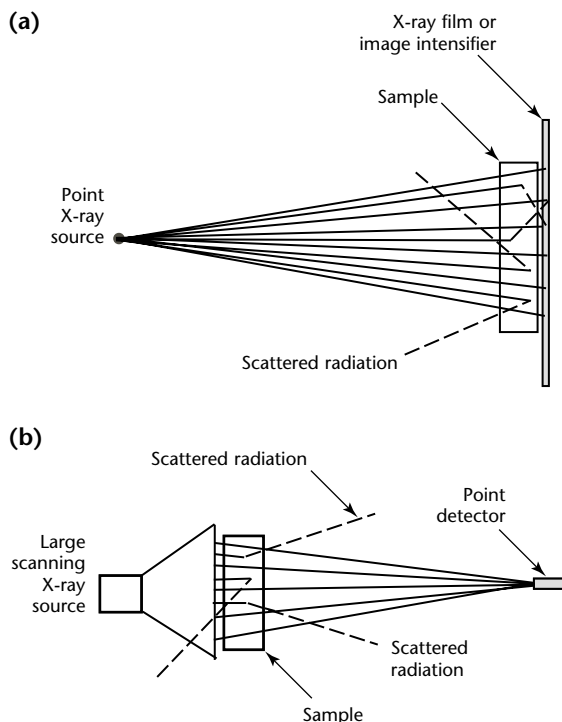
A simplified schematic in Fig. 12 compares the reversed geometry system to a conventional radiographic setup. The reversed geometry, scanning source radiographic system uses a large, electronically raster scanning X-ray source positioned near the object to be tested and a discrete detector for video radiographic imaging of a structure. A large portion of X-ray scatter (noise) bypasses the small, distant point sensors, thus improving the signal-to-noise ratio. A computer controls both the X-ray tube and the pixel-by-pixel image construction.<sup>24,25</sup>

The following description is given by the patent for the technique: "Radiographic images of high definition and clarity are produced quickly and with

reduced radiation exposure of the subject by using a scanning X-ray source in which a moving point source of X-rays is created by sweeping an electron beam in a raster pattern on a broad anode. A radiation detector having a very small radiation sensitive area is situated on the opposite side of the subject from the source. The output of the detector controls electron beam intensity within a cathode ray type display tube wherein the raster pattern is synchronized with that of the X-ray source to produce an image of internal structure of the subject. In some embodiments of the invention, the small radiation detector is mounted on a probe suitable for insertion into internal regions of a living body or into recesses in mechanical structure to be examined. Stereo images may be produced by using two spaced apart detectors controlling two separate images directed to separate eyes of the observer or by using a single detector alternately controlling each of the two images while the raster pattern at the source is alternately shifted between two at least partially separate areas of the anode. As the detector output is an electronic signal, the image data may be stored on magnetic tape or the like and may also be readily processed by electronic techniques for such purposes as image enhancement and addition, subtraction or superimposition of images. Automatic brightness control may also be provided to produce uniform contrast in different areas of the image where the corresponding different regions of the subject have different average densities.<sup>26</sup>

Reversed geometry has several possible advantages compared to conventional radiography. First, the X-ray detector can be miniaturized and easily positioned inside a complex structure (such as an aircraft wing) enabling images of each surface of the structure to be obtained separately. Second, multiple detectors enable the simultaneous acquisition of data from several different perspectives without moving the structure or the measurement system. Data from several different perspectives provide a means for locating the position of discontinuities and enhance separation of features at the surface from features inside the structure. Finally, the amount of secondary scattered radiation contributing to the noise in the radiograph is reduced compared to

FIGURE 12. Comparison of radiographic test setups: (a) conventional radiography; (b) scanning source radiography with reversed geometry.



conventional radiography. This simplifies the conversion of the radiographs to quantitative images of the integrated material density along the ray paths between the source and the detector.

The intensity of the X-ray flux is recorded with a relatively small thallium activated sodium iodide scintillation detector coupled to a photomultiplier tube. The photomultiplier tube output is amplified and offset before being digitized by a data acquisition computer. This enables optimizing the dynamic range of the digitizer to the dynamic range of the acquired signal. A detector is placed 0.81 m (32 in.) above the center of the tube. Seven other detectors are placed at positions around the tube at distances varying from 290 to 380 mm (11 to 15 in.) from the center and at a height of 360 mm (14 in.) above the surface of the tube. The detectors enable the acquisition of three dimensional data about a specimen. The data acquisition computer is connected to all eight detectors through a multiplexer enabling electronic switching between detectors.

The specimen of interest is placed on top of the X-ray source. This is the opposite of conventional radiography where the object is placed near an imaging detector and the source is approximately a point source. The data acquisition computer also controls the rastering of the electron beam. By acquiring the output of the detector as a function of electron beam position, the computer is able to generate an electronic image of the specimen of interest.

### Technique Setup

See Table 1 lists features of the reversed geometry, scanning source system. The most unique feature of the system is the large scanning X-ray source with a target diameter of about 250 mm (10 in.). The X-ray source operates in a manner similar to a video monitor. An electron beam is electronically rastered over the inner surface of the front of the X-ray source. Where the electrons collide with the inner surface of the tube, X-rays are generated. By electronically scanning the electron beam, the instantaneous position of the X-ray source scans an area of the front surface of the tube. The size and location of the scanned region is user definable and varies from the whole front surface to an area of about 50 × 50 mm (2.0 × 2.0 in.). The repetition rate of the scan is user definable, variable from 0.25 to 16 s. The acceleration voltage is also user definable from 55 to 160 kV with an electron beam current up to about 0.5 mA. The diameter of the electron beam spot at the inner surface of the tube is about 25 µm (0.001 in.).

## Applications

### Crack Detection<sup>23</sup>

An aircraft manufacturer conducted a series of experiments, ranging from imaging crack simulations with the laboratory system to imaging real fatigue cracks under fastener heads with the portable system in the maintenance hangar. In May 1998, this system examined airliner aircraft wings in a hangar. The array of eight detectors were suspended about 0.61 m (24 in.) above the aircraft wing and the 250 mm (10 in.) diameter scanning X-ray tube rested on a mobile arm adjacent to the lower surface of the wing.

Another reversed geometry system capability is the use of eight simultaneous detectors in conjunction with tomographic software. This enables the resolution of discrete layers within the structure with a single exposure and no mechanical motion. The X-ray system is on a rolling platform with variable height. The platform supports the X-ray source and the articulating arm supports the X-ray detectors. Each X-ray detector consists of eight scintillators mounted on a photomultiplier tube. Primary X-rays

**TABLE 1. Features of reversed geometry, scanning source system.**

Feature	Specification
<b>System</b>	
Operating current	0 to 0.5 mA, selectable
Power	120 V, 60 Hz, 20 A
Speed	≤ 4 s (512 to 2048 bits, selectable)
<b>Detector</b>	
Type	sodium iodide (> 99 percent efficient)
Diameter	25 mm (1 in.)
Length	100 mm (4 in.)
Extender diameter	3.2 mm (0.125 in.) diameter
<b>Image</b>	
Area magnification	×1 to ×100
Focal spot size	< 25 µm (0.001 in.)
Linear imaging	256 to 2000 lines
Overall field of view	75 to 250 mm (3 to 10 in.)
Off-axis alignment	± 0.7854 rad (± 45 degrees)
Penetrameter power	2-2T for aluminum
<b>Resolution</b>	
Contrast resolution	0.5 percent for plastics and composites; 0.3 percent for 4.19 mm (0.165 in.) thick aluminum
Contrast control	×1 to ×1000 signal gain
Image resolution	1 to 80 pixels per millimeter (25 to 2000 pixels per inch)
Spatial resolution	4.5 to 10 line pairs per millimeter



from the source pass through the rib of the wing and reach the X-ray detectors. Simultaneous image acquisition from eight different angles facilitates crack detection and increased test throughput. The system completed the entire test in less than 2 h and detected foreign objects and a large rib crack.

Using this setup on another occasion, the radiographer found fatigue cracks propagating from rivet heads that had not been previously detected. In one case, a fatigue crack ran the length between two rivet heads. These cracks were later verified by removing the skin and performing eddy current testing. However, compared to eddy current testing, the large area X-ray system provided the advantage in both throughput and depth of penetration.

One rivet, shown in Fig. 13a as a peak in a three-dimensional density plot, displayed what appeared to be a crack (white line protruding at an angle 60 degrees from vertical). Before removing the skin to begin repairs, however, the radiographer decided to determine whether the feature could be a slit in the sealant. Using the system's postacquisition image processing software, the radiographer made a slice graph (Fig. 13b and 13c).

The reversed geometry scanning source system has been mounted on a dual robotic system for scanning of an entire aircraft wing (Fig. 14). Cracks and corrosion were detected.

### Corrosion Detection<sup>22</sup>

A common technique for detecting corrosion in aircraft is visual testing for surface distortions or pillowing of the outer skin. Advanced nondestructive testing techniques are used when regions are partially or completely inaccessible for testing because of the overlying structure. Most of these techniques have difficulty accurately quantifying the corrosion, particularly in complex or multilayered structures.

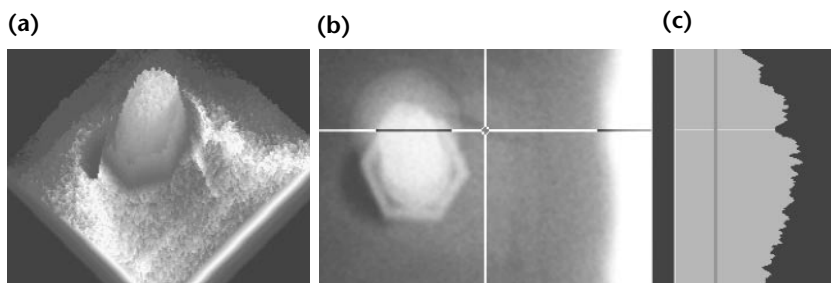
Reversed geometry scanning source X-radiography has been applied to the detection of corrosion.<sup>27,28</sup> A technique has been presented for reducing data from a reversed geometry system to provide images of material thickness by calibrating the data using known thicknesses within the images. Using a second order approximation of Beer's equation, good agreement was achieved between the radiographic and mechanical measurements of thickness. Details of this technique are discussed elsewhere.<sup>22</sup>

Figure 15 shows material loss due to corrosion in an aircraft crown. Researchers calibrated the thickness of the remaining aluminum portions by comparing the gray scale values with known values of a calibrated step wedge they measured under the same conditions. To test the contrast sensitivity of the system, researchers tested a 1.3 mm (0.05 in.) thick aluminum panel with slight corrosion. The thickness values over the selected area of corrosion vary between 1.1 to 1.3 mm (0.045 to 0.050 in.). This measurement indicates a contrast

FIGURE 14. Setup for inspection of wing structure.



FIGURE 13. Sealant slit: (a) three-dimensional density plot; (b) radiograph showing angular rivet and line that indicates slice; (c) metal thickness in slice (relative scale).



sensitivity of about two percent for material loss resulting from corrosion.

Detection and quantification of corrosion in real aircraft specimens is considerably more difficult than quantifying variations in thickness in a fabricated specimen. The image of a typical lap joint specimen in Fig 15a illustrates this difficulty. The specimen, obtained from an aircraft fuselage, has several different thicknesses. Linear scaling of the image contrast to enable the visualization of the variable thicknesses in the specimen masks the slight variation resulting from the corrosion in the sample. Improved visualization of the corrosion is obtained by performing a linear stretch of the contrast, which scales the image to enable visualization of the corrosion for a single thickness of the specimen.

An alternate technique that enables the rapid visualization of corrosion in a specimen with multiple thicknesses is histogram equalization. Histogram

equalization gives the best gray scale presentation of the corrosion. Because histogram equalization is nonlinear, the quantitative nature of the data is lost.

Examination of the images in Fig. 15 illustrates a difficulty in quantification of corrosion in real specimens. The corroded areas of the specimen have the appearance of having more material rather than less. This can be readily seen in an alternate representation of the data. Following calibration of the data, a three-dimensional volume can be constructed by assuming a flat bottom for the sample and a voidless, homogeneous structure. The vertical voxels of the volume representation are filled with fixed values until the projection through the volume representation is equal to the measured projection through the specimen. This reconstructed volume is then displayed with a volume visualization algorithm. For the specimen in Fig. 15a, the results of this procedure are shown in Fig. 15b. The region of corrosion appears as an increase in the apparent thickness of the material.

The apparent increase in material thickness is a result of the radiographic intensities being a function of the total mass along the ray path between the source and the detector. As the material corrodes, the aluminum of the structure combines with other elements to produce corrosion byproducts. These byproducts are sometimes trapped within the structure. The net mass along the ray path is the mass of the residual material plus the mass of the byproducts. This increase in net mass results in an increase rather than a decrease in the attenuation of the X-rays, which gives the appearance of an increase in material thickness rather than a decrease. The profile of thickness can be plotted in menu generated charts along user selectable lines.

X-ray tomographic images help to provide insight into the nature of corrosion and the difficulty of quantifying it with radiographic techniques. X-ray tomography enables viewing cross sections of the material, without disturbing either the delicate structure of the residual material or the location of the byproducts. The nature of corrosion, as illustrated in these cross sections, makes it difficult to quantify with any technique. However, the increase in apparent thickness is a good indicator as to the presence of corrosion.

The detectability of the corrosion with radiography can be further improved with digital laminography. Laminography is performed by imaging the specimen from several different angles. These images are all back projected and summed to yield an image that highlights the information at a selected depth in the measurement

**FIGURE 15.** Enhancement of corrosion data: (a) scaled radiographic image; (b) three-dimensional rendering from detector of reversed geometry, scanning source system.

(a)



(b)



volume. This is advantageous for increasing the detectability of corrosion that exists at a known location — for example, at the interface between two layers. The reversed geometry system is ideally suited to digital laminography as the source position is electronically made to scan a selected area. Several detectors collect data at different locations around the specimen to provide the different angles required for laminography.

---

## Closing

A reversed geometry portable system has the capability to detect fatigue cracks in aircraft structure. The system also can distinguish between cracks, which reduce the base level thickness, and irregularities in sealant, which do not.

The reversed geometry technique can present images of the effects of corrosion on a real aircraft specimen. Because of the nature of the corrosion, the radiograph gives the appearance of increased thickness in the corroded area, making quantification of the extent of corrosion difficult. Using data from the eight detectors laminographic image reconstruction of planes of interest within the lap joint can increase the detectability of the corrosion effects. Digital removal of surface features from images of interior planes of interest can improve corrosion boundary definition.

## PART 4. Stereo Radiography<sup>1</sup>

### Background

Radiographic discontinuity depth determination is important because fracture mechanics helps determine product serviceability. Fracture mechanics uses information on the character, size, shape and location of discontinuities. The present discussion deals with (1) parallax techniques for determining discontinuity depth in a part or weldment<sup>1,29</sup> and (2) stereo imaging, which takes advantage of human binocular vision.<sup>30</sup>

Stereo radiography is a radiographic technique using two separate radiographic images with a source shift exactly parallel to the imaging plane; the movement of the source between exposures is about the same as the distance between pupils of human eyes. When the processed images are viewed, the right eye sees one image and the left eye sees the other. The brain combines the images, giving the impression of a three-dimensional radiograph. The possibilities of stereo radiographs has intrigued investigators for many years.<sup>30-32</sup> Advances in microprocessor technology and concurrent software development in the 1990s have widened the range of applications for which three-dimensional imaging is practical.<sup>33-36</sup>

### Purpose of Stereo Radiographic Testing<sup>30</sup>

The main purposes of stereo radiographic testing are (1) to provide depth information and (2) to aid in the interpretation of complex radiographic images.

1. As with binocular vision, a pair of radiographic images permits the viewer to estimate the relative distances from a reference point to various objects of interest in the field of view. Triangulation provides precise depth measurements.
2. Radiographs of complex objects are often difficult to interpret when the images of many features are superimposed. Stereo radiographic testing lets the viewer separate overlapping features according to their depths, greatly improving the probability that each item will be properly identified and evaluated.

Innovations in radioscopy and microprocessing have made it possible to obtain images instantly and to store them indefinitely. These innovations have made *dynamic* imaging practical. Dynamic stereo imaging entails movement of the test piece or sensors, making it easier to distinguish overlapping items and making it possible to see *around* or *behind* some items. The detection of contraband in cargo containers is one application.

### Parallax Principle

Parallax techniques are based on the principle that from two exposures made with different positions of the X-ray tube, the depth of the discontinuity is computed from the shift of the shadow of the discontinuity.<sup>30</sup>

The shadows of objects closest to the source will have the largest shadow projection. An object close to the background does not appear to change position whereas an object farther from the background appears to shift a moderate amount.

The amount of left or right movement of the projected shadows is directly proportional to the closeness of the object to the light source. Visual and radiographic parallax principles are compared in Fig. 16.

### Similar Triangle Relationship

A similar triangle relationship is the basis for most of the calculations used in the radiographic parallax techniques: the height  $D$  divided by the height  $T - D$  is equal to base  $B$  divided by base  $A$ . All of the radiographic parallax techniques discussed here maintain this fundamental relationship.

Radiographic parallax techniques use three variations of the similar triangle relationship. These three techniques are discussed next: (1) the *rigid formula*, (2) the *single marker approximate formula* and (2) the *double marker approximate formula* (Fig. 17). The data for the similar triangle relationship are derived from the displacement of the image from the sensor plane.

The sensor plane is used rather than the depth below the surface, for it is not

always possible to have the sensor in contact with the surface of the part.

In addition to problems encountered in calculating the object's height above the sensor surface, certain orientation or discontinuity geometries can cause measurement errors; these errors are not due to failure of the technique but to failure of the radiographer to recognize and compensate for variations in object displacement.

## Rigid Formula

Figure 17a shows the rigid formula parallax technique, which is also defined in Eqs. 2 to 4.

$$(2) \quad \frac{D}{T - D} = \frac{B}{A}$$

$$(3) \quad D = \frac{BT}{A + B}$$

$$(4) \quad H_s = D - K = \frac{BT}{A + B} - K$$

and where  $A$  is the source's shift between exposures;  $B$  is the parallax or image shift of the discontinuity;  $D$  is the distance of the discontinuity above the image plane;  $K$  is the distance from the test object to the sensor plane (assuming those surfaces are parallel); and  $T$  is the distance from source to sensor.<sup>30,31</sup>

By measuring or knowing the first three parameters, the fourth parameter can be calculated based on the similar

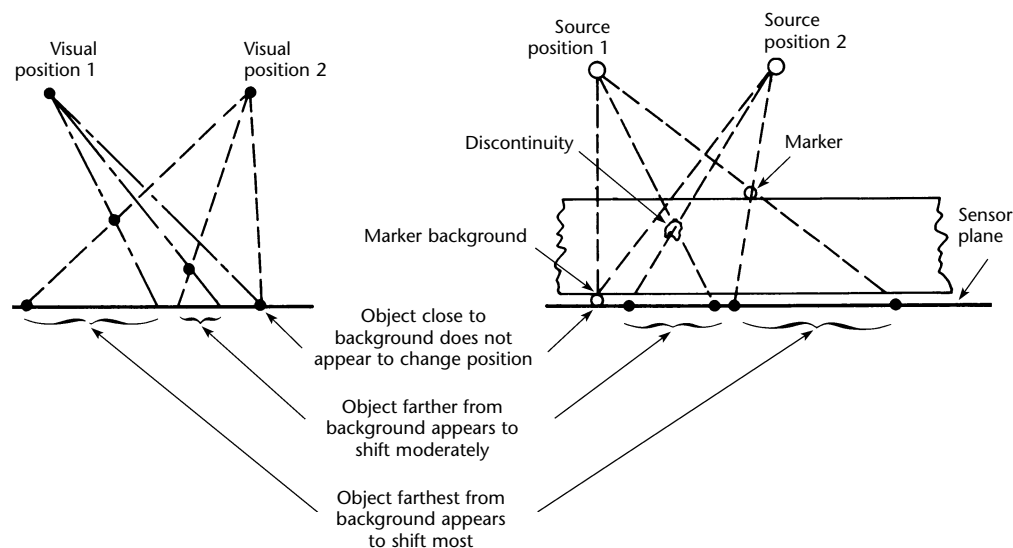
triangle relationship. With the rigid parallax technique, no markers are necessary. However, the part thickness, the distance from source to sensor and the source shift must be accurately known. In addition to knowing these measurements, the image of the discontinuity must be present on a twice exposed radiograph.

Normally, this radiograph is made by (1) calculating the necessary exposure time; (2) making one part of the radiograph with half of this exposure time; (3) moving the source parallel to (and a specified distance along) the sensor plane; and then (4) making the second half of the exposure. The rigid parallax technique can be used when the sensor surface is placed in contact with the part bottom and when there are no limitations on the height of the source above the sensor plane. It is important to have a significantly large ratio of (1) the distance from source to sensor over (2) the distance from sensor side of object to sensor when using the rigid parallax technique.

Three other important points should be remembered when using rigid formula parallax radiography.

1. The fundamental relationship between discontinuity height and image shift is nonlinear.
2. As the discontinuity height approaches the distance from source to sensor, the image shift increases without limit.
3. When the discontinuity height is small compared to the distance from source to sensor, the curve of accuracy approaches linearity.

FIGURE 16. Comparison of visual and radiographic parallax.



## Single Marker Approximate Formula

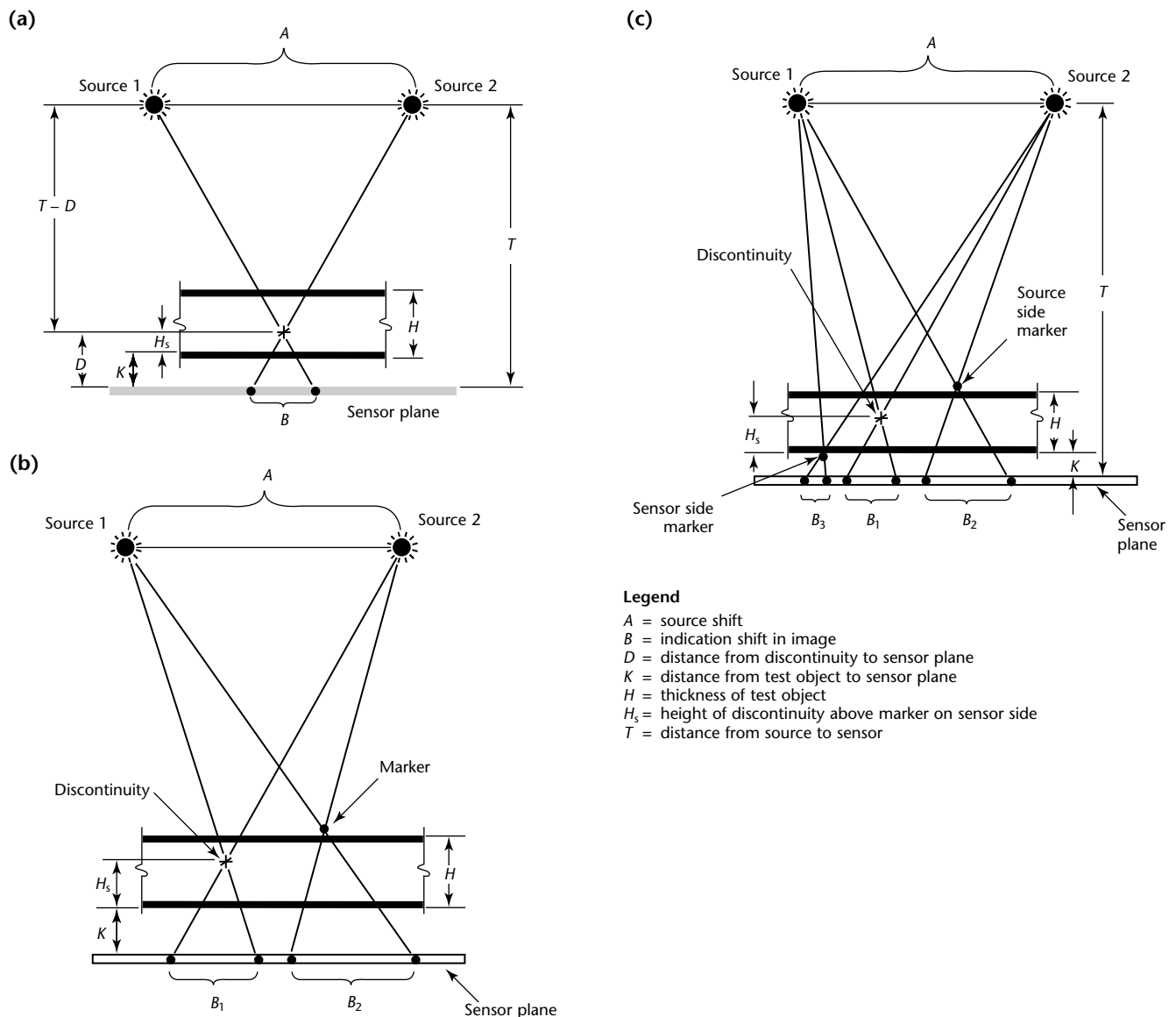
When the part thickness and discontinuity height are small relative to the distance from source to sensor, the relationship between  $B$  and  $D$  approaches linearity and the height of the discontinuity above the sensor plane becomes approximately proportional to its parallax. A proportional relationship offers certain advantages in that an artificial discontinuity or marker can be placed on the source side of an object as shown in Fig. 17b.

The height of the discontinuity can be estimated or calculated by comparing the

shift of its radiographic image with that of the marker. For example, if the single marker shift is twice the shift of the discontinuity, this indicates that the discontinuity is about in the middle of the wall. This parallax technique eliminates the need for detailed measurement of the part thickness, of the distance from source to sensor and of the source shift as required by the rigid technique.

With distances from source to sensor at least ten times greater than the part thicknesses, maximum errors on the order of three percent (of the part thicknesses) can be expected. These errors are based on the premise that the sensor is in intimate contact with the part being radiographed.

FIGURE 17. Stereo technique diagrams: (a) rigid formula parallax technique; (b) single marker approximate technique; (c) double marker approximate technique.





If the sensor is not in intimate contact with the part, the error will be increased because the proportional ratio is based on the discontinuity height above the sensor plane.

## Double Marker Approximate Formula

When the sensor cannot be placed in intimate contact with the object or when the image of the discontinuity is not present on a double exposed radiograph, the double marker approximate technique should be used (see Fig. 17c).

If both markers are thin, neglect their thickness and assume that they represent the top and bottom of the test piece. By measuring the parallax or image shift of each marker, as well as that of the discontinuity, the relative position of the discontinuity between the two surfaces of the test object can be obtained by linear interpolation, using Eqs. 5 to 9.

$$(5) \quad B_1 - B_3 \cong \Delta B_d$$

$$(6) \quad B_2 - B_3 \cong \Delta B_s$$

$$(7) \quad \frac{\Delta B_d}{\Delta B_s} \cong \frac{B_1 - B_3}{B_2 - B_3}$$

$$(8) \quad \frac{H_s}{H} \cong \frac{\Delta B_d}{\Delta B_s}$$

$$(9) \quad H_s \cong H_s \times \frac{\Delta B_d}{\Delta B_s}$$

where  $H_s$  is the height of the discontinuity above the sensor side marker and  $H$  is the distance between the source side marker and the sensor side marker.

Listed in Table 2 are the various parallax formulas, the triangulation measurement requirements and the general areas of application for the double-marker, single-marker and rigid formula parallax techniques.

## Effects of Discontinuity Geometry on Parallax Accuracy

The effect of discontinuity geometry on the accuracy of parallax calculations is common to all three of these techniques. Calculations typically indicate the center line dimension of the discontinuity above the sensor plane. However, in those cases where the geometry of the discontinuity is not cylindrical or rectilinear, its shape can influence the accuracy and detectability of discontinuities. If the general shape of the discontinuity can be determined by viewing a standard radiograph, proper allowances can be made.

Figure 18 shows three cases where the approximate, average displacement of the discontinuity on the sensor plane can be calculated by using Eq. 10.

$$(10) \quad \text{Parallax shift} = \frac{L \times R}{2}$$

where  $R$  and  $L$  are indication widths caused by sources 1 and 2 respectively.

If the discontinuity geometry is similar to one of those in Fig. 19, averaging the

TABLE 2. Triangulation measurement requirements.

Formula	Flaw and Marker Shifts (B)	Distance from Source to Sensor (T)	Source Shift (A)	Sensor Separation (K)	Application Notes
Rigid formula	yes	yes	yes	yes	for relatively short distances from source to sensor or where marker placement is difficult where part thickness is unknown or difficult to measure
Approximate formula: source side marker	yes	no	no	yes	also requires that part thickness $D_2$ plus sensor separation $K$ be known for relatively long distances for situations where sensor side marker placement is difficult
Approximate formula: source side and sensor side markers	yes	no	no	no	also requires that part thickness $H$ be known most accurate approximate formula best for long distances from source to sensor simplifies data retrieval

discontinuity shift does not show the true discontinuity dimension location.

## Source Movement

The correct movement is parallel to the sensor plane. This principle is further illustrated in Fig. 20, which shows incorrect source movements and changes in distance from source to sensor for a flat object or a tapered surface.

When the source position is not perpendicular to the sensor plane, the approximate angle of the sensor plane (to the source) must be known and compensated for in the calculations, even with correct source movement.

Care must also be exercised when using the parallax technique of discontinuity depth determination on cylindrical parts. It is important to maintain the angle of source to sensor or plane as closely as possible to 90 degrees, particularly in those cases where flexible film cassettes (or sensors embedded in fabric that conforms to test object surfaces) are used. This is also true when radiography of

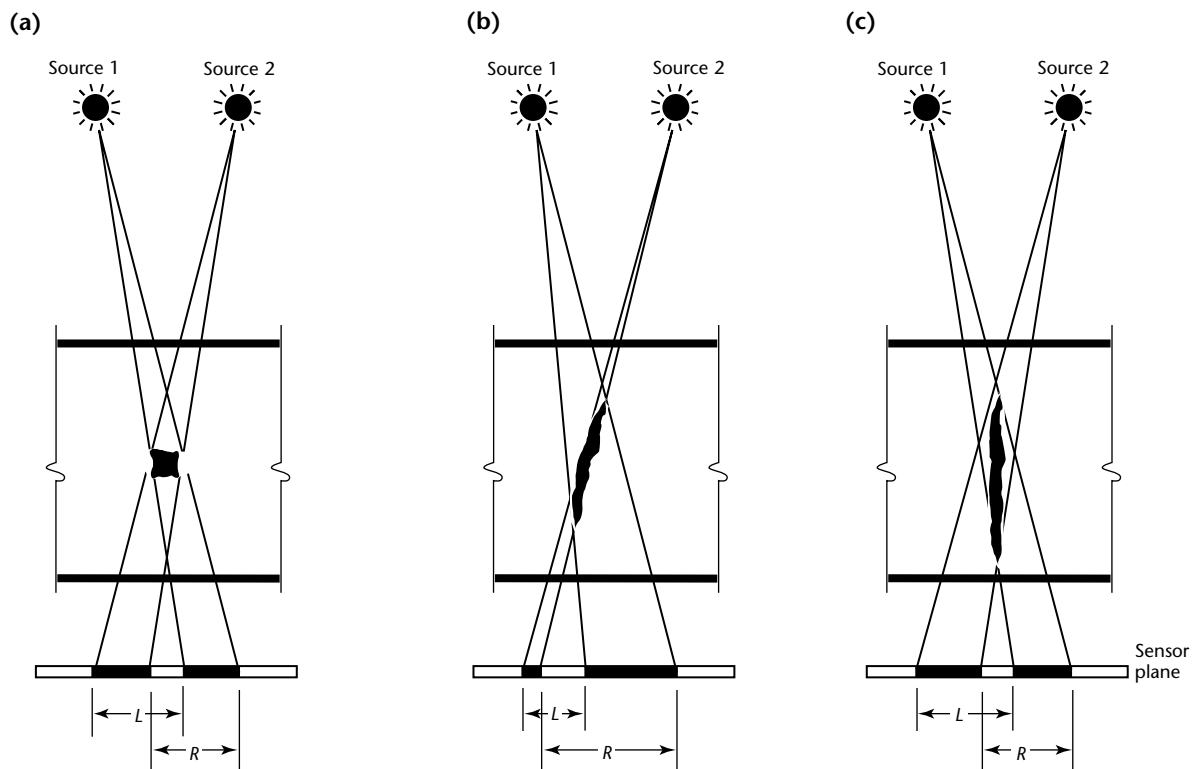
cylindrical parts is made using a rigid cassette. The radiographer must be aware of and maintain to the maximum extent possible, a normal relationship of the sensor plane to the source. Additionally, when rigid sensor planes (including film cassettes) are used, the standoff or separation distance between the rigid sensor planes and the inside or outside of the cylindrical object must be known and compensated for in the calculations.

## Flickered Image Technique for Depth Measurement<sup>30</sup>

Quantitative depth information can be extracted from a pair of stereo images through parallax calculations or by means of the radiosopic *flickered image* technique. The flickered image technique uses a pair of radiosopic images stored in a computer, a single video monitor and software.

1. Identifying markers are placed on the front and back surfaces of the test object.

**FIGURE 18.** Flaw geometries that permit calculation of average flaw displacement: (a) discontinuity with no difficult orientation; (b) oblique discontinuity creates larger indication for source 1 than source 2; (c) indication from long discontinuity resembles indication in Fig. 18a.



### Legend

$L$  = width of indication created by source 2 on sensor plane  
 $R$  = width of indication created by source 1 on sensor plane

2. A pair of stereo radioscopic images with adequate separation are acquired and stored in the digital image processor.
3. The computer recalls the two images and alternately displays first the right image and the left image at a rate of about two images per second. Using a keyboard or other input device the operator shifts one of the flickering images until the front surface markers are superimposed. A keystroke records the magnitude of the lateral shift of the image of the moved marker.
4. Similarly, the images of the back surface markers are superimposed and the magnitude of lateral shift is recorded.
5. The projected distance between the front and back surface markers is usually the test object thickness and is entered in the computer.
6. The images of a feature of interest (a discontinuity, foreign object or surface) within the test object are superimposed and this position is entered in the computer.
7. The computer calculates and displays the distance or depth from the front surface to the feature of interest.

This technique is fast, simple and accurate. Repeatability within  $\pm 3$  percent has been demonstrated.

**FIGURE 19.** Examples of flaw geometries where center line of discontinuity is not determined by shift averaging: (a) discontinuity with tail; (b) discontinuity shaped like cylindrical or conic section.

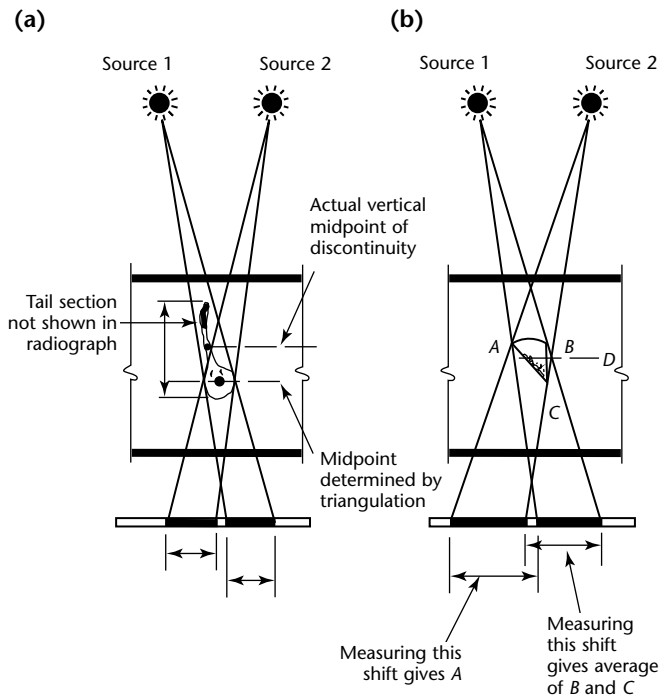
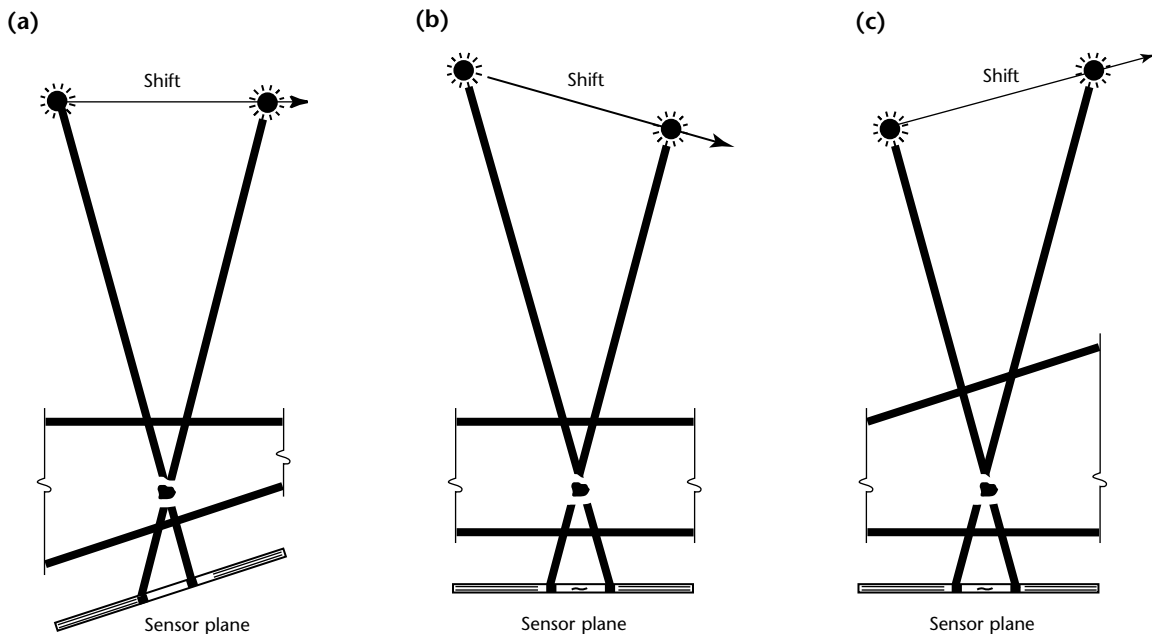


**FIGURE 20.** Incorrect source shifts: (a) oblique sensor plane; (b) oblique source shift; (c) source shift oblique to sensor plane.



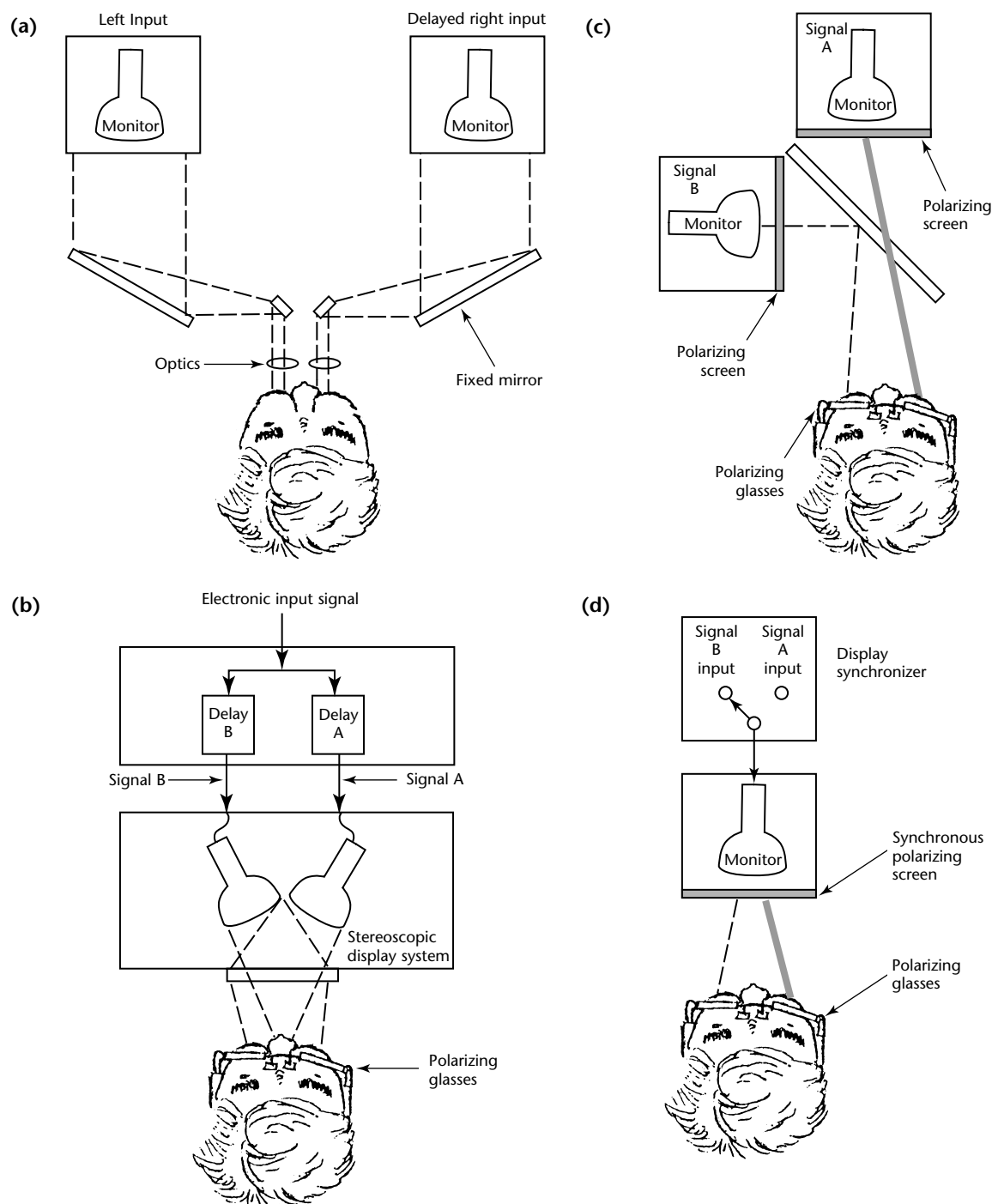
## Approaches for Stereo Viewing<sup>30</sup>

Various arrangements have been used to achieve stereoscopic vision of radiographic tests (Fig. 21). Before the

1990s, stereo radiographs have used film as both the recording and viewing medium. A video hard copy printer reproduced pairs of images that could be viewed with an optical stereoscope.

An extension of this technique displays two images, left and right, on a matched

**FIGURE 21.** Designs for stereo radiographic displays: (a) two video monitors and prismatic specular stereoscope; (b) signals from moving test object assigned to separate monitors for stereo image; (c) two video monitors, partially silvered mirror and polarized filters; (d) liquid crystal synchronous polarizing screen covering entire monitor screen, producing different polarizations for right and left images.



pair of video monitors, placed side by side so that their screens could be viewed through a prismatic stereo scope (Fig. 21a).

One dynamic stereo system, not illustrated here, used an X-ray tube with a double filament with double control grids and a rotating anode. The tube produced two focal spots separated by about 20 mm (0.8 in.). The grids controlled the flow of electrons from the two filaments to activate the left focal spot and then the right one, creating a series of left and right images in the intensifier tube.

The setup shown in Fig. 21b permits viewing by several people at once. Two cathode ray tube monitors are oriented perpendicularly to each other; a partially silvered, 45 degree mirror beam splitter is placed between the monitors; and a linear polarizing filter is placed over the face of each monitor. When the filters are properly adjusted, observers wearing polarized glasses can observe the image in the right monitor with the right eye and the image in the left monitor with the left eye.

The viewing system in Fig. 21c uses a single display monitor with a liquid crystal modulator. The right and left image are input to an external modulator frame synchronizer and then to the display monitor. A screen sized liquid crystal modulator mounted on the screen provides a different polarization for the left image than for the right. The observer's polarized eyewear decodes the circularly polarized images in such a way that the left eye sees only the left image and the right eye sees only the right image. Head orientation does not affect the stereo effect and many people can watch simultaneously.

In another configuration (Fig. 21d), the radiation source and imaging system remain stationary while the test object is translated or rotated at a constant velocity. A continuous series of images is acquired and stored. Selected images are displayed to produce the same spatial separation as achieved when a stationary object is viewed from two positions.

## PART 5. X-Ray Diffraction and X-Ray Fluorescence<sup>1</sup>

### Principles of Analytic Techniques

X-rays are a form of electromagnetic radiation produced in an atom when inner orbital electrons are ejected and the outer electrons move to fill the positions near the nucleus. This transition takes the outer electrons from states of high to low energy, energy that is released in the form of X-rays.

When a beam of this X-ray energy falls onto a specimen, three basic phenomena may result: absorption, scatter or fluorescence. These phenomena form the basis of several important X-ray analytical techniques.

### Absorption Analysis

The absorption of X-rays increases with the atomic number of the absorbing matter. This property of X-rays was quickly established and applied to medical diagnosis. At one time, it was also used for the analysis of materials but these techniques have now been superseded by X-ray fluorescence. Today, absorption techniques are only found in more specialized fields, such as X-ray absorption edge fine structure analysis. The absorption effect is still important in establishing a relationship between X-ray intensity and element composition or phase. In X-ray diffraction and fluorescence, *phase* is any chemically homogenous, physically distinct constituent of a substance.

### X-Ray Fluorescence Spectrometry

*Fluorescence* occurs when an intense X-ray beam irradiates a specimen and characteristic X-ray spectra are emitted. *Spectrometry* may be defined as the recording of these emission spectra and its separation into its component parts, each part being characteristic of an element.

X-ray fluorescence spectrometry consists of two techniques. The first of these is *wavelength dispersive spectrometry*, which uses the diffracting power of a crystal to isolate narrow wavelength bands from the polychromatic characteristic radiation excited in the sample. The second, *energy dispersive spectrometry*, uses a proportional detector to isolate the energy bands.

Because of the known relationship between emission wavelength and atomic number, identification of an element can be made by isolating individual characteristic lines and elemental concentrations can be estimated from characteristic line intensities. Thus, these two techniques are means of materials characterization in terms of chemical composition.

### X-Ray Diffraction

The discovery of X-ray diffraction was made by Max von Laue in 1913<sup>39</sup> and may be defined as changes in the scattering characteristics of X-rays due to collision with some object in their path. Diffraction is a special case of X-ray scattering that can be used for the identification of elemental phases.

Scattering occurs when an X-ray photon interacts with the loosely bound outer electrons of an element. When this collision is elastic (no energy is lost in the collision process), the scatter is said to be coherent (or rayleigh) scatter. Coherently scattered photons may undergo subsequent interactions with other scattered photons, causing reinforcement or interference.

Under certain geometric conditions, scattered wavelengths may reinforce one another if exactly in phase or may cancel one another if exactly out of phase. The coherently scattered photons that constructively interfere with each other give diffraction maxima (peaks in the X-ray diffraction diagram). *Phase* here denotes a uniform motion varying according to simple harmonic laws.

A crystal lattice, for example, consists of a regular arrangement of atoms and, when a monochromatic beam of radiation falls onto these atomic layers, scattering will occur. To satisfy the requirements for interference, it is necessary that the scattered waves originating from the individual atoms (the scattering points) be in phase with one another.

The geometric conditions necessary for the waves to be in phase are illustrated in Fig. 22. Two parallel rays strike a set of crystal planes at an angle  $\theta$  and are scattered. (Diffraction angles are labeled  $\theta$  for the angle of specimen to source and  $2\theta$  for the angle of source to specimen to detector.)



Reinforcement will occur when the difference in the path lengths of the two waves is equal to a whole number of wavelengths. This path length difference is equal to  $\overline{BC} + \overline{BD}$  (Fig. 22). For reinforcement to occur,  $\overline{BC}$  must equal  $\overline{BD}$ ; and if  $\overline{BC} = \overline{BD} = X$ , then  $2X$  must equal  $n\lambda$ , where  $n$  is an integer and  $\lambda$  is the wavelength.

It will also be seen that  $X = d \times \sin\theta$ , where  $d$  is the interplanar atomic spacing. Hence, the overall condition for reinforcement is a statement of Bragg's law:<sup>40</sup>

$$(11) \quad n\lambda = 2d \times \sin\theta$$

## Role of Crystal Structure in X-Ray Scattering and Diffraction

All substances are made of individual atoms and nearly all substances have some degree of order, or periodicity, in the arrangement of these atoms.

A crystal is a highly ordered substance that can be defined as a homogeneous, anisotropic body (exhibiting properties with values that vary when measured on different axes), having the natural shape of polyhedron.

In practical terms, determining the homogeneity of a substance depends on the means available for measuring the crystallinity. In general, the shorter the diffracted wavelength, the smaller the recognizable crystalline region.

Even noncrystalline materials have a degree of order and each will give some

sort of a diffraction pattern. For example, glassy materials and liquids will generally give diffraction patterns in the form of one or more broad diffuse peaks or halos. X-ray powder diffractometry usually deals exclusively with crystalline materials. Because every ordered material is made up of a unique arrangement and number of atoms, every ordered material will give a diffraction pattern that is, to all intents and purposes, also unique. The diffraction pattern can, moreover, be used to determine the degree of crystallinity; that is, the dimensions of the crystalline regions in otherwise amorphous substances.<sup>41</sup>

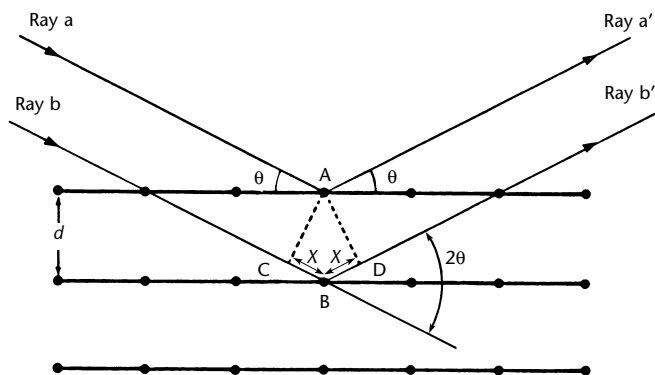
## Positioning of Analytical Instrumentation

There are many similarities between the instrumentation used for diffraction and spectrographic measurements, particularly in the case of the wavelength dispersive spectrometer.

As examples, the high voltage generator used to power the X-ray tube is generally of the same type; the digital and analog counting electronics and goniometer (angle measurement or control) circuitry are almost identical. It is often found that in a given laboratory, the high voltage generator and counting electronics are actually shared between the diffractometer and wavelength dispersive spectrometer.

Shown in Fig. 23 are layout diagrams of the instrumentation used in the three different analytical techniques.

FIGURE 22. Geometric conditions for diffraction of X-rays.



### Legend

- A = point where ray a is diffracted
- B = point where ray b is diffracted
- C = point in incident ray b
- D = point in diffracted ray b'
- $d$  = interplanar atomic spacing
- $X$  = variable denoting distance from point B to point C or D
- $\theta$  = angle of incidence

## X-Ray Diffraction for Measurement of Stress

One of the important metallurgical applications of X-ray diffraction is in the determination of residual stress.<sup>42</sup> When a polycrystalline piece of metal is deformed, the lattice plane spacings will change their values, the new values corresponding to the applied stress. If the stress is uniform, this value change will manifest itself as a shift in the observed  $2\theta$  angle of the appropriate diffraction line. If the stress is nonuniform, the effect will appear as a broadening of the appropriate diffracted line profile.

As far as uniform strain is concerned, it is a rather simple procedure to correlate the line shift with the stress in the system, by using measured elastic constants or by calibration with materials of known stress. It should be realized, however, that in either instance the diffraction technique is actually measuring strain, not stress; it is thus an indirect technique of

measurement. When an applied stress is removed and the deformation persists, the material is said to have *residual stress*. Determination of residual stress in metals is one of the most common applications of X-ray stress measurement. Automated X-ray machines are available for the rapid measurement of stress, both on laboratory specimens as well as on large samples, such as weldments in pipe lines, aircraft wings and so on.

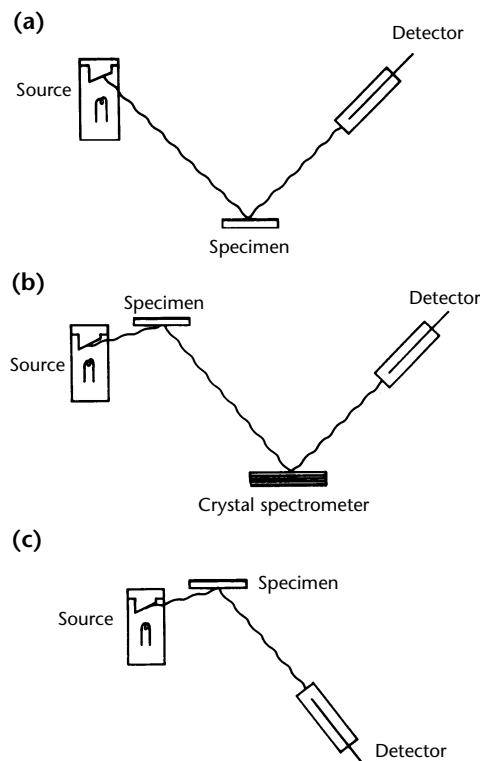
## Elemental Analysis by X-Ray Fluorescence

### Principles of X-Ray Fluorescence

The basis of the X-ray fluorescence technique lies in the relationship between the atomic number  $Z$  and the wavelength  $\lambda$  (or energy  $E$ ) of the X-ray photons emitted by the sample element:

$$(12) \quad \frac{E}{12.4} = \frac{1}{\lambda} = K(Z - s)^2$$

**FIGURE 23.** X-ray analytical instrumentation: (a) X-ray powder diffraction; (b) wavelength dispersive X-ray spectrometry; (c) energy dispersive X-ray spectrometry.



where  $K$  and  $s$  are constants dependent on the spectral series of the emission line in question.<sup>40</sup>

Most commercial X-ray spectrometers have a range of about 0.02 to 2.01 nm (0.6 to 60 keV), which will allow measurement of the K series from fluorine ( $Z = 9$ ) to lutetium ( $Z = 71$ ) and for the L series from manganese ( $Z = 25$ ) to uranium ( $Z = 92$ ).

Other line series can occur from the M and N levels but these have little use in analytical X-ray spectrometry. Although almost any high energy particle can be used to excite characteristic radiation from a specimen, an X-ray source offers a reasonable compromise between efficiency, stability and cost. Commercial X-ray spectrometers use an X-ray source. Because primary (source) X-ray photons are used to excite secondary (specimen) radiation, the technique is referred to as *X-ray fluorescence spectrometry*.

Commercially available X-ray spectrometers fall roughly into two categories: wavelength dispersive instruments and energy dispersive instruments. The wavelength dispersive system was introduced in the early 1950s and has developed into a widely accepted analytical tool; energy dispersive spectrometers became commercially available in the early 1970s. By the twenty-first century thousands of units of both types have been in use.

### Qualitative Analysis with X-Ray Spectrometer

The output from a wavelength dispersive spectrometer may be either analog or digital. For qualitative work, an analog output is traditionally used and in this instance a rate meter integrates the pulses over short time intervals, typically on the order of a second or so. The output from the rate meter is fed to a strip chart recorder that scans at a speed conveniently coupled with the goniometer scan speed. The recorder displays a diagram of intensity versus time, which becomes a diagram of  $2\theta$  versus intensity. Tables are used to interpret the resulting wavelengths.

For quantitative work, it is more convenient to use digital counting. A combination of timer and scaler is provided that allows pulses to be integrated over a period of several tens of seconds and then displayed as count or count rate.

Most modern wavelength dispersive spectrometers are controlled in some way by a minicomputer or microprocessor. Specimen changers make them capable of very high specimen throughput. Once they are set up, the spectrometers can run unattended for several hours.

## Quantitative Techniques

The great flexibility and range of the various X-ray fluorescence spectrometers, coupled with their high sensitivity and good inherent precision, makes them ideal for quantitative analysis. As with all instrumental analysis techniques, high precision can be translated into high accuracy only by compensating for the various systematic errors in the analysis process.

The precision of a well designed X-ray spectrometer is typically on the order of one tenth of a percent, the major contributor to the random error being the X-ray source (the high voltage generator plus the source element). In addition, there is an error arising from the statistics of the actual counting process.

Systematic errors in quantitative X-ray spectrometry arise mainly from absorption and specimen related phenomena (matrix effects). This is also the case in X-ray powder diffraction, except that in spectrometry, the systematic errors are much more complicated.

Diffraction deals with a single wavelength — for example, the diffracted, monochromatic line scattered from the primary source. In spectrometry, many wavelengths are involved. Although these *matrix effects* are somewhat complicated, many excellent techniques have been developed for handling them. The advent of the minicomputercontrolled spectrometer has done much to enhance the application of correction procedures. In most cases, the presence of elements of atomic number  $Z = 9$  and greater can be quantified to an accuracy of a few tenths of a percent. The areas of application for the X-ray fluorescence technique now cover almost all areas of inorganic analysis.

## Trace Analysis

The wavelength dispersive X-ray fluorescence technique is a reasonably sensitive technique with detection limits (for most elements) in the low parts per million range. Figure 24 shows a curve for the lower limit of detection as a function of atomic number, for a typical system. The curve is a smooth U shape, which is repeated above atomic number  $Z = 50$  (tin) and displaced upward by about one order of magnitude. Below atomic number  $Z = 13$  (aluminum), the sensitivity drops quite sharply until at the conventional low atomic number limit of the technique (fluorine,  $Z = 9$ ) the achievable detection limit is only about  $500 \mu\text{g}\cdot\text{g}^{-1}$ . With energy dispersive spectrometers, detection limits are typically five to ten times worse than the wavelength dispersive instruments. The

lower limit of detection is defined as *that concentration equivalent to two standard deviations of the background count rate*. In practical terms, the lower limit of detection (LLD) is given by Eq. 13:

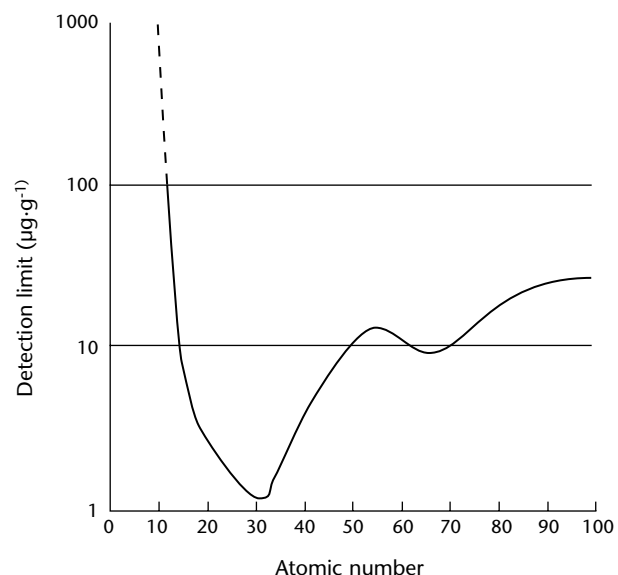
$$(13) \quad \text{LLD} = \frac{3}{m} \left( \frac{R_b}{t_b} \right)^{\frac{1}{4}}$$

where  $m$  is the counting rate per unit concentration of the analyte element;  $R_b$  the background counting rate; and  $t_b$  is the analysis time spent counting the background (effectively one half the total analysis time).

For example, in steel, the element phosphorus would give a sensitivity of about 2000 counts per second for each percent, over a background of 35 counts per second. For a total analysis time of 100 s,  $t_b$  would equal 50 s, giving a detection limit of about  $12 \mu\text{g}\cdot\text{g}^{-1}$ .

Generally, the ultimate detection limits can only be obtained where a large sample is available, typically several tenths of a gram. Very small samples can be handled, though with much poorer element detection limits. Samples as small as a few milligram will give measurable signals for concentration levels of  $10 \mu\text{g}\cdot\text{g}^{-1}$  or greater. Special instrumentation has been used for ultra trace analysis. Under favorable circumstances, detection limits down to  $10 \mu\text{g}\cdot\text{g}^{-1}$  can be obtained.

FIGURE 24. Lower limits of detection obtainable with wavelength dispersive spectrometer.



## Instrumentation for X-Ray Fluorescence Analysis

**Wavelength Dispersive Spectrometry.** All conventional X-ray spectrometers comprise three basic parts: the primary source unit; the spectrometer itself; and the measuring electronics. The primary source unit consists of a sealed X-ray tube, plus a very stable high voltage generator, capable of providing up to 3 kW of power at a typical potential of 60 to 80 kV. The sealed X-ray tube has an anode of chromium, rhodium, tungsten, silver, gold or molybdenum and delivers an intense source of continuous radiation that impinges on the specimen, producing characteristic radiation.

In the wavelength dispersive spectrometer, a single crystal of known spacing is used to disperse the polychromatic beam of characteristic wavelengths coming from the sample, such that each wavelength will diffract at a discrete angle. A portion of the characteristic fluorescence radiation is then collected by the actual spectrometer, where the beam is passed, via a collimator or slit, onto the surface of an analyzing crystal. Individual wavelengths are then diffracted in accordance with Bragg's law.

A photon detector, typically a gas flow proportional counter or a scintillation counter, is used to convert the diffracted characteristic photons into voltage pulses that are integrated and displayed as a measure of the characteristic line intensity. To maintain the required geometric conditions, a goniometer is used to ensure that the angle of source to crystal and the angle of crystal to detector are kept the same.

**Energy Dispersive Spectrometry.** Like the wavelength dispersive spectrometer, the energy dispersive spectrometer also consists of the three basic units: excitation source; spectrometer; and detection system. In this case, however, the detector itself acts as the dispersion agent. The detector is typically a lithium activated silicon detector, a proportional detector of high intrinsic resolution. The lithium activated silicon detector diode serves as a solid state version of the gas flow detector in the wavelength dispersive system.

When an X-ray photon is stopped by the detector a cloud of ionization is generated in the form of electron hole pairs. The number of electron/hole pairs created (or the total electric charge released) is proportional to the energy of the incident X-ray photon. The charge is swept from the diode by a high voltage applied across it. A preamplifier is responsible for collecting this charge on a feedback capacitor to produce a voltage pulse proportional to the original X-ray

photon energy. Thus when a range of photon energies is incident on the detector, an equivalent range of voltage pulses is produced as detector output. A multichannel analyzer is used to sort the arriving pulses to produce a histogram representation of the X-ray energy spectrum.

The output from an energy dispersive spectrometer is generally given on a visual display unit. The operator is able to display the contents of the various channels as an energy spectrum. Provisions are often made to allow zooming, to overlay spectra, to subtract background and so on in a rather interactive manner. As is the case with modern wavelength dispersive systems, nearly all energy dispersive spectrometers will incorporate some form of minicomputer for spectral stripping, peak identification, quantitative analysis and a host of other useful functions.

## Materials Certification

The energy dispersive spectrometer plays an important role in the area of materials certification, covering the range from scrap metal sorting to alloy identification and certification.

In the identification of specific product types, it may be necessary only to identify a few key elements and use these to *fingerprint* the product.

Sometimes this is done by deliberately adding tracer elements at low concentration. The technique has been used successfully in the sorting of finished polymer pieces by tagging them with the elements chlorine and chromium, at concentration levels of about 0.1 percent. A very short counting time, perhaps a few seconds, is all that the energy dispersive spectrometer requires to establish the source of the polymer product.

Another example of the spectrometer's use is in the analysis of plating on sheet steel, where it is necessary to control the thickness of a coated layer.<sup>44-45</sup> A calibration curve of X-ray line intensity, as a function of coating thickness, can be easily established from a few standard samples. This curve is then used for quality control purposes by comparison with online count data from the energy dispersive system.

## Closing

Since the 1950s, X-ray analytical techniques have been widely used in materials research, quality control and certification. Although there are alternatives to the X-ray fluorescence technique for elemental analysis, the ability of the technique to give fast,

accurate analyses over wide concentration ranges, coupled with its excellent qualitative capability, makes the technique very attractive. As far as phase analysis is concerned, the X-ray diffraction technique's capacity for identification of multiphase mixtures is unique and is enhanced by its ability to give data on stress, strain, texture, topography and so on.

The minicomputer has played an important role in the development of instrumentation, both for X-ray diffraction and X-ray fluorescence. Modern diffractometer and spectrometer systems are highly automated and most of the tedium and complexity of data interpretation are being reduced by the computer. Fast and efficient programs are available for peak hunting, profile deconvolution, data plotting and other functions. The rapid growth in computer technology will undoubtedly continue to give impetus to the X-ray analytical field.

In the realm of instrumentation, a fruitful area has been high power sources. Rotating anode X-ray tubes, operating at 15 to 20 kW, are available for diffraction measurements and give higher X-ray intensities (by an order of magnitude) than do sealed tubes of the 1970s. Two-dimensional position sensitive detectors have been applied in stress and low angle scatter measurements. The X-ray analytical field has traditionally been quick to implement technologies, making the role of X-ray techniques in materials characterization secure for years to come.



# References

1. *Nondestructive Testing Handbook*, second edition: Vol. 3, *Radiography and Radiation Testing*. Columbus, OH: American Society for Nondestructive Testing (1985).
2. "Projection Microfocus Radiography." *Nondestructive Testing Handbook*, second edition: Vol. 3, *Radiography and Radiation Testing*. Sec. 19, "Specialized Radiographic Methods." Columbus, OH: American Society for Nondestructive Testing (1985): p 801-807.
3. McDaniel, G.A. "Recent Developments in High Output Microfocus X-Ray Systems." *Automated Nondestructive Testing: Proceedings of a Topical Seminar* [Idaho Falls, ID, June 1983]. New York, NY: Gordon and Breach Science Publishers (1986): p 209-212.
4. Spaulding, W.H. and J.J. Schuldies. "Microfocus Radiography and Computer Image Enhancement Applied to Non-Metallics." *Paper Summaries: ASNT National Fall Conference* [Denver, CO, October 1978]. Columbus, OH: American Society for Nondestructive Testing (1978): p 127-130.
5. Peugeot, R.S. "Theoretical and Practical Considerations of Microfocus Radiography." *Materials Evaluation*. Vol. 40, No. 2. Columbus, OH: American Society for Nondestructive Testing (February 1982): p 150, 152.
6. Bagnell, M.J. and B. Kotzian. "Microfocus Radiography of Jet Engines." *Materials Evaluation*. Vol. 44, No. 13. Columbus, OH: American Society for Nondestructive Testing (December 1986): p 1466-1467.
7. Marchese, M. and K.A. Glodowski. "Real-Time Microfocus Radiography for Electronic Failure Analysis." *Materials Evaluation*. Vol. 49, No. 12. Columbus, OH: American Society for Nondestructive Testing (December 1991): p 1481-1485.
8. Silver, M.D. and N.R. Schreiber. "Microfocus Volume CT of Aluminum Castings." *1992 ASNT Spring Conference* [Orlando, FL]. Columbus, OH: American Society for Nondestructive Testing (March-April 1992): p 124.
9. Ellingson, W.A., E.A. Sivers, D.A. Holloway, J.R. Ling, J.P. Pollinger and H.C. Yeh. "Application of 3-D Microfocus X-Ray Computed Tomography for Mapping Density Variations in Pressure Slip Cast  $\text{Si}_3\text{N}_4$  Ceramics." *ASNT 1993 Spring Conference*. Columbus, OH: American Society for Nondestructive Testing (March-April 1993): p 129.
10. Isaacson, B. "Microfocus Radiography." *Proceedings of the Radiologic NDT III: Advancements, Automation and Imaging* [Atlantic City, NJ]. Columbus, OH: American Society for Nondestructive Testing (August 1993): p 88.
11. Renwick, S. and H. Hansen. "High-Energy Microfocus X-Ray Source." *ASNT 1994 Fall Conference and Quality Testing Show* [Atlanta, GA]. Columbus, OH: American Society for Nondestructive Testing (September 1994): p 47.
12. Biagi, E., A. Forti, L. Masotti and C. Cappabianca. "Ultrasonic High Resolution Images and X-Ray Microfocus Testing for Defect Detection in Ceramic Materials." *ASNT 1996 Spring Conference/Fifth Annual Research Symposium* [Norfolk, MD]. Columbus, OH: American Society for Nondestructive Testing (March 1996): p 171.
13. Silva, F. "Automated X-Ray Inspection Strategies." *Real-Time Radioscopy and Digital Imaging* [Mashantucket, CT]. Columbus, OH: American Society for Nondestructive Testing (August 1998): Appendix, p 1-15.
14. Ely, R.V. *Microfocus Radiography*. New York, NY: Academic Press (1980).
15. Charbonnier, F. "Flash Radiography." *Nondestructive Testing Handbook*, second edition: Vol. 3, *Radiography and Radiation Testing*. Columbus, OH: American Society for Nondestructive Testing (1985): p 491-531.
16. Jamet, F. and G. Thomer. *Flash Radiography*. Elsevier Publishing Company (1976).
17. Bryant, L.E., ed. *Proceedings of the Flash Radiography Symposium* [Houston, TX]. Columbus, OH: American Society for Nondestructive Testing (1976).



18. Marilleau, J., ed. *Proceedings of the First European Conference on Cineradiography with Photons or Particles* [Paris, 1981]. Bellingham, WA: International Society for Optical Engineering (1983).
19. Webster, E.A., Jr. and A.M. Kennedy. *Proceedings of the 1986 Flash Radiography Topical* [Portland, OR, July 1986]. Columbus, OH: American Society for Nondestructive Testing (1986).
20. Charbonnier, F.M. et al. *Radiology*. Vol. 117. Easton, PA: Radiological Society of North America (1975): p 165-172.
21. Bryant, L.E. "Flash Radiography of Electron Beam Welding." *Materials Evaluation*. Vol. 29, No. 10. Columbus, OH: American Society for Nondestructive Testing (October 1971): p 237-240.
22. Winfree, W.P., N.A. Cmar-Mascis and F.R. Parker. "Enhanced Imaging of Corrosion in Aircraft Structures with Reverse Geometry X-Ray ®." Paper 7C2. *Third Joint Conference on Aging Aircraft* [Albuquerque, NM]. Arlington, VA: Galaxy Scientific for the Federal Aviation Administration, Airworthiness Assurance Nondestructive Inspection Validation Center, Sandia National Laboratories, Albuquerque, NM (September 1999).
23. Albert, R., W. Pember, J. Garrison and D. Reyna. "Aircraft Inspection with a Portable, Filmless X-Ray System Using Reverse Geometry." *Materials Evaluation*. Vol. 58, No. 5. Columbus, OH: American Society for Nondestructive Testing (May 2000): p 634-638.
24. Albert, T.M. "X-Ray System Applications Using Reverse Geometry for High Sensitivity." *Materials Evaluation*. Vol. 51, No. 12. Columbus, OH: American Society for Nondestructive Testing (September 1993): p 1020-1027.
25. Albert, R.D. and T.M. Albert. "Aerospace Applications of X-Ray System Using Reverse Geometry." *Materials Evaluation*. Vol. 51, No. 12. Columbus, OH: American Society for Nondestructive Testing (December 1993): p 1350-1352.
26. Albert, R.D. *X-Ray Scanning Method and Apparatus*. United States Patent 3 949 229 (April 1976).
27. Albert, T.M. "Reverse Geometry X-Ray Imaging: An Emerging QNDE Technology." *Review of Progress in Quantitative Nondestructive Evaluation*. Vol. 13. Plenum, NY: Plenum (1994): p 587.
28. Birt, E.A., F.R. Parker and W.P. Winfree. "Quantification of Corrosion Damage in Aircraft Skin Using a Novel X-Ray Radiography System." *Review of Progress in Quantitative Nondestructive Evaluation*. Vol. 13. Plenum, NY: Plenum (1994): p 1963.
29. Landolt, J.F., W.D. Stump and J.L. Summers. "A Visual Comparative Method for Radiographic Determination of Defect Thickness." *Materials Evaluation*. Vol. 36, No. 11. Columbus, OH: American Society for Nondestructive Testing (October 1978): p 33.
30. Barry, R.C., M.D. Barker and L.M. Klynn. "Real-Time Stereo Radiography." *Materials Evaluation*. Vol. 50, No. 2. Columbus, OH: American Society for Nondestructive Testing (February 1992): p 247-252.
31. Burbank, B.B. "Improved Stereoscopic Radiography." *Industrial Radiography*. Vol. 2, No. 2. Columbus, OH: American Society for Nondestructive Testing (Fall 1943): p 20-23, 31-32.
32. Dudley, L.P. "Stereoscopic Radiography." *Industrial Radiography and Nondestructive Testing*. Vol. 5, No. 1. Columbus, OH: American Society for Nondestructive Testing (Summer 1946): p 23-25, 39.
33. Lipton, L. "Stereo-Vision Formats for Video and Computer Graphics." White paper. San Rafael, CA: StereoGraphics Corporation (1997).
34. Lipton, L. *StereoGraphics Developers' Handbook*. San Rafael, CA: StereoGraphics Corporation (1997).
35. Lipton, L. "A Little History; and HP's Link to Stereoscopic Visualization." *The HP Chronicle*. Austin, TX: Publications and Communications (March 2000).
36. Lipton, L. and M. Feldman. "A New Autostereoscopic Display Technology: The SynthaGram™." White paper. San Rafael, CA: StereoGraphics (2001).
37. *Radiography in Modern Industry*, fourth edition. Rochester, NY: Eastman Kodak Company (1980): p 114-116.
38. McMaster, R.C., ed. *Nondestructive Testing Handbook*, first edition. Vol. 1, Sec. 20. Columbus, OH: American Society for Nondestructive Testing (1959): p 49.
39. Henry, N.F.M. and K. Lonsdale, eds. *International Tables for X-Ray Crystallography*, third edition: Vol. 1, *Symmetry Groups*. Birmingham, AL: Kynoch Press (1969).
40. Moseley, H.G.J. "The High Frequency Spectra of the Elements." *Philosophical Magazine*, sixth series. Vol. 26. London, United Kingdom: Taylor and Francis, Limited (1913): p 1024.

41. Hentschel, M.P., A. Lange, J. Schors, O. Wald and K.W. Harbich. "Wide Angle X-Ray Diffraction Topography of Polycrystalline Materials." *Nondestructive Characterization of Materials IX*. AIP Proceedings 497. Melville, NY: American Institute of Physics (1999): p 655-660.
42. Ruud, C.O., M.E. Jacobs, J.A. Josef, D.J. Snoha and A.L. Moran. "X-Ray Diffraction Techniques for the Assessment of Residual Stress and Microstrain in Carbon Graphite Materials." *Materials Evaluation*. Vol. 48, No. 7. Columbus, OH: American Society for Nondestructive Testing (July 1990): p 894-897.
43. Nondestructive Thickness Gaging Method for Thin Layers Using X-Ray Fluorescence, Chesney, H.L., E.P. Papadakis and J.M. Brinkerhoff. *Materials Evaluation*. Vol. 39, No. 8. Columbus, OH: American Society for Nondestructive Testing (July 1981): p 726-738.
44. Light, G.M., G.P. Singh and E.D. McDaniel. "Ultrasonic and X-Ray Fluorescence Measurement of the Thickness of Metal Foils." *Materials Evaluation*. Vol. 47, No. 3. Columbus, OH: American Society for Nondestructive Testing (March 1989): p 322-324, 326-328, 330.
45. Adams, L. "X-Ray Fluorescence Measures Coating Thickness." *Quality*. Vol. 40, No. 11. Bensenville, IL: Business News Publishing (November 2001): p 30-33.



# 16

## C H A P T E R

# Neutron Radiography

---

John P. Barton, Consultant, San Diego, California

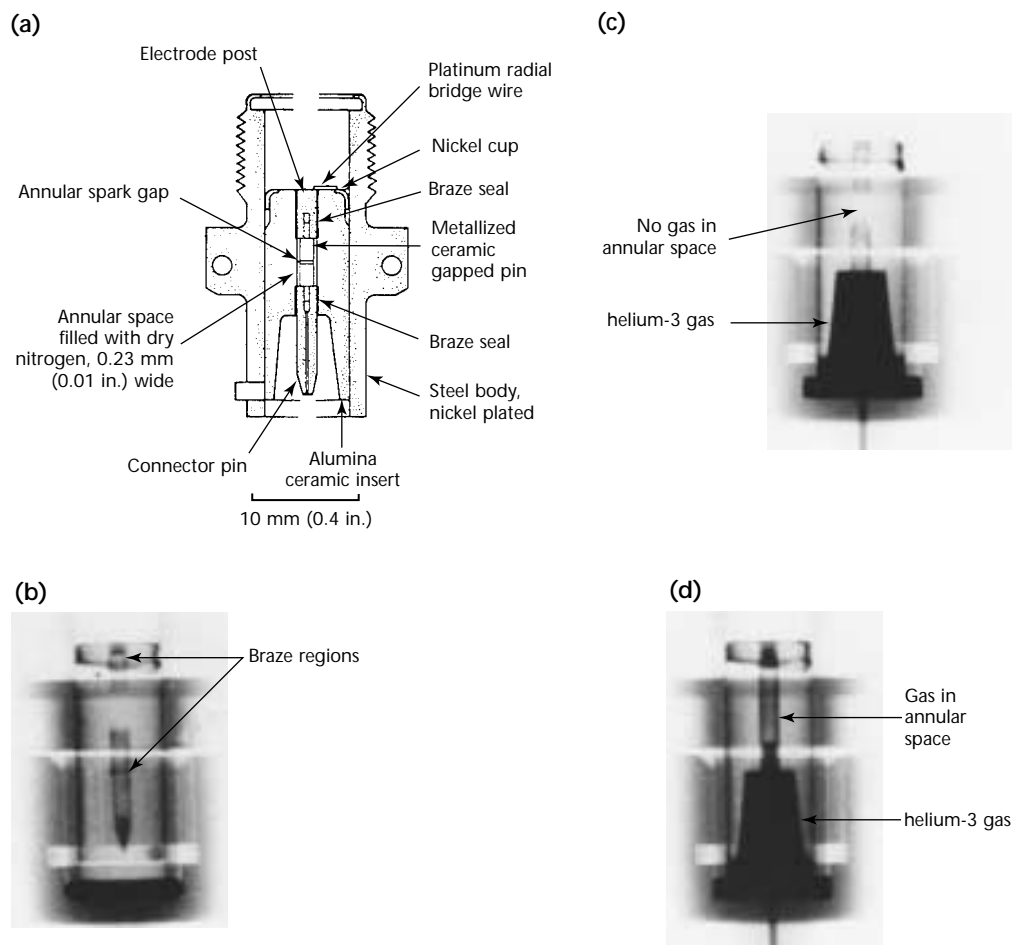
## PART 1. Applications of Neutron Radiography

Neutron radiation is similar to X-radiation. The radiation can originate from an effective point source or can be collimated to shine through an object in a coherent beam. The pattern of penetrating radiation can then be studied to reveal clues about the internals of the object. The information conveyed can be very different from that obtainable with X-rays. Whereas X-rays are attenuated by dense metals more than by hydrocarbons, neutrons are attenuated more by hydrocarbons than by most metals. The difference can mean much more than the reversal of a positive image to a negative

image. Neutrons, for example, can reveal details within high density surroundings that cannot be revealed by other means.<sup>1-13</sup>

A typical application for neutron radiography is shown in the images of a pyrotechnic device (Fig. 1), where the small explosive charge is encased in metal. Other applications include inspection of explosive cords used in pilot ejector mechanisms; inspection of gaskets, seals and O-rings inside metallic valves; confirmation that coolant channels in jet engine turbine blades are free of blockage; studies of coking in jet engine fuel

FIGURE 1. Electric bridge wire squid: (a) drawing and (b) neutron radiograph of part as aid to interpretation; (c) helium-3 gaseous penetrant applied to serviceable unit; (d) penetrant applied to dysfunctional unit.



nozzles; and screening of aircraft panels to detect low level moisture or early stage corrosion in aluminum honeycomb (Fig. 2).

## User's Guide

Unlike many other forms of nondestructive testing, neutron radiography is not a do-it-yourself technique. There have been neutron radiography service centers in the United States since 1968. To try out neutron radiography on an object of interest, it is simply necessary to locate the services currently available and, if agreed, mail your item to them. Typically, the neutron radiograph and your item will be mailed back within a day or two. The cost could be less than 1 or 2 h of an engineer's time. If assistance is required to interpret the findings, this too may be requested on a service basis, as may referrals to more specialized neutron radiographic techniques.

The providers of neutron radiography services use equipment and expertise that is highly specialized. Even though one or more neutron radiography service centers have been operating successfully for over 30 years, there has been no in-house neutron radiography available at any general service, commercial

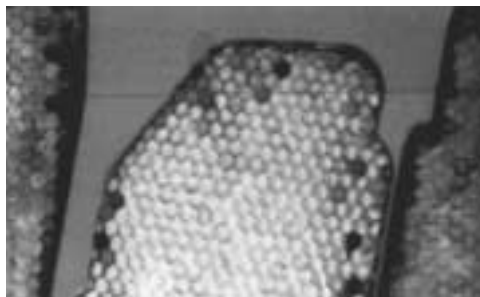
nondestructive testing center. The interested user is therefore advised to seek a supplier of neutron radiographic services using leads such as society directories or the published literature.

Because neutrons are fundamentally different from X-rays, any object that is a candidate for inspection by X-radiography could also be a candidate for neutron radiography. If X-rays cannot give sufficient information, then trials with neutron techniques may be prudent. The most frequently successful complement to X-radiography is static radiography with thermal neutrons. This approach is reviewed next.

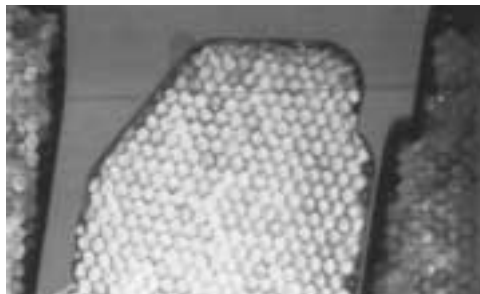
Then more specialized neutron radiology techniques are reviewed, such as neutron computed tomography, dynamic neutron imaging, high frame rate neutron imaging, neutron induced autoradiography and neutron gaging. For each of the neutron radiology techniques different neutron energies may be selected. The user should be aware that many of the specialized services are only available at one or two centers worldwide. It is therefore important to shop in the global market and to take advantage of the excellent communications existing between neutron radiography centers in various countries.

FIGURE 2. Comparison of neutron radiographs of moisture globules in aluminum honeycomb panel, later dried: (a) before processing; (b) after processing.

(a)



(b)



## PART 2. Static Radiography with Thermal Neutrons

### Neutron Energy

Thermal energy neutrons are those that have collided repeatedly with a moderator material, typically graphite or water, such that they reach an equilibrium energy with the thermal energy of the moderator nuclei.

The attenuation coefficients for thermal neutrons differ from material to material in a way that is different from X-rays as shown in Table 1. As a consequence, a high degree of contrast between the elements in an object is possible. In addition, thermal neutrons are relatively easy to obtain and easy to detect.<sup>11-15</sup>

### Neutron Collimation

Because the source of thermal neutrons is a dispersed moderator volume, rather than a point source, it is necessary to use a collimator between the source and the object. In preference to a single tube parallel sided collimator or a multiple slit collimator, the most frequently used design uses divergent beam geometry.<sup>16</sup>

The collimator may be used to extract a beam in any one of a variety of different geometries including horizontal or vertical, radial or tangential to the source. A collimator that is tangential to the source can provide a thermal neutron beam relatively free of fast neutron and gamma ray contamination. An incidental consequence of the divergent collimator

principal is that even very large objects can be radiographed using an array of side-by-side films (Fig. 3).

### Neutron Imaging

#### Collimation Ratio

The collimation ratio is the ratio  $L \cdot D^{-1}$  of the collimator length  $L$  to aperture diameter  $D$ . This ratio helps to predict image sharpness.

#### Imaging Processes

For static thermal neutron radiography of nonradioactive objects, two important imaging processes are (1) the gadolinium converter with single emulsion X-ray film and (2) the neutron sensitive storage phosphor (neutron imaging plate). For static neutron radiography of radioactive objects, additional imaging processes are (1) dysprosium foil activation transfer to film, (2) indium foil activation transfer to

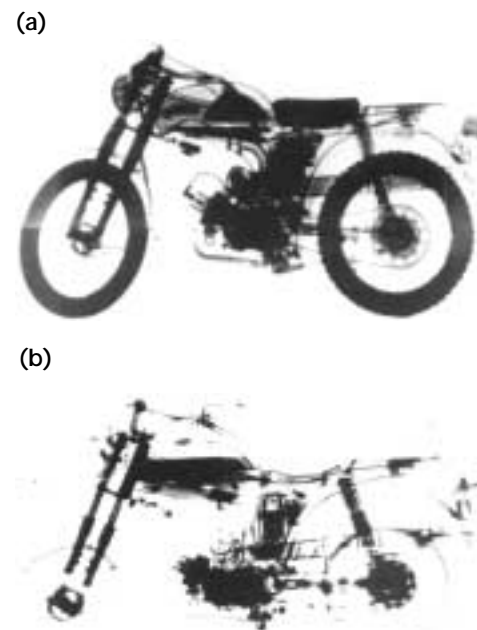
TABLE 1. Comparison of X-ray and thermal neutron attenuation.

Element	Density (g·cm <sup>-3</sup> )	Relative X-Ray Attenuation	Relative Thermal Neutron Attenuation
Lead <sup>a</sup>	11.3	High	Low
Cadmium	7.9	Medium	Very high
Iron	7.8	Medium	Medium
Aluminum	2.7	Low	Low
Water <sup>b</sup>	1	Low	High

a. Other materials relatively transparent to thermal neutrons include gold, silver, platinum, titanium, silicon, tin and zinc.

b. Other materials relatively opaque to thermal neutrons include hydrogenous oils, plastics, rubbers, explosives and light elements boron and lithium.

FIGURE 3. Radiographs of full size motorcycle: (a) neutron radiograph; (b) x-radiograph.





film and (3) track etch imaging using a boron converter and cellulose nitrate film.

The established direct imaging technique uses thin gadolinium layer vapor deposited on a solid converter screen, which is held flat against a single emulsion film inside a vacuum cassette of thin aluminum construction. An exposure of  $10^9$  neutrons per square centimeter can give a high resolution, high contrast radiograph if careful dust free film darkroom procedures are used.

Neutron sensitive imaging plates consist of a thin phosphor layer containing a mixture of storage phosphor, neutron converter and organic binder. Following the neutron exposure stage is the information readout phase, in which the plate is scanned by a thin laser beam stimulating the emission of a pattern of light. Merits of this neutron imaging technique include five decades of linearity, wide dynamic range, direct availability of digital data for processing converter efficiencies of 30 to 40 percent, and spatial resolution acceptable for some applications.<sup>17,18</sup>

For neutron radiography of highly radioactive objects, dysprosium and indium foil activation transfer to film and track etch imaging each offer complete discrimination against gamma ray fogging.<sup>19</sup> Examples of nuclear fuel neutron radiography are shown in Fig. 4. Dysprosium transfer can be combined with a cadmium indium foil sandwich for dual energy radiography. Alternative track etch techniques have been developed to yield more precise dimensional measurements.<sup>20</sup>

### Image Quality Indicators

For any nondestructive system, the best measure of quality is to compare the image of the test object with an image of a similar object that contains a known artificial discontinuity, a *defect standard*, or *reference standard*. However, neutron radiography has the same problems as other nondestructive testing methods: the quantity of reference standards required is too large to obtain and maintain. In lieu of a reference standard, neutron radiographers have chosen to fabricate a resolution indicator that emulates the worst case scenario with gaps placed between and holes placed beneath different plastic thicknesses.<sup>12</sup> For defining the neutron beam characteristics a beam purity indicator has been devised to accompany the sensitivity indicator.

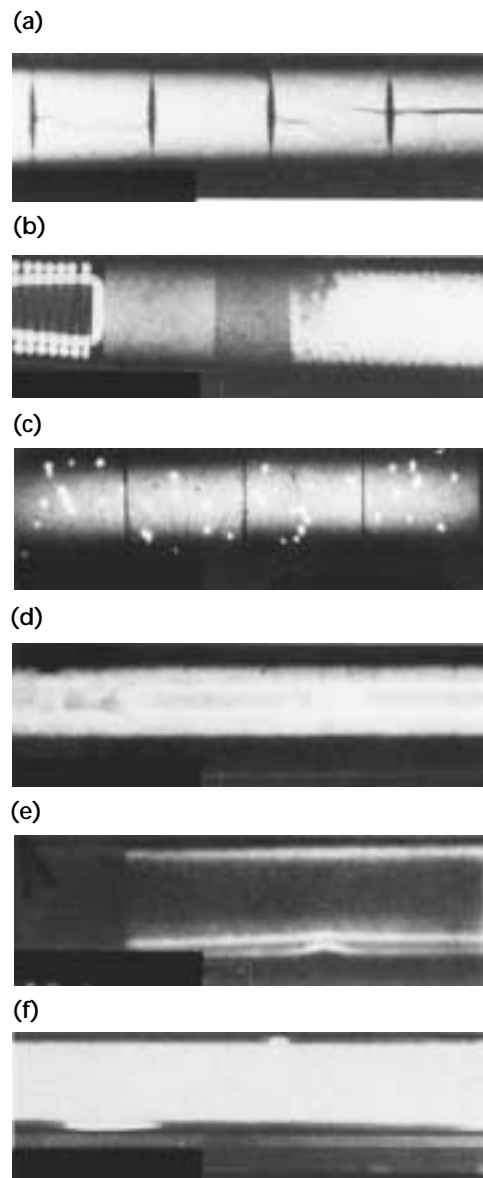
The image quality indicator system of ASTM International has become the primary or alternate system for most manufacturing specifications on an international basis. The *no umbra* device, a device to measure resolution, is described

in ASTM E 803-91 and can be used to determine the collimation ratio  $L \cdot D^{-1}$  of the neutron radiography facility.<sup>13</sup>

## Nuclear Reactor Systems

A nuclear reactor system operated for over 30 years solely to provide a commercial neutron radiographic service is illustrated in Fig. 5. The reactor core, positioned underground in a tank of water, is only about 0.38 m (15 in.) in diameter and

FIGURE 4. Neutron radiographs of nuclear fuel: (a) longitudinal cracks in pellets; (b) missing chips in compacted fuels; (c) inclusions of plutonium in pellets; (d) accumulation of plutonium in central void; (e) deformed cladding; (f) hydrides in cladding.



operates at 250 kW power. The tangential beam tube is orientated vertically with air displaced by helium. Parts for neutron radiography can therefore be supported on horizontal trays. Usually the neutron imaging uses a gadolinium converter with fine grain radiographic film and the exposure time at a selected collimation is typically about 2 min.<sup>21</sup>

Another reactor that has provided neutron radiography services since 1968 is illustrated in Fig. 6. It is above ground and the fuel of the 100 kW core is arranged in an annulus with a moderator region in the center. Two horizontal beams are extracted from the central moderator, one for direct film neutron

radiography of nonradioactive objects, the other for dysprosium activation transfer neutron radiography of radioactive nuclear fuel.<sup>22</sup>

Another service for static neutron radiography of radioactive nuclear fuel has been provided by a 250 kW nuclear reactor installed in a hot cell complex (Fig. 7). Also several university reactors in the United States have been equipped for neutron radiography. Worldwide, over fifty nuclear reactors have contributed to development of this field.

## Accelerator Based Systems

An initial user of neutron radiography need not, in general, be concerned with accelerator source options unless there is an established need either for an in-house system or for a transportable system. Almost all neutron radiography service providers use a nuclear reactor source. One exception has been the powerful spallation type accelerator in Switzerland; the accelerator is a multipurpose facility comparable in complexity and cost to a research reactor.

An in-house system that was operated successfully for over 15 years at the United States Department of Energy's Pantex Plant used a van de graaff accelerator. The operation of this machine, which accelerates over 200  $\mu$ A of deuterons at 3 MeV into a beryllium target, is illustrated in Fig. 8. The system provided a peak thermal neutron flux of about  $10^9$  neutrons per square centimeter

FIGURE 5. Representative neutron radiographic service center for nonnuclear applications.

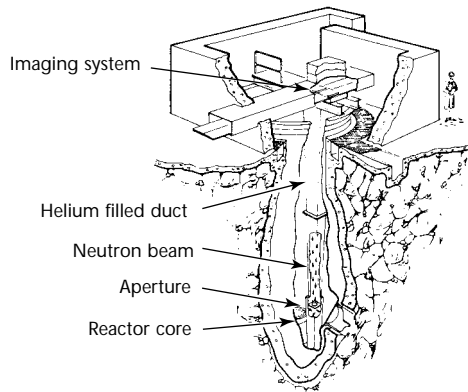
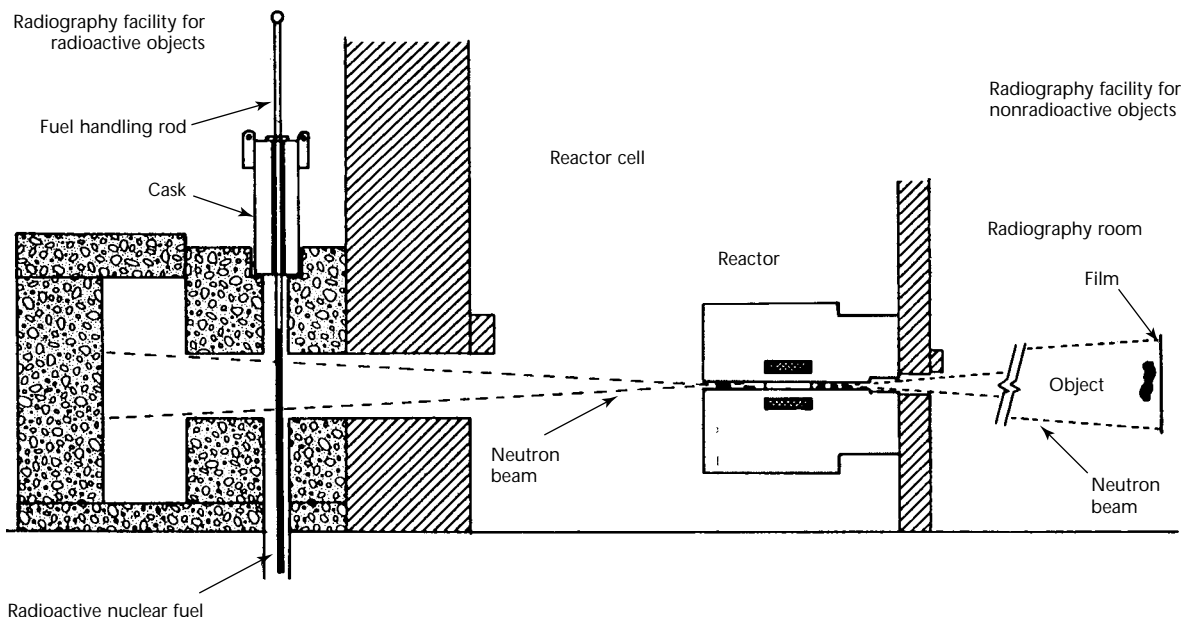


FIGURE 6. Representative neutron radiographic service center for nuclear and nonnuclear applications.



second, two orders of magnitude less than the reactor systems described above but sufficient for low throughput work using 2 h exposure times and a relatively low beam collimation ratio.

Cyclotrons and radio frequency quadrupole accelerators are other candidates for a potential custom designed in-house neutron radiographic system. Neutron radiographic performance data have been reported for designs with a variety of sizes, neutron yields and costs.<sup>23</sup>

For transportable systems much of the development work has used sealed tube acceleration of deuterium tritium mixtures. This can consist of a source head that is maneuverable with long high tension cable linking it to the high voltage power supply and control unit as illustrated (Fig. 9). The particular type shown yields a peak thermal neutron flux of about  $10^8$  neutrons per square

centimeter second with a tube operation half life of about 200 h.<sup>24-25</sup>

## High Intensity Californium-252 Systems

Of the many radioactive neutron sources, such as polonium-210 beryllium and americium-244 beryllium, one has dominated interest for neutron radiography: californium-252. This transplutonic isotope is produced as a byproduct of basic research programs. In the United States, some government centers have been able to obtain the source on a low cost loan basis from the Department of Energy. The isotope yields neutrons by spontaneous fission at a rate of  $2 \times 10^9$  neutrons per second per milligram and has a half life of 2.5 years.

FIGURE 7. Hot cell fuel inspection system.

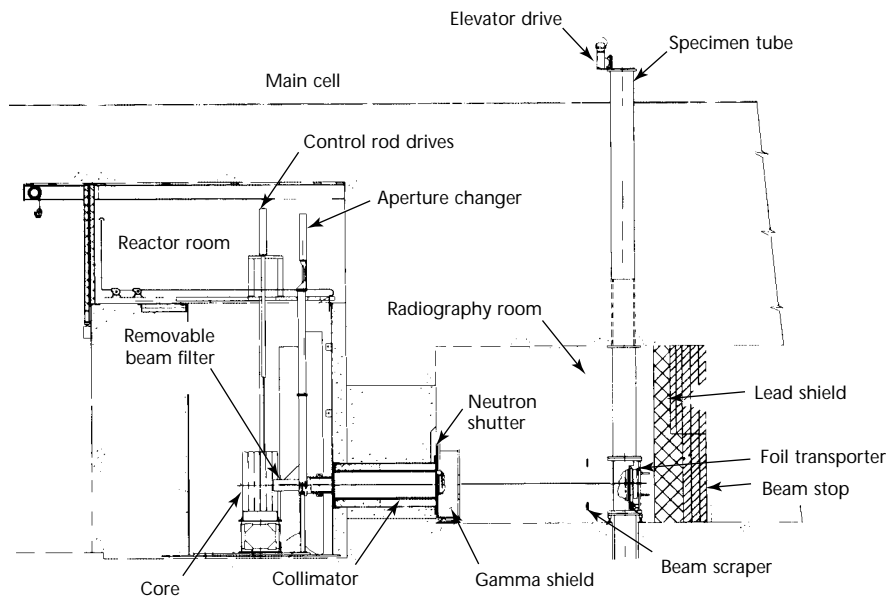
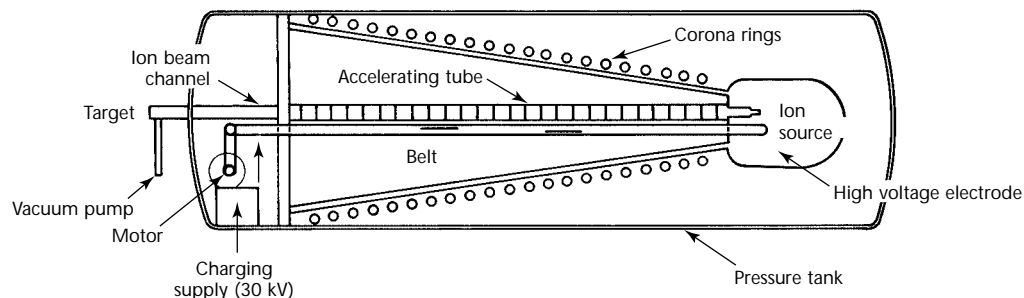


FIGURE 8. Cross section showing van de graaff principle.



A high yield source of up to 50 mg can be smaller than a tube of lipstick (Fig. 10).

An in-house stationary system has operated at the United States Department of Energy's installation at Pantex with a total source strength of 150 mg californium-252. It provided sets of nine films, each  $350 \times 425$  mm ( $14 \times 17$  in.), approaching reactor quality by using gadolinium with a very fine grain X-ray film; a collimator ratio of 65; and exposure time of under 24 h.

A maneuverable source system has operated at McClellan Air Force Base with a total source strength of 50 mg californium-252. It provided single neutron radiographs using a fast scintillator screen; high speed, light sensitive film; a collimator ratio of 30; and an exposure time of 12 min. This system was designed for the specific application of scanning intact aircraft to

detect hidden problems at an early stage, such as moisture or corrosion in aluminum honeycomb.<sup>26</sup>

Another example of a high yield californium-252 system design uses a subcritical multiplier to amplify the central neutron flux. This design (Fig. 11) produces a peak central flux of  $7 \times 10^8$  neutrons per square centimeter second when loaded with 40 mg californium-252.

### Low Cost In-House System

There is evidence that an extremely low intensity californium-252 neutron source could provide a convenient, low cost in-house system. A source size of only 100  $\mu$ g can provide useful quality neutron radiographs by using highly efficient imaging systems that need only  $10^5$  neutrons per square centimeter exposure. This is 10 000 times less than

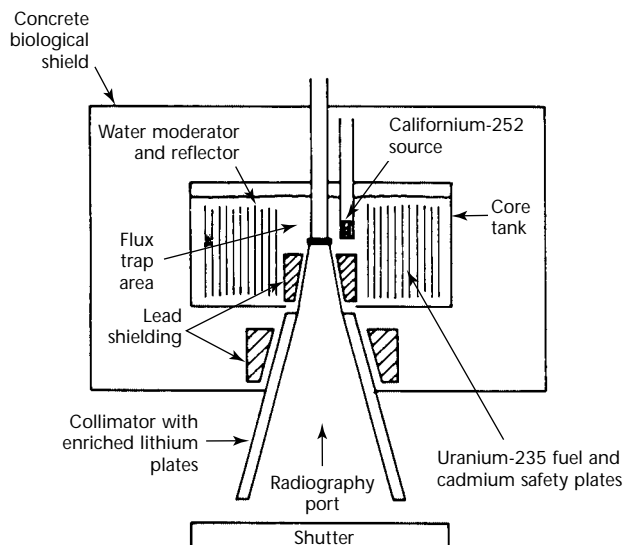
FIGURE 9. Components of mobile deuterium tritium neutron radiographic system: (a) deuterium tritium source head, typically on 6 m (20 ft) cables; (b) cooling unit (left) and power supply; (c) control unit.



FIGURE 10. Californium-252 sources compared in size to postage stamp.



FIGURE 11. Elevation of subcritical multiplier system.



the exposure used typically with gadolinium and single emulsion film. The small source size would mean an inexpensive source and also inexpensive shielding, handling and interlock requirements.<sup>26</sup> Therefore, a nondestructive testing center with a variety of X-ray, ultrasonic and other inspection capabilities could easily incorporate a small californium-252 based neutron radiographic capability using an underground storage geometry in an existing radiographic bay. Because neutron radiography yields unique information, such an inexpensive in-house capability could be an important complement to an otherwise full service nondestructive testing center.

## PART 3. Special Techniques of Neutron Radiography

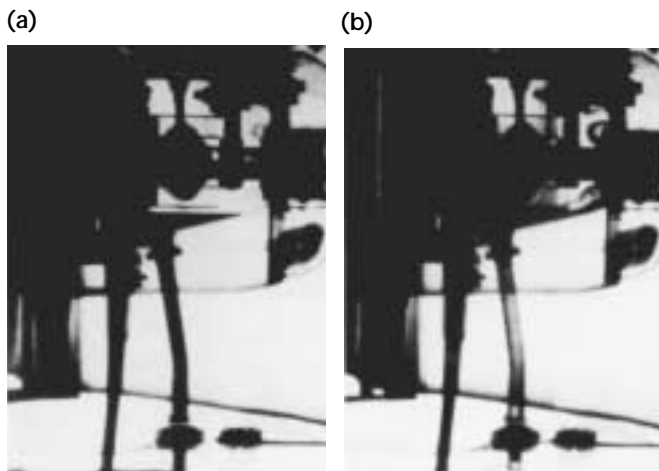
### Dynamic Neutron Radioscopy

Services that provide different types of dynamic neutron radioscopy have been developed at numerous nuclear reactor centers worldwide. They cover frame rates that range from 30 frames per second (real time motion display similar to television) to 1000 frames per second range (a high frame rate) or to 10 000 frames per second (a very high frame rate).<sup>27-28</sup>

An example of a real time dynamic neutron radioscopy application is illustrated in Figure 12. A beam from a 28 MW reactor was used to study the flow characteristics of lubricant inside an operating jet engine. Other applications have included studies of absorption and compression refrigerator designs, studies of automotive parts in motion and a large range of two-phase flow studies.

For high throughput dynamic neutron imaging one reactor center has been equipped with three separate beams, each with its neutron imaging system and digital image interpretation system.<sup>29</sup> Other reactor centers have developed techniques for simultaneous neutron and gamma ray dynamic imaging using a pair of scintillator screens in conjunction with a low light level television camera and video processing.<sup>30</sup>

FIGURE 12. Frames from real time studies of operating aircraft engine: (a) first view; (b) second view.



The development of dynamic neutron radioscopy services with a high frame rate of 1000 frames per second has capitalized on the availability of very high intensity steady state neutron beams (with a flux of  $10^8$  neutrons per square centimeter second) and very high frame rate video cameras used with rapid response neutron sensitive scintillator screens. A very high frame rate capability, up to 10 000 frames per second, uses the ability of certain reactors to be pulsed, giving a high neutron yield for a time duration of a few milliseconds. The event to be studied, such as the burn cycle of a pyrotechnic event, is synchronized to the neutron pulse time.<sup>31</sup>

### Subthermal Neutron Radiology

The neutron attenuation coefficient of a particular material can change significantly as the neutron energy is changed. The pattern of this variation also changes abruptly from one element to another. Therefore, selection of different energy neutrons provides possibilities for quite different neutron radiology penetration and contrast.

Neutron radiology service reactors have developed neutron beams of selected subthermal or cold neutrons using three techniques: (1) beam filtration by polycrystal beryllium, which passes only long wavelength, low energy neutrons below 0.005 eV, (2) a refrigerated moderator volume and (3) selection of longer wavelength, low energy neutrons by multiple internal reflection in a gently curved guide tube.<sup>32,33</sup>

The effect of this energy selection is typically to increase the transparency of certain materials while simultaneously increasing the contrast or detectability of hydrogenous materials (see Table 2 and Fig. 13). Just as thermal neutron radiography gives different information to X-radiography, so subthermal or cold neutron radiography gives information different from that of regular thermal neutron techniques. An example is given in Fig. 14. It is possible, using a guide tube, to select only very cold neutrons (that is, energies below 0.001 eV) and this can provide high sensitivity for very thin hydrogenous specimens.



## Epithermal and Fast Neutron Radiology

A reactor beam, although consisting primarily of thermal neutrons, will contain a proportion of both subthermal and epithermal (high energy) neutrons. With a filter such as cadmium, the thermal and subthermal neutrons can be removed and only the epithermal part of the neutron energy spectrum will be transmitted.<sup>33</sup>

For the inspection of enriched nuclear fuel the higher penetration of epithermal neutrons provides a valuable difference from thermal or subthermal neutron radiography. Indium has a high resonance capture cross section at about 1.4 eV epithermal energy. Cadmium wrapped indium foil activation transfer imaging techniques have been used for this application.

Another epithermal neutron technique uses an indium foil filter in the incident beam to remove neutrons close to the specific resonance energy. This beam is passed through the object and an indium detector is used on the far side. The technique can provide high sensitivity to small quantities of hydrogen in the object because hydrogen can change the energy of an incident neutron more than heavier elements.

The term fast neutron radiography refers normally to those neutron energies yielded by an unmoderated accelerator source or radioactive source. Fast neutron radiography provides high penetration but little contrast between elements. The accelerator can provide a point source. Tantalum is one of several detector materials for direct exposure and scintillator screens can be used. Alternatively, foil activation transfer with holmium has been demonstrated.<sup>34</sup>

TABLE 2. Relative neutron attenuation coefficients.

Element	Thermal Neutrons	Cold Neutrons
Beryllium	0.861	0.055
Silicon	0.092	0.050
Iron	1.160	0.568
Nickel	1.980	1.350
Zirconium	0.340	0.047
Lead	0.370	0.049
Bismuth	0.250	0.126

## Neutron Computed Tomography

Computed axial tomography has been developed for neutron radiography and can provide detailed cross sectional slices of the object to be analyzed. Although the principle is similar to that of X-ray computed tomography, the information conveyed by neutrons can be unique. In a typical facility the object is rotated in the

FIGURE 13. Attenuation of materials for thermal and cold neutrons.

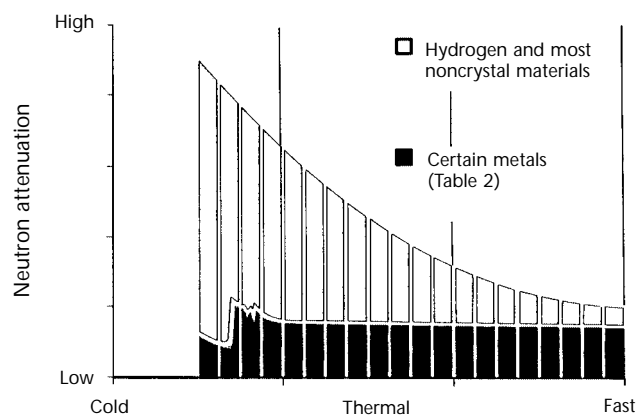
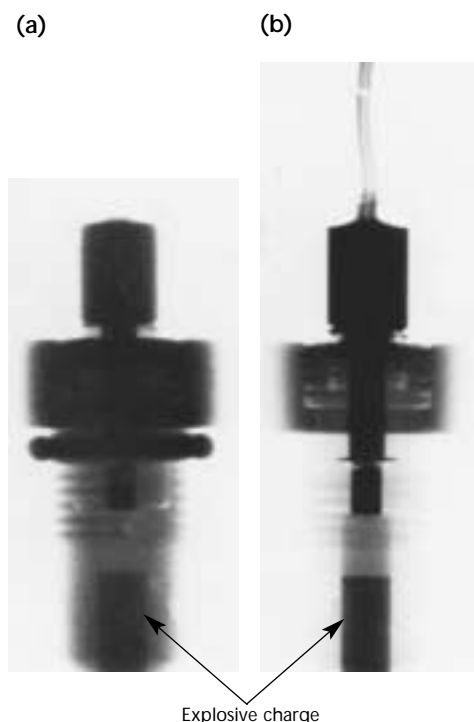


FIGURE 14. Neutron radiographs of explosive bridge wire igniter: (a) thermal neutron image; (b) cold neutron image.



neutron beam and data are stored for upward of 200 angles. Detectors used have included a scintillator screen  $^6\text{LiF-ZnS}$  (Ag), viewed by a cooled charge coupled device camera and alternatively a storage phosphor image plate loaded with  $\text{Gd}_2\text{O}_3$  combined with an automatic laser beam scanner. Using a high intensity neutron radiography beam of over  $10^8$  neutrons per square centimeter second, computed tomography of two-phase flow volumes has been processed as a time averaged three-dimensional analysis.<sup>35-37</sup>

been used for this neutron induced autoradiography of paintings.<sup>42</sup> Typically, a series of autoradiographs is taken using a range of neutron exposure times and different decay times before imaging. This, combined with a range of scintillator screen and film sensitivities, can provide extensive information about successive layers of each painting.

---

## Closing

Industry standards have been published on neutron radiographic testing.<sup>11-13,43-45</sup>

---

## Neutron Gaging and Neutron Probe Techniques

Neutron gaging is the measurement of attenuation of a collimated small diameter beam of radiation as it is transmitted by a specimen. A neutron radiology service center equipped with a nuclear reactor has demonstrated that the imaging techniques can be complemented by the more quantitative techniques of gaging.<sup>38,39</sup> The gaging technique can inspect items of greater thickness than can be inspected with neutron radiography. It has been used for static gaging of discrete assemblies and for continuous scanning of long objects for acceptable uniformity.

There are also a variety of neutron probe techniques in which radiation, typically gamma, is observed as a result of neutron radiation incident on the object. For example the associated particle sealed tube neutron generator enables the flight time of the incident neutron to be used in conjunction with gamma ray spectroscopy to indicate the chemical composition within an object. This technique has been developed for identification of hidden explosives, drugs or nuclear materials.<sup>40</sup>

Another example of a neutron probe is neutron interferometry to detect phase shifts of the neutron wave properties. This neutron phase topography has been proposed for very high sensitivity material testing.<sup>41</sup>

## Neutron Induced Autoradiography

By exposing a painting to thermal or cold neutrons and later imaging the radioactivity induced in the various paint components, a technique has been developed sensitive to many elements including manganese, potassium, copper, sodium, arsenic, phosphorus, gold, iron, mercury, antimony and cobalt. The neutron exposures were originally performed in a moderator block (thermal column), close to a reactor core. However, beams similar to those used for transmission neutron radiography have

## References

1. Barton, J.P. et al., eds. *Neutron Radiography: Proceedings of the First World Conference*. Dordrecht, Netherlands: D. Reidel Publishers (1982).
2. Barton, J.P. et al., eds. *Neutron Radiography: Proceedings of the Second World Conference*. Dordrecht, Netherlands: Kluwer Academic Publishers (1987).
3. Fujine, S. et al., eds. *Neutron Radiography: Proceedings of the Third World Conference*. Dordrecht, Netherlands: D. Reidel Publishers (1990).
4. Barton, J.P. et al., eds. *Neutron Radiography: Proceedings of the Fourth World Conference*. Yverdon, Switzerland: Gordon and Breach Science Publishers (1994).
5. Fischer C.O. et al., eds. *Neutron Radiography: Proceedings of the Fifth World Conference*. Berlin, Germany: Deutsche Gesellschaft für Zerstörungsfreie Prüfung (1997).
6. Fujine, S. et al., eds. *Neutron Radiography: Proceedings of the Sixth World Conference*. Yverdon, Switzerland: Gordon and Breach Science Publishers (2001).
7. Kobayashi, H. et al., eds. *Neutron Radiography System Design and Characterization: Proceedings of Second International Topical Meeting*. Reprinted in *Nuclear Instruments and Methods in Physics Research, Section A*. Amsterdam, Netherlands: Elsevier/North Holland (1996).
8. Lehmann, E. et al., eds. *Neutron Detectors, Imaging Techniques and Applications: Proceedings of the Third International Topical Meeting on Neutron Radiography*. Reprinted in *Nuclear Instruments and Methods in Physics Research, Section A*. Amsterdam, Netherlands: Elsevier/North Holland (1999).
9. Berger, H., ed. *Practical Applications of Neutron Radiography and Gaging*. West Conshohocken, PA: ASTM International (1975).
10. Domanus, J.C., ed. *Practical Neutron Radiography*. Dordrecht, Netherlands: Kluwer Academic Publishers (1992).
11. ASTM E 748, *Standard Practices for Thermal Neutron Radiography of Materials*. West Conshohocken, PA: ASTM International (1995).
12. ASTM E 545, *Standard Method for Determining Image Quality in Direct Thermal Neutron Radiographic Examination*. West Conshohocken, PA: ASTM International (1999).
13. ASTM E 803-91, *Standard Method for Determining the L/D Ratio of Neutron Radiography Beams*. West Conshohocken, PA: ASTM International (1996).
14. Hawkesworth, M.R. et al. "Basics of Thermal Neutron Radiography." *Neutron Radiography: Proceedings of the First World Conference*. Dordrecht, Netherlands: D. Reidel Publishers (1982): p 5-21.
15. Whittemore, W.L. "Neutron Sources and Facilities." *Neutron Radiography: Proceedings of the Sixth World Conference*. Yverdon, Switzerland: Gordon and Breach Science Publishers (2001): p 3-10.
16. Domanus, J.C., ed. *Collimators for Thermal Neutron Radiography*. Dordrecht, Netherlands: D. Reidel Publishers (1987).
17. Rant, J.J. "Imaging Techniques." *Neutron Radiography: Proceedings of the Sixth World Conference*. Yverdon, Switzerland: Gordon and Breach Science Publishers (2001): p 23-34.
18. Kobayashi, H. et al. "Basic Performance of a Neutron Sensitive Photo-Stimulated Luminescence Device for Neutron Radiography." *Neutron Detectors, Imaging Techniques and Applications: Proceedings of the Third International Topical Meeting on Neutron Radiography*. Reprinted in *Nuclear Instruments and Methods in Physics Research, Section A*. Amsterdam, Netherlands: Elsevier/North Holland (1999): p 1-8.
19. McClellan, G.C. et al. "Neutron Radiography Applications and Techniques at the Hot Cell Examination Facility." *Neutron Radiography: Proceedings of the First World Conference*. Dordrecht, Netherlands: D. Reidel Publishers (1982): p 437-443.
20. Markgraf, J.F.W. "The Practical Utilization of Nitrocellulose Film in Neutron Radiography." *Neutron Radiography: Proceedings of the Third World Conference*. Dordrecht, Netherlands: D. Reidel Publishers (1990): p 353-364.

21. Newacheck, R.L. "Applications and Trends of Industrial Neutron Radiography." *Neutron Radiography: Proceedings of the First World Conference*. Dordrecht, Netherlands: D. Reidel Publishers (1982): p 77-84.
22. Leighty, C.E. "Neutron Radiography at the General Electric Nuclear Test Reactor." *Neutron Radiography: Proceedings of the First World Conference*. Dordrecht, Netherlands: D. Reidel Publishers (1982): p 153-162.
23. Hamm, R.S. "Status of the Lansar Neutron Generators." *Neutron Radiography: Proceedings of the Fifth World Conference*. Berlin, Germany: Deutsche Gesellschaft für Zerstörungsfreie Prüfung (1997): p 540-567.
24. Cluzeau, S. "Thermal Neutron Source Using a Sealed Neutron Tube." *Neutron Radiography: Proceedings of the Fourth World Conference*. Yverdon, Switzerland: Gordon and Breach Science Publishers (1994): p 453-460.
25. Barton, J.P. et al. "Experience with Aircraft Inspected in MNRS Using Film and Electronic Imaging." *Neutron Radiography: Proceedings of the Fourth World Conference*. Yverdon, Switzerland: Gordon and Breach (1994): p 133-142.
26. Barton, J.P. et al. "Lessons from Pantex Cf-252 Wide Angle Beam Characterization." *Neutron Radiography: Proceedings of the Sixth World Conference*. Yverdon, Switzerland: Gordon and Breach Science Publishers (2001): p 124-136.
27. Lindsay, J.T. et al. "Fifteen Years of Neutron Radioscopy Applications in Transmission Lubrication Studies for the Automotive Industry." *Neutron Radiography: Proceedings of the Sixth World Conference*. Yverdon, Switzerland: Gordon and Breach Science Publishers (2001): p 67-76.
28. Takenaka, N. et al. "Application of Neutron Radiology to Thermal Hydraulic Phenomena." *Neutron Radiography: Proceedings of the Sixth World Conference*. Yverdon, Switzerland: Gordon and Breach Science Publishers (2001): p 503-506.
29. Polichar, R. et al. "A Quantitative Neutron Radioscopic Image Acquisition and Processing System for SNRS." *Neutron Radiography: Proceedings of the Fourth World Conference*. Yverdon, Switzerland: Gordon and Breach Science Publishers (1994): p 195-206.
30. Balasko, M. "Dynamic Neutron Radiography Instrumentation and Application in Central Europe." *Neutron Radiography System Design and Characterization: Proceedings of Second International Topical Meeting*. Reprinted in *Nuclear Instruments and Methods in Physics Research*, Section A. Amsterdam, Netherlands: Elsevier/North Holland (1996): p 140-143.
31. Mishima, K. "Multiphase Flow Measurements." *Neutron Radiography: Proceedings of the Sixth World Conference*. Yverdon, Switzerland: Gordon and Breach Science Publishers (2001): p 35-50.
32. Bayon, G. "Review on Use of Neutron Radiography at Saclay Nuclear Research Centre." *Neutron Radiography: Proceedings of the Fifth World Conference*. Berlin, Germany: Deutsche Gesellschaft für Zerstörungsfreie Prüfung (1997): p 25-31.
33. Whitemore, W.L. et al. "Physics of Neutron Radiography Using Selected Energy Neutrons." *Neutron Radiography: Proceedings of the First World Conference*. Dordrecht, Netherlands: D. Reidel Publishers (1982): p 23-33.
34. Klahn, R.T. et al. "Fast Neutron Radiography Research at ANL-W." *Neutron Radiography: Proceedings of the Fifth World Conference*. Berlin, Germany: Deutsche Gesellschaft für Zerstörungsfreie Prüfung (1997): p 382-390.
35. Schillenger, G. "Improved Neutron Radiography and 3D Tomography Due to Better Beam Geometry." *Neutron Radiography: Proceedings of the Sixth World Conference*. Yverdon, Switzerland: Gordon and Breach Science Publishers (2001): p 601-606.
36. McFarland, E. et al. "Quantitative Evaluation of a Neutron Radiography and Tomography System." *Neutron Radiography: Proceedings of the Fourth World Conference*. Yverdon, Switzerland: Gordon and Breach Science Publishers (1994): p 561-574.
37. Kobayashi, H. "Recent Development of Cooled CCD Camera for Neutron Radiography Imaging — Tomography." *Neutron Radiography: Proceedings of the Fourth World Conference*. Yverdon, Switzerland: Gordon and Breach Science Publishers (1994): p 553-560.
38. Reynolds, G.M. "Neutron Gaging Systems." *Practical Applications of Neutron Radiography and Gaging*. West Conshohocken, PA: ASTM International (1975): p 58-73.

39. Newacheck, R.L. et al. "Computerized Neutron Gaging Adds a New Dimension to Neutron Radiography." *Neutron Radiography: Proceedings of the Second World Conference*. Dordrecht, Netherlands: D. Reidel Publishers (1987): p 821-828.
40. Rhodes, E. et al. "Neutron Interrogation for Detection of Nuclear Materials, Explosives and Drugs." *Neutron Radiography: Proceedings of the Fourth World Conference*. Yverdon, Switzerland: Gordon and Breach Science Publishers (1994): p 827-836.
41. Rauch, H. "Neutron Phase Topography for High Sensitive Material Testing." *Neutron Radiography: Proceedings of the Fifth World Conference*. Berlin, Germany: Deutsche Gesellschaft für Zerstörungsfreie Prüfung (1997): p 61-68.
42. Fischer, C.O. et al. "Autoradiography of Large Scale Paintings." *Neutron Radiography: Proceedings of the Sixth World Conference*. Yverdon, Switzerland: Gordon and Breach Science Publishers (2001): p 563-571.
43. E 2023-99, *Standard Practice for Fabrication of Neutron Radiographic Sensitivity Indicators*. West Conshohocken, PA: ASTM International (1999).
44. E 1496-97, *Standard Test Method for Neutron Radiographic Dimensional Measurements*. West Conshohocken, PA: ASTM International (1997).
45. E 2003-98e1, *Standard Practice for Fabrication of the Neutron Radiographic Beam Purity Indicators*. West Conshohocken, PA: ASTM International (1998).



# 17

## C H A P T E R

# Radiographic Testing of Metal Castings<sup>1</sup>

---

George R. Strabel, Howmet Research Corporation,  
Whitehall, Michigan



# PART 1. Introduction to Radiographic Testing of Metal Castings

Casting is a metals fabrication method chosen primarily because it produces complex shapes with a minimum of finished weight. In addition, casting permits the manufacture of a desired product with fewer components, thus minimizing the amount of joining (by fasteners or welds). Possible casting problems are often associated with the mold, the molten metal or patterns in the cast object; these must be properly considered to avoid difficulties and to ensure required quality levels. These problems can be addressed by radiographic testing.

## Casting Discontinuities

Pouring of castings is simplified when the melt fluidity is high. This is achieved by superheating the material above its melting range to a point where associated gas absorption is kept to a reasonable minimum; this is especially important for molten practices with ordinary air. Failure to superheat creates the possibility of gas pocket formation in some portions of the casting. Gas pockets tend to occur in the heavier cast sections while gas porosity occurs under an initial layer of solidified metal near the mold or core walls. Large pockets of gas are obviously detrimental to the strength of the casting unless it is designed to allow pocket formation only in portions discarded during finishing.

Subsurface gas may be unacceptable because finish machining may produce surface openings that act as locations of stress concentration. Subsurface porosity occurs because the gas takes some time to move toward the mold and core walls and, in that time, heat loss causes metal skins to form, preventing the gas from escaping. The extent of subsurface porosity varies with mold type. Sand molds, depending on their degree of dryness, have a greater tendency to produce solid metal skins near mold walls, when compared to shell and plastic (precision casting) molds. Possible sources of such discontinuities should be eliminated during the casting process.

## Reasons for Radiographic Testing

The major goal of radiographic testing of castings is to help control the production process and product quality. The latter is especially true when the number of castings is high and the production of pilot castings is possible and practical.

Film radiography has been one of the most effective nondestructive testing techniques for quality control of castings. Film radiography uses penetrating ionizing radiation and provides permanent reference data. The image, in principle, is a record of variation in the total thickness of radiation absorbing material displayed in a single plane; or a planar projection of conditions prevailing in the three-dimensional space of the item tested.

Other common nondestructive testing methods are affected by the metallographic structure and degree of working to which the metal has been subjected; generally these considerations have no effect on the radiation transmission or subsequent legibility of the radiographic indications. The only exceptions are grain and the condition called *mottling*, as described in some detail below. Hence radiography is the most effective nondestructive testing method for castings, which generally are studied for presence of volumetric defect types. As is true of any important engineering fabrication where stress concentrations may cause trouble, surface methods such as magnetic particle or liquid penetrant testing should supplement radiography because discontinuities such as surface cracks are difficult to detect radiographically.

To be effective, the radiographic method requires proper interpretation of resulting images. Interpretation, in turn, demands a familiarity with the types of discontinuities generated. Important things to consider include the method of casting; mold and core materials and design; melting and pouring temperatures; cooling rates and time; and possible interaction of the particular metallographic structure with the test radiation.

## PART 2. General Radiographic Techniques for Metal Castings

### Radiation Sources Used

Gamma ray sources, especially as used in casting radiography, have the following advantages over X-rays: (1) simple apparatus; (2) compactness; (3) independence from external power; (4) ability to provide simultaneous testing of many objects and complete circumferences of large cylindrical objects; (5) practicality when access to the interior of the object is difficult; and (6) usability when testing must occur in confined spaces. Radium, a naturally occurring gamma ray source, came into use in the late 1930s; it has since been replaced by artificial isotopes (see Table 1).

X-rays, however, are essential for some applications. Low (kilovolt) X-ray energies are needed for obtaining required radiographic sensitivities in light metals (such as aluminum) and in thin material thicknesses of steel. High energy (megavolt) X-rays are necessary for penetration of steel thicknesses in excess of 200 mm (8.0 in.). As with all nondestructive testing, casting inspection is best done with the method that produces the desired results for the specific application.

Gamma ray sources, unlike X-ray machines, emit penetrating radiation having only one or a few discrete wavelengths. Sources are commonly specified by the energy of the individual quantum (using units of *electronvolts*) rather than by wavelength. Thus a gamma ray with an energy of 1.25 MeV is

equivalent in wavelength and penetrating power to the most penetrating radiation emitted by an X-ray tube operating at 1.2 MeV. The total penetrating power of the gamma radiation source is about equal to that of a 3 MeV X-ray machine that emits a spectrum or wide range of energies.

The wavelengths (or energies) emitted by a gamma ray source depend only on the nature of the emitter and are not variable at the will of the operator, as X-rays are.

Important gamma source characteristics include: (1) the curie value and specific activity, (2) half life, (3) energy of quanta, (4) dosage rate and (5) application thickness limit. The intensity of gamma radiation depends on the number of radioactive atoms that disintegrate per second in the source. For small or moderate sources, this intensity is proportional to the source activity in becquerel (1 disintegration per second) or curie ( $3.7 \times 10^{10}$  disintegrations per second). The proportionality fails for large sources or for those emitting low energy gamma rays because of self-absorption.

The *specific activity*, expressed in becquerel (or curie) per gram, is important because it influences geometrical unsharpness of the images. Higher specific activity allows shorter source-to-sensor distances without a loss of image sharpness.

*Gamma ray dosage* is expressed in microsievert per gigabecquerel hour at one meter ( $\mu\text{Sv} \cdot \text{GBq}^{-1} \cdot \text{h}^{-1}$  at 1 m), or roentgen per curie hour at one meter

TABLE 1. Gamma ray sources used in industrial radiography.

Radioactive Element	Energy (MeV)	Half Life	Dosage Rate		Metallurgical Application and Thickness of Steel or Equivalent	
			mSv·GBq <sup>-1</sup> ·h <sup>-1</sup> at 1 m	(R·Ci <sup>-1</sup> ·h <sup>-1</sup> at 1 m)	mm	(in.)
Cesium-137	0.66 <sup>a</sup>	33 yr	0.1053	(0.39)	12 to 88	(0.5 to 3.5)
Cobalt-60	1.17 and 1.33	5.3 yr	0.3645	(1.35)	25 to 200	(1.0 to 8.0)
Iridium-192	0.137 to 0.651 <sup>b</sup>	75 dy	0.1485	(0.55)	12 to 75	(0.5 to 3.0)
Thulium-170	0.048 and 0.054 <sup>c</sup>	127 dy	0.0081	(0.003)	0.75 to 13	(0.03 to 0.5)

a. Usual form used is cesium chloride, soluble powder calling for special precautions to prevent leakage, such as double encapsulation in welded stainless steel.

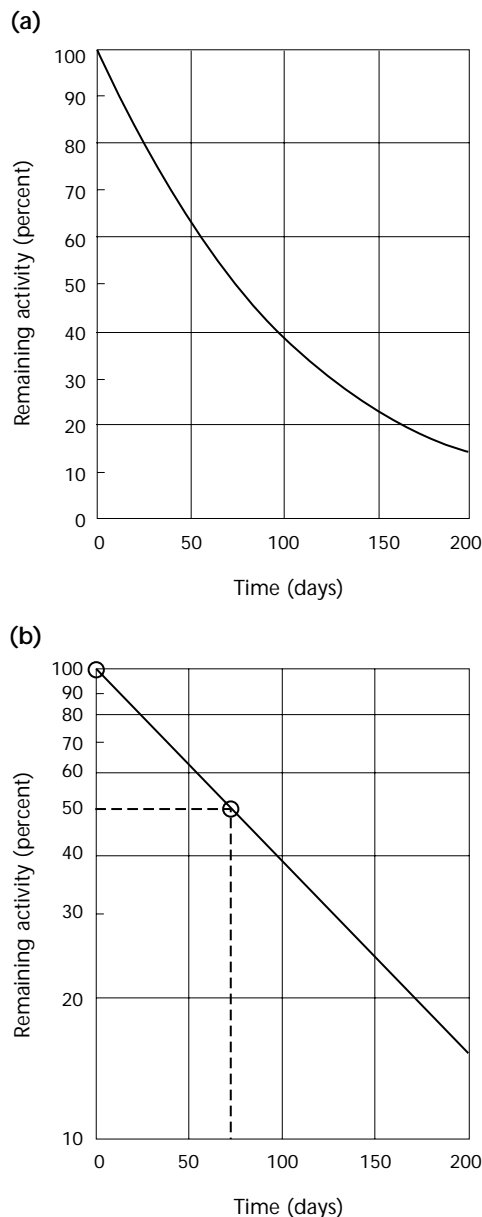
b. Has at least 12 gamma rays, principal ones at 0.310, 0.470 and 0.600 keV.

c. Produced in limited intensities for desired energies, so use is not widespread. Has excellent portability and may be used at two percent sensitivity down to 13 mm (0.5 in.) aluminum and for light nonmetals.

( $\text{R}\cdot\text{Ci}\cdot\text{h}^{-1}$  at 1 m). Gamma ray sources lose activity with time, the rate depending on the material *half life* shown in Table 1. Knowing the half life of the isotope allows preparation of *decay curves* as illustrated for iridium-192 in Fig. 1. This graph of activity versus time permits revised calculation of exposure time as the activity of the gamma ray source diminishes.

X-rays are made by using electrical energy to produce electrons accelerated to very high velocities. X-rays are emitted by deceleration of the electrons when they strike a target, which for industrial radiography is usually made of tungsten.

FIGURE 1. Decay curves for iridium-192: (a) linear plot; (b) logarithmic plot.



The higher the voltage of the applied energy, the greater the speed of the electrons striking the focal spot. The result is a decrease in wavelength of the X-rays emitted, with a simultaneous increase in penetrating power and intensity. Thus, unlike gamma ray sources, X-ray machine radiations may be varied at the will of the operator within the range of the equipment used.

The various X-ray machines commercially available may be very roughly classified according to their maximum voltage. Table 2 is a generalized guide for typical X-ray machines by voltage ranges and applications.<sup>2</sup> The table must be used with the understanding that particular machines differ in their specifications from model to model.

Although most commonly used X-ray machines are less mobile than radioisotopes and depend on electric current, they are available in portable designs. In addition, those with rod anode tubes (in which the target is perpendicular to the electron stream) can be used to produce radiographs with circumferential coverage of appropriate items. The major advantages of X-rays are their ability to generate higher intensities of penetrating radiation and their variability in radiation intensity (quantity) and energy (quality) as determined by the operator and the application.

TABLE 2. Representative energies of X-ray machines and their applicable thickness limits.

Maximum Voltage (kV)	Screens	Approximate Thickness Limits <sup>a</sup>
50	none	thin sections of most metals <sup>b</sup>
	none or lead foil	125 mm (5.0 in.) aluminum <sup>c</sup>
150	none or lead foil	25 mm (1.0 in.) steel <sup>c</sup>
	fluorescent	38 mm (1.5 in.) steel <sup>c</sup>
250	lead foil	50 mm (2.0 in.) steel <sup>c</sup>
	fluorescent	75 mm (3.0 in.) steel <sup>c</sup>
400	lead foil	75 mm (3.0 in.) steel <sup>c</sup>
	fluorescent	100 mm (4.0 in.) steel <sup>c</sup>
1000	lead foil	125 mm (5.0 in.) steel <sup>c</sup>
	fluorescent	200 mm (8.0 in.) steel <sup>c</sup>
2000	lead foil	200 mm (8.0 in.) steel <sup>c</sup>
8000 to 25000	lead foil	400 mm (16.0 in.) steel <sup>c</sup>

a. Also used for important nonmetallics such as moderate thicknesses of graphite and small electronic components, wood and plastics.

b. Lower limit depends on particular machine and how secondary voltage may be adjusted.

c. Or equivalent.

## Specification Requirements

Radiographic testing of castings provides information about the quality of the product within the limits of the test method. Hence, the contract between producer and consumer should, for their mutual benefit, refer to time proven specifications. Among the most widely used specifications are those of ASTM International with emphasis on technique and interpretation of radiographic indications<sup>3</sup> and those of the American Society of Mechanical Engineers (ASME) with emphasis on product quality and in-process weld repairs.<sup>4</sup>

During the preparation of radiographic test requirements, it is essential to recognize that radiographic coverage has its limitations, especially when inspecting castings with complex geometries or part configurations. Geometry or part configurations that do not allow complete coverage with normal radiographic techniques should be acknowledged by supplier and user before the start of work. Supplementary nondestructive testing methods should be clearly agreed on from the outset.

It should be noted that the radiographic method is particularly effective for discontinuities that displace a volume of cast material. Cracks and planar discontinuities that do not displace an appreciable volume of material may not be detected by radiography unless the radiation is favorably oriented. Additional nondestructive test methods and criteria for acceptability must be agreed on by supplier and user.

## Radiographic Setup

Radiographic coverage is determined by the casting geometry, especially those portions to which gates and risers are connected during casting; cylindrical portions; flanges; bosses; and portions inaccessible to radiation and to film or sensing apparatus. The inaccessible portions always call for special considerations in nondestructive testing contract dealings. All radiographic testing (especially of portions critical to use or loading) requires the making of *radiographic shooting sketches* (RSS) and the compilation of associated data. Recommended radiographic shooting sketch types (for example, Fig. 2) are covered by ASTM International.<sup>1,3,5</sup>

Shooting sketches may take into consideration such aspects as simultaneous coverage of cylindrical portions, completely or by sectors; and single or double wall shots when inside diameters are relatively small, 100 mm

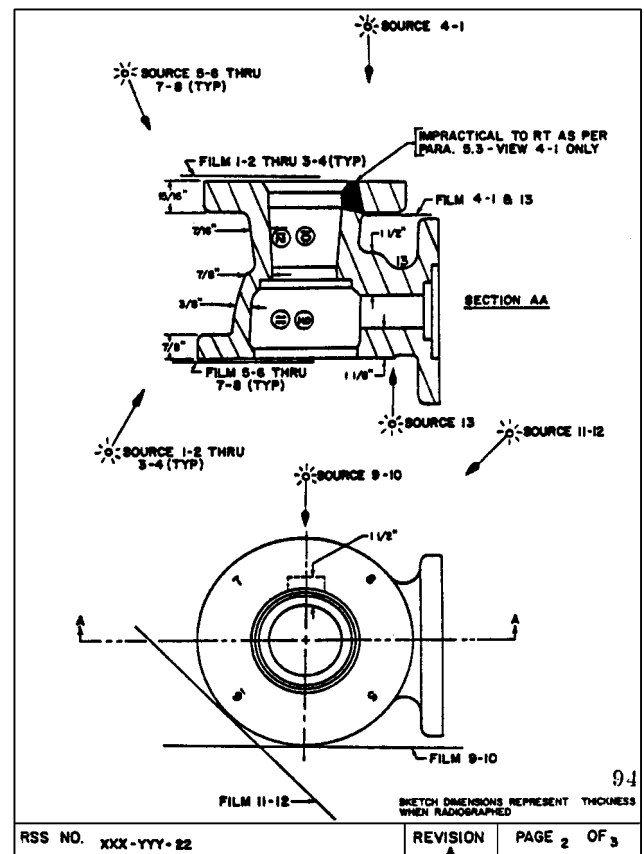
(4 in.) or less). With isotope radiography, it is often convenient to examine a number of castings simultaneously. In all cases, special consideration must be given to proper identification of the images. This is usually done using lead letters attached to the object under test. Because sources are never actually ideal point sources, the source-to-sensor distance should be such that it limits geometric unsharpness  $U_g$  with reasonably economical exposure times. This unsharpness is given by:

$$(1) \quad U_g = \frac{F \cdot t}{D}$$

where  $D$  is the source-to-object distance,  $F$  is the effective focal spot size and  $t$  is the object-to-sensor distance.

The equipment parameters for digital acquisition, processing and display of test results must be applicable to the inspection goals. [This technology is discussed elsewhere.](#)

FIGURE 2. Sample of radiographic shooting sketch (RSS), showing film placement and Identification.<sup>1,3,5</sup>



## Penetrameters

### Plaque Penetrameters<sup>5</sup>

A relatively simple way to determine whether the radiographic testing procedure has met the required quality level (even without detailed consideration of the many factors involved) is by the proper choice and use of penetrameters. The penetrameter (also referred to as the *image quality indicator*, or *IQI*) is simply a metal plaque with holes. Its material is chosen to have radiation absorption characteristics close to those of the material under test. Its thickness and hole sizes are predetermined percentages of the section thickness to be radiographed. The plaque, as most commonly used in casting radiography, is 2 percent of the section thickness and its three holes have diameters of 1, 2 and 4 percent of the plaque thickness. Where casting thickness and/or exposures vary appreciably, more than one penetrameter must be used to indicate image sensitivity.

Penetrameters are usually placed on the portion radiographed. If this is not possible, because of curvature of the part or possible interference with radiographic legibility, the penetrameters are placed as close as possible to the portion radiographed, on blocks of the same material and a similar thickness and as close to the casting as possible. In addition, penetrameters are usually placed

on the source side of the casting. When they are placed on the sensor side, it should be indicated on the radiograph with a lead marker and the comparability of penetrameter size to the one required for the source side must be suitably demonstrated.

### Wire Penetrameters<sup>6</sup>

Wire penetrameters, originally introduced in Germany and known as Deutsche Institut für Normung (DIN) types, have been used in the United States as an alternative means of radiographic quality control. Such a device is illustrated in Fig. 3. When a wire penetrameter is used, the size must be equivalent to the customarily specified plaque type. Table 3 shows equivalence data that compare wire penetrameters to plaque types for the 2-2T level. This designation signifies that radiographs must show, as a minimum, a plaque thickness within two percent (that is, the first 2 in 2-2T) and a hole diameter within twice the plaque thickness, or 2T.

## Discontinuity Detection and Radiographic Sensitivity

For optimum radiographic sensitivity the image must meet contrast requirements. Film density requirements and image

FIGURE 3. Wire penetrameter, shown in positive image radiograph of 19 mm (0.75 in.) thick casting.



TABLE 3. Wire penetrameter sizes equivalent to 2-2T hole levels.<sup>6</sup>

Minimum Specimen Thickness		Wire Diameter	
mm	(in.)	mm	(in.)
6.35	(0.250)	0.08 <sup>a</sup>	(0.0032) <sup>a</sup>
7.95	(0.313)	0.10 <sup>a</sup>	(0.0040) <sup>a</sup>
9.50	(0.375)	0.13 <sup>a</sup>	(0.0050) <sup>a</sup>
12.7	(0.500)	0.16	(0.0063)
15.9	(0.625)	0.20	(0.008)
19.1	(0.750)	0.25	(0.010)
22.2	(0.875)	0.33	(0.013)
25.4	(1.00)	0.40	(0.016)
31.8	(1.25)	0.51	(0.020)
38.1	(1.50)	0.64	(0.025)
44.4	(1.75)	0.81	(0.032)
50.8	(2.00)	1.02	(0.040)
63.5	(2.50)	1.27	(0.050)
76.2	(3.00)	1.60	(0.063)
88.9	(3.50)	2.03	(0.080)
102.0	(4.00)	2.50	(0.100)
114.0	(4.50)	3.20	(0.126)
127.0	(5.00)	4.06	(0.160)

a. Wire diameters for use with specimens less than 12.7 mm (0.5 in.) in thickness do not represent true 2-2T level. They follow the same relationship as hole type.



signal levels are used to quantify this parameter. It must be remembered that a penetrometer is used to indicate the quality level of the radiographic technique and not necessarily to provide a measurement of the size of minimum discontinuity that can be shown in the object. Thus, if required penetrometer details are visible in the radiograph, there is no certainty that an equivalent flaw in the casting will be revealed. This is because the penetrometer holes have sharp boundaries while natural casting holes of the same size may have boundaries that are more or less rounded, with sides gradually merging into surrounding casting portions. Hence, the hole of the penetrometer may be readily discerned, even though its density differs only slightly from that of the surrounding casting area.

Similar considerations apply to linear or crack like indications. If the plane of the linear discontinuity is inclined away from the beam (by at least 7 degrees), the crack may not be visible on the radiograph because of the relatively gradual transition of densities in the image. Similarly, the visibility of a wire penetrometer does not guarantee that a casting discontinuity of the same cross section will actually be visible. The human eye discerns a long boundary more readily than it does a short one, even if the density increase and image sharpness are the same. Nevertheless, it is true that the probability of flaw detection in the object radiographed (to ensure the required quality) is related to the discernibility of penetrometer features, when all other factors are the same.<sup>6-9</sup>

## Considerations Specific to Castings

### Mold Type

As castings progress from sand mold castings to shell mold, permanent mold, investment, precision, plastic mold and die castings, the radiographic procedure must be changed to accommodate more castings with more complex shapes and thinner sections. All these factors provide justification for using one or more pilot runs designed to improve yields and minimize or eliminate systematic flaws.

Mold type also determines the amount and frequency of radiographic testing. For sand castings, sections are relatively thicker with rougher skins; there is more allowance for machining, especially for surfaces joined to other system components. Difficulties in radiographic interpretation are increased by surface roughness and by sections with

dimensions substantially thicker than when finished.

Exposures must be made in such a way that penetrometer sensitivity, as dictated by finished section thicknesses, is not compromised. This is usually done by using penetrameters based on finished rather than rough wall thicknesses. As foundry techniques improve, precision and die cast sections become thinner and smoother; the interpretation of radiographs is improved and radiation energies must be reduced. Of course, in the more precise casting techniques, cost of all production steps must be watched. Systematic flaws must be determined using pilot runs of sufficient number to ensure the required quality levels. It should be noted that smoother surfaces also tend to considerably reduce random flaws.

Individual sand castings generally require more radiography because the possibility of nonsystematic (random) flaws is larger than for the more precise casting techniques. Important sand castings, however, require individual radiography, especially of critical portions, to locate both systematic and random flaws. It may be pointed out that systematic flaws are generally associated with the casting details (gates, risers, junctions of heavy to thin portions and other locations). Random flaws may be due to accidental conditions (local gas due to mold moisture; local stresses causing incidence of linear flaws and other anomalies).

### Alloy Castings

When testing alloys, the major factor affecting the radiography is alloy density, which determines the energy levels needed in the radiation sources. It is well known that alloys are prone to reaction with the atmosphere or mold material. The general solidification peculiarities of alloys may affect the indication types that are discernible in their radiographs. Industrial casting alloys fall into the following major types according to atomic number: (1) light metals (including magnesium, aluminum and tin); (2) intermediate alloy types (including zinc, cast iron, steels, brasses and bronzes); and (3) heavy metals (including lead and tantalum). The densities of some of the most common alloys are shown in Table 4.

Of the heavy alloys, tantalum may be used as an example for a typical castings application. Tantalum castings are used in acid resistant chemical equipment such as heat exchangers, centrifugal pumps and valves. Tantalum has a combination of characteristics not found in many refractory metals. These characteristics



include ease of fabrication, low ductile-to-brittle transition temperature and high melting point.

Tantalum oxidizes in air above 299 °C (570 °F). Because of its high density, it requires longer exposures or a different choice of radiation energy than needed for less dense materials. Thus a section 7.5 mm (0.30 in.) thick requires an exposure of about half an hour with a medium size cesium-137 source when fast industrial films or sensitive sensors are used with intensifying screens.

## Superalloys

Superalloys have requirements unique to their physical characteristics. Test personnel must consult applicable standards and specifications when conducting radiographic tests of these materials.

## Radiographic Standards

Standards for radiographic testing of castings have been written (with the help of producers, consumers, government and educational institutions) for radiographic practices and image quality control.<sup>3-27</sup> Following the standards ensures the production of reference radiographic images that can be meaningfully read by representatives of both producer and consumer interests.

Of course, the reading leads to an interpretation of the casting's soundness

and interpretation requires some sort of standardized guideline. ASTM International's work on reference radiograph documents (beginning in 1950 and continuing to the present) has led to the development of standards that encourage relatively unbiased determination of casting quality for use in meeting contractually required acceptance criteria.<sup>14</sup> Reference radiograph documents published by ASTM International include information on fabrication material of the hardware used; section thickness ranges; discontinuity types represented; and numbers of discontinuities shown in graded types.<sup>15-27</sup>

Reference radiographs for steel castings were first issued by the United States Navy Bureau of Engineering in 1938 as *Gamma Ray Radiographic Standards for Steam Pressure Service*.<sup>15</sup> These were reissued in 1942 by the Bureau of Ships as *Reference Radiographic Standards for Steel Castings* and adopted in 1952 by ASTM International.<sup>16</sup>

ASTM International has also developed improved techniques for mass production and monitoring of document illustrations, either in the form of actual radiographs or photographic copies of originally selected radiographs. Its recent work involves reference radiographs for titanium alloys.

Documents for ductile and gray iron castings<sup>13,25</sup> have been produced. Another document discusses how images change as certain radiographic parameters vary.<sup>8</sup>

TABLE 4. Common alloy casting densities versus radiographic sources used and American Society for Testing and Materials (ASTM) reference radiograph documents.

Element or Alloy	Density Range (g·cm <sup>-3</sup> )	Radiographic Sources Commonly Used	Available ASTM Reference Radiographs
Magnesium	1.79 to 1.86	X-rays <sup>a</sup>	E 155 <sup>17</sup> and E 505 <sup>24</sup>
Aluminum	2.57 to 2.95	X-rays <sup>a</sup>	E 155 <sup>17</sup> and E 505 <sup>24</sup>
Titanium	4.43 to 4.65	X-rays and iridium-192	see note <sup>b</sup>
Cast iron	5.54 to 7.48	X-rays, iridium-192, cobalt-60	E 802 <sup>25</sup> plus applicable steel documents
Zinc	6.60 to 6.70	X-rays, iridium-192, cobalt-60	none <sup>c</sup>
Carbon steels	7.81 to 7.84	X-rays, iridium-192, cobalt-60	E 192, <sup>19</sup> E 446, <sup>16</sup> E 186 <sup>18</sup> and E 280 <sup>21</sup>
Stainless steels	7.53 to 7.75	X-rays, iridium-192, cobalt-60	E 192, <sup>19</sup> E 446, <sup>16</sup> E 186 <sup>18</sup> and E 280 <sup>21</sup>
Aluminum bronze	7.50 to 7.80	X-rays, iridium-192, cobalt-60	E 272 <sup>20</sup>
Manganese bronze	7.70 to 8.30	X-rays, iridium-192, cobalt-60	E 272 <sup>20</sup>
Silicon bronze	8.30	X-rays, iridium-192, cobalt-60	E 272 <sup>20</sup>
Tin bronze	8.70 to 8.80	X-rays, iridium-192, cobalt-60	E 310 <sup>22</sup>
Navy bronze	8.70	X-rays, iridium-192, cobalt-60	E 272 <sup>20</sup>
Nickel silver	8.85 to 8.95	X-rays, iridium-192, cobalt-60	E 272 <sup>20</sup>
Tantalum	16.60	cesium-137	none

a. Up to about 300 kV peak.

b. Depending on thickness involved, use applicable documents for aluminum or steel including source type.

c. Use available documents closest in density.

## PART 3. Radiographic Indications for Metal Castings

The major objective of radiographic testing of castings is the disclosure of discontinuities (with emphasis on volumetric types) that adversely affect the strength of the product. These discontinuities, of course, are related to casting process deficiencies which, if properly understood, can lead to accurate accept/reject decisions as well as to suitable corrective measures. Following is a brief description of the most common discontinuity types included in existing reference radiograph documents (in graded types or as single illustrations). The discontinuities in Figs. 4 to 10 are offered for illustrative purposes only and may exhibit appearances different from those of other cast materials.

[More information on discontinuity types may be found in this volume's chapter on radiographic interpretation.](#)

### Radiographic Indications from Casting Process

*Gas porosity* is a form of more or less spherical voids within the cast metal. These voids are usually due to occluded gas in the melt, gas that had no chance to rise and escape through the casting top or its risers. Gas porosity often comes from the atmosphere or from interactions between mold and metal. Overheating of melt and excessive moisture in molds and/or cores tends to promote this flaw type (Figs. 4 and 5).

*Sand inclusions* and *dross* are nonmetallic oxides, appearing on the radiograph as irregular, dark blotches. These come from disintegrated portions of mold or core walls and/or from oxides (formed in the melt) that have not been skimmed off before metal is introduced into the mold gates. Careful control of the melt, proper holding time in the ladle and skimming of the melt during pouring will minimize or obviate this source of trouble.

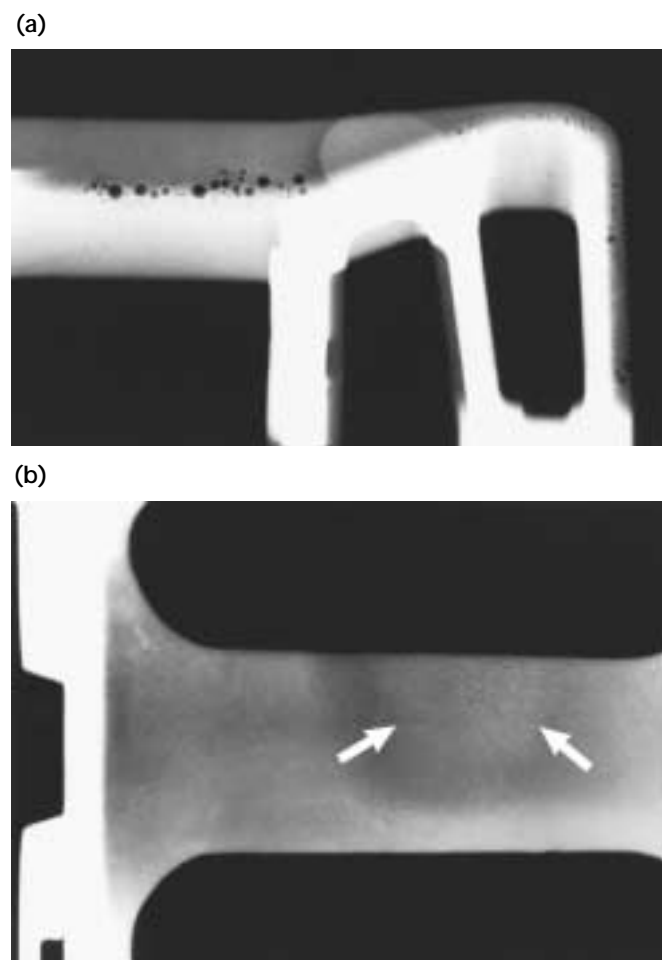
*Shrinkage* is a form of discontinuity that appears as dark regions on the radiograph. Individual shrinks assume various forms but in all cases shrinkage occurs because molten metal shrinks as it solidifies in all portions of the final casting. Shrinkage is avoided by making sure that the volume of the casting is

adequately fed by risers that sacrificially retain the shrinkage.

Shrinkage can be recognized in a number of characteristic but varying appearances on radiographs. There are at least five types: (1) cavity, (2) dendritic, (3) filamentary, (4) sponge types and (5) microshrinkage. Some documents designate these types by numbers, without actual names, to avoid possible misunderstanding.

*Cavity shrinkage* appears as areas with distinct jagged boundaries. It may be produced when metal solidifies between two original streams of melt, coming from opposite directions to join a common

FIGURE 4. Radiographs of 6.4 mm (0.25 in.) aluminum casting: (a) gas voids; (b) elongated gas porosity.



front; cavity shrinkage usually occurs at a time when the melt has almost reached solidification temperature and there is no source of supplementary liquid to feed possible cavities.

*Dendritic shrinkage* is a treelike distribution of very fine lines or small elongated cavities that may vary in density and are usually unconnected.

*Filamentary shrinkage* usually occurs as a continuous structure of connected lines or branches of variable length, width and density or occasionally as a network.

*Sponge shrinkage* shows itself as areas of lacy texture with diffuse outlines, generally toward the mid thickness of heavier casting sections. Sponge shrinkage may be dendritic or filamentary shrinkage; filamentary sponge shrinkage appears more blurred because it is projected through the relatively thick coating between the discontinuities and the sensor surface (Fig. 6).

Groups of tiny shrinks are referred to as *microshrinkage* (Fig. 7).<sup>28</sup>

FIGURE 5. Gas discontinuities in 6.4 mm (0.25 in.) thick castings: (a) gas voids in steel; (b) round gas porosity in aluminum.<sup>28</sup>

(a)



(b)

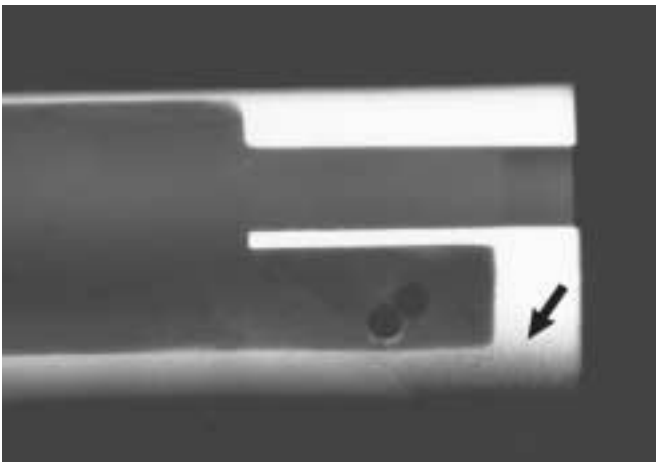
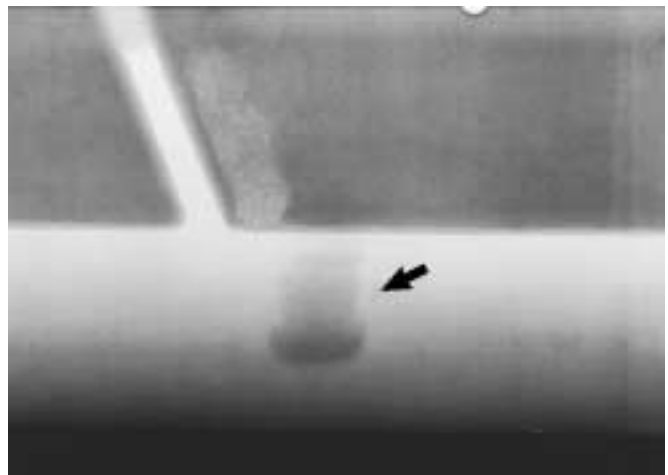


FIGURE 6. Sponge shrinkage in 13 mm (0.5 in.) aluminum casting.



FIGURE 7. Microshrinkage in 6.3 mm (0.25 in.) thick magnesium base alloy castings: (a) sponge microshrink; (b) feathery microshrink.<sup>28</sup>

(a)



(b)



*Cracks* are thin (straight or jagged) linearly disposed discontinuities that occur after the melt has solidified. They generally appear singly and originate at casting surfaces.

*Cold shuts* generally appear on or near a surface of cast metal as a result of two streams of liquid meeting and failing to unite (Fig. 8).

*Inclusions* are other materials in a supposedly uniform metallic matrix. They may be less or more dense than the matrix alloy and will appear on the radiograph, respectively, as darker or lighter indications. The latter type is more common in light metal castings (Figs. 9 and 10).

Chills, chaplets and other inserts used to support cores or cool casting metal appear as discontinuities when they are not united with the poured metal. They appear as broken lines or concentric circles in the image.

*Core shift* shows itself as a variation in section thickness, usually on radiographic views representing diametrically opposite portions of cylindrical casting portions.

*Hot tears* are linearly disposed indications that represent fractures formed in a metal during solidification because of hindered contraction. The latter may occur because of overly hard (completely unyielding) mold or core walls. The effect of hot tears, as a stress concentration, is similar to that of an ordinary crack; hot tears are usually systematic flaws. If flaws are identified as hot tears in larger runs of a casting type, they may call for explicit improvements in technique.

*Misruns* occur as a result of molten metal's failure to fill a mold cavity:

misruns appear on the radiograph as prominent dense areas of variable dimensions with a definite smooth outline. They are mostly random in occurrence and not readily eliminated by specific remedial actions in the process.

*Mottling* is a radiographic indication that appears as an indistinct area of more or less dense images. The condition is a diffraction effect that occurs on relatively vague, thin section radiographs, most often with austenitic stainless steel. Mottling is caused by interaction of the

FIGURE 9. Inclusion less dense than surrounding material in 3.2 mm (0.125 in.) aluminum casting.

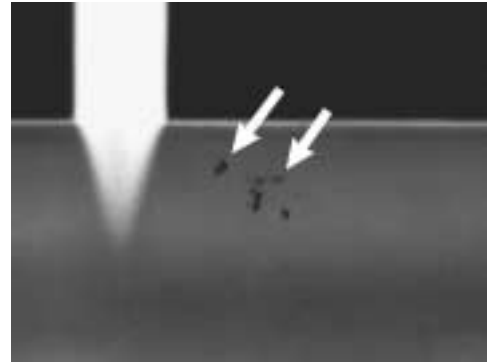


FIGURE 10. Inclusion more dense than surrounding material in 6.4 mm (0.25 in.) aluminum casting.

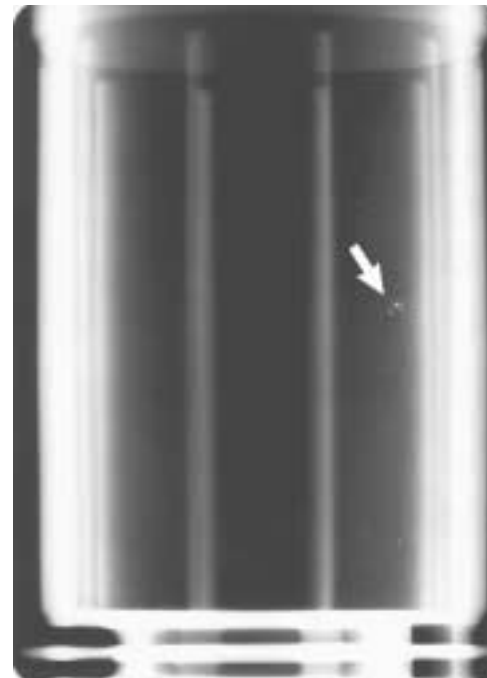
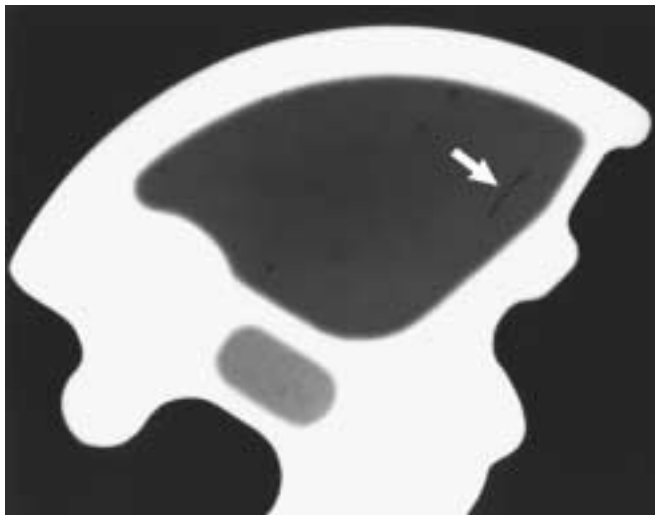


FIGURE 8. Cold shut in 3.2 mm (0.125 in.) aluminum casting.



object's grain boundary material with low energy X-rays (300 kV or lower). Inexperienced interpreters may incorrectly consider mottling as indications of unacceptable casting flaws. Even experienced interpreters often have to check the condition by reradiography from slightly different source-to-sensor angles. Shifts in mottling are then very pronounced, while true casting discontinuities change only slightly in appearance.

---

## Radiographic Indications in Casting Repair Welds

Most common alloy castings require welding either in their upgrading from anomalous conditions or in joining them to other system parts. It is mainly for reasons of casting repair that these descriptions of the more common weld discontinuities are given. The terms appear as indication types in ASTM E 390.<sup>23</sup> [For additional information, see the chapter on welds in this volume.](#)

*Slag* is nonmetallic solid material entrapped in weld metal or between weld material and base metal.

*Porosity* shows gas pockets or voids in the weld metal.

*Undercut* is a groove melted in the base metal at the edge of a weld and left unfilled by weld metal. It represents a stress concentration that often must be corrected.

*Incomplete penetration*, as the name implies, is a lack of weld penetration through the thickness of the joint (or penetration less than specified).

*Incomplete fusion* is lack of complete fusion of some portions of the metal in a weld joint with adjacent metal; either base or previously deposited weld metal.

*Arc strike* is an indication from a localized heat affected zone or a change in surface contour of a finished weld or adjacent base metal. Arc strikes are caused by the heat generated when electrical energy passes between surfaces of the finished weld or base metal and the current source.

*Weld spatter* occurs in arc or gas welding as metal particles that are expelled during welding and do not form part of the actual weld.

*Tungsten inclusion* is usually more dense than base metal particles.

*Oxidation* is the condition of a surface that is heated during welding, resulting in oxide formation on the surface, because of partial or complete lack of purge of the weld atmosphere.

## PART 4. Radiographic Testing and Process Scheduling

It is important to determine when radiographic testing should be done, with respect to required heat treatment, necessary repair welding and rough or finish machining. The timing of such tests is usually determined by mutual agreement between producer and user, with due consideration to the costs.

If a casting could possibly be rejected, further steps in its manufacture and testing should be minimized or eliminated. In addition, it is also known that heat treatment, especially drastic temperature changes, may cause aggravation of some discontinuity types.

On the other hand, the closer the casting surfaces are to their finished condition, the easier it is to read radiographic images and disclose linear surface flaws; these tend to act as stress concentrations and could be the most damaging discontinuities in service. All other things being equal, however, radiographic testing is performed as early

in the process as possible, to permit necessary weld repairs. Consequently, radiographic interpreters must have the actual casting available for their inspection to make allowance for surface irregularities.

In addition, experience has shown that castings should be examined in their final form with surface nondestructive testing methods, usually magnetic particle or liquid penetrant testing. The coverage and test frequency (if many castings of a single type are involved) is subject to mutual agreement between producer and user, with a logical statistical basis for the number and exact locations to be tested.

### Factors Influencing Choice of Acceptance Criteria

The advent of reference radiographs has done much to improve the measurement of casting quality, especially as applied to

TABLE 5. Statistical correlation data between tensile properties and severity of representative types of radiographic indications in 75 mm (3.0 in.) thick steel and manganese-nickel-aluminum bronze plate castings.<sup>14</sup>

Discontinuity	Tensile		Yield		Percent Elongation <sup>b</sup>	
	Slope	Tolerance <sup>c</sup>	Slope	Tolerance <sup>c</sup>	Slope	Tolerance <sup>c</sup>
<b>Class B Steel (MIL-S-15083)</b>						
Gas porosity	-3.28	±5.2	-0.43	— <sup>d</sup>	-3.65	+5.0
Inclusions	-0.03	— <sup>d</sup>	-0.03	— <sup>d</sup>	-1.36	— <sup>d</sup>
Linear shrinks	-8.11	±6.2	1.76	±2.3	-3.38	±4.8
Dendritic shrinkage	-8.11	±9.2	-0.69	±3.0	-1.22	±3.8
Worm hole shrinkage	-7.60	±5.4	-1.43	±2.2	-3.46	±5.6
Hot tears	-8.06	±6.8	-1.23	±2.0	-4.40	±5.8
Chill inserts	-2.58	±5.2	-0.08	— <sup>d</sup>	-2.59	±4.3
Chaplet inserts	-4.93	±5.4	-0.061	±1.9	-3.26	±3.8
<b>Manganese-Nickel-Aluminum Bronze (MIL-B-21250A, Alloy #2)</b>						
Gas porosity	-4.07	±6.4	— <sup>e</sup>	— <sup>e</sup>	— <sup>d</sup>	— <sup>d</sup>
Sand inclusions	-0.06	±7.2	— <sup>e</sup>	— <sup>e</sup>	— <sup>d</sup>	— <sup>d</sup>
Dross inclusions	-3.85	±9.0	— <sup>e</sup>	— <sup>e</sup>	-1.20	±3.9
Linear shrinkage	-3.62	±8.4	— <sup>e</sup>	— <sup>e</sup>	-1.10	±2.6
Spongy shrinkage	-3.58	±10.1	— <sup>e</sup>	— <sup>e</sup>	-0.93	±3.0

a. At 6.9 MPa (1000 lb<sub>f</sub>-in.<sup>-2</sup>).

b. At 100 mm (4.0 in.) gage length.

c. 95 percent tolerance limit.

d. No significant relationship indicated.

e. Data not taken.



important technological applications. It must be remembered that reference radiographs are sets of illustrations (especially of the graded severity discontinuity types), which cover a wide range of attainable casting quality levels. There is no recommendation of acceptability criteria for particular applications.

The ASME *Boiler and Pressure Vessel Code*<sup>4</sup> does point out accept/reject criteria for various graded steel casting discontinuity types. Briefly, accept/reject criteria for castings should be based on the following considerations: (1) alloy type; (2) section thickness; (3) pressure (including temperature and superheat when steam is involved); (4) service stress; (5) presence of impact and vibration; (6) fatigue; (7) exposure to penetrating radiation; (8) accessibility for maintenance and replacement during expected life; and (9) alloy solidification peculiarities, if any. At best, however, the acceptance criteria are largely qualitative.

Table 5 presents data to illustrate the advantages of correlating radiographic discontinuity indications with destructive test results. The term *slope* in Table 5 is the deterioration  $Y$  per grade of severity and is expressed by Eq. 2:

$$(2) \quad Y = a - bX$$

where  $a$  is average value for substantially sound plates and  $X$  is indication severity.

The radiographer has little say in determining criteria for acceptance or rejection. Establishing such criteria is the responsibility of the customers. Criteria are frequently specified by using a standardized grading system — for example, AMS-STD-2175,<sup>29</sup> radiographic grades A, B, C and D.

---

---

---

---

---

## PART 5. Problems in Radiographic Testing of Metal Castings

The important decisions in casting radiography involve setup, actual radiographic procedures and interpretation. Each of these may at times become problems in actual practice. The intent of the present discussion is to consolidate the discussion of casting control problems and to indicate various solutions.

---

### Radiographic Source

The choice of radiographic source is based on many considerations. Often the source is determined by availability. If this is the case, care must be taken to ensure that the penetrameter sensitivity required by contractual agreement can be met. The usual limits for most commonly used radiation sources, as far as metal section thickness is concerned, are cited in Tables 1 and 2. When deviation from these limits is considered for available sources, trial shots with carefully chosen compensating parameters should be made to determine whether the required sensitivity can be achieved. These parameters include higher resolution image settings (or finer grained film), larger source-to-sensor distance for improved sharpness and proper base density.

When a choice of source can be made, the preferred one is determined by a combination of factors, including: section thickness; the ability to produce simultaneous, complete coverage of a cylindrical casting portion; and the desirability for simultaneous radiography of several castings at one time. A reasonably small gamma ray source is often the best choice for the heavier metals, especially when portability is desired and the radiography is scheduled for raw castings — that is, before surface preparations, necessary machining and repair or assembly welding.

---

### Radiographic Coverage

Contrary to a common misconception, there is no such thing as 100 percent radiographic coverage for all castings. To make sure that no coverage problems arise between producer and purchaser, it is essential to follow proper and early

planning of the radiography. Decisions on the radiographic techniques, especially for castings produced in considerable quantities, can best be made by shooting sketches and associated tabular data (for example, see Fig. 2).

In the control of castings, radiographic coverage is recognized to be a problem with certain configurations of the mold and core; these include portions connecting flanges with bodies and include transition portions between relatively thin bodies and heavy bosses, especially when source location (with respect to sensor) is limited by casting geometry and details. Thus, for example, the blackened portion in the casting of Fig. 2 cannot be radiographed properly. Placement of the source on the inside of the cylinder is prohibited by the size of the inside diameter; placement of the source on the outside is made practically impossible by the limited space between the other flange and the portion of interest.

---

### Radiographic Scheduling

Scheduling of radiography is also an important aspect that should be agreed on by all concerned parties before actual production. Scheduling requires such coordination especially if the casting requires considerable machining and welding. Radiography performed early in the manufacturing process has the advantage of saving further production expenses on castings that may ultimately be rejected or may require extensive repair and associated, unplanned heat treatments. Where an appreciable number of a particular casting is produced, pilot castings may yield valuable information for corrective action, even if they are radiographed in the as-cast condition (with gates and risers attached and section thicknesses considerably greater than finished dimensions). Note, however, that required penetrameter sensitivities are often based on the finished thickness rather than on the as-cast thickness.

Once major problems in the pilot castings(s) have been suitably solved, future castings can be radiographed in the nearly finished and weld repaired condition, thereby obtaining the best penetrameter sensitivity and optimized

sensor or film sensitivity. The interpretation of a pilot radiograph often includes consideration of how the casting process might have caused a given flaw. Thus, radiographic interpretation is not simply a search for casting discontinuities; it also allows the discovery and eventual repair of major systematic flaws.

## Radiographic Interpretation

The interpretation of radiographic images must be performed by trained and certified personnel. Proper reading of images demands that the casting be available for reference purposes. Regardless of when the radiography is performed, visual testing of the part may help decide whether indications on the radiograph are true internal flaws or indications caused by surface finish or other conditions.

Knowledge of gate and riser locations, if the casting is radiographed after their removal, can also help image interpretation. Shrinkage is more likely to occur near risers, if they are of small volume or if the melt solidifies quickly. Gas inclusions are more likely to be found near gates because of the influx of melt when other portions have partially solidified. Interior casting surfaces may at times cause false indications on radiographs because of surface or near surface conditions of the wall; moisture in the core may introduce gas into the melt before it has time to move upward and out through the risers. At other times, brittle components of the core surface may be carried by the melt stream into the casting wall and may then result in near surface density differences; these also could be incorrectly interpreted as discontinuities.

The hot tear is another discontinuity whose positive recognition is sometimes difficult but nonetheless important. This defect is linear in nature and has all the adverse effects of a crack. It occurs when the melt is nearly solidified and is the result of an applied force in excess of what the just solidified metal could withstand at considerably higher temperatures. This is the clue for determining the accuracy of a *hot tear* interpretation.

There must exist in the casting, as confined by mold and core, a source of suitably directed stress to make this type of defect possible. In a cylindrical casting, for example, a relatively unyielding core may cause an outward force as the metal shrinks and thus produce a hot tear. When interpreting a linear discontinuity as a hot tear, it must be verified that the

geometry and mold configuration are capable of providing corresponding stresses during the last stages of solidification.

## Choice of Reference Radiographs

There is at present a wide range of reference documents for various alloy types and section thicknesses, though not all alloys are represented. Because of this, a decision must be made by producer and user on the document mutually considered appropriate for judging discontinuities. For example, ASTM E 310, based on leaded bronze hardware, should not be used for bronzes that tend to solidify more rapidly (those containing little or no lead).<sup>22</sup> A separate set of reference radiographs are available for titanium alloy castings.<sup>27</sup>

## Conclusion

Specific problems in the radiographic control of castings are difficult to enumerate because of the wide variety of casting materials, configurations and techniques. To ensure that problems are kept to an absolute minimum, the radiographic testing of castings in all its aspects should be specified in contracts, purchase orders, product specifications and drawings.

# References

1. Goldspiel, S. "Radiographic Control of Castings." *Nondestructive Testing Handbook*, second edition: Vol. 3, *Radiography and Radiation Testing*. Columbus, OH: American Society for Nondestructive Testing (1985): p 458-490.
2. Quinn, R.A. and C.C. Sigl, eds. *Radiography in Modern Industry*, fourth edition. Rochester, NY: Eastman Kodak Company (1980).
3. ASTM E 1030-00, *Standard Test Method for Radiographic Examination of Metallic Castings*. West Conshohocken, PA: ASTM International (2000).
4. ASME *Boiler and Pressure Vessel Code*: Section VIII, *Pressure Vessels*. Division 1, "Examination of Steel Castings," Appendix VII. New York: American Society of Mechanical Engineers.
5. ASTM E 94-00, *Standard Guide for Radiographic Examination*. West Conshohocken, PA: ASTM International (2000).
6. ASTM E 747-97, *Standard Practice for Design, Manufacture and Material Grouping Classification of Wire Image Quality Indicators (IQI) Used for Radiology*. West Conshohocken, PA: ASTM International (1997).
7. ANSI PH2.8-1975, *Sensitometry of Industrial X-Ray Films for Energies Up to 3 Million Electron Volts*. New York, NY: American National Standards Institute (1997).
8. ASTM E 592-99, *Standard Guide to Obtainable ASTM Equivalent Penetrameter Sensitivity for Radiography of Steel Plates 1/4 to 2 in. (6 to 51 mm) Thick with X Rays and 1 to 6 in. (25 to 152 mm) Thick with Cobalt-60*. West Conshohocken, PA: ASTM International (1999).
9. ASTM E 746-93 (1998), *Standard Test Method for Determining Relative Image Quality Response of Industrial Radiographic Film*. West Conshohocken, PA: ASTM International (1998).
10. ASTM E 1734-98, *Standard Practice for Radioscopic Examination of Castings*. West Conshohocken, PA: ASTM International (1998).
11. ASTM E 1814-96, *Standard Practice for Computed Tomographic (CT) Examination of Castings*. West Conshohocken, PA: ASTM International (1996).
12. ASTM F 629-97, *Standard Practice for Radiography of Cast Metallic Surgical Implants*. West Conshohocken, PA: ASTM International (1997).
13. Goldspiel, S. "Development of Radiographic Standards for Castings." *Third International Conference on Nondestructive Testing* [Osaka, Japan]. Tokyo, Japan: Japanese Society for Nondestructive Testing, for the International Committee for Nondestructive Testing (1960).
14. Goldspiel, S. "Development of Radiographic Standards for Castings." *Materials Research and Standards* (July 1969).
15. Goldspiel, S. and W.N. Roy. "Reference Radiographs." *Standardization News*. Vol. 10, No. 11. West Conshohocken, PA: ASTM International (November 1982).
16. ASTM E 446-98, *Standard Reference Radiographs for Steel Castings Up to 2 in. (51 mm) in Thickness*. [Supersedes E 71.] West Conshohocken, PA: ASTM International (1998).
17. ASTM E 155-00, *Standard Reference Radiographs for Inspection of Aluminum and Magnesium Castings*. West Conshohocken, PA: ASTM International (2000).
18. ASTM E 186-98, *Standard Reference Radiographs for Heavy-Walled (2 to 4 1/2-in. [51 to 114-mm]) Steel Castings*. West Conshohocken, PA: ASTM International (1998).
19. ASTM E 192-95 (1999), *Standard Reference Radiographs for Investment Steel Castings of Aerospace Applications*. West Conshohocken, PA: ASTM International (1999).
20. ASTM E 272-99, *Standard Reference Radiographs for High-Strength Copper-Base and Nickel-Copper Alloy Castings*. West Conshohocken, PA: ASTM International (1999).
21. ASTM E 280-98, *Standard Reference Radiographs for Heavy-Walled (4 1/2 to 12-in. [(114 to 305-mm)]) Steel Castings*. West Conshohocken, PA: ASTM International (1998).

22. ASTM E 310-99, *Standard Reference Radiographs for Tin Bronze Castings*. West Conshohocken, PA: ASTM International (1999).
23. ASTM E 390-01, *Standard Reference Radiographs for Steel Fusion Welds*. West Conshohocken, PA: ASTM International (2001).
24. ASTM E 505-96, *Standard Reference Radiographs for Inspection of Aluminum and Magnesium Die Castings*. West Conshohocken, PA: ASTM International (1996).
25. ASTM E 689-95, *Standard Reference Radiographs for Ductile Iron Castings*. West Conshohocken, PA: ASTM International (1999).
26. ASTM E 802-95 (1999), *Standard Reference Radiographs for Gray Iron Castings Up to 4 1/2 in. [114 mm] in Thickness*. West Conshohocken, PA: ASTM International (1999).
27. ASTM E 1320-00, *Standard Reference Radiographs for Titanium Castings*. West Conshohocken, PA: ASTM International (2000).
28. *Casting Inspection Handbook*. Arlington, TX: GAF Corporation (1968).
29. SAE AMS-STD-2175, *Castings, Classification and Inspection of*. Warrendale, PA: SAE International (1998).
- Bland, J. and S. Goldspiel. "X-Ray Determination of the Cladding Thickness of Clad Metals." *Industrial Radiography*. Vol. 1, No. 4. Columbus, OH: American Society for Nondestructive Testing (April 1943): p 25-28.
- Burrill, E.A. "Radiography of Small Castings with High Cobalt or Nickel Content." *Nondestructive Testing*. Vol. 13, No. 3. Columbus, OH: American Society for Nondestructive Testing (May-June 1955): p 19-21.
- Busk, R.S. "A Correlation of the Mechanical Properties and Radiographic Appearance of Magnesium Alloy Castings." *Industrial Radiography*. Vol. 2, No. 3. Columbus, OH: American Society for Nondestructive Testing (Winter 1943-1944): p 33-37.
- Clark, G.L. and R.W. Eyler. "Development of a Monochromatic Radiographic Method for Locating Small Defects in Aluminum Alloy Castings." *Industrial Radiography*. Vol. 3, No. 1. Columbus, OH: American Society for Nondestructive Testing (Summer 1944): p 13-18.
- Clarke, E.T. "Gamma Radiography of Light Metals." *Nondestructive Testing*. Vol. 16, No. 3. Columbus, OH: American Society for Nondestructive Testing (May-June 1958): p 265-268.
- Cohen, J., E. Hall, L. Leonard and R. Ogilvie. "Investigation of Segregation in Cast Irons by Radiographic Techniques." *Nondestructive Testing*. Vol. 13, No. 2. Columbus, OH: American Society for Nondestructive Testing (March-April 1955): p 33-34.
- Dively, R.W. "Radiography in the Die Casting Industry." *Industrial Radiography and Nondestructive Testing*. Vol. 6, No. 1. Columbus, OH: American Society for Nondestructive Testing (Summer 1947): p 20-21, 39.
- Droegkamp, R.E. "Van de Graaff Radiography of High Density Alloys." *Nondestructive Testing*. Vol. 13, No. 5. Columbus, OH: American Society for Nondestructive Testing (September-October 1955): p 27-30.
- Field, N.M. "Foundry X-Ray Service." *Industrial Radiography*. Vol. 3, No. 4. Columbus, OH: American Society for Nondestructive Testing (Spring 1945): p 23-25, 28.
- Foster, B.E. and R.W. McClung. "A Study of X-Ray and Isotopic Techniques for Borehole Radiography of Tube-to-Tubesheet Welds." *Materials Evaluation*. Vol. 35, No. 7. Columbus, OH: American Society for Nondestructive Testing (July 1977): p 43-46, 51.

## Bibliography

- Applegate, R.L. "The Use of X-Ray Inspection to Identify Alloy Materials." *Nondestructive Testing*. Vol. 21, No. 5. Columbus, OH: American Society for Nondestructive Testing (September-October 1963): p 311-312.
- Baer, W.H. "Radiographic Tests of Gun Metal Castings." *Nondestructive Testing*. Vol. 6, No. 4. Columbus, OH: American Society for Nondestructive Testing (Spring 1948): p 33-39.
- Balakrishnan, B.R. and V. Balasubramanian. "Analysis of the Heavy Element in Alloys and Ores by Beta Ray Backscattering." *Materials Evaluation*. Vol. 25, No. 7. Columbus, OH: American Society for Nondestructive Testing (July 1967): p 173-176.
- Ball, L.W. "X-Ray Micrography As a Tool for Foundry Control." *Industrial Radiography*. Vol. 4, No. 1. Columbus, OH: American Society for Nondestructive Testing (Summer 1945): p 29-36.



- Isaacson, B.G. and B. Krohn. "Digital Radiography Pinpoints Casting Defects Automatically." *Materials Evaluation*. Vol. 45, No. 8. Columbus, OH: American Society for Nondestructive Testing (August 1987): p 884-885.
- Klein, F.D. "Comments and Observations on Experimental X-Ray Diffraction Stress Methods and Technique for Sand Cast Magnesium Alloy Structures." *Industrial Radiography*. Vol. 4, No. 4. Columbus, OH: American Society for Nondestructive Testing (Spring 1946): p 41-46, 49.
- Kuttemperoor, V.Z. "Photon Activation of Alloys and Elements Used in Industrial Parts Requiring High-Energy X-Ray Radiography." *Materials Evaluation*. Vol. 33, No. 5. Columbus, OH: American Society for Nondestructive Testing (May 1975): p 113-119.
- Lueckerath, W., K. Fink and R. Flossmann. "A Nondestructive Method to Detect Pipes and Cavities in Hot Steel Blooms during the Rolling-Process by Means of Betatron, X-Ray-Image-Intensifier and Television-Setup." *Nondestructive Testing*. Vol. 18, No. 1. Columbus, OH: American Society for Nondestructive Testing (January-February 1960): p 27-34.
- Lutts, C.G. "An X-Ray Method for Studying Skin Thickness of Bronze Castings." *Nondestructive Testing*. Vol. 6, No. 4. Columbus, OH: American Society for Nondestructive Testing (Spring 1948): p 13-14, 21.
- Munro, J.J. "Calculation of Scattered Radiation Intensities of 192 Iridium Gamma Rays from a Steel Slab." *Materials Evaluation*. Vol. 35, No. 2. Columbus, OH: American Society for Nondestructive Testing (February 1977): p 51-53.
- Strecker, H. "Scatter Imaging of Aluminum Castings Using an X-Ray Fan Beam and a Pinhole Camera." *Materials Evaluation*. Vol. 40, No. 10. Columbus, OH: American Society for Nondestructive Testing (September 1982): p 1050-1056.
- Struk, D. *NDT in the Foundry*. Columbus, OH: American Society for Nondestructive Testing (1995).
- Trout, E.D., J.P. Kelley and V.L. Larson. "Transmitted and Scattered X Rays for Aluminum and Steel 50 to 300 kVp." *Materials Evaluation*. Vol. 32, No. 8. Columbus, OH: American Society for Nondestructive Testing (August 1974): p 163-168.
- Wilsey, R.B., D.H. Strangways and G.M. Corney. "The Photographic Monitoring of Stray X-Rays in the Radiography of Metals." *Nondestructive Testing*. Vol. 14, No. 2. Columbus, OH: American Society for Nondestructive Testing (March-April 1956): p 18-23.



# Radiographic Testing of Welds

Stanislav I. Rokhlin, Ohio State University, Columbus, Ohio

George L. Becker, Newark, Delaware (Part 6)

Roy L. Buckrop, United States Army Operations Support Command, Rock Island Arsenal, Rock Island, Illinois (Part 6)

Herbert Chapman, Scarborough, Ontario, Canada (Parts 2 to 6)

Tosiyasu Fukui, Kobe, Japan (Part 8)

Eiichi Hirose, Nagoya, Japan (Part 8)

Masahisa Naoe, Nagoya, Nagoya, Japan (Part 8)

# PART 1. Introduction to Radiographic Testing of Welds<sup>1</sup>

Radiographic testing is applied to a new product to provide assurance that the product will be free of discontinuities significant enough to be considered defects and justify rejection of the product. Wherever people work on products, it is normal for things to go wrong. This is the case for all industrial processes, from the historically established trades to modern production systems.

The quality of welds may be partly determined visually; there are general requirements of workmanship that are most easily met by having the welds *appear correct*. The main reason for concern with welds, however, is that they must be as sound throughout as their intended use demands. In determining the requirements for intended use, when some minor discontinuities might be present, radiographic testing has very special advantages. The radiographic process provides good information on the precise nature of a discontinuity. Some discontinuities are not inherently hazardous, so this ability to identify them with some assurance becomes very important. For example, cases of isolated spherical porosity are seldom considered serious in themselves because they do not constitute stress risers within the component. Linear and clustered porosity, however, can be serious failure anomalies. It is important that porosity be evaluated because its presence could indicate that the welding process has gone awry and presage other serious difficulties.

In the hierarchy of quality functions, radiography comes at the functional peak. A welding procedure would usually be regarded as a proven routine although certain unexpected events may occur. For instance, a welding process could gradually change, such as drift in an instrument. There might be no external indication that the process had been altered. Radiographic testing can contribute very meaningfully here because of the detailed record it provides of the internal condition of a weld.

Radiographic testing is useful in welding technique development. In addition, many standards require radiographic testing in the final inspection.<sup>2-9</sup> In some cases, when welds become hidden in complex assemblies, this final inspection can occur fairly early in the component's manufacturing cycle.

## PART 2. Weld Design<sup>1</sup>

Most weldments consist of two pieces of metal joined in a way that satisfies a specification, a drawing or some other means of stating a requirement. In industry, welded joints are most often secured by fusion welding.

### Butt Joints

The basic type of welded assembly is the *square butt joint* in which the original square cut faces are butted or prespaced. When there is some space left between the faces, which is the common form of assembly, this space is referred to as a *groove*. In the case of butt joints, the groove is square; its shape involves only right angles. It is possible to make a weld in a square cut joint with the joint faces fitted tightly together (with no groove). Such a tight joint can lead to the entrapment of nonweld materials in the weld metal because the joint is not open to let these materials float away.

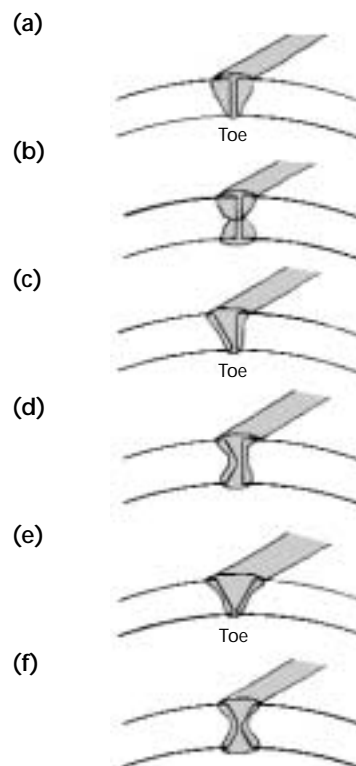
A square groove joint made without the addition of filler metal can contain discontinuities typical of the material being welded, joint configuration and the welding process. In a radiograph, these discontinuities usually appear as straight lines when gross quantities of entrapped solids are present as linear slag. Inasmuch as they usually will have lower mass than the metal involved, they will appear as darker zones in the radiographic image.

Another type of butt joint has a prepared groove. Figure 1 shows six welded assemblies made up of a single type of joint, the butt joint, and a single type of weld, the groove weld. The shape of the groove serves to classify the set still further. In Figs. 1a, 1c and 1e, the groove is limited to one side of the joint, the top side as drawn. These make up the single groove set, with groove shapes as follows: (1) square, because of 90 degree rectangular shape (Fig. 1a); (2) bevel, with one angled face (Fig. 1c); (3) V, a pair of angled surfaces facing one another (Fig. 1e). Figures 1b, 1d and 1f repeat the previous three but are doubled through the thickness. The double joint is used mainly for thick material but can be specified for thinner members when it is desired to have a better balance of material on the two sides, to minimize distortion.

These grooves can be symmetrical or asymmetrical. The groove form is a necessity for joints in thicker materials where there must be access for maintaining an arc and allowing metal to be deposited under controlled conditions. Usually, economic choice will determine whether the V groove or the bevel groove is used. Note that the smaller bevel groove requires less electrode material to make the joint. Less weld metal means less distortion. In these simple joints, metal is added from one side only; when distortion occurs, the assembly bends in the direction shown in Fig. 2.

In order of increasing complexity, the next form of joint is the double V or double bevel preparation shown in Figs. 1d and 1f. These include mirror images of the single bevel joints and are used when the material is too thick to be

FIGURE 1. Butt joints with groove welds: (a) square groove single weld; (b) square groove double weld; (c) single bevel groove; (d) double bevel groove; (e) single V groove; (f) double V groove.



welded from one side without serious distortion. A root pass is again performed but this time in the midsection of the weld. This midsection is a small, square groove butt joint and requires checking, as above, for the similar geometry.

When fitness-for-purpose criteria are applied, fairly large discontinuities might be tolerated in the midsection. In the case of the bevel weld preparation, there is a vertical face involved, when the weld is to be made in the flat position (Figs. 1c and 1d). This configuration can lead to some difficulties in welding. When the square face is oriented vertically and weld metal is being deposited, there could be problems in developing a uniform fusion layer on this face. The resulting discontinuity is referred to as incomplete fusion. When it is feasible to position the joint so that the square face is horizontal during welding, this sort of difficulty may be avoided.

## Other Joints and Welds

There are some further joints of more complex geometry not as well suited to radiographic testing as the butt joint.

The T joint, for example, may be assembled with one or two fillet welds (Fig. 3). This is the weld most commonly used with the T joint. It would provide the most economic assembly because no special preparation (machining) is required. The T joint with fillet welds is not an easy assembly to inspect because it

is not easy to set up for reliable radiography. In its most rudimentary form, a single fillet weld, confined to one side, would be a candidate for radiography. While this weld may be radiographed by shooting from above (with respect to the orientation of Fig. 3), such welds should be subjected to refined techniques of testing with caution because an unfused zone exists in the original joint interface and this thin gap looks very much like an internal crack.

More refined models of the T joint are shown in Figs. 4a and 4b, where prepared welds are illustrated. Some options available to the weld designer are shown in this figure. Other forms of preparation (shown in Fig. 1) might also be used. The welds shown would be amenable to radiography by positioning the sensor under the base plate. Joints such as this may be expected to carry dynamic loads in service, as in bridges.

Another fundamental joint, the corner joint, may be bonded by several kinds of weld. A corner totally welded with a prepared weld is shown in Fig. 5. This weld is one of several for joining at the corner. The simplest method is a fillet weld on the inside corner, such as those fillets shown in Fig. 3. Any of the other single groove shapes in Fig. 1 could be used here as well. For static service (buildings not subject to variable wind loads, for example) the simpler fillet weld could be used on the inside corner; this case parallels the T joint illustrated in Fig. 3.

Another complex joint is the lap joint, usually assembled with a pair of fillet welds as shown in Fig. 6. This unbalanced looking joint is a natural for the fillet

FIGURE 2. Potential distortion with welding done from one side only.

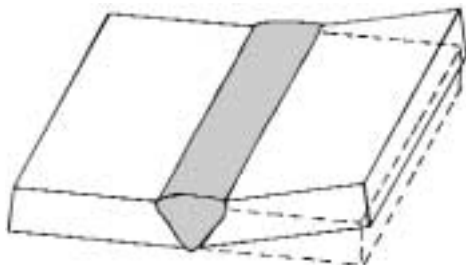


FIGURE 3. T joint with fillet welds.

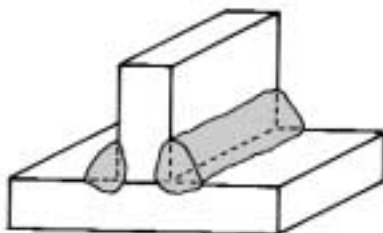
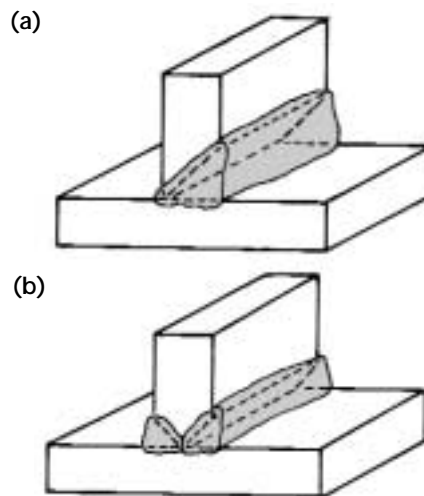


FIGURE 4. T joints with groove welds: (a) single bevel groove; (b) double bevel groove.



weld. There would be no point in cutting any groove shapes as a preparation. A similar joint can be used to join two extended plates by butting them and adding a pad bonded by fillet welds; the plate junction is made by including one of the groove welds associated with the butt joint.

A final edge joint requires the simplest form of weld. As shown in Figs. 7, this joint is ordinarily secured by melting existing flanges. Note that the configuration in Fig. 7a could be welded on the reverse side, using the natural groove there; it would then be classed among the groove welds.

## Weldment Material and Thickness

The material involved in a weldment influences radiography mainly through its density and, more importantly, its atomic number.

Welded materials ordinarily range in density from  $1.78 \text{ g}\cdot\text{cm}^{-3}$  for magnesium to  $8.57 \text{ g}\cdot\text{cm}^{-3}$  for niobium. Comparisons of density alone are not sufficient when comparing materials; the absorption of ionizing radiation by a specimen is also affected by the atomic structure of the material.

The thickness of the material under examination has an influence that acts in parallel with the specimen density. As the thickness increases, the energy level of the radiation source and exposure time must be increased.

Another effect related to the thickness of the material has to do with how close the zone of interest is to the plane of the detector. This distance has a direct influence on the sharpness of the image.

The geometrical unsharpness is also controlled by the size of the radiation source and its distance from the object. In X-ray devices it is the size of the X-ray

tube target interrupting the electron flow; in a gamma ray source, it is the physical size of the isotope. Increases in distance from source to object can compensate for large source sizes.

When butt joints are examined, one side of the weld could be of more interest than another. In this case, to reduce the unsharpness, the detector is positioned so that the potential discontinuities are closer to the sensor. This applies to the single-V or bevel groove, when the root of the joint, or toe of the weld, is virtually at the back surface of the weld. This portion of any groove weld is the most susceptible to discontinuities.

FIGURE 6. Lap joint with double fillet welds.

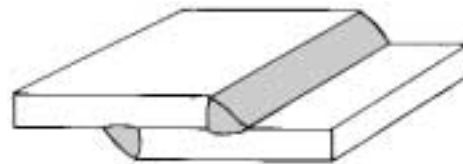


FIGURE 7. Edge joints: (a) normal fused edge; (b) thin sheet before welding; (c) thin sheet after welding with flange consumed.

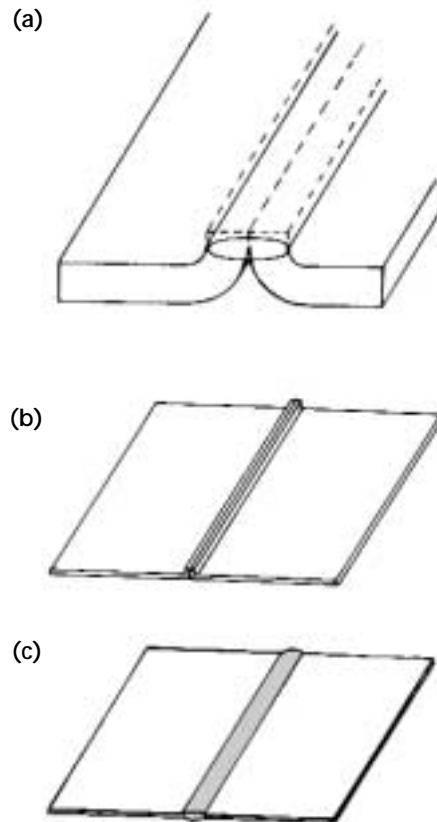
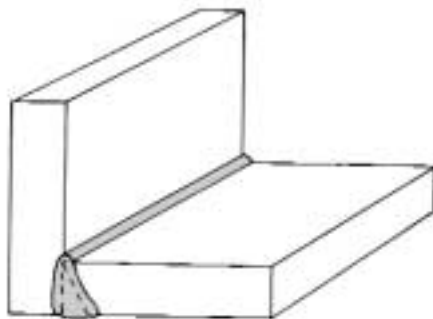


FIGURE 5. Corner joint with single bevel groove.



## PART 3. Discontinuities in Welds<sup>1</sup>

Although many of the following discontinuities occur in several types of welded joints, the differences in joint geometry produce differences in the location and orientation of the discontinuities. Thus, the radiographic procedure for imaging one discontinuity might not be useful for another.

Weld discontinuities that can be found by radiography are mainly porosity, inclusions, inadequate penetration, incomplete fusion, cracks, underfill, undercut and arc strikes.

Some weld discontinuities not commonly found by radiography include underbead cracks, lamellar tearing, lamination and delamination.

### Porosity

Porosity is a condition in which the metal has voids containing gases; most welds contain a certain percentage of porosity. These gases are dissolved in the metal while it is hot and then separate as it cools. The solubility of gases in metals can be very high at high temperatures.

The gases result from chemical and physical reactions during welding. A certain amount of gas is always generated in standard welding but is usually not detectable radiographically. At times, however, excessive gas is produced and leads to the discontinuity called *porosity*.

Most porosity is spherical but can take on other shapes, depending on welding conditions. It can also be distributed in ways that are again related to welding condition.

Porosity may be found anywhere throughout the weld metal. It will not be found in the unmelted heat affected zone of the material.

The restrictions on porosity in some welds may be rather lenient. This condition does not seriously weaken a welded joint. There are two aspects contributing to this apparent lenience.

First, spherical porosity does not act as a stress riser, meaning that it does not behave like a sharp notch that would indeed weaken a joint. Secondly, the strength of weld metal is customarily greater than the nominal strength of the material being joined. Welding electrodes, with their special coatings, are designed to deposit a relatively high strength material,

one with a very fine cast structure as a result of an extremely rapid cooling rate. Most weldments then can accommodate a fair amount of porosity, especially when the service conditions are predictable. An exception to this lenience is for severe linear and clustered porosity in highly stressed and fatigued sensitive joints.

### Common Types of Porosity

Uniformly distributed, spherical porosity indicates that the cause of the difficulty has been averaged over the entire weld.

Clustered spherical porosity occurs in zones where there has been a perturbation in the welding process, especially when welding has been stopped and started up again. In such cases the pores would be spherical.

Linear spherical porosity is confined to the earlier portions of the weld, often following a joint edge. Linear spherical porosity usually indicates contaminated material.

Damaging porosity is usually easy to identify in a radiographic image and, although inclusions can be similarly shaped, will usually be less symmetrical and more contrasting.

### Piping

*Piping* is a term applied to porosity of a teardrop shape; it usually has a linear distribution. The condition is easily recognized in a properly oriented radiograph because of its streamlined shape and customary grouping.

### Herring Bone Porosity

Herring bone porosity is a special case, occurring in automatic arc welding processes. It has a tear drop shape, similar to piping porosity, and is distributed in linear fashion with a high degree of regularity. Herring bone porosity is caused by contamination, generally the presence of air. In the gas metal arc process, a special atmosphere provided by the equipment helps avoid this discontinuity.

### Inclusions

Inclusions are pieces of slag or other solid materials that have been trapped by weld metal. This form of discontinuity, like



porosity, is consistently found by the radiographic process. It can occur in nearly spherical, isolated cases but the tendency is for inclusions to accumulate linearly. Most inclusions consist of residual slag from the electrode coatings or fluxes in welding. The trapped material tends to occur in the welding direction and therefore normally appears in a line.

In building up a weld, a channel effect occurs on both sides of the bead. If through a fault in the process some slag is trapped, there could be two affected zones, corresponding to the weld bead width. When such parallel slag lines occur they are called *wagon tracks*.

In multipass welding, the slag covering will remain on the as welded work piece, just as it does on properly completed welds, and measures must be taken to ensure its removal.

If this interbead slag is not completely removed before the next pass, inclusions will result. In a radiograph, this type of slag is not distinguishable from slag material trapped during single-pass welds.

All the welding processes involving flux can exhibit slag inclusions. Just as for porosity, the automatic processes, when they go awry, tend to exhibit long, regular discontinuities.

The spherical type of slag inclusion may often be distinguished from porosity because there is a major density difference between the solid slag and the open void. When both appear in the same image, confirmation is easier. A major slag inclusion may also have a structure that can be resolved in a radiograph and will not be smooth.

The limits on slag are more stringent than for porosity because the linear form of the inclusion can act as a stress riser. The interpreter is usually directed by the applicable code in determining the allowable length and width of such inclusions.

An intermittent slag line is actually a single slag deposit with gaps. The accumulated length of the broken run plus the gap space may be used to determine the total discontinuity length, in some specifications.

## Inadequate Penetration

The discontinuity called *inadequate penetration* may or may not constitute a *defect*. One definition states inadequate penetration of the joint constitutes *penetration less than that specified*. Thus it is possible to have an incompletely bonded (or incompletely filled) joint that would still be allowed by specification. This is especially true for partial penetration weld joints, discussed below. Should such a weld be radiographed, clear

geometric indications of the unwelded zone would be obtained. However, if the radiation source is angularly adjusted, the unwelded joint may not show and the anomalies can be evaluated. Inadequate penetration must be monitored and measured to determine limits.

On a radiograph, this indication is usually a straight sided, dark zone. In the case of joints welded from one side only, the image will be well defined, assuming the detector is on the root side. When inadequate penetration occurs in thicker joints welded from both sides or piping welds, the outlines will not be sharp. This unsharpness occurs because (1) the zone of interest is further from the detector or (2) the discontinuity is a smaller percentage of the total specimen thickness.

The effect of this condition on the weldment can be very serious: a pair of sharp notches may be present, extending for a considerable distance. The joint would be weak in bending across the weld, especially for repeating loads or cycles. In these cases, specifications such as those in AWS D1.1<sup>3</sup> impose strict limits on the length permitted.

## Incomplete Fusion

Incomplete fusion is a discontinuity characterized by unbonded zones in a weld where weld metal is cast in place but not bonded to a prepared surface or to a previous bead. The shape may then be precisely or roughly linear. In its usual form, the discontinuity exhibits a gap over some of its width, gradually closing to zero. The typical radiographic appearance shows evidence of tapering (the image would be longitudinal and shaded across its width). Note that when incomplete fusion comprises only weld metal in complete contact with another material, the thickness of the discontinuity could be near zero. In this arrangement, the discontinuity might not be detectable radiographically unless the beam were directed along the unfused zone. Radiographic techniques might not detect this type of discontinuity. In ordinary weld sampling, with the beam directed at the weld bead, the result would be negative. If the radiographic requirements are designed to detect incomplete fusion, a requirement for the appropriate beam direction (Fig. 8) would be included.

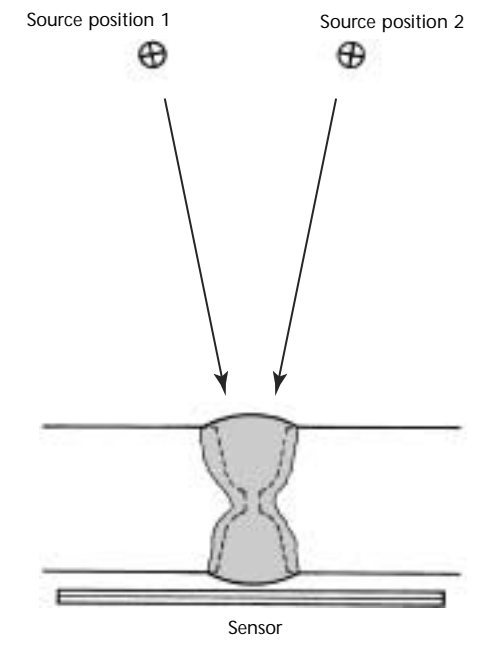
Incomplete fusion can occur in all types of fusion welds. The limits for incomplete fusion are generally equivalent to those for incomplete penetration and specifications might group the two conditions together, classed as fusion discontinuities.

## Cracks

A crack may be defined as a split, exhibiting a sharp tip and typically a very small opening. Its detectability by radiography is a function of the orientation of the beam to the crack. As in the case of incomplete fusion, cracks are ordinarily detectable only by ensuring that the beam direction is in line with the crack. Typically, when cracking is suspected but cannot be confirmed, more radiography will be required to confirm the indication. When clearly detected in a radiograph, the typical crack will appear as a narrow, irregular line.

Cracks exposed by radiography are always considered discontinuities and rejection follows, with repair being an option. They are the most serious form of discontinuity because their sharp tip acts as a severe stress riser. For cyclic loading, cracks are always dangerous. Note that in interpreting radiographs, the very presence of a crack is sufficient evidence for rejection; there is no guarantee that the actual limits of a crack will match the visible length of its radiographic image. Further portions of cracks can be closed very tightly because of weld shrinkage stresses and no tightly closed crack would be detectable.

FIGURE 8. Radiography of weld joint based on double U groove; both source positions in line with prepared faces.



## Hot Cracks

A form of cracking, referred to as hot cracking or hot tearing, is radiographically detectable. This discontinuity originates during or just after the hardening of the metal when shrinkage is excessive. When narrow, deep welds are made, the weld metal does not stay molten long enough to fill the normal shrinkage spaces.

Hot cracks have some visible width and are therefore more easily detected with radiography.

## Crater Crack

A variation on the hot crack is the crater crack. These occur if the electrode is removed too soon at the point where a weld is terminated. Crater cracks usually consist of sets of radial cracks and are recognizable in a radiograph by this typical pattern.

## Other Separations

Other cracks may develop adjacent to the weld metal, in the heat affected zone. Such cracks may be associated with hydrogen in the metal and may appear up to several hours after the completion of the weld. Hydrogen cracking is almost always associated with high strength materials because of their susceptibility to alloy modifications during welding and inherent ductility. They may not be open and will generally not be oriented in a predictable direction. The radiographic method should not be used for their detection.

Other serious forms of separation not ordinarily detectable with radiography include (1) the underbead crack (a cold crack sloped away from the plate surface), (2) lamellar tearing (separation within the plane of the plate) and (3) delamination (opening of an in-plate separation).

## Tungsten Inclusion

Tungsten inclusions are particles from the tungsten electrodes that become deposited in weld metal through faulty procedures. The particles may be spherical and appear much denser than the material being welded, typically aluminum alloys and stainless steels. The very high density serves as positive identification.

Tungsten inclusions are not considered especially harmful in stainless steel and are usually counted with porosity. The condition does indicate some processing or procedural problem and should thus be monitored. However, in titanium alloys, such inclusions require removal and rework.

---

## Undercut

Undercut refers to a groove melted into base metal directly adjacent to a weld bead. External undercut is ordinarily evident visually. Internal undercut occurs in pipe welds. When undercut occurs in assemblies, the original surface may not be accessible and the need for radiographic interpretation may arise. Undercut is a processing fault and may be repaired by adding an extra, narrow weld bead.

The condition is generally recognizable because the plate thickness will exhibit a definite tone on a radiograph, whereas adjacent to the weld there will be a darker area where the plate thickness has actually been reduced.

In some standards, a certain amount of undercut is permitted. As an example, AWS Standard D1.1-83<sup>3</sup> permits undercut to a depth of 1.6 mm (0.063 in.) for material thicker than 15.9 mm (0.625 in.). In more critical cases, no undercut is permitted and a radiographic determination leads to rejection.

---

## Arc Strikes

Arc strikes are discontinuities that result from establishing the welding arc in zones other than a weld. They consist of remelted metal or portions of electrode metal in unscheduled places. Their potential danger arises from steep changes in metal properties that develop when a material such as steel has been subjected to very rapid heating and cooling. Excessive hardness can result, leading to possible fracture during welding or service.

The condition is identified by its position (away from the weld metal) and by a small patch of extra thickness that is often intermittent but linear.

Arc strikes are usually cause for rejection on critical weldments because of the possible effect on service life. Repairs are possible and would generally involve grinding through the thin affected layer, with fine grinding as a finishing operation; no further welding would be scheduled.

[A collection of radiographs showing special conditions for weldments is presented elsewhere.](#)

## PART 4. Technique Development<sup>1</sup>

### Radiation Sources

Equipment that could be used for the radiography of weldments is usually one of three types: (1) standard, low voltage X-ray generators, (2) gamma ray sources and (3) high energy X-ray generators.

#### Standard X-Ray Generators

All X-ray units are high voltage devices. The standard equipment recommended for weldments ranges from 25 kV peak to 420 kV constant potential. This range covers weldment materials with densities of 1.8 to 8.6 g·cm<sup>-3</sup>. Because of the attenuation coefficients and thicknesses, there are limitations in thicknesses that can be adequately covered. Figure 9 presents some thickness limits for X-ray machines both in the regular voltage ranges and for high energy X-ray generators. High energy X-ray generators are primarily electron accelerators that do not use standard X-ray tube heads. Their energies range from 1 to 25 MeV.

#### Gamma Ray Sources

The exposure time with radioactive isotopes depends on the available activity and on the amount of material in the

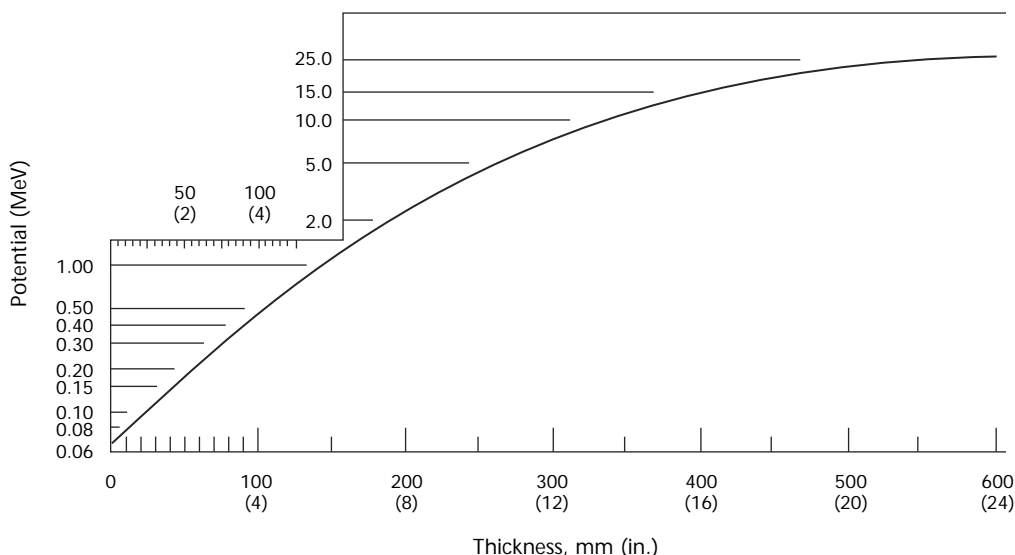
capsule. This activity level is presented in becquerel (Bq) or curie (Ci).

The shape of the isotopic pellet also affects its usefulness in radiography. Only the atoms near the outside of the pellet contribute fully to the exposure. For atoms in the interior, the radiation emitted first penetrates part of the pellet itself. Because the materials are dense, with a medium to high atomic number, intensity diminishes significantly.

### Film

An important factor influencing the choice of film is the total cost of the operation. Slow, fine grained film costs roughly the same as other film but can end up costing much more because of the longer exposures it demands. The time cost can be twofold: (1) radiographic personnel are required for a longer time and (2) the working areas of fabricating shops may have to be shut down for safety reasons. With isotopic radiation sources it is customary to operate hazardous equipment on off shifts. This procedure can be very safe but it can add materially to the interval between the actual exposure and the repair of the component.

FIGURE 9. X-ray potential and general thickness limits for steel.



With film, there is also a choice to be made for the type of radiation being used (high or low energy) and for the weld material density. The information available from film is contained in its optical density variations. If this *variation* is reduced by the quality of the radiation, whether the film is light or dark, the information content also decreases. To optimize contrast, film selection and exposure parameters are determined by using film characteristic curves and exposure charts [as discussed elsewhere](#).

## Setup for Exposure of Various Weld Types

The choice of a radiographic technique is usually based on sensitivity. It is usually given in terms of percentages of the radiation, with two percent or less applying to fairly critical projects and four percent to less critical work. As an example of scaling, in a steel section 100 mm (4 in.) thick, a 2 percent sensitivity would correspond to 2.0 mm (0.08 in.).

Following are examples showing how the radiography of specific weldments could be handled.

### Butt Joint

Consider a butt joint in 76 mm (3.0 in.) steel, as might occur in the wall of a pressure vessel. The welding technique should be in accordance with the *ASME Boiler and Pressure Vessel Code*, Section VIII.<sup>2</sup>

To ensure weld quality, the designer might have the joint prepared for welding from two sides, with the initial welding pass made at the midsection, which becomes the root of the joint. This weld preparation is called *U groove preparation*, similar to the double-V groove weld (Fig. 1f). Such a configuration permits access to the root for welding and requires much less material to fill than a V shaped opening. Good practice requires that the backside of the root pass be ground or gouged, leaving a groove for the first pass on the second side. Such a weld usually requires at least five passes on each side. The passes would be sequenced to minimize stress and distortion but the sequence of passes does not influence the radiographic method.

If the initial root pass and the first pass on the second side have been performed properly (and confirmed by visual observation at the time) then there should be no radiographic indications associated with the root of the joint. The most likely areas for difficulty are on the steeply sloping sides of the groove — it is for these zones that the radiographic test is designed. The radiography can require

two exposures, with the beam directed in line with the preparation angle of the groove. The symmetry of the joint will ensure that one shot on either side of the weld can be used to sample the two flanks (Fig. 8). The image will be evaluated according to the code requirements.<sup>2</sup> The actual length of the weld being sampled affects the exposure geometry.

The beam direction has a further effect on the test because as it shifts from the 90 degree orientation, a discontinuity's projected shape and position change. The visibility of a plaque image quality indicator will serve to show whether the distortion significantly affects the image. The specified film density is broad enough to accommodate the variation arising from this projection effect. In some cases, the finished weld bead must be ground to make the weld region flush. In the case chosen here, grinding is not required; instead, a maximum bead height is indicated. If this were not taken into account, the extra bead metal could lead to some underexposure of the image; exposure parameters must be based on the total thickness.

### Joint with Varying Thicknesses

Another common variation occurs when two members of differing thicknesses are fastened by a butt joint. For such a case, the weld area is a tapered zone. Although there are limits set for the angle of such a taper, the difference between the two thicknesses has a critical effect on the radiographic process. Accommodating such a difference may require a special arrangement, such as using films with different speeds for a single exposure. By this means, the thinner steel section will be captured on slower film and the thicker section on faster film. To evaluate such a radiograph, the two films can be viewed together.

### Joining Different Materials

Only one type of material is involved in the previous example but another variable can arise in a welded joint when more than one type of material is involved. A typical case of this sort involves joints that will be exposed to significant magnetic fields, such as in large electrical equipment. These configurations often include two parts fabricated from steel joined by a nonmagnetic weld of stainless steel. The weld serves to break the continuity of the magnetic field that occurs when the component is in service. To the radiographer, there will be a noticeable change in radiographic density between the steel and the stainless steel. It is important that the form of the joint be known so that the change in density will



not be interpreted as a change in thickness.

## Lap Joints

The butt joint with a groove weld is the simplest welding arrangement and is easily interpreted because of the general uniformity of the assembly. A less uniform weldment is the lap joint secured by two fillet welds (Fig. 6).

This type of joint is used on vessels fabricated according to specifications in the *ASME Boiler and Pressure Vessel Code*, Section VIII.<sup>2</sup> If the requirement were for an opening already fitted with a nozzle, a pipe might be slipped over and attached using a lap joint. Being integral with its vessel, such a joint is subject to loading and will have some low strength requirements. The assurance requirement for this joint could include verifying that sufficient weld metal is present in the joint.

It is possible to make a fillet weld that, from the outside, appears full sized but is actually hollow. Ultrasonic testing can be used to ensure bond.

Because of the weld configuration, there is no means of directing a beam so that a constant thickness is examined. Also, the sensor plane is not close to the weld zone. The interpretation of the image from this seemingly simple joint is quite complex because there is a large film density gradient over a small dimension (the projected width of the weld). In this case then, the radiographer could expect only to confirm the presence of relatively large discontinuities.

## T Joints

A further increase in complexity occurs with the T joint, of which there are two types: one with full penetration making a completely welded assembly (Fig. 4) and the simpler case with fillet welds in the corners (Fig. 3). When there are only two fillets involved (or even one) the radiographic assessment becomes very similar to that for the lap joint: a varying thickness of material is presented to the beam and the sensor plane is separated from the weld metal by the thickness of the lower plate. Again, however, if radiography is required, the sensitivity does not have to be of an extremely high order because a joint of this type is only partially welded and would never be used in a critical application.

A more refined T joint involves a groove weld, or welds, rather than simple fillets. The vertical member is prepared from one or both sides. The complete weld is made through the thickness of the web, as shown in Figs. 4a and 5a. Such a weld would be amenable to radiography.

There is still some variation in the effective thickness across the weld but this variation is much less than for the plane fillet weld. Note that a plane fillet is usually present in a practical T joint but any extra fill material is cosmetic and does not contribute to the strength of the joint.

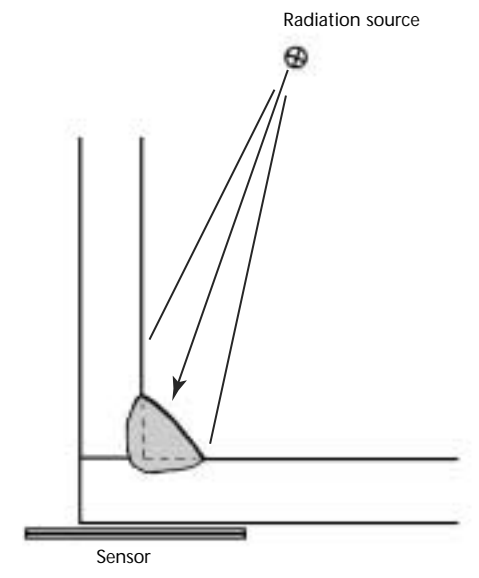
The weld in a prepared T joint can be considered fully load bearing and may therefore have performance requirements that will justify a sensitive radiographic technique.

## Corner Joint

As with the lap joint and the simple T joint, the corner joint may be assembled with a minimum of welding using a fillet weld in the corner. This weld is not used when full loading is required and thus does not require refined radiography. If radiography is used, the joint has one special advantage: there could be a preferred direction for the beam that would not involve the unwelded portion of the joint (see Fig. 10). There is still a variable thickness presented to the beam but this effect may be minimized by having the beam come in at about 20 degrees.

The unwelded portion presents a large open notch that limits the usefulness of such a simple assembly. The corner joint may also be prepared as a groove weld, just as for the T joint (Fig. 5). For a groove weld, the preparation usually involves work on one member of the joint. When welded, the corner must be solid metal. The source and the sensor are positioned as shown in Fig. 10 but with the joint

FIGURE 10. Radiography of fillet weld on corner joint.





oriented as shown in Fig. 5, so the sensor plane and weld metal are virtually in contact.

### Fillet Welds

The fillet weld is commonly used with the lap joint, the corner joint and the T joint; the fillet weld may be used in conjunction with a groove weld in a corner or T joint.

For a 90 degree T joint with a symmetrical fillet weld, the shortest path through the weld is that bisecting the 90 degree angle, giving a radiation beam angle of 45 degrees. If the sensor plane (film holder or detector assembly) is positioned in contact with the flange of the T joint (the top of the T), then the radiation beam must pass through a relatively large thickness of metal.

Another approach to the radiography of fillet welds is to position the sensor on the weld side of the joint. In this case, the thickness of the sensor plane will have some considerable influence on the radiographic resolution. This limitation only applies when the sensor is flat. Flexible film holders and detector arrays are available that can be bent to conform to the weldment and thereby bring the sensor closer to the weld bead. The extra metal in the radiation path does not fall between the weld zone and the sensor and resolution will usually be improved. In this setup, the beam is at right angles to the weld surface. This arrangement is the best for detecting centerline cracking. A similar arrangement is useful for T joints in which the web (the stem of the T) is prepared for welding.

Other arrangements may be used to compensate for the uneven geometry of the fillet weld. One example is the introduction of metal wedges, prepared with shapes complementary to the fillet shape and fitted between the sensor and the radiation source. The wedges may be in contact with the weld surface or on the opposite side, where they should be in contact with the sensor plane. This setup can be used with any of the three joint types using the fillet weld.

### Edge Joint

The edge joint is illustrated in Fig. 7. This form of joint is usually intended for sealing and is not considered structural. When the weld is completed, there is a severe notch on one side that reaches to the root of the weld and precludes any significant bending or tensile loading. The edge joint has an evident deficiency in load bearing capacity but may be radiographically tested when sealing is a crucial factor. The total geometry of the joint discourages radiography: although the weld is fairly thin, it is mounted on

legs that act as a thick section when viewed from directly above. When sealing a cylindrical object with an edge weld, tangential radiography is frequently used.

A form of the edge joint made with flanges could be readily checked radiographically (Figs. 7a and 7c). If made from thin material, when fairly sharp bending might be assumed in the weld preparation, a careful weld could be designed to use up all the projected material and melt through to the back, rather like the consumable insert. The resulting weld is somewhat thicker than the sheet and is suited to the radiographic examination process. Such welds are used on articles made of precious metal, where the amount of material is always a great part of the total cost.

## Image Quality Indicators

There are two basic image quality indicators for indicating the quality of a radiograph: the *plaque* image quality indicator (a flat rectangular plate) and the *wire* image quality indicator. In North America, quality is judged by checking for the discernibility of (1) the outline of the plaque itself and either (2) wires or (3) certain small holes in the thin plaque. At one end of the plaque there are lead characters that identify the material of the plaque and its thickness (see Figs. 11a and 12).

The plaque image quality indicator first functions in a thickness mode, the thickness being a percentage of the weldment thickness. A second aspect of this sensitivity indicator is related to the actual hole diameter. Customarily, because many codes so require, the plaque thickness will be 2 percent of the weld thickness and a hole whose diameter is two times the plaque thickness (2T) will be required.

ASTM E 1025, *Standard Practice for Design, Manufacture, and Material Grouping Classification of Hole-Type Image Quality Indicators (IQI) Used for Radiology*,<sup>10</sup> is a standard for plaque image quality indicators. Image quality indicators that are made to ASTM E 142, *Standard Method for Controlling Quality of Radiographic Testing*,<sup>11</sup> will incorporate the 2T hole and two other holes, one with diameter equal to the plaque thickness (1T) and one with a diameter four times the plaque thickness (4T). For more critical applications, a contract could require that the smallest hole be used. Alternatively, plaques could be prepared with other versions of the hole diameters. The 2 percent level, however, has the advantage of international recognition because of its presence in the ASTM standards and

because many codes refer to the 2 percent level.

The next most common form of image quality indicator is the wire type (Fig. 11b). The wires are arranged by diameter and are all of the same length. The wire material is chosen to match the material in the weldment. In use, a specification will state the smallest diameter that should be visible on a finished radiograph. The wire package is of a standard design and information about the wire set is presented in lead characters. Customarily it would be stated that at least two thirds of the significant wire length should be resolved on the image. See Table 1 for some details on the design of the wire set.<sup>12</sup>

An image quality indicator portrays the material thicknesses and identity on each device, with the 1T, 2T and 4T holes (Fig. 12).<sup>13</sup>

FIGURE 11. Image quality indicators: (a) plaque; (b) wire.

(a)



(b)



## Purpose of Image Quality Indicators

All forms of the image quality indicator have one basic purpose: displaying a measure of the radiographic quality and thereby some measure of the quality of the radiographic process.

Some of the most critical radiographic test objects are pressure containing zones in nuclear reactors. These zones comprise the main pressure vessels, heat exchangers, pipe fittings, valves and piping and are linked with one another by welds. Because of the extremes in pressure and temperature these components must withstand, they are built from very thick metal. They are, however, not much thicker than they need to be and no large safety factors are

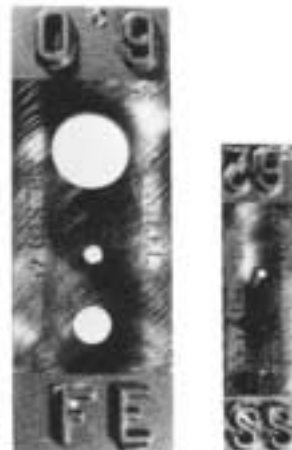
TABLE 1. Comparison of plaque and wire image quality indicator sensitivity.

Plaque Thickness		Wire Diameter	
mm	(in.)	mm	(in.)
0.13	(0.005)	0.13	(0.005)
0.16	(0.006)	0.16	(0.006)
0.20	(0.008)	0.20	(0.008)
0.23	(0.009)	0.25	(0.010)
0.25	(0.010)	0.33	(0.013)
0.28	(0.011)	0.40	(0.016)
0.31	(0.012)	0.51	(0.020)
0.51	(0.020)	0.64	(0.025)
2.54	(0.100)	0.81	(0.032)
3.81	(0.150)	1.02	(0.040)

1. Plaque thicknesses are arbitrary in this example.

2. Wire diameters are in geometric series, each multiplied by tenth root of 10 (1.2589).

FIGURE 12. Image quality indicator of type described in ASTM E 1742, ASTM E 2104 and MIL-STD-453.<sup>13,20,21</sup>



involved. Exceeding minimum standards could make these components so thick and heavy that the material and fabrication costs would be prohibitive. The aim is to ensure that the assembly is of high enough quality that it can function in complete safety. The welds involved are expected to be as sound as the materials being joined. The materials are subjected to quality assurance systems throughout their manufacture and the welded joints become equally important. When radiography is used to determine the quality of the welds, the test system itself logically becomes subject to question and to similar control.

## Area Coverage

The area to be covered by the sensor (either film or detector array) is a major concern. For one thing, the sensor size must be adequate for the size of the weld zone involved. The sensor must also be large enough to gather information on radiographic quality (the image quality indicator and any shims must be visible). Larger sensor sizes may be required when complex sensor identification systems are involved.

The area to be covered is directly affected by the geometry of the arrangement. The radiation source images precisely only when the object and the sensor plane are normal to the beam. With flat work pieces, this becomes a definite limitation on the length of a weld that can be covered in a single exposure. Often a specification will incorporate a limit here — for example, a maximum of 27 degrees half angle in such a case.

Such exposure angles have two important effects and both tend to degrade the image. First, the true shape of an indication will not be presented because the beam will generate a shadow that is elongated in the plane common to the weld metal and the axis of the radiation beam. The second effect has to do with the position of an image compared with the actual position of the discontinuity that generates the image. An indication in the image will always be projected away from the true position of the discontinuity causing the image. Like the distortion effect above, this can become quite severe if limits are not imposed.

Specifications usually incorporate clauses covering exposure geometry and may even go a step further in demanding that the image quality indicators be placed at the outboard end of the joint, where the effect is intensified. Presuming that the image quality indicator is sufficiently visible, the radiograph is judged accordingly.

## Screens

For weldments of steel and other dense metals, a lead foil screen between the sensor and the radiation source is usually required. The screen improves the image quality by filtering out longer wavelength radiation, which causes general fogging, by filtering out scatter and by intensifying the image. A companion screen, fitted on the back side of the sensor, also acts positively to reinforce the image forming process and minimize backscattered radiation.

The lead screen is not used for light alloy weldments because, with aluminum and other light metals, the softer radiation must reach the sensor unimpeded to yield an adequate contrast range through the material. A screen on the back side of the sensor, however, acts positively and is often used. In this position, it contributes to latent image exposure (1) by electron intensification and (2) by blocking secondary radiation (backscatter). Such radiation is always lower in energy when compared to the primary beam; if not stopped, it could cause general image fogging. The specifications in *ASME Boiler and Pressure Vessel Code*<sup>2</sup> require that a lead character B be present on the back of the cassette as evidence that a screen was used. If a significant amount of backscattered radiation impinges on the wrong side of the cassette, the B is imaged.

## Section Thickness

The quality of any radiography is very much dependent on the object's effective section thickness. A simple geometric concept governs here; the farther the zone of interest is from the film or other detector, the less distinct the shadow will be. This is a very real effect. The result is a moderate loss of resolution when a thick weld is considered and the effect can be very pronounced when complex shapes are involved, such as some forms of corner and T joints. The image quality indicator image becomes very important as a monitor and the radiographic procedure must make it clear that the image quality indicator should not be positioned where it would yield misinformation. It is often required to position the image quality indicator on the top surface of the part, creating the largest unsharpness in the image quality indicator image.

The ultimate sensitivity is not expected to be constant over a wide range of weldment thicknesses. The sensitivity parameter is presented as a percentage of the object thickness. See Table 1 for a

comparison of plaque and wire image quality indicator sizes.<sup>1</sup> Specifications that present acceptance limits for radiography also present the scaling of the acceptable indication sizes.

---

## Identifying Welds and Images

Because a radiograph is a permanent reference of a weldment's condition, it is usually required that the finished image be traceable to the specific joint. This need is generally met with a marking system consisting of lead characters that appear clearly on the image through the thickness range involved. As evidence that coverage is complete, records made at the time of the radiography must adequately show how to match the image (1) to the weld, (2) to the location on the weld and (3) to the position of the sensor plane and the beam direction of the original exposure. Careful marking and record keeping are necessary, especially if checks are made later to determine whether some condition is developing into a significant discontinuity.

Devices that mark by imprinting an image from the radiation must be considerably more dense than the material under study. Lead is commonly used for overprinting on steel and such numbers, letters and symbols are available in many sizes and thicknesses. On very thick welds, even quite thick lead markers can virtually disappear on the image; they can be mounted on a block of steel or sheet of lead. A similar case exists when a weld specimen is smaller in area than the sensor plane. If the numbers are thin, they could disappear in the image and should be positioned on a separate lead shim or on a shim of thickness similar to that of the weld material.

In ASTM E 94, *Recommended Practice for Radiographic Testing*, there are suggestions for the type of information that should be retrievable from image marking systems.<sup>14</sup>

In large radiographic projects, a few simple identifying numbers are not sufficient for permanent reference; on occasion the image identity scheme could require as much storage medium (either in bytes or as part of the film mass) as the weld zone itself. There are refined coding systems that print information on the image using visible light as the exposure medium. These systems have the disadvantage of being indirect compared to the identity scheme using lead characters exposed simultaneously on the radiograph.

For some welds, the area of interest is not limited to the weld metal. For example, a form of cracking can occur

adjacent to a weld, rather than directly in the weld. The identifying symbols must be positioned so as not to obscure a possible discontinuity.

With light materials, identifying the image with lead characters is quite easy because of the difference in density between low density materials (such as aluminum) and lead.

---

## Film Handling

All of the standard precautions for film handling apply when radiographing welds. Extreme care should be taken in loading, unloading and handling the film cassette. Cleanliness is essential for screens and during the processing phase.

During exposure, the film seems safe in its cassette, yet there can be mishandling at this stage too. A special case for welds occurs when a high weld bead, coupled with a heavy load, imposes on the film a pattern (pressure mark) that will be visible after processing.



## PART 5. Standards and Specifications for Radiographic Testing of Welds<sup>1</sup>

There is much published material on radiographic testing, its controls and limits of acceptance. Publications are available with specific information on radiographic testing as it applies to weldments. The welds in question are means of joining metal products, including (1) pressure vessels, boilers and heat exchangers, (2) buildings, industrial structures and bridges, (3) ships and marine structures, (4) transmission pipelines, (5) industrial pipe, (6) storage tanks, (7) rail vehicles, (8) machinery, (9) aircraft and spacecraft and (10) road vehicles. [See elsewhere in this volume for more about standards for radiographic testing.](#)

A specification is a document that states in some detail the requirements of the test method and techniques. The source of such a specification is usually the buyer of the product. Instead of composing a complex technical document, such a buyer could choose a particular standard document that adequately covers the particular method.

A standard is a published specification, test technique, classification or practice that has been prepared by an issuing body. To satisfy the needs of a contract, a standard or parts of a standard can function as a specification.

A code is a collection of related standards and specifications given the force of law by government regulation. An example is the *ASME Boiler and Pressure Vessel Code*,<sup>2</sup> which consists of many specifications covering pressure vessels, their manufacture and inspection, their licensing and their inservice inspection; it incorporates scores of ASTM standards.<sup>15</sup> Another example is the *National Building Code of Canada*, incorporating Canadian Standards Association design standards, Canadian Standards Association welded construction requirements and construction safety measures to ensure public safety in buildings.<sup>16</sup>

The ASTM standards do not presume to set acceptance standards for radiography because these vary according to the product. The *ASME Boiler and Pressure Vessel Code*<sup>2</sup> contains such limits, as does the American Welding Society's *Structural Welding Code*<sup>3</sup> and the American Bureau of Shipping's *Rules for Building and Classing Steel Vessels*.<sup>4</sup> Piping and pipelines are covered by the American Society of

Mechanical Engineerings' piping standards<sup>8,17</sup> and by API 1104, *Standard for Welding Pipelines and Related Facilities*.<sup>6</sup> For storage tanks refer to American Waterworks Association's D100, *Welded Steel Tanks for Water Storage*,<sup>18</sup> and API 650, *Standard for Welded Steel Tanks for Oil Storage*.<sup>9</sup> Requirements for rail vehicles refer to the AWS Standard D1.1 already mentioned.<sup>3</sup> Machinery is typically incorporated into existing standards. A typical standard that could apply to road vehicles is AWS D14.3/D14.3M, *Specification for Welding Earthmoving and Construction Equipment*.<sup>19</sup>

For aircraft and aerospace, specifications are more specialized. ASTM E 2104, *Standard Practice for Radiographic Examination of Advanced Aero and Turbine Materials and Components*,<sup>20</sup> covers some important test situations. Standards have been issued by the National Aeronautics and Space Administration and by the United States Department of Defense. Since the 1990s, however, many United States military standards have been superseded by standards of SAE International and ASTM International. MIL-STD-453C, *Inspection, Radiographic*,<sup>21</sup> for example, has been superseded by ASTM E 1742.<sup>13</sup>

### Radiographic Requirements for Welds in Selected Standards

The radiographic testing of welds in particular is covered by ASTM E 1032, *Standard Test Method for Radiographic Examination of Weldments*.<sup>22</sup> Although there is some commonality in the standards cited for the radiographic control of welds, there is variation in the acceptance limits. For the method and control, respectively, it is normal to see a reference to ASTM E 94, *Recommended Practice for Radiograph Testing*,<sup>14</sup> and ASTM E 142, *Standard Method for Controlling Quality of Radiographic Testing*.<sup>11</sup> The acceptance limits are, not unnaturally, associated with the type of product involved, so those products that are deemed more critical will carry more stringent requirements.

The acceptance criteria are usually expressed in graded words and numbers,

occasionally with a graphical presentation as a backup for estimating the extent of porosity. Where porosity charts are included, there is also an absolute limit based on total area and individual diameters.



## PART 6. Radiography of Weld Discontinuities<sup>1,23,24</sup>

### Crack Detectability in Steel Weld Specimens<sup>23</sup>

#### Background

Whenever penetrating radiation is used to search for discontinuities in solids, an appropriate exposure technique must be established. Variables governing the exposure, such as kilovoltage, milliamperage, time and distance, must be judiciously selected to exceed minimum test sensitivity requirements. The effect that each variable has on overall sensitivity is generally understood and appreciated. However, overall test sensitivity is often judged on the visibility of holes in image quality indicators (penetrameters) and such judgment can be misleading. For example, how closely does the flat, pancake shaped hole of the indicator simulate a thin canyon shaped crack? Was it ever intended to do this? Perhaps not, yet the indicator is understood to communicate a 2 percent discontinuity detectability level, regardless of the shape of the discontinuity itself, to all who can see the 2T hole.

It was known from earlier work<sup>25</sup> that the recording of an image of a crack or a cracklike discontinuity on a radiograph was a more exacting task than was generally acknowledged. It was also suspected that the image of a crack on any given medium might not necessarily be observable when the image of the 2T hole in the image quality indicator was visible.<sup>25</sup> These observations motivated the review of exposure variables to understand better how crack detectability sensitivity related to overall test sensitivity.

Kilovoltage and radiation source positioning were chosen as the exposure variables that earlier studies<sup>25-27</sup> had indicated as having the greatest effect on crack detectability. Since cobalt-60 and iridium-192 were the two isotopes most commonly used for radiographic purposes, each was selected to supplement the energy range of the X-ray generating equipment, producing high energy test data.

The effects of energy level and radiation source position changes on crack detectability were evaluated on an

actual crack in a steel weld. The weld was machined in steps to present various crack depths on the radiographs. Steel plates were added progressively beneath this cracked wedge until the crack image was no longer discernible on the image. Both X-radiation and gamma radiation were used and standard image quality indicators were added to correlate crack detectability with indicator sensitivity. Detectability parameters were established for the various energies and positions used.

#### Test Object

A cracked steel weld, supplied by the Subcommittee for Nondestructive Testing of Unfired Pressure Vessels of the American Society of Mechanical Engineers (ASME), was used for these tests. It had been fabricated as part of a proposal to have this specimen used in an investigation of the effectiveness of radiographic techniques.

Originally, two double beveled plates measuring  $152 \times 483$  mm ( $6.0 \times 19.0$  in.) by 38 mm (1.5 in.) thick were butt welded and purposely cracked during welding. The bottom of the welded assembly was machined to expose the crack along the full length of the weld. It was then machined to the configuration observed in Fig. 13. Widths of the crack were measured at the bottom surface of the crack using a visual measuring comparator with  $6\times$  magnification. The following values represent an average of the widths found at each of the four machined steps: (1) 1.59 mm (0.063 in.) deep, 0.08 mm (0.003 in.) wide; (2) 3.18 mm (0.125 in.) deep, 0.08 mm (0.003 in.) wide; (3) 4.76 mm (0.188 in.) deep, 0.09 mm (0.0035 in.) wide; (4) 6.35 mm (0.25 in.) deep, 0.127 mm (0.005 in.) wide.

An approximation of the cross sectional shape of the crack was obtained by photographing the end view of the crack at the end of the weld closest to the 1.59 mm (0.063 in.) thick portion of the test object. Figure 14 is a tracing of this photograph. Note this crack closely resembles two parallel 0.79 mm (0.031 in.) deep cracks, radiographically, because of the severe bend it exhibits. The crack presents a mere  $75\text{ }\mu\text{m}$  (0.003 in.) reduction in radiation path length through the test plate along the horizontal portion of the bend. This is

much less than two percent of the radiation path and would not be expected to show.

Different thicknesses of smaller steel plates were used as filler plates and placed on top of each of the four sections of cracked weld so that the four steps would be equal in total crack-plus-filler thickness.

A series of eight ASTM image quality indicators was placed on top of the filler plates, facing the radiation. Slits measuring 0.25 mm (0.010 in.) by 6.35 mm (0.250 in.) were cut into each image quality indicator in an attempt to relate slit visibility, in addition to hole visibility, with crack detectability. One image quality indicator in each series was the correct thickness for the total thickness of steel under test. The seven additional image quality indicators were used to determine the precise level of hole and slit sensitivity existing whenever a crack detectability limit was reached.

### Exposure and Film Processing Controls

The following parameters remained constant throughout the testing.

**Isotope Source Collimation.** The cobalt and iridium sources were used directly, without collimation, to duplicate extreme field conditions when collimation was not feasible.

**Screens.** A combination of 0.13 mm (0.005 in.) thick front and 0.25 mm (0.010 in.) back lead screens was used to conform to the standard practice of the industry.

**Film Type.** An industrial X-ray film was used that had both very fine grain size characteristics and relatively fast exposure speed.

**Film Density.** The exposures were calculated to produce a resultant film density of 2.0. This figure is usually accepted as a suitable level for film interpretation.

**Film Processing.** A 240 s (4 min) drying cycle was established to expedite testing results. A conventional industrial X-ray film processor was modified to obtain this faster processing.

**Solutions.** To ensure consistent and uniform film and solution compatibility, the same developer and fixer were used and temperature was held constant at 31 °C (88 °F) throughout the tests.

### Testing Procedure

The cracked weld, with the filler plates installed, was radiographed at five separate energy levels. At each level, steel plates were added in 1.59 mm (0.063 in.) thick increments beneath the full length

FIGURE 14. End view of crack in test object.<sup>23</sup>

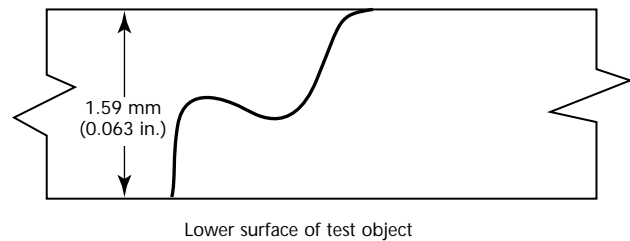
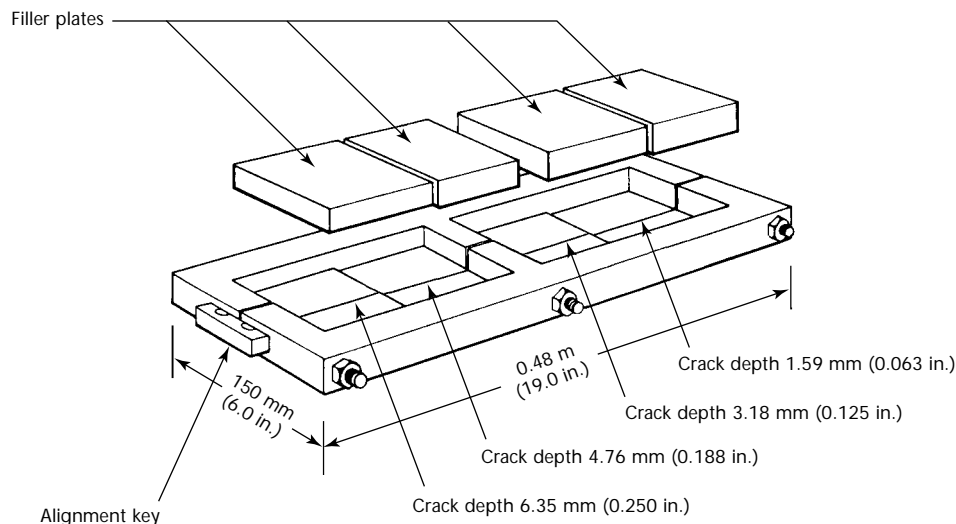


FIGURE 13. Radiographic test object. Cracked weld used for natural crack threshold determinations.<sup>23</sup>



of the weld. Exposures were made at each new thickness and this process continued until the image of a 1.59 mm (0.063 in.) deep crack was no longer distinguishable on the radiograph. The 1.59 mm (0.063 in.), or shallowest, crack was chosen as the standard for these tests so that the penetration of the total thicknesses of steel required for crack obliteration would fall within the practical working range of the X-ray equipment.

In addition, many different source angles were used at each energy level to determine effect of angle on the detection of the shallowest crack. Plates were again added, at each angle, until the crack became undetectable to the radiographer. The angles were measured as degrees of inclination from the vertical or central portion of the beam, which was considered to be zero degrees. The radiation source-to-sensor distance increased slightly as the angle of inclination increased. All sources were shifted laterally at a constant 914 mm (36.0 in.) level; however, the X-ray tube was also angled toward the crack. Earlier work<sup>25</sup> indicated that such relatively minor changes in source-to-film distance had no appreciable effect on crack detectability. This lateral approach provides a more precise way to duplicate critical source angles using conventional industrial equipment.

The resultant film radiographs were reviewed by experienced radiographers to determine limits of crack detectability for each energy level and source position. This limit was expressed as the maximum number of thicknesses  $t$  of steel (each thickness was equal to the depth of the crack) that could be placed in the path of radiation, along with the cracked plate, without losing the image of the crack.

To relate these  $t$  values to the familiar concept of image quality indicator detectability, it would require 50  $t$  to produce a crack depth-to-thickness added ratio of 1:50, the detectability level of standard, 2 percent, hole type image quality indicators.

The  $t$  values were used to calculate crack detectability sensitivity as follows:

$$(1) \quad \frac{\text{Crack detectability}}{\text{sensitivity}} = \frac{d_c}{t + d_c}$$

The image quality indicator (IQI) hole and slit sensitivities at each  $t$  value are calculated as follows:

$$(2) \quad \frac{\text{Hole sensitivity}}{\text{sensitivity}} = \frac{\text{Thinnest IQI thickness with visible 2T hole}}{\text{Thickness under penetrometer}}$$

$$(3) \quad \frac{\text{Slit sensitivity}}{\text{sensitivity}} = \frac{\text{Thickness of thinnest IQI with visible slit}}{\text{Thickness under IQI}}$$

## Test Results

Table 2 lists the  $t$  values found at the various energy levels and source angles. Table 3 shows the results of the sensitivity calculations.

None of the  $t$  values reported in Table 2 approached the 50  $t$  limit, indicative of 2 percent image quality indicator hole sensitivity, but the values themselves might be used as crack detection thresholds for exposure technique determinations. For example, to detect a 1.59 mm (0.063 in.) crack in 51 mm (2.0 in.) of steel (32  $t$  total), an energy level at or close to 250 kV and a near zero source angle must be used. If only iridium-192 was available as a source of radiation, this same crack could be detected whenever the total thickness to be penetrated was 23.8 mm (0.88 in.) or less and the source was positioned directly over the crack.

All of the sensitivity calculations were based on a 1.59 mm (0.063 in.) deep crack, although the crack more closely resembled a 0.79 mm (0.0313 in.) crack radiographically because of the severe bend it exhibited at nearly this distance up from the lower surface (Fig. 14). The test crack was considered to be a 1.59 mm (0.063 in.) deep crack because it was probably the cross sectional shape that would be most difficult to detect radiographically.

If the sensitivity calculations had been based on a 0.79 mm (0.031 in.) crack depth, all but three of the crack detectability sensitivity levels in the X-ray energy range would have been 2 percent or less and these three exceptions were at the extreme source position angles of 17 and 30 degrees. If the percent

TABLE 2. Limits of detectability obtained for 1.6 mm (0.063 in.) deep crack in steel are expressed as thicknesses of steel that can be placed with cracked plate in radiation path without losing crack image, where  $t$  = crack depth.

Energy Level	Radiation Source Angle (degrees inclination)			
	0	8	17	30
250 kV	31 $t$	31 $t$	28 $t$	27 $t$
275 kV	29 $t$	26 $t$	25 $t$	24 $t$
300 kV	28 $t$	25 $t$	24 $t$	19 $t$
Iridium-192	14 $t$	12 $t$	11 $t$	11 $t$
Cobalt-60	8 $t$	8 $t$	7 $t$	5 $t$

sensitivity of an X-ray passing through a 0.08 mm (0.003 in.) wide slit were calculated at these extreme angles as a ratio of the distance traveled through the air gap of the slit to the travel distance through sound metal, then these three sensitivity levels would have been 2 percent or less, as well.

Although none of the crack detectability sensitivity values approached the 2 percent level, a generally accepted level of overall test sensitivity,<sup>28</sup> there is no inexplicable loss of sensitivity. Radiation travels in straight lines and penetrates significant amounts of metal by passing in and out of the side walls of the crack before it reaches the sensor. Accordingly, there is less of a difference in the intensity of radiation reaching the sensor between the cracked and uncracked areas than there would have been if the crack had been a smooth, straight walled slit or image quality indicator hole. It is these differences in intensities that are recorded as images of the crack and slit or hole; therefore, it is only a less than expected change in the intensity of the emerging radiation in the cracked area that occurs and not a loss of test sensitivity.

An examination of the image quality indicator thickness listed in Table 3 shows that all but two of the thicknesses listed for hole type image quality indicators within the X-ray energy range are identical at 0.38 mm (0.015 in.) thickness.

Similarly, with iridium-192, the 2T hole in a 0.45 mm (0.0175 in.) thick image quality indicator is always visible along with the test crack. With cobalt-60, the 0.51 mm (0.020 in.) thick image quality indicator is visible. From these data the rudiments of a positive correlation can be seen forming between the visibility of a 2T hole in a thinner (than 2 percent of the metal it is placed on) image quality indicator and crack detectability.

## Conclusions

The image of the 2T hole in the image quality indicator whose thickness was correct for the thickness of steel being radiographed would always be discernible on the image on which the crack was no longer visible. This meant the 2T hole in the correct 2 percent thick image quality indicator could not be considered as a reliable indicator of a 2 percent crack depth detectability level.

The slit also could be readily shown on the correct 2 percent thick image quality indicator after an image of the crack had disappeared. The slit, in fact, reacted more like a line of fine, aligned porosity to radiation and became easier to detect than the 2T hole. It too was not a reliable indicator of 2 percent crack depth detectability sensitivity.

Crack detectability did increase as the energy level decreased, as was evidenced by the increasing *t* values in Table 2.

TABLE 3. Crack detectability and image quality indicator sensitivity.

Energy Level	Source Position (degree)	t Value		Total Thickness		Image Quality Indicator				Sensitivity		
		mm	(in.)	mm	(in.)	Hole		Slit		Crack (percent)	Hole (percent)	Slit (percent)
250 kV	0	49.19	(1.938)	50.76	(2.000)	0.38	(0.0150)	0.32	(0.0125)	3.23	0.750	0.625
	8	49.19	(1.938)	50.76	(2.000)	0.38	(0.0150)	0.38	(0.0150)	3.23	0.750	0.750
	17	44.42	(1.750)	46.02	(1.813)	0.38	(0.0150)	0.38	(0.0150)	3.57	0.827	0.827
	30	42.84	(1.688)	44.42	(1.750)	0.38	(0.0150)	0.32	(0.0125)	3.71	0.857	0.715
275 kV	0	46.02	(1.813)	47.59	(1.875)	1.97	(0.0775)	0.38	(0.0150)	3.45	0.932	0.800
	8	41.24	(1.625)	42.84	(1.688)	0.38	(0.0150)	0.32	(0.0125)	3.85	0.885	0.740
	17	39.67	(1.563)	41.24	(1.625)	0.38	(0.0150)	0.32	(0.0125)	4.00	0.923	0.768
	30	38.07	(1.500)	39.67	(1.563)	0.38	(0.0150)	0.32	(0.0125)	4.18	0.960	0.800
300 kV	0	44.42	(1.750)	46.02	(1.813)	0.44	(0.0175)	0.44	(0.0175)	3.57	0.963	0.963
	8	39.67	(1.563)	41.24	(1.625)	0.38	(0.0150)	0.38	(0.0150)	4.00	0.922	0.922
	17	38.07	(1.500)	39.67	(1.563)	0.38	(0.0150)	0.38	(0.0150)	4.18	0.958	0.958
	30	30.15	(1.188)	31.73	(1.250)	0.38	(0.0150)	0.32	(0.0125)	5.27	1.200	1.000
Iridium-192	0	22.21	(0.875)	23.81	(0.938)	0.44	(0.0175)	0.38	(0.0150)	7.15	1.865	1.600
	8	19.04	(0.750)	20.63	(0.813)	0.44	(0.0175)	0.38	(0.0150)	8.32	2.150	1.845
	17	17.46	(0.688)	19.04	(0.750)	0.44	(0.0175)	0.44	(0.0175)	9.10	2.330	2.330
	30	17.46	(0.688)	19.04	(0.750)	0.44	(0.0175)	0.38	(0.0150)	9.10	2.330	2.000
Cobalt-60	0	12.69	(0.500)	14.29	(0.563)	0.51	(0.020)	0.51	(0.020)	12.5	4.000	4.000
	8	12.69	(0.500)	14.29	(0.563)	0.51	(0.020)	0.51	(0.020)	12.5	4.000	4.000
	17	11.12	(0.438)	12.69	(0.500)	0.51	(0.020)	0.51	(0.020)	14.3	4.560	4.560
	30	7.94	(0.313)	9.52	(0.375)	0.51	(0.020)	0.51	(0.020)	20.0	6.380	6.380

A decrease in the source position angle also increased crack detectability, again as evidenced by increasing  $t$  values in Table 2.

The cross sectional shape, or directional changing, of the crack in a plane parallel to the direction of radiation affects crack detectability.

Standard hole type image quality indicators may be used to measure the technique's ability to provide cracklike indications. Within the 250 to 300 kV X-ray energy range, the 1.59 mm (0.063 in.) crack was visible whenever the 2T hole in a standard image quality indicator 0.38 mm (0.015 in.) thick was visible. At iridium and cobalt energies, the 2T holes in the 0.45 mm (0.018) and 0.51 mm (0.020 in.) thick image quality indicators, respectively, were reliable indicators of the detectability of a 1.59 mm (0.063 in.) crack.

## Typical Weld Joint Discontinuities<sup>21</sup>

To conduct an effective test, it is necessary for the inspector to understand the circumstances of manufacturing and service and to know what to look for.

For any test process, realistic standards of acceptability must be established. These standards will depend on many aspects of the welded component, such as its application to the base material and its cost. Because the perfect weld has never existed and only degrees of weld perfection are obtainable, the following examples of weld discontinuities are presented.

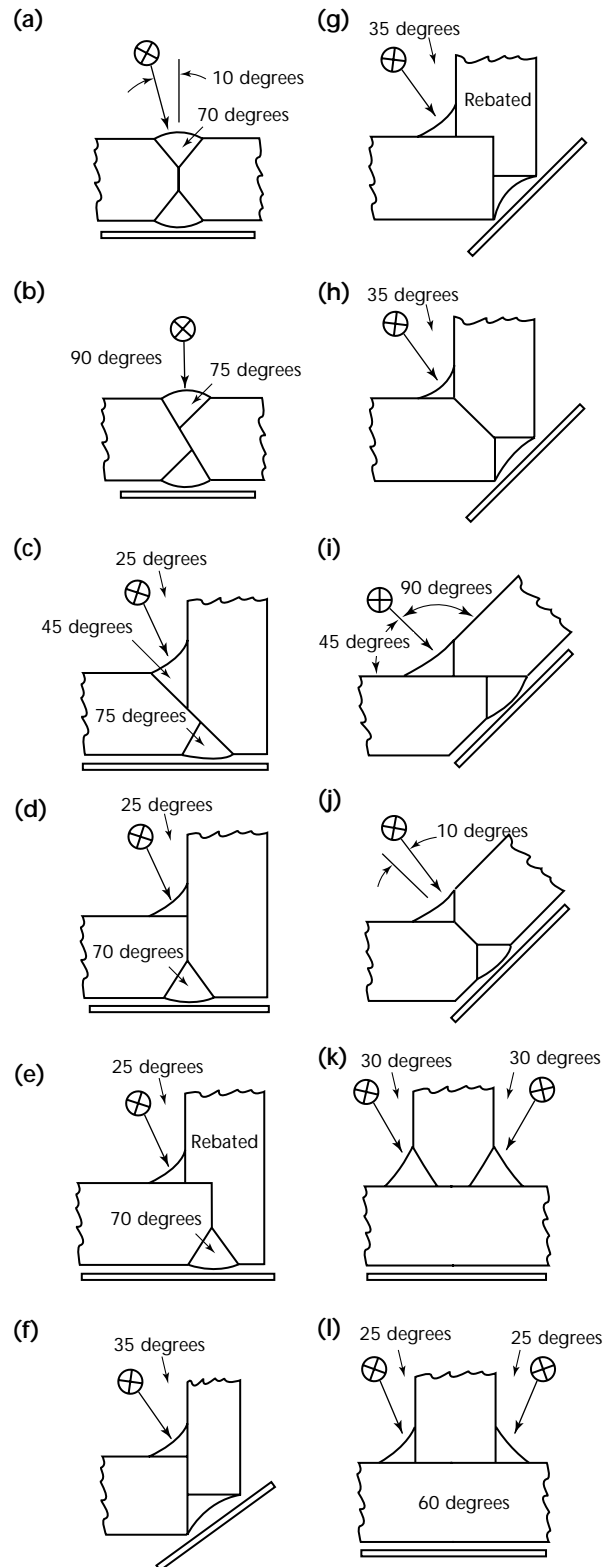
Figure 15 shows the recommended radiographic procedures for partial penetration weld joint designs. Partial penetration welds differ from full penetration welds and require more care when being radiographed to ensure complete or maximum weld coverage with minimum interference from the normal unfused weld joint land. Figures 16 and 17 illustrate radiation angles for two typical weld joint designs.

The joint may be incomplete for various reasons. Figure 18 shows gas cavities in an aluminum weld. Figures 19 and 20 show incomplete penetration in aluminum and steel welds, respectively. Figures 21 and 22 show lack of fusion in aluminum and steel welds, respectively.

Figure 23 shows ungraded conditions (discontinuities that are not due to welding process but do affect weld quality) in aluminum welds — poor plate fitup and cleaning brush bristle inclusions.

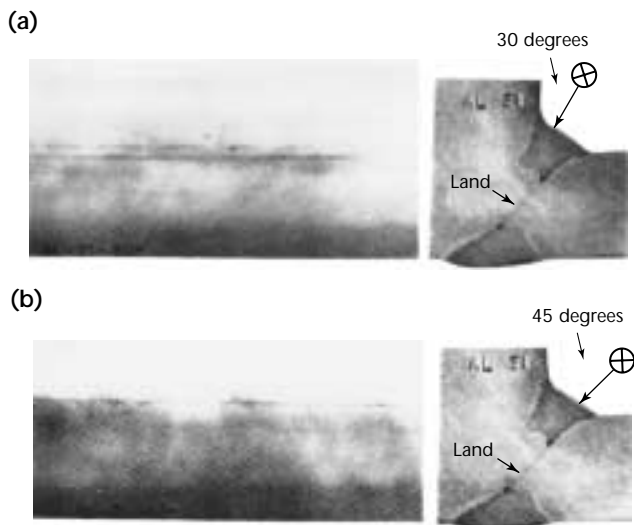
Porosity is frequently visible in weld radiographs. Figure 24 shows fine

FIGURE 15. Recommended radiographic procedures for partial penetration joint designs: (a) double V groove; (b) offset double V groove; (c) corner; (d) corner; (e) corner; (f) corner; (g) corner; (h) corner; (i) 135 degree corner; (j) 135 degree corner; (k) T joint with groove; (l) T joint.<sup>24</sup>





**FIGURE 16.** Correct and incorrect radiographic procedure for joint design in Fig. 15c: (a) correct procedure, incomplete penetration at both roots separated from land image; (b) incorrect procedure, incomplete penetration in line with land image and cannot be evaluated.<sup>24</sup>



**FIGURE 17.** Correct and incorrect radiographic procedure for joint design in Fig. 15a: (a) correct procedure, incomplete penetration at both roots separated from land image; (b) incorrect procedure, incomplete penetration in line with land image cannot be evaluated.<sup>24</sup>

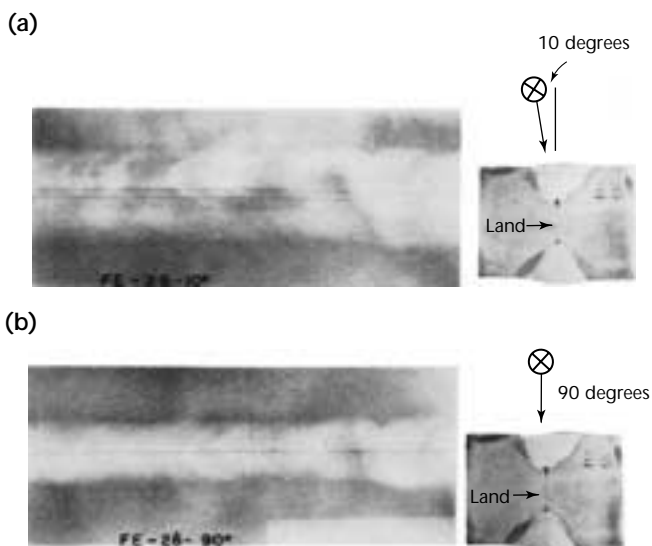


**FIGURE 18.** Reference standards for gas cavities in aluminum welds: (a) cross section of joint in Fig. 15a, showing gas cavity; (b) 2-1T sensitivity; (c) standard 1; (d) standard 2.<sup>24</sup>

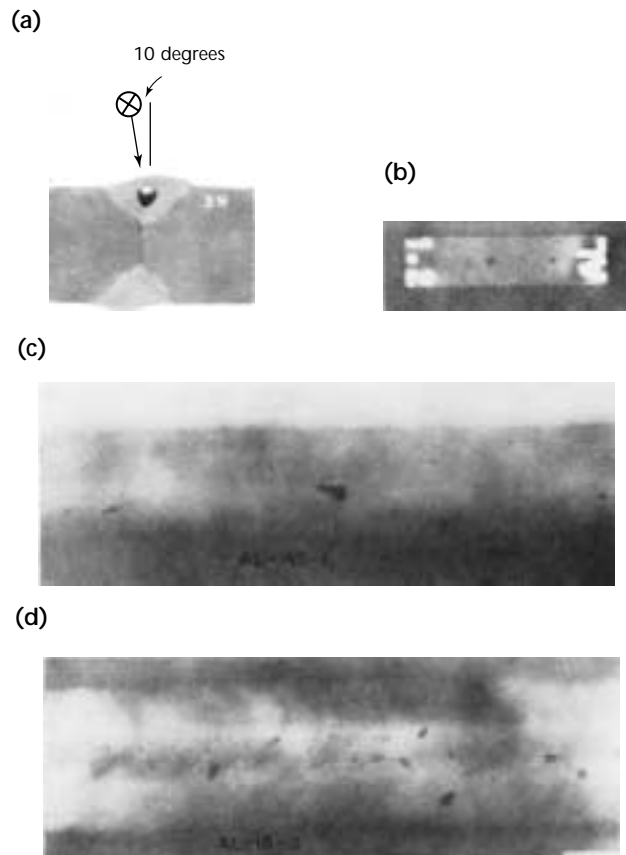


**FIGURE 19.** Examples of incomplete penetration correlated with weld cross sections in aluminum welds: (a) joint in Fig. 15c, incomplete penetration due to welding gun misalignment, and lack of fusion also present; (b) joint in Fig. 15b, 60 degrees, incomplete penetration resulting from low current setting.<sup>24</sup>

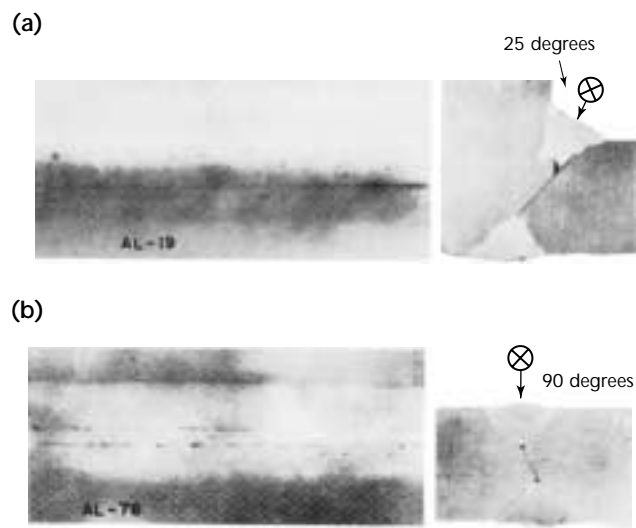




**FIGURE 20.** Varying degrees of incomplete penetration in steel welds correlated with weld cross sections: (a) slight condition normal for joint in Fig. 15b made with stick electrode; (b) moderate condition in joint in Fig. 15c resulting from too large electrode on root pass; (c) gross condition in joint of Fig. 15a, resulting from low heat and too large electrode.<sup>24</sup>

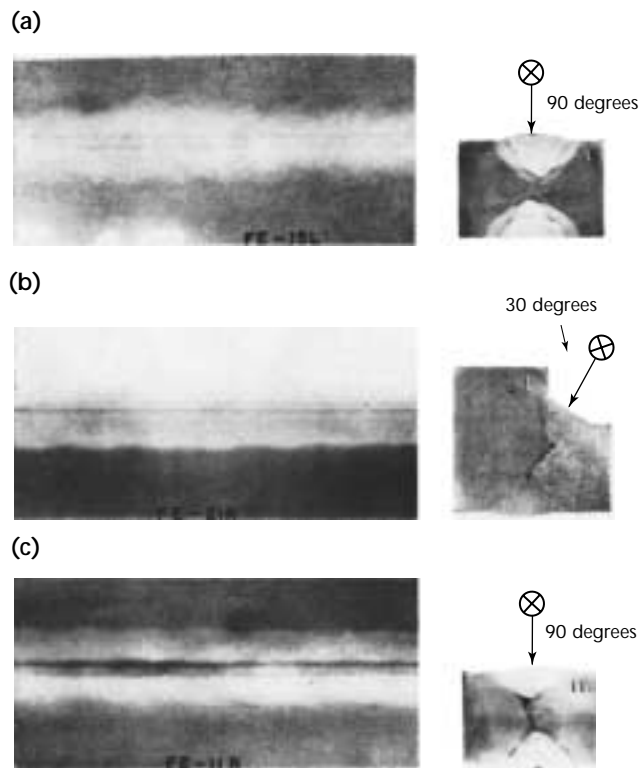


**FIGURE 21.** Examples of lack of fusion correlated with cross sections of aluminum welds: (a) lack of fusion, resulting from welding gun misalignment; (b) lack of fusion, resulting from low current setting.<sup>24</sup>

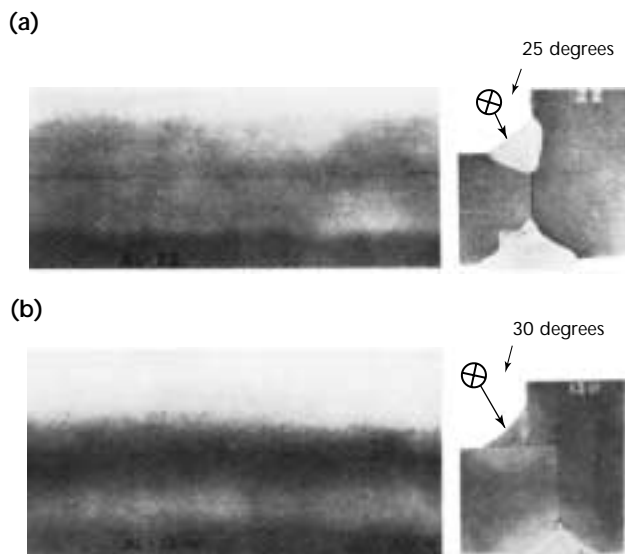


**FIGURE 22.** Examples of lack of fusion in steel welds, correlated with weld cross sections: (a) lack of fusion caused by trapped slag in joint of Fig. 15a; (b) slag trapped in sharp notches made by high crown bead in joint of Fig. 15b; (c) severe condition due to poor gun angle and sharp notch in joint of Fig. 15a.<sup>24</sup>

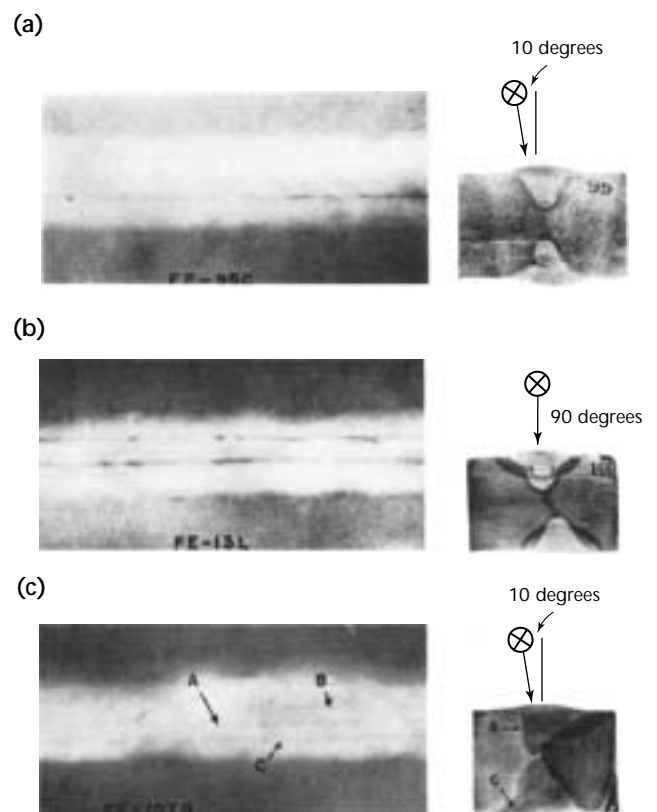


**FIGURE 23.** Examples of ungraded conditions correlated with weld cross sections in aluminum welds: (a) plate separation, appearing similar to incomplete penetration; (b) wire inclusion trapped during cleaning operation.<sup>24</sup>

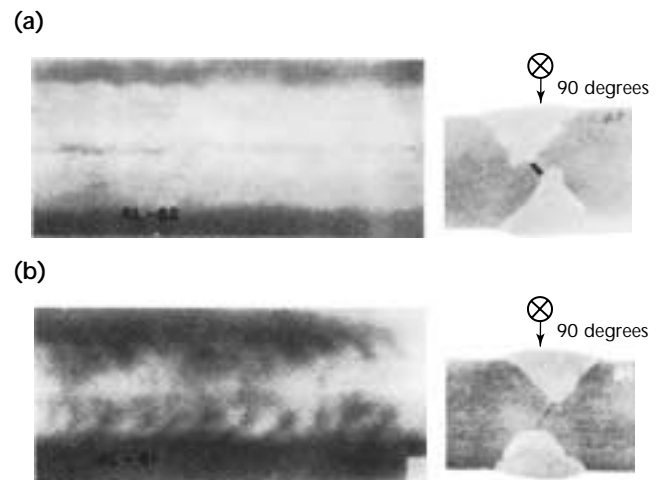


**FIGURE 24.** Reference standards for fine scattered porosity in steel welds: (a) cross section of fine scattered porosity in joint of Fig. 15b; (b) 2-1T radiographic sensitivity; (c) standard 1, about 1 pore per 1 cm<sup>2</sup> (6 pores per 1 in.<sup>2</sup>); (d) standard 2, about 2 pores per 1 cm<sup>2</sup> (12 pores per 1 in.<sup>2</sup>).<sup>24</sup>

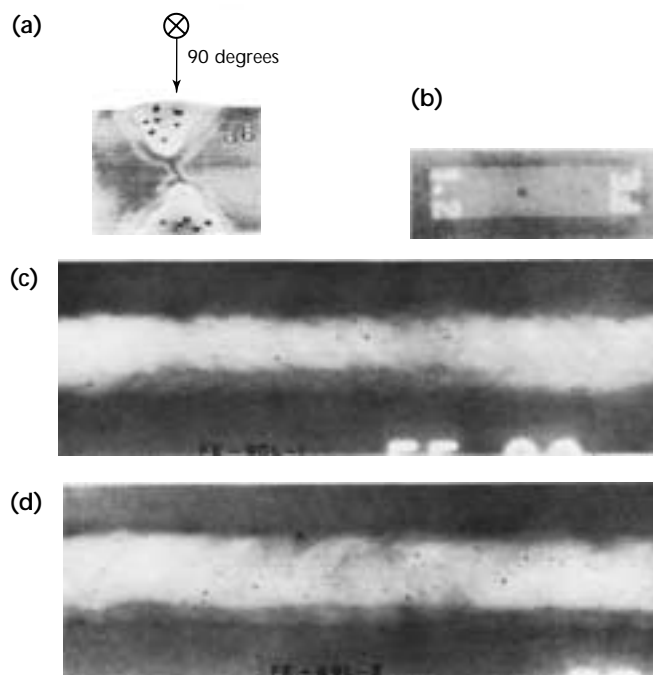


**FIGURE 25.** Reference standards for coarse scattered porosity in steel welds: (a) cross section of coarse, scattered porosity in joint of Fig. 15b; (b) 2-1T sensitivity; (c) standard 1, about 0.3 pore per 1 cm<sup>2</sup> (2 pores per 1 in.<sup>2</sup>); (d) standard 2, about 0.7 pore per 1 cm<sup>2</sup> (4 pores per 1 in.<sup>2</sup>).<sup>24</sup>

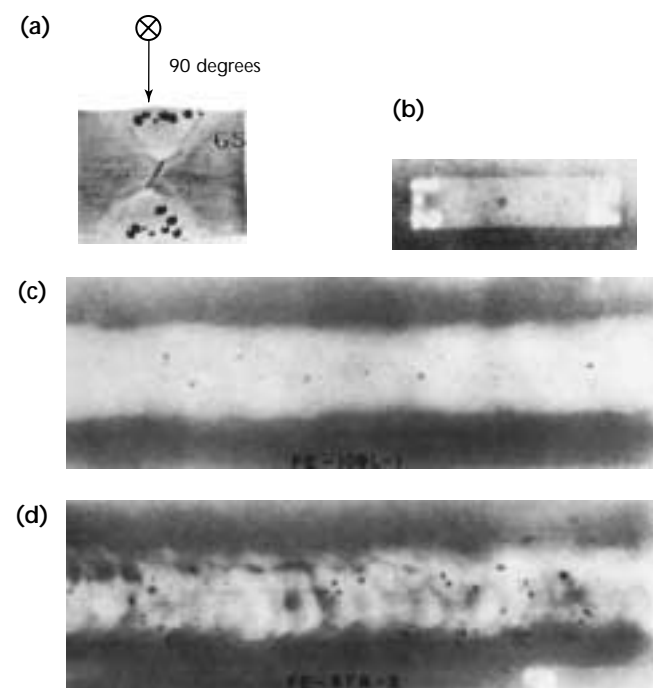


**FIGURE 26.** Reference standards for linear porosity in steel welds: (a) cross section of linear porosity in joint of Fig. 15a; (b) sensitivity 2-1T; (c) standard 1; (d) standard 2.<sup>24</sup>

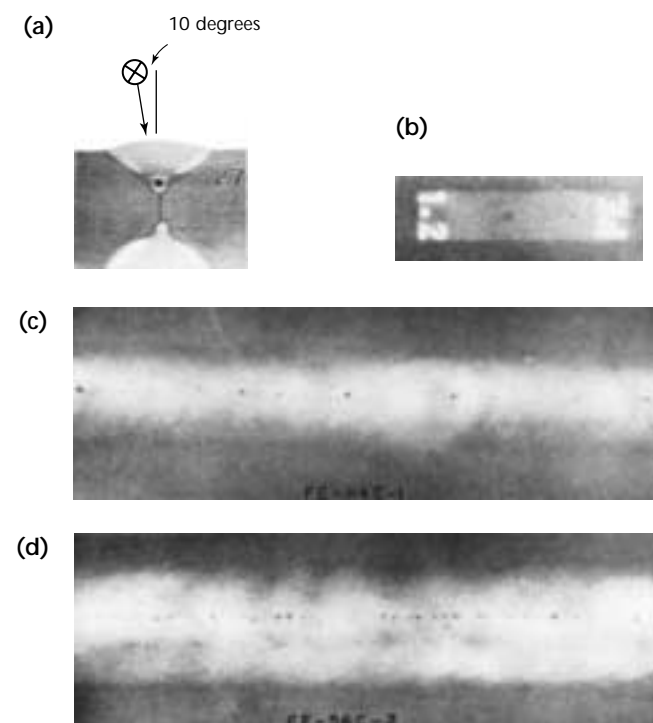
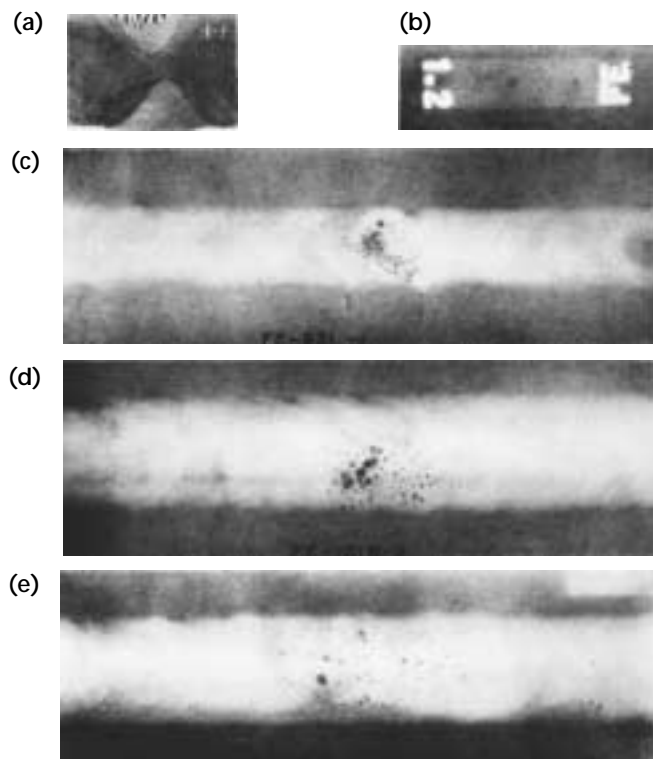


**FIGURE 27.** Reference standards for clustered porosity in steel welds: (a) cross section; (b) 2-1T sensitivity; (c) standard 1; (d) standard 2; (e) standard 3.<sup>24</sup>



scattered porosity in steel welds. Figure 25 shows coarse scattered porosity in steel welds. Figure 26 shows linear porosity and Fig. 27 shows clustered porosity in steel welds. Figure 28 shows scattered slag inclusions in steel welds for two intensity levels.

### Selected Pipe Weld Discontinuities<sup>1,29</sup>

Selected pipe weld discontinuities are reproduced in Figs. 29 to 34. With some images an iridium-192 radiograph shows the identical discontinuity in projection. Discontinuities were deliberately introduced into the specimens, which were based on 250 mm (10 in.), schedule 80 stainless steel pipe, designation type 316. The complete report also includes a comparison of ultrasonic testing indications, with photographs of the response signals.<sup>29</sup> Additional illustrations of pipe welding discontinuities can be found in the chapter on radiographic interpretation.

**Arc Strikes.** Arc strikes (Fig. 29<sup>29</sup>) are disturbances left on the surface of the base metal where a welder has momentarily touched an arc welding

electrode to start the arc. Arc strikes can cause failure of the affected material. These failures initiate at the abnormal structural conditions produced by the arc strike. The careful welder strikes the arc in the joint where the base metal will be melted by penetration, as the operation progresses beyond the striking point. The welder may also use a scrap of metal as a starting tab or use a high frequency arc starter. Severe metallurgical conditions can exist when the careless welder makes an arc strike on the surface of the base metal adjacent to the weld and then quickly moves the electrode into the joint to perform the welding operation. Arc strikes often harbor minute cracks, porosity and hard zones. Arc strikes are damaging primarily for heat treatable carbon steels and high strength alloyed steels. Mild carbon steel is practically unaffected.

**Drop-Through.** Weld drop-through (Fig. 30<sup>1,29</sup>) is an undesirable sagging or surface irregularity at the weld root, usually encountered when the welding

FIGURE 28. Reference standards for scattered slag inclusions in steel welds: (a) cross section showing slag inclusion in joint of Fig. 15b; (b) sensitivity 2-1T; (c) standard 1; (d) standard 2.<sup>24</sup>

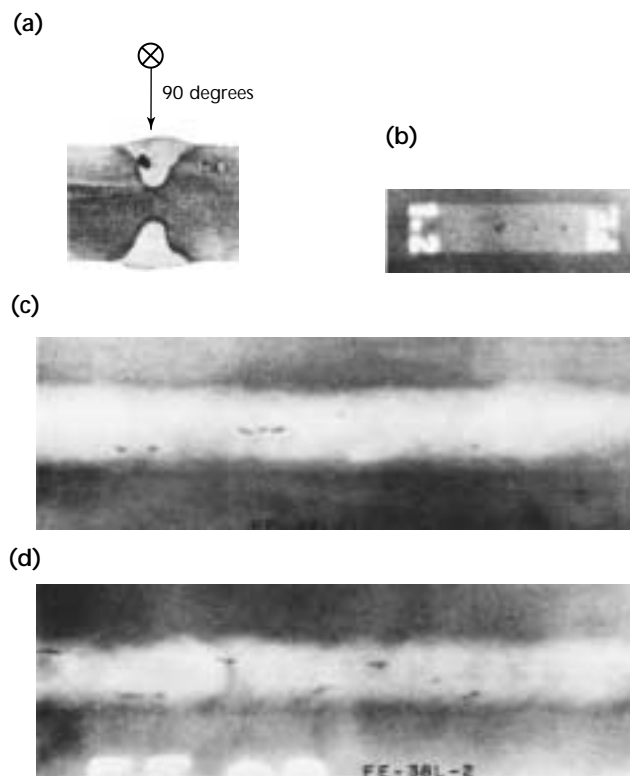


FIGURE 29. Arc strike: (a) photomacrograph at 2 $\times$ ; (b) radiograph at 1 $\times$ .<sup>29</sup>

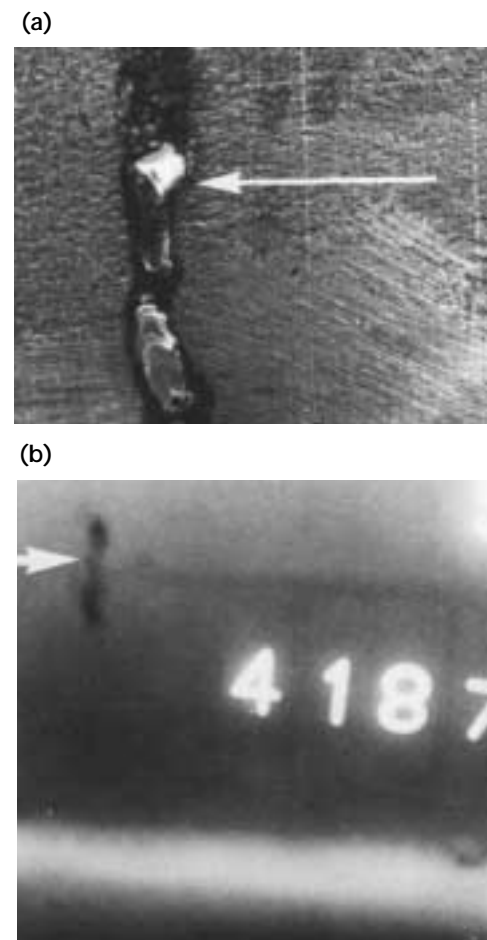


FIGURE 30. Drop-through:  
(a) photomacrograph at 4 $\times$ ; (b) radiograph at 1 $\times$ .<sup>29</sup>

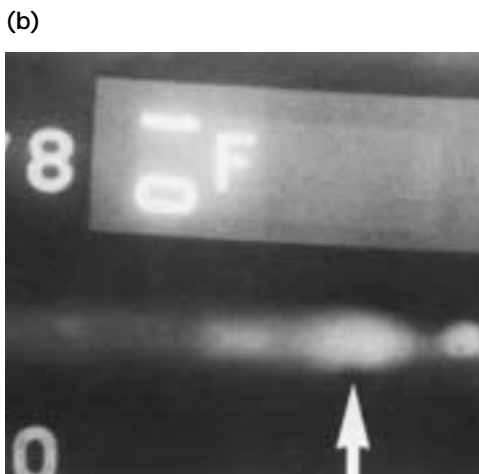
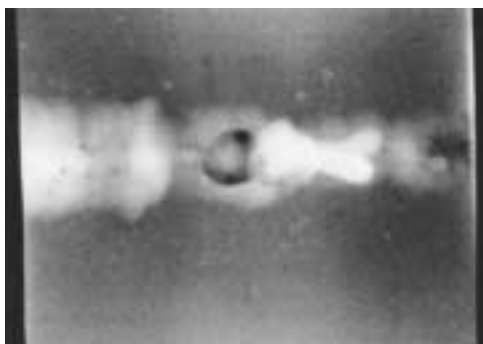


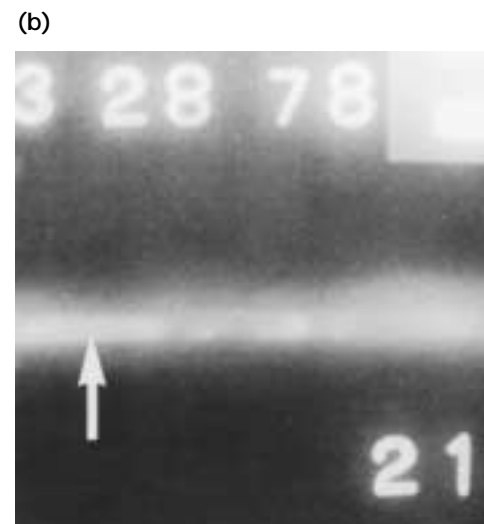
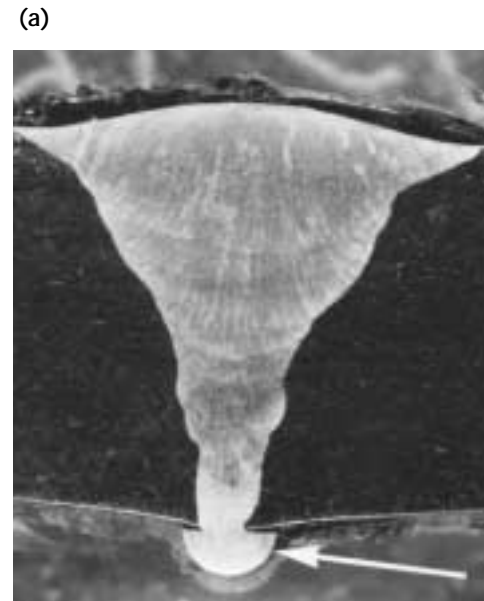
FIGURE 31. Radiograph of severe case of drop-through.



amperage is too high for the rate of travel, causing overheating of the weld joint and bead deposit. Drop-through is characterized by excessive root bead width and a slumping of weld metal on the back side of the weld. The condition in Fig. 31 is much more severe, as evidenced by the weld material hanging inside the pipe wall. The droplet shape is easily identified, together with the cavity remaining after the material was dislodged. Figure 31 shows a pipe with diameter of 150 mm (6.0 in.) and wall thickness of 11 mm (0.43 in.).

**Unconsumed Insert.** An unconsumed insert (Fig. 32<sup>29</sup>) results from preplaced filler metal that is not completely melted and fused in the root joint. This condition

FIGURE 32. Unconsumed Insert:  
(a) photomacrograph at 4 $\times$ ; (b) radiograph at 1 $\times$ .<sup>29</sup>

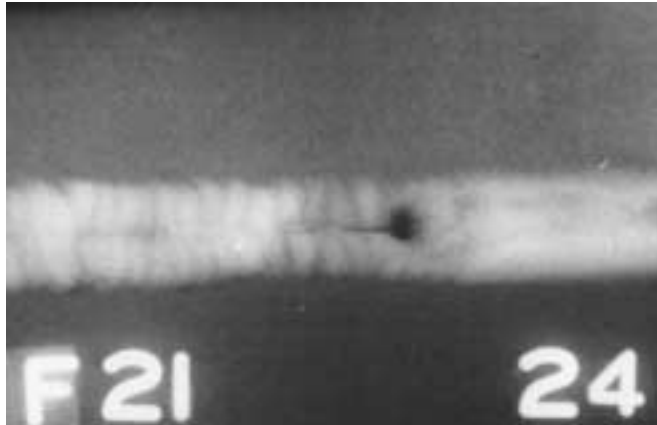


is caused by low welding current, improper electrode manipulation, improper joint design and improper welding speed. Considerable welder technique and skill must be developed to ensure high quality root beads when using inserts with the gas tungsten arc welding process. Proper welding parameters and sufficient skill of the welder will produce melting and fusion of the insert and the side walls of the joint preparation. This results in a satisfactory root bead profile.

**Incomplete Penetration.** Figure 33 illustrates a major blowhole with associated incomplete penetration in a large stainless steel pipe. The bead shape, which changes from a smooth to a rippled form, further shows that there was a

perturbation in the welding process, such as a change in heat input or speed. The image is a contact shot of an object measuring 400 mm (16.0 in.) in diameter and 10 mm (0.37 in.) in wall thickness. Figure 34 portrays what is probably a case of 100 percent incomplete penetration around a butt joint in a pipe. The image shows about 80 percent of the pipe diameter. A very uniform indication extends along the weld centerline. It seems to disappear toward the edges of the image but this is the section in which poor projection geometry prevails, so that the effective wall thickness, as seen by the beam, increases very rapidly. The image demonstrates the loss in image definition as the optical conditions degrade. The pipe measures 150 mm (6.0 in.) in diameter and 11 mm (0.43 in.) in wall thickness.

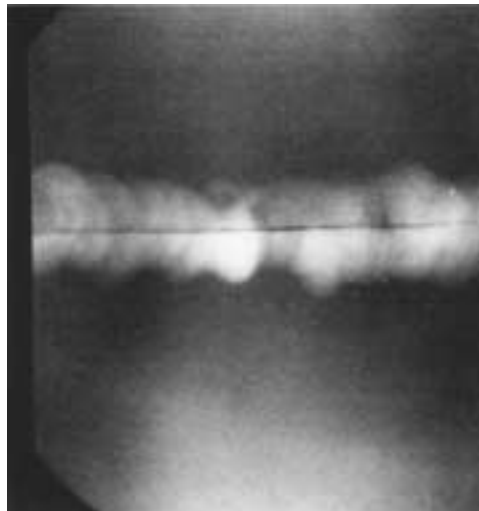
FIGURE 33. Radiograph showing blowhole and associated incomplete penetration.



## Closing

Weldments are often subjected to high pressure, high temperature and cyclic loading. These stresses are usually strongest in structures that can least tolerate the possibility of failure (nuclear reactors, for example). Because of the variety of welding techniques and the variety of joined materials, nondestructive testing of welds is difficult but vitally important.

FIGURE 34. Radiograph showing indication of continuous incomplete penetration.





## PART 7. In-Process Radioscopy of Arc Welding<sup>30–32</sup>

### Introduction<sup>30,31</sup>

Two different approaches may be applied to the nondestructive testing of welds. The conventional one consists in the application of nondestructive testing after welding without relation to the process itself. The second, new, approach is in-process nondestructive inspection, in which the production and testing operations are integrated into a single procedure. In this combined approach, information received from nondestructive testing may be used in feedback with other process parameters for process control. Such a concept gives significant cost savings.<sup>33</sup> Because the nondestructive testing system is included as a part of the sensing system in the feedback loop of the process control, the quality control is integrated with the process itself.

The ultimate goal of welding process control is to achieve good weld quality and high weld productivity. Different control techniques for automated welding have been used to reach this goal<sup>34,35</sup> but lack of direct information on weld quality has been a weak point in these techniques. A different approach to solve this problem is *in-process nondestructive inspection*, which aims to integrate radioscopic nondestructive testing techniques with welding process control techniques. Such an approach may improve weld quality and provide significant cost reduction.<sup>33</sup>

The dynamic nature of the arc welding process and the different types of weld discontinuities produced during arc welding create difficulties for radioscopic quality control. For real time application of radiography to weld process control, the acquisition and processing of information must be fast enough to extract useful features before any major change occurs in the welding process. This prohibits some sophisticated but slow image processing algorithms.

One approach is to use radioscopy as a vision system in remote arc welding process monitoring.<sup>30</sup> Direct information on weld penetration extracted from real time radiographic images of the solidified weld has been used in feedback to adjust the welding conditions to maintain weld quality.<sup>36</sup> The disadvantage of this technique is the time (and space) delay in extracting information on weld

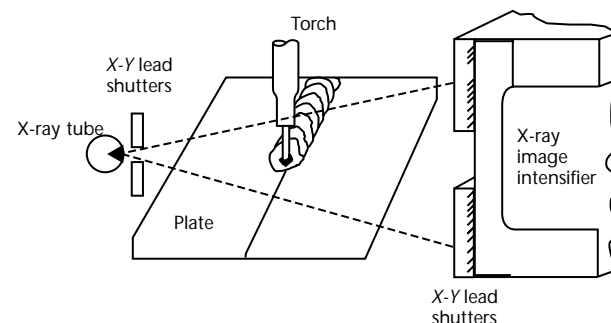
penetration. The delay leads to the appearance of small weld areas with lack of penetration.

In another technique, weld penetration is controlled by radiographic information on weld pool depression to eliminate the time delay — thus providing feedback before weld solidification.<sup>31</sup> Integration of weld quality control with welding process control is achieved by in-process radiographic information on the depression of the butt joint welding pool and the weld properties in the solidified areas. During the welding process, the welding conditions are automatically controlled to maintain the required pool depression and, hence, weld penetration. Butt joint weld penetration in the solidified weld is simultaneously tested by extracting information from real time radiographic images in the area of the welding path behind the liquid pool. This information is also used in feedback for weld process control. Butt joint weld quality maintenance and penetration control have been demonstrated.

### Experimental Concept<sup>30</sup>

Two system setups for radioscopic observation of the welding process are one horizontal (Fig. 35) and one vertical (Fig. 36). In the horizontal setup, the X-ray beam is oriented parallel to the welded piece and the image intensifier receiver is positioned on the side. This setup is appropriate for studying metal and flux transfer and solidification of the

FIGURE 35. Horizontal setup for radioscopic observation of metal and flux transfer and solidification in welding process.





weld pool. Testing in this position usually requires soft X-rays (about 30 to 50 kV peak) and therefore a miniature X-ray unit may be used.

In the second, vertical, setup, the X-ray beam is perpendicular to the weld surface or at small angles to the welding torch. This configuration is appropriate for studying discontinuity formation in the weld (cracks, cavities and porosities) and for monitoring lack of fusion and weld penetration. Weld pool dynamics and weld penetration may also be studied and monitored in this configuration of the system. The energy of the X-ray required in this case is determined by the penetration requirement and is usually higher than in the horizontal case. In this setup, the X-ray unit was mounted above the welding piece and the image intensifier was mounted below it.

The radiosopic unit may be used not only for online quality control but as a vision system in feedback control of the welding power supply or used for manual remote control.

The radiographic monitoring method is distinguished from optical monitoring in two ways: (1) there is no effect of the welding arc on visibility and, more important, (2) internal discontinuities of the weld and weld penetration are visible and therefore complete information on weld quality is available for weld control. Also, welding processes such as submerged arc welding are accessible by this technique.

Automatic weld quality and process control is also possible in the framework of the radiographic method. In this approach, the radiosopic image is digitized and analyzed by computer. The welding electrode position can be observed in the image together with the

depressed welding pool and the welding gap. Therefore, one branch of control may include tracking and torch positioning algorithms that will control the welding manipulator.

A second branch of control is weld quality control. Here the digitized image is analyzed by different pattern recognition algorithms for identification of weld quality and type of weld discontinuities (if they exist). Next, information on weld characteristics is fed to the decision algorithm. Information from other sensors is also accumulated in this unit for analyzing weld current, voltage and other parameters. Here the appropriate schedule for changing the welding parameters should be established: for example, appropriate current and weld speed.

## Radioscopic Control of Arc Weld Penetration<sup>31</sup>

Change of welding conditions such as current, voltage and speed of welding can affect the thickness and width of the weld reinforcement and penetration. They also determine the existence and depth of incomplete weld penetration. The lack of weld penetration lowers the weld bearing capacity and hence is a discontinuity that may be considered a weld defect.

An example of a frozen image (one frame) from sequences of radiosopic images taken during submerged arc welding is shown in Fig. 37. As usual in radioscopy the image is represented in

FIGURE 36. Vertical setup for radiosopic observation of welding process monitors formation of discontinuities (cracks, cavities and porosity) and monitors lack of fusion and weld penetration.

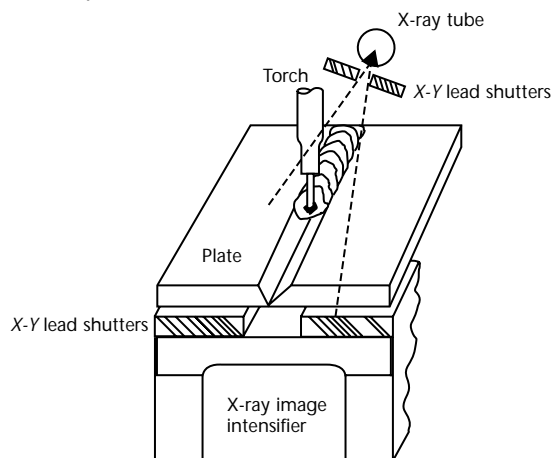
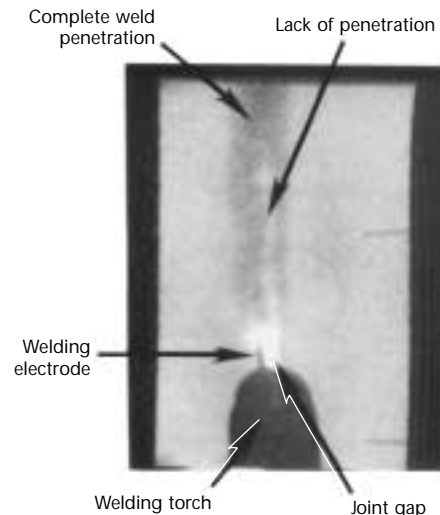


FIGURE 37. Example showing one frame of radiosopic image of submerged arc welding. Lack of weld penetration is due to incorrect position of welding electrode relative to joint gap.



positive form rather than as a film image. The base metal, the weldment and the melted pool are shown in the image. The weld and the pool are covered by the welding flux and by molten flux (slag). However, the flux affects an image only slightly because of its low density. The dark region in the center of the image is the weld. The upper part of this region corresponds to the weld with complete penetration. The lower part corresponds to the weld with inadequate penetration, seen as a long light strip along the joint. The lower dark area with the semicircular shape is the welding gun; the welding wire can also be seen. In front of the welding gun is the joint gap, a totally white area. The gray area surrounding the weld is the base metal.

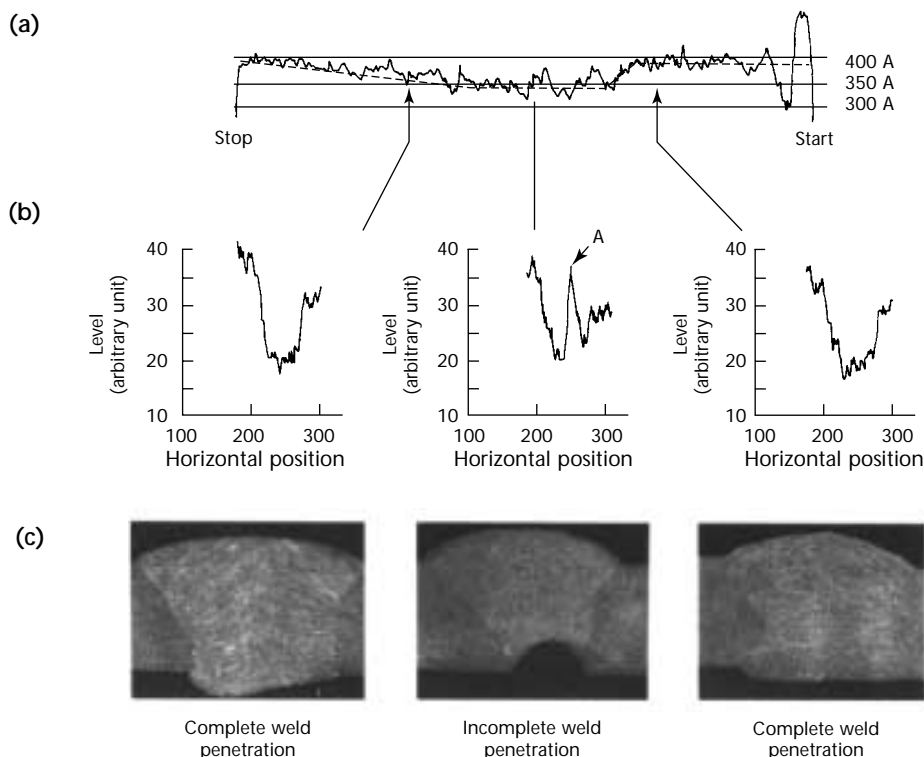
The radiographic images were digitized in real time at the speed of 30 frames per second. To establish a relation between a gray value of a pixel and the actual thickness of the material, the apparatus was calibrated by measuring, for a given X-ray intensity, the output brightness level as a function of material thickness. The weld profile (weld reinforcement and depth of weld penetration) was measured from radiographic images. Such measurements showed good agreement with actual measurements from metallographs of the weld cross sections.

Visual observation of radiosopic images and the digital information on depth of weld penetration received from these images were used for process control of the weld. For this, the welding current was adjusted in such a way that full penetration occurred. An example of the results of such an experiment is summarized in Fig. 38. Figure 38a shows the welding current and Fig. 38b shows the image profiles. These profiles show the changes of the values of the gray levels along a particular horizontal line of the digitized image. The deep, wide minimum of the profile corresponds to the weld's increased thickness due to weld reinforcement.

Figure 38c shows microphotographs of the weld cross sections corresponding to the image profiles. At a welding current of about 390 A, full weld penetration is observed. This follows from the image profile and is supported by the photograph of the weld cross section, both shown in the rightmost column.

When the current is reduced to 340 A, there is incomplete weld penetration, indicated by the peak on the image profile. The corresponding weld cross section is shown below in the middle column. The information on incomplete weld penetration can be extracted by computer from the appearance and height

FIGURE 38. Remote process control: (a) welding current; (b) image profiles; (c) microradiographs corresponding to image profiles in Fig. 38b.



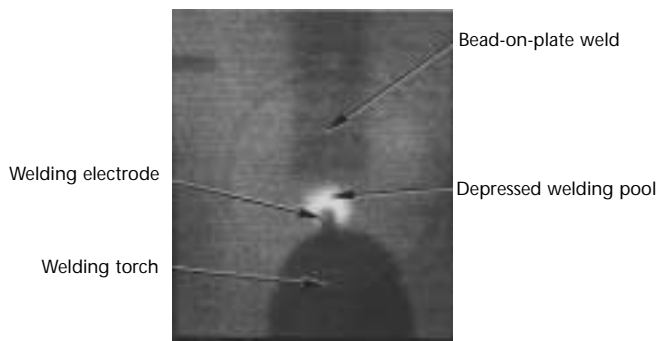
of the profile peak. The depth of the weld penetration was calculated from the height of this peak. If the incomplete penetration occurs, the welding current must be increased. When the current is increased above 360 A, the peak disappears, indicating full penetration, as shown on the microphotograph of the corresponding weld cross section.

## Radioscopic Weld Penetration Control with Feedback on Weld Pool Depression<sup>32</sup>

Above was described the technique of automatic control of weld penetration. In that technique the weld was monitored at some distance behind the welding pool.<sup>36</sup> The time (and space) delay in extraction of information on weld penetration leads to the appearance of small areas of weld with lack of penetration. The technique discussed next is free from this disadvantage. In this technique the control of weld penetration is accomplished by radiographic information on pool depression in system feedback for bead-on-plate and butt welds.

Figure 39 shows one frame from a sequence of radiographic images of a molten pool of a bead-on-plate (no weld joint) weld taken during submerged arc welding. The image is positive, therefore a thinner section of the depressed weld pool is represented as a lighter area. The welding torch and welding electrode are seen in the bottom of the image. The circular white area in front of the welding torch is the welding pool. The solidified weld and the molten pool are covered by the welding flux and by the molten flux (slag). However, the flux affects an image

**FIGURE 39.** One frame of radioscopic image of bead-on-plate depressed molten pool. X-ray tube voltage 150 kV, tube current 10 mA, welding arc current 410 A, arc voltage 30 V, welding speed 11.0 mm·s<sup>-1</sup> (0.43 in·s<sup>-1</sup>).



only slightly because of its low density and thickness. The gray area surrounding the weld is the base metal.

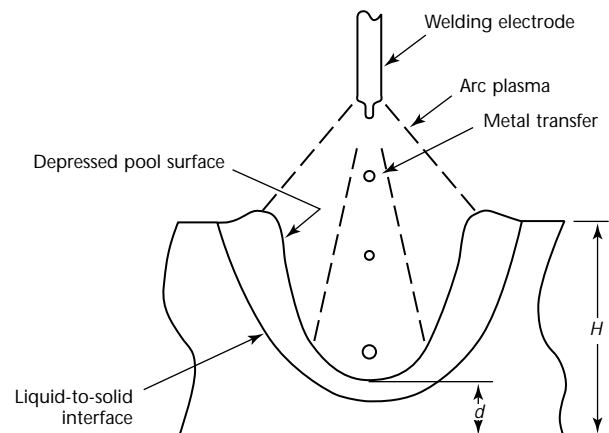
Figure 40 is the schematic showing the consumable welding electrode, electric arc, metal transfer, depressed pool surface, liquid pool, weld penetration and base metal.  $H$  is the plate thickness and  $d$  is the thickness of liquid and solid metal together at the bottom of the welding pool. Because of the heat of the arc, which melts the plate, and the arc pressure on the molten pool, the welding pool is depressed during welding and the material thickness is reduced from  $H$  to  $d$ . The depressed pool surface becomes deeper and wider when a higher welding current is used because of the expansion of the welding arc at a higher current.

In Fig. 40, because of the thinner material under the welding arc, the attenuation of X-rays is less in the welding pool area than in the surrounding base metal. Hence, it is seen as a lighter area on a positive radiographic image (Fig. 39). The material thickness can be reconstructed from the image by knowing the brightness level and the X-ray attenuation coefficient. The relation between the brightness level and the material thickness in this work is obtained experimentally. This three-dimensional information on the welding pool helps characterize weld penetration.

## Depression and Weld Geometry<sup>32</sup>

Knowledge of the relation between weld penetration and pool dimensions is necessary to control weld penetration using the method described. Weld penetration could be changed by

**FIGURE 40.** Cross section showing welding electrode, depressed pool surface and liquid-to-solid interface.



### Legend

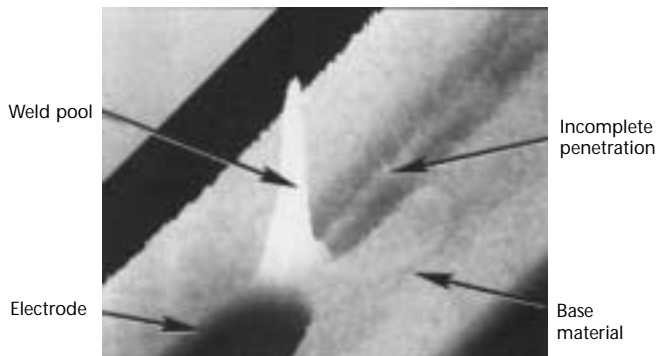
$d$  = thickness of solid and liquid metal at bottom of welding pool  
 $H$  = plate thickness

changing the welding current. A greater welding current resulted in a larger pool diameter and deeper weld penetration. As an example, three-dimensional radiographic images of a welding pool are shown in Fig. 41. Light areas correspond to reduced thickness of the material; peaks are images of the depressed pool. The brightness of the welding pool area means that molten metal was pushed by plasma pressure away from the electrode, which also is visible in these images. When the welding current is insufficient, melting of the base metal is less intense and the light area becomes narrower. In Fig. 41a, lack of weld penetration can be seen in the solidified area behind the pool as a white stripe (indicated by an arrow in the figure). A butt weld with lack of weld penetration shows the pool diameter to be about the width of the butt weld gap.

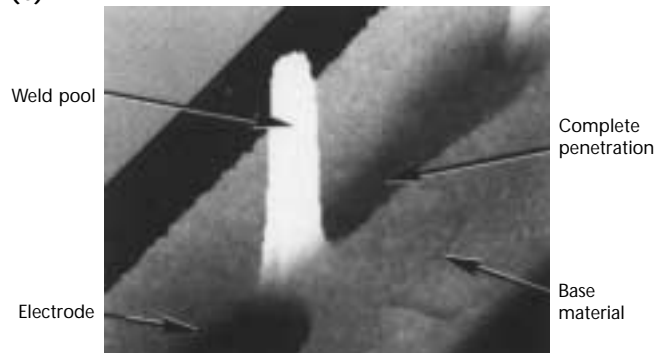
The relation between weld pool depression and weld current and arc force are described elsewhere.<sup>37,38</sup> The examples of implementation and computerized weld process control by these means are described elsewhere.<sup>31,36</sup>

**FIGURE 41.** Three-dimensional radioscopic image of depressed pool for butt weld: (a) incompletely penetrated butt weld; (b) completely penetrated butt weld.

(a)



(b)



## PART 8. False Indications in Radiographs of Aluminum Alloy Welds<sup>39</sup>

### Introduction

An indication is valid if it corresponds to a real discontinuity. *False* indications (sometimes called *ghost defects*) in aluminum alloy welds may lead to errors in radiographic interpretation. Investigations have been reported on false indications observed in radiographs of aluminum alloy welds. W.D. Rummel and B.E. Gregory<sup>40</sup> and M.S. Tucker and P.A. Larssen<sup>41</sup> report linear dark markings similar to lack of fusion in radiographs of 2014 aluminum alloy welds and indicate that these linear markings are caused by the X-ray diffraction effect from particular dendritic grain structures in the weld metals. Rabkin<sup>42</sup> also reports dark bands in radiographs of aluminum magnesium alloy welds, which correspond to the regions with increased magnesium content. Issiki<sup>43</sup> discusses the occurrence of macrostructure in a radiograph of aluminum alloy castings and its mechanism in detail. Furthermore, Irie<sup>44</sup> has shown the false indications due to grain structure in stainless steel welds.

These false indications are caused by either macro grain structure or by segregation of alloying elements. In radiographs of aluminum zinc magnesium alloy plates welded with aluminum magnesium filler metals. Another type of false indication is discussed; these discontinuities are associated with neither particular grain structures nor segregation of constituents. They appear in radiographs as linear dark markings quite similar to lack of fusion but have no influence on mechanical properties of the welds.

### Study

False indications observed in radiographs of aluminum zinc magnesium alloy plates welded with aluminum magnesium filler metals appear to be linear discontinuities such as *lack of fusion* or *undercuts*. The cause is neither a particular grain structure nor segregation of alloying elements but rather the interaction of two factors in X-ray absorption. One cause is the compositional difference between weld metal (magnesium rich) and parent metal (zinc rich); the other cause is the geometrical form and size of reinforcement of the weld beads.

False indications are observed in both ends of lapped penetrations only under a critical condition wherein the compositional effect exceeds the size effect of reinforcement. The condition is theoretically formulated as follows:

$$(4) \quad \frac{\mu_p}{\mu_w} = 1 + \left( \frac{\tan \theta}{\tan \theta_p} \right)_{x=x_1}$$

where the term at the left side is the ratio of the X-ray attenuation coefficient of parent metal  $\mu_p$  to that of weld metal  $\mu_w$  and where the second term on the right side is the ratio of gradient of reinforcement  $\theta$  to that of penetration of the fused zone  $\theta_p$  at the position  $x_1$  of the false indication.

### Chemical and Geometrical Factors of Fused Zone

From observation of a number of radiographs of aluminum zinc magnesium alloy welds, it was found that aluminum zinc magnesium alloy plates welded with aluminum magnesium filler metal exhibited the clear false indications but welds made with parent metal filler did not. When an aluminum magnesium plate and an aluminum zinc magnesium alloy plate are welded with aluminum magnesium filler metal, only one linear dark line appears in the side of the aluminum zinc magnesium alloy plate. In addition, welds with relatively high reinforcement do not always exhibit false indications.

It was also found that the false indications disappeared when the reinforcement of the weld bead was removed, as shown in Fig. 42. These facts suggest that both chemical compositions of the filler metal and geometry of the weld metal are concerned with the occurrence of the false indications.

### Analysis of False Indication

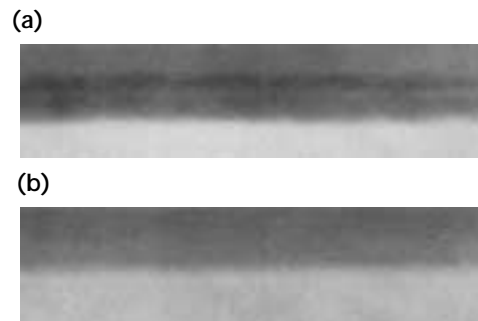
There are two factors affecting the transmitted X-ray intensity in welds. One is the constitutional factor  $F_C$ , resulting from the compositional difference between weld and parent metals, and the other is the shape or size factor  $F_S$ .

resulting from the geometry of reinforcement and penetration of welds.

Figure 43 shows a cross section of the weld. The shaded area in Fig. 44 shows the range where false indications are formed. The left end of the range ( $\tan \theta = 0$ ) corresponds to the flat welds (without reinforcement), whereas the

boundary on the right ( $F_C = F_S$  gives the critical angles of inclination of reinforcement and penetration corresponding to the visible limit of the false indication. Therefore, in the middle of the two boundary lines, there should exist the optimum condition under which the false indication will be observed most clearly.

FIGURE 42. Effect of reinforcement on ghost discontinuities in radiographs of welds made with filler metal (aluminum with five percent magnesium by weight) joining aluminum zinc magnesium (above) to aluminum magnesium (below): (a) bead on; (b) bead off.<sup>39</sup>

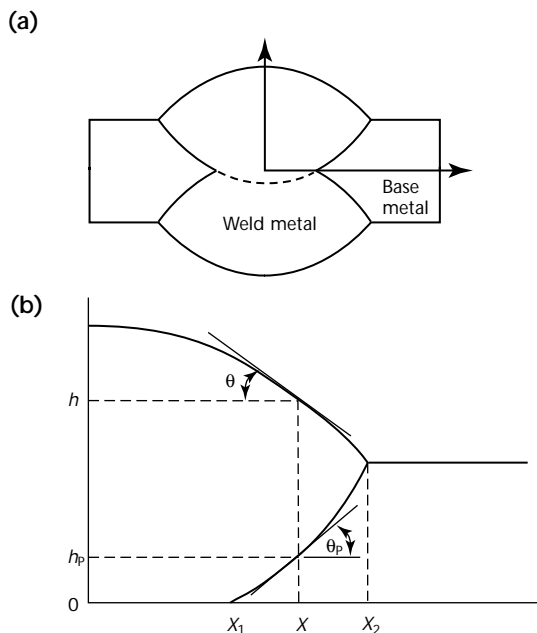


## Formation of False Indication Due to Block Model of Welds

To confirm the above hypothesis, the formation of false indications was investigated by radiography of block models. These models were composed of two kinds of wedge pieces representing the weld metal and parent metal close to the fusion zone.

Compositions of the wedge pieces representing the weld metal and parent metal were aluminum (4 percent magnesium and 2 percent zinc by weight) and aluminum (6 percent zinc and 1 percent magnesium by weight), respectively. The angle of inclination of penetration was 45 degrees and those of reinforcement were 45, 30, 15 and 0 degrees. One of the radiographs of these

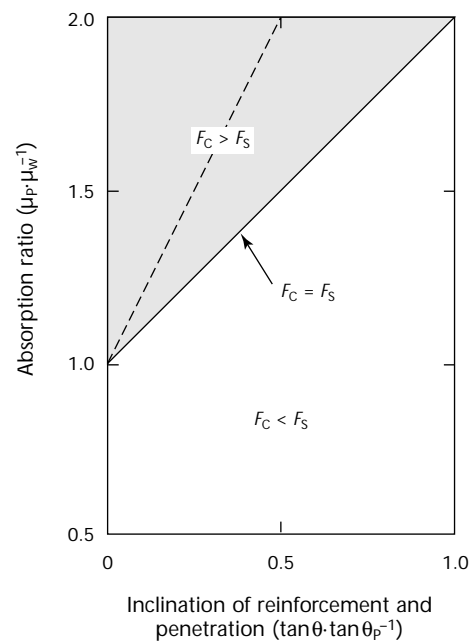
FIGURE 43. Coordinates of cross section in welds: (a) cross section of weld; (b) enlarged view of quadrant shown in Fig. 43a.<sup>39</sup>



### Legend

$h$  = height of weld metal  
 $X$  = width lapped in penetration  
 $\theta$  = Inclination of reinforcement (degrees)

FIGURE 44. Conditions for appearance of ghost discontinuities in radiographs of welds.<sup>39</sup>



### Legend

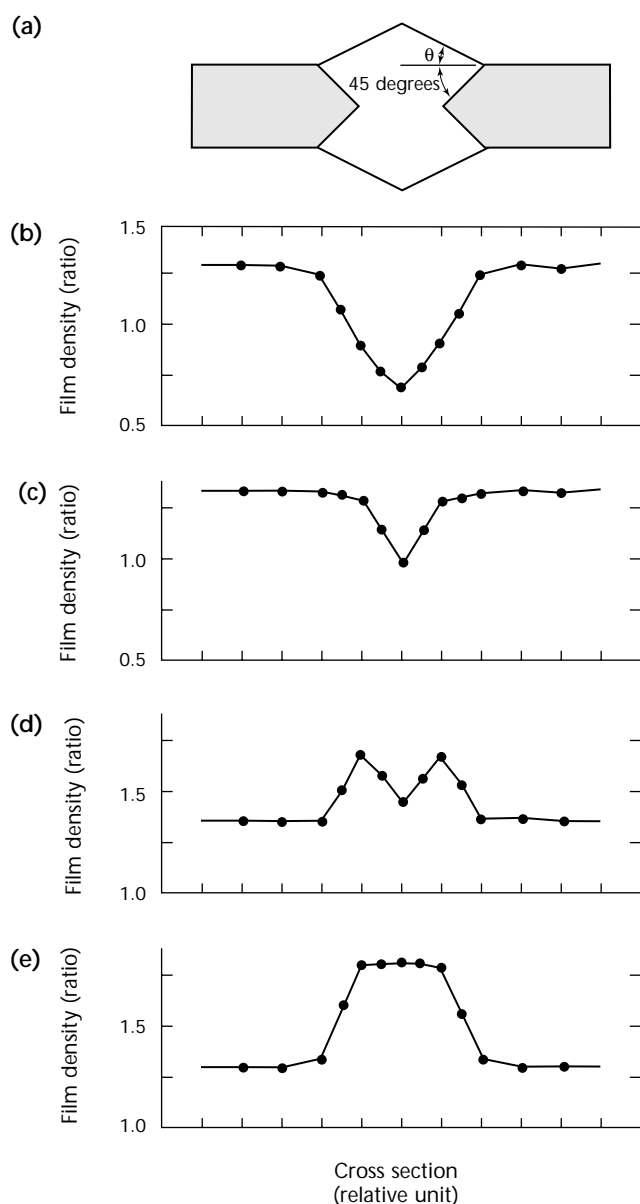
$F_C$  = constitutional factor resulting from compositional difference between weld metal and parent metals  
 $F_S$  = size factor resulting from geometry of reinforcement and penetration of welds  
 $\mu_p$  = absorption coefficient of parent metal  
 $\mu_w$  = absorption coefficient of weld metal  
 $\theta$  = angle



block models showed dark lines similar to false indications in radiographs of welds. The false indications were clearly observed as two parallel dark lines for  $\theta = 15$  degrees but were not observed for larger angles of inclination. The results of measurements of film density are shown in Fig. 45.

It is apparent from these results that the formation of false indications depends on the interaction of geometrical and constitutional factors in welds.

FIGURE 45. Film density in radiographs of block models with aluminum zinc magnesium alloy quasi welds with various angles  $\theta$  of penetration: (a) schematic diagram; (b) penetration angle  $\theta = 45$  degrees; (c)  $\theta = 30$  degrees; (d)  $\theta = 15$  degrees; (e)  $\theta = 0$  degree.<sup>39</sup>



## Discrimination of False from Valid Indications

From the cause of the formation of the false indications, it is clear that the presence of the false indications does not reduce the mechanical properties of the welded joints. The aluminum zinc magnesium alloy welds with false indications are nearly as strong as the same alloy welds without false indications and do not show large changes in mechanical properties. The slight difference of mechanical properties depends on the compositions of weld metal and not on the false indications.

As mentioned above, the false indications themselves are not harmful; nevertheless, it is quite important to judge whether the linear markings observed in radiographs are the false indications themselves or whether they contain real welding discontinuities as well as false indications. If the condition of formation of the false indication expressed is not satisfied, the linear markings are real discontinuities. If the condition is satisfied, it is very difficult to determine whether they contain real discontinuities or not. In this case, it is necessary to observe in detail the location and form of linear dark markings in X-radiographs, because false indications appear about in the middle between the bead center and the bead edge whereas weld discontinuities such as cracking, lack of fusion, undercut and others appear as comparatively sharp lines and in many cases tend to show their specific forms in radiographs.

To further discriminate between false indications and valid indications, the ultrasonic test method can be used. No ultrasonic echo should be obtained from false indications.

# References

1. Chapman, H. "Radiographic Control of Welds." *Nondestructive Testing Handbook*, second edition: Vol. 3, *Radiography and Radiation Testing*. Columbus, OH: American Society for Nondestructive Testing (1985): p 418-457.
2. *ASME Boiler and Pressure Vessel Code*. New York, NY: American Society of Mechanical Engineers (2000).
3. AWS D1.1/D1.1M, *Structural Welding Code — Steel*. Miami, FL: American Welding Society (2002).
4. ABS 2, *Rules for Building and Classing Steel Vessels*. New York, NY: American Bureau of Shipping (2001).
5. ABS 14, *Nondestructive Inspection of Hull Welds*. New York, NY: American Bureau of Shipping (1986).
6. API STD 1104, *Welding Pipelines and Related Facilities*. Washington, DC: American Petroleum Institute (1999).
7. CSA W59-M1989 (R2001), *Welded Steel Construction (Metal Arc Welding)*, metric version. Toronto, Ontario: Canadian Standards Association (2001).
8. ASME B31.1, *Power Piping*. New York, NY: American National Standards Institute (2001).
9. API 650, *Standard for Welded Steel Tanks for Oil Storage*. Washington, DC: American Petroleum Institute (1998).
10. ASTM E 1025, *Standard Practice for Design, Manufacture, and Material Grouping Classification of Hole-Type Image Quality Indicators (IQI) Used for Radiology*. West Conshohocken, PA: ASTM International (1998).
11. ASTM E 142, *Standard Method for Controlling Quality of Radiographic Testing*. West Conshohocken, PA: ASTM International (1992).
12. ASTM E 747, *Design, Manufacture and Material Grouping Classification of Wire Image Quality Indicators (IQI) Used for Radiology*. West Conshohocken, PA: ASTM International (1997).
13. ASTM E 1742, *Standard Practice for Radiographic Examination*. West Conshohocken, PA: ASTM International (2000).
14. ASTM E 94, *Recommended Practice for Radiographic Testing*. West Conshohocken, PA: ASTM International (1977).
15. *Annual Book of ASTM Standards*. West Conshohocken, PA: ASTM International (2002).
16. NRC-BLDG CODE-95, *National Building Code of Canada 1995*. Ottawa, Ontario, Canada: National Research Council Canada, Institute for Research in Construction (1995).
17. ASME B31.3, *Process Piping*. New York, NY: American National Standards Institute (2001).
18. D100, *Welded Steel Tanks for Water Storage*. Denver, CO: American Waterworks Association (1996).
19. AWS D14.3/D14.3M, *Specification for Welding Earthmoving and Construction Equipment*. Miami, FL: American Welding Society (2000).
20. E 2104, *Standard Practice for Radiographic Examination of Advanced Aero and Turbine Materials and Components*. West Conshohocken, PA: ASTM International (2001).
21. MIL-STD-453C, *Inspection, Radiographic*. Washington, DC: Department of Defense (1996). Superseded by ASTM E 1742.<sup>13</sup>
22. E 1032, *Standard Test Method for Radiographic Examination of Weldments*. West Conshohocken, PA: ASTM International (2001).
23. Becker, G.L. "Factors Governing Radiographic Crack Detectability in Steel Weld Specimens." *Materials Evaluation*. Vol. 30, No. 7. Columbus, OH: American Society for Nondestructive Testing (July 1972): p 149-152.
24. Buckrop, R.L. "What Makes a Good Weld ... and Radiography Can Prove It." *Materials Evaluation*. Vol. 30, No. 5. Columbus, OH: American Society for Nondestructive Testing (May 1972): p 25A-31A.
25. Becker, G.L. and W.T. Granett. "The Use of Crack Simulators to Assure X-Ray Inspection Technique Reliability." *Proceedings of the Sixth Symposium on Nondestructive Evaluation of Aerospace and Weapons System Components and Materials*. North Hollywood, CA: Western Periodicals Company (1967): p 533-559.
26. Criscuolo, E.L. "Slit Detection by Radiography." *Materials Evaluation*. Vol. 24, No. 4. Columbus, OH: American Society for Nondestructive Testing (April 1966): p 201-205.

27. Dutili, J.W. and G.H. Tenney. "A Preliminary Investigation of the Radiographic Visualization of Cracks." *Nondestructive Testing*. Vol. 12, No. 2. Columbus, OH: American Society for Nondestructive Testing (March-April 1954): p 13-15.
28. McMaster, R.C. "Radiographic Sensitivity." *Nondestructive Testing Handbook*, first edition. Vol. 1, Section 15. Columbus, OH: American Society for Nondestructive Testing (1959): p 31-37.
29. *NDE Characteristics of Pipe Weld Defects*. Special Report NP-1590-SR. Palo Alto, CA: Electric Power Research Institute (1980).
30. Rokhlin, S.I. "In-Process Radiographic Evaluation of Arc Welding." *Materials Evaluation*. Vol. 47, No. 2. Columbus, OH: American Society for Nondestructive Testing (February 1989): p 219-224. Erratum, *Materials Evaluation*, Vol. 47, No. 12 (December 1989): p 1424.
31. Guu, A.C. and S.I. Rokhlin. "Arc Weld Process Control Using Radiographic Sensing." *Materials Evaluation*. Vol. 50, No. 11. Columbus, OH: American Society for Nondestructive Testing (November 1992): p 1344-1348, 1356.
32. Guu, A.C. and S.I. Rokhlin. "Computerized Radiographic Weld Penetration Control with Feedback on Weld Pool Depression." *Materials Evaluation*. Vol. 47, No. 10. Columbus, OH: American Society for Nondestructive Testing (October 1989): p 1204-1210.
33. Watkins, A.D., J.A. Johnson and H.B. Smart. "Economic Evaluation of Concurrent Welding and Nondestructive Testing." *Welding Journal*. Vol. 65, No. 6. Miami, FL: American Welding Society (June 1986): p 17-21.
34. Richardson, R.W. "Robotic Weld Joint Tracking Systems — Theory and Implementation Methods." *Welding Journal*. Vol. 21, No. 11. Miami, FL: American Welding Society (November 1986): p 43-51.
35. Chen, W.H., P. Banerjee and B.A. Chin. "Study of Penetration Variation in Automated Gas Tungsten Arc Welding." *Recent Trends in Welding Science and Technology* [Gatlinburg, TN]. Materials Park, OH: ASM International (1989): p 517-522.
36. Rokhlin, S.I., K. Cho and A.C. Guu. "Closed-Loop Process Control of Weld Penetration Using Real-Time Radiography." *Materials Evaluation*. Vol. 47, No. 3. Columbus, OH: American Society for Nondestructive Testing (March 1989): p 363-369.
37. Guu, A.C. and S.I. Rokhlin. "Technique for Simultaneous Real-Time Measurements of Weld Pool Surface Geometry and Arc Force." *Welding Journal*. Vol. 71, No. 12. Miami, FL: American Welding Society (December 1992): p 473-482.
38. Guu, A.C. and S.I. Rokhlin. "A Study of Arc Force, Weld Pool Depression, and Penetration during Gas Tungsten Arc Welding." *Welding Journal*. Vol. 72, No. 8. Miami, FL: American Welding Society (August 1993): p 381-390.
39. Hirosawa, E., M. Naoe and T. Fukui. "'Ghost Defects' in Radiographs of Aluminum Alloy Welds." *Materials Evaluation*. Vol. 29, No. 5. Columbus, OH: American Society for Nondestructive Testing (May 1971): p 99-104.
40. Rummel, W.D. and B.E. Gregory. "Ghost Lack of Fusion in Aluminum Alloy Butt Fusion Welds." *Materials Evaluation*. Vol. 23, No. 12. Columbus, OH: American Society for Nondestructive Testing (December 1965): p 586-588.
41. Tucker, M.S. and P.A. Larssen. "Markings in Radiographs of 2014 Aluminum Alloy Gas Tungsten-Arc Welds." *Welding Journal*. Vol. 47, No. 5. Miami, FL: American Welding Society (May 1968): p 223-225.
42. Rabkin, D.M., L.A. Bukalo, V.T. Korzbova and A.S. Deniyanchuk. "Weld Heterogeneity in Aluminum Magnesium Alloys." *Avtomaticheskaya Svarka* [Automatic Welding]. In Russian. No. 5. Kiev, Ukraine: Instytut Elektrozvarivannia of Akademiia nauk Ukraïns'koï RSR (1966): p 74-75.
43. Issiki, S., J. Ko, K. Kataoka and T. Yamazawa. "The Abnormal Pattern in Radiographs of Aluminum Alloy Castings." In Japanese. *Hihakai-Kensa* [Journal of NDI]. Vol. 15. Tokyo, Japan: Japanese Society for Non-Destructive Inspection (July 1966): p 257-265.
44. Irie, M., M. Fujii and S. Yamashita. "The Influence of Structure on the X-ray Radiograph of Stainless Steel Welds." In Japanese. *Hihakai-Kensa* [Journal of NDI]. Vol. 12. Tokyo, Japan: Japanese Society for Non-Destructive Inspection (June 1963): p 263.

# Radiographic Testing in Utility, Petroleum and Chemical Industries

---

Frank J. Sattler, Sattler Consultants, Incorporated,  
Akron, Ohio

---

---

---

---

---

---

## PART 1. Overview

In the utility, nuclear, chemical and petroleum industries there are a variety of applications of penetrating radiation and radiographic testing. Many of these applications will not be covered here because they are in common practice or detailed in other parts of this book. Radiography is required in many of these applications because it is specified by codes and standards in federal, state and local governing regulations. Most of the radiographic requirements come about during fabrication and construction of chemical and petroleum plants and power generation facilities such as boilers, pressure vessels, nuclear power plant components and gas and oil transmission pipelines. However, some of these same requirements come into effect when repairs, replacements or additions are made to the facilities. Radiography also has become a valuable tool for accessing deterioration caused by corrosion and erosion in many pipes, vessels and other components that are part of today's complex plants. Penetrating radiation has seen many applications in detecting and measuring fluids and their movement, leak detection gages, liquid level gages and other important monitoring instrumentation.

In addition to the radiography for nuclear power plant components, several applications exist where radiographic testing is performed on nuclear fuel or fuel rods during manufacture, after service or to gather additional test information. Some of these examinations involve autoradiography where the component itself provides radiation to expose the radiographic film or other media.

Other uses of radiography include a move to eliminate film through imaging where the radiographic image is formed radioscopically and recorded on magnetic or optical media. Digital enhancement brings additional benefits to image quality. Tomography adds a third dimension to radiographic imaging and expands the uses of penetrating radiation tests.

## PART 2. Pipe and Tubing Applications

### Pipelines

#### History

Before 1946 it was common practice in gas and oil pipeline construction to cut out a certain number of pipe welds made each day. Test specimens were cut from these welds and mechanical tests were made. If the weld failed these tests, the contractor was required to replace the welds at no cost to the owner and, if they passed, the owner paid the cost of replacement. It was apparent to many pipeline engineers that a nondestructive method of testing pipeline welds would be more economical and dependable.

During World War II radiography was used extensively as a means of measuring weld quality in various industries. The same principles were used in applying radiography to pipeline welding problems. The first recorded use of radiography for the examination of pipeline welding occurred in 1945.<sup>1</sup> At that time radium was used as a radiographic source because X-ray equipment available was not adaptable for the job. With radium, the radiographic quality was poor but the portability presented many advantages over other pipeline weld inspection methods then available.

In 1946 a 621 km (385 mi), 457 mm (18 in.) diameter petroleum line was constructed in California. Radiographic testing of the circumferential pipe welds was accomplished by drilling a 19 mm (0.75 in.) hole about 76 mm (3 in.) from the weld. An 11 GBq (300 mCi) capsule of radium, mounted on a device that would support it at the center of the pipe in line with the weld, was then placed through this hole. In this manner a complete circumferential weld radiograph was made in one exposure. The method had the further advantage of having to penetrate only one wall thickness of pipe as the radium sources available were usually less than 37 GBq (1 Ci) in strength.

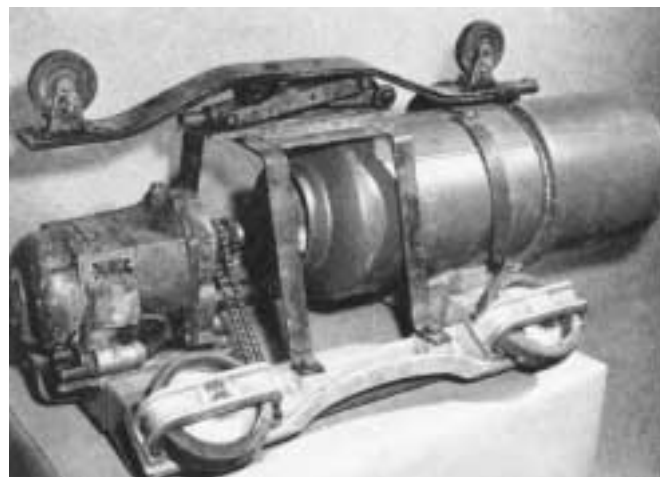
The disadvantages of the radium technique were the cost and time required to cut the hole and patch weld the opening. The quality of the plug weld was an unknown factor. Another disadvantage of the gamma rays produced by radium and its radon gas was the low radiographic contrast obtained, resulting

in radiographic sensitivities of four to five percent. Yet, in comparison with the destructive testing previously used, it had definite advantages in monitoring weld quality.

With the advent of iridium-192 production, an even better radioisotope source for pipeline radiography was available. It had the same advantages of portability without an external power source but was available in higher source sizes and smaller physical sizes to improve its specific activity. Because of its energy spectrum and strength, it could be used both internally and externally, through single or double walls to expose radiographic film.

With the availability of portable X-ray generators capable of generating X-rays 360 degrees around a pipe, it was now possible to radiograph an entire circumferential line weld. It was also feasible to select the energy best suited to provide the sensitivity required. Crawlers were developed that could carry the X-ray tube or isotope source hundreds of meters (thousands of feet) back into welded sections of a pipeline fed by portable generators carried onto the right of way. A typical X-ray crawler device is shown in Fig. 1.<sup>1</sup> The unit has a sensing system to identify the weld and stop at the right distance to make an exposure or a detector senses a low level gamma isotope

FIGURE 1. Internal pipeline X-ray generator and crawler device.<sup>1</sup>





on the outside of the pipe and stops the crawler. A technician identifies the weld with lead numbers and letters on the external pipe surface beneath a film cassette that is wrapped around the weld. Depending on the number of welds to examine, either hand processing or automatic processors may be used to process the film.

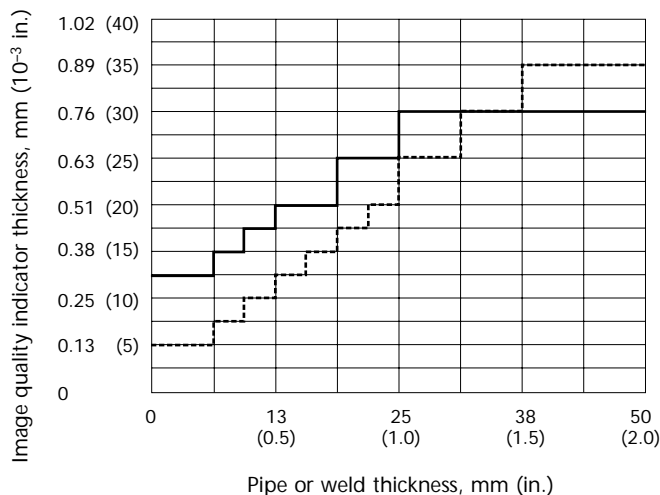
Most of the welding and inspections on pipelines are governed by ANSI/API Recommended Practice 1104.<sup>2</sup> However, many companies supplement this standard with additional or supplemental requirements. Requirements range from finer grain film to higher film density requirements, to specifications that detail that only X-ray generators can be used in single wall exposures except where tie in welds or repair welds are to be radiographed. ANSI/API Recommended Practice 1104 requires that one of three types of image quality indicators be used to confirm the quality of the radiograph. Two of these are plaque type image quality indicators, ASTM E 1025 and API,<sup>2,3</sup> whereas the third type references ASTM E 747 wire image quality indicators.<sup>4</sup> In most cases, because the inside of the pipe wall is inaccessible, image quality indicators are placed on the outside surface of the pipe adjacent to the weld. The plaque image quality indicators as well as the wire image quality indicators used represent a range of sensitivities depending on thickness. Figure 2 is a plot of pipe or weld thickness

and the maximum thickness of the plaque image quality indicators allowed for the pipe or wall thickness.<sup>2,3</sup> Figure 3 shows the maximum allowable source and sensor side equivalent image quality indicator sensitivity for wall or weld thicknesses from 1.27 mm (0.050 in.) to 51 mm (2.0 in.) for the plaque image quality indicators. For most of the common weld or wall thicknesses found in pipeline work, below 19 mm (0.75 in.), the maximum equivalent image quality indicator sensitivity allowed by API 1104<sup>2</sup> is about 3 percent or greater, all less than 2-4T sensitivity. Investigations of welding quality on lines subjected to seismic activity have suggested that additional radiographic sensitivity, smaller values of equivalent image quality indicator sensitivity, may be warranted because of the better images provided in revealing discontinuities.<sup>5</sup>

### Assessing Pipe Weld Quality

In most codes and standards, the rejection limits are based on workmanship standards. As a result, the radiographic standards of API 1104<sup>2</sup> and other codes and standards require the measurement of length or width or both to access the severity of a discontinuity indication. (The [interpretation and identification of these indications is discussed elsewhere in this volume](#) and the evaluation of the type of indication is detailed in the specifications.) These requirements are based on judgments about the levels of weld and examination quality that can be attained and maintained in field or shop

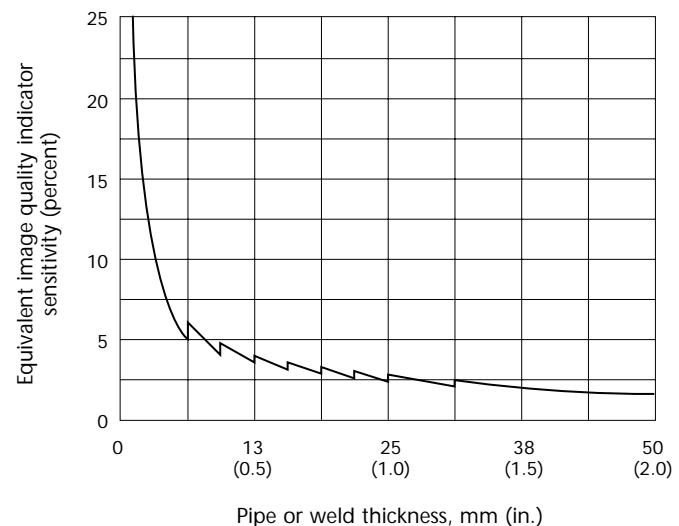
FIGURE 2. Image quality indicator (IQI) thickness as function of pipe or weld thickness for plaque image quality indicators as specified per American Petroleum Institute for both API 1104 and ASTM E 1025 image quality indicators.<sup>2,3</sup>



#### Legend

- = ASTM International image quality indicators
- = American Petroleum Institute image quality indicators

FIGURE 3. Maximum allowed source and sensor side equivalent image quality indicator sensitivity as function of pipe or weld thickness per API 1104.<sup>2</sup>



applications. The quality achieved must not compromise the pipe or other component integrity.

Steels with improved strength and fracture toughness have been used in new pipeline construction. With these improvements, it may be possible to replace the workmanship standards with a fracture mechanics based approach to determine weld quality on a fitness for purpose criterion.<sup>6</sup> Such an approach places increased demands on the nondestructive tests performed because additional discontinuity information is needed. At most, radiographic testing has traditionally required only two-dimensional determination of a discontinuity's extent, that is, the length and width dimensions of an indication. For fracture mechanics evaluations, a third dimension is necessary, indication depth (through-wall thickness), to properly evaluate a discontinuity's effect on serviceability.

Studies by the United States Department of Transportation<sup>6</sup> were conducted to determine if it is possible to measure a discontinuity's dimensions (through-wall thickness as revealed by film density differences) in production pipeline radiographs. These studies reveal that tighter controls are needed on various radiographic variables such as kilovoltage, film processing, film types and intensifying screens and source-to-sensor geometry before sufficient information is obtained from production radiographic film. Studies have been conducted to look at controls to be placed on these variables and at other supplementary testing methods that can be used to obtain the required information.

### Video Technique for Sizing Discontinuities

In other work to determine discontinuity dimension radiographically, a radioscopy system image intensifier system with a vidicon camera has been used to radiograph pipe segments containing artificial and welding discontinuities.<sup>7</sup> The radiographic images produced were recorded on a video recorder and then the voltage of one of the horizontal raster lines was measured with an oscilloscope at various locations in and adjacent to several types of discontinuities in the image. This study had several conclusions. Radioscopy is an alternative to film radiography for the inspection of pipeline girth welds fabricated to API 1104.<sup>2</sup> Permanent records can be made on video tape with identification information superimposed by an alphanumeric video writer. Immediate hard copies of rejectable discontinuities can be generated for repair

operations. Existing technology for remote mechanized inspection can be readily used for moving the real time detector module around the pipe and providing X and Y motion. All equipment except the detector head can be housed in a truck with 30.5 m (100 ft) of cabling to the detector. Electric power is provided from a brushless motor generator set. Volumetric discontinuities can be accurately sized electronically.

## Power and Process Piping

### ASME Codes

Electric power plants today can be powered by coal, oil, gas or nuclear fuel. Many of the large coal and oil boilers have been supplemented with combined cycle systems or newer natural gas stand alone turbine generators. Chemical and petroleum plants have extensive piping and vessels, some built to ASME or API standards. Nuclear power plants built in earlier years have extensive piping systems to support various functions to turn turbine generators. Most piping in these systems is built to requirements of the *ASME Boiler and Pressure Vessel Code* of the American Society of Mechanical Engineers (ASME).<sup>8,9</sup> Among these requirements are those for B31.1, *Power Piping*;<sup>10</sup> B31.3, *Process Piping*;<sup>11</sup> and several sections of the *ASME Boiler and Pressure Vessel Code* (Section I, *Rules for the Construction of Power Boilers*; Section VIII, *Rules for the Construction of Pressure Vessels*; and Section III, *Nuclear Components*).<sup>8,9</sup> These standards invoke the *ASME Boiler and Pressure Vessel Code*, Section V, Article 2, for radiography; some have supplemental requirements for radiography; and each contains acceptance standards for evaluating any indications found in radiographs. In B31.3,<sup>11</sup> acceptance standards are based on several design service categories with tighter acceptance requirements for more severe service.

Section V, Article 2,<sup>8</sup> contains the methodology for producing the radiographic images of welds and base metal for piping, vessels and other components. An essential part of any radiographic requirement is the resolution of specific features of a penetrameter's image, or *image quality indicator* features, that must be resolved in the radiographic image.

Article 2 provides a table, like the previous API 1104,<sup>2</sup> which details what image quality indicator is to be used for a given thickness range and what essential hole (2T) or wire size must be resolved. Table T-276 has both source side and

sensor side image quality indicator requirements. The source side image quality indicator requirements for thickness of 51 mm (2.0 in.) and less give very similar equivalent image quality indicator sensitivities as for the API requirements shown in Fig. 3.<sup>2</sup> The sensor side image quality indicators may be used only where inaccessibility prevents hand placement of the image quality indicators on the source side. When sensor side image quality indicators are used a lead letter F shall be placed next to or on the image quality indicator.

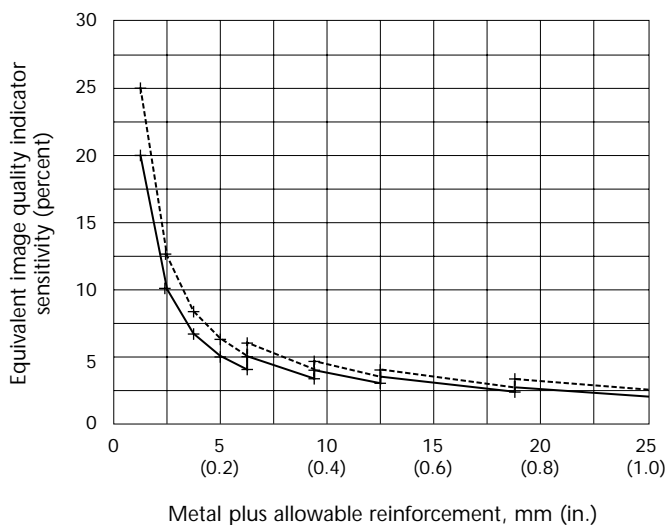
The maximum values of equivalent image quality indicator sensitivity for the *ASME Boiler and Pressure Vessel Code*, Article 2,<sup>8</sup> for source side image quality indicators are very similar to those of API 1104.<sup>2</sup> The maximum values of equivalent image quality indicator sensitivity for the *ASME Boiler and Pressure Vessel Code*, Article 2,<sup>8</sup> for sensor side image quality indicators are 10 to 20 percent below those of the source side image quality indicators. (Smaller equivalent image quality indicator percent values indicate greater sensitivity.) Maximum equivalent image quality indicator sensitivity for source and sensor side plaque type image quality indicators for 0 to 25 mm (0 to 1.0 in.) thick are shown in Fig. 4.<sup>8</sup> Piping thicknesses in ASME work can run as high as 75 to 100 mm (3.0 to 4.0 in.) so these rules

apply, in many cases, to piping much thicker than normal in pipeline work.

Figure 5 illustrates maximum equivalent image quality indicator sensitivity allowed for thicknesses over 25 mm (1.0 in.) in pipe or vessel wall plus applicable reinforcement for both source side and sensor side image quality indicators. At total thicknesses (base metal plus allowable reinforcement) of 51 mm (2.0 in.) or more, the maximum equivalent image quality indicator sensitivity for either sensor side or source side image quality indicators is 2 percent or less. At 102 mm (4.0 in.) and above, the maximum equivalent image quality indicator sensitivity is below 1.5 percent for both source side and sensor side image quality indicators and drops to below 1 percent for sensor side image quality indicators at 152 mm (6 in.) and greater thicknesses.<sup>8</sup>

Article 2, Table T-276, serves all of the *ASME Boiler and Pressure Vessel Code* work for weld radiography image quality indicator selection except for Section III, Division 1, nuclear work in Classes NB and NC, Class 1 and Class 2, components respectively.<sup>9</sup> Class 1 and 2 component image quality indicator requirements are detailed in Tables NB and NC 5111-1.<sup>9</sup> Requirements are included for ASTM plaque image quality indicators (ASTM E 1025) as well as ASTM wire image quality indicators (E 747).<sup>3,4</sup> When plaque image quality indicators are used on the source side of the object, little

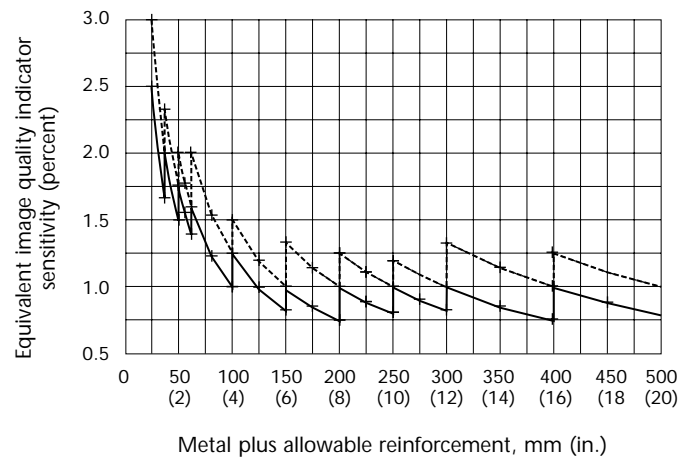
FIGURE 4. Maximum allowed source and sensor side equivalent image quality indicator sensitivity as function of wall thickness plus allowable reinforcement for *ASME Boiler and Pressure Vessel Code*, Article 2, for total thickness of 25 mm (1.0 in.) and less.<sup>8</sup>



#### Legend

- = Source side image quality indicators
- = Sensor side image quality indicators

FIGURE 5. Maximum allowed source and sensor side equivalent image quality indicator sensitivity as function of wall thickness plus allowable reinforcement for *ASME Boiler and Pressure Vessel Code*, Article 2, for thicknesses of 25 to 500 mm (1.0 to 20 in.).<sup>7</sup>



#### Legend

- = Source side image quality indicators
- = Sensor side image quality indicators

difference in sensitivity is noted except for some deviations at lower thicknesses. A plot of both the nuclear Class 1 and Class 2 maximum equivalent image quality indicator sensitivity allowable as well as those of Article 2 are shown in Fig. 6 for source side image quality indicators. The dashed lines are Article 2 requirements and coincide with NB and NC requirements for most of the thickness range. However, the sensor side image quality indicator requirements are very different in the nuclear work compared to those in Article 2 for 16.0 mm (0.63 in.) thickness and above. The equivalent image quality indicator sensitivity maximum averages about 25 percent lower than their counterpart allowables in Article 2 at the large thicknesses and approaches equal values at the 16.0 mm (0.63 in.) thickness. A comparison of maximum sensor side equivalent image quality indicator sensitivities for Article 2 and Nuclear Class 1 and Class 2 are shown in Fig. 7. Sensor side maximum equivalent image quality indicator sensitivities allowable are all below 2 for thicknesses greater than about 22 mm (0.88 in.) and below 1 for total thicknesses greater than about 110 mm (4.5 in.).<sup>8</sup>

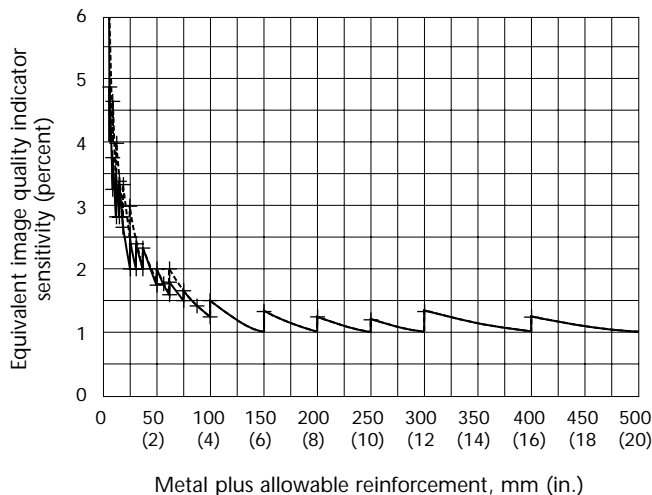
### Detection of Corrosion and Erosion

There are many applications of radiographic testing that require thought and ingenuity to apply code rules to

comply with sensitivity requirements. The code rules for piping assume that access to both the inside or outside of the pipe is possible and are generally made to do weld testing during construction or for repair or replacement. However, radiography has been found very useful in doing piping wall thickness surveys in both power plants and chemical and petrochemical facilities during shutdown outages and even during operation. These uses range from identifying areas that have had thickness reductions to actually determining remaining wall thicknesses.

One of the popular techniques for detection of erosion or corrosion is tangential radiography<sup>12,13</sup> illustrated for external corrosion in Fig. 8.<sup>12</sup> Normally erosion and corrosion are hidden from viewing by either being on the pipe's inside surface or by external corrosion being covered by insulation. In tangential radiography, a view of the pipe's cross section, including a view of the pipe wall, is projected on the sensor, enabling direct measurement of the remaining pipe wall thickness. The extremities of the pipe wall cross section projected onto the sensor may be defined by a line drawn from the source to the sensor through a tangent point on the pipe's outside diameter and from the source to the sensor through a tangent point on the pipe's inside diameter. The thickest portion of the pipe through which the radiation passes is therefore a cord bisected by the inside diameter tangent point. The cross section

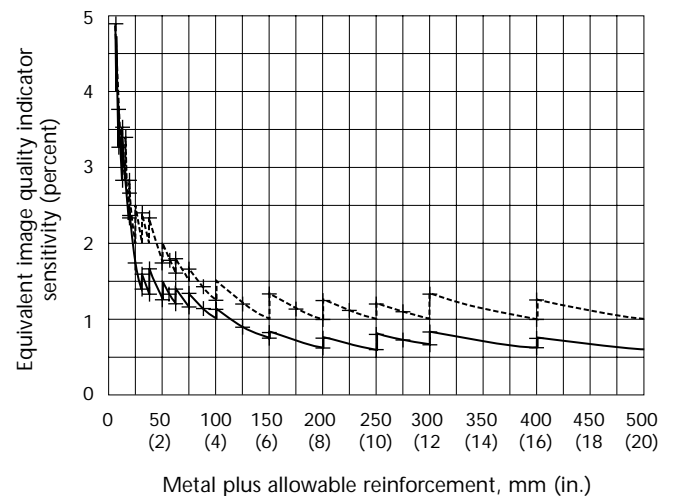
FIGURE 6. Comparison of maximum allowed source side equivalent image quality indicator sensitivity as function of wall thickness plus allowable reinforcement for ASME Boiler and Pressure Vessel Code.<sup>8</sup>



#### Legend

- = Article 2 image quality indicators, Table T-276
- = Section III, NB and NC Table 5111-1

FIGURE 7. Comparison of maximum allowed sensor side equivalent image quality indicator sensitivity as function of wall thickness plus allowable reinforcement for ASME Boiler and Pressure Vessel Code.<sup>8</sup>



#### Legend

- = Article 2 image quality indicators, Table T-276
- = Section III, NB and NC Table 5111-1

of the pipe wall that appears in the image is approximately that which occurs perpendicular to the center of the cord.

As the image of the cross section is projected onto the sensor, the image is enlarged somewhat as shown in Fig. 9.<sup>13</sup> This enlargement is proportional to the source-to-sensor distance and source-to-object distance. (Source-to-sensor distance is the same as source-to-film distance in other contexts, film being a kind of analog sensor.) The enlargement may be calculated and taken into consideration in the direct wall measurement as follows:

$$(1) \quad I_c = \frac{I_a (SSD - 0.5 d)}{SSD}$$

FIGURE 8. Tangential radiographic technique to determine wall thickness.<sup>12</sup>

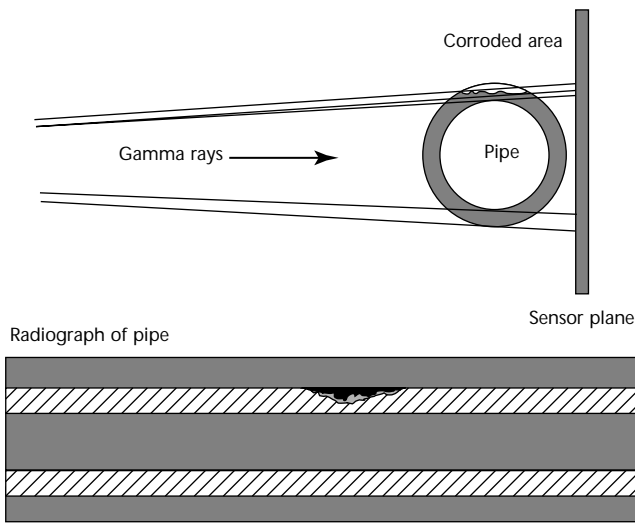
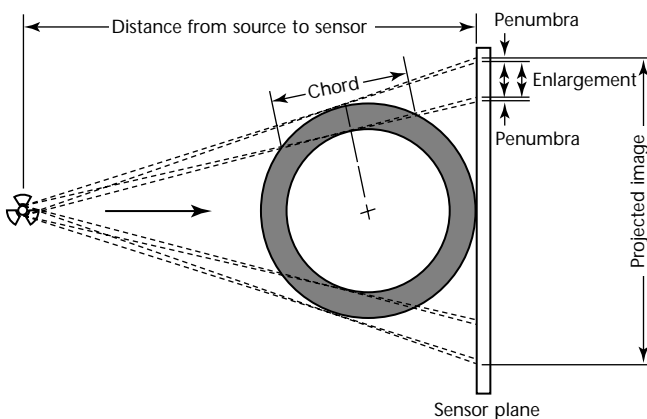


FIGURE 9. Enlargement of pipe wall and resulting penumbra.<sup>13</sup>



in which  $I_c$  = corrected image dimension,  $I_a$  = apparent image dimension, SSD = source-to-sensor distance and  $d$  = pipe outside diameter.

Because the radiation does not actually emanate from a point source, a penumbra (shadow image of the edges of the cross section) will also appear on the image. The extent of the penumbra may be calculated as follows, and a further correction may be made to the direct wall reading:

$$(2) \quad U_g = \frac{2(F \times 0.5 d)}{SSD - 0.5 d}$$

in which  $U_g$  is the width of total penumbra and  $F$  is the radiation source focal spot size.

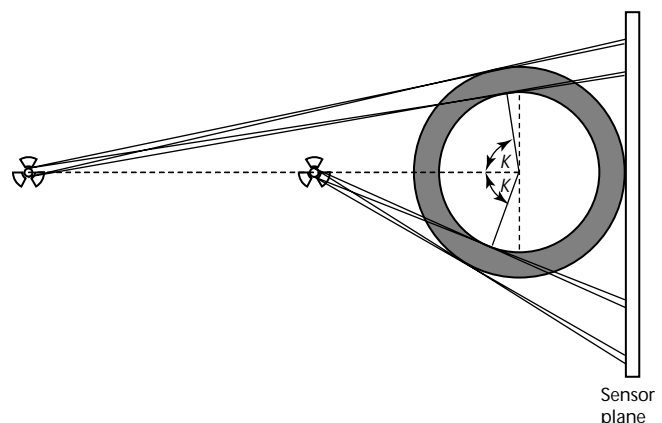
The source-to-sensor distance, film type and exposure density all significantly influence the accuracy of tangential radiography. The locations of the tangent points will vary with the source-to-sensor distance (Fig. 10) as follows:

$$(3) \quad K = \cos^{-1} \frac{0.5 d}{SSD - 0.5 d}$$

in which  $K$  is the angle of rotation of tangent point as shown in Fig. 10.<sup>13</sup>

One of the problems encountered is that of undercut or *burnoff* where the thinner or outer thickness of the pipe is darkened considerably over the thicker inner portion of the wall and may be too dark at higher film densities or image contrast settings. For optimized results, the source-to-sensor distance should be as large as practical. Ratios of source-to-sensor distance to outside diameter of six or more produce low unsharpness values. High contrast image settings and fine

FIGURE 10. Variation of tangent point on pipe outside diameter with different source-to-sensor distances and pipe outside diameters. Sharpness varies with interrogation angle  $K$ .<sup>13</sup>



grained films produce more accurate results when developed to medium range film densities around 2.0.

A comparator block can also reduce the calculations needed to provide corrections to the measurement. In one study,<sup>13</sup> a comparator block was developed that had several artificially drilled holes of various sizes to simulated metal loss. With the simulator block, the calculations of metal

loss are simplified by direct comparison to known losses in the comparator block sample. The comparator block used is shown in Fig. 11 and its placement at the tangent point can be determined with a straight edge or string stretched from the source to the pipe.<sup>13</sup> The placement of the comparator at the tangent point is shown in Fig. 12.<sup>13</sup> Another problem with these measurements is that the maximum wall

FIGURE 11. Comparator block having three differently sized drilled holes and slot.<sup>13</sup>

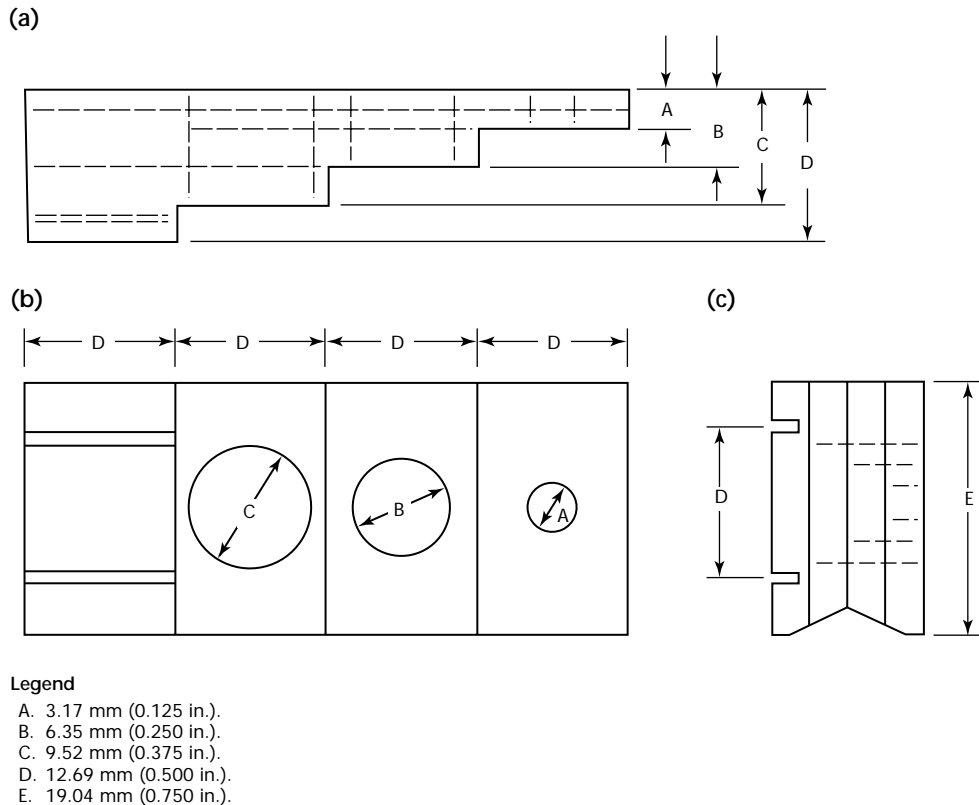
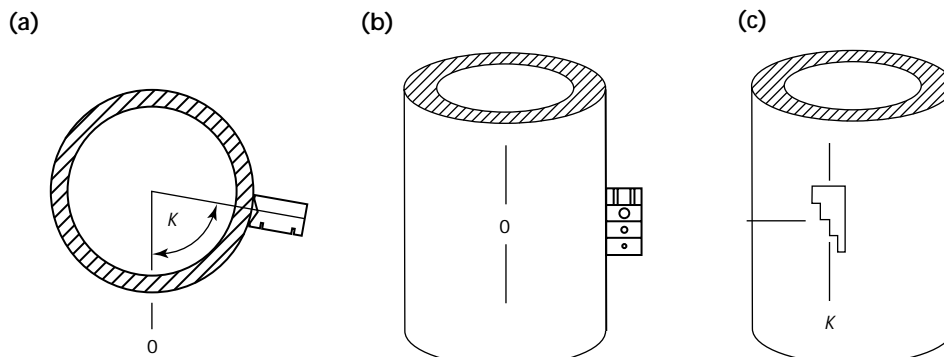


FIGURE 12. Placement of comparator block on pipe at tangent point from source: (a) axial cross section; (b) side view; (c) side view with pipe rotated about 90 degrees from position in Fig. 12b. Tangent point may be determined with straight edge or taught string from source holder to pipe.  $K$  = interrogation angle.<sup>13</sup>





thickness loss must be perpendicular to the radiation beam. If it is not, significant errors can be made in determining wall loss that may be either greater than the actual loss or much less than the actual loss.

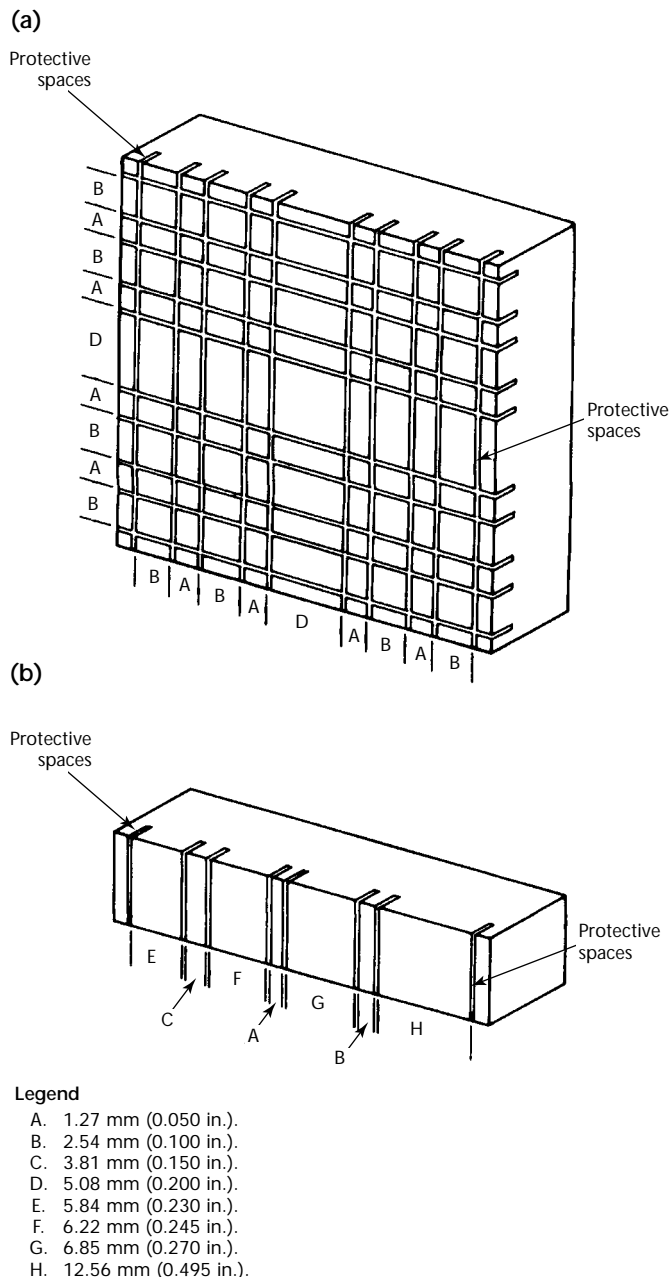
Other types of calibrated reference blocks<sup>14</sup> have been used in performing tangential radiographic thickness measurements. A dense metal calibration block with milled slots separated at known distances is machined and placed

on each exposure. Typical reference blocks are shown in Fig. 13.<sup>14</sup> The slots are separated by known dimensions of the wall thickness to be measured and are imaged at the tangent locations where the pipe wall is measured. Calculations of the wall thickness are based on the measurement of the thickness of the pipe wall as seen in the radiographic image and picking a dimension off the radiographic image of the reference block similar or closest to the pipe thickness dimension measured. The actual thickness is determined by multiplying the measured wall thickness in the radiograph by the actual physical separation of the lines chosen from the reference block divided by the separation of the reference lines on the reference block as seen in the radiograph.

A third approach<sup>15</sup> to measuring wall thickness by the tangential technique and using computed radiography uses a step block or tapered thickness block to measure thickness in other areas of the wall. The burnout or undercut that occurs because scatter and the primary beam from the source darken the outer wall thickness can be reduced by a 1.6 mm (0.06 in.) lead screen on the source side of the cassette. Other scatter reducing techniques may also help. A round ball of high density metal is used to determine the source location in the radiograph and the enlargements that occur in different parts of the images. With this technique, the tangential thicknesses are measured but the additional density information in the radiograph is used to determine thickness in other areas.

Another approach to radiography for wall thickness measurements<sup>16</sup> involves a nonfilm technique and computer processing of image data using an iridium-192 source. The cassette contains a linear array of X-ray detectors and a linear motion system to drive the array the length of the frame. The cassette system detector is optimized for use with the energies of the iridium-192 source. The detector scintillators are a photodiode based solid state line array with a separation between the array elements. An excellent photon capture efficiency is maintained because of the thickness of each scintillator. The array provides for the measurement of the radiographic intensities emerging from the pipe with 16-bit accuracy as it moves, sending the data to a portable computer for storage and processing. The radiation profile provides pipe wall measurements and a radiographic image display as shown in Fig. 14.<sup>16</sup> The intensity measurements represent the thickness of the pipe and can be calibrated for double-wall measurements. The detectors can also be used to take profile or tangent wall shots

FIGURE 13. Another concept for calibrated reference block for tangential radiography of pipe wall: (a) square block; (b) rectangular block. Material is lead based alloy or other high density metal.<sup>14</sup>



to provide single-wall measurements. Figure 15 is a single-wall and double-wall pipe scan where both profile and double-wall thickness data are presented.<sup>16</sup>

### Monitoring Methods and Techniques

There are many other uses of penetrating radiation to perform functions that are not related to finding discontinuities, thickness changes and thickness measurements. Radiation is attenuated to varying degrees depending on the energy of the source and the thickness and density of matter through which it passes. It has many other uses in monitoring processes, leak detection, flow measurement and detecting and measuring fluids in containment systems. These methods have found uses in power plants and chemical and petroleum plants.

One of these applications<sup>17</sup> uses sealed radioactive sources of cobalt-60 and cesium-137 to perform a series of level and density measurements. Sources used typically have strengths from 0.37 to 3.7 GBq (10 to 100 mCi) whereas the radiation intensity measurements are made with scintillation detectors. The source holder has a collimator through which the beam emerges and is guided to a detector on the opposite side of the object. The beam is placed so that it is transmitted through a column or reactor to take a series of density measurements by measuring the transmitted radiation. The beam of radiation is made to scan through the diameter of the column as depicted in Figure 16.<sup>17</sup> When a column is operating properly, it has the right mix of liquid and gases at various elevations along with its internals at their proper

FIGURE 14. Pipe wall scan through both pipe walls showing radiographic image (upper) and thickness presentation (lower).<sup>16</sup>

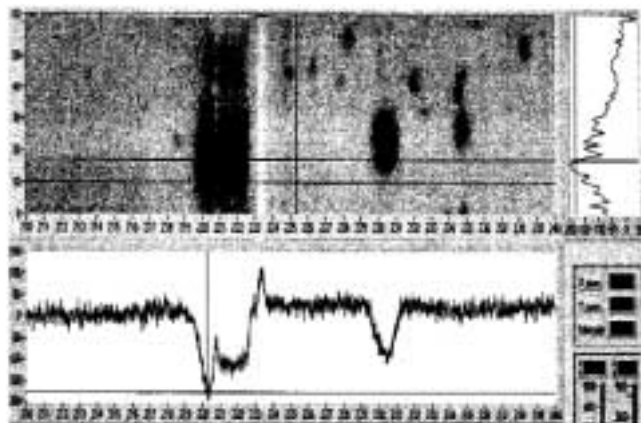


FIGURE 15. Pipe wall scan through both pipe walls: (a) radiographic image; (b) wall profiles and thickness presentation across one pipe scan line.<sup>16</sup>

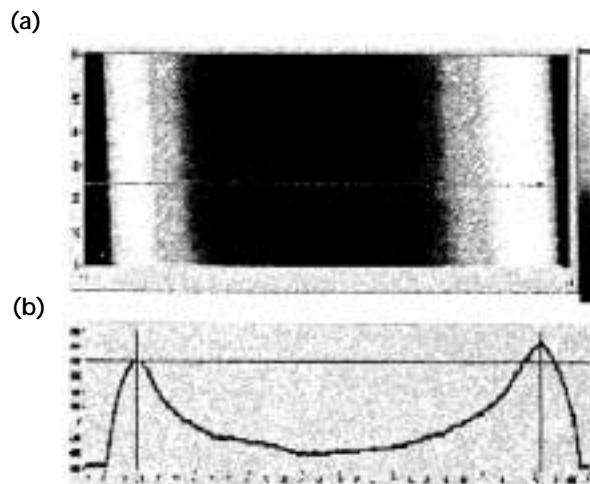
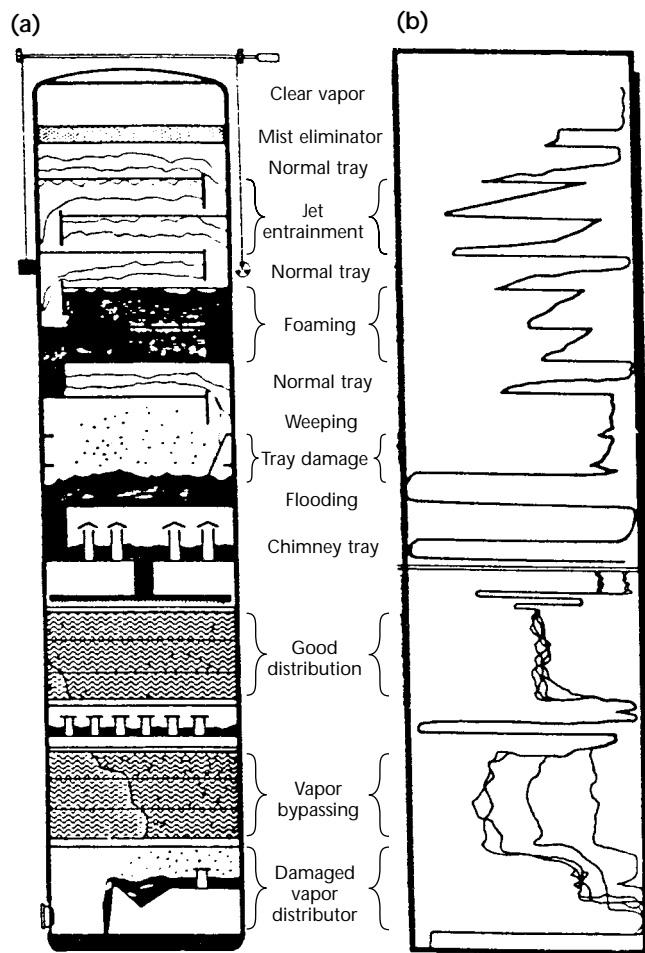


FIGURE 16. Distillation column: (a) schematic cross section; (b) trace from scan with gamma radiation.<sup>17</sup>



locations. The radiation transmitted at each elevation is a function of the density and thickness of the materials in its path. Higher transmissions of radiation are indicative of higher amounts of gas whereas lower transmissions are caused by higher densities and thicknesses of liquid and metal. A drawing of a representative radiation intensity pattern for a column is shown in Fig. 16b,<sup>17</sup> with a description of the internal conditions that caused the levels in transmitted radiation intensity. The scan can detect existing problems that result in density differences. These problems may include anomalies that result from the column's hydraulic performance, fouling and coking deposits and damaged or missing trays and packing. A scan of the column when the column is operating properly can form the base signature against which problems can be identified when the column is not functioning properly.

Another application in monitoring operations<sup>17</sup> involves unsealed sources or tracers to perform invasive measurements. In the sealed source technique, the measurement remains external to the process and is affected by transmission in and out of the vessel. In the process world, it is often meaningful to determine volumes, speeds and frequency in reactions. This can be accomplished by introducing a radioactive tracer gas into the process while measuring where the material goes and how fast it moves. Radioactive tracers are used to locate and size leaks in heat exchangers; discover mean residence time, velocity and plug flow attributes of a process; determine leakage past relief and block valves; and learn mass/flow relationships through flare lines or piping systems.

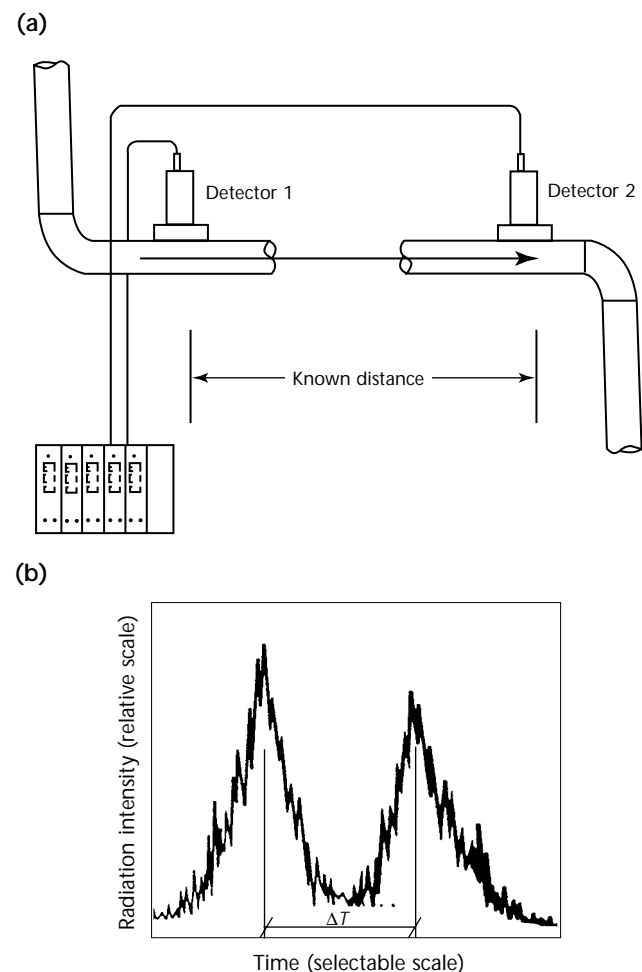
Radioactive isotopes that are normally possible for these types of tests are iodine-131, sodium-24, bromine-82 and krypton-85. Which isotope is right for the job depends on the physical character of the system. Figure 17 illustrates a piping system with two scintillation detectors at least 10 pipe diameters downstream from the injection point of the isotope.<sup>17</sup> The first detector's measurements provide a starting point for the timing sequence. The transport of the tracer material is being measured at two locations a fixed distance apart. The flow rate is determined by the time difference between the peaks of intensity curve for the two sensors as shown in the lower half of Fig. 17.<sup>17</sup>

Neutron radiography<sup>18</sup> has been used to detect fluids in process pipes that normally carry gases. This study determined that it was possible to detect fluids in small diameter pipe, 6.0 to 14.3 mm (0.25 to 0.563 in.) outside diameter with a ratio of outside diameter

to inside diameter of 3. Fluid thicknesses from 0.08 to 0.89 mm (0.003 to 0.035 in.) in thickness were detectable. Although these studies were conducted with a reactor using transfer techniques, it was felt that in-plant tests could be performed with the neutron isotope source californium-252. Better detectability was obtained by angling the beam (in the tests angling the pipe) at a sufficient angle to the neutron beam to effectively increase the thickness of liquid to make it more attenuating to the radiation.

Liquid level gages<sup>19</sup> using radiation transmission principles have several applications in determining liquid heights and fluid density values. In simple applications, a radiation gage can be installed to determine when the liquid in a tank has reached a certain level. When a source is installed on one side of a tank and the detector on the other, the radiation in air is much larger than when

FIGURE 17. Flow rate measurements at two pipe locations: (a) downstream from injection point; (b) resulting intensity measurements from both detectors as function of time duration  $\Delta T$ .<sup>17</sup>



that radiation is attenuated by a liquid. The gage can provide a feedback signal to turn off the flow of liquid as the radiation level drops. This gage is called a predetermined liquid level gage. Another type of liquid level gage uses changes in distance to constantly monitor the liquid level in tanks or other containers. In this type of gage, the radioactive source is enclosed in a float guided by suitable guides inside a tank or other storage device while the detector is some distance away at a higher elevation. As the liquid moves up or down, the source moves up or down, changing the distance between it and the detector. Because radiation intensity changes as a function of the square of the distance, the change in radiation intensity provides a measure of the liquid height. This type of float gage has several advantages over other approaches. Some of the advantages are that the level can be accurately detected in totally enclosed containers, the change in level can be continuously monitored and high accuracies can be obtained over selected portions of the range.

## PART 3. Vessel and Component Applications

### Pressure Vessels

#### *ASME Boiler and Pressure Vessel Code*

The radiography requirements of various ASME code items was detailed above, in the power and process piping section of this chapter. Requirements for vessels or piping concerning radiography are the same, except that because of the thicknesses involved and the manner in which the examinations can be conducted, they result in greater sensitivity for thicker components. This increased sensitivity results in a higher quality, as smaller thicknesses and densities are now resolved in these radiographic images. Vessels in boiler construction such as the mud and steam drums fabricated to the *ASME Boiler and Pressure Vessel Code*, Section I, as well as other pressure vessels constructed to the *ASME Boiler and Pressure Vessel Code*, Section VIII, requirements are radiographed to ASME Section V, Article 2,<sup>8</sup> requirements — other requirements being provided by the referencing code sections along with acceptance standards for any resulting indications. Nuclear codes and the *ASME Boiler and Pressure Vessel Code*, Section III,<sup>9</sup> use the *ASME Boiler and Pressure Vessel Code*, Article 2,<sup>8</sup> for most of their requirements except that they have a separate image quality indicator table that applies for Class 1 and 2 components. Acceptance standards are in relatively close agreement for these three code sections.

#### Nuclear Vessels and Components

Nuclear construction requires other methods of nondestructive testing but places responsibility for volumetric examinations on radiography. Because of the thicknesses involved, high energy isotopes and linear accelerators must be used to penetrate the carbon steel wall thicknesses that may exceed 406 mm (16.0 in.) in the nozzle belts of pressurized water reactor vessels. Cobalt-60 has an upper limit of about 200 mm (8.0 in.) of equivalent carbon steel thickness and is suitable for most applications in boiling water reactors (BWRs). However, to reduce

exposure times and to radiograph thicknesses exceeding 200 mm (8.0 in.) in pressurized water reactor (PWR) vessels, linear accelerators are used. (Isotope sources require long exposure times for thick materials.) Betatrons were popular in the 1950s and early 1960s but were replaced by linear accelerators, with at first 10×, then 20× and even greater increases in radiation intensity. A 13 MeV linear accelerator<sup>20</sup> is shown in Fig. 18, where film placement and beam alignment are being performed to set up an exposure on a nozzle weld in a boiling water reactor vessel.<sup>20</sup> These linear accelerators reduced the time required for radiography and therefore its cost while maintaining the sensitivity required. A 7.5 MeV linear accelerator is shown with its smaller size head being set up for the examination of a pressure vessel weld in Fig. 19.<sup>20</sup>

#### Inservice Inspection of Components

In general, radiography does not work very well in inservice examinations in nuclear and other plants because of the need to have access to both sides of a component. In a nuclear power plant, the component is likely to contain water or contaminated water of some type on the

FIGURE 18. Placing film and aligning 13 MeV linear accelerator beam for examination of boiling water reactor nozzle weld.<sup>20</sup>





internal side of the component or pipe. Ultrasonic angle beam examinations are more suitable, in most instances because they require access to only one side. However, nuclear plants have materials and fabrications that contain austenitic cast and wrought components, that offer limited physical access, that limit the sensitivity of the test or that prevent an effective examination of the material. Several applications of radiography have been made and unique equipment or techniques developed where ultrasonic applications are limited.

The main coolant pipe in some pressurized water reactors (PWRs) is some form of austenitic stainless steel that is usually cast conventionally or centrifugally or that may be wrought pipe. This pipe is joined to the carbon steel reactor, steam generators and pressurizer vessels by some form of safe end weld. The weld has either high temperature nickel chromium alloy or austenitic stainless buttering on the carbon steel nozzle and then is joined by welding with austenitic filler metal. Arc welding produces a cast structure in the weld that, along with the austenitic stainless pipe, make for a difficult if not impossible ultrasonic examination. A unique radiographic examination of this

weld is performed in French nuclear unit pressurized water reactor vessels by means of a special manipulator. This manipulator provides for placing under water an isotope source internally within the center of the pipe-to-nozzle weld surrounded by an inflatable diaphragm that replaces water with air. Film is manually placed around the pipe-to-nozzle weld and the exposure is made of the weld circumference.

To determine if radiography has the sensitivity to detect planar discontinuities in austenitic materials, a study was conducted to see if the minimum size discontinuity was detectable by radiography.<sup>21</sup> One of the conclusions of the study was that minimum through-wall thickness detectable using a portable miniature linear accelerator is essentially equal to or less than the values permitted by the *ASME Boiler and Pressure Vessel Code, Section XI, Inservice Inspection of Nuclear Plants*.

In a nuclear power plant in Tennessee,<sup>22</sup> radiography with a miniature linear accelerator provided the information needed to confirm the position of valve disks in two separate valves. Each valve was 965 mm (38.0 in.) in diameter with a wall thickness of 102 mm (4.0 in.) and an additional 102 mm (4.0 in.) of insulation on the outside surfaces. This meant that the radiation beam would have to travel through 204 mm (8 in.) of carbon steel before producing an image on the sensing plane at a minimum source-to-sensor of 1.17 m (46.0 in.). Additional material was expected internally as the disk was about 0.76 m (30 in.) in diameter and 76 mm (3.0 in.) thick. The valves were in the main steam piping system with full steam flow operating at temperatures above 200 °F (93 °C). With these thicknesses, radiography with conventional X-ray sources or even the most powerful of isotope sources would be impractical. Even with the miniature linear accelerator, exposure times were 45 min long. The radiographs showed that one disk had become detached and was lodged in the valve body whereas the second disk was detached and eventually found some 152 m (500 ft) downstream where it lodged in a reducer section.

In another nuclear power plant,<sup>23</sup> access was the determining factor in developing a radiographic technique to perform examinations of main steam piping. The main steam piping that transports steam from four steam generators to the turbine is enclosed within a guard pipe (Fig. 20).<sup>23</sup> The guard pipe is designed to prevent damage to surrounding components in the event of a rupture of a main steam pipe. Some of the circumferential welds in this piping are

FIGURE 19. Radiographic examination of pressure vessel welds is conducted with 7.5 MeV linear accelerator.<sup>20</sup>





required to be examined during the ten year inservice inspection interval. Because of the access limitations, ultrasonic examination of only part of the weld is possible. Radiographic techniques were developed to perform the examinations. The welds are both vertical and horizontal. Access to the pipe welds is restricted to two hand holes located 180 degrees apart on each weld to be radiographed as shown in Fig. 20.<sup>23</sup> The hand holes are 305 mm (12 in.) in diameter and are covered with a flange plate when the power plant is in operation. Each of the welds has two gamma holes, one hole underneath each of the flange plates. An iridium-192 source is positioned in the center of the pipe with a special guide tube and plug shown in Fig. 21.<sup>23</sup> The identification markers and number belt to mark locations around the pipe were placed on a steel banding strap and fed around the pipe. Because of problems with the source having to pass close to the sensing plane if a panoramic film belt was used, two exposures were made on each weld from each side of the pipe. Figure 22 illustrates how the exposures were made<sup>23</sup> except that film cassettes were placed only on

180 degrees of the pipe circumference farthest from the hand hole being used. A lead backing of the cassettes was used to hold the film in place and limit backscatter from the guard pipe.

## Tanks

Nondestructive testing of welded steel tanks for oil storage is specified for fabrication in API 650, *Welded Steel Tanks for Oil Storage*.<sup>24</sup> For butt welded tank shells with thicknesses less or equal to 25 mm (1.0 in.) in thickness, only spot radiographs are required. Spots at junctions of vertical and horizontal seams

FIGURE 20. Steam generator and piping within guard pipe.<sup>23</sup>

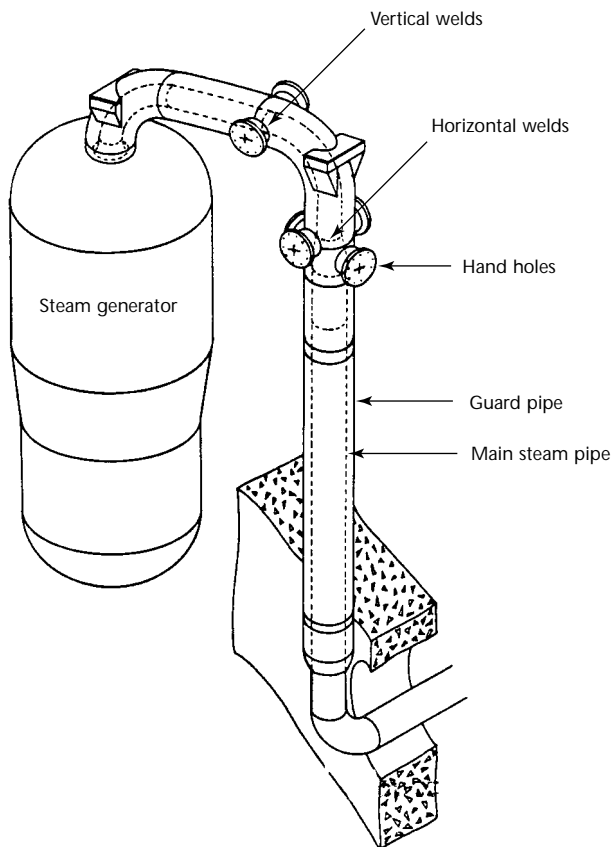


FIGURE 21. Isotope source tube: (a) guide tube; (b) access hole plug.<sup>23</sup>

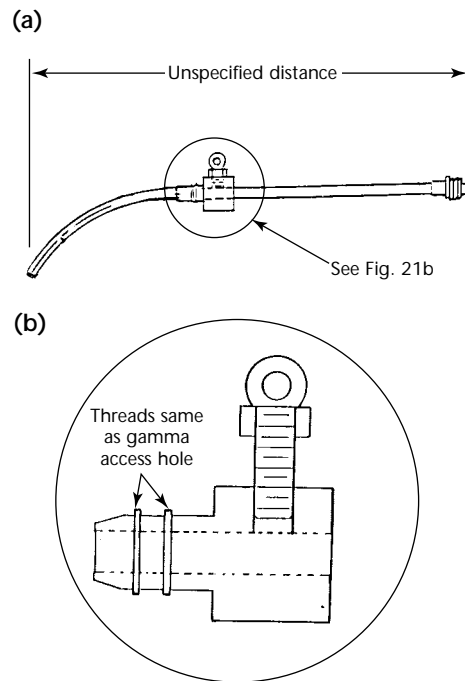
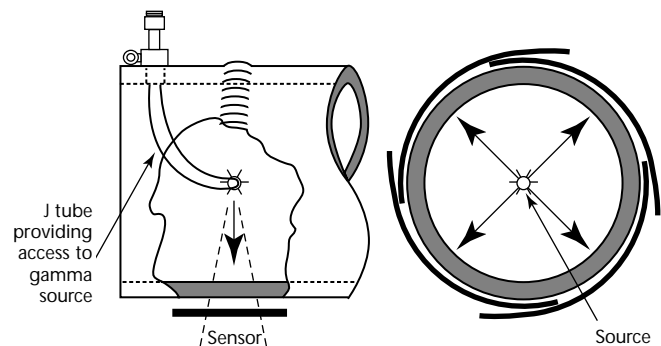


FIGURE 22. Panoramic technique using J tube guide tube and gamma access hole holder.<sup>23</sup>



required are to include 51 mm (2 in.) of the horizontal seams. Vertical joints in walls that exceed 25 mm (1 in.) in thickness shall be completely radiographed as well as butt welds around the periphery of a manhole or nozzle in any wall thickness. Radiographs are to be made in accordance with the requirements of the *ASME Boiler and Pressure Vessel Code*, Section V, Article 2,<sup>8</sup> except for unsharpness requirements. Acceptance of radiographs is to be based on resolving the prescribed image quality indicator. Acceptance of radiographs is based on the acceptance standards of the *ASME Boiler and Pressure Vessel Code*, Section VIII, Division 1, Paragraph UW-51(b). API Standard 653, *Tank Inspection, Repair, Alteration, and Reconstruction*<sup>25</sup> also defers to the same *ASME Boiler and Pressure Vessel Code* sections for radiographic requirements and acceptance standards.

Some types of tanks present unique problems for detecting corrosion internally. Double-walled insulated tanks are used in petrochemical plants in several processes. When these vessels are operated at fill levels below their maximum capability, the volume above the liquid is occupied by entrained air or vapors. Exposure of the inner wall to the resulting boundary between gas and fluid has caused erosion in some processes. Because the exterior of the inner shell is not available for ultrasonic testing, the only effective method of examination is to enter the tank when it is shut down and examine the surfaces visually. Even conventional radiography is not effective because of the great image unsharpness that would be present in any image. Access into the tank requires venting and draining, removing it from service. Down time for these actions can take the tank out of service for up to two days.

To determine an acceptable technique to detect and measure erosion damage, a feasibility study<sup>26</sup> was conducted on laminography to image and provide measurement of any wall thickness losses. A 19 mm (0.75 in.) plate specimen containing several different types of wall loss was fabricated for the inner wall. Polystyrene foam was used to simulate the heating fluid occupying the layer between the inner and outer vessels and then a 6.0 mm (0.25 in.) thick plate for the outer shell and another layer of polystyrene foam to simulate the outer insulation. Several iridium-192 exposures were made at a source-to-sensor distance of 1.8 m (72 in.) and at 0, 305 and 610 mm (0, 12 and 24 in.) offsets from the center of the specimen. The resulting radiographs were scanned and digitized. The digital information was analyzed using a laminography algorithm along with a

conventional computer graphics program. Comparison of the actual sharp edged fabrications versus the image processed data showed a greater than 98 percent correlation. Examination of the large erosion gouge showed a +6.7 percent, -5.3 percent variance from the actual depths. These techniques may provide a noninvasive means of measuring inner erosion with acceptable accuracy.

## PART 4. Nuclear Fuel Applications

One of the critical areas in a nuclear reactor is the fuel and its containment. Poor containment of the fuel in the fuel rods will cause erosion and dispersion of the uranium throughout the reactor system and cause higher radiation levels wherever it is trapped. Many items go into maintaining the quality of the fuel from the individual microspheres to compaction of the fuel in the fuel element to producing a good seal weld on the fuel element. Examinations of fuel after use can reveal characteristics that caused problems and that must be addressed in future fabrications. Radiography has also been used to characterize nuclear waste materials without having to open the waste drums.

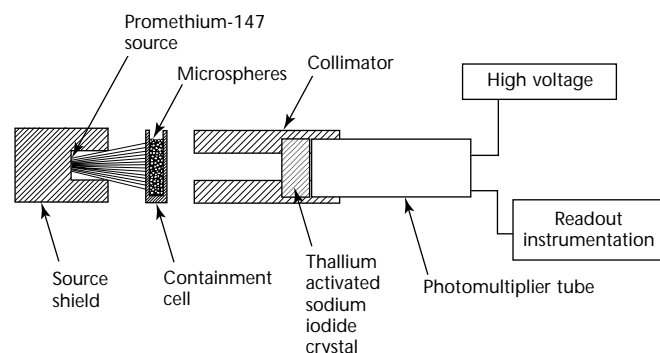
Microradiographic techniques have been used for many years to measure coating thicknesses of nuclear fuel microspheres. This measurement typically involves using very low energies with a beryllium window tube. At low energies it may use an inert gas instead of air to reduce attenuation while placing the spheres on bare single-emulsion film or photographic plates. The resultant image can be enlarged many times to accurately determine the coating thickness. It was desirable, however, to have a technique<sup>27</sup> that could have faster feedback in order to change processing parameters if necessary. It was required to measure pyrolytic carbon thickness on approximately 0.25 mm (0.010 in.) diameter thorium microspheres on small samples during the coating operation to prevent overcoating.

Experiments were set on a series of thorium dioxide particles with 0.23 mm (0.009 in.) diameters having coating thicknesses in the range of 0.013 to 0.173 mm (0.0005 to 0.0068 in.) to determine the optimum X-ray energy with microradiographic techniques. Two sizes of acrylic containment cells were constructed to hold the particles during radiography with each coating thickness having its own containment cells. The best sensitivity was obtained with 50 kV constant potential radiation and a thinner 1.588 mm (0.0625 in.) acrylic containment cell. The 50 kV constant potential polychromatic X-ray beam has an *effective energy* of about 38 keV. Effective energy is defined as the energy of monochromatic (single-wavelength) radiation that would produce the same

absorption measurement as obtained from polychromatic X-rays emitted at a given X-ray tube voltage. Because the measurements were to be made on a production line, an isotopic radiation source was desirable. Promethium-147 was investigated and chosen as the radiation source because it produces a characteristic X-ray of 38 keV when bombarded by its own 0.223 MeV beta radiation. This radioactive isotope is a more stable radiation source than an X-ray generator and is quite portable while being available in 3.7 GBq (100 Ci) source sizes. Figure 23 represents a pictorial diagram of the thickness measuring system developed to measure the coating thickness.<sup>27</sup> By scanning the particles and averaging the voltages, a thickness measurement was determined from a calibration curve with a total measurement time of 2 min. At the latter stages of the program, a direct reading thickness instrument was developed, as shown in Fig. 24,<sup>27</sup> which provided a measurement accuracy on the coatings within  $2.0\text{ }\mu\text{m}$  ( $8 \times 10^{-5}$  in.) over a range of carbon coating thicknesses from 0.016 mm (0.0006 in.) to 0.168 mm (0.0066 in.).

Acceptance standards often call for limits of acceptability of an item such as *no cracks* or *no tungsten inclusions*. What this limit implies is that no detectable cracks or tungsten inclusions are acceptable in the radiographs. However, the sensitivity in a radiograph will determine what is detectable so that personnel performing examinations to

FIGURE 23. Pictorial diagram of thickness measuring system for coated nuclear fuel microspheres.<sup>27</sup>



different criteria can get different results. Such a problem<sup>28</sup> was faced in the examination of thin, stainless steel clad, 5 to 7 mm (0.20 to 0.28 in.) diameter, fuel pin tube-to-end plug, tungsten insert gas welds. A similar problem existed in 14 to 15 mm (0.55 to 0.59 in.) diameter zirconium alloy clad fuel pins welded in the same manner. Tungsten wires and powders were used to simulate tungsten inclusions found in the radiographs. Wire sizes chosen were 0.05 and 0.1 mm (0.002 and 0.004 in.) and particles whose larger dimensions were 0.05, 0.1, 0.15 and 0.2 mm (0.002, 0.004, 0.006 and 0.008 in.) were chosen for the study. The end cap welds are examined with shape corrected blocks to reduce the scatter that would come from the cylindrical configuration. It was possible to detect both the 0.05 mm (0.002 in.) and 0.1 mm (0.004 in.) diameter wires in the 5.5 mm (0.22 in.) thick stainless steel radiographs made on very fine grain, fine grain and medium grain films. The limit of detection in the steel zirconium alloy welds was determined to be 0.1 mm (0.004 in.) as shown on fine and medium grain films. Microdensitometer scans of the latter films are shown in Fig. 25.<sup>28</sup>

Densitometric measurements in film are analogous to contrast measurements in electronic images, which measurements provide monochromatic data for the description of density in the test object. Work in the 1990s was conducted to control and quantify gray levels for densitometry. An unprocessed image may be compared with a reference image to help identify vignetting and other distortions caused by incident radiation patterns and by gain in the image intensifier and elsewhere in the system.<sup>29,30</sup>

Radiation gaging applications can measure densities of materials with a fairly high accuracy. This technique assumes that all other conditions that might affect the amount of radiation

being transmitted through the material are under control and that the only variable affecting the radiation intensity is density. In the production of fuel elements,<sup>31</sup> there are different means of placing the nuclear fuel particles within the metal tubes, usually zirconium alloy or stainless steel tubes. One of these filling techniques uses vibratory energy to compact the fuel particles. Another technique is to insert cold pressed and sintered oxide pellets into similar tubing. The fuel particle density and distribution play an important roll in the performance of the fuel element. Development engineers studied the effects of various manufacturing parameters on fuel homogeneity and density. These variables included fuel particle size distribution, vibratory energy, rod loading techniques as well as pressing pressure and sintering temperatures. Seamless tubing can have relatively large wall thickness variations that can be more pronounced in smaller diameters. As a billet is pierced to start the tube process, the mandrel that pierces the tube can float providing thick and thin areas on opposite sides of the tube. If the diameter is unaffected, the wall will be

FIGURE 25. Microdensitometric scans over 0.1 mm (0.004 in.) diameter tungsten wire on 15.5 mm (0.61 in.) thick zirconium alloy block: (a) extra fine grain film with average speed and high contrast; (b) high speed, medium grain film.<sup>28</sup> In film radiography, film density is expressed as ratio in base 10 logarithm of  $I_0 \cdot I_x^{-1}$ , where  $I_0$  is radiation reaching the densitometric detector without intervening film and where  $I_x$  is radiation through film. These measurements correspond to contrast or relative brightness differences in radioscopy, which in some cases can be adjusted by using different amounts of gain.

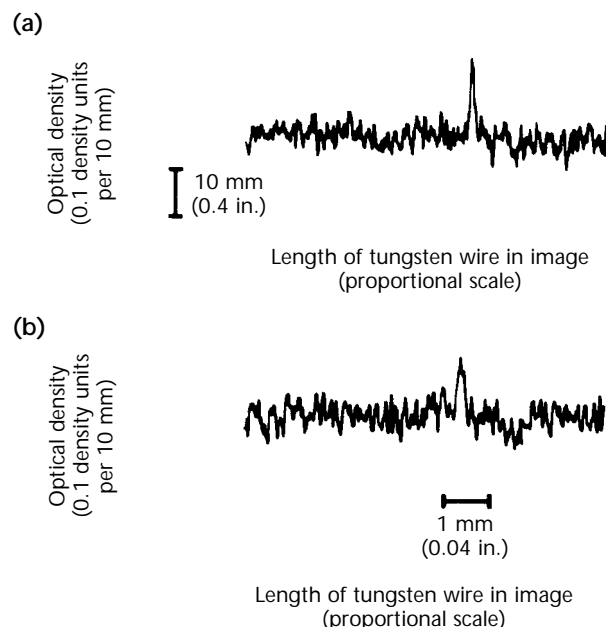


FIGURE 24. Gaging system for direct readout process monitor for carbon coating thickness on nuclear fuel microspheres.<sup>27</sup>



heavy on one side and light on the other or vice versa but contain the same amount of metal. If the diameter changes, the total wall thickness across two walls 180 degrees apart will not be the same. These wall thickness variations and diameter variations can affect radiation transmission measurements and interfere with the density determination. Commercial tubing 13 mm (0.5 in.) outside diameter by 0.89 mm (0.035 in.) wall may have a wall thickness tolerance of  $\pm 10$  percent and an inside diameter tolerance of 0.27 mm ( $\pm 0.005$  in.).

Figure 26a is a diagram of the technique with the radiation sources on the bottom and the detector on top.<sup>31</sup> The radiation energies used were those from cobalt-60 (1.17 and 1.33 MeV) and cesium-137 (0.662 MeV) obtained from 74 GBq (2 Ci) of cobalt-60 and 185 GBq (5 Ci) of cesium-137. The two sources were housed in a two-compartment uranium pig. The detection system for measuring the radiation intensity is a sodium iodide (thallium activated) crystal optically coupled to a photomultiplier tube. The collimation of the beam occurs in the pig where the radiation beams are 5 mm (0.2 in.) wide by 16 mm (0.63 in.) long and then in lead cylinders measuring 64 mm (2.5 in.) diameter by 152 mm (6.0 in.) long. The long dimension of the collimators is lined up in the axial direction of the fuel rod. The output of the detector is fed to a strip chart recorder.

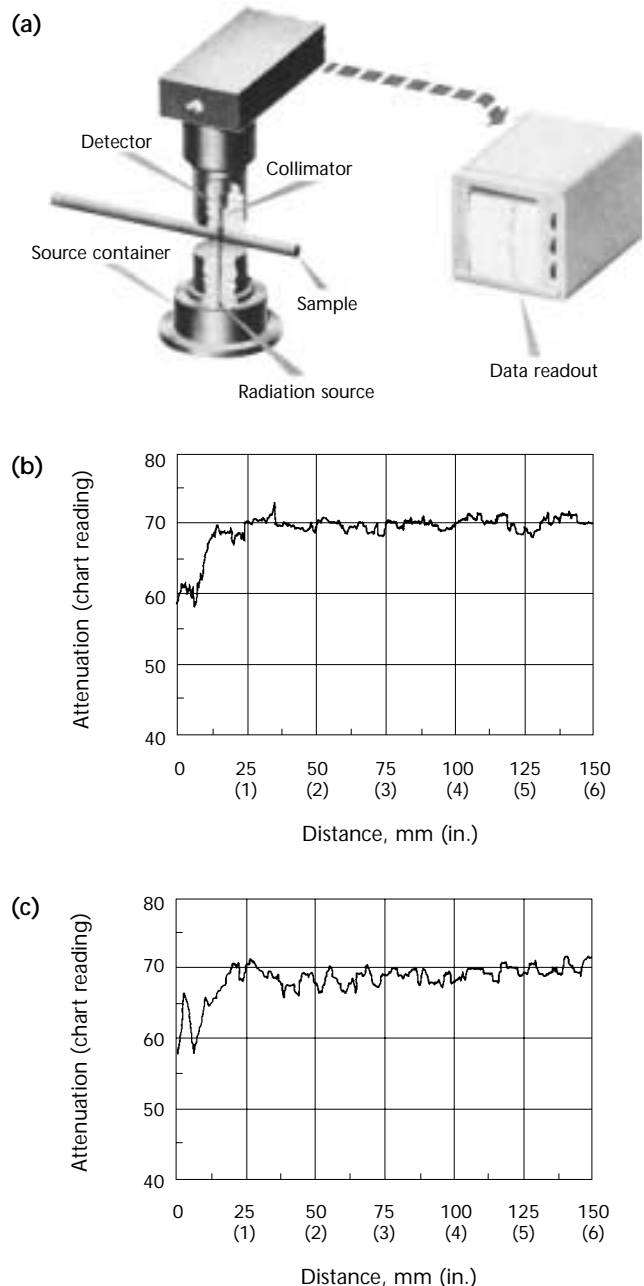
Two collimator dimensions,  $3.0 \times 3.0$  mm ( $0.13 \times 0.13$  in.) and  $3 \times 13$  mm ( $0.125 \times 0.5$  in.), were evaluated as well as various scanning speeds. A larger collimator reduces the resolution as shown in Figs. 26b and 26c.<sup>31</sup> With the larger collimator, the signals are higher but show less resolution to changes evident in the smaller collimator scan.

Figure 27 shows the difference in attenuation between the cobalt-60 and cesium-137 radiation sources. The attenuations are close at lower concentrations and deviate at higher concentrations. This difference in source attenuation is expected because of the source energies.

From calculations using mass absorption coefficients of the various materials at the effective energy of cobalt-60, it was determined that 0.025 mm (0.001 in.) of stainless steel was equivalent in attenuation to 0.018 mm (0.0007 in.) of thorium uranium dioxide (3 percent thorium) fuel. Stainless steel shims 0.025 mm to 0.25 mm (0.001 to 0.010 in.) thick were placed on the tubes containing 13 and 19 mm (0.5 and 0.75 in.) diameter pellets during scanning. Figure 28 shows the attenuation curves as a function of fuel density with no shims

and with the 0.25 mm (0.010 in.) thick shim in the beam.<sup>31</sup> As the plots show, the additional thickness of stainless steel has an equivalence in attenuation to a 1.66 percent change in fuel content, a 0.178 mm (0.007 in.) wall thickness

FIGURE 26. Radiation attenuation technique for evaluation of fuel concentration in metal clad nuclear fuel rod: (a) setup; (b) strip chart recorder trace showing attenuation with  $3.2 \times 12.7$  mm ( $0.13 \times 0.5$  in.) collimator; (c) same, showing reduced resolution with  $3.2 \times 3.2$  mm ( $0.13 \times 0.13$  in.) collimator. Outside diameter of compacted rod = 12.7 mm (0.5 in.). Thickness of stainless steel wall = 0.89 mm (0.035 in.). Diameter of compacted thorium uranium dioxide (3 percent thorium) fuel = 10.92 mm (0.430 in.).<sup>31</sup>





change on the 13 mm (0.5 in.) diameter rod.

The gamma ray attenuation technique developed in this study had a reproducibility better than 1 percent for evaluating fuel heterogeneities in vibratory compacted and sintered pellet fuel rods with metal cladding. Heterogeneities appearing as fuel concentration changes result from particle and compaction density variations as well as variations in tube wall and diameter. If better precision is required, tubing with special tolerances must be used.

Computed tomography (CT) was first developed and used in the medical field. The technique is starting to become popular in industrial radiography but several differences between medical and industrial radiography have restricted its use. In industrial radiography, a higher range of film densities or contrast settings are used for a large range of objects, many of which are not suitable for computed tomography or would greatly multiply the cost of performing computed tomography. In general, industrial radiography is performed with requirements for smaller detail in the radiographs, detail that can be hard to achieve in each of the multiple radiographs required.

Normally in a radiograph, the details of a three dimensional object are displayed in two dimensions. The cross sectional details are piled on each other, the film

density or contrast setting at any given location being a function of the thickness and density seen as the radiation traverses the object. Computed tomography presents the radiographic exposure data in a cross section of the object, revealing details as if the object were sliced perpendicularly to the axis about which the multiple radiographs were made.

To produce the computed tomographic image, multiple exposures are made at multiple angles around a selected axis of the specimen. Processed film images can be digitized by scanning and recording the film densities within the imaged object for each angled exposure. Various other digital imaging techniques can be used to produce digital image data. The digitized data are then imported to a computed tomographic image reconstruction process in a computer.

With suitable calibration, computed tomography can have higher sensitivity to smaller changes in density or thickness than in conventional radiography. Medical systems routinely claim the ability to achieve sensitivities within 0.5 percent of thickness or material density. Computed tomography has been used with X-ray, gamma ray and neutron beams in examining fuel and other nuclear materials. A few of the applications are discussed next.

Experiments<sup>32</sup> were performed on nuclear fuel rod assemblies to determine debris formation and relocation (DFR) in simulated accidents to study the effects of

FIGURE 27. Comparison of attenuation of radiation from cobalt-60 and cesium-137 versus changes in fuel concentration, using  $3.2 \times 3.2$  mm ( $0.13 \times 0.13$  in.) collimator.<sup>31</sup>

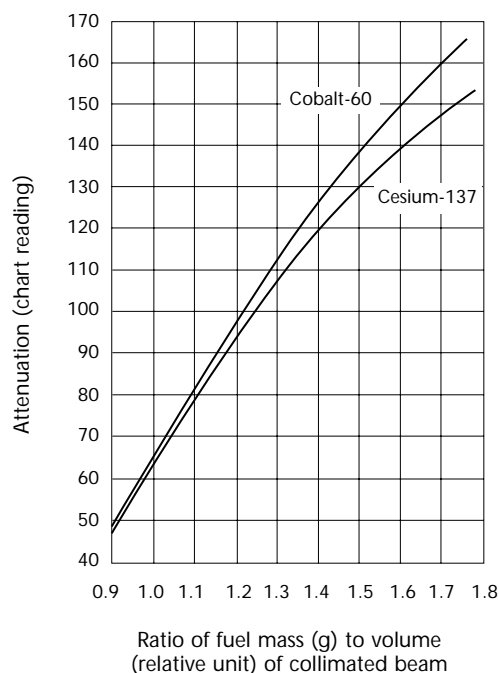
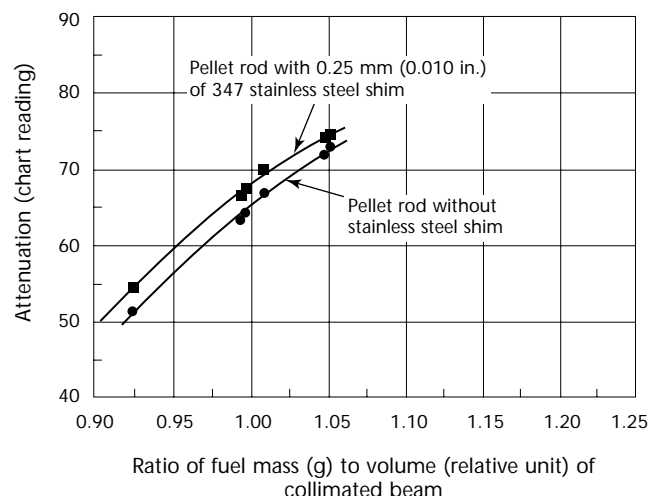


FIGURE 28. Radiation attenuation curves obtained with cobalt-60, showing influence of variations in metal cladding thickness on apparent fuel concentration, with  $3.2 \times 3.2$  mm ( $0.13 \times 0.13$  in.) collimator. Scan speed =  $3.4 \text{ mm} \cdot \text{s}^{-1}$  ( $8 \text{ in.} \cdot \text{min}^{-1}$ ). Outside diameter of pellet rod = 12.7 mm (0.5 in.). Thickness of stainless steel wall = 0.89 mm (0.035 in.). Diameter of thorium uranium dioxide (3 percent thorium) pellet = 10.82 mm (0.426 in.).<sup>31</sup>





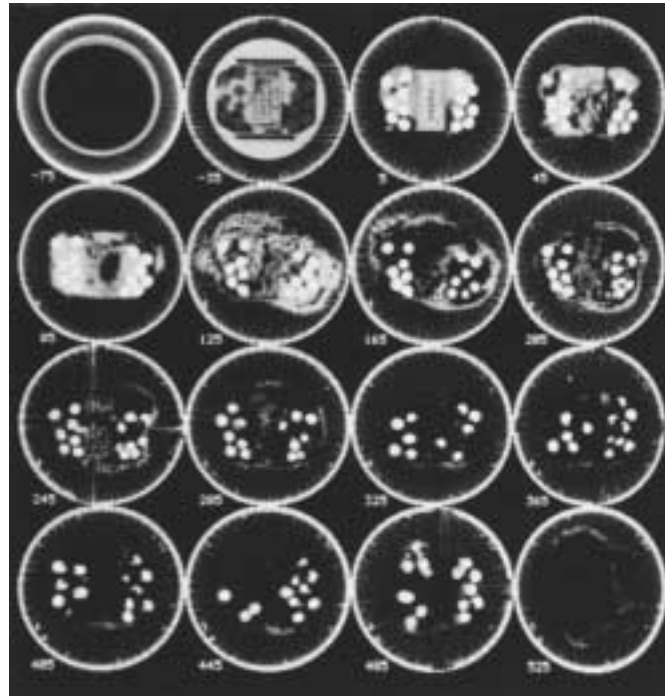
overheated conditions on the assemblies. Light water reactor (LWR) fuel rod assemblies are placed in the core of a research reactor and where the fuel is fission heated. The assembly is then exposed to superheated steam to create conditions that might exist in a core damage accident. After the assemblies have been exposed to the high temperatures, a low density potting material is poured into the assembly to stabilize the debris in its condition immediately after testing. The assembly was contained in a steel can about 180 mm (7.1 in.) in diameter and 1.00 m (39 in.) long. The part of the fuel assembly in the can that contained the fuel and where molten fuel might have flowed was about 100 mm (3.9 in.) by 650 mm (25 in.) long. Because of the thickness and density of the fuel, a high energy source, 7.5 MeV linear accelerator was selected to perform the radiography. At the time of this work, no electronic or digital screens could record this radiation so a fine grain film was used. Because the fuel in the can was giving off some radiation, the film had to be separated from the can about 1.00 m (39 in.) and that required that a long source-to-object distance of 12 m (39 ft) also be used to reduce unsharpness. The film cassette had 0.5 mm (0.020 in.) front and back lead screens contacting the film while 6 mm (0.25 in.) lead sheets protected the cassette from forward scatter and backscatter. The exposures were each 0.5 Gy (50 rad) at the film and required about 8 min to accomplish each exposure with a minimum film density of about 1.5.

Four assemblies were radiographed. The first can was radiographed every 10 degrees whereas succeeding cans were radiographed every 5 degrees. Only 180 degrees was covered, as the 180 degree exposure contained the same information as at 0 degrees. The films were digitized using a microdensitometer with a resolution of 0.4 mm (0.016 in.) in both directions. The digitizing produced 512 points per scan and 1400 to 1630 scans per area of interest in the four sets of either 19 or 37 radiographs.

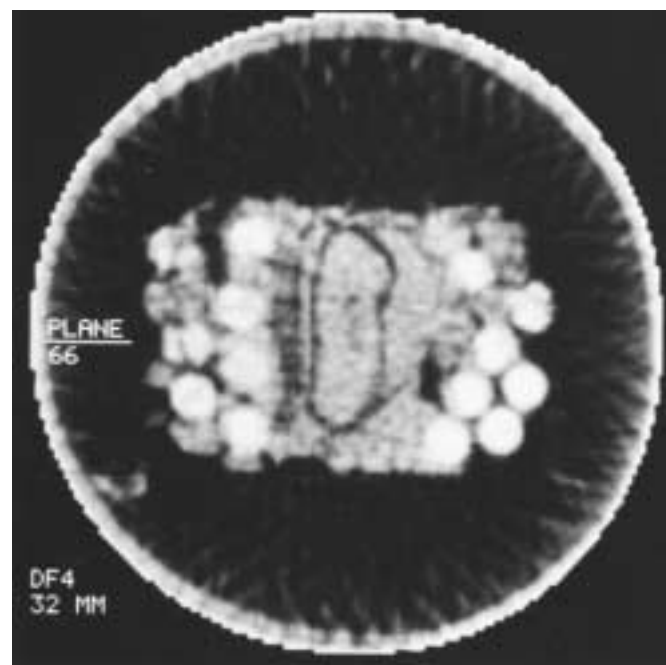
Figure 29 shows some typical tomographic images of the last fuel element assembly.<sup>32</sup> These images were produced on a display device having  $512 \times 512$  pixel resolution. The array of 16 separate images (Fig. 29a) is displayed at the reconstructed resolution of  $128 \times 128$  pixels per image. In particular, note that the shapes and locations of the eroded rods, as well as cracks such as that in the rod nearest the plane 66 markers in Fig. 29b, are visible in these images. Each tomographic image of each can consists of 1400 to 1600 slices like those in Fig. 29a.

FIGURE 29. Typical slice images from last fuel assembly tested: (a) array of 16 images of rod cross sections at resolution of  $128 \times 128$  pixels; (b) magnification by interpolation of one cross section image to  $128 \times 128$  pixels.<sup>32</sup> Interpolation does not improve genuine resolution but avoids pixelization of image.

(a)



(b)



Computed radiography has proven useful in the posttest analysis of the debris formation and relocation nuclear fuel experiment packages. The film based technique provides relatively high resolution images but is expensive because of the time required to handle and digitize the radiographs.

Similar tomographic work was done on irradiated fuel elements at another facility.<sup>33</sup> However, these fuel elements have up to  $2.78 \text{ Sv}\cdot\text{s}^{-1}$  ( $10^6 \text{ R}\cdot\text{h}^{-1}$ ) gamma activity so that isotope or X-ray exposures are out of the question as the large gamma intensity would expose the film or saturate any other detector. This work called for neutron radiographic tomography with transfer foils. In neutron radiography, transfer foils are used in high intensity gamma beams. Neutrons are absorbed in the transfer foil, in this case 0.13 mm (0.024 in.) thick indium. Neutron radiography of large nuclear fuel bundles requires neutron beam energies of sufficient energy to penetrate the full array of fuel pins in the bundle. In most neutron radiography, the images are formed by the capture of thermal or lower energy neutrons. However, in this case, the reactor needed to produce epithermal neutrons. These neutrons provide sufficient penetration of the fuel bundles and are imaged by the 1.46 eV resonance of indium. Because indium has a large thermal neutron cross section, the indium must be shielded with a thermal neutron filter such as cadmium or gadolinium. Because the gamma radiation from the fuel bundles is quite large, positioning adjustments to the specimen and rotation for the various radiographs must be accomplished

remotely. Also the indium foils must be placed remotely for each exposure. A drawing (Fig. 30) shows one part of the reactor for neutron radiography and other features.<sup>33</sup>

Exposures of the indium foil in the reactor required 18 min with a collimator length-to-diameter ratio of 125. The activated transfer screens were placed against a medium grain radiographic film in a vacuum cassette (so intimate contact results) immediately following exposure. The transfer screen must be left in contact with the film for at least four half lives (indium half life = 54 min) but normally these exposures were left overnight. The resultant beta particle emission from the indium screen exposes the film, which in turn is processed in an automatic processor. Thirty-six films were exposed for each fuel bundle. Figure 31 shows a reconstruction of the neutron tomographic image of one cross section in a 91-pin fuel bundle using the 36 neutron radiographs to form the image.<sup>33</sup>

Neutron tomography of irradiated fuel bundles is an expensive form of nondestructive testing and it would probably not find general application for examination of routine fuel bundles. However, there are safety tests being conducted on fuel bundles in which there is a very large capital investment and where the expected results have warranted the cost of tomography. In these instances, the irradiation effects on the fuel under the deliberately induced severe operating conditions have caused very gross displacement of the internal components. These features would obviously be lost or disturbed during disassembly of the bundle. Neutron tomography thus becomes a valuable and effective way to study the relationship of

FIGURE 30. Neutron radiographic facility used for neutron tomography of hot fuel assemblies.<sup>33</sup>

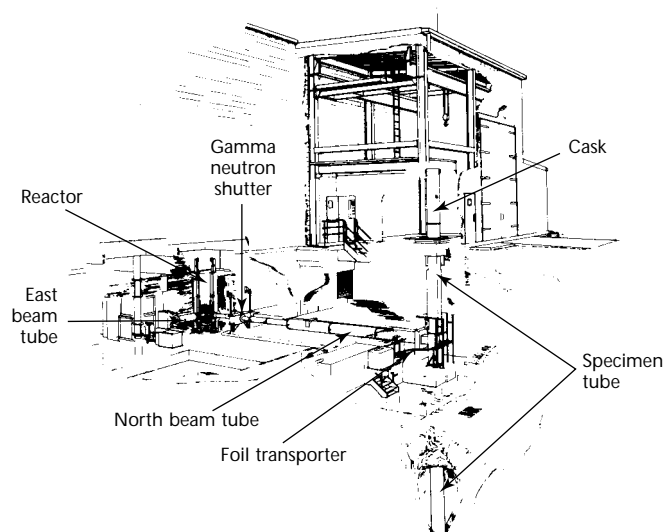
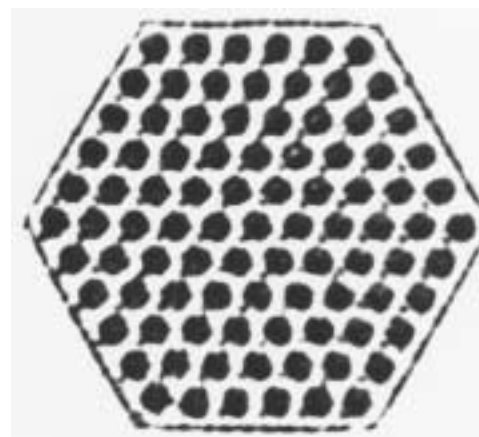


FIGURE 31. Tomographic reconstruction of 91-pin fuel bundle using 36 neutron radiographs.<sup>33</sup>



these internal components before disassembly.

In another development,<sup>34</sup> a mobile computed tomographic system has been developed to provide gamma and 2 MeV X-ray images of nuclear waste materials. The mobile feature of the waste inspection tomography program allows inspections to be performed at the storage sites without the need to ship the nuclear waste to another facility for characterization. With the detectors built into the system, the radioactive gamma rays from the stored material can be measured for intensity and wavelength and the specific radioactive isotopes identified. Without opening waste drums, tomography can inspect and characterize radioactive waste as low level waste, transuranic waste or mixed waste. With externally transmitted X-ray techniques, waste inspection tomography can identify high density waste materials like heavy metals, define drum contents in two-dimensional and three-dimensional space, quantify free liquid volumes through density and X-ray attenuation coefficient discrimination and measure drum wall thickness. With waste emitting gamma ray assay techniques, tomography can locate gamma emitting radioactive sources in two-dimensional and three-dimensional space and identify gamma emitting isotopic species. It can also identify the external activity levels of emitting gamma ray sources, correct for waste matrix attenuation, provide internal activity approximations and provide the data needed for waste classification.

The tomographic linear detector array is curved and consists of 896 individual channels of cadmium tungstate ( $\text{CdWO}_4$ ) crystals mounted on individual photodiodes with thin septa between channels to eliminate crosstalk, blooming and in-plane scatter. These detectors have an 18-bit dynamic range (262 144 gray levels) for analog-to-digital conversion. The wide dynamic range is used in waste inspection tomography to image the variety of material densities and geometries found in Department of Energy waste streams, including combustibles, glass, cement, sludges and metals that may be present in the same drum. The linear array has a 2 MeV high energy accelerator as an externally transmitted radiation source, using a thin fan beam output with a measured flux of  $11.7 \text{ mGy}\cdot\text{s}^{-1}$  ( $70 \text{ rad}\cdot\text{min}^{-1}$ ) at 1 m (39 in.). This high energy source is needed to penetrate the denser and thicker Department of Energy waste forms like glass logs, sludge and cemented drums while allowing for an optimum inspection throughput. A three-dimensional volume rendering of waste drum computed tomography slices are shown in Fig. 32.<sup>34</sup>

Three-dimensional visualization software has been used to cut away the front portion of the drum to reveal its internal structures.

FIGURE 32. Volume rendered 100-slice display of 2 MeV transmission computed tomographic data taken from waste drum phantom.<sup>34</sup>



## PART 5. Other Uses for Radiographic Testing

Often radiographic testing is used because a specification or code requires it to verify that fabrication activities have been completed to some level specified in the standard. However, there are a few applications where nondestructive tests are used because they provide information not obtainable from visual or physical tests performed to determine continued performance. A few uses of radiography in some nonroutine applications are cited below.

Radiography was first used on wooden poles<sup>35</sup> by utilities to locate decay in the 1930s. The cost of radiographic testing was expensive so the method was replaced by ultrasonic tests in the 1960s. Video X-ray units and other electronic imaging means may make radiography a more economical test today.

Cables used for electric power transmission operate in hostile environments. Fatigue damage results from dynamic conditions imposed by these environments. Radiography is used in the field to detect partial failures and damage to cables and hardware.<sup>36</sup> In the 1950s utilities performed radiographic tests on transmission lines. In most cases, these tests were performed on deenergized lines and all used aerial lifts. These field tests were normally performed with gamma radiation. In the 1960s X-ray techniques were developed that provided lower energies to be used for the radiography. For field inspections, a pulsed X-ray system with remote tube head and a 30 m (100 ft) tube head extension cable was developed. The remote tube head minimizes the size and weight of the components, which must be used by linemen on the transmission line structure. The total weight of the aerial components is under 13.6 kg (30 lb<sub>m</sub>), including all fixtures and cable. An assembly drawing of the aerial components is shown in Fig. 33.<sup>36</sup>

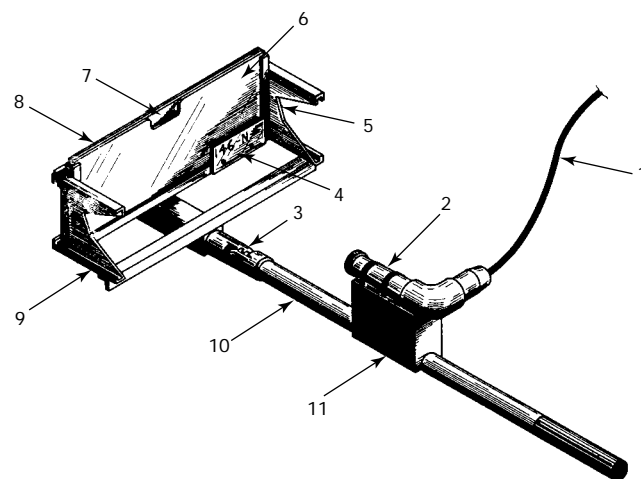
A battery operated, inverter power supply was constructed to provide the 1200 W surges required by the X-ray system. This rechargeable battery power supply makes the system completely portable and eliminates the need for a cumbersome gasoline generator. An overnight charge provides sufficient power for a full day of operation (50 or more 15 pulse radiographs). The battery power supply, in its convenient carrying

case, weighs 28 kg (61 lb<sub>m</sub>) and is easily shipped or carried to a field location.

The X-ray tube voltage is 150 kV and the effective current per pulse is 0.06 mC (0.06 mA·s). This pulsed X-ray system produces 14 pulses of radiation per second. Pulse duration is 60 ns. Any number of pulses up to 99 can be preset on the automatic pulse number selector. When the exposure is initiated, the equipment automatically counts the pulses and stops at the preset number.

The fixture shown in Fig. 34<sup>36</sup> was designed primarily for use on energized power lines. All fixture parts are mounted on an insulated stick (*hot stick*), which is commonly used by linemen for work on energized lines. A 2.4 m (8.0 ft) fiber glass hot stick is used. Other lengths can be used depending on specific requirements of the job. A splined fitting on the film carrier and an adjustable hose clamp on the tube head fixture allow various length hot sticks and provide fast and

FIGURE 33. Hot line X-ray fixture.<sup>36</sup>



### Legend

1. 30 m (100 ft) high voltage extension cable.
2. Remote X-ray tube head assembly.
3. Splined joint.
4. Lead film markers in plastic pocket.
5. Special cutout for supporting and positioning fixture on cables.
6. Protective plastic sheet.
7. Film and screen cassette.
8. Reinforced backup plate.
9. Light weight film carrier assembly.
10. Fiber glass hot stick.
11. Adjustable tube head mount for setting distance from focal point to sensor plane.



convenient assembly. The tube head can be positioned easily anywhere along the length of the hot stick.

Industrial radiographic film is not used in this application, because of the higher doses of radiation required. Instead, medical screens and film provide adequate sensitivity for the application. Typical exposures using focus film distances of 760 mm (30 in.) are 15 to 20 pulses (1 to 1.5 s). After 30 pulse exposures, a dosimeter located 0.3 m (1 ft) behind the tube head did not show any dose accumulation. A second dosimeter 0.3 m (1 ft) to the side of the tube head also showed no dose accumulation. Another dosimeter placed 4 m (13 ft) directly in front of the tube head had a reading of  $1.3 \mu\text{C}\cdot\text{kg}^{-1}$  (5 mR). During field inspections, linemen using pocket dosimeters have had no more than  $0.5 \mu\text{C}\cdot\text{kg}^{-1}$  (2 mR) recorded for a full day's work. Examples of radiographs made on hot lines in the field are shown in Figs. 35 and 36.<sup>36</sup>

## Closing

Radiographic testing has a long history of significant applications in the electric power and related industries.<sup>37-43</sup> Innovations in detector technology, digital processing and signal transmission and storage hold the promise of further development and more applications in the twenty-first century.

FIGURE 34. Lineman using hot line X-ray equipment.<sup>36</sup>



FIGURE 35. Radiograph of splice made on energized line reveals splice applied incorrectly. Outer aluminum sleeve (arrow 1) should be centered over steel core splice (arrow 2).<sup>36</sup>

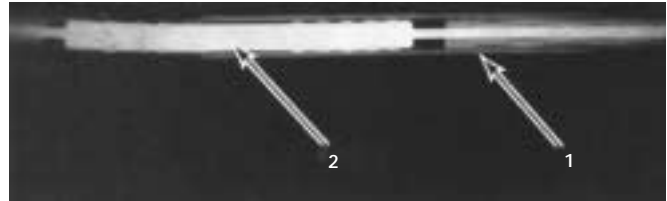


FIGURE 36. Radiograph showing multiple breaks under suspension clamp in field X-ray.<sup>36</sup>



## References

1. McMaster, R.C. *Nondestructive Testing Handbook*, first edition. Vol. 1, Sec. 25. Columbus, OH: American Society for Nondestructive Testing (1959): p 16-27.
2. API Recommended Practice 1104, *Welding of Pipelines and Related Facilities*, eighteenth edition. Washington, DC: American Petroleum Institute (1994).
3. ASTM E 1025, *Standard Practice for Design, Manufacture, and Material Grouping Classification of Hole-Type Image Quality Indicators (IQI) Used for Radiology*. West Conshohocken, PA: ASTM International (1998).
4. ASTM E 747, *Standard Practice for Design, Manufacture and Material Grouping Classification of Wire Image Quality Indicators (IQI) Used for Radiology*. West Conshohocken, PA: ASTM International (1997).
5. Bagarry, A. and A. Sambrarov. "Seismic Activity Calls for Modified Radiographic Technique in Piping System Inspection." *Materials Evaluation*. Vol. 55, No. 4. Columbus, OH: American Society for Nondestructive Testing (April 1997): p 452-453.
6. Placious, R.C., D.A. Garrett, M.B. Kasen and H. Berger. "Dimensioning Flaws in Pipeline Girth Welds by Radiographic Methods." *Materials Evaluation*. Vol. 39, No. 8. Columbus, OH: American Society for Nondestructive Testing (July 1981): p 755-760.
7. Wenk, S.A. "Radiographic Video Technique for Sizing Defects in Pipe Welds." *Materials Evaluation*. Vol. 39, No. 8. Columbus, OH: American Society for Nondestructive Testing (July 1981): p 748-751. Errata, *Materials Evaluation*, Vol. 39, No. 10 (September 1981): p 938.
8. ASME Boiler and Pressure Vessel Code: Section V, *Nondestructive Examination*. Article 2, "Radiographic Examination." New York, NY: American Society of Mechanical Engineers (2001): p 16-59.
9. ASME Boiler and Pressure Vessel Code: Section III, *Rules for Construction of Nuclear Facility Components*. Div. 1, Subsections NB and NC, Class 1 and Class 2 Components. New York, NY: American Society of Mechanical Engineers (2001).
10. ANSI/ASME B 31.1, *Power Piping*. New York, NY: American Society of Mechanical Engineers (1998).
11. ANSI/ASME B 31.3, *Process Piping*. New York, NY: American Society of Mechanical Engineers (1999).
12. Marks, P.T. "The Generation of Error in Interpretation." *1993 International Chemical and Petroleum Industry Inspection Technology III Topical Conference* [Houston, TX]. Columbus, OH: American Society for Nondestructive Testing (June 1993): p 90-91.
13. Burkle, W.S. "Application of Tangential Radiographic Technique for Evaluating Pipe System Erosion/Corrosion." *Materials Evaluation*. Vol. 47, No. 10. Columbus, OH: American Society for Nondestructive Testing (October 1989): p 1184, 1186-1188.
14. Krollicki, R.P. "Internal Corrosion Examination and Wall Thickness Measurement of Pipe by Radiographic Method." *Materials Evaluation*. Vol. 35, No. 2. Columbus, OH: American Society for Nondestructive Testing (February 1977): p 32-33, 44.
15. Loftus, T. "Integrating Profile and Computed Radiography for Internal and External Corrosion Detection, Evaluation and Monitoring." *ASNT's International Chemical and Petroleum Industry Inspection Technology (ICPIIT) VI Topical Conference: The Challenges to NDT in the New Millennium* [Houston, TX]. Columbus, OH: American Society for Nondestructive Testing (June 1999): p 77-86.
16. Gupta, N. and B. Isaacson. "Near Real Time In-Service Pipe Component Inspection without Removing Insulation." *The 9th Asia-Pacific Conference on Nondestructive Testing in Conjunction with ASNT's 1998 Spring Conference and 7th Annual Research Symposium* [Anaheim, CA]. Columbus, OH: American Society for Nondestructive Testing (March 1998): p 217-220.



17. Winfield, C. and J.D. Bowman. "Radiotracer Methods for Flow Measurement and Online Leak Detection." *1993 International Chemical and Petroleum Industry Inspection Technology III Topical Conference* [Houston, TX]. Columbus, OH: American Society for Nondestructive Testing (June 1993): p 86-89.
18. Winn, W.G. "Neutron Radiographic Detection Limits of Fluids in Metal Pipes." *Materials Evaluation*. Vol. 34, No. 9. Columbus, OH: American Society for Nondestructive Testing (September 1976): p 207-212.
19. Regas, S. "Industrial Applications of Radioisotopes, Nuclear Liquid Level Gauges." *Nondestructive Testing*. Vol. 16, No. 6. Columbus, OH: American Society for Nondestructive Testing (November-December 1958): p 493-494.
20. Forrer, G.R. and F. J. Sattler. "State-of-the-Art Review of Nondestructive Testing as Applied to Nuclear Pressure Vessels and Components." *Materials Evaluation*. Vol. 33, No. 10. Columbus, OH: American Society for Nondestructive Testing (October 1975): p 20A-23A, 25A-27A.
21. Lapides, M.E. "Radiographic In-Service Inspection of Cast Austenitic Nuclear Plant Components." *Materials Evaluation*. Vol. 44, No. 1. Columbus, OH: American Society for Nondestructive Testing (January 1986): p 108-113.
22. Freeman, W.E. and M.L. Turnbow. "Miniature Linear Accelerator for Radiography of Nuclear Plant Components." *Materials Evaluation*. Vol. 49, No. 10. Columbus, OH: American Society for Nondestructive Testing (October 1991): p 1341-1342.
23. Cabe, D. "Radiography of Main Steam Piping Welds Enclosed within Guard Pipe." *Materials Evaluation*. Vol. 47, No. 10. Columbus, OH: American Society for Nondestructive Testing (October 1989): p 1126-1128.
24. API Standard 650, *Welded Steel Tanks for Oil Storage*, tenth edition. Washington, DC: American Petroleum Institute (1998).
25. API Standard 653, *Tank Inspection, Repair, Alteration, and Reconstruction*, third edition. Washington, DC: American Petroleum Institute (2001).
26. Knight, R.B., Jr., C. Maucher and T.S. Jones. "A Method to Determine Erosion in Sealed Double Walled Vessels Using Gamma Ray Sources and Laminographic Tomosynthesis." *The 9th Asia-Pacific Conference on Nondestructive Testing in Conjunction with ASNT's 1998 Spring Conference and 7th Annual Research Symposium* [Anaheim, CA]. Columbus, OH: American Society for Nondestructive Testing (March 1998): p 217-220.
27. Foster, B.E. and S.D. Snyder. "Measurement of Carbon Coating Thickness on Microspheres of Nuclear Fuels." *Materials Evaluation*. Vol. 28, No. 1. Columbus, OH: American Society for Nondestructive Testing (January 1970): p 13-16.
28. Panakkal, J.P., K.N. Chandrasekharan and J.K. Ghosh. "Radiographic Detection of Tungsten in Nuclear Fuel Pin End-Plug Welds." *Materials Evaluation*. Vol. 43, No. 8. Columbus, OH: American Society for Nondestructive Testing (July 1985): p 1005-1007.
29. Stupin, D.M. "Filmless Radiographic Detection of Microscopic Wires and Very Small Areal Density Variations." *Materials Evaluation*. Vol. 45, No. 12. Columbus, OH: American Society for Nondestructive Testing (November 1987): p 1315-1319.
30. Scott, D.M. "Density Measurements from Radioscopic Images." *Materials Evaluation*. Vol. 47, No. 10. Columbus, OH: American Society for Nondestructive Testing (October 1989): p 1113-1114, 1116-1119.
31. Foster, B.E. and S.D. Snyder. "Evaluation of Variables in the Measurement of Fuel Concentration." *Materials Evaluation*. Vol. 26, No. 2. Columbus, OH: American Society for Nondestructive Testing (February 1968): p 27-32.
32. Hansche, B.D. "Film-Based Computed Tomography of Nuclear-Fuel-Damaged Experiments." *Materials Evaluation*. Vol. 47, No. 6. Columbus, OH: American Society for Nondestructive Testing (June 1989): p 741-745.
33. Richards, W.J., G.C. McClellan and D.M. Tow. "Neutron Tomography of Nuclear Fuel Bundles." *Materials Evaluation*. Vol. 40, No. 12. Columbus, OH: American Society for Nondestructive Testing (November 1982): p 1263-1267.
34. Bernardi, R.T. and H. Martz, Jr. "Nuclear Waste Drum Characterization with 2 MeV X-Ray and Gamma-Ray Tomography." *Materials Evaluation*. Vol. 53, No. 10. Columbus, OH: American Society for Nondestructive Testing (October 1995): p 1121-1122, 1124-1126.

35. Collins, R.V. "The Role of NDT in an Electric Utility." *Materials Evaluation*. Vol. 30, No. 5. Columbus, OH: American Society for Nondestructive Testing (August 1972): p 174-180.
36. Strange, W.F., G.H. Ault and E.A. Capadona. "Radiographic Testing of Cables and Hardware for Power Transmission and Oceanography." *Materials Evaluation*. Vol. 27, No. 1. Columbus, OH: American Society for Nondestructive Testing (January 1969): p 16-22.
37. Carpenter, O.R. "Some Results of Advances in Welding and Radiography on the Welding of Pressure Vessels" [1945 Lester Honor Lecture]. *Industrial Radiography and Nondestructive Testing*. Vol. 5, No. 1. Columbus, OH: American Society for Nondestructive Testing (Summer 1946): p 9-17.
38. Moriarty, C.D. "Progress in Nondestructive Testing of Steam Turbine-Generator Components" [1960 Mehl Honor Lecture]. *Nondestructive Testing*. Vol. 19, No. 1. Columbus, OH: American Society for Nondestructive Testing (January-February 1961): p 29-38.
39. Hovland, H. "Developments in Field X-Radiography, 1931-62." *Materials Evaluation*. Vol. 43, No. 11. Columbus, OH: American Society for Nondestructive Testing (October 1985): p 1386-1390.
40. Moore, P.O. "A Gamma-Radiographer of Pipeline Welds." *Materials Evaluation*. Vol. 43, No. 9. Columbus, OH: American Society for Nondestructive Testing (August 1985): p 1084-1086, 1088-1089.
41. *Neutron Radiography: Proceedings of the First World Conference* (San Diego, CA, December 1981). Dordrecht, Netherlands: D. Reidel Publishing Company (1983).
42. *Neutron Radiography: Proceedings of the Second World Conference* (Paris, France, June 1986). Dordrecht, Netherlands: D. Reidel Publishing Company (1987).
43. Ross, A.M. "Neutron Radiographic Inspection of Nuclear Fuels." *Atomic Energy Review*. Vol. 15, No. 2. Vienna, Austria: International Atomic Energy Agency (1977): p 221-247.



# 20

C H A P T E R

## **Aerospace Applications of Radiographic Testing<sup>1</sup>**

---

Lisa Brasche, Iowa State University, Ames, Iowa

Donald J. Hagemmaier, Huntington Beach, California

# PART 1. Film Radiography of Aviation Components

Radiography inspection plays a critical role in the life cycle management of aviation components with applications during production and service. Initial applications of radiography to aerospace inspections occurred over 50 years ago. During the years from 1955 to 1965, the aircraft industry produced the first commercial jet transports with expansion in the aerospace field to ballistic missiles, research rocket aircraft and the beginning of manned space flight. The rapid growth in engineered systems placed new demands on nondestructive testing.<sup>2,3</sup>

Initial routine applications used radiographic testing to check castings and weldments for discontinuities as part of fabrication quality control.<sup>4,5</sup> Many small, lightweight aluminum castings were inspected semiautomatically by fluoroscopy. Nationally, commercial aircraft and military aircraft were periodically X-rayed to detect fatigue cracks (Fig. 1) and corrosion (Fig. 2). Lightweight portable X-ray machines were not available at this time, which required specialized designs like the boom mounted, mobile X-ray unit (Fig. 3) that allowed placement of the X-ray source in the proper position for each exposure. It was especially useful for radiography of wings and empennage structures. In the 1970s, the aerospace industry was engaged in the moon projects, wide body commercial transports, research and military satellites, advanced ballistic

missiles and the beginning of the space shuttle program. These advances placed new demands on radiographic testing.

## Automated Inspection<sup>5,6</sup>

Computers are used in all aspects of inspection, for data gathering, processing, transmission and storage. Automation of radiographic testing can take any of several forms.<sup>6</sup>

FIGURE 2. Radiograph showing corrosion in bonded honeycomb.

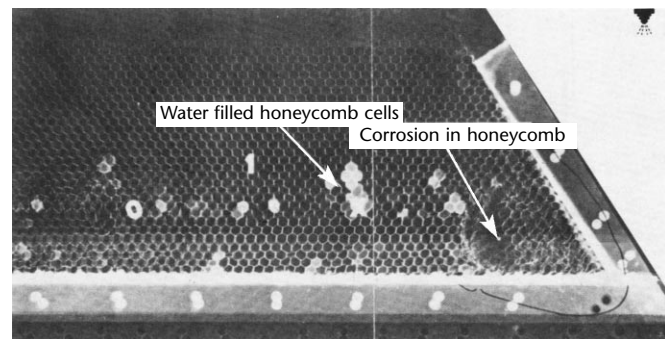
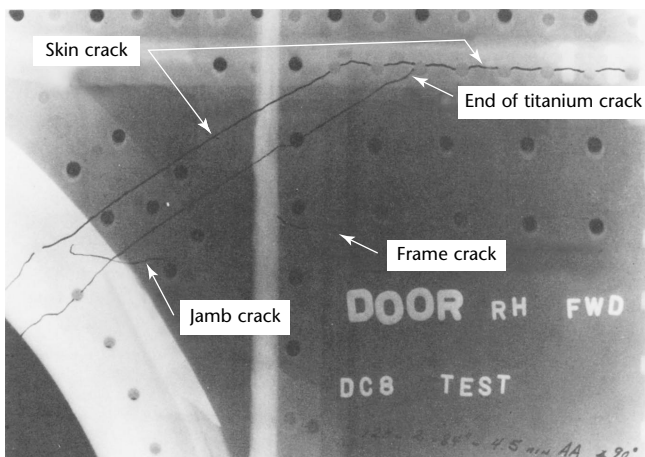


FIGURE 3. Mobile X-ray system.



FIGURE 1. Radiograph showing cracks at door corner.



1. Radioscopic inspection may take place in assembly lines for mass production of components, such as printed circuits, that are later integrated into aircraft.
2. Robotic inspection calls for programmed control of test object position, including loading into, orientation with and offloading from test system.
3. Automatic inspection involves programmed manipulation and indexing of source or sensor system components relative to a test object *in situ*.

### In-Motion Radiography<sup>5</sup>

Applications of radiography have involved inspection in support of the manufacture of intermediate range ballistic missiles. A major problem is to provide techniques for the X-ray inspection of large tank weldments — imperative to meet schedule requirements for reliability, to make timely delivery of missile components and to keep costs commensurate with those of an average product development.

In-motion radiography of weldments in one case has required that an X-ray facility be built and special equipment designed or purchased. In the absence of packaged strip film, engineers have designed and built a machine to cassette 70 mm roll film. The technique consists of placing two rod anode X-ray tubes on a boom and porting the X-rays through an aperture that projects a narrow beam to the longitudinal welds of the tank. The welded tank was placed on a carriage that rode a track anchored on the floor of the exposure room (Fig. 4). An electrical variable speed drive propelled the carriage and tank along the track at a speed of  $0.15 \text{ m} \cdot \text{min}^{-1}$  ( $0.5 \text{ ft} \cdot \text{min}^{-1}$ ). Simultaneously, the three longitudinal weldments were exposed to the X-ray beams.

Two 150 kV X-ray units were used to reduce the exposure time by half. One tube was located at the end of the boom and a second was located half the tank length behind it. With this arrangement, it was necessary to propel the tank only half its length to obtain complete exposure of the three longitudinal welds. The aft X-ray tube was positioned inside the boom to compensate for the two different tank lengths. The carriage drive mechanism and X-ray machines were synchronized to operate simultaneously when the start button was pushed in the control room. Three lead ports were used to restrict the X-ray beams to the three longitudinal welds. The slits in the port ends were 3.2 mm (0.13 in.) long and 25.4 mm (1.00 in.) wide, producing a beam 25.4 mm (1.00 in.) long and

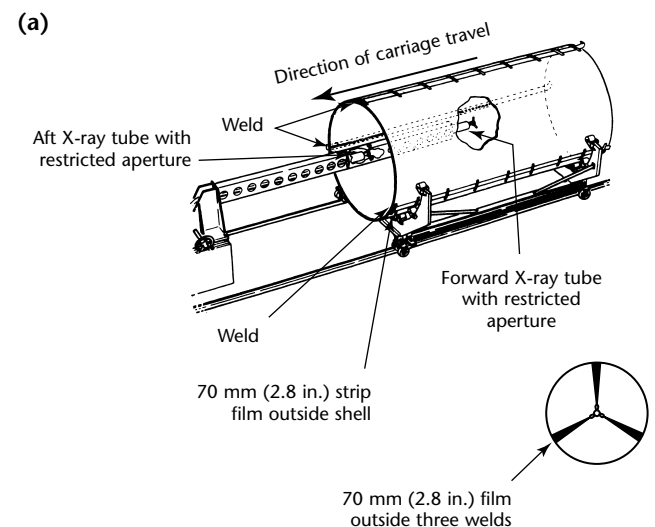
203 mm (8.0 in.) wide, at a 1.22 m (48 in.) source-to-film distance. Table 1 compares the techniques used.

In-motion radiography has also been used for liquid hydrogen tanks in solid rocket motors (Fig. 5).

### Flight Test Aircraft Inspection<sup>7</sup>

Applications also include a nondestructive testing unit to perform inspections of flight test passenger jet aircraft. To address issues that arise with performing nondestructive testing in the field, such as the transportation of equipment to the job, a mobile laboratory was designed specifically to house portable equipment and to serve as an X-ray film processing darkroom. The system was used for inspection of jetliners and military aircraft. An elaborate, accelerated test program was undertaken during the flight test phase of the passenger jet in 1957.

FIGURE 4. In-motion radiography of welded steel tanks: (a) schematic; (b) photograph.



(b)

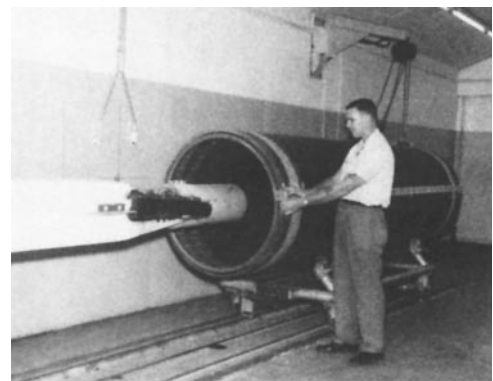




TABLE 1. Comparison of techniques used for in-motion radiography of longitudinal welds.

Material	Thickness		Length		Voltage (kV)	Amperage (mA)	Distance from Focal Point to Sensor		Travel	
	mm	(in.)	m	(ft)			m	(in.)	mm·s <sup>-1</sup>	(in.·min <sup>-1</sup> )
2014 aluminum	9.53	(0.375)	6.1	(20.0)	90	15.0	1.22	(48)	2.5	(6.0)
2014 aluminum	9.53	(0.375)	4.6	(15.1)	90	15.0	1.22	(48)	2.5	(6.0)
4340 steel	2.29	(0.090)	3.7	(12.1)	150	3.5	0.46	(18)	1.7	(4.0)
4340 steel	1.65	(0.065)	2.0	(6.6)	140	3.5	0.46	(18)	1.9	(4.5)
4340 steel	3.81	(0.150)	4.3	(14.1)	160	4.0	0.51	(20)	1.5	(3.5)

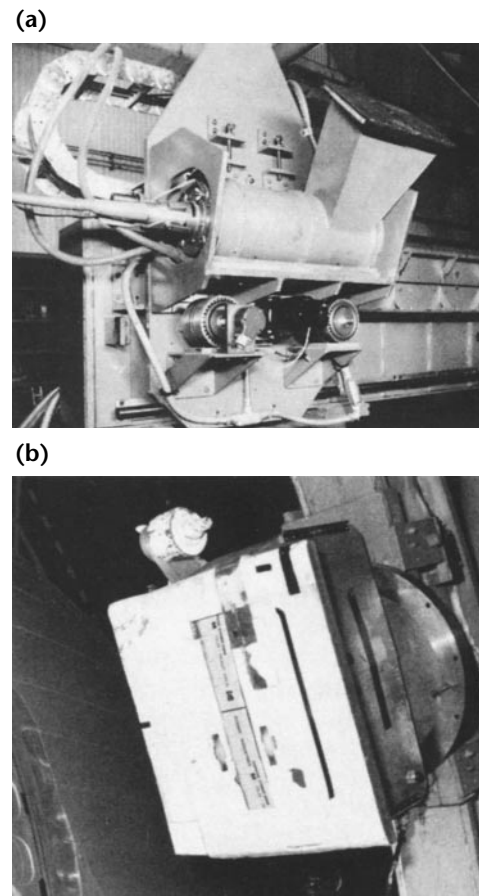
The equivalent of 40 to 120 years of endurance (depending on the type of operation) under simulated service loads was imposed on the test specimens. In this way, damage propagation rates and failsafe characteristics of the structure were studied under deliberately prolonged exposures to fatigue beyond that permissible in actual service. From this information, the company decided what areas to survey with nondestructive testing.

The passenger jet was X-rayed to ascertain that all extraneous material (debris) had been removed from all control surfaces — ailerons, flaps, elevators, rudder and vertical or horizontal stabilizers. It required 480 films of 360 by 430 mm (15 × 17 in.) each to cover the necessary areas. The airplanes were then turned over to a testing division for evaluation and certification. In flight tests aircraft were subjected to stress levels above those normally encountered in regular service. Hence, all critical areas were periodically surveyed 100 percent. The technician placed the film on one side of the vertical stabilizer and then moved the bucket to the opposite side to make the exposure (Fig. 6).

The closed areas and control surfaces of jet aircraft are also radiographed for debris or discontinuities as part of final assembly inspection. Figure 7a shows the placement of 360 by 430 mm film over the structure to be inspected. The X-ray source is positioned to expose a large area of the assembly, as shown in Fig. 8. The film is read and discrepancies are reported. The area is opened up and the debris is removed and compared with the object indicated by the film images. Typical debris includes tools, springs, wire clips, flashlights, nuts, bolts and paint brushes.

Routine inspection for fabrication errors or discontinuities in closed areas is accomplished simultaneously with the debris survey. Defective areas are reported and corrective action is implemented. Film evaluation and corrective action are performed in the shortest possible time. The radiographs may show both debris

FIGURE 5. In-motion radiography of liquid hydrogen tanks: (a) X-ray tube, collimating slit and drive mechanism; (b) film transport mechanism for stop frame radiographic system used on forward dome.



and workmanship errors consisting of inadequate rivet shank-to-hole fit and short hole-to-edge distances. Radiographs of aircraft structure contain a wide range of densities and complicated geometrical images.

Aircraft X-ray inspection can readily locate the following discrepancies: cracks, corrosion, double drilled holes, oversized holes, short hole-to-edge distances, loose



rivets and loose hardware. It is also used to check for missing assemblies and used for general inspection of closed areas.

## Composites

Radiographic testing has found various applications in the inspection of engineered materials such as composite laminates.<sup>4,8-10</sup>

### Brazed Honeycomb Structures

In the 1960s in-motion radiographic inspection of brazed honeycomb structures was developed for military aircraft. A radiation collimator was designed and fabricated with an

adjustable aperture for controlling the radiation pattern and hence the unsharpness gradient necessary for blurring of all preselected details nearest to the radiation source without causing unsharpness of the image surface adjacent to the film. The focal-to-film distance was established at 910 mm (36 in.). The optima in definition, area coverage, radiation potential and speed of travel were considered in determining the focal-to-film distance for brazed honeycomb. The X-ray exposure was accomplished by controlled linear movement of the brazed assembly across the area of radiation emitted by the stationary collimated X-ray source (see Fig. 9).

**FIGURE 6.** Radiographic inspection of aircraft stabilizer.

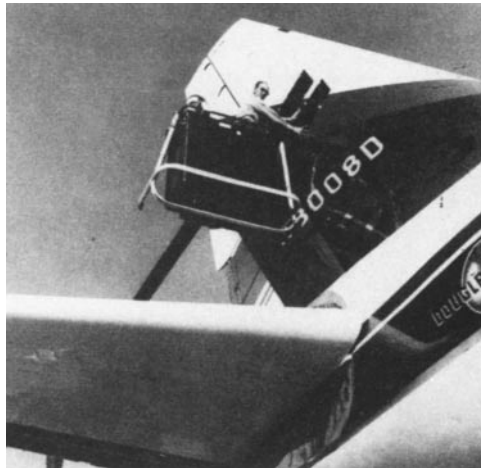


**FIGURE 7.** X-ray film placement on vertical stabilizer for debris and structural inspection.

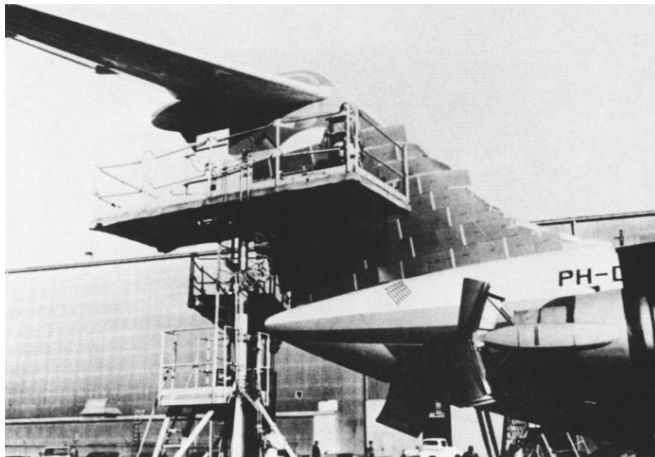
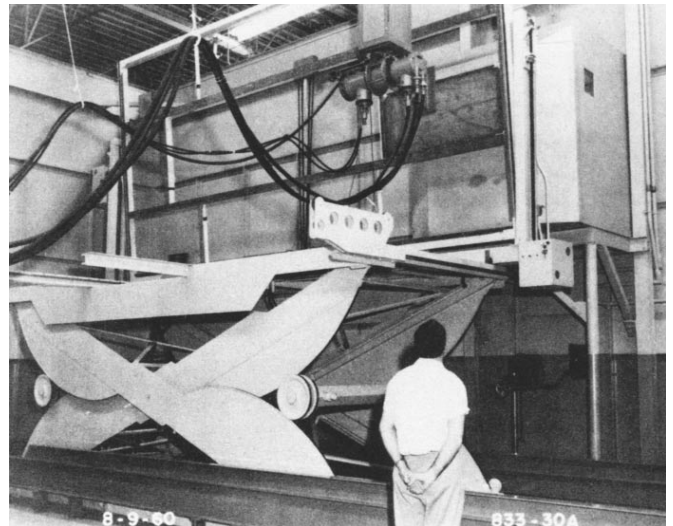


**FIGURE 8.** Position of X-ray source to expose maximum area of structure being radiographed.



**FIGURE 9.** In-motion radiography facility for brazed honeycomb structure.

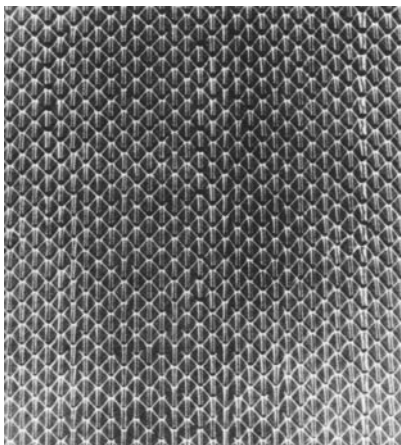


The fine grained, high contrast film was cut in widths of 300 mm (1 ft) and varied in length. Cassettes to accommodate the various lengths of X-ray film were designed and fabricated from a special plastic material suitable for radiographic work. The plastic cassettes were secured in intimate contact with the honeycomb panel by precut lengths of magnetic rubber strips placed on the cassette and magnetically attached to the honeycomb panel.

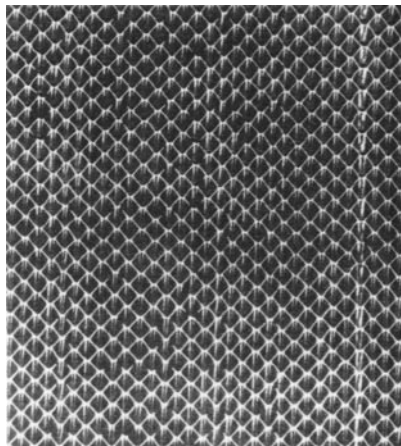
In all phases of the operation, in-motion radiography was less time consuming than conventional X-radiography. The ease of operation was particularly noted in the interpretation of the radiographs. Figure 10a is a conventional (still) radiograph showing brazed fillets on the source and film side (double surface) of the panel. Figure 10b is an in-motion

**FIGURE 10.** Brazed honeycomb structure: (a) conventional (not moving) radiograph of two surfaces; (b) in-motion radiograph of one surface.

(a)



(b)



radiograph showing only the brazed fillets on the film side (single surface) of the panel. It is much easier to detect lack of braze and to measure the fillet width on the latter radiograph.

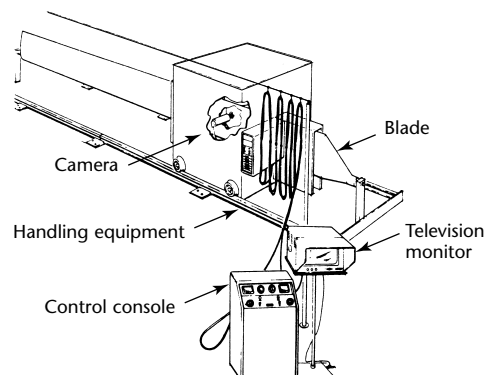
## Helicopter Composite Rotor/Propeller Blades<sup>11</sup>

Significant performance improvements in rotor/propeller blades were realized by proper use of composite materials. From 1954 to 1962, intensive research into materials and fabrication techniques were performed and backed up by component and sample fatigue testing. The successful use of fiber reinforced composite materials in helicopter rotor blades leads naturally to an improved capability for a successful V/STOL propeller design.

To fully appreciate the enormity and importance of the nondestructive inspection to be done, one must be aware of the types of loads that rotor blades bear and the general construction of the blade. Rotor blades in service are subjected to a variety of static and cyclic loads. These loads include beam, centrifugal, torsional and flatwise and cordwise bending.

One of the most important tasks in the use of composites is the development of the nondestructive testing capability to ensure that the hardware to be tested is of known quality. Some of the most challenging efforts come not in the selection of nondestructive test technique to use but in the mechanism necessary for practical application of that technique to the complex structure of a rotor/propeller blade. Figure 11 shows a concept of the automated penetrating radiation inspection equipment provided for an X-ray sensitive vidicon and image intensifier presentation. The system was basically a mobile X-ray unit in which the blade is fixed within two tracks and the

**FIGURE 11.** X-ray structure sensitive vidicon and image intensifier system concept.

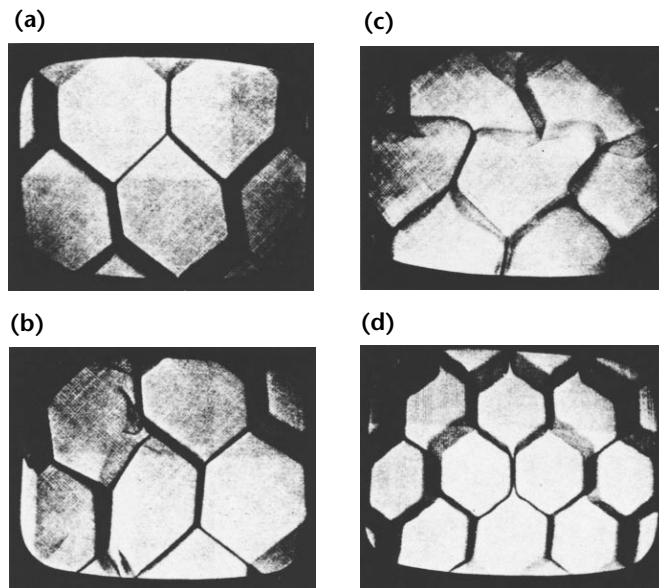


enclosed generator-and-detector system traverses the length of the rotor blade.

The X-ray vidicon image was presented on a remote 430 mm (17 in.) video screen at about 30 $\times$ . The image amplification system also presented a view on the same screen at 1:1. The viewing area using the vidicon tube was about 13 by 13 mm (0.5  $\times$  0.5 in.) with 1 to 2 percent image quality indicator sensitivity whereas the viewing area of the image amplifier is about 200  $\times$  200 mm (8  $\times$  8 in.) with 3 to 4 percent image quality indicator sensitivity.

Both the X-ray generator and pickup tubes had free 90 degree movement to allow for selection of the viewing angle that proved to be most desirable. Viewing speed was variable, the maximum speed being limited by interpreter perception. All controls and viewing apparatus were remote. Figure 12 shows some photographs taken of the video screen showing various conditions and discontinuities.

**FIGURE 12.** Typical vidicon monitor presentations: (a) image of honeycomb structure; (b) cell wall fracture and separation; (c) cell structure deformation; (d) cell wall separation.





## PART 2. Radiographic Testing of Space Flight Components

### Solid Propellant Rocket Motors

#### Saturn Fuel and Oxidizer Tank Weldments

During the early 1960s, many engineering talents were applied to the National Aeronautics and Space Administration's efforts for manned space flight. This included fabrication of 6.7 m (22 ft) diameter tanks for the Saturn moon rocket (Fig. 13). The weld joint configuration for the SIV-B is illustrated in Fig. 14. Initially, the in-motion technique using the welding fixture was used on the dome welds but was discontinued because smooth movement of the fixture was not achieved. The conventional techniques located a 100 kV beryllium window X-ray tube on a fixture inside the dome.<sup>12</sup> About 1.2 m (4 ft) of extra fine grain film was covered in each exposure. Circular dome movement was used between exposures to align each of nine segment welds with the X-ray beam. In Fig. 15, the operator is placing 70 mm (2.8 in.) strip film over each weld. After the nine films are exposed, the operation was repeated three

times to cover the full length of each weld. The cylindrical section welds, or tank welds, were similarly radiographed.

#### Large Rocket Motors

During a time of international tension in the 1950s and 1960s, solid propellant rockets became an important part of the United States arsenal. These missile systems consisted of ground, air and submarine launched vehicles. They were used in intercontinental and intermediate range missiles, where high performance and immediate readiness were required. Discontinuities in the propellant and propellant-to-liner joint affect the performance, reliability and safety of these motors.

Radiography of large, 0.75 to 1.5 m (2.5 to 5 ft) diameter, solid propellant motors can be accomplished in several ways. If the central perforation is of a design that permits the insertion of a cassette, radiography can be accomplished with a 2000 kV X-ray source or a cobalt-60 gamma ray source located on the exterior and the film placed inside the motor (Fig. 16a). If the motor design does not permit the insertion of a cassette, then radiography can only be accomplished by radiation penetrating the entire unit (Fig. 16b). For thicknesses greater than 760 mm (30 in.), X-ray energies above 2 MeV are required. Therefore, most of the earlier work was done with 10, 22 and 31 MeV betatrons.<sup>13</sup>

In the 0.5 to 6 MeV range, the van de graff and resonant transformer types of X-ray equipment were capable of providing the intensity and penetrating power necessary for high quality radiography in propellant thickness range up to 760 mm (30 in.). Above about 5 MeV, however, and for heavier propellant sections, these two direct acceleration techniques became impractical. In their stead, the betatron and microwave linear electron accelerator (linac) were required. The radiation output from betatrons is in the 25 to 50 mC.kg<sup>-1</sup> (100 to 200 R) per minute range, whereas the linear accelerator radiation output ranges from 130 mC.kg<sup>-1</sup> to 2.5 C.kg<sup>-1</sup> (0.5 to 10.0 kR) per minute and can thus rapidly radiograph thick propellant sections as illustrated in Fig. 17. High energy equipment was developed in the 1950s.<sup>14</sup>

FIGURE 13. Liquid propellant rocket engines used to launch Apollo Saturn moon rocket.

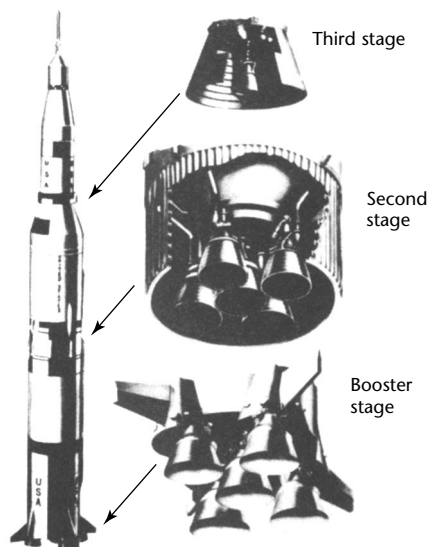
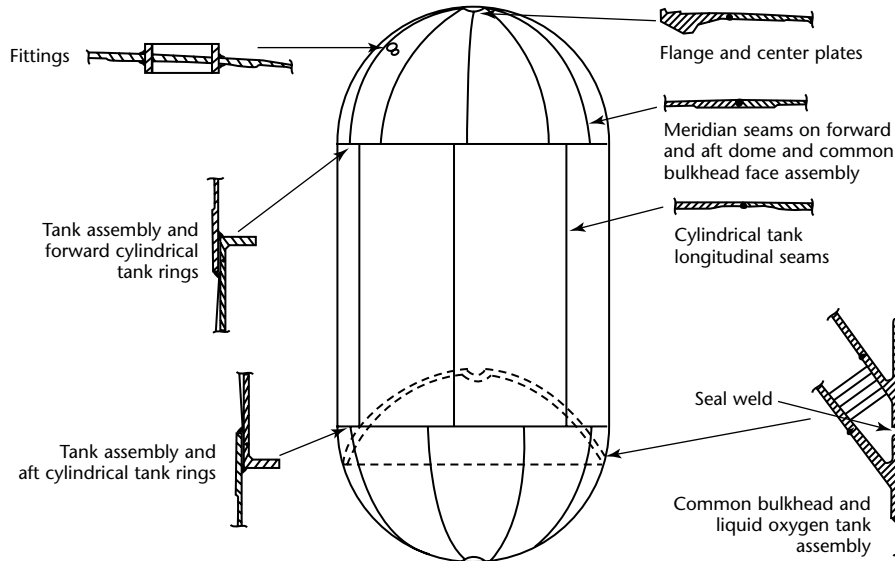


**FIGURE 14.** Weld joint configuration for Saturn SIV-B rocket.



**MOVIE.**  
Automated  
inspection of  
rocket motor.

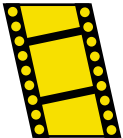


**FIGURE 15.** X-ray technician placing film on dome segment welds before radiographic inspection.

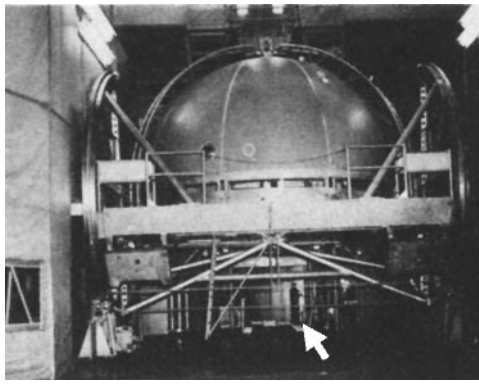


**FIGURE 16.** Radiography of solid propellant rocket motors: (a) single-wall radiography; (b) double-wall radiography.

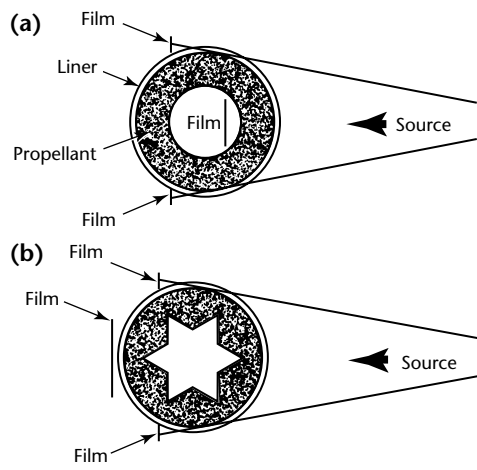
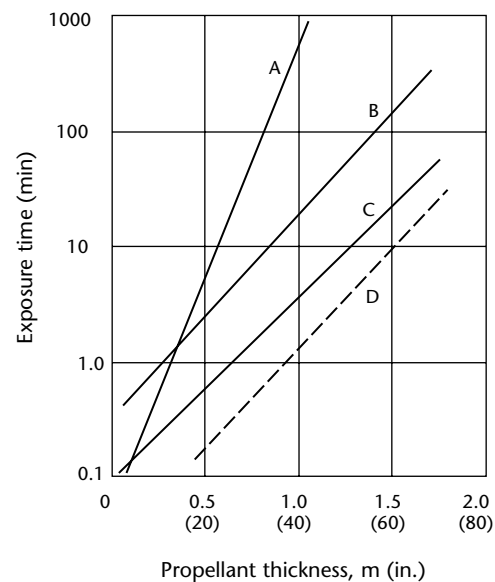


**FIGURE 17.** Exposure thickness data for propellant at various X-ray energies.



**Legend**

- A. 2000 kV peak at 1.5 mA
- B. 10 MeV betatron at  $7.0 \text{ Sv} \cdot \text{min}^{-1}$  (700 R $\cdot$ min $^{-1}$ )
- C. 22 MeV betatron at  $1.4 \text{ Sv} \cdot \text{min}^{-1}$  (140 R $\cdot$ min $^{-1}$ )
- D. 10 MeV linear accelerator at  $10 \text{ Sv} \cdot \text{min}^{-1}$  (1000 R $\cdot$ min $^{-1}$ )

## Jet Engine Inspection<sup>14,15</sup>

On-aircraft, periodic gamma ray inspection of jet engines is used for detection of compressor and turbine blade damage, including hot gas damage of burner cans. Possibly one of the greatest assets of the inspection is the ability to judge turbine blade alignment. The flexible isotope guide is inside a rigid aluminum tube and inserted through the axial engine drive shaft to a predetermined distance. The iridium-192 source is stopped at the selected longitudinal locations along the engine axis, as illustrated in Fig. 18. The film is placed on the outside of the area to be inspected. The film (as shown in Fig. 19a) is evaluated for evidence of excessive wear, misalignment or other unsatisfactory conditions. Figure 19b, photographed after engine disassembly, shows that a stator blade had worn its slot excessively and the resulting vibration had caused a crack in the retainer ring. If not detected, the resulting internal damage to the engine can cause complete failure.

## Small Ablative Thrust Chambers<sup>16</sup>

Silica phenolic materials have been used extensively in the manufacture of exhaust nozzles for solid propellant rocket motors. In this particular application, the material must withstand high intensity, short time ablation and erosion. In spacecraft engines for Gemini or Apollo, however, the motor is pulse fired at intervals throughout the mission to a total accumulated time of 10 to 20 min. The hypergolic engines are designed to produce from 111 to 445 kN (25 to 100 lb<sub>m</sub>) of thrust in environments found

at over 160 km (100 mi) above sea level. It is apparent that the quality reliability of these small engines must be ensured for the intended mission of the spacecraft. An illustration of the type and number of motors in the Gemini vehicle is shown in Fig. 20.

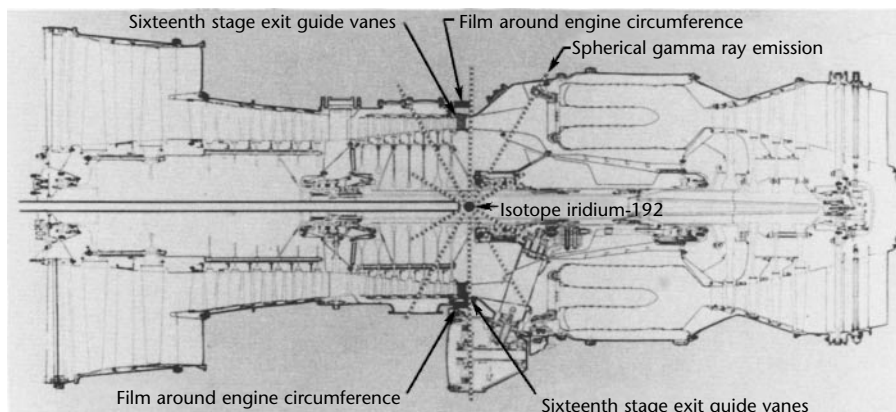
The radiographic testing of ablative materials has revealed various discontinuities, such as delaminations, porosity, cracks and resin rich or resin starved bands. Detail parts inspection revealed discontinuities similar to those found in the billets. These discontinuities were undetected because the original billets were not radiographed or were improperly radiographed. Tangential radiographs also revealed case-to-ablative adhesive voids and porosity.

Tangential radiographic inspection of the case-to-ablative bondline is illustrated in Fig. 21. Measurement of the film density at an interface is not possible unless a separation of 0.75 mm (0.030 in.) or greater exists, because the minimum aperture on a standard densitometer is 0.75 mm (0.030 in.). Measurements of gaps less than this require an automatic scanning microdensitometer.

It was found generally that the X-ray absorption of most adhesives was very low, causing interpretation problems of case-to-ablative and other bond joint interfaces. Thick or thin bond joints yielded different radiographic results that were difficult to interpret. To compensate for the problem, a small percentage of antimony trioxide was added to the adhesives. This material did not affect the cohesive bond strength but made the joint more opaque to X-ray and bondline discontinuities became more apparent by revealing the presence of adhesives as illustrated in Fig. 22.

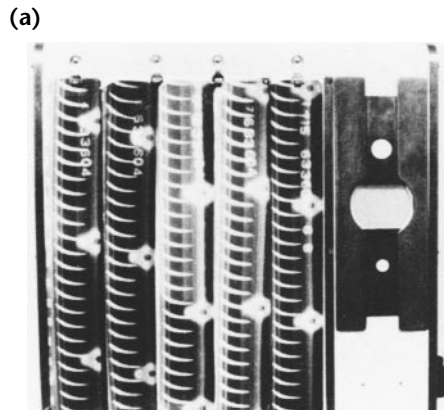
The verification of delaminations and location of leakage paths was proved by radiographing various specimens and

FIGURE 18. Iridium-192 gamma ray inspection of jet engine.





**FIGURE 19.** Gamma radiography of vane segments in jet engine: (a) gamma radiographs; (b) visual crack indication previously revealed by gamma ray inspection of vane guide.



**FIGURE 20.** Gemini vehicle space engines.

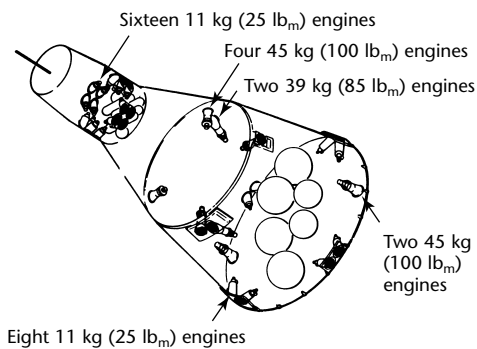


**FIGURE 21.** Tangential radiographic technique for case bond using a microphotometer: (a) setup; (b) recording.

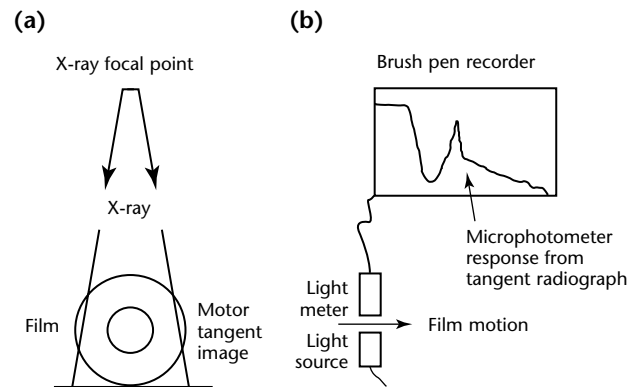
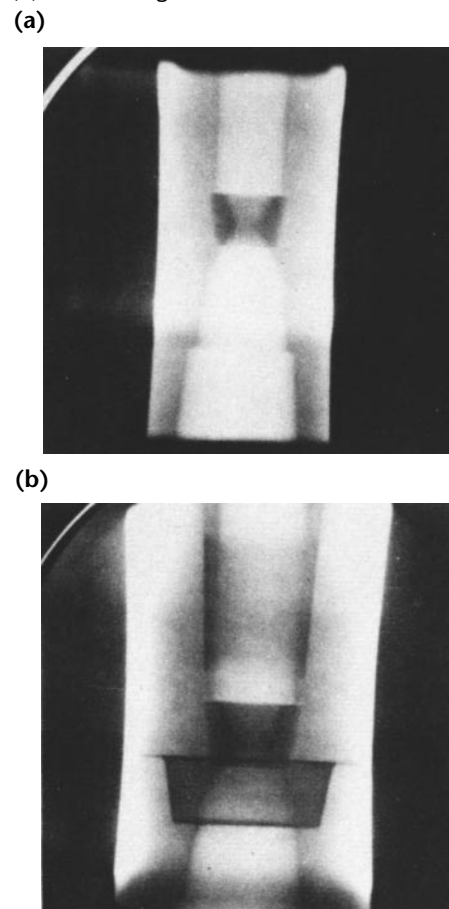


**FIGURE 22.** Case-to-ablative bond discontinuities are revealed by radiopaque additive in adhesive: (a) first image; (b) closer image.



motors before and after soaking in X-ray opaque solutions. Different solutions were tried but the one yielding the best results was a concentrated water solution of lead acetate and lead nitrate. All delaminations and leakage paths were detected after a 1 h soak period and rinse (Fig. 23). Motors showing delaminations and leakage paths were rinsed thoroughly with deionized water to remove most of the lead solution and were then dried and pressure impregnated with resin. Reradiographing after resin impregnation usually indicated that the void was filled, thereby making the part acceptable for use. Motors repaired in this way were hot fired successfully, indicating the adequacy of the repair procedure.

### Video Radioscopy and X-Ray Image Intensifier Tests<sup>17</sup>

The normal technique of inspecting small ablative thrust chambers requires that each chamber be radiographed before hot firing and also at subsequent intervals during the test program. This plan entails disassembly of the chamber and shipping it to the X-ray laboratory for radiographic

testing. After inspection, the chamber is returned to the cell for further testing. The prime factor of discovering discontinuities when they occur and before they can lead to failure is missed by this technique of using X-ray image equipment in conjunction with motion picture film. Sequencing of the thrust chamber image during hot firing will ensure that complete failure analysis data are obtained.

Cinefluorography has been used successfully to establish the mode of failure in small solid propellant rocket engines during hot firing.<sup>18</sup> A similar study on solid propellant rocket engines was reported.<sup>13</sup> Cinefluorography of solid propellant engines reveals the flame front pattern and burning rate as a function of contrast differential in the test object. The failure analysis of liquid hypergolic ablative engines by cinefluorography is more concerned with the detail resolution of discontinuities as they develop in the test object.

The equipment consisted of a fractional focus X-ray tube, full wave rectified voltage transformer, X-ray control panel, high gain, image intensifier tube and an optical system for viewing. Additional accessory equipment can be used for special purpose applications. Such equipment consists of a 16, 35 or 70 mm motion picture camera capable of 7.5, 16, 30 or 60 frames per second (Fig. 24a). In this way, cinefluorographic time lapse studies may be made of systems while functioning. Such studies may include the analysis of small solid or liquid propellant engines during hot firing. Other techniques include the use of a television camera (kinefluorography) in place of the positive print and

**FIGURE 23.** Soaking in saturated solution of lead acetate and lead nitrate: (a) before soaking; (b) after soaking.

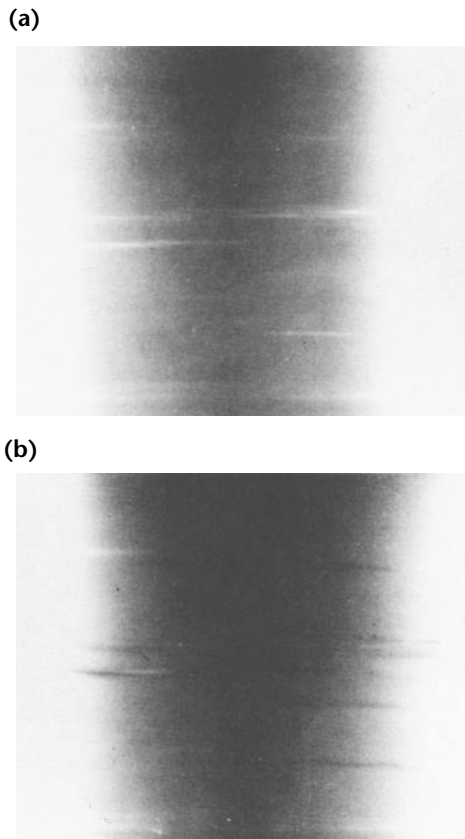
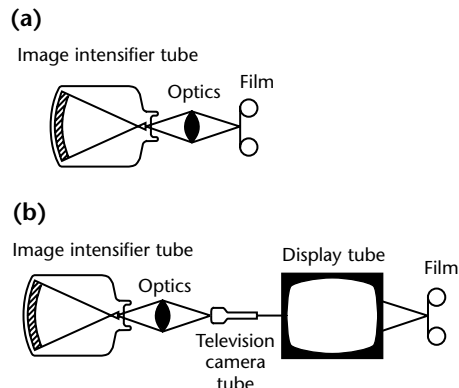


**FIGURE 24.** Comparison of cinefluorography and kinefluorography: (a) cinefluorography, direct photography of output phosphor of image intensifier tube; (b) kinefluorography, photography of picture tube image of output phosphor.



transmitting the image to a television monitor (Fig. 24b).

An X-ray image intensifier system has proved successful in determining the mode and sequence of failure of ablative thrust chamber during actual firing. Delaminations, bond joint separations and cracks were readily detected in test materials and assemblies. A high gain X-ray image system was installed at the Rocketdyne test facility for hot fire studies. Excellent results were obtained using a 150 kV, 4 mA, 0.3 mm (0.012 in.) fractional focus X-ray tube in conjunction with a 230 mm (9.1 in.) diameter, high gain image intensifier.

Radiographic results of a chamber fired to failure are shown in Fig. 25. Test results of the failure mode were recorded on 16 mm motion picture film at 32 frames per second.

Used as a process and quality control device during manufacturing operations, the X-ray image intensifier has many applications involving direct viewing of the image tube. Thus, the cost of film and the time involved for film processing are avoided. Unusual phenomena might be photographed with a positive print or regular camera when required. Cylindrical objects can be rotated through 360 degrees during viewing; in film radiography, they would likely have to be X-rayed in two exposures at 90 degrees. Confidence in the detection of discontinuities is greatly improved by the 360 degree scan.

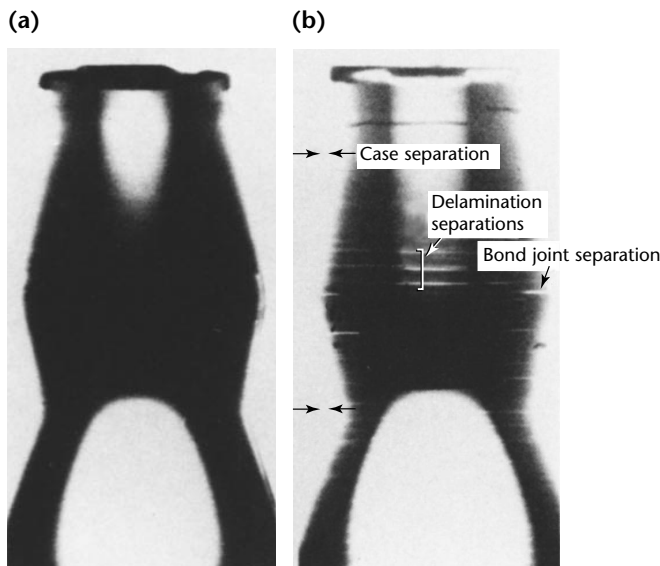
Parts to be inspected are placed on a 130 mm (5 in.) turntable capable of supporting and rotating a 23 kg (50 lb<sub>m</sub>) assembly in either direction at 1 rotation

per minute. The turntable can be elevated and depressed over a 250 mm (10 in.) travel. It can be positioned within about 100 mm (4 in.) of the input phosphor for best detail resolution of as far as 760 mm (30 in.) away for direct geometric magnification. A horizontal travel of 250 mm (10 in.) transverse to the X-ray beam also is provided. The X-ray tube head itself can be traveled horizontally to provide a range of 150 to 760 mm (6 to 30 in.) from the input phosphor. This range permits the use of very high radiation intensities at short focal lengths or improved image sharpness at greater focal length, as different test problems dictate.

In selecting parameters for a specific test, the technician first positions the item on the turntable and adjusts the electrically driven lead shutters to confine radiation to the area of interest. Then, while observing the image tube, the technician selects the geometric relationship best suited for the test objectives. Next, the energy level (kV) is adjusted for the desired contrast and the tube current (mA) is adjusted for brightness. The component then is scanned on either axis or is rotated, or combinations might be used. When a significant anomaly is observed, it can be recorded in a variety of ways for later observation.

A functional multienvironmental fluoroscopic facility has been used for the evaluation of valves, switches, actuators and other components. The system can reveal the operation of internal components under various dynamic and environmental conditions expected to be encountered during flight. The temperature and pressure of the inspection chamber can be varied to meet environmental requirements. A general view of the test room and inspection cabinet is shown in Fig. 26a and the control console and X-ray image monitor are shown in Fig. 26b. Radioscopic results can be seen on the monitor and images are recorded on video media that provide playback capability for the system engineers responsible for analysis of each component tested.

**FIGURE 25.** Ablative thrust chamber: (a) before firing; (b) after firing.



## Large Liquid Propellant Rocket Engines<sup>19-21</sup>

Throughout the modern era of rocketry, liquid propellant rocket engines have demonstrated their ability to provide high performance, high reliability and operational flexibility. It is mandatory to have highly reliable launch vehicles.

The engine reliability program begins with design and manufacture to ensure

accurate, high strength, failure free hardware. Extensive inspection procedures further assist this phase. Engine component testing follows inspection and finally the liquid propellant rocket engine can be subjected to extensive testing in the development phase to uncover any potential weakness. This extensive test effort provides a high degree of confidence in the engine reliability. Liquid propellant rocket engines also provide the capability of testing the article that will be used during the actual launch. Also, each engine is tested before it is delivered to the customer and later each stage and engine is tested as a unit and completely checked out before the launch. Fig. 27 shows a completed engine. Five of these 6.67 MN (1 500 000 lb<sub>f</sub>) thrust engines were used on the manned Saturn moon rocket booster stage.<sup>19</sup>

Radiography is used to detect internal discontinuities in weldments and high strength castings, to determine braze alloy distribution in brazed thrust chambers (Fig. 28) or components and to internally inspect electrical assemblies for missing or broken components. Special radiographic

procedures have been developed for unique problems as indicated in the following paragraphs.

## Neutron Radiography of Special Aerospace Components

Typical aerospace items that have been neutron radiographed include jet engine

**FIGURE 27.** Apollo space vehicle booster engine, 6.67 MN ( $1.5 \times 10^6$  lb<sub>f</sub>).

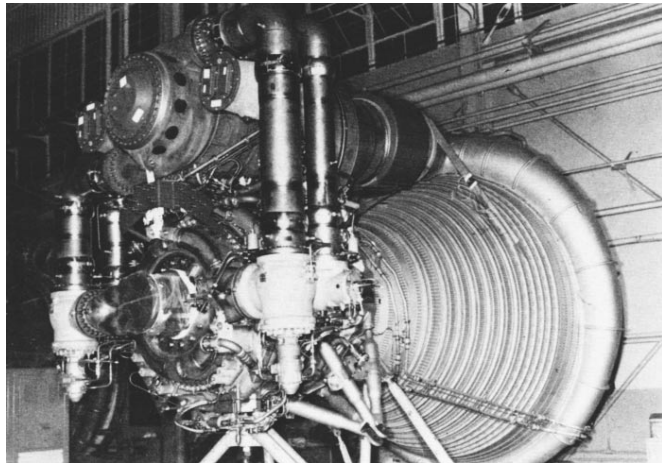
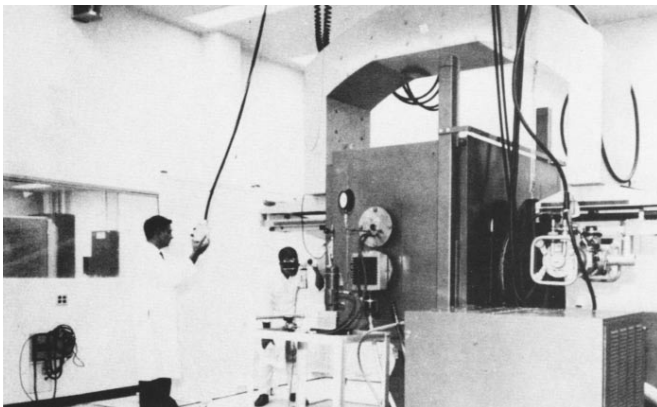


**FIGURE 26.** Functional multienvironmental fluoroscopic system: (a) installation; (b) control console.

(a)



(b)

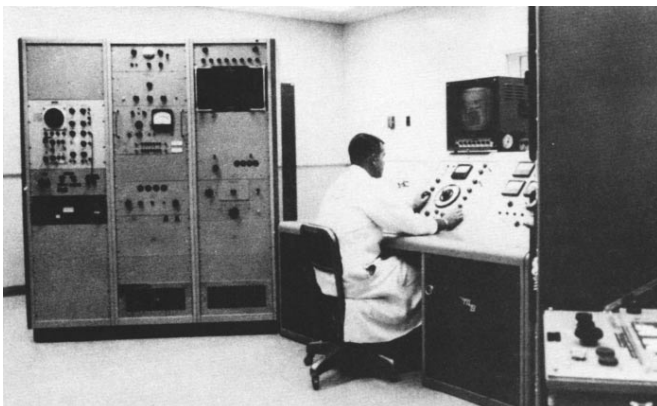
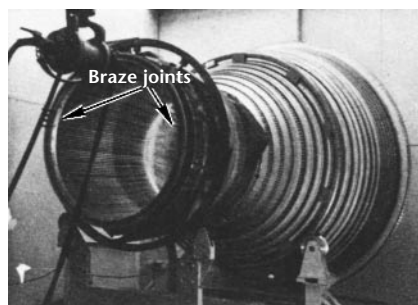


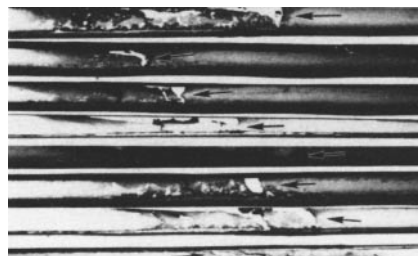
**FIGURE 28.** Radiographic testing of thrust chamber tube-to-tube braze joints:

(a) technique setup; (b) positive prints of radiographs, arrows marking indications.

(a)



(b)





turbine blades, adhesively bonded honeycomb and laminates, ordnance or pyrotechnic devices, flight controls and metal assemblies containing nonmetal O rings or seals.<sup>22-24</sup> Inspection of such parts is possible because neutron radiographic testing can detect certain low density materials through heavy metal sections.

Attenuation of X-radiation is determined largely by the electron density of the material being examined, so that thicker and/or denser materials appear more opaque. Neutrons undergo two main types of reactions with atomic nuclei: absorption (capture) and scattering. The mass attenuation coefficient for thermal neutrons is thus a function of both the scattering and capture probabilities for each element; the density of a particular material or component is a poor predictor whether it will be relatively transparent or opaque to the passage of neutrons.<sup>25</sup>

High attenuation coefficients for thermal neutrons are exhibited by hydrogen and boron. Hydrogen has the highest scattering coefficient whereas boron, cadmium, samarium and gadolinium have unusually high neutron capture probabilities. For this reason, hydrogenous or boron containing materials being inspected by neutron radiography can be *seen* or delineated from other elements in many cases where X-radiography is inadequate. It is thus possible to expose a specimen (for example, a hydrogenous or borated explosive or a fuel sealed in a metallic container) to a beam of thermal neutrons and to project an image having excellent resolution and contrast, thereby distinguishing between the charge material and its container while revealing any imperfections in the specimen. Similarly, neutron radiography permits detection of hydrides,<sup>26</sup> which can cause hydrogen embrittlement in welds and can be used for nondestructive testing of ordnance (explosive) devices to determine the relative density of the charge material and/or the presence of voids or cracks.

### Explosive and Pyrotechnic Devices

One of the important applications of neutron radiography is the quality control of certain critical explosive devices, such as pilot seat ejection cartridges, detonating cords and pressure cartridges for aerospace applications. These devices normally contain explosives or propellants of low atomic numbers. In most instances, they also have metal housings. Therefore, it is nearly impossible to inspect them effectively with postassembly X-ray examination. However, because hydrogenous materials

have a high neutron scatter rate, a neutron radiograph will image gaps, cracks, low density areas or other discontinuities that could prevent normal operation.

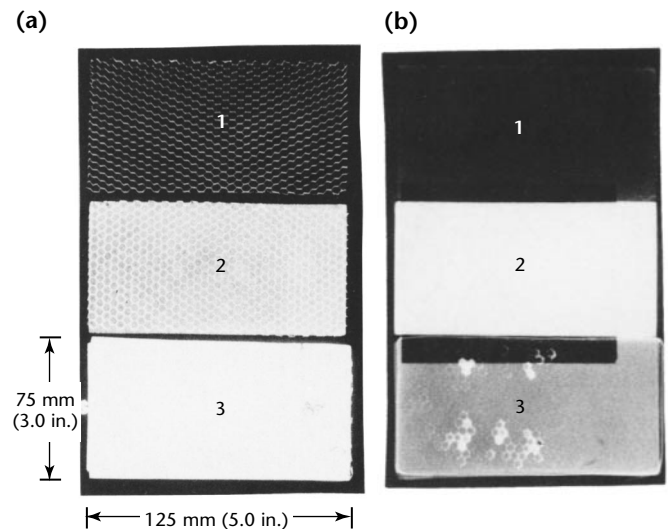
A neutron radiograph will image certain materials of low atomic number whereas the X-radiograph does not. The powder train inside an explosive device is well defined in the neutron radiograph, for example, but is not shown in the X-radiograph. Hence, neutron radiography has played a major role in yielding a *no failure* reliability for ordnance devices in aerospace programs.

### Adhesive Bonded Composite Structures<sup>27</sup>

Thermal neutrons are highly attenuated by boron and hydrogen atoms. Therefore, when an adhesive bonded laminate or honeycomb specimen is neutron radiographed, the hydrocarbon adhesive becomes very apparent because of its high neutron scatter. This condition is reversed for X-radiography where metal components are high attenuators. A high density boron fiber composite would be completely opaque to a thermal neutron beam, as shown in Fig. 29.

In Fig. 29, specimens have aluminum honeycomb cores with adhesive bonded skins of graphite epoxy, boron epoxy and fiberglass.

**FIGURE 29.** Attenuation in adhesive bonded, aluminum honeycomb core, fiber matrix facing sheet, composite specimens: (a) low kilovoltage X-rays; (b) thermal neutrons.



**Legend**  
 1. graphite  
 2. boron  
 3. fiber glass

## Investment Castings

Investment casting, also known as the *lost wax* process, is a manufacturing method used to produce near net shape metal articles. A wax pattern is produced by injection molding into a die cavity typically machined into aluminum. The die cavity replicates the desired casting shape. After molding, the wax pattern is dipped into a series of slurries that contain ceramic particles. Multiple coatings of ceramic slurries are applied to build a sufficiently thick mold layer. The dip layers are allowed to dry and harden between applications.

The first layer of the mold is referred to as the *face coat*, important because it is in contact with the molten metal and determines the quality of the casting. Subsequent layers are referred to as *backup* layers. After sufficient layers have been applied, the wax is melted from the shell, leaving a cavity whose shape is an exact replica of the desired metal article.

The ceramic mold is sintered to make it denser and stronger. Metal is then melted and poured into the mold. After solidification and cooling, the ceramic shell is removed leaving a metallic casting of the same geometry as the wax pattern. After shell removal, the casting is nondestructively tested to reveal inclusions of mold material. These discontinuities are removed by grinding and subsequently repaired by welding.

Investment casting has been used to produce precise, high quality aerospace engine components that range from 0.1 to 1.2 m (a few inches to several feet) and are cast in a variety of alloys including steel, nickel, cobalt and titanium.

## Titanium Castings for Aerospace Structures

Airframe manufacturers have been exploring the use of titanium investment castings to replace components traditionally produced from forgings. Titanium investment castings in these applications reduce weight, costs and lead time. The fatigue driven, fracture critical environment of these aerospace structures requires a quality level higher than necessary for titanium castings in aerospace engines. The design of these fracture critical titanium castings is driven by the ability to detect mold face coat inclusions in the components. The required thicknesses have challenged the limits of radiographic testing.

## Investment Casting of Titanium

The investment casting of titanium poses several challenges due to the high

reactivity of molten titanium. Ceramic materials used to produce face coats for the investment casting of titanium must be stable and have low reactivity with molten titanium. If the ceramic face coat materials are reduced by the molten and solidifying titanium a type of brittle, oxygen enriched titanium called *alpha case* is generated. The amount of alpha case produced on a casting must be limited as mechanical properties are negatively affected. This in turn restricts the candidate ceramic face coat materials that can be used.



## PART 3. Techniques for Advanced Materials

In the decade from 1975 to 1985, the aerospace industry was busy launching the space shuttle,<sup>28</sup> producing high performance jet fighters, attack helicopters, missiles and satellites. Considerable work was accomplished in developing fiber reinforced plastic composite aircraft structures. In the 1980s and 1990s, radiography, particularly X-ray based imaging techniques and applications, saw tremendous growth.<sup>29</sup> As with many technologies, advances in speed of data acquisition/analysis were enabled by the improvements made in computers and semiconductors. Advances in digital radiography continue to affect the aerospace industry, with many benefits leveraged from medical applications. The Air Force Research Laboratory has served as a major funding source<sup>30-32</sup> driving the development of all three of the main components of a penetrating radiation system: a source of radiation, a manipulation system for the test object and a detector system. Air Force Research Laboratory investments have focused on improvements in sensitivity with emphasis on cost effective applications. Simulation tools have been a focus of work at several research laboratories.<sup>33,34</sup> Recent aerospace applications are provided in the remaining section.

### Advanced Materials

#### Adhesively Bonded Honeycomb Structures

In-motion fluoroscopic inspection of metallic bonded honeycomb structures has been done for years by several prominent manufacturers.<sup>35,36</sup> In-motion radiographic techniques have been used to inspect a variety of bonded honeycomb structures. These structures are composed of aluminum core bonded to either aluminum, boron epoxy or carbon epoxy skins. The inspections are performed to detect crushed core, core node separation, foreign objects, core splice discontinuities and core tie-ins at closures.

A collimator is used to limit the X-ray beam in the direction of motion. Roll films of required lengths and 70, 120, 254 and 355 mm wide are used. The films are

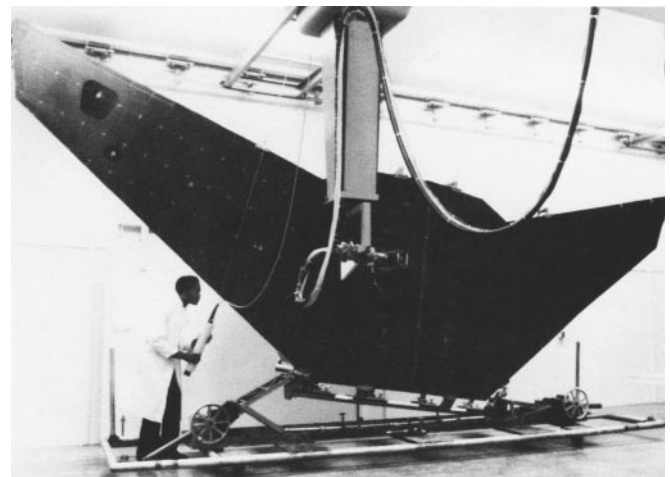
processed in automatic film processing equipment and special film reading boxes have been fabricated, some of which provide for viewing up to 1.5 m (5 ft) of film at one time. The assemblies are oriented with the honeycomb cells parallel with the X-ray beam and the direction of motion is parallel to the ribbon direction.

#### Composites

Figure 30 shows in-motion radiography being performed on carbon to epoxy composite upper wing skin. The composite skin is about 8 m (26 ft) tip to tip and 1.8 m (71 in.) forward to aft at the centerline. The stainless steel tool is designed to manipulate the assembly in five axes to permit orientation of the contoured surface perpendicular to the X-ray beam. The X-ray tube head has a lead shielded cone attached to the port to limit radiation onto a narrow line about 13 mm (0.5 in.) wide in the direction of tube motion. The tube support is mounted on the ceiling and has an extension up to 12 m (40 ft).

A more detailed view of the gooseneck tube support and in-motion cone is shown in Fig. 31a. This figure shows a bonded honeycomb assembly with boron epoxy skins on 360 mm wide roll film that is on 3 mm (0.12 in.) vinyl lead backup material. The pendant control

FIGURE 30. In-motion radiography of composite wing skin.



permits movement of the tube support in three directions.

The control console for a representative in-motion radiography system has the standard X-ray control panel modified to provide kilovoltage slope control during the in-motion exposure (see Fig. 31b). As many aircraft structures taper in thickness from inboard to outboard, it is impossible to maintain constant film density without adjusting X-ray parameters during the in-motion exposure. Kilovoltage was chosen as the variable because it can be changed to match energy level with the thickness of the part. Another improvement in the in-motion control is constant speed control, which automatically compensates for varying loads and maintains a constant speed readout on a digital tachometer. The television monitor (Fig. 31b) displays the area of the assembly being subjected to radiation. It does not provide an X-ray image but is used to aid in alignment of the assembly.

## Microfocus Radiography

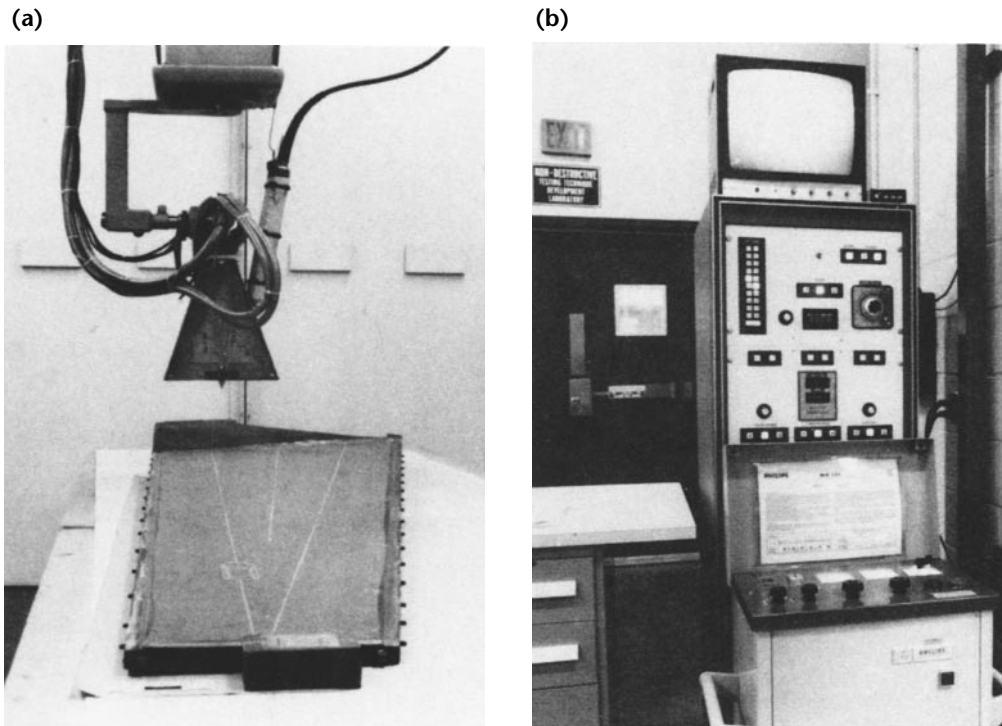
Normal radiography is accomplished using 1 to 3 mm (0.04 to 0.12 in.) focal spots. Projection radiography can be accomplished with a true microfocus X-ray source; that is, an X-ray tube with

an electron focal spot smaller than 0.1 mm (0.004 in.). In practice, focal spots from 0.002 to 0.25 mm ( $8 \times 10^{-5}$  in. to 0.01 in.) have proven to be useful for radiosopic systems<sup>37</sup> and spots from 0.025 to 0.075 mm (0.001 to 0.003 in.) have proven satisfactory for film techniques using magnification.

A typical system might contain a 160 kV constant potential microfocus X-ray tube capable of continuous operation at 0.5 mA with a focal spot size of 12  $\mu\text{m}$  ( $5 \times 10^{-4}$  in.). Using a 12  $\mu\text{m}$  ( $5 \times 10^{-4}$  in.) focal spot size, the system can resolve details as small as 25  $\mu\text{m}$  (0.001 in.) without magnification. The system may also contain a 230 mm (9.0 in.) X-ray image intensifier optically coupled to a 15 MHz closed circuit television fitted with a 25 mm (1.0 in.) vidicon image tube. With low absorbing materials, projection magnification of 50 $\times$  or more may be obtained.

A useful technique that can be achieved with radiosopic projection microfocus radiography is that of zooming or dynamically positioning the object with a manipulation between the X-ray tube and image receptor.<sup>38</sup> In this technique, magnification is achieved when the object is moved away from image receptor and toward the X-ray tube. Figure 32 illustrates a single integrated circuit that was initially situated for low

**FIGURE 31.** In-motion radiography: (a) gooseneck tube support and cone assembly; (b) control panel.



projection magnification of 2×. The integrated circuit was then zoomed toward the X-ray tube through 10×, 50× and 250× magnification. It is evident that the higher the magnification, the more detail one can see on the video monitor.

A similar test, done on a metal jet engine turbine blade is shown in Fig. 33a and at 10× magnification in Fig. 33b. Jet engine turbine blade inspection using radioscopic microfocus radiography has been performed for jet engine manufacturers. The blades are inspected for cracks, voids, inclusions and plugged cooling passages.

## Computed Tomography

Computed tomography (CT) combines the capabilities of the computer with an X-ray source for the inspection and analysis of the internal structure of objects. Very minor changes in density can be accurately detected by a computed tomography system. Ordinary film radiography inspection systems have some major weaknesses. One is that they create only superimposed images of artifacts. The superpositioning of images — lying one on top of another — distorts the inspection results. Computed tomography eliminates superposition by examining an object in a series of cross sectional slices from different views along the length of the object.

A computer calculates an image based on the information in all the slices and reconstructs a two-dimensional picture of a slice through the object. This precise, highly accurate, two-directional data package can be viewed on a cathode ray tube screen, printed out in hard copy and stored on optical or magnetic media.<sup>39</sup>

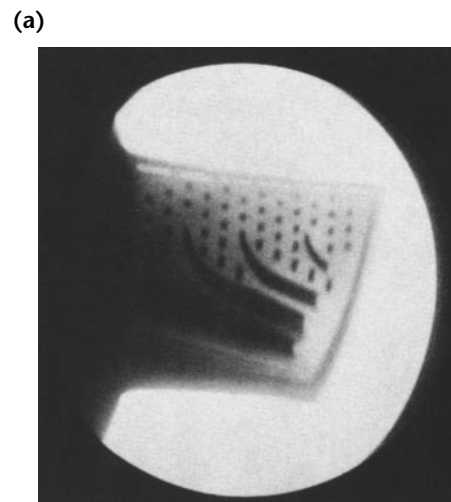
In the 1980s computed tomography was developed for industrial applications. Solid rocket motor components were

inspected, including cases, propellants, liners and igniters (Fig. 34).

The inspection system features a 420 kV X-ray source to inspect objects up to 1 m (40 in.) diameter (Fig. 35). The range of measurable signal levels produced is about  $10^6$  to 1, superior to that offered by alternative techniques at the time of testing. The information is more complete, detailed and accurate and the computer sorted images can be manipulated and analyzed by design, manufacturing and quality engineers or stored for future reference.

Work has been completed for the United States Air Force to develop and implement an automated device to X-ray inspect turbine blades and vanes.<sup>40</sup> This radiographic inspection module uses a gas ionization X-ray detector as the image medium. A computer processes the detector output signal to generate digital X-ray images. Advanced image processing

**FIGURE 33.** Microfocus radioscopic images: (a) jet engine blade; (b) enlargement.



(b)

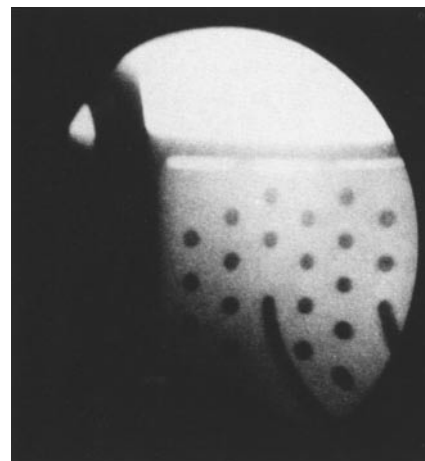
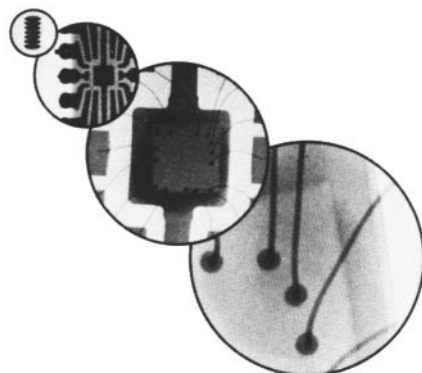


**FIGURE 32.** Microfocus radioscopic images of integrated circuit.



software, operates on these digital images to make automated accept/reject decisions. The handling of the part during X-ray exposure is carried out robotically under computer control.

To detect internal material and manufacturing discontinuities and to make inspection decisions, the computer operates on two data representations, depending on the application. The first is digital fluoroscopy, or digital radiography, and results in a filmlike image (Fig. 36a). Digital fluoroscopy allows quick identification of internal anomalies and other features of interest. The second is computed tomography (CT) and results in a cross sectional image (Fig. 36b). This latter data format, although requiring more time to generate, yields significantly higher material discontinuity sensitivity and a better ability to resolve internal anomalies such as *thin wall* discontinuities. Computed tomography provides additional geometric detail not available with conventional film radiography. Computer based X-ray inspection is expected to yield significant improvements in productivity, reliability and sensitivity for airfoils. In addition, the new industrial computed tomography capability provides new inspection capability and offers new freedom to design engineers, allowing them to be more innovative. Advanced nondestructive testing techniques, like computed X-ray tomography, will be a key to the practical realization of optimum designs.

## Neutron Tomography

Neutron radiography has already proven itself as a reliable method for the

detection of hydrogenous substances, such as moisture and corrosion in aircraft components. The advantage of neutrons is that low atomic number nuclei, in particular hydrogen, have higher interaction cross sections than the surrounding material. Figure 37 shows a neutron radiograph of an aerospace valve, in which the O rings are clearly visible as light horizontal bands.

A neutron tomography system generally consists of an intense neutron source, object turntable, a scintillator screen, a mirror, a cooled charge coupled device camera, and computer imaging and processing support. With such an arrangement, the actual distribution of materials across a given path can be determined.

FIGURE 35. Computed tomography system.

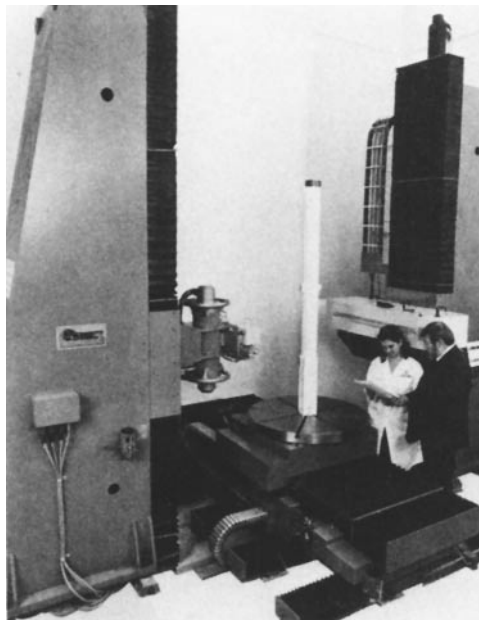


FIGURE 34. Simplified illustration of computed tomography for aerospace structures.

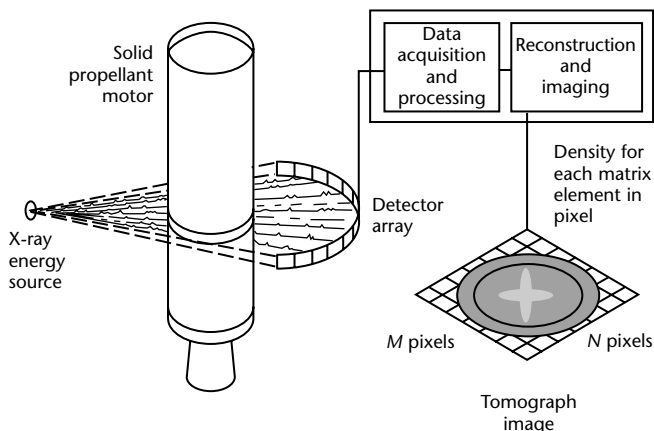
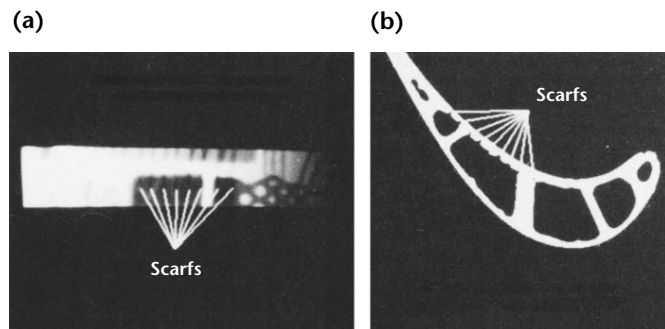


FIGURE 36. Digital images of turbine blade: (a) fluoroscopic; (b) tomographic.





As aerospace and nondestructive test engineers have become more familiar with the capabilities of neutron radiography and tomography, the techniques have been used more. Neutron tomography systems have been used to determine the hydrogen content in aircraft compressor blades<sup>41</sup> and the exact placement and shape of O rings in critical components of spacecraft (Fig. 38).

An Air Force Research Laboratory program<sup>42</sup> was initiated to develop and evaluate advanced radiographic and radiosopic systems. To ensure broad applicability to many aerospace inspection needs, a diverse team was assembled consisting of commercial companies and government contractors. The program evaluates detectors that are proven in other industries and that are fast and easy to use. To reduce reliance on more costly film techniques and enhance inspection productivity, these detectors include large area, flat panel, X-ray detectors modified from medical applications, recently available dental sensors and photographic industry digital charge coupled devices modified for radiography.

## Reversed Geometry, Scanning Beam Technique

The National Aeronautics and Space Administration has explored a technique, reversed geometry scanning beam

radiographic testing.<sup>43</sup> The technique uses an electronically scanning X-ray source and a discrete detector for radiosopic imaging of a structure.

The scanning source system has several advantages. Miniaturization of the discrete X-ray detector enables easy positioning inside a complex structure (such as an aircraft wing) allowing images of each surface of the structure to be obtained separately. Additional advantages include multiple detectors that enable the simultaneous acquisition of data from several different perspectives without moving the structure or the measurement system. This provides a means for locating the position of discontinuities and enhances separation of features at the surface from features inside the structure. Finally, the amount of secondary scattered radiation contributing to the noise in the image is reduced compared to conventional radiography. Noise reduction facilitates the acquisition and analysis of quantitative data about the integrated material density along the ray path between the source and the detector.

Details of the techniques and application to crack detection in aircraft structures have been published.<sup>43,44</sup> Results are shown for different crack sizes in a range of thicknesses. Application to honeycomb structures is also being presented. A honeycomb specimen with a fatigue crack in one of the face sheets was imaged with the scanned X-ray system. It was shown that the variation in contrast as a function of incident angle can be used to remove some of the image clutter due to the effects from the underlying honeycomb structure, thereby improving the detectability of the crack. A

**FIGURE 37.** Neutron radiograph of aerospace valve. O rings are visible as light bands.

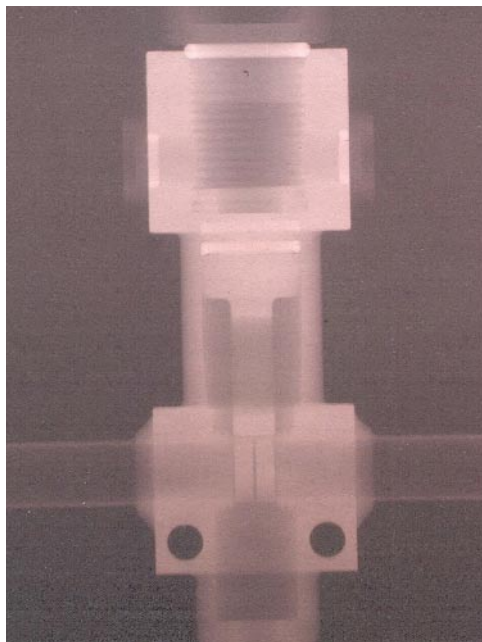
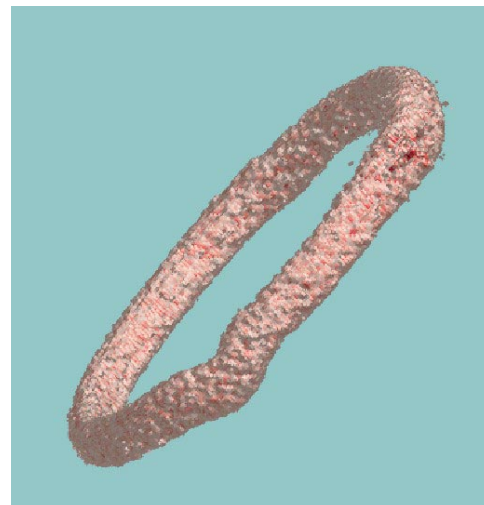


**FIGURE 38.** Neutron tomographic image of aerospace valve, showing bend in O ring.



differential laminography image produced from examining the difference in laminographic images at different depths gave the best image of the crack.

[The reversed geometry, scanning beam technique is discussed at greater length elsewhere in this book.](#)

## Simulation Tools

Advances in computational power has enabled not only new capabilities in the inspection systems but in the physics calculations used to design and optimize X-ray techniques.<sup>45</sup> Validated inspection models offer an opportunity to design inspection techniques for a given component.

Advances include the development of an X-ray computer simulation program capable of accurately simulating the output of an X-ray imaging system and involves a number of components, including X-ray beam models for isotope sources and bremsstrahlung sources, the interaction of that beam with the part including material effects, complex geometry issues and finally the conversion of the beam into a visible form, in the case of radiography, film or image intensifiers. Tools developed include the ability to insert a discontinuity of any size into the part at any location, which provides a powerful tool to evaluate the capabilities of a particular inspection. The use of a computer assisted design representation for the discontinuities allows realistic cracks, shrink cavities and inclusions to be evaluated. The limit of detectability for a discontinuity at a particular location can be calculated simply by varying the size of the discontinuity and calculating the resulting image. The location can be changed at will and a detectability map can be computed for the entire part at particular kilovoltage, setup, orientation, sensor type and all other parameters currently modeled in the simulation program.

Techniques to consider the probability of detection as a function of position have been developed. The application of a quantitative X-ray simulation code has applications at the earliest stage of design where inspectability issues can be evaluated. The simulation code can be used to optimize an inspection to ensure adequate coverage with the best sensitivity at a minimum cost and can be used as a training tool. Applications to aerospace castings<sup>46,47</sup> and other components are being explored.

## Closing

Initially, radiographic testing was used for the quality control of weldments and castings — it is still used for this purpose. Various publications cover the history of nondestructive testing in the aerospace industry,<sup>1,48</sup> including radiographic testing of aircraft during World War II.<sup>49</sup> Every decade since then has seen major advances in technology. Applications of the method have been expanded to include the inspection of components and materials for experimental rocket and jet aircraft, missiles, solid propellant and liquid propellant rocket engines, space vehicles (Fig. 39) and satellites.

**FIGURE 39.** Space shuttle: (a) *Atlantis* touches down, 1992; (b) *Discovery* is launched, 1995.

(a)



(b)





The high reliability of these vehicles and systems can be directly attributed to proper application of nondestructive testing as a whole and industrial radiography in particular. This reliability has been made possible through the dedication of scientists, engineers and technicians of the aerospace nondestructive testing community. Radiographic testing continues to be important for aerospace quality and safety in the twenty-first century.

## References

1. Hagemmaier, D.J. "Aerospace Radiography — The Last Three Decades" [1984 Lester Honor Lecture]. *Materials Evaluation*. Vol. 43, No. 10. Columbus, OH: American Society for Nondestructive Testing (September 1985): p 1262-1264+.
2. Hagemmaier, D.J. "Nondestructive Testing Developments in the Aircraft Industry." *Materials Evaluation*. Vol. 49, No. 12. Columbus, OH: American Society for Nondestructive Testing (December 1991): p 1470-1472, 1474-1476, 1478.
3. Dodge, D.O. "A Time of Opportunity" [1980 Lester Honor Lecture]. *Materials Evaluation*. Vol. 39, No. 1. Columbus, OH: American Society for Nondestructive Testing (January 1981): p 32-35.
4. Chitty, F. "Radiography as a Control in Aluminum Alloy Spotwelding and the Fabrication of Plastic Honeycomb Panels for Aircraft." *Nondestructive Testing*. Vol. 6, No. 4. Columbus, OH: American Society for Nondestructive Testing (Spring 1948): p 11-12.
5. Hitt, W.C. and D.J. Hagemmaier. "Radiography of Weldments In-Motion." *Symposium on Nondestructive Testing in the Missile Industry* [San Francisco, October 1959]. Special Technical Publication 278. West Conshohocken, PA: ASTM International (1960).
6. Gallar, J.J. "Modular Robotic Manipulation in Radiographic Inspection." *Materials Evaluation*. Vol. 46, No. 11. Columbus, OH: American Society for Nondestructive Testing (October 1988): p 1397-1399.
7. Hagemmaier, D.J. and A. Barath. "Mobile Field Testing of Missiles and Aircraft." *Symposium on Nondestructive Testing in the Missile Industry* [San Francisco, October 1959]. Special Technical Publication 278. West Conshohocken, PA: ASTM International (1960).
8. Hastings, C.H. and M.V. Grund. "Radiographic Inspection of Reinforced Plastics and Resin-Ceramic Composites." *Nondestructive Testing*. Vol. 19, No. 5. Columbus, OH: American Society for Nondestructive Testing (September-October 1961): p 347-351.
9. Hasenkamp, F.A. "Radiographic Laminography." *Materials Evaluation*. Vol. 32, No. 8. Columbus, OH: American Society for Nondestructive Testing (August 1974): p 169-174, 180.
10. Becker, G.L. "A Brief Look at the Low-Energy Radiography of Composite Materials." *Materials Evaluation*. Vol. 43, No. 6. Columbus, OH: American Society for Nondestructive Testing (May 1985): p 596, 598.
11. Whealy, R.D. "NDT of an Advanced Geometry Composite Blade." *Proceedings, Aerospace — AFML Conference on NDT of Plastic/Composite Structures* [Dayton, OH]. Wright Patterson Air Force Base, OH: Air Force Materials Laboratory (March 1969).
12. McFaul, H.J. "Automated Radiographic Film Interpretations." Presented at *Voordrachten: 5th International Symposium on Industrial Radiography* [Antwerp, Belgium]. Mortsel, Belgium: Gevaert-Agfa (1969).
13. Criscuolo, E. et al. "Radiography of Large Solid Propellant Rocket Motors." *Symposium on Nondestructive Testing in the Missile Industry* [San Francisco, October 1959]. Special Technical Publication 278. West Conshohocken, PA: ASTM International (1960): p 3-11.
14. Burrill, E.A. "High-Energy Nuclear Radiations — Their Implications for Industry" [1961 Lester Honor Lecture]. *Nondestructive Testing*. Vol. 19, No. 3. Columbus, OH: American Society for Nondestructive Testing (May-June 1961): p 167-176.
15. Failor, J.A. "Life Beyond the Limits: Radiography and Aircraft Turbine Repair." *Materials Evaluation*. Vol. 54, No. 6. Columbus, OH: American Society for Nondestructive Testing (June 1996): p 659-660, 662.
16. Hagemmaier, D.J. *Nondestructive Testing of Silica-Phenolic Materials for Small Ablative Thrust Chambers*. AFML-TR-66-274. Wright-Patterson Air Force Base, OH: Air Force Materials Laboratory (1966).
17. Hagemmaier, D.J. and R. Kleint. "Cinefluorography of Small Ablative Thrust Chambers during Hot Firing." *Materials Evaluation*. Vol. 24, No. 4. Columbus, OH: American Society for Nondestructive Testing (April 1966): p 186-191.

18. Weiley, R.G. "Photo Recording Internal Ballistics and Flame Fronts of Solid Propellant Engines by Cine-X Data Process." Presented at Symposium for the Society of Photo-Optical Instrumentation Engineers [Miami Beach, FL]. Bellingham, WA: International Society for Optical Engineering (August 1964).
19. Hagemmaier, D.J. "Testing Rocket Engine Materials." *Metal Progress*, Vol. 94, No. 2. Materials Park, OH: ASM International (August 1968): p 87-90.
20. Barclay, J.L. "X-Ray and Ballistic Missiles" [1958 Lester Honor Lecture]. *Nondestructive Testing*. Vol. 17, No. 2. Columbus, OH: American Society for Nondestructive Testing (March-April 1959): p 73-79.
21. Viswanathan, K., K.V. Rao, C. Subbiah and M.C. Uttam. "Performance Characteristics of Conventional X-Ray Generator, Isotope Source, and High-Energy Accelerator in Rocket Motor Evaluation." *Materials Evaluation*. Vol. 44, No. 1. Columbus, OH: American Society for Nondestructive Testing (January-February 1987): p 86-90.
22. Tomlinson, R.L. and P.E. Underhill. "Production Neutron Radiography Facility for the Routine NDT Inspection of Special Aerospace Components." *AGNTP-29*. San Ramon, CA: Aerojet-General Corporation, Nuclear Division (March 1969).
23. Lewis, W.J. and L.G.I. Bennett. "The Use of Neutron Radiography in the Inspection of Aircraft Composite Flight Control Surfaces." *The First Pan-American Conference on Nondestructive Testing: Alliance of the Americas* [Toronto, Canada, September 1998]. Columbus, OH: American Society for Nondestructive Testing (1998): p 51-55.
24. DeVolpi, A. and E.A. Rhodes. "Neutron and Gamma-Ray Tomographic Imaging of LMFBR SAREF-Program Safety-Test Fuel Assemblies." *Materials Evaluation*. Vol. 40, No. 12. Columbus, OH: American Society for Nondestructive Testing (November 1982): p 1273-1279.
25. Berger, H. *Neutron Radiography*. New York, NY: Elsevier Publishing (1965).
26. Hagemmaier, D.J., J. Halchak and G. Basl. "Detection of Titanium Hydride by Neutron Radiography." *Materials Evaluation*. Vol. 27, No. 9. Columbus, OH: American Society for Nondestructive Testing (September 1969): p 193-198.
27. Hagemmaier, D.J., H.J. McFaul and J.T. Parks. "Nondestructive Testing Techniques for the Fiberglass, Graphite Fiber and Boron Fiber Composite Aircraft Structures." *Materials Evaluation*. Vol. 28, No. 9. Columbus, OH: American Society for Nondestructive Testing (September 1970): p 194-204.
28. Buetzow, G.C. "Automated Radiography of Space Shuttle Motor." *Materials Evaluation*. Vol. 47, No. 6. Columbus, OH: American Society for Nondestructive Testing (June 1989): p 686-687, 690-691.
29. Gray, J.N. and G.R. Tillack. "X-Ray Imaging Methods over the Last 25 Years — New Advances and Capabilities." *Review of Progress in Quantitative NDE*. New York, NY: Plenum Press (2000).
30. Kropas-Hughes, C.V. and S. Trent Neel. "Basics of Computed Tomography." *Materials Evaluation*. Vol. 58, No. 5. Columbus, OH: American Society for Nondestructive Testing (May 2000): p 630-633.
31. Maranville, C. "Requirements for Radioscopy of Aerospace Structures." *Real-Time Radioscopy and Digital Imaging* [Mashantucket, CT, August 1998]. Columbus, OH: American Society for Nondestructive Testing (1998): p 37-43.
32. Jones, T. "Evaluation of Digital X-Ray Imaging Systems for US Air Force Applications." *ASNT Fall Conference and Quality Testing Show Paper Summaries* [Phoenix, AZ, October 1999]. Columbus, OH: American Society for Nondestructive Testing (1999): p 137-139.
33. Gray, J. "Three Dimensional Modeling of Projection X-Ray Radiography." *Review of Progress in Quantitative Nondestructive Evaluation*. Vol. 7A. New York, NY: Plenum (1988): p 343-348.
34. Inanc, F. and J.N. Gray. "New Developments in the Computer Simulation of X-Ray NDE Process." *Review of Progress in Quantitative Nondestructive Evaluation*. Vol. 10A. New York, NY: Plenum (1991): p 355-362.
35. Hoppins, W.K. "In-Motion Radiography." *Precision Metal*. Cleveland, OH: Industrial Publishing Company (August 1968).
36. Bulban, E.J. "Fluoroscopic Inspection Assures Quality." *Aviation Week and Space Technology*. New York, NY: McGraw-Hill (August 1979).

37. McDaniel, G.A. "Recent Developments in High Output Microfocus X-Ray Systems." *Automated Nondestructive Testing: Proceedings of a Topical Seminar* [Idaho Falls, ID, June 1983]. Sponsored by American Society for Nondestructive Testing South Idaho Section. Amsterdam, Netherlands: Gordon and Breach Science Publishers (1986): p 209-212.
38. Chapter 19, "Specialized Radiographic Methods." *Nondestructive Testing Handbook*, second edition: Vol. 3, *Radiography and Radiation Testing*. Columbus, OH: American Society for Nondestructive Testing (1985): p 759-835.
39. London, B., R.N. Yancey and J.A. Smith. "High-Resolution X-Ray Computed Tomography of Composite Materials." *Materials Evaluation*. Vol. 48, No. 5. Columbus, OH: American Society for Nondestructive Testing (May 1990): p 604-608, 629.
40. Wojciechowski, C. "Automated X-Ray Inspection of Air Foils." Presented at Qual-Test®-3 [Cincinnati, OH, October 1984]. Program, *Materials Evaluation*, Vol. 42, No. 10 (September 1984): p 19.
41. Richards, W.J., M.R. Gibbons and K.C. Shields. "Neutron Tomography of Aerospace Structures." *Fifth World Conference on Neutron Radiography* [Berlin, Germany, June 1996]. Berlin, Germany: Deutsche Gesellschaft für Zerstörungsfreie Prüfung (1997): p 644-649.
42. Bueno, C., M.D. Barker, R.A. Betz, R.C. Barry and R.A. Buchanan. "Nondestructive Evaluation of Aircraft Structures using High Resolution Real Time Radiography." *Nondestructive Evaluation of Aging Aircraft, Airports, Aerospace Hardware and Materials*. SPIE Proceedings 2455. Bellingham, WA: International Society for Optical Engineering (1995): p 114-124.
43. Winfree, W., R. Parker and P. Howell. "Detection of Cracks in Aircraft Structures with Reverse Geometry X-Ray®." *Proceedings of the 5th Joint DOD/FAA/NASA Aging Aircraft Conference* (September 2001).
44. Albert, R., W. Pember, J. Garrison and D. Reyna. "Aircraft Inspection with a Portable, Filmless X-Ray System Using Reverse Geometry." *Materials Evaluation*. Vol. 58, No. 5. Columbus, OH: American Society for Nondestructive Testing (May 2000): p 634-638.
45. Xu, J., R. Wallingford, T. Jensen and J. Gray. "Recent Developments in the X-Ray Radiography Simulation Code: XRSIM." *Review of Progress in Quantitative Nondestructive Evaluation*. Vol. 13A. New York, NY: Plenum (1994): p 557-562.
46. Conley, J., B. Moran and J. Gray. "A New Paradigm for the Design of Safety Critical Castings." *Aluminum in Automotive Applications*. SP 1350. Warrendale, PA: SAE International (1998) p 25-38.
47. Gray, J. "Recent Developments of an X-Ray NDE Simulation Tool." *Modeling of Casting, Welding and Advanced Solidification Processes*. Vol. 9. Aachen, Germany: Shaker-Verlag (2000): p xxxvi-xliii.
48. Straw, R. "Voices in the Air — The Early Days of Aircraft NDT." *Materials Evaluation*. Vol. 42, No. 2. Columbus, OH: American Society for Nondestructive Testing (February 1984): p 152-160.
49. Ito, G. "A Review of the History of Nondestructive Testing in Japan." *Materials Evaluation*. Vol. 40, No. 11. Columbus, OH: American Society for Nondestructive Testing (October 1982): p 1138, 1140-1141.

# Other Applications of Radiographic Testing

Bruce E. Bolliger, Agilent Technologies, Singapore, Republic of Singapore (Part 2)

Gary G. Korkala, Security Defense Systems, Nutley, New Jersey (Parts 3 and 4)

Andreas F. Kotowski, Rapiscan Security Products, Hawthorne, California (Part 4)

Stig Oresjo, Agilent Technologies, Loveland, Colorado (Part 2)

Samuel G. Snow, Oak Ridge, Tennessee (Part 1)

# PART 1. Radiation Gaging of Density or Thickness<sup>1</sup>

Radiation gaging does not use shadow image formation yet is a nondestructive testing technique by which density, thickness and composition can be determined using the interaction of ionizing radiation with a test material. Applications of radiation gaging range from high accuracy measurements of coating thickness to detection of termite damage. Radiation gaging may be used online to enable real time control of processing equipment or may involve extensive scanning and analysis to construct three-dimensional images of internal density variations in materials.

## Gaging Techniques

Radiation gaging includes a wide variety of measurement types. Gamma rays, X-rays, beta particles, neutrons and positive ions can all be used for radiation gaging. These radiations interact with the test material in a number of useful ways.

Despite the wide diversity of techniques that can be used, one technique, gamma or X-ray attenuation gaging, has found the widest application because of its general applicability to all materials and many component configurations. Gamma and X-ray attenuation techniques are particularly well suited for process monitoring applications such as control of thickness in a rolling mill or monitoring density of a solution in process piping. As an inspection tool for fabricated components, attenuation gaging can be used to ensure that density, composition and thickness of a wide variety of materials have been kept under control.

Attenuation gaging can achieve extremely high accuracies for some applications; or operational parameters can be adjusted for rapid testing on an assembly line basis.

Interactions of radiation with matter that are useful for gaging are listed in Table 1, along with an indication of measurement applications. For convenience, these may be classed in two categories: (1) those involving gamma rays and X-rays and (2) radiations based on interactions of nuclear particles (neutrons, positive ions and beta particles).

Gaging with particles from the atomic nucleus gives the name *nucleonic* to nucleonic gaging, widely used for the online gaging of low density and thin film materials, such as paper and other materials manufactured in sheets and rolls. Nucleonic gaging is a well established family of quality control techniques with a long history in nondestructive testing.<sup>2-6</sup>

## Attenuation Gaging

Gaging by measuring the attenuation of gamma and X-ray photon beams is used to determine the product of density  $D$  times thickness  $T$ . In many applications, the density may be assumed to be nonvarying and this gaging technique is used for thickness measurements, often in continuous automatic systems for control of production equipment. Conversely, if thickness is held constant, density can be measured. Use of more than one radiation energy makes possible the measurement of the density thickness product of individual elemental components in a

TABLE 1. Applications of radiation measurement for gaging of density or thickness.

Technique	Application
Absorption edge densitometry	coating thickness; composites of two materials
Attenuation gaging of density	paper and wood pulp; cigarettes
Attenuation gaging of thickness	metal sheet, foil, pipes and tubes; plastic film, sheet and tubing
Beta backscatter	coating thickness (for example, vinyl on wood)
Compton scattering	density or thickness of nondense materials; high and low density discontinuities; testing from one side
Computed tomography	multidirectional location of internal discontinuities
Neutron gaging	objects or discontinuities with high hydrogen content (for example, damp regions)
X-ray fluorescence	coating thickness



multicomponent material such as a layered structure or a composite.

The basic gamma or X-ray attenuation gage, in its simplest form, consists of an X-ray or gamma source, source shielding and collimation, an air gap where samples can be introduced and a collimated detector as shown in Fig. 1. The principle of operation is simple and is described by a single basic equation. If the intensity of the radiation measured by the detector with no sample in place is  $I_0$ , then when a sample of thickness  $T$  is introduced into the air gap so as to intercept the radiation beam, the intensity  $I$  measured by the detector is given by the exponential attenuation law:

$$(1) \quad I = I_0 \exp(-\mu_M \rho T)$$

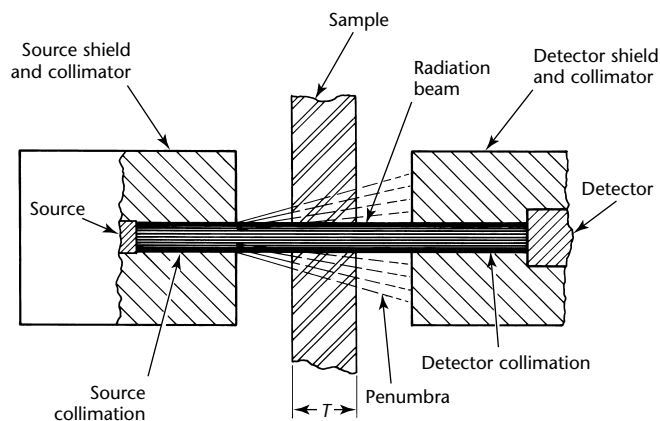
where  $\rho$  is the density of the sample and  $\mu_M$  is the mass attenuation coefficient of the sample material for gamma or X-rays of the energy used.

Measurements of radiation intensity  $I$  can be used to determine sample characteristics that depend on the product  $\mu\rho T$ . Most commonly, radiation attenuation gaging is used to measure thickness when coefficient  $\mu$  and density  $\rho$  are controlled or known.

Other applications include monitoring density when thickness is held constant and monitoring composition variation through its effect on  $\mu$ ,  $\rho$  or both. Although the basic principles of these measurements are simple, they must be thoroughly understood in order to select the proper approach to a given measurement problem.

The technique of gaging density and thickness by attenuation measurement is the basis for most of the applications discussed below (Figs. 2 and 3).

**FIGURE 1.** Basic gamma attenuation gage for sample of thickness  $T$ .<sup>1</sup>



## X-Ray Fluorescence

X-ray fluorescence (XRF) gaging is based on excitation and detection of characteristic X-ray emission ( $K$  or  $L$  X-rays). Because the energy of the radiation emitted is unique to the emitting element, X-ray fluorescence is commonly used for elemental analysis. [X-ray fluorescence as an analytical tool is described elsewhere in this volume.](#)

When used for gaging, X-ray fluorescence generally uses an isotopic gamma source and a semiconductor (energy dispersive) detector. Cadmium-109, americium-241, gadolinium-153 and cobalt-57 are suitable excitation sources, the choice depending on the elements to be excited. The semiconductor detector is usually lithium drifted silicon [Si(Li)].

An X-ray fluorescence gage can be used to measure the thickness of coatings for a variety of material combinations of coating and substrate. Coating thickness can be measured by measuring (1) the increase in X-ray intensity from the coating material with increasing coating thickness, (2) the attenuation of substrate X-rays by the coating or (3) a combination of both.<sup>7</sup>

## Compton Scattering

Compton scattering is used to measure material density, including detection of high and low density discontinuities, and can also be used for one-sided thickness gaging. The equipment used for Compton scatter gaging is very similar to that used for X-ray fluorescence gaging. In fact X-ray fluorescence and Compton scattering measurements can be combined in a single gage.

Compton scattering can be used to measure density or thickness of low atomic number materials. The configurations of source and detector and sample are similar to those used for X-ray fluorescence. Source energy must be high enough to ensure that (1) Compton scattering is the predominant interaction with the material and (2) the radiation penetrates adequately to the desired gaging depth. Best sensitivity is obtained for the lowest energy that satisfies these requirements.

The energy  $E'$  of the scattered radiation is related to the energy  $E$  of the incident radiation and the scattering angle  $\theta$  according to the relationship:<sup>19</sup>

$$(2) \quad \frac{1}{E'} - \frac{1}{E} = \frac{1}{\mu_e C^2} (1 - \cos \theta)$$

where  $\mu_e$  is the electron rest mass and  $C$  is the speed of light ( $\mu_e C^2 = 0.51$  MeV).

Thus, the energy of the scattered radiation is selected by choice of scattering angle and source energy. This can be important for separating Compton scattered radiation from interfering X-ray fluorescence radiation.

The intensity of the scattered radiation is usually so low that a spectrometric detector can be used. A scintillation

detector has adequate energy resolution for many applications.

Examples of the application of Compton scattering gages include measuring the thickness of composite structures with a low energy system<sup>8</sup> (40 and 100 keV from gadolinium-153) and detection of termite damage to railway ties with a system using 662 keV gamma rays from cesium-137.<sup>9</sup>

**FIGURE 2.** Automated applications of X-ray density gaging: (a) measurement of thickness of coiled stainless steel; (b) measurement of thickness of hot strip steel; (c) measurement of moisture content of paper at paper mill; (d) measurement of packaging tape after application of adhesive coating.<sup>14</sup>



## Other Radiation Gaging Techniques

**Tomography.** Tomography is a specialized form of attenuation gaging by which multidirection attenuation measurements are computer analyzed to reconstruct images of the internal distribution of mass in the test object. This technique is extremely valuable when internal discontinuities need to be located as well as detected or when the shape of the test object is irregular enough to obscure internal density variations in conventional radiography or radiation attenuation gaging.

**Absorption Edge Densitometry.** The very good energy resolution of semiconductor detectors makes possible absorption edge spectrometry in a practical gage.<sup>10</sup> This can be used for coating thickness measurements or composition of a two-element composite material. The basis for this measurement is the abrupt change in X-ray attenuation that occurs at the photoelectric absorption edge of one of the two elements. By gaging with two energies, one above and one below the absorption edge, it is possible to determine the mass per area of both elements.

**Beta Backscatter.** Beta backscatter is a well established technique for measuring coating thicknesses. Its applicability is based on the increased backscattering of beta particles as a function of increasing atomic number. As coating thickness increases from zero, the backscatter response varies smoothly from the response characteristic of the substrate atomic number to the response characteristic of the coating atomic number. Intermediate values of backscatter response can be calibrated

directly in terms of coating thickness. The sensitivity of this technique improves as the difference between the atomic numbers of the coating and the substrate increases.

Details of beta backscatter for thickness gaging are discussed elsewhere.<sup>1</sup> Backscatter imaging is [discussed elsewhere](#) in this book.

**Neutron Gaging.** Neutron gaging is a very specialized technique most often used for measuring hydrogen content (usually in the form of water), or less often, the content of other isotopes with high neutron cross sections. Neutron gages can be simple, inexpensive systems for measuring moisture in food, soil or other bulk materials. The basis of the measurement technique can be attenuation of thermal or fast neutrons, moderation of fast neutrons, or scattering of thermal neutrons. For some applications, such as moisture measurements, neutron gaging is the best or only available technique. However, neutron gages are of limited and specialized use. A published review provides an excellent summary of neutron gaging.<sup>11</sup>

**Rutherford Scattering.** Rutherford scattering, elastic scattering of positively charged particles from atomic nuclei, is a useful surface analysis technique. The energy loss upon scattering at a specific angle is an easily calculable function of atomic weight of the scattering material. This technique can be used to identify surface contaminants and determine composition of materials at the surface. However, applicability of this technique is generally limited to samples because positive ions are readily absorbed in air and measurements must therefore be made in vacuum.

**FIGURE 3.** Scanner searches for holes, discolorations and protrusions in cigarette rod. After passing through scanner, cigarette rod is divided into cigarettes.<sup>14</sup>



## Detector Types

The operation of all gamma and X-ray detectors is based on the effect of energy deposited in the detector. Photons deposit their energy primarily by three types of interaction with the detector material: photoelectric absorption, scattering from atomic electrons and pair production.

In all three mechanisms, some or all of the photon energy is transferred to kinetic energy of electrons and some of the energy may escape from the detector. It is in the means by which different types of detectors transfer the kinetic energy of these electrons into measurable voltage or current signals that detectors differ. The different types of detection include gas filled detectors, scintillation phototube systems and semiconductor detectors.<sup>12</sup>

## Gas Filled Detectors

A gas filled detector consists of a chamber containing gas in which an electric field is maintained. Geometry may be planar or coaxial. The primary electrons from the interaction of photons with the detector lose their energy by ionizing gas molecules along their paths, leaving tracks of electron positive ion pairs. The electrons are quickly swept out of the gas to the anode. The relationship between the negative charge collected at the anode and the energy deposited in the detector by the radiation is dependent on the electric field strength in the chamber. At very low voltages the field strength is insufficient to separate all of the electrons from the positive ions before recombination occurs. In this *recombination region*, the relationship between energy deposited and charge collected is complicated and difficult to predict.

Gas filled chambers are relatively inefficient because of the low density of gas. For radiation attenuation gaging, only the ionization chamber has an offsetting advantage for specific applications. An ionization chamber can be an extremely stable detector for measuring very intense radiation fields that would damage other types of detectors. For highest efficiency, a high atomic number gas such as xenon should be used.

## Ionization Chambers

For voltages sufficiently high to prevent recombination of electrons and positive ions, the charge collected is independent of the voltage and proportional to the energy deposited. This is the *ionization chamber* region of operation. Ionization chambers are used in the *current mode*. That is, rather than trying to detect the extremely small charge collected from a single photon interaction, the integrated current of many interactions is measured. This current is proportional to the energy deposited in the detector per unit time and hence, for constant photon energy, to the radiation flux.

## Proportional Counters

As the electric field in a gas filled chamber is increased further, secondary electrons are accelerated to energies that ionize other molecules in the gas, producing additional electron-and-ion pairs. In this *proportional region*, the charge collected is proportional to the energy deposited and increases with increasing voltage. By measuring the collected charge from a single interaction, proportional counters are used for energy spectrometry. That is, individual photons are detected and sorted according to charge. Because charge

is proportional to energy, this sorting results in an energy spectrum.

## Geiger Counters

As voltage is further increased, the gas multiplication continues to increase until each photon interaction produces a complete electrical breakdown of the gas, providing a large pulse of charge independent of the deposited energy. This is the *geiger region* of a gas filled tube. In this region, individual photon interactions are detected as with proportional counters but energy information is lost.

## Scintillator Phototubes

As the primary electrons from a photon interaction pass through a material, they ionize atoms and excite atomic or molecular energy levels. Some materials give up a portion of their excitation energy as light, a process called *scintillation*. Scintillation materials transparent to their own light can be coupled to a photodetector and used as a radiation detector.

The phototube has a glass front window through which light passes to a photoemissive surface on the inside of the tube. Because the photoemissive surface is at negative potential relative to other parts of the tube, it is called the *photocathode*. In the presence of the impressed electric field, light striking the photocathode causes electrons to be ejected and accelerated to the anode. The charge transferred from cathode to anode is proportional to the light intensity on the photocathode and hence to the energy deposited in the scintillator.

**Current Mode.** When the scintillator phototube detector is used in the current mode, the anode current is measured to determine the average radiation flux. The currents generated are on the order of  $10^{-10}$  to  $10^{-7}$  A. To measure these small currents accurately, the dark current (the background current measured in the absence of radiation) must be small. Because tubes not designed for low level measurements may have large dark currents, care should be exercised in selecting a phototube. Phototubes with dark currents less than  $10^{-11}$  A should be used.

**Spectrometry Mode.** A scintillator can also use a photomultiplier tube to operate in a spectrometric mode. In a photomultiplier tube, the charge from the photocathode is accelerated to the first dynode of a dynode chain, ejecting more electrons from the surface of the dynode. These electrons are accelerated to the second dynode, ejecting additional electrons. The process continues down the



dynode chain, multiplying the charge at each dynode, so that the charge reaching the anode is many times that ejected from the cathode. The collected charge due to a single pulse of light in the scintillator can be measured and related to the energy deposited by the initial photon interaction. Thus, a scintillator photomultiplier can be used for energy spectrometry.

### Semiconductor Detectors

Unlike gas filled detectors and scintillation detectors that can either be operated in a current mode or spectrometry mode, semiconductor detectors are always used in the spectrometry mode. The advantage of semiconductor detectors is the superior resolution for energy spectrometry. Semiconductor detectors have the additional advantage of being more stable than scintillation photomultiplier detectors.

A semiconductor radiation detector can be described as the solid state analogy to a gas filled detector. Charge carriers in a semiconductor are electron hole pairs created by ionizing radiation, much as electron positive ion pairs are created in the gas detector. In semiconductors, electrons exist in energy bands separated by band gaps. In the absence of any excitation, the valence band is completely filled with electrons and the conduction band is empty. The band gap is an energy range in which electrons cannot exist. Electrons can be excited, either by thermal energy or by an interaction with radiation, leaving a positive hole in the valence band and an electron in the conduction band. In the presence of an applied field, the mobile electrons and holes migrate through the semiconductor, creating a current.

Silicon and germanium detectors can be made to incorporate large volumes in which electron hole pairs are formed and can readily migrate to electrical contacts. By collecting the charge generated by a detected photon, the photon's energy can be measured with precision. To minimize thermally generated noise, detectors are cooled to liquid nitrogen temperature. In addition to cooling the detector, the liquid nitrogen operates a pump that maintains an insulating vacuum around the detector. An integral preamplifier collects the small charge generated by individual photons and outputs a corresponding voltage pulse to the external electronics.

## Selection of Detector Type

Radiation detection can be grouped in two categories: current mode types and spectrometers. Depending on the specific detector and detector electronics, the upper limit of count rates that can be handled by a spectrometer system is between  $10^4$  and  $10^5$  counts per second. As a general rule, a radiation gaging application that requires intensities greater than  $10^4$  counts per second (to achieve the required accuracy in acceptable measurement time) should not be attempted with a spectrometer system. For most of these applications, a scintillator phototube system, operated in the current mode, is best.

### Current Mode Detectors

A typical scintillator used for gamma detection is thallium activated sodium iodide. Thallium activated sodium iodide has two characteristics that make it unsuitable for attenuation gaging applications requiring current mode operation.

1. A long decay contributes to slow detector response.<sup>13</sup>
2. Thallium activated sodium iodide darkens under intense gamma exposure, reducing the amount of light reaching the photocathode. This slow recovery makes response even slower.

Europium activated calcium fluoride,  $\text{CaF}_2(\text{Eu})$ , is one scintillator that has been found to exhibit neither of these effects. The only drawback of europium activated calcium fluoride over thallium activated sodium iodide is a lower efficiency because of its lower atomic number, lower density and somewhat less light output for the same energy deposition. Current mode measurements should use either a europium activated calcium fluoride scintillator or an alternative also free of slow response effects.

### Spectrometer Mode Detectors

Spectrometer detectors can be used when high intensity is not required. Their energy selection capability makes it possible to choose the desired gaging energy. For example, a spectrometric source makes it possible to gage with 43 keV X-rays from gadolinium-153 while discriminating against the 100 keV gammas. Energy spectrometry also allows discrimination against lower energy scattered radiation that can be a source of measurement error.

Germanium and silicon detectors offer good energy resolution. For energies up to about 100 keV, lithium activated silicon

detectors are satisfactory. Germanium detectors are preferred for higher energies because of their higher efficiency. Germanium detectors may be either planar or coaxial. Coaxial detectors are preferred for higher energies because, with their greater detector volume, they are more efficient at high energies. For applications where 15 to 20 percent energy resolution is adequate, a scintillator photomultiplier detector provides a less expensive alternative that does not require liquid nitrogen cooling. For spectrometry, thallium activated sodium iodide is an acceptable scintillator.

## Application Case Histories<sup>14</sup>

Nucleonic measurement gages have been used since the 1950s for nondestructive testing in the manufacture of diverse products, including paper, metals, plastics, tires and cigarettes. These gages have been integrated into programs for quality control and statistical process control.

Radiation density gaging and radioscopy taken together are applicable to online testing for various anomalies in various consumer goods (Table 1).

### Steel

Steel gaging can use X-ray sources or isotopes. Radiation particles are beamed into the steel as it passes through the production line and sensors are used to calculate the radiation absorbed by the steel and the radiation passing through it. Calculating mathematical difference between the two provides a rapid, accurate thickness measurement. In the 1950s, X-ray thickness gages were used almost exclusively to measure product thickness. Since then, computer based electronics have modernized the manufacturing process so that thickness measurement data are fed directly into a mill's control systems, resulting in automated statistical process control. The same technology is used for quality monitoring and for final testing of steel products.

**Thickness.** Gamma ray gages and nucleonic measurement devices are used by steel manufacturers to monitor thickness in castings, coiled steel (Fig. 2a), steel plate, sheet, hot strip steel (Fig. 2b), cold strip steel and walls of pipe products. These gages provide feedback to mill control. Their accuracy depends on the calibration and application of the gaging system being used, as well as on the material's temperature. A multiple-point area of measurement can be documented

at high speed to monitor the full width thickness profile of steel.

For strip steel, data are used to make manual adjustments along the production lines. X-ray gages are integrated into automated process control to help the company make steel thinner than normally specified. With an automated system, rapid adjustments can be made to the production lines to eliminate waste.

**Liquid Metal Level.** The technology is used also to measure liquid level in continuously cast bolts as dross is being poured into the slab. Radiation is used by casters to measure levels of molten metal in molds

**Coating Thickness.** Radiation devices are used to measure coating thickness on coated steel.

**Moisture.** Moisture affects the density of materials used in steel making. Radiation is gaged to measure the amount of moisture content in coke.

**Furnace Monitoring.** Isotopes are embedded in blast furnace walls to measure the thickness of refractory walls and radiation sensors are used to track the positions of slab.

### Aluminum

Nucleonic measurement gages are used on a wide range of aluminum products, including foil, house coverings, armor, automotive bodies and aircraft bodies. Many aluminum products are actually a combination of aluminum and plastic. Because both materials are expensive, thickness variation is critical. Aluminum manufacturers have incentive to produce thinner materials to save material costs and to achieve weight objectives. X-ray thickness gaging is very important for these objectives.

A major manufacturer of aluminum cans has used beta ray gages to guarantee that products meet the industry's specifications for thickness. The manufacturer has used these thickness gages on all aluminum sheet made and additional gages are used for final quality testing.

### Paper and Pulp

In the paper and pulp industries, radiation gages and sensors are used mainly to measure density or basis weight, moisture content (Fig. 2c), thickness and ash content. Nonionizing frequencies of radiation (such as infrared and visible radiation) are used to evaluate the glossiness, smoothness, opacity and brightness of paper.

A manufacturer of fine papers, including bond, carbonless and coated papers for use in stationery and printed matter, has used beta ray gages to measure



paper weight. Another paper manufacturer uses a krypton-80 beta gage to measure the mass (organic, inorganic and water content) of its paper products. In some of the company's production areas, the gages are used to automate the manufacturing process. The company makes printing paper for use in advertisements and brochures and uncoated papers for use in making trade books.

Nucleonic measurement gages have been used for the evaluation of paper products. The technology is used to measure basis weight and moisture content. Measurement data are automatically transmitted into a computer, which adjusts the production line.

The gaging systems help cut down on energy in the final stage of drying the paper. A scanner, placed near the end of the production line, identifies wet spots on the paper so that automatic adjustments can be made to the drying process. Without the gages, there was no accurate way to predict efficiently the amount of energy necessary to dry the paper and in many cases the paper could be overdried.

In the manufacture of wood particle board, an isotope device with promethium and americium sources has been used to measure the density (thickness and weight) of the mat (layers of resin and wax) before it is pressed into board. Mounted on a frame, the scanner moves horizontally over the product as the wood passes through the production line.

## Plastics

Hot melt plastic is used to make packaging tape. In one factory, the tape was processed on two webs, in which unwound base paper is run through a coating section. Two scanners were used on each roll of tape as it passed through the production line: one scanned the product before adhesive coating was applied; the other scanned the tape after the coating was applied (Fig. 2d). The statistical difference between both measurements indicates the thickness of the adhesive coating.

Measurement data are fed automatically into production control and immediate, automatic adjustments are made to the production line. The same data appear on a control screen, alerting plant operators of these changes (Fig. 3). In addition, all measurement data are fed into a personal computer and archived for analysis. The system provides actual data on the products. Accurate measurement is important because adhesive coating is very expensive and because customers

want a consistent product. The gages have reduced waste and downtime.

Beta ray thickness measurement gages have been used to measure extruded vinyl used to cover wooden window frames. Even with variations in the process, the technique is 99.9 percent accurate, an improvement over production without the gages.

Chemical companies have used nucleonic gages to measure the thickness of extruded plastic sheets formed by forcing melted plastic through dies.

## Other Industries

Radiation measurement gages are also used in the production of fiber glass, textiles, fabrics and pharmaceuticals. In the tire industry, the gages are used on steel radial tires to measure the top and bottom coats of rubber on the tire and to measure the number of cords across the tire's surface.

The technology is also used in the production of cigarettes to measure weight, as well as to measure filter size and weight. Similar infrared gages measure circumference to verify that the cigarette is not too thin or too thick. An optical rod scanner (Fig. 3) searches for visible discontinuities, including holes, discolorations and protrusions.

---

## Closing

Radiation thickness gages have helped manufacturers of many products to reduce costs and to guarantee their products with confidence. The need for precision and product uniformity have made radiation gaging devices a vital part of the production process, especially within automated or statistical process control systems.

## PART 2. Radioscopy of Electronics

Printed circuit assemblies undergo digital X-radiographic testing during assembly, including components after placement and solder joints after solder curing. The following discussion focuses on production radiographic testing, not on the collection of measurements in process development during research and development.

### Solder Joint Automated Process Test Systems

Solder joints have much more complex shapes than do solder paste depositions and components, so taking measurements of solder joints normally requires more complex imaging techniques than do solder paste and components. Automated process test systems for solder joints have tried a variety of imaging technologies, including visual, radiographic, thermographic and ultrasonic testing and profilometry of laser heated solder joints as they cool. Two radiographic technologies have dominated in these systems: (1) transmission X-ray imaging and (2) cross sectional X-ray imaging.

#### Transmission X-Ray Systems

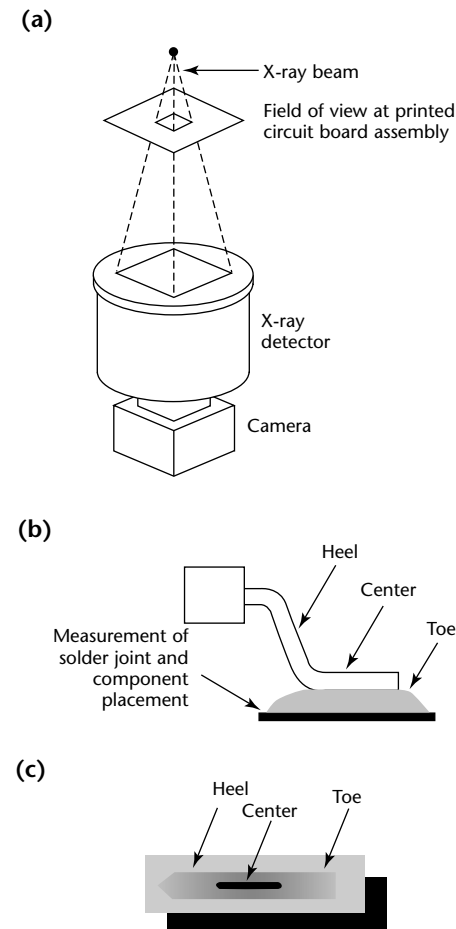
**Operating Principles.** Transmission X-ray systems radiate X-rays from a point source perpendicularly through the printed circuit assembly being inspected, as depicted in Fig. 4. An X-ray detector picks up a varying amount of X-rays depending on the thickness of metals that the X-rays are penetrating and converts the X-rays to light photons for a camera to create a grayscale image. The X-ray source is filtered so that metals of only a certain density range — typically lead, tin, gold and silver — will absorb the X-rays. The copper leads and frames of components sitting on top of solder joints do not absorb the X-rays and are therefore practically invisible to the X-ray detector. Thus, X-ray systems can easily see the entire solder joint, no matter what component material may be on top of the joint and blocking the operator's view of it.

The resulting X-ray image will be darker wherever the lead and tin solder is thicker in the solder joint. The image processing capability of the systems then

searches for features, such as the heel and toe fillets, the sides of the solder joint and even voids internal to the joint based on grayscale readings of the solder joint X-ray image. The systems then use predetermined decision rules to compare the grayscale readings to acceptance criteria to automatically accept or reject a solder joint. For example, the system would compare the relative grayscale

**FIGURE 4.** In transmission X-ray automated process, camera converts light photons to image and processes image to find solder joint features and detect anomalies:

(a) X-ray detector converts varying amount of X-rays to light, based on radiation absorbed by various parts of solder joint;  
(b) diagram of gull wing solder joint;  
(c) resultant density profile of solder joint.



reading for the heel fillet region, the center of the solder joint and the toe fillet region. The acceptance criteria might state that the heel fillet reading should be twice that of the center and that the toe fillet reading should be 50 percent higher than that of the center. If the actual readings do not meet these criteria, then the solder joint is reported as being anomalous.

Figure 4c shows an X-ray image of a gull wing solder joint that shows the center of the joint as much darker than the heel fillet region. This solder joint is clearly anomalous as the heel fillet region should always be darker and with a higher grayscale reading than the center of the joint, where the solder is thinnest for mechanically good solder joints. (The system's image processing capability can detect much more subtle changes in grayscales than can the human eye, allowing very accurate relative readings from one solder joint to the next.)

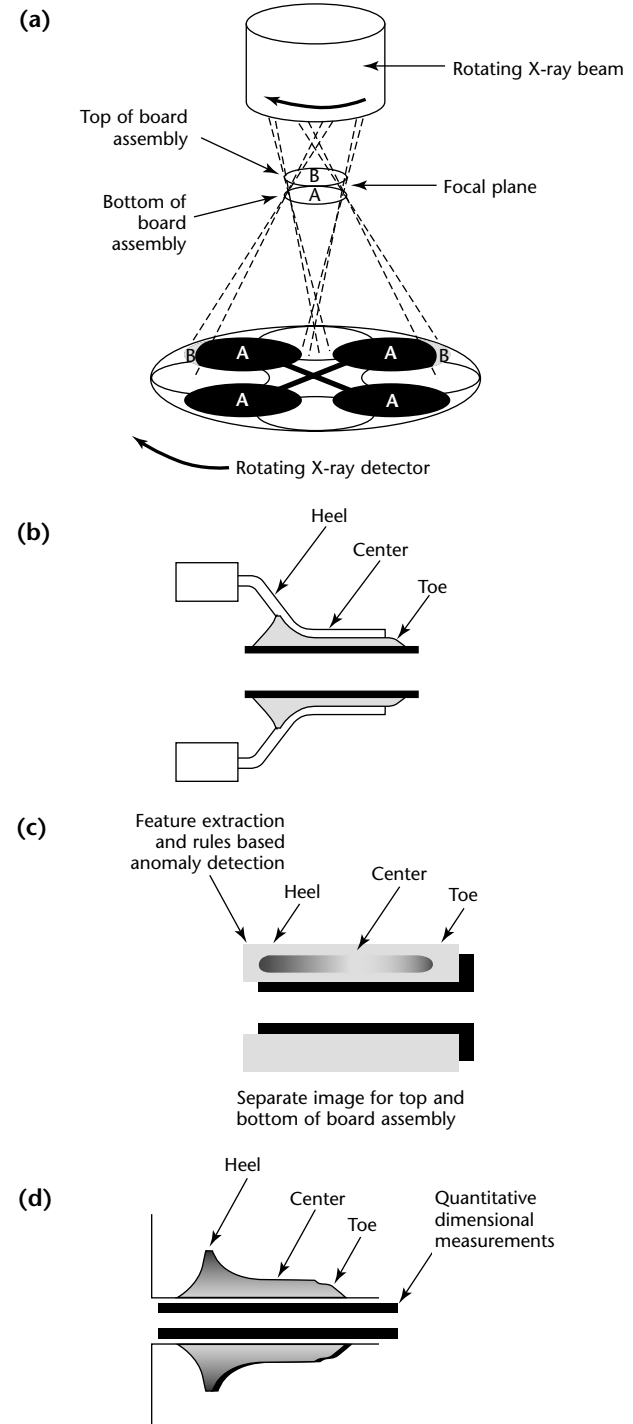
**Application.** Transmission X-ray technology works well for single-sided surface mount assemblies. These automated process test systems will accurately detect solder joint discontinuities such as open joints, insufficient solder, excess solder, bridges, misalignment between pin and pad and voids for most surface mount solder joint types, including J leads, gull wings, passive chips and small outline transistors. These systems also detect missing components and reversed tantalum capacitors. Based on trends in grayscale reading, these systems also can accurately detect process drifts through process control charting.

For double-sided assemblies, however, the transmission X-ray images of solder joints on the topside will overlap with the images of solder joints on the bottom side. The X-rays are absorbed by any solder in their path through the printed circuit assembly from the source to the detector. These overlapping images make accurate solder joint measurement impossible. Transmission X-ray imaging also cannot easily distinguish between the top, bottom and barrel of plated through-hole (PTH) solder joints, nor the bottom and ball of ball grid array (BGA) solder joints. So transmission X-ray systems cannot be used for accurate measurement and discontinuity detection of solder joints on double-sided assemblies nor for plated through-hole and ball grid array solder joints.

## Cross Sectional X-Ray Systems

**Operating Principles.** Cross sectional X-ray systems radiate X-rays at an acute angle from vertical through the printed circuit assembly being inspected. As Fig. 5 indicates, images from all around the

**FIGURE 5.** Schematic of cross sectional X-ray automated process test system for solder joint measurement: (a) adding images around circle from rotating X-ray beam and detector creates focal plane that captures only solder joints of interest, minimizing what is below or above; (b) diagram of solder joint; (c) density profile with feature extraction and rules based anomaly detection, separately for top and bottom of assembly; (d) resultant density profile with dimensional measurements. Image processing software then finds solder joint features and detect anomalies.



particular view being inspected are added together or integrated to create in effect an X-ray focal plane in space. This focal plane creates a cross sectional image, about 0.2 to 0.4 mm (0.008 to 0.016 in.) in thickness, right at the focal plane by blurring everything above and below the focal plane into the background, or noise, of the image. By moving the topside of an assembly into the focal plane, cross sectional images of only the solder joints on the topside are created. By moving the bottom side of an assembly into the focal plane, cross sectional images of only the solder joints on the bottom side are created. Separate images of top and bottom sides are always created, preventing any image overlap from the two sides.

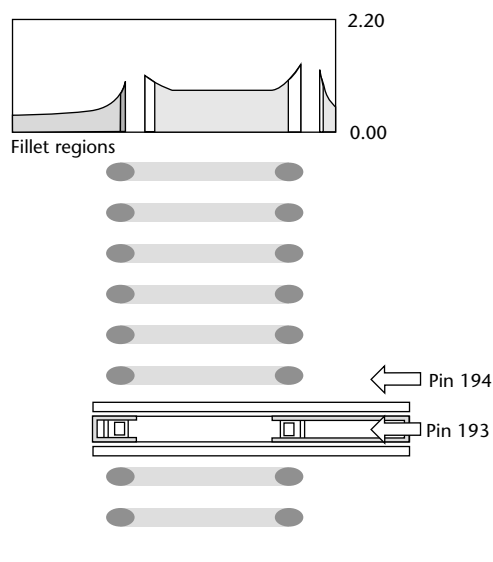
**Application.** Cross sectional X-ray automated process test systems work well for all types of printed circuit assemblies, including single-sided and double-sided, surface mount, through-hole and mixed technology assemblies. These systems accurately detect the same solder joint and component discontinuities as do transmission X-ray systems but, in addition, the cross sectional X-ray systems accurately detect insufficient solder

conditions for ball grid array and pin through-hole solder joints.

Some cross sectional X-ray automated process test systems go beyond just grayscale readings of specific solder joint features. By carefully calibrating grayscale readings to actual solder thickness, it is possible to generate repeatable measurements, in physical units rather than grayscale numbers, of fillet heights, solder and void volume and average solder thickness for the entire joint. Figure 6 shows an example of these calibrated measurements and includes a cross sectional representation of tape automated bonded (TAB) solder joints. The profile shown at the top of the X-ray image is generated by the system in physical dimensional units by interpreting and calibrating the grayscale readings of pin 193 in the X-ray image. Table 2 lists representative measurements for both pin 193 and pin 194.

Analysis of these physical thickness measurements of solder joints provides the information required for process characterization and improvement. For instance, variations in average solder thickness or volume for the solder joints across a single assembly or from assembly to assembly provide insight into the quality level of the paste printing process as well as sources of discontinuities.

**FIGURE 6.** Cross sectional X-ray image of tape automated bond (TAB) solder joints. Image processing software converts the grayscale readings of pin 193 image into side profile of solder thickness shown above image. Actual calibrated measurements of average solder thickness across pad, heel fillet height, center thickness and toe fillet height processed from images of pins 193 and 194 are shown in Table 2 and indicate that both solder joints are good.



## Advantages and Disadvantages of Radioscopic Testing

X-ray solder joint test systems can reach average inspection speeds of around 80 to 120 joints per second. X-ray solder joint inspection systems also have higher prices, typically about 50 to 100 percent more than the price of optical solder joint systems with the fastest testing speed capability.

**TABLE 2.** Example of measurement results from inspection of pins in printed circuit board. (See Fig. 6.)

Pin	Inspection Point	Thickness	
		$\mu\text{m}$	( $10^{-3}$ in.)
193	Pad	15.0	(0.59)
	Heel	29.9	(1.18)
	Center	17.5	(0.69)
	Toe	34.0	(1.34)
194	Pad	14.7	(0.58)
	Heel	30.5	(1.20)
	Center	17.3	(0.68)
	Toe	33.0	(1.30)

Automated X-ray testing of solder joints has the following major advantages: (1) extremely high discontinuity detection capability; (2) obviation of visual testing by automating solder joint discontinuity detection, thereby also reducing unnecessary rework due to false reject calls; (3) reduction of rework analysis time by pinpointing discontinuities to the exact solder joint; (4) real time process control of all three process steps (paste printing, component placement and solder cure) to lower discontinuity rates and rework costs; (5) quantitative measurements to help permanently eliminate the causes of discontinuities from all three process steps; (6) reduction of failures at final assembly and in the field, failures due to anomalous hidden solder joints and marginal solder joints due to insufficient solder, misalignment or excessive voids; and (7) applicability to lead free solder systems.

Automated radioscopy of solder joints has some limitations. Test throughput is not always fast enough to inspect all solder joints within the manufacturing cycle time for the printed circuit assembly. Also, automated radioscopy requires a significant learning curve to become expert at developing solder joint tests with low rates both of false calls (incorrect rejections) and of missed calls (incorrect acceptances).

## Implementation of Automated Process Test Systems

Successful implementation of automated process test systems into printed circuit assembly production lines requires a significant investment in training, process analysis and system integration. The implementation can be a lengthy process that requires concerted effort by engineers or skilled technicians. Listed here are highlights of what several manufacturers have learned are key aspects of successfully implementation of automated test systems such as X-radiographing testing.

1. Assess requirements carefully. Start by carefully assessing the requirements for automated process test in the particular production environment into which the system will be integrated. Determine exactly what kind of discontinuities are most important for the test system to detect, what measurements will most help with process improvement and what benefits will generate the quickest financial return on investment.<sup>15</sup> This assessment must consider the test and measurement

capability that already has been implemented as well as new requirements arising from future printed circuit assembly designs.

2. Select a small number of automated process test systems to evaluate thoroughly and compare against the system requirements. The evaluation should include a benchmark using printed circuit assemblies from production to determine the system's capabilities to accurately detect the important discontinuity types within the required false reject rate, repeatedly making the required measurements and not exceeding the required test time. Elements of cost of ownership should be well understood, including test development time, maintenance skills and cost, expected system downtime and supplier maintenance services and prices.
3. Consider and plan carefully for interfaces to other factory systems. These systems include board handling equipment, barcode reading systems, computer aided design systems for automatic download of board layout and component package information and quality data management systems for statistical process control and historical quality tracking.
4. Start with a focus on statistical process control measurements instead of discontinuity detection. Until the process variation is reduced, most manufacturers will encounter a rate higher than desired — either a false rejection rate or a false acceptance rate. Allowing one or the other rate to be too high while focusing on reducing the process variation first will avoid time consuming, unproductive tweaking of acceptance thresholds. Reducing process variation requires correlating measurements to the process parameters causing the variation and discontinuities and then properly adjusting these process parameters.<sup>16</sup>
5. With an understanding of the selected system's capability, carefully define the defects that must be detected for product quality and reliability. Many of the visual testing criteria used in the past are not appropriate for automated test systems because the system takes objective and different measurements.
6. Do not underestimate the initial resource investment required to obtain optimum benefit from an automated process test system. The implementation plan should include dedicated technical support for the first six months of operation and test development. Developing a thorough understanding of the measurement



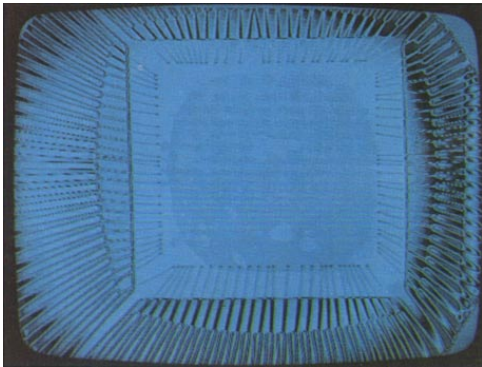
results and correlating the data with process parameters is key to successful use of the system. Implementation should also address the fact that production personnel will have to be convinced of the accuracy of the system's test results before full benefit can be obtained from the system.

## Image Processing for Qualitative Assessment of Electronics

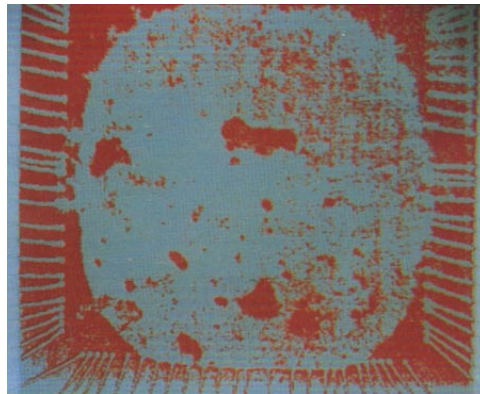
Radioscopic systems incorporating image processing software and images may be enhanced by color coding of density data, displaying the test object with colors

**FIGURE 7.** Contrast enhancement in microfocus radioscopic images of printed circuit board: (a) automatic contrast enhancement revealing bonding pattern and voids in quasi pack; (b) manual contrast enhancement of quasi pack; (c) measurements line between two voids on quad flat pack; (d) gray range highlighted in red; (e) colors selected by trackball to enhance contrast; (f) contour enhancement of density differences.

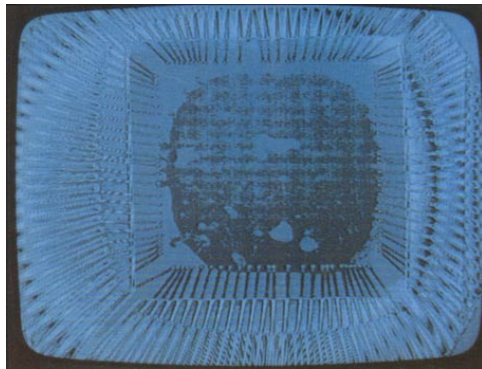
(a)



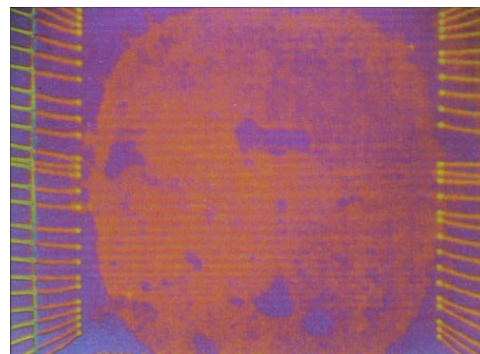
(d)



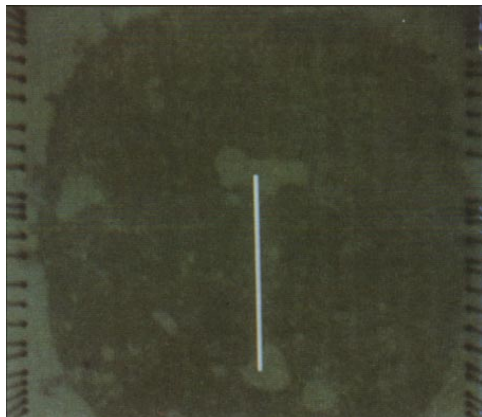
(b)



(e)



(c)



(f)

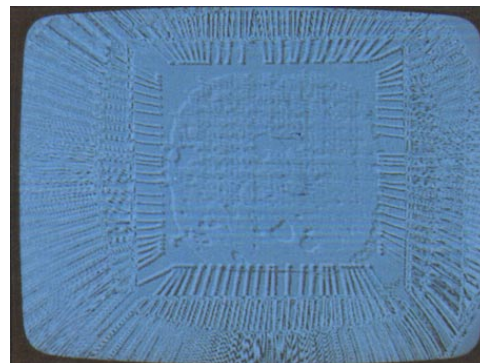
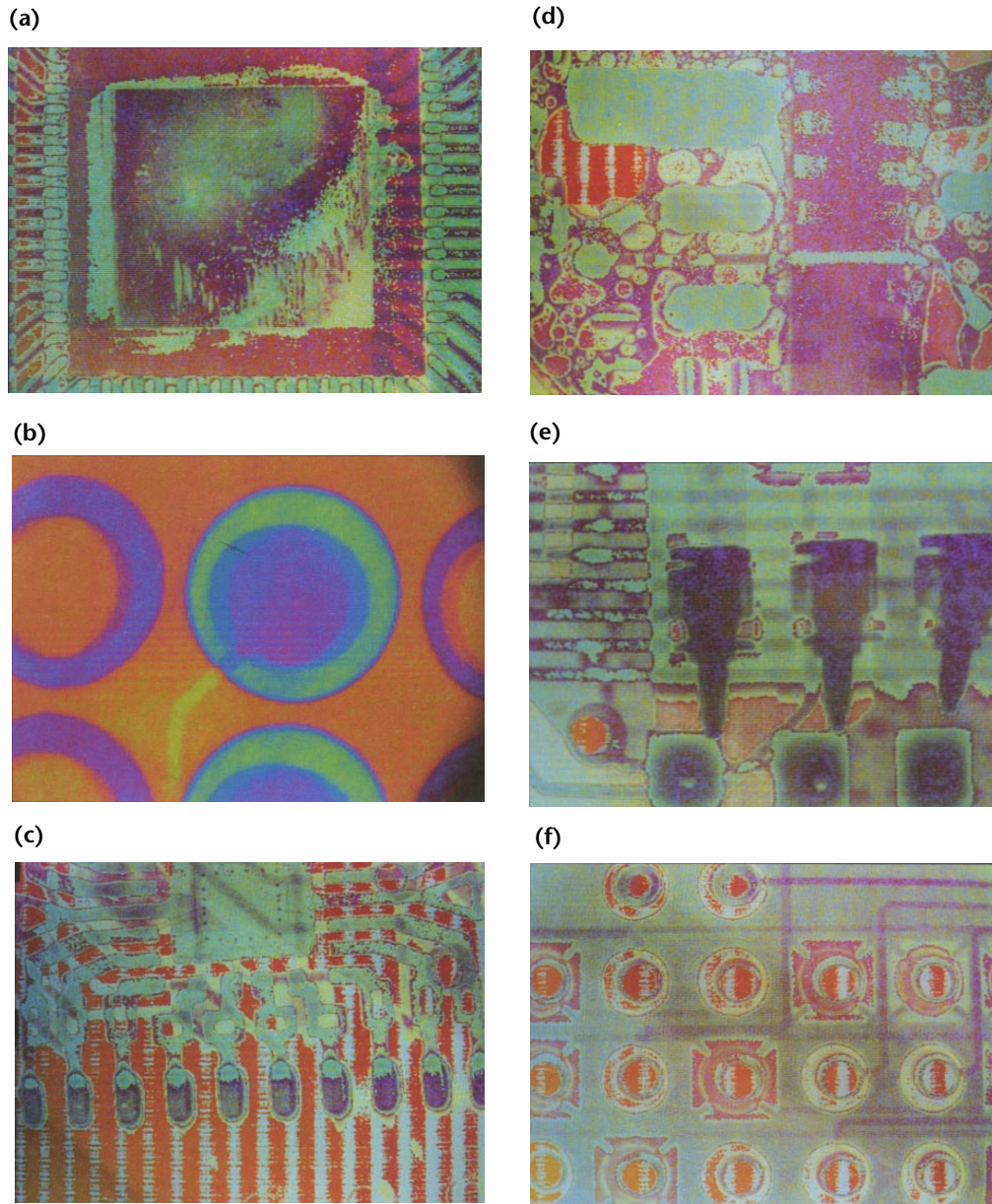


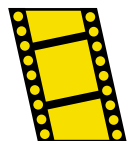
**FIGURE 8.** Color enhancement of images on computer screen: (a) poor bonding on surface mounted component; (b) colorized highlight of misregistered areas of printed circuit board; (c) solder voids and registration placement on surface mounted component; (d) heat delamination, registration and placement of surface mounted component; (e) connections, component placement, registration accuracy and solder voids in surface mounted printed circuit board; (f) accurate registration of printed circuit board.



assigned according to thresholds selected by the user. Figure 7 shows six images of the same printed circuit to illustrate several options for contrast enhancement.<sup>17</sup> Image enhancement can also be used to detect anomalies that occur during assembly (Fig. 8).<sup>17</sup> Color versions of the images in Figs. 7 and 8 may be seen in a journal article<sup>17</sup> or in the CD-ROM version of this book.

The application of radiographic testing to electronics testing is documented in the technical literature.<sup>15-21</sup>

**MOVIE.**  
Inspection  
of printed  
circuit  
boards.





## PART 3. Radiographic Testing of Consumer Goods

Demand for pharmaceutical and food safety has prompted industry to look beyond electromagnetic metal detectors to other nondestructive means of detecting contaminants in consumer product. Conventional radiography has been used in industry since the first half of the twentieth century. In the 1990s, radioscopy has also been used, especially in the electronics industry, where a few manufacturers are offering fully computerized systems.

Radioscopic testing has been primarily with image intensifiers and charge coupled device cameras. Images are displayed on a closed circuit television monitor; often an image processor with frame averaging removes noise and uses additional image enhancement features. This operation has generally been manual: the operator views the images and makes an accept/reject decision. In systems of this type the component or product being inspected is usually stopped in order for the image processing to be effective. In certain food inspection applications a conveyor is used at a continuous speed where the product flow is slow enough to give the operator time to view the displayed image.

Since 1990 X-ray sensitive linear arrays have seen increasing applications for testing and screening of commercial and consumer products. The advent of the linear diode array (LDA) and very sophisticated image analysis software products permit tests at production line flow capacities. Systems are available with enough resolution to detect wire down to 0.28 mm (0.011 in.) diameter with operating speeds greater than  $1.5 \text{ m}\cdot\text{s}^{-1}$  ( $300 \text{ ft}\cdot\text{min}^{-1}$ ).

These systems use a low energy constant potential X-ray source, linear array detector, computer, conveyor and a radiation safe enclosure. The X-ray energy levels vary from 50 to 140 kV peak. The image processing software provides a system less dependent on operators' qualitative assessments and capable of detecting a wide variety of contaminants. In addition these systems may be used for checking tamper evident seals, fill level, missing product, improper packaging and more. Product size generally ranges from small processed cartons and bottles to actual full cases. The detectors are available in almost any size and many

vendors offer standard enclosures that will accommodate many different products. Washdown enclosures are used for processed meat, poultry and dairy products.

Radioscopy and radiation density measurement together are applicable to a wide variety of quality control applications for many types of consumer goods (Table 3).

### Linear Arrays

The commercial use of linear arrays has slowly emerged in industrial and consumer food and pharmaceutical applications. These systems are available in various conveyor widths, X-ray energy levels and speeds in excess of  $1.5 \text{ m}\cdot\text{s}^{-1}$  ( $300 \text{ ft}\cdot\text{min}^{-1}$ ) are attainable. Resolution and sensitivity is based on the selection of the array's pixel size, ranging from 0.225 mm (0.01 in.) up to 2.5 mm (0.1 in.) with little limitation in the array's length, especially in the larger detector size.

A typical linear array based X-ray system consists of a variable energy X-ray source with collimator, detector module with image processor, personal computer, power supply, conveyor to transport the items to be inspected and an image display monitor. Software ranges from that required to produce an image to

TABLE 3. Applications of radiographic testing to online inspection of consumer products.

Category	Problem
Foreign objects	stones metals plastics bone fragments glass
Anomalous products	deformed products clod formations size errors water logged products defrosted frozen products
Missing items	missing constituents missing packages product missing from carton bag or box missing from case

advanced detection programs to fully automate the test process. The components are usually housed in a shielded cabinet or in some cases enclosures are manufactured that incorporate an existing production type conveyor used in the firms manufacturing process.

The operation is based on an array of light sensitive silicon photo diodes coated with a scintillator along with the signal processing electronics. The detectors provide a standard digital data output to a frame storage card and personal computer. Energy levels of the X-ray source are typically in the 20 to 160 kV peak with current values from 0.20 to 20 mA, depending on the pixel pitch of the array and the speed of the conveyor.

Resolution is determined by the pixel pitch of the detector but processing speed is also important in selecting the proper detector. As an example, a 2.5 mm (0.1 in.) pixel detector has a maximum scanning speed of  $1.1 \text{ m}\cdot\text{s}^{-1}$  (210 ft·min<sup>-1</sup>) and a 0.8 mm (0.03 in.) pixel detector has a maximum speed of only  $0.3 \text{ m}\cdot\text{s}^{-1}$  (57 ft·min<sup>-1</sup>). Currently detectors are available with a pixel pitch of 0.225 mm ( $8.9 \times 10^{-3}$  in.), 0.4 mm (0.016 in.), 0.8 mm (0.03 in.), 1.5 mm (0.06 in.) and 2.5 mm (0.10 in.). The standard detector length varies between manufactures with the higher resolution detectors (lower pixel pitch) generally not exceeding 0.40 m (16 in.) in length.

## Applications

Radiography is widely used for the study of biological specimens. The instrumentation and techniques are familiar from medical applications. Medical radiology and industrial radiography were closely allied technologies in the middle of the twentieth century but drifted apart, in part because industrial test objects required ionizing radiation with greater penetrating power than do thin biological tissues. Each field developed its own hardware, technical literature and procedures.

### Food

Computerized systems have been manufactured to inspect various consumer food products, including candy, tobacco, fresh baked goods, cheese, butter, canned meats, snack foods and numerous other packaged or cased products.<sup>22</sup> The layers of an onion are clearly visible in Fig. 9a.<sup>23</sup>

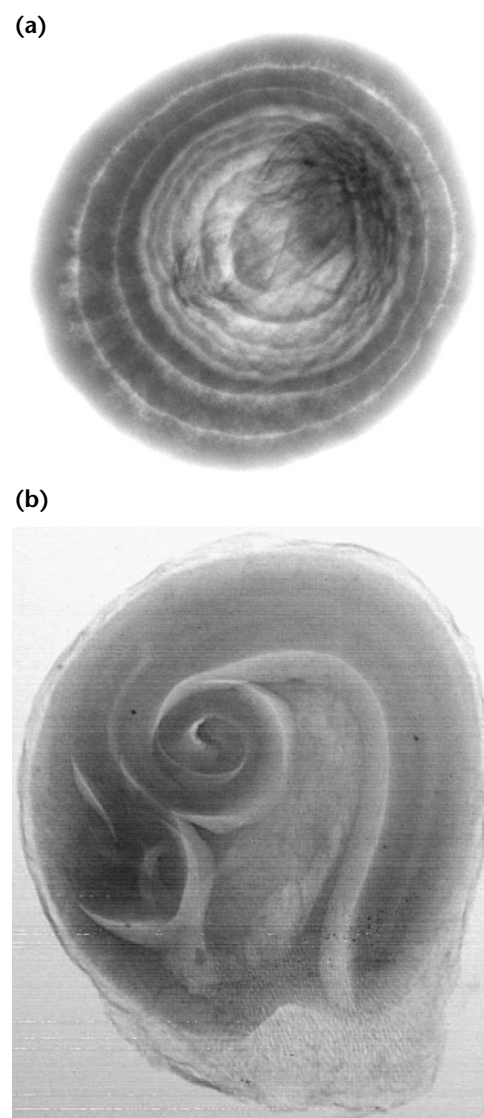
Online systems incorporate object recognition software for swift, automated accept/reject decision making.

Representative of such systems is one reported that can test marmalade jars for uniform fill and for foreign objects, such as glass splinters. The system can also count the slices of pepperoni on frozen pizza. As soon as a grocery item passes the X-ray sensor, the program can interpret the resulting image and cause an anomalous item to be ejected from the assembly line.<sup>24</sup>

### Seed

As with all sorts of biological specimens, radiographic testing can be applied to the study of seeds.<sup>25,26</sup> The image can be examined to determine the following.

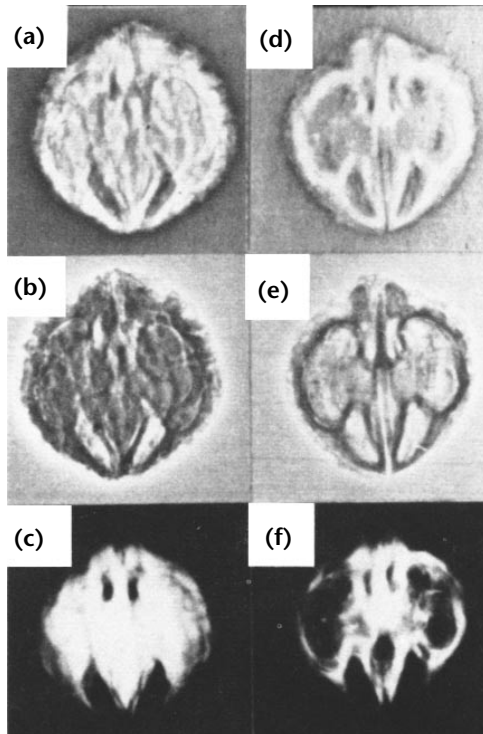
**FIGURE 9.** Radiographic images of vegetables: (a) radioscopic image of onion; (b) microfocus radioscopic image of tomato seed.



1. Radiography can show that the embryo has germinated to produce a seedling (see Fig. 9b).
2. Radiography can show whether a seed or shell is full or empty (Fig. 10). Some seeds are empty because of genetic deficiency.
3. Full seeds may not germinate because of rough handling or other trauma that causes cracking in the seed coat. Such cracking can be seen with radiography.
4. Stereo radiography makes it possible to view internal features of seed morphology. A stereo image can be produced by taking one image, then moving either the image plane or the test object and then taking the other image. Depth is seen when the two images are viewed simultaneously with a stereoscope or prism.
5. Tomography can be used to provide images of selected planes in the seed.
6. A radiopaque dye can be added to selectively enhance the visibility of structures according to their ability to absorb the dye's vehicle.

Figure 10 shows radiographs of walnut seeds.

**FIGURE 10.** Black walnut seeds: (a) nut 1, dry photostatic negative radiograph; (b) nut 1, dry photostatic positive radiograph; (c) nut 1, conventional film radiograph, negative; (d) nut 2, dry photostatic negative radiograph; (e) nut 2, dry photostatic positive radiograph; (f) nut 2, conventional film radiograph, negative.<sup>26</sup>



## Cellulose

Wood products can be radiographically tested for discontinuities in various shapes.<sup>27</sup> as well as for consistent thickness as paper.<sup>14</sup>

Cigarettes are inspected for uniformity of fill and packing by online density gages as described above.<sup>14</sup> Radioscopic techniques have been applied in combustion studies.<sup>28</sup>

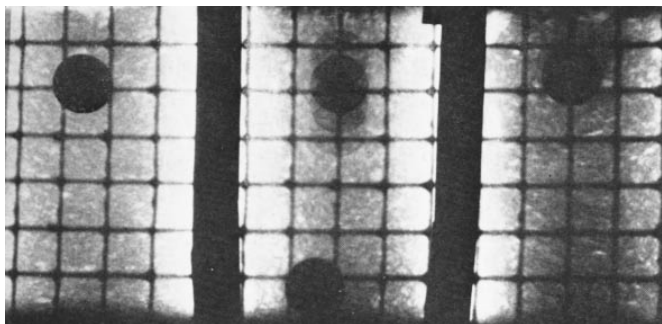
## Pharmaceuticals

Pharmaceutical applications include packaged catheter kits, saline solution dispensers, metal film drug packaging. Systems are used for inspecting engine components, aluminum castings, electronic assemblies, computers, consumer electronic packaging, wire harness assemblies and numerous additional packaged products.

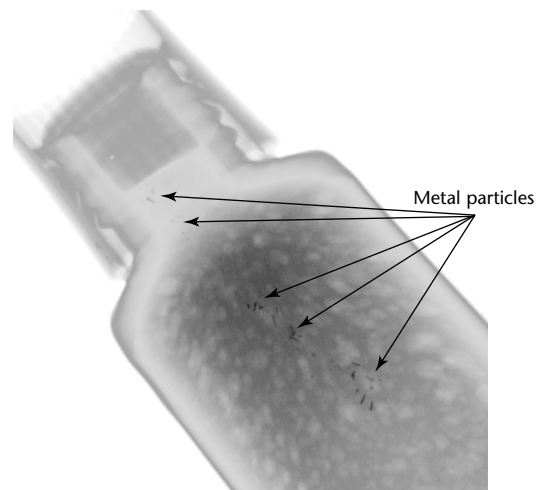
Radiographic testing can provide various sorts of information useful to quality control of pharmaceutical and hygiene products. Figure 11a shows radiographic images used to measure the

**FIGURE 11.** Radiographic testing of toothpaste: (a) five exposures show ball bearing sinks to bottom in center sample;<sup>23</sup> (b) radioscopic image reveals metal particles in toothpaste tube.

(a)



(b)





density of toothpaste by tracking a metal ball falling through the paste.<sup>23</sup> Figure 11b shows metal shavings discovered inside a tube of toothpaste.

### Packaging

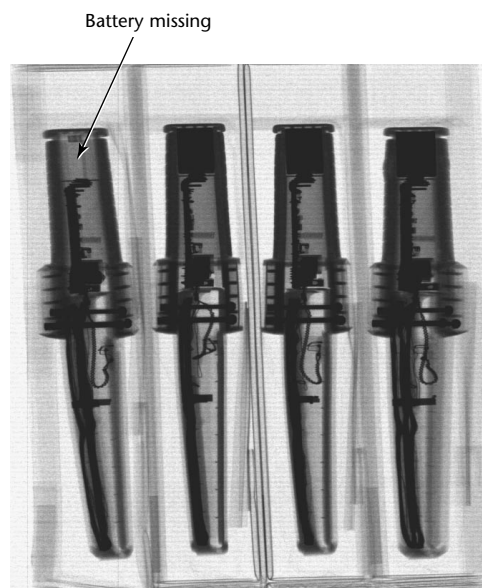
The increased usage of decorative metal film packaging in consumer food manufacturing has mandated an increased use of X-ray testing because metal detectors will no longer function because of the metal film. Linear arrays are capable of detecting metal contaminants down to 0.5 mm (0.02 in.) as well as identifying plastic, stones, rubber and related possible contaminants.

In addition, linear X-ray testing makes it possible to inspect products by the case rather than by the individual box, something metal detectors usually cannot do. Another advantage of the automatic computer processing is that several tests may be conducted simultaneously. Although the original intent may have been to detect a metal contaminant, the computer program can also look for numerous packaging anomalies, missing product, duplicate product, anomalous package integrity and even product count verification.

Figure 12 shows how radioscopy can reveal that a battery is missing in a handheld device. In essence each image may be subject to highly advanced processing, if required, while obviating an operator.

The image in Fig. 13 shows the filaments in a light bulb.

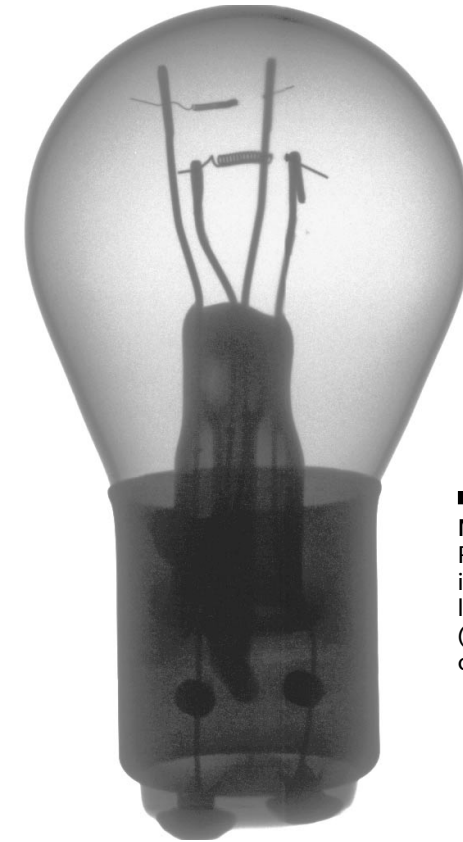
**FIGURE 12.** Radioscopic image of metal detector wands reveals assembly error.



### Sports Equipment

Radiography can be used to test sports equipment for departures from specification, because of either tampering or manufacturing discontinuities. Radiography can detect corking or other illegal cores in baseball bats, for example. Figure 14 shows images of golf balls in a film radiograph made circa 1930.<sup>23</sup>

**FIGURE 13.** Radioscopic image of light bulb reveals connections.



**MOVIE.**  
Radiographic inspection of light bulb.  
(Press escape to close.)

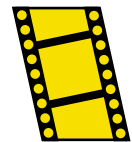
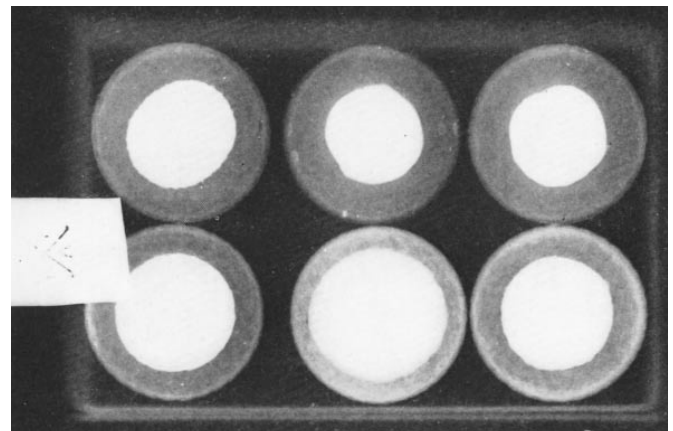


**FIGURE 14.** Radiograph of golf balls.<sup>23</sup>



## PART 4. Radiographic Testing in Security Systems

### X-Ray Screening for Airport Security

X-ray screening systems became widely used in the early 1970s following incidents of hijacking. The airline

FIGURE 15. Radioscopic scanner typically used for airport security.



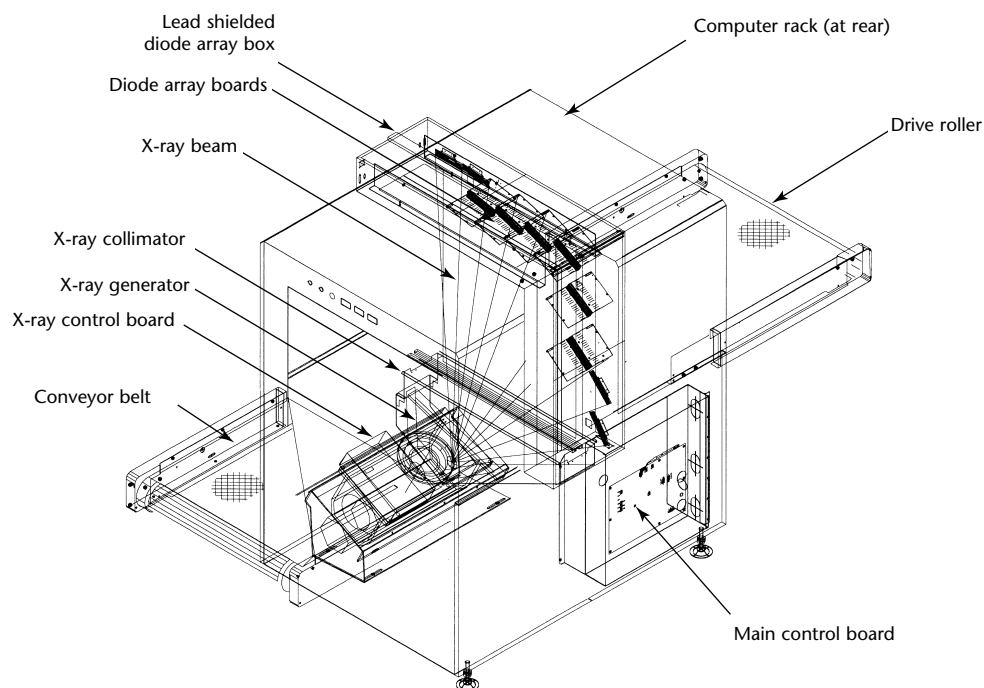
industry was required to conduct X-ray screening of passenger carryon baggage.<sup>29</sup>

Twentieth century X-ray screening systems were radiosopes, either fluoroscopes with cathode ray tube outputs or closed circuit television screens with video compatible outputs.<sup>30,31</sup>

By the year 2000, virtually all X-ray systems had become based on linear detector arrays. Thousands are in use throughout the world. In the twenty-first century, airport baggage X-ray scanners provide high resolution digital imaging, with sophisticated image analysis and enhancement software that can detect and identify explosive materials, weapons and other contraband seconds after the luggage enters the X-ray machine.

A variety of techniques offer possibilities for imaging and visualization for aircraft security. Planar transmission imaging techniques using X-rays and nuclear radiation have been investigated. Means for distinguishing materials by using multiple radiation sources are available, along with techniques for simulating materials with mixtures of other materials. Tomographic

FIGURE 16. Schematic diagram of conveyor belt radioscopic scanner.



reconstruction techniques have been derived and estimates have been made of their performance. X-ray diffraction techniques offer an alternative to transmission imaging.<sup>32</sup>

The enclosure of a representative installation (Figs. 15 and 16) contains a conveyor and a 140 to 160 kV peak, 0.2 to 2.0 mA X-ray generator. A folded linear

diode array is used to ensure 100 percent screening of anything in the tunnel and a computer with image analysis and enhancement software with image display monitor enables the operator to observe the flow of luggage. The high dynamic range of the systems provides for penetration in steel from 25 mm (1 in.) to over 400 mm (16 in.) in the larger cargo systems. Linear array technology provides for low scatter, high dynamic range and excellent quantum efficiency and low dose, typically 1  $\mu$ Sv (0.1 mR) per test. Systems are available from familiar luggage screening systems (Fig. 17) to those capable of inspecting a fully loaded sea freight container or a semi tractor trailer (Fig. 18). The larger systems use high energy X-ray generators from 320 kV peak to 9 MeV.<sup>33</sup>

[The use of Compton backscatter imaging for mine detection and baggage scanning is discussed elsewhere in this volume.](#)

Small wand shaped metal detectors and low intensity radiation detectors of other designs are available for frisking and other low intensity searches of individuals.<sup>34</sup>

### Threat Recognition Software

Software can identify and separate objects with specific material characteristics, including explosives, narcotics, gold, other metals, currency and even agricultural products.

An operator training program is designed to daily test the operator with known X-ray images of contraband. Threat assessment software provides real time operator training and performance monitoring. The threat projection software inserts numerous types of threat objects at predefined settings and intervals into otherwise *clean* bags, allowing supervisors to monitor the operator's recognition response. This training may also be networked to several

**FIGURE 17.** Radioscopic image of suitcase contents: (a) detailed image; (b) image thresholded to view items of greatest density.

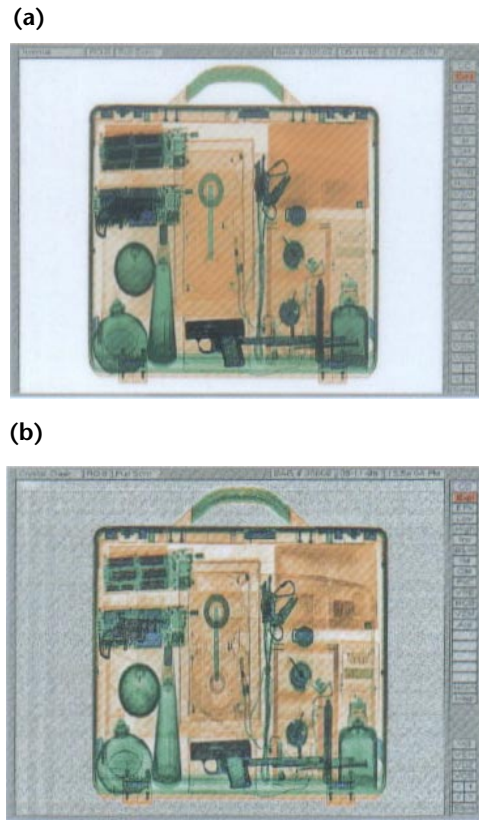
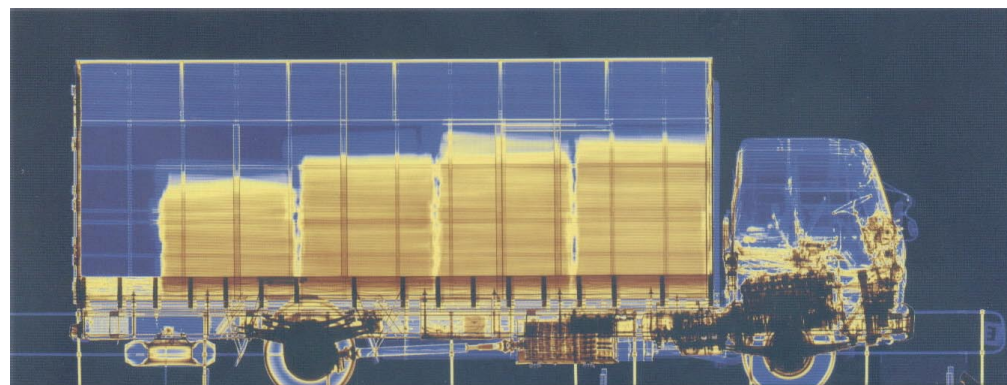
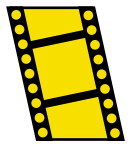


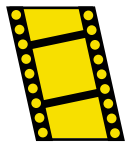
**FIGURE 18.** Radioscopic security inspection of vehicle.



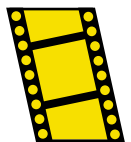
**MOVIE.**  
Cargo  
scanning.



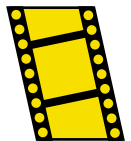
**MOVIE.**  
Image  
acquisition  
and  
evaluation.



**MOVIE.**  
Images at  
3 MV and  
6 MV.



**MOVIE.**  
Contraband  
in water  
tank.



machines for testing and downloading of data.

Images may be saved or transmitted to distant security stations for further analysis without allowing the suspect bag to exit the system. These systems may also be networked so that an entire airport terminal could have all X-ray units also sending images to a central location for observation, backup or additional analysis of suspect bags.

## Radiological Detection and Identification of Material

Through Compton scatter and photoelectric absorption, dual energy X-ray technology makes it possible to separate organic from inorganic materials. The photoelectric effect is very energy dependent; Compton scattering is only mildly energy dependent. The ratio of photoelectric effect to Compton scattering depends on atomic number ( $Z$  number). Using two X-ray energies permits the determination of this ratio and so provides the average (or mean) effective  $Z$  number along the line of sight. Compton scattering is effective in imaging of water, hydrocarbons and other organic materials — generally composed of hydrogen, carbon, oxygen and nitrogen and typically displayed as orange. Metals, steel and copper are displayed as blue. Aluminum is on the boundary of the metals, typically identified as a material of mixed high and low atomic number and displayed as green. Explosives and drugs tend to be low atomic number whereas weapons have a high atomic number. The effective  $Z$  number aids in identification of these materials by the system operator.

A prototype system used at United States southern point of entries for cargo truck and railroad freight car inspections has prompted development of other vehicle inspection systems that are cost effective, transportable, fast and reliable and that use low level radiation exposures. A high resolution 13 mm (0.5 in.) system that scans an entire cargo truck, including the van, can conduct normal as well as oblique scans in 90 s. A system that scans railroad cars at  $8 \text{ km}\cdot\text{h}^{-1}$  ( $5 \text{ mi}\cdot\text{h}^{-1}$ ) has been under development. It has the option of using a cobalt-60 source for inspecting heavier cargoes. In addition, a system has been planned that will be mounted on a small vehicle with an extendable detector tower and deployable gamma ray source to scan a suspect vehicle, either a passenger car or cargo truck, for contraband.<sup>33</sup>

## Pulsed Fast Neutron Analysis

Several techniques have been advanced for detection of explosive devices by using interactions of specific nuclei with gamma rays or fast neutrons. Techniques using these interactions identify the device by measuring the densities or relative concentrations of the elemental constituents of explosives.<sup>35,36</sup>

Pulsed fast neutron analysis<sup>37</sup> has been advanced as a technology that can interrogate large (truck sized) containers and conveyances for user specified chemicals or materials such as drugs, explosives and hazardous materials. The test object is subjected to short pulses of fast neutrons that pass through container walls and produce gamma rays as they strike the cargo. Gamma sensors measure the radiation, which permits identification of elements (carbon, oxygen and nitrogen) present in small, specific areas of the test object. The system then assembles the small images into a composite image that shows the contents of the container.

Studies have reported that the technique can work. As of the turn of the century, however, the cost of the technology has limited its implementation.<sup>38</sup>



## PART 5. Infrastructure Applications of Radiographic Testing

In their broadest sense, infrastructure installations include transportation systems such as railroads, tunnels, streets, highways and bridges; civil engineering structures such as dams, walkways, arenas and other public buildings; utilities systems for the conveyance of liquid and gas materials, such as petroleum, natural gas, water and sewage; energy systems such as towers, high tension lines, underground cables and piping. Most infrastructures either, like architecture, are hyperengineered to avoid failure or, like structural steel and electric power, have evolved specialized and codified technologies apart from other parts of infrastructure. As a result, discussions of infrastructure nondestructive testing typically concentrate on highways and bridges.

### Soil

Radiation techniques have been applied to the testing of soil.<sup>39,40</sup> These techniques are valuable for comparative research on aggregates such as concrete and for imaging of objects irradiated *in situ* in soil.

### Concrete

Because concrete is an aggregate that severely scatters acoustic waves, the applicability of nonacoustic test methods, such as radiographic and microwave testing, has long been of interest.<sup>23,41-43</sup> The ability of gamma rays to provide images of steel rebars inside concrete (Fig. 19) has been demonstrated<sup>44-47</sup> although access problems prevent widespread implementation of the technique in highway maintenance programs. Obstacles include (1) the desirability of testing from two sides, often difficult, (2) safety considerations associated with high energy radiation in public places and (3) expense.

Research by the United States Department of Transportation has included the evaluation of the following techniques for inspecting concrete, steel and asphalt: (1) X-ray computed tomography for determination of crack propagation, void percentage and distribution in concrete;<sup>48</sup> (2) validation

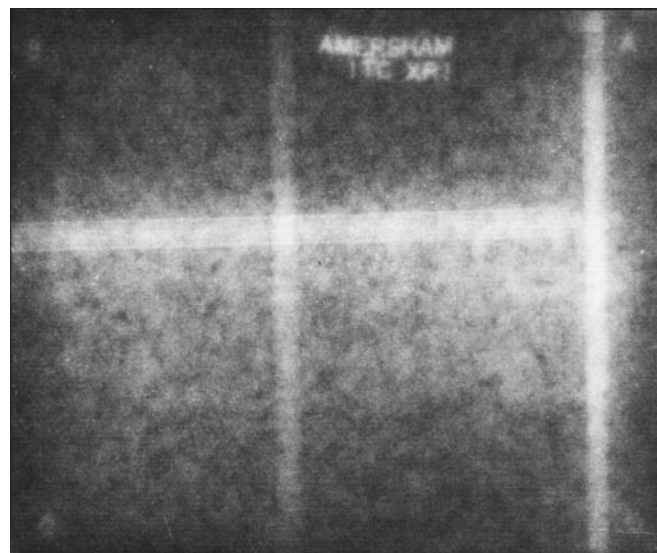
of X-ray radiography techniques for inspection of bridge cables; (3) development of codes, standards and specifications for radiography and tomography of concrete; (4) measuring cement hydration using a neutron scattering technique;<sup>49</sup> and (5) determination of chloride concentration and depth profiles in concrete using prompt gamma neutron activation analysis.<sup>50-52</sup>

### Chloride Contamination

Chloride contamination is a major contributor to road deterioration. A portable prompt gamma neutron activation spectroscopy system has been developed to analyze the elemental composition (calcium, silicon, aluminum and others) of reinforced concrete and to measure chloride contamination. The portable system consists of a high purity germanium gamma detector with a 70 percent relative efficiency, a californium-252 neutron source and moderator subsystem and a portable multichannel analyzer system integrated with a laptop computer.

Two types of activation experiments were performed to evaluate the device:

FIGURE 19. Radiograph of 13 mm (0.5 in.) reinforcement bars and 16 mm (0.6 in.) steel conduit in 0.46 m (18 in.) thick concrete slab.<sup>44</sup>





(1) a detector calibration and (2) an evaluation of the actual performance of the complete system with the californium-252 source using full scale test slabs containing known amounts of chloride. Both techniques indicate that it is feasible to use this technique to measure the chloride content of reinforced concrete in the field. The chloride level for the corrosion threshold can be measured with a precision of 10 percent for a counting time of roughly 6 min. The prompt gamma neutron activation technique is competitive with the conventional destructive method.<sup>51</sup>

## Bridges

The approach of design engineers for bridges — as for elevators, skyscrapers and amusement park rides — is to *hyperengineer*, that is, to specify secondary supports and materials stronger than required by the worst scenarios of the civil architect's imagination so that material failures remain noncritical. However, despite hyperengineering, the passage of decades has made bridges a matter of urgent and ongoing concern. Radiographic testing plays several critical roles in the inspection of thousands of bridges in the United States.<sup>53</sup>

1. Structural steel needs to be inspected during forging.
2. Welds during fabrication need to be inspected using applicable codes standards.
3. In maintenance testing during the lifetime of the bridge, radiographic testing may be used selectively to analyze corrosion rates and monitor other material conditions. In particular, radiographic testing has been used to test welds, cables and cable caps.<sup>54</sup> Special applications may arise for particular bridges, such as a drainage pump inspected with a linear accelerator.<sup>55</sup>
4. More generally, laboratory studies contribute to an understanding of material behavior.

The greatest obstacle for radiographic testing occurs when the structural members requiring attention are buried under concrete (Fig. 20). There has been an economic incentive to develop other methods — such as visual testing, microwave testing or acoustic methods — for maintenance tests after initial fabrication.

## Other Civil Structures

Radiographic testing finds application in the testing of a great variety of civil structures. Any sort of structural steel, for example, may be inspected during fabrication or years later during maintenance.

### Penstocks

In dams, valves control the flow of water in penstocks, large conduits that convey water to hydroelectric generators. Radiographic testing has been used to test penstocks installed in water projects in Colorado and Washington (Fig. 21).<sup>56</sup>

FIGURE 20. Setup for radiographic test of bridge splice.<sup>53</sup>

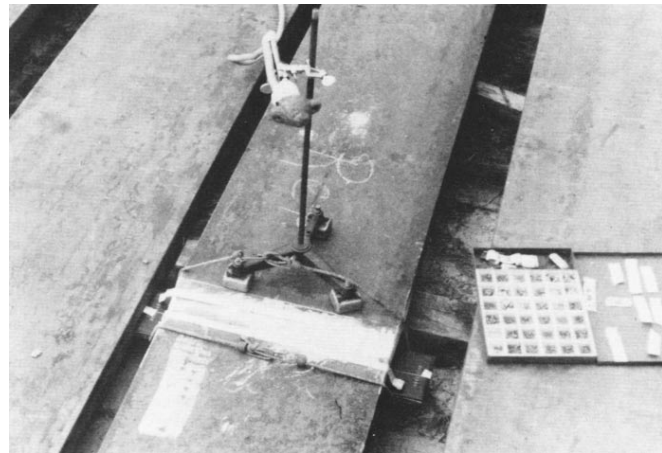


FIGURE 21. Inspector positions X-ray film holder for radiographic test of section of longitudinal seam in penstock.<sup>56</sup>



## Light Poles<sup>57</sup>

Radiographic testing has been used to test light poles for discontinuities that might lead to material failure and expensive or dangerous accidents. In one case in Texas, lamps had been mounted on poles 24 m (80 ft) high (Fig. 22). Each pole was constructed by butt welding together four sections of 6 m (20 ft) each. After one weld failed in service, all welds were inspected.

Ultrasonic testing was unhelpful because waves passed through the welds and reflected from the inside surface of the hollow poles. Many of the welds failed to comply with requirements of AWS D1.1, *Structural Welding Code*.<sup>58</sup> Radiographic testing revealed several discontinuities: porosity, slag, incomplete penetration and lack of penetration.

## Buildings

The nondestructive testing of buildings is a concern of both infrastructure and conservation. The radiographic testing of some historic buildings is discussed below.

**FIGURE 22.** Inspector in aerial personnel lift radiographically tests welded part of lamp post.<sup>57</sup>



## PART 6. Radiographic Testing in Conservation of Historic Buildings and Museum Objects

### Archaeology

Radiographic testing has found a wide variety of applications in the investigation of artifacts for their preservation and for research in the fields of anthropology, archaeology and history.<sup>59-62</sup> Studies have focused on particular materials such as glass,<sup>63</sup> wood<sup>64</sup> and metals<sup>65-67</sup> and on particular techniques such as computed tomography,<sup>68</sup> compton scattering<sup>69</sup> and X-ray fluorescence.<sup>70</sup>

### Bones and Fossils

In anthropology radiographic testing is applied to the examination of funerary remains, particularly mummies.<sup>71-74</sup> This test object is not unlike those in the more familiar applications of medical and forensic investigations.

Radiographic testing has also been used to examine fossils and coral.<sup>75-76</sup>

### Structures

Gamma radiography has been popular for the testing of buildings and outdoor structures because isotopes are portable and do not require electric power.

### Statue of Liberty<sup>77,78</sup>

The Statue of Liberty stands 46 m (151 ft) tall and weighs 254 000 kg (560 000 lb<sub>m</sub>). A special design was necessary to support a statue of this size. Its external envelope of 300 copper plates, joined by 300 000 rivets, is secured by 1500 copper saddles to an armature of 600 vertical iron ribs, each 50 mm (2 in.) thick. This flexible design permits the structure to *breathe*, that is, to expand and contract with temperature and other weather conditions. The monument was renovated in 1986 because years of corrosion and strain had caused 600 saddles to fail (Fig. 23).

Gamma radiography was performed as part of the diagnostic work. A gamma ray projector with a 3.7 TBq (100 Ci) iridium-192 isotope and radiographic film of three speeds were selected for the job. Most exposures were made in 5 min. A tungsten collimator was used to control radiation scatter. Attention was paid to tie rods, rivets, bolts, welds and pylons,

particularly the tie rod assembly at the base, where the statue is anchored to a central pylon. The radiographic testing confirmed discontinuity severity and locations needing repair.

### Buildings

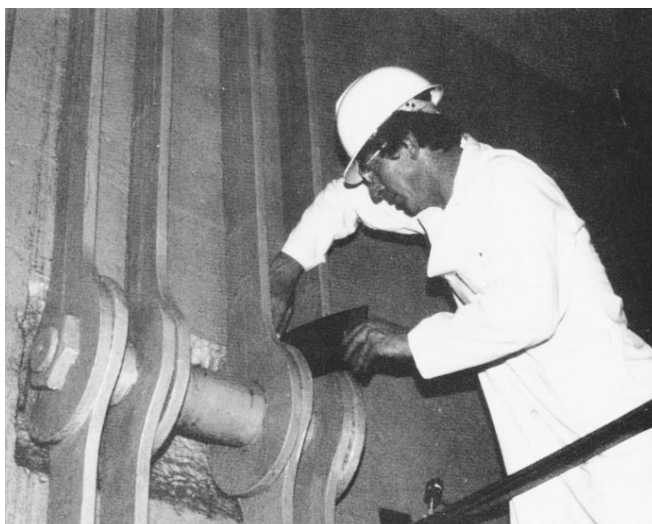
Radiographic testing has been used to inspect ancient buildings, looking

FIGURE 23. Statue of Liberty: (a) seen from above, statue enclosed in scaffolding, May 1984; (b) radiographer prepares to expose film to 3.7 TBq (100 Ci) iridium-192 source.<sup>92</sup>

(a)



(b)





diagnostically for hidden structures and discontinuities to guide renovation, conservation and restoration.<sup>79</sup> One example is the gamma radiography performed on the Acropolis, in Athens, Greece.<sup>80</sup>

**Capitol.** The Capitol building in Washington, District of Columbia, needed renovation in 1983. Before drilling holes in two walls the architects needed to know where utility lines and ventilation ducts and flues were located. The walls, like much of the building, were rebuilt after being destroyed in the War of 1812; lines for electricity, water and telephone were installed years later and no drawings remained to show where.

The walls were X-radiographed with a small, mobile linear accelerator. The first wall was 0.6 m (24 in.) thick and the X-ray head was positioned 1 m (39 in.) from the wall for a source-to-film distance of 1.6 m (63 in.). The linear accelerator was operated for 1.5 h at 50 percent power: 0.5 Gy·min<sup>-1</sup> at 1 m (50 rad·min<sup>-1</sup> at 39 in.); total dose to the film was 18 mGy (1.8 rad). To shorten the exposure time, the equipment was operated at 100 percent power for the second wall, 0.46 m (18 in.) thick. The radiographic testing showed that utility lines could be installed in the walls.<sup>81</sup>

**Roofs and Hidden Apertures.** In the field of building conservation, radiographic testing shares at least two applications with another method, infrared thermography: one is looking for hidden apertures in walls, as in the case of the Capitol described above; another is surveying rooftops for moisture ingress and retention. A neutron moisture gage is feasible because of the opacity of water molecules to neutron radiation.<sup>82</sup>

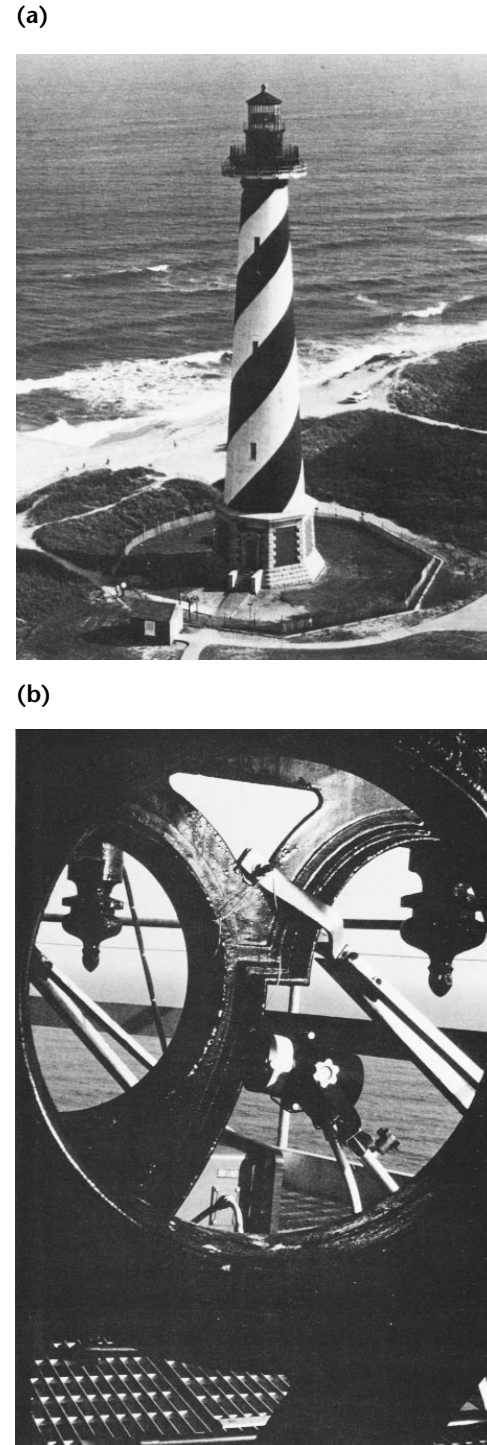
**Lighthouse.** The Cape Hatteras Lighthouse, Cape Hatteras, North Carolina, was built around 1867 and suffered damage in an 1886 earthquake. In 1976 a painting contractor noticed cracks in the brackets supporting the cast iron gallery. In 1979 a platform was constructed beneath the gallery for testing and repairs. In radiographic testing, the inspector used a 9.37 TBq (252 Ci) cobalt-60 source and a 1.8 m (6 ft) source-to-film distance to obtain images through 0.6 m (2 ft) of masonry and 50 mm (2 in.) of iron (see Fig. 24). The film radiographs revealed severe cracks in seven brackets behind the masonry. Subsequent repairs compensated for these discontinuities and made the gallery safe to walk on.<sup>83,84</sup>

### Cosmic Radiography

Cosmic radiography is distinguished from other types of radiography by its radiation source. Cosmic rays are emitted by stars in

outer space and can be recorded with detector arrays on Earth. Cosmic rays comprise electrons of about 700 pC·kg<sup>-1</sup>·h<sup>-1</sup> (2.7 μR·h<sup>-1</sup>) and photons of about 200 pC·kg<sup>-1</sup>·h<sup>-1</sup> (0.8 μR·h<sup>-1</sup>).

**FIGURE 24.** Cape Hatteras Lighthouse: (a) aerial view; (b) portion of ornamental support system, with isotope head visible at bottom of structure's circular aperture.<sup>83</sup>



Intensities on Earth vary with altitude, latitude and sun spot activity. Because cosmic radiation is emitted from all directions in the Universe, the Earth itself serves as a radiation shield, partly limiting the source to the sky overhead. The atmosphere also helps to reduce radiation from directions other than directly overhead.

**Limitations.** Limitations include the following:

1. The inspectors cannot control the wavelength and intensity of the rays. Material data are quantified only approximately. Cosmic radiography could not be used to gage the thickness of piping, for example.
2. The inspectors cannot select source location and so cannot control the angle of incidence of rays. Consequently, the radiation is difficult to collimate and scatter is difficult to control. The resulting images lack resolution; they are fuzzy because radiation comes from different parts of the sky.

These considerations limit cosmic radiography to preliminary, qualitative assessment of massive objects.

**Advantages.** The advantages of cosmic rays are (1) their extremely great penetrating power, (2) low cost, (3) greater safety than with other forms of ionizing radiation and (4) availability in remote locations.

**Applications.** The main gate of a temple in Nagoya, Japan, was examined to investigate the practicality of applying cosmic rays to structural analysis of large objects (Fig. 25). Cosmic ray intensity data were collected at a number of positions around and under the gate with a thallium activated sodium iodide scintillation counter. A threshold of 3 MeV was used to distinguish cosmic ray spectra from terrestrial radiation from elements such as uranium and potassium in the environment. The resulting cosmic radiographic image corresponded to the known structure.<sup>85</sup>

Cosmic radiography was used in 1968 to look for hidden rooms in the Pyramid of Khafre, the second largest pyramid at Giza, Egypt. Cosmic ray particles reaching the sensor were counted from different directions and made it possible to estimate the amount of material throughout the pyramid. No hidden rooms were found.<sup>86,87</sup>

Cosmic radiography could be used for qualitative surveys of dams, some bridges and other massive structures.<sup>87</sup>

## Historic Ships

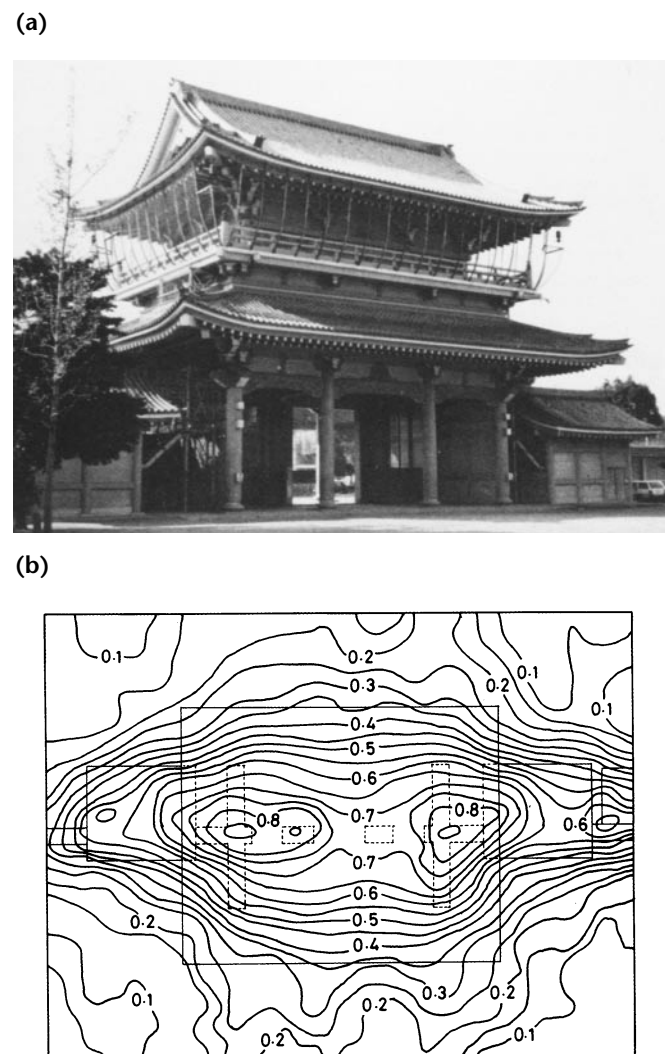
Historic ships present a particular challenge to conservationists because of

their age and because exposure to sea water and weather is destructive to metal parts. The following case histories illustrate the benefits of radiographic testing for these vessels.

**Joseph Conrad.** The fully rigged *Joseph Conrad*, moored in Mystic Seaport, Connecticut, was built in 1882 and underwent inspection and repairs in 1978. Gamma radiography with a 1.5 TBq (40 Ci) iridium-192 source was conducted to inspect the riveted hull, which had undergone repairs in 1962. After further repairs in 1978, the hull was replated, radiographically tested and then coated with tar.<sup>88</sup>

**Belle.** Underwater archeology can present special problems. Ships can sink and remain on the ocean floor for decades, even centuries. Wood rots and metal corrodes. The *Belle*, a ship in French

**FIGURE 25.** Higashi Honganji Temple: (a) photograph of temple; (b) planar view of cosmic ray pattern.<sup>85</sup>





explorer La Salle's final expedition, sank in 1886 along the coast of Texas and was discovered in 1995. Conservators have used radiographic testing to examine thousands of corroded objects, to identify them and decide how they can be restored. For a variety of speeds both medical and industrial film was used. Each artifact was radiographed three times to provide images from different angles.<sup>89,90</sup>

**Hunley.** The submarine *H.L. Hunley* served the Confederacy in the American Civil War, sinking the Union warship *Houstatonic* in Charleston Harbor, South Carolina, in 1964. The *Hunley* sank while returning from that mission. Its wreck was discovered in 1995 and salvaged with the help of radiographic testing (Fig. 26). When new, the submarine weighed 6800 kg (15000 lb<sub>m</sub>) and was 12 m (39 ft) long.

The salvaged vessel was full of sediment. A primary goal of the radiographic testing was to measure the width of the submarine's plates and find the seam line to help decide the best point of entry. Confronted with the need to create an image through 1.2 m (46 in.) of sand and silt, the radiographers used 2.5 h exposures with a cobalt-60 source. Digital images were manipulated to make particular features more visible. Using this information, conservators removed several of the hull's plates and excavated the sediment inside the hull carefully, much as an archeologist excavates a site on dry land.

As with the *Belle*, corroded objects that were discovered were then radiographed to identify them and determine how best to restore them. Recovered objects, in addition to human bones, included canteens, buttons, a thimble and a lantern.<sup>91</sup>

## Liberty Bell<sup>78,92,93</sup>

The Liberty Bell in Philadelphia rang to celebrate the United States' independence in 1776. Gamma radiography was performed with film in 1975 to assess the bell's integrity before a planned move from Independence Hall to a different building across the street (Fig. 27). The radiographic testing used took place in two phases: (1) a series of small sections and (2) one large image of the entire bell.

The small radiographs were made with standard 0.36 × 0.43 m (14 × 17 in.) film exposed to a 1.9 TBq (52 Ci) iridium-192 source. Because of thickness variations in the bell, exposure times ranged from 1.75 min at 1.9 TBq (52 Ci) to 17 min at 3.7 TBq (100 Ci).

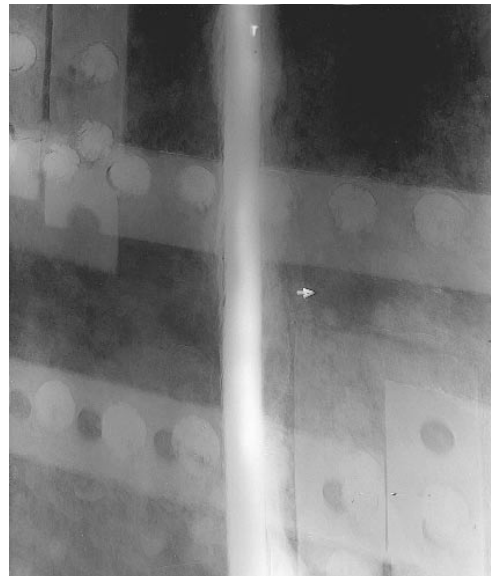
The full size radiograph was made with a vinyl covered package containing

**FIGURE 26.** Radiography of submarine *Hunley*: (a) positioning a radiosopic image plate on hull exterior; (b) computed radiograph of hull's rivets (the vessel was riveted from the inside and sanded to improve its hydrodynamics); (c) setting up exposure of iridium-192.<sup>91</sup>

(a)



(b)



(c)

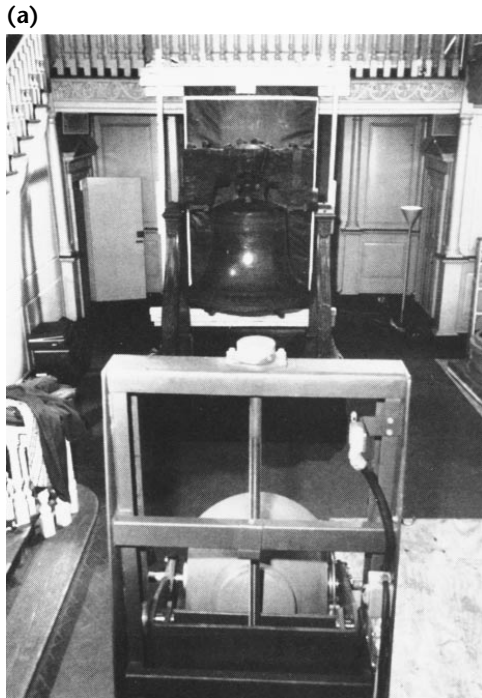


14 sheets of  $1.3 \times 2.1$  m ( $52 \times 84$  in.) film. The sheets were made by slicing 2.1 m (7 ft) sections from rolls of film in a width of 1.3 m (52 in.), the width in which they are manufactured before being cut to normal size. A 25 TBq (670 Ci) gamma ray projector containing cobalt-60 in a 900 kg (2000 lb<sub>m</sub>), 0.6 m (24 in.) diameter lead

ball was positioned at a distance of 15 m (50 ft) from the film.

The bell was radiographically tested with film again in 2001 and the images have been compared with those from 1975 to check for crack propagation and other changes.<sup>94</sup>

**FIGURE 27.** Gamma radiography of Liberty Bell in 1976: (a) setup showing lead ball containing cobalt-60; (b) film image.<sup>92</sup>



## Marble Statues

### Caligula<sup>95</sup>

In the 1980s, the Virginia Museum of Fine Arts, Richmond, acquired a statue of the Roman Emperor Caligula dating from the first century of the Christian Era. A fracture had separated the head from the shoulders of the statue and a conservator in 1970 had reconnected them using a metal pin and glue. Radiography was undertaken to determine the extent of the 1970 conservation efforts and, by examination of the marble grain, to verify that the head was originally part of the rest of the statue. One of only two complete statues of that emperor, the statue is worth more if the head is original. The radiographic tests helped further studies to verify the head's authenticity (Fig. 28).

An iridium-192 source of 3.3 to 37 TBq (90 to 1000 Ci) was placed 1.2 m (48 in.) from the film cassettes taped to the head. It required a series of 4 h exposures to get images through 0.20 m (8 in.) of marble.

### Pietà<sup>96</sup>

At the New York World's Fair, in 1964, the Vatican exhibited Michelangelo Buonarroti's *Pietà*. Before moving the statue to the United States, the Vatican commissioned a radiographer from the United States to document its condition. (Fig. 29a) The technician practiced by radiographing stacks of marble window sills but the Carera marble chosen by Michelangelo proved harder and more absorbing than the samples.

Radiographic work in the Basilica was timed to avoid interference with Lenten services. Film radiographs were made in the day with a portable X-ray machine operating up to 200 kV peak and exposure times ranging from 30 s to 10 min. Additional exposures were made overnight with gamma equipment, using a cobalt-60 source for the thickest parts of the statue.

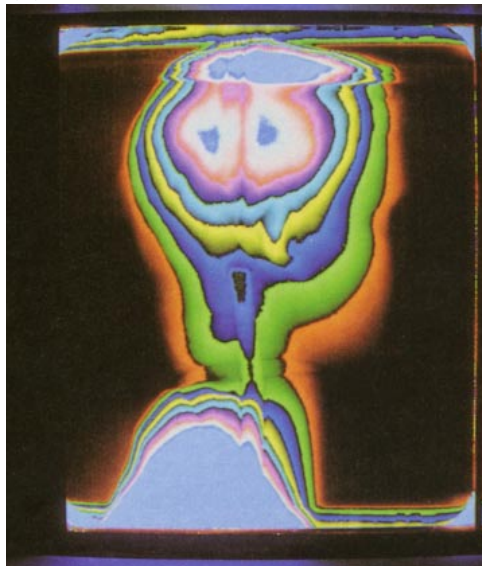
Fragile parts were of concern. The statue had been moved in the past but there was no record about the moves or of damage to the statue. Radiographs of the outstretched left hand of Mary revealed that the fingers had been broken and repaired using interior pins (Fig. 29b).

FIGURE 28. Statue of Caligula: (a) placement of film cassette; (b) digitized film image.<sup>95</sup>

(a)



(b)



Shipping experts used this information for packing the statue.

## Paintings<sup>97</sup>

The scientific examination of art can be divided into two basic categories: destructive and nondestructive. Among the destructive methods are those that involve sampling, taking a small slice or scraping for closer scrutiny, perhaps by microscopy or spectroscopy. A conservator's goal, however, is carefully to maintain valuable works of art and to slow the inevitable deterioration. Nondestructive testing is an invaluable tool to this end. The art historian also finds nondestructive testing an important asset in the pursuit of information of historical value — for example, about creative techniques of a particular artist or a certain period of art.

FIGURE 29. Michelangelo Buonarroti's *Pietà*, Saint Peter's Basilica, Vatican: (a) film cassette placement; (b) image of hand, showing pins used to repair broken fingers.<sup>96</sup>

(a)



(b)





As part of the creative evolution of a painting, an artist will often reconsider during composition and paint over the original idea. The artist may even paint over an earlier works simply because the artist considers the earlier painting less important than the need for another canvas. A change can also be made by someone other than the original artist. From the art historian's point of view, these underpaintings can afford insight into artistic development or the techniques used to achieve a particular effect. They can also help determine the artist or the authenticity of a painting.

Three nondestructive methods derived from the electromagnetic spectrum are used in the testing of two-dimensional art: (1) ultraviolet fluorescent photography, for study of chemistry on the surface; (2) infrared reflectography and thermography, sensitive to relatively emissive hues near the surface; and (3) X-radiography, suited for revealing subsurface layers. X-radiography records the distribution of pigments that have a high absorption coefficient for X-rays. The X-rays used in X-radiography will completely penetrate a canvas. However, if pigments such as white lead or vermillion with high absorption coefficients are present,<sup>98</sup> their distribution will be indicated on a photographic plate placed behind the canvas.

X-radiography has been used to examine paintings since early in the twentieth century.<sup>23</sup> By revealing hidden layers of a painting, the method can provide valuable information about artistic techniques and materials. This information can help conservators preserve or restore paintings.<sup>99-103</sup>

### Flemish Art<sup>104,105</sup>

Film radiography has been used for the examination and restoration of several masterpieces of Flemish art.

1. Van Eyck's *Altarpiece of the Mystic Lamb* (1432), Saint Bavo's Cathedral, Ghent, consists of seven paintings on three oaken boards. Radiographic testing has shown where apertures in the wood grain had been filled with pigment and mounting glue and revealed several layers in the painting process.
2. Peter Paul Rubens' *Portrait of Gaspard Gevartius* (1628), Royal Museum of Fine Arts, Antwerp, was painted on a panel consisting of five boards joined by dowel pins. Radiographic testing has revealed various details of Rubens' technique. For example, a thick layer of paint confirmed a technique called "wet in wet" (*alla prima*).

3. The original canvas of Rubens' *The Virgin and Child Enthroned with Saints* (1628), Royal Museum of Fine Arts, Antwerp, had deteriorated and been mounted on a second canvas, so radiography is the only way to examine the original canvas. Radiographic testing has revealed few corrections to the original, suggesting a high level of mastery.
4. *The Oyster Eater* (1882), Royal Museum of Fine Arts, Antwerp, is a work from James Ensor's youth. It uses less opaque commercial oils from tubes. Radiographic testing has revealed that Ensor mixed paints on the canvas more than on the palette.

### Vermeer<sup>97</sup>

Infrared reflectography and X-radiography have been applied in relating the painting techniques of seventeenth century Flemish artist Jan Vermeer to his distinctive style.<sup>106,107</sup> *View of Delft*, known for the realistic impression it gives, was examined by Wheelock. The painting is a cityscape of the seventeenth century mirrored in the still waters of a harbor. Using infrared and X-radiography, conservators were able to determine the changes made in the length and positioning of the reflections in the water and in the outlining of the city's profile: changes that Vermeer made to achieve his realistic effect.

In addition to learning more about Vermeer's working techniques, conservators attempted to determine compositional changes and also to learn more of actual physical condition — that is, abrasion, restorations or any sort of size alteration. Some changes to a painting can result in questions of authenticity, especially when they appear to be done by someone other than the original artist.<sup>106,107</sup>

### Baum<sup>97</sup>

Some of the examination procedures used in the Intermuseum Conservation Association laboratory are illustrated by the infrared photographs of Charles Baum's *Boy with Still Life*, owned by the Butler Institute of American Art. Fig. 30a shows the portrait using normal light. No images other than that of the title are apparent. An infrared photograph of the same painting shows the sketch, or underdrawing, for the face of the young boy and the faint image of a young woman slightly above and to the right. Figure 30b, the result of X-radiography, is a third image and appears to be that of an older man. In addition, darker areas slightly below center and lower left indicate some restoration.

## Higgins<sup>97</sup>

The painting *Randall's Mill* (1922-23), by American artist Victor Higgins, was examined by the Intermuseum Conservation Association laboratory (Fig. 31a).<sup>107</sup> The painting was still on the original canvas stretcher and in a frame with a brass label, which reads: "VICTOR HIGGINS NA [sic] / 1884-1949 / RANDALL'S MILL."

In light from a window, the raised surface of another painting appeared on the canvas. After examining *Randall's Mill* under a raking light, the laboratory conservators assayed the oil painting with various methods including X-radiography

and infrared reflectography. The painting appears as a depopulated landscape but, when it is viewed with infrared reflectography, the structure of a mill appears, along with carriages filled with figures, horsedrawn wagons and the figure of a saddled donkey being led by a man. Photographic images of the infrared reflectography examination were made from the black and white monitor as the camera scanned various portions of the canvas. With X-radiography, the structure of the mill is the dominant element of Fig. 31b.

A painting of this description by Higgins was detailed in the Indianapolis *Star* in 1924 but the painting subsequently disappeared. In an interview in 1975, Helen Spiess Ferris, daughter of Benjamin G. Randall, related the tale explaining the painting beneath a

**FIGURE 30.** Charles Baum's *Boy with Still Life*, previously attributed to Severin Roesen: (a) visible light photograph; (b) X-radiograph of entire canvas showing image apparently of older man.<sup>97</sup>

(a)



(b)

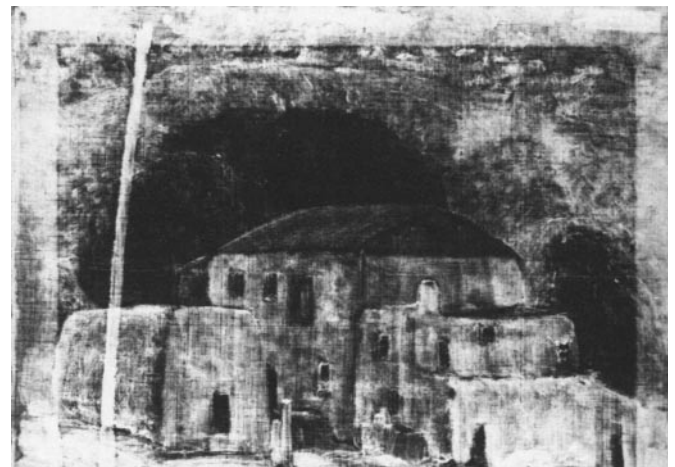


**FIGURE 31.** Victor Higgins' *Randall's Mill*: (a) visible light photograph; (b) X-radiograph showing mill of title.<sup>97</sup>

(a)



(b)





painting. Randall had built the mill of the title. In the vicinity of the mill, he owned a cabin that he made available to the artist Higgens. Higgens painted the picture of Randall's Mill from that cabin. On seeing the picture, Randall pronounced it "the worst picture Higgens ever painted." The statement must have bothered Higgens for some time, for the overpainting is in a style that Higgens used much later during the 1940s.

---

## Closing

The applications in this chapter illustrate the versatility of radiographic testing.

# References

1. Snow, S.G. and R.A. Morris. "Radiation Gaging." *Nondestructive Testing Handbook*, second edition: Vol. 3, *Radiography and Radiation Testing*. Chapter 16. Columbus, OH: American Society for Nondestructive Testing (1985): p 674-704.
2. Davis, R.S. "Early Development of Process Automation with Nucleonic Measurement Gages." *Materials Evaluation*. Vol. 47, No. 10. Columbus, OH: American Society for Nondestructive Testing (October 1989): p 1190-1191.
3. Trout, E.D., R.M. Gager and A.L. Pace. "Possible Industrial Applications of Soft X-Radiation 15 to 100 Kilovolts." *Nondestructive Testing*. Vol. 7, No. 3. Columbus, OH: American Society for Nondestructive Testing (Winter 1948-1949): p 20-24.
4. Reider, J.E. "Industrial Nucleonic Gaging." *Nondestructive Testing*. Vol. 15, No. 6. Columbus, OH: American Society for Nondestructive Testing (November-December 1957): p 360-365.
5. Clayton, J.D. "Thickness Gaging by Gamma Ray Attenuation." *Materials Evaluation*. Vol. 31, No. 2. Columbus, OH: American Society for Nondestructive Testing (February 1973): p 27-32.
6. Ball, E. "A Method for Non-Contact Thickness and Conductivity Gaging." *Materials Evaluation*. Vol. 33, No. 9. Columbus, OH: American Society for Nondestructive Testing (September 1975): p 54A, 57A.
7. Coulter, J.E. *X-Ray Fluorescence Technique for Measuring Coating Thickness*. Y-1927. Oak Ridge, TN: Oak Ridge Y-12 Plant (1974).
8. White, J.D. *Compton Scattering Technique for Measuring the Area Density of Glass-Reinforced Structures*. Y-1714. Oak Ridge, TN: Oak Ridge Y-12 Plant (1970).
9. Foukes, R.A., J.S. Watt, B.W. Seatonberry, A. Davison, R.A. Greig, H.W.G. Lowe and A.C. Abbott. *International Journal of Applied Radiation and Isotopes*. Vol. 29, No. 12 (1978): p 721.
10. Whittaker, J.W. and S.G. Snow. "A Radiation Attenuation Technique for Simultaneous Determination of Layer Thickness in a Bi-Layered Structure." *Materials Evaluation*. Vol. 34, No. 10. Columbus, OH: American Society for Nondestructive Testing (October 1976): p 224-229.
11. Reynolds, G.M. "Neutron Gaging Systems." *Practical Applications of Neutron Radiography and Gauging*. Special Technical Publication 586. ASTM International (1976): p 58.
12. Knoll, G.F. *Radiation Detection and Measurement*, third edition. New York: John Wiley and Sons (2000).
13. Koicki, S., A. Koicki and V. Aydacic. *Nuclear Instrumentation and Methods* (1973): p 297.
14. Davis, R.S. "Nondestructive Gaging with Radiation Sources." *Materials Evaluation*. Vol. 47, No. 9. Columbus, OH: American Society for Nondestructive Testing (September 1989): p 1054, 1056, 1058, 1060.
15. Baird, D.L. "Using 3D X-Ray Inspection for Process Improvements." *Proceedings of NEPCON West Conference*. Des Plaines, IL: Cahnners Publishing (1993).
16. Sack, T. "Implementation Strategy for an Automated X-Ray Inspection Machine." *Proceedings of Nepcon West Conference*. Des Plaines, IL: Cahnners Publishing (1991).
17. Olsen, R. "More Than Just a Pretty Picture: Real-Time X-Ray Image Enhancement in the Electronics Industry." *Materials Evaluation*. Vol. 46, No. 11. Columbus, OH: American Society for Nondestructive Testing (October 1988): p 1403-1408.
18. Silva, F. "Automated X-Ray Inspection Strategies." *Real-Time Radioscopy and Digital Imaging* [Mashantucket, CT, August 1998]. Columbus, OH: American Society for Nondestructive Testing (1998): appendix.

19. Buechler, D.W. "Real-Time Radiography for Electronics Reliability Assessment." *Materials Evaluation*. Vol. 45, No. 11. Columbus, OH: American Society for Nondestructive Testing (November 1987): p 1326-1329.
20. Marchese, M. and K.A. Glodowski. "Real-Time Microfocus Radiography for Electronic Failure Analysis." *Materials Evaluation*. Vol. 49, No. 12. Columbus, OH: American Society for Nondestructive Testing (December 1991): p 1481-1485.
21. "X-Ray Technology Digital Detector Based Systems." Technical note. Bohemia, NY: V.J. Technologies (2000).
22. Tollner, E. and M. Shahin. "X-Ray Imaging for Classifying Food Products Based on Internal Defects." *ASNT Spring Conference and 9th Annual Research Symposium Abstracts* [Birmingham, AL]. Columbus, OH: American Society for Nondestructive Testing (March 2000): p 89-90.
23. St. John, A. and H.R. Isenburger. *Industrial Radiography*. New York, NY: John Wiley and Sons (1934).
24. Schmitt, P. "Lebensmittelscanner." *Arbeitskreis Industrielle Röntgenprüfverfahren*. Ausgabe 1 [ZfP-Zeitung, Ausgabe 79]. Berlin, Germany: Deutsche Gesellschaft für Zerstörungsfreie Prüfung (April 2002): p 4.
25. Katz, R., M.R. Lee and M. Milner. "X-Ray Inspection of Wheat." *Nondestructive Testing*. Vol. 9, No. 2. Columbus, OH: American Society for Nondestructive Testing (Fall 1950): p 16-18.
26. Vozzo, J.A. "Seed Radiography." *Materials Evaluation*. Vol. 46, No. 11. Columbus, OH: American Society for Nondestructive Testing (October 1988): p 1450, 1452-1455.
27. Beaton, J.A., W.B. White and F.H. Berry. "Radiography of Trees and Wood Products." *Materials Evaluation*. Vol. 30, No. 10. Columbus, OH: American Society for Nondestructive Testing (October 1972): p 14A-17A.
28. Brenizer, J.S., K.W. Tobin, J.M. Hylko, D.D. McRae and R.W. Jenkins, Jr. "Quantitative Measurement of Equivalent Water Density in a Burning Cigarette." *Materials Evaluation*. Vol. 45, No. 11. Columbus, OH: American Society for Nondestructive Testing (November 1987): p 1310-1314.
29. "Mobile X-Ray Unit (on a Trailer) 'Eyes' Airport Luggage, Packages." *Materials Evaluation*. Vol. 30, No. 5. Columbus, OH: American Society for Nondestructive Testing (May 1972): p 54A.
30. Battema, J.P. "Nondestructive Testing Fights Terrorism." *Materials Evaluation*. Vol. 44, No. 11. Columbus, OH: American Society for Nondestructive Testing (October 1986): p 1304, 1310, 1314, 1316.
31. Tsacoumis, T.P., ed. *Access Security Screening: Challenges and Solutions*. Special Technical Publication 1127. West Conshohocken, PA: ASTM International (1992).
32. Lanza, R.C. "Visualization and Imaging." *Aviation Security Problems and Related Technologies*. SPIE Proceedings, Vol. CR42. Bellingham, WA: International Society for Optical Engineering (1992): p 104-125.
33. Verbinski, V.V., J. Payne and M. Snell. "Recent Developments in the VACIS Gamma Radiography Systems." *Enforcement and Security Technologies*. SPIE Proceedings, Vol. 3575. Bellingham, WA: International Society for Optical Engineering (1998): p 368-374.
34. De Moulpied, D.S., P.J. Rothschild and G.J. Smith. "X-Ray BodySearch Eliminates Strip Search in Montana Prison." *Enforcement and Security Technologies*. SPIE Proceedings, Vol. 3575. Bellingham, WA: International Society for Optical Engineering (1998): p p 175-181.
35. Bell, C.J. "Nuclear Technologies for Explosives Detection." *Aviation Security Problem and Related Technologies*. SPIE Proceedings, Vol. CR42. Bellingham, WA: International Society for Optical Engineering (1992): p 137-166.
36. Hussein, E.M. "Detection of Explosive Materials Using Nuclear Radiation: A Critical Review." *Aviation Security Problem and Related Technologies*. SPIE Proceedings, Vol. CR42. Bellingham, WA: International Society for Optical Engineering (1992): p 126-136.
37. Fishbein, R.H. "Pulsed Fast Neutron Analysis May Help Quench Terrorism." *Materials Evaluation*. Vol. 55, No. 12. Columbus, OH: American Society for Nondestructive Testing (December 1997): p 1330, 1332, 1334.

38. Baltzer, K.R. "Is There a Role for Nondestructive Testing in Preventing Terrorism and Increasing Homeland Security?" *Materials Evaluation*. Vol. 60, No. 4. Columbus, OH: American Society for Nondestructive Testing (April 2002): p 513-517.
39. Marr, W.A. and C. Fairhurst, eds. *Nondestructive and Automated Testing for Soil and Rock*. Special Technical Publication 1350. West Conshohocken, PA: ASTM International (1999).
40. Bernhard, R.K. and M. Chasek. "Soil Density Determination by Means of Radioactive Isotopes." *Nondestructive Testing*. Vol. 11, No. 8. Columbus, OH: American Society for Nondestructive Testing (November-December 1953): p 17-23. Errata, Vol. 12, No. 1 (January-February 1954): p 40.
41. Ritz, V.H. "Broad and Narrow Beam Attenuation of Ir-192 Gamma Rays in Concrete, Steel, and Lead." *Nondestructive Testing*. Vol. 16, No. 3. Columbus, OH: American Society for Nondestructive Testing (May-June 1958): p 269-272.
42. Runkiewicz, L. "Application the Radiographical Testing for Control of Building Constructions of Concrete in Poland." *3rd European Conference on Nondestructive Testing* [Florence, Italy]. Vol. 1. Brescia, Italy: Italian Society for Non-Destructive Testing, for the European Societies for Nondestructive Testing (October 1984): p 142-153.
43. Mitchell, T.M. "Radioactive/Nuclear Methods." *CRC Handbook on Nondestructive Testing of Concrete*. Boca Raton, LA: CRC Press (1990): p 227-252.
44. Clarke, E.T. "Cobalt-60 Radiography of Concrete." *Materials Evaluation*. Vol. 47, No. 10. Columbus, OH: American Society for Nondestructive Testing (October 1989): p 1200-1203.
45. Niehous, F., G. Coen, R. Kretschmer and M. Biercher. "Radiographic Inspection of Prestressed Concrete up to 1600 mm Wall Thickness Using a 9 MeV Linear Accelerator." *11th World Conference on Nondestructive Testing* [Las Vegas, Nevada]. Vol. 1. Columbus, OH: American Society for Nondestructive Testing (November 1985): p 528-534.
46. Sakine, I. and M. Fujinawa. "Exploratory Tests of Corrosion of Reinforcing Steel in Concrete by X-Radiography." *Materials Evaluation*. Vol. 42, No. 1. Columbus, OH: American Society for Nondestructive Testing (January 1984): p 121-126.
47. Forbis, J.E. "Radiography for Building Renovation." *Materials Evaluation*. Vol. 59, No. 6. Columbus, OH: American Society for Nondestructive Testing (June 2002): p 685-686, 688, 690, 692-694.
48. Saleh, H.H., G. Washer and M. Moore. "The Use of X-Ray Computed Tomography for Highway Applications." *ASNT Fall Conference and Quality Testing Show 2000 Paper Summaries Book* [Indianapolis, IN]. Columbus, OH: American Society for Nondestructive Testing (November 2000): p 126.
49. Livingston, A. and H. Saleh. "Development of an Epithermal Neutron Detector for Nondestructive Measurement of Concrete Hydration." *Nondestructive Characterization of Materials VIII: Proceedings of the Eighth International Symposium held in Boulder, Colorado, June 15-20, 1997*. New York, NY: Plenum Press (1998): p 535-540.
50. Livingston, R.A. and H.H. Saleh. "Specification and Design of a Portable Prompt Gamma/Neutron Activation System for Nondestructive Determination of Chloride in Reinforced Concrete." *Topics on Nondestructive Evaluation: Vol. 2, Nondestructive Testing and Evaluation of Infrastructure*. Columbus, OH: American Society for Nondestructive Testing (1998): p 83-96.
51. Saleh, H.H. and R.A. Livingston. "Experimental Evaluation of a Portable Neutron-Based Gamma-Spectroscopy System for Chloride Measurements in Reinforced Concrete." *Journal of Radioanalytical and Nuclear Chemistry*. Vol. 244, No. 2. Lausanne, Switzerland: Elsevier Sequoia (May 2000): p 367-371.
52. Livingston, R.A., H.H. Saleh, R.C. Block and P.J. Brand. "Time of Flight Calibration of Li-6 Glass Epithermal Neutron Detectors." *Applied Radiation and Isotopes*. Vol. 53, No. 4-5. Oxford, United Kingdom: Pergamon Press (May-June 2000): p 773-777.

53. Hellier, C. "Who Will Inspect Our Bridges?" *Materials Evaluation*. Vol. 41, No. 12. Columbus, OH: American Society for Nondestructive Testing (November 1983): p 1352-1355.
54. Thomas, G., S. Benson, P. Durbin, N. Del Grande, J.J. Haskins, A. Brown and D.J. Schneberk. "Nondestructive Evaluation Techniques for Enhanced Bridge Inspection." *Review of Progress in Nondestructive Evaluation*. Vol. 13B. New York, NY: Plenum Press (1994): p 2083-2090.
55. Newell, R.S. and P.J. Stolarski. "Use of a Portable Linear Accelerator to Radiograph a Bridge Drainage Pump." *Materials Evaluation*. Vol. 50, No. 9. Columbus, OH: American Society for Nondestructive Testing (September 1992): p 1084, 1086-1087.
56. Bell, R.D. "Field Radiography — Images from the Past." *Materials Evaluation*. Vol. 42, No. 7. Columbus, OH: American Society for Nondestructive Testing (June 1984): p 849-851.
57. "Radiography Saves Baseball Season." *Materials Evaluation*. Vol. 47, No. 10. Columbus, OH: American Society for Nondestructive Testing (October 1989): p 1162. See also Vol. 48, No. 4 (April 1990): p 504.
58. AWS D1.12, *Structural Welding Code — Steel*. Section 8, "Buildings." Miami, FL: American Welding Society (1986).
59. Reimers, P. and J. Riederer. "Zerstörungsfreie Prüfung Kulturgeschichtlicher Objekte durch Computertomographie (CT)." *3rd European Conference on Nondestructive Testing* [Florence, Italy]. Vol. 1. Brescia, Italy: Italian Society for Non-Destructive Testing, for the European Societies for Nondestructive Testing (October 1984): p 305-313.
60. Boutaine, J.L. "Radiography Applied to Non Destructive Examination of Cultural Objects." *7th European Conference on Non-Destructive Testing* [Copenhagen, Denmark]. Vol. 1. Copenhagen, Denmark: 7th ECNDT (May 1998): p 391.
61. Lavayssiére, B. and N. Lacoudre. "Application of Radiography for the Conservation and Restoration of Archaeological Objects." *7th European Conference on Non-Destructive Testing* [Copenhagen, Denmark]. Vol. 1. Copenhagen, Denmark: 7th ECNDT (May 1998): p 416-419.
62. Yang, J. "X-Ray Radiography Applied to the Study of the Ancient Manufacturing Technique and the State of Conservation of Cultural Relics." *15th World Conference on Non-Destructive Testing* [Rome, Italy]. Brescia, Italy: Italian Society for Non-Destructive Testing Monitoring Diagnostics (October 2000): p 170.
63. Schiekkel, M., G. Haase, A. Meister and M. Seibitz. "Investigation of Historical Glasses Using Natural Born Radioactivity." *15th World Conference on Non-Destructive Testing* [Rome, Italy]. Brescia, Italy: Italian Society for Non-Destructive Testing Monitoring Diagnostics (October 2000): p 174.
64. Alonso, M.A. M Arroyo, V. Gil, E.M. de Salinas and G. Delojo. "A Radiographic Study of Insect Attacks in Woods." *7th European Conference on Non-Destructive Testing* [Copenhagen, Denmark]. Vol. 1. Copenhagen, Denmark: 7th ECNDT (May 1998): p 400-408.
65. Míšek, B. and L. Ptáček. "Some Data Obtained on X-Ray and Neutronographic Examination of Heat Resistant Ni-Base Alloys." *3rd European Conference on Nondestructive Testing* [Florence, Italy]. Vol. 1. Brescia, Italy: Italian Society for Non-Destructive Testing, for the European Societies for Nondestructive Testing (October 1984): p 246-251.
66. Ptáčková, M. and L. Ptáček. "Complex Examination of Corrosion Damage in Archaeological Finds of Etruscan Bronze Jewels." *3rd European Conference on Nondestructive Testing* [Florence, Italy]. Vol. 1. Brescia, Italy: Italian Society for Non-Destructive Testing, for the European Societies for Nondestructive Testing (October 1984): p 252-261.
67. Gottlieb, B. "NDT Examination of Bronze Lurs." *7th European Conference on Non-Destructive Testing* [Copenhagen, Denmark]. Vol. 1. Copenhagen, Denmark: 7th ECNDT (May 1998): p 436-443.
68. Rossi, M. "High Resolution 3D Computed Tomography of Small Archaeological Sculptures." *7th European Conference on Non-Destructive Testing* [Copenhagen, Denmark]. Vol. 1. Copenhagen, Denmark: 7th ECNDT (May 1998): p 409-415.



69. Tartari, A. "Compton Scattering Elemental Imaging of a Deep Layer Performed with the Principal Component Analysis." *15th World Conference on Non-Destructive Testing* [Rome, Italy]. Brescia, Italy: Italian Society for Non-Destructive Testing Monitoring Diagnostics (October 2000): p 158.
70. Caneva, C. "XRF Spectrometers for Non-Destructive Investigations in Art and Archaeology." *15th World Conference on Non-Destructive Testing* [Rome, Italy]. Brescia, Italy: Italian Society for Non-Destructive Testing Monitoring Diagnostics (October 2000): p 171.
71. Rossi, M., D. Romani and D. Picchi. "Investigation of Small Egyptian Mummies by 3D Computed Tomography." *15th World Conference on Non-Destructive Testing* [Rome, Italy]. Brescia, Italy: Italian Society for Non-Destructive Testing Monitoring Diagnostics (October 2000): p 159.
72. "NSWC X-Rays Mummified Bull." *Materials Evaluation*. Vol. 36, No. 5. Columbus, OH: American Society for Nondestructive Testing (April 1978): p 58.
73. Lombardo, B., G. Conlogue and R. Colten. "The Use of Computed Radiography to Survey Mummified Remains." *ASNT Fall Conference and Quality Testing Show 2000: Paper Summaries Book* [Indianapolis, IN]. Columbus, OH: American Society for Nondestructive Testing (November 2000): p 127.
74. Paderni, L. and M. Micheli. "X-Ray Study of Peruvian Funeral 'Fardos' of the Museo Preistorico Etnografico 'Luigi Pignorini.'" *3rd European Conference on Nondestructive Testing* [Florence, Italy]. Vol. 1. Brescia, Italy: Italian Society, for Non-Destructive Testing, for the European Societies for Nondestructive Testing (October 1984): p 263-275.
75. Zangerl, R. "The Use of X-Rays in the Study of Fossils." *Nondestructive Testing*. Vol. 7, No. 1. Columbus, OH: American Society for Nondestructive Testing (Summer 1948): p 29-31.
76. "X Rays Provide Researcher with Views of Coral Growth Patterns." *Materials Evaluation*. Vol. 37, No. 9. Columbus, OH: American Society for Nondestructive Testing (August 1979): p 26-27.
77. "The Statue of Liberty: The Restoration in Retrospect." *Materials Evaluation*. Vol. 44, No. 8. Columbus, OH: American Society for Nondestructive Testing (July 1986): p 891-895.
78. Berntson, C.M. "Nondestructive Testing Sheds Light on Preserving America's Past." *Materials Evaluation*. Vol. 43, No. 10. Columbus, OH: American Society for Nondestructive Testing (September 1985): p 1180-1182, 1184-1186.
79. Hatzianeandreu, L. and G. Ladopoulos. "Use of Radiography for Solution of Diagnostic Problems Existing in Marble Monuments." *Materialprüfung*. Vol. 22. Berlin, Germany: Bundesanstalt für Materialforschung und Prüfung (July 1980): p 298-300.
80. Clarke, E.T. "Radiography of Ancient Structures on the Acropolis of Athens." *Technology and Conservation*. Vol. 8, No. 3. Boston, MA: Technology Organization (Fall 1983): p 18-22.
81. "Radiography Aids Renovation of Capitol." *Materials Evaluation*. Vol. 43, No. 10. Columbus, OH: American Society for Nondestructive Testing (September 1985): p 1148, 1150-1151.
82. Bonin, H.W. and C.J. Thorp. "Neutron Moisture Gage for Roofing Surveys: Experiment and Simulation." *3rd European Conference on Nondestructive Testing* [Florence, Italy]. Vol. 1. Brescia, Italy: Italian Society for Non-Destructive Testing, for the European Societies for Nondestructive Testing (October 1984): p 224-229.
83. Blancato, R.J. "Radiography Finds 'Broken Bones' in Cape Hatteras Lighthouse." *Materials Evaluation*. Vol. 38, No. 3. Columbus, OH: American Society for Nondestructive Testing (March 1980): p 13-15.
84. Clarke, E.T. "Radiography of the Cape Hatteras Lighthouse." *Technology and Conservation*. Vol. 5, No. 1. Boston, MA: Technology Organization (Spring 1980): p 20-24.
85. Minato, S. "Feasibility of Cosmic-Ray Radiography: A Case Study of a Temple Gate as a Testpiece." *Materials Evaluation*. Vol. 46, No. 11. Columbus, OH: American Society for Nondestructive Testing (October 1988): p 1468-1470.

86. Livingston, R.A. "Transferring Technology from Conservation Science to Infrastructure Renewal." *Public Roads*. Vol. 58, No. 1. McLean, VA: Federal Highway Administration (Summer 1994).
87. Alvarez, L.W. "Search for Hidden Chambers in the Pyramids." *Science*. Vol. 167. Washington, DC: American Association for the Advancement of Science (1970): p 832-839.
88. "Hellier Examines Historic Vessel with Modern NDT Tests." *Materials Evaluation*. Vol. 36, No. 7. Columbus, OH: American Society for Nondestructive Testing (June 1978): p 70-71.
89. Kleven, S. "Use of Computed Radiology during the Archaeological Conservation of LaSalle's Ship — The Belle." *15th World Conference on Non-Destructive Testing* [Rome, Italy]. Brescia, Italy: Italian Society for Non-Destructive Testing Monitoring Diagnostics (October 2000): p 157.
90. "Uncovering Historical Treasures Using NDT." *Materials Evaluation*. Vol. 57, No. 7. Columbus, OH: American Society for Nondestructive Testing (July 1999): p 736.
91. Fanning, D.F. "The Confederate Submarine H.L. Hunley and Nondestructive Testing." *Materials Evaluation*. Columbus, OH: American Society for Nondestructive Testing (March 2002): p 409-413, 416-419.
92. "How They Did It — Radiographing the Liberty Bell." *Materials Evaluation*. Vol. 34, No. 2. Columbus, OH: American Society for Nondestructive Testing (February 1976): p 14A-16A, 18A, 26A.
93. Clarke, E.T. "Radiographing the Liberty Bell." *Foundry Trade Journal*. Vol. 141. London, United Kingdom: Institute of British Foundrymen (August 1976): p 223-228.
94. "Examining the Liberty Bell." *The NDT Technician*. Vol. 1, No. 3. Columbus, OH: American Society for Nondestructive Testing (July 2002): p 1-5.
95. "Radiography Aids Art Conservation of Caligula Statue." *Materials Evaluation*. Vol. 47, No. 10. Columbus, OH: American Society for Nondestructive Testing (October 1989): p 1129-1131.
96. "George Corney's Radiographs Help Move Vatican's Pieta." *Materials Evaluation*. Vol. 22, No. 6. Columbus, OH: American Society for Nondestructive Testing (June 1964): p 279.
97. Humphries, H. "Infrared Testing in Art Conservation." *Materials Evaluation*. Vol. 45, No. 4. Columbus, OH: American Society for Nondestructive Testing (April 1987): p 426-428, 430.
98. Van Asperen de Boer, J.R.J. "Infrared Reflectography: A Contribution to the Examination of Earlier European Paintings." Dissertation. Amsterdam, Netherlands: University of Amsterdam (July 1970): p 11-15.
99. Graham, D. and T. Eddie. *X-Ray Techniques in Art Galleries and Museums*. Boston: Adam Hilger Limited (1985).
100. Rossi, M., F. Casali, A. Bacchilega and D. Romani. "An Experimental X-Ray Digital Detector for Investigation of Paintings." *15th World Conference on Non-Destructive Testing* [Rome, Italy]. Brescia, Italy: Italian Society for Non-Destructive Testing Monitoring Diagnostics (October 2000): p 160.
101. Panczyk, E., M. Ligeza, K. Pytel, A. Kalicki, L. Rõwinska, B. Sartowska and L. Walis. "Neutron-Induced Autoradiography in the Study of Oil Paintings by Tintoretto, Marieschi and Bellotto." *15th World Conference on Non-Destructive Testing* [Rome, Italy]. Brescia, Italy: Italian Society for Non-Destructive Testing Monitoring Diagnostics (October 2000): p 179.
102. "The Mysterious Paintings of Francis Picabia." *Worldwide*. Vol. 7. Mortsel, Belgium: Agfa-Gavaert NV [n.d.].
103. "The Hermitage Museum Conservation Project: Titian's *The Flight into Egypt*." *Worldwide*. Vol. 8/9. Mortsel, Belgium: Agfa-Gavaert NV [n.d.].
104. *Flemish Masterpieces X-Rayed with Structurix Industrial X-Ray Film*. Press release. Mortsel, Belgium: Agfa-Gavaert NV [n.d.].
105. *The Ingenuity of Flemish Art and NDT Technology Combined*. Brochure. Mortsel, Belgium: Agfa-Gavaert NV [1988].
106. Wheelock, Arthur K., Jr. "NEA Fellows' Diary: Vermeer's Painting Technique." *Art Journal*. Vol. 41, No. 2. New York, NY: Hearst Corporation (Summer 1981): p 162-164.
106. Wheelock, A.K., Jr. *Vermeer and the Art of Painting*. New Haven, CT: Yale University Press (1995).
107. Porter, D. Correspondence (January 1987).



# 22

## C H A P T E R

# Attenuation Coefficients

---

Frank A. Iddings, San Antonio, Texas

## PART 1. Introduction to Attenuation Coefficients

The attenuation of an X-ray or gamma ray beam passing through matter (and the beam's resulting attenuation) is the consequence of a series of single events. During each event a photon is removed from the beam after interaction with a nucleus or an orbital electron in the attenuating material. The total probability (per atom) for scattering or absorption of a photon of the original energy is given by a proportionality constant  $\sigma$ . This is often referred to as the *cross section* because it has the dimensions of an area. Such cross sections are measured in a unit of  $10^{-28} \text{ m}^2$ . In physics, this unit has been called *barn* (b), where  $1 \text{ b} = 100 \text{ fm}^2 = 10^{-28} \text{ m}^2 = 10^{-24} \text{ cm}^2$ .

The total attenuation coefficient is the sum of the attenuation coefficients due to Compton scattering, the photoelectric effect and pair production. The *photoelectric effect* is that process in which a photon transfers its total energy to an electron in some shell of an atom. It is most significant at lower photon energies. As photon energy increases, *Compton scattering* becomes the main process contributing to attenuation. Very high energy photons are absorbed by *pair production*, in which a photon is converted into an electron and a positron. This process occurs in the electrical field of a nucleus and requires a minimum photon energy of 1.02 MeV.

The total attenuation coefficient can be expressed in three different forms:

1. The *atomic attenuation coefficient* measures the probability of absorption, per atom of absorbing material, in barn ( $10^{-28} \text{ m}^2$ ).
2. The *mass attenuation coefficient* measures the probability of absorption per gram of absorbing material in a square centimeter of the beam ( $\text{cm}^2 \cdot \text{g}^{-1}$ ).
3. The *linear attenuation coefficient* measures the probability of absorption per centimeter of the absorbing material's thickness ( $\text{cm}^{-1}$ ).

### Linear Attenuation Coefficient

The linear attenuation coefficient  $\mu_L$  can be expressed as:

$$(1) \quad \mu_L = \mu_M \times \rho$$

where  $\mu_M$  is the mass attenuation coefficient and where  $\rho$  is the density of the absorbing material. The linear attenuation coefficient has a dimension of  $\text{cm}^{-1}$ .

The linear attenuation coefficient  $\mu_L$  of water at 1 MeV, for example, is:

$$0.0705 \text{ cm}^2 \cdot \text{g}^{-1} \times 1 \text{ g} \cdot \text{cm}^{-3} = 0.0705 \text{ cm}^{-1}$$

where 1 is the density  $\rho$  in gram per cubic centimeter at standard temperature and pressure and where 0.0705 is the mass attenuation coefficient  $\mu_M$  for water.

The linear attenuation coefficient  $\mu_L$  for air at 0.020 MeV is:

$$0.761 \times 0.0012 = 0.91 \times 10^{-3} \text{ cm}^{-1}$$

where 0.0012 is the density  $\rho$  of air in gram per cubic centimeter and 0.761 is its mass attenuation coefficient  $\mu_M$ . Calculation of the mass attenuation coefficients for air and water is shown below).

### Mass Attenuation Coefficient

The mass attenuation coefficient  $\mu_M$  of a compound or mixture is the sum of the mass attenuation coefficients of the constituent *elements*, weighted in proportion to their relative abundance  $R$ .

$$(2) \quad (\mu_M)_{\text{total}} = (\mu_M)_a R_a + (\mu_M)_b R_b + \dots$$

The total mass attenuation coefficient for a compound, water, at 1 MeV, is:

$$\begin{aligned} (\mu_M)_{\text{water}} &= 0.126 \left( \frac{2}{18} \right) \\ &+ 0.0636 \left( \frac{16}{18} \right) \\ &= 0.0705 \text{ cm}^2 \cdot \text{g}^{-1} \end{aligned}$$

where 0.126 and 0.0636 are the mass attenuation coefficients of hydrogen and oxygen at 1 MeV. The relative abundance is figured using the relative atomic mass  $A_r = 1$  for hydrogen and  $A_r = 16$  for oxygen. *Relative atomic mass* (formerly

called *atomic weight*) is the ratio of the average mass per atom of an element to one twelfth of the mass of the atom of the nuclide carbon 12.

The same method can be used to calculate the mass attenuation coefficient at 0.02 MeV for air (a mixture), which consists in percentages by weight primarily of N<sub>2</sub> (75.6 percent), O<sub>2</sub> (23.1 percent) and Ar (1.3 percent). The mass attenuation coefficients are as follows: nitrogen, 0.598 cm<sup>2</sup>·g<sup>-1</sup>; oxygen, 0.840 cm<sup>2</sup>·g<sup>-1</sup>; and argon, 8.87 cm<sup>2</sup>·g<sup>-1</sup>. Therefore the total mass attenuation coefficient for air at 0.02 MeV is:

$$\begin{aligned}(\mu_M)_{\text{air}} &= (0.598 \times 0.756) \\ &+ (0.840 \times 0.231) \\ &+ (8.87 \times 0.013) \\ &= 0.761 \text{ cm}^2 \cdot \text{g}^{-1}\end{aligned}$$

sharp change occurs for K electrons is called the *K absorption edge* and is used to identify the situation where kinetic energy of the ejected K electron is zero. Further increase of the photon energy causes the absorption to decrease almost inversely with the cube of the energy.

## Linear Coefficient Tables

Tables 1 to 40 are based on a narrow beam absorption. The calculated atomic, mass and linear attenuation coefficients for various elements are given in the energy range of 0.01 to 30 MeV.

The tables were prepared for a previous edition by the Radiation Physics Committee of the American Society for Nondestructive Testing, under the direction of C. Robert Emigh of Los Alamos National Laboratory, New Mexico. The tabulations provide data for the photoelectric component; data for the pair production component, which includes both nuclear and orbital electron contributions; data for the scattering component; and a correction for electronic binding energies. Values were obtained from G.R. White's calculated values in the *Handbook of Radiology*<sup>1</sup> and other sources.<sup>2-4</sup> Corrections to these values and values for other elements were obtained by graphical interpolation. For convenience, the values are presented to no more than three significant figures, although the estimated probable error is no larger than one-half unit in the last place, or three percent, whichever is greater. The linear attenuation coefficients are calculated with the density most commonly used for the given element.

## K Absorption Edge

Tables 21 to 40 include information on the element's K absorption edge. When the transmitted photon energy reaches the binding energy of a particular shell of electrons, there is an abrupt increase in the absorption. The energy at which this



## PART 2. Attenuation Coefficient Tables

TABLE 1. Attenuation coefficients for hydrogen (atomic number  $Z = 1$ ).

Energy (MeV)	Cross Section ( $10^{-28} \text{ m}^2$ )			Attenuation Coefficient $\mu$		
	Scattering	Photoelectric	Pair	Atomic ( $10^{-28} \text{ m}^2$ )	Mass <sup>a</sup> ( $\text{cm}^2\text{-g}^{-1}$ )	Linear <sup>b</sup> ( $\text{cm}^{-1}$ )
0.01	0.637	0.005	—	0.642	0.384	$32.1 \times 10^{-6}$
0.015	0.627	0.001	—	0.628	0.375	$31.4 \times 10^{-6}$
0.02	0.616	—	—	0.616	0.368	$30.8 \times 10^{-6}$
0.03	0.596	—	—	0.596	0.356	$29.8 \times 10^{-6}$
0.04	0.578	—	—	0.578	0.345	$28.9 \times 10^{-6}$
0.05	0.561	—	—	0.561	0.335	$28.1 \times 10^{-6}$
0.06	0.546	—	—	0.546	0.326	$27.3 \times 10^{-6}$
0.08	0.517	—	—	0.517	0.309	$25.9 \times 10^{-6}$
0.10	0.493	—	—	0.493	0.295	$24.7 \times 10^{-6}$
0.15	0.444	—	—	0.444	0.265	$22.2 \times 10^{-6}$
0.20	0.407	—	—	0.407	0.243	$20.4 \times 10^{-6}$
0.30	0.354	—	—	0.354	0.212	$17.8 \times 10^{-6}$
0.40	0.317	—	—	0.317	0.189	$15.8 \times 10^{-6}$
0.50	0.289	—	—	0.289	0.173	$14.5 \times 10^{-6}$
0.60	0.268	—	—	0.268	0.160	$13.4 \times 10^{-6}$
0.80	0.235	—	—	0.235	0.140	$11.7 \times 10^{-6}$
1.0	0.211	—	—	0.211	0.126	$10.6 \times 10^{-6}$
1.5	0.172	—	—	0.172	0.103	$8.63 \times 10^{-6}$
2.0	0.146	—	—	0.146	0.0873	$7.31 \times 10^{-6}$
3.0	0.115	—	0.001	0.116	0.0693	$5.80 \times 10^{-6}$
4.0	0.0960	—	0.0010	0.0970	0.0580	$4.86 \times 10^{-6}$
5.0	0.0828	—	0.0014	0.0842	0.0503	$4.21 \times 10^{-6}$
6.0	0.0732	—	0.0019	0.0751	0.0449	$3.76 \times 10^{-6}$
8.0	0.0599	—	0.0027	0.0626	0.0374	$3.13 \times 10^{-6}$
10.0	0.0510	—	0.0033	0.0543	0.0325	$2.72 \times 10^{-6}$
15.0	0.0377	—	0.0046	0.0423	0.0253	$2.12 \times 10^{-6}$
20.0	0.0302	—	0.0056	0.0358	0.0214	$1.79 \times 10^{-6}$
30.0	0.0220	—	0.0071	0.0291	0.0174	$1.46 \times 10^{-6}$

a. Mass attenuation coefficient is calculated by using relative atomic mass  $A_r = 1.008$ .

b. Linear attenuation coefficient is calculated by using density  $\rho = 8.38 \times 10^{-5} \text{ g}\cdot\text{cm}^{-3}$ .

TABLE 2. Attenuation coefficients for beryllium (atomic number  $Z = 4$ ).

Energy (MeV)	Cross Section ( $10^{-28} \text{ m}^2$ )			Attenuation Coefficient $\mu$		
	Scattering	Photoelectric	Pair	Atomic ( $10^{-28} \text{ m}^2$ )	Mass <sup>a</sup> ( $\text{cm}^2\text{-g}^{-1}$ )	Linear <sup>b</sup> ( $\text{cm}^{-1}$ )
0.01	3.54	5.42	—	8.96	0.599	1.09
0.015	3.01	1.39	—	4.40	0.294	0.535
0.02	2.77	0.52	—	3.29	0.220	0.400
0.03	2.53	0.13	—	2.66	0.178	0.324
0.04	2.38	0.05	—	2.43	0.162	0.295
0.05	2.28	0.02	—	2.30	0.154	0.280
0.06	2.21	0.01	—	2.22	0.148	0.269
0.08	2.09	—	—	2.09	0.140	0.255
0.10	1.99	—	—	1.99	0.133	0.242
0.15	1.78	—	—	1.78	0.119	0.217
0.20	1.63	—	—	1.63	0.109	0.198
0.30	1.41	—	—	1.41	0.0943	0.172
0.40	1.27	—	—	1.27	0.0849	0.155
0.50	1.16	—	—	1.16	0.0775	0.141
0.60	1.07	—	—	1.07	0.0715	0.130
0.80	0.940	—	—	0.940	0.0628	0.114
1.0	0.845	—	—	0.845	0.0565	0.103
1.5	0.686	—	0.001	0.687	0.459	0.0835
2.0	0.586	—	0.003	0.589	0.0394	0.0717
3.0	0.460	—	0.008	0.468	0.0313	0.0570
4.0	0.384	—	0.014	0.398	0.0266	0.0484
5.0	0.331	—	0.019	0.350	0.0234	0.0426
6.0	0.293	—	0.024	0.317	0.0212	0.0386
8.0	0.240	—	0.031	0.271	0.0181	0.0329
10	0.204	—	0.039	0.243	0.0162	0.0295
15	0.151	—	0.051	0.202	0.0135	0.0246
20	0.121	—	0.061	0.182	0.0122	0.0222
30	0.0880	—	0.075	0.163	0.0109	0.0198

a. Mass attenuation coefficient is calculated by using relative atomic mass  $A_r = 9.013$ .

b. Linear attenuation coefficient is calculated by using density  $\rho = 1.82 \text{ g}\cdot\text{cm}^{-3}$ .

TABLE 3. Attenuation coefficients for carbon (atomic number  $Z = 6$ ).

Energy (MeV)	Cross Section ( $10^{-28} \text{ m}^2$ )			Attenuation Coefficient $\mu$		
	Scattering	Photoelectric	Pair	Atomic ( $10^{-28} \text{ m}^2$ )	Mass <sup>a</sup> ( $\text{cm}^2\text{-g}^{-1}$ )	Linear <sup>b</sup> ( $\text{cm}^{-1}$ )
0.01	6.90	38.6	—	45.5	2.28	5.06
0.015	5.30	10.2	—	15.5	0.778	1.73
0.02	4.64	3.91	—	8.55	0.429	0.952
0.03	4.04	0.99	—	5.03	0.252	0.559
0.04	3.71	0.38	—	4.09	0.205	0.455
0.05	3.53	0.18	—	3.71	0.186	0.413
0.06	3.38	0.10	—	3.48	0.175	0.389
0.08	3.18	0.04	—	3.22	0.162	0.360
0.10	3.02	0.02	—	3.04	0.153	0.340
0.15	2.69	—	—	2.69	0.135	0.300
0.20	2.46	—	—	2.46	0.123	0.273
0.30	2.13	—	—	2.13	0.107	0.238
0.40	1.90	—	—	1.90	0.0953	0.212
0.50	1.74	—	—	1.74	0.0873	0.194
0.60	1.61	—	—	1.61	0.0808	0.179
0.80	1.41	—	—	1.41	0.0707	0.157
1.0	1.27	—	—	1.27	0.0637	0.141
1.5	1.03	—	—	1.03	0.0517	0.115
2.0	0.878	—	0.006	0.884	0.0444	0.0986
3.0	0.691	—	0.018	0.709	0.0356	0.0790
4.0	0.576	—	0.031	0.607	0.0305	0.0677
5.0	0.497	—	0.042	0.539	0.0270	0.0599
6.0	0.439	—	0.052	0.491	0.0246	0.0546
8.0	0.359	—	0.068	0.427	0.0214	0.0475
10	0.306	—	0.083	0.389	0.0195	0.0433
15	0.226	—	0.110	0.336	0.0169	0.0375
20	0.181	—	0.130	0.311	0.0156	0.0346
30	0.132	—	0.160	0.292	0.0146	0.0324

a. Mass attenuation coefficient is calculated by using relative atomic mass  $A_r = 12.010$ .

b. Linear attenuation coefficient for graphite form of carbon is calculated by using density  $\rho = 2.22 \text{ g}\cdot\text{cm}^{-3}$ .

TABLE 4. Attenuation coefficients for nitrogen (atomic number  $Z = 7$ ).

Energy (MeV)	Cross Section ( $10^{-28} \text{ m}^2$ )			Attenuation Coefficient $\mu$		
	Scattering	Photoelectric	Pair	Atomic ( $10^{-28} \text{ m}^2$ )	Mass <sup>a</sup> ( $\text{cm}^2 \cdot \text{g}^{-1}$ )	Linear <sup>b</sup> ( $\text{cm}^{-1}$ )
0.01	9.0	79.4	—	88.4	3.80	$44.3 \times 10^{-4}$
0.015	6.7	21.2	—	27.9	1.20	$14.0 \times 10^{-4}$
0.02	5.73	8.21	—	13.9	0.598	$6.97 \times 10^{-4}$
0.03	4.84	2.15	—	6.99	0.301	$3.51 \times 10^{-4}$
0.04	4.45	0.81	—	5.26	0.226	$2.63 \times 10^{-4}$
0.05	4.14	0.38	—	4.52	0.194	$2.26 \times 10^{-4}$
0.06	3.98	0.21	—	4.19	0.180	$2.10 \times 10^{-4}$
0.08	3.73	0.08	—	3.81	0.164	$1.91 \times 10^{-4}$
0.10	3.54	0.04	—	3.58	0.154	$1.79 \times 10^{-4}$
0.15	3.15	0.01	—	3.16	0.136	$1.58 \times 10^{-4}$
0.20	2.87	—	—	2.87	0.123	$1.43 \times 10^{-4}$
0.30	2.48	—	—	2.48	0.107	$1.25 \times 10^{-4}$
0.40	2.22	—	—	2.22	0.0955	$1.11 \times 10^{-4}$
0.50	2.02	—	—	2.02	0.0869	$1.01 \times 10^{-4}$
0.60	1.87	—	—	1.87	0.0804	$0.937 \times 10^{-4}$
0.80	1.65	—	—	1.65	0.0710	$0.827 \times 10^{-4}$
1.0	1.48	—	—	1.48	0.0637	$0.742 \times 10^{-4}$
1.5	1.20	—	—	1.20	0.0516	$0.601 \times 10^{-4}$
2.0	1.03	—	0.01	1.04	0.0447	$0.521 \times 10^{-4}$
3.0	0.806	—	0.025	0.831	0.0357	$0.416 \times 10^{-4}$
4.0	0.672	—	0.042	0.714	0.0307	$0.358 \times 10^{-4}$
5.0	0.580	—	0.057	0.637	0.0274	$0.319 \times 10^{-4}$
6.0	0.512	—	0.071	0.583	0.0251	$0.292 \times 10^{-4}$
8.0	0.419	—	0.092	0.511	0.0220	$0.256 \times 10^{-4}$
10	0.357	—	0.111	0.468	0.0201	$0.234 \times 10^{-4}$
15	0.264	—	0.148	0.412	0.0177	$0.206 \times 10^{-4}$
20	0.212	—	0.174	0.386	0.0166	$0.193 \times 10^{-4}$
30	0.154	—	0.213	0.367	0.0158	$0.184 \times 10^{-4}$

a. Mass attenuation coefficient is calculated by using relative atomic mass  $A_r = 14.088$ .

b. Linear attenuation coefficient is calculated by using density  $\rho = 1.165 \times 10^{-3} \text{ g} \cdot \text{cm}^{-3}$ .

TABLE 5. Attenuation coefficients for oxygen (atomic number  $Z = 8$ ).

Energy (MeV)	Cross Section ( $10^{-28} \text{ m}^2$ )			Attenuation Coefficient $\mu$		
	Scattering	Photoelectric	Pair	Atomic ( $10^{-28} \text{ m}^2$ )	Mass <sup>a</sup> ( $\text{cm}^2\text{-g}^{-1}$ )	Linear <sup>b</sup> ( $\text{cm}^{-1}$ )
0.01	11.3	146	—	157	5.91	$78.7 \times 10^{-4}$
0.015	8.3	39.6	—	47.9	1.80	$24.0 \times 10^{-4}$
0.02	6.9	15.4	—	22.3	0.840	$11.2 \times 10^{-4}$
0.03	5.77	4.09	—	9.86	0.371	$4.94 \times 10^{-4}$
0.04	5.18	1.55	—	6.73	0.253	$3.37 \times 10^{-4}$
0.05	4.86	0.73	—	5.59	0.211	$2.81 \times 10^{-4}$
0.06	4.62	0.40	—	5.02	0.189	$2.52 \times 10^{-4}$
0.08	4.31	0.15	—	4.46	0.168	$2.24 \times 10^{-4}$
0.10	4.06	0.07	—	4.13	0.156	$2.08 \times 10^{-4}$
0.15	3.61	0.02	—	3.63	0.137	$1.82 \times 10^{-4}$
0.20	3.29	0.01	—	3.30	0.124	$1.65 \times 10^{-4}$
0.30	2.84	—	—	2.84	0.107	$1.43 \times 10^{-4}$
0.40	2.54	—	—	2.54	0.0957	$1.27 \times 10^{-4}$
0.50	2.31	—	—	2.31	0.0870	$1.16 \times 10^{-4}$
0.60	2.14	—	—	2.14	0.0806	$1.07 \times 10^{-4}$
0.80	1.88	—	—	1.88	0.0708	$0.943 \times 10^{-4}$
1.0	1.69	—	—	1.69	0.0636	$0.847 \times 10^{-4}$
1.5	1.37	—	—	1.37	0.0516	$0.687 \times 10^{-4}$
2.0	1.17	—	0.01	1.18	0.0444	$0.591 \times 10^{-4}$
3.0	0.921	—	0.033	0.954	0.0359	$0.478 \times 10^{-4}$
4.0	0.768	—	0.054	0.822	0.0310	$0.413 \times 10^{-4}$
5.0	0.663	—	0.074	0.737	0.0278	$0.370 \times 10^{-4}$
6.0	0.586	—	0.091	0.677	0.0255	$0.340 \times 10^{-4}$
8.0	0.479	—	0.119	0.598	0.0225	$0.300 \times 10^{-4}$
10	0.408	—	0.143	0.551	0.0208	$0.277 \times 10^{-4}$
15	0.302	—	0.190	0.492	0.0185	$0.246 \times 10^{-4}$
20	0.242	—	0.224	0.466	0.0175	$0.233 \times 10^{-4}$
30	0.176	—	0.273	0.449	0.0169	$0.225 \times 10^{-4}$

a. Mass attenuation coefficient is calculated by using relative atomic mass  $A_r = 16.000$ .

b. Linear attenuation coefficient is calculated by using density  $\rho = 1.332 \times 10^{-3} \text{ g}\cdot\text{cm}^{-3}$ .



TABLE 6. Attenuation coefficients for sodium (atomic number  $Z = 11$ ).

Energy (MeV)	Cross Section ( $10^{-28} \text{ m}^2$ )			Attenuation Coefficient $\mu$		
	Scattering	Photoelectric	Pair	Atomic ( $10^{-28} \text{ m}^2$ )	Mass <sup>a</sup> ( $\text{cm}^2\text{-g}^{-1}$ )	Linear <sup>b</sup> ( $\text{cm}^{-1}$ )
0.01	20.6	588	—	609	16.0	15.5
0.015	14.0	169	—	183	4.79	4.65
0.02	11.3	67.5	—	78.8	2.06	2.00
0.03	8.91	18.1	—	27.0	0.707	0.686
0.04	7.71	7.0	—	14.7	0.385	0.374
0.05	7.07	3.3	—	10.4	0.272	0.264
0.06	6.67	1.90	—	8.57	0.225	0.218
0.08	6.08	0.74	—	6.82	0.179	0.174
0.10	5.66	0.32	—	5.98	0.157	0.152
0.15	5.01	0.09	—	5.10	0.134	0.130
0.20	4.54	0.04	—	4.58	0.120	0.117
0.30	3.92	0.01	—	3.93	0.103	0.100
0.40	3.50	—	—	3.50	0.0917	0.0890
0.50	3.19	—	—	3.19	0.0836	0.0812
0.60	2.94	—	—	2.94	0.0770	0.0748
0.80	2.59	—	—	2.59	0.0679	0.0659
1.0	2.32	—	—	2.32	0.0608	0.0590
1.5	1.89	—	—	1.89	0.0495	0.0481
2.0	1.61	—	0.02	1.63	0.0427	0.0415
3.0	1.27	—	0.06	1.33	0.0348	0.0338
4.0	1.06	—	0.10	1.16	0.0304	0.0295
5.0	0.911	—	0.139	1.05	0.0275	0.0267
6.0	0.805	—	0.170	0.975	0.0255	0.0248
8.0	0.659	—	0.221	0.880	0.0231	0.0224
10	0.561	—	0.266	0.827	0.0217	0.0211
15	0.415	—	0.351	0.766	0.0201	0.0195
20	0.333	—	0.413	0.746	0.0195	0.0189
30	0.242	—	0.500	0.742	0.0194	0.0188

a. Mass attenuation coefficient is calculated by using relative atomic mass  $A_r = 22.997$ .

b. Linear attenuation coefficient is calculated by using density  $\rho = 0.971 \text{ g}\cdot\text{cm}^{-3}$ .

TABLE 7. Attenuation coefficients for magnesium (atomic number  $Z = 12$ ).

Energy (MeV)	Cross Section ( $10^{-28} \text{ m}^2$ )			Attenuation Coefficient $\mu$		
	Scattering	Photoelectric	Pair	Atomic ( $10^{-28} \text{ m}^2$ )	Mass <sup>a</sup> ( $\text{cm}^2\text{-g}^{-1}$ )	Linear <sup>b</sup> ( $\text{cm}^{-1}$ )
0.01	24.3	851	—	875	21.7	37.8
0.015	16.4	244	—	260	6.44	11.2
0.02	13.0	99.0	—	112	2.77	4.82
0.03	10.1	27.4	—	37.5	0.929	1.62
0.04	8.71	10.5	—	19.2	0.476	0.829
0.05	7.88	5.13	—	13.0	0.322	0.561
0.06	7.37	2.84	—	10.2	0.253	0.440
0.08	6.70	1.10	—	7.80	0.193	0.336
0.10	6.25	0.53	—	6.78	0.168	0.292
0.15	5.48	0.14	—	5.62	0.139	0.242
0.20	4.96	0.06	—	5.02	0.124	0.216
0.30	4.28	0.02	—	4.30	0.107	0.186
0.40	3.82	0.01	—	3.83	0.0949	0.165
0.50	3.48	—	—	3.48	0.0862	0.150
0.60	3.22	—	—	3.22	0.0798	0.139
0.80	2.82	—	—	2.82	0.0699	0.122
1.0	2.53	—	—	2.53	0.0627	0.109
1.5	2.06	—	0.01	2.07	0.0513	0.0893
2.0	1.76	—	0.02	1.78	0.0441	0.0768
3.0	1.38	—	0.08	1.46	0.0362	0.0630
4.0	1.15	—	0.12	1.27	0.0315	0.0548
5.0	0.994	—	0.165	1.16	0.0287	0.0500
6.0	0.878	—	0.201	1.08	0.0268	0.0467
8.0	0.719	—	0.261	0.980	0.0243	0.0423
10	0.612	—	0.314	0.926	0.0229	0.0399
15	0.452	—	0.415	0.867	0.0215	0.0374
20	0.362	—	0.490	0.852	0.0211	0.0367
30	0.264	—	0.593	0.857	0.0212	0.0369

a. Mass attenuation coefficient is calculated by using relative atomic mass  $A_r = 24.32$ .

b. Linear attenuation coefficient is calculated by using density  $\rho = 1.741 \text{ g-cm}^{-3}$ .

TABLE 8. Attenuation coefficients for aluminum (atomic number  $Z = 13$ ).

Energy (MeV)	Cross Section ( $10^{-28} \text{ m}^2$ )			Attenuation Coefficient $\mu$		
	Scattering	Photoelectric	Pair	Atomic ( $10^{-28} \text{ m}^2$ )	Mass <sup>a</sup> ( $\text{cm}^2\text{-g}^{-1}$ )	Linear <sup>b</sup> ( $\text{cm}^{-1}$ )
0.01	29	1170	—	1200	26.8	72.4
0.015	19	343	—	362	8.08	21.8
0.02	15	141	—	156	3.48	9.40
0.03	11.7	39.0	—	50.7	1.13	3.05
0.04	9.7	15.2	—	24.9	0.556	1.50
0.05	8.7	7.3	—	16.0	0.357	0.964
0.06	8.1	4.0	—	12.1	0.270	0.729
0.08	7.34	1.60	—	8.94	0.200	0.540
0.10	6.82	0.78	—	7.60	0.170	0.459
0.15	5.96	0.21	—	6.17	0.138	0.373
0.20	5.39	0.08	—	5.47	0.122	0.329
0.30	4.64	0.02	—	4.66	0.104	0.281
0.40	4.14	0.01	—	4.15	0.0927	0.250
0.50	3.78	—	—	3.78	0.0844	0.228
0.60	3.49	—	—	3.49	0.0779	0.210
0.80	3.06	—	—	3.06	0.0683	0.184
1.0	2.75	—	—	2.75	0.0614	0.166
1.5	2.23	—	0.01	2.24	0.0500	0.135
2.0	1.90	—	0.03	1.93	0.0431	0.116
3.0	1.50	—	0.09	1.59	0.0355	0.0959
4.0	1.25	—	0.14	1.39	0.0310	0.0837
5.0	1.08	—	0.19	1.27	0.0284	0.0767
6.0	0.952	—	0.237	1.19	0.0266	0.0718
8.0	0.778	—	0.311	1.09	0.0243	0.0656
10	0.663	—	0.365	1.03	0.0230	0.0621
15	0.490	—	0.484	0.974	0.0217	0.0586
20	0.393	—	0.570	0.963	0.0215	0.0581
30	0.286	—	0.690	0.976	0.0218	0.0589

a. Mass attenuation coefficient is calculated by using relative atomic mass  $A_r = 26.98$ .

b. Linear attenuation coefficient is calculated by using density  $\rho = 2.70 \text{ g}\cdot\text{cm}^{-3}$ .

TABLE 9. Attenuation coefficients for silicon (atomic number  $Z = 14$ ).

Energy (MeV)	Cross Section ( $10^{-28} \text{ m}^2$ )			Attenuation Coefficient $\mu$		
	Scattering	Photoelectric	Pair	Atomic ( $10^{-28} \text{ m}^2$ )	Mass <sup>a</sup> ( $\text{cm}^2\text{-g}^{-1}$ )	Linear <sup>b</sup> ( $\text{cm}^{-1}$ )
0.01	33	1580	—	1610	34.5	81.1
0.015	22	470	—	492	10.6	24.9
0.02	17	194	—	211	4.53	10.6
0.03	12.8	54.4	—	67.2	1.44	3.38
0.04	10.8	21.4	—	32.2	0.691	1.62
0.05	9.6	10.3	—	19.9	0.427	1.00
0.06	8.9	5.8	—	14.7	0.315	0.740
0.08	8.0	2.3	—	10.3	0.221	0.519
0.10	7.38	1.10	—	8.48	0.182	0.428
0.15	6.44	0.29	—	6.73	0.144	0.338
0.20	5.82	0.12	—	5.94	0.127	0.298
0.30	5.01	0.04	—	5.05	0.108	0.254
0.40	4.46	0.02	—	4.48	0.0961	0.226
0.50	4.07	—	—	4.07	0.0873	0.205
0.60	3.75	—	—	3.75	0.0804	0.189
0.80	3.30	—	—	3.30	0.0708	0.166
1.0	2.96	—	—	2.96	0.0635	0.149
1.5	2.40	—	0.01	2.41	0.0517	0.121
2.0	2.05	—	0.04	2.09	0.0448	0.105
3.0	1.61	—	0.10	1.71	0.0367	0.0862
4.0	1.34	—	0.16	1.50	0.0322	0.0757
5.0	1.16	—	0.23	1.39	0.0298	0.0700
6.0	1.03	—	0.28	1.31	0.0281	0.0660
8.0	0.84	—	0.35	1.19	0.0255	0.0599
10	0.714	—	0.426	1.14	0.0245	0.0576
15	0.528	—	0.565	1.09	0.0234	0.0550
20	0.423	—	0.663	1.09	0.0234	0.0550
30	0.308	—	0.793	1.10	0.0236	0.0555

a. Mass attenuation coefficient is calculated by using relative atomic mass  $A_r = 28.09$ .

b. Linear attenuation coefficient is calculated by using density  $\rho = 2.35 \text{ g}\cdot\text{cm}^{-3}$ .

TABLE 10. Attenuation coefficients for argon (atomic number  $Z = 18$ ).

Energy (MeV)	Cross Section ( $10^{-28} \text{ m}^2$ )			Attenuation Coefficient $\mu$		
	Scattering	Photoelectric	Pair	Atomic ( $10^{-28} \text{ m}^2$ )	Mass <sup>a</sup> ( $\text{cm}^2\text{-g}^{-1}$ )	Linear <sup>b</sup> ( $\text{cm}^{-1}$ )
0.01	56	4280	—	4340	65.4	$10.9 \times 10^{-2}$
0.015	36	1320	—	1360	20.5	$3.41 \times 10^{-2}$
0.02	27	561	—	588	8.87	$1.48 \times 10^{-2}$
0.03	19	164	—	183	2.76	$0.459 \times 10^{-2}$
0.04	15.6	64.5	—	80.1	1.21	$0.201 \times 10^{-2}$
0.05	13.6	31.6	—	45.2	0.682	$0.113 \times 10^{-2}$
0.06	12.4	18.0	—	30.4	0.458	$0.0762 \times 10^{-2}$
0.08	10.8	7.2	—	18.0	0.271	$0.0451 \times 10^{-2}$
0.10	9.85	3.60	—	13.5	0.204	$0.0339 \times 10^{-2}$
0.15	8.43	0.98	—	9.41	0.142	$0.0236 \times 10^{-2}$
0.20	7.57	0.41	—	7.98	0.120	$0.0200 \times 10^{-2}$
0.30	6.48	0.12	—	6.60	0.0995	$0.0165 \times 10^{-2}$
0.40	5.76	0.05	—	5.81	0.0876	$0.0146 \times 10^{-2}$
0.50	5.24	0.03	—	5.27	0.0795	$0.0132 \times 10^{-2}$
0.60	4.84	0.02	—	4.86	0.0733	$0.0122 \times 10^{-2}$
0.80	4.24	—	—	4.24	0.0639	$0.0106 \times 10^{-2}$
1.0	3.81	—	—	3.81	0.0575	$0.00956 \times 10^{-2}$
1.5	3.09	—	0.02	3.11	0.0469	$0.00780 \times 10^{-2}$
2.0	2.64	—	0.06	2.70	0.0407	$0.00677 \times 10^{-2}$
3.0	2.07	—	0.17	2.24	0.0338	$0.00562 \times 10^{-2}$
4.0	1.73	—	0.27	2.00	0.0302	$0.00502 \times 10^{-2}$
5.0	1.49	—	0.37	1.86	0.0280	$0.00466 \times 10^{-2}$
6.0	1.32	—	0.45	1.77	0.0267	$0.00444 \times 10^{-2}$
8.0	1.08	—	0.59	1.67	0.0252	$0.00419 \times 10^{-2}$
10	0.918	—	0.691	1.61	0.0243	$0.00404 \times 10^{-2}$
15	0.679	—	0.913	1.59	0.0240	$0.00399 \times 10^{-2}$
20	0.544	—	1.06	1.60	0.0241	$0.00401 \times 10^{-2}$
30	0.396	—	1.29	1.69	0.0255	$0.00424 \times 10^{-2}$

a. Mass attenuation coefficient is calculated by using relative atomic mass  $A_r = 39.944$ .b. Linear attenuation coefficient is calculated by using density  $\rho = 1.663 \times 10^{-3} \text{ g}\cdot\text{cm}^{-3}$ .



TABLE 11. Attenuation coefficients for calcium (atomic number  $Z = 20$ ).

Energy (MeV)	Cross Section ( $10^{-28} \text{ m}^2$ )			Attenuation Coefficient $\mu$		
	Scattering	Photoelectric	Pair	Atomic ( $10^{-28} \text{ m}^2$ )	Mass <sup>a</sup> ( $\text{cm}^2\text{-g}^{-1}$ )	Linear <sup>b</sup> ( $\text{cm}^{-1}$ )
0.01	69	6380	—	6450	96.9	149
0.015	44	2010	—	2050	30.8	47.4
0.02	33	859	—	892	13.4	20.6
0.03	24	254	—	278	4.18	6.44
0.04	19	102	—	121	1.82	2.80
0.05	15.8	50.6	—	66.4	0.098	1.54
0.06	14.3	28.8	—	43.1	0.648	0.998
0.08	12.3	11.6	—	23.9	0.359	0.553
0.10	11.2	6.0	—	17.2	0.259	0.399
0.15	9.48	1.60	—	11.1	0.167	0.257
0.20	8.47	0.67	—	9.14	0.137	0.211
0.30	7.23	0.20	—	7.43	0.112	0.172
0.40	6.42	0.09	—	6.51	0.0978	0.151
0.50	5.84	0.05	—	5.89	0.0885	0.136
0.60	5.38	0.03	—	5.41	0.0813	0.125
0.80	4.72	0.01	—	4.73	0.0711	0.109
1.0	4.24	—	—	4.24	0.0637	0.0981
1.5	3.43	—	0.02	3.45	0.0518	0.0798
2.0	2.93	—	0.07	3.00	0.0451	0.0695
3.0	2.30	—	0.21	2.51	0.0377	0.0581
4.0	1.92	—	0.33	2.25	0.0338	0.0521
5.0	1.66	—	0.45	2.11	0.0317	0.0488
6.0	1.46	—	0.55	2.01	0.0302	0.0465
8.0	1.20	—	0.72	1.92	0.0289	0.0445
10	1.02	—	0.84	1.86	0.0280	0.0431
15	0.755	—	1.12	1.88	0.0283	0.0436
20	0.605	—	1.31	1.92	0.0289	0.0445
30	0.440	—	1.57	2.01	0.0302	0.0465

a. Mass attenuation coefficient is calculated by using relative atomic mass  $A_r = 40.08$ .

b. Linear attenuation coefficient is calculated by using density  $\rho = 1.54 \text{ g}\cdot\text{cm}^{-3}$ .

TABLE 12. Attenuation coefficients for titanium (atomic number  $Z = 22$ ).

Energy (MeV)	Cross Section ( $10^{-28} \text{ m}^2$ )			Attenuation Coefficient $\mu$		
	Scattering	Photoelectric	Pair	Atomic ( $10^{-28} \text{ m}^2$ )	Mass <sup>a</sup> ( $\text{cm}^2\text{-g}^{-1}$ )	Linear <sup>b</sup> ( $\text{cm}^{-1}$ )
0.01	84	9150	—	9230	116	527
0.015	53	2900	—	2950	37.1	168
0.02	39	1250	—	1290	16.2	73.5
0.03	27	374	—	401	5.04	22.9
0.04	22	154	—	176	2.21	10.0
0.05	18.3	76.3	—	94.6	1.19	5.40
0.06	16.3	43.9	—	60.2	0.757	3.44
0.08	14.0	17.9	—	31.9	0.401	1.82
0.10	12.5	9.2	—	21.7	0.273	1.24
0.15	10.6	2.5	—	13.1	0.165	0.749
0.20	9.40	1.04	—	10.4	0.131	0.595
0.30	7.99	0.31	—	8.30	0.104	0.472
0.40	7.09	0.13	—	7.22	0.0908	0.412
0.50	6.43	0.07	—	6.50	0.0818	0.371
0.60	5.94	0.05	—	5.99	0.0754	0.342
0.80	5.19	0.02	—	5.21	0.0655	0.297
1.0	4.66	0.01	—	4.67	0.0587	0.266
1.5	3.78	0.01	0.02	3.81	0.0479	0.217
2.0	3.22	—	0.09	3.31	0.0416	0.189
3.0	2.53	—	0.25	2.78	0.0350	0.159
4.0	2.11	—	0.41	2.52	0.0317	0.144
5.0	1.82	—	0.54	2.36	0.0297	0.135
6.0	1.61	—	0.67	2.28	0.0287	0.130
8.0	1.32	—	0.86	2.18	0.0274	0.124
10	1.12	—	1.02	2.14	0.0269	0.122
15	0.829	—	1.34	2.17	0.0273	0.124
20	0.664	—	1.58	2.24	0.0282	0.128
30	0.484	—	1.90	2.38	0.0299	0.136

a. Mass attenuation coefficient is calculated by using relative atomic mass  $A_r = 47.9$ .

b. Linear attenuation coefficient is calculated by using density  $\rho = 4.54 \text{ g}\cdot\text{cm}^{-3}$ .

TABLE 13. Attenuation coefficients for vanadium (atomic number  $Z = 23$ ).

Energy (MeV)	Cross Section ( $10^{-28} \text{ m}^2$ )			Attenuation Coefficient $\mu$		
	Scattering	Photoelectric	Pair	Atomic ( $10^{-28} \text{ m}^2$ )	Mass <sup>a</sup> ( $\text{cm}^2\text{-g}^{-1}$ )	Linear <sup>b</sup> ( $\text{cm}^{-1}$ )
0.01	92	10 700	—	10 800	128	763
0.015	58	3430	—	3490	41.3	246
0.02	43	1490	—	1530	18.1	108
0.03	29	449	—	478	5.65	33.7
0.04	23	185	—	208	2.46	14.7
0.05	19.6	92.7	—	112	1.32	7.87
0.06	17.4	53.3	—	70.7	0.836	4.98
0.08	14.8	21.8	—	36.6	0.443	2.58
0.10	13.3	11.1	—	24.4	0.289	1.72
0.15	11.1	3.1	—	14.2	0.168	1.00
0.20	9.85	1.27	—	11.1	0.131	0.781
0.30	8.36	0.38	—	8.74	0.103	0.614
0.40	7.41	0.16	—	7.57	0.0896	0.534
0.50	6.73	0.09	—	6.82	0.0807	0.481
0.60	6.20	0.06	—	6.26	0.0741	0.442
0.80	5.44	0.03	—	5.47	0.0647	0.386
1.0	4.88	0.02	—	4.90	0.0580	0.346
1.5	3.96	0.01	0.03	4.00	0.0473	0.282
2.0	3.37	—	0.09	3.46	0.0409	0.244
3.0	2.65	—	0.28	2.93	0.0347	0.207
4.0	2.21	—	0.44	2.65	0.0313	0.187
5.0	1.90	—	0.60	2.50	0.0296	0.176
6.0	1.68	—	0.73	2.41	0.0285	0.170
8.0	1.38	—	0.94	2.32	0.0274	0.163
10	1.17	—	1.12	2.29	0.0271	0.162
15	0.867	—	1.46	2.33	0.0276	0.164
20	0.695	—	1.74	2.44	0.0289	0.172
30	0.506	—	2.06	2.57	0.0304	0.181

a. Mass attenuation coefficient is calculated by using relative atomic mass  $A_r = 50.95$ .

b. Linear attenuation coefficient is calculated by using density  $\rho = 5.96 \text{ g}\cdot\text{cm}^{-3}$ .

TABLE 14. Attenuation coefficients for chromium (atomic number  $Z = 24$ ).

Energy (MeV)	Cross Section ( $10^{-28} \text{ m}^2$ )			Attenuation Coefficient $\mu$		
	Scattering	Photoelectric	Pair	Atomic ( $10^{-28} \text{ m}^2$ )	Mass <sup>a</sup> ( $\text{cm}^2\text{-g}^{-1}$ )	Linear <sup>b</sup> ( $\text{cm}^{-1}$ )
0.01	101	12 500	—	12 600	146	1050
0.015	64	4040	—	4100	47.5	342
0.02	47	1760	—	1810	21.0	151
0.03	32	533	—	565	6.54	47.0
0.04	25	221	—	246	2.85	20.5
0.05	21	111	—	132	1.53	11.0
0.06	18.5	63.9	—	82.4	0.954	6.86
0.08	15.7	26.3	—	42.0	0.486	3.49
0.10	14.0	13.5	—	27.5	0.318	2.29
0.15	11.7	3.75	—	15.5	0.179	1.29
0.20	10.3	1.55	—	11.9	0.138	0.992
0.30	8.74	0.46	—	9.20	0.107	0.769
0.40	7.75	0.20	—	7.95	0.0921	0.662
0.50	7.03	0.11	—	7.14	0.0827	0.595
0.60	6.48	0.07	—	6.55	0.0758	0.545
0.80	5.67	0.03	—	5.70	0.0660	0.475
1.0	5.09	0.02	—	5.11	0.0592	0.426
1.5	4.13	0.01	0.03	4.17	0.0483	0.347
2.0	3.51	0.01	0.11	3.63	0.0420	0.302
3.0	2.76	—	0.30	3.06	0.0354	0.255
4.0	2.30	—	0.48	2.78	0.0322	0.232
5.0	1.99	—	0.65	2.64	0.0306	0.220
6.0	1.76	—	0.79	2.55	0.0295	0.212
8.0	1.44	—	1.02	2.46	0.0285	0.205
10	1.22	—	1.21	2.43	0.0281	0.202
15	0.905	—	1.59	2.50	0.0290	0.209
20	0.725	—	1.87	2.60	0.0301	0.216
30	0.528	—	2.24	2.77	0.0321	0.231

a. Mass attenuation coefficient is calculated by using relative atomic mass  $A_r = 52.01$ .

b. Linear attenuation coefficient is calculated by using density  $\rho = 7.19 \text{ g}\cdot\text{cm}^{-3}$ .

TABLE 15. Attenuation coefficients for manganese (atomic number  $Z = 25$ ).

Energy (MeV)	Cross Section ( $10^{-28} \text{ m}^2$ )			Attenuation Coefficient $\mu$		
	Scattering	Photoelectric	Pair	Atomic ( $10^{-28} \text{ m}^2$ )	Mass <sup>a</sup> ( $\text{cm}^2\text{-g}^{-1}$ )	Linear <sup>b</sup> ( $\text{cm}^{-1}$ )
0.01	110	14 400	—	14 500	159	1180
0.015	70	4690	—	4760	52.2	388
0.02	51	2051	—	2100	23.0	171
0.03	34	626	—	660	7.24	53.8
0.04	27	263	—	290	3.18	23.6
0.05	22	132	—	154	1.69	12.6
0.06	19.7	76.2	—	95.9	1.05	7.80
0.08	16.6	31.4	—	48.0	0.527	3.92
0.10	14.7	16.2	—	30.9	0.339	2.52
0.15	12.2	4.51	—	16.7	0.183	1.36
0.20	10.8	1.88	—	12.7	0.139	1.03
0.30	9.13	0.56	—	9.69	0.106	0.788
0.40	8.09	0.24	—	8.33	0.0914	0.679
0.50	7.33	0.13	—	7.46	0.0818	0.608
0.60	6.76	0.08	—	6.84	0.0750	0.557'
0.80	5.91	0.04	—	5.95	0.0653	0.485
1.0	5.30	0.03	—	5.33	0.0585	0.435
1.5	4.30	0.01	0.03	4.34	0.0476	0.354
2.0	3.66	0.01	0.12	3.79	0.0416	0.309
3.0	2.88	—	0.33	3.21	0.0352	0.262
4.0	2.40	—	0.52	2.92	0.0320	0.238
5.0	2.07	—	0.70	2.77	0.0304	0.226
6.0	1.83	—	0.86	2.69	0.0295	0.219
8.0	1.50	—	1.11	2.61	0.0286	0.212
10	1.28	—	1.31	2.59	0.0284	0.211
15	0.943	—	1.72	2.66	0.0292	0.217
20	0.755	—	2.02	2.78	0.0305	0.227
30	0.55	—	2.43	2.98	0.0327	0.243

a. Mass attenuation coefficient is calculated by using relative atomic mass  $A_r = 54.93$ .

b. Linear attenuation coefficient is calculated by using density  $\rho = 7.43 \text{ g}\cdot\text{cm}^{-3}$ .



TABLE 16. Attenuation coefficients for iron (atomic number  $Z = 26$ ).

Energy (MeV)	Cross Section ( $10^{-28} \text{ m}^2$ )			Attenuation Coefficient $\mu$		
	Scattering	Photoelectric	Pair	Atomic ( $10^{-28} \text{ m}^2$ )	Mass <sup>a</sup> ( $\text{cm}^2\text{-g}^{-1}$ )	Linear <sup>b</sup> ( $\text{cm}^{-1}$ )
0.01	120	16 500	—	16 600	179	1410
0.015	75	5380	—	5460	58.9	464
0.02	55	2380	—	2440	26.3	207
0.03	37	729	—	766	8.27	65.1
0.04	29	308	—	337	3.64	28.6
0.05	24	155	—	179	1.93	15.2
0.06	20.9	90.7	—	112	1.21	9.52
0.08	17.5	38.0	—	55.5	0.599	4.71
0.10	15.4	19.1	—	34.5	0.372	2.93
0.15	12.8	5.4	—	18.2	0.196	1.54
0.20	11.3	2.2	—	13.5	0.146	1.15
0.30	9.50	0.66	—	10.2	0.110	0.866
0.40	8.42	0.29	—	8.71	0.0940	0.740
0.50	7.63	0.16	—	7.79	0.0841	0.662
0.60	7.03	0.10	—	7.13	0.0769	0.605
0.80	6.15	0.05	—	6.20	0.0669	0.527
1.0	5.52	0.03	—	5.55	0.0599	0.471
1.5	4.46	0.02	0.03	4.51	0.0487	0.383
2.0	3.81	0.01	0.12	3.94	0.0425	0.334
3.0	2.99	—	0.35	3.34	0.0360	0.283
4.0	2.50	—	0.57	3.07	0.0331	0.260
5.0	2.15	—	0.76	2.91	0.0314	0.247
6.0	1.90	—	0.92	2.82	0.0304	0.239
8.0	1.56	—	1.20	2.76	0.0298	0.235
10	1.33	—	1.41	2.74	0.0296	0.233
15	0.981	—	1.86	2.84	0.0306	0.241
20	0.786	—	2.17	2.96	0.0319	0.251
30	0.572	—	2.61	3.18	0.0343	0.270

a. Mass attenuation coefficient is calculated by using relative atomic mass  $A_r = 55.85$ .

b. Linear attenuation coefficient is calculated by using density  $\rho = 7.87 \text{ g}\cdot\text{cm}^{-3}$ .

TABLE 17. Attenuation coefficients for cobalt (atomic number  $Z = 27$ ).

Energy (MeV)	Cross Section ( $10^{-28} \text{ m}^2$ )			Attenuation Coefficient $\mu$		
	Scattering	Photoelectric	Pair	Atomic ( $10^{-28} \text{ m}^2$ )	Mass <sup>a</sup> ( $\text{cm}^2\text{-g}^{-1}$ )	Linear <sup>b</sup> ( $\text{cm}^{-1}$ )
0.01	130	18 800	—	18 900	193	1720
0.015	82	6170	—	6250	63.9	569
0.02	60	2760	—	2820	28.8	256
0.03	40	848	—	888	9.08	80.8
0.04	31	360	—	391	4.00	35.6
0.05	25	181	—	206	2.11	18.8
0.06	22	106	—	128	1.31	11.7
0.08	18.5	43.8	—	62.3	0.637	5.67
0.10	16.3	22.5	—	38.8	0.397	3.53
0.15	13.4	6.40	—	19.8	0.202	1.80
0.20	11.8	2.65	—	14.5	0.148	1.32
0.30	9.91	0.80	—	10.7	0.109	0.970
0.40	8.75	0.34	—	9.09	0.0929	0.827
0.50	7.94	0.19	—	8.13	0.0831	0.740
0.60	7.30	0.12	—	7.42	0.0758	0.675
0.80	6.39	0.06	—	6.45	0.0659	0.587
1.0	5.73	0.04	—	5.77	0.0590	0.525
1.5	4.64	0.02	0.03	4.69	0.0479	0.426
2.0	3.96	0.01	0.14	4.11	0.0420	0.374
3.0	3.11	0.01	0.38	3.50	0.0358	0.319
4.0	2.59	—	0.61	3.20	0.0327	0.291
5.0	2.24	—	0.82	3.06	0.0313	0.279
6.0	1.98	—	1.00	2.98	0.0305	0.271
8.0	1.62	—	1.29	2.91	0.0297	0.264
10	1.38	—	1.53	2.91	0.0297	0.264
15	1.02	—	2.00	3.02	0.0309	0.275
20	0.815	—	2.35	3.17	0.0324	0.288
30	0.594	—	2.82	3.41	0.0349	0.311

a. Mass attenuation coefficient is calculated by using relative atomic mass  $A_r = 58.94$ .

b. Linear attenuation coefficient is calculated by using density  $\rho = 8.90 \text{ g}\cdot\text{cm}^{-3}$ .

TABLE 18. Attenuation coefficients for nickel (atomic number  $Z = 28$ ).

Energy (MeV)	Cross Section ( $10^{-28} \text{ m}^2$ )			Attenuation Coefficient $\mu$		
	Scattering	Photoelectric	Pair	Atomic ( $10^{-28} \text{ m}^2$ )	Mass <sup>a</sup> ( $\text{cm}^2\text{-g}^{-1}$ )	Linear <sup>b</sup> ( $\text{cm}^{-1}$ )
0.01	141	21 300	—	21 400	220	1950
0.015	89	7020	—	7110	73.0	646
0.02	65	3160	—	3230	33.2	294
0.03	43	984	—	1030	10.6	93.8
0.04	33	418	—	451	4.63	41.0
0.05	27	210	—	237	2.43	21.5
0.06	23	123	—	146	1.50	13.3
0.08	19.4	51.1	—	70.5	0.724	6.41
0.10	17.1	26.4	—	43.5	0.447	3.96
0.15	14.0	7.52	—	21.5	0.221	1.96
0.20	12.3	3.12	—	15.4	0.158	1.40
0.30	10.3	0.95	—	11.3	0.116	1.03
0.40	9.10	0.41	—	9.51	0.0977	0.865
0.50	8.24	0.22	—	8.46	0.0869	0.769
0.60	7.58	0.14	—	7.72	0.0793	0.702
0.80	6.63	0.07	—	6.70	0.0688	0.609
1.0	5.94	0.04	—	5.98	0.0614	0.543
1.5	4.81	0.02	0.04	4.87	0.0500	0.443
2.0	4.11	0.01	0.15	4.27	0.0439	0.389
3.0	3.22	0.01	0.41	3.64	0.0374	0.331
4.0	2.69	0.01	0.65	3.35	0.0344	0.304
5.0	2.32	—	0.88	3.20	0.0329	0.291
6.0	2.05	—	1.07	3.12	0.0320	0.283
8.0	1.68	—	1.39	3.07	0.0315	0.279
10	1.43	—	1.64	3.07	0.0315	0.279
15	1.06	—	2.14	3.20	0.0329	0.291
20	0.846	—	2.52	3.37	0.0346	0.306
30	0.616	—	3.02	3.64	0.0374	0.331

a. Mass attenuation coefficient is calculated by using relative atomic mass  $A_r = 58.69$ .

b. Linear attenuation coefficient is calculated by using density  $\rho = 8.85 \text{ g}\cdot\text{cm}^{-3}$ .

TABLE 19. Attenuation coefficients for copper (atomic number  $Z = 29$ ).

Energy (MeV)	Cross Section ( $10^{-28} \text{ m}^2$ )			Attenuation Coefficient $\mu$		
	Scattering	Photoelectric	Pair	Atomic ( $10^{-28} \text{ m}^2$ )	Mass <sup>a</sup> ( $\text{cm}^2\cdot\text{g}^{-1}$ )	Linear <sup>b</sup> ( $\text{cm}^{-1}$ )
0.01	150	23 600	—	23 800	226	2010
0.015	96	8000	—	8100	76.8	684
0.02	70	3580	—	3650	34.6	308
0.03	46	1120	—	1170	11.1	98.8
0.04	35	474	—	509	4.83	43.0
0.05	29	242	—	271	2.57	22.9
0.06	24	143	—	167	1.58	14.1
0.08	20.5	60.2	—	80.7	0.765	6.81
0.10	17.9	30.7	—	48.6	0.461	4.10
0.15	14.5	8.9	—	23.4	0.222	1.98
0.20	12.8	3.7	—	16.5	0.156	1.39
0.30	10.7	1.1	—	11.8	0.112	0.997
0.40	9.43	0.48	—	9.91	0.0940	0.837
0.50	8.54	0.26	—	8.80	0.0834	0.742
0.60	7.86	0.16	—	8.02	0.0760	0.676
0.80	6.87	0.08	—	6.95	0.0659	0.587
1.0	6.16	0.05	—	6.21	0.0589	0.524
1.5	4.98	0.02	0.04	5.04	0.0478	0.425
2.0	4.25	0.02	0.16	4.43	0.0420	0.374
3.0	3.34	0.01	0.44	3.79	0.0359	0.320
4.0	2.78	0.01	0.71	3.50	0.0332	0.295
5.0	2.40	0.01	0.95	3.36	0.0319	0.284
6.0	2.12	—	1.16	3.28	0.0311	0.277
8.0	1.74	—	1.48	3.22	0.0305	0.271
10	1.48	—	1.75	3.23	0.0306	0.272
15	1.09	—	2.29	3.38	0.0320	0.285
20	0.877	—	2.69	3.57	0.0339	0.302
30	0.638	—	3.23	3.87	0.0367	0.327

a. Mass attenuation coefficient is calculated by using relative atomic mass  $A_r = 63.54$ .

b. Linear attenuation coefficient is calculated by using density  $\rho = 8.90 \text{ g}\cdot\text{cm}^{-3}$ .

TABLE 20. Attenuation coefficients for zinc (atomic number  $Z = 30$ ).

Energy (MeV)	Cross Section ( $10^{-28} \text{ m}^2$ )			Attenuation Coefficient $\mu$		
	Scattering	Photoelectric	Pair	Atomic ( $10^{-28} \text{ m}^2$ )	Mass <sup>a</sup> ( $\text{cm}^2\text{-g}^{-1}$ )	Linear <sup>b</sup> ( $\text{cm}^{-1}$ )
0.01	164	26 400	—	26 600	245	1750
0.015	103	8920	—	9020	83.1	593
0.02	75	4060	—	4140	38.2	272
0.03	49	1280	—	1330	12.3	87.7
0.04	37	549	—	586	5.40	38.5
0.05	29	276	—	305	2.81	20.0
0.06	26	163	—	189	1.74	12.4
0.08	21.5	68.5	—	90.0	0.829	5.91
0.10	18.7	35.5	—	54.2	0.499	3.56
0.15	15.2	10.2	—	25.4	0.234	1.67
0.20	13.2	4.28	—	17.5	0.161	1.15
0.30	11.1	1.29	—	12.4	0.114	0.83
0.40	9.77	0.56	—	10.3	0.0949	0.677
0.50	8.85	0.30	—	9.15	0.0843	0.601
0.60	8.14	0.19	—	8.33	0.0768	0.548
0.80	7.11	0.09	—	7.20	0.0663	0.473
1.0	6.38	0.06	—	6.44	0.0593	0.423
1.5	5.16	0.03	0.04	5.23	0.0482	0.344
2.0	4.40	0.02	0.17	4.59	0.0423	0.302
3.0	3.45	0.01	0.47	3.92	0.0361	0.258
4.0	2.88	0.01	0.74	3.63	0.0335	0.239
5.0	2.48	0.01	1.01	3.50	0.0323	0.230
6.0	2.20	0.01	1.22	3.43	0.0316	0.225
8.0	1.80	—	1.59	3.39	0.0312	0.223
10	1.53	—	1.87	3.40	0.0313	0.223
15	1.13	—	2.45	3.58	0.0330	0.235
20	0.906	—	2.87	3.78	0.0348	0.248
30	0.660	—	3.45	4.11	0.0379	0.270

a. Mass attenuation coefficient is calculated by using relative atomic mass  $A_r = 65.38$ .b. Linear attenuation coefficient is calculated by using density  $\rho = 7.133 \text{ g}\cdot\text{cm}^{-3}$ .



TABLE 21. Attenuation coefficients for germanium (atomic number  $Z = 32$ ).

Energy (MeV)	Cross Section ( $10^{-28} \text{ m}^2$ )			Attenuation Coefficient $\mu$		
	Scattering	Photoelectric	Pair	Atomic ( $10^{-28} \text{ m}^2$ )	Mass <sup>a</sup> ( $\text{cm}^2\text{-g}^{-1}$ )	Linear <sup>b</sup> ( $\text{cm}^{-1}$ )
0.01	189.0	3690	—	3880	32.2	173
0.01112	170.0	3000	—	3170	26.3	141
K 0.01112 <sup>c</sup>	170.0	27500	—	27700	230	1230
0.015	119.0	11100	—	11200	93.0	498
0.02	86.0	5130	—	5220	43.3	232
0.03	56.0	1640	—	1700	14.1	75.6
0.04	42.0	708	—	750	6.23	33.4
0.05	34.0	356	—	390	3.24	17.4
0.06	29.0	212	—	241	2.00	10.7
0.08	23.7	89.9	—	114	0.946	5.07
0.10	20.5	46.6	—	67.1	0.557	2.99
0.15	16.4	13.5	—	29.9	0.248	1.33
0.20	14.3	5.70	—	20.0	0.166	0.890
0.30	11.9	1.74	—	13.6	0.113	0.606
0.40	10.5	0.76	—	11.3	0.0938	0.503
0.50	9.45	0.41	—	9.86	0.0818	0.438
0.60	8.70	0.26	—	8.96	0.0744	0.399
0.80	7.59	0.13	—	7.72	0.0641	0.344
1.0	6.80	0.08	—	6.88	0.0571	0.306
1.5	5.51	0.04	0.05	5.60	0.0465	0.249
2.0	4.69	0.03	0.19	4.91	0.0408	0.219
3.0	3.69	0.01	0.54	4.24	0.0352	0.189
4.0	3.07	0.01	0.86	3.94	0.0327	0.175
5.0	2.65	0.01	1.15	3.81	0.0316	0.169
6.0	2.34	0.01	1.39	3.74	0.0310	0.166
8.0	1.92	0.01	1.81	3.74	0.0310	0.166
10	1.63	—	2.13	3.76	0.0312	0.167
15	1.21	—	2.78	3.99	0.0331	0.177
20	0.966	—	3.25	4.22	0.0350	0.188
30	0.704	—	3.91	4.61	0.0383	0.205

a. Mass attenuation coefficient is calculated by using relative atomic mass  $A_r = 72.60$ .

b. Linear attenuation coefficient is calculated by using density  $\rho = 5.36 \text{ g}\cdot\text{cm}^{-3}$ .

c. K = K absorption edge.

TABLE 22. Attenuation coefficients for selenium (atomic number  $Z = 34$ ).

Energy (MeV)	Cross Section ( $10^{-28} \text{ m}^2$ )			Attenuation Coefficient $\mu$		
	Scattering	Photoelectric	Pair	Atomic ( $10^{-28} \text{ m}^2$ )	Mass <sup>a</sup> ( $\text{cm}^2\text{-g}^{-1}$ )	Linear <sup>b</sup> ( $\text{cm}^{-1}$ )
0.01	215	4410	—	4630	35.3	170.0
0.01268	172	2530	—	2700	20.6	99.1
K 0.01268 <sup>c</sup>	172	22 300	—	22 500	172	827
0.015	137	13 600	—	13 700	105	505
0.02	98	6360	—	6460	49.3	237
0.03	63	2050	—	2110	16.1	77.4
0.04	47	895	—	942	7.19	34.6
0.05	38	454	—	492	3.75	18.0
0.06	32	270	—	302	2.30	11.1
0.08	26	116	—	142	1.08	5.19
0.10	22.3	60.2	—	82.5	0.629	3.03
0.15	17.7	17.7	—	35.4	0.270	1.30
0.20	15.1	7.45	—	22.6	0.172	0.827
0.30	12.7	2.28	—	15.0	0.114	0.548
0.40	11.2	1.00	—	12.2	0.0931	0.448
0.50	10.1	0.54	—	10.6	0.0809	0.389
0.60	9.26	0.34	—	9.60	0.0732	0.352
0.80	8.07	0.17	—	8.24	0.0629	0.303
1.0	7.23	0.11	—	7.34	0.0560	0.269
1.5	5.85	0.05	0.06	5.96	0.0455	0.219
2.0	4.99	0.03	0.22	5.24	0.0400	0.192
3.0	3.92	0.02	0.61	4.55	0.0347	0.167
4.0	3.26	0.01	0.96	4.23	0.0323	0.155
5.0	2.82	0.01	1.30	4.13	0.0315	0.152
6.0	2.49	0.01	1.57	4.07	0.0311	0.150
8.0	2.04	0.01	2.04	4.09	0.0312	0.150
10.0	1.73	0.01	2.39	4.13	0.0315	0.152
15.0	1.28	—	3.12	4.40	0.0336	0.162
20	1.03	—	3.66	4.69	0.0358	0.172
30	0.748	—	4.39	5.14	0.0392	0.189

a. Mass attenuation coefficient is calculated by using relative atomic mass  $A_r = 78.96$ .

b. Linear attenuation coefficient is calculated by using density  $\rho = 4.81 \text{ g}\cdot\text{cm}^{-3}$ .

c. K = K absorption edge.

TABLE 23. Attenuation coefficients for zirconium (atomic number  $Z = 40$ ).

Energy (MeV)	Cross Section ( $10^{-28} \text{ m}^2$ )			Attenuation Coefficient $\mu$		
	Scattering	Photoelectric	Pair	Atomic ( $10^{-28} \text{ m}^2$ )	Mass <sup>a</sup> ( $\text{cm}^2\text{-g}^{-1}$ )	Linear <sup>b</sup> ( $\text{cm}^{-1}$ )
0.01	309	9220	—	9530	62.9	411
0.015	196	2820	—	3020	19.9	130
0.01760	171	1790	—	1960	12.9	84.2
K 0.01760 <sup>c</sup>	171	15800	—	16000	106	692
0.02	140	11000	—	11100	73.3	479
0.03	88	3710	—	3800	25.1	164
0.04	65	1650	—	1720	11.4	74.4
0.05	51	850	—	901	5.95	38.9
0.06	43	512	—	555	3.67	24.0
0.08	33	226	—	259	1.71	11.2
0.10	28	117	—	145	0.958	6.26
0.15	21.8	35.3	—	57.1	0.377	2.46
0.20	18.5	15.2	—	33.7	0.223	1.46
0.30	15.2	4.68	—	19.9	0.131	0.855
0.40	13.3	2.08	—	15.4	0.102	0.666
0.50	11.9	1.13	—	13.0	0.0859	0.561
0.60	11.0	0.71	—	11.7	0.0773	0.505
0.80	9.53	0.36	—	9.89	0.0653	0.426
1.0	8.53	0.23	—	8.76	0.0579	0.378
1.5	6.89	0.11	0.08	7.08	0.0468	0.306
2.0	5.88	0.07	0.32	6.27	0.0414	0.270
3.0	4.61	0.04	0.85	5.50	0.0363	0.237
4.0	3.84	0.03	1.35	5.22	0.0345	0.225
5.0	3.31	0.02	1.80	5.13	0.0339	0.221
6.0	2.93	0.02	2.17	5.12	0.0338	0.221
8.0	2.40	0.01	2.79	5.20	0.0343	0.224
10	2.04	0.01	3.28	5.33	0.0352	0.230
15	1.51	0.01	4.26	5.78	0.0382	0.249
20	1.21	—	5.00	6.21	0.0410	0.268
30	0.88	—	6.00	6.88	0.0454	0.296

a. Mass attenuation coefficient is calculated by using relative atomic mass  $A_r = 91.22$ .

b. Linear attenuation coefficient is calculated by using density  $\rho = 6.53 \text{ g}\cdot\text{cm}^{-3}$ .

c. K = K absorption edge.

TABLE 24. Attenuation coefficients for niobium (atomic number  $Z = 41$ ).

Energy (MeV)	Cross Section ( $10^{-28} \text{ m}^2$ )			Attenuation Coefficient $\mu$		
	Scattering	Photoelectric	Pair	Atomic ( $10^{-28} \text{ m}^2$ )	Mass <sup>a</sup> ( $\text{cm}^2\text{-g}^{-1}$ )	Linear <sup>b</sup> ( $\text{cm}^{-1}$ )
0.01	326	10 300	—	10 600	68.7	589
0.015	208	3140	—	3350	21.7	186
0.01902	152	1490	—	1640	10.6	90.8
K 0.01902 <sup>c</sup>	152	13 000	—	13 200	85.6	734
0.02	148	11 900	—	12 000	77.8	667
0.03	93	4070	—	4160	27.0	231
0.04	69	1810	—	1880	12.2	105
0.05	54	936	—	990	6.42	55.0
0.06	45	563	—	608	3.94	33.8
0.08	35	251	—	286	1.85	15.9
0.10	29	130	—	159	1.03	8.83
0.15	22.5	39.3	—	61.8	0.401	3.44
0.20	19.1	16.9	—	36.0	0.233	2.00
0.30	15.6	5.23	—	20.8	0.135	1.16
0.40	13.6	2.32	—	15.9	0.103	0.883
0.50	12.3	1.25	—	13.6	0.0882	0.756
0.60	11.2	0.79	—	12.0	0.0778	0.667
0.80	9.78	0.40	—	10.2	0.0661	0.566
1.0	8.75	0.26	—	9.01	0.0584	0.500
1.5	7.08	0.13	0.09	7.30	0.0473	0.405
2.0	6.02	0.08	0.33	6.43	0.0417	0.357
3.0	4.73	0.05	0.90	5.68	0.0368	0.315
4.0	3.95	0.03	1.41	5.39	0.0350	0.300
5.0	3.40	0.03	1.89	5.32	0.0345	0.296
6.0	3.00	0.02	2.27	5.29	0.0343	0.294
8.0	2.46	0.02	2.93	5.41	0.0351	0.301
10	2.09	0.01	3.43	5.53	0.0359	0.308
15	1.55	0.01	4.48	6.04	0.0392	0.336
20	1.24	0.01	5.24	6.49	0.0421	0.361
30	0.90	—	6.27	7.17	0.0465	0.398

a. Mass attenuation coefficient is calculated by using relative atomic mass  $A_r = 92.91$ .

b. Linear attenuation coefficient is calculated by using density  $\rho = 8.57 \text{ g}\cdot\text{cm}^{-3}$ .

c. K = K absorption edge.

TABLE 25. Attenuation coefficients for molybdenum (atomic number  $Z = 42$ ).

Energy (MeV)	Cross Section ( $10^{-28} \text{ m}^2$ )			Attenuation Coefficient $\mu$		
	Scattering	Photoelectric	Pair	Atomic ( $10^{-28} \text{ m}^2$ )	Mass <sup>a</sup> ( $\text{cm}^2\text{-g}^{-1}$ )	Linear <sup>b</sup> ( $\text{cm}^{-1}$ )
0.01	340	11 400	—	11 700	73.5	750
0.015	220	3480	—	3700	23.2	240
0.02004	160	1510	—	1670	10.5	107
K 0.02004 <sup>c</sup>	160	13 000	—	13 200	82.9	846
0.03	98	4390	—	4490	28.2	288
0.04	71	1960	—	2030	12.7	130
0.05	56	1030	—	1090	6.85	69.9
0.06	47	620	—	667	4.19	42.7
0.08	36	274	—	310	1.95	19.9
0.10	30	144	—	174	1.09	11.1
0.15	23.2	43.4	—	66.6	0.418	4.26
0.20	19.8	18.7	—	38.5	0.242	2.47
0.30	16.1	5.8	—	21.9	0.138	1.41
0.40	14.0	2.6	—	16.6	0.104	1.06
0.50	12.6	1.4	—	14.0	0.0879	0.897
0.60	11.5	0.88	—	12.4	0.0779	0.795
0.80	10.0	0.45	—	10.5	0.0659	0.672
1.0	8.96	0.29	—	9.25	0.0581	0.593
1.5	7.25	0.14	0.09	7.48	0.0470	0.479
2.0	6.15	0.09	0.35	6.59	0.0414	0.422
3.0	4.83	0.05	0.94	5.82	0.0365	0.372
4.0	4.03	0.04	1.50	5.57	0.0350	0.357
5.0	3.48	0.03	1.98	5.49	0.0345	0.352
6.0	3.08	0.01	2.38	5.47	0.0344	0.351
8.0	2.52	0.01	3.06	5.59	0.0351	0.358
10	2.14	0.01	3.59	5.74	0.0360	0.367
15	1.59	0.01	4.68	6.28	0.0394	0.402
20	1.27	0.01	5.47	6.75	0.0424	0.432
30	0.92	—	6.57	7.49	0.0470	0.479

a. Mass attenuation coefficient is calculated by using relative atomic mass  $A_r = 95.95$ .

b. Linear attenuation coefficient is calculated by using density  $\rho = 10.2 \text{ g}\cdot\text{cm}^{-3}$ .

c. K = K absorption edge.



TABLE 26. Attenuation coefficients for silver (atomic number  $Z = 47$ ).

Energy (MeV)	Cross Section ( $10^{-28} \text{ m}^2$ )			Attenuation Coefficient $\mu$		
	Scattering	Photoelectric	Pair	Atomic ( $10^{-28} \text{ m}^2$ )	Mass <sup>a</sup> ( $\text{cm}^2\text{-g}^{-1}$ )	Linear <sup>b</sup> ( $\text{cm}^{-1}$ )
0.01	443	18 500	—	18 900	106	1110
0.015	285	5670	—	5960	33.3	349
0.02	202	2460	—	2660	14.9	156
0.025 59	156	1180	—	1340	7.48	78.5
K 0.025 59 <sup>c</sup>	156	10 000	—	10 200	57.0	598
0.03	125	6590	—	6720	37.5	393
0.04	91	2960	—	3050	17.0	178
0.05	70	1580	—	1650	9.22	96.7
0.06	57	952	—	1010	5.64	59.2
0.08	44	427	—	471	2.63	27.6
0.10	36	225	—	261	1.46	15.3
0.15	27.1	68.6	—	95.7	0.534	5.60
0.20	22.6	30.4	—	53.0	0.296	3.11
0.30	18.3	9.49	—	27.8	0.155	1.63
0.40	15.8	4.27	—	20.1	0.112	1.17
0.50	14.2	2.32	—	16.5	0.0922	0.967
0.60	13.0	1.46	—	14.5	0.0810	0.850
0.80	11.3	0.75	—	12.1	0.0676	0.709
1.0	10.1	0.48	—	10.6	0.0592	0.621
1.5	8.13	0.24	0.12	8.49	0.0474	0.497
2.0	6.91	0.15	0.45	7.51	0.0419	0.440
3.0	5.43	0.09	1.20	6.72	0.0375	0.393
4.0	4.52	0.06	1.87	6.45	0.0360	0.378
5.0	3.90	0.05	2.50	6.45	0.0360	0.378
6.0	3.44	0.04	2.99	6.47	0.0361	0.379
8.0	2.82	0.03	3.81	6.66	0.0372	0.390
10.0	2.40	0.02	4.47	6.89	0.0385	0.404
15.0	1.77	0.01	5.81	7.59	0.0424	0.445
20.0	1.42	0.01	6.79	8.22	0.0459	0.481
30.0	1.03	0.01	8.14	9.18	0.0513	0.538

a. Mass attenuation coefficient is calculated by using relative atomic mass  $A_r = 107.88$ .

b. Linear attenuation coefficient is calculated by using density  $\rho = 10.49 \text{ g}\cdot\text{cm}^{-3}$ .

c. K = K absorption edge.

TABLE 27. Attenuation coefficients for cadmium (atomic number  $Z = 48$ ).

Energy (MeV)	Cross Section ( $10^{-28} \text{ m}^2$ )			Attenuation Coefficient $\mu$		
	Scattering	Photoelectric	Pair	Atomic ( $10^{-28} \text{ m}^2$ )	Mass <sup>a</sup> ( $\text{cm}^2\text{-g}^{-1}$ )	Linear <sup>b</sup> ( $\text{cm}^{-1}$ )
0.01	466	20 200	—	20 700	111	960
0.015	322	6220	—	6540	35.1	304
0.02	212	2700	—	2910	15.6	135
0.026 76	159	1170	—	1330	7.13	61.7
K 0.026 76 <sup>c</sup>	159	9700	—	9860	52.8	457
0.03	131	7080	—	7210	38.6	334
0.04	95	3210	—	3310	17.7	153
0.05	73	1710	—	1780	9.54	82.5
0.06	60	1030	—	1090	5.84	50.5
0.08	46	461	—	507	2.72	23.5
0.10	38	245	—	283	1.52	13.1
0.15	27.9	74.9	—	103	0.552	4.77
0.20	23.3	33.4	—	56.7	0.304	2.63
0.30	18.7	10.4	—	29.1	0.156	1.35
0.40	16.2	4.66	—	20.9	0.112	0.969
0.50	14.5	2.55	—	17.1	0.0917	0.793
0.60	13.3	1.60	—	14.9	0.0799	0.691
0.80	11.5	0.83	—	12.3	0.0659	0.570
1.0	10.3	0.53	—	10.8	0.0579	0.501
1.5	8.30	0.26	0.13	8.69	0.0466	0.403
2.0	7.06	0.17	0.47	7.70	0.0413	0.357
3.0	5.54	0.10	1.25	6.89	0.0369	0.319
4.0	4.62	0.07	1.95	6.64	0.0356	0.308
5.0	3.98	0.05	2.61	6.64	0.0356	0.308
6.0	3.51	0.05	3.12	6.68	0.0358	0.310
8.0	2.88	0.03	3.98	6.89	0.0369	0.319
10	2.45	0.03	4.66	7.14	0.0383	0.331
15	1.81	0.02	6.05	7.88	0.0422	0.365
20	1.45	0.01	7.08	8.54	0.0458	0.396
30	1.06	0.01	8.47	9.54	0.0511	0.442

a. Mass attenuation coefficient is calculated by using relative atomic mass  $A_r = 112.41$ .

b. Linear attenuation coefficient is calculated by using density  $\rho = 8.65 \text{ g}\cdot\text{cm}^{-3}$ .

c. K = K absorption edge.

TABLE 28. Attenuation coefficients for tin (atomic number  $Z = 50$ ).

Energy (MeV)	Cross Section ( $10^{-28} \text{ m}^2$ )			Attenuation Coefficient $\mu$		
	Scattering	Photoelectric	Pair	Atomic ( $10^{-28} \text{ m}^2$ )	Mass <sup>a</sup> ( $\text{cm}^2\text{-g}^{-1}$ )	Linear <sup>b</sup> ( $\text{cm}^{-1}$ )
0.01	510	24 000	—	24 500	124	905
0.015	330	7410	—	7740	39.3	287
0.02	240	3220	—	3460	17.6	128
0.02925	150	1050	—	1200	6.09	44.5
K 0.02925 <sup>c</sup>	150	8580	—	8730	44.3	323
0.03	143	8150	—	8290	42.1	307
0.04	103	3700	—	3800	19.3	141
0.05	79	1990	—	2070	10.5	76.7
0.06	65	1210	—	1280	6.50	47.5
0.08	49	539	—	588	2.98	21.8
0.10	40	286	—	326	1.65	12.0
0.15	29.6	88.8	—	118	0.599	4.37
0.20	24.6	39.3	—	63.9	0.324	2.37
0.30	19.7	12.4	—	32.1	0.163	1.19
0.40	17.0	5.6	—	22.6	0.115	0.840
0.50	15.2	3.0	—	18.2	0.0924	0.675
0.60	13.8	1.9	—	15.7	0.0797	0.582
0.80	12.0	1.0	—	13.0	0.0660	0.482
1.0	10.7	0.64	—	11.3	0.0574	0.419
1.5	8.65	0.32	0.14	9.11	0.0462	0.337
2.0	7.36	0.20	0.51	8.07	0.0410	0.299
3.0	5.76	0.12	1.35	7.23	0.0367	0.268
4.0	4.80	0.08	2.14	7.02	0.0356	0.260
5.0	4.14	0.06	2.82	7.02	0.0356	0.260
6.0	3.66	0.05	3.37	7.08	0.0359	0.262
8.0	2.99	0.04	4.29	7.32	0.0372	0.272
10	2.55	0.03	5.04	7.62	0.0387	0.283
15	1.89	0.02	6.54	8.45	0.0429	0.313
20	1.51	0.01	7.63	9.15	0.0464	0.339
30	1.10	0.01	9.15	10.3	0.0523	0.382

a. Mass attenuation coefficient is calculated by using relative atomic mass  $A_r = 118.70$ .

b. Linear attenuation coefficient is calculated by using density  $\rho = 7.30 \text{ g}\cdot\text{cm}^{-3}$ .

c. K = K absorption edge.

TABLE 29. Attenuation coefficients for antimony (atomic number  $Z = 51$ ).

Energy (MeV)	Cross Section ( $10^{-28} \text{ m}^2$ )			Attenuation Coefficient $\mu$		
	Scattering	Photoelectric	Pair	Atomic ( $10^{-28} \text{ m}^2$ )	Mass <sup>a</sup> ( $\text{cm}^2\text{-g}^{-1}$ )	Linear <sup>b</sup> ( $\text{cm}^{-1}$ )
0.01	535	25 900	—	26 400	131	867
0.015	344	8010	—	8350	41.3	273
0.02	244	3490	—	3730	18.5	122
0.03050	148	1000	—	1150	5.69	37.7
K 0.03050 <sup>c</sup>	148	8140	—	8290	41.0	271
0.04	108	3970	—	4080	20.2	134
0.05	82	2140	—	2220	11.0	72.8
0.06	67	1300	—	1370	6.78	44.9
0.08	51	580	—	631	3.12	20.7
0.10	42	311	—	353	1.75	11.6
0.15	30.4	93.5	—	124	0.614	4.06
0.20	25.1	42.8	—	67.9	0.336	2.22
0.30	20.1	13.5	—	33.6	0.166	1.10
0.40	17.3	6.11	—	23.4	0.116	0.768
0.50	15.5	3.34	—	18.8	0.0930	0.616
0.60	14.1	2.09	—	16.2	0.0802	0.531
0.80	12.3	1.09	—	13.4	0.0663	0.439
1.0	10.9	0.71	—	11.6	0.0574	0.380
1.5	8.82	0.34	0.15	9.31	0.0461	0.305
2.0	7.51	0.22	0.54	8.27	0.0409	0.271
3.0	5.89	0.13	1.42	7.44	0.0368	0.244
4.0	4.91	0.09	2.21	7.21	0.0357	0.236
5.0	4.23	0.07	2.95	7.25	0.0359	0.238
6.0	3.73	0.06	3.51	7.30	0.0361	0.239
8.0	3.06	0.04	4.47	7.57	0.0375	0.248
10	2.60	0.03	5.22	7.85	0.0388	0.257
15	1.92	0.02	6.79	8.73	0.0432	0.286
20	1.54	0.01	7.90	9.45	0.0468	0.310
30	1.12	0.01	9.49	10.6	0.0524	0.347

a. Mass attenuation coefficient is calculated by using relative atomic mass  $A_r = 121.76$ .

b. Linear attenuation coefficient is calculated by using density  $\rho = 6.62 \text{ g}\cdot\text{cm}^{-3}$ .

c. K = K absorption edge.

TABLE 30. Attenuation coefficients for iodine (atomic number  $Z = 53$ ).

Energy (MeV)	Cross Section ( $10^{-28} \text{ m}^2$ )			Attenuation Coefficient $\mu$		
	Scattering	Photoelectric	Pair	Atomic ( $10^{-28} \text{ m}^2$ )	Mass <sup>a</sup> ( $\text{cm}^2\text{-g}^{-1}$ )	Linear <sup>b</sup> ( $\text{cm}^{-1}$ )
0.01	590	29 800	—	30 400	144	710
0.015	380	9360	—	9740	46.2	228
0.02	270	4130	—	4400	20.9	103
0.03	164	1260	—	1420	6.74	33.2
0.033 23	150	933	—	1080	5.13	25.3
K 0.033 23 <sup>c</sup>	150	7510	—	7660	36.4	179
0.04	117	4490	—	4610	21.9	108
0.05	89	2470	—	2560	12.2	60.1
0.06	72	1500	—	1570	7.45	36.7
0.08	54	677	—	731	3.47	17.1
0.10	44	360	—	404	1.92	9.47
0.15	32	113	—	145	0.688	3.39
0.20	26.5	50.0	—	76.5	0.363	1.79
0.30	21.0	16.0	—	37.0	0.176	0.868
0.40	18.1	7.2	—	25.3	0.120	0.592
0.50	16.2	3.9	—	20.1	0.0954	0.470
0.60	14.8	2.5	—	17.3	0.0821	0.405
0.80	12.8	1.3	—	14.1	0.0669	0.330
1.0	11.4	0.84	—	12.2	0.0579	0.285
1.5	9.18	0.41	0.17	9.76	0.0463	0.228
2.0	7.81	0.26	0.59	8.66	0.0411	0.203
3.0	6.10	0.16	1.53	7.79	0.0370	0.182
4.0	5.09	0.11	2.41	7.61	0.0361	0.178
5.0	4.39	0.08	3.17	7.64	0.0363	0.179
6.0	3.88	0.07	3.78	7.73	0.0367	0.181
8.0	3.17	0.05	4.81	8.03	0.0381	0.188
10	2.70	0.04	5.63	8.37	0.0397	0.196
15	2.00	0.02	7.30	9.32	0.0442	0.218
20	1.60	0.01	8.51	10.1	0.0479	0.236
30	1.17	0.01	10.2	11.4	0.0541	0.267

a. Mass attenuation coefficient is calculated by using relative atomic mass  $A_r = 126.92$ .b. Linear attenuation coefficient is calculated by using density  $\rho = 4.93 \text{ g}\cdot\text{cm}^{-3}$ .

c. K = K absorption edge.



TABLE 31. Attenuation coefficients for cesium (atomic number  $Z = 55$ ).

Energy (MeV)	Cross Section ( $10^{-28} \text{ m}^2$ )			Attenuation Coefficient $\mu$		
	Scattering	Photoelectric	Pair	Atomic ( $10^{-28} \text{ m}^2$ )	Mass <sup>a</sup> ( $\text{cm}^2\text{-g}^{-1}$ )	Linear <sup>b</sup> ( $\text{cm}^{-1}$ )
0.01	633	34 700	—	35 300	160	299
0.015	411	11 000	—	11 400	51.7	96.7
0.02	290	4830	—	5120	23.2	43.4
0.03	177	1480	—	1660	7.52	14.1
0.036 03	146	881	—	1030	4.67	8.73
K 0.036 03 <sup>c</sup>	146	7100	—	7250	32.9	61.5
0.04	127	5160	—	5290	24.0	44.9
0.05	96	2840	—	2940	13.3	24.9
0.06	78	1720	—	1800	8.16	15.3
0.08	58	765	—	823	3.73	6.98
0.10	47	414	—	461	2.09	3.91
0.15	34	129	—	163	0.739	1.38
0.20	27.8	58.4	—	86.2	0.391	0.731
0.30	21.9	18.6	—	40.5	0.184	0.344
0.40	18.8	8.46	—	27.3	0.124	0.232
0.50	16.8	4.64	—	21.4	0.0970	0.181
0.60	15.3	2.93	—	18.2	0.0825	0.154
0.80	13.3	1.54	—	14.8	0.0671	0.125
1.0	11.8	1.00	—	12.8	0.0580	0.108
1.5	9.53	0.49	0.18	10.2	0.0462	0.0864
2.0	8.10	0.31	0.64	9.05	0.0410	0.0767
3.0	6.36	0.18	1.66	8.20	0.0372	0.0696
4.0	5.29	0.13	2.59	8.01	0.0363	0.0679
5.0	4.56	0.10	3.42	8.08	0.0366	0.0684
6.0	4.04	0.08	4.07	8.19	0.0371	0.0694
8.0	3.30	0.06	5.17	8.53	0.0387	0.0724
10	2.81	0.05	6.04	8.90	0.0403	0.0754
15	2.07	0.03	7.82	9.92	0.0450	0.0842
20	1.66	0.02	9.12	10.8	0.0490	0.0916
30	1.21	0.01	10.9	12.1	0.0548	0.102

a. Mass attenuation coefficient is calculated by using relative atomic mass  $A_r = 132.91$ .

b. Linear attenuation coefficient is calculated by using density  $\rho = 1.87 \text{ g}\cdot\text{cm}^{-3}$ .

c. K = K absorption edge.

TABLE 32. Attenuation coefficients for barium (atomic number  $Z = 56$ ).

Energy (MeV)	Cross Section ( $10^{-28} \text{ m}^2$ )			Attenuation Coefficient $\mu$		
	Scattering	Photoelectric	Pair	Atomic ( $10^{-28} \text{ m}^2$ )	Mass <sup>a</sup> ( $\text{cm}^2\text{-g}^{-1}$ )	Linear <sup>b</sup> ( $\text{cm}^{-1}$ )
0.01	662	37 000	—	37 700	165	624
0.015	371	11 900	—	12 300	53.9	204
0.02	303	5190	—	5490	24.1	91.1
0.03	185	1590	—	1780	7.81	29.5
0.037 48	145	837	—	982	4.31	16.3
K 0.037 48 <sup>c</sup>	145	6720	—	6870	30.1	114
0.04	132	5510	—	5640	24.7	93.4
0.05	100	3030	—	3130	13.7	51.8
0.06	81	1834	—	1920	8.42	31.8
0.08	60	815	—	875	3.84	14.5
0.10	49	444	—	493	2.16	8.16
0.15	35	138	—	173	0.759	2.87
0.20	28.4	62.8	—	91.2	0.400	1.51
0.30	22.4	20.0	—	42.4	0.186	0.703
0.40	19.2	9.14	—	28.3	0.124	0.469
0.50	17.1	5.02	—	22.1	0.0969	0.366
0.60	15.6	3.18	—	18.8	0.0825	0.312
0.80	13.5	1.67	—	15.2	0.0667	0.252
1.0	12.1	1.09	—	13.2	0.0579	0.219
1.5	9.70	0.53	0.19	10.4	0.0456	0.172
2.0	8.25	0.34	0.67	9.26	0.0406	0.153
3.0	6.47	0.20	1.73	8.40	0.0368	0.139
4.0	5.39	0.14	2.68	8.21	0.0360	0.136
5.0	4.65	0.11	3.59	8.35	0.0366	0.138
6.0	4.11	0.09	4.21	8.41	0.0369	0.139
8.0	3.35	0.07	5.35	8.77	0.0385	0.146
10	2.86	0.05	6.26	9.17	0.0402	0.152
15	2.11	0.03	8.09	10.2	0.0447	0.169
20	1.69	0.02	9.45	11.2	0.0491	0.186
30	1.23	0.02	11.3	12.6	0.0553	0.209

a. Mass attenuation coefficient is calculated by using relative atomic mass  $A_r = 137.36$ .

b. Linear attenuation coefficient is calculated by using density  $\rho = 3.78 \text{ g}\cdot\text{cm}^{-3}$ .

c. K = K absorption edge.

TABLE 33. Attenuation coefficients for thulium (atomic number  $Z = 69$ ).

Energy (MeV)	Cross Section ( $10^{-28} \text{ m}^2$ )			Attenuation Coefficient $\mu$		
	Scattering	Photoelectric	Pair	Atomic ( $10^{-28} \text{ m}^2$ )	Mass <sup>a</sup> ( $\text{cm}^2\text{-g}^{-1}$ )	Linear <sup>b</sup> ( $\text{cm}^{-1}$ )
0.015	705	27 400	—	28 100	100	935
0.02	496	12 200	—	12 700	45.2	423
0.03	300	3790	—	4090	14.5	136
0.04	210	1690	—	1900	6.76	63.2
0.05	156	884	—	1040	3.70	34.6
0.059 45	126	497	—	623	2.22	20.8
K 0.059 45 <sup>c</sup>	126	3880	—	4010	14.3	134
0.06	124	3860	—	3980	14.2	133
0.08	89	1750	—	1840	6.54	61.1
0.10	74	970	—	1040	3.70	34.6
0.15	48	313	—	361	1.28	12.0
0.20	38	144	—	182	0.647	6.05
0.30	29.0	47.2	—	76.2	0.271	2.53
0.40	24.4	22.4	—	46.8	0.166	1.55
0.50	21.6	12.5	—	34.1	0.121	1.13
0.60	19.6	8.05	—	27.7	0.0985	0.921
0.80	16.9	4.35	—	21.3	0.0758	0.709
1.0	15.0	2.85	—	17.9	0.0637	0.596
1.5	12.0	1.38	0.33	13.7	0.0487	0.455
2.0	10.2	0.89	1.11	12.2	0.0434	0.406
3.0	7.99	0.51	2.73	11.2	0.0398	0.372
4.0	6.65	0.36	4.15	11.2	0.0398	0.372
5.0	5.73	0.28	5.41	11.4	0.0405	0.379
6.0	5.05	0.23	6.36	11.6	0.0413	0.386
8.0	4.14	0.17	7.97	12.3	0.0438	0.410
10	3.52	0.13	9.27	12.9	0.0459	0.429
15	2.60	0.08	11.9	14.6	0.0519	0.485
20	2.08	0.06	13.9	16.0	0.0569	0.532
30	1.52	0.04	16.5	18.1	0.0644	0.602

a. Mass attenuation coefficient is calculated by using relative atomic mass  $A_r = 169.4$ .

b. Linear attenuation coefficient is calculated by using density  $\rho = 9.35 \text{ g}\cdot\text{cm}^{-3}$ .

c. K = K absorption edge.

TABLE 34. Attenuation coefficients for tantalum (atomic number  $Z = 73$ ).

Energy (MeV)	Cross Section ( $10^{-28} \text{ m}^2$ )			Attenuation Coefficient $\mu$		
	Scattering	Photoelectric	Pair	Atomic ( $10^{-28} \text{ m}^2$ )	Mass <sup>a</sup> ( $\text{cm}^2\text{-g}^{-1}$ )	Linear <sup>b</sup> ( $\text{cm}^{-1}$ )
0.015	808	34 000	—	34 800	116	1930
0.02	569	15 200	—	15 800	52.6	873
0.03	342	4750	—	5090	17.0	282
0.04	238	2120	—	2360	7.86	130
0.05	176	1110	—	1290	4.30	71.4
0.06	140	638	—	778	2.59	43.0
0.067 51	124	440	—	564	1.88	31.2
K 0.067 51 <sup>c</sup>	124	3360	—	3480	11.6	193
0.08	101	2140	—	2240	7.46	124
0.10	79	1180	—	1260	4.20	69.7
0.15	53	387	—	440	1.47	24.4
0.20	41	179	—	220	0.733	12.2
0.30	31.1	59.3	—	90.6	0.302	5.01
0.40	26.1	28.4	—	54.5	0.182	3.02
0.50	23.0	15.9	—	38.9	0.130	2.16
0.60	20.9	10.3	—	31.2	0.104	1.73
0.80	17.9	5.60	—	23.5	0.0783	1.30
1.0	15.9	3.69	—	19.6	0.0653	1.08
1.5	12.7	1.78	0.39	14.9	0.0496	0.823
2.0	10.8	1.15	1.28	13.2	0.0440	0.730
3.0	8.45	0.66	3.08	12.2	0.0406	0.674
4.0	7.04	0.47	4.67	12.2	0.0406	0.674
5.0	6.06	0.36	6.06	12.5	0.0416	0.691
6.0	5.35	0.29	7.08	12.7	0.0423	0.702
8.0	4.37	0.21	8.86	13.4	0.0446	0.740
10	3.72	0.17	10.3	14.2	0.0473	0.785
15	2.75	0.11	13.2	16.1	0.0536	0.890
20	2.20	0.08	15.4	17.7	0.0590	0.979
30	1.61	0.05	18.4	20.1	0.0670	1.11

a. Mass attenuation coefficient is calculated by using relative atomic mass  $A_r = 180.88$ .

b. Linear attenuation coefficient is calculated by using density  $\rho = 16.6 \text{ g}\cdot\text{cm}^{-3}$ .

c. K = K absorption edge.

TABLE 35. Attenuation coefficients for tungsten (atomic number  $Z = 74$ ).

Energy (MeV)	Cross Section ( $10^{-28} \text{ m}^2$ )			Attenuation Coefficient $\mu$		
	Scattering	Photoelectric	Pair	Atomic ( $10^{-28} \text{ m}^2$ )	Mass <sup>a</sup> ( $\text{cm}^2\text{-g}^{-1}$ )	Linear <sup>b</sup> ( $\text{cm}^{-1}$ )
0.015	840	36 000	—	36 800	121	2260
0.02	590	16 000	—	16 600	54.4	1020
0.03	350	5040	—	5390	17.7	331
0.04	245	2220	—	2470	8.09	151
0.05	180	1160	—	1340	4.39	82.1
0.06	145	674	—	819	2.68	50.1
0.06964	122	437	—	559	1.83	34.2
K 0.06964 <sup>c</sup>	122	3230	—	3350	11.0	206
0.08	104	2250	—	2350	7.70	144
0.10	80	1250	—	1330	4.36	81.5
0.15	54	408	—	462	1.51	28.2
0.20	42	186	—	228	0.747	14.0
0.30	31.5	63.1	—	94.6	0.310	5.80
0.40	26.5	29.8	—	56.3	0.184	3.44
0.50	23.4	16.7	—	40.1	0.131	2.45
0.60	21.2	11.0	—	32.2	0.105	1.96
0.80	18.2	5.9	—	24.1	0.0790	1.48
1.0	16.1	3.9	—	20.0	0.0655	1.22
1.5	12.9	1.9	0.40	15.2	0.0498	0.931
2.0	10.9	1.2	1.32	13.4	0.0439	0.821
3.0	8.57	0.71	3.20	12.5	0.0410	0.767
4.0	7.10	0.50	4.81	12.4	0.0406	0.759
5.0	6.13	0.38	6.23	12.7	0.0416	0.778
6.0	5.42	0.31	7.34	13.0	0.0426	0.797
8.0	4.43	0.23	9.06	13.7	0.0449	0.840
10	3.77	0.18	10.6	14.6	0.0478	0.894
15	2.79	0.11	13.5	16.4	0.0537	1.00
20	2.24	0.08	15.7	18.0	0.0590	1.10
30	1.63	0.06	18.8	20.5	0.0672	1.26

a. Mass attenuation coefficient is calculated by using relative atomic mass  $A_r = 183.92$ .

b. Linear attenuation coefficient is calculated by using density  $\rho = 18.7 \text{ g}\cdot\text{cm}^{-3}$ .

c. K = K absorption edge.

TABLE 36. Attenuation coefficients for platinum (atomic number  $Z = 78$ ).

Energy (MeV)	Cross Section ( $10^{-28} \text{ m}^2$ )			Attenuation Coefficient $\mu$		
	Scattering	Photoelectric	Pair	Atomic ( $10^{-28} \text{ m}^2$ )	Mass <sup>a</sup> ( $\text{cm}^2\text{-g}^{-1}$ )	Linear <sup>b</sup> ( $\text{cm}^{-1}$ )
0.015	940	43 800	—	44 700	138	2950
0.02	670	19 700	—	20 400	63.0	1350
0.03	400	6240	—	6640	20.5	439
0.04	280	2720	—	3000	9.26	198
0.05	188	1440	—	1630	5.03	108
0.06	163	836	—	999	3.08	65.9
0.07858	117	381	—	498	1.54	33.0
K 0.07858 <sup>c</sup>	117	2830	—	2950	9.10	195
0.08	115	2680	—	2800	8.64	185
0.10	88	1500	—	1590	4.91	105
0.15	59	498	—	557	1.72	36.8
0.20	45	226	—	271	0.836	17.9
0.30	34	77.3	—	111	0.343	7.34
0.40	28.3	37.1	—	65.4	0.202	4.32
0.50	24.8	21.1	—	46.0	0.142	3.04
0.60	22.5	13.9	—	36.4	0.112	2.40
0.80	19.2	7.6	—	26.8	0.0827	1.77
1.0	17.0	4.9	—	21.9	0.0676	1.45
1.5	13.6	2.4	0.47	16.5	0.0509	1.09
2.0	11.6	1.5	1.51	14.6	0.0451	0.965
3.0	9.04	0.90	3.55	13.5	0.0417	0.892
4.0	7.52	0.63	5.37	13.5	0.0417	0.892
5.0	6.46	0.48	6.92	13.9	0.0429	0.918
6.0	5.71	0.39	8.07	14.2	0.0438	0.937
8.0	4.67	0.29	9.98	14.9	0.0460	0.984
10	3.98	0.22	11.7	15.9	0.0491	1.05
15	2.94	0.14	14.9	18.0	0.0555	1.19
20	2.36	0.10	17.3	19.8	0.0611	1.31
30	1.72	0.07	20.6	22.4	0.0691	1.48

a. Mass attenuation coefficient is calculated by using relative atomic mass  $A_r = 195.23$ .

b. Linear attenuation coefficient is calculated by using density  $\rho = 21.4 \text{ g}\cdot\text{cm}^{-3}$ .

c. K = K absorption edge.



TABLE 37. Attenuation coefficients for gold (atomic number  $Z = 79$ ).

Energy (MeV)	Cross Section ( $10^{-28} \text{ m}^2$ )			Attenuation Coefficient $\mu$		
	Scattering	Photoelectric	Pair	Atomic ( $10^{-28} \text{ m}^2$ )	Mass <sup>a</sup> ( $\text{cm}^2\text{-g}^{-1}$ )	Linear <sup>b</sup> ( $\text{cm}^{-1}$ )
0.015	977	45 500	—	46 500	142	2740
0.02	681	20 700	—	21 400	65.4	1260
0.03	412	6550	—	6960	21.3	412
0.04	285	2890	—	3180	9.71	188
0.05	210	1510	—	1720	5.25	101
0.06	165	880	—	1050	3.21	62.0
0.08	118	382	—	500	1.53	29.6
0.08091	117	368	—	485	1.48	28.6
K 0.08091 <sup>c</sup>	117	2740	—	2860	8.74	169
0.10	92	1570	—	1600	5.07	98.0
0.15	60	520	—	580	1.77	34.2
0.20	46	241	—	287	0.877	16.9
0.30	34.5	80.9	—	115	0.351	6.78
0.40	28.7	39.4	—	68.1	0.208	4.02
0.50	25.2	22.5	—	47.7	0.146	2.82
0.60	22.8	14.7	—	37.5	0.115	2.22
0.80	19.5	8.03	—	27.5	0.0840	1.62
1.0	17.3	5.29	—	22.6	0.0690	1.33
1.5	13.8	2.56	0.48	16.8	0.0513	0.991
2.0	11.7	1.65	1.56	14.9	0.0455	0.879
3.0	9.17	0.95	3.65	13.8	0.0422	0.815
4.0	7.62	0.67	5.50	13.8	0.0422	0.815
5.0	6.56	0.50	7.10	14.2	0.0434	0.838
6.0	5.80	0.41	8.22	14.4	0.0440	0.850
8.0	4.74	0.30	10.2	15.2	0.0464	0.896
10	4.04	0.24	11.9	16.2	0.0495	0.956
15	2.98	0.15	15.2	18.3	0.0559	1.08
20	2.39	0.11	17.7	20.2	0.0617	1.19
30	1.74	0.08	21.2	23.0	0.0703	1.36

a. Mass attenuation coefficient is calculated by using atomic weight  $Z = 197.2$ .

b. Linear attenuation coefficient is calculated by using density  $\rho = 19.32 \text{ g}\cdot\text{cm}^{-3}$ .

c. K = K absorption edge.

TABLE 38. Attenuation coefficients for lead (atomic number  $Z = 82$ ).

Energy (MeV)	Cross Section ( $10^{-28} \text{ m}^2$ )			Attenuation Coefficient $\mu$		
	Scattering	Photoelectric	Pair	Atomic ( $10^{-28} \text{ m}^2$ )	Mass <sup>a</sup> ( $\text{cm}^2\text{-g}^{-1}$ )	Linear <sup>b</sup> ( $\text{cm}^{-1}$ )
0.02	750	24 000	—	24 800	72.1	818
0.03	450	7620	—	8070	23.5	266
0.04	310	3310	—	3620	10.5	119
0.05	230	1740	—	1970	5.73	65.0
0.06	180	1040	—	1220	3.55	40.3
0.08	127	444	—	571	1.66	18.8
0.08823	113	334	—	447	1.30	14.7
K 0.08823 <sup>c</sup>	113	2510	—	2620	7.62	86.4
0.10	100	1780	—	1880	5.47	62.0
0.15	64	596	—	660	1.92	21.8
0.20	49	275	—	324	0.942	10.7
0.30	36.2	93.4	—	130	0.378	4.29
0.40	30.1	45.7	—	75.8	0.220	2.49
0.50	26.3	26.1	—	52.4	0.152	1.72
0.60	23.8	17.3	—	41.1	0.120	1.36
0.80	20.3	9.5	—	29.8	0.0867	0.983
1.0	18.0	6.2	—	24.2	0.0704	0.798
1.5	14.4	3.0	0.5	17.9	0.0521	0.591
2.0	12.2	2.0	1.7	15.9	0.0462	0.524
3.0	9.51	1.1	4.0	14.6	0.0425	0.482
4.0	7.91	0.80	6.02	14.7	0.0427	0.484
5.0	6.79	0.60	7.63	15.0	0.0436	0.494
6.0	6.00	0.49	8.84	15.3	0.0445	0.505
8.0	4.91	0.35	11.0	16.3	0.0474	0.538
10	4.18	0.28	12.8	17.3	0.0503	0.570
15	3.09	0.18	16.3	19.5	0.0567	0.643
20	2.48	0.13	18.9	21.5	0.0625	0.709
30	1.80	0.09	22.6	24.5	0.0712	0.807

a. Mass attenuation coefficient is calculated by using atomic weight  $Z = 207.21$ .

b. Linear attenuation coefficient is calculated by using density  $\rho = 11.34 \text{ g}\cdot\text{cm}^{-3}$ .

c. K = K absorption edge.

TABLE 39. Attenuation coefficients for uranium (atomic number  $Z = 92$ ).

Energy (MeV)	Cross Section ( $10^{-28} \text{ m}^2$ )			Attenuation Coefficient $\mu$		
	Scattering	Photoelectric	Pair	Atomic ( $10^{-28} \text{ m}^2$ )	Mass <sup>a</sup> ( $\text{cm}^2\text{-g}^{-1}$ )	Linear <sup>b</sup> ( $\text{cm}^{-1}$ )
0.03	590	12 000	—	12 600	31.9	597
0.04	400	5250	—	5650	14.3	267
0.05	300	2780	—	3080	7.79	146
0.06	230	1640	—	1870	4.73	88.5
0.08	163	716	—	879	2.22	41.5
0.10	123	374	—	497	1.26	23.6
0.1163	103	239	—	342	0.866	16.2
K 0.1163 <sup>c</sup>	103	1790	—	1890	4.78	89.4
0.15	78	905	—	983	2.49	46.6
0.20	59	417	—	476	1.20	22.4
0.30	42	146	—	188	0.0476	8.90
0.40	34.7	73.2	—	108	0.273	5.11
0.50	30.2	43.1	—	73.3	0.186	3.48
0.60	27.1	29.2	—	56.3	0.142	2.66
0.80	23.0	16.0	—	39.0	0.0987	1.85
1.0	20.3	10.5	—	30.8	0.0779	1.46
1.5	16.2	5.1	0.8	22.1	0.0559	1.05
2.0	13.7	3.3	2.3	19.3	0.0488	0.913
3.0	10.7	1.9	5.21	17.8	0.0450	0.842
4.0	8.88	1.3	7.62	17.8	0.0450	0.842
5.0	7.62	1.0	9.73	18.4	0.0466	0.871
6.0	6.74	0.81	11.1	18.6	0.0471	0.881
8.0	5.51	0.59	13.5	19.6	0.0496	0.928
10	4.69	0.46	15.7	20.9	0.0529	0.989
15	3.47	0.30	20.0	23.8	0.0602	1.13
20	2.78	0.22	23.1	26.1	0.0661	1.24
30	2.02	0.15	27.6	29.8	0.0754	1.41

a. Mass attenuation coefficient is calculated by using atomic weight  $Z = 238.07$ .

b. Linear attenuation coefficient is calculated by using density  $\rho = 18.7 \text{ g}\cdot\text{cm}^{-3}$ .

c. K = K absorption edge.

TABLE 40. Attenuation coefficients for plutonium (atomic number  $Z = 94$ ).

Energy (MeV)	Cross Section ( $10^{-28} \text{ m}^2$ )			Attenuation Coefficient $\mu$		
	Scattering	Photoelectric	Pair	Atomic ( $10^{-28} \text{ m}^2$ )	Mass <sup>a</sup> ( $\text{cm}^2\text{-g}^{-1}$ )	Linear <sup>b</sup> ( $\text{cm}^{-1}$ )
0.03	627	13 200	—	13 800	34.8	679
0.04	426	5700	—	6130	15.5	302
0.05	312	3020	—	3330	8.39	164
0.06	243	1780	—	2020	5.09	99.3
0.08	171	778	—	949	2.39	46.6
0.10	130	409	—	539	1.36	26.5
0.12256	101	222	—	323	0.814	15.9
K 0.12256 <sup>c</sup>	101	1660	—	1760	4.44	86.6
0.15	81	976	—	1060	2.67	52.1
0.20	61	455	—	516	1.30	25.4
0.30	44	159	—	203	0.512	9.98
0.40	35.7	80.0	—	116	0.292	5.69
0.50	31.0	47.0	—	78.0	0.197	3.84
0.60	27.9	31.9	—	59.8	0.151	2.94
0.80	23.6	17.5	—	41.1	0.104	2.03
1.0	20.8	11.6	—	32.4	0.0817	1.59
1.5	20.6	5.60	0.81	27.0	0.0681	1.33
2.0	14.0	3.63	2.46	20.1	0.0507	0.989
3.0	10.9	2.08	5.45	18.4	0.0464	0.905
4.0	9.09	1.46	8.04	18.6	0.0469	0.915
5.0	7.82	1.09	10.1	19.0	0.0479	0.934
6.0	6.91	0.90	11.5	19.3	0.0487	0.950
8.0	5.65	0.65	14.0	20.3	0.0512	0.998
10	4.80	0.50	16.3	21.6	0.0545	1.06
15	3.54	0.33	20.7	24.6	0.0620	1.21
20	2.84	0.24	23.9	27.0	0.0681	1.33
30	2.07	0.17	27.8	30.0	0.0756	1.47

a. Mass attenuation coefficient is calculated by using atomic weight  $A_r = 239$ .

b. Linear attenuation coefficient is calculated by using density  $\rho = 19.5 \text{ g}\cdot\text{cm}^{-3}$ .

c. K = K absorption edge.

---

## References

1. White, G.R. "Absorptive Components of the Mass Absorption Coefficients." National Bureau of Standards Report No. 1003. Gaithersburg, MD: National Institute of Standards and Technology (n.d.).
2. Victoreen, J.A. "The Absorption of Incident Quanta by Atoms As Defined by the Mass Photoelectric Absorption Coefficient and the Mass Scattering Coefficient." *Journal of Applied Physics*. Vol. 19. Melville, NY: American Institute of Physics (1948): p 855.
3. Victoreen, J.A. "The Calculation of X-Ray Mass Absorption Coefficients." *Journal of Applied Physics*. Vol. 20. Melville, NY: American Institute of Physics (1949): p 1141.
4. Zemaný, P.D. and H.A. Liebhafsky. "Plating Thickness by the Attenuation of Characteristic X-Rays." *Journal of the Electrochemical Society*. Vol. 103. New York, NY: Electrochemical Society (1956).

# Radiographic Testing Glossary

---

Ringo Beaumont, Tempe, Arizona

Richard H. Bossi, The Boeing Company, Seattle,  
Washington

Lawrence R. Lawson, Bradford, Pennsylvania

William E.J. McKinney, Naples, Florida

George Wheeler, Materials and Processes Consultants,  
Schenectady, New York



## Introduction

This glossary is based on volumes of the *Nondestructive Testing Handbook*,<sup>1-10</sup> published by the American Society for Nondestructive Testing.

The definitions in this glossary have been modified to satisfy peer review and editorial style. For this reason, references given in this glossary should be considered not attributions but rather acknowledgments and suggestions for further reading.

The definitions in this *Nondestructive Testing Handbook* volume should not be referenced for inspections performed according to standards or specifications or in fulfillment of contracts. Standards writing bodies take great pains to ensure that their documents are definitive in wording and technical accuracy. People working to written contracts or procedures should consult definitions referenced in those standards when appropriate.

This glossary is provided for instructional purposes. No other use is intended.

## Terms

### A

**Å:** *Angstrom*.

**absorbed dose:** Amount of energy imparted to matter by an ionizing event per unit mass of irradiated material at the place of interest. *Absorbed dose* is expressed in *gray* (Gy) or *rad*.<sup>11</sup>

**absorption:** Event where photons in a beam of radiation interact with atoms of a material the photons pass through and are reduced in energy by this interaction.<sup>7,12</sup>

**absorption coefficient, linear ( $\mu_l$ ):** Fractional decrease in transmitted intensity per unit of absorber thickness. Expressed in units of  $\text{cm}^{-1}$ .<sup>7,12</sup>

**accelerator:** (1) Device that accelerates charged particles to high energies. Examples are X-ray tubes, linear accelerators and betatrons. (2) Linear accelerator.

**acceptable quality level (AQL):** Maximum percentage of defective units of the total units tested in an acceptable lot.

**acceptance criteria:** Standard against which test results are to be compared for purposes of establishing the functional acceptability of a part or system being examined.

**acceptance level:** Average or standard test level above or below which test objects are acceptable, in contrast to *rejection level*.<sup>4,13</sup>

**acceptance standard:** Specimen similar to the test object containing natural or artificial discontinuities that are well defined and similar in size or extent to the maximum acceptable in the product. See *reference standard* and *standard*.<sup>4,6,7</sup>

**accommodation:** Of the eye, adjustment of the lens' focusing power by changing the thickness and curvature of the lens by the action of tiny muscles attached to the lens.<sup>8</sup> Accommodation facilitates the viewing of objects near and far.

**accuracy:** Degree of conformity of a particular measurement to a standard or true value.

**activation:** Process by which neutrons bombard stable atoms and make them radioactive.

**activity:** Degree of radioactivity of a particular isotope. Activity is expressed as the number of atoms disintegrating per unit of time. Measured in *becquerel*.

**actual throat:** See *throat*, *actual*.

**acuity:** See *neural acuity*; *vision acuity*.

**adaptive thresholding:** Threshold value varying with inconstant background gray level.<sup>8</sup>

**agency:** Organization selected by an authority to perform nondestructive testing, as required by a specification or purchase order.<sup>2</sup>

**algorithm:** Prescribed set of well defined rules or processes for the solution of a mathematical problem in a finite number of steps.<sup>4,14</sup>

**alpha particle:** Positively charged helium ion emitted by certain radioactive materials. It is made up of two neutrons and two protons; hence it is identical with the nucleus of a helium atom.<sup>11</sup>

**alternating current:** Electrical current that reverses its direction of flow at regular intervals.<sup>6</sup>

**alternating current field:** Varying magnetic field produced around a conductor by an alternating current flowing in the conductor.<sup>6</sup>

**ampere (A):** Unit of electric current.<sup>6</sup>

**analog-to-digital converter:** Circuit whose input is information in analog form and whose output is the same information in digital form.<sup>4,14</sup>

**angstrom (Å):** Unit of distance once used to express wavelengths of electromagnetic radiation. The SI unit nanometer (nm) is now preferred; 1 nm = 10 Å.<sup>2,8</sup>

**anode:** (1) In radiography, the positive electrode of a cathode ray tube that generates ionizing radiation. (2) Positively charged terminal, which may corrode electrochemically during production of an electric current. Compare *cathode*.<sup>8</sup>

**anomaly:** Variation from normal material or product quality.<sup>4</sup>

**AOQ:** Average outgoing quality.

**AOQL:** Average outgoing quality limit.

**AQL:** See *acceptable quality level*.

**arc welding:** See *electric arc welding*.

**artifact:** In nondestructive testing, an indication that may be interpreted incorrectly as a discontinuity.<sup>2</sup>

**artificial discontinuity standard:** See *acceptance standard*.

**artificial discontinuity:** Reference point, such as a hole, groove or notch, that is introduced into a reference standard to provide accurately reproducible sensitivity levels for nondestructive test equipment.<sup>4,13</sup> A manufactured material anomaly. See *acceptance standard* and *reference standard*.<sup>6</sup>

**artificial flaw standard:** See *acceptance standard*.

**ASNT:** American Society for Nondestructive Testing.

**ASNT Recommended Practice No. SNT-TC-1A:** Set of guidelines for employers to establish and conduct a nondestructive testing personnel qualification and certification program. *SNT-TC-1A* was first issued in 1968 by the Society for Nondestructive Testing (SNT, now ASNT) and has been revised every few years since.<sup>8</sup>

**attenuation:** (1) Decrease in energy or signal magnitude in transmission from one point to another. Can be expressed in decibels or as a scalar ratio of the input magnitude to the output magnitude.<sup>4,14</sup> (2) Change in signal strength caused by an electronic device such as an attenuator.<sup>7</sup> (3) In radiography, the decrease in radiation intensity caused by distance, by passage through material or by both.<sup>11</sup>

**austenite:** Face centered cubic phase of iron, which phase is stable between 906 °C (1663 °F) and 1390 °C (2535 °F) and which often acts as a solvent for carbon. Also called *gamma iron*.

**austenite, retained:** Face centered cubic solid solution in iron or iron-nickel, stable at room temperature.

**automated system:** Acting mechanism that performs required tasks at a determined time and in a fixed sequence in response to certain conditions.<sup>8</sup> *Robotic system*.

## B

**back reflection:** Signal received from the far boundary or back surface of a test object.<sup>7,10</sup>

**back scatter:** See *backscatter*.

**background noise:** Signals that originate from the test object, the test instrument and their surroundings and that interfere with test signals of interest. The higher the level of background noise, the more difficult it is to distinguish a discontinuity. Sometimes called *grass* or *hash*.<sup>5,7,8,10</sup>

**background signal:** Steady or fluctuating output signal of a test instrument caused by the presence of acoustic, chemical, electrical or radiation conditions to which the sensing element responds.<sup>1</sup>

**backscatter:** (1) Interaction of radiation with matter such that the direction of travel after scattering is over 90 degrees and often close to 180 degrees to the original direction of travel. (2) In transmission radiography, interaction of radiation with matter behind the image plane such that scattered radiation returns to the image plane, often adding fog and noise that interfere with production of an image of the specimen. (3) Of scatter imaging, interaction of incident radiation with a specimen that scatters the radiation through large angles frequently greater than 90 degrees to the original direction of travel. Such radiation is used to form an image or to measure a parameter of the specimen, usually through digital techniques.

**backscatter imaging:** In radiographic testing, a family of radiosopic techniques that use *backscatter*.

**barium clay:** Molding clay containing barium, used to eliminate or reduce the amount of scattered or secondary radiation reaching the film.<sup>3</sup>

**baseline:** Standard, average, prior measurements or other criteria used in quality control for comparison and evaluation.

**beam:** Defined stream of radiation particles in which stream all particles are traveling in parallel paths.

**beam quality:** Penetrating energy of a radiation beam.

**beam spread:** Divergence from a beam of radiation in which all particles are traveling in parallel paths.

**becquerel (Bq):** SI unit for measurement of radioactivity, equivalent to one disintegration per second. Replaces *curie*.

**beta particle:** Electron or positron emitted from a nucleus during decay.<sup>11</sup>

**beta ray:** Radiation stream consisting of *beta particles*.

**betatron:** Circular electron accelerator that is a source of either high energy electrons or X-rays. The electrons are injected by periodic bursts into a region of an alternating magnetic field.<sup>11</sup> Sometimes the electrons are used directly as the radiation.

**billet:** Solid semifinished round or square product that has been hot worked for forging, rolling or extrusion.<sup>2</sup>

**bleed:** Refers to molten metal oozing out of a casting. Stripped or removed from the mold before complete solidification.<sup>3</sup>

**blind riser:** Internal riser that does not reach to the exterior of the mold.<sup>3</sup>

**blister:** Discontinuity in metal, on or near the surface, resulting from the expansion of gas in a subsurface zone. Very small blisters are called pinheads or pepper blisters.<sup>2</sup>

**blowhole:** Hole in a casting caused by gas expanding in molten metal.

**Bq:** *Becquerel*.

**brazing:** Joining of metals and alloys by fusion of nonferrous alloys that have melting points above 430 °C (806 °F), but below melting points of materials being joined.<sup>2</sup>

**bremsstrahlung:** Electromagnetic radiation produced when electrons' path and kinetic energy brings them close to the positive fields of atomic nuclei — as when, for example, electrons strike a target provided for this purpose. The electrons slow down, giving up kinetic energy as X-radiation.

**bridging:** Premature solidification of metal across a mold section before the metal below or beyond solidifies.<sup>3</sup>

**brinelling:** Stripe indentations made by a spherical object. *False brinelling* refers to a type of surface wear.<sup>8</sup>

**brittle crack propagation:** Very sudden propagation of a crack with the absorption of no energy except that stored elastically in the body. Microscopic examination may reveal some deformation even though it is not visible to the unaided eye.<sup>2</sup>

**brittleness:** Quality of a material that may lead to crack formation and propagation without appreciable plastic deformation.<sup>2</sup>

**burning:** Extreme overheating. Makes metal grains excessively large and causes the more fusible constituents of steel to melt and run into the grain boundaries or it may leave voids between the grains. Steel may be oxidized to the extent that it is no longer useful and cannot be corrected by heat treating but it can be remelted.<sup>2</sup>

**burnt-in sand:** Discontinuity consisting of a mixture of sand and metal cohering to the surface of a casting.<sup>3</sup>

**burr:** Raised or turned over edge occurring on a machined part and resulting from cutting, punching or grinding.<sup>8,15</sup>

**burst:** In metal, external or internal rupture caused by improper forming.<sup>8</sup> See also *crack, forging*.

**butt weld or butt joint:** Weld joining two metal pieces in the same plane.<sup>8</sup>

## C

**C:** *Coulomb*.

**calcium tungstate:** Fluorescent chemical compound that emits visible blue violet light when irradiated by X-rays or gamma rays.

**calibration reflector:** See *reference reflector*.

**camera:** Device that contains a sealed radiation source, where the source or shielding can be moved so that the source becomes unshielded (to make a radiographic exposure) or shielded (for safe storage).

**case crushing:** Mechanism producing fracture of the case, like subcase fatigue but attributable to static overloading rather than to fatigue alone. In many instances the movement of the subcase causes the case to crack or spall.<sup>8</sup>

**casing:** Many strings of pipe that are used to line the hole during and after drilling of a gas or oil well.<sup>8</sup>

**casing string:** Tubular structure on the outer perimeter of a gas or oil well hole. The casing string is a permanent part of the well and many are cemented into the formation.<sup>8</sup>

**cassette, film:** Lightproof container that is used for holding radiographic film in position during the radiographic exposure. The cassette may be rigid or flexible and may contain intensifying screens, filter screens, both or neither.<sup>11</sup>

**cast structure:** Internal physical structure of a casting evidenced by shape, orientation of grains and segregation of impurities.<sup>2,3</sup>

**cast weld assembly:** Assembly formed by welding one casting to another.<sup>3</sup>

**casting:** Object of shape obtained by solidification of a substance in a mold.

**casting shrinkage:** Total shrinkage includes the sum of three types:  
(1) liquid shrinkage (the reduction in volume of liquid metal as it cools through the liquidus to the solidus);  
(2) solidification shrinkage (the change in volume of metal from the beginning to ending of solidification);  
and (3) solid shrinkage (the reduction in volume of metal from the solidus to room temperature).<sup>2,3</sup>

**casting strains:** Strains in a casting caused by casting stresses that develop as the casting cools.<sup>3</sup>

- casting stresses:** Stresses set up in a casting because of geometry and casting shrinkage.<sup>3</sup>
- cathode:** (1) Negatively charged terminal in an arrangement that produces current by chemical reactions. Compare *anode*.<sup>8</sup> (2) In radiography, the negative electrode of an X-ray tube, the electrode from which electrons are emitted.
- cathode ray:** Stream of electrons emitted by a heated filament and projected in a more or less confined beam under the influence of a magnetic or electric field.<sup>7,12</sup>
- cathode ray tube:** Vacuum tube in which an electron beam of *cathode rays* are projected on a fluorescent screen to produce an image or spot.
- cavitation fatigue:** Form of pitting caused by erosion from vibration and movement in liquid environments.<sup>8</sup>
- cementite:** Iron carbide ( $\text{Fe}_3\text{C}$ ), present in steels.<sup>8</sup>
- centrifugal casting:** Casting made in a mold (sand, plaster or permanent) that rotates while the metal solidifies under the pressure developed by centrifugal force.<sup>3</sup>
- certification:** Process of providing written testimony that an individual (or test technique, process or equipment) is qualified. See also *certified*.<sup>8</sup>
- certified:** Having written testimony of qualification. See also *certification*.<sup>8</sup>
- cesium-137:** Radioactive isotope of element cesium, having a half life of 30 years and photon energy of about 660 keV.
- chaplet:** Metal support used to hold a core in place on a mold.<sup>3</sup>
- characteristic curve:** Curve that expresses film density as function of log relative exposure. These curves are useful in determining exposure correction factors and to define the gamma characteristics of the film.
- chill:** (1) Metal insert embedded in the surface of a sand mold or core or placed in a mold cavity to increase the cooling rate at that point. (2) White iron occurring on a gray iron casting, such as the chill in the wedge test.<sup>3</sup>
- chipping:** (1) Removing seams and other surface discontinuities in metals manually with chisel or gouge or by continuous machining, before further processing. (2) Removing excessive metal.<sup>2,3</sup>
- Ci:** *Curie*.
- cire perdue process:** *Lost wax process*.<sup>3</sup>
- clean:** Free from interfering solid or liquid contamination on the test surface and within voids or discontinuities.<sup>2</sup>
- cleavage fracture:** Fracture, usually of a polycrystalline metal, in which most of the grains have failed by cleavage, resulting in bright reflecting facets. It is one type of crystalline fracture. Contrast with *shear fracture*.<sup>2</sup>
- closing:** In image processing, dilation followed by erosion. A single pixel closing connects a broken feature separated by one pixel. See also *opening*.<sup>8</sup>
- closure:** Process by which a person cognitively completes patterns or shapes that are incompletely perceived.<sup>8</sup>
- cobalt-60:** Radioactive isotope of element cobalt, having half life of 5.3 years and photon energies of 1.17 and 1.33 MeV.
- code:** Standard enacted or enforced as a law.<sup>8</sup>
- coefficients of the filter:** Values in a mask that serves as a filter in image formation and processing.<sup>8</sup>
- coherent radiation:** Radiation at the same energy and phase.
- coherent scatter:** Form of scatter where no energy is lost.
- cold cathode ionization gage:** Pressure measuring gage for low pressures, in the range of 13.3 mPa to below 0.13 nPa ( $10^{-4}$  torr to below  $10^{-12}$  torr), that works by measuring a discharge current associated with the ionization of gas by electrons confined in a magnetic field. Also called a *philips discharge gage* or *penning gage*.
- cold chamber machine:** Die casting machine where the metal chamber or plunger are not heated.<sup>3</sup>
- cold cracks:** Discontinuities appearing as straight lines usually continuous throughout their length and generally existing singly. Cold cracks start at the surface and result from cold working or stressing of metallic materials.<sup>2</sup>
- cold shut:** (1) Casting discontinuity caused by two streams of semimolten metal coming together inside a mold but failing to fuse. Cold shuts are sometimes called misruns but the latter term correctly describes incomplete filling of the mold.<sup>3</sup> (2) A discontinuity that appears on the surface of metal as a result of two streams of liquid meeting and failing to unite. A cracklike discontinuity caused by forging, where two surfaces of metal fold against each other to produce a discontinuity at the point of folding. This is usually at some angle to the surface. It may also be a separate piece of metal forged into the main component. See *lap*. (3) A portion of the surface of a forging that is separated in part from the main body of metal by oxide.<sup>2,3</sup>



- cold work:** Permanent deformation produced by an external force in a metal at temperature below its recrystallization temperature.<sup>2</sup>
- collimator:** Device for restricting the size, shape and direction of the irradiating beam, thereby limiting beam spread and its consequences.
- color discrimination:** Perception of differences between two or more hues.<sup>8</sup>
- compensator:** Electrical matching network to compensate for electrical impedance differences.<sup>7,12</sup>
- compensator blocks:** Material added to regions of a test object to flatten its radiographic image.
- complete testing:** Testing of an entire production lot in a prescribed manner. Sometimes complete testing entails the inspection of only the critical regions of a part. One hundred percent testing requires the inspection of the entire part by prescribed methods. Compare *sampling, partial*.<sup>8</sup>
- compton scatter:** Reduction of energy of incident photon by its interaction with an electron. Part of the photon energy is transferred to the electron, giving it kinetic energy, and the remaining photon is redirected with reduced energy.
- computed tomography:** Technique by which radiation passing through an object is displayed as one slice or layer of that object at a time. Image data are processed in three dimensions.
- contrast:** (1) In film radiography, the measure of differences in the film blackening or density resulting from various radiation intensities transmitted by the object and recorded as density differences in the image. Thus, difference in film blackening from one area to another.<sup>11</sup> (2) The difference in visibility between an indication and the surrounding area.
- contrast, subject:** Ratio of radiation intensities transmitted by selected portions of object being radiographed.
- control:** See *in control, process control* and *quality control*.
- control cable:** Cable connected to isotopic radiographic source and used to move the source in and out of the exposure device.
- core:** (1) Specially formed material inserted in a mold to shape the interior of another part of a casting that cannot be shaped as easily by the pattern. (2) In a ferrous alloy, the inner portion that is softer than the outer portion or case.<sup>3</sup>
- corrosion:** Deterioration of a metal by chemical or electrochemical reaction with its environment. Removal of material by chemical attack, such as the rusting of automobile components.<sup>2</sup>
- corrosion, crevice:** Type of galvanic corrosion caused by a difference in partial pressure of oxygen between the occluded interior and exposed exterior of a notchlike geometry. Active metal ions are usually present.
- corrosion embrittlement:** Severe loss of ductility of a metal, resulting from corrosive attack, usually intergranular and often not visually apparent.<sup>2</sup>
- corrosion fatigue:** Fatigue cracking caused by repeated load applications on metal in a corrosive environment.<sup>2</sup>
- corrosion, fretting:** Corrosion facilitated by fretting, particularly where a protective surface has been chafed in a corrosive environment.<sup>8</sup>
- corrosion-erosion:** Simultaneous occurrence of erosion and corrosion.<sup>8</sup>
- coulomb (C):** SI unit for electric charge, replacing faraday and ampere hour, where 1 A·h = 3600 C. X-ray or gamma ray intensity is measured in coulomb per kilogram (C·kg<sup>-1</sup>).
- coupon:** Piece of material from which a test object is prepared, often an extra piece, as on a casting or forging.<sup>3</sup>
- crack:** (1) Break, fissure or rupture, usually V shaped and relatively narrow and deep. A discontinuity that has a relatively large cross section in one direction and a small or negligible cross section when viewed in a direction perpendicular to the first.<sup>2</sup> (2) Propagating discontinuities caused by stresses such as heat treating or grinding. Difficult to detect unaided because of fineness of line and pattern (may have a radial or latticed appearance).<sup>6</sup>
- crack, base metal:** Cracks existing in base metal before a manufacturing or welding operation or occurring in base metal during the operation.<sup>2</sup>
- crack, cold:** Cracks that occur in a casting or weld after solidification and that are caused by excessive stress generally from nonuniform cooling.<sup>2</sup>
- crack, cooling:** Cracks in bars of alloy or tool steels resulting from uneven cooling after heating or hot rolling. They are usually deep and lie in a longitudinal direction, but are usually not straight.<sup>2</sup>
- crack, crater:** Multisegment crack in a weld crater. Segments radiate from a common point, often called star cracks.
- crack, fatigue:** Progressive cracks that develop in the surface and are caused by the repeated loading and unloading of the object.<sup>2</sup>

**crack, forging:** Crack developed in the forging operation due to forging at too low a temperature, resulting in rupturing of the metal.<sup>2</sup> Also called *forging burst*.

**crack, hot:** Crack that develops before the casting has completely cooled, as contrasted with cold cracks, that develop after solidification.<sup>2</sup>

**crack, longitudinal:** Crack parallel to the length of the test object.<sup>2</sup>

**crack, machining:** Crack caused by too heavy a cut, a dull tool or chatter. Typically called *machining tears*.<sup>2</sup>

**crack, quenching:** Ruptures produced during quenching of hot metal due to more rapid cooling and contraction of one portion of a test object than occurs in adjacent portions.<sup>2</sup>

**crack, transverse:** Cracks at right angles to the length of the test object.<sup>2</sup>

**crack, weld:** Cracks in weld fusion zones or adjacent base metal. Usually a result of thermal expansion or contraction stresses related to temperature changes during welding.<sup>2</sup>

**crater:** In arc or gas fusion welding, a cavity in the weld bead surface, typically occurring when the heat source is removed and insufficient filler metal is available to fill the cavity.<sup>2</sup>

**crevice corrosion:** See *corrosion, crevice*.

**CRT:** See *cathode ray tube*.

**crush:** Casting discontinuity caused by a partial destruction of the mold before the metal was poured.<sup>3</sup>

**curie (Ci):** Unit for measurement of the quantity of radioactivity, corresponding originally to radiation from atomic disintegrations from 1 g of radium; replaced by *becquerel* (Bq) in SI, where 1 Ci =  $3.7 \times 10^{10}$  Bq.

## D

**decay curve:** Graph showing radioactive strength as a function of time for an isotope. Decay curves are used in determining exposure times in radiographic testing.

**defect:** Discontinuity whose size, shape, orientation or location make it detrimental to the useful service of its host object or which exceeds the accept/reject criteria of an applicable specification.<sup>6,10,17</sup> Note that some discontinuities may not affect serviceability and are therefore not defects.<sup>2</sup> All defects are discontinuities.<sup>2</sup> Compare *discontinuity* and *indication*.<sup>8,15</sup>

**definition:** Description of linear demarcation sensitivity, or the detail sharpness of object outline in a radiographic image. It is a function of screen type, exposure geometry, radiation energy and characteristics of film or sensor.

**deformation:** Change of shape under load. See also *creep*.<sup>8</sup>

**delamination:** Laminar discontinuity, generally an area of unbonded materials.<sup>7</sup>

**depth of field:** Range of distance over which an imaging system gives satisfactory definition when its lens is in the best focus for a specific distance.<sup>8</sup>

**depth of focus:** Distance a sensor may be moved from a lens system and still produce a sharp image.

**depth of fusion:** Depth to which base metal has melted during welding.<sup>2</sup>

**detail:** In radiography, the degree of sharpness of outline of an image, or the clear definition of an object or discontinuity in the object. See also *definition*.

**detector, X-ray:** *Sensor, X-ray*.

**developer:** In radiography, a chemical solution that reduces exposed silver halide crystals to metallic silver.<sup>11</sup>

**dewaxing:** Removing the expendable wax pattern from an investment mold by heat or solvent.<sup>3</sup>

**die casting:** (1) Casting made in a die. (2) Casting process where molten metal is forced under high pressure into the cavity of a metal mold.<sup>3</sup>

**diffraction:** Special case of scatter, where coherently scattered photons undergo interference or reinforcement, resulting in patterns indicative of the scattering medium. See also *X-ray diffraction*.

**dilation:** In image processing, the condition of a binary image where the pixel in the output image is a 1 if any of its eight closest neighbors is a 1 in the input image. See also *closing*, *erosion* and *opening*.<sup>8</sup>

**discontinuity:** Intentional or unintentional interruption in the physical structure or configuration of a part.<sup>6,8,16</sup> After nondestructive testing, unintentional discontinuities interpreted as detrimental in the host object may be called *flaws* or *defects*.<sup>6</sup> Compare *defect*, *dislocation* and *indication*.

**discontinuity, artificial:** Reference discontinuities such as holes, indentations, cracks, grooves or notches that are introduced into a reference standard to provide accurately reproducible indications for determining sensitivity levels.<sup>2</sup>



**discontinuity, inherent:** Material anomaly originating from solidification of cast metal. Pipe and nonmetallic inclusions are the most common and can lead to other types of discontinuities in fabrication.<sup>8,15</sup>

**discontinuity, primary processing:** Material anomaly produced from the hot or cold working of an ingot into forgings, rod and bar.<sup>8,15</sup>

**discontinuity, secondary processing:** Material anomaly produced during machining, grinding, heat treating, plating or other finishing operations.<sup>8,15</sup>

**discontinuity, service induced:** Material anomaly caused by the intended use of the part.<sup>8</sup>

**dose:** See *absorbed dose*.

**dose rate:** Radiation dose delivered per a specified unit of time and measured, for instance, in sievert per minute (or in rem per hour). See also *absorbed dose*.<sup>11</sup>

**dosimeter:** Device that measures radiation dose, such as a film badge or ionization chamber.<sup>11</sup>

**drop:** Discontinuity in a casting due to a portion of the sand dropping from the cope or overhanging section of the mold.<sup>3</sup>

**drop out:** Falling away of green sand from the walls of a mold cavity when the mold is closed.<sup>3</sup>

**dross:** Scum that forms on the surface of molten metals largely because of oxidation but sometimes because of the rising of impurities to the surface.<sup>3</sup>

**element:** Chemical substance that cannot be divided into simpler substances by chemical means. Examples are hydrogen, lead and uranium.<sup>2</sup>

**erosion:** (1) Loss of material or degradation of surface quality through friction or abrasion by moving fluids, made worse by solid particles in those fluids or by cavitation in the moving fluid. (2) In image processing, condition of a binary image where the pixel in the output image is a 1 if each of its eight neighbors is a 1 in the input image. See also *closing*, *dilation* and *opening*.<sup>8</sup>

**erosion-corrosion:** Simultaneous occurrence of erosion and corrosion.<sup>8</sup>

**eV:** *Electronvolt*.

**evaluation:** Process of determining the magnitude and significance of a discontinuity after the indication has been interpreted as relevant. Evaluation determines if the test object should be rejected, repaired or accepted. See *indication* and *interpretation*.<sup>2,6,7</sup>

**exfoliation:** Corrosion that progresses approximately parallel to the outer surface of the metal, causing layers of the metal to be elevated by the formation of corrosion product.<sup>2</sup>

**exposure factor:** In X-radiography, the quantity that combines source strength (milliamperage), time (usually minute) and distance. It is the product of milliamperage and time divided by distance squared and determines the degree of film density.

## E

**effective focal spot:** Size and geometry of focal spot after target interaction.

Viewed from along the primary beam central axis at the target the effective focal spot would appear nearly square and smaller than the actual focal spot area covered by the electron stream.

**effective throat:** In welding, the weld throat including the amount of weld penetration but ignoring excess metal between the theoretical face and the actual face.<sup>8</sup>

**electric arc welding:** Joining of metals by heating with electric arc. Also called *arc welding*.<sup>8</sup>

**electrochemical corrosion:** Corrosion that occurs when current flows between cathodic and anodic areas on metallic surfaces.<sup>2</sup>

**electronvolt (eV):** Kinetic energy acquired by an electron in passing through a potential difference of 1 V in vacuum; 1 eV = ~1.60 J. The electronvolt is commonly used to express the energy of X-rays.

## F

**false brinelling:** Fretting wear indentations. Compare *brinelling*.<sup>8</sup>

**false indication:** Indication that could be interpreted as originating from a discontinuity but which actually originates where no discontinuity exists.<sup>7</sup> Distinct from nonrelevant indication.<sup>2</sup> Compare *defect*.<sup>8</sup>

**fatigue fracture:** Progressive fracture of a material that begins at a discontinuity and increases under repeated cycles of stress. The phenomenon leading to fracture under repeated or fluctuating stresses having a maximum value less than the tensile strength of the material.<sup>2</sup>

**feature extraction:** From an enhanced image, derivation of some feature values, usually parameters for distinguishing objects in the image.<sup>8</sup>

- ferromagnetic material:** Material such as iron, nickel or cobalt whose relative permeability is considerably greater than unity and depends on the magnetizing force.<sup>4,14</sup> Materials that are most strongly affected by magnetism are called ferromagnetic.<sup>2</sup>
- field:** In video technology, one of two video picture components that together make a frame. Each picture is divided into two parts called *fields* because a frame at the rate of thirty frames per second in a standard video output would otherwise produce a flicker discernible to the eye. Each field contains one half of the total picture elements. Two fields are required to produce one complete picture or frame so the field frequency is sixty fields per second and the frame frequency is thirty frames per second.<sup>8</sup>
- field of view:** Range or area that can be seen through an imaging system, lens or aperture.<sup>8</sup>
- fillet weld:** Weld at vertex or corner formed by two metal pieces.<sup>8</sup>
- film badge:** Package of photographic film worn as a badge by radiographic personnel (and by workers in the nuclear industry) to measure exposure to ionizing radiation. Absorbed dose can be calculated by degree of film darkening caused by irradiation.<sup>11</sup>
- film holder:** See *cassette, film*.
- film speed:** Relative exposure required to attain a specified film density.<sup>11</sup>
- film undercut:** See *undercut, film*.
- filter:** (1) Network that passes electromagnetic wave energy over a described range of frequencies and attenuates energy at all other frequencies.<sup>4,13</sup> (2) Processing device or function that excludes a selected kind of signal or part of a signal.<sup>8</sup> (3) In radiography, the thickness of absorbing material placed in a primary radiation beam to selectively remove longer wavelength radiation, thereby adjusting the quality of the radiographic image.
- fine crack:** Discontinuity in a solid material with a very fine opening to the surface, but possessing length and depth greater than the width of this opening. Usually the depth is many times the width.<sup>2</sup>
- finite element analysis:** Numerical technique for the analysis of a continuous system whereby that system is decomposed into a collection of finite sized elements.<sup>4</sup>
- fit up:** To secure one or more joint members with special external fixturing to prevent movement during welding.<sup>8,15</sup>
- fixing:** Procedure used in film processing that removes undeveloped silver salts in the emulsion from the surface of the film, leaving only the developed black silver of the image on the film.
- flakes:** Short discontinuous internal fissures in ferrous metals attributed to stresses produced by localized transformation and/or decreased solubility of hydrogen during cooling usually after hot working. On a fractured surface, flakes appear as bright silvery areas; on an etched surface they appear as short, discontinuous cracks.<sup>8,15</sup> Also called *shatter cracks* and *snowflakes*.<sup>2</sup>
- flaw:** Rejectable anomaly or unintentional discontinuity. See also *defect* and *discontinuity*.<sup>2</sup>
- focal spot:** Area on target that receives bombardment of electrons. See also *effective focal spot*.
- focus:** Position of a viewed object and a lens system relative to one another to offer a distinct image of the object as seen through the lens system. See *accommodation* and *depth of field*.<sup>8</sup>
- focus, principal plane of:** Single plane actually in focus in a photographic scene.<sup>8</sup>
- fog:** Increase of film density caused by sources other than from the intended primary beam exposure. Heat, humidity, pressure and scatter radiation can all cause fogging of the film.
- foil:** Metal in sheet form less than 0.15 mm ( $6 \times 10^{-3}$  in.) thick.<sup>2</sup>
- foreign materials:** Inclusions that may be sand, slag, oxide or dross metal or any dissimilar material in the material being examined. In radiographic film, foreign materials may appear as isolated, irregular or elongated variations of film density not corresponding to variations in thickness of material or to cavities.<sup>3</sup>
- forging burst:** Also called *forging crack*. See *crack, forging*.
- forging crack:** Also called *forging burst*. See *crack, forging*.
- foundry:** Establishment or building where metal castings are produced.<sup>3</sup>
- fracture:** Break, rupture or crack large enough to cause a full or partial partition of a casting.<sup>2,3</sup>
- frame:** Complete raster scan projected on a video screen. There are thirty frames per second in a standard video output. A frame may be comprised of two fields, each displaying part of the total frame. See also *field*.<sup>8</sup>

**fretting:** Action that results in surface damage, especially in a corrosive environment, when there is low amplitude motion between solid surfaces in contact under pressure. Also called *fretting corrosion*.<sup>2</sup>

**fretting corrosion:** See *corrosion, fretting*.

## G

**galling:** Type of adhesive wear more gross than fretting.<sup>8</sup>

**gamma iron:** *Austenite*.

**gamma rays:** High energy, short wavelength electromagnetic radiation emitted by the nucleus of a radioactive isotope. Energies of gamma rays are usually between 0.01 and 10 MeV. X-rays also occur in this energy range but are of nonnuclear origin.<sup>11</sup>

**gas holes:** Holes created by a gas evolving from molten metal.<sup>2</sup> Appear as dark spots occurring individually, in clusters or distributed throughout a casting.<sup>3</sup>

**gas porosity:** Gas pockets or voids in metal. Refers to porous sections in metal that appear as round or elongated dark spots corresponding to minute voids usually distributed through the entire casting.<sup>3</sup> Spherical or elongated internal cavities caused by evolution of dissolved gases from molten metal or slag trapped during cooling and solidification of castings or fusion welds.<sup>2</sup>

**gas tungsten arc welding (GTAW):** Inert gas shielded arc welding using a tungsten electrode. Also called *tungsten inert gas (TIG) welding*.<sup>8</sup>

**gated pattern:** Pattern designed to include gating in the mold.<sup>3</sup>

**general examination:** Test or examination of a person's knowledge, typically (in the case of nondestructive testing personnel qualification) a written test on the basic principles of a nondestructive testing method and general knowledge of basic equipment used in the method. (According to ASNT's guidelines, the general examination should not address knowledge of specific equipment, codes, standards and procedures pertaining to a particular application.) Compare *practical examination* and *specific examination*.<sup>8</sup>

**geometric unsharpness:** See *unsharpness, geometric*.

**gouge:** Surface indentation caused by forceful abrasion or impact or flame cutting. Also called *nick*. Compare *tool mark*.<sup>8</sup>

**gradient:** Slope of *characteristic curve* for specified film density.

**graininess:** Film characteristic that results from improper film processing and that consists of the grouping or clumping together of many small silver grains into masses visible to the naked eye or with slight magnification.<sup>11</sup>

**grains:** (1) Solid particle or crystal of metal. As molten metal solidifies grains grow and lattices intersect, forming irregular grain boundaries.<sup>8</sup> (2) Individual crystals that make up the crystalline structure of metal.<sup>2</sup>

**gray (Gy):** SI unit for measurement of the dose of radiation absorbed per unit mass at a specified location. Replaces the *rad* where *rad* denotes *radiation absorbed dose*, not *radian*.

1 Gy = 1 J·kg<sup>-1</sup> = 100 rad.

**gray level:** Integer number representing the brightness or darkness of a pixel or, as a composite value, of an image comprised of pixels.<sup>8</sup>

**gross porosity:** In weld metal or in a casting, pores, gas holes or globular voids that are larger and in greater number than obtained in good practice.<sup>2,3</sup>

**guide tube:** Cable connected to isotopic radiographic source and used to move the source in and out of the exposure device.

**Gy:** *Gray*.

## H

**halation:** Spreading of light around a bright image on a fluorescent screen or developed film.

**hardness:** (1) Of metals, temper or stiffness or resistance to plastic deformation, usually by indentation. (2) Of metals, temper or resistance to scratching, abrasion or cutting.<sup>2</sup>

**heat affected zone (HAZ):** Base metal not melted during brazing, cutting or welding, but whose microstructure and physical properties were altered by the heat.<sup>2</sup>

**heat checking:** Surface cracking caused when metal rapidly heated (or cooled and heated repeatedly) is prevented from expanding freely by colder metal below the surface. Friction may produce the heat. Sometimes called *thermal fatigue*.<sup>8</sup>

**holes:** Any voids remaining in an object as a result of improper manufacturing processing. Often called *gas holes*, *cavities* or *air locks*.<sup>2</sup>

**hot cracks:** Ragged dark lines of variable width and numerous branches. They have no definite line of continuity and may exist in groups. They may originate internally or at the surface.<sup>3</sup> Cracks occurring in hot solid metals, caused by stresses of thermal expansion or contraction and originating either internally or at the surface.<sup>2</sup>

**hot tears:** Fractures formed in a metal during solidification because of hindered contraction. Surface cracks on castings produced by contraction of the metal during cooling.<sup>2,3</sup> Hot tears often occur where areas of different thickness adjoin.<sup>8</sup>

**hundred percent testing:** See *one hundred percent testing*.

**I**

**icicles:** Coalescence of metal protruding beyond the root of the weld. Sometimes called *burn through*.<sup>2</sup>

**image:** Visual representation of a test object or scene.<sup>8</sup>

**image enhancement:** Any of a variety of image processing steps, used singly or in combination to improve the detectability of objects in an image.<sup>8</sup>

**image orthicon:** Television tube that uses the photoemission method. Compare *vidicon tube*.<sup>8</sup>

**image processing:** Actions applied singly or in combination to an image, in particular the measurement and alteration of image features by computer. Also called *picture processing*.<sup>8</sup>

**image quality indicator:** Strip of material the same composition as that of the material being tested, representing a percentage of object thickness and provided with a combination of steps, holes or slot or alternatively made as a series of wires. When placed in the path of the rays, its image provides a check on the radiographic technique employed.<sup>3-11</sup>

**image segmentation:** Process in which the image is partitioned into regions, each homogeneous.<sup>8</sup>

**impregnation:** (1) Treatment of porous castings with a sealing medium to stop pressure leaks. (2) The process of filling the pores of a sintered compact, usually with a liquid such as a lubricant. (3) The process of mixing particles of a nonmetallic substance in a matrix of metal powder, as in diamond impregnated tools.<sup>3</sup>

**impurities:** Elements or compounds whose presence in a material is unintentional.<sup>2,3</sup>

**in control:** Within prescribed limits of process control.<sup>8</sup>

**in-motion radiography:** Technique in which either the object being radiographed or the source of radiation is in motion during the exposure.<sup>3,11</sup>

**incident radiation:** Primary radiation striking an object at closest point.

**inclusion:** Foreign particles or impurities, usually oxides, sulfides, silicates and such, that are retained in metal (welds or castings) during solidification or that are formed by subsequent reaction of the solid metal.<sup>2,3</sup>

**incomplete fusion:** Fusion that is less than complete. Failure of weld metal to fuse completely with and bond to the base metal or preceding bead.<sup>2</sup>

**incomplete penetration:** In welding, root penetration that is less than complete or failure of a root pass and a backing pass to fuse with each other.<sup>2</sup> Also called *lack of fusion*.<sup>2</sup>

**index of refraction:** Ratio of velocity of light in a vacuum to velocity of light in a material.

**indication:** Nondestructive testing discontinuity response that requires interpretation to determine its relevance. Compare *defect*, *discontinuity* and *false indication*.<sup>8</sup>

**indication, discontinuity:** Visible evidence of a material discontinuity. Subsequent interpretation is required to determine the significance of an indication.<sup>2</sup>

**indication, false:** (1) Indication produced by something other than a discontinuity.<sup>6</sup> (2) Indication due to misapplied or improper testing.<sup>2</sup>

**indication, nonrelevant:** Indication caused by a condition that does not affect the usability of the object (a change of section, for instance).<sup>2</sup>

**indication, relevant:** Indication from a discontinuity (as opposed to a nonrelevant indication) requiring evaluation by a qualified inspector, typically with reference to an acceptance standard, by virtue of the discontinuity's size or location.<sup>8,16</sup>

**inherent discontinuities:** Discontinuities that are produced in the material at the time it is formed (for example, during solidification from the molten state).<sup>2</sup>

**intergranular corrosion:** Corrosion occurring preferentially at grain boundaries.<sup>2</sup>

**intergranular stress corrosion cracking:** Anomaly caused by intergranular corrosion as a result of sensitized material, stress and corrosive environment (typical in the heat affected zone of stainless steel welds).



**interlaced scanning:** Process whereby the picture appearing on a video screen is divided into two parts. Interlaced scanning reduces flicker by increasing the electron beam's downward rate of travel so that every other line is sent. When the bottom is reached, the beam is returned to the top and the alternate lines are sent. The odd and even line scans are each transmitted at 1/60 s, totaling 1/30 s per frame and retaining the standard rate of 30 frames per second. The eye's persistence of vision allows the odd and even lines to appear as a single image without flicker.<sup>8</sup>

**interpretation:** Determination of the significance of test indications from the standpoint of their relevance or irrelevance. The determination of the cause of an indication or the evaluation of the significance of discontinuities from the standpoint of whether they are detrimental or inconsequential.<sup>2</sup>

**inverse square law:** From a point source of radiation, the intensity of energy decreases as the inverse square of distance from source.<sup>3,11</sup>

**investment casting:** (1) Casting metal into a mold produced by surrounding (investing) an expendable pattern with a refractory slurry that sets at room temperature after which the wax, plastic or frozen mercury pattern is removed. Also called *precision casting* or *lost wax process*. (2) A casting made by the process.<sup>3</sup>

**ion chambers:** Device for measuring radiation due to ionization of a gas in a chamber.

**ionizing radiation:** Form of radiation that can displace orbital electrons from atoms. Types include X-rays, gamma rays and particles such as neutrons, electrons and alpha particles.<sup>11</sup>

**IQI:** *Image quality indicator*.

**irradiance:** Power of electromagnetic radiant energy incident on the surface of a given unit area. Compare *radiance*.<sup>8</sup>

## J

**joint:** (1) Part of the mold where the cope and cheek, cope and drag or cheek and drag come together.<sup>3</sup> (2) Part of weld where two welded parts meet.

**joint efficiency:** Strength of a welded joint expressed as a percentage of the strength of the unwelded base metal.<sup>2</sup>

**joint penetration:** Distance weld metal and fusion extend into a joint.<sup>2</sup>

## L

**lack of fusion:** Discontinuity due to lack of union between weld metal and parent metal or between successive weld beads.<sup>2</sup> Also called *incomplete penetration*.

**lamination:** Discontinuity in plate, sheet or strip caused by pipe, inclusions or blowholes in the original ingot. After rolling, laminations are usually flat and parallel to the outside surface. Laminations may also result from pipe, blisters, seams, inclusions or segregation elongated and are made directional by working. Lamination discontinuities may also occur in metal powder compacts.<sup>2</sup> May appear in the form of rectangles or plates as inclusion stringers between rolled surfaces. Short, intermittent laminations may be detrimental if the object is subjected to high bending stresses in service.<sup>6</sup>

**lap:** Surface discontinuity, usually parallel to the surface, appearing as a fold or tangential seam in a wrought product and caused by folding over of a hot metal fin or sharp corner in a thin plate, then rolling or forging it into the surface but not welding it. See also *cold shut*.<sup>2,6</sup>

**level, acceptance:** In contrast to rejection level, test level above or below which, depending on the test parameter, test objects are acceptable.<sup>2</sup>

**level, rejection:** Value established for indication or test signal above or below which, depending on the test parameter, test objects are rejectable or otherwise distinguished from the remaining objects.<sup>2</sup> See *level, acceptance*.

**light metal:** Low density metal such as aluminum, magnesium, titanium, beryllium or one of their alloys.<sup>2</sup>

**limited certification:** Individuals who are certified only for specific operations are usually called *limited Level* (I, II or III) or are designated as having *limited certification* because they are not qualified to perform the full range of activities expected of personnel at that level of qualification.<sup>8</sup>

**linac:** *Linear accelerator*.

**linear accelerator:** Device that accelerates atomic particles in a straight line through a series of magnetic fields.

**line pair:** Pair of adjacent, parallel lines used to evaluate the resolution of a specific imaging system. See also *minimum line pair*.<sup>8</sup>

**lost-wax process:** Investment casting process in which a wax pattern is used.<sup>3</sup>

**lot tolerance percent defective:** In quality control, the percent defective at which there is a 10 percent probability of acceptance in a production run.<sup>8</sup>

**low pass filtering:** Linear combination of pixel values to smoothen abrupt transitions in a digital image. Also called *smoothing*.<sup>8</sup>

## M

**machine vision:** Automated system function of acquiring, processing and analyzing images to evaluate a test object or to provide information for human interpretation. A typical system consists of a light source, a video camera, a video digitizer, a computer and an image display.<sup>8</sup>

**macroshrinkage:** Casting discontinuity consisting of voids in the form of stringers shorter than shrinkage cracks. This discontinuity results from contraction during solidification where there is not an adequate opportunity to supply filler material to compensate for the shrinkage. It is usually associated with abrupt changes in section size.<sup>2,3</sup> See *shrink*.

**mask:** (1) Square matrix of  $n \times n$  with different values that serves as a filter in image processing.<sup>8</sup> (2) In radiography, a cover with an aperture to view a specific area; *mask plate*. (3) In radiographic testing, a selective radiation filter.

**match plate:** Device used in a high intensity illuminator to limit the light to a specific area, typically less than the size of the film radiograph. See *mask*.

**material noise:** Random signals caused by the material structure of the test object.<sup>10</sup> A component of background noise.<sup>7</sup>

**mathematical morphology:** Image processing technique of expanding and shrinking. The basic operators in mathematical morphology are dilation (expanding), erosion (shrinking), opening and closing.<sup>8</sup>

**measurement system:** Entire system from sensor to display inclusive.<sup>1</sup>

**mechanical properties:** Properties of a material that reveal its elastic and inelastic behavior where force is applied, thereby indicating its suitability for mechanical applications (for example, modulus of elasticity, tensile strength, elongation, hardness and fatigue limit).<sup>2</sup>

**metallic discontinuity:** Break in the continuity of the metal of an object. May be located on the surface (such as a crack) or deep in the interior of the object (such as a gas pocket or inclusion).<sup>2</sup>

**metallography:** Science dealing with the constitution and structure of metals and alloys as revealed by the unaided eye or by such tools as low powered magnifications, optical microscope, electron microscope and X-ray diffraction.<sup>2</sup>

**metallurgy:** Science and technology of metals.<sup>2</sup>

**micro:** Prefix that divides a basic unit of measure by one million.<sup>2</sup>

**microcrack:** Crack less than about 50  $\mu\text{m}$  (0.002 in.) in largest surface dimension. See also *microfissure*.

**microfissure:** Crack of microscopic proportions. See also *microcrack*.

**microporosity:** Porosity visible only with the aid of a microscope.<sup>2</sup>

**microscopic stresses:** Residual stresses that vary from tension to compression in a distance (presumably approximating the grain size) that is small compared to the gage length in ordinary strain measurement. Hence, not detectable by dissection method. Microscopic stresses can sometimes be measured by X-ray shift.<sup>2</sup>

**microsegregations:** (1) Segregation within a grain, crystal or small particle. Also called *coring*.<sup>2</sup> (2) Extremely narrow cracks, usually long and straight, on the surfaces of highly finished wrought metals. Often very shallow, their identity must be established to ensure that the indications are not from detrimental cracks, deep laps or long inclusion stringers.<sup>6</sup>

**microshrinkage:** Casting discontinuity, not detectable at magnifications lower than ten diameters, consisting of interdendritic voids. This discontinuity results from contraction during solidification where there is not an adequate opportunity to supply filler material to compensate for shrinkage. Alloys with a wide solidification temperature range are particularly susceptible.<sup>2,3</sup>

**minimum line pair:** Closest distance that a specific imaging system can resolve between a pair of adjacent, parallel lines (line pair) used to evaluate system resolution.<sup>8</sup>

**misrun:** Casting not fully formed, resulting from the metal solidifying before the mold is filled.<sup>3</sup>

**MKSA:** System of units for mechanics and electromagnetics in which the basic units are meter, kilogram, second and ampere. It is a constituent part of the SI system of units.<sup>4,14</sup>



**model, analytical:** Representation of a process or phenomenon by a set of solvable equations.<sup>4,14</sup>  
**mottle:** In radiographic testing, nonuniform density where it should be uniform, resulting from scattered radiation, secondary radiation, forward scatter and film irregularities. Often confused with *graininess*.

## N

**NDC:** Nondestructive characterization.  
**NDE:** (1) Nondestructive evaluation.  
 (2) Nondestructive examination.<sup>8</sup>  
**NDI:** Nondestructive inspection.<sup>8</sup>  
**NDT:** Nondestructive testing.<sup>8</sup>  
**near ultraviolet radiation:** Ultraviolet radiation with wavelengths ranging from about 320 to about 400 nm. Sometimes called *black light*.<sup>8</sup>  
**necking down:** Localized reduction in area of a specimen or structural member during welding or overloading.<sup>8,15</sup>  
**neural acuity:** Ability of the eye and brain together to discriminate patterns from background. Discrimination is influenced by knowledge of the target pattern, by the scanning technique and by the figure/ground relationship of a discontinuity.<sup>8</sup>  
**neutron:** Uncharged elementary particle with mass nearly equal to that of the proton.<sup>11</sup>  
**neutron fluence:** Integrated exposure (product of current and time) of neutrons per unit area.  
**neutron flux:** Neutron current; quantity of neutrons passing through a unit area per unit time.  
**neutron radiography:** Radiographic testing using a neutron beam.  
**neutron radioscopy:** Radioscopy using a neutron beam.  
**nick:** Surface indentation caused by forceful abrasion or impact. Also called *gouge*. Compare *tool mark*.<sup>8</sup>  
**noise:** Any undesired signals that tend to interfere with normal detection or processing of a desired signal. See *graininess* and *mottle*.  
**nondestructive characterization (NDC):** Branch of nondestructive testing concerned with the description and prediction of material properties and behaviors of components and systems.  
**nondestructive evaluation (NDE):** Another term for *nondestructive testing*. In research and academic communities, the word *evaluation* is often preferred because it connotes quantitative interpretation of nondestructive test data based on understanding of nondestructive test process.

**nondestructive examination (NDE):** Another term for *nondestructive testing*. In the utilities and nuclear industry, *examination* is sometimes preferred because *testing* can imply performance trials of pressure containment or power generation systems.<sup>8</sup>  
**nondestructive inspection (NDI):** Another term for *nondestructive testing*. In some industries (utilities, aviation), the word *inspection* often implies maintenance for a component that has been in service.<sup>8</sup>  
**nondestructive testing (NDT):** Determination of the physical condition of an object without affecting that object's ability to fulfill its intended function. Nondestructive testing techniques typically use a probing energy form to determine material properties or to indicate the presence of material discontinuities (surface, internal or concealed). See also *nondestructive evaluation*, *nondestructive examination* and *nondestructive inspection*.<sup>8</sup>  
**nonrelevant indication:** See *indication*, *nonrelevant*.  
**normalizing:** Heating a ferrous alloy to a suitable temperature above the transformation range and then cooling in air to a temperature substantially below the transformation range.<sup>3</sup>  
**numerical analysis:** Technique to generate numbers as the solution to a mathematical model of a physical system. Used in place of a closed form analytic expression. Usually requires digital computation.<sup>4</sup>

## O

**oil country tubular goods (OCTG):** Hollow cylindrical components used to convey petroleum and related products.<sup>8</sup>  
**one hundred percent testing:** Testing of all parts of an entire production lot in a prescribed manner. Sometimes, *complete testing* entails the testing of only the critical portions of the part. Compare *sampling*, *partial*.<sup>8</sup>  
**opening:** Image processing operation of erosion followed by dilation. A single opening eliminates isolated single pixels. See also *closing*.<sup>8</sup>  
**organoleptic:** Relying on or using sense organs, such as the human eye.<sup>8</sup>  
**orientation:** Angular relationship of a surface, plane, discontinuity or axis to a reference plane or surface.<sup>7,10</sup>  
**orthicon:** See *image orthicon*.<sup>8</sup>

## P

**parallax:** Apparent difference in position of an imaged point according to two differently positioned sensors.<sup>8</sup>

**parting line:** Mark left on the casting where the die halves meet. Also, the surface between the cover and ejector portions of the die.<sup>3</sup>

**pass:** In welding, a single bead along the entire weld length or the process of laying down that bead.<sup>8</sup>

**pearlite:** Platelet mixture of cementite and ferrite in steels or in alpha and beta phases in nonferrous alloys.<sup>8</sup>

**peeling:** (1) Dropping away of sand from the casting during shakeout. (2) The detaching of one layer of a coating from another or from the basic metal, because of poor adherence.<sup>3</sup>

**penetrameter:** See *image quality indicator*.

**penning gage:** *Cold cathode ionization gage.*

**period:** Absolute value of the minimum interval after which the same characteristics of a periodic waveform or a periodic feature return.<sup>4,14</sup>

**peripheral vision:** Seeing of objects displaced from the primary line of sight and outside the central visual field.<sup>8,17</sup>

**phase shift:** Change in the phase relationship between two alternating quantities of the same frequency.<sup>4,13</sup>

**philips discharge gage:** *Cold cathode ionization gage.*

**photoconduction:** Method by which a vidicon television camera tube produces an electrical image, in which conductivity of the photosensitive surface changes in relation to intensity of the light reflected from the scene focused onto the surface. Compare *photoemission*.<sup>8</sup>

**photoelectric effect:** Emission of free electrons from a surface bombarded by sufficiently energetic photons. Such emissions may be used in an illuminance meter, calibrated in lux.<sup>8,17</sup> Interaction of photons with atoms in which the full energy of the photon is absorbed by an orbital electron, removing the electron from the atom.

**photoemission:** Method by which an image orthicon television camera tube produces an electrical image, in which a photosensitive surface emits electrons when light reflected from a viewed object is focused on that surface. Compare *photoconduction*.<sup>8</sup>

**photometry:** Science and practice of the measurement of light or photon-emitting electromagnetic radiation.<sup>8</sup>

**photon:** Particle of electromagnetic radiation.

**photoreceptor:** Photon sensor. Examples include film and electronic detector elements.<sup>8</sup>

**physical properties:** Nonmechanical properties such as density, electrical conductivity, heat conductivity and thermal expansion.<sup>2</sup>

**picture element:** See *pixel*.

**picture processing:** See *image processing*.

**pigtail:** In gamma radiography, flexible cable to which an isotope bearing capsule may be attached for movement in and out of a shielding container.

**pill:** In gamma radiography, capsule containing isotopic source of radiation.

**pinhole porosity:** Porosity, in either castings or metal formed by electrodeposition, resulting from numerous small holes distributed throughout the metal.<sup>3</sup>

**pipe:** (1) Central cavity formed during solidification of metal, especially ingots, by thermal contraction. (2) Discontinuity in wrought or cast products resulting from such a cavity. (3) Extrusion discontinuity due to the oxidized surface of the billet flowing toward the center of the rod at the back end. (4) Cast, wrought or welded metal tube.<sup>2</sup>

**pitting:** Discontinuity consisting of surface cavities. See also *cavitation fatigue* and *pitting fatigue*.<sup>8</sup>

**pitting fatigue:** Discontinuity consisting of surface cavities typically due to fatigue and abrasion of contacting surfaces undergoing compressive loading. See also *cavitation fatigue* and *pitting*.<sup>8</sup>

**pixel:** One element of a digital picture. Each pixel represents a finite area in the scene being imaged. See *picture element*.

**plane of focus:** See *focus, principal plane of*.

**pores:** (1) Small voids within a metal. (2) Minute cavities, sometimes intentional, in a powder metallurgy compact. (3) Minute perforations in an electroplated coating.<sup>2</sup>

**porosity:** Discontinuity in metal resulting from the creation or coalescence of gas. Very small pores are called pinholes.<sup>8,15</sup>

**positive sliding:** Rolling and sliding of meshing gears or rollers when directions of rolling and sliding are the same.<sup>8</sup>

**pouring basin:** Basin on top of a mold to receive the molten metal before it enters the sprue or downgate.<sup>3</sup>

**pouring:** Transferring molten metal from a furnace or a ladle to a mold.<sup>3</sup>

**practical examination:** In certification of nondestructive testing personnel, a hands-on examination using test equipment and sample test objects. Compare *general examination* and *specific examination*.<sup>8</sup>

**primary radiation:** Radiation emitting directly from the target of an X-ray tube or from a radioactive source.<sup>11</sup>

**principal plane of focus:** See *focus*, *principal plane of*.

**process:** Repeatable sequence of actions to bring about a desired result.<sup>8</sup>

**process control:** Application of quality control principles to the management of a repeated process.<sup>8</sup>

**process testing:** Initial product testing to establish correct manufacturing procedures and then by periodic tests to ensure that the process continues to operate correctly.<sup>2</sup>

**proof test:** *Structural integrity test*.

## Q

**qualification:** Process of demonstrating that an individual (or test technique, process or instrument) has the required amount and the required type of training, experience, knowledge and abilities. See also *qualified*.<sup>8</sup>

**qualified:** Having demonstrated the required amount and the required type of training, experience, knowledge and abilities. See also *qualification*.<sup>8</sup>

**quality:** Ability of a process or product to meet specifications or expectations of its users in terms of efficiency, appearance, longevity and ergonomics.<sup>8</sup>

**quality assurance:** Administrative actions that specify, enforce and verify a quality control program.<sup>8</sup>

**quality control:** Physical and administrative actions required to ensure compliance with the quality assurance program. May include nondestructive testing in the manufacturing cycle.<sup>8</sup>

## R

**R:** *Roentgen*.

**rad:** Radiation absorbed dose. Unit of absorbed dose of ionizing radiation. One rad is equal to the absorption of  $10^{-5}$  J (100 erg) of radiation energy per gram of matter.<sup>11</sup> Replaced by the *gray* (Gy).

**radiance:** Radiant flux per unit solid angle and per unit projected area of the source. Measured in watts per square meter steradian. Compare *irradiance*.<sup>8</sup>

**radiant energy:** Energy emitting as electromagnetic waves. Also known as *radiation*.<sup>8</sup>

**radiant flux:** Radiant energy's rate of flow, measured in watts.<sup>8</sup>

**radiant intensity:** Electromagnetic energy emitted per unit time per unit solid angle.

**radiant power:** Total radiant energy emitted per unit time.<sup>8</sup>

**radiation safety officer:** Individual supervising program to provide radiation protection. The representative appointed by the licensee for liaison with the applicable regulatory agency.<sup>11</sup>

**radiographer:** Person that performs, supervises and is responsible for industrial radiographic testing operations.

**radiographic interpretation:** Determination of the cause and significance of subsurface discontinuities indicated on a radiograph.

**radiographic screens:** Thin sheets used to intensify the effect of radiation on films.<sup>11</sup> The screens can be made of a fluorescent material or a metal such as lead. Metallic screens absorb secondary and scattered radiation, which helps to improve image quality.

**radiographic testing (RT):** Use of penetrating radiant energy in the form of X-rays, gamma rays or neutrons for nondestructive testing of objects to provide images of the objects' interiors. Also called *radiography*.

**radiography:** *Radiographic testing*.

**radiology:** (1) That branch of medicine which uses ionizing radiation for diagnosis and therapy. (2) Science of electromagnetic radiation, particularly ionizing radiation.

**radiometer:** Instrument for measuring radiant power of specified frequencies. Different radiometers exist for different frequencies.<sup>8</sup>

**radiometric photometer:** Radiometer for measuring radiant power over a variety of wavelengths.<sup>8</sup>

**radioscopy:** Radiographic testing technique in which gamma rays, X-rays or neutrons are used to produce an image on a video or screen display as opposed to a latent image on a film. The test object or interrogating optics may move in real time to present a moving radiographic image.

- raster:** Repetitive pattern whereby a directed element (a robotic arm or a flying dot on a video screen) follows the path of a series of adjacent parallel lines, taking them successively in turn, always in the same direction (from top to bottom or from left to right), stopping at the end of one line and beginning again at the start of the next line. Following a raster pattern makes it possible for electron beams to form video pictures or frames and for a sensor bearing armature to cover a predetermined part of the surface of a test object.<sup>8</sup>
- real time:** Playback of video or audio streams at frame rate replicating the event originally recorded.
- real time radiography:** *Radioscopy*. See also *real time*.
- recommended practice:** Set of guidelines or recommendations.<sup>8</sup>
- Recommended Practice SNT-TC-1A:** See *ASNT Recommended Practice No. SNT-TC-1A*.
- reference reflector:** Reflector with known dimensioned surface established to provide an accurately reproducible reference level.<sup>7</sup>
- reference standard:** Typical test object with known artificial or natural discontinuities of various specific sizes, used as a basis for test comparisons, equipment calibration or determining the efficiency of the discontinuity detection process. Also called *reference* or *test panel*, *reference* or *test block* and *reference* or *test piece*.<sup>2</sup> See also *acceptance standard*.
- reinforcement of weld:** (1) In a butt joint, weld metal on the face of the weld that extends out beyond a surface plane common to the members being welded. (2) In a fillet weld, weld metal that contributes to convexity. (3) In a flash, upset or gas pressure weld, weld metal exceeding base metal diameter or thickness.<sup>2</sup>
- rejection level:** See *level*, *rejection*.
- relevant indication:** See *indication*, *relevant*.
- rem:** Roentgen equivalent man. Unit of absorbed radiation dose in biological matter. It is equal to the absorbed dose in rads multiplied by the quality factor of the radiation.<sup>11</sup>
- remote viewing:** Viewing of a test object not in the viewer's immediate presence. The word *remote* previously implied either closed circuit television or fiber optic systems remote enough so that, for example, the eyepiece and the objective lens could be in different rooms. High resolution video and digital signals can now be transmitted around the world with little loss of image quality. Compare *direct viewing*.<sup>8</sup>
- repeatability:** Ability to reproduce a detectable indication in separate processings and tests from a constant source.<sup>1,2</sup>
- reserve vision acuity:** Ability of an individual to maintain vision acuity under poor viewing conditions. A visual system with 20/20 near vision acuity under degraded viewing conditions has considerable reserve vision acuity compared to that of an individual with 20/70 near vision acuity.<sup>8</sup>
- residual elements:** Elements present in an alloy in small quantities, but not added intentionally.<sup>2</sup>
- resolution:** Aspect of image quality pertaining to a system's ability to reproduce objects, often measured by resolving a pair of adjacent objects or parallel lines. See also *minimum line pair* and *resolving power*.<sup>8</sup>
- resolution, discontinuity:** Property of a test system that enables the separation of indications due to discontinuities located in close proximity to each other in a test object.<sup>2</sup>
- resolution test:** Procedure wherein a line or series of lines or line pairs are detected to verify or evaluate a system's sensitivity.<sup>8</sup>
- resolution threshold:** Minimum distance between a pair of points or parallel lines when they can be distinguished as two, not one, expressed in minutes of arc. Vision acuity in such a case is the reciprocal of one half of the period expressed in minutes.<sup>8,17</sup>
- resolving power:** Ability of detection systems to separate two points in time or distance. Resolving power depends on the angle of vision and the distance of the sensor from the test surface. Resolving power in vision systems is often measured using parallel lines. Compare *resolution*.<sup>8</sup>
- robotic system:** Automated system programmed to perform purposeful movements in variable sequences.<sup>8</sup> See *automated system*.
- roentgen (R):** Unit for measurement of radiation intensity; amount of radiation that will generate one electrostatic unit in 1 cm<sup>-3</sup> of air at *standard atmospheric conditions*. The roentgen (R) has been replaced by an SI compound unit, coulomb per kilogram (C·kg<sup>-1</sup>).
- root crack:** Crack in either the weld or heat affected zone at the root of a weld.<sup>2</sup>
- root penetration:** Depth to which weld metal extends into the root of a joint.<sup>2</sup>
- RT:** *Radiographic testing*.



## S

**salvage tests:** Testing after salvage operations or testing objects that can be repaired.<sup>2</sup>

**sampling, partial:** Testing of less than one hundred percent of a production lot. See also *one hundred percent testing*.<sup>8</sup>

**sampling, random partial:** Partial sampling that is fully random.<sup>8</sup>

**sampling, specified partial:** Partial sampling in which a particular frequency or sequence of sample selection is prescribed. An example of specified partial sampling is the testing of every fifth unit.<sup>8</sup>

**scattering:** Random reflection and refraction of radiation caused by interaction with material it strikes or penetrates.

**scintillation:** Emission of light of specific frequencies after the absorption of electromagnetic radiation, such as X-rays or gamma rays.

**scintillation detector:** Radiation measuring device based on use of a scintillating material.

**scrap:** (1) Manufactured materials not suitable for intended use.  
(2) Discarded metallic material that may be reclaimed through melting and refining.<sup>3</sup>

**seam:** (1) On the surface of metal, an unwelded fold or lap that appears as a crack, usually resulting from a discontinuity obtained in casting or working. (2) Mechanical or welded joints.<sup>3</sup> (3) Longitudinal surface discontinuity on metal originating from a surface crack or blowhole near the surface of the ingot, that is drawn out during rolling and follows the rolling direction. Also due to overfill while rolling. After forging, seams generally follow the direction of flow lines.<sup>2</sup>

**seeability:** Characteristic of an indication that enables an observer to see it against the adverse conditions of background, outside light and others.<sup>2</sup>

**segregation:** Nonuniform distribution of alloying elements, impurities or microphases.<sup>2,3</sup>

**selectivity:** Characteristic of a test system that is a measure of the extent to which an instrument can distinguish the desired signal from disturbances of other frequencies or phases.<sup>4,13</sup>

**sensitivity:** Measure of a sensor's ability to detect small signals. Limited by the *signal-to-noise ratio*.<sup>7</sup>

**sensitization:** Condition of exposed silver halide emulsion in radiographic film before development.

**sensor, X-ray:** In radiographic testing, device or material that changes with and provides evidence of contact with ionizing radiation. Examples include X-ray film, X-ray sensitive phosphors and electronic devices such as linear detector arrays. See *detector, X-ray*.

**shallow discontinuity:** Discontinuity open to the surface of a solid object that possesses little depth in proportion to the width of this opening. Scratch or nick may be a shallow discontinuity in this sense.<sup>2</sup>

**shielding:** Material or object used to reduce intensity of or exposure to penetrating radiation.

**shrink:** Internal rupture occurring in castings due to contraction during cooling, usually caused by variations in solidification rates in the mold. Includes shrinkage sponge, small voids (stringers or bunches) or a fingerprint pattern of semifused seams. Also applied to surface shrinkage cracks.<sup>2,6</sup>

**shrink mark:** Surface depression on a casting that sometimes occurs next to a thick section that cools more slowly than adjacent sections.<sup>3</sup>

**shrinkage cavities:** Cavities in castings caused by lack of sufficient molten metal as the casting cools.<sup>2,3</sup>

**shrinkage cracks:** Hot tears associated with shrinkage cavities.<sup>2,3</sup>

**shrinkage porosity or sponge:** Porous metal often with a network of fine cracks formed during solidification of molten metal. At surface, may form a localized, lacy or honeycombed penetrant indication.<sup>2</sup>

**SI:** International System of units of measurement. An international system of measurement based on seven units: meter (m), kilogram (kg), second (s), kelvin (K), ampere (A), candela (cd) and mole (mol). See also *MKSA*.<sup>4,14</sup>

**sievert (Sv):** SI unit for measurement of exposure to ionizing radiation, replacing rem.  
 $1 \text{ Sv} = 1 \text{ J} \cdot \text{kg}^{-1} = 100 \text{ rem}$ .

**signal:** Response containing relevant information.<sup>4,13</sup>

**signal electrode:** Transparent conducting film on the inner surface of a vidicon's faceplate and a thin photoconductive layer deposited on the film.<sup>8</sup>

**signal processing:** Acquisition, storage, analysis, alteration and output of digital data through a computer.<sup>8</sup>

**signal-to-noise ratio:** Ratio of signal values (responses that contain relevant information) to baseline noise values (responses that contain nonrelevant information). See *noise*.<sup>4,7,13</sup>

**slag:** Nonmetallic product resulting from the mutual dissolution of flux and nonmetallic impurities in smelting, refining and welding operations.<sup>3</sup>

- slag inclusions:** Nonmetallic solid material entrapped in weld metal or between weld metal and base metal.<sup>2,3</sup>
- slag lines:** Elongated cavities containing slag or other foreign matter in fusion welds.<sup>2,3</sup>
- SNT-TC-1A:** See *ASNT Recommended Practice No. SNT-TC-1A*.
- source:** Machine or material from which ionizing radiation emanates.
- spalling:** Cracking or flaking of small particles of metal, usually in thin layers, from the surface of an object.<sup>2</sup>
- spatial resolution:** Width of smallest region from which reliable data can be extracted.<sup>9</sup>
- specific examination:** In certification of nondestructive testing personnel, a written examination that addresses the specifications and products pertinent to the application. Compare *general examination* and *practical examination*.<sup>8</sup>
- specification:** Set of instructions or standards to govern the results or performance of a specific set of tasks or products.<sup>8</sup>
- spectral power distribution:** Radiant power per unit wavelength as a function of wavelength. Also known as *spectral energy distribution*, *spectral density* and *spectral distribution*.<sup>8</sup>
- spectral reflectance:** Radiant flux reflected from a material divided by the incident radiant flux.<sup>8</sup>
- spectral transmittance:** Radiant flux passing through a medium divided by the incident radiant flux.<sup>8</sup>
- spectrophotometer:** Instrument used for *spectrophotometry*.<sup>8</sup>
- spectrophotometry:** Measurement of the luminance or illuminance produced by electromagnetic radiation as a function of wavelength.
- spectroradiometer:** Instrument used for *spectroradiometry*.<sup>8</sup>
- spectroradiometry:** Measurement of electromagnetic radiant power and spectral emittance, used particularly to examine colors and to measure the spectral emittance of light sources.<sup>8</sup>
- spectroscope:** Instrument used for *spectroscopy*.<sup>8</sup>
- spectroscopy:** Spectrophotometry or spectroradiometry in which the spectrum, rather than being analyzed only by a processing unit, is presented in a visible form to the operator for organoleptic examination.<sup>8</sup>
- spectrum:** (1) Amplitude distribution of frequencies in a signal.<sup>7</sup> (2) Representation of radiant energy in adjacent bands of hues in sequence according to the energy's wavelengths or frequencies. A rainbow is a well known example of a visible spectrum.<sup>8</sup>
- spectrum response:** Amplification (gain) of a receiver over a range of frequencies.<sup>7</sup>
- speed of light:** Speed of all radiant energy, including light, is  $2.997925 \times 10^8 \text{ m}\cdot\text{s}^{-1}$  in vacuum (approximately  $186\,000 \text{ mi}\cdot\text{s}^{-1}$ ). In all transparent materials the speed is less and varies with the material's index of refraction, which itself varies with wavelength.<sup>8,17</sup>
- speed of vision:** Reciprocal of the duration of the exposure time required for something to be seen.<sup>8,17</sup>
- spot check tests:** Testing a number of objects from a lot to determine the lot's quality, the sample size being chosen arbitrarily, such as five or ten percent. This does not provide accurate assurance of the lot's quality.<sup>2</sup>
- spot examination:** Local examination of welds or castings.<sup>2</sup>
- standard:** (1) Physical object with known material characteristics used as a basis for comparison, specification or calibration. (2) Concept established by authority, custom or agreement to serve as a model or rule in the measurement of quantity or the establishment of a practice or procedure.<sup>7,12</sup> (3) Document to control and govern practices in an industry or application, applied on a national or international basis and usually produced by consensus. See also *acceptance standard*, *working standard* and *reference standard*.<sup>4,8,13</sup>
- standard atmospheric conditions:** Standard temperature and pressure. Atmospheric pressure of  $101.325 \text{ kPa}$  ( $14.6959 \text{ lb}_f\cdot\text{in}^{-2}$ ). Temperature of  $20^\circ\text{C}$  ( $293.15 \text{ K}$ ,  $68^\circ\text{F}$  or  $527.67^\circ\text{R}$ ). The density of dry air at these conditions is  $1.2041 \text{ kg}\cdot\text{m}^{-3}$  ( $0.07517 \text{ lb}_m\cdot\text{ft}^{-3}$ ).<sup>1</sup>
- steel:** Iron alloy, usually with less than two percent carbon.<sup>8</sup>
- Stefan-Boltzmann law:** Relationship governing the wavelength independent rate of emission of radiant energy per unit area. The law relates the total radiation intensity to the fourth power of absolute temperature and emissivity of the material surface. For example, intensity (heat flow) from a copper block at  $100^\circ\text{C}$  ( $212^\circ\text{F}$ ) is  $300 \text{ W}\cdot\text{m}^{-2}$  ( $95 \text{ BTU}\cdot\text{ft}^{-2}\cdot\text{h}^{-1}$ ). (Stefan-Boltzmann constant for photon emission =  $1.52041 \times 10^{15} \text{ photon}\cdot\text{s}^{-1}\cdot\text{m}^{-2}\cdot\text{K}^{-2}$ ).<sup>9</sup>
- step wedge:** *Stepped wedge*.
- stepped wedge:** Reference object, with steps of various thicknesses in the range of tested parts' thicknesses, for the radiographic testing of parts having thickness variations or complex geometries. The stepped wedge must be made of material radiographically similar to that of the radiographic test object and may include penetrametric features (such as calibrated holes) in any or all steps.



**stereo imaging:** Imaging technique involving the capture and display of two images of the same object from different angles. Binocular viewing simultaneously of the two images simulates a three-dimensional viewing.

**stereo radiography:** *Radiographic testing* using *stereo imaging*.

**strain:** Alteration of the shape of a material by external forces.

**stress:** (1) In physics, the force in a material that resists external forces such as tension and compression. (2) Force per unit area.<sup>8</sup>

**stress corrosion cracking:** Failure by cracking under combined action of corrosion and stress, either applied or residual. Cracking may be either intergranular or transgranular, depending on the metal and corrosive medium.<sup>2</sup>

**stress raiser:** Contour or property change that causes local concentration of stress.<sup>8</sup>

**stress riser:** See *stress raiser*.

**stringer:** In wrought materials, an elongated configuration of microconstituents or foreign material aligned in the direction of working. Commonly, the term is associated with elongated oxide or sulfide inclusions in steel.<sup>2</sup>

**strobe:** Of or pertaining to irradiation or lighting that flashes intermittently at a rate that may be adjusted, that is often perceived as a flicker and that is used to image moving objects or still objects with potential movement.<sup>8</sup>

**structural integrity test (SIT):** Test that demonstrates the capability of a vessel to withstand specified internal pressure loads. *Proof test*.

**subcase fatigue:** Fatigue originating below the case depth. Compare *case crushing*. Also called *spalling fatigue*.<sup>8</sup>

**subcase origin fatigue:** See *subcase fatigue*.

**substrate:** Layer of metal underlying a coating, regardless of whether the layer is base metal.<sup>2</sup>

**subsurface discontinuity:** Any discontinuity that does not extend through the surface of the object in which it exists.<sup>2</sup> See *near surface discontinuity*.

**subsurface fatigue:** Fatigue cracking that originates below the surface. Usually associated with hard surfaced or shot peened parts but may occur anytime subsurface stresses exceed surface stresses.<sup>8</sup>

**suppression:** See *reject*.

**survey meter:** Portable instrument that measures rate of exposure dose or ionizing radiation intensity.<sup>11</sup>

**Sv:** *Sievert*.

## T

**test piece:** Part subjected to testing.

**test quality level:** See *level, rejection*.

**test surface:** Exposed surface of a test object.<sup>2,7</sup>

**thermoluminescent dosimetry:** Means of measuring radiation dose by using a material that stores energy due to irradiation, which energy can be measured as light emission when the material is heated.

**threshold:** See *adaptive thresholding, resolution threshold* and *threshold level*.

**threshold level:** Setting of an instrument that causes it to register only those changes in response greater or less than a specified magnitude.<sup>4,13</sup>

**thresholding:** (1) Digital data processing technique that reduces a gray level image into a binary image.<sup>8</sup> (2) Filtering out signals below a selected energy or amplitude.

**throat, actual:** Shortest distance from the root of a fillet weld to its face, as opposed to theoretical throat or weld size.<sup>8</sup>

**throat, theoretical:** Distance from the beginning of the root of the weld perpendicular to the hypotenuse of the largest right triangle that can be inscribed within the cross section of the fillet weld. Compare *weld size*.<sup>8</sup>

**throat, weld:** Distance from the root of a fillet weld to its face. Compare *weld size* and *throat, actual*.<sup>8</sup>

**toe crack:** Base metal crack at the toe of a weld.<sup>2</sup>

**tolerance:** Permissible deviation or variation from exact dimensions or standards.<sup>2</sup>

**tool mark:** Shallow indentation or groove made by the movement of manufacturing tools over a surface. Compare *gouge* or *nick*.<sup>8</sup>

**trace:** Line formed by an electron beam scanning from left to right on a video screen to generate a picture.<sup>8</sup>

**tungsten inclusions:** Inclusions in welds resulting from solidified droplets, particles or splinters of tungsten from welding electrodes.<sup>2</sup>

**tungsten inert gas (TIG) welding:** See *gas tungsten arc welding*.

## U

**underbead crack:** Subsurface crack in the base metal adjacent to the weld fusion zone.<sup>2</sup>

**undercut:** Undesirable depression or groove left unfilled by weld metal, created by melting during welding and located in base material at the toe of a weld.<sup>2,8</sup>

**undercut, film:** Scattering phenomenon in X-ray film where the edges of a high contrast feature are blurred.

**unit die:** Die block that contains several cavity inserts for making different kinds of die castings.<sup>3</sup>

**unsharpness, geometric:** Fuzziness or lack of definition in a radiographic image resulting from the source size, object-to-film distance and the source-to-object distance.<sup>11</sup>

**upper confidence limit:** Calculated value constructed from sample data with the intention of placing a statistical upper boundary on a true leakage rate.<sup>1</sup>

## V

**video:** Pertaining to the transmission and display of images in an electronic format that can be displayed on a screen.<sup>8</sup>

**video presentation:** Electronic screen presentation in which radiofrequency signals have been rectified and usually filtered.<sup>7,12</sup>

**vidicon tube:** Television tube that uses the *photoconduction* method. Compare *image orthicon*.<sup>8</sup>

**visible light:** Radiant energy in the 400 to 700 nm wavelength range.<sup>6</sup>

**vision acuity:** Ability to distinguish fine details visually. Quantitatively, it is the reciprocal of the minimum angular separation in minutes of two lines of width subtending one minute of arc when the lines are just resolvable as separate.<sup>8</sup>

**voids:** Hollow volumes, depressions or cavities. See also *discontinuity* and *dislocation*.<sup>8</sup>

## W

**weld bead:** Deposit of filler metal from a single welding pass.<sup>2</sup>

**weld crack:** Crack in weld metal.<sup>2</sup>

**weld line:** Junction of the weld metal and the base metal or the junction of base metal parts when filler metal is not used.<sup>2</sup>

**weld metal:** That portion of a weld that has been melted during welding.<sup>2</sup>

**weld nugget:** Weld metal in spot, seam or projection welding.<sup>2</sup>

**weld size:** Thickness of weld metal — in a fillet weld the distance from the root to the toe of the largest isosceles right triangle that can be inscribed in a cross section of the weld.<sup>8</sup>

**weld throat:** See *throat, weld*.

**working standard:** Work piece or energy source calibrated and used in place of expensive reference standards. In the calibrating of photometers, the standard would be a light source.<sup>8</sup>

**worm holes:** Elongated or tubular cavities due to entrapped gas. Also called *pipes*.<sup>2</sup>

## X

**X-ray:** Penetrating electromagnetic radiation emitted when the inner orbital electrons of an atom are excited and release energy. Radiation is nonisotopic in origin and is generated by bombarding a metallic target with high speed charged particles, usually electrons.

**X-ray diffraction (XRD):** Radiographic testing technique used for material characterization, based on change in scattering of X-radiation as a result of interaction with test material. See also *diffraction*.

**X-ray fluorescence (XRF):** Radiographic testing technique used for material characterization, based on wavelengths of fluorescence from material irradiated by X-rays.

**XRD:** *X-ray diffraction*.

**XRF:** *X-ray fluorescence*.

## Z

**zircon sand:** Highly absorptive material used as a blocking or masking medium for drilled holes, slots and highly irregular geometries to reduce scattering during radiography.<sup>3</sup>

## References

1. *Nondestructive Testing Handbook*, third edition: Vol. 1, *Leak Testing*. Columbus, OH: American Society for Nondestructive Testing (1998).
2. *Nondestructive Testing Handbook*, third edition: Vol. 2, *Liquid Penetrant Testing*. Columbus, OH: American Society for Nondestructive Testing (1999).
3. *Nondestructive Testing Handbook*, second edition: Vol. 3, *Radiography and Radiation Testing*. Columbus, OH: American Society for Nondestructive Testing (1985).
4. *Nondestructive Testing Handbook*, second edition: Vol. 4, *Electromagnetic Testing*. Columbus, OH: American Society for Nondestructive Testing (1986).
5. *Nondestructive Testing Handbook*, second edition: Vol. 5, *Acoustic Emission Testing*. Columbus, OH: American Society for Nondestructive Testing (1987).
6. *Nondestructive Testing Handbook*, second edition: Vol. 6, *Magnetic Particle Testing*. Columbus, OH: American Society for Nondestructive Testing (1989).
7. *Nondestructive Testing Handbook*, second edition: Vol. 7, *Ultrasonic Testing*. Columbus, OH: American Society for Nondestructive Testing (1991).
8. *Nondestructive Testing Handbook*, second edition: Vol. 8, *Visual and Optical Testing*. Columbus, OH: American Society for Nondestructive Testing (1993).
9. *Nondestructive Testing Handbook*, second edition: Vol. 9, *Special Nondestructive Testing Methods*. Columbus, OH: American Society for Nondestructive Testing (1995).
10. *Nondestructive Testing Handbook*, second edition: Vol. 10, *Nondestructive Testing Overview*. Columbus, OH: American Society for Nondestructive Testing (1996).
11. *NDT Terminology*. Wilmington, DE: E.I. du Pont de Nemours & Company, Photo Products Department (n.d.).
12. *Nondestructive Testing Methods*. TO33B-1-1 (NAVAIR 01-1A-16) TM43-0103. Washington, DC: Department of Defense, United States Air Force (June 1984): p 1.25.
13. E 268-81, *Definitions Approved for Use by Agencies of the Department of Defense as Part of Federal Test Method Standard No. 151b and for Listing in the DoD Index of Specifications and Standards*. Philadelphia, PA: American Society for Testing and Materials (1981).
14. *IEEE Standard Dictionary of Electrical and Electronic Terms*. New York, NY: Institute of Electrical and Electronics Engineers, distributed by Wiley-Interscience, a division of John Wiley and Sons (1984).
15. *EPRI Learning Modules*. Charlotte, NC: Electric Power Research Institute (various years).
16. *1992 Annual Book of ASTM Standards*. Section 3, *Metals Test Methods and Analytical Procedures*: Vol. 03.03, *Nondestructive Testing*. Philadelphia, PA: ASTM International (1992).
17. *IES Lighting Handbook: Reference Volume*. New York, NY: Illuminating Engineering Society of North America (1984).

# Index

Users of the CD-ROM version of this book are urged to read its instructions and take advantage of its search function, a powerful indexing tool that can, with a single command, provide access to all occurrences of a given word throughout the entire book. The following printed index is necessarily more selective.

Page references in *italic* type indicate illustrations. Page references followed by *table* indicate material in tables.

Readers are encouraged to consult this volume's glossary: glossary entries are not entered in the index.

## A

A 4907. *See* Korean Standards Association

A 4921. *See* Korean Standards Association

ablative thrust chamber radiography, 552-555

absorbed dose, 119

absorbers, 49, 131

absorption

alpha particles, 45

beta particles, 45

and film radiography, 152-153

neutrons, 45-47

and photoelectric effect, 48-49

X-rays, 57-58

absorption analysis, 427

absorption edge densitometry, 573

absorption edges, 49, 611

selected elements, 612-651 *table*

accelerator neutron sources, 53, 442-443

safety aspects, 134

*See also* linear accelerators

acceptance criteria, 14

castings, 465-466

nuclear fuel rods, 530

power and process piping, 516

welds, 489-490

*See also* reference standards

acid stop bath, 234

acoustic emission testing, 10, 10-11

acoustic methods, 11

Acropolis, gamma radiography, 595

acrylic, hounsfield value, 314 *table*

actinium series, 52

activation foils, 104-105

activator, in film development, 234

adhesive bonded composite structures, 557, 559, 559-560

adhesives, X-ray absorption, 552, 553

aerospace applications, 543-544

advanced material techniques, 559-565

aviation component radiography, 544-549

inspection with thulium-170, 78

simulation tools, 564

space flight component radiography, 550-558

Aerospace Material Specification (AMS). *See* SAE International

afterglow, 293

agreement states, 114, 117-118

air

hounsfield value, 314 *table*

mass attenuation coefficient, 611

air bells, 205

aircraft

backscatter imaging of aluminum skin, 390

backscatter imaging of corrosion, 396-397

brazed honeycomb structures, 547, 547-548, 549

corrosion detection using reversed beam scanning, 416-418, 417

dynamic neutron radioscopy of engines, 446

fatigue cracking of fuselage, 3

flight test inspection, 545-547, 547

helicopter composite rotor/propeller blades, 548-549

panel neutron radiography, 439

radioscopic imaging, 254

residual stress measurement, 429

wing crack detection using reversed beam scanning, 415-416, 416

*See also* jet engine turbine blades

air image, 293

airport security screening, 588, 588-590, 589

ALARA (As Low As Reasonably Achievable) dose, 120, 133

alarming rate meters, 98-99

alarm signals, 127

alloy castings, 459. *See also* castings

alloy identification, 590

by energy dispersive spectrometry, 431

alpha case, 558

alpha particles

absorption by matter, 45

discovery, 38

emission, 43

*Altarpiece of the Mystic Lamb* (Van Eyck), radiographic evaluation, 600

aluminum

adhesive bonded composite structures, 557

attenuation coefficients, 383, 619 *table*

aviation component radiography, 544

backscatter imaging of aircraft skin, 390

backscatter tomography of sheets, rivets and pellets, 392-393, 393

casting density *versus* radiographic sources, 460 *table*

cold shuts in castings, 463

contrast sensitivity phantom, 333

digital radiography of tube welds, 297

dimensional measurement phantoms, 338

exfoliate corrosion, 396

false radiographic indications in welds, 507-509, 508

gas cavities in welds, 496

honeycomb panel neutron radiography, 439

hounsfield value, 314 *table*

image analysis of casting, 358

inclusions in castings, 463

incomplete penetration in welds, 496

inspection with thulium-170, 78

lack of fusion in welds, 497

lead foil screens for, 159

maximum filter thickness, 157

microfocus radioscopy of aircraft honeycomb, 408

porosity in castings, 461, 462

radiation gaging, 576

radiographic equivalence factors, 153 *table*

radiological detection and identification, 590

scattered radiation, 153

shrinkage in castings, 462

step wedge image analysis, 364-365

tungsten inclusions in welds, 480

X-ray and thermal neutron attenuation, 440 *table*

- aluminum bronze, casting density *versus* radiographic sources, 460*table*
- ambient dose equivalent, 32, 119
- American National Standards Institute (ANSI)
- ANSI/API Recommended Practice 1104, 516
  - ANSI/ASME B31.1, 17*table*
  - ANSI/ASME B31.3, 17*table*
  - ANSI/ASNT CP-189, 15, 17*table*
  - ANSI N43.9-1991, 17*table*
  - ANSI PH2.8-1975, 17*table*
  - ANSI film standards bibliography, 251
  - ANSI Type I exposure devices, 79, 80, 80-83
  - ANSI Type II exposure devices, 83, 83-84, 84
- American Petroleum Institute (API)
- API 510, 17*table*
  - API 570, 17*table*
  - API 650, 17*table*, 489, 528
  - API 653, 529
  - API 1104, 17*table*, 489, 516, 516
- American Society for Nondestructive Testing (ASNT)
- ASNT Central Certification Program (ACCP), 15
  - ASNT Recommended Practice No. SNT-TC-1A, 15, 17*table*, 18
  - history of, 26-27
  - Industrial Radiography Radiation Safety Personnel (IRRSP) program, 117-118
- American Society for Testing and Materials (ASTM). *See* ASTM International
- American Society of Mechanical Engineers. *See* ASME Boiler and Pressure Vessel Code
- American Welding Society (AWS)
- AWS D1.1, 17*table*, 479, 481, 489
  - AWS D14.3/D14.3M, 489
- amorphous selenium detectors
- for digital radiography, 284, 287, 290-291, 298, 298
  - discontinuity centers, 293
  - for microfocus radiography, 404
  - properties, 286*table*
- amorphous silicon detectors
- calibration, 356
  - for digital radiography, 284, 287, 290, 294, 296, 296-298, 297
  - for microfocus radiography, 404, 407
  - properties, 286*table*
  - for radioscopy, 279
- AMS (Aerospace Material Specification). *See* SAE International
- annihilation, 45
- and pair production, 50
- anode grounded circuit, 65
- anodes, 57
- X-ray tubes, 61, 61-62, 63, 63
- ANSI. *See* American National Standards Institute
- antimony, attenuation coefficients, 640*table*
- antiparticles, 39
- API. *See* American Petroleum Institute
- Apollo booster engine, 556
- archaeology applications, 596
- archival storage of film, 178, 243
- arc strikes
- castings, 464
  - welds, 481, 499, 499
- arc welding
- flash radiography, 412-413
  - radioscopy, 502, 502-506, 503, 504
- area detectors, image digitization, 350
- area monitoring, 123, 125, 127
- area viewers, 191
- argon, attenuation coefficients, 621*table*
- artifacts. *See* radiographic artifacts
- artillery shells, 21
- backscatter imaging, 380, 395
  - scanning microdensitometry of fuses, 197
- art radiography, 598-601
- ASME Boiler and Pressure Vessel Code, 17*table*
- butt joints, 483
  - castings acceptance criteria, 466
  - and image quality indicators (penetrameters), 174
  - lap joints, 484
  - lead foil screens, 487
  - nuclear pressure vessels, 527
  - power and process piping, 517, 518
  - pressure vessels, 526
  - tanks, 529
  - weld acceptance criteria, 489
- ASNT. *See* American Society for Nondestructive Testing
- asphalt radiography, 591
- ASTM International (formerly American Society for Testing and Materials).
- ASTM C 638, 16*table*
  - ASTM E 94, 16*table*, 488, 589
  - ASTM E 142, 485, 589
  - ASTM E 155, 16*table*
  - ASTM E 170, 16*table*
  - ASTM E 186, 16*table*
  - ASTM E 192, 16*table*
  - ASTM E 242, 16*table*
  - ASTM E 272, 16*table*
  - ASTM E 280, 16*table*
  - ASTM E 310, 16*table*, 468
  - ASTM E 390, 16*table*, 464
  - ASTM E 431, 16*table*
  - ASTM E 446, 16*table*
  - ASTM E 505, 16*table*
  - ASTM E 592, 16*table*
  - ASTM E 666, 16*table*
  - ASTM E 689, 16*table*
  - ASTM E 746, 16*table*
  - ASTM E 747, 16*table*, 174, 175, 516, 518
  - ASTM E 748, 16*table*
  - ASTM E 802, 16*table*
  - ASTM E 803, 16*table*, 441
  - ASTM E 975, 16*table*
  - ASTM E 999, 16*table*
  - ASTM E 1000, 16*table*
  - ASTM E 1025, 16*table*, 173, 175, 485, 516, 516, 517, 518
  - ASTM E 1030, 16*table*
  - ASTM E 1032, 16*table*, 589
  - ASTM E 1114, 16*table*
  - ASTM E 1161, 16*table*
  - ASTM E 1165, 16*table*
  - ASTM E 1254, 16*table*, 178
  - ASTM E 1255, 16*table*
  - ASTM E 1320, 16*table*
  - ASTM E 1390, 16*table*
  - ASTM E 1411, 16*table*
  - ASTM E 1441, 16*table*
  - ASTM E 1453, 16*table*
  - ASTM E 1475, 16*table*
  - ASTM E 1496, 16*table*
  - ASTM E 1570, 16*table*
  - ASTM E 1647, 16*table*
  - ASTM E 1648, 16*table*
  - ASTM E 1672, 16*table*
  - ASTM E 1734, 16*table*
  - ASTM E 1735, 16*table*
  - ASTM E 1742, 16*table*, 486, 489
  - ASTM E 1814, 16*table*
  - ASTM E 1815, 16*table*, 228
  - ASTM E 1894, 16*table*
  - ASTM E 1931, 16*table*
  - ASTM E 1936, 16*table*
  - ASTM E 1955, 16*table*
  - ASTM E 2002, 16*table*
  - ASTM E 2033, 16*table*
  - ASTM E 2104, 486, 489
  - ASTM E 2116, 16*table*
  - ASTM F 629, 16*table*
  - ASTM F 947, 16*table*
  - ASTM F 1035, 16*table*
  - Committee E-7 on Nondestructive Testing, 27
  - image quality indicators (penetrameters). *See* image quality indicators
  - international standards, 15, 16*table*
  - ISO *versus* ASTM film classifications, 228*table*
  - standards for metal castings, 460
  - test standards, 15, 16*table*
- atomic attenuation coefficient
- defined, 50, 610
  - selected elements, 612-651*table*
- atomic mass unit, 31
- atomic number, 39
- atomic structure, 38-41, 57
- atomic weight (relative atomic mass), 610-611
- attenuation, 44-45, 48-51
- gaging, 570-571
  - and image analysis, 347
  - See also* absorption; scattering



attenuation coefficients  
 defined, 50-51, 610-611  
 gamma attenuation with and without scatter, 51  
 neutrons, 440*table*, 447*table*  
 selected elements, 612-651*table*  
 audit, of radiation safety procedures, 115-117  
 automatic defect recognition, 406-407  
 image analysis, 371-374  
 automotive applications  
 assembly line radiology, 278  
 digital radiography, 300  
 radioscopic security inspection of truck, 589, 590  
 spark plug microfocus radiology, 407  
 tire radiation gaging, 577  
 wheel radiology, 279  
 aviation component radiography, 544-549. *See also* aircraft  
 AWS. *See* American Welding Society

## B

background scatter, 348  
 backscattered radiation, 154, 154  
 backscatter imaging, 28  
 applications, 395-399  
 multiaperture collimator, 388  
 principles, 379-387  
 for radiation gaging, 392, 573  
 reconstruction and image processing techniques, 392-394  
 sensitivity, 393-394  
 techniques, 388-391  
 backscatter tomography, 392  
 badge plants, 133  
 badges  
 body, 103  
 film, 108, 121-122  
 bad pixels, 357  
 baggage scanners, 588-590  
 ball grid arrays  
 image analysis, 356-357, 357, 361, 362  
 solder joints, 579  
 barium, attenuation coefficients, 643*table*  
 barium clay diaphragms, 155  
 barium fluorobromide, europium activated, 287, 294  
 barrels, digital radiography of contents, 300  
 barriers, 127  
 baseball bat radiography, 587  
 battery flashlight computed tomography, 327  
 battery powered densitometer, 194  
 beam focusing, X-ray tubes, 60-61  
 beam hardening  
 and computed tomography, 336  
 and image analysis, 349, 360, 365, 392-393  
 becquerel (Bq), 31, 42, 119  
 Belle (ship), radiography of artifacts, 596-597  
 beryllium  
 attenuation coefficients, 613*table*  
 grid diaphragms for radiography of, 157  
 neutron attenuation coefficients, 447*table*  
 beta disintegration, 46  
 beta particles  
 absorption by matter, 45  
 discovery, 38  
 emission, 43-44  
 maximum range *versus* energy, 131  
*See also* electrons  
 betatron generator, 69  
 betatrons, 68, 68-69  
 for nuclear vessel radiography, 526  
 bismuth germanate, 100*table*, 260*table*  
 bitmapped graphics, 276*table*  
 blob analysis, 362, 372  
 blowholes  
 interpretation in castings, 214, 214  
 interpretation in welds, 501  
 body badges, 103  
 body scan tomography. *See* laminography  
 bohr atom, 38, 39-41, 40  
 Boiler and Pressure Vessel Code. *See* ASME Boiler and Pressure Vessel Code  
 boilers, 514  
 effect of discontinuities, 3  
 boiling water reactor radiography, 526, 526-527

bone  
 hounsfield value, 314*table*  
 radiography, 596  
 boron  
 attenuation coefficients, 557  
 capture cross section, 47*table*  
 boron fiber composites  
 attenuation in adhesive bonded, 557  
 backscatter imaging, 390  
 boron trifluoride neutron detector tubes, 104, 122, 123  
 bouwers-schmidt lenses, 271  
 Boy with Still Life (Baum), radiographic evaluation, 600, 601, 601  
 branching, 43  
 brass  
 inspection with cobalt-60, 75  
 radiographic equivalence factors, 152, 153*table*  
 brass filters, 156  
 brazed honeycomb structures, 547, 547-548, 549  
 brazing, automatic defect recognition, 406  
 bremsstrahlung, 44, 56-57  
 bridge radiography, 591, 592, 596  
 bridge wire igniter, 447  
 bridge wire squid, 438  
 broad beam shielding, 133  
 bronze  
 casting density *versus* radiographic sources, 460*table*  
 tensile property relation to radiographic indications, 465*table*  
 brumlein line generators, 411  
 building materials, density of selected commercial, 133*table*  
 building radiography, 593  
 historic buildings, 594-596  
 burnthrough, interpretation in welds, 211, 211  
 butt joints, 475, 475-476  
 exposure setup, 483-484  
 in-process radiology of arc-welded, 502, 506

## C

cable radiography, 537  
 cadmium  
 attenuation coefficients, 638*table*  
 capture cross section, 47*table*  
 neutron absorption by, 47  
 X-ray and thermal neutron attenuation, 440*table*  
 cadmium tungstate, properties, 260*table*  
 calcium, attenuation coefficients, 622*table*  
 calcium fluoride, europium-activated  
 properties, 260*table*  
 for radiation gaging, 575  
 calcium tungstate  
 properties, 257*table*  
 relative light yield, 257*table*  
 spectral emission, 258  
 calibration  
 densitometers, 194-195  
 low level transforms, 356-359  
 radiation detection instruments, 126  
 californium-252, 104  
 for neutron radiography, 443-445, 444  
 spontaneous fission, 44  
 californium-252 exposure devices, 134  
 Caligula statue radiography, 598, 599, 599  
 Canadian General Standards Board  
 CAN/CGSB-48.3-92, 17*table*  
 CAN/CGSB-48.5-95, 17*table*  
 CAN/CGSB-48.9712-95, 17*table*  
 CAN/CGSB-48-GP-2M, 17*table*  
 capacitor microfocus radiography, 407  
 Cape Hatteras Lighthouse, radiographic testing of gallery, 595, 595  
 Capitol building, radiographic testing of walls, 595  
 capping, 319  
 carbon  
 attenuation coefficients, 614*table*  
 hounsfield value, 314*table*  
 carbon-to-carbon composites, computed tomography, 335  
 cargo transport, digital radiography application, 300



castings, 453-454  
 aerospace components, 556, 558  
 computed tomography of turbine blades, 326  
 flash radiography, 412, 412-413  
 image analysis of aluminum, 358  
 interpretation of discontinuities, 213-217  
 interpretation report, 201  
 radiographic indications, 461-464  
 radiographic techniques for, 455-460  
 radiographic testing and process scheduling, 465-466, 467-468  
 radiographic testing problems, 467-468  
 repair welds, 464, 465

cast iron, 459  
 Cape Hatteras Lighthouse, 595  
 casting density *versus* radiographic sources, 460*table*

cathode grounded circuit, 65

cathode rays, 21

cathodes, 57  
 X-ray tubes, 60

cavity shrinkage, 461-462

cellulose radiography, 586

CEN 584, 17*table*

center grounded circuit, 65

centimeter-gram-second (CGS) units, 29

certification. *See* personnel qualification and certification

cesium, attenuation coefficients, 642*table*

cesium-137, 53, 74*table*, 75-76  
 attenuation by fuel rods, 533  
 bibliography, 86  
 disintegration, 76  
 gamma ray source, 128*table*  
 gamma ray transmission through lead and concrete, 131  
 gamma spectra, 75  
 half value thickness, 51*table*  
 source for castings, 455*table*

cesium iodide scintillators, 266  
 in digital radiography, 289, 297  
 discontinuity centers, 293  
 properties, 257*table*, 260*table*  
 spectral emission, 258

channel electron multipliers, 266-267

characteristic curve, 167, 167-169, 222, 224, 223-227, 242-243  
 gamma, 232, 233, 243  
 intensifying salt screen exposed, 243  
 of films exposed with lead foil screens, 169  
 typical industrial film, 224, 225  
 characteristic X-rays, 44, 57

charge coupled devices, 269  
 for digital radiography, 294, 298, 298-300  
 for film digitization systems, 180-181  
 intensified, 271, 279  
 properties, 286*table*  
 for radioscopy, 269-271  
 sensitivity compared to vidicons, 270

chemical industry applications. *See* utility, petroleum and chemical industry applications

chemical spot testing, 11

chemical streaks, 204, 204

chill inserts, 463

chloride contamination detection, in roads, 591-592

chlorine, capture cross section, 47*table*

chromium, attenuation coefficients, 625*table*

chromium-51, gamma ray source, 128*table*

cigarette radiation gaging, 573, 577, 586

cin fluorography, rocket engines, 554, 554-555

civil structure radiography, 591, 592-593

clustered porosity  
 interpretation in welds, 498  
 welds, 478

coarse scattered porosity, in steel welds, 498

coatings  
 backscatter imaging, 381  
 thickness gaging, 571, 573, 576

cobalt  
 attenuation coefficients, 628*table*  
 capture cross section, 47*table*

cobalt-60, 52, 74*table*, 74-75  
 attenuation with fuel rods, 533  
 bibliography, 86-87  
 disintegration, 75  
 exposure devices, 82, 82-83  
 gamma ray source, 128*table*  
 gamma ray transmission through lead and concrete, 131  
 gamma spectra, 75  
 half value thickness, 51*table*  
 for nuclear vessel radiography, 526  
 source for castings, 455*table*  
 temporary field site *versus* permanent facility, 116

codes, 187-188, 489. *See also* ASME Boiler and Pressure Vessel Code; reference standards

coherent scattering. *See* elastic scattering

cold cracks, interpretation in welds, 212

cold neutrons, attenuation by selected elements, 447

cold shuts, 463, 463  
 interpretation in castings, 216-217

collimation  
 in computed tomography, 305  
 and image analysis, 351  
 in megavolt radiography, 158  
 neutrons, 440  
 in radioscopy, 262, 271

color conditioning, 240

color lookup tables, 354, 354-356, 355, 359

coloumb per kilogram (C\*kg<sup>-1</sup>; replaces roentgen), 31-32, 119

compact disk (CD) data storage, 275

comparator, with etched glass reticle, 192

comparator block, 521, 521-522

composites  
 adhesive bonded, 557  
 aviation component radiography, 547, 547-548  
 backscatter imaging, 390, 397-398  
 computed tomography, 335  
 inspection with thulium-170, 78  
*See also* honeycomb structures

compound units, 32, 120

compton scattering, 49, 347  
 attenuation coefficient, 610  
 defined, 49, 380-382, 382  
 for radiation gaging, 571-572  
 for radiological material detection, 590

computed tomography, 28, 303-305  
 aerospace components, 561-562, 562  
 applications, 323-327  
 back projection filtering, 314  
 body scan method, 304  
 capabilities, 323*table*  
 with collimated fan beam and linear detector array, 305  
 contrast, 316-317, 332-334  
 contrast discrimination curves, 334  
 data acquisition and reconstruction, 312  
 effective aperture, 308  
 fuel rods, 533-536  
 imaging process, 346, 347, 349  
 and material density, 334-335  
 mechanical handling, 320  
 principles of, 310-315  
 probability distribution for feature detection, 332  
 for radiation gaging, 573  
 reference standards, 328-338  
 resolution, 316-317  
 shape inspectability *versus* conventional radiography, 325*table*  
 source-object-detector configurations and effective beam widths, 316  
 system design, 318-322, 321, 321*table*  
 system generations, 319  
 system size *versus* cost, 322  
 system size *versus* sensitivity to detail, 322  
 tradeoffs in detectors, 351  
*See also* laminography; phantoms

concavity, in welds, 211, 212, 212

concrete  
 backscatter imaging, 398-399  
 gamma ray transmission through, 131  
 and infrastructure radiography, 591, 591-592  
 shielding equivalents, 132*table*  
 X-ray transmission under broad beam conditions, 133

concrete shooting booth, 130

cone beam computed tomography, 320

- Conference for Radiation Control Program Directors, 118  
 confined space, 19  
 consultants, 13  
 consumer goods radiography, 584-587  
 contrast detail dose curves, 328  
 contrast discrimination curves, 329  
 contrast sensitivity, 346, 348  
   computed tomography, 317, 332-334  
 control strips, 242  
 convexity (excessive penetration), in welds, 210-211  
 convolution function, in computed tomography, 313-314  
 Coolidge Award, 27  
 copper  
   attenuation coefficients, 630*table*  
   dimensional analysis of pipe, 367-370, 367-370  
   inspection with cobalt-60, 75  
   radiographic equivalence factors, 153*table*  
   radiological detection and identification, 590  
   segregation in castings, 217  
 copper diaphragms, 155  
 copper filters, 156  
 core shift, 463  
   interpretation in castings, 217, 217  
 corner joints, 476, 477  
   exposure setup, 484, 484-485  
   radiographic procedure, 495  
 corrosion  
   backscatter imaging of aircraft, 396-397  
   backscatter imaging of pipelines, 397  
   in power and process piping, 519-523  
   reversed geometry scanning beam radiography of aircraft, 416-418, 417  
 cosmic radiography, 595-596  
 cosmic rays, 39, 52  
 cost benefit analysis, 13  
 crack detection, 2, 5*table*, 6*table*  
   aircraft wings, using reversed beam scanning, 415-416, 416  
   aviation components, 544  
   backscatter imaging, 387  
   first uses of radiography, 26  
   interpretation in castings, 216, 216  
   interpretation in welds, 212  
   nuclear fuel rods, 530, 534  
   steel welds, 491-495, 492  
   visibility and image quality indicators (penetrameters), 175-176  
   *See also* castings; discontinuities; welds  
 cracks  
   types in castings, 463  
   types in welds, 480  
 crater cracks, 480  
   interpretation in welds, 212  
 crimp marks, 177, 202, 202  
 crookes tube, 21, 23  
 cross sections, 46-47, 50  
   selected elements, 47*table*, 612-651*table*  
   *See also* individual elements  
 crown (static mark), 240, 240  
 cruise missile computed tomography, 326, 327  
 crystals  
   latent image site, 221  
   residual stresses, 428-429  
   X-ray diffraction, 427-428, 428  
 cupping, 319  
 curie (Ci), 31, 42, 119  
 current mode detectors, 574, 575  
 cyclotrons, 53, 443
- D**
- dam radiography, 593, 596  
 darkroom technique, 237  
 debris formation and relocation, in nuclear fuel rods, 533-535  
 decay constant, 42  
 deexcitation, 100  
 defects. *See* discontinuities  
 defect standard, 441  
 definition, 170, 171
- delamination  
   ablative thrust chambers, 555  
   surface mounted components, 582  
   welds, 478, 480  
 delayed cracks, interpretation in welds, 212  
 delay streaks, 205  
 dendritic shrinkage, 461, 462  
 dense inclusions, 208, 215, 215  
 densitometers, 165, 194-198  
 density  
   backscatter based estimation, 385, 398  
   castings, *versus* radiographic sources, 460*table*  
   and computed tomography, 334-335  
   limitations of radiographic testing, 12  
   optical, of film, 141, 164-165, 190-198  
   selected building materials, 133*table*  
   *See also* radiation gaging  
 density phantoms, 335, 336  
 dental work, microfocus radioscopy, 408  
 Department of Transportation (United States)  
   concrete radiography research, 591  
   pipeline radiography research, 517  
   radioactive material transportation regulations, 118  
 depleted uranium shields, 132  
   for ANSI Type I exposure devices, 81  
   for ANSI Type II exposure devices, 83  
 depth profiling, 390-391, 392  
   computed tomography, 311  
 detectors. *See* radiation detectors  
 deuterium, 42  
 Deutsche Industrie Norm (DIN) standards, 17*table*  
   for castings radiography, 458  
   DIN 6814, 17*table*  
   DIN 6832-2, 17*table*  
   DIN 25430, 17*table*  
   DIN 54109, EN 462 P1 (DIN) and ASTM E 747, 174, 175, 183  
   DIN 54115, 17*table*  
   DIN EN 444, 17*table*  
   DIN EN 12681, 17*table*  
   DIN EN 14096, 17*table*  
   image quality indicators (penetrameters), 174, 175, 458  
   for radioscopy, 277  
   *See also* image quality indicators, wire type  
 Deutsche Institut für Normung. *See* Deutsche Industrie Norm (DIN) standards  
 developer, 163, 241-242  
   faults from, 233*table*  
   MQ and PQ, 232  
   and spotting artifacts, 204, 205  
 development. *See* film development  
 diaphragms, for reduction of scattering, 155  
   grid type, 157-158  
 diffused *p-n* junction detector, 106-107, 107  
 digital audio tape (DAT) data storage, 275  
 digital fluoroscopy, aerospace structures, 562  
 digital images, 349-351  
   colorizing, 354  
   practical considerations, 351-352  
   transform techniques, 356-366, 357*table*  
   visual enhancement, 353-356  
   *See also* computed tomography  
 digital laminography. *See* laminography  
 digital radiographic imaging, 283-284  
   detectors for, 284-288, 296-300, 351  
   image contrast and signal statistics, 289-295  
   imaging process, 346, 347, 349  
   substitute for flash radiography, 410  
 digital transmission densitometer, 194  
 digital video disk (DVD) data storage, 275, 276  
 dimensional measurements  
   image analysis, 366-370  
   phantoms for, 336-338, 337  
 DIN standards. *See* Deutsche Industrie Norm  
 directional dose equivalent, 32, 119  
 direct reading dosimeters, 94  
 dirt, radiographic artifacts caused by, 203, 205  
 discontinuities  
   heat treatment effects, 465  
   types in castings, 461-464  
   types in welds, 478-481

discontinuity detection, 2, 26, 5*table*, 6*table*  
 depth detection using stereo radiography, 419-426  
 and imaging method selection, 14  
 interpretation for castings, 213-217  
 interpretation for welds, 207-212  
 limiting factors in detection, 12  
 in pipelines, 517  
 and radiographic sensitivity, 458-459  
 reliability, 19-20  
 visibility and image quality indicators (penetrameters), 175-176  
*See also* automatic defect recognition; castings; crack detection; welds

disintegration, 42  
 disintegration rate, 119  
 disposal, radioactive materials, 118  
 distillation column radiography, 523  
 dose. *See* radiation dose  
 dosimeters, 121-122, 123  
 direct reading, 94  
 energy dependence of response, 94  
 performance specifications, 95*table*  
 DOT. *See* Department of Transportation (United States)  
 double beam microdensitometry, 196  
 dross, 461  
 interpretation in castings, 214-215  
 drugs. *See* pharmaceuticals  
 drying, of film, 230, 244  
 dual energy techniques, 28  
 dynamic neutron radioscopy, 446  
 dynodes, 101  
 dysprosium, capture cross section, 47*table*

## E

eddy current testing, 8, 8-9  
 edge joints, 477, 477  
 exposure setup, 485  
 edge spread function  
 computed tomography, 329, 331, 332  
 and image quality indicators (penetrameters), 277  
 effective apertures, 308  
 elastic scattering  
 defined, 380  
 neutrons, 46  
 electromagnetic radiation, 48-51  
 electromagnetic spectrum, 48  
 electron beam welding, flash radiography, 412-413  
 electron capture, 44  
 electronic components  
 image analysis, 359, 360  
 laminography, 306  
 radioscopy, 578-583, 584  
 surface mounted, 582  
 tantalum capacitor microfocus radiography, 407  
 electronic dosimeters, 122  
 electronic quenching, in geiger-müller counters, 97  
 electronic radiation sources, 55-58  
 generator construction, 59-66  
 for high voltage radiography, 63, 63-66, 66  
 for megavolt radiography, 67-70  
 standards, 14  
 electronic radioscopy, 28  
 electron linear accelerators, 69, 69-70, 70  
 electrons  
 atomic structure, 38  
 capture, 44  
 and latent image formation, 108  
 production from incident photon, 50  
 radiation detection instruments, 123  
 radiation protection measurement, 121-122  
*See also* beta particles  
 electronvolt, 31  
 electrostatic generators, 67, 67-68, 68  
 elemental analysis, by X-ray fluorescence spectrometry, 429-431  
 elementary particles, 38-41  
 EN 12679, 17*table*  
 encapsulated isotope sources, 79, 79-80  
 enclosed installations, 127-128  
 energy conservation, 56  
 energy dispersive spectrometry, 427, 429, 429  
 instrumentation for, 431  
 energy levels, 40-41

epithermal neutron radiography, 447  
 epithermal neutrons, 104*table*  
 equivalent dose, 32  
 equivalent sensitivity of image quality indicator (penetrameter), 174-175  
 erosion, of power and process piping, 519-523  
 European wire image quality indicators (penetrameters), 174, 175  
 europium, capture cross section, 47*table*  
 examinations, for certification, 18  
 excessive penetration (convexity), in welds, 210-211, 211  
 excitation, 45  
 exfoliate corrosion, 396  
 explosives  
 aerospace, 557  
 backscatter imaging, 381  
 flash radiography, 410  
 neutron radiography, 438, 447  
 exposure, 119, 243  
 for castings, 459  
 in film radiography, 139-151, 221-222, 231  
 exposure charts, 165-167  
 exposure control, 127-129  
 exposure devices  
 with crankout and tube guide, 87  
 guide tube collimators for, 82  
 isotope radiation sources, 77, 80, 80-84  
 safety considerations, 116-117  
 with source exchanger, 83  
 exposure factor, 149-150, 166

## F

fabric radiation gaging, 577  
 false indications, 202  
 aluminum alloy welds, 507-509, 508  
*See also* radiographic artifacts  
 faraday (unit of charge), 38  
 fast neutron radiography, 447  
 fast neutrons, 46, 104*table*  
 shielding, 134  
 fatigue corrosion, 396  
 feature space, 356  
 females, radiation exposure, 120  
 fermi distribution, 43  
 fiber glass  
 attenuation in adhesive bonded composites, 557  
 radiation gaging, 577  
 fiber optic scintillators, 290, 291, 298, 299  
 fiber optic tapers, 299  
 field emission, 410  
 FIFO (first-in, first out) system, of film storage, 240  
 filamentary shrinkage, 461, 462  
 fillet welds, 476  
 on corner joints, 484  
 exposure setup, 485  
 film badges, 121-122, 122  
 film, radiographic  
 artifacts, 202  
 base, 231  
 contrast, 170, 171  
 emulsion, 231  
 graininess, 171-172, 227  
 handling, 177  
 film development  
 artifacts associated with, 204-205  
 chemistry, 230-236, 231-234  
 darkroom technique, 237  
 equipment and practice, 238-240  
 latent image, 108-109, 219-229, 230  
 processing technique, 241-246  
 silver recovery, 247-249  
 film digitization systems  
 charge coupled device, 180-181  
 laser, 181

- film radiography
  - absorption and scattering, 152-158
  - automatic processing, 233-234, 236, 245-246
  - characteristic curve, 167, 167-169, 169, 222, 224-226
  - equivalent exposure ratios, 168*table*
  - exposure, 139-151, 221-222, 222, 231
  - exposure charts, 165, 165-167, 166
  - film choice for castings, 458-459
  - film choice for welds, 482-483
  - film classification, 228*table*
  - film digitization, 180-182
  - film handling and storage, 177-179, 240, 488
  - image quality and detail visibility, 170-176
  - industrial X-ray films, 163-169
  - screens for, 154-155, 159-162
  - sensitivity, 151
  - source strength, distance and time relations, 147-149
  - transmittance, opacity and density relationships, 162*table*
  - X-ray spectral sensitivity curve, 228
- film scratches
  - after processing, 206
  - before processing, 202
- film shipping, 177
- film speed, 226, 243-244
  - relative values, 226*table*
  - shifts in curve position with salt screens, 243
- filmless radiography. *See* radioscopy
- filters, 155-157
  - effect on X-ray intensity, 156
- final edge joints, 477
- fine scattered porosity, in steel welds, 498
- finger marks, 177, 204
- fingerprints, 204
- fire-on-position data acquisition, 320
- fission fragments, 53
- fission track counting systems, 122
- fixation, 230, 235
- fixer, 234-235, 244
- flashlight computed tomography, 327
- flash radiography, 28, 409-413
  - flash X-ray diffraction, 413
  - flash X-ray tubes, 410-411, 411
- flaws. *See* discontinuities
- Flemish art, radiographic evaluation, 600
- flickered imaged technique, 423-424, 424
- flight test aircraft inspection, 545-547
- fluid flow radiography, 524, 524-525
- fluorescence scattering, 381, 384
- fluorescent screens, 161-162, 162, 164
  - artifacts associated with dirt, 203, 205
  - and graininess, 227
  - for radioscopy, 254, 256-259, 279
- fluoroscopy, 254-255
  - fluoroscope, 23, 24
  - See also* radioscopy
- flying spot scanning, 389, 389-390
- focus cup, X-ray tubes, 60
- fog, 203, 225
  - and darkroom technique, 237, 238
  - and development, 233
- food radiography, 585, 585
- digital, 300
- fossil radiography, 596
- fourier transforms
  - in backscatter imaging, 388, 392
  - in computed tomography, 310, 314, 329, 332
  - and image analysis, 348
  - and modulation transfer function, 292
- frame averaging, in imaging systems, 352
- freeman chain code algorithms, 356, 356, 363
- fuel injector image analysis, 355
- fuel rods/elements. *See* nuclear fuel
- future usefulness, and nondestructive testing, 2
- gadolinium, capture cross section, 47*table*
- gadolinium oxysulfide, 266, 290
  - relative light yield, 257*table*
  - spectral emission, 258
- gaging. *See* radiation gaging
- gain decrease, 293-294
- gamma (of characteristic curve), 232, 243
  - gamma *versus* temperature curve, 233
- gamma ray attenuation gaging, 570, 570-571
- gamma radiography
  - audit procedures, 116-117
  - backscatter imaging, 398
  - bibliography, 85-88
  - of buildings and structures, 594, 595, 597
  - exposure charts, 167
  - infrastructure applications, 591
  - jet engine inspection, 552, 553
  - and pulsed fast neutron analysis, 590
  - See also* isotope radiation sources
- gamma rays, 38
  - attenuation, 48-51
  - attenuation with and without scatter, 57
  - dissipation in matter, 152
  - dosage, 455-456
  - as electromagnetic radiation, 48
  - emission, 44, 142
  - exposure control installations, 127-128
  - exposure factor, 150
  - and ionization, 91
  - radiation damage from, 293-294
  - radiation detection instruments, 123, 124, 125
  - radiation protection measurement, 121-122
  - radiographic equivalence factors, 153*table*
  - transmission through concrete, 131
  - transmission through lead, 131
- gamma ray sources
  - bibliography, 86-88
  - for castings, 455-456
  - output, 128*table*, 129
  - shielding equivalents, 132*table*
  - skyshine from, 131
  - for welds, 482
- gas discharge tubes, 410
- gas filled detectors, for radiation gaging, 574
- gas ionization detectors, 91-99
- gaskets, neutron radiography, 438
- gas void porosity
  - castings, 454, 461, 462
  - interpretation in castings, 214, 214, 468
  - interpretation in welds, 496
  - welds, 478
- geiger-müller counters, 97, 125
  - described, 96-99
  - energy response curves, 98
  - quenching in, 97
  - for radiation gaging, 574
  - resolving time, 96
- Gemini space vehicle, 552, 553
- geometric enlargement, 146, 147
- geometric unsharpness, 60, 145-146, 146
  - welds, 477
- germanium, attenuation coefficients, 632*table*
- germanium detectors
  - gamma ray efficiency, 107
  - for radiation gaging, 575-576
  - sodium iodide (thallium-activated) compared, 101
  - surface barrier, 106
- ghost defects, 507, 508
- glass, high density, 290
  - properties, 260*table*
- glass dosimeters, 122
- glass X-ray tube, 59
- gold
  - attenuation coefficients, 648*table*
  - capture cross section, 47*table*
- gold-198
  - gamma ray source, 128*table*
  - gamma ray transmission through lead and concrete, 131
- golf ball radiography, 587
- go/no-go gage, 175. *See also* image quality indicators
- government licensing, 114, 118
- government regulations, 117-118, 514
- graetz circuit, 64, 64
- graphite composites
  - attenuation in adhesive bonded, 557
  - epoxy woven stiffener computed tomography, 326
- gray (Gy; replaces rad), 32, 119
- gray wedge, 195-196
- greinacker circuit, 64, 64-65

grid diaphragms, 157-158  
groove welds, 475, 475-476, 477  
radiographic procedure, 495

## H

H and D (Hurter and Driffield) curve. *See* characteristic curve  
half life, 42-43  
half value layer (thickness), 131, 132*table*, 264*table*  
    common materials, 51*table*  
    defined, 51  
hard disk data storage, 275  
hardener, in film development, 234  
Hatteras Lighthouse, radiographic testing of gallery, 595, 595  
helicopter composite rotor/propeller blades, 548-549  
herring bone porosity, 478  
Higashi Honganji Temple, cosmic radiography, 596, 596  
high intensity illuminators, 190-192, 191  
high low defect, 211, 212, 212  
high voltage radiography, 67  
    pulsed sources for flash radiography, 411  
    radiation sources for, 63, 63-66, 66  
    *See also* megavolt radiography  
highway radiography, 591  
histogram equalization, 417  
historic building radiography, 594-596  
historic ship radiography, 596-597  
hole image quality indicators (penetrameters), 172-174  
hollow bead porosity, 207, 208  
holmium, capture cross section, 47*table*  
holography, 11  
honeycomb structures  
    aerospace components, 557, 559, 559-560  
    aviation components, 544, 547, 547-548, 549  
    backscatter imaging, 390  
    microfocus radioscopy, 408  
    neutron radiography of aluminum, 439  
hot cells, 79, 84, 442, 443  
hot cracks, 480  
    interpretation in welds, 212  
    hot line X-ray fixture, 537  
hot stick, 537-538, 538  
hot tears, 216, 216, 463, 468, 480  
hounsfield values, 314*table*  
Hunley (Civil War submarine), radiography of artifacts, 597, 597  
Hurter and Driffield (H and D) curve. *See* characteristic curve  
hydride detection, 557  
hydrogen, attenuation coefficients, 557, 612*table*  
hydrogen cracking, 480  
hyperons, 39  
hypo retention, 234, 235-236

## I

icicles, 211  
illuminators, 190-192, 191  
image analysis, 345-346  
    automated testing techniques, 371-374  
    digital images and processing schemes, 346-352  
    techniques and radiographic tests, 353-370  
image intensifier tubes, 254, 265, 265-266, 271-273  
    for aviation component radiography, 548  
    spectral matching, 267-268  
image isocons, 272-273, 273, 274*table*, 279  
image processing  
    backscatter imaging, 392-394  
    qualitative assessment of electronics, 582-583  
image quality indicators *and* penetrameters, 486-487  
    ASTM E 747, 516, 518  
    for castings, 458  
    film radiography, 172-176  
    and image analysis, 353  
    for microfocus radioscopy, 408  
    for neutron radiography, 441  
    for computed tomography, 328-338, 329*table*, 330, 333, 335, 337  
    plaque type, 172, 174, 458, 485, 486  
    for power and process piping, 516, 517, 518, 518, 519  
    for radioscopy, 277  
    sensitivity *and* discontinuity visibility, 175, 486*table*  
    for weld radiography, 485-487, 486  
    wire type, 173-175, 174, 277, 458, 458*table*, 486, 486,

image transform techniques, 356-366  
inadequate penetration. *See* incomplete penetration  
inclusions  
    castings, 463, 463, 468  
    interpretation in castings, 214-215  
    interpretation in welds, 207-208, 219  
    welds, 478-479  
incomplete fusion  
    castings, 464  
    welds, 479-480  
incomplete penetration  
    castings, 464  
    interpretation in welds, 208-209, 209, 496, 497, 501  
    welds, 479  
indium, capture cross section, 47*table*  
industrial radiography. *See* specific applications, materials and techniques  
inelastic scattering, 46  
infrared testing, 11, 11  
infrastructure radiography, 591-593  
inherent geometry, 338  
in-house programs, 13  
in-motion radiography, 28  
    aerospace components, 559, 559-560, 560  
    aviation components, 545, 545-549  
in-process nondestructive inspection, 502  
integrated circuits. *See* printed circuits  
integrating instruments, 93, 123  
intensified charge coupled device cameras, 271, 279  
intensified silicon intensifier targets, 272  
interactive image enhancement, 353-354, 359  
Inter-Governmental Maritime Consultative Organization (IMCO), radioactive  
    material transportation requirements, 118  
interlacing, 275  
intermediate neutrons, 104*table*  
International Air Transport Association, radioactive material transportation  
    requirements, 118  
International Atomic Energy Agency, radioactive material transportation  
    requirements, 118  
International Committee for Weights and Measures, 31  
International Organization for Standardization (ISO), 18-19  
    ISO 2504, 17*table*  
    ISO 3999, 17*table*  
    ISO 7004, 17*table*  
    ISO 9712, 17*table*, 19  
    ISO 9915, 17*table*  
    ISO 11699, 17*table*, 228  
    ISO *versus* ASTM film classifications, 228*table*  
    Technical Committee 135, 19  
interpretation. *See* radiographic interpretation  
inverse square law, for radiation attenuation, 23, 44-45  
    and radiographic exposure, 146-147, 147  
investment castings, 558  
iodine, attenuation coefficients, 641*table*  
ionization, 91, 91  
    by alpha particles, 45  
    by electromagnetic radiation, 49  
ionization chambers, 91, 121, 125  
    current amplifier for, 93  
    described, 91-93  
    energy and directional response, 92  
    externally located on survey instruments, 93  
    for radiation gaging, 574  
ionizing radiation, 56, 90  
    effect on scintillators, 100  
    effect on semiconductors, 106  
ion pair, 91  
iridium, capture cross section, 47*table*  
iridium-192, 41*table*, 74, 76-77  
    bibliography, 87  
    decay curves, 456  
    disintegration, 76  
    exposure devices, 80, 81  
    gamma ray exposure chart, 166  
    gamma ray source, 128*table*, 455*table*  
    gamma ray transmission through lead and concrete, 131  
    gamma spectra, 75, 77  
    half value thickness, 51*table*  
    for pipeline radiography, 515  
    production, 52



- iron  
 attenuation coefficients, 383, 627*table*  
 casting density *versus* radiographic sources, 460*table*  
 hounsfield value, 314*table*  
 inspection with cobalt-60, 75  
 X-ray and thermal neutron attenuation, 440*table*  
*See also* stainless steel; steel
- ISO. *See* International Organization for Standardization
- isocon cameras, 272-273, 273, 274*table*, 279
- isotope radiation sources, 73-74  
 encapsulation, 79-80  
 exposure devices, 77, 80, 80-84  
 leak testing of sealed, 126  
 selection of isotopes, 74-78  
 semiannual audits, 116-117  
 source handling equipment, 79-84  
 source tube for pipe radiography, 528  
 standards, 14  
 temporary field site *versus* permanent facilities, 116
- J**
- Japanese Standards Association (JSA)  
 JSA K 7091, 17*table*  
 JSA K 7521, 17*table*  
 JSA Z 4560
- jet engines  
 flash radiography, 413  
 inspection, 552, 552, 553
- jet engine turbine blades  
 computed tomography, 305, 323, 326, 561-562, 562  
 flash radiography, 413  
 microfocus radiography, 406, 560-561, 561  
 neutron radiography, 438, 556-557
- joints, 475-477  
*Joseph Conrad*, radiographic testing of hull, 596  
 JSA. *See* Japanese Standards Association
- K**
- K 7091. *See* Japanese Standards Association  
 K 7521. *See* Japanese Standards Association
- K absorption edge, 49, 611  
 fluorescent screens, 259  
 selected elements, 612-651*table*
- K capture, 44
- kinefluorography, 554, 554-555
- kissing, 205
- knowledge-of-position systems, 320
- Korean Standards Association (KSA)  
 KSA A 4907, 17*table*  
 KSA A 4921, 17*table*  
 KSA M 3910, 17*table*
- KSA. *See* Korean Standards Association
- L**
- L absorption edge, 49
- lack of fusion, 496, 497, 503  
 aluminum alloy welds, 507, 509  
 interpretation in welds, 209, 210
- lag, 293
- lamellar tearing, 478, 480
- laminography, 28, 305  
 corrosion detection in aircraft with reversed geometry scanning, 417-418  
 described, 304, 306-309  
 effective aperture, 308  
 generalized mathematical solution, 307  
 scanned beam system, 306  
 for tank radiography, 529  
*See also* digital radiographic imaging
- lanthanum bromide, relative light yield, 257*table*
- lanthanum hypobromite, spectral emission, 258
- lap joints, 476-477, 477  
 exposure setup, 484
- laser film digitization systems, 181
- lateral migration radiography, 395-396
- lead  
 attenuation coefficients, 383, 649*table*  
 filters, 156, 158  
 gamma ray transmission through, 131  
 masks and diaphragms, 155  
 for overprinting to identify radiographs, 488  
 radiographic equivalence factors, 152, 153*table*  
 radiographic quality, 155  
 shielding equivalents, 132*table*  
 X-ray and thermal neutron attenuation, 440*table*
- lead foil screens, 154-155, 159-161  
 artifacts associated with dirt, 203  
 characteristic curves of films exposed with, 167, 169  
 and film graininess, 172, 227  
 kilovoltage effect on intensification properties, 160  
 for radioscopy, 259-260  
 uniformity of electrons emitted, 161  
 for weld radiography, 487
- lead resolution tester, 405
- leak testing, 10  
 of isotope sealed sources, 126
- lenard tube, 23
- Lester Honor Lecture, 27
- Liberty Bell, radiographic testing prior to moving, 597, 598
- licensing, 114, 118
- light bulb radiography, 587
- lighthouse radiography, 595, 595
- light leaks, 203, 203-204
- light pole radiography, 593, 593
- lightroom, 237
- limited angle tomography, 320
- linacs, 69
- linatrons, 53
- linear accelerators  
 for flash radiography, 411-412  
 for megavolt radiography, 69-70  
 for nuclear vessel radiography, 70, 526, 526-528  
 for radioscopy, 264
- linear attenuation coefficient  
 defined, 50, 610  
 selected elements, 612-651*table*
- linear detector arrays  
 for computed tomography, 305  
 for digital radiography, 286*table*, 288, 290, 294, 300  
 image digitization, 349  
 for nuclear fuel tomography, 536
- linear diode arrays  
 for airport bagging screening, 589  
 for consumer goods radiography, 584
- linear porosity  
 interpretation in welds, 207, 498  
 welds, 478  
 line focusing, X-ray tubes, 60, 60
- line pair gages, 329
- line pair resolution phantom, 330, 330
- line spread function  
 computed tomography, 328, 329-332, 331  
 and image analysis, 368
- liquid level gages, 524-525
- liquid penetrant testing, 8, 8, 27  
 castings, 465
- liquid propellant rocket motors, 555-556
- lithium, capture cross section, 47*table*
- lithium drifted detectors, 107, 107
- lithium-6 fluoride dosimeters, 122  
 properties, 102-103
- lithium iodide scintillators, 100*table*  
 for neutron detection, 104
- locks, 127
- longitudinal cracks, in welds, 212, 213, 213
- lookup tables, 354, 354-356, 355, 359
- low level transforms, 356
- luminescent dosimetry, 102-103, 122



## M

M 3910. See Korean Standards Association

magnesium

- attenuation coefficients, 618*table*
- casting density *versus* radiographic sources, 460*table*
- radiographic equivalence factors, 153*table*
- shrinkage in castings, 462

magnetic particle testing, 8, 27

- castings, 465

magnifiers, 192, 193

manganese, attenuation coefficients, 626*table*

manganese bronze, casting density *versus* radiographic sources, 460*table*

manganese-nickel-aluminum bronze, tensile property relation to radiographic indications, 465*table*

marble statue radiography, 598, 599

marx-surge generators, 411

masks and diaphragms, 155

- and interpretation, 192

mass attenuation coefficient

- defined, 50, 610-611
- selected elements, 612-651*table*

matrix effects, in spectrometry, 430

measure, units of, 29-32

medical radiography

- computed tomography, 305
- first use of radiography, 21, 24
- interpretation reproducibility, 186
- market size, 28

megavolt radiography

- electronic radiation sources, 67-70
- film storage, 178
- microfocus radioscopy, 406
- scattering in, 158
- See also high voltage radiography

Mehl Honor Lecture, 26, 27

mercury, capture cross section, 47*table*

mesons, 39

- metal ceramic X-ray tube, 59

metal detector wands, 587

microchannel plates, 266-267, 267

- in intensified charge coupled devices, 271

microfilm, 178-179

microfocus radiography, 28, 404, 404-408

- aerospace components, 560-561, 561
- of electronics, 578-583
- microfocus X-ray tubes, 62

microshrinkage. See shrinkage

microshrinks. See shrinkage

MIL-STD. See military specifications

military specifications

- MIL-B-21250A, 465*table*
- MIL-S-15083, 465*table*
- MIL-STD-453, 486, 489

mine detection, backscatter imaging for, 395-396

mine rock anchor bolts, scanning microdensitometry, 198

mismatch, interpretation in welds, 211, 212

misruns, 463

- interpretation in castings, 217, 217

mobile neutron radiography system, 444

mobile radiation sources, 14

moderators, 46

modular radiation enclosure, 130

modulation transfer function

- computed tomography, 328, 329-332, 331, 332*table*
- and imaging, 277, 277-279, 290, 292, 292-293, 348-349
- and laser film digitization systems, 181

moiré imaging, 11

moisture measurement, 572, 573

molybdenum, attenuation coefficients, 636*table*

monitors, 354

- for radioscopy, 275

morphological transforms, 356, 360-363

motion blur, in radioscopy, 262

motorcycle neutron radiography, 440

mottling, 454, 463-464

- and film radiography, 158
- quantum, 227, 262, 289
- screen mottle, 162, 171-172

moving detector depth scanning, 388-389, 389

MQ developers, 232

multiscale, multiresolution transforms, 356, 363-364, 364

mummy radiography, 594

munitions. See explosives; ordnance

## N

narrow beam shielding, 133

National Building Code of Canada, 489

National Institute of Standards and Technology, 125

natural radioactivity, 52

navy bronze, casting density *versus* radiographic sources, 460*table*

NCRP 61, 17*table*

neutrinos, 39

neutron absorbers, 47

neutron activation, 52

neutron capture, 46, 52

neutron detectors, 104-105

neutron gaging, 448, 573

neutron induced autoradiography, 448

neutron interferometry, 448

neutron radiography

- aerospace components, 556-557
- applications, 437-439
- dynamic radioscopy, 446
- epithelial, 447
- fast, 447
- for fluid flow measurements, 524
- for high and low density materials, 12
- imaging, 264, 440-441
- radiation safety, 134-135
- special techniques, 446-448
- static radiography with thermal neutrons, 440-445
- subthermal, 446
- training and experience recommended, 18*table*

neutrons

- atomic structure, 39
- capture, 46, 52
- classification, 104*table*
- interactions, 45-47
- radiation detection instruments, 126
- radiation protection measurement, 122

neutron sensitive screens, 259

neutron sources, 53, 441-443

- radiographic isotope creation, 74-78
- safety aspects, 134

neutron tomography, 447-448, 530, 534-536, 535

- aerospace components, 562-563

newvicon, 272, 273

- characteristics, 274*table*

nickel

- attenuation coefficients, 629*table*
- digital radiography of bucket blades, 300
- radiographic equivalence factors, 153*table*

nickel silver, casting density *versus* radiographic sources, 460*table*

niobium, attenuation coefficients, 635*table*

nitrogen, attenuation coefficients, 615*table*

nondestructive testing

- applications, 4
- defined, 2
- methods classification, 4-6
- methods overview, 7-12
- objectives, 5*table*, 6*table*
- purposes, 2-4
- specifying tests, 186-187
- test objects, 5-6
- value of, 7

Nondestructive Testing Handbook series, 27

nonmetallics, 207

nonrelevant indications, 202

no umbra device, 441

NRC. See Nuclear Regulatory Commission

nuclear cross sections. See cross sections

nuclear fission, 46

nuclear fuel, 530-536

- cesium-137 recovery from, 76
- digital radiography, 300
- flash radiography, 413
- neutron radiography, 441
- scanning microdensitometry, 197
- thickness measuring system for microspheres, 530, 531

nuclear magnetic resonance imaging (MRI), 311

nuclear neutron absorption, 46  
 nuclear power plants  
   inservice inspection with linear accelerator, 70, 526-528  
   piping radiography, 517, 518  
   pressure vessel radiography, 526  
 nuclear radiographic service centers, 442  
 nuclear reactor neutron sources, 441-442  
   radiographic isotope creation, 74-78  
   safety aspects, 134  
 Nuclear Regulatory Commission (NRC), 114  
   permissible doses, 120  
   reporting of leaking isotope sources, 126  
   safety personnel certification, 117-118  
   waste disposal licensing, 118  
 nuclear transmutation, 46  
 nuclear waste  
   computed tomography, 536  
   disposal licensing, 118  
 nucleonic gaging, 570, 576-577

## O

object scatter, 348  
 observed contrast, in radioscopy, 261-262  
*Occupational Safety and Health Standards*, 17table, 19  
 onion radiography, 585  
 open installation, 128  
 optical coupling  
   digital radiography, 299  
   radioscopy, 269, 271  
 optical density, 141, 164-165, 190-198  
 optically stimulated luminescence dosimetry, 103  
 optical testing methods, 11  
 optotype, 189  
 ordnance  
   aerospace, 557  
   backscatter imaging, 388, 395-396  
   microfocus radioscopy, 406  
 O-rings  
   neutron radiography, 438, 557  
   neutron tomography of aerospace, 562, 563  
 overlap, interpretation in welds, 210  
 oxidation, repair welds in castings, 464  
 oxtail, 63  
 oxygen, attenuation coefficients, 616table  
*The Oyster Eater* (Ensor), radiographic evaluation, 600

## P

packaging radiography, 587  
 packaging tape, attenuation gaging, 572  
 paintings, radiographic testing, 598-601  
 pair production, 347  
   attenuation coefficient, 610  
   defined, 49, 50  
 paper  
   moisture content gaging, 572  
   radiation gaging, 576-577  
 paper radiographs  
   density, 195  
   viewing, 192-193  
 parallax, and stereo radiography, 419-423, 420  
 partial volume effect, 317  
 particle physics  
   electromagnetic radiation, 48-51  
   elementary particles, 38-41  
   radioactive material production, 52-63  
   radioactive material properties, 42-47  
 passenger jet flight test radiography, 545-546, 547  
 pellet implosion studies, flash radiography application, 413  
 penetrameters. *See* image quality indicators  
 penetrating radiation, 22, 23, 48  
 penstock radiography, 592, 592  
 perception, 189-190  
 periodic table, 40, 41  
 permissible doses, 120  
 persistence curves, 257-258  
 personal dose equivalent, 32  
 personnel dosimetry, 121-122  
   clip-on devices, 122  
 personnel monitoring, 127  
 personnel monitoring instruments  
   dose rate *versus* effective energy, 98  
   geiger-müller counters, 98-99  
   ionization chambers, 93-94  
 personnel qualification and certification, 13, 15, 18-19, 186  
   ANSI/ASNT CP-189, 17table  
   ASNT Recommended Practice No. SNT-TC-1A, 17table, 18table  
   ISO 9712, 17table  
   for radiation safety, 19, 117-118  
   *See also* training  
 petroleum industry applications. *See* utility, petroleum and chemical industry applications  
 phantoms, 310, 335-338  
   categories and measurement technique, 329table  
   for contrast sensitivity, 333  
   for dimensional measurement, 336-338, 337  
   and image analysis, 351  
   line pair resolution, 330  
   for material density, 335, 336  
   for medical computed tomography, 328  
   nuclear waste drum, 536  
 pharmaceuticals  
   backscatter imaging, 381  
   radiation gaging, 577  
   radiographic testing, 586-587  
 phosphors, 256, 257table  
   for digital radiography, 284, 286, 290-291, 291  
   in neutron detection, 104  
   for personnel dosimetry, 122  
   spectral emission, 267  
   typical glow curve, 102  
 photocathodes, 101, 574  
   response spectrum in image intensifiers, 267  
 photocurrent signal, 270  
 photoelectric effect, 347  
   attenuation coefficient, 610  
   defined, 48-49  
 photographic density, 141, 164-165  
   density *versus* exposure, 226  
   and exposure, 226  
   paper radiographs, 195  
   quality control, 242-243  
 photoluminescent glass dosimeters, 122  
 photomultiplier tubes, 100-101, 101  
   with laser film digitization systems, 181  
   in thermoluminescent dosimeters, 103  
 photon attenuation coefficients. *See* attenuation coefficients  
 photons, 48-50, 56-57  
   characteristics, 48table  
   pair production from incident, 50  
   photoelectric interaction of incident with orbital electron, 49  
*Pietà* statue radiography, 598, 599, 599  
 pigtail, 79, 79, 80, 81, 83  
 pillowing, 396-397  
 pi marks, 205, 205  
 pinhole cameras, for backscatter imaging, 388  
 pipeline radiography, 515-517  
   backscatter imaging of corrosion, 397  
   radioscopic imaging, 254  
   residual stress measurement, 429  
 pipe radiography  
   automated defect recognition in welds, 372, 372-374, 373  
   dimensional analysis of copper, 367-370, 367-371  
   nuclear power plants, 527-528, 528  
   power and process piping, 517-525  
 piping (weld porosity type), 478  
   interpretation, 478  
 pixel pitch, 292  
 plaque penetrameters. *See* image quality indicators  
 plastics, radiation gaging, 577  
 plastic scintillators, 100  
   for neutron detection, 104  
 plated through-hole (PTH) solder joints, 579  
 platinum, attenuation coefficients, 647table  
 plumbicon, 272, 273  
 plutonium, attenuation coefficients, 651table  
 pocket ionization chambers, 93-94, 94  
 pocket knife, digital laminography, 308, 309  
 point clouds, 363, 369  
 point spread function, 348-349  
   computed tomography, 328, 329

polonium, 38  
 porosity, 2  
   castings, 454, 461, 464  
   interpretation in castings, 213-214, 214  
   interpretation in welds, 207, 207-208, 495, 496, 498, 499  
   repair welds in castings, 464  
   welds, 478  
*Portrait of Gaspard Gevartius* (Rubens), radiographic evaluation, 600  
 positron emission tomography (PET), 311  
 positrons, 39  
   production from incident photon, 50  
 potassium-40, 52  
 power line radiography, 537-538  
 power piping radiography, 517-525  
 PQ developers, 232  
 predetermined liquid level gage, 525  
 pressure marks, 203, 203, 205, 205  
 pressure vessel radiography, 526-528, 527  
 pressurized water reactor radiography, 526-527  
   primary X-ray photons, 347  
 printed circuits  
   laminography, 306  
   microfocus radiography, 405  
   radioscopy, 578-583  
 process piping radiography, 517-525  
 projection microfocus radiography, 264, 404-408  
 proportional counters, 94-95  
   for neutron detection, 104  
   for radiation gaging, 574  
 proportional region, 574  
 protective enclosures, 130-131  
 protective installation, 127  
 protons, 38-39  
 pulsed fast neutron analysis, 590  
 pulsed high voltage sources, for flash radiography, 411  
 Pyramid of Khafre, cosmic radiography, 596  
 pyrotechnic devices  
   aerospace, 557  
   neutron radiography, 438, 446, 447

## Q

qualification. *See* personnel qualification and certification  
 quality control, 188  
   of film processing, 242-244  
 quality factor, 119-120  
 quantum mottle, 227, 262, 289  
 quantum noise, 360  
 quantum theory, 48  
 quartz fiber pocket dosimeter, 94

## R

rad (radiation absorbed dose), 32, 119  
 radiation absorption. *See* absorption  
 radiation attenuation. *See* attenuation  
 radiation conversion material, 287  
 radiation damage, 293-294  
   thresholds, 265 *table*  
 radiation detectors, 122-123  
   calibration, 126  
   choice, 123-125, 350 *table*  
   *See also* radiation gaging; radiation measurement; radiation safety; and  
   *specific detectors*  
 radiation dose  
   definitions, 32, 119-120  
   dosage rate, 32, 74-75, 120, 128-129, 455-456  
   dose equivalent, 32, 119  
   *See also* personnel certification; radiation safety  
 radiation gaging, 28, 570-573  
   application case histories, 576-577  
   backscatter imaging application, 392, 573  
   detector types, 573-576. *See also* radiation detectors;  
   *See also* radiation detectors; radiation measurement; radiation safety  
 radiation measurement, 89-90, 122-126. *See also* radiation detectors; radiation  
   gaging; radiation safety

radiation safety, 19  
   doses, 119-120  
   exposure control, 127-129  
   exposure levels, 119-120  
   management, 114-118  
   neutron radiography, 134-135  
   protection measurements, 121-126  
   shielding, 130-133  
   standards and practices, 17 *table*  
   *See also* dosimeters; personnel certification; radiation dose  
 radiation safety officer, 114-117  
   and changes to protective enclosures, 130  
 radiation sources, 14, 55-88  
   for flash radiography, 411  
   for metal castings, 455-456, 467  
   output, 129  
   for radioscopy, 263-264  
   for welds, 482  
   *See also* electronic radiation sources; isotope radiation sources  
 radiation surveys, 123, 125, 127  
   and shielding wall thickness, 123, 125, 127  
   survey meter, 121  
 radiation, units of measure for, 29-32, 42, 119-120  
 radiation weighting factors, 119 *table*  
 radioactive decay, 43, 43-44  
 radioactive materials  
   production, 52-63  
   properties, 42-47  
   transportation and disposal, 118  
 radioactive neutron sources, safety aspects, 134  
 radio frequency quadrupole accelerators, 443  
 radiographer certification, 15, 18-19, 117-118  
 radiographic artifacts  
   aluminum alloy welds, 507-509, 508  
   computed tomography, 336  
   in digital radiography, 295  
   radioscopic, 206  
   types of, 202-206  
   viewing accessories for interpreting, 192  
 radiographic contrast  
   defined, 170, 243  
   and film development, 223-225, 226-227  
   and film exposure, 150-151  
   and kilovoltage, 151  
 radiographic equivalence factors, 152-153, 153 *table*  
 radiographic interpretation, 14, 185-188  
   castings, 213-217, 468  
   densitometers for, 194-198  
   reporting, 198-201  
   reproducibility, 186  
   viewing equipment, 190-193  
   vision acuity and perception, 189-193  
   welds, 207-212  
   *See also* radiographic artifacts  
 radiographic parallax, 420  
 radiographic sensitivity  
   defined, 170  
   and discontinuity detection, 458-459  
   and film exposure, 151  
 radiographic shadows, 143, 143-144, 144  
 radiographic shooting sketches, 199  
   castings, 457  
 radiographic testing  
   advances in, 28  
   advantages and disadvantages, 12, 454  
   audit procedures, 115-117  
   essential steps of, 186  
   history, 21-28  
   imaging and viewing, 14, 189-193  
   management, 12-20  
   personnel qualification and certification, 15, 18-19, 18 *table*  
   reliability, 19-20  
   representative setup, 7  
   test procedures, 13-15, 16-17 *table*  
 radiographs  
   identification, 177  
   setup for making with X-rays, 140  
   subtleties, 364-366  
 radioscopic artifacts, 206  
 radioscopic imaging system, 255  
 radioscopic weld penetration control, 505, 505-506

radioscopy, 14, 253-255  
     arc welding, in-process, 502, 502-506, 503, 504  
     cameras for, 269-274  
     consumer goods, 584-587  
     of electronics, 578-583, 584  
     image quality, 261-264  
     image systems, 265-268  
     light conversion, 254, 256, 256-260  
     optical coupling, 269, 271  
     of pipeline weld quality, 517  
     projection microfocus, 404-408  
     recording equipment, 275-276  
     sources for, 263-264  
     systems, 277-279  
     viewing and recording, 275-276  
     *See also* digital radiographic imaging; fluoroscopy  
 radium, 38  
     bibliography, 88  
     gamma ray source, 128*table*  
     gamma ray transmission through lead and concrete, 131  
     radium-226, 52, 74  
 radon, publications on 88  
 railroad car security inspection, 590  
*Randall's Mill* (Higgins), radiographic evaluation, 600-601, 601  
 rate instruments, 123  
 rayleigh scattering. *See* elastic scattering  
 reader's sheet, 199  
 real time radiography. *See* radioscopy  
 rebar, gamma radiography of steel, 591  
 recertification, 18  
 reciprocity law, 148, 149  
     failure of, 228-229, 229  
 recombination region, 574  
 reconstruction  
     in backscatter imaging, 392-394  
     in computed tomography, 312, 312-314  
 reference standards, 187-188  
     for automated defect recognition, 374  
     for casting radiography, 460, 468  
     for computed tomography, 328-338  
     for radiographic testing, 14-15, 16-17*table*  
     for weld radiography, 489-490  
     *See also* image quality indicators; phantoms; specific standards  
 regulations, 12, 514  
 relative atomic mass (atomic weight), 610-611  
 relative biological effect, 119  
 relative film speed, 244  
 relativistic neutrons, 104*table*  
 reliability, of radiographic testing results, 19-20  
 rem (roentgen equivalent man), 32, 119  
 replenishers, 233, 242  
 residual hypo, 234  
     residual stress, X-ray diffraction measurement, 428-429  
 resistor spark plugs, microfocus radioscopy, 407  
 resonance fluorescence scattering, 381  
 resonance peaks, 47  
     resonant transformer X-ray machines (resotrons), 67, 67  
 restricted areas, 120  
 reticulation, 244  
 reversed geometry scanning beam technique, 288, 414, 414-418  
     aerospace components, 563-564  
     aircraft wing crack detection, 415-416, 416  
     for digital radiography, 286*table*, 294  
 reverse engineering, by computed tomography, 324  
 rhenium, capture cross section, 47*table*  
 rhodium, capture cross section, 47*table*  
 robotics  
     assembly line radioscopy of automotive parts, 278, 279  
     use in radioscopic imaging, 254, 255, 264  
 rocket engines and motors  
     computed tomography, 323  
     liquid propellant, 555-556  
     small ablative thrust chambers, 552-555  
     solid propellant, 550-552  
     rod anode, X-ray tubes, 63, 63  
 roentgen (R), 31-32, 119, 120  
 roentgen rays, 22  
 root cracks, interpretation in welds, 212, 214, 214  
     rotating anode X-ray tubes, 67, 432  
 rutherford scattering, for radiation gaging, 573

## S

SAE International (formerly Society of Automotive Engineers) standards, 489  
     SAE AMS-STD-2175, 466, 470  
     SAE AMS 2635C, 17*table*  
     SAE ARP 1611A, 17*table*  
     SAE AS 7114/4, 17*table*  
     SAE AS 1613A, 17*table*  
 safety  
     film development, 244-245  
     increased public demand for, and nondestructive testing, 4  
     *See also* radiation safety  
 safety factor, 3  
 salting, 353, 374  
 samarium, capture cross section, 47*table*  
 sand castings, 459  
 sand inclusions, 461  
     interpretation in castings, 214  
 Saturn rocket motor radiography, 550  
 scanned beam laminography system, 306  
 scanning microdensitometry, 195-198  
     example graphs, 197  
 scattering  
     and film radiography, 153-158, 154  
     and image analysis, 347-349  
     material, scattering as function of, 382-384  
     and megavolt radiography, 158  
     and radioscopic imaging, 262  
     reduction, 154-158, 155  
     and resolved diameter, 386  
     single and multiple, 382, 384-387, 385  
     types of, 45-47, 49, 380-382  
     *See also* backscatter imaging; compton scattering; elastic scattering  
 scatter-to-primary ratios, 348  
 scintillation, 100, 100, 574  
 scintillation detectors, 125  
     described, 100-101  
     image digitization, 349-351  
     for neutron detection, 104  
     for radiation gaging, 574-575  
 scintillator plates, 260  
 scintillators, 100*table*  
     and beam hardening, 349  
     degradation, 366  
     properties, 260*table*  
 scrambling, 127  
 scrap film, 248  
 scratches, 202, 206  
     screen effect, X-ray tubes, 60-61, 61  
 screen gamma, 259  
 screen marks, 203  
 screen mottle, 162  
 SDRAM (synchronous dynamic random access memory) chips, 355  
 seals  
     neutron radiography, 557  
     radiography of tamper evident, 584  
 security applications, 28  
     digital radiography, 300  
     radioscopic detection of contraband (circa 1910), 23  
     X-ray screening for airport security, 588, 588-590, 589  
 seeds, radiographic testing, 585-586  
 segregation, interpretation in castings, 217  
 selenium  
     attenuation coefficients, 633*table*  
     selenium-75, properties, 78  
     selenium-75, publications on, 87-88  
 self-quenching gas, in geiger-müller counters, 97  
 semiconductor detectors  
     described, 106-107  
     for radiation gaging, 575  
     *See also* amorphous selenium detectors; amorphous silicon detectors;  
     germanium detectors; silicon detectors  
 sensitometric curve, 167  
 sensitometric density, 141, 164-165  
 sensitometry, 230, 242-243  
 service companies, 12-13, 439  
 shearography, 11  
 shielding, 130-133  
     neutron radiography, 134-135  
 shields, 127

shifts, 463  
     interpretation in castings, 217  
 ship radiography, 596-597  
 shooting sketches, 199, 457  
 shrinkage  
     castings, 461-462  
     interpretation in castings, 215-216, 468  
     microshrinkage, 215, 461, 462, 462  
 shrinks. *See* shrinkage  
 shrinkwrap codes, 356, 356, 363  
 sievert (Sv; replaces rem), 32, 119, 120  
 sight developing, 245  
 signal-to-noise ratio  
     computed tomography, 333-334  
     for digital radiography, 294  
     and image analysis, 346  
 silicon, attenuation coefficients, 620*table*  
 silicon bronze, casting density *versus* radiographic sources, 460*table*  
 silicon detectors  
     gamma ray efficiency, 107  
     for radiation gaging, 575-576  
     surface barrier, 106  
     *See also* amorphous silicon detectors  
 silicon intensifier targets, 272, 273  
     characteristics, 274*table*  
 silver  
     attenuation coefficients, 637*table*  
     capture cross section, 47*table*  
     recovery in film development, 247-249  
     sludge, 249  
 silver bromide, 163, 221, 221, 227, 231  
     developed grain, 223  
 silver flake, 249  
 silver halide film, 231  
     industrial X-ray films, 163  
     latent image formation, 108-109, 220, 220-222  
     *See also* film development  
 silver sulfide, 220, 234, 244  
 simulation, aerospace applications, 564  
 single-pixel noise, 360  
 SI units, 29-32  
 skyshine, 130, 130-131  
 slag inclusions  
     castings, 464  
     interpretation in castings, 214, 215  
     interpretation in welds, 207-208, 208, 499  
     welds, 478-479  
 slit collimated linear detector arrays, 350  
 slit imaging, for backscatter imaging, 388-389  
 slow neutrons, 46, 104*table*  
 smudge (static mark), 240, 240  
 SNARK, 311  
 Society of Automotive Engineers. *See* SAE International  
 sodium, attenuation coefficients, 617*table*  
 sodium iodide scintillators, 100*table*  
     for digital radiography, 288  
     germanium detectors compared, 101  
     properties, 260*table*  
     for radiation gaging, 575, 576  
 soil, and infrastructure radiography, 591  
 solder joints  
     automated process test systems, 578-580, 579  
     automatic defect recognition, 406  
 solid propellant rocket motors, 550-552, 551  
 solid state detectors. *See* semiconductor detectors  
 sonde length, 398  
 source. *See* radiation sources  
 source shutdown mechanisms, 127  
 space charge, 57  
 space flight component radiography, 550-558  
 spallation, 46  
 spark plugs, microfocus radioscopy, 407  
 spark testing, 11  
 spatially invariant transforms, 356, 359, 359-360  
 spatial resolution, 346, 348-349  
     digital radiography, 292-293  
 specific activity, 455  
 specifications, 14-15, 187-188  
     castings, 457  
     welds, 489-490  
     *See also* reference standards  
 specific ionization, 91  
 spectrometer mode detectors, 574, 575-576  
 spectroscopy, 11  
 speed of light, 31  
 sponge shrinkage, 216, 461, 462, 462  
 spontaneous fission, 44  
 spontaneous fission neutron sources, safety aspects, 134  
 sports equipment radiography, 587  
 spotting, 204, 204-205  
 spot viewers, 191  
 stainless steel  
     casting density *versus* radiographic sources, 460*table*  
     density gaging, 572  
     fuel rod radiography, 531  
     mottling, 463  
     nuclear vessel radiography, 527  
     pipe weld discontinuities, 499-501  
     tungsten inclusions in welds, 480  
     *See also* steel  
 standards. *See* reference standards  
 starter solution, 233  
 state licensing, 114  
 state regulations, 117-118, 514  
 static marks, 161, 203, 239, 240, 240  
 statistics  
     digital radiographic imaging, 289, 289-295  
     radioscopy, 268  
 Statue of Liberty, gamma radiography, 594  
 steam generator radiography, 528  
 steel  
     aviation component radiography, 544  
     backscatter imaging, 387, 395  
     casting density *versus* radiographic sources, 460*table*  
     crack detectability in welds, 491-495  
     energy dispersive spectrometry of sheet, 431  
     exposure of part containing two thicknesses, 171  
     fluorescent screens for, 161-162  
     fuel injector image analysis, 355  
     gamma radiography of rebar in concrete, 591  
     incomplete penetration in welds, 497  
     in-motion radiography of aviation components, 545  
     inspection with cobalt-60, 75  
     inspection with iridium-192, 76-77  
     inspection with thulium-170, 78  
     lack of fusion in welds, 497  
     lead foil screens for, 159  
     line resolution phantom, 330  
     maximum filter thickness, 157  
     nuclear fuel rods in steel can, 534-535  
     optical density obtained through 13 to 16 mm, 225*table*  
     pipe weld radiography, 517  
     porosity in castings, 462  
     porosity in welds, 498  
     radiation gaging, 576, 577  
     radiographic equivalence factors, 152, 153*table*  
     radiological detection and identification, 590  
     scattered radiation, 153  
     slag inclusions in welds, 499  
     tensile property relation to radiographic indications, 465*table*  
     tungsten inclusions in welds, 480  
     X-ray exposure chart, 165  
     X-ray potential and general thickness limit, 482  
     *See also* stainless steel  
 steel diaphragms, 155  
 step wedge, 364-365, 365, 366  
 stereo radiography, 419-426, 421  
     display designs, 425  
     flaw geometries permitting calculation of average flaw displacement, 423  
     flickered imaged technique, 423-424, 424  
 storage phosphors, 287-288, 294  
     properties, 286*table*  
 strain gaging, 11  
 streak artifacts, 348  
 stress corrosion, 396  
 stress riser, 209, 210, 478, 479, 480  
 strip film viewers, 191  
 subject contrast, 170-171  
     in radioscopy, 261  
 subthermal neutron radiography, 446  
 superalloys, 460  
 surface barrier detectors, 106-107, 107



## T

tamper evident seal radiography, 584  
 tangential radiography, 519-523, 520, 522  
   ablativ thrust chambers, 552, 553  
 tank radiography, 528-529  
 tantalum  
   attenuation coefficients, 645*table*  
   capacitor microfocus radiography, 407  
   casting density *versus* radiographic sources, 460*table*  
   inspection with cobalt-60, 75  
 tantalum-182, gamma ray source, 128*table*  
 tantalum screens, 259  
 tape automated bonded (TAB) solder joints, 580  
 tapping, 11  
 television cameras, 254, 255, 269  
   common adjustments for, 274*table*  
   output *versus* light input, 273  
 television monitors, 275, 354  
 tenth value layer, 131, 132*table*  
 textile radiation gaging, 577  
 thermal neutrons, 46, 104*table*  
   attenuation by selected elements, 440*table*, 447  
   shielding, 134-135  
   static radiography with, 440-445  
 thermal testing, 11  
 thermionic emission, 57  
 thermoluminescence, 102  
 thermoluminescent dosimeters, 122  
   described, 102-103  
 thermoluminescent dosimetry, 102  
 thermometers, in film development, 241  
 thin film transistors, 287  
 thiosulfate, 234  
 thorium series, 52  
 threat recognition software, in airport security, 589-590  
 thresholding transforms, 356, 358, 359  
   for automated defect recognition, 372  
 thulium-170, 77-78  
   attenuation coefficients, 644*table*  
   bibliography, 88  
   disintegration, 77  
   source for castings, 455*table*  
 tin, attenuation coefficients, 639*table*  
 tin bronze, casting density *versus* radiographic sources, 460*table*  
 titanium  
   aerospace castings, 558  
   attenuation coefficients, 623*table*  
   casting density *versus* radiographic sources, 460*table*  
   compton scattering intensity, 383, 384  
   in image intensifier tubes, 266  
   radiographic equivalence factors, 153*table*  
   tungsten inclusions in welds, 480  
 T joints, 476  
   exposure setup, 484, 485  
   radiographic procedure, 495  
 toe cracks, interpretation in welds, 212  
 tomato radiography, 585  
 tomograms, 305  
 tomography. *See* computed tomography; laminography; neutron tomography  
 tomosynthesis, 304, 306-309. *See also* laminography  
 toothpaste radiography, 586  
 trace analysis, by wavelength dispersive spectrometry, 430  
 track etch neutron detectors, 105  
 training, 18-19  
   security threat recognition, 589  
   *See also* personnel qualification and certification  
 transmission images  
   components, 346-349  
   digitizing, 349-351  
   subtleties, 364-366  
   transmission X-ray system, 578  
 transportation, radioactive materials, 118  
 transverse cracks, interpretation in welds, 212, 213, 213  
 tree (static mark), 240, 240  
 trend removal, 371, 372  
 tritium, 42  
 tube gamma, 273  
 tubes welds, 372, 372-374, 373  
 tungsten, attenuation coefficients, 646*table*  
 tungsten inclusions

castings, 464  
 interpretation in welds, 208, 209, 209  
 nuclear fuel rods, 530-531  
 welds, 480  
 tungsten screens, 259  
 turbine blades. *See* jet engine turbine blades  
 two-gain coefficient technique, 367

## U

ultrasonic testing, 9, 9-10  
 unattended installation, 128  
 unconsumed insert, 500, 500-501  
 underbead cracks, 478, 480  
   interpretation in welds, 212  
 undercut  
   castings, 464  
   interpretation in welds, 210  
   piping welds, 520  
   welds, 481, 507  
 undercut (scattered radiation effect), 153-154  
 underfill, interpretation in welds, 209, 210  
 unfused chaplets, 463  
   interpretation in castings, 216-217, 217  
 unfused inserts, 463  
   interpretation in castings, 216  
 unified atomic mass unit, 31  
 units of measure, 29-32, 42, 119-120  
 unsharp mask transforms, 360  
 unsharpness  
   effect on discontinuity detection, 258  
   geometric, 145-146  
   and object-film-source orientation, 145  
   radioscopy, 258-259  
   welds, 477  
 uranium, 38  
   absorption and scattering curves, 49  
   attenuation coefficients, 650*table*  
   inspection with cobalt-60, 75  
   radiographic equivalence factors, 153*table*  
 uranium-235, 52  
 uranium-238, 52  
   resonance peaks, 47  
   spontaneous fission, 44  
 uranium series, 52  
 utility, petroleum and chemical industry applications, 513-514  
   nuclear fuel radiography, 530-536  
   pipeline radiography, 515-517  
   power and process piping radiography, 517-525  
   power line radiography, 537-538  
   pressure vessel radiography, 526-528  
   tank radiography, 528-529

## V

vacuum discharges, 410  
 valves  
   neutron radiography, 438  
   neutron radiography of aerospace, 563  
 vanadium  
   attenuation coefficients, 624*table*  
   compton scattering intensity, 383, 384  
 van de graaff generators, 53, 67, 67-68, 442-443, 443  
 veiling glare, 356  
 vessel radiography, 526-528  
 vibrating reed electrometers, 93, 93  
 vibration analysis, 11  
 video cameras, 254, 255  
 video capture card, 276  
 video cassette recorder (VCR) data storage, 275  
 vidicons, 272, 272, 273  
   for aviation component radiography, 548  
   characteristics, 274*table*  
   sensitivity compared to charge coupled devices, 270  
 viewing conditions, 190-192  
 viewing room, 237  
*View of Delft* (Vermeer), radiographic evaluation, 600  
 vignetting, 271  
 villard circuit, 64, 64  
*The Virgin and Child Enthroned with Saints* (Rubens), radiographic evaluation, 600



vision acuity, 189-190  
vision acuity tests, 189  
visual parallax, 420  
visual testing, 7, 7-8  
volume computed tomography, 320, 327  
V/STOL propeller blade radiography, 548

## W

wagon tracks, 479  
walnut seed radiography, 586  
washing, film, 230, 244  
water  
    in film development, 232, 235-236, 241  
    hounsfield value, 314 *table*  
    and spotting artifacts, 204, 205, 205  
    X-ray and thermal neutron attenuation, 440 *table*  
wavelength dispersive spectrometry, 427, 429, 429  
    detection lower limits, 430  
    instrumentation for, 431  
weld drop-through, 499-500, 500  
welds, 473-474  
    arc weld in-process radioscopy, 502, 502-506, 503, 504  
    automated defect recognition, 372, 372-374, 373  
    crack detectability in steel, 491-495  
    design, 475-477  
    digital laminography, 308, 309  
    digital radiography of aluminum tubes, 297  
    discontinuities in, 478-481  
    discontinuity depth detection using stereo radiography, 419  
    discontinuity radiography, 491-501  
    exposure setup for various types, 483-485  
    false indications in aluminum alloys, 507-509, 508  
    flash radiography, 412-413  
    image analysis, 362  
    in-motion radiography of aviation tanks, 545, 546, 546 *table*  
    inspection of bridge, 592  
    interpretation of discontinuities, 207-212  
    interpretation report, 200  
    light poles, 593  
    liquid propellant rockets, 556  
    material and thickness, 477  
    image quality indicators (penetrameters), 485-487  
    penetration control by in-process radioscopy, 505, 505-506  
    in pipelines, 515-517  
    in pipes, 499-502  
    radiographic techniques, 482-488  
    repair welds in castings, 464, 465  
    residual stress measurement, 429  
    Saturn rocket motor, 550, 551  
    scanning microdensitometry, 197  
weld spatter, 464  
whole body irradiation, 120  
wire mesh, 277  
wire image quality indicators (penetrameters), 172-174  
    for castings radiography, 458  
    sensitivity, 486 *table*  
    for weld radiography, 485, 486  
    *See also* image quality indicators (penetrameters)  
working distance, 129  
working time, 129  
wormhole porosity  
    interpretation in castings, 214  
    interpretation in welds, 207

## X

X-ray crawler device, 515  
X-ray diffraction, 25, 28, 384  
    and crystal structure, 427-428, 428  
    flash, 413  
    mottling caused by, 158  
    for residual stress measurement, 428-429  
X-ray exposure charts, 165, 165-167, 166  
X-ray fluorescence gaging, 571  
X-ray fluorescence spectrometry, 427  
    elemental analysis by, 429-431  
X-ray lithography, 28  
X-ray photon, 57  
X-ray powder diffractometry, 429  
X-ray radiography. *See* radiographic testing

## X-rays

absorption, 57-58  
attenuation, 48-51, 440 *table*  
discovery, 22-23  
dissipation in matter, 152  
effect of metal filters on intensity, 156, 156 *table*, 157  
as electromagnetic radiation, 48  
and electron capture, 44  
emission, 141-142  
exposure control installations, 127-128  
exposure factor, 150  
forward intensity from optimum target, 129  
and ionization, 91  
radiation damage from, 293-294  
radiation detection instruments, 12, 124, 125  
radiation protection measurement, 121-122  
radiographic equivalence factors, 153 *table*  
Roentgen demonstrates, 23  
spectral sensitivity, 227-228  
wavelength *versus* intensity, 141, 142  
X-ray sensitive cameras, 273  
X-ray sources  
    advances in, 28  
    for castings, 456, 457 *table*  
    output, 129 *table*  
    shielding equivalents, 132 *table*  
    for welds, 482  
    *See also* electronic radiation sources; isotope radiation sources  
X-ray spectrum, 56  
X-ray tomography. *See* computed tomography  
X-ray tubes  
    construction, 59, 59-63  
    electron beam distribution, 62  
    flash, 410-411, 411  
    high voltage, 63-66  
    invention, 24-25, 25  
    projected focal spot, 187, 188  
    rotating anode, 61, 432  
X-ray distribution, 62

## Z

Z 4560. *See* Japanese Standards Association  
zinc  
    attenuation coefficients, 631 *table*  
    casting density *versus* radiographic sources, 460 *table*  
    radiographic equivalence factors, 153 *table*  
zinc cadmium sulfide, 265  
    properties, 257 *table*  
    relative light yield, 257 *table*  
    spectral emission, 258  
zinc sulfide, silver-activated, 100 *table*  
zirconium  
    attenuation coefficients, 634 *table*  
    radiographic equivalence factors, 153 *table*  
zooming (in microfocus radiography), 405-406  
    aerospace structures, 560

# Figure Sources

## Chapter 1. Introduction to Radiographic Testing

Figure 11 — Warner-Lambert Company, Morris Plains, NJ.

## Chapter 3. Electronic Radiation Sources

Figure 22 — Varian Associates, Palo Alto, CA.

## Chapter 4. Isotopes for Gamma Radiography

Figures 7c, 9a, 11, 13b, 14, 16 — Source Production and Equipment Company, Saint Rose, LA.

Figures 10, 12, 13a — AEA Technology PLC, Arlington Heights, IL.

## Chapter 5. Radiation Measurement

Figure 4 — Victoreen, Solon, OH.

## Chapter 6. Radiation Safety

Figures 1, 3, 5 — Thermo Eberline, Santa Fe, NM.

Figure 2 — Landauer, Incorporated, Glenwood, IL.

Figures 4a, 4e — Industrial Nuclear Company, San Leandro, CA.

Figures 4b, 4c, 4d — NDS Products, Pasadena, TX.

Figure 6b — InnospeXion APS, Hvalsoe, Denmark.

## Chapter 7. Principles of Film Radiography

Figures 1-24 — Eastman Kodak, Rochester, NY.

## Chapter 8. Radiographic Interpretation

Figure 3 — National Institute of Standards and Technology, Gaithersburg, MD.

Figure 6 — Edmund Scientific, Tonawanda, NY.

Figure 7 — Macbeth Division of Kollmorgen Company, Newburgh, NY.

Figure 8 — X-Rite, Incorporated, Grandville, MI.

Figure 14-23 — Eastman Kodak Company, Rochester, NY.

Figure 24, 25, 28, 32, 36, 37 — Southwest Research Institute, San Antonio, TX.

Figure 26, 27, 29-31, 33-35 — Electric Power Research Institute, Charlotte, NC.

## Chapter 10. Radioscopy

Figures 1, 16 — Agfa Pantak Seifert GmbH, Ahrensburg, Germany.

Figure 14 — From R. Halmshaw. Reprinted with permission.

Figure 15 — Yxlon International, Hamburg, Germany.

## Chapter 11. Digital Radiographic Imaging

Figures 2 — Eastman Kodak, Rochester, NY.

Figure 14, 15 — V.J. Technologies, Bohemia, NY.

## Chapter 12. Computed Tomography

Figure 5 — C.V. Mosby Company, Saint Louis, MO.

Figures 6, 7 — R. Schulte.

## Chapter 14. Backscatter Imaging

Figure 10 — American Science and Engineering, Billerica, MA.

## Chapter 16. Neutron Radiographic Testing

Figure 4 — Risø National Laboratory, Roskilde, Denmark.

Figure 5 — Aerotest Operations, San Ramon, CA.

Figure 6 — General Electric Company, Schenectady, NY.

Figure 9 — Kaman Sciences, Utica, NY.

Figure 11 — IRT Corporation, San Diego, CA.

Figure 12 — Rolls Royce Limited.

## Chapter 17. Radiographic Testing of Metal Castings

Figure 2 — American Society for Testing and Materials, West Conshohocken, PA.

## Chapter 18. Welding Applications of Radiographic Testing

Figures 29, 30b, 32 — Electric Power Research Institute, Palo Alto, CA.

## Chapter 19. Applications of Radiographic Testing in Utility, Petroleum and Chemical Industries

Figures 2-3 — After the American Petroleum Institute, Washington, DC.

Figures 4-7 — After the American Society of Mechanical Engineers, New York, NY.

Figure 16 — After Tru-Tec Services, La Porte, TX.

## Chapter 20. Aerospace Applications of Radiographic Testing

Figures 1-4, 6-8, 14-18, 20 — Boeing Company, Long Beach, CA.

Figure 5 — Martin Marietta, Denver, CO.

Figures 9-10, 13, 20-23, 25, 27-28, 39-40 — Rocketdyne, Canoga Park, CA.

Figures 11-12 — Boeing Company, Philadelphia, PA.

Figure 19 — Eastern Airlines, Miami, FL.

Figure 24 — Picker International, Cleveland, OH.

Figure 26 — Northrop Grumman, Los Angeles, CA.

Figure 29-31 — Boeing Company, Saint Louis, MO.

Figure 32 — FeinFocus USA, Stamford, CT.

Figure 33, 36 — General Electric, Cincinnati, OH.

Figures 34-35 — United States Air Force; Aerojet Strategic Propulsion, Sacramento, CA.

Figure 37 — White Sands Testing Station, NM.

Figure 38 — University of California Davis, McClellan Nuclear Radiation Center, CA.

Figure 39 — National Aeronautics and Space Administration, Washington, DC.

## Chapter 21. Other Applications of Radiographic Testing

Figures 9a, 11b, 13 — Rad-Icon, Santa Clara, CA.

Figures 9b — V.J. Technologies, Bohemia, NY.

Figure 19 — Intermountain Testing Company (Carl E. Fox), Englewood, CO.

Figures 20 — Virginia Department of Transportation, Richmond, VA.

Figure 23a — Prints and Photographs Division, Library of Congress, Washington, DC.

# Movie Sources

## Chapter 4

Movie. Isotopic source — United States Nuclear Regulatory Commission, Washington, DC

Movie. Collimators — United States Nuclear Regulatory Commission, Washington, DC

## Chapter 6

Movie. Radiation injury — United States Nuclear Regulatory Commission, Washington, DC

Movie. Survey meters — United States Nuclear Regulatory Commission, Washington, DC

Movie. Check equipment — United States Nuclear Regulatory Commission, Washington, DC

Movie. Personnel monitoring devices — United States Nuclear Regulatory Commission, Washington, DC

Movie. Warning tape and signs — United States Nuclear Regulatory Commission, Washington, DC

## Chapter 7

Movie. Conventional radiography gives shadow image — The Boeing Company, Seattle, WA

## Chapter 10

Movie. Automated wheel inspection — Agfa, Mortsel, Belgium

## Chapter 12

Movie. Second generation (rotate and translate) — The Boeing Company, Seattle, WA

Movie. Third generation (rotate only) — The Boeing Company, Seattle, WA

Movie. Electronic device on turntable — Lockheed Missiles and Space Company, Sunnyvale, CA

Movie. Images of electronic device — Lockheed Missiles and Space Company, Sunnyvale, CA

Movie. Tomographic data image of electronic device — Lockheed Missiles and Space Company, Sunnyvale, CA

Movie. Image slices of electronic device, top to bottom — Lockheed Missiles and Space Company, Sunnyvale, CA

Movie. Slices show delaminations in composite fastener hole — The Boeing Company, Seattle, WA

Movie. Transverse image of delaminations in fastener hole — The Boeing Company, Seattle, WA

## Chapter 13

Movie. Exfoliation corrosion, thin to thick — Lockheed Missiles and Space Company, Sunnyvale, CA

Movie. General corrosion, thin to thick — Lockheed Missiles and Space Company, Sunnyvale, CA

Movie. Cracks around fasteners — Lockheed Missiles and Space Company, Sunnyvale, CA

Movie. Cracks around fasteners, in layers from top — Lockheed Missiles and Space Company, Sunnyvale, CA

## Chapter 14

Movie. Backscatter scan of undamaged area — Lawrence R. Lawson, Bradford, PA

Movie. Moving source and sensor into place — Lawrence R. Lawson, Bradford, PA

Movie. Pillowing and corrosion — Lawrence R. Lawson, Bradford, PA

## Chapter 20

Movie. Automated inspection of rocket motor — Agfa, Mortsel, Belgium

## Chapter 21

Movie. Inspection of printed circuit boards — Agilent Technologies, Loveland, CO

Movie. Radiographic inspection of light bulb — Rad-Icon Imaging Corporation, Santa Clara, CA

Movie. Cargo scanning — ARACOR, Sunnyvale, CA

Movie. Image acquisition and evaluation — ARACOR, Sunnyvale, CA

Movie. Images at 3 MV and 6 MV — ARACOR, Sunnyvale, CA

Movie. Contraband in water tank — ARACOR, Sunnyvale, CA